INFECTION AND CONTROL OF VECTOR-BORNE DISEASES

EDITED BY: Lubin Jiang, Jun Feng, Xiaojun Chen, Khalid B. Beshir, Tianmu Chen and Xiaoxiao Wang

PUBLISHED IN: Frontiers in Cellular and Infection Microbiology, Frontiers in Medicine and Frontiers in Public Health

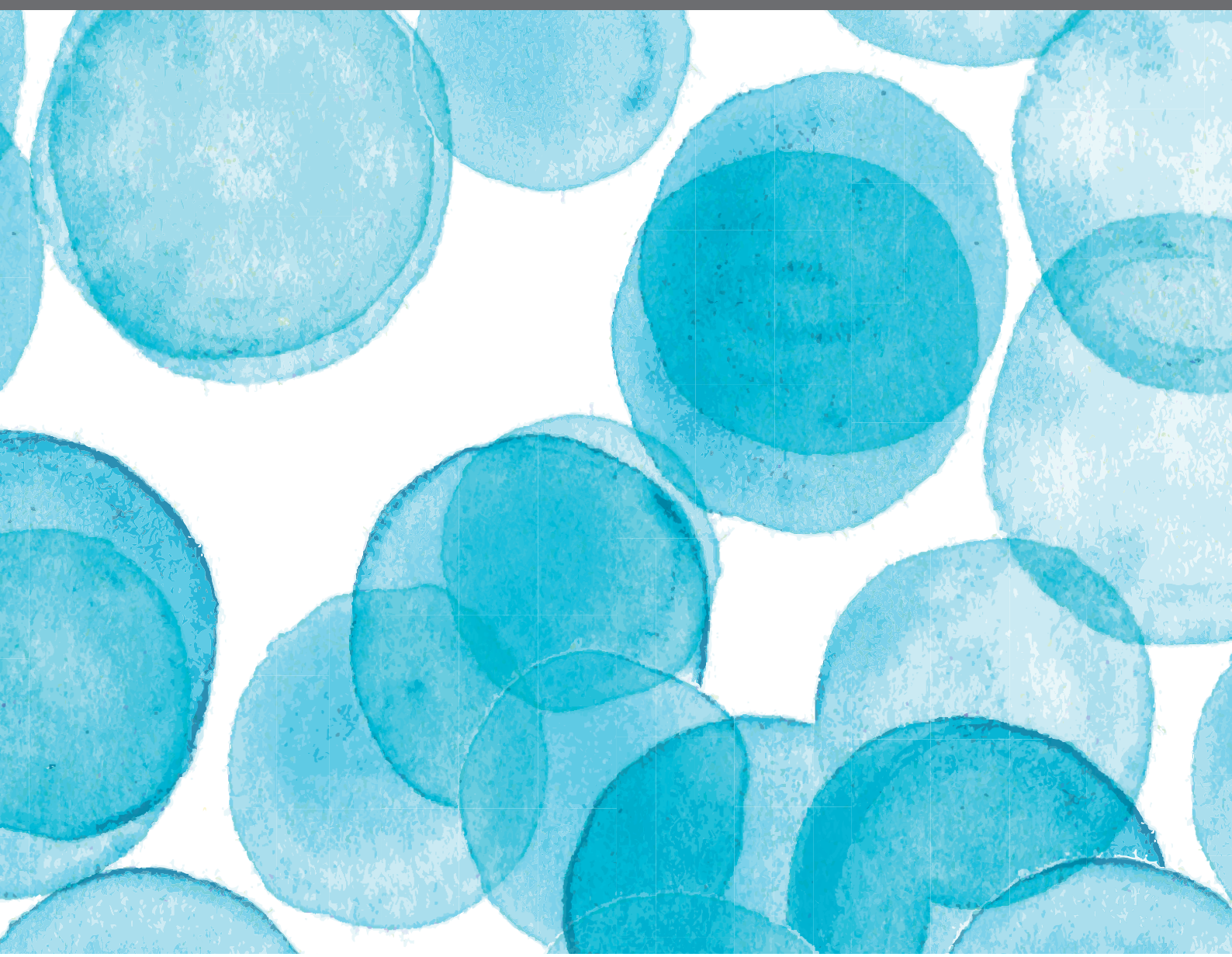

frontiers Research Topics

ISSN 1664-8714
ISBN 978-2-88976-116-6
DOI 10.3389/978-2-88976-116-6

About Frontiers

Frontiers is more than just an open-access publisher of scholarly articles: it is a pioneering approach to the world of academia, radically improving the way scholarly research is managed. The grand vision of Frontiers is a world where all people have an equal opportunity to seek, share and generate knowledge. Frontiers provides immediate and permanent online open access to all its publications, but this alone is not enough to realize our grand goals.

Frontiers Journal Series

The Frontiers Journal Series is a multi-tier and interdisciplinary set of open-access, online journals, promising a paradigm shift from the current review, selection and dissemination processes in academic publishing. All Frontiers journals are driven by researchers for researchers; therefore, they constitute a service to the scholarly community. At the same time, the Frontiers Journal Series operates on a revolutionary invention, the tiered publishing system, initially addressing specific communities of scholars, and gradually climbing up to broader public understanding, thus serving the interests of the lay society, too.

Dedication to Quality

Each Frontiers article is a landmark of the highest quality, thanks to genuinely collaborative interactions between authors and review editors, who include some of the world's best academicians. Research must be certified by peers before entering a stream of knowledge that may eventually reach the public - and shape society; therefore, Frontiers only applies the most rigorous and unbiased reviews.
Frontiers revolutionizes research publishing by freely delivering the most outstanding research, evaluated with no bias from both the academic and social point of view. By applying the most advanced information technologies, Frontiers is catapulting scholarly publishing into a new generation.

What are Frontiers Research Topics?

Frontiers Research Topics are very popular trademarks of the Frontiers Journals Series: they are collections of at least ten articles, all centered on a particular subject. With their unique mix of varied contributions from Original Research to Review Articles, Frontiers Research Topics unify the most influential researchers, the latest key findings and historical advances in a hot research area! Find out more on how to host your own Frontiers Research Topic or contribute to one as an author by contacting the Frontiers Editorial Office: frontiersin.org/about/contact

INFECTION AND CONTROL OF VECTOR-BORNE DISEASES

Topic Editors:
Lubin Jiang, Chinese Academy of Sciences (CAS), China
Jun Feng, Shanghai Municipal Center for Disease Control and Prevention (SCDC), China
Xiaojun Chen, Nanjing Medical University, China
Khalid B. Beshir, London School of Hygiene and Tropical Medicine, United Kingdom
Tianmu Chen, Xiamen University, China
Xiaoxiao Wang, Zhejiang Center for Disease Control and Prevention (Zhejiang CDC), China

Citation: Jiang, L., Feng, J., Chen, X., Beshir, K. B., Chen, T., Wang, X., eds. (2022). Infection and Control of Vector-Borne Diseases. Lausanne: Frontiers Media SA. doi: 10.3389/978-2-88976-116-6

Table of Contents

frontiers in Cellular and Infection Microbiology

ORIGINAL RESEARCH
published: 02 November 2020
doi: 10.3389/fcimb.2020.587708

Dynamic of Composition and Diversity of Gut Microbiota in *Triatoma rubrofasciata* in Different Developmental Stages and Environmental Conditions

Yue Hu[1,2,3†], Hanguo Xie[4†], Minzhao Gao[1], Ping Huang[1,2,3], Hongli Zhou[1,3], Yubin Ma[1,3], Minyu Zhou[1,3], Jinying Liang[1,3], Jun Yang[2] and Zhiyue Lv[1,2,3*]*

[1] Joint Program of Pathobiology, Fifth Affiliated Hospital, Zhongshan School of Medicine, Sun Yat-sen University, Guangzhou, China, [2] Key Laboratory of Tropical Translational Medicine of Ministry of Education, Hainan Medical University, Haikou, China, [3] Key Laboratory of Tropical Disease Control (Sun Yat-sen University), Ministry of Education, Guangzhou, China, [4] Provincial Key Laboratory of Zoonosis Research, Fujian Center for Disease Control and Prevention, Fuzhou, China

OPEN ACCESS

Edited by:
Xiaojun Chen,
Nanjing Medical University, China

Reviewed by:
Xiao-Nong Zhou,
National Institute of Parasitic Diseases, China
Jiraporn Ruangsittichai,
Mahidol University, Thailand

***Correspondence:**
Zhiyue Lv
lvzhiyue@mail.sysu.edu.cn
Jun Yang
hyyj0101@hainmc.edu.cn

[†]These authors have contributed equally to this work

Specialty section:
This article was submitted to Parasite and Host, a section of the journal Frontiers in Cellular and Infection Microbiology

Received: 27 July 2020
Accepted: 09 October 2020
Published: 02 November 2020

Citation:
Hu Y, Xie H, Gao M, Huang P, Zhou H, Ma Y, Zhou M, Liang J, Yang J and Lv Z (2020) Dynamic of Composition and Diversity of Gut Microbiota in Triatoma rubrofasciata in Different Developmental Stages and Environmental Conditions. Front. Cell. Infect. Microbiol. 10:587708. doi: 10.3389/fcimb.2020.587708

Triatoma rubrofasciata (*T. rubrofasciata*), one kind of triatomine insects, is the vector of *Trypanosoma cruzi* (*T. cruzi*), which lead to American trypanosomiasis. Although the gut microbiome may play an essential role in the development and susceptibility of triatomine, there is limited research on the gut microbiota of *T. rubrofasciata*. To elucidate the effect of the vector's developmental stages and environmental conditions on the gut microbiome, we employed *16S* rRNA gene sequencing to profile the gut bacterial community diversity and composition of *T. rubrofasciata*. Significant shifts were observed in the overall gut microbe diversity and composition across the development of *T. rubrofasciata* and specific bacteria were detected in different stages. *Serratia* and *Burkholderia-Caballeronia-Paraburkholderia* were dominant in the 1st nymphal stage, while the abundance of *Staphylococcus* was low in the 1st nymphal stage. *Oceanicaulis* were undetectable in the adult stage and *Odoribacter* peaked in the 2nd nymphal stage. Moreover, *Staphylococcus* was correlated negatively with *Serratia*. Likewise, the total gut microbiota diversity and composition of *T. rubrofasciata* differentiated significantly by environmental conditions. The ingestion of a bloodmeal increased alpha diversity of gut bacterial communities, and *Staphylococcus* was more abundant in laboratory-reared bugs whereas *Enterococcus* enriched in wild-caught bugs. Furthermore, *Pantoea* was negatively correlated with *Staphylococcus*, and positively related to *Bacillus* only. The phylogenetic Investigation of Communities by Reconstruction of Unobserved States (PICRUSt) algorithm showed obvious metagenomic functional differences by environmental conditions, and Chagas disease relevant pathway was enriched in wild-caught *T. rubrofasciata*.

Keywords: *Triatoma rubrofasciata*, gut microbiota, developmental stages, environmental conditions, *16S* rRNA gene sequencing

INTRODUCTION

American trypanosomiasis, also named Chagas disease, is a vector-borne disease for which the causative agent is the protozoan parasite *Trypanosoma cruzi* (*T. cruzi*), which is mainly transmitted by triatomines. Chagas disease is also one of the chronic, systemic and neglected tropical diseases (NTDs); with 8 million people infected worldwide, mostly in Latin America, at least 70 million people are at risk of contagion (Gourbière et al., 2012; Orantes et al., 2018; WHO, 2020). Chagas disease had been commonly recorded in Latin American and Caribbean (LAC) region in the past decades, however, it is being increasingly reported as an emerging infectious disease in North America, Europe and the Indo-Pacific region because of the frequent international migration of population and global invasion of the widespread kissing-bug (Hotez et al., 2012; Dujardin et al., 2015). Furthermore, Chagas disease ranks near the top in terms of annual deaths and disability-adjusted life years (DALYs) lost among all NTDs in the Americas because of its highly debilitating chronic course with alteration of the cardiovascular, digestive and nervous systems (Hotez et al., 2012; Sassera et al., 2013). Since a vaccine or effective treatment for Chagas disease is still unavailable, adequate prevention and control of the disease may be achieved by control of the vectors.

Currently, triatomine insects are composed of 151 species that are grouped into 17 genera and organized into 5 tribes, that is, Aberproseniini, Bolboderini, Cavernicolini, Rhodiniini and Triatomini (Galvão and Justi, 2015; Vieira et al., 2018). Most triatomine species occur in the Americas, while six species belonging to the genus *Linshcosteus* are found in India; moreover, the species of the genus *Triatoma* are distributed in Africa, the Middle East, South-East Asia and the Western Pacific (Vieira et al., 2018).

Triatoma is one of the most diverse genera, including the species *Triatoma rubrofasciata* (*T. rubrofasciata*), which is widespread throughout southern China, such as in Guangdong, Guangxi, Hainan and Taiwan (Ibarra-Cerdeña et al., 2009; Huang et al., 2018). *T. rubrofasciata* is a domiciliated species with urban characteristics and exists in close association with rodents that act as reservoirs of *T. cruzi*. It is naturally infected by *T. cruzi* as well as *Trypanosoma conorrhini*, which is pathogenic to *Rattus rattus* but not to humans (Braga et al., 1998; Cortéz and Gonçalves, 1998). Due to the wide distribution of *T. rubrofasciata* in South China, which suggests the possibility of introduction and transmission of Chagas disease in China, further study of this vector is urgently required.

Triatomines are hemipteran (true) bugs and obligate hematophagous insects with five nymphal stages before the egg reaches adulthood (Gourbière et al., 2012; Oliveira et al., 2018; Vieira et al., 2018). Because both nymphs and adults feed on the blood of vertebrates, so they may become infected and are likely to transmit *T. cruzi* after they ingest blood from infected mammalian hosts. Once the parasites arrive at the gut of the triatomine, they multiply and are able to infect a new host during a subsequent blood meal; they also come in contact with the local gut microbiota and avoid detrimental interactions with the microbiome to survive and develop inside the bug gut (Azambuja et al., 2005; Gourbière et al., 2012; Oliveira et al., 2018).

Various studies of triatomine gut microbes have been conducted, and to date, more than 57 species of cultivable bacteria have been identified (Lima et al., 2018). Previous studies have shown that the most common bacteria in eight species of wild-caught and laboratory-reared triatomines were Gram-negative rods (Azambuja et al., 2005). Interestingly, bacteria of the genus *Rhodococcus* in the triatomine gut are believed to play an important role in the metabolism of the vector, such as by participating in the synthesis of group B vitamins or by being digested by the bugs directly to provide missing nutrients (Sassera et al., 2013). Moreover, the most attractive aspect is the host-symbiont relationship between triatomines and *Rhodococcus*; since *Rhodococcus* bacteria can be easily cultured and genetically modified to harm the pathogen in vector gut, they are probably suitable tools for the control of trypanosomiasis (Sassera et al., 2013). Another study found that the SM365 and RPH strains of *Serratia marcescens*, which is a common symbiont of various triatomine species, exhibit trypanolytic activity toward several *T. cruzi* strains (Azambuja et al., 2004).

However, previous studies of the triatomine gut microbiome have been based mostly on the isolation and identification of cultivable bacteria, did not reflect the relative abundances of these species under natural conditions, and inevitably missed many taxa that could not be cultivated (da Mota et al., 2012; Oliveira et al., 2018). On the other hand, cultivation-independent methods, such as high-throughput DNA sequencing, allow fast and accurate description of bacterial diversity, especially for uncultivable microbes, which are impossible to detect with cultivation-dependent methods (da Mota et al., 2012; Oliveira et al., 2018).

To date, *16S* ribosomal RNA (rRNA) gene sequencing has been applied in the characterization of the gut microbiota in some triatomine species (Gumiel et al., 2015; Díaz et al., 2016; Dumonteil et al., 2018; Oliveira et al., 2018; Orantes et al., 2018; Rodríguez-Ruano et al., 2018); to the best of our knowledge, the gut microbiome of *T. rubrofasciata* has not yet been investigated. Hence, in this study, we applied this technology to determine and compare the relative abundance of both cultivable and uncultivable bacteria in the gut of *T. rubrofasciata* from 1st instar nymphs to adults for the first time and tried to elucidate the potential interactions between the vector and colonizing bacteria during vector development. In addition, we used *16S* rRNA gene sequencing to examine the gut flora of wild-caught and laboratory-reared *T. rubrofasciata* for the first time to explore and compare the diversity and composition of the gut microbes of triatomines and reveal the correlations between environmental conditions and specific gut microbiota profiles.

MATERIALS AND METHODS

Bug Collection and DNA Extraction

The four wild adult triatomines used in this study were captured in Huping village (E 117°38′, N 24°39′), Fengshan town, Hua'an county, Zhangzhou city, Fujian province, China, by technicians from the Fujian Center for Disease Control and Prevention, China, in August 2017. A set of 45 randomly selected laboratory-reared triatomines at each developmental stage (1st to 5th instar nymphs plus male and female adults) were reared from eggs of local *T. rubrofasciata* caught in Huping village between July and August 2017.

DNA extraction from the entire gut of individual bugs was performed by using a QIAamp DNA Mini Kit (cat. no. 51306, QIAGEN, Hilden, Germany) according to the manufacturer's protocols. The quality and quantity of the DNA were determined by agarose gel electrophoresis and a Nanodrop 2000 spectrophotometer (Thermo Scientific, Waltham, MA, USA), respectively. Then, the extracted DNA was partly diluted to a concentration of 1 ng/μL and stored at -20°C until use.

Detection of *T. rubrofasciata* Feeding Sources and *T. cruzi* Infection

To determine the feeding sources of wild-caught and laboratory-reared adult triatomines, we used the primer set BM1/BM2 (**Table 1**) synthesized by Sangon Biotech (Shanghai, China) to amplify the mitochondrial cytochrome *b* (*cytb*) gene of all vertebrates. Polymerase chain reactions (PCRs) were performed in a total volume of 50 μL containing approximately 30 ng of DNA template, 1.1 × Golden Star T6 Super PCR Mix (Tsingke, China) and 0.4 μmol/L each primer. Sterile water was used as a negative control to avoid contamination during PCR. Amplifications were performed in a Bio-Rad PCR C1000 Touch instrument (Bio-Rad, USA), with an initial denaturation at 98°C for 2 min, followed by 35 cycles of denaturation at 98°C for 10 s, annealing at 56°C for 30 s, and extension at 72°C for 15 s and a final extension at 72°C for 3 min.

To determine the natural infection status of wild-caught triatomines, the *T. cruzi*-specific TCZ1/TCZ2 nuclear satellite repeat and Tc121/Tc122 minicircle fragment were amplified with the primers listed in **Table 1**. The mixture and conditions used to amplify these two targets were the same as those for *cytb* except that the annealing temperature of the nuclear satellite repeat was different and was set as 60°C.

All PCR products were observed by electrophoresis on 2% agarose gels stained with ethidium bromide, and then the products of all positive reactions were purified using an Agarose Gel DNA Extraction Kit (Takara, Japan). Sequencing reactions were performed using the primers listed in **Table 1** in an Automated DNA Analyzer (ABI 3730XL, Applied Biosystems, Foster City, CA, USA) with the BigDye Terminator v3.1 Cycle Sequencing Kit (cat. no. 4337457, Applied Biosystems, Foster City, CA, USA) by Tsingke Biotechnology Ltd., Co. (Guangzhou, China). Then, the sequences were submitted to the GenBank database for homology searches using BLAST[1].

[1] http://blast.ncbi.nlm.nih.gov/Blast.cgi

16S rRNA Gene Amplification, Library Construction, and Next-Generation Sequencing

The V3-V4 variable regions of the *16S* rRNA gene were amplified with the primers 343F (5'-TACGGRAGGCAGCAG-3') and 798R (5'-AGGGTATCTAATCCT-3') in combination with the barcoded primers and Takara Ex Taq DNA polymerase (cat. no. RR001Q, Takara, Japan), while the diluted DNA was used as a template. The quality of the PCR amplicon products and the relative intensity of the bands were determined by agarose gel electrophoresis, and then, Agencourt AMPure XP beads (cat. no. A63881, Beckman Coulter, Brea, CA, USA) were applied to purify the amplicon, and another round of PCR was subsequently performed. After purification with Agencourt AMPure XP beads once again, the final amplicon was quantified by a Qubit® dsDNA HS Assay Kit (cat. no. Q32852, Life Technologies, Waltham, MA, USA). Purified amplicons from each sample were pooled together in equal amounts for next-generation sequencing on the Illumina MiSeq platform following the manufacturer's guidelines.

Quality Control of Sequencing Data and Bacterial Classification

Raw sequencing data were obtained in FASTQ format. Paired-end reads were then preprocessed with Trimmomatic software[2] (Bolger et al., 2014) to detect and cut off ambiguous bases from the N terminus. Low quality sequences with average quality scores lower than 20 were also removed using the sliding window trimming approach. Then, paired-end reads were assembled by Fast Ligation-Based Automatable Solid-Phase High-Throughput (FLASH) software (version 1.2.11) (Reyon et al., 2012). The parameters for assembly were set as 10 base pairs (bp) of minimum overlap, 200 bp of maximum overlap and 20% maximum mismatch rate. Furthermore, reads with ambiguous, homologous sequences and a total length of less than 200 bp were abandoned, while reads with 75% bases above Q20 were retained. Next, reads with chimeras were detected and removed by Quantitative Insights Into Microbial Ecology (QIIME) software (version 1.8.0) (Caporaso et al., 2010).

Clean reads were subjected to primer sequence removal and clustering to generate operational taxonomic units (OTUs) (Blaxter et al., 2005) using Vsearch software[3] (Rognes et al., 2016) with a 97% sequence similarity cutoff (equal to the bacterial species level). The representative read was chosen from each OTU by selecting the most abundant sequence using the QIIME package. All high-quality representative sequences were annotated and blasted against the Silva database (version 123) on the basis of the Ribosomal Database Project (RDP) classifier with the confidence threshold set as 70% (Wang et al., 2007).

Sequences identified as DNA from non-bacterial sources, such as chloroplasts, mitochondria, Archaea, and Eukarya, as well as singletons, were filtered out. Then, the rarefied OTU table

[2] http://www.usadellab.org/cms/index.php?page=trimmomatic
[3] https://github.com/torognes/vsearch

TABLE 1 | Primers used to amplify the specific genes in this study.

Gene target	Primer name	Forward primer (5′→3′)	Reverse primer (5′→3′)	Expected length (bp)
Vertebrate mtDNA *cytb*	BM1/BM2	CCCCTCAGAATGATATTTGTCCTCA (Boakye et al., 1999)	CCATCCAACATCTCAGCATGATGAAA (Boakye et al., 1999)	358
Trypanosoma cruzi nDNA satellite repeat	TCZ1/ TCZ2	CGAGCTCTTGCCCACACGGGTGCT (Moser et al., 1989)	CCTCCAAGCAGCGGATAGTTCAGG (Moser et al., 1989)	188
Trypanosoma cruzi minicircle kDNA	Tc121/ Tc122	AAATAATGTACGGG(T/G)GAGATGCATGA (Wincker et al., 1994)	GGTTCGATTGGGGTTGGTGTAATATA (Wincker et al., 1994)	330

was applied to illustrate the composition of the gut bacteria in each bug and for further analysis.

Alpha Diversity and Beta Diversity

To estimate within-sample diversity, alpha diversity estimators, such as the number of observed species, Chao1 richness estimator, Shannon-Wiener index, Good's coverage estimator and phylogenetic diversity index, were obtained by using Mothur[4] (Schloss et al., 2009) for each individual. The number of observed species indicated the number of OTUs that were actually observed, while the Chao1 richness estimator was used to estimate the number of OTUs that were actually present in the bacterial community. The Shannon-Wiener index reflected both the richness and the evenness of species in the community; the higher the value was, the higher the diversity of the community. Sample coverage was revealed by the Good's coverage estimator, and the depth of sequencing substantially covered all the species in the sample if the value was close to one. The phylogenetic diversity index based on random sampling of OTUs indicated the evolutionary distance relationship among OTUs; the higher the value was, the greater the evolutionary distance of the species.

Beta diversity, that is, between-sample diversity, was then monitored with principal coordinate analysis (PCoA) and nonmetric multidimensional scaling (NMDS), two kinds of ordination analyses, based on weighted UniFrac distance metrics or Bray-Curtis distance metrics. Moreover, one-way analysis of similarity (ANOSIM) was performed to assess whether the differences among the groups identified by NMDS were significant with 1,000 Monte Carlo permutation tests. In addition, the relative levels of gut bacterial community dispersal from each group were visualized by bar plots at both the phylum level and the genus level.

Statistical Analysis

One-way analysis of variance (ANOVA) or Student's *t* test was performed to distinguish differences in gut microbial communities among multiple groups or between two groups, respectively, and differences were considered statistically significant at a *p*-value lower than 0.05. Linear discriminant analysis (LDA) coupled with effect size (LEfSe) measurement[5] (Segata et al., 2011) was applied to identify gut microbiome that were distinct from different groups. To identify the key signature gut flora of triatomines, a random forest (RF) classification model was built to estimate the importance of the top 30 dominant genera with the mean decrease gini, a measure applied to rank each genus in the model. Finally, Spearman correlation coefficients among the top 30 predominant bacterial genera were calculated to demonstrate the relationships among these genera. Unless otherwise stated, statistical analyses and plotting were carried out using R software (version 3.5.1).

Functional Profile Prediction for Gut Bacterial Communities

The functional profiles of gut bacterial communities were predicted with Phylogenetic Investigation of Communities by Reconstruction of Unobserved States (PICRUSt)[6] (Langille et al., 2013) on the basis of *16S* sequencing data annotated by the Greengenes reference database[7] (DeSantis et al., 2006). Then, the predicted functions in combination with functional categorization were obtained by mapping the normalized OTU data in the Kyoto Encyclopedia of Genes and Genomes (KEGG) database[8]. The differences between samples and groups were calculated by the Kruskal-Wallis (KW) rank sum test and visualized by a heatmap in level 3 of KEGG pathways.

RESULTS

Identification of Feeding Sources and Natural Infection

Using the primer set BM1/BM2, we successfully amplified the *cytb* gene of vertebrates from the digestive tract of laboratory-reared adult triatomines, obtaining the characteristic 358-bp product, but this amplification failed in wild-caught triatomines. The feeding source of the laboratory-reared triatomines was identified as *Mus musculus*, as the triatomines were fed on the blood of ICR mice in our laboratory. Additionally, neither the *T. cruzi*-specific TCZ1/2 nuclear satellite repeat nor the Tc121/122 minicircle fragment was amplified from the gut of wild-caught triatomines, which suggested that the four bugs did not host *T. cruzi*.

Summary of High-Throughput Sequencing Data

A total of 1,479,154 high-quality sequences were yielded using *16S* rRNA gene amplicon sequencing from 49 extracted DNA samples of the triatomine gut, with an average of 30,186 reads per

[4] http://www.mothur.org
[5] http://huttenhower.org/galaxy
[6] http://picrust.github.com
[7] http://greengenes.lbl.gov
[8] http://www.genome.jp/kegg/pathway.html

sample after quality and abundance filtering, and the average sequence length was 438 bp. Among these reads, 1,765 OTUs were identified at a sequence similarity threshold of 97% (**Supplementary Table 1**). The high value of Good's coverage index in all the triatomine samples indicated that the sequencing depth was sufficient for profiling of the bacterial communities present (**Supplementary Table 2**).

Dynamic Alteration in the Gut Microbiota Across *T. rubrofasciata* Developmental Stages

First, alpha diversity estimators were used to reveal marked differences in the richness and diversity of species in the community during triatomine development. Statistically significant differences were observed in the Chao1 index, Shannon-Wiener index, observed species and phylogenetic diversity index among the bug development stages. All four of the alpha diversity estimates increased in young nymphs (1^{st}-3^{rd} stages) but decreased obviously from 4^{th} stage nymphs, reaching the lowest value in nymphs of the fifth instar; however, the value rebounded to the highest value in adults, especially in the female adults (**Figure 1**, KW test, $p < 0.05$ for all comparisons), which indicated that the gut bacteria of *T. rubrofasciata* were affected by aging, and the gut communities in adults were more rich and even than those at earlier stages. Then, PCoA plots based on weighted UniFrac distances demonstrated that the composition of the bug gut flora was related to the development stage, with 65.12% and 18.07% variation explained by principal component (PC) 1 and PC 2, respectively; 1^{st} stage nymphs were distant from the other nymphs and adults, and this result was mainly driven by the largest differences in the abundances of *Staphylococcus* and *Serratia* between 1^{st} stage nymphs and the others (**Figure 2A**). Obvious separation of nymphs of the first instar was also found in the NMDS plot on the basis of Bray-Curtis dissimilarities; moreover, the separation of 1^{st}-2^{nd} stage nymphs from older nymph stages and adults became evident, although older nymph stages and adults seemed closely related to each other, samples were still clustered according to developmental stage (**Figure 2B**). The stress value of NMDS in combination with the one-way ANOSIM results (R = 0.1822, p = 0.001) suggested that the grouping of NMDS was reliable. Overall, diversity analyses indicated that the gut microbes of *T. rubrofasciata* differ with age, in both the richness and evenness of the community in the microbiota structure.

Subsequently, bar plots were generated based on the relative abundances of the top 15 dominant gut bacteria at the phylum level (**Figure 3A**) and the genus level (**Figure 3B**) in different groups to

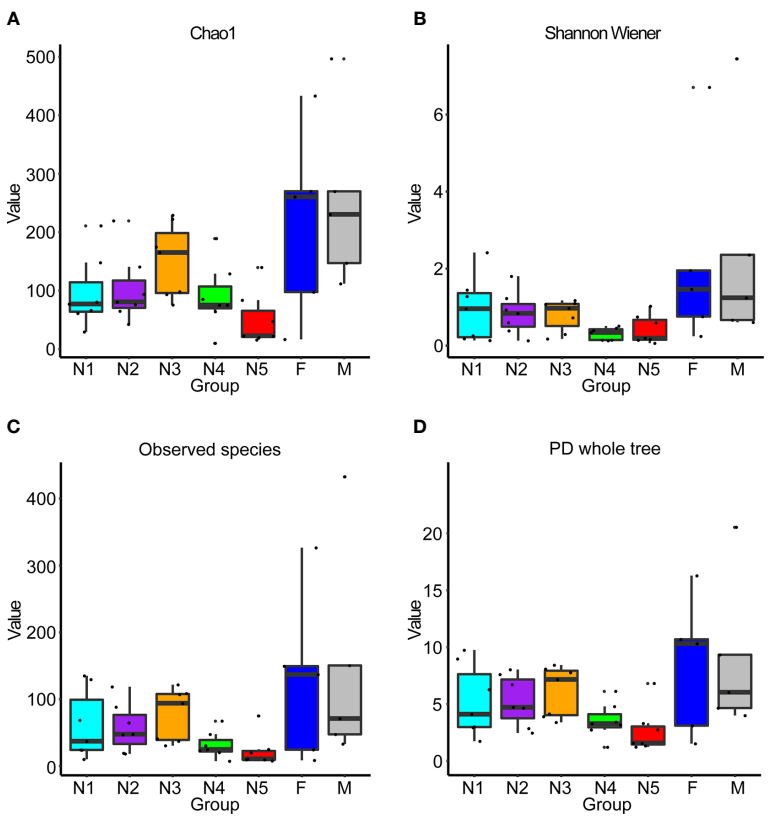

FIGURE 1 | Box plots of *16S* rRNA gene sequences obtained from gut samples of *T. rubrofasciata* across developmental stages based on alpha diversity analyses. Each column represents one group (N1, 1^{st} stage nymphs; N2, 2^{nd} stage nymphs; N3, 3^{rd} stage nymphs; N4, 4^{th} stage nymphs; N5, 5^{th} stage nymphs; F, female adult; M, male adult). The top and bottom whiskers indicate the maximum and minimum values, respectively, and the hyphen represents the median value. **(A)** Chao1. **(B)** Shannon Wiener. **(C)** Observed species. **(D)** PD whole tree.

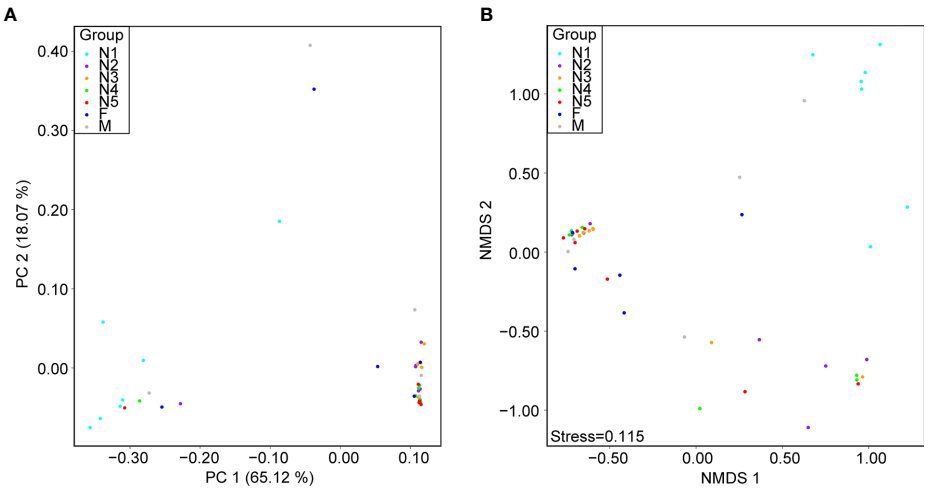

FIGURE 2 | Beta diversity differences in *T. rubrofasciata* gut samples across developmental stages on the basis of *16S* rRNA gene sequencing (N1, 1st stage nymphs; N2, 2nd stage nymphs; N3, 3rd stage nymphs; N4, 4th stage nymphs; N5, 5th stage nymphs; F, female adult; M, male adult). Each point represents an individual. **(A)** Principal coordinate analysis (PCoA) plot of weighted UniFrac distances. **(B)** Nonmetric multidimensional scaling (NMDS) plot of Bray-Curtis distance.

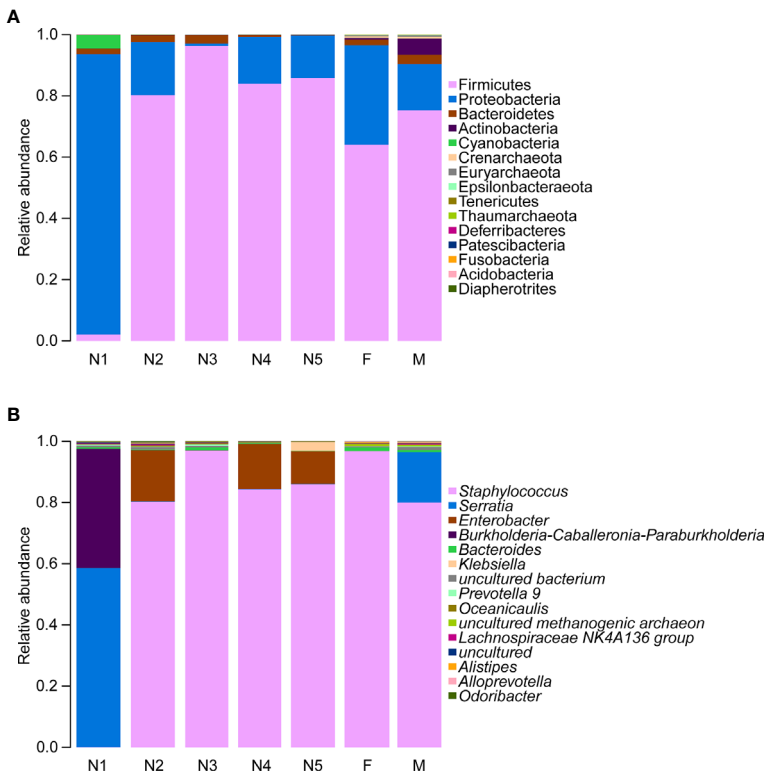

FIGURE 3 | Relative abundances of the 15 most important gut microbiota constituents at the phylum level **(A)** and genus level **(B)** across development stages of *T. rubrofasciata*, as assessed by *16S* rRNA sequencing. Each column represents the composition of the microbial taxa in one group (N1, 1st stage nymphs; N2, 2nd stage nymphs; N3, 3rd stage nymphs; N4, 4th stage nymphs; N5, 5th stage nymphs; F, female adult; M, male adult).

observe the alteration in the gut microbiota composition during the development of *T. rubrofasciata*. Meanwhile, one-way ANOVA was performed to identify significantly altered gut bacterial phyla and genera across the developmental stages. Firmicutes, Proteobacteria, Bacteroidetes and Actinobacteria were the prevalent gut bacterial phyla of the bugs, accounting for more than 95% of the average relative abundances at different ages of *T. rubrofasciata*. Among these phyla, the average abundances of Firmicutes, Proteobacteria and Actinobacteria were altered significantly ($p < 0.05$, **Supplementary Table 3**). The average abundance of Proteobacteria was the highest in the 1st nymphal stage, while the average abundance of Firmicutes was the lowest. However, the opposite result was obtained in the 3rd nymphal stage (**Figures 4A, B**). Furthermore, Actinobacteria, which was almost undetectable in nymphs, increased markedly in adults, particularly in male adults (**Figure 4C**). Moreover, *Staphylococcus*, *Serratia*, *Enterobacter*, *Burkholderia-Caballeronia-Paraburkholderia* and *Bacteroides* were the 5 most important gut bacterial genera in triatomines (**Figure 3B**); nevertheless, the average relative abundance of *Staphylococcus* was low in nymphs of the first instar, whereas *Serratia* was significantly more abundant in 1st stage nymphs (**Figures 5A, B**, $p < 0.05$; see also **Supplementary Table 4**). Interestingly, *Burkholderia-Caballeronia-Paraburkholderia*, which showed the highest average abundance in the 1st nymphal stage, as well as *Oceanicaulis*, was undetectable in the adult stage (**Figures 5C, D**, $p < 0.05$; see also **Supplementary Table 4**). Additionally, the average abundance of *Odoribacter* peaked in the 2nd nymphal stage (**Figure 5E**, $p < 0.05$; see also **Supplementary Table 4**). Taken together, the results showed that not only gut bacterial genera but also gut bacterial phyla changed significantly across *T. rubrofasciata* developmental stages.

Next, LEfSe was applied to identify taxa from the phylum to genus level that were distinct among the developmental stages of triatomines. The cladogram in **Figure 6** shows that *Burkholderia-Caballeronia-Paraburkholderia*, a bacterium from the class Gammaproteobacteria, phylum Proteobacteria, was markedly enriched in the 1st nymphal stage, while *Oceanicaulis* and *Altererythrobacter*, bacteria belonging to the class Alphaproteobacteria, phylum Proteobacteria, were significantly associated with the 2nd nymphal stage. *Staphylococcus*, within the phylum Firmicutes, was identified as the key marker of the 3rd nymphal stage; because it showed higher abundance in nymphs of the third instar than in other stages. Similarly, *Enterobacter*, a member of the class Gammaproteobacteria, phylum Proteobacteria, was linked to the 4th nymphal stage due to its highest average abundance in that stage. *Bacteroides*, in addition to some members from the order Clostridiales, phylum Firmicutes, was the significant bacterial genus related to the adult stage. Nevertheless, no discriminative gut microbiome was found in the 5th nymphal stage.

Finally, the correlation analysis results for the top 30 dominant bacterial genera were plotted (**Figure 7**). Notably, a majority of the bacteria were significantly positively related to each other, which revealed a symbiotic relationship of the gut microbiota in *T. rubrofasciata*. Even so, most negative correlations were found between the 5 most abundant gut bacteria and the remaining bacteria; most importantly, *Staphylococcus* was negatively correlated with *Serratia* ($p < 0.001$).

Comparison of the Gut Microbiota in Wild-Caught and Laboratory-Reared *T. rubrofasciata*

Based on the boxplot of Chao1, observed species and phylogenetic diversity, we found that the alpha diversity of wild-caught *T. rubrofasciata* was significantly lower than that of laboratory-reared *T. rubrofasciata* (**Figures 8A–C**, KW test, $p < 0.05$ for all comparisons); because the wild-caught triatomines had not ingested a blood meal before we captured them. In addition, differences in gut bacterial communities between wild-caught and laboratory-reared insects were visualized by a three-dimensional PCoA plot on the basis of weighted UniFrac distances. A clear separation was observed between the gut microbiome of wild-caught and laboratory-reared insects, with all three variables together explaining 95.92% of the total variance (**Figure 8D**).

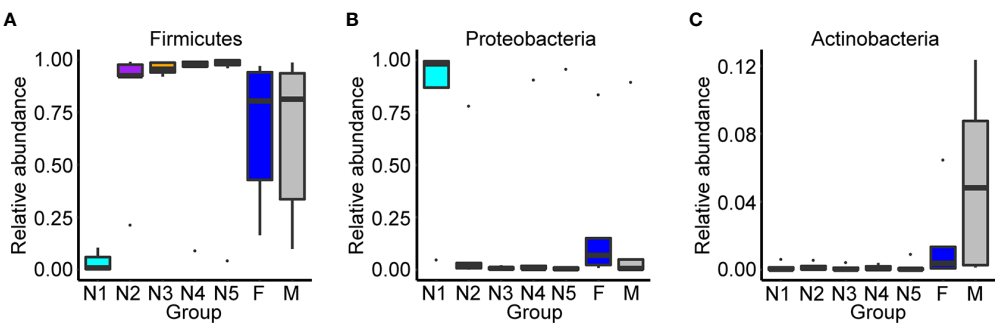

FIGURE 4 | Relative abundances of the significantly altered 15 most important gut phyla across developmental stages of *T. rubrofasciata*. Each column represents one group (N1, 1st stage nymphs; N2, 2nd stage nymphs; N3, 3rd stage nymphs; N4, 4th stage nymphs; N5, 5th stage nymphs; F, female adult; M, male adult). The top and bottom whiskers indicate the maximum and minimum values, respectively, and the hyphen represents the median value. **(A)** Firmicutes. **(B)** Proteobacteria. **(C)** Actinobacteria.

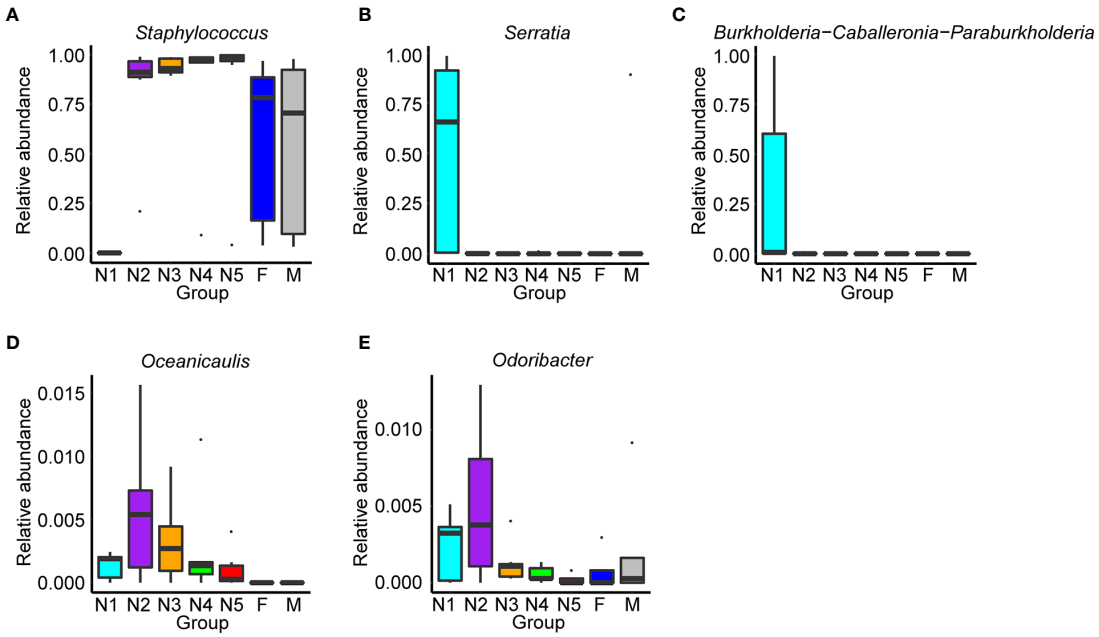

FIGURE 5 | Relative abundances of the significantly altered 15 most important gut genera across developmental stages of *T. rubrofasciata*. Each column represents one group (N1, 1st stage nymphs; N2, 2nd stage nymphs; N3, 3rd stage nymphs; N4, 4th stage nymphs; N5, 5th stage nymphs; F, female adult; M, male adult). The top and bottom whiskers indicate the maximum and minimum values, respectively, and the hyphen represents the median value. **(A)** *Staphylococcus*. **(B)** *Serratia*. **(C)** *Burkholderia-Caballeronia-Paraburkholderia*. **(D)** *Oceanicaulis*. **(E)** *Odoribacter*.

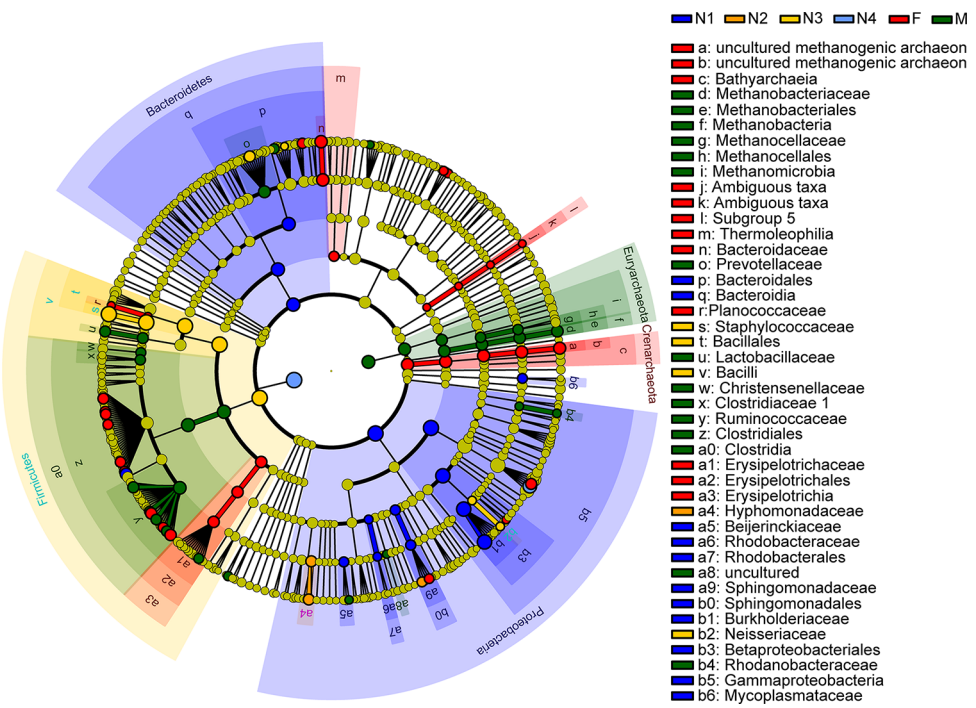

FIGURE 6 | Cladogram showing discriminated taxa at different ages of *T. rubrofasciata* (N1, 1st stage nymphs; N2, 2nd stage nymphs; N3, 3rd stage nymphs; N4, 4th stage nymphs; N5, 5th stage nymphs; F, female adult; M, male adult). Regions with different colors represent different groups. Different colored nodes in the branches represent the microbial groups that play an important role in the corresponding groups, whereas yellow nodes indicate bacterial groups that are nonsignificant in all groups.

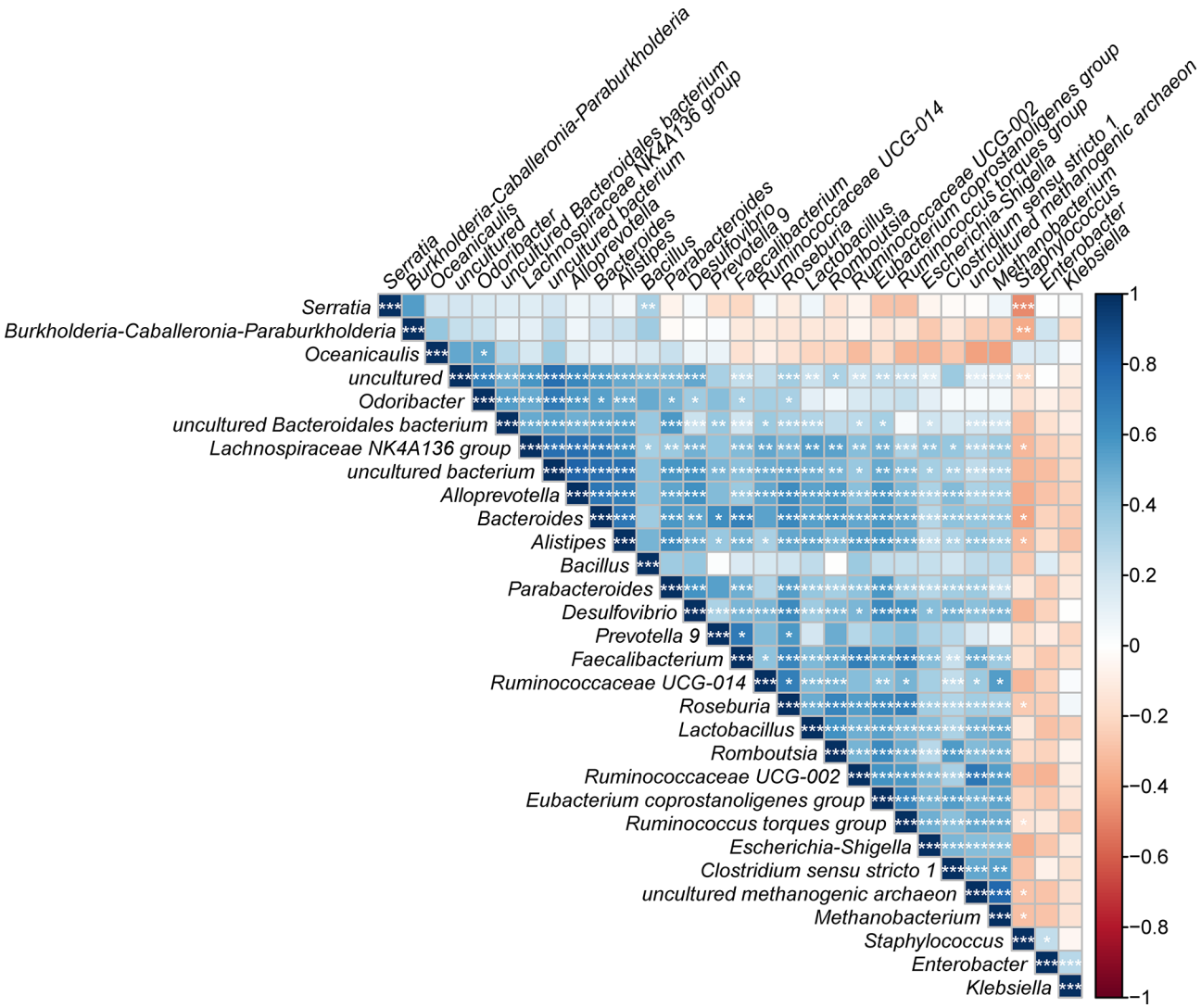

FIGURE 7 | Correlation plot showing the relationship among the top 30 predominant gut bacteria across developmental stages of *T. rubrofasciata*. The correlations between the bacteria are indicated by colors; blue indicates positive correlation, while red indicates negative correlation, with a darker color indicating a stronger correlation (*$p < 0.05$, **$p < 0.01$, ***$p < 0.001$).

Alterations in the gut flora were determined based on the relative proportions of different taxa, with a sharp reduction in the relative abundance of Proteobacteria ($p < 0.05$) and an increase in the abundance of Firmicutes, but the difference between laboratory-reared bugs and wild-caught bugs at the phylum level was not significant (**Figure 9A**; see also **Supplementary Table 5**). At the genus level, significant differences in bacterial abundances of the 15 most important genera were observed only in *Staphylococcus* and *Enterococcus*. The former was more abundant in laboratory-reared bugs than in wild-caught bugs, while the latter was relatively highly enriched in wild-caught bugs (**Figure 9B**, $p < 0.05$; see also **Supplementary Table 6**).

LEfSe identified 20 biomarkers, of which *Pantoea*, belonging to the phylum Proteobacteria, was markedly associated with wild-caught insects because of its absence in laboratory-reared insects, whereas *Staphylococcus*, within Firmicutes phylum, was closely linked with laboratory-reared insects (**Figure 10**). To establish a prediction model to distinguish laboratory-reared triatomines from wild-caught triatomines according to the abundance of genera as measured in the gut, we applied machine learning combined with RF analysis. The results demonstrated that the genera *Pantoea* and *Lactobacillus* were the variables with the highest importance in the model, which indicated that these two taxa had the strongest prediction power (**Figure 11**).

Using the calculated Spearman correlation coefficients for the top 30 dominant gut microbes at the genus level, we observed both positive and negative correlations among these microbes, with the former being more common (**Figure 12**). Interestingly, *Pantoea* was negatively correlated with *Staphylococcus* and other taxa and positively related to *Bacillus* only ($p > 0.05$).

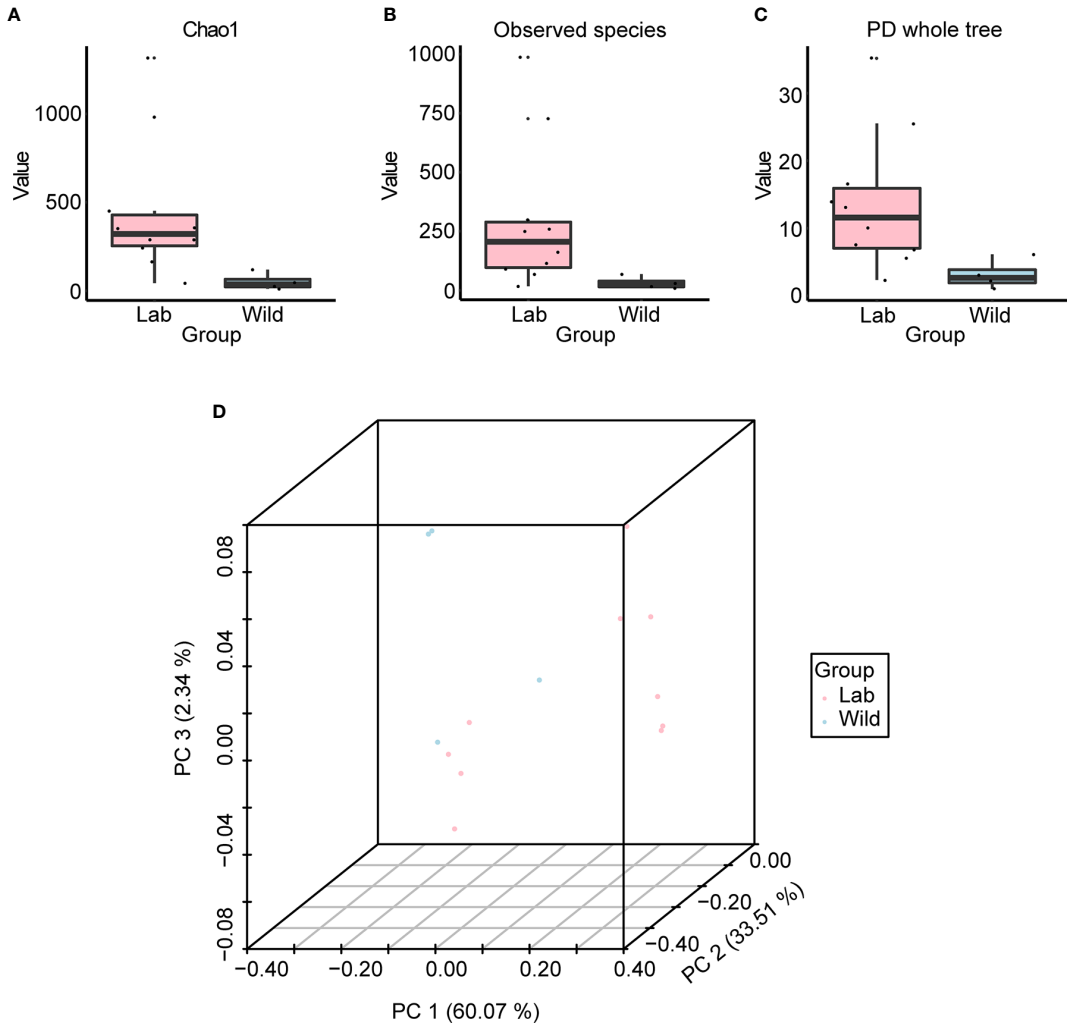

FIGURE 8 | Alpha diversity and beta diversity of laboratory-reared and wild-caught *T. rubrofasciata*. **(A)** Chao1. **(B)** Observed species. **(C)** Phylogenetic diversity index. **(D)** Principal coordinate analysis (PCoA) plot of weighted UniFrac distances.

In addition, to predict the functional differences in the gut bacterial community between laboratory-reared and wild-caught *T. rubrofasciata*, a hierarchical clustering heat map was plotted by utilizing the PICRUSt algorithm to map the KEGG pathways (**Supplementary Figure 1**). The results demonstrated that pathways associated with metabolism of amino acids (D-arginine and D-ornithine metabolism, ko00472), metabolism of lipids (primary bile acid biosynthesis, ko00120; and secondary bile acid biosynthesis, ko00121), metabolism of terpenoids and polyketides (carotenoid biosynthesis, ko00906) and infectious disease (*Staphylococcus aureus* infection, ko05150) were upregulated in laboratory-reared triatomines ($p < 0.05$). In contrast, pathways such as those associated with glycan biosynthesis and metabolism (N-glycan biosynthesis, ko00510; glycosphingolipid biosynthesis - ganglio series, ko00604; and lipopolysaccharide biosynthesis, ko00540), carbohydrate metabolism (starch and sucrose metabolism, ko00500; and ascorbate and aldarate metabolism, ko00053), amino acid metabolism (glutathione metabolism, ko00480), lipid metabolism (alpha-linolenic acid metabolism, ko00592), terpenoid and polyketide metabolism (biosynthesis of siderophore group nonribosomal peptides, ko01053), the immune system (RIG-I-like receptor signaling pathway, ko04622; antigen processing and presentation, ko04612; and NOD-like receptor signaling pathway, ko04621), cell motility (flagellar assembly, ko02040; and bacterial chemotaxis, ko02030), membrane transport (bacterial secretion system, ko03070), and infectious disease (Chagas disease, ko05142; and African trypanosomiasis, ko05143) were enriched in wild-caught triatomines ($p < 0.05$).

DISCUSSION

Based on the adaptation of triatomines to human dwellings, these insects have traditionally been classified into four categories: sylvatic species, intrusive species, domiciliary species and domestic species (Carbajal-de-la-Fuente et al., 2019).

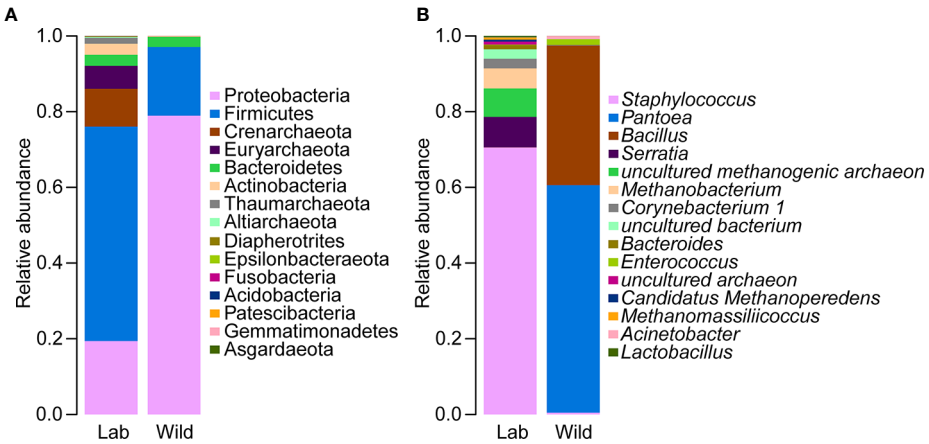

FIGURE 9 | Relative abundances of the 15 most important gut microbiota constituents of laboratory-reared and wild-caught *T. rubrofasciata* at the phylum level **(A)** and genus level **(B)**, as assessed by *16S* rRNA sequencing.

T. rubrofasciata, as one kind of domiciliary species, has recently been frequently captured in human houses or near living areas in southern China (Liu et al., 2017; Huang et al., 2018; Hu et al., 2019; Shi et al., 2020), and residents who were reportedly bitten by this insect showed some clinical symptoms, including an urticaria-like systemic skin response or anaphylactic shock (Huang et al., 2018; Shi et al., 2020). Although *T. cruzi* has not been detected in wild-caught *T. rubrofasciata* in China to date, increased attention should be paid to the prevention and control of this vector due to the living habit of *T. rubrofasciata*. In addition, the feeding sources of wild-caught *T. rubrofasciata* were not identified in the present study, possibly because the

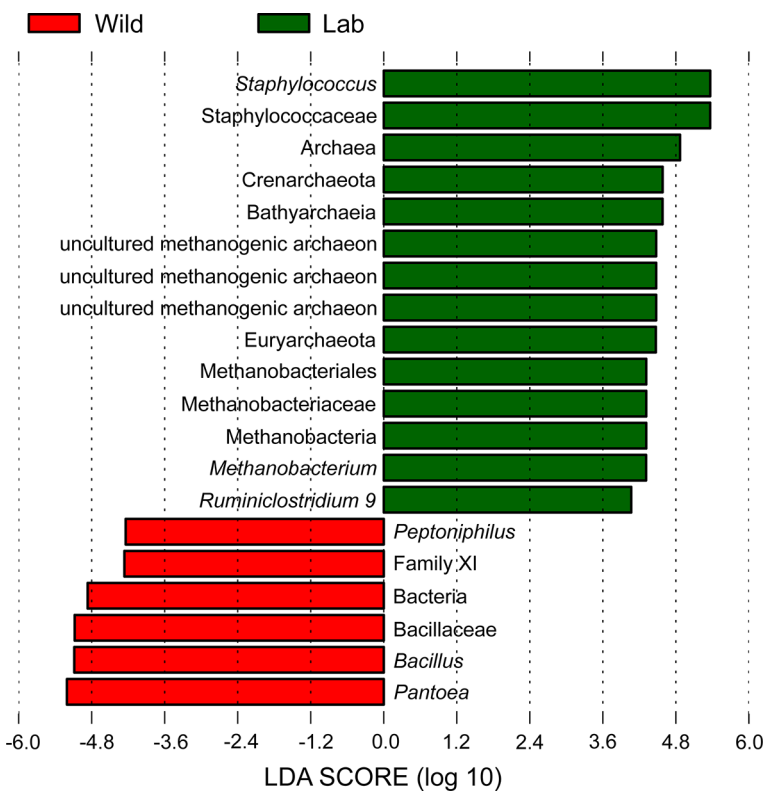

FIGURE 10 | Histogram with LDA scores (threshold > 4) showing differentially abundant gut bacteria between laboratory-reared and wild-caught *T. rubrofasciata*. Taxa highlighted in green are overrepresented in laboratory-reared bugs, while those in red are overrepresented in wild-caught bugs.

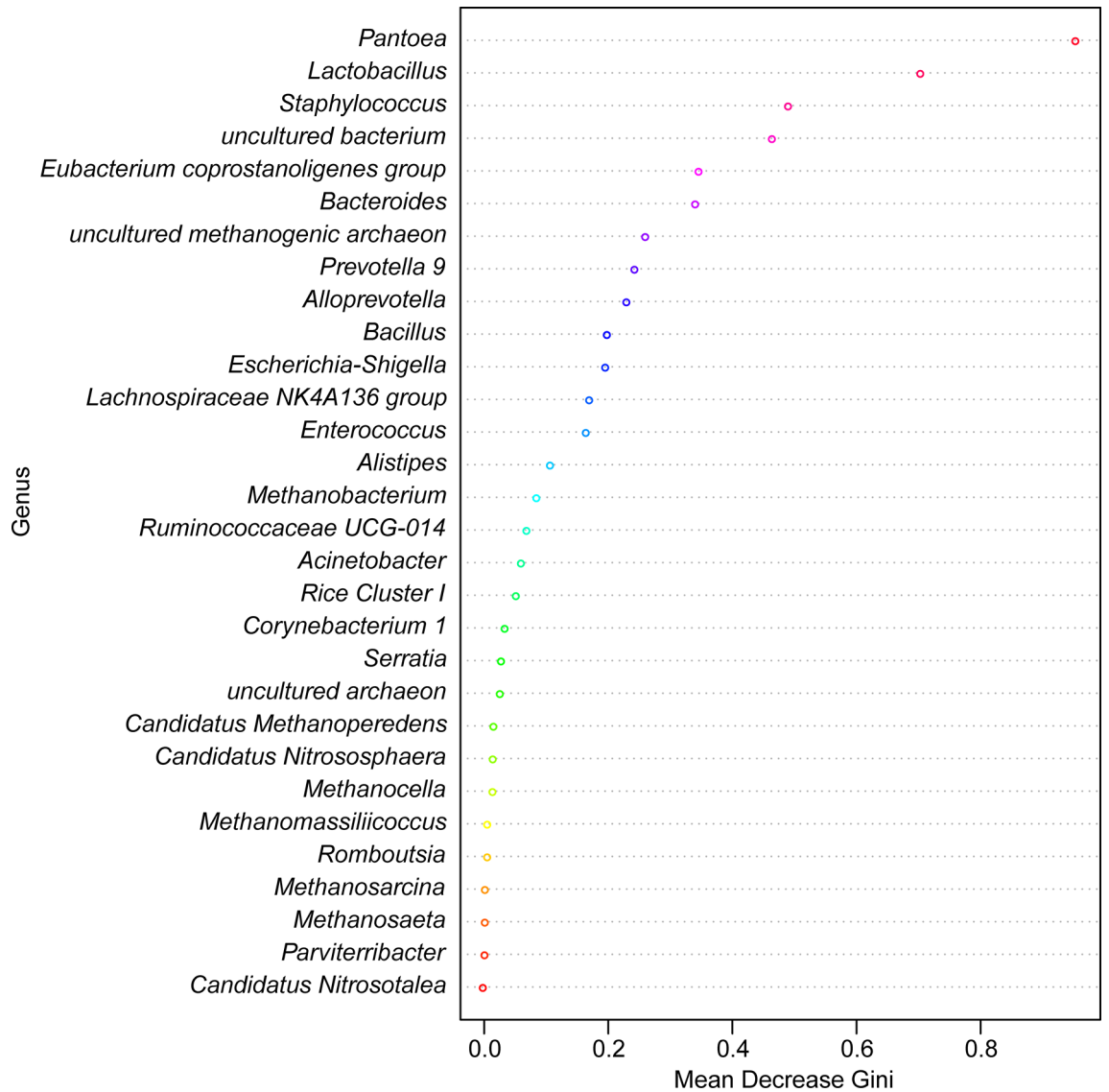

FIGURE 11 | Random forest model classifying laboratory-reared and wild-caught *T. rubrofasciata* at the genus level. The importance levels are represented by the data for the mean decrease gini. Various bacterial genera are indicated by corresponding colors.

triatomines that we caught were starved at that time, so there was limited blood in their guts, making it difficult to extract DNA and perform PCRs. Therefore, we could not draw the conclusion that these wild-caught triatomines did not ingest blood meals, because they have high resistance to starvation, and the volume of blood ingested by adults was proportionally lower than that ingested by nymphs (Cortéz and Gonçalves, 1998; Orantes et al., 2018; Hieu et al., 2019).

In this study, we demonstrated continuous dramatic changes in the gut microbes of *T. rubrofasciata* during development with *16S* rRNA sequencing. Diversity analyses revealed a relative increase in alpha diversity, whereas a relative reduction in beta diversity was observed during bug development, which indicated that the composition of the gut microbiota in *T. rubrofasciata* became increasingly similar with age, which is consistent with a previous study of *Triatoma sordida* (*T. sordida*) (Oliveira et al., 2018). Notably, the triatomines that we used for this part of the study were laboratory reared. Although the environmental conditions during feeding, such as temperature, humidity and blood meal sources, were all the same, the differences in the gut microbiome across developmental stages were still distinct, which indicated that some significant microbes were tightly linked to the development and growth of *T. rubrofasciata*, such as maturation of the immune system, selection of specific bacterial taxa, supplementation of nutrient or digestion (Oliveira et al., 2018).

The predominant phylum among the gut microbes of *T. rubrofasciata* was Firmicutes, which was consistent with the bacterial community in the salivary glands of *Rhodnius prolixus*

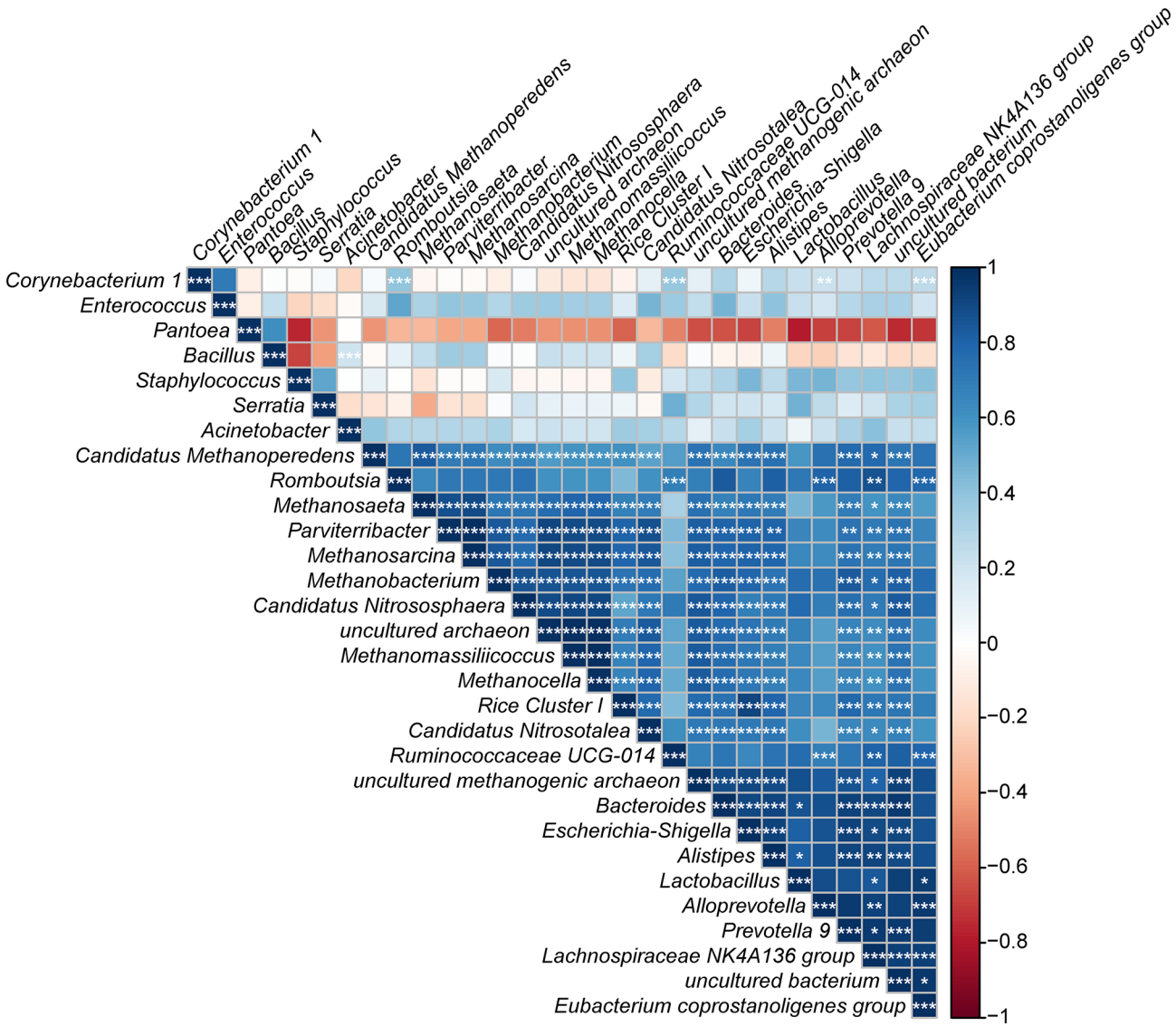

FIGURE 12 | Correlation plot showing the relationship among the top 30 predominant gut bacteria in laboratory-reared and wild-caught *T. rubrofasciata*. The correlations between the bacteria are indicated by colors; blue indicates positive correlation, while red indicates negative correlation, and a darker color indicates a stronger correlation (*$p < 0.05$, **$p < 0.01$, ***$p < 0.001$).

(*R. prolixus*) (Lima et al., 2018). In addition, the abundance of this phylum increased markedly after the 1st nymphal stage, and the same phenomenon was also observed in *T. sordida* (Oliveira et al., 2018). Conversely, the phylum Proteobacteria, which had the highest relative abundance in the salivary glands of *Triatoma brasiliensis*, *Triatoma infestans* (*T. infestans*), *Triatoma rubrovaria* and *Rhodnius milesi* (Lima et al., 2018), as well as in the gut of *Triatoma maculata* and *Rhodnius pallescens* (Montoya-Porras et al., 2018; Kieran et al., 2019), was highly depleted upon reaching the 2nd nymphal stage of *T. rubrofasciata*, this result was opposite to that for *T. sordida* (Oliveira et al., 2018). Furthermore, the variance in gut bacteria between *T. rubrofasciata* and *T. sordida* was also reflected in the abundance of the phylum Actinobacteria, which increased significantly through the development of the former. The gut microbes found in different triatomines form a symbiotic relationship, and the presence of symbiotic organisms can affect the development and survival of both hosts and parasites (Garcia et al., 2010; de Fuentes-Vicente et al., 2018; Salcedo-Porras and Lowenberger, 2019). Among these symbionts, Actinobacteria can provide B complex vitamins, extracellular enzymes, secondary metabolites and antimicrobial bioactive compounds to the host, while Proteobacteria can inhibit the growth of pathogens transmitted by insect vectors (Gumiel et al., 2015; Oliveira et al., 2018). In addition, the results of LEfSe demonstrated that Proteobacteria was the main biomarker in the nymphal stage of *T. rubrofasciata*, whereas Firmicutes that produce antimicrobial

molecules including polyketides and lipopeptides (Aleti et al., 2015) became dominant in the adult stage. Thus, further studies of the complex and dynamic gut microbes may be helpful in finding their potential effects on the host fitness.

Previous studies of the gut bacteria in *Triatoma dimidiata* showed that *Staphylococcus* was identified as the main bacterial genus (Dumonteil et al., 2018), and it was common to all the developmental stages of *T. sordida* but without obvious differences in abundance (Oliveira et al., 2018); however, our study found that *Staphylococcus* had a high relative abundance from the 1st nymphal stage onwards. Interestingly, its abundance was associated with that of *Serratia*. Moreover, *Serratia* and *Enterobacter* were prevalent in the gut microbiome of *T. rubrofasciata*, and the result is consistent with that of a prior study of triatomines, including *T. infestans*, *Triatoma pseudomaculata*, *Panstrongylus megistus*, and *R. prolixus* (Azambuja et al., 2004). Both *Serratia* and *Enterobacter* are members of the family Enterobacteriaceae, which appears frequently in insect vectors, particularly in those whose diets are restricted to a few food sources, and Enterobacteriaceae may play an important role in host fitness by resisting pathogenic microbes. Some members of Enterobacteriaceae are able to kill closely related bacteria to reduce competition for essential nutrients (da Mota et al., 2012; da Mota et al., 2018; Montoya-Porras et al., 2018). Nevertheless, various studies have focused on *Serratia* because it is thought to decrease the population of *T. cruzi* by attacking the parasite's membrane to impede the establishment of this pathogen (Flores-Villegas et al., 2015). The trypanocidal activity of *Serratia* was reported only under *in vitro* conditions, and its protective effect, preventing colonization by *T. cruzi in vivo*, was not distinct. It was hypothesized that the expression of bacterial cytotoxic genes varied among specific regions of the digestive tract (Gumiel et al., 2015; da Mota et al., 2018). Moreover, the diversity of *Serratia* species defines the influence of this genus on the pathogen or the host. While *Serratia* Y1 has the ability to inhibit the development of *Plasmodium berghei* in *Anopheles* by activating the mosquito immune system, *Serratia odorifera* enhances the susceptibility of *Aedes aegypti* to DENV-2 infection, and *Serratia marcescens* is pathogenic to honey bees (Raymann et al., 2018; Bai et al., 2019; Wu et al., 2019). Our results revealed that *Serratia* was enriched in 1st stage nymphs, and as we could not artificially infect *T. rubrofasciata* with *T. cruzi*, the relationship between *Serratia* and *T. cruzi in vivo* was not clear. Likewise, *Enterobacter* was the common bacterium in the gut of *Aedes*, *Anopheles*, and *Culex*, and it could inhibit invasion by and the development of *Plasmodium falciparum via* the generation of reactive oxygen species (ROS) in *Anopheles* (Cirimotich et al., 2011; Jayakrishnan et al., 2018), but its impact on *T. cruzi* has not yet been studied. The abundance of *Enterobacter* in *T. rubrofasciata* did not change significantly, which suggested that this bacterium may play a vital role in the biology of the vector or in the transmission of pathogens. *Enterobacter* species have shown strong hemolytic activity and are capable of performing red blood cell lysis to accelerate blood meal digestion (Muturi et al., 2019). More importantly, the potential of *Enterobacter* and *Serratia* in the paratransgenic control of malaria has been reported widely (Eappen et al., 2013; Koosha et al., 2019a; Koosha et al., 2019b).

In other instances, diversity analyses between wild-caught and laboratory-reared *T. rubrofasciata* suggested that the gut bacterial populations increased dramatically in the latter, contributing to the ingested blood meal. Previous researches have shown that after blood ingestion, the number of gut bacteria increased rapidly, probably due to the richness of iron and protein in the blood meal (Azambuja et al., 2004; Castro et al., 2012). Hence, the restriction of blood feeding may contribute to the low diversity in the gut microbiota of wild-caught triatomines (Gumiel et al., 2015). Similarly, the PCoA plot suggested that the alterations in bacterial communities were also influenced by the bloodmeal of *T. rubrofasciata*, which was explained by the most significant phylum Proteobacteria, with the majority of these bacteria belonging to the class Gammaproteobacteria, while the differentiating genus was *Staphylococcus*, followed by *Enterococcus*, members of the class Bacilli, and the phylum Firmicutes.

Under laboratory conditions, *Staphylococcus* demonstrated a stronger colonization capacity in the gut of *T. rubrofasciata* than other natural bacteria, such as *Pantoea*, but the opposite result was detected in the gut flora of *Aedes albopictus* and *Culex quinquefasciatus* (Gazzoni Araújo Gonçalves et al., 2019). One of the possible reasons is that our wild-caught triatomines had not ingested blood. For the same reason, *Serratia* was not detected in the gut flora of field-caught *T. rubrofasciata*. Because *Staphylococcus* is a common constituent of the natural skin flora of animals, it would proliferate rapidly in the guts of triatomines after a blood meal. Notably, *Staphylococcus* is also an opportunistic pathogen; once people are bitten by *T. rubrofasciata*, secondary bacterial infection occurs, since the vector that transports pathogenic microbes could facilitate colonization by and multiplication of opportunistic invaders by providing an ideal environment. An analogous situation was observed in canid species infected with *Sarcoptes scabiei* mites (DeCandia et al., 2019). Therefore, based on the functional profile of gut bacterial communities predicted by the PICRUSt algorithm, we should pay more attention to the potential of interspecies transmission of the microbiota.

Under natural conditions, *Pantoea* and *Bacillus* were the dominant genera in the gut of *T. rubrofasciata*, which is opposite to the result of a previous study of *T. infestans* (Waltmann et al., 2019), and interestingly, *Pantoea* was absent in the gut bacteria of *T. rubrofasciata*. These phenomena indicated that these genera can be strongly influenced by environmental changes and the consequent immune responses of triatomines. Moreover, *Pantoea* and *Bacillus* are common in *Anopheles* as well as in natural and laboratory-reared sand flies; these bacteria are able to regulate the immune responses of sand fly larvae and could be used as paratransgenic tools against malaria or leishmaniasis (Dinparast Djadid et al., 2011; Akhoundi et al., 2012; Heerman et al., 2015; Karimian et al., 2019). Nevertheless, due to the limited number of natural *T. rubrofasciata* analyzed in the present study, the variations in the gut microbiome composition of wild populations across a

wider geographic area and their correlation with *T. cruzi* infection will require further investigation.

In summary, we profiled the gut microbiome alterations of *T. rubrofasciata* across developmental stages, as well as its gut microbiota succession, under natural and laboratory conditions. Importantly, we observed significant differences in both the diversity and composition of the gut microbes of *T. rubrofasciata* at different ages and environmental statuses. The specific gut bacteria may be modulated by feeding type and may have an effect on *T. cruzi* infection; however, further exploration is essential for determining whether the microbiota changes identified are causal and identifying the important metabolic pathways of gut microbes using metagenomics. Moreover, understanding the interactions among vectors-*T. cruzi*-symbionts (including *Serratia*, *Enterobacter*, *Pantoea* and *Bacillus*), along with understanding the biological functions and potential antiparasitic activity *in vivo* of gut symbionts might lead to the application of these bacteria in paratransgenic control of American trypanosomiasis.

DATA AVAILABILITY STATEMENT

The sequencing data for the *16S* rRNA gene have been deposited in the NCBI Sequence Read Archive under project number PRJNA645287.

AUTHOR CONTRIBUTIONS

ZL, JY, and HX conceived and designed the experiments. ZL, YH, and HX drafted the manuscript. HX collected the samples. YH and MG performed the experiments. YH, MG, and PH collected and analyzed the data. HZ, YM, MZ, and JL participated in study design, technological guidance, and coordination. All authors contributed to the article and approved the submitted version.

FUNDING

This work was supported by grants from the National Natural Science Foundation of China (grant no. 81572023 and 81371836), the National Parasitic Resources Center of China (grant no. NPRC-2019-194-30), Science and Technology Planning Project of Guangdong Province (grant no. 2019B030316025), Natural Science Foundation of Guangdong Province (grant no. 2019A1515011541), the National Key Research and Development Program of China (grant no. 2016YFC1202000 and 2016YFC1200500), the Open Foundation of Key Laboratory of Tropical Translational Medicine of Ministry of Education, Hainan Medical University (grant no. 2020TTM007), the 111 Project (grant no. B12003), Teaching Reform Project of Guangdong Province (grant no. 2017001) and Construction of Fujian Provincial Scientific and Technological Innovation Platform (2019Y2001).

SUPPLEMENTARY MATERIAL

The Supplementary Material for this article can be found online at: https://www.frontiersin.org/articles/10.3389/fcimb.2020.587708/full#supplementary-material

SUPPLEMENTARY FIGURE 1 | Hierarchical clustering heatmap of PICRUSt analysis with annotated *16S* sequencing data demonstrates significant level 3 KEGG pathways between laboratory-reared and wild-caught *T. rubrofasciata*. Samples are shown in columns, and KEGG pathways are shown in rows.

SUPPLEMENTARY TABLE 1 | OTU tables and taxonomic classifications of the *16S* rRNA gene.

SUPPLEMENTARY TABLE 2 | Good's coverage estimators of *T. rubrofasciata* gut samples (N1, 1st stage nymphs; N2, 2nd stage nymphs; N3, 3rd stage nymphs; N4, 4th stage nymphs; N5, 5th stage nymphs; F, female adult; M, male adult).

SUPPLEMENTARY TABLE 3 | One-way ANOVA of relative abundances of gut microbiome constituents across developmental stages of *T. rubrofasciata* at the phylum level (N1, 1st stage nymphs; N2, 2nd stage nymphs; N3, 3rd stage nymphs; N4, 4th stage nymphs; N5, 5th stage nymphs; F, female adult; M, male adult).

SUPPLEMENTARY TABLE 4 | One-way ANOVA of relative abundances of gut microbiome constituents across developmental stages of *T. rubrofasciata* at the genus level (N1, 1st stage nymphs; N2, 2nd stage nymphs; N3, 3rd stage nymphs; N4, 4th stage nymphs; N5, 5th stage nymphs; F, female adult; M, male adult).

SUPPLEMENTARY TABLE 5 | One-way ANOVA of relative abundances of gut microbiome constituents in laboratory-reared and wild-caught *T. rubrofasciata* at the phylum level.

SUPPLEMENTARY TABLE 6 | One-way ANOVA of relative abundances of gut microbiome constituents in laboratory-reared and wild-caught *T. rubrofasciata* at the genus level.

REFERENCES

Akhoundi, M., Bakhtiari, R., Guillard, T., Baghaei, A., Tolouei, R., Sereno, D., et al. (2012). Diversity of the bacterial and fungal microflora from the midgut and cuticle of phlebotomine sand flies collected in North-Western Iran. *PloS One* 7 (11), e50259. doi: 10.1371/journal.pone.0050259

Aleti, G., Sessitsch, A., and Brader, G. (2015). Genome mining: Prediction of lipopeptides and polyketides from Bacillus and related Firmicutes. *Comput. Struct. Biotechnol. J.* 13, 192–203. doi: 10.1016/j.csbj.2015.03.003

Azambuja, P., Feder, D., and Garcia, E. S. (2004). Isolation of Serratia marcescens in the midgut of Rhodnius prolixus: impact on the establishment of the parasite Trypanosoma cruzi in the vector. *Exp. Parasitol.* 107 (1-2), 89–96. doi: 10.1016/j.exppara.2004.04.007

Azambuja, P., Garcia, E. S., and Ratcliffe, N. A. (2005). Gut microbiota and parasite transmission by insect vectors. *Trends Parasitol.* 21 (12), 568–572. doi: 10.1016/j.pt.2005.09.011

Bai, L., Wang, L., Vega-Rodríguez, J., Wang, G., and Wang, S. (2019). A Gut Symbiotic Bacterium Serratia marcescens Renders Mosquito Resistance to Plasmodium Infection Through Activation of Mosquito Immune Responses. *Front. Microbiol.* 10, 1580. doi: 10.3389/fmicb.2019.01580

Blaxter, M., Mann, J., Chapman, T., Thomas, F., Whitton, C., Floyd, R., et al. (2005). Defining operational taxonomic units using DNA barcode data. *Philos. Trans. R Soc. Lond. B Biol. Sci.* 360 (1462), 1935–1943. doi: 10.1098/rstb.2005.1725

Boakye, D. A., Tang, J., Truc, P., Merriweather, A., and Unnasch, T. R. (1999). Identification of bloodmeals in haematophagous Diptera by cytochrome B

heteroduplex analysis. *Med. Vet. Entomol.* 13 (3), 282–287. doi: 10.1046/j.1365-2915.1999.00193.x

Bolger, A. M., Lohse, M., and Usadel, B. (2014). Trimmomatic: a flexible trimmer for Illumina sequence data. *Bioinformatics* 30 (15), 2114–2120. doi: 10.1093/bioinformatics/btu170

Braga, M. V., Pinto, Z. T., and Lima, M. M. (1998). Life cycle and reproductive patterns of Triatoma rubrofasciata (De Gee) (Hemiptera: Reduviidae), under laboratory conditions. *Mem. Inst. Oswaldo Cruz* 93 (4), 539–542. doi: 10.1590/s0074-02761998000400022

Caporaso, J. G., Kuczynski, J., Stombaugh, J., Bittinger, K., Bushman, F. D., Costello, E. K., et al. (2010). QIIME allows analysis of high-throughput community sequencing data. *Nat. Methods* 7 (5), 335–336. doi: 10.1038/nmeth.f.303

Carbajal-de-la-Fuente, A. L., Fernández, M. D. P., Piccinali, R. V., Rodríguez-Planes, L. I., Duarte, R., and Gürtler, R. E. (2019). Occurrence of domestic and intrusive triatomines (Hemiptera: Reduviidae) in sylvatic habitats of the temperate Monte Desert ecoregion of Argentina. *Acta Trop.* 196, 37–41. doi: 10.1016/j.actatropica.2019.04.028

Castro, D. P., Moraes, C. S., Gonzalez, M. S., Ratcliffe, N. A., Azambuja, P., and Garcia, E. S. (2012). Trypanosoma cruzi immune response modulation decreases microbiota in Rhodnius prolixus gut and is crucial for parasite survival and development. *PloS One* 7 (5), e36591. doi: 10.1371/journal.pone.0036591

Cirimotich, C. M., Dong, Y., Clayton, A. M., Sandiford, S. L., Souza-Neto, J. A., Mulenga, M., et al. (2011). Natural microbe-mediated refractoriness to Plasmodium infection in Anopheles gambiae. *Science* 332 (6031), 855–858. doi: 10.1126/science.1201618

Cortéz, M. G., and Gonçalves, T. C. (1998). Resistance to starvation of Triatoma rubrofasciata (De Geer 1773) under laboratory conditions (Hemiptera: Reduviidae: Triatominae). *Mem. Inst. Oswaldo Cruz* 93 (4), 549–554. doi: 10.1590/s0074-02761998000400024

da Mota, F. F., Marinho, L. P., Moreira, C. J., Lima, M. M., Mello, C. B., Garcia, E. S., et al. (2012). Cultivation-independent methods reveal differences among bacterial gut microbiota in triatomine vectors of Chagas disease. *PloS Negl. Trop. Dis.* 6 (5), e1631. doi: 10.1371/journal.pntd.0001631

da Mota, F. F., Castro, D. P., Vieira, C. S., Gumiel, M., de Albuquerque, J. P., Carels, N., et al. (2018). In vitro Trypanocidal Activity, Genomic Analysis of Isolates, and in vivo Transcription of Type VI Secretion System of Serratia marcescens Belonging to the Microbiota of Rhodnius prolixus Digestive Tract. *Front. Microbiol.* 9:3205:3205. doi: 10.3389/fmicb.2018.03205

de Fuentes-Vicente, J. A., Gutiérrez-Cabrera, A. E., Flores-Villegas, A. L., Lowenberger, C., Benelli, G., Salazar-Schettino, P. M., et al. (2018). What makes an effective Chagas disease vector? Factors underlying Trypanosoma cruzi-triatomine interactions. *Acta Trop.* 183, 23–31. doi: 10.1016/j.actatropica.2018.04.008

DeCandia, A. L., Leverett, K. N., and vonHoldt, B. M. (2019). Of microbes and mange: consistent changes in the skin microbiome of three canid species infected with Sarcoptes scabiei mites. *Parasit. Vectors* 12 (1), 488. doi: 10.1186/s13071-019-3724-0

DeSantis, T. Z., Hugenholtz, P., Larsen, N., Rojas, M., Brodie, E. L., Keller, K., et al. (2006). Greengenes, a chimera-checked 16S rRNA gene database and workbench compatible with ARB. *Appl. Environ. Microbiol.* 72 (7), 5069–5072. doi: 10.1128/aem.03006-05

Díaz, S., Villavicencio, B., Correia, N., Costa, J., and Haag, K. L. (2016). Triatomine bugs, their microbiota and Trypanosoma cruzi: asymmetric responses of bacteria to an infected blood meal. *Parasit. Vectors* 9 (1), 636. doi: 10.1186/s13071-016-1926-2

Dinparast Djadid, N., Jazayeri, H., Raz, A., Favia, G., Ricci, I., and Zakeri, S. (2011). Identification of the midgut microbiota of An. stephensi and An. maculipennis for their application as a paratransgenic tool against malaria. *PloS One* 6 (12), e28484. doi: 10.1371/journal.pone.0028484

Dujardin, J. P., Pham Thi, K., Truong Xuan, L., Panzera, F., Pita, S., and Schofield, C. J. (2015). Epidemiological status of kissing-bugs in South East Asia: A preliminary assessment. *Acta Trop.* 151, 142–149. doi: 10.1016/j.actatropica.2015.06.022

Dumonteil, E., Ramirez-Sierra, M. J., Pérez-Carrillo, S., Teh-Poot, C., Herrera, C., Gourbière, S., et al. (2018). Detailed ecological associations of triatomines revealed by metabarcoding and next-generation sequencing: implications for triatomine behavior and Trypanosoma cruzi transmission cycles. *Sci. Rep.* 8 (1), 4140. doi: 10.1038/s41598-018-22455-x

Eappen, A. G., Smith, R. C., and Jacobs-Lorena, M. (2013). Enterobacter-activated mosquito immune responses to Plasmodium involve activation of SRPN6 in Anopheles stephensi. *PloS One* 8 (5), e62937. doi: 10.1371/journal.pone.0062937

Flores-Villegas, A. L., Salazar-Schettino, P. M., Córdoba-Aguilar, A., Gutiérrez-Cabrera, A. E., Rojas-Wastavino, G. E., Bucio-Torres, M. I., et al. (2015). Immune defence mechanisms of triatomines against bacteria, viruses, fungi and parasites. *Bull. Entomol. Res.* 105 (5), 523–532. doi: 10.1017/s0007485315000504

Galvão, C., and Justi, S. A. (2015). An overview on the ecology of Triatominae (Hemiptera:Reduviidae). *Acta Trop.* 151, 116–125. doi: 10.1016/j.actatropica.2015.06.006

Garcia, E. S., Genta, F. A., de Azambuja, P., and Schaub, G. A. (2010). Interactions between intestinal compounds of triatomines and Trypanosoma cruzi. *Trends Parasitol.* 26 (10), 499–505. doi: 10.1016/j.pt.2010.07.003

Gazzoni Araújo Gonçalves, G., Feitosa, A. P. S., Portela-Júnior, N. C., de Oliveira, C. M. F., de Lima Filho, J. L., Brayner, F. A., et al. (2019). Use of MALDI-TOF MS to identify the culturable midgut microbiota of laboratory and wild mosquitoes. *Acta Trop.* 200, 105174. doi: 10.1016/j.actatropica.2019.105174

Gourbière, S., Dorn, P., Tripet, F., and Dumonteil, E. (2012). Genetics and evolution of triatomines: from phylogeny to vector control. *Heredity (Edinb).* 108 (3), 190–202. doi: 10.1038/hdy.2011.71

Gumiel, M., da Mota, F. F., Rizzo Vde, S., Sarquis, O., de Castro, D. P., Lima, M. M., et al. (2015). Characterization of the microbiota in the guts of Triatoma brasiliensis and Triatoma pseudomaculata infected by Trypanosoma cruzi in natural conditions using culture independent methods. *Parasit. Vectors* 8, 245. doi: 10.1186/s13071-015-0836-z

Heerman, M., Weng, J. L., Hurwitz, I., Durvasula, R., and Ramalho-Ortigao, M. (2015). Bacterial Infection and Immune Responses in Lutzomyia longipalpis Sand Fly Larvae Midgut. *PloS Negl. Trop. Dis.* 9 (7), e0003923. doi: 10.1371/journal.pntd.0003923

Hieu, H. V., Do, L. T., Pita, S., Ha, H., Khoa, P. T., Tuan, P. A., et al. (2019). Biological attributes of the kissing bug Triatoma rubrofasciata from Vietnam. *Parasit. Vectors* 12 (1), 585. doi: 10.1186/s13071-019-3844-6

Hotez, P. J., Dumonteil, E., Woc-Colburn, L., Serpa, J. A., Bezek, S., Edwards, M. S., et al. (2012). Chagas disease: "the new HIV/AIDS of the Americas". *PloS Negl. Trop. Dis.* 6 (5), e1498. doi: 10.1371/journal.pntd.0001498

Hu, Y., Gao, M. Z., Huang, P., Zhou, H. L., Ma, Y. B., Zhou, M. Y., et al. (2019). Taxonomic integrative and phylogenetic identification of the first recorded Triatoma rubrofasciata in Zhangzhou, Fujian Province and Maoming, Guangdong Province, China. *Infect. Dis. Poverty* 8 (1), 70. doi: 10.1186/s40249-019-0579-8

Huang, Y. L., Huang, D. N., Wu, W. H., Yang, F., Zhang, X. M., Wang, M., et al. (2018). Identification and characterization of the causative triatomine bugs of anaphylactic shock in Zhanjiang, China. *Infect. Dis. Poverty* 7 (1), 127. doi: 10.1186/s40249-018-0509-1

Ibarra-Cerdeña, C. N., Sánchez-Cordero, V., Townsend Peterson, A., and Ramsey, J. M. (2009). Ecology of North American Triatominae. *Acta Trop.* 110 (2-3), 178–186. doi: 10.1016/j.actatropica.2008.11.012

Jayakrishnan, L., Sudhikumar, A. V., and Aneesh, E. M. (2018). Role of gut inhabitants on vectorial capacity of mosquitoes. *J. Vector Borne Dis.* 55 (2), 69–78. doi: 10.4103/0972-9062.242567

Karimian, F., Vatandoost, H., Rassi, Y., Maleki-Ravasan, N., Mohebali, M., Shirazi, M. H., et al. (2019). Aerobic midgut microbiota of sand fly vectors of zoonotic visceral leishmaniasis from northern Iran, a step toward finding potential paratransgenic candidates. *Parasit. Vectors* 12 (1):10. doi: 10.1186/s13071-018-3273-y

Kieran, T. J., Arnold, K. M. H., Thomas, J. C. T., Varian, C. P., Saldaña, A., Calzada, J. E., et al. (2019). Regional biogeography of microbiota composition in the Chagas disease vector Rhodnius pallescens. *Parasit. Vectors* 12 (1), 504. doi: 10.1186/s13071-019-3761-8

Koosha, M., Vatandoost, H., Karimian, F., Choubdar, N., Abai, M. R., and Oshaghi, M. A. (2019a). Effect of Serratia AS1 (Enterobacteriaceae: Enterobacteriales) on the Fitness of Culex pipiens (Diptera: Culicidae) for Paratransgenic and RNAi Approaches. *J. Med. Entomol.* 56 (2), 553–559. doi: 10.1093/jme/tjy183

Koosha, M., Vatandoost, H., Karimian, F., Choubdar, N., and Oshaghi, M. A. (2019b). Delivery of a Genetically Marked Serratia AS1 to Medically Important Arthropods for Use in RNAi and Paratransgenic Control Strategies. *Microb. Ecol.* 78 (1), 185–194. doi: 10.1007/s00248-018-1289-7

Langille, M. G., Zaneveld, J., Caporaso, J. G., McDonald, D., Knights, D., Reyes, J. A., et al. (2013). Predictive functional profiling of microbial communities using 16S rRNA marker gene sequences. *Nat. Biotechnol.* 31 (9), 814–821. doi: 10.1038/nbt.2676

Lima, M. S., Laport, M. S., Lorosa, E. S., Jurberg, J., Dos Santos, K. R. N., da Silva Neto, M. A. C., et al. (2018). Bacterial community composition in the salivary glands of triatomines (Hemiptera: Reduviidae). *PloS Negl. Trop. Dis.* 12 (9), e0006739. doi: 10.1371/journal.pntd.0006739

Liu, Q., Guo, Y. H., Zhang, Y., Zhou, Z. B., Zhang, L. L., Zhu, D., et al. (2017). First records of Triatoma rubrofasciata (De Gee) (Hemiptera, Reduviidae) in Foshan, Guangdong Province, Southern China. *Infect. Dis. Poverty* 6 (1), 129. doi: 10.1186/s40249-017-0342-y

Montoya-Porras, L. M., Omar, T. C., Alzate, J. F., Moreno-Herrera, C. X., and Cadavid-Restrepo, G. E. (2018). 16S rRNA gene amplicon sequencing reveals dominance of Actinobacteria in Rhodnius pallescens compared to Triatoma maculata midgut microbiota in natural populations of vector insects from Colombia. *Acta Trop.* 178, 327–332. doi: 10.1016/j.actatropica.2017.11.004

Moser, D. R., Kirchhoff, L. V., and Donelson, J. E. (1989). Detection of Trypanosoma cruzi by DNA amplification using the polymerase chain reaction. *J. Clin. Microbiol.* 27 (7), 1477–1482. doi: 10.1128/JCM.27.7.1477-1482.1989

Muturi, E. J., Dunlap, C., Ramirez, J. L., Rooney, A. P., and Kim, C. H. (2019). Host blood-meal source has a strong impact on gut microbiota of Aedes aegypti. *FEMS Microbiol. Ecol.* 95 (1), fiy213. doi: 10.1093/femsec/fiy213

Oliveira, J. L., Cury, J. C., Gurgel-Gonçalves, R., Bahia, A. C., and Monteiro, F. A. (2018). Field-collected Triatoma sordida from central Brazil display high microbiota diversity that varies with regard to developmental stage and intestinal segmentation. *PloS Negl. Trop. Dis.* 12 (8), e0006709. doi: 10.1371/journal.pntd.0006709

Orantes, L. C., Monroy, C., Dorn, P. L., Stevens, L., Rizzo, D. M., Morrissey, L., et al. (2018). Uncovering vector, parasite, blood meal and microbiome patterns from mixed-DNA specimens of the Chagas disease vector Triatoma dimidiata. *PloS Negl. Trop. Dis.* 12 (10), e0006730. doi: 10.1371/journal.pntd.0006730

Raymann, K., Coon, K. L., Shaffer, Z., Salisbury, S., and Moran, N. A. (2018). Pathogenicity of Serratia marcescens Strains in Honey Bees. *mBio* 9 (5), e01649–18. doi: 10.1128/mBio.01649-18

Reyon, D., Tsai, S. Q., Khayter, C., Foden, J. A., Sander, J. D., and Joung, J. K. (2012). FLASH assembly of TALENs for high-throughput genome editing. *Nat. Biotechnol.* 30 (5), 460–465. doi: 10.1038/nbt.2170

Rodríguez-Ruano, S. M., Škochová, V., Rego, R. O. M., Schmidt, J. O., Roachell, W., Hypša, V., et al. (2018). Microbiomes of North American Triatominae: The Grounds for Chagas Disease Epidemiology. *Front. Microbiol.* 9, 1167. doi: 10.3389/fmicb.2018.01167

Rognes, T., Flouri, T., Nichols, B., Quince, C., and Mahé, F. (2016). VSEARCH: a versatile open source tool for metagenomics. *PeerJ* 4, e2584. doi: 10.7717/peerj.2584

Salcedo-Porras, N., and Lowenberger, C. (2019). The innate immune system of kissing bugs, vectors of chagas disease. *Dev. Comp. Immunol.* 98, 119–128. doi: 10.1016/j.dci.2019.04.007

Sassera, D., Epis, S., Pajoro, M., and Bandi, C. (2013). Microbial symbiosis and the control of vector-borne pathogens in tsetse flies, human lice, and triatomine bugs. *Pathog. Glob. Health* 107 (6), 285–292. doi: 10.1179/2047773213y.0000000109

Schloss, P. D., Westcott, S. L., Ryabin, T., Hall, J. R., Hartmann, M., Hollister, E. B., et al. (2009). Introducing mothur: open-source, platform-independent, community-supported software for describing and comparing microbial communities. *Appl. Environ. Microbiol.* 75 (23), 7537–7541. doi: 10.1128/aem.01541-09

Segata, N., Izard, J., Waldron, L., Gevers, D., Miropolsky, L., Garrett, W. S., et al. (2011). Metagenomic biomarker discovery and explanation. *Genome Biol.* 12 (6), R60. doi: 10.1186/gb-2011-12-6-r60

Shi, Y., Wei, Y., Feng, X., Liu, J., Jiang, Z., Ou, F., et al. (2020). Distribution, genetic characteristics and public health implications of Triatoma rubrofasciata, the vector of Chagas disease in Guangxi, China. *Parasit. Vectors* 13 (1), 33. doi: 10.1186/s13071-020-3903-z

Vieira, C. B., Praça, Y. R., Bentes, K., Santiago, P. B., Silva, S. M. M., Silva, G. D. S., et al. (2018). Triatomines: Trypanosomatids, Bacteria, and Viruses Potential Vectors? *Front. Cell Infect. Microbiol.* 8, 405. doi: 10.3389/fcimb.2018.00405

Waltmann, A., Willcox, A. C., Balasubramanian, S., Borrini Mayori, K., Mendoza Guerrero, S., Salazar Sanchez, R. S., et al. (2019). Hindgut microbiota in laboratory-reared and wild Triatoma infestans. *PloS Negl. Trop. Dis.* 13 (5), e0007383. doi: 10.1371/journal.pntd.0007383

Wang, Q., Garrity, G. M., Tiedje, J. M., and Cole, J. R. (2007). Naive Bayesian classifier for rapid assignment of rRNA sequences into the new bacterial taxonomy. *Appl. Environ. Microbiol.* 73 (16), 5261–5267. doi: 10.1128/aem.00062-07

WHO (2020).Chagas disease (American trypanosomiasis). In: *Epidemiology*. Available at: https://www.who.int/chagas/en/ (Accessed 16 March 2020).

Wincker, P., Britto, C., Pereira, J. B., Cardoso, M. A., Oelemann, W., and Morel, C. M. (1994). Use of a simplified polymerase chain reaction procedure to detect Trypanosoma cruzi in blood samples from chronic chagasic patients in a rural endemic area. *Am. J. Trop. Med. Hyg.* 51 (6), 771–777. doi: 10.4269/ajtmh.1994.51.771

Wu, P., Sun, P., Nie, K., Zhu, Y., Shi, M., Xiao, C., et al. (2019). A Gut Commensal Bacterium Promotes Mosquito Permissiveness to Arboviruses. *Cell Host Microbe* 25 (1), 101–112.e105. doi: 10.1016/j.chom.2018.11.004

Conflict of Interest: The authors declare that the research was conducted in the absence of any commercial or financial relationships that could be construed as a potential conflict of interest.

frontiers in Cellular and Infection Microbiology

ORIGINAL RESEARCH
published: 25 November 2020
doi: 10.3389/fcimb.2020.588107

Prevalence and Genetic Characterization of Two Mitochondrial Gene Sequences of Strobilocercus Fasciolaris in the Livers of Brown Rats (*Rattus norvegicus*) in Heilongjiang Province in Northeastern China

Fengnian Zhao[†], *Yun Zhou*[†], *Yanchen Wu*, *Kexin Zhou*, *Aiqin Liu*, *Fengkun Yang*[*] *and Weizhe Zhang*[*]

Department of Parasitology, Harbin Medical University, Harbin, China

Rodents constitute the largest and most successful group of mammals worldwide. Brown rats (*Rattus norvegicus*) are one of the most common rodent species, and they serve as intermediate hosts of *Hydatigera taeniaeformis.* Although there have been a few studies reporting on the presence of the larval form of *H. taeniaeformis* (strobilocercus fasciolaris) in brown rats worldwide, little information is available on the genetic characterization of this parasite, with no molecular data from China. Therefore, from April 2014 to March 2016, this study was carried out to understand the prevalence and genetic characters of strobilocercus fasciolaris in brown rats captured in Heilongjiang Province in northeastern China. The livers of brown rats were collected and examined for the presence of cysts. Each cyst was identified based on morphological observation: the larvae with the naked eye and the scolexes under a microscope. The results were confirmed by polymerase chain reaction (PCR) and sequencing of the cytochrome *c* oxidase subunit 1 (*cox1*) and NADH dehydrogenase subunit 4 (*nad4*) genes. At the investigated sites, 11.8% (13/110) of the brown rats were infected with strobilocercus fasciolaris. Based on sequence analysis, there were 10 and six haplotypes regarding the *cox1* and the *nad4* loci, with 24 and 42 polymorphic sites, respectively (degree of intraspecific variation: 0.3%–4.4% and 0.6%–4.7%, respectively). Twelve nucleotide sequences (six of the 10 at the *cox1* locus and all six at the *nad4* locus) have not previously been described. Base differences in three of the six novel *cox1* gene sequences and five of the six novel *nad4* gene sequences caused amino acid changes. Phylogenetic analyses of the *cox1* and *nad4* gene

OPEN ACCESS

Edited by:
Jun Feng,
National Institute of Parasitic Diseases, China

Reviewed by:
Hiroshi Sato,
Yamaguchi University, Japan
Raquel Simões,
Universidade Federal Rural do Rio de Janeiro, Brazil

***Correspondence:**
Fengkun Yang
yangfk99@hotmail.com
Weizhe Zhang
zhangweizhe526@163.com

[†]*These authors have contributed equally to this work*

Specialty section:
This article was submitted to Parasite and Host, a section of the journal Frontiers in Cellular and Infection Microbiology

Received: *28 July 2020*
Accepted: *21 October 2020*
Published: *25 November 2020*

Citation:
Zhao F, Zhou Y, Wu Y, Zhou K, Liu A, Yang F and Zhang W (2020) Prevalence and Genetic Characterization of Two Mitochondrial Gene Sequences of Strobilocercus Fasciolaris in the Livers of Brown Rats (Rattus norvegicus) in Heilongjiang Province in Northeastern China. Front. Cell. Infect. Microbiol. 10:588107. doi: 10.3389/fcimb.2020.588107

sequences based on neighbor-joining and Bayesian inference trees indicated that all the strobilocercus fasciolaris isolates belonged to *Hydatigera taeniaeformis* sensu stricto (s.s.). This is the first report on the genetic characterization of strobilocercus fasciolaris in brown rats in China. The findings of novel *cox1* and *nad4* nucleotide and amino acid sequences may reflect the region-specific genetic characterization of the parasite. The data will be useful to explore the biological and epidemiological significance of the intraspecific variation within *H. taeniaeformis* s.s.

Keywords: strobilocercus fasciolaris, *Hydatigera taeniaeformis*, brown rats, prevalence, genetic characterization

INTRODUCTION

Taeniidae is one of the most important families of the order Cyclophyllidea, which contains most of the zoonotic parasites of medical significance. Some members of the genus *Taenia* are responsible for taeniasis and/or cysticercosis in humans (Sharma et al., 2016). The resurrection of the genus *Hydatigera* was proposed in a recent revision of the family Taeniidae; *Hydatigera* consists of four valid species, *Hydatigera taeniaeformis* sensu stricto (s.s.), *Hydatigera krepkogorski*, *Hydatigera parva*, and *Hydatigera kamiyai* (Nakao et al., 2013a; Nakao et al., 2013b; Catalano et al., 2019). *H. taeniaeformis* is found in the small intestine of cats and other felids, which are the definitive hosts. They acquire the parasitic infection by consuming the livers of rats and mice (the intermediate hosts) infected with the larval form of *H. taeniaeformis* (strobilocercus fasciolaris) (Singla et al., 2008; Moudgil et al., 2016). Brown rats (*Rattus norvegicus*) are one of the most widely known and most common rat species. Natural infections involving strobilocercus fasciolaris have been reported in brown rats in many countries/regions (Sharma et al., 2017). To date, several human cases have been documented: strobilocercus fasciolaris infection in the liver of a 77-year-old man from Czechoslovakia (Sterba and Barus, 1976) and *H. taeniaeformis* infection in the small intestine of individuals from Argentina, Japan and Sri Lanka (Sterba and Barus, 1976; Ekanayake et al., 1999; Hoberg, 2002).

The use of polymerase chain reaction (PCR)-based molecular tools has contributed to accurate species differentiation and a better understanding of the genetic characterization of *H. taeniaeformis*. As mitochondrial (mt) DNA is known to have a faster evolutionary rate than nuclear DNA, mt genes have been widely used to identify taeniid species and strains and to assess the genetic relationships among them (Okamoto et al., 1995; Dai et al., 2012). However, there is limited information on the genetic variation and phylogenetic relationships regarding *H. taeniaeformis* population worldwide (Lavikainen et al., 2016). In China, *H. taeniaeformis* adults have been found in cats (Xu et al., 1994; Lin et al., 1995; Wang et al., 1995; Wang et al., 1997), while the larvae have been found in rats and mice (based on morphological analysis), including brown rats (11.6%–53.6%) (Wu and Yin, 2005; Tan et al., 2008), buff-breasted rats (*Rattus flavipectus*) (3.3%–38.0%) (Huang, 1991; Yuan et al., 2000), lesser rice-field rats (*Rattus losea*) (16.3%) (Yuan et al., 2000), black rats (*Rattus rattus*) (15.0%) (Huang, 1991), and house mice (*Mus musculus*) (16.2%) (La and Zhao, 1989). However, there are no available reports on the genetic characterization of strobilocercus fasciolaris in brown rats in China. Therefore, we carried out this epidemiological study of the parasite in brown rats in Heilongjiang Province, northeastern China, and conducted a genetic characterization of the isolates.

MATERIALS AND METHODS

Study Sites and Collection of Rats

From April 2014 to March 2016, 110 brown rats were captured in cage traps baited with sunflower seeds and peanut/sesame butter in four areas in Heilongjiang Province, northeastern China: 23 in a granary in Xingren Town, 27 in a pig farm in Mingshui County, 27 in a pig farm in Qinggang County, and 33 in a sheep farm in Baoqing County. All the captured rats were euthanized by CO_2 inhalation and transported to our laboratory in coolers with ice packs. Procedures involving the rats were strictly conducted according to the Chinese Laboratory Animal Administration Act of 1998.

Collection of Liver Samples and Examination of Cysts

After euthanasia, the liver was collected from each rat and examined for the presence of cysts. Each cyst was opened by making a small slit. If a single larva was released with liquid, and a large scolex could be observed with four lateral suckers and double rows of hooks using a light microscope at 400× magnification, the larva was suspected to be strobilocercus fasciolaris. They were preserved in 70% ethanol at 4°C for further molecular analysis.

Extraction of Genomic DNA

Prior to DNA extraction, each parasite specimen was washed three times with phosphate-buffered saline to remove the ethanol. Parasitic genomic DNA was extracted from approximately 25 mg of each larva using a DNeasy Blood & Tissue Kit (Qiagen, Hilden, Germany) according to the manufacturer's instructions. DNA was eluted in 200 μl of AE elution buffer (provided with the kit) and stored at −20°C until further PCR analysis.

PCR Amplification

The partial cytochrome *c* oxidase subunit 1 (*cox1*) and NADH dehydrogenase subunit 4 (*nad4*) genes (approximately 450 and 660 bp, respectively) of *H. taeniaeformis* were amplified using the primers and protocols described previously by Bowles and

McManus (1994) and Dai et al. (2012), respectively. TaKaRa Taq DNA polymerase (TaKaRa Bio Inc., Tokyo, Japan) was used for all PCR amplifications. Sterile deionized water served as the negative control. The PCR products were subjected to electrophoresis in 1.5% agarose gel and visualized by staining the gel with GelStain (TransGen Biotech, Beijing, China).

DNA Sequencing and Molecular Analysis

The PCR products were then sequenced with PCR primers for each gene on an ABI PRISM 3730 XL DNA Analyzer (Applied Biosystems, Carlsbad, CA, USA) using a Big Dye Terminator v3.1 Cycle Sequencing kit (Applied Biosystems). The accuracy of the sequencing data was confirmed by sequencing the PCR products from forward and reverse directions. The nucleotide sequences were then used in Basic Local Alignment Search Tool (BLAST) searches (http://www.ncbi.nlm.nih.gov/blast.cgi). They were aligned with each other and with reference sequences that were downloaded from GenBank using ClustalX v1.83 (http://www.clustal.org/).

Phylogenetic Analysis

To explore the genetic and geographical relationships of *H. taeniaeformis* isolates, phylogenetic analyses of the *cox1* and *nad4* gene sequences were performed using two common phylogenetic methods: the neighbor-joining method with MEGA v6.0 (http://www.megasoftware.net) and Bayesian inference with MrBayes v3.2.6 (http://phylosuite.jushengwu.com/). For the countries for which there were more than two *H. taeniaeformis* sequences in GenBank, the two sequences with the largest base difference were selected for each locus being analyzed. However, for some countries, we only used one sequence, as there was only one sequence deposited in GenBank. The reliability of the neighbor-joining trees was assessed using bootstrap analysis with 1000 replicates, and the evolutionary distances were calculated using the Kimura-2-parameter model. The Jukes–Cantor model was used for Bayesian inference. Bayesian posterior probability values were determined after running the Markov chains (two runs, four chains) for 2 million generations and discarding the first 25% of samples as burn-in. The consensus tree was rooted at its midpoint and visualized using FigTree v1.4.2 (http://tree.bio.ed.ac.uk/software/figtree/).

RESULTS AND DISCUSSION

Thirteen of the 110 brown rats (11.8%) were confirmed to be infected with strobilocercus fasciolaris in the livers based on morphological observation (the larvae in the cysts with the naked eye and the scolexes under a microscope) and by sequence analysis of the partial *cox1* and *nad4* genes. The prevalence of 11.8% was lower than that reported in brown rats in the Philippines (100%) (Claveria et al., 2005), India (36.0%) (Singla et al., 2008), Korea (33.8%) (Lee et al., 2016), Serbia (29.9%) (Kataranovski et al., 2010), and Grenada, West Indies (29.6%–67.6%) (Chikweto et al., 2009; Sharma et al., 2017). The prevalence has been reported to be in the range of 11.6%–53.6% in another six Chinese provinces (Wu and Yin, 2005; Tan et al., 2008). The prevalence is complex and related to many factors. For example, regarding the rat age, 25–60-day-old albino rats were observed to be more susceptible to the parasite than younger or older albino rats in a study of age-related resistance to strobilocercus fasciolaris (Greenfield, 1942). However, Lee et al. (2016) pointed out that the prevalence was more closely related to infection accumulation with age, rather than host age-dependent differences in susceptibility to the parasite, and host body weight was positively associated with the prevalence. Additionally, Sharama et al. (2017) believed that human population density influenced the prevalence of strobilocercus fasciolaris in brown rats in the two study sites in Grenada, West Indies.

By comparing the *cox1* and *nad4* gene sequences of the 13 isolates, 10 and six haplotypes were found, with 24 and 42 polymorphic sites being observed, respectively; the degree of intraspecific variation was 0.3%–4.4% (1–18 base differences) at the *cox1* locus and 0.6%–4.7% (4–31 base differences) at the *nad4* locus (**Tables 1**, **2**). Intraspecific variation within *H. taeniaeformis* has been described previously. In 2016, 150 specimens of *Hydatigera taeniaeformis* sensu lato (s.l.) from various definitive and intermediate hosts in Eurasia, Africa and Australia were analyzed and a new species, *H. kamiyai*, was separated from *H. taeniaeformis* s.l. (Lavikainen et al., 2016). This finding supported the earlier discovery in 1995 of a presumed novel species, the TtACR isolate, from the grey red-backed vole (*Myodes rufocanus bedfordiae*) in Japan (Okamoto

TABLE 1 | Values of nucleotide variation in the *cox1* gene detected between pairs of strobilocercus fasciolaris sequences, expressed as percentages.

Accession no.	MF380373	MF380374	MF380375	MF380376	MF380377	MF380378	MF380379	MF380380	MF380381	MF380382
MF380373	——									
MF380374	0.5	——								
MF380375	1.0	1.5	——							
MF380376	1.2	1.7	0.3	——						
MF380377	1.8	1.9	0.5	0.7	——					
MF380378	2.5	2.9	3.2	3.4	3.7	——				
MF380379	1.5	1.9	1.2	1.5	1.7	3.7	——			
MF380380	0.3	0.7	1.2	1.5	1.7	2.7	1.7	——		
MF380381	1.2	1.7	0.3	0.5	0.3	3.4	1.5	1.5	——	
MF380382	3.2	3.7	1.2	4.2	4.4	0.7	3.9	3.4	4.2	——

TABLE 2 | Values of nucleotide variation in the *nad4* gene detected between pairs of strobilocercus fasciolaris sequences, expressed as percentages.

Accession no.	MF380383	MF380384	MF380385	MF380386	MF380387	MF380388
MF380383	——					
MF380384	2.3	——				
MF380385	4.7	4.0	——			
MF380386	2.1	1.4	4.1	——		
MF380387	0.6	2.0	4.7	1.8	——	
MF380388	4.7	4.0	0.6	4.1	4.7	——

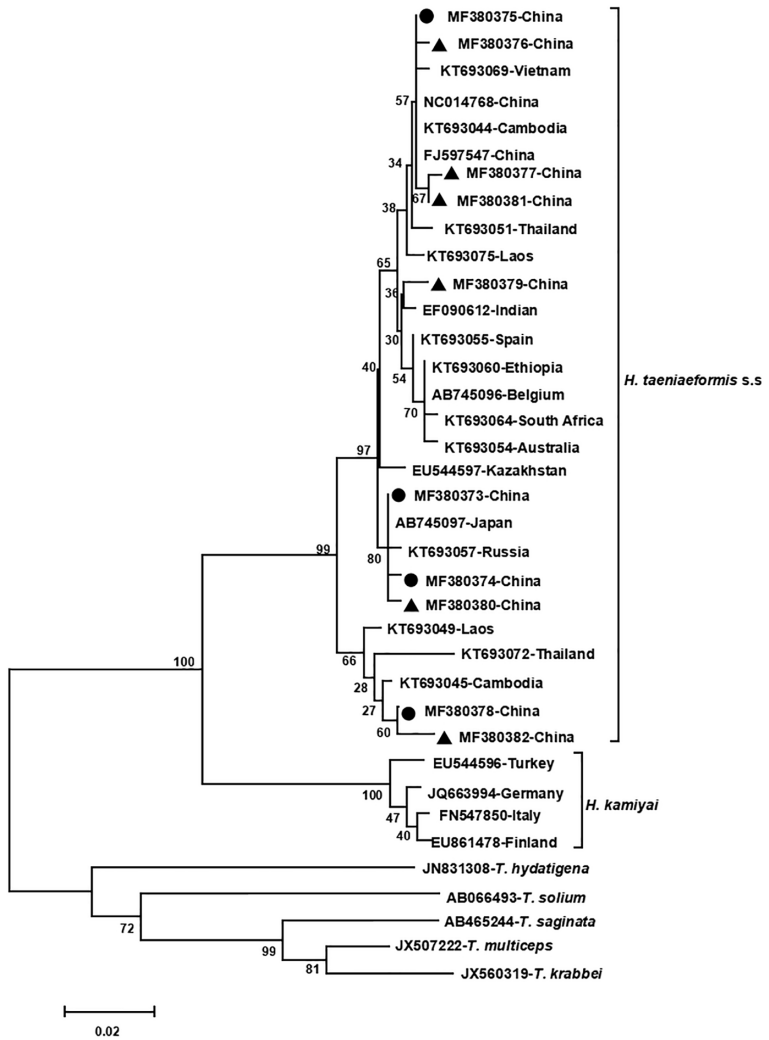

FIGURE 1 | Genetic and geographical relationships of *H. taeniaeformis* s.l. isolates based on a neighbor-joining analysis of the *cox 1* locus. The relationships were inferred by a neighbor-joining analysis of *cox1* gene sequences of *H. taeniaeformis* s.l. isolates from different countries based on genetic distance calculated using the Kimura 2-parameter model. The numbers on the branches are percent bootstrapping values from 1,000 replicates. Each *H. taeniaeformis* s.s. or *H. kamiyai* sequence is identified by its accession number and geographical location (country). Novel and known nucleotide sequences of strobilocercus fasciolaris isolates obtained in the present study are represented by black triangles and black circles, respectively.

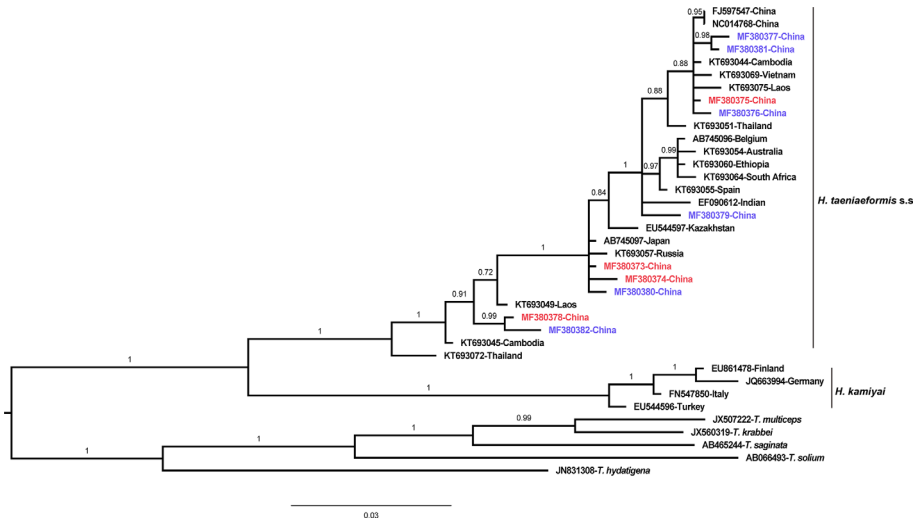

FIGURE 2 | Genetic and geographical relationships of *H. taeniaeformis* s.l. isolates based on a Bayesian inference analysis of the *cox 1* locus. The relationships were inferred by Bayesian inference analysis of *cox1* gene sequences of *H. taeniaeformis* s.l. isolates from different countries based on the Jukes–Canto model. Posterior probability values were produced using MrBbayes. The scale bar displays branch length in units of evolutionary distance. Each *H. taeniaeformis* s.s. or *H. kamiyai* sequence is identified by its accession number and geographical location (country). Novel and known nucleotide sequences obtained in the present study are shown in blue and red, respectively.

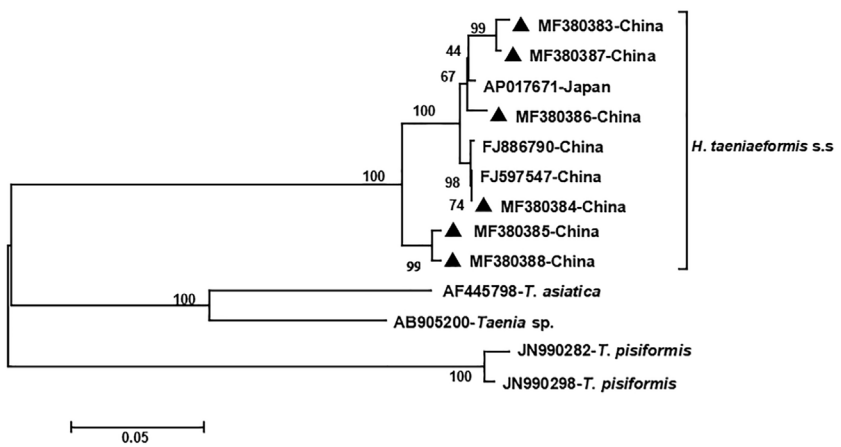

FIGURE 3 | Genetic and geographical relationships of *H. taeniaeformis* s.s. isolates based on a neighbor-joining analysis of the *nad4* locus. The relationships were inferred by a neighbor-joining analysis of the *nad4* gene sequences of *H. taeniaeformis* s.s. isolates from different countries based on genetic distance calculated using the Kimura 2-parameter model. The numbers on the branches are percent bootstrapping values from 1,000 replicates. Each *H. taeniaeformis* s.s. sequence is identified by its accession number and geographical location (country). Novel nucleotide sequences obtained in the present study are represented by black triangles.

et al., 1995). The TtACR isolate was observed to have a degree of variation of 9.0%–9.5% at the *cox1* locus compared to isolates from other murine species including brown rats in Japan (n = 1) and Malaysia (n = 1), house mice in Belgium (n = 1) and China (n = 1), and small Japanese field mice (*Apodemus argenteus*) in Japan (n = 2) (Okamoto et al., 1995). In 2008, an analysis of the *cox1* locus showed that a Turkish isolate (TtaTu) from a wood mouse (*Apodemus sylvaticus*) and a Finnish isolate (TtaFi) from a cat (*Felis catus*) were genetically close to the divergent isolate from Japan (TtACR), and the three isolates were genetically distant from a Kazakhstan isolate (TtaKa) from a wood mouse (which had a *cox1* gene sequence that resembled the majority of the previously published *cox1* gene sequences of *H. taeniaeformis*) (Lavikainen et al., 2008). Variation has been

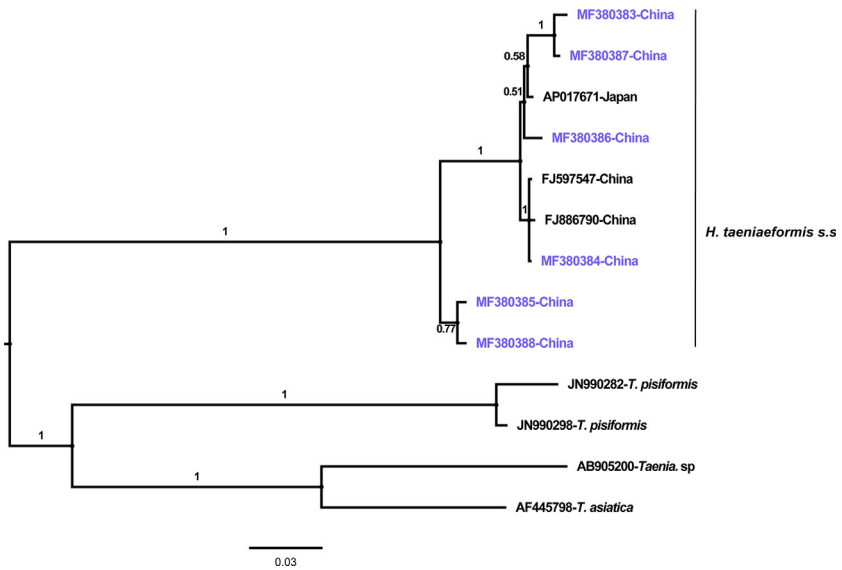

FIGURE 4 | Genetic and geographical relationships of *H. taeniaeformis* s.s. isolates based on a Bayesian inference analysis of the *nad4* locus. The relationships were inferred by Bayesian inference analysis of *nad4* gene sequences of *H. taeniaeformis* s.s. isolates from different countries based on the Jukes–Canto model. Posterior probability values were produced using MrBayes. The scale bar displays branch length in units of evolutionary distance. Each *H. taeniaeformis* s.s. sequence is identified by its accession number and geographical location (country). Novel nucleotide sequences obtained in the present study are shown in blue.

clearly observed at the *cox1* locus: 0.3%–5.1% within *H. taeniaeformis* s.s., and 9.1%–13.3% between *H. taeniaeformis* s.s. and *H. kamiyai* (including the TtACR, TtaFi and TtaTu isolates) (Lavikainen et al., 2016). Due to the rarity of data on the *nad4* gene sequences of *H. taeniaeformis* from other countries/regions, we did not conduct a corresponding comparative analysis in this study.

The phylogenetic analyses based on the sequence data of the *cox1* and *nad4* genes revealed that all the haplotypes were grouped with *H. taeniaeformis* s.s., confirming the results of PCR amplification and sequencing. The phylogenetic trees based on neighbor-joining and Bayesian inference analyses were broadly congruent. Regarding the *cox1* locus analysis, all 10 haplotypes belonged to *H. taeniaeformis* s.s.: eight were grouped with those from Europe (Spain, Belgium and Russia), Africa (Ethiopia and South Africa), Oceania (Australia), and Asia (Vietnam, Cambodia, Thailand, Laos, India, Japan, Kazakhstan and China), and two with those from Asia (Cambodia, Thailand, Laos and China). However, several isolates from Europe (Turkey, Germany, Finland and Italy) belonged to *H. kamiyai*, which was recently separated from *H. taeniaeformis* s.l. (Lavikainen et al., 2016) (**Figures 1**, **2**). The *H. kamiyai* isolates were in a single clade, and the results confirmed that *H. kamiyai* is genetically distant from *H. taeniaeformis* s.s. Based on nucleotide sequence comparisons, Catalano et al. found that a *H. taeniaeformis* isolate from a Nile rat (*Arvicanthis niloticus*) in Senegal showed identity to what was described as *H. taeniaeformis* s.s., a lineage that might have originated in Southeast Asia and rapidly invaded Australia, the Americas, Europe and Africa, where it has been identified in Ethiopia and South Africa in *Rattus* spp. (Catalano et al., 2019). Lavikainen et al. (2016) has also speculated that *H. taeniaeformis* probably originated in Asia and has spread worldwide, given its linkage to the Rattini tribe. Regarding the *nad4* locus analysis, all six haplotypes obtained in the present study were grouped with *H. taeniaeformis* s.s. isolates from China (FJ886790 and FJ597547) and Japan (AP017671) (**Figures 3**, **4**). All of these genetic relationships were supported by high Bayesian inference posterior probability values and most of them by moderate-to-high neighbor-joining bootstrap values.

Based on homology analysis of the 10 *cox1* gene sequences identified in the present study, four sequences (MF380373, MF380374, MF380375, and MF380378) have been previously described, while the remaining six (MF380376, MF380377, and MF380379–MF380382) are novel. All of the six *nad4* gene sequences identified in the present study (MF380383–MF380388) are novel. However, only three of the six novel *cox1* gene sequences and five of the six novel *nad4* gene sequence caused amino acid changes relative to their respective reference sequences (the reference sequences were selected on the basis that they had the highest similarity to the representative sequences obtained in the present study) **(Table 3)**. These findings of novel nucleotide and amino acid sequences might reflect the region-specific genetic characterization of *H. taeniaeformis* s.s. Currently, the significance of these changes at the nucleotide and amino acid levels is unclear. However, *Echinococcus granulosus* research has shown that genetic variation could affect host infectivity, epidemiology and control strategies (Carmena and Cardona, 2014). Similarly, studies on the *Taenia saginata* and *Taenia solium* mt genomes have also demonstrated intraspecific variation that may influence the pathological presentations exhibited in different hosts (Vega et al., 2003; Rostami et al., 2015).

TABLE 3 | Homology analysis of the *cox1* and *nad4* loci in strobilocercus fasciolaris isolates from brown rats.

Amplified gene	Accession no. (n) [a](no of isolates)	Accession no. [b]/host/country	Homology (%)	Codon[c]/amino acid (nucleotide Position)[d]
cox1	MF380373 (3)	KT693056/leopard cat/Russia; AB221484/brown rat/Japan	100	
	MF380374 (1)	KT693059/striped field mouse/Russia	100	
	MF380375 (1)	FJ597547/cat/China; KT693044/brown rat/Cambodia	100	
	MF380378 (2)	KT693062/leopard cat/Russia	100	
	MF380376 (1)	FJ597547/cat/China	99.8	(T to C)TT/F to L (103)
	MF380377 (1)	FJ597547/cat/China	99.5	(A to G)TT/I to V (310)
	MF380379 (1)	KT693053/small white-toothed rat/Thailand	99.2	
	MF380380 (1)	AB745097/brown rat/Japan	99.8	
	MF380381 (1)	FJ597547/cat/China	99.8	(A to G)TT/I to V (310)
	MF380382 (1)	KT693062/leopard cat/Russia	99.2	
nad4	MF380383 (4)	AP017671/unspecific/Japan	98.2	(G to A)CT/(A to T) (355); (T to C)TT/(F to L) (415); AT(A to G)/(I to M) (621)
	MF380384 (5)	FJ597547/cat/China	99.9	
	MF380385 (1)	FJ597547/cat/China	95.9	(A to G)TA/I to V(88); (G to A)AT/D to N (94); AT (A to G)/I to M (330)
	MF380386 (1)	AP017671/unspecific/Japan	98.8	(C to T)CC/(P to S) (124)
	MF380387 (1)	AP017671/unspecific/Japan	98.5	(T to C)TT/F to L (415); AT(A to G)/I to M (621)
	MF380388 (1)	AP017671/unspecific/Japan	95.9	(A to G)TA/I to V (88); (C to T)C(C to T)/P to S (124; 126); AT(A to G)/I to M (330); A(C to T)A/T to I (386)

[a]Accession no. of the representative sequences obtained in the present study.
[b]Accession no. of the reference sequences, which had the highest similarity with the representative sequences obtained in the present study.
[c]The nucleotide change (in brackets for each codon) represents the change from the reference sequence to the representative sequence obtained in the present study.
[d]Nucleotide position numbers according to the representative sequence, with the beginning of the coding region being position no. 1.

CONCLUSION

This is the first report on the genetic characterization of strobilocercus fasciolaris in brown rats in China. High genetic heterogeneity was found across the 13 identified isolates: 10 haplotypes (intraspecific variation: 0.3%–4.4%) at the *cox1* locus and six haplotypes (intraspecific variation: 0.6%–4.7%) at the *nad4* locus. Based on phylogenetic and homology analyses, all 13 isolates belonged to *H. taeniaeformis* s.s. The findings of novel nucleotide and amino acid sequences might reflect the endemic genetic characterization of strobilocercus fasciolaris. The molecular data will be useful to further explore the biological and epidemiological significance of intraspecific variation within *H. taeniaeformis* s.s.

DATA AVAILABILITY STATEMENT

The datasets presented in this study can be found in online repositories. The names of the repository/repositories and accession number(s) can be found below: https://www.ncbi.nlm.nih.gov/genbank/, MF380373–MF380382 (*cox1* gene) and MF380383–MF380388 (*nad4* gene).

ETHICS STATEMENT

The animal study was reviewed and approved by Research Ethics Committee and the Animal Ethical Committee of Harbin Medical University. Procedures involving animals were strictly conducted according to the Chinese Laboratory Animal Administration Act of 1998.

AUTHOR CONTRIBUTIONS

AL and WZ conceived and designed the study. FY, FZ, and YZ performed the study and analyzed the data. FY wrote the first draft of the manuscript. WZ, YW, and KZ provided strategic advice and assisted with editing the manuscript. All authors contributed to the article and approved the submitted version.

FUNDING

This work was financially supported by the Heilongjiang Province Education Bureau of Foundation (No. 12531266) and by the Natural Science Foundation of Heilongjiang Province of China (No. H2017006). The funding sponsors had no role in study design, data collection and analysis, decision to publish or preparation of the manuscript.

REFERENCES

Bowles, J., and McManus, D. P. (1994). Genetic characterization of the Asian Taenia, a newly described taeniid cestode of humans. *Am. J. Trop. Med. Hyg.* 50, 33–44.

Carmena, D., and Cardona, G. A. (2014). Echinococcosis in wild carnivorous species: epidemiology, genotypic diversity, and implications for veterinary public health. *Vet. Parasitol.* 202, 69–94. doi: 10.1016/j.vetpar.2014.03.009

Catalano, S., Bâ, K., Diouf, N. D., Léger, E., Verocai, G. G., and Webster, J. P. (2019). Rodents of Senegal and their role as intermediate hosts of Hydatigera spp. (Cestoda: Taeniidae). *Parasitol.* 146, 299–304. doi: 10.1017/S0031182018001427

Chikweto, A., Bhaiyat, M. I., Macpherson, C. N., Deallie, C., Pinckney, R. D., Richards, C., et al. (2009). Existence of Angiostrongylus cantonensis in rats (Rattus norvegicus) in Grenada, West Indies. *Vet. Parasitol.* 162, 160–162. doi: 10.1016/j.vetpar.2009.02.020

Claveria, F. G., Causapin, J., de Guzman, M. A., Toledo, M. G., and Salibay, C.. (2005). Parasite biodiversity in Rattus spp caught in wet markets. *Southeast Asian J. Trop. Med. Public Health* 36 Supp 4, 146–148.

Dai, R. S., Liu, G. H., Song, H. Q., Lin, R. Q., Yuan, Z. G., Li, M. W., et al. (2012). Sequence variability in two mitochondrial DNA regions and internal transcribed spacer among three cestodes infecting animals and humans from China. *J. Helminthol.* 86, 245–251. doi: 10.1017/s0022149x11000319

Ekanayake, S., Warnasuriya, N, D., Samarakoon, P. S., Abewickrama, H., Kuruppuarachchi, N. D., and Dissanaike, A. S. (1999). An unusual 'infection' of a child in Sri Lanka, with Taenia taeniaeformis of the cat. *Ann. Trop. Med. Parasitol.* 93, 869–873. doi: 10.1080/00034989957871

Greenfield, S. H. (1942) Age resistance of the albino rat to Cysticercus fasciolaris. *J. Parasitol.* 28, 207–211.

Hoberg, E. P. (2002). Taenia tapeworms: their biology, evolution and socioeconomic significance. *Microbes. Infect.* 4, 859–866. doi: 10.1016/s1286-4579(02)01606-4

Huang, Z. M. (1991). Investigation of natural infection with strobilocercus fasciolaris in rats. *Sichuan J. Zool.* 10, 39. (in Chinese).

Kataranovski, M., Zolotarevski, L., Belij, S., Mirkov, I., and Kataranovski, D. (2010). First record of Calodium hepaticum and Taenia taeniaeformis liver infection in wild Norway rats (Rattus norvegicus) in Serbia. *Arch. Biolo. Sci.* 62.

La, Y., and Zhao, S. C. (1989). Strobilocercus fasciolaris in cats was found for the first time in Qinghai rats. *Chin. J. Zool.* 24, 40–41. (in Chinese).

Lavikainen, A., Haukisalmi, V., Lehtinen, M. J., Henttonen, H., Oksanen, A., and Meri, S. (2008). A phylogeny of members of the family Taeniidae based on the mitochondrialcox1 and nad1 gene data. *Parasitol.* 135, 1457–1467. doi: 10.1017/S003118200800499X

Lavikainen, A., Iwaki, T., Haukisalmi, V., Konyaev, S. V., Casiraghi, M., Dokuchaev, N.E., et al. (2016). Reappraisal of Hydatigera taeniaeformis (Batsc) (Cestoda: Taeniidae) sensu lato with description of Hydatigera kamiyai n. sp. *Int. J. Parasitol.* 46, 361–374. doi: 10.1016/j.ijpara.2016.01.009

Lee, B. W., Jeon, B. S., Kim, H. S., Kim, H. C., and Yoon, B. I. (2016) Cysticercus fasciolaris infection in wild rats (Rattus norvegicus) in Korea and formation of cysts by remodeling of collagen fibers. *J. Vet. Diagn. Invest.* 28, 263–270. doi: 10.1177/1040638716643129

Lin, M. L., Jiang, S. Z., Hu, T. Y., Jiang, Y. C., Hu, Y. J., and Zhang, Y. Q. (1995). Investigation on the parasitic helminth Fauna in dogs and cats in Suifen River basin. *Heilongjiang Anim. Sci. Vet. Med.* 9, 40–42. in Chinese.

Moudgil, A. D., Singla, L. D., Gupta, K., Daundkar, P. S., and Vemu, B. (2016). Histopathological and morphological studies on natural Cysticercus fasciolaris infection in liver of Wistar rats. *J. Parasitol. Dis.* 40, 255–258. doi: 10.1007/s12639-014-0488-5

Nakao, M., Lavikainen, A., Iwaki, T., Haukisalmi, V., Konyaev, S., Oku, Y., et al. (2013a). Molecular phylogeny of the genus Taenia (Cestoda: Taeniidae): proposals for the resurrection of Hydatigera Lamarck 1816 and the creation of a new genus Versteria. *Int. J. Parasitol.* 43, 427–237. doi: 10.1016/j.ijpara.2012.11.014

Nakao, M., Lavikainen, A., Yanagida, T., and Ito, A. (2013b). Phylogenetic systematics of the genus Echinococcus (Cestoda: Taeniidae). *Int. J. Parasitol.* 43, 1017–1029. doi: 10.1016/j.ijpara.2013.06.002

Okamoto, M., Bessho, Y., Kamiya, M., Kurosawa, T., and Horii, T. (1995). Phylogenetic relationships within Taenia taeniaeformis variants and other taeniid cestodes inferred from the nucleotide sequence of the cytochrome c oxidase subunit I gene. *Parasitol. Res.* 81, 451–458. doi: 10.1007/bf00931785

Rostami, S., Salavati, R., Beech, R. N., Babaei, Z., Sharbatkhori, M., and Harandi, M. F. (2015). Genetic variability of Taenia saginata inferred from mitochondrial DNA sequences. *Parasitol. Res.* 114, 1365–1376. doi: 10.1007/s00436-015-4314-5

Sharma, R., Tiwari, K., Birmingham, K., Armstrong, E., Montanez, A., Guy, R., et al. (2017). Cysticercus fasciolaris in Brown Rats (Rattus norvegicus) in Grenada, West Indies. *J. Parasitol. Res.* 2017, 1723406. doi: 10.1155/2017/1723406

Sharma, S., Lyngdoh, D., Roy, B., and Tandon, V. (2016). Molecular phylogeny of Cyclophyllidea (Cestoda: Eucestoda): an in-silico analysis based on mtCOI gene. *Parasitol. Res.* 115, 3329–3335. doi: 10.1007/s00436-016-5092-4

Singla, L. D., Singla, N., Parshad, V. R., Juyal, P. D., and Sood, N. K. (2008). Rodents as reservoirs of parasites in India. *Integr. Zool.* 3, 21–26. doi: 10.1111/j.1749-4877.2008.00071.x

Sterba, J., and Barus, V. (1976). First record of Strobilocercus fasciolaris (Taenidae-larvae) in man. *Folia. Parasitol (Praha.)* 23, 221–226.

Tan, Q. M., Chen, D. X., Zhang, Y., and Zhan, X. M. (2008). Investigation on the infection of Angiostrongylus cantonensis and strobilocercus fasciolaris in Jiangmen city in 2007. *Prev. Med. Trib.* 14, 208–209. (in Chinese).

Vega, R., Piñero, D., Ramanankandrasana, B., Dumas, M., Bouteille, B., Fleury, A., et al. (2003). Population genetic structure of Taenia solium from Madagascar and Mexico: implications for clinical profile diversity and immunological technology. *Int. J. Parasitol.* 33, 1479–1485. doi: 10.1016/s0020-7519(03)00206-6

Wang, D. D., Liu, X. M., and Han, X. Y. (1995). Investigation on parasitic helmiths in dogs and cats in Guizhou Province. *Chin. J. Vet. Sci. Tech.* 25, 13–15. (in Chinese).

Wang, Y. Q., Xu, S. K., Zhou, Y. C., Li, S. S., Zhu, W., Li, Z. M., et al. (1997). Investigation report of the helminth fauna in cats in the county of Luobei in Heilongjiang Province, China. *Heilongjiang. Anim. Sci. Vet. Med.* 3, 38–39. (in Chinese).

Wu, J., and Yin, W. X. (2005). Investigation on parasitic infection in rodents in Bitang town, Foshan city. *Chin. J. Parasitol. Dis. Con.* 18, 367–370. (in Chinese).

Xu, S. K., Wang, Y. Q., Zhu, Y. C., Li, S. S., Zhao, X. C., Liu, L. G., et al. (1994). Investigation report of the helminth fauna in cats in the county of Xunke in Heilongjiang Province, China. *Heilongjiang Anim. Sci. Vet. Med.* 10, 32–33. (in Chinese).

Yuan, G. L., Li, X. Y., and Chen, W. J. (2000). Investigation of parasite infection in the livers of garden mice in Ningde city. *Chin. J. Vec. Biol. Control.* 11, 301–302. (in Chinese).

Conflict of Interest: The authors declare that the research was conducted in the absence of any commercial or financial relationships that could be construed as a potential conflict of interest.

frontiers in Cellular and Infection Microbiology

ORIGINAL RESEARCH
published: 26 November 2020
doi: 10.3389/fcimb.2020.586466

iTRAQ-Based Phosphoproteomic Analysis of *Toxoplasma gondii* Tachyzoites Provides Insight Into the Role of Phosphorylation for its Invasion and Egress

Cheng He[1], *Mei-zhen Xu*[1], *Shuai Pan*[1], *Hui Wang*[1], *Hong-juan Peng*[2*] *and Zhuan-zhuan Liu*[1*]

[1] Jiangsu Key Laboratory of Immunity and Metabolism, Department of Pathogen Biology and Immunology, Xuzhou Medical University, Xuzhou, China, [2] Department of Pathogen Biology, Guangdong Provincial Key Laboratory of Tropical Disease Research, School of Public Health, Southern Medical University, Guangzhou, China

OPEN ACCESS

Edited by:
Tania F. De Koning-Ward,
Deakin University, Australia

Reviewed by:
Daniel Adesse,
Oswaldo Cruz Foundation (Fiocruz), Brazil
Fred David Mast,
Seattle Children's Research Institute, United States

***Correspondence:**
Hong-juan Peng
floriapeng@hotmail.com
Zhuan-zhuan Liu
liouzhuanzhuan12@163.com

Specialty section:
This article was submitted to Parasite and Host, a section of the journal Frontiers in Cellular and Infection Microbiology

Received: 23 July 2020
Accepted: 27 October 2020
Published: 26 November 2020

Citation:
He C, Xu M-z, Pan S, Wang H, Peng H-j and Liu Z-z (2020) iTRAQ-Based Phosphoproteomic Analysis of Toxoplasma gondii Tachyzoites Provides Insight Into the Role of Phosphorylation for its Invasion and Egress. Front. Cell. Infect. Microbiol. 10:586466. doi: 10.3389/fcimb.2020.586466

The invasion and egress are two key steps in lytic cycle vital to the propagation of *Toxoplasma gondii* infection, and phosphorylation is believed to play important roles in these processes. However, the phosphoproteome of *T. gondii* at these two stages has not been characterized. In this study, we profiled the phosphoproteome of tachyzoites at the stages of "just invading" (JI) and "prior to egress" (PE) based on iTRAQ quantitative analysis, in which a total of 46 phosphopeptides, 42 phosphorylation sites, and 38 phosphoproteins were detected. In the comparison of PE vs. JI, 10 phosphoproteins were detected with their phosphorylation level significantly changed, and four of them were demonstrated to be significantly down-regulated at the transcriptional level. Bioinformatic analysis of these identified phosphoproteins suggested that phosphorylation-mediated modulation of protein function was employed to regulate the pathway of toxoplasmosis and metabolism and cellular processes correlated with tachyzoite's binding, location, and metabolism, and thus play vital roles in the parasite lytic cycle. Moreover, cytoskeletal network (CN)-associated Inner Membrane Complex (IMC1, IMC4, IMC6 and IMC12), Intravascular Network (IVN)-related GRAs (GRA2, GRA3, GRA7 and GRA12), and Parasitophorous Vacuole Membrane (PVM)-localized ROP5 were shown to be enriched at the central nodes in the protein interaction network generated by bioinformatic analysis, in which the phosphorylation level of IMC4, GRA2, GRA3, and GRA12 were found to be significantly regulated. This study revealed the main cellular processes and key phosphoproteins crucial for the invasion and egress of *T. gondii*, which will provide new insights into the developmental biology of *T. gondii in vitro* and contribute to the understanding of pathogen-host interaction from the parasite perspective.

Keywords: *Toxoplasma gondii*, iTRAQ, phosphoproteomic analysis, bioinformatic analysis, invasion, egress

INTRODUCTION

Toxoplasma gondii is an obligate intracellular apicomplexan parasite that chronically infects approximately one-third of the world's human population, and the toxoplasmosis caused by its infection has been regarded as one of the major neglected parasitic infections (Hotez, 2014; Wei et al., 2016). Fortunately, most infections in healthy people do not show obvious clinical symptoms. However, severe complications, such as encephalitis and eye disease, even death can be caused by the infection of *T. gondii* in immunocompromised patients (Weiss and Dubey, 2009). Moreover, primary infection of *T. gondii* in pregnant women can be vertically transmitted to infect the fetus and result in miscarriage, premature birth, stillbirth, malformations, and other adverse pregnancy outcomes (Li et al., 2014). As an obligate intracellular parasite, the successful invasion and egress of *T. gondii* from its host cell are critical for survival, dissemination and transmission, and thus are believed to be essential for the propagation of parasite infection (Lavine and Arrizabalaga, 2007; Hortua Triana et al., 2018).

Phosphorylation is a key post-translational protein modification for regulating protein function, which is considered to regulate almost all aspects of cell life (Olsen et al., 2006; Schulze, 2010; Broncel and Treeck, 2020). The critical roles of phosphorylation in the lytic cycle of *T. gondii* have also been demonstrated in the previous studies. For example, preventing the phosphorylation of *Tg*IF2α with point mutation (S71A) lead to a significant delay in producing acute toxoplasmosis *in vivo* and a defect in adapting to the extracellular environment while the parasite searched for a new host cell *in vitro* (Joyce et al., 2010). Moreover, *Tg*MyoA is reported to regulate the initiation of motility and egress in the *T. gondii*'s lytic cycle, which largely depends on its phosphorylation (Gaji et al., 2015; Powell et al., 2018). Till now, however, only a few phosphorylated proteins of *T. gondii* have been identified, and the quantitative phosphoproteomic analysis of *T. gondii* at the different lytic cycle stages is also very few.

T. gondii invasion of its host is a rapid process, and to accomplish this process, complex signaling events within the parasite must occur. Meanwhile, the egress of *T. gondii* is an active process to rupture the PVM, which contributes to its dissemination and associates with the pathogenesis of its infection (Frénal et al., 2017). Here, the first 30 min post infection was defined as the phase of "just invasion", when most of the *T. gondii* tachyzoites invade the host cell and the parasitophorous vacuoles (PVs) are newly formed. Moreover, since the tachyzoites have been thoroughly proliferated and are ready to egress at 28 h post infection (PI), this phase was termed as the phase of "prior to egress" (Treeck et al., 2011). In our study, we performed phosphoproteomic analysis of *T. gondii* to characterize the complicated events mediated by phosphorylation of *T. gondii* at these two infection stages, and also analyzed mRNA expression of the significantly regulated phosphoproteins that significantly changed between JI and PE. This current study will be helpful to elucidate the invasion and egress mechanisms of *T. gondii* and understand the role of phosphorylation in host-pathogen interactions from the perspective of the pathogen.

MATERIALS AND METHODS

Cell and Parasite Culture

RH tachyzoites were maintained by serial passages in human foreskin fibroblast (HFFs) monolayers grown in Dulbecco's modified Eagle's medium (DMEM, Gibco) supplemented with 10% fetal calf serum (FBS; Gibco) and 100 μg/ml gentamicin.

Sample Preparation

The HFF cells were infected with *T. gondii* RH tachyzoites with a multiplicity of infection (MOI) of 3 for 30 min and 28 h, respectively. After infection for 30 min, the unrecruited tachyzoites were washed off with phosphate buffered saline (PBS) for three times, and the JI groups were then harvested with cell scrapers. The PE groups were cultured for another 27.5 h and harvested with the same method. All six groups of cells were pelleted by centrifugation, stored in dry CO_2, and sent to the Beijing Genomic Institute (BGI) for total protein extraction and subsequent analysis.

Protein Extraction and Digestion

Protein extraction and digestion procedures were performed essentially as described previously (He et al., 2019). Briefly, the cells were suspended in lysis buffer (7 M urea, 2 M thiourea, 4% CHAPS, 40 mM Tris-HCl, pH 8.5, 1 mM PMSF, 2 mM EDTA) and sonicated on ice. The protein mixtures were precipitated by adding 4× volume of chilled acetone and leaving the mixtures overnight at -20°C. After centrifugation at 30,000 g and 4°C, each pellet was dissolved in 0.5 M triethylamine borane (TEAB; Applied Biosystems, Milan, Italy) and sonicated on ice. After centrifuging again at 30,000 g and 4°C, an aliquot of the supernatant was taken for determination of protein concentration by the Bradford method using BSA as a standard. For each example, 100 μg of the extracted proteins were digested at 37°C for 4 h with Trypsin Gold (Promega, Madison, WI, USA) with a protein-to-trypsin ratio of 40:1. Trypsin Gold was then added to each sample again with the same ratio, and the protein was digested for another 8 h. The digested peptides were desalted using a Strata X C18 column (Phenomenex, Torrance, CA, USA) and vacuum-dried.

iTRAQ Labeling and Phosphopeptide Enrichment

The vacuum dried peptides from each group were reconstituted in 0.5 M TEAB and isotope labeling was carried out according to the manufacturer's protocol for the iTRAQ Reagent 8-Plex Kit (Applied Biosystems, Foster City, CA, USA). The labeled samples were desalted using a Strata X C18 column (Phenomenex, Torrance, CA, USA) and vacuum-dried.

The dried peptides were reconstituted in a solution containing 65% (v/v) acetonitrile (ACN) and 3.5% (v/v) trifluoroacetic acid (TFA) and then saturated with glutamic acid. Phosphopeptides were enriched using TiO_2, as previously described (He et al., 2017a). Briefly, iTRAQ-labeled peptides were added into the freshly prepared TiO_2 beads (GL Sciences) at peptides-to-beads ratio of 1:4 (mass/mass) and then incubated for 20 min at 37°C with end-over-end rotation. The mixture was

first washed with 65% ACN and 0.5% TFA (pH 2.0-3.5) and then with 65% ACN and 0.1% TFA (pH 2.0–3.5). The phosphopeptides were eluted with 0.3 M NH_4OH solution in 50% (v/v) ACN (diluted from a 25% NH_4OH solution) and vacuum-dried.

Peptide Fractionation

The enriched peptide mixtures were reconstituted with 300 µl 1%TFA and separated according to the manufacturer's protocol for the High pH Reversed-Phase Peptide Fractionation Kit (Thermo Scientific Pierce, #84868). The eluted peptides were pooled into six fractions and vacuum-dried.

Liquid Chromatography-Tandem Mass Spectrometry Analysis Using Q Exactive

Each fraction was resuspended in buffer A (2% ACN, 0.1% FA) and centrifuged at 20, 000 g for 10 min. The supernatant was loaded by the auto sampler onto a trap column on a LC-20AD nanoHPLC (Shimadzu, Kyoto, Japan) for trapping and desalting. The peptides were then eluted onto a 15 cm analytical C18 column (inner diameter 75 µm, column particle size 3.6 µm) that was packed in-house. The samples were loaded and subjected to the following conditions: 8 min at a flow rate of 300 nl/min maintaining at 5% buffer B (98% ACN, 0.1% FA), followed by 68 min linear gradient to 21%, 6 min linear gradient to 32%, and 3 min linear gradient to 80%, and then maintenance at 80% buffer B for 5 min, and finally a return to 5% buffer B for 5 min.

The peptides were then subjected to ionization with nano-electrospray ionization (nanoESI) followed by analysis with a Q Exactive Tandem Mass Spectrometer (Thermo Fisher Scientific, MA, USA) in a data-dependent acquisition mode. The electrospray voltage applied was 1.6 kV. MS1 spectra were collected in the range 350–1,500 m/z at a resolution of 70,000 and MS2 spectra were collected in the fixed starting 100 m/z at a resolution of 17,500. The 20 most intense precursors with a charge state of 2+ to 5+ were selected for MS2 fragmentation with 20 s dynamic exclusion setting. Peptides were selected for MS2 using the high-energy collision dissociation operating mode with a normalized collision energy setting of 30, and the ion fragments were detected in the Orbitrap. The AGC target value for MS1 and MS2 was set at 3E6 and 1E5, respectively.

Phosphoproteomic Data Analysis

For iTRAQ phosphorylated protein identification, raw MS/MS spectra were processed with Proteome Discoverer 1.4 (Thermo Fisher Scientific) and searched using in-house Mascot 2.3 (Matrix Science, London, UK) against the download protein sequences from *Toxo*DB database (https://toxodb.org/toxo/). The search parameters were as follows: enzyme, trypsin; peptide mass tolerance, 20 ppm; fragment mass tolerance, 0.05 Da; fixed modifications, Carbamidomethyl (C), iTRAQ8plex (N-term), iTRAQ8plex (K); variable modifications, Oxidation (M), Acetyl (Protein N-term), Deamidated (NQ), Phospho (ST), Phospho (Y), and iTRAQ8plex (Y); and max missed cleavage, 2. The search results were further processed using Percolator and a peptide false discovery rate (FDR) ≤0.05 was used as the criterion for defining confidential peptides. The phosphorylation sites of identified phosphopeptides were scored with Proteome Discoverer applying in-house phosphoRS 3.1, and the confidence was set at a phosphoRS site probability ≥0.75 (Taus et al., 2011). For iTRAQ quantification, the peptide for quantification was automatically selected by the algorithm to calculate the reporter peak area, error factor (EF), and p-value (default parameters in Mascot software package). Student's t-test was performed using the Mascot software. The resulting data set was auto bias-corrected to the biological replicates. The peptide ratios were normalized by dividing by the median ratio of all the peptides identified (Wu et al., 2015). A phosphoprotein with a between-group 1.5-fold change in phosphorylation level at $p \leq 0.05$ was considered to be a significantly regulated phosphoprotein (Nguyen et al., 2012).

Functional Analysis of the Phosphorylation Data Set

All the identified phosphoproteins between the two comparison groups (JI and PE) were subjected to bioinformatic analysis. Gene Ontology (GO) annotation and enrichment analysis were completed using the web-based GO software (http://www.geneontology.org) (Ashburner et al., 2000). A pathway analysis was performed at the Kyoto Encyclopedia of Genes and Genomes database (KEGG, http://www.genome.p/kegg) (Kanehisa and Goto, 2000). Hypergeometric tests were used for identifying significantly enriched GO terms and KEGG pathways. A significance level of $p < 0.05$ was used as the enrichment cut off threshold for GO terms and KEGG pathways (Nguyen et al., 2012). All the identified proteins were used as the backgrounds of GO and KEGG analyses with all the identified *T. gondii* phosphorylated proteins. Additionally, interaction networks for all the identified phosphoproteins in these two groups were conducted using STRING 11.0 (http://string-db.org).

Transcript Expression Analysis With qPCR

Total RNA was isolated from HFF cells infected with *T. gondii* for 30 min and 28 h by Trizol (Invitrogen), and then reversely transcribed using Reverse Transcriptase (*Vazyme*). Each biological replicate was analyzed in triplicates by SYBR green-based quantitative real-time PCR using Top Green qPCR SuperMix (*TransGen* Biotech) on Light Cycler 480II (*Roche*) with the primers shown in **Table S1**. Mean fold-changes from three independent experiments were calculated from $\Delta\Delta CT$ values using actin transcript as a housekeeping gene (Buguliskis et al., 2010; Blume et al., 2015).

RESULTS

Phosphoproteomic Identification of *T. gondii* Tachyzoites at Different Infection Phases

All six samples were labeled with iTRAQ reagents, and the phosphopeptides were enriched by TiO_2, which were then analyzed with LC-MS/MS. The workflow of this study is presented in **Figure 1**. As a result, a total of 46 phosphopeptides

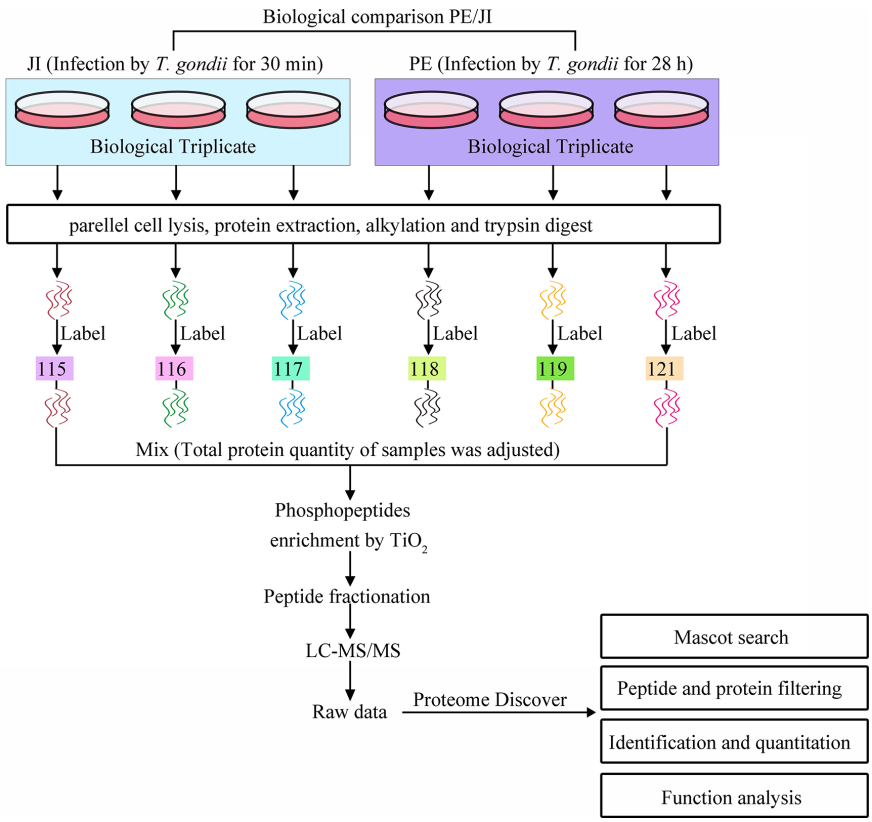

FIGURE 1 | Processes of the iTRAQ-based phosphoproteomic analysis of *T. gondii* tachyzoites at the stages of "just invading" and "prior to egress". Two biological triplicates of cells infected with *T. gondii* RH tachyzoites for 30 min or 28 h, respectively, at a MOI of 3 were collected for the phosphoproteomic analysis of *T. gondii* tachyzoites. All the six samples were digested with trypsin and labeled with iTRAQ. The labeled phosphopeptides were enriched with TiO2, and subjected to LC-MS/MS analysis. The generated phosphoproteomic data were then qualitatively, quantitatively, and functionally analyzed.

matching to 38 phosphoproteins were identified with a false-discovery rate (FDR) ≤0.01 in phosphopeptide level, and 42 phosphorylation sites were detected with phosphoRS probability ≥0.75 in phosphorylation site level (**Figure 2A**). The detected 42 phosphorylation sites consisted of 33 (78.57%) serine phosphorylation (pSer), 8 (19.05%) threonine phosphorylation (pThr), and 1 (2.38%) tyrosine phosphorylation (pTyr) (**Figure 2B**). The detailed information of all the identified phosphoproteins is shown in **Table S2**.

Identification and Quantification of the Significantly Regulated Tachyzoite Phosphoproteins

The phosphopeptides identified in the two groups (JI and PE) were quantified using Mascot software, and between these two groups, the comparative analysis of phosphorylation level change was further performed based on PE/JI ratio. The comparative phosphorylation level analysis led to the identification of 8 up-regulated (TGGT1_311480, GRA12, IMC4, TGGT1_273460, TGGT1_230940, GRA2, TGGT1_257530, GRA3) and 2 down-regulated phosphoproteins (TGGT1_239800, TGGT1_228360) ($p < 0.05$). The detailed information of phosphoproteins with phosphorylation level significantly changed is shown in **Table S2**.

Function Analysis of the Identified Phosphoproteins

To gain a better understanding of the phosphoproteins' role in the lytic cycle processes of *T. gondii* tachyzoites, we performed GO and KEGG enrichment analysis with the identified phosphoproteins. The enriched GO terms were assigned to molecular function (MF), biological process (BP), cellular component (CC), and the results are shown in **Figure 3**. The terms of the MF were significantly enriched with the identified phosphoproteins including "transporter activity", "catalytic activity", and "binding". In the BP, the terms were significantly enriched with the identified phosphoproteins including "single-organism process", "metabolic process", "localization", "establishment of localization", and "cellular process". While in the CC, terms of "organelle part", "organelle", "membrane part", "membrane", "macromolecular complex", "extracellular region", "cell part", and "cell" were significantly enriched. Unfortunately, since the number of identified phosphoproteins with phosphorylation level significantly changed was few, no term in MF and CC was significantly enriched, except for the terms of "single-organism cellular process", "single-organism process", and "cellular process" in BP enriched with the significantly regulated phosphoproteins.

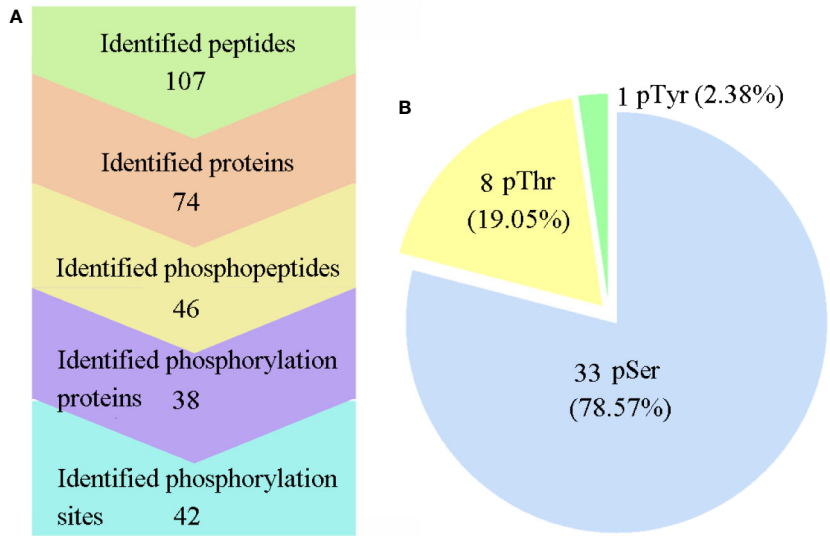

FIGURE 2 | Large-scale mass spectra information regarding the phosphoproteome data. **(A)** Information on the identified proteins, phosphoproteins, peptides, phosphopeptides, and phosphosites. **(B)** Distribution of the pSer/pThr/pTyr phosphoproteome. Phospho-Ser was the most abundant site, and it accounted for 78.57% of all phosphorylated amino acids, followed by phospho-Thr (19.05%) and phospho-Tyr (2.38%).

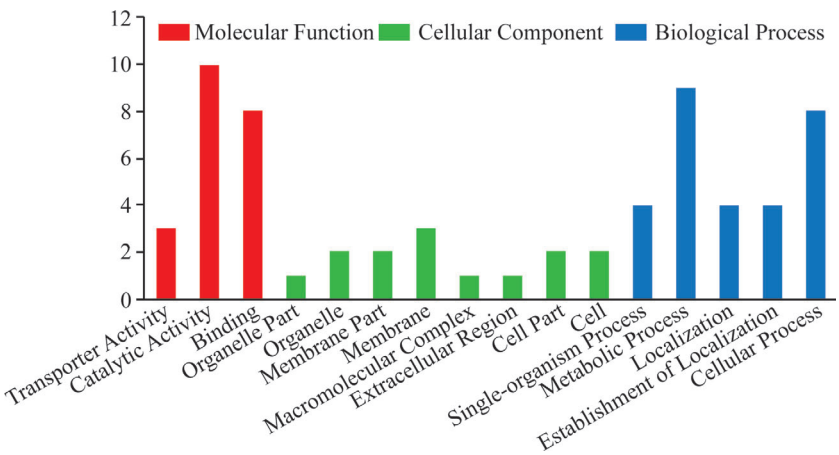

FIGURE 3 | GO enrichment analysis of all the identified *T. gondii* phosphoproteins. GO analysis of all the 38 identified phosphoproteins revealed that proteins in the "biological process", "cellular component", and "molecular function" categories were enriched. These phosphoproteins were suggested to be involved in the regulation of cellular processes including binding, location, and metabolism correlated with *T. gondii* invasion and egress.

The KEGG pathway analysis with all the identified phosphoproteins revealed that the enriched pathways were closely associated with the pathogenicity of *T. gondii*, such as "toxoplasmosis", "metabolic pathways", and "glycerophospholipid metabolism" (**Table S3**, **Figure S1**). For the same reason with GO analysis, however, only one pathway correlated with "toxoplasmosis" was enriched with the significantly regulated phosphoproteins in the comparison group of PE vs. JI (**Figure 4**).

Protein–Protein Interaction Analysis

The protein–protein interaction (PPI) network of the identified phosphoproteins were analyzed using STRING 11.0, and the resulting PPI network included 16 nodes and 37 edges and was then constructed by removing unconnected proteins and self-loops as shown in **Figure 4**. The PPI network was constructed by setting the minimum required interaction score to medium confidence (0.4). Based on the results of PPI network analysis,

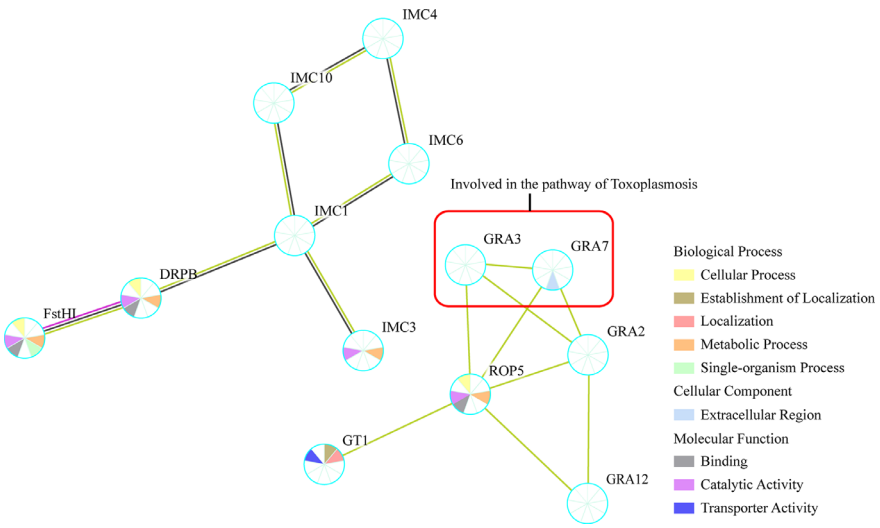

FIGURE 4 | Protein–protein interaction (PPI) networks of all the identified phosphoproteins. The PPI network was generated with the identified tachyzoites phosphoproteins *via* STRING v11.0 with a confidence score over 0.7. GRA3 and GRA7 within red box were suggested to be involved in the regulation of Toxoplasmosis pathway.

phosphoproteins of GRA2, GRA3, GRA7, GRA12, and ROP5 were shown to be enriched at the central nodes in the PPI network, which were demonstrated to be important to suppress the immune recognition by the host cell (Rommereim et al., 2019). In addition, some other phosphoproteins with unknown function such as IMC1, IMC4, IMC6, IMC12, and GT1 were also shown as important node proteins in the PPI network (**Figure 4**).

Transcription Level Assay of the Significantly Regulated Phosphoproteins

The transcription level of ten phosphoproteins with phosphorylation level significantly changed in the comparison group of PE vs. JI were analyzed with qPCR. Four of the ten *T. gondii* phosphoproteins (TGGT1_311480, GRA12, TGGT1_273460, and TGGT1_239800) were demonstrated to be significantly down-regulated at the transcription level, while the other 6 phosphoproteins were revealed with no significant change (**Figure 5**).

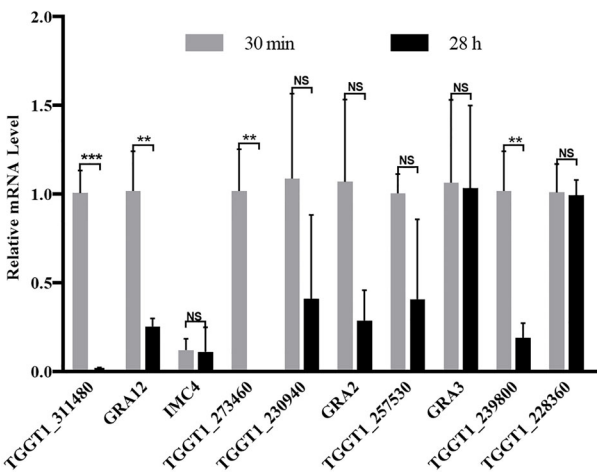

FIGURE 5 | Relative transcription level of the genes with their protein's phosphorylation level significantly changed. The transcription level of ten phosphoproteins with the phosphorylation level significantly changed were detected with qPCR, ant the Actin was used as an internal control. Error bars represent SD from three independent replicates, and statistical values were determined by t test. **p < 0.01; ***p < 0.001; NS, no significant difference.

DISCUSSION

The invasion and egress of *T. gondii* tachyzoites are two basic processes of the lytic cycle, which entails complex signaling events within both the parasite and its host (Treeck et al., 2011; Blader et al., 2015). As a key post-translational modification in mediating the protein function, the phosphorylation was considered to be involved in regulating almost all the signaling events, and the phosphorylation has been proved to play important roles in regulating the invasion and egress processes of *T. gondii* (Tang et al., 2014; Krishnamurthy et al., 2016; Stewart et al., 2016; Wallbank et al., 2019). For example, phosphorylation of host Irga6 by *Tg*ROP18 inhibits its accumulation and action on the PVM, thereby promoting *T. gondii* escape from host immune clearance (Steinfeldt et al., 2010). Moreover, the phosphorylation-mediated activation of host STAT3 induced by *Tg*ROP16 enhances the production of proinflammatory cytokines, including IL-6 and IL-12, to eliminate the parasites (Yamamoto et al., 2009). Corresponding to the essential roles of phosphorylation in modifying the

function of a host protein, the crucial role of phosphorylation of *T. gondii* protein in mediating the invasion and egress processes of *T. gondii* has also been reported (Tang et al., 2014; Krishnamurthy et al., 2016). For example, Tang's group has demonstrated that enhanced phosphorylation of *Tg*MyoA increases the efficiency of invasion and accelerates the process of calcium-induced egress (Tang et al., 2014). Additionally, the dephosphorylation of *Tg*AMA1 is demonstrated to be necessary for the optimal invasion of *T. gondii* (Krishnamurthy et al., 2016). Therefore, phosphorylation is a double-edged sword, which can play both positive and negative regulatory roles in mediating the interaction between *T. gondii* and its host. Recently, iTRAQ based phosphoproteomic quantitative analysis has emerged as an efficient approach to screen key phosphoproteins essential for the pathogenesis of *T. gondii*. Intriguingly, our previous iTRAQ-based phosphoproteomic analysis with respect to the host cell at the infection stages of JI and PE manifests that *T. gondii* manipulates host cell processes including apoptosis, metabolism, cytoskeleton reorganization through phosphorylation (He et al., 2019). Based on the results of our phosphoproteomic analysis, we found that the phosphorylation levels of host cell vimentin were significantly modulated by *T. gondii* at the two infection stages. Further functional analysis revealed that vimentin inhibits the invasion of *T. gondii* (He et al., 2017b). Consequently, the phosphoproteomic analysis of *T. gondii* at the infection phases of JI and PE may provide new clues to unravel the mechanisms controlling the parasite's invasion and egress processes. However, the phosphoproteome data and its quantitative information with respect to *T. gondii* tachyzoite at the infection phases of just invasion and prior to egress have not been identified yet.

With the illustration of the vital roles of phosphorylation for *T. gondii* infection, the phosphoproteomic analysis of *T. gondii* has been gradually explored. For example, Wang et al. analyzed the phosphoproteome of three different strains *of T. gondii* tachyzoites (RH strain, PRU stain, and PYS strain), and identified several hundreds of phosphoproteins. This phosphoproteomic analysis is therefore beneficial for explaining the contribution of phosphorylation in regulating the virulence heterogeneity of the three parasite strains (Wang et al., 2019). In our study, however, only 38 phosphoproteins were identified, which were much less than the reported number of phosphoproteins in *T. gondii* tachyzoites. The discrepancy between the number of identified *T. gondii* phosphoproteins may be due to the far below amount of loading protein of *T. gondii* for the analysis performed with the same approach, completely different lytic cycles of tachyzoites and various sources of parasite collection (Wang et al., 2019). Since the phosphoproteome data generated in this study was confirmed by western blot from the aspect of human cells (He et al., 2019), the phosphoproteome data reported in this study therefore is very reliable. Interestingly, most of these identified phosphoproteins were revealed with low mean phenotype scores based on the genome-wide CRIPSR screened results performed by Sidik's group (**Table S2**), which suggested that the phosphorylation could be employed to modulate these protein's function thereby controlling the invasion and egress processes of *T. gondii* (Sidik et al., 2016). Additionally, among the ten significantly regulated phosphoproteins, four of them were demonstrated to be significantly down-regulated at the transcriptional level in the comparison group of PE vs. JI, which suggested that some phosphoproteins were involved in the regulation of the invasion and egress processes of *T. gondii* not only through modifying the phosphorylation status, but also by regulating the mRNA expression.

The results of the bioinformatic analysis in our study showed that these identified phosphoproteins were mainly involved in the regulation of the processes of metabolism and location, and their function emphasized on "transporter activity", "catalytic activity", and "binding". Our analysis is in agreement with previous studies, which demonstrated that multiple phosphoproteins played crucial roles in modulating the enriched biological processes. For example, GRA2 is reported to be involved in the formation of IVN in the PV, which allows nutrients transportation to nourish the parasites (Nam, 2009). Deletion of GRA2 lead to failed formation of the IVN and also decreases the infection rate *in vitro* (Rommereim et al., 2016). Intriguingly, the phosphorylation level of GRA2 was detected to be up-regulated significantly in the comparison group of PE vs. JI, which suggested that phosphorylation may be one of the important mechanisms in mediating the function of GRA2. Surprisingly, both GRA3 and GRA12 were identified with enhanced phosphorylation level in this study yet were shown to be dispensable for the lytic cycle of *T. gondii in vitro*, however, they play essential roles in acute infection of *T. gondii in vivo* (Craver and Knoll, 2007; Rommereim et al., 2016; Fox et al., 2019; Wang et al., 2020). The explanation of this discrepancy may be that GRA3 and GRA12 do not play their roles independently in the lytic cycle process of tachyzoites but interdependently, just as other GRA proteins (Rommereim et al., 2016). Consequently, double knockout stains of GRA3 and GRA12, or even more GRAs, need to be generated to explore their roles in the lytic cycle of *T. gondii*. Moreover, another significantly regulated phosphoprotein, ApiAT5-3 (TGGT1_257530), identified in this work has been shown to play an essential role in the lytic cycle of *T. gondii* other than egress, despite it being rapidly phosphorylated at Ser56 after induction of egress with ionophore (Wallbank et al., 2019). Wallbank et al. reports that the phosphorylation of ApiAT5-3 at the process of PE is prepared for the extracellular milieu, or reinvasion of tachyzoites. However, how the phosphorylation of ApiAT5-3 functions during the lytic cycle of *T. gondii*, and whether there are other phosphorylation sites involving in the regulation of its function need to be further explored. In our study, we found the phosphorylation level of ApiAT5-3 at Ser24 was significantly up-regulated prior to egress compared to the stage of just invasion of *T. gondii*. This may provide new insight into the mechanism of how ApiAT5-3 works in the lytic cycle of *T. gondii*.

KEGG pathway analysis showed that the identified phosphoproteins were annotated into pathways with direct

relevance to toxoplasmosis and metabolism, such as "Glycerophospholipid metabolism" and "Metabolic pathways" (**Table S3**, **Figure S1**), which is consistent with the reported phosphoproteins function in the phosphoproteomic analysis of different *T. gondii* strains (Wang et al., 2019). This result suggests that phosphoprotein-mediated pathway regarding toxoplasmosis and metabolism may be critical for the pathogenesis of *T. gondii*. Further analysis of the key phosphoproteins involved in the regulation of these shared pathways may provide potential clues to illustrate the mechanism of the invasion and egress, such as GRA3, GRA7, and TGGT1_306540. Moreover, five phosphoproteins ROP5, GRA7, GRA2, GRA3, and GRA12, were shown to locate at the central nodes in the PPI network. All these five phosphoproteins were demonstrated to play essential roles in reducing T cell recognition (Rommereim et al., 2019), which could further avoid the clearance of parasite by the host immune system. What is interesting is that three of the five phosphoproteins, GRA2, GRA3, and GRA12, were found to be significantly up-regulated at the phosphorylation level in the comparison group of PE vs. JI. Some of other phosphoproteins were shown to locate at the central nodes in the PPI network, such as IMC1, IMC4, and IMC12, and they may have important roles in the regulation of *T. gondii* lytic cycle. Unfortunately, the biological significance of these identified phosphorylation has not been explored yet. Therefore, further work is required to unravel the function of these identified phosphoproteins in the process of parasite lytic cycle.

In conclusion, iTRAQ-based phosphoproteomic analysis in this research will supplement the phosphoproteome data of *T. gondii* at the different lytic cycle stages. Moreover, the identified phosphoproteins and enriched cellular processes will contribute to understanding the mechanism of *T. gondii* invasion and egress and future studies should aim to clarify the precise function of these identified phosphoproteins as well as characterize the phosphoproteome data of other lytic cycle processes besides the present two stages.

DATA AVAILABILITY STATEMENT

All datasets generated for this study are included in the article/ **Supplementary Material**. All the original mass spectrometry data have been deposited to the ProteomeXchange Consortium (http://proteomecentral.proteomexchange.org) *via* the iProX partner repository (Ma et al., 2019) with the dataset identifier PXD020655.

AUTHOR CONTRIBUTIONS

CH performed the experiments, analyzed the data, and wrote the paper. MX and SP performed the experiments and data analysis. HW revised the paper. HP and ZL helped conceive and design the experiments. ZL provided advice on data interpretation and edited the paper. All authors contributed to the article and approved the submitted version.

FUNDING

This research was provided by the Natural Science Foundation of Jiangsu Province (BK20190983), the Natural Science Foundation of the Jiangsu Higher Education Institutions of China (19KJB310022), and the Research Foundation of Xuzhou Medical University (D2019018) to CH.

SUPPLEMENTARY MATERIAL

The Supplementary Material for this article can be found online at: https://www.frontiersin.org/articles/10.3389/fcimb.2020.586466/full#supplementary-material

SUPPLEMENTARY FIGURE 1 | Enriched KEGG pathways with all the identified phosphoproteins in the comparison group of PE vs. JI. Yellow nodes represent the identified phosphoproteins involved in the regulation of enriched KEGG pathways, which was denoted with the surrounding blue nodes. Protein with red color indicated the phosphoprotein with the phosphorylation level significantly changed.

SUPPLEMENTARY TABLE 1 | qPCR primers for the transcription level detection of the genes with their protein's phosphorylation level significantly changed.

SUPPLEMENTARY TABLE 2 | Quantitative and the mean phenotype score information of all the identified *T. gondii* phosphoproteins.

SUPPLEMENTARY TABLE 3 | Enriched KEGG pathways with all the identified *T. gondii* phosphoproteins and the information of phosphoproteins involved in the regulation of these pathways.

REFERENCES

Ashburner, M., Ball, C. A., Blake, J. A., Botstein, D., Butler, H., Cherry, J. M., et al. (2000). Gene ontology: tool for the unification of biology. The Gene Ontology Consortium. *Nat. Genet.* 25, 25–29. doi: 10.1038/75556

Blader, I. J., Coleman, B.II, Chen, C. T., and Gubbels, M. J. (2015). Lytic Cycle of *Toxoplasma gondii*: 15 Years Later. *Annu. Rev. Microbiol.* 69, 463–485. doi: 10.1146/annurev-micro-091014-104100

Blume, M., Nitzsche, R., Sternberg, U., Gerlic, M., Masters, S. L., Gupta, N., et al. (2015). A *Toxoplasma gondii* Gluconeogenic Enzyme Contributes to Robust Central Carbon Metabolism and Is Essential for Replication and Virulence. *Cell Host Microbe.* 18, 210–220. doi: 10.1016/j.chom.2015.07.008

Broncel, M., and Treeck, M. (2020). Label-Based Mass Spectrometry Approaches for Robust Quantification of the Phosphoproteome and Total Proteome in *Toxoplasma gondii*. *Methods Mol. Biol.* 2071, 453–468. doi: 10.1007/978-1-4939-9857-9_23

Buguliskis, J. S., Brossier, F., Shuman, J., and Sibley, L. D. (2010). Rhomboid 4 (ROM4) affects the processing of surface adhesins and facilitates host cell invasion by *Toxoplasma gondii*. *PloS Pathog.* 6, e1000858. doi: 10.1371/journal.ppat.1000858

Craver, M. P., and Knoll, L. J. (2007). Increased efficiency of homologous recombination in *Toxoplasma gondii* dense granule protein 3 demonstrates that GRA3 is not necessary in cell culture but does contribute to virulence. *Mol. Biochem. Parasitol.* 153, 149–157. doi: 10.1016/j.molbiopara.2007.02.013

Fox, B. A., Guevara, R. B., Rommereim, L. M., Falla, A., Bellini, V., Pètre, G., et al. (2019). *Toxoplasma gondii* Parasitophorous Vacuole Membrane-Associated Dense Granule Proteins Orchestrate Chronic Infection and GRA12 Underpins Resistance to Host Gamma Interferon. *mBio* 10, e00589–e00519. doi: 10.1128/mBio.00589-19

Frénal, K., Dubremetz, J. F., Lebrun, M., and Soldati-Favre, D. (2017). Gliding motility powers invasion and egress in Apicomplexa. *Nat. Rev. Microbiol.* 15, 645–660. doi: 10.1038/nrmicro.2017.86

Gaji, R. Y., Johnson, D. E., Treeck, M., Wang, M., Hudmon, A., and Arrizabalaga, G. (2015). Phosphorylation of a Myosin Motor by *Tg*CDPK3 Facilitates Rapid Initiation of Motility during *Toxoplasma gondii* egress. *PloS Pathog.* 11, e1005268. doi: 10.1371/journal.ppat.1005268

He, C., Chen, A. Y., Wei, H. X., Feng, X. S., and Peng, H. J. (2017a). Phosphoproteome of *Toxoplasma gondii* Infected Host Cells Reveals Specific Cellular Processes Predominating in Different Phases of Infection. *Am. J. Trop. Med. Hyg.* 97, 236–244. doi: 10.4269/ajtmh.16-0901

He, C., Kong, L., Zhou, L., Xia, J., Wei, H., Liu, M., et al. (2017b). Host Cell Vimentin Restrains *Toxoplasma gondii* Invasion and Phosphorylation of Vimentin is Partially Regulated by Interaction with *Tg*ROP18. *Int. J. Biol. Sci.* 13, 1126–1137. doi: 10.7150/ijbs.21247

He, C., Kong, L., Puthiyakunnon, S., Wei, H. X., Zhou, L. J., and Peng, H. J. (2019). iTRAQ-based phosphoproteomic analysis reveals host cell's specific responses to *Toxoplasma gondii* at the phases of invasion and prior to egress. *Biochim. Biophys. Acta Proteins Proteom.* 1867, 202–212. doi: 10.1016/j.bbapap.2018.12.004

Hortua Triana, M. A., Márquez-Nogueras, K. M., Vella, S. A., and Moreno, S. N. J. (2018). Calcium signaling and the lytic cycle of the Apicomplexan parasite *Toxoplasma gondii*. *Biochim. Biophys. Acta Mol. Cell Res.* 1865, 1846–1856. doi: 10.1016/j.bbamcr.2018.08.004

Hotez, P. J. (2014). Neglected parasitic infections and poverty in the United States. *PloS Negl. Trop. Dis.* 8, e3012. doi: 10.1371/journal.pntd.0003012

Joyce, B. R., Queener, S. F., Wek, R. C., and Sullivan, W. J. Jr. (2010). Phosphorylation of eukaryotic initiation factor-2{alpha} promotes the extracellular survival of obligate intracellular parasite *Toxoplasma gondii*. *Proc. Natl. Acad. Sci. U. S. A.* 107, 17200–17205. doi: 10.1073/pnas.1007610107

Kanehisa, M., and Goto, S. (2000). KEGG: kyoto encyclopedia of genes and genomes. *Nucleic Acids Res.* 28, 27–30. doi: 10.1093/nar/28.1.27

Krishnamurthy, S., Deng, B., Del Rio, R., Buchholz, K. R., Treeck, M., Urban, S., et al. (2016). Not a Simple Tether: Binding of *Toxoplasma gondii* AMA1 to RON2 during Invasion Protects AMA1 from Rhomboid-Mediated Cleavage and Leads to Dephosphorylation of Its Cytosolic Tail. *mBio* 7, e00754–e00716. doi: 10.1128/mBio.00754-16

Lavine, M. D., and Arrizabalaga, G. (2007). Invasion and egress by the obligate intracellular parasite *Toxoplasma gondii*: potential targets for the development of new antiparasitic drugs. *Curr. Pharm. Des.* 13, 641–651. doi: 10.2174/138161207780162854

Li, X. L., Wei, H. X., Zhang, H., Peng, H. J., and Lindsay, D. S. (2014). A meta analysis on risks of adverse pregnancy outcomes in *Toxoplasma gondii* infection. *PloS One* 9, e97775. doi: 10.1371/journal.pone.0097775

Ma, J., Chen, T., Wu, S., Yang, C., Bai, M., Shu, K., et al. (2019). iProX: an integrated proteome resource. *Nucleic Acids Res.* 47, D1211–D1217. doi: 10.1093/nar/gky869

Nam, H. W. (2009). GRA proteins of *Toxoplasma gondii*: maintenance of host-parasite interactions across the parasitophorous vacuolar membrane. *Korean J. Parasitol.* 47 Suppl, S29–S37. doi: 10.3347/kjp.2009.47.S.S29

Nguyen, T. H., Brechenmacher, L., Aldrich, J. T., Clauss, T. R., Gritsenko, M. A., Hixson, K. K., et al. (2012). Quantitative phosphoproteomic analysis of soybean root hairs inoculated with *Bradyrhizobium japonicum*. *Mol. Cell Proteomics* 11, 1140–1155. doi: 10.1074/mcp.M112.018028

Olsen, J. V., Blagoev, B., Gnad, F., Macek, B., Kumar, C., Mortensen, P., et al. (2006). Global, *in vivo*, and site-specific phosphorylation dynamics in signaling networks. *Cell* 127, 635–648. doi: 10.1016/j.cell.2006.09.026

Powell, C. J., Ramaswamy, R., Kelsen, A., Hamelin, D. J., Warshaw, D. M., Bosch, J., et al. (2018). Structural and mechanistic insights into the function of the unconventional class XIV myosin MyoA from *Toxoplasma gondii*. *Proc. Natl. Acad. Sci. U. S. A.* 115, E10548–e10555. doi: 10.1073/pnas.1811167115

Rommereim, L. M., Bellini, V., Fox, B. A., Pètre, G., Rak, C., Touquet, B., et al. (2016). Phenotypes Associated with Knockouts of Eight Dense Granule Gene Loci (GRA2-9) in Virulent *Toxoplasma gondii*. *PloS One* 11, e0159306. doi: 10.1371/journal.pone.0159306

Rommereim, L. M., Fox, B. A., Butler, K. L., Cantillana, V., Taylor, G. A., and Bzik, D. J. (2019). Rhoptry and Dense Granule Secreted Effectors Regulate CD8(+) T Cell Recognition of *Toxoplasma gondii* Infected Host Cells. *Front. Immunol.* 10, 2104. doi: 10.3389/fimmu.2019.02104

Schulze, W. X. (2010). Proteomics approaches to understand protein phosphorylation in pathway modulation. *Curr. Opin. Plant Biol.* 13, 280–287. doi: 10.1016/j.pbi.2009.12.008

Sidik, S. M., Huet, D., Ganesan, S. M., Huynh, M. H., Wang, T., Nasamu, A. S., et al. (2016). A Genome-wide CRISPR Screen in *Toxoplasma* Identifies Essential Apicomplexan Genes. *Cell* 166, 1423–1435.e1412. doi: 10.1016/j.cell.2016.08.019

Steinfeldt, T., Könen-Waisman, S., Tong, L., Pawlowski, N., Lamkemeyer, T., Sibley, L. D., et al. (2010). Phosphorylation of mouse immunity-related GTPase (IRG) resistance proteins is an evasion strategy for virulent *Toxoplasma gondii*. *PloS Biol.* 8, e1000576. doi: 10.1371/journal.pbio.1000576

Stewart, R. J., Ferguson, D. J., Whitehead, L., Bradin, C. H., Wu, H. J., and Tonkin, C. J. (2016). Phosphorylation of αSNAP is Required for Secretory Organelle Biogenesis in *Toxoplasma gondii*. *Traffic* 17, 102–116. doi: 10.1111/tra.12348

Tang, Q., Andenmatten, N., Hortua Triana, M. A., Deng, B., Meissner, M., Moreno, S. N., et al. (2014). Calcium-dependent phosphorylation alters class XIVa myosin function in the protozoan parasite *Toxoplasma gondii*. *Mol. Biol. Cell.* 25, 2579–2591. doi: 10.1091/mbc.E13-11-0648

Taus, T., Köcher, T., Pichler, P., Paschke, C., Schmidt, A., Henrich, C., et al. (2011). Universal and confident phosphorylation site localization using phosphoRS. *J. Proteome Res.* 10, 5354–5362. doi: 10.1021/pr200611n

Treeck, M., Sanders, J. L., Elias, J. E., and Boothroyd, J. C. (2011). The phosphoproteomes of *Plasmodium falciparum* and *Toxoplasma gondii* reveal unusual adaptations within and beyond the parasites' boundaries. *Cell Host Microbe* 10, 410–419. doi: 10.1016/j.chom.2011.09.004

Wallbank, B. A., Dominicus, C. S., Broncel, M., Legrave, N., Kelly, G., Macrae, J.II, et al. (2019). Characterisation of the *Toxoplasma gondii* tyrosine transporter and its phosphorylation by the calcium-dependent protein kinase 3, *Mol. Microbiol.* 111, 1167–1181. doi: 10.1111/mmi.14156

Wang, Z. X., Zhou, C. X., Calderón-Mantilla, G., Petsalaki, E., He, J. J., Song, H. Y., et al. (2019). iTRAQ-Based Global Phosphoproteomics Reveals Novel Molecular Differences Between *Toxoplasma gondii* Strains of Different Genotypes. *Front. Cell Infect. Microbiol.* 9:307. doi: 10.3389/fcimb.2019.00307

Wang, J. L., Bai, M. J., Elsheikha, H. M., Liang, Q. L., Li, T. T., Cao, X. Z., et al. (2020). Novel roles of dense granule protein 12 (GRA12) in *Toxoplasma gondii* infection. *FASEB J.* 34, 3165–3178. doi: 10.1096/fj.201901416RR

Wei, H. X., He, C., Yang, P. L., Lindsay, D. S., and Peng, H. J. (2016). Relationship Between Cat Contact and Infection by *Toxoplasma gondii* in Humans: A Meta-Analysis. *Comp. Parasitol.* 83, 11–19. doi: 10.1654/1525-2647-83.1.11

Weiss, L. M., and Dubey, J. P. (2009). Toxoplasmosis: A history of clinical observations. *Int. J. Parasitol.* 39, 895–901. doi: 10.1016/j.ijpara.2009.02.004

Wu, L., Wang, S., Wu, J., Han, Z., Wang, R., Wu, L., et al. (2015). Phosphoproteomic analysis of the resistant and susceptible genotypes of maize infected with *sugarcane mosaic virus*. *Amino Acids* 47, 483–496. doi: 10.1007/s00726-014-1880-2

Yamamoto, M., Standley, D. M., Takashima, S., Saiga, H., Okuyama, M., Kayama, H., et al. (2009). A single polymorphic amino acid on *Toxoplasma gondii* kinase ROP16 determines the direct and strain-specific activation of Stat3. *J. Exp. Med.* 206, 2747–2760. doi: 10.1084/jem.20091703

Conflict of Interest: The authors declare that the research was conducted in the absence of any commercial or financial relationships that could be construed as a potential conflict of interest.

frontiers in Cellular and Infection Microbiology

REVIEW
published: 10 December 2020
doi: 10.3389/fcimb.2020.610121

Accelerator or Brake: Immune Regulators in Malaria

Chunmei Cai[1,2†], *Zhiqiang Hu*[3†] *and Xiao Yu*[3,4*]

[1] Research Center for High Altitude Medicine, School of Medical, Qinghai University, Xining, China, [2] Key Laboratory of Application and Foundation for High Altitude Medicine Research in Qinghai Province, Qinghai University, Xining, China, [3] Department of Immunology, School of Basic Medical Sciences, Southern Medical University, Guangzhou, China, [4] Guangdong Provincial Key Lab of Single Cell Technology and Application, Southern Medical University, Guangzhou, China

Malaria is a life-threatening infectious disease, affecting over 250 million individuals worldwide each year, eradicating malaria has been one of the greatest challenges to public health for a century. Growing resistance to anti-parasitic therapies and lack of effective vaccines are major contributing factors in controlling this disease. However, the incomplete understanding of parasite interactions with host anti-malaria immunity hinders vaccine development efforts to date. Recent studies have been unveiling the complexity of immune responses and regulators against *Plasmodium* infection. Here, we summarize our current understanding of host immune responses against *Plasmodium*-derived components infection and mainly focus on the various regulatory mechanisms mediated by recent identified immune regulators orchestrating anti-malaria immunity.

Keywords: malaria, immune regulators, immune responses, type I interferon, signaling mechanisms, protective immunity

OPEN ACCESS

Edited by:
Xiaojun Chen,
Nanjing Medical University, China

Reviewed by:
Gaoqian Feng,
Burnet Institute, Australia
Celio Geraldo Freire-de-Lima,
Federal University of Rio de Janeiro, Brazil

***Correspondence:**
Xiao Yu
xiaoyu523@smu.edu.cn

[†]*These authors have contributed equally to this work*

Specialty section:
This article was submitted to Parasite and Host, a section of the journal Frontiers in Cellular and Infection Microbiology

Received: *25 September 2020*
Accepted: *09 November 2020*
Published: *10 December 2020*

Citation:
Cai C, Hu Z and Yu X (2020) Accelerator or Brake: Immune Regulators in Malaria. Front. Cell. Infect. Microbiol. 10:610121. doi: 10.3389/fcimb.2020.610121

INTRODUCTION

Malaria, caused by *Plasmodium*, is one of the deadly infectious diseases worldwide (Battle et al., 2015; Howes et al., 2016). According to the World Health Organization report (WHO, 2019), this infectious disease affected up to 260 million individuals, and caused about half a million deaths in 2018. When female *Anopheles* mosquitoes inject *Plasmodium* sporozoites into mammalian hosts skin, the malaria infection is initiated, leading to a complex life cycle (Ross, 1896; Grassi et al., 1899). After that, the sporozoites travel through the bloodstream to the liver (Tavares et al., 2013). Once sporozoites reach the liver, they infect hepatocytes and replicate to about 30,000 merozoites, which are then released back into the peripheral blood (Mota et al., 2001). Merozoites infect red blood cells (RBCs) rapidly, and the repeated cycle, including invasions, replication and release, leads to exponential growth of parasites and disease (Amino et al., 2006; Sturm et al., 2006). The complex and multi-staged life cycle of malaria parasites evokes a slow development of immunity to protect parasites from being eliminated.

Over the past decade, the malaria disease, death, and transmission rates significantly decreased in most endemic countries. However, this stunning progress has been halted by emergence of drug resistance (WHO, 2019). Besides, the lack of an effective vaccine has been a major constraint in the

prevention of malaria infection, which largely due to the underlying mechanism of host-parasite interactions is poorly understood (Riley and Stewart, 2013; Arama and Troye-Blomberg, 2014; Ouattara and Laurens, 2015). Malaria infection triggers a systemic immune response, and results in the increase of inflammatory cytokines production that leads to parasite elimination or disease (Stevenson and Riley, 2004; Parroche et al., 2007; Coban et al., 2010; Sharma et al., 2011; Gazzinelli et al., 2014; Kalantari et al., 2014; Wu et al., 2014; Mendonca and Barral-Netto, 2015). A fine-tuned regulation of immune responses is crucial for developing protective immunity to effectively eliminate malaria parasites and preventing overreacted damage to host. Hence, a comprehensive understanding of the molecular and regulatory mechanisms that modulate the immunity against *Plasmodium* is pivotal to develop effective therapeutics and vaccines.

In this Review, we briefly summarize the activation and function of immune responses to malaria invasion, and mainly focus on the immune regulators in anti-malaria immunity. We describe parasites recognition by host, and the following initiation as well as function of host immune responses. Additionally, we discuss how the known regulators manipulate above immune activation and direct our attention on our group's findings. These include that an early spike of type I interferon (IFN-I) is protective against blood stages in *Plasmodium* infection, which is modulated by CD40, SOCS1, FOSL1, MARCH1, as well as RTP4, regulators identified by our group and collaborators.

Abbreviations: AIM2, absent in melanoma 2; AP-1, activating protein-1; APCs, antigen presenting cells; ATF, activating transcription factor; BCR, B cell receptor; BTLA, B and T lymphocyte attenuator; BTNL2, Butyrophilin-like 2; cGAS, cyclic GMP-AMP synthase; CCL, The chemokine (C-C motif) ligand; cDCs, conventional dendritic cells; CLAG2, cytoadherence-linked asexual gene 2; CTLA-4, Cytotoxic T lymphocyte antigen-4; CXCL, Chemokine (C-X-C motif) ligand; DAMPs, danger-associated molecular patterns; DC, dendritic cell; ECM, experimental cerebral malaria; ERK, extracellular signal-regulated kinases; FOXP3, Forkhead Box P3; GC, germinal center; gDNA, genomic-DNA; GPCR, G-protein-coupled receptors; GPI, glycosylphosphatidylinositol; HVEM, Herpes virus entry mediator; IDO, Indoleamine 2,3-dioxygenase; IFN-I, type I interferon; IL, interleukin; iRBCs, infected red blood cells; IRAK, IL-1 receptor associated kinase; IRF, IFN regulatory factor; JAK, Janus kinase; JNK, c-Jun N-terminal kinases; LAG-3, Lymphocyte Activation Gene-3; MAF, musculoaponeurotic fibrosarcoma; MAPK, mitogen-activated protein kinases; MARCH1, Membrane-associated ring-CH–type finger 1; MDA-5, melanoma differentiation-associated protein 5; MAVS, mitochondrial antiviral-signaling protein; MHC, major histocompatibility complex; MSP1, merozoite surface protein 1; MyD88, myeloid differentiation factor 88; NETs, neutrophil extracellular traps; NFAT1, Nuclear factor of activated T cell 1; NF-κB, nuclear factor κB; NK cells, natural killer cells; NKT cells, NK T cells; NLRP3, NLR family pyrin domain containing 3; PAMPs, pathogen-associated molecular patterns; PD-1, programmed cell death protein 1; pDCs, plasmacytoid dendritic cells; PI3K, phosphatidylinositol 3-kinase; PRRs, pathogen recognition receptors; PyHEUL, *Plasmodium yoelii* HECT-like E3 ubiquitin ligase; RBCs, red blood cells; ROS, reactive oxygen species; SOCS, suppressors of cytokine signaling; STAT, Signal transducer and activator of transcription; STING, stimulator of IFN genes; TBK1, TRAF family member-associated NF-κB activator (TANK)–binding kinase 1; TCR, T cell receptor; Tfh cells, T follicular helper cells; Th cells, helper T cells; TIGIT, T cell immunoglobulin and ITIM domain; Tim-3, T-cell immunoglobulin- and mucin-domain-containing molecule 3; TLR, Toll-like receptor; TNF, Tumor necrosis factor; TNFRSF5, TNF receptor superfamily member 5; TRAF, tumor necrosis factor receptor-associated factor; Treg cells, regulatory T cells.

ANTI-MALARIA IMMUNITY

Malaria infection is initiated by the bite of mosquitoes carrying *Plasmodium* sporozoites. Those sporozoites target liver and infect hepatocytes when they enter the bloodstream at the first step, referred to as the liver stage. After that, merozoites released from the infected hepatocytes invade RBCs, which is called the blood stage infection. During infection, the host immune system senses the invading of *Plasmodium* at both liver stage and blood stage, and initiates the innate immune responses to produce cytokines and chemokines, which further activates antigen presenting cells to bridge the innate and adaptive immunity against malaria (**Figure 1**).

Parasite Sensing

Host detects *Plasmodium*-derived components [known as pathogen-associated molecular patterns (PAMPs)], including hemozoin, glycosylphosphatidylinositol (GPI) anchors, and immunostimulatory nucleic acid motifs, and host-derived damage-associated molecular patterns (DAMPs), including uric acid, microvesicles, and haem, through pathogen-recognition receptors (PRRs) (Gazzinelli and Denkers, 2006; Figueiredo et al., 2007; Schroder and Tschopp, 2010; Takeuchi and Akira, 2010; Barbalat et al., 2011; O'neill et al., 2013; Gallego-Delgado et al., 2014; Mantel and Marti, 2014). During liver stage, *Plasmodium* inside hepatocytes are detected by macrophages and dendritic cells (DCs) through the interaction of parasite RNA with melanoma differentiation-associated protein 5 (MDA5), resulting in production of MDA5-MAVS-IRF3/IRF7-mediated IFN-I (Combes et al., 2004; Couper et al., 2010). At the blood stage, the GPI anchors from *P. falciparum* could stimulate pro-inflammatory responses by macrophages through recognition via TLR1/TLR2 or TLR2/TLR6 and to a much lesser extent through TLR4 (Krishnegowda et al., 2005; Walther et al., 2006; Clark et al., 2008; Riley and Stewart, 2013; Singh and Daneshvar, 2013), resulting in several downstream signaling pathways activation, including MAPK (JNK, p38, and ERK) and NF-κB signaling (Zhu et al., 2005). Hemozoin-combined genomic DNA (gDNA) induces TLR9 translocation on mouse DCs and macrophages and human B lymphocytes, subsequently initiates the activation of NF-κB and MAPK signaling pathways, as well as the release of chemokines and cytokines (Coban et al., 2005; Coban et al., 2010). On the other hand, accumulated studies demonstrate that hemozoin-gDNA complex could also induce NLRP3/AIM2 inflammasomes (Shio et al., 2009; Kalantari et al., 2014). Besides, our results show that the activation of NLRP3/AIM2 dependent inflammasome in plasmacytoid DCs (pDCs), conventional DCs (cDCs), and macrophages during *P. yoelii* YM infection (Yu et al., 2018). We also demonstrate that the *P. yoelii* YM gDNA initiates low level of IFN-I induction via cGAS-STING-TBK1-IRF3 (Yu et al., 2016). Our and other studies indicate that during both the liver and blood stage, parasites RNA activates MDA5-MAVS-mediated IFN-I production with murine parasites (such as *P. yoelii* and *P. berghei*) or human *Plasmoidums* (such as *P. falciparum*) treatment in DCs and macrophages (Baccarella et al., 2013; Liehl et al., 2014; Wu et al., 2014; Yu et al., 2016).

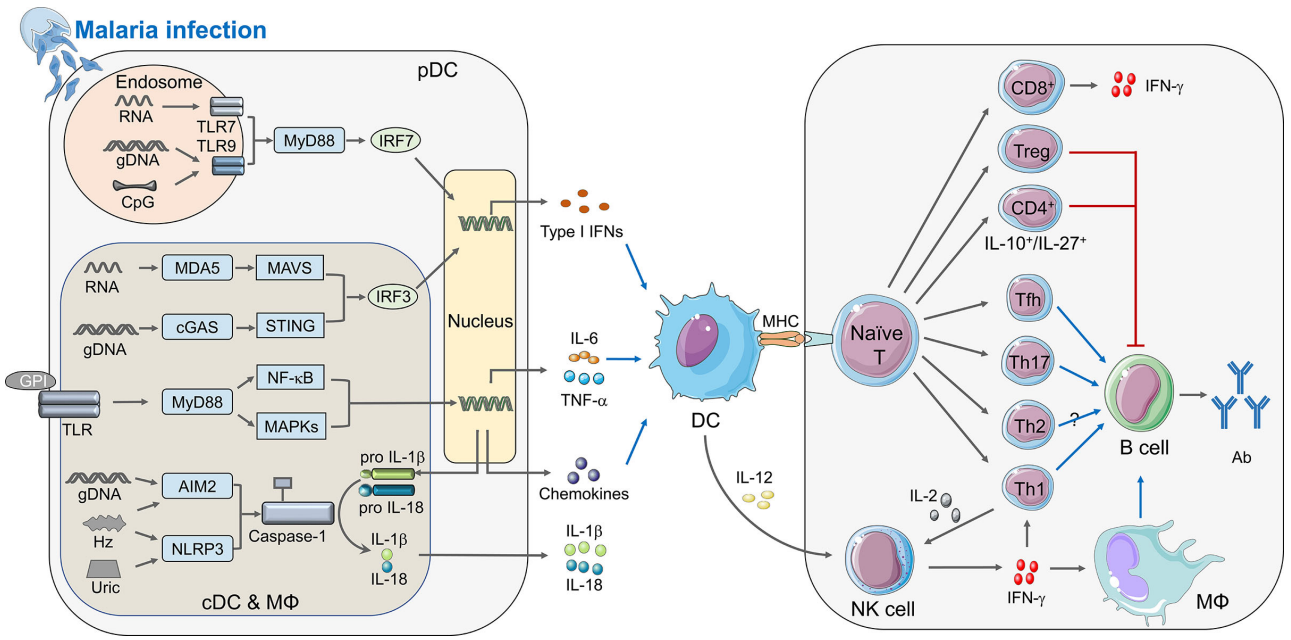

FIGURE 1 | Immune responses elicited by *Plasmodium* infection. During malaria infection, different PAMPs secreted from merozoites can be sensed by PRRs and activate the innate immunity (left panel). cDCs, macrophages, and pDCs are the crucial innate immune cells to defend malaria infection. Within the cytosol of these cells, pathogenic RNA interacts with MDA5 and recruits the adaptor protein MAVS, and *Plasmodium* gDNA can be detected by cGAS or other DNA sensors to activate adaptor protein STING. Both MAVS and STING could recruit serine/threonine-protein kinase TBK1 to phosphorylate IRF3 which translocate to nucleus and induce the expression of IFN-I. Furthermore, parasitic nucleic acid gDNA can also be sensed by inflammasome sensors AIM2, whereas haemozoin and uric acid activates NLRP3, leading to activation of inflammasomes and Caspase-1, which cleave pro-IL-1β and pro-IL-18 to form mature IL-1β and IL-18. Besides, parasite glycosylphosphatidylinositol (GPI) anchors to TLRs, including TLR2-TLR6 or TLR1-TLR2 heterodimers and TLR4 homodimers. TLRs signal transduces through MyD88, which finally causes the activation of NF-κB and MAPKs, and induces the secretion of pro-inflammatory cytokines, such as TNF-α and IL-6, as well as chemokines. Specifically, both CpG and hemozoin-combined gDNA can induce TLR9 translocation, and TLR7 can sense parasite RNA in the endosome of pDCs during the early infection stage, TLR9 as well as TLR7 recruit adaptor protein MyD88 and kinases TRAFs to phosphorylate IRF7 and induce the early robust production of IFN-I. After the innate immune responses, DC acts as a vital APC receiving stimulation via cytokines described upon, is activated and presents the antigens to naïve T cell through combination of MHC and TCR, which builds a bridge between innate and adaptive immunity. During adaptive immunity (right panel), naïve T cells differentiate into different subtypes with unique functions in anti-malaria immunity. Tfh, Th1, and Th17 could facilitate function of B cells, while Treg and IL-10$^+$/IL-27$^+$ CD4$^+$ T cell can suppress B cell function; CD8$^+$ T cells mainly express IFN-γ, and leaving function of Th2 is still uncertain. Activated DCs can also secrete IL-12 to promote the expression of IFN-γ from NK cell, which can enhance function of Th1 and macrophage thus help B cells to secrete antibody. Besides, IL-2 produced by Th1 can help NK cell to kill parasites. The diagram depicts a simplified version of indicated signaling pathway and immune cells involved in anti-malaria immunity. The abbreviations are defined in footnote.

In addition, our and other studies denote that the RNA of blood stage parasites induces IFN-I responses through TLR7 signaling pathway (Torgler et al., 2008; Baccarella et al., 2013; Soulat and Bogdan, 2017; Ding et al., 2018). Uric acid, released in large amounts by dying cells, is a byproduct of purine metabolism (Kordes et al., 2011). The pathogenic role of uric acid arises from NLRP3 activation and the inflammatory responses during malaria (Artavanis-Tsakonas and Riley, 2002; Baratin et al., 2007; Griffith et al., 2009; Chen et al., 2014). Host cell-derived microvesicles and haem also trigger inflammatory responses and pathogenesis of malaria (Couper et al., 2010; Ferreira et al., 2011; Mantel and Marti, 2014).

Innate Immunity

The innate immune responses provide a powerful front line defense against invasive malaria by inhibiting parasite growth and initiating the development of adaptive immunity (Deroost et al., 2016; Thaiss et al., 2016). During the liver stage of malaria infection, recent studies have demonstrated that sporozoites can be phagocytized by neutrophils, which are usually the first circulating cells to respond to an invading *Plasmodium* sporozoites through a mosquito bite (Segal, 2005; Peters et al., 2008; Hopp and Sinnis, 2015). At the blood stage infection, neutrophils clear merozoites via phagocytosis by producing reactive oxygen species (ROS) and other antimicrobial products or by formatting neutrophil extracellular traps (NETs) (Kumaratilake and Ferrante, 2000; Baker et al., 2008; Dale et al., 2008; Dupre-Crochet et al., 2013; Kapelski et al., 2014; Manfredi et al., 2018). The monocytes/macrophages are also important in eliminating parasite to protect host from disease (Chua et al., 2013). Kupffer cells play a pivotal role in preventing the severity of malaria and the release of the parasite into the bloodstream (Tweedell et al., 2015; Tweedell et al., 2018). During the blood stage of malaria, the circulating monocytes are pivotal to control parasitemia by phagocytose merozoite and asexual infected RBCs (iRBCs), as well as by increased inflammatory cytokines (IFN-α, IFN-γ, TNF-α, and IL-6) and chemokines (CCL2, CCL3, CCL4, and

CXCL10) (Huang et al., 2014; Colborn et al., 2015; Bansal et al., 2016; Hommel et al., 2018). Besides, the splenic macrophages play a key role in reducing blood stage parasitemia by phagocytosing iRBCs and producing reactive oxygen intermediates (Sponaas et al., 2009).

Type I IFNs play important roles in controlling malaria infection. An early spike of IFN-I is protective against some *P. yoelii* or *P. berghei* models (Liehl et al., 2014; Wu et al., 2014; Yu et al., 2016). Although the mechanisms remain largely unknown, studies have also shown that chronically high levels of IFN-I inhibit T cell activation, IFN-γ production and humoral immunity; as well as promote DCs death (Haque et al., 2011; Haque et al., 2014; Tamura et al., 2015; Montes De Oca et al., 2016; Zander et al., 2016). During liver stage of malaria infection, IFN-I could be induced by sporozoites in hepatocytes through cytosolic sensing of RNA (Liehl et al., 2014; Miller et al., 2014). At the blood stage, type I IFNs are the earliest cytokines produced by pDCs via TLR7-MyD88-IRF7 signaling pathway. By using lethal model of *P. yoelii* YM infection, our studies have showed that production of early type I IFNs are mediated by TLR7-MyD88-IRF7 signaling pathway and cytosolic sensing mechanisms, which include AIM2/NLRP3-Caspase1-IL-1β-TRAF3-TBK1-IRF3, cGAS-STING, and MDA5-MAVS associated TBK1-IRF3 signaling pathways (Yu et al., 2016; Yu et al., 2018). We further identified SOCS1, expressed in response to cytosolic sensing mechanisms, as a vital regulator to inhibit TLR7-MyD88-dependent IFN-I signaling (Yu et al., 2018). Type I IFNs contribute to the killing of parasite-infected hepatocytes by priming efficient cytokines and chemokines as well as activating γδT, T, natural killer (NK), and NKT cells to induce IFN-γ and other inflammatory cytokines production (Mcnab et al., 2015). The IFN-γ is an important effector that contributes to activating immune cells and indirectly eliminating parasite-infected cells (Liehl et al., 2014; Miller et al., 2014; Stegmann et al., 2015).

Bridging Innate and Adaptive Immunity

DCs exist in all clinically relevant sites related to the life stage of the malaria parasites and play a vital role in bridging the innate and adaptive immune system (Wykes and Good, 2008). Upon taking up foreign antigens or infecting by malaria parasites, DCs undergo a process of maturation and efficiently present antigen to pathogen-specific T cells via major histocompatibility complex (MHC) surface molecules (Stevenson et al., 1995; Stevenson and Riley, 2004; Orsini et al., 2012). Besides, the DCs secrete several cytokines and chemokines to recruit other immune cells and regulate T and B cells responses, ultimately resulting in clearance of malaria parasites (Wykes et al., 2007; Gowda et al., 2012; Orsini et al., 2012; Wu et al., 2014). An important mechanism for mice to resist *Plasmodium* infection is that the production of IL-12 in DCs, which then initiates the NK cells release IFN-γ to polarize $CD4^+$ T helper cell 1 (Th1) (Stevenson et al., 1995; Stevenson and Riley, 2004; Wykes et al., 2007; Gowda et al., 2012). The $CD4^+$ Th1 cells evoke effector responses and maintain the memory T cell pool to protect host from *Plasmodium* infection for a long-term (Da Silva et al., 2013). The DCs can be roughly divided into pDCs and cDCs population according to the expression of CD11c and CD123 (Macri et al., 2018). pDCs are the main sources of IFN-α, while cDCs are specifically used to prime and present antigens to T cells (Orsini et al., 2012; Macri et al., 2018). Besides, our studies suggest that pDCs, cDCs, and macrophages are required for generating IFN-I responses against *P. yoelii* YM infection in a stage-specific manner (Yu et al., 2016).

Adaptive Immunity

Upon DCs presenting processed antigens to naïve T cells, adaptive immunity is activated. Parasite-specific cytotoxic $CD8^+$ T cells are essential for the liver-stage protection upon recognition of *Plasmodium* antigens present on MHC class I expressed by DCs and infected hepatocytes (Sedegah et al., 1992; Doolan et al., 1997; Doolan et al., 2003). Yet, at the blood stage of malaria infection, iRBCs have lost the ability to express MHC-I leading to little contribution of $CD8^+$ T cell-mediated cytotoxicity to control malaria infection (Kumar and Miller, 1990; Vinetz et al., 1990; Miyakoda et al., 2012). Besides, the function of $CD8^+$ T cells in controlling cerebral *Plasmodium* in human is still controversial (Hunt et al., 2010; White et al., 2010). $CD4^+$ T cells can be activated by specific polarized cytokines to differentiate into functionally diverse subsets. $CD4^+$ Th cells are able to target MHC class II molecules, and play a crucial role in orchestrating innate and adaptive immunity during malaria infection (Roestenberg et al., 2009; Seder et al., 2013; Ishizuka et al., 2016; Mordmuller et al., 2017). IFN-γ and IL-2 are the $CD4^+$ Th1-associated cytokines (Shear et al., 1989; Su and Stevenson, 2000; Horowitz et al., 2010). During blood stage *Plasmodium* infection, IFN-γ is essential to activate macrophages and tune class-switch recombination in parasite-specific B cells to evoke antibody response, while IL-2 is critical for activating NK cells (Su and Stevenson, 2000; Jaramillo et al., 2003; Horowitz et al., 2010). The contribution of $CD4^+$ Th2 cells remains unknown in anti-malaria immunity (Perez-Mazliah and Langhorne, 2014; Coomes et al., 2015; Walker and Mckenzie, 2018). The T follicular helper (Tfh) cells broadly express the chemokine receptor CXCR5, the transcriptional repressor BCL-6, and the inhibitory receptor programmed cell death protein 1 (PD-1) (Vinuesa and Cyster, 2011). Multiple reports have suggested that Tfh cells, locating at germinal center (GC), can promote protective antibody responses against malaria via providing selection, survival and maturation signal to differentiate GC B cells (Obeng-Adjei et al., 2015; Ryg-Cornejo et al., 2016; Figueiredo et al., 2017; Perez-Mazliah et al., 2017). However, in human malaria, unlike GC Tfh cells, the subsets of circulating Tfh (cTfh) cells play diverse role in anti-malaria immunity. Th1-cTfh cells exhibit a negative role in eliminating parasite, while Th2-cTfh positively correlates with functional antibodies in anti-malaria immune responses (Crotty, 2019; Chan et al., 2020). The Th17 subset is expanded and meaningfully protects host from malaria infection through supporting GC reactions as well as $CD8^+$ T cell responses (Wei et al., 2007; Moretto et al., 2017). Another subsets $CD4^+$-derived T cells, including those expressing IL-27 and IL-10, appear to inhibit parasite control and protective immunity during *Plasmodium*

infection (Couper et al., 2008; Freitas Do Rosario et al., 2012; Gwyer Findlay et al., 2014; Kimura et al., 2016). Treg cells are a subset of $CD4^+$ T cells that specifically express the transcription factor FOXP3. In the clinical studies, the Treg cell populations expand after malaria infection. In addition, Treg cell frequency was positively correlated with parasite load (Jangpatarapongsa et al., 2008; Torcia et al., 2008; Hansen and Schofield, 2010). Several experimental studies have shown that during blood-stage malaria, Treg cells block effective interactions between Tfh and B cells in GC responses during blood-stage infection (Abel et al., 2012; Kurup et al., 2017).

During a primary infection, antibody-independent immune mechanism can usually limit the severity of malaria infection. However, the B cells and antibodies are essential for complete parasite clearance and providing protection against reinfection, which are coordinated by $CD4^+$ Th1 cells via indirectly targeting iRBCs, lacking expression of MHC molecules (Mendis and Targett, 1979; Osier et al., 2008; Fowkes et al., 2010; Perez-Mazliah et al., 2015; Stone et al., 2018). Hence, studying B-cell responses to *Plasmodium* at the monoclonal level has great potential for the development of effective vaccines and therapies (Imkeller et al., 2018; Murugan et al., 2018; Alanine et al., 2019; Mcleod et al., 2019). The antibody-dependent immune responses target circulating parasites and infected host cells expressing parasite antigens on their surfaces (Doolan et al., 2009). Several studies have indicated that the protective antibody titers could not be efficiently induced to against malaria both at liver- and blood-stage, which arise from no time for maturation of long-lived antibody-secreting plasmablasts and highly variable antigen-mediated immune escape of merozoites, respectively (Hoffman et al., 1987; Wahlgren et al., 2017; Aliprandini et al., 2018). Besides, multiple studies hypothesized that B cell responses might be suboptimal or dysfunctional after malaria parasites infection, resulting in defective long-lasting humoral memory (Marsh et al., 1989; Gupta et al., 1999; Silveira et al., 2018). To support above assumption, a series of field studies have indicated that *Plasmodium*-specific antibody responses retain a much shorter lifespan than their homologous memory B cell responses, especially in children (Crompton et al., 2010; Weiss et al., 2010; Ndungu et al., 2012; Ndungu et al., 2013). Recent advance has suggested that during the blood stage, the short-lived plasmablasts expand to constrain GC-dependent humoral immunity both in human and mice (Vijay et al., 2020). Interestingly, several reports have shown that antibodies could activate the complement system to against parasites (Ratelade and Verkman, 2014; Kurtovic et al., 2020). Antibody-mediated complement activation can protect and enhance antibody efficacy by exploiting Fc-mediated neutralization and lysis of target cells. Notably, complement-mediated lysis is strongly observed in human, guinea pig, and rat serum, except for mouse. Furthermore, The AMB, T-bet-expressing B cells, expands in blood stage during *Plasmodium* infection (Weiss et al., 2009). The function of T-bet^+ AMB (atypical memory B cells) on host protection from malaria infection is still undetermined (Barnett et al., 2016; Rivera-Correa et al., 2017).

REGULATORS IN ANTI-MALARIA IMMUNE RESPONSES

Anti-malaria immune responses are tightly modulated to maintain host defense and immune balance. These include positive regulators to accelerate the immune responses and negative regulators to attenuate the immunity. Over the past decades, many immune regulators have been identified (**Figure 2**), which could lead to beneficial or detrimental outcomes for the host. Understanding how anti-malaria immune responses are regulated by these regulators will obviously facilitate the development of new effective vaccines and therapies. Next, we summarize the current knowledge of the positive and negative regulators involved in anti-malaria immune responses and discuss the mechanism by which these regulators orchestrate host immunity against malaria.

Positive Regulators

CD40

CD40 (or TNFRSF5), a member of TNF receptor superfamily, is broadly expressed on the surfaces of many cell types, including monocytes, DCs, B cells, endothelial cells, and epithelial cells (Van Kooten and Banchereau, 2000). The signal transduction mediated by CD40-CD40L interaction could activate NF-κB, STAT3, MAPK, and other kinases (Van Kooten and Banchereau, 2000; Elgueta et al., 2009). Accumulated studies have indicated that CD40 is responsible for promoting cellular and humoral adaptive immunity and inflammatory responses (Van Kooten and Banchereau, 2000; Benveniste et al., 2004; Elgueta et al., 2009; Carlring et al., 2011). Besides, interaction of CD40 and CD40L between the DCs and $CD4^+$ T cells triggers DCs to activate cytotoxic $CD8^+$ cells (Bennett et al., 1998; Ridge et al., 1998; Schoenberger et al., 1998). Recent advances suggested that CD40-CD40L ligation could initiate the activation TRAF2/3 mediated NF-κB pathways and production of IRF1 to eventually induce IFN-β expression (Stirnweiss et al., 2010; Moschonas et al., 2012). CD40 was reported to help eliminating the malaria parasites to reduce the severity of disease (Inoue et al., 2012; Murray et al., 2015; Gramaglia et al., 2017; Parmar et al., 2018). Yao et al. found that CD40 could compete with STING to bind TRAF2/3 and/or TRAF6 to reduce STING ubiquitination, leading to dampen STING degradation and increase STING protein level (Yao et al., 2016). The increase of CD40 expression by *P. yoelii* N67 infection could enhance the protein level of STING, which in turn promotes the IFN-I production during early stage of infection and results in better host survival (Yao et al., 2016). It is also indicated that iRBCs, parasite DNA/RNA, and various TLR ligands, could induce CD40 expression. After malaria infection, a signaling axis of TLR recognition and signaling is established, leading to increase CD40 and STING levels, enhance IFN-I production, and prolong host survival (Yao et al., 2016).

CD28

CD28 constitutively expresses on T cells surface (Gross et al., 1992). The CD80/86-CD28 interaction between APCs and T cells is an important costimulatory signal for T cell

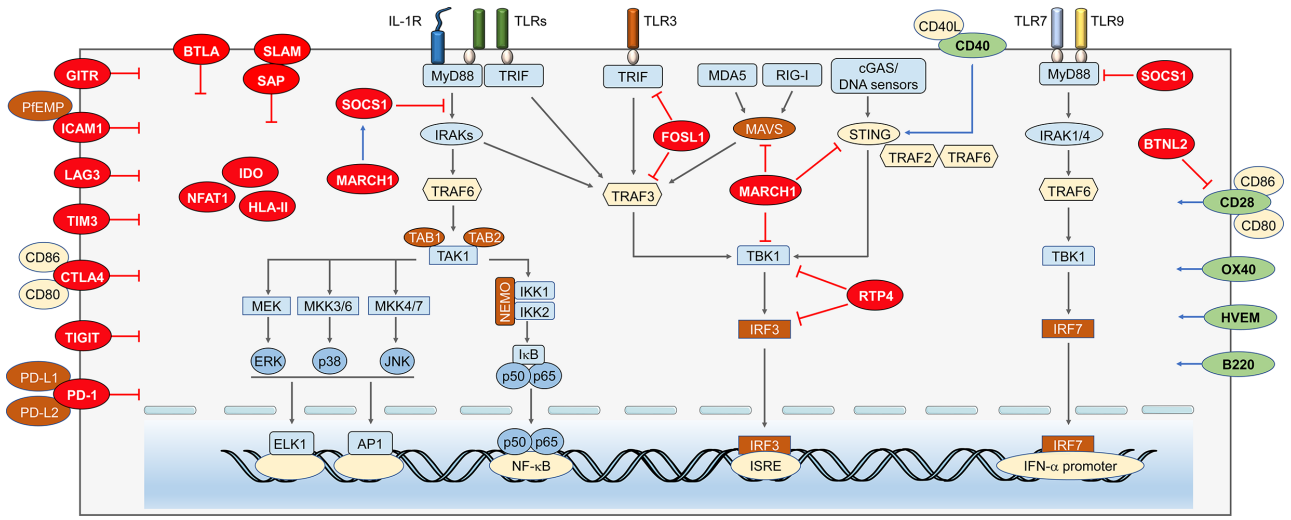

FIGURE 2 | Immune regulators in anti-malaria immunity. Anti-malaria immunity is tightly regulated by cytosolic and cell surface molecules at multiple levels. *Negative regulators within cytosol.* As a negative molecule binds to MyD88, SOCS-1 can not only suppress the NF-κB and MAPKs signaling, but also inhibits MyD88-mediated IFN-I signaling. MARCH1 can reduce IFN-I through increasing expression of SOCS-1. Besides, its target proteins, MAVS, STING, and TBK1, possibly are degraded through ubiquitination. FOSL1 inhibits the K63 ubiquitination of TRAF3 and TRIF and disrupts TBK1/TRAF3/TRIF complexes formation, which results in reduced phosphorylation of IRF3 and suppresses IFN-I production. RTP4 inhibits the expression of TBK1 and IRF3 and/or activation by binding with TBK1 to reduce IFN-I production. *Negative regulators on the cell membrane*. Binding of ICAM1 and PfEMP leads to static adhesion of parasite and evades immune clearance. LAG3 inhibits T cell responses and antibody secreting B cell responses. CTLA-4 expressed on activated T cells could suppress the $CD4^+$ Th and humoral immune responses. TIM3 can inhibit T lymphocytes, NK cells, and macrophages responses. TIGIT proteins mainly suppress the function of T cell and NK cell. The activation of PD-1 pathway dramatically inhibits TCR-mediated proliferation and function of T cells. *Positive regulators on the cell membrane.* CD40 could compete with STING to bind TRAF2/3 and/or TRAF6 to reduce STING ubiquitination, which leads to increased expression of IFN-I. CD28 can enhance $CD4^+$ T cell responses, but the CD28-B7 signals can also be inhibited by BTNL2. OX40 enhances *Plasmodium* specific CD4 T cell activity. B220 expressed on the surface of B and T cells can help promoting the maturation of both T and B cell.

activation, which serves as a crucial second signal for T cell activation along with the MHC-TCR signaling (Carreno and Collins, 2002). CD28 could promote transcription signaling transduction, activation of cytokines or cytokine receptors, as well as activation and differentiation of naïve $CD4^+$ and $CD8^+$ T cells, to protect host from a variety of pathogens (Sharpe and Freeman, 2002; Elias et al., 2005; Butty et al., 2007; Cong et al., 2014; Niknam et al., 2017). During malaria infection, CD28 plays an essential role in enhancing $CD4^+$ T cell responses and $CD4^+$ T cell-driven antibody class switch (Falanga et al., 1984; Langhorne et al., 1989; Sanchez-Torres et al., 2001). Besides, CD28-CD80/CD86 signals increase the survival and proliferation of γδ T cells to reduce severity of malaria infection (Dieli et al., 2001; D'ombrain et al., 2007; Ribot et al., 2012).

OX40

OX40 receptor, transiently expressed on T cells, is an important co-stimulatory molecule that interacts with TCRs and MHC complexes on APCs (Croft, 2010). Previous reports have denoted that OX40 promotes proliferation and survival of T cell, as well as differentiation of $CD4^+$ T cells into Th1, Th2 and Tfh cell subsets; and reportedly reverses the hyperactivity of $CD4^+$ T cell (Walker et al., 1999; Bansal-Pakala et al., 2001; Croft, 2010). Recent studies have demonstrated that OX40 would enhance *Plasmodium* specific $CD4^+$ and $CD8^+$ T cell activity, as well as parasite specific humoral immunity (Zander et al., 2015; Zander et al., 2017; Othman et al., 2018; Xia et al., 2018).

Other Positive Regulators

Herpes virus entry mediator (HVEM), a co-stimulatory receptor, expresses on the surface of B cells, T cells, endothelial cells and mast cells (Chang et al., 2005; Guo et al., 2015; Sibilano et al., 2016). Upon bacterial and viral infections, HVEM-mediated signaling pathway enhances T cell expansion and is necessary for persistence of memory T cell (Soroosh et al., 2011; Flynn et al., 2013; Steinberg et al., 2013; Desai et al., 2017). Recent findings of Muscate et al. indicated that HVEM is required to provide pro-survival signals for stabilizing $CD8^+$ T effector cells during malaria infection (Muscate et al., 2018). During *P. berghei* ANKA infection, the HVEM-CD160 ligation is crucial for the delicate regulation of stimulatory and inhibitory signals in $CD8^+$ T cells.

B220 is a high-molecular mass alternative splicing isoform of the tyrosine phosphatase CD45 (Renno et al., 1998). Its expression is found not only in B cell, including precursors, mature and memory B cells, but also in a subset activated T cells and pDCs (Marvel and Mayer, 1988; Hathcock et al., 1992; Renno et al., 1998; Rodig et al., 2005). Several studies have suggested that malaria exposure increased frequencies of B220, which is essential for promoting both T and B cells maturation

(Asensi et al., 1990; Bakir et al., 2006; Niikura et al., 2008; Kanda et al., 2010; Bao et al., 2015; Ubillos et al., 2017).

Negative Regulators

PD-1

Unlike other CD28 family members, the expression of PD-1 (CD279) could be induced on activated monocytes, NK cells, DCs, myeloid cells, $CD4^+$ T cells, $CD8^+$ T cells, B cells, and a subset of thymocytes through TCR or BCR mediated signaling; as well as being augmented by stimulation of tumor necrosis factor (TNF) (Agata et al., 1996; Nakae et al., 2006; Okazaki and Honjo, 2006). The activation of PD-L1/PD-1 pathway dramatically inhibits TCR-mediated proliferation and function of $CD4^+$ and $CD8^+$ T cells (Freeman et al., 2000; Latchman et al., 2001; Rodig et al., 2003; Grosso et al., 2009). Several studies have demonstrated that pathogens including bacteria, viruses (such as HIV), protozoan parasites (including *Plasmodium*), and tumor cells could exploit above PD-1 inhibitory function on T cells to evade host adaptive immunity (Day et al., 2006; Horne-Debets et al., 2013; Gubin et al., 2014). In malaria infection, the number and function of parasite-specific $CD4^+$ T cells (including Th1 and Tfh), $CD8^+$ T cells, and memory T cells are significantly inhibited by PD-1 with decelerated parasite clearance (Horne-Debets et al., 2013; Karunarathne et al., 2016; Liu T. et al., 2018; Pan et al., 2020). However, the inhibition of B cell function by PD-1 is controversial. During *P. chabaudi* infection, PD-1 elimination does not improve primary B cell responses (Horne-Debets et al., 2013). In contrast, multiple studies have indicated that PD-1 deficiency substantially promoted expansion of GC B cells and humoral immunity in ITV (infection treatment vaccine)–immunized mice (Liu T. et al., 2015; Liu T. et al., 2018); and PD-1 elimination significantly increased long-lived plasma cells by *P. berghei* ANKA infection (Pan et al., 2020).

SOCS1

SOCS1 is one of the members of suppressors of cytokine signaling (SOCS) family, which regulates signal transduction pathways triggered by activation of cytokine and hormone receptors (Machado et al., 2006; Dimitriou et al., 2008). *Socs1*$^{-/-}$ mice die within 3 weeks after birth, due to the high level of JAK/STAT-mediated inflammation, which could be significantly inhibited by SOCS1 (Naka et al., 1997; Starr et al., 1997; Naka et al., 1998; Starr et al., 1998), and this mice are highly susceptible to sepsis comparing to WT mice (Kinjyo et al., 2002; Nakagawa et al., 2002). *Socs1*$^{-/-}$ macrophages produce high amount of proinflammatory cytokines and nitric oxide after LPS and CpG stimulation. Moreover, SOCS1 seems to inhibit LPS- but not TNF-mediated NF-κB signaling through promoting the degradation of IRAK and NF-κB (Dimitriou et al., 2008).

Our studies have demonstrated that SOCS1 could interact with MyD88 to inhibit TLR7-MyD88-IRF7 dependent IFN-I signaling after lethal malaria infection (Yu et al., 2016; Yu et al., 2018; Cai and Yu, 2020). During malaria infection, *Plasmodium* gDNA and RNA activate cGAS/STING and MDA5/MAVS to induce IRF3-dependent SOCS1 production, respectively, which, in turn, bind to MyD88 to suppress MyD88-IRF7 dependent IFN-I response, leading to fast parasite growth and host death (Yu et al., 2016). Furthermore, *Plasmodium* gDNA, RNA, and hemozoin also activate inflammasome signaling and lead to production of IL-1β, which subsequently induces SOCS1 expression to inhibit MyD88 dependent IFN-I production (Yu et al., 2018). Moreover, a recent study further illustrated the delicate cross-regulation between several IFN-I signaling pathways and inflammasome signaling pathways during lethal *P. yoelii* YM infection. Inflammasome-, MAVS-, and STING-mediated signaling pathways have diverse impacts on regulating MyD88-dependent IFN-I responses after *P. yoelii* YM infection; and the dosage of *P. yoelii* YM has significant effect on the differences of resistance among inflammasome, MAVS, and STING deficiency (Cai and Yu, 2020).

It has been reported that SOCS1 could simultaneously inhibit MyD88-dependent IFN-I production and downstream IFN-dependent production of IFN-γ. However, SOCS1 deficiency could not protect host from infection in *Myd88*$^{-/-}$ mice, suggesting that SOCS1 controls the host resistance to malaria mainly through MyD88-mediated IFN-I production (Yu et al., 2018). Importantly, SOCS1 could be induced by IRF3-dependent signaling, LPS, and CpG DNA, as well as the downstream IFN-stimulating pathway, indicating a negative-feedback regulatory mechanism to sustain its inhibitory function.

FOSL1

FOSL1 belongs to a gene family that encode proteins containing leucine zippers (Macchia et al., 2012), which are identified as regulators in trophoblast migration and invasion (Renaud et al., 2014). The FOSL1 contributes to several cellular processes, including proliferation, differentiation, and apoptosis via serving as a member of transcription factors and musculoaponeurotic fibrosarcoma (MAF) (Macchia et al., 2012). It has been reported that FOSL1 is a key downstream effector of the phosphatidylinositol 3-kinase (PI3K)/AKT signaling pathway to control *Mmp9* gene expression and trophoblast lineages development (Kent et al., 2011). In addition, FOSL1 also plays a pivotal role in diverse cancers (Young and Colburn, 2006).

FOSL1 is normally expressed in the nucleus, while Cai et al. showed that cGAS-STING-, TRIF-, or RIG-I/MDA5-MAVS-mediated IFN-I production could evoke the "translocation" of FOSL1 into the cytoplasm after iRBCs stimulations. The cytoplasmic FOSL1 inhibits the formation of TBK1/TRAF3/TRIF complexes by suppressing K63 ubiquitination of TRAF3 and TRIF. The inhibition of FOSL1 on TBK1 complexes leads to suppression of IFN-I production (Cai et al., 2017). Hence, these reports identified FOSL1 as a negative regulator of IFN-I production during early infection and liver stages, resulting in fast parasite growth and host death (Liehl et al., 2014; Wu et al., 2014; Yu et al., 2016; Yu et al., 2018).

MARCH1

Membrane-associated ring-CH–type finger 1 (MARCH1) is a member of membrane-bound E3 ubiquitin ligases expressed mostly by DCs and B cells (Ohmura-Hoshino et al., 2006; Wu et al., 2020). The MARCH1 production is initiated by IL-10 after

TLR4 and CD40 signaling (Galbas et al., 2012; Mittal et al., 2015). Besides, stimulating the monocyte-derived macrophages could enhance endogenous expression of MARCH1 (Zhang et al., 2019b). Previous studies, focusing on MARCH1 function, have shown that MARCH1 ubiquitinates CD86 and MHC-II molecules for degradation to down-regulate adaptive immunity; and may influence CD28, CTLA4, and PD-L1 signaling by regulating relative protein levels of CD80/CD86 on antigen-presenting cells (APCs) (Ishido et al., 2009; Samji et al., 2014; Ablack et al., 2015).

Wu et al. have recently indicated that upon *P. yoelii* N67 or *P. yoelii* YM treatment, mice deficient in *March1* had significant better survival rates than WT mice, indicating the negative function of MARCH1 in generating protective immunity against malaria infection (Liehl et al., 2014; Wu et al., 2014; Yu et al., 2016). Clustered with several ISGs in the Ts-eQTL analysis, MARCH1 deficient mice produce higher amount of IFN-I than WT mice in response to cGAMP and poly(I:C), accompany with increased protein levels of STING, MAVS, TRAF3 and TRAF6 in uninfected condition. However, reduced production level of IFN-I was observed in MARCH1 deficient mice during early malaria infection. The mechanism by which MARCH1 regulates IFN-I remains obscure and several factors may include increased expression of genes encoding SOCS1, SOCS3, SIKE1, CACTIN, TRIM24, IL-10RA, USP18, and mir-21 that are known to suppress IFN-I responses (Huang et al., 2005; Yu and Hayward, 2010; Liu D. et al., 2015; Arimoto et al., 2017) and changes in DCs, Macs, and other cell populations can may also affect the levels of proteins critical for IFN-I production (Wu et al., 2020). In addition, MARCH1 deficiency significantly increased numbers of both $CD86^+$ DCs population, which could promote CD86-CD28 interaction and T cell activation, leading to enhanced Th1-mediated response and IFN-γ production (Wu et al., 2020).

RTP4

Receptor transporter family is known to promote cell surface expression of a group of G-protein-coupled receptors (GPCR). RTP4, a member of the RTP family, can be induced after viral infection (Nair S. R. et al., 2017; Dang et al., 2018). In addition, RTP4 plays an important role in mediating pain relief, bitterness, or odor sensing (Behrens et al., 2006; Decaillot et al., 2008). Su's group has suggested that the IFN-I and IFN-I pathways can induce RTP4 expression after parasite infection. Besides, RTP4 significantly inhibits IFN-I response through inhibition of TBK1 and IRF3 expression and activation by binding with TBK1 to reduce IFN-I production. Inhibition of RTP4 expression may help reduce parasitemia and help to alleviate symptoms of cerebral malaria (CM) and other diseases with neuropathology (He et al., 2020). Besides, Su's group also demonstrated that *P. yoelii* HECT-like E3 ubiquitin ligase (*Py*HEUL) encoding by malaria genome may indirectly affect host immune response and parasite infection by regulating the expression levels of proteins, such as merozoite surface protein 1 (MSP1) and/or cytoadherence-linked asexual gene 2 (CLAG2) (Nair S. C. et al., 2017).

Other Negative Regulators

Butyrophilin-like 2 (BTNL2) is a butyrophilin family member. Previous studies have demonstrated that BTNL2 inhibits T cells proliferation and is involved in a variety of autoimmune diseases (Lin et al., 2015; Tian et al., 2019). Besides, BTNL2 promotes Tregs generation through modifying B7/CD28 signaling (Swanson et al., 2013). Recent study has shown that BTNL2 also dampens T cells proliferation and activation in the *P. berghei* model of experimental cerebral malaria (ECM) (Subramaniam et al., 2015).

Indoleamine 2,3-dioxygenase (IDO) is induced by pro-inflammatory mediators, such as endotoxin and IFN-γ, in several tissues. IDO is a tryptophan-degrading enzyme; and has been identified an inhibitory function on proliferation of facultative intracellular pathogens and tumor cells (Taylor and Feng, 1991). In addition, IDO could suppress responses of T cells and promote tolerance (Mellor and Munn, 2004). Several studies have denoted that IDO is involved in CM (Medana et al., 2002; Medana et al., 2003; Mitchell et al., 2005).

Nuclear factor of activated T cell 1 (NFAT1) is a member of NFAT transcription factors, which are required for regulating the activation and differentiation of T cells (Macian, 2005). Multiple field reports, including malaria infection, have indicated that NFAT1-regulated gene expression is essential in efficient Treg-mediated $CD4^+$ T cell suppression (Soto-Nieves et al., 2009; Shin et al., 2014; Ames et al., 2017; Kadziolka et al., 2017).

CD160 is expressed by NK, NKT, $CD8^+$ T, γδ T, iIELs, ILC1, mast, and a minority of $CD4^+$ T cells (Maeda et al., 2005; Ortonne et al., 2011; Fuchs et al., 2013). The function of CD160 on T cells remains controversial, some studies have suggested that CD160 is a co-inhibitory molecule, while others have indicated that it has co-stimulative functions that promote proliferation and cytotoxicity of T cells, as well as inflammatory cytokine production (Le Bouteiller et al., 2002; Barakonyi et al., 2004; Cai et al., 2008). Strikingly, during malaria, CD160 is crucially involved in restricting $CD8^+$ T cytotoxicity and IFN-γ production (Muscate et al., 2018).

B and T lymphocyte attenuator (BTLA) (CD272), a co-inhibitory receptor, is expressed by most leukocytes (Muscate et al., 2018). The BTLA is required for maintenance of peripheral tolerance by inhibiting lymphocytes activation. In malaria model, BTLA dampens innate immune responses and T/B cell-mediated immune response to malaria infection (Sun et al., 2009; Vendel et al., 2009; Adler et al., 2011).

Once T cells are activated by CD28-CD80/CD86 signal, they enhance expression of cytotoxic T lymphocyte antigen-4 (CTLA-4, also named CD152), which is another receptor for CD80/CD86. CTLA-4 is shown to be involved in maintenance of peripheral tolerance; inhibition of immune response against tumors and infectious diseases; as well as increased severity of autoimmune diseases (Gregor et al., 2004; Martins et al., 2004).

T-cell immunoglobulin- and mucin-domain-containing molecule 3 (TIM-3) is expressed by monocytes, macrophages, NK cells, DCs, and Th1 and Tc1 lymphocytes (Sakuishi et al., 2011). The binding of TIM-3 and galectin-9 negatively regulates

T-cell and NK-cell activation in many diseases (Sabatos et al., 2003; Ju et al., 2010; Bi et al., 2011; Hou et al., 2012). Accumulated findings indicated that TIM-3 was responsible for inhibiting T lymphocytes ($CD4^+$ Th1/Th2, $CD8^+$, and γδ T cells), NK cells, and macrophages responses to malaria treatment (Hou et al., 2016; Hou et al., 2017; Sabins et al., 2017; Schofield et al., 2017; Otterdal et al., 2018).

T cell immunoglobulin and ITIM domain (TIGIT) is expressed on the surface of NK cells and T cells (Yu et al., 2009). It has reported that TIGIT as an inhibitor controls the function of NK cells, $CD4^+$ T cells, and $CD8^+$ T cells (Johnston et al., 2014). During *P. berghei* ANKA infection, the upregulation of TIGIT proteins results in inhibition on T and NK cells (Villegas-Mendez et al., 2016; Zhang et al., 2019a).

The Signaling Lymphocytic Activation Molecule (SLAM)–Associated Protein (SAP), a small intracellular adaptor protein, could interact with the SLAM family and mediate downstream signaling of these receptors (Cannons et al., 2011). The deficient of SAP promotes the activation of Tfh and GC B cells, as well as IgG response against malaria infection (Perez-Mazliah et al., 2017).

Lymphocyte Activation Gene-3 (LAG-3) is expressed by many cells, including NK cells, T cells, B cells, and tumor infiltrating lymphocytes (Huang et al., 2004). As the T cell receptors, LAG-3 directly and indirectly induces transcriptional changes, which negatively modulates proliferation and pro-inflammatory cytokines expression by virus-specific $CD8^+$ T cells (Barber et al., 2006; Blackburn et al., 2009). Butler et al. recently have shown that LAG-3 substantially inhibits T-cell responses and antibody secreting B cell responses to malaria infection (Butler et al., 2011).

Intracellular adhesion molecule 1(ICAM1, also named CD54) belongs to immunoglobulin superfamily; and is expressed by endothelial cells and leukocytes (Rowe et al., 2009). Binding of ICAM1 and malaria ligands, members of the PfEMP1 family, leads to static adhesion of parasite (Chattopadhyay et al., 2004; Springer et al., 2004). This adhesion occludes blood flow, leads to inflammation, and evades immune clearance (Lennartz et al., 2017; Lennartz et al., 2019).

The MHC [human leukocyte antigen (HLA) in humans] class II heterodimers are major participants in generating an immune response against microorganisms for providing exogenous peptides to activate and differentiate $CD4^+$ T cells (Rothbard and Gefter, 1991). Previously, $CD4^+$ Th1, Th2, and Th17 cells have been reported to be essential for coordinating the cellular and/or humoral response to clear pathogens, while the Treg cells downregulate those responses via secretion of suppressive cytokines or through direct cell-cell interactions (Surls et al., 2010; Ma et al., 2012; Issa et al., 2013). Importantly, during malaria infection, the HLA-II molecules evoke expansion and activation of Tregs to suppress antibody production by direct cell-cell interaction with B cells (Storti-Melo et al., 2012; Wijayalath et al., 2014).

Glucocorticoid-induced tumor necrosis factor receptor (GITR) constitutively expresses on cell surface of natural Tregs (Yagi et al., 2004; Belkaid and Rouse, 2005; Nocentini et al., 2007). The interaction of GITR and agonist antibody or GITR ligand (GITRL) appears to abrogate suppressive activity of Tregs (Mchugh et al., 2002; Shimizu et al., 2002; Shevach and Stephens, 2006). However, engagement of GITR promotes proliferation and suppressive function of Tregs (Shevach and Stephens, 2006; Nocentini et al., 2007; Nishioka et al., 2008). In malaria infection, GITR is involved in the escape of parasites from host T cell immune responses (Hisaeda et al., 2005).

CONCLUDING REMARKS

Nearly 160 years post the discovery of *Plasmodium* in 1861, malaria is still a serious threat to global health that accounts for about 0.5 million deaths every year. Although significant progress has been done in most endemic area, eliminating malaria is still halted by emergence of drug resistance. Furthermore, the lack of an effective vaccine has been one of the major limiting factors in the prevention of malaria infection, which mainly due to the incomplete understanding of the underlying mechanism of host-parasite interactions.

During the past 10 years, stepwise progresses have been achieved in understanding the immune responses to malaria infection and their contribution to eliminating parasites. Yet, malaria infection triggers a systemic immune response, which in turn induces an increase in the production of inflammatory cytokines that lead to parasite elimination and/or immune pathology. *Plasmodium* infection induces host balanced responses in which activating signaling for anti-malaria states and promoting immunity counterbalanced by suppressive signaling that limit toxicity and enable chronic infection. Hence, a fine-tuned regulation of immune responses is crucial for developing protective immunity to effectively eliminate malaria parasites and preventing damage to host.

Plasmodium also exploits regulatory mechanisms to escape immune responses, including enhancing negative regulators and inhibiting positive regulators. We noticed that much more negative regulators are discovered than the positive regulators due to date, which may indicate that *Plasmodium* infection initiates multiple tools or signaling to evade host immune responses. Advances in these areas would aid the development of malaria vaccines and therapeutics that could selectively target pathogenic regulators while leaving defensive regulators intact. Here, we highlight our studies indicating the crucial role of early spike of IFN-I in protecting host from *Plasmodium* infection, and focus on discussing the regulatory network of immune responses against to malaria infection. Besides, we also emphasize our results demonstrating the importance of regulators mediated tune modulation of immune responses during malaria treatment. The search for more efficient vaccines and novel treatment strategies is a major objective in reducing the burden of malaria. Hence, any effort to control and eradicate malaria requires a better understanding of the contribution and regulation of immune responses to *Plasmodium* infection. In addition, new technologies, including whole genome-wide analysis in a single immune cell level and application of Mass Cytometry would offer

promise for a more comprehensive investigation of immune responses and regulations in responses to malaria, and should facilitate the development of new effective vaccines and therapies.

AUTHOR CONTRIBUTIONS

CC wrote the manuscript. ZH drew the figures and wrote the manuscript. XY wrote the manuscript and supervised the entire project. All authors contributed to the article and approved the submitted version.

FUNDING

This work was supported by grants from the National Science Foundation of China (No. 81801579), Science and Technology Planning Project of Guangzhou (No. 201904010064), Guangdong Basic and Applied Basic Research Foundation (No. 2019B1515120033), Zhujiang Youth Scholar Funding, and the Start-up Fund for High-level Talents of Southern Medical University to XY. This work was also supported by the National Natural Science Foundation of China (No. 81960292) to CC.

REFERENCES

Abel, S., Luckheide, N., Westendorf, A. M., Geffers, R., Roers, A., Muller, W., et al. (2012). Strong impact of CD4+ Foxp3+ regulatory T cells and limited effect of T cell-derived IL-10 on pathogen clearance during Plasmodium yoelii infection. *J. Immunol.* 188, 5467–5477. doi: 10.4049/jimmunol.1102223

Ablack, J. N., Metz, P. J., Chang, J. T., Cantor, J. M., and Ginsberg, M. H. (2015). Ubiquitylation of CD98 limits cell proliferation and clonal expansion. *J. Cell Sci.* 128, 4273–4278. doi: 10.1242/jcs.178129

Adler, G., Steeg, C., Pfeffer, K., Murphy, T. L., Murphy, K. M., Langhorne, J., et al. (2011). B and T lymphocyte attenuator restricts the protective immune response against experimental malaria. *J. Immunol.* 187, 5310–5319. doi: 10.4049/jimmunol.1101456

Agata, Y., Kawasaki, A., Nishimura, H., Ishida, Y., Tsubata, T., Yagita, H., et al. (1996). Expression of the PD-1 antigen on the surface of stimulated mouse T and B lymphocytes. *Int. Immunol.* 8, 765–772. doi: 10.1093/intimm/8.5.765

Alanine, D. G. W., Quinkert, D., Kumarasingha, R., Mehmood, S., Donnellan, F. R., Minkah, N. K., et al. (2019). Human Antibodies that Slow Erythrocyte Invasion Potentiate Malaria-Neutralizing Antibodies. *Cell* 178, 216–228.e221. doi: 10.1016/j.cell.2019.05.025

Aliprandini, E., Tavares, J., Panatieri, R. H., Thiberge, S., Yamamoto, M. M., Silvie, O., et al. (2018). Cytotoxic anti-circumsporozoite antibodies target malaria sporozoites in the host skin. *Nat. Microbiol.* 3, 1224–1233. doi: 10.1038/s41564-018-0254-z

Ames, R. Y., Ting, L. M., Gendlina, I., Kim, K., and Macian, F. (2017). The Transcription Factor NFAT1 Participates in the Induction of CD4(+) T Cell Functional Exhaustion during Plasmodium yoelii Infection. *Infect. Immun.* 85, e00364-17. doi: 10.1128/IAI.00364-17

Amino, R., Thiberge, S., Martin, B., Celli, S., Shorte, S., Frischknecht, F., et al. (2006). Quantitative imaging of Plasmodium transmission from mosquito to mammal. *Nat. Med.* 12, 220–224. doi: 10.1038/nm1350

Arama, C., and Troye-Blomberg, M. (2014). The path of malaria vaccine development: challenges and perspectives. *J. Intern. Med.* 275, 456–466. doi: 10.1111/joim.12223

Arimoto, K. I., Lochte, S., Stoner, S. A., Burkart, C., Zhang, Y., Miyauchi, S., et al. (2017). STAT2 is an essential adaptor in USP18-mediated suppression of type I interferon signaling. *Nat. Struct. Mol. Biol.* 24, 279–289. doi: 10.1038/nsmb.3378

Artavanis-Tsakonas, K., and Riley, E. M. (2002). Innate immune response to malaria: rapid induction of IFN-gamma from human NK cells by live Plasmodium falciparum-infected erythrocytes. *J. Immunol.* 169, 2956–2963. doi: 10.4049/jimmunol.169.6.2956

Asensi, V., Himeno, K., Kawamura, I., Sakumoto, M., and Nomoto, K. (1990). In vivo treatment with anti B-220 monoclonal antibody affects T and B cell differentiation. *Clin. Exp. Immunol.* 80, 268–273. doi: 10.1111/j.1365-2249.1990.tb05246.x

Baccarella, A., Fontana, M. F., Chen, E. C., and Kim, C. C. (2013). Toll-like receptor 7 mediates early innate immune responses to malaria. *Infect. Immun.* 81, 4431–4442. doi: 10.1128/IAI.00923-13

Baker, V. S., Imade, G. E., Molta, N. B., Tawde, P., Pam, S. D., Obadofin, M. O., et al. (2008). Cytokine-associated neutrophil extracellular traps and antinuclear antibodies in Plasmodium falciparum infected children under six years of age. *Malar. J.* 7, 41. doi: 10.1186/1475-2875-7-41

Bakir, H. Y., Tomiyama-Miyaji, C., Watanabe, H., Nagura, T., Kawamura, T., Sekikawa, H., et al. (2006). Reasons why DBA/2 mice are resistant to malarial infection: expansion of CD3int B220+ gammadelta T cells with double-negative CD4- CD8- phenotype in the liver. *Immunology* 117, 127–135. doi: 10.1111/j.1365-2567.2005.02273.x

Bansal, G. P., Weinstein, C. S., and Kumar, N. (2016). Insight into phagocytosis of mature sexual (gametocyte) stages of Plasmodium falciparum using a human monocyte cell line. *Acta Trop.* 157, 96–101. doi: 10.1016/j.actatropica.2016.01.033

Bansal-Pakala, P., Jember, A. G., and Croft, M. (2001). Signaling through OX40 (CD134) breaks peripheral T-cell tolerance. *Nat. Med.* 7, 907–912. doi: 10.1038/90942

Bao, L. Q., Nhi, D. M., Huy, N. T., Kikuchi, M., Yanagi, T., Hamano, S., et al. (2015). Splenic CD11c+ cells derived from semi-immune mice protect naive mice against experimental cerebral malaria. *Malar. J.* 14, 23. doi: 10.1186/s12936-014-0533-y

Barakonyi, A., Rabot, M., Marie-Cardine, A., Aguerre-Girr, M., Polgar, B., Schiavon, V., et al. (2004). Cutting edge: engagement of CD160 by its HLA-C physiological ligand triggers a unique cytokine profile secretion in the cytotoxic peripheral blood NK cell subset. *J. Immunol.* 173, 5349–5354. doi: 10.4049/jimmunol.173.9.5349

Baratin, M., Roetynck, S., Pouvelle, B., Lemmers, C., Viebig, N. K., Johansson, S., et al. (2007). Dissection of the role of PfEMP1 and ICAM-1 in the sensing of Plasmodium-falciparum-infected erythrocytes by natural killer cells. *PloS One* 2, e228. doi: 10.1371/journal.pone.0000228

Barbalat, R., Ewald, S. E., Mouchess, M. L., and Barton, G. M. (2011). Nucleic acid recognition by the innate immune system. *Annu. Rev. Immunol.* 29, 185–214. doi: 10.1146/annurev-immunol-031210-101340

Barber, D. L., Wherry, E. J., Masopust, D., Zhu, B., Allison, J. P., Sharpe, A. H., et al. (2006). Restoring function in exhausted CD8 T cells during chronic viral infection. *Nature* 439, 682–687. doi: 10.1038/nature04444

Barnett, B. E., Staupe, R. P., Odorizzi, P. M., Palko, O., Tomov, V. T., Mahan, A. E., et al. (2016). Cutting Edge: B Cell-Intrinsic T-bet Expression Is Required To Control Chronic Viral Infection. *J. Immunol.* 197, 1017–1022. doi: 10.4049/jimmunol.1500368

Battle, K. E., Guerra, C. A., Golding, N., Duda, K. A., Cameron, E., Howes, R. E., et al. (2015). Global database of matched Plasmodium falciparum and P. vivax incidence and prevalence records from 1985-2013. *Sci. Data* 2, 150012. doi: 10.1038/sdata.2015.12

Behrens, M., Bartelt, J., Reichling, C., Winnig, M., Kuhn, C., and Meyerhof, W. (2006). Members of RTP and REEP gene families influence functional bitter taste receptor expression. *J. Biol. Chem.* 281, 20650–20659. doi: 10.1074/jbc.M513637200

Belkaid, Y., and Rouse, B. T. (2005). Natural regulatory T cells in infectious disease. *Nat. Immunol.* 6, 353–360. doi: 10.1038/ni1181

Bennett, S. R., Carbone, F. R., Karamalis, F., Flavell, R. A., Miller, J. F., and Heath, W. R. (1998). Help for cytotoxic-T-cell responses is mediated by CD40 signalling. *Nature* 393, 478–480. doi: 10.1038/30996

Benveniste, E. N., Nguyen, V. T., and Wesemann, D. R. (2004). Molecular regulation of CD40 gene expression in macrophages and microglia. *Brain Behav. Immun.* 18, 7–12. doi: 10.1016/j.bbi.2003.09.001

Bi, S., Hong, P. W., Lee, B., and Baum, L. G. (2011). Galectin-9 binding to cell surface protein disulfide isomerase regulates the redox environment to enhance T-cell migration and HIV entry. *Proc. Natl. Acad. Sci. U.S.A.* 108, 10650–10655. doi: 10.1073/pnas.1017954108

Blackburn, S. D., Shin, H., Haining, W. N., Zou, T., Workman, C. J., Polley, A., et al. (2009). Coregulation of CD8+ T cell exhaustion by multiple inhibitory receptors during chronic viral infection. *Nat. Immunol.* 10, 29–37. doi: 10.1038/ni.1679

Butler, N. S., Moebius, J., Pewe, L. L., Traore, B., Doumbo, O. K., Tygrett, L. T., et al. (2011). Therapeutic blockade of PD-L1 and LAG-3 rapidly clears established blood-stage Plasmodium infection. *Nat. Immunol.* 13, 188–195. doi: 10.1038/ni.2180

Butty, V., Roy, M., Sabeti, P., Besse, W., Benoist, C., and Mathis, D. (2007). Signatures of strong population differentiation shape extended haplotypes across the human CD28, CTLA4, and ICOS costimulatory genes. *Proc. Natl. Acad. Sci. U.S.A.* 104, 570–575. doi: 10.1073/pnas.0610124104

Cai, C., and Yu, X. (2020). A mathematic model to reveal delicate cross-regulation between MAVS/STING, inflammasome and MyD88-dependent type I interferon signalling. *J. Cell Mol. Med.* 24, 11535–11545. doi: 10.1111/jcmm.15768

Cai, G., Anumanthan, A., Brown, J. A., Greenfield, E. A., Zhu, B., and Freeman, G. J. (2008). CD160 inhibits activation of human CD4+ T cells through interaction with herpesvirus entry mediator. *Nat. Immunol.* 9, 176–185. doi: 10.1038/ni1554

Cai, B., Wu, J., Yu, X., Su, X. Z., and Wang, R. F. (2017). FOSL1 Inhibits Type I Interferon Responses to Malaria and Viral Infections by Blocking TBK1 and TRAF3/TRIF Interactions. *mBio* 8, e02161–16. doi: 10.1128/mBio.02161-16

Cannons, J. L., Tangye, S. G., and Schwartzberg, P. L. (2011). SLAM family receptors and SAP adaptors in immunity. *Annu. Rev. Immunol.* 29, 665–705. doi: 10.1146/annurev-immunol-030409-101302

Carlring, J., Altaher, H. M., Clark, S., Chen, X., Latimer, S. L., Jenner, T., et al. (2011). CD154-CD40 interactions in the control of murine B cell hematopoiesis. *J. Leukoc. Biol.* 89, 697–706. doi: 10.1189/jlb.0310179

Carreno, B. M., and Collins, M. (2002). The B7 family of ligands and its receptors: new pathways for costimulation and inhibition of immune responses. *Annu. Rev. Immunol.* 20, 29–53. doi: 10.1146/annurev.immunol.20.091101.091806

Chan, J. A., De Labastida Rivera, F., Loughland, J., Engel, J. A., Lee, H. J., Sheelanair, A., et al. (2020). Th2-like T-follicular helper cells promote functional antibody production during Plasmodium falciparum infection. *bioRxiv*. doi: 10.1101/2020.05.18.101048

Chang, Y. H., Hsieh, S. L., Chao, Y., Chou, Y. C., and Lin, W. W. (2005). Proinflammatory effects of LIGHT through HVEM and LTbetaR interactions in cultured human umbilical vein endothelial cells. *J. BioMed. Sci.* 12, 363–375. doi: 10.1007/s11373-005-1360-5

Chattopadhyay, R., Taneja, T., Chakrabarti, K., Pillai, C. R., and Chitnis, C. E. (2004). Molecular analysis of the cytoadherence phenotype of a Plasmodium falciparum field isolate that binds intercellular adhesion molecule-1. *Mol. Biochem. Parasitol.* 133, 255–265. doi: 10.1016/j.molbiopara.2003.08.014

Chen, Q., Amaladoss, A., Ye, W., Liu, M., Dummler, S., Kong, F., et al. (2014). Human natural killer cells control Plasmodium falciparum infection by eliminating infected red blood cells. *Proc. Natl. Acad. Sci. U.S.A.* 111, 1479–1484. doi: 10.1073/pnas.1323318111

Chua, C. L., Brown, G., Hamilton, J. A., Rogerson, S., and Boeuf, P. (2013). Monocytes and macrophages in malaria: protection or pathology? *Trends Parasitol.* 29, 26–34. doi: 10.1016/j.pt.2012.10.002

Clark, I. A., Alleva, L. M., Budd, A. C., and Cowden, W. B. (2008). Understanding the role of inflammatory cytokines in malaria and related diseases. *Travel Med. Infect. Dis.* 6, 67–81. doi: 10.1016/j.tmaid.2007.07.002

Coban, C., Ishii, K. J., Kawai, T., Hemmi, H., Sato, S., Uematsu, S., et al. (2005). Toll-like receptor 9 mediates innate immune activation by the malaria pigment hemozoin. *J. Exp. Med.* 201, 19–25. doi: 10.1084/jem.20041836

Coban, C., Igari, Y., Yagi, M., Reimer, T., Koyama, S., Aoshi, T., et al. (2010). Immunogenicity of whole-parasite vaccines against Plasmodium falciparum involves malarial hemozoin and host TLR9. *Cell Host. Microbe* 7, 50–61. doi: 10.1016/j.chom.2009.12.003

Colborn, J. M., Ylostalo, J. H., Koita, O. A., Cisse, O. H., and Krogstad, D. J. (2015). Human Gene Expression in Uncomplicated Plasmodium falciparum Malaria. *J. Immunol. Res.* 2015, 162639. doi: 10.1155/2015/162639

Combes, V., Taylor, T. E., Juhan-Vague, I., Mege, J. L., Mwenechanya, J., Tembo, M., et al. (2004). Circulating endothelial microparticles in malawian children with severe falciparum malaria complicated with coma. *JAMA* 291, 2542–2544. doi: 10.1001/jama.291.21.2542-b

Cong, J., Zhang, S., and Gao, X. (2014). Quantitative assessment of the associations between CD28 T > C polymorphism (rs3116496) and cancer risk. *Tumour Biol.* 35, 9195–9200. doi: 10.1007/s13277-014-2204-6

Coomes, S. M., Pelly, V. S., Kannan, Y., Okoye, I. S., Czieso, S., Entwistle, L. J., et al. (2015). IFNgamma and IL-12 Restrict Th2 Responses during Helminth/Plasmodium Co-Infection and Promote IFNgamma from Th2 Cells. *PloS Pathog.* 11, e1004994. doi: 10.1371/journal.ppat.1004994

Couper, K. N., Blount, D. G., Wilson, M. S., Hafalla, J. C., Belkaid, Y., Kamanaka, M., et al. (2008). IL-10 from CD4CD25Foxp3CD127 adaptive regulatory T cells modulates parasite clearance and pathology during malaria infection. *PloS Pathog.* 4, e1000004. doi: 10.1371/journal.ppat.1000004

Couper, K. N., Barnes, T., Hafalla, J. C., Combes, V., Ryffel, B., Secher, T., et al. (2010). Parasite-derived plasma microparticles contribute significantly to malaria infection-induced inflammation through potent macrophage stimulation. *PloS Pathog.* 6, e1000744. doi: 10.1371/journal.ppat.1000744

Croft, M. (2010). Control of immunity by the TNFR-related molecule OX40 (CD134). *Annu. Rev. Immunol.* 28, 57–78. doi: 10.1146/annurev-immunol-030409-101243

Crompton, P. D., Kayala, M. A., Traore, B., Kayentao, K., Ongoiba, A., Weiss, G. E., et al. (2010). A prospective analysis of the Ab response to Plasmodium falciparum before and after a malaria season by protein microarray. *Proc. Natl. Acad. Sci. U.S.A.* 107, 6958–6963. doi: 10.1073/pnas.1001323107

Crotty, S. (2019). T Follicular Helper Cell Biology: A Decade of Discovery and Diseases. *Immunity* 50, 1132–1148. doi: 10.1016/j.immuni.2019.04.011

Da Silva, H. B., De Salles, E. M., Panatieri, R. H., Boscardin, S. B., Rodriguez-Malaga, S. M., Alvarez, J. M., et al. (2013). IFN-gamma-induced priming maintains long-term strain-transcending immunity against blood-stage Plasmodium chabaudi malaria. *J. Immunol.* 191, 5160–5169. doi: 10.4049/jimmunol.1300462

Dale, D. C., Boxer, L., and Liles, W. C. (2008). The phagocytes: neutrophils and monocytes. *Blood* 112, 935–945. doi: 10.1182/blood-2007-12-077917

Dang, W., Xu, L., Yin, Y., Chen, S., Wang, W., Hakim, M. S., et al. (2018). IRF-1, RIG-I and MDA5 display potent antiviral activities against norovirus coordinately induced by different types of interferons. *Antiviral Res.* 155, 48–59. doi: 10.1016/j.antiviral.2018.05.004

Day, C. L., Kaufmann, D. E., Kiepiela, P., Brown, J. A., Moodley, E. S., Reddy, S., et al. (2006). PD-1 expression on HIV-specific T cells is associated with T-cell exhaustion and disease progression. *Nature* 443, 350–354. doi: 10.1038/nature05115

Decaillot, F. M., Rozenfeld, R., Gupta, A., and Devi, L. A. (2008). Cell surface targeting of mu-delta opioid receptor heterodimers by RTP4. *Proc. Natl. Acad. Sci. U.S.A.* 105, 16045–16050. doi: 10.1073/pnas.0804106105

Deroost, K., Pham, T. T., Opdenakker, G., and Van Den Steen, P. E. (2016). The immunological balance between host and parasite in malaria. *FEMS Microbiol. Rev.* 40, 208–257. doi: 10.1093/femsre/fuv046

Desai, P., Abboud, G., Stanfield, J., Thomas, P. G., Song, J., Ware, C. F., et al. (2017). HVEM Imprints Memory Potential on Effector CD8 T Cells Required for Protective Mucosal Immunity. *J. Immunol.* 199, 2968–2975. doi: 10.4049/jimmunol.1700959

Dieli, F., Troye-Blomberg, M., Farouk, S. E., Sireci, G., and Salerno, A. (2001). Biology of gammadelta T cells in tuberculosis and malaria. *Curr. Mol. Med.* 1, 437–446. doi: 10.2174/1566524013363627

Dimitriou, I. D., Clemenza, L., Scotter, A. J., Chen, G., Guerra, F. M., and Rottapel, R. (2008). Putting out the fire: coordinated suppression of the innate and adaptive immune systems by SOCS1 and SOCS3 proteins. *Immunol. Rev.* 224, 265–283. doi: 10.1111/j.1600-065X.2008.00659.x

Ding, H., Yang, X., and Wei, Y. (2018). Fusion Proteins of NKG2D/NKG2DL in Cancer Immunotherapy. *Int. J. Mol. Sci.* 19 (1), 177. doi: 10.3390/ijms19010177

Doolan, D. L., Hoffman, S. L., Southwood, S., Wentworth, P. A., Sidney, J., Chesnut, R. W., et al. (1997). Degenerate cytotoxic T cell epitopes from P. falciparum restricted by multiple HLA-A and HLA-B supertype alleles. *Immunity* 7, 97–112. doi: 10.1016/S1074-7613(00)80513-0

Doolan, D. L., Southwood, S., Freilich, D. A., Sidney, J., Graber, N. L., Shatney, L., et al. (2003). Identification of Plasmodium falciparum antigens by antigenic

analysis of genomic and proteomic data. *Proc. Natl. Acad. Sci. U.S.A.* 100, 9952–9957. doi: 10.1073/pnas.1633254100

Doolan, D. L., Dobano, C., and Baird, J. K. (2009). Acquired immunity to malaria. *Clin. Microbiol. Rev.* 22, 13–36. doi: 10.1128/CMR.00025-08

D'ombrain, M. C., Hansen, D. S., Simpson, K. M., and Schofield, L. (2007). gammadelta-T cells expressing NK receptors predominate over NK cells and conventional T cells in the innate IFN-gamma response to Plasmodium falciparum malaria. *Eur. J. Immunol.* 37, 1864–1873. doi: 10.1002/eji.200636889

Dupre-Crochet, S., Erard, M., and Nubetae, O. (2013). ROS production in phagocytes: why, when, and where? *J. Leukoc. Biol.* 94, 657–670. doi: 10.1189/jlb.1012544

Elgueta, R., Benson, M. J., De Vries, V. C., Wasiuk, A., Guo, Y., and Noelle, R. J. (2009). Molecular mechanism and function of CD40/CD40L engagement in the immune system. *Immunol. Rev.* 229, 152–172. doi: 10.1111/j.1600-065X.2009.00782.x

Elias, R. M., Sardinha, L. R., Bastos, K. R., Zago, C. A., Da Silva, A. P., Alvarez, J. M., et al. (2005). Role of CD28 in polyclonal and specific T and B cell responses required for protection against blood stage malaria. *J. Immunol.* 174, 790–799. doi: 10.4049/jimmunol.174.2.790

Falanga, P. B., Franco Da Silveira, J. F., and Pereira Da Silva, L. (1984). Protective immune response to Plasmodium chabaudi, developed by mice after drug controlled infection or vaccination with parasite extracts: analysis of stage specific antigens from the asexual blood cycle. *Parasite Immunol.* 6, 529–543. doi: 10.1111/j.1365-3024.1984.tb00823.x

Ferreira, A., Marguti, I., Bechmann, I., Jeney, V., Chora, A., Palha, N. R., et al. (2011). Sickle hemoglobin confers tolerance to Plasmodium infection. *Cell* 145, 398–409. doi: 10.1016/j.cell.2011.03.049

Figueiredo, R. T., Fernandez, P. L., Mourao-Sa, D. S., Porto, B. N., Dutra, F. F., Alves, L. S., et al. (2007). Characterization of heme as activator of Toll-like receptor 4. *J. Biol. Chem.* 282, 20221–20229. doi: 10.1074/jbc.M610737200

Figueiredo, M. M., Costa, P. A. C., Diniz, S. Q., Henriques, P. M., Kano, F. S., Tada, M. S., et al. (2017). T follicular helper cells regulate the activation of B lymphocytes and antibody production during Plasmodium vivax infection. *PloS Pathog.* 13, e1006484. doi: 10.1371/journal.ppat.1006484

Flynn, R., Hutchinson, T., Murphy, K. M., Ware, C. F., Croft, M., and Salek-Ardakani, S. (2013). CD8 T cell memory to a viral pathogen requires trans cosignaling between HVEM and BTLA. *PloS One* 8, e77991. doi: 10.1371/journal.pone.0077991

Fowkes, F. J., Richards, J. S., Simpson, J. A., and Beeson, J. G. (2010). The relationship between anti-merozoite antibodies and incidence of Plasmodium falciparum malaria: A systematic review and meta-analysis. *PloS Med.* 7, e1000218. doi: 10.1371/journal.pmed.1000218

Freeman, G. J., Long, A. J., Iwai, Y., Bourque, K., Chernova, T., Nishimura, H., et al. (2000). Engagement of the PD-1 immunoinhibitory receptor by a novel B7 family member leads to negative regulation of lymphocyte activation. *J. Exp. Med.* 192, 1027–1034. doi: 10.1084/jem.192.7.1027

Freitas Do Rosario, A. P., Lamb, T., Spence, P., Stephens, R., Lang, A., Roers, A., et al. (2012). IL-27 promotes IL-10 production by effector Th1 CD4+ T cells: a critical mechanism for protection from severe immunopathology during malaria infection. *J. Immunol.* 188, 1178–1190. doi: 10.4049/jimmunol.1102755

Fuchs, A., Vermi, W., Lee, J. S., Lonardi, S., Gilfillan, S., Newberry, R. D., et al. (2013). Intraepithelial type 1 innate lymphoid cells are a unique subset of IL-12- and IL-15-responsive IFN-gamma-producing cells. *Immunity* 38, 769–781. doi: 10.1016/j.immuni.2013.02.010

Galbas, T., Steimle, V., Lapointe, R., Ishido, S., and Thibodeau, J. (2012). MARCH1 down-regulation in IL-10-activated B cells increases MHC class II expression. *Cytokine* 59, 27–30. doi: 10.1016/j.cyto.2012.03.015

Gallego-Delgado, J., Ty, M., Orengo, J. M., Van De Hoef, D., and Rodriguez, A. (2014). A surprising role for uric acid: the inflammatory malaria response. *Curr. Rheumatol. Rep.* 16, 401. doi: 10.1007/s11926-013-0401-8

Gazzinelli, R. T., and Denkers, E. Y. (2006). Protozoan encounters with Toll-like receptor signalling pathways: implications for host parasitism. *Nat. Rev. Immunol.* 6, 895–906. doi: 10.1038/nri1978

Gazzinelli, R. T., Kalantari, P., Fitzgerald, K. A., and Golenbock, D. T. (2014). Innate sensing of malaria parasites. *Nat. Rev. Immunol.* 14, 744–757. doi: 10.1038/nri3742

Gowda, N. M., Wu, X., and Gowda, D. C. (2012). TLR9 and MyD88 are crucial for the development of protective immunity to malaria. *J. Immunol.* 188, 5073–5085. doi: 10.4049/jimmunol.1102143

Gramaglia, I., Velez, J., Combes, V., Grau, G. E., Wree, M., and Van Der Heyde, H. C. (2017). Platelets activate a pathogenic response to blood-stage Plasmodium infection but not a protective immune response. *Blood* 129, 1669–1679. doi: 10.1182/blood-2016-08-733519

Grassi, B., Bignami, A., and Bastianelli, G. (1899). Medical Zoology: Further Researches upon the Cycle of Human Malaria in the Body of the Mosquito. *Ind. Med. Gaz.* 34, 104–107.

Gregor, P. D., Wolchok, J. D., Ferrone, C. R., Buchinshky, H., Guevara-Patino, J. A., Perales, M. A., et al. (2004). CTLA-4 blockade in combination with xenogeneic DNA vaccines enhances T-cell responses, tumor immunity and autoimmunity to self antigens in animal and cellular model systems. *Vaccine* 22, 1700–1708. doi: 10.1016/j.vaccine.2003.10.048

Griffith, J. W., Sun, T., Mcintosh, M. T., and Bucala, R. (2009). Pure Hemozoin is inflammatory in vivo and activates the NALP3 inflammasome via release of uric acid. *J. Immunol.* 183, 5208–5220. doi: 10.4049/jimmunol.0713552

Gross, J. A., Callas, E., and Allison, J. P. (1992). Identification and distribution of the costimulatory receptor CD28 in the mouse. *J. Immunol.* 149, 380–388.

Grosso, J. F., Goldberg, M. V., Getnet, D., Bruno, T. C., Yen, H. R., Pyle, K. J., et al. (2009). Functionally distinct LAG-3 and PD-1 subsets on activated and chronically stimulated CD8 T cells. *J. Immunol.* 182, 6659–6669. doi: 10.4049/jimmunol.0804211

Gubin, M. M., Zhang, X., Schuster, H., Caron, E., Ward, J. P., Noguchi, T., et al. (2014). Checkpoint blockade cancer immunotherapy targets tumour-specific mutant antigens. *Nature* 515, 577–581. doi: 10.1038/nature13988

Guo, H., Pang, K., Wei, Y., Yi, C., and Wu, X. (2015). Herpes virus entry mediator in human corneal epithelial cells modulates the production of inflammatory cytokines in response to HSV type 1 challenge. *Ophthalmic Res.* 54, 128–134. doi: 10.1159/000437209

Gupta, S., Snow, R. W., Donnelly, C. A., Marsh, K., and Newbold, C. (1999). Immunity to non-cerebral severe malaria is acquired after one or two infections. *Nat. Med.* 5, 340–343. doi: 10.1038/6560

Gwyer Findlay, E., Villegas-Mendez, A., O'regan, N., De Souza, J. B., Grady, L. M., Saris, C. J., et al. (2014). IL-27 receptor signaling regulates memory CD4+ T cell populations and suppresses rapid inflammatory responses during secondary malaria infection. *Infect. Immun.* 82, 10–20. doi: 10.1128/IAI.01091-13

Hansen, D. S., and Schofield, L. (2010). Natural regulatory T cells in malaria: host or parasite allies? *PloS Pathog.* 6, e1000771. doi: 10.1371/journal.ppat.1000771

Haque, A., Best, S. E., Ammerdorffer, A., Desbarrieres, L., De Oca, M. M., Amante, F. H., et al. (2011). Type I interferons suppress CD4(+) T-cell-dependent parasite control during blood-stage Plasmodium infection. *Eur. J. Immunol.* 41, 2688–2698. doi: 10.1002/eji.201141539

Haque, A., Best, S. E., Montes De Oca, M., James, K. R., Ammerdorffer, A., Edwards, C. L., et al. (2014). Type I IFN signaling in CD8- DCs impairs Th1-dependent malaria immunity. *J. Clin. Invest.* 124, 2483–2496. doi: 10.1172/JCI70698

Hathcock, K. S., Hirano, H., Murakami, S., and Hodes, R. J. (1992). CD45 expression by B cells. Expression of different CD45 isoforms by subpopulations of activated B cells. *J. Immunol.* 149, 2286–2294.

He, X., Ashbrook, A. W., Du, Y., Wu, J., Hoffmann, H. H., Zhang, C., et al. (2020). RTP4 inhibits IFN-I response and enhances experimental cerebral malaria and neuropathology. *Proc. Natl. Acad. Sci. U.S.A.* 117, 19465–19474. doi: 10.1073/pnas.2006492117

Hisaeda, H., Hamano, S., Mitoma-Obata, C., Tetsutani, K., Imai, T., Waldmann, H., et al. (2005). Resistance of regulatory T cells to glucocorticoid-induced [corrected] TNFR family-related protein (GITR) during Plasmodium yoelii infection. *Eur. J. Immunol.* 35, 3516–3524. doi: 10.1002/eji.200526073

Hoffman, S. L., Oster, C. N., Plowe, C. V., Woollett, G. R., Beier, J. C., Chulay, J. D., et al. (1987). Naturally acquired antibodies to sporozoites do not prevent malaria: vaccine development implications. *Science* 237, 639–642. doi: 10.1126/science.3299709

Hommel, M., Chan, J. A., Umbers, A. J., Langer, C., Rogerson, S. J., Smith, J. D., et al. (2018). Evaluating antibody functional activity and strain-specificity of vaccine candidates for malaria in pregnancy using in vitro phagocytosis assays. *Parasit. Vectors* 11, 69. doi: 10.1186/s13071-018-2653-7

Hopp, C. S., and Sinnis, P. (2015). The innate and adaptive response to mosquito saliva and Plasmodium sporozoites in the skin. *Ann. N Y Acad. Sci.* 1342, 37–43. doi: 10.1111/nyas.12661

Horne-Debets, J. M., Faleiro, R., Karunarathne, D. S., Liu, X. Q., Lineburg, K. E., Poh, C. M., et al. (2013). PD-1 dependent exhaustion of CD8+ T cells drives chronic malaria. *Cell Rep.* 5, 1204–1213. doi: 10.1016/j.celrep.2013.11.002

Horowitz, A., Newman, K. C., Evans, J. H., Korbel, D. S., Davis, D. M., and Riley, E. M. (2010). Cross-talk between T cells and NK cells generates rapid effector responses to Plasmodium falciparum-infected erythrocytes. *J. Immunol.* 184, 6043–6052. doi: 10.4049/jimmunol.1000106

Hou, N., Zhao, D., Liu, Y., Gao, L., Liang, X., Liu, X., et al. (2012). Increased expression of T cell immunoglobulin- and mucin domain-containing molecule-3 on natural killer cells in atherogenesis. *Atherosclerosis* 222, 67–73. doi: 10.1016/j.atherosclerosis.2012.02.009

Hou, N., Zou, Y., Piao, X., Liu, S., Wang, L., Li, S., et al. (2016). T-Cell Immunoglobulin- and Mucin-Domain-Containing Molecule 3 Signaling Blockade Improves Cell-Mediated Immunity Against Malaria. *J. Infect. Dis.* 214, 1547–1556. doi: 10.1093/infdis/jiw428

Hou, N., Jiang, N., Zou, Y., Piao, X., Liu, S., Li, S., et al. (2017). Down-Regulation of Tim-3 in Monocytes and Macrophages in Plasmodium Infection and Its Association with Parasite Clearance. *Front. Microbiol.* 8, 1431. doi: 10.3389/fmicb.2017.01431

Howes, R. E., Battle, K. E., Mendis, K. N., Smith, D. L., Cibulskis, R. E., Baird, J. K., et al. (2016). Global Epidemiology of Plasmodium vivax. *Am. J. Trop. Med. Hyg.* 95, 15–34. doi: 10.4269/ajtmh.16-0141

Huang, C. T., Workman, C. J., Flies, D., Pan, X., Marson, A. L., Zhou, G., et al. (2004). Role of LAG-3 in regulatory T cells. *Immunity* 21, 503–513. doi: 10.1016/j.immuni.2004.08.010

Huang, J., Liu, T., Xu, L. G., Chen, D., Zhai, Z., and Shu, H. B. (2005). SIKE is an IKK epsilon/TBK1-associated suppressor of TLR3- and virus-triggered IRF-3 activation pathways. *EMBO J.* 24, 4018–4028. doi: 10.1038/sj.emboj.7600863

Huang, H., Lamikanra, A. A., Alkaitis, M. S., Thezenas, M. L., Ramaprasad, A., Moussa, E., et al. (2014). Interleukin-10 regulates hepcidin in Plasmodium falciparum malaria. *PloS One* 9, e88408. doi: 10.1371/journal.pone.0088408

Hunt, N. H., Grau, G. E., Engwerda, C., Barnum, S. R., Van Der Heyde, H., Hansen, D. S., et al. (2010). Murine cerebral malaria: the whole story. *Trends Parasitol.* 26, 272–274. doi: 10.1016/j.pt.2010.03.006

Imkeller, K., Scally, S. W., Bosch, A., Marti, G. P., Costa, G., Triller, G., et al. (2018). Antihomotypic affinity maturation improves human B cell responses against a repetitive epitope. *Science* 360, 1358–1362. doi: 10.1126/science.aar5304

Inoue, S., Niikura, M., Takeo, S., Mineo, S., Kawakami, Y., Uchida, A., et al. (2012). Enhancement of dendritic cell activation via CD40 ligand-expressing gammadelta T cells is responsible for protective immunity to Plasmodium parasites. *Proc. Natl. Acad. Sci. U.S.A.* 109, 12129–12134. doi: 10.1073/pnas.1204480109

Ishido, S., Goto, E., Matsuki, Y., and Ohmura-Hoshino, M. (2009). E3 ubiquitin ligases for MHC molecules. *Curr. Opin. Immunol.* 21, 78–83. doi: 10.1016/j.coi.2009.01.002

Ishizuka, A. S., Lyke, K. E., Dezure, A., Berry, A. A., Richie, T. L., Mendoza, F. H., et al. (2016). Protection against malaria at 1 year and immune correlates following PfSPZ vaccination. *Nat. Med.* 22, 614–623. doi: 10.1038/nm.4110

Issa, F., Robb, R. J., and Wood, K. J. (2013). The where and when of T cell regulation in transplantation. *Trends Immunol.* 34, 107–113. doi: 10.1016/j.it.2012.11.003

Jangpatarapongsa, K., Chootong, P., Sattabongkot, J., Chotivanich, K., Sirichaisinthop, J., Tungpradabkul, S., et al. (2008). Plasmodium vivax parasites alter the balance of myeloid and plasmacytoid dendritic cells and the induction of regulatory T cells. *Eur. J. Immunol.* 38, 2697–2705. doi: 10.1002/eji.200838186

Jaramillo, M., Gowda, D. C., Radzioch, D., and Olivier, M. (2003). Hemozoin increases IFN-gamma-inducible macrophage nitric oxide generation through extracellular signal-regulated kinase- and NF-kappa B-dependent pathways. *J. Immunol.* 171, 4243–4253. doi: 10.4049/jimmunol.171.8.4243

Johnston, R. J., Comps-Agrar, L., Hackney, J., Yu, X., Huseni, M., Yang, Y., et al. (2014). The immunoreceptor TIGIT regulates antitumor and antiviral CD8(+) T cell effector function. *Cancer Cell* 26, 923–937. doi: 10.1016/j.ccell.2014.10.018

Ju, Y., Hou, N., Meng, J., Wang, X., Zhang, X., Zhao, D., et al. (2010). T cell immunoglobulin- and mucin-domain-containing molecule-3 (Tim-3) mediates natural killer cell suppression in chronic hepatitis B. *J. Hepatol.* 52, 322–329. doi: 10.1016/j.jhep.2009.12.005

Kadziolka, B., Lesniak, W., and Filipek, A. (2017). Regulation of CacyBP/SIP expression by NFAT1 transcription factor. *Immunobiology* 222, 872–877. doi: 10.1016/j.imbio.2017.05.002

Kalantari, P., Deoliveira, R. B., Chan, J., Corbett, Y., Rathinam, V., Stutz, A., et al. (2014). Dual engagement of the NLRP3 and AIM2 inflammasomes by plasmodium-derived hemozoin and DNA during malaria. *Cell Rep.* 6, 196–210. doi: 10.1016/j.celrep.2013.12.014

Kanda, Y., Kawamura, H., Matsumoto, H., Kobayashi, T., Kawamura, T., and Abo, T. (2010). Identification and characterization of autoantibody-producing B220(low) B (B-1) cells appearing in malarial infection. *Cell Immunol.* 263, 49–54. doi: 10.1016/j.cellimm.2010.02.015

Kapelski, S., Klockenbring, T., Fischer, R., Barth, S., and Fendel, R. (2014). Assessment of the neutrophilic antibody-dependent respiratory burst (ADRB) response to Plasmodium falciparum. *J. Leukoc. Biol.* 96, 1131–1142. doi: 10.1189/jlb.4A0614-283RR

Karunarathne, D. S., Horne-Debets, J. M., Huang, J. X., Faleiro, R., Leow, C. Y., Amante, F., et al. (2016). Programmed Death-1 Ligand 2-Mediated Regulation of the PD-L1 to PD-1 Axis Is Essential for Establishing CD4(+) T Cell Immunity. *Immunity* 45, 333–345. doi: 10.1016/j.immuni.2016.07.017

Kent, L. N., Rumi, M. A., Kubota, K., Lee, D. S., and Soares, M. J. (2011). FOSL1 is integral to establishing the maternal-fetal interface. *Mol. Cell Biol.* 31, 4801–4813. doi: 10.1128/MCB.05780-11

Kimura, D., Miyakoda, M., Kimura, K., Honma, K., Hara, H., Yoshida, H., et al. (2016). Interleukin-27-Producing CD4(+) T Cells Regulate Protective Immunity during Malaria Parasite Infection. *Immunity* 44, 672–682. doi: 10.1016/j.immuni.2016.02.011

Kinjyo, I., Hanada, T., Inagaki-Ohara, K., Mori, H., Aki, D., Ohishi, M., et al. (2002). SOCS1/JAB is a negative regulator of LPS-induced macrophage activation. *Immunity* 17, 583–591. doi: 10.1016/S1074-7613(02)00446-6

Kordes, M., Matuschewski, K., and Hafalla, J. C. (2011). Caspase-1 activation of interleukin-1beta (IL-1beta) and IL-18 is dispensable for induction of experimental cerebral malaria. *Infect. Immun.* 79, 3633–3641. doi: 10.1128/IAI.05459-11

Krishnegowda, G., Hajjar, A. M., Zhu, J., Douglass, E. J., Uematsu, S., Akira, S., et al. (2005). Induction of proinflammatory responses in macrophages by the glycosylphosphatidylinositols of Plasmodium falciparum: cell signaling receptors, glycosylphosphatidylinositol (GPI) structural requirement, and regulation of GPI activity. *J. Biol. Chem.* 280, 8606–8616. doi: 10.1074/jbc.M413541200

Kumar, S., and Miller, L. H. (1990). Cellular mechanisms in immunity to blood stage infection. *Immunol. Lett.* 25, 109–114. doi: 10.1016/0165-2478(90)90100-5

Kumaratilake, L. M., and Ferrante, A. (2000). Opsonization and phagocytosis of Plasmodium falciparum merozoites measured by flow cytometry. *Clin. Diagn. Lab. Immunol.* 7, 9–13. doi: 10.1128/CDLI.7.1.9-13.2000

Kurtovic, L., Boyle, M. J., Opi, D. H., Kennedy, A. T., Tham, W. H., Reiling, L., et al. (2020). Complement in malaria immunity and vaccines. *Immunol. Rev.* 293, 38–56. doi: 10.1111/imr.12802

Kurup, S. P., Obeng-Adjei, N., Anthony, S. M., Traore, B., Doumbo, O. K., Butler, N. S., et al. (2017). Regulatory T cells impede acute and long-term immunity to blood-stage malaria through CTLA-4. *Nat. Med.* 23, 1220–1225. doi: 10.1038/nm.4395

Langhorne, J., Gillard, S., Simon, B., Slade, S., and Eichmann, K. (1989). Frequencies of CD4+ T cells reactive with Plasmodium chabaudi chabaudi: distinct response kinetics for cells with Th1 and Th2 characteristics during infection. *Int. Immunol.* 1, 416–424. doi: 10.1093/intimm/1.4.416

Latchman, Y., Wood, C. R., Chernova, T., Chaudhary, D., Borde, M., Chernova, I., et al. (2001). PD-L2 is a second ligand for PD-1 and inhibits T cell activation. *Nat. Immunol.* 2, 261–268. doi: 10.1038/85330

Le Bouteiller, P., Barakonyi, A., Giustiniani, J., Lenfant, F., Marie-Cardine, A., Aguerre-Girr, M., et al. (2002). Engagement of CD160 receptor by HLA-C is a triggering mechanism used by circulating natural killer (NK) cells to mediate cytotoxicity. *Proc. Natl. Acad. Sci. U.S.A.* 99, 16963–16968. doi: 10.1073/pnas.012681099

Lennartz, F., Adams, Y., Bengtsson, A., Olsen, R. W., Turner, L., Ndam, N. T., et al. (2017). Structure-Guided Identification of a Family of Dual Receptor-Binding PfEMP1 that Is Associated with Cerebral Malaria. *Cell Host. Microbe* 21, 403–414. doi: 10.1016/j.chom.2017.02.009

Lennartz, F., Smith, C., Craig, A. G., and Higgins, M. K. (2019). Structural insights into diverse modes of ICAM-1 binding by Plasmodium falciparum-infected erythrocytes. *Proc. Natl. Acad. Sci. U.S.A.* 116, 20124–20134. doi: 10.1073/pnas.1911900116

Liehl, P., Zuzarte-Luis, V., Chan, J., Zillinger, T., Baptista, F., Carapau, D., et al. (2014). Host-cell sensors for Plasmodium activate innate immunity against liver-stage infection. *Nat. Med.* 20, 47–53. doi: 10.1038/nm.3424

Lin, Y., Wei, J., Fan, L., and Cheng, D. (2015). BTNL2 gene polymorphism and sarcoidosis susceptibility: a meta-analysis. *PloS One* 10, e0122639. doi: 10.1371/journal.pone.0122639

Liu, D., Sheng, C., Gao, S., Yao, C., Li, J., Jiang, W., et al. (2015). SOCS3 Drives Proteasomal Degradation of TBK1 and Negatively Regulates Antiviral Innate Immunity. *Mol. Cell Biol.* 35, 2400–2413. doi: 10.1128/MCB.00090-15

Liu, T., Cheng, X., Ding, Y., Zhu, F., Fu, Y., Peng, X., et al. (2018). PD-1 deficiency promotes TFH cells expansion in ITV-immunized mice by upregulating cytokines secretion. *Parasit. Vectors* 11, 397. doi: 10.1186/s13071-018-2984-4

Liu, T., Lu, X., Zhao, C., Fu, X., Zhao, T., and Xu, W. (2015). PD-1 deficiency enhances humoral immunity of malaria infection treatment vaccine. *Infect. Immun.* 83, 2011–2017. doi: 10.1128/IAI.02621-14

Ma, C. S., Deenick, E. K., Batten, M., and Tangye, S. G. (2012). The origins, function, and regulation of T follicular helper cells. *J. Exp. Med.* 209, 1241–1253. doi: 10.1084/jem.20120994

Macchia, G., Trombetta, D., Moller, E., Mertens, F., Storlazzi, C. T., Debiec-Rychter, M., et al. (2012). FOSL1 as a candidate target gene for 11q12 rearrangements in desmoplastic fibroblastoma. *Lab. Invest.* 92, 735–743. doi: 10.1038/labinvest.2012.46

Machado, F. S., Johndrow, J. E., Esper, L., Dias, A., Bafica, A., Serhan, C. N., et al. (2006). Anti-inflammatory actions of lipoxin A4 and aspirin-triggered lipoxin are SOCS-2 dependent. *Nat. Med.* 12, 330–334. doi: 10.1038/nm1355

Macian, F. (2005). NFAT proteins: key regulators of T-cell development and function. *Nat. Rev. Immunol.* 5, 472–484. doi: 10.1038/nri1632

Macri, C., Pang, E. S., Patton, T., and O'keeffe, M. (2018). Dendritic cell subsets. *Semin. Cell Dev. Biol.* 84, 11–21. doi: 10.1016/j.semcdb.2017.12.009

Maeda, M., Carpenito, C., Russell, R. C., Dasanjh, J., Veinotte, L. L., Ohta, H., et al. (2005). Murine CD160, Ig-like receptor on NK cells and NKT cells, recognizes classical and nonclassical MHC class I and regulates NK cell activation. *J. Immunol.* 175, 4426–4432. doi: 10.4049/jimmunol.175.7.4426

Manfredi, A. A., Ramirez, G. A., Rovere-Querini, P., and Maugeri, N. (2018). The Neutrophil's Choice: Phagocytose vs Make Neutrophil Extracellular Traps. *Front. Immunol.* 9, 288. doi: 10.3389/fimmu.2018.00288

Mantel, P. Y., and Marti, M. (2014). The role of extracellular vesicles in Plasmodium and other protozoan parasites. *Cell Microbiol.* 16, 344–354. doi: 10.1111/cmi.12259

Marsh, K., Otoo, L., Hayes, R. J., Carson, D. C., and Greenwood, B. M. (1989). Antibodies to blood stage antigens of Plasmodium falciparum in rural Gambians and their relation to protection against infection. *Trans. R Soc. Trop. Med. Hyg.* 83, 293–303. doi: 10.1016/0035-9203(89)90478-1

Martins, G. A., Tadokoro, C. E., Silva, R. B., Silva, J. S., and Rizzo, L. V. (2004). CTLA-4 blockage increases resistance to infection with the intracellular protozoan Trypanosoma cruzi. *J. Immunol.* 172, 4893–4901. doi: 10.4049/jimmunol.172.8.4893

Marvel, J., and Mayer, A. (1988). CD45R gives immunofluorescence and transduces signals on mouse T cells. *Eur. J. Immunol.* 18, 825–828. doi: 10.1002/eji.1830180526

Mchugh, R. S., Whitters, M. J., Piccirillo, C. A., Young, D. A., Shevach, E. M., Collins, M., et al. (2002). CD4(+)CD25(+) immunoregulatory T cells: gene expression analysis reveals a functional role for the glucocorticoid-induced TNF receptor. *Immunity* 16, 311–323. doi: 10.1016/S1074-7613(02)00280-7

Mcleod, B., Miura, K., Scally, S. W., Bosch, A., Nguyen, N., Shin, H., et al. (2019). Potent antibody lineage against malaria transmission elicited by human vaccination with Pfs25. *Nat. Commun.* 10, 4328. doi: 10.1038/s41467-019-11980-6

Mcnab, F., Mayer-Barber, K., Sher, A., Wack, A., and O'garra, A. (2015). Type I interferons in infectious disease. *Nat. Rev. Immunol.* 15, 87–103. doi: 10.1038/nri3787

Medana, I. M., Hien, T. T., Day, N. P., Phu, N. H., Mai, N. T., Chu'ong, L. V., et al. (2002). The clinical significance of cerebrospinal fluid levels of kynurenine pathway metabolites and lactate in severe malaria. *J. Infect. Dis.* 185, 650–656. doi: 10.1086/339009

Medana, I. M., Day, N. P., Salahifar-Sabet, H., Stocker, R., Smythe, G., Bwanaisa, L., et al. (2003). Metabolites of the kynurenine pathway of tryptophan metabolism in the cerebrospinal fluid of Malawian children with malaria. *J. Infect. Dis.* 188, 844–849. doi: 10.1086/377583

Mellor, A. L., and Munn, D. H. (2004). IDO expression by dendritic cells: tolerance and tryptophan catabolism. *Nat. Rev. Immunol.* 4, 762–774. doi: 10.1038/nri1457

Mendis, K. N., and Targett, G. A. (1979). Immunisation against gametes and asexual erythrocytic stages of a rodent malaria parasite. *Nature* 277, 389–391. doi: 10.1038/277389a0

Mendonca, V. R., and Barral-Netto, M. (2015). Immunoregulation in human malaria: the challenge of understanding asymptomatic infection. *Mem. Inst. Oswaldo Cruz* 110, 945–955. doi: 10.1590/0074-02760150241

Miller, J. L., Sack, B. K., Baldwin, M., Vaughan, A. M., and Kappe, S. H. I. (2014). Interferon-mediated innate immune responses against malaria parasite liver stages. *Cell Rep.* 7, 436–447. doi: 10.1016/j.celrep.2014.03.018

Mitchell, A. J., Hansen, A. M., Hee, L., Ball, H. J., Potter, S. M., Walker, J. C., et al. (2005). Early cytokine production is associated with protection from murine cerebral malaria. *Infect. Immun.* 73, 5645–5653. doi: 10.1128/IAI.73.9.5645-5653.2005

Mittal, S. K., Cho, K. J., Ishido, S., and Roche, P. A. (2015). Interleukin 10 (IL-10)-mediated Immunosuppression: MARCH-I INDUCTION REGULATES ANTIGEN PRESENTATION BY MACROPHAGES BUT NOT DENDRITIC CELLS. *J. Biol. Chem.* 290, 27158–27167. doi: 10.1074/jbc.M115.682708

Miyakoda, M., Kimura, D., Honma, K., Kimura, K., Yuda, M., and Yui, K. (2012). Development of memory CD8+ T cells and their recall responses during blood-stage infection with Plasmodium berghei ANKA. *J. Immunol.* 189, 4396–4404. doi: 10.4049/jimmunol.1200781

Montes De Oca, M., Kumar, R., Rivera, F. L., Amante, F. H., Sheel, M., Faleiro, R. J., et al. (2016). Type I Interferons Regulate Immune Responses in Humans with Blood-Stage Plasmodium falciparum Infection. *Cell Rep.* 17, 399–412. doi: 10.1016/j.celrep.2016.09.015

Mordmuller, B., Surat, G., Lagler, H., Chakravarty, S., Ishizuka, A. S., Lalremruata, A., et al. (2017). Sterile protection against human malaria by chemoattenuated PfSPZ vaccine. *Nature* 542, 445–449. doi: 10.1038/nature21060

Moretto, M. M., Hwang, S., and Khan, I. A. (2017). Downregulated IL-21 Response and T Follicular Helper Cell Exhaustion Correlate with Compromised CD8 T Cell Immunity during Chronic Toxoplasmosis. *Front. Immunol.* 8, 1436. doi: 10.3389/fimmu.2017.01436

Moschonas, A., Ioannou, M., and Eliopoulos, A. G. (2012). CD40 stimulates a "feed-forward" NF-kappaB-driven molecular pathway that regulates IFN-beta expression in carcinoma cells. *J. Immunol.* 188, 5521–5527. doi: 10.4049/jimmunol.1200133

Mota, M. M., Pradel, G., Vanderberg, J. P., Hafalla, J. C., Frevert, U., Nussenzweig, R. S., et al. (2001). Migration of Plasmodium sporozoites through cells before infection. *Science* 291, 141–144. doi: 10.1126/science.291.5501.141

Murray, S. A., Mohar, I., Miller, J. L., Brempelis, K. J., Vaughan, A. M., Kappe, S. H., et al. (2015). CD40 is required for protective immunity against liver stage Plasmodium infection. *J. Immunol.* 194, 2268–2279. doi: 10.4049/jimmunol.1401724

Murugan, R., Buchauer, L., Triller, G., Kreschel, C., Costa, G., Pidelaserra Marti, G., et al. (2018). Clonal selection drives protective memory B cell responses in controlled human malaria infection. *Sci. Immunol.* 3, eaap802. doi: 10.1126/sciimmunol.aap8029

Muscate, F., Stetter, N., Schramm, C., Schulze Zur Wiesch, J., Bosurgi, L., and Jacobs, T. (2018). HVEM and CD160: Regulators of Immunopathology During Malaria Blood-Stage. *Front. Immunol.* 9, 2611. doi: 10.3389/fimmu.2018.02611

Nair, S. C., Xu, R., Pattaradilokrat, S., Wu, J., Qi, Y., Zilversmit, M., et al. (2017). A Plasmodium yoelii HECT-like E3 ubiquitin ligase regulates parasite growth and virulence. *Nat. Commun.* 8, 223. doi: 10.1038/s41467-017-00267-3

Nair, S. R., Abraham, R., Sundaram, S., and Sreekumar, E. (2017). Interferon regulated gene (IRG) expression-signature in a mouse model of chikungunya virus neurovirulence. *J. Neurovirol.* 23, 886–902. doi: 10.1007/s13365-017-0583-3

Naka, T., Narazaki, M., Hirata, M., Matsumoto, T., Minamoto, S., Aono, A., et al. (1997). Structure and function of a new STAT-induced STAT inhibitor. *Nature* 387, 924–929. doi: 10.1038/43219

Naka, T., Matsumoto, T., Narazaki, M., Fujimoto, M., Morita, Y., Ohsawa, Y., et al. (1998). Accelerated apoptosis of lymphocytes by augmented induction of Bax in SSI-1 (STAT-induced STAT inhibitor-1) deficient mice. *Proc. Natl. Acad. Sci. U.S.A.* 95, 15577–15582. doi: 10.1073/pnas.95.26.15577

Nakae, S., Suto, H., Iikura, M., Kakurai, M., Sedgwick, J. D., Tsai, M., et al. (2006). Mast cells enhance T cell activation: importance of mast cell costimulatory molecules and secreted TNF. *J. Immunol.* 176, 2238–2248. doi: 10.4049/jimmunol.176.4.2238

Nakagawa, R., Naka, T., Tsutsui, H., Fujimoto, M., Kimura, A., Abe, T., et al. (2002). SOCS-1 participates in negative regulation of LPS responses. *Immunity* 17, 677–687. doi: 10.1016/S1074-7613(02)00449-1

Ndungu, F. M., Olotu, A., Mwacharo, J., Nyonda, M., Apfeld, J., Mramba, L. K., et al. (2012). Memory B cells are a more reliable archive for historical antimalarial responses than plasma antibodies in no-longer exposed children. *Proc. Natl. Acad. Sci. U.S.A.* 109, 8247–8252. doi: 10.1073/pnas.1200472109

Ndungu, F. M., Lundblom, K., Rono, J., Illingworth, J., Eriksson, S., and Farnert, A. (2013). Long-lived Plasmodium falciparum specific memory B cells in naturally exposed Swedish travelers. *Eur. J. Immunol.* 43, 2919–2929. doi: 10.1002/eji.201343630

Niikura, M., Kamiya, S., Kita, K., and Kobayashi, F. (2008). Coinfection with nonlethal murine malaria parasites suppresses pathogenesis caused by Plasmodium berghei NK65. *J. Immunol.* 180, 6877–6884. doi: 10.4049/jimmunol.180.10.6877

Niknam, A., Karimi, M. H., Geramizadeh, B., Roozbeh, J., Yaghobi, R., and Salehipour, M. (2017). Polymorphisms of the Costimulatory Genes CTLA-4, CD28, PD-1, and ICOS and Outcome of Kidney Transplants in Iranian Patients. *Exp. Clin. Transplant.* 15, 295–305. doi: 10.6002/ect.2014.0253

Nishioka, T., Nishida, E., Iida, R., Morita, A., and Shimizu, J. (2008). In vivo expansion of CD4+Foxp3+ regulatory T cells mediated by GITR molecules. *Immunol. Lett.* 121, 97–104. doi: 10.1016/j.imlet.2008.09.003

Nocentini, G., Ronchetti, S., Cuzzocrea, S., and Riccardi, C. (2007). GITR/GITRL: more than an effector T cell co-stimulatory system. *Eur. J. Immunol.* 37, 1165–1169. doi: 10.1002/eji.200636933

Obeng-Adjei, N., Portugal, S., Tran, T. M., Yazew, T. B., Skinner, J., Li, S., et al. (2015). Circulating Th1-Cell-type Tfh Cells that Exhibit Impaired B Cell Help Are Preferentially Activated during Acute Malaria in Children. *Cell Rep.* 13, 425–439. doi: 10.1016/j.celrep.2015.09.004

Ohmura-Hoshino, M., Goto, E., Matsuki, Y., Aoki, M., Mito, M., Uematsu, M., et al. (2006). A novel family of membrane-bound E3 ubiquitin ligases. *J. Biochem.* 140, 147–154. doi: 10.1093/jb/mvj160

Okazaki, T., and Honjo, T. (2006). The PD-1-PD-L pathway in immunological tolerance. *Trends Immunol.* 27, 195–201. doi: 10.1016/j.it.2006.02.001

O'neill, L. A., Golenbock, D., and Bowie, A. G. (2013). The history of Toll-like receptors - redefining innate immunity. *Nat. Rev. Immunol.* 13, 453–460. doi: 10.1038/nri3446

Orsini, G., Legitimo, A., Failli, A., Massei, F., Biver, P., and Consolini, R. (2012). Enumeration of human peripheral blood dendritic cells throughout the life. *Int. Immunol.* 24, 347–356. doi: 10.1093/intimm/dxs006

Ortonne, N., Ram-Wolff, C., Giustiniani, J., Marie-Cardine, A., Bagot, M., Mecheri, S., et al. (2011). Human and mouse mast cells express and secrete the GPI-anchored isoform of CD160. *J. Invest. Dermatol.* 131, 916–924. doi: 10.1038/jid.2010.412

Osier, F. H., Fegan, G., Polley, S. D., Murungi, L., Verra, F., Tetteh, K. K., et al. (2008). Breadth and magnitude of antibody responses to multiple Plasmodium falciparum merozoite antigens are associated with protection from clinical malaria. *Infect. Immun.* 76, 2240–2248. doi: 10.1128/IAI.01585-07

Othman, A. S., Franke-Fayard, B. M., Imai, T., Van Der Gracht, E. T. I., Redeker, A., Salman, A. M., et al. (2018). OX40 Stimulation Enhances Protective Immune Responses Induced After Vaccination With Attenuated Malaria Parasites. *Front. Cell Infect. Microbiol.* 8, 247. doi: 10.3389/fcimb.2018.00247

Otterdal, K., Berg, A., Michelsen, A. E., Patel, S., Tellevik, M. G., Haanshuus, C. G., et al. (2018). Soluble markers of neutrophil, T-cell and monocyte activation are associated with disease severity and parasitemia in falciparum malaria. *BMC Infect. Dis.* 18, 670. doi: 10.1186/s12879-018-3593-8

Ouattara, A., and Laurens, M. B. (2015). Vaccines against malaria. *Clin. Infect. Dis.* 60, 930–936. doi: 10.1093/cid/ciu954

Pan, Y., Sun, X., Li, D., Zhao, Y., Jin, F., and Cao, Y. (2020). PD-1 blockade promotes immune memory following Plasmodium berghei ANKA reinfection. *Int. Immunopharmacol.* 80, 106186. doi: 10.1016/j.intimp.2020.106186

Parmar, R., Patel, H., Yadav, N., Parikh, R., Patel, K., Mohankrishnan, A., et al. (2018). Infectious Sporozoites of Plasmodium berghei Effectively Activate Liver CD8alpha(+) Dendritic Cells. *Front. Immunol.* 9, 192. doi: 10.3389/fimmu.2018.00192

Parroche, P., Lauw, F. N., Goutagny, N., Latz, E., Monks, B. G., Visintin, A., et al. (2007). Malaria hemozoin is immunologically inert but radically enhances innate responses by presenting malaria DNA to Toll-like receptor 9. *Proc. Natl. Acad. Sci. U.S.A.* 104, 1919–1924. doi: 10.1073/pnas.0608745104

Perez-Mazliah, D., and Langhorne, J. (2014). CD4 T-cell subsets in malaria: TH1/TH2 revisited. *Front. Immunol.* 5, 671. doi: 10.3389/fimmu.2014.00671

Perez-Mazliah, D., Ng, D. H., Freitas Do Rosario, A. P., Mclaughlin, S., Mastelic-Gavillet, B., Sodenkamp, J., et al. (2015). Disruption of IL-21 signaling affects T cell-B cell interactions and abrogates protective humoral immunity to malaria. *PloS Pathog.* 11, e1004715. doi: 10.1371/journal.ppat.1004715

Perez-Mazliah, D., Nguyen, M. P., Hosking, C., Mclaughlin, S., Lewis, M. D., Tumwine, I., et al. (2017). Follicular Helper T Cells are Essential for the Elimination of Plasmodium Infection. *EBioMedicine* 24, 216–230. doi: 10.1016/j.ebiom.2017.08.030

Peters, N. C., Egen, J. G., Secundino, N., Debrabant, A., Kimblin, N., Kamhawi, S., et al. (2008). In vivo imaging reveals an essential role for neutrophils in leishmaniasis transmitted by sand flies. *Science* 321, 970–974. doi: 10.1126/science.1159194

Ratelade, J., and Verkman, A. S. (2014). Inhibitor(s) of the classical complement pathway in mouse serum limit the utility of mice as experimental models of neuromyelitis optica. *Mol. Immunol.* 62, 104–113. doi: 10.1016/j.molimm.2014.06.003

Renaud, S. J., Kubota, K., Rumi, M. A., and Soares, M. J. (2014). The FOS transcription factor family differentially controls trophoblast migration and invasion. *J. Biol. Chem.* 289, 5025–5039. doi: 10.1074/jbc.M113.523746

Renno, T., Attinger, A., Rimoldi, D., Hahne, M., Tschopp, J., and Macdonald, H. R. (1998). Expression of B220 on activated T cell blasts precedes apoptosis. *Eur. J. Immunol.* 28, 540–547. doi: 10.1002/(SICI)1521-4141(199802)28:02<540::AID-IMMU540>3.0.CO;2-Y

Ribot, J. C., Debarros, A., Mancio-Silva, L., Pamplona, A., and Silva-Santos, B. (2012). B7-CD28 costimulatory signals control the survival and proliferation of murine and human gammadelta T cells via IL-2 production. *J. Immunol.* 189, 1202–1208. doi: 10.4049/jimmunol.1200268

Ridge, J. P., Di Rosa, F., and Matzinger, P. (1998). A conditioned dendritic cell can be a temporal bridge between a CD4+ T-helper and a T-killer cell. *Nature* 393, 474–478. doi: 10.1038/30989

Riley, E. M., and Stewart, V. A. (2013). Immune mechanisms in malaria: new insights in vaccine development. *Nat. Med.* 19, 168–178. doi: 10.1038/nm.3083

Rivera-Correa, J., Guthmiller, J. J., Vijay, R., Fernandez-Arias, C., Pardo-Ruge, M. A., Gonzalez, S., et al. (2017). Plasmodium DNA-mediated TLR9 activation of T-bet (+) B cells contributes to autoimmune anaemia during malaria. *Nat. Commun.* 8, 1282. doi: 10.1038/s41467-017-01476-6

Rodig, N., Ryan, T., Allen, J. A., Pang, H., Grabie, N., Chernova, T., et al. (2003). Endothelial expression of PD-L1 and PD-L2 down-regulates CD8+ T cell activation and cytolysis. *Eur. J. Immunol.* 33, 3117–3126. doi: 10.1002/eji.200324270

Rodig, S. J., Shahsafaei, A., Li, B., and Dorfman, D. M. (2005). The CD45 isoform B220 identifies select subsets of human B cells and B-cell lymphoproliferative disorders. *Hum. Pathol.* 36, 51–57. doi: 10.1016/j.humpath.2004.10.016

Roestenberg, M., Mccall, M., Hopman, J., Wiersma, J., Luty, A. J., Van Gemert, G. J., et al. (2009). Protection against a malaria challenge by sporozoite inoculation. *N Engl. J. Med.* 361, 468–477. doi: 10.1056/NEJMoa0805832

Ross, R. (1896). Dr. Manson's Mosquito-Malaria Theory. *Ind. Med. Gaz.* 31, 264.

Rothbard, J. B., and Gefter, M. L. (1991). Interactions between immunogenic peptides and MHC proteins. *Annu. Rev. Immunol.* 9, 527–565. doi: 10.1146/annurev.iy.09.040191.002523

Rowe, J. A., Claessens, A., Corrigan, R. A., and Arman, M. (2009). Adhesion of Plasmodium falciparum-infected erythrocytes to human cells: molecular

mechanisms and therapeutic implications. *Expert Rev. Mol. Med.* 11, e16. doi: 10.1017/S1462399409001082

Ryg-Cornejo, V., Ioannidis, L. J., Ly, A., Chiu, C. Y., Tellier, J., Hill, D. L., et al. (2016). Severe Malaria Infections Impair Germinal Center Responses by Inhibiting T Follicular Helper Cell Differentiation. *Cell Rep.* 14, 68–81. doi: 10.1016/j.celrep.2015.12.006

Sabatos, C. A., Chakravarti, S., Cha, E., Schubart, A., Sanchez-Fueyo, A., Zheng, X. X., et al. (2003). Interaction of Tim-3 and Tim-3 ligand regulates T helper type 1 responses and induction of peripheral tolerance. *Nat. Immunol.* 4, 1102–1110. doi: 10.1038/ni988

Sabins, N. C., Chornoguz, O., Leander, K., Kaplan, F., Carter, R., Kinder, M., et al. (2017). TIM-3 Engagement Promotes Effector Memory T Cell Differentiation of Human Antigen-Specific CD8 T Cells by Activating mTORC1. *J. Immunol.* 199, 4091–4102. doi: 10.4049/jimmunol.1701030

Sakuishi, K., Jayaraman, P., Behar, S. M., Anderson, A. C., and Kuchroo, V. K. (2011). Emerging Tim-3 functions in antimicrobial and tumor immunity. *Trends Immunol.* 32, 345–349. doi: 10.1016/j.it.2011.05.003

Samji, T., Hong, S., and Means, R. E. (2014). The Membrane Associated RING-CH Proteins: A Family of E3 Ligases with Diverse Roles through the Cell. *Int. Sch. Res. Notices* 2014, 637295. doi: 10.1155/2014/637295

Sanchez-Torres, L., Rodriguez-Ropon, A., Aguilar-Medina, M., and Favila-Castillo, L. (2001). Mouse splenic CD4+ and CD8+ T cells undergo extensive apoptosis during a Plasmodium chabaudi chabaudi AS infection. *Parasite Immunol.* 23, 617–626. doi: 10.1046/j.1365-3024.2001.00422.x

Schoenberger, S. P., Toes, R. E., Van Der Voort, E. I., Offringa, R., and Melief, C. J. (1998). T-cell help for cytotoxic T lymphocytes is mediated by CD40-CD40L interactions. *Nature* 393, 480–483. doi: 10.1038/31002

Schofield, L., Ioannidis, L. J., Karl, S., Robinson, L. J., Tan, Q. Y., Poole, D. P., et al. (2017). Synergistic effect of IL-12 and IL-18 induces TIM3 regulation of gammadelta T cell function and decreases the risk of clinical malaria in children living in Papua New Guinea. *BMC Med.* 15, 114. doi: 10.1186/s12916-017-0883-8

Schroder, K., and Tschopp, J. (2010). The inflammasomes. *Cell* 140, 821–832. doi: 10.1016/j.cell.2010.01.040

Sedegah, M., Sim, B. K., Mason, C., Nutman, T., Malik, A., Roberts, C., et al. (1992). Naturally acquired CD8+ cytotoxic T lymphocytes against the Plasmodium falciparum circumsporozoite protein. *J. Immunol.* 149, 966–971.

Seder, R. A., Chang, L. J., Enama, M. E., Zephir, K. L., Sarwar, U. N., Gordon, I. J., et al. (2013). Protection against malaria by intravenous immunization with a nonreplicating sporozoite vaccine. *Science* 341, 1359–1365. doi: 10.1126/science.1241800

Segal, A. W. (2005). How neutrophils kill microbes. *Annu. Rev. Immunol.* 23, 197–223. doi: 10.1146/annurev.immunol.23.021704.115653

Sharma, S., Deoliveira, R. B., Kalantari, P., Parroche, P., Goutagny, N., Jiang, Z., et al. (2011). Innate immune recognition of an AT-rich stem-loop DNA motif in the Plasmodium falciparum genome. *Immunity* 35, 194–207. doi: 10.1016/j.immuni.2011.05.016

Sharpe, A. H., and Freeman, G. J. (2002). The B7-CD28 superfamily. *Nat. Rev. Immunol.* 2, 116–126. doi: 10.1038/nri727

Shear, H. L., Srinivasan, R., Nolan, T., and Ng, C. (1989). Role of IFN-gamma in lethal and nonlethal malaria in susceptible and resistant murine hosts. *J. Immunol.* 143, 2038–2044.

Shevach, E. M., and Stephens, G. L. (2006). The GITR-GITRL interaction: co-stimulation or contrasuppression of regulatory activity? *Nat. Rev. Immunol.* 6, 613–618. doi: 10.1038/nri1867

Shimizu, J., Yamazaki, S., Takahashi, T., Ishida, Y., and Sakaguchi, S. (2002). Stimulation of CD25(+)CD4(+) regulatory T cells through GITR breaks immunological self-tolerance. *Nat. Immunol.* 3, 135–142. doi: 10.1038/ni759

Shin, D. S., Jordan, A., Basu, S., Thomas, R. M., Bandyopadhyay, S., De Zoeten, E. F., et al. (2014). Regulatory T cells suppress CD4+ T cells through NFAT-dependent transcriptional mechanisms. *EMBO Rep.* 15, 991–999. doi: 10.15252/embr.201338233

Shio, M. T., Eisenbarth, S. C., Savaria, M., Vinet, A. F., Bellemare, M. J., Harder, K. W., et al. (2009). Malarial hemozoin activates the NLRP3 inflammasome through Lyn and Syk kinases. *PloS Pathog.* 5, e1000559. doi: 10.1371/journal.ppat.1000559

Sibilano, R., Gaudenzio, N., Degorter, M. K., Reber, L. L., Hernandez, J. D., Starkl, P. M., et al. (2016). A TNFRSF14-FcvarepsilonRI-mast cell pathway contributes to development of multiple features of asthma pathology in mice. *Nat. Commun.* 7, 13696. doi: 10.1038/ncomms13696

Silveira, E. L. V., Dominguez, M. R., and Soares, I. S. (2018). To B or Not to B: Understanding B Cell Responses in the Development of Malaria Infection. *Front. Immunol.* 9, 2961. doi: 10.3389/fimmu.2018.02961

Singh, B., and Daneshvar, C. (2013). Human infections and detection of Plasmodium knowlesi. *Clin. Microbiol. Rev.* 26, 165–184. doi: 10.1128/CMR.00079-12

Soroosh, P., Doherty, T. A., So, T., Mehta, A. K., Khorram, N., Norris, P. S., et al. (2011). Herpesvirus entry mediator (TNFRSF14) regulates the persistence of T helper memory cell populations. *J. Exp. Med.* 208, 797–809. doi: 10.1084/jem.20101562

Soto-Nieves, N., Puga, I., Abe, B. T., Bandyopadhyay, S., Baine, I., Rao, A., et al. (2009). Transcriptional complexes formed by NFAT dimers regulate the induction of T cell tolerance. *J. Exp. Med.* 206, 867–876. doi: 10.1084/jem.20082731

Soulat, D., and Bogdan, C. (2017). Function of Macrophage and Parasite Phosphatases in Leishmaniasis. *Front. Immunol.* 8, 1838. doi: 10.3389/fimmu.2017.01838

Sponaas, A. M., Freitas Do Rosario, A. P., Voisine, C., Mastelic, B., Thompson, J., Koernig, S., et al. (2009). Migrating monocytes recruited to the spleen play an important role in control of blood stage malaria. *Blood* 114, 5522–5531. doi: 10.1182/blood-2009-04-217489

Springer, A. L., Smith, L. M., Mackay, D. Q., Nelson, S. O., and Smith, J. D. (2004). Functional interdependence of the DBLbeta domain and c2 region for binding of the Plasmodium falciparum variant antigen to ICAM-1. *Mol. Biochem. Parasitol.* 137, 55–64. doi: 10.1016/j.molbiopara.2004.03.019

Starr, R., Willson, T. A., Viney, E. M., Murray, L. J., Rayner, J. R., Jenkins, B. J., et al. (1997). A family of cytokine-inducible inhibitors of signalling. *Nature* 387, 917–921. doi: 10.1038/43206

Starr, R., Metcalf, D., Elefanty, A. G., Brysha, M., Willson, T. A., Nicola, N. A., et al. (1998). Liver degeneration and lymphoid deficiencies in mice lacking suppressor of cytokine signaling-1. *Proc. Natl. Acad. Sci. U.S.A.* 95, 14395–14399. doi: 10.1073/pnas.95.24.14395

Stegmann, K. A., De Souza, J. B., and Riley, E. M. (2015). IL-18-induced expression of high-affinity IL-2R on murine NK cells is essential for NK-cell IFN-gamma production during murine Plasmodium yoelii infection. *Eur. J. Immunol.* 45, 3431–3440. doi: 10.1002/eji.201546018

Steinberg, M. W., Huang, Y., Wang-Zhu, Y., Ware, C. F., Cheroutre, H., and Kronenberg, M. (2013). BTLA interaction with HVEM expressed on CD8(+) T cells promotes survival and memory generation in response to a bacterial infection. *PloS One* 8, e77992. doi: 10.1371/journal.pone.0077992

Stevenson, M. M., and Riley, E. M. (2004). Innate immunity to malaria. *Nat. Rev. Immunol.* 4, 169–180. doi: 10.1038/nri1311

Stevenson, M. M., Tam, M. F., Wolf, S. F., and Sher, A. (1995). IL-12-induced protection against blood-stage Plasmodium chabaudi AS requires IFN-gamma and TNF-alpha and occurs via a nitric oxide-dependent mechanism. *J. Immunol.* 155, 2545–2556.

Stirnweiss, A., Ksienzyk, A., Klages, K., Rand, U., Grashoff, M., Hauser, H., et al. (2010). IFN regulatory factor-1 bypasses IFN-mediated antiviral effects through viperin gene induction. *J. Immunol.* 184, 5179–5185. doi: 10.4049/jimmunol.0902264

Stone, W. J. R., Campo, J. J., Ouedraogo, A. L., Meerstein-Kessel, L., Morlais, I., Da, D., et al. (2018). Unravelling the immune signature of Plasmodium falciparum transmission-reducing immunity. *Nat. Commun.* 9, 558. doi: 10.1038/s41467-017-02646-2

Storti-Melo, L. M., Da Costa, D. R., Souza-Neiras, W. C., Cassiano, G. C., Couto, V. S., Povoa, M. M., et al. (2012). Influence of HLA-DRB-1 alleles on the production of antibody against CSP, MSP-1, AMA-1, and DBP in Brazilian individuals naturally infected with Plasmodium vivax. *Acta Trop.* 121, 152–155. doi: 10.1016/j.actatropica.2011.10.009

Sturm, A., Amino, R., Van De Sand, C., Regen, T., Retzlaff, S., Rennenberg, A., et al. (2006). Manipulation of host hepatocytes by the malaria parasite for delivery into liver sinusoids. *Science* 313, 1287–1290. doi: 10.1126/science.1129720

Su, Z., and Stevenson, M. M. (2000). Central role of endogenous gamma interferon in protective immunity against blood-stage Plasmodium chabaudi AS infection. *Infect. Immun.* 68, 4399–4406. doi: 10.1128/IAI.68.8.4399-4406.2000

Subramaniam, K. S., Spaulding, E., Ivan, E., Mutimura, E., Kim, R. S., Liu, X., et al. (2015). The T-Cell Inhibitory Molecule Butyrophilin-Like 2 Is Up-regulated in Mild Plasmodium falciparum Infection and Is Protective During Experimental Cerebral Malaria. *J. Infect. Dis.* 212, 1322–1331. doi: 10.1093/infdis/jiv217

Sun, Y., Brown, N. K., Ruddy, M. J., Miller, M. L., Lee, Y., Wang, Y., et al. (2009). B and T lymphocyte attenuator tempers early infection immunity. *J. Immunol.* 183, 1946–1951. doi: 10.4049/jimmunol.0801866

Surls, J., Nazarov-Stoica, C., Kehl, M., Casares, S., and Brumeanu, T. D. (2010). Differential effect of CD4+Foxp3+ T-regulatory cells on the B and T helper cell responses to influenza virus vaccination. *Vaccine* 28, 7319–7330. doi: 10.1016/j.vaccine.2010.08.074

Swanson, R. M., Gavin, M. A., Escobar, S. S., Rottman, J. B., Lipsky, B. P., Dube, S., et al. (2013). Butyrophilin-like 2 modulates B7 costimulation to induce Foxp3 expression and regulatory T cell development in mature T cells. *J. Immunol.* 190, 2027–2035. doi: 10.4049/jimmunol.1201760

Takeuchi, O., and Akira, S. (2010). Pattern recognition receptors and inflammation. *Cell* 140, 805–820. doi: 10.1016/j.cell.2010.01.022

Tamura, T., Kimura, K., Yui, K., and Yoshida, S. (2015). Reduction of conventional dendritic cells during Plasmodium infection is dependent on activation induced cell death by type I and II interferons. *Exp. Parasitol.* 159, 127–135. doi: 10.1016/j.exppara.2015.09.010

Tavares, J., Formaglio, P., Thiberge, S., Mordelet, E., Van Rooijen, N., Medvinsky, A., et al. (2013). Role of host cell traversal by the malaria sporozoite during liver infection. *J. Exp. Med.* 210, 905–915. doi: 10.1084/jem.20121130

Taylor, M. W., and Feng, G. S. (1991). Relationship between interferon-gamma, indoleamine 2,3-dioxygenase, and tryptophan catabolism. *FASEB J.* 5, 2516–2522. doi: 10.1096/fasebj.5.11.1907934

Thaiss, C. A., Levy, M., Itav, S., and Elinav, E. (2016). Integration of Innate Immune Signaling. *Trends Immunol.* 37, 84–101. doi: 10.1016/j.it.2015.12.003

Tian, X., Lin, Y., Cui, C., Su, M., and Lai, L. (2019). BTNL2-Ig Protein Attenuates Type 1 Diabetes in Non-Obese Diabetic (NOD) Mice. *Adv. Healthc. Mater.* 8, e1800987. doi: 10.1002/adhm.201800987

Torcia, M. G., Santarlasci, V., Cosmi, L., Clemente, A., Maggi, L., Mangano, V. D., et al. (2008). Functional deficit of T regulatory cells in Fulani, an ethnic group with low susceptibility to Plasmodium falciparum malaria. *Proc. Natl. Acad. Sci. U.S.A.* 105, 646–651. doi: 10.1073/pnas.0709969105

Torgler, R., Bongfen, S. E., Romero, J. C., Tardivel, A., Thome, M., and Corradin, G. (2008). Sporozoite-mediated hepatocyte wounding limits Plasmodium parasite development via MyD88-mediated NF-kappa B activation and inducible NO synthase expression. *J. Immunol.* 180, 3990–3999. doi: 10.4049/jimmunol.180.6.3990

Tweedell, R., Tao, D., and Dinglasan, R. R. (2015). The cellular and proteomic response of primary and immortalized murine Kupffer cells following immune stimulation diverges from that of monocyte-derived macrophages. *Proteomics* 15, 545–553. doi: 10.1002/pmic.201400216

Tweedell, R. E., Qi, L., Sun, Z., and Dinglasan, R. R. (2018). Kupffer Cells Survive Plasmodium berghei Sporozoite Exposure and Respond with a Rapid Cytokine Release. *Pathogens* 7, 91. doi: 10.3390/pathogens7040091

Ubillos, I., Campo, J. J., Requena, P., Ome-Kaius, M., Hanieh, S., Rose, H., et al. (2017). Chronic Exposure to Malaria Is Associated with Inhibitory and Activation Markers on Atypical Memory B Cells and Marginal Zone-Like B Cells. *Front. Immunol.* 8, 966. doi: 10.3389/fimmu.2017.00966

Van Kooten, C., and Banchereau, J. (2000). CD40-CD40 ligand. *J. Leukoc. Biol.* 67, 2–17. doi: 10.1002/jlb.67.1.2

Vendel, A. C., Calemine-Fenaux, J., Izrael-Tomasevic, A., Chauhan, V., Arnott, D., and Eaton, D. L. (2009). B and T lymphocyte attenuator regulates B cell receptor signaling by targeting Syk and BLNK. *J. Immunol.* 182, 1509–1517. doi: 10.4049/jimmunol.182.3.1509

Vijay, R., Guthmiller, J. J., Sturtz, A. J., Surette, F. A., Rogers, K. J., Sompallae, R. R., et al. (2020). Infection-induced plasmablasts are a nutrient sink that impairs humoral immunity to malaria. *Nat. Immunol.* 21, 790–801. doi: 10.1038/s41590-020-0678-5

Villegas-Mendez, A., Inkson, C. A., Shaw, T. N., Strangward, P., and Couper, K. N. (2016). Long-Lived CD4+IFN-gamma+ T Cells rather than Short-Lived CD4+IFN-gamma+IL-10+ T Cells Initiate Rapid IL-10 Production To Suppress Anamnestic T Cell Responses during Secondary Malaria Infection. *J. Immunol.* 197, 3152–3164. doi: 10.4049/jimmunol.1600968

Vinetz, J. M., Kumar, S., Good, M. F., Fowlkes, B. J., Berzofsky, J. A., and Miller, L. H. (1990). Adoptive transfer of CD8+ T cells from immune animals does not transfer immunity to blood stage Plasmodium yoelii malaria. *J. Immunol.* 144, 1069–1074.

Vinuesa, C. G., and Cyster, J. G. (2011). How T cells earn the follicular rite of passage. *Immunity* 35, 671–680. doi: 10.1016/j.immuni.2011.11.001

Wahlgren, M., Goel, S., and Akhouri, R. R. (2017). Variant surface antigens of Plasmodium falciparum and their roles in severe malaria. *Nat. Rev. Microbiol.* 15, 479–491. doi: 10.1038/nrmicro.2017.47

Walker, J. A., and Mckenzie, A. N. J. (2018). TH2 cell development and function. *Nat. Rev. Immunol.* 18, 121–133. doi: 10.1038/nri.2017.118

Walker, L. S., Gulbranson-Judge, A., Flynn, S., Brocker, T., Raykundalia, C., Goodall, M., et al. (1999). Compromised OX40 function in CD28-deficient mice is linked with failure to develop CXC chemokine receptor 5-positive CD4 cells and germinal centers. *J. Exp. Med.* 190, 1115–1122. doi: 10.1084/jem.190.8.1115

Walther, M., Woodruff, J., Edele, F., Jeffries, D., Tongren, J. E., King, E., et al. (2006). Innate immune responses to human malaria: heterogeneous cytokine responses to blood-stage Plasmodium falciparum correlate with parasitological and clinical outcomes. *J. Immunol.* 177, 5736–5745. doi: 10.4049/jimmunol.177.8.5736

Wei, L., Laurence, A., Elias, K. M., and O'shea, J. J. (2007). IL-21 is produced by Th17 cells and drives IL-17 production in a STAT3-dependent manner. *J. Biol. Chem.* 282, 34605–34610. doi: 10.1074/jbc.M705100200

Weiss, G. E., Crompton, P. D., Li, S., Walsh, L. A., Moir, S., Traore, B., et al. (2009). Atypical memory B cells are greatly expanded in individuals living in a malaria-endemic area. *J. Immunol.* 183, 2176–2182. doi: 10.4049/jimmunol.0901297

Weiss, G. E., Traore, B., Kayentao, K., Ongoiba, A., Doumbo, S., Doumtabe, D., et al. (2010). The Plasmodium falciparum-specific human memory B cell compartment expands gradually with repeated malaria infections. *PloS Pathog.* 6, e1000912. doi: 10.1371/journal.ppat.1000912

White, N. J., Turner, G. D., Medana, I. M., Dondorp, A. M., and Day, N. P. (2010). The murine cerebral malaria phenomenon. *Trends Parasitol.* 26, 11–15. doi: 10.1016/j.pt.2009.10.007

WHO. *World Malaria Report 2019*. Available at: https://www.who.int/publications/i/item/9789241565721.

Wijayalath, W., Danner, R., Kleschenko, Y., Majji, S., Villasante, E. F., Richie, T. L., et al. (2014). HLA class II (DR0401) molecules induce Foxp3+ regulatory T cell suppression of B cells in Plasmodium yoelii strain 17XNL malaria. *Infect. Immun.* 82, 286–297. doi: 10.1128/IAI.00272-13

Wu, J., Tian, L., Yu, X., Pattaradilokrat, S., Li, J., Wang, M., et al. (2014). Strain-specific innate immune signaling pathways determine malaria parasitemia dynamics and host mortality. *Proc. Natl. Acad. Sci. U.S.A.* 111, E511–E520. doi: 10.1073/pnas.1316467111

Wu, J., Xia, L., Yao, X., Yu, X., Tumas, K. C., Sun, W., et al. (2020). The E3 ubiquitin ligase MARCH1 regulates antimalaria immunity through interferon signaling and T cell activation. *Proc. Natl. Acad. Sci. U.S.A.* 117, 16567–16578. doi: 10.1073/pnas.2004332117

Wykes, M. N., and Good, M. F. (2008). What really happens to dendritic cells during malaria? *Nat. Rev. Microbiol.* 6, 864–870. doi: 10.1038/nrmicro1988

Wykes, M. N., Liu, X. Q., Beattie, L., Stanisic, D. I., Stacey, K. J., Smyth, M. J., et al. (2007). Plasmodium strain determines dendritic cell function essential for survival from malaria. *PloS Pathog.* 3, e96. doi: 10.1371/journal.ppat.0030096

Xia, L., Wu, J., Pattaradilokrat, S., Tumas, K., He, X., Peng, Y. C., et al. (2018). Detection of host pathways universally inhibited after Plasmodium yoelii infection for immune intervention. *Sci. Rep.* 8, 15280. doi: 10.1038/s41598-018-33599-1

Yagi, H., Nomura, T., Nakamura, K., Yamazaki, S., Kitawaki, T., Hori, S., et al. (2004). Crucial role of FOXP3 in the development and function of human CD25+CD4+ regulatory T cells. *Int. Immunol.* 16, 1643–1656. doi: 10.1093/intimm/dxh165

Yao, X., Wu, J., Lin, M., Sun, W., He, X., Gowda, C., et al. (2016). Increased CD40 Expression Enhances Early STING-Mediated Type I Interferon Response and Host Survival in a Rodent Malaria Model. *PloS Pathog.* 12, e1005930. doi: 10.1371/journal.ppat.1005930

Young, M. R., and Colburn, N. H. (2006). Fra-1 a target for cancer prevention or intervention. *Gene* 379, 1–11. doi: 10.1016/j.gene.2006.05.001

Yu, Y., and Hayward, G. S. (2010). The ubiquitin E3 ligase RAUL negatively regulates type i interferon through ubiquitination of the transcription factors IRF7 and IRF3. *Immunity* 33, 863–877. doi: 10.1016/j.immuni.2010.11.027

Yu, X., Harden, K., Gonzalez, L. C., Francesco, M., Chiang, E., Irving, B., et al. (2009). The surface protein TIGIT suppresses T cell activation by promoting the generation of mature immunoregulatory dendritic cells. *Nat. Immunol.* 10, 48–57. doi: 10.1038/ni.1674

Yu, X., Cai, B., Wang, M., Tan, P., Ding, X., Wu, J., et al. (2016). Cross-Regulation of Two Type I Interferon Signaling Pathways in Plasmacytoid Dendritic Cells Controls Anti-malaria Immunity and Host Mortality. *Immunity* 45, 1093–1107. doi: 10.1016/j.immuni.2016.10.001

Yu, X., Du, Y., Cai, C., Cai, B., Zhu, M., Xing, C., et al. (2018). Inflammasome activation negatively regulates MyD88-IRF7 type I IFN signaling and anti-malaria immunity. *Nat. Commun.* 9, 4964. doi: 10.1038/s41467-018-07384-7

Zander, R. A., Obeng-Adjei, N., Guthmiller, J. J., Kulu, D. I., Li, J., Ongoiba, A., et al. (2015). PD-1 Co-inhibitory and OX40 Co-stimulatory Crosstalk Regulates Helper T Cell Differentiation and Anti-Plasmodium Humoral Immunity. *Cell Host. Microbe* 17, 628–641. doi: 10.1016/j.chom.2015.03.007

Zander, R. A., Guthmiller, J. J., Graham, A. C., Pope, R. L., Burke, B. E., Carr, D. J., et al. (2016). Type I Interferons Induce T Regulatory 1 Responses and Restrict Humoral Immunity during Experimental Malaria. *PloS Pathog.* 12, e1005945. doi: 10.1371/journal.ppat.1005945

Zander, R. A., Vijay, R., Pack, A. D., Guthmiller, J. J., Graham, A. C., Lindner, S. E., et al. (2017). Th1-like Plasmodium-Specific Memory CD4(+) T Cells Support Humoral Immunity. *Cell Rep.* 21, 1839–1852. doi: 10.1016/j.celrep.2017.10.077

Zhang, Y., Jiang, N., Zhang, T., Chen, R., Feng, Y., Sang, X., et al. (2019a). Tim-3 signaling blockade with alpha-lactose induces compensatory TIGIT expression in Plasmodium berghei ANKA-infected mice. *Parasit. Vectors* 12, 534. doi: 10.1186/s13071-019-3788-x

Zhang, Y., Tada, T., Ozono, S., Yao, W., Tanaka, M., Yamaoka, S., et al. (2019b). Membrane-associated RING-CH (MARCH) 1 and 2 are MARCH family members that inhibit HIV-1 infection. *J. Biol. Chem.* 294, 3397–3405. doi: 10.1074/jbc.AC118.005907

Zhu, J., Krishnegowda, G., and Gowda, D. C. (2005). Induction of proinflammatory responses in macrophages by the glycosylphosphatidylinositols of Plasmodium falciparum: the requirement of extracellular signal-regulated kinase, p38, c-Jun N-terminal kinase and NF-kappaB pathways for the expression of proinflammatory cytokines and nitric oxide. *J. Biol. Chem.* 280, 8617–8627. doi: 10.1074/jbc.M413539200

Conflict of Interest: The authors declare that the research was conducted in the absence of any commercial or financial relationships that could be construed as a potential conflict of interest.

frontiers in Cellular and Infection Microbiology

ORIGINAL RESEARCH
published: 23 February 2021
doi: 10.3389/fcimb.2021.631545

Full-Length Transcriptome Analysis of *Plasmodium falciparum* by Single-Molecule Long-Read Sequencing

Mengquan Yang[1,2,3†], Xiaomin Shang[1†], Yiqing Zhou[3], Changhong Wang[1], Guiying Wei[1], Jianxia Tang[4], Meihua Zhang[4], Yaobao Liu[4], Jun Cao[4,5] and Qingfeng Zhang[1*]*

[1] Research Center for Translational Medicine, Key Laboratory of Arrhythmias of the Ministry of Education of China, East Hospital, Tongji University School of Medicine, Shanghai, China, [2] State Key Laboratory of Drug Research, Shanghai Institute of Materia Medica, Chinese Academy of Sciences, Shanghai, China, [3] CAS Key Laboratory of Synthetic Biology, CAS Center for Excellence in Molecular Plant Sciences, Chinese Academy of Sciences, Shanghai, China, [4] National Health Commission Key Laboratory of Parasitic Disease Control and Prevention, Jiangsu Provincial Key Laboratory on Parasite and Vector Control Technology, Jiangsu Institute of Parasitic Diseases, Wuxi, China, [5] Center for Global Health, School of Public Health, Nanjing Medical University, Nanjing, China

OPEN ACCESS

Edited by:
Xiaojun Chen,
Nanjing Medical University, China

Reviewed by:
Feng Tan,
Wenzhou Medical University, China
Bang Shen,
Huazhong Agricultural University, China

***Correspondence:**
Qingfeng Zhang
qfzhang@tongji.edu.cn
Jun Cao
caojuncn@hotmail.com

[†]These authors have contributed equally to this work

Specialty section:
This article was submitted to Parasite and Host, a section of the journal Frontiers in Cellular and Infection Microbiology

Received: 20 November 2020
Accepted: 05 January 2021
Published: 23 February 2021

Citation:
Yang M, Shang X, Zhou Y, Wang C, Wei G, Tang J, Zhang M, Liu Y, Cao J and Zhang Q (2021) Full-Length Transcriptome Analysis of Plasmodium falciparum by Single-Molecule Long-Read Sequencing. Front. Cell. Infect. Microbiol. 11:631545. doi: 10.3389/fcimb.2021.631545

Malaria, an infectious disease caused by *Plasmodium* parasites, still accounts for amounts of deaths annually in last decades. Despite the significance of *Plasmodium falciparum* as a model organism of malaria parasites, our understanding of gene expression of this parasite remains largely elusive since lots of progress on its genome and transcriptome are based on assembly with short sequencing reads. Herein, we report the new version of transcriptome dataset containing all full-length transcripts over the whole asexual blood stages by adopting a full-length sequencing approach with optimized experimental conditions of cDNA library preparation. We have identified a total of 393 alternative splicing (AS) events, 3,623 long non-coding RNAs (lncRNAs), 1,555 alternative polyadenylation (APA) events, 57 transcription factors (TF), 1,721 fusion transcripts in *P. falciparum*. Furthermore, the shotgun proteome was performed to validate the full-length transcriptome of *P. falciparum*. More importantly, integration of full-length transcriptomic and proteomic data identified 160 novel small proteins in lncRNA regions. Collectively, this full-length transcriptome dataset with high quality and accuracy and the shotgun proteome analyses shed light on the complex gene expression in malaria parasites and provide a valuable resource for related functional and mechanistic researches on *P. falciparum* genes.

Keywords: *Plasmodium falciparum*, small protein, long non-coding RNA, alternative splicing, full-length RNA-seq

Abbreviations: AS, alternative splicing; APA, alternative polyadenylation; LncRNA, long non-coding RNA; TF, transcription factor; NR, NCBI non-redundant protein sequences; NT, NCBI non-redundant nucleotide sequences; Pfam, protein family; KOG/COG, Clusters of Orthologous Groups of proteins; Swiss-Prot, SWISS-PROT Protein Sequence Data Bank; KO, KEGG Ortholog database; GO, Gene Ontology; NCBI, National Center for Biotechnology Information; iProx, Integrated Proteome Resources.

INTRODUCTION

Malaria is still a major threat to public health globally caused by *Plasmodium* genus with the occurrence of artemisinin resistance (van der Pluijm et al., 2020). *Plasmodium*, especially *P. falciparum*, is one of the deadliest pathogens that causes malaria in humans which is a disease transmitted by *Anopheles* mosquitoes. Therefore, potential mechanistic regulation pathways should be researched urgently (White et al., 2014). *P. falciparum* as a research model specie of malaria disease was widely studied in a long period, however, the infection and resistance mechanism are still unclear entirely, which attributes to the great adaptation ability of *P. falciparum* to evade host immunity and develop drug resistance. Further understanding of *P. falciparum* will give us clues on discovering the new therapy to cure malaria.

In the last two decades, second-generation sequencing approaches were widely used in genome and transcriptome sequencing which assisted us furtherly understanding the molecular mechanism and function of unknown genes. However, sequences obtained by second-generation short reads assembly always lead to errors so that we could not obtain the full-length transcripts directly and characterize the gene structure accurately, such as the alternative splicing events. RNA-seq as a routine approach was widely used in research of gene discovery and biological functions. Recently, the full-length RNA-seq platform showed advantages in biological research, especially in gene structure identification, gradually taking the place of short-read RNA sequencing in transcriptome profiling.

The understanding of the infection was hindered by high variable and repetitive sequences in the *P. falciparum* genome in previous genetic studies by using short-read sequencing platform. As known, gene structural variations (alternative splicing, alternative polyadenylation, lncRNA and gene fusion, etc.) in transcriptional process resulted in transcriptome complexity which affects the gene function and gene expression regulation (Ma et al., 2018). Gene structural variations were proved to drive genomic diversity in *P. falciparum* (Miles et al., 2016). Besides, mRNA polyadenylation is a universal phenomenon in the transcriptional process in eukaryotes. For the understanding of the mRNA polyadenylation, the high throughout sequencing study of *Sarcocystis neurona*, a unicellular parasite, was performed and it indicated that alternative polyadenylation (APA) is a common phenomenon in unicellular parasites that has the potential to impact growth and development.

Recently, it was revealed that non-coding RNAs play an important role in biological processes and gene function regulation in Apicomplexan parasites by experimental and sequencing technologies (Li et al., 2020). As for *Plasmodium* species, various strategies were carried out for non-coding RNA characterization (Mourier et al., 2008; Raabe et al., 2010; Liao et al., 2014; Siegel et al., 2014; Broadbent et al., 2015; Chappell et al., 2020). Gene fusion is a common phenomenon which was overlooked for a long time. This phenomenon was confirmed with the development of long reads sequencing approach (Rhoads and Au, 2015). For decades, open reading frames (ORF, > 100 codons) were considered as coding sequences which can be translated into proteins (Cabrera-Quio et al., 2016; Yin et al., 2019). However, amounts of small open reading frames (<100 codons) were also produced in the transcriptional stages which were dismissed by current bioinformatic algorithms and always considered meaningless because known functional proteins longer than 100 amino acids (Frith et al., 2006; Ladoukakis et al., 2011). The first research on sORFs were carried out on baker's yeast, revealing 299 sORFs not annotated before (Kastenmayer et al., 2006). Later, sORFs with high potential of encoding microproteins were found in kinds of organisms like bacteria, insects, plants, and human (Cabrera-Quio et al., 2016; Hsu and Benfey, 2018; Fesenko et al., 2019; Miravet-Verde et al., 2019; Ruiz-Orera and Alba, 2019; Segonzac and Monaghan, 2019; Orr et al., 2020; Patraquim et al., 2020). Among them, it was reported that one small peptide that regulates metabolism and reduces obesity (Lee et al., 2015). Based on these research results, we predicted that sORFs or small proteins probably play an important role in growth development and infection processes in *P. falciparum* which were ignored for a long period. To further understand the functional genes and exploit the infection mechanism of *P. falciparum* for drug discovery and new therapy development, it is necessary to obtain the full-length transcriptional isoforms of its genes and characterize the gene structures.

Defining all the transcripts expressing in the whole asexual blood stages of *P. falciparum* with full length would avoid the assembly errors and assist significantly in understanding the malaria infection process. Herein, we performed the full-length transcriptome sequencing to characterize the full-length transcripts and uncovered alternative splicing, long non-coding RNA, alternative polyadenylation (APA) sites. Besides, combining the full-length transcriptome and the shotgun proteome approaches were used to validate the small proteins coded by CDS in long non-coding RNA. In this process, a modified cDNA library construction procedure for TA-rich species and mixtures of samples at six time points in the whole asexual blood stages were applied into *P. falciparum* resequencing. This work broadens our knowledge far beyond the existing resources in terms of accuracy (full-length sequencing without assembly). Collectively, we not only systematically characterize the complexity of the transcriptome and proteome but also provide a valuable resource for investigating the infection mechanisms of *Plasmodium* parasites.

MATERIALS AND METHODS

Parasites Culture and Collection

P. falciparum 3D7 strains were used in this study. *P. falciparum* parasites were grown in 5% O^+ human erythrocytes in RPMI1640/25 mM Hepes supplemented with 0.5% Albumax I, and were cultured *in vitro* at 37°C under a gaseous mixture of 5% O_2, 5% CO_2, and 90% N_2. Parasites were repeatedly synchronized with 5% sorbitol treatment in ring stage during two consecutive lifecycles when grown at 3–5% parasitemia and then maintained culturing in 175 cm^2 flasks. After reinvasion, the parasites were started to collect mainly in ring stage when grown at 5–8% parasitemia and then collected by every 8 h. We collected six time-point (8, 16, 24, 32, 40, and 48 hpi) samples

with a time window of ~8 h which may cover all stages of parasites in an intraerythrocytic lifecycle. Two biological replicates of pelleted parasites were stored in TRIzol reagent (Invitrogen) at −80°C prior to RNA isolation. Meanwhile, aliquots of the mixed samples were also used for total protein extraction. The proteome extracted from *P. falciparum* mixtures of two biological replicates were used for proteome profiling.

RNA Preparation and cDNA Library Construction

Total RNA from six time-points (8, 16, 24, 32, 40, and 48 hpi) were prepared by treated in TRIzol reagent and processing according to the manufacturer's instruction of Zymo RNA Extract kit. To remove genomic DNA, each sample was treated with RNase-free DNase I digestion for 15 min at room temperature and eluted with 50 ul RNase-free water (Invitrogen). Each total RNA was quantified and assessed using an Agilent Bioanalyzer 2100, and then the six RNA samples were pooled into one sample with equal amounts for further library construction. The full-length cDNA was synthesized and library amplified by using the SMARTer PCR cDNA Synthesis Kit (Clontech, CA, USA). After purification, the BluePippin Size Selection System (Sage Science, MA, USA) was used for selection and the cDNA library was constructed by using SMARTbell Template Prep kit (Clontech, CA, USA). The cDNA library was sequenced on PacBio Sequel platform. To obtain the sequencing data with better quality, the optimized method for TA-rich species was applied: an AT-rich optimized KAPA protocol using KAPA HiFi HotStart ready mix (KAPA Biosystems, KM2602) with the following PCR program: 95°C for 5 min; 14 cycles of 95°C for 10 s, 65°C for 1 min; 65°C for 5 min to reduce the bias in the process of cDNA library construction, which improved the coverage of RNA-seq notably.

PacBio Sequencing Processing and Transcriptome Analysis Pipeline

Sequencing data were processed using the SMRTlink 5.0 software. Circular consensus sequence (CCS) were generated from subread BAM files, parameters: min_length 200, max_drop_fraction 0.8, no_polish TRUE, min_passes 1, min_zscore -9999, min_passes 1. Min_predicted_accuracy 0.8, max_length 18000. CCS.BAM files were output, which were then classified into full length (as defined by reads both with 5' primer, 3' primer, and a polyA tail) and non-full length reads using pbclassify.py script, ignore polyA false, minSeq Length 200. Non-full length and full-length fasta files produced were then fed into the cluster step, which dose isoform-level clustering (ICE), followed by final Arrow polishing, hq_quiver_min_accuracy 0.99, bin_by_primer false, bin_size_kb 1, qv_trim_5p 100, qv_trim_3p 30. The misread of nucleobases are much higher in PacBio sequencing reads than in shorter Illumina sequencing reads and can lead to incorrectly detected gene structures. The sequencing errors in the consensus reads were corrected using the Illumina RNA-seq data with the software LoRDEC (Salmela and Rivals, 2014). The corrected consensus reads were then aligned to reference genome using GMAP with parameters: –no-chimeras –cross-species –expand-offsets 1 –B 5 –K 50000 –f samse –n 1 against reference genome (Wu and Watanabe, 2005). The GMAP output bam format file and gff/gtf format genome annotation file were used for gene and transcript determination. All transcripts were mapped on reference genome of *P. falciparum* and unmapped transcripts without overlapping were considered as novel genes. Novel gene transcripts function were annotated based on the following databases: NR, NT, Pfam, KOG/COG, Swiss-Prot, KO, and GO database.

Characterization of Alternative Splicing Events

SUPPA was used to calculate expression weight (Psi) of alternative splice based on transcript TPM values (Alamancos et al., 2015). Differential alternative splice of two conditions was performed using significance test of Psi. The dpsi value was adjusted using the Mann-Whitney U test method. The absolute dpsi value of 0.1 and p-value of 0.05 were set as the threshold for significantly differential alternative splice. Alternative splicing events were classified into SE (skipped exon), MX (mutually exclusive exon), A5 (alternative 5' splice site), A3 (alternative 3' splice site), RI (retained intron), AF (alternative first exon), AL (alternative last exon).

Alternative Polyadenylation Sites Detection and Transcription Factor Identification

Alternative polyadenylation (APA) sites detection was performed using TAPIS pipeline (Abdel-Ghany et al., 2016). Transcription factors (TFs) were identified and assigned into different families by HMMER 3.0 (Eddy, 2009).

Gene Fusion Characterization

Fusion transcripts were determined as transcripts mapping to two or more long-distance range genes (Weirather et al., 2015). All the consensus sequences were used for fusion transcripts identification and the criteria used in the process was as follows: (a) a full-length transcript must be mapped to two or more loci on the *P. falciparum* genome; (b) minimum coverage for each locus is 10% of the full-length transcripts; (c) > = 99% total coverage of the full-length transcript was mapped on the *P. falciparum* genome; (d) the distance between each locus mapped on the *P. falciparum* genome is more than 100 kb.

LncRNA Identification From PacBio Sequences

We used CNCI (Coding-Non-Coding-Index), CPC (Coding Potential Calculator), Pfam-scan, and PLEK four tools to predict the coding potential of transcripts. We use CNCI with default parameters (Sun et al., 2013). We used the NCBI eukaryotes' protein database and set the e-value "1e-10" in CPC analysis (Kong et al., 2007). Pfam searches used default parameters of –E 0.001 –domE 0.001 (Finn et al., 2016). PLEK used parameters of –minlength 200 (Li et al., 2014). Transcripts predicted with coding potential by either/all of the three tools above were filtered out, and those without coding potential were our candidate set of lncRNAs.

Global Proteomic Profiling of *Plasmodium falciparum*

P. falciparum cultures in different growth stages (8, 16, 24, 32, 40, and 48 hpi) were collected. The proteomics experiment was performed in biological duplicates. Then the cultures were washed with PBS, harvested and lysed with SDT lysis buffer (100 mM Tris-HCl pH 7.6, 4% SDS, 0.1 M DTT) at 95°C for 3 min. The lysates were centrifuged at 14,000 g for 15 min and the supernatants were collected. Each of 300 μg of protein was alkylated with 55 mM of iodoacetamide and subjected to in-solution tryptic digestion utilizing the FASP (filter aided sample preparation) protocol (Wisniewski et al., 2009). The digested peptides were combined and fractionated by high-pH reversed-phase chromatography on a 1-mm Xbridge column (Waters), and eight fractions were collected. Each fraction was evaporated to dryness on a SpeedVac and dried peptides were resuspended in 15 μl of ddH2O containing 0.1% formic acid with sonication for subsequent MS analysis. A volume of 1 μl of each sample was desalted by loading on a Thermo C18 PepMap100 precolumn (300 μm × 5 mm) and eluted on a Thermo Acclaim PepMap RSLC analytical column (75 μm × 15 cm). Mobile phase A (0.1% formic acid in H2O) and mobile phase B (0.1% formic acid in acetonitrile) were used to establish the 120 min gradient comprised of 85 min of 4–30% B, 15 min of 30–50% B, and 5 min of 90% B, followed by re-equilibrating at 4% B for 15 min. The flow rate was 0.3 μl/min. Peptides were then analyzed on Thermo Orbitrap Fusion Lumos proteomic mass spectrometer (Thermo Scientific) in a data-dependent manner, with automatic switching between MS and MS/MS scans using a cycle time 3 s. MS spectra were acquired at a resolution of 120,000 with AGC target value of 4 × 105 ions or a maximum integration time of 50 ms. The scan range was limited from 375 to 1,500 m/z. Peptide fragmentation was performed *via* high energy collision dissociation (HCD) with the energy set at 38 NCE. The MS/MS spectra were acquired at a resolution of 50,000 with AGC target value of 1×10^5 ions or a maximum integration time of 105 ms. The fixed first m/z was 120, and the isolation window was 0.7 m/z.

Protein identification and quantification were performed using Proteome Discoverer 2.1 software (Thermo Scientific). Peptide sequences (and hence protein identity) were searched against the protein database constructed by using the PacBio sequencing and the database of small protein (<100 amino acids) from identified lncRNA with the acquired fragmentation pattern by SEQUEST HT algorithm. The precursor mass tolerance was set to 10 ppm and fragment ion mass tolerance to 0.02 Da. One missed cleavage site of trypsin was allowed. Oxidation (M) was used as variable modifications. All spectra were searched against protein database using a target false discovery rate (FDR) of 1%. The proteins identified in both channels were additionally filtered by at least two spectral counts and one unique peptide in each experimental replicate. Protein ratios were calculated as the median of peptide with S/N ratio higher than 10 of a protein.

Proteome Analysis and Potential Small Proteins Validation

For global profiling of *P. falciparum* and validating the transcripts identified by full-length transcriptome sequencing, the transcripts with open reading frames (ORF, >300 bp) were translated to construct the protein database. Firstly, all the proteins characterized by liquid chromatography-mass spectrometry were discovered by searching against the protein datasets. And then, these sequences were annotated by KEGG database (Kyoto encyclopedia of genes and genomes) by using BLAST and classified into different KEGG pathway.

To identify small ORFs with high coding potential, the long non-coding RNA (lncRNA) sequences were used to predict the small proteins by selecting the sequences with small open reading frames (ORF, <300 bp). It is considered that these small open reading frames were likely to be translated into small proteins. And then, all of the small ORFs were translated as the small protein (<100 amino acids) database. For small protein detection and validation, these small proteins were validated by using the peptides searching against the small protein database.

Gene Structure Visualization

The structures of chromosomes, alternative splicing sites, alternative polyadenylation, novel transcripts distribution, novel genes distribution, lncRNA density, and gene fusion were visualized by Circos (Krzywinski et al., 2009).

RESULTS

Sample Preparation and PacBio Sequencing

To further understand the mechanism and discover the novel genes in *P. falciparum*, the study was designed to perform the full-length transcriptome sequencing by collecting the samples at six time points over the whole asexual blood stages (6, 12, 18, 24, 36, and 48 h). The time window of each sample is 6 h. Two approaches were applied into cDNA library construction and the transcriptome sequencing was performed on PacBio Sequel. For the conventional library construction (1st-PacBio), a total of 18.69 Gb clean data were generated by the mixed sample. The genome of *P. falciparum* is extremely TA-rich, so we carried out the sequencing again by using optimized method (2nd-PacBio) for cDNA library construction and a total of 24.56 Gb clean data was generated. The length distribution of the PacBio sequencing reads from the PacBio sequencing data by using the different cDNA library construction approaches were compared (**Figure 1A**), and it indicated that the optimized library construction method improved the transcriptome data quality a lot. Thus, the sequencing data obtained from the optimized cDNA library approach was used for following analysis.

PacBio Sequencing and GAMP Mapping

After filtering using the subreads, 7,309,966 subreads were obtained. Next, the Circular consensus sequence (CCS) was generated using the SMRTlink software and the CCS was classified into full-length and non-full length reads according to the 5′ and 3′ adapters and the poly(A) tails. A total of 376,592 circular consensus sequences (CCS) reads were generated and 299,462 (79.5%) sequences were considered as full-length transcripts. A total of 145,469 polished CCS reads with average size 2,387 bp ranging from 155 to 14,521 bp

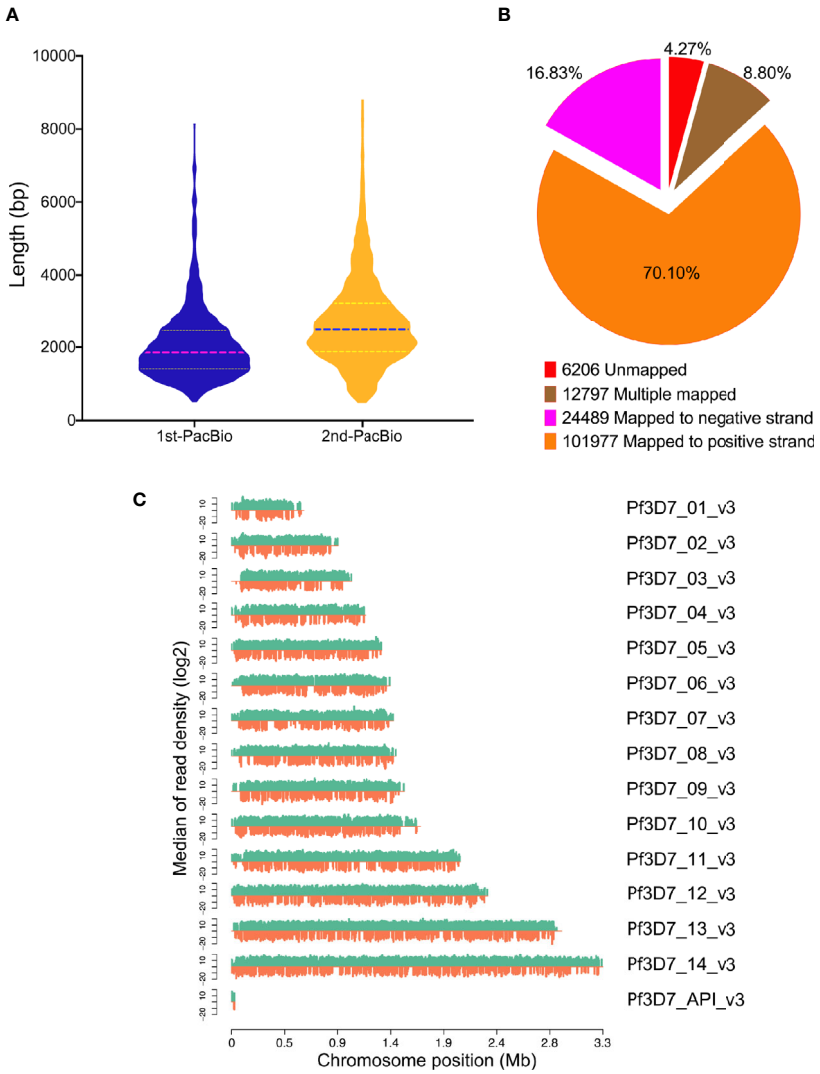

FIGURE 1 | Mapping results of PacBio sequencing. **(A)** Reads length distribution of PacBio sequencing by two different library construction methods; **(B)** GMAP mapping rates; **(C)** Reads distribution on chromosomes of *P. falciparum*. X-axis indicates the chromosome position, y-axis indicates the median of reads density.

were obtained. The statistics information of transcriptome in detail were summarized in **Supplementary Table 1**.

A total of 145,469 polished CCS reads were searched against *P. falciparum* genome and 139,263 (95.73%) transcripts were mapped on reference genome by GMAP (**Figure 1B**) and the results were summarized in **Supplementary Table 2**. In addition, the reads density showed that all the reads were distributed on the chromosomes homogeneously (**Figure 1C**).

Alternative Splicing Events Analysis

As known, alternative splicing plays an important role in the process of differentiation and growth in multicellular organisms. For the unicellular protozoa, the study in *P. berghei* indicates that alternative splicing is a stage-specific phenomenon regulating the cellular differentiation into variable cell types (Yeoh et al., 2019). Although alternative splicing events have been studied in *P. falciparum*, only short-read sequencing technologies were applied into detecting the AS events by short reads assembly. In this study, long-read sequencing platform was employed to improve the detection accuracy. The results provide an accurate AS events of all the genes by aligning all the transcripts on the reference genome. Usually, AS events will be classified into seven categories (**Figure 2A**): SE (skipping exon), MX (mutually exclusive exons), A5 (alternative 5' splice-site), A3 (alternative 3' splice-site), RI (retained intron), AF (alternative first exon), and AL (alternative last exon). In our study, a total of 393 AS events were detected in *P. falciparum* (**Supplementary Table 3**). Based on the classification and statistics, the AS events were divided into different types. Among these types, A3 (24%), A5 (33%), and RI (31%) were dominant in these AS events (**Figure 2B**). Among them, Apetala 2 (AP2) encode a set of transcription factors in Apicomplexa including *P. falciparum* and the AS events of these

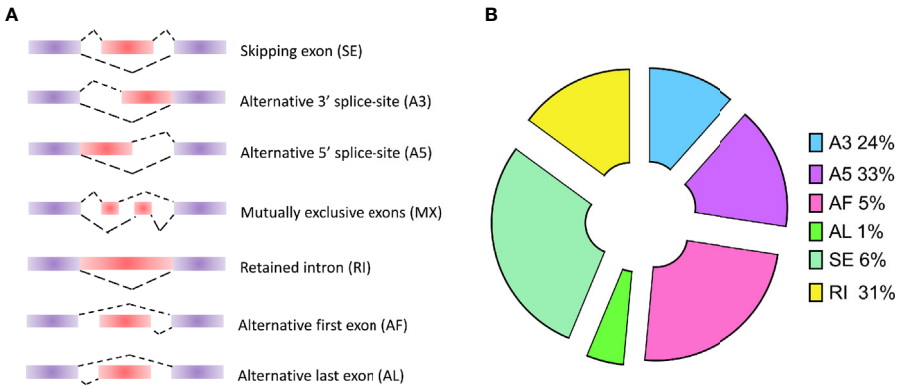

FIGURE 2 | Types of alternative splicing (AS) events and the classification of AS events in *P. falciparum*. **(A)** Types of AS events: SE (skipping exon), MX (mutually exclusive exons), A5 (alternative 5′ splice-site), A3 (alternative 3′ splice-site), RI (retained intron), AF (alternative first exon), and AL (alternative last exon). **(B)** The distribution of AS events in *P. falciparum*.

genes were visualized: PF3D7_0730300 (A5), PF3D7_0420300 (RI), PF3D7_0613800 (A5), and PF3D7_1239200 (AF) (**Supplementary Figure 3**).

Long Non-coding RNA Analysis

In previous study, unlike those protein-coding RNAs, non-coding RNAs especially lncRNAs are still not well investigated. Though lots of lncRNAs were characterized by the second-generation sequencing, amounts of lncRNAs are still not fully characterized as well as un-correctly because of sequencing shortness. We compared the length distribution (**Supplementary Figure 4A**) and the exon number (**Supplementary Figure 4B**) of mRNA and lncRNA in PacBio sequencing data. To identify lncRNAs in the full-length sequencing transcriptome and obtain the high-confidence lncRNA dataset, four algorithms including Coding-Noncoding Index (CNCI), Pfam-scan (Pfam), the predictor of long non-coding RNAs and messenger RNAs based on an improved k-mer scheme (PLEK), and Coding Potential Calculator (CPC) were employed to characterize the lncRNAs. Among 12,553 potential lncRNAs predicted by four algorithms, the intersection of 3,623 lncRNAs (**Figure 3A**, **Supplementary Table 4**) were identified and were divided into four categories: Antisense (2,023, 55.84%), lncRNA (1,071, 29.56%), sense-overlapping (394, 10.87%), and sense-intronic (135, 3.73%) (**Figure 3B**, **Supplementary Table 4**).

Alternative Polyadenylation and Transcription Factors Identification

Differential alternative polyadenylation (APA) of mRNAs has been proved to play an important regulatory role in different species (Shen et al., 2011; Elkon et al., 2013). In this study, 1,555 APA events were detected and annotated in **Supplementary Table 5**. Genes with different number of Poly(A) sites were visualized in **Figure 4A** and 478 genes contain 1 poly(A) sites

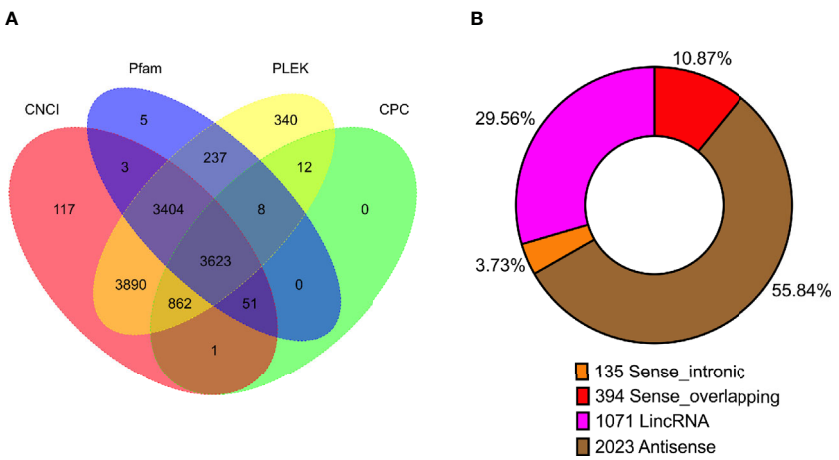

FIGURE 3 | Statistics of long non-coding RNA (lncRNA) in *P. falciparum*. **(A)** Venn diagram showing the number of lncRNAs predicted using four algorithms (CNCI, Pfam, PLEK, and CPC). **(B)** The number of lncRNA classified into sense intronic, sense overlapping, lncRNA, and antisense.

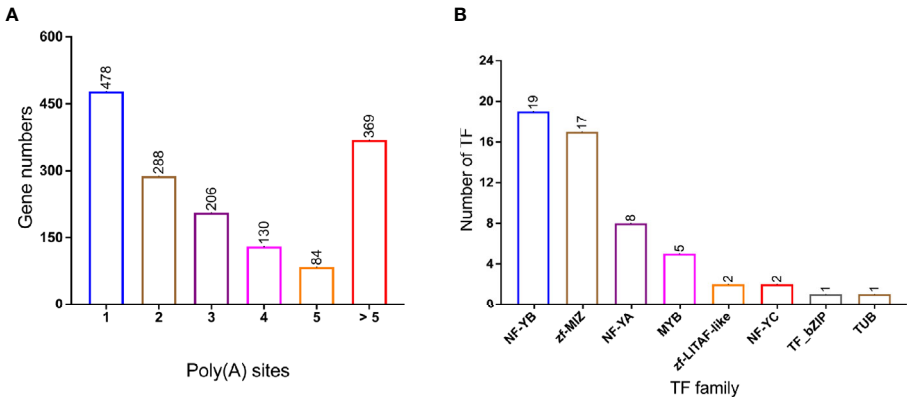

FIGURE 4 | Alternative polyadenylation (APA) and transcription Factor (TF) in PacBio transcriptome. **(A)** Distribution of poly(A) with different poly(A) sites' number; **(B)** TF family classification of genes. Number of TF genes in each families, NF-YB and zf-MIZ proteins make up a large proportion.

were dominant in all APA events. In addition, 369 genes contain more than five poly(A) sites. A total of 55 variant transcripts of TFs were identified and assigned into different families (**Figure 4B**, **Supplementary Table 6**): NF-YB (19 members), zf-MIZ (17 members), NF-YA (8 members), and MYB (5 members) were the most abundant in *P. falciparum*.

Full Scan of Proteome

To validate the full-length sequencing data, the full scan genome was performed with the mixed samples containing the whole asexual blood stages. Proteins in the mixed sample were characterized by Lumos and the spectrums were searched against the protein database constructed by full length sequencing data of *P. falciparum*. A total of 1,535 proteins with high confidence were characterized and list in **Supplementary Table 7**. And then, KEGG analysis was performed by using the proteome data which were classified into six main categories: human diseases, organismal systems, cellular processes, environmental information processing, genetic information processing, and metabolism (**Figure 5**).

Small Proteins in Long Non-coding RNA

Recently, small proteins (<100 amino acids) were characterized in different species and proved to be functional (Kastenmayer et al., 2006; Fesenko et al., 2019; Sberro et al., 2019; Martinez et al., 2020). *P. falciparum* as a very important species related to human health, however, the small proteins in *P. falciparum* are still unexplored. Thus, small proteins were analyzed in this study and 160 small proteins (<100 aa) were validated by searching against the small protein database (**Supplementary Table 8**).

Fusion Transcript Identification

Fusion transcripts, usually caused by chromosomal rearrangements, have been proved to play an important role in oncogenesis (Friedrich and Sonnhammer, 2020). In our study, a total of 1,721 fusion transcripts were identified by long-read sequencing. The fusion transcripts were distributed in different chromosomes and shown in **Figure 6**. Among them, 84 and 1,636 fusion transcripts were located in the intra- and inter-chromosomic region (**Supplementary Table 9**).

DISCUSSION

Currently, the mechanisms of *Plasmodium* parasite invasion and hijacking of host cells, transmission, and immune evasion remain largely elusive. These processes are regulated precisely by a complex dynamic system. Fortunately, a full genome sequence of *P. falciparum* has been sequenced and partial genes have been annotated functionally, which may reveal some underlying mechanisms for physiological activities of malaria parasites (Gardner et al., 2002). However, in most cases, the routine approach of sequencing is not capable of generating reads corresponding to entire transcripts because of the short reads which will result in mistakes during the assembly (van Dijk et al., 2014). Now, the single-molecule, real-time (SMRT) sequencing technique producing kilobase-sized reads has been developed (Eid et al., 2009), which help us obtain the entire transcripts without assembly easily (Sharon et al., 2013). As for the malaria parasites, though the genome annotation of *P. falciparum* has been updated frequently based on more and more microarray or RNA-seq data since 2002 (Gardner et al., 2002), there are still many annotation mistakes. This interferes those researches on gene function or underlying mechanism. Here, the updated full-length transcriptome provides a valuable resource for further studies on gene regulation and protein functions in the human malaria parasites.

Long non-coding RNA (lncRNA) were proved to play a role in transcriptional regulation in eukaryotic organisms including *P. falciparum* (Broadbent et al., 2015). For instance, the antisense lncRNAs produced by the intronic promoters of *var* genes were involved in the transcriptional activation of these virulence genes (Jing et al., 2018). To date, the non-coding transcriptome and their biological functions remain largely unknown. In our study, 3,623 full-length lncRNA were characterized by using four algorithms (CNCI, Pfam, PLEK, and CPC) and were divided

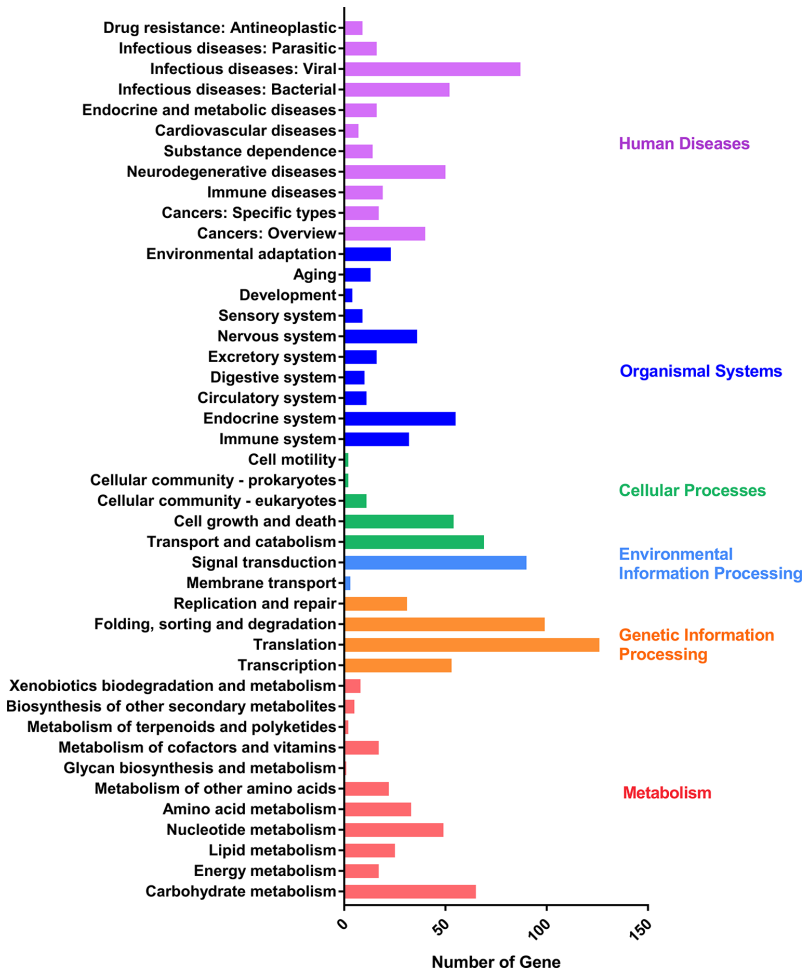

FIGURE 5 | KEGG pathway assignment of proteins characterized by liquid chromatography-mass spectrometry. The bottom x-axis indicates the number of proteins. The left y-axis indicates the categories in detail, the right y-axis indicates the main clustered group of the specific categories.

into four categories including Antisense, lncRNA, sense-overlapping, and sense-intronic transcripts. This data will facilitate the functional studies of lncRNAs in malaria parasites. More importantly, lncRNA-derived small proteins have been validated by integration of full-length transcriptomic and proteomic data in this study. Until then, small proteins are often ignored in transcriptome. Here, the proteome profiling was applied successfully to characterize 1,535 proteins with high confidence. Besides, 160 small proteins were validated by liquid chromatography-mass spectrometry corresponding to lncRNA regions of *P. falciparum*. These results not only provide an updated proteome database within the whole asexual blood stages, but also assist the small protein discovery and functional investigation in *P. falciparum*.

Finally, to our knowledge, this is the first report of the PacBio full-length transcriptome in *Plasmodium*, which compensates the deficiency of the conventional sequencing methods using Illumina-generated short reads in terms of gene expression. Many of the predicted transcripts that did not correspond to the annotated transcripts may potentially regulate *P. falciparum* development and reveal a complex transcriptional landscape in the asexual blood stage. However, the underlying molecular mechanism of alternative splicing, long non-coding RNAs, alternative polyadenylation, and fusion transcripts still requires more sufficient research to investigate in the future, especially how these novel proteins identified by multi-omics analysis are involved in parasites growth and development process. We believe this work provides a novel and valuable genetic resource for functional and mechanistic studies of genes of interest in *P. falciparum*.

CONCLUSION

In our study, full-length RNA sequencing was used to reconstruct the transcriptome of *P. falciparum*. An improved transcriptomic dataset covering the whole asexual blood stages without short-read assembly was obtained. This is the first time

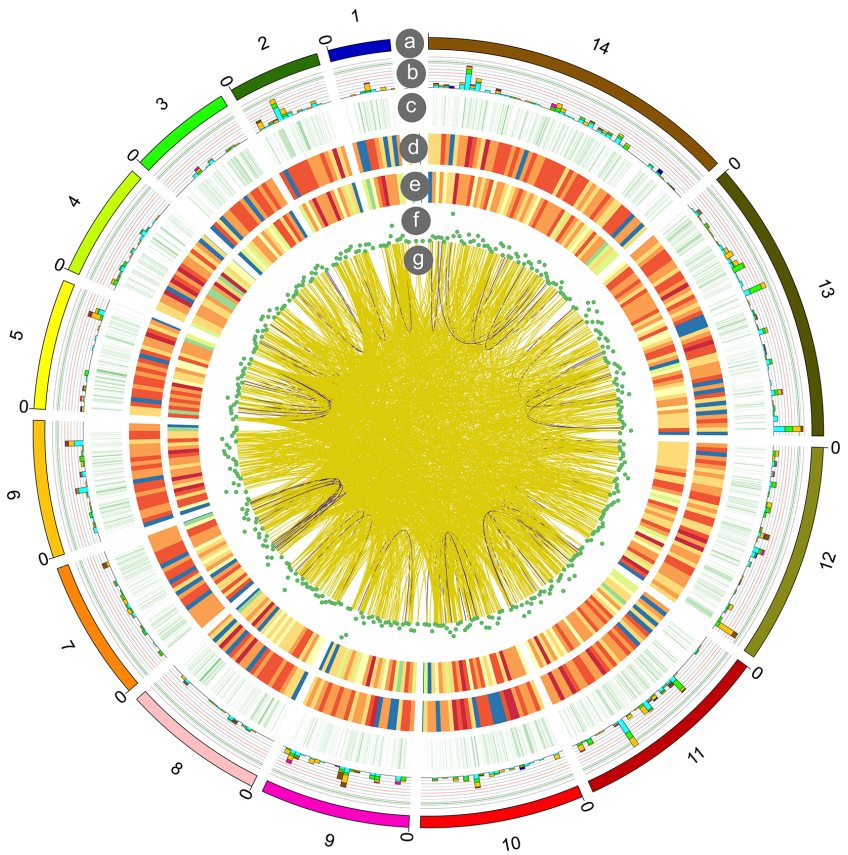

FIGURE 6 | Circos visualization of *P. falciparum* PacBio sequencing results. From outside to inside, the circles represent chromosomes (a); alternative splicing (AS) sites (b); alternative polyadenylation (APA) (c); novel transcripts distribution (d); novel genes distribution (e); long non-coding RNA (lncRNA) density (f); gene fusion distribution (g): intra-chromosome (purple), inter-chromosome (yellow).

to reveal the full-length transcriptome in *P. falciparum*. Among 145,469 transcripts, 139,263 (95.73%) of them were mapped on reference genome, and 393 alternative splicing (AS) events, 3,623 long non-coding RNAs (lncRNA), 1,555 alternative polyadenylation (APA) events, 57 transcription factors (TF), 1,721 fusion transcripts were identified, respectively. In addition, 1,535 proteins with high confidence were validated by liquid chromatography-mass spectrometry. Notably, 160 small proteins were identified by liquid chromatography-mass spectrometry searching against the small protein database. This study not only provides an improved full-length transcriptomic dataset with high quality and accuracy, but also contributes to better understanding of structural variations in the transcription process.

DATA AVAILABILITY STATEMENT

The raw sequence of transcriptomic data reported in this paper have been deposited in the Genome Sequence Archive in the BIG Data Center (http://bigd.big.ac.cn/gsa/s/4dvmackj), Beijing Institute of Genomics (BIG), Chinese Academy of Sciences, under accession number: CRA003525. Proteomic data are available *via* ProteomeXchange with identifier PXD022618.

AUTHOR CONTRIBUTIONS

QZ and JC designed the study. MY, XS, YZ, GW, CW, JT, MZ, and YL performed the experiments and analyzed the data. MY and QZ wrote the manuscript with contributions from the other authors. All authors contributed to the article and approved the submitted version.

FUNDING

This work was supported by the National Key R&D Program of China Grant (2018YFA0507300) and National Natural Science Foundation of China (NSFC) (81630063, 81971959, and 31671353) to QZ, National Key R&D Program of China Grant (2020YFC1200105), National Natural Science Foundation of China (NSFC) (81971967), and Jiangsu Provincial Project of Invigorating Health Care Through Science, Technology and Education and the

Jiangsu Provincial Commission of Health to JC, National Natural Science Foundation of China (NSFC) (22077011) to YZ.

ACKNOWLEDGMENTS

We thank Dr. Youli Xiao valuable supports on this work.

SUPPLEMENTARY MATERIAL

The Supplementary Material for this article can be found online at: https://www.frontiersin.org/articles/10.3389/fcimb.2021.631545/full#supplementary-material

Supplementary Figure 1 | Saturation curve of alignment by GMAP. X-axis indicates the number of full-length reads, y-axis indicates the number of genes.

Supplementary Figure 2 | Number of mapped reads in chromosomes. X-axis indicates the chromosome length, y-axis indicates the number of mapped reads.

Supplementary Figure 3 | The representative AS events identified in PacBio transcriptome. The AS events of Apetala 2 (AP2) genes: PF3D7_0730300 (A5), PF3D7_0420300 (RI), PF3D7_0613800 (A5), and PF3D7_1239200 (AF).

Supplementary Figure 4 | Comparison of the lncRNA and mRNA. **(A)** Length distribution of lncRNA and mRNA; **(B)** Distribution of exons in lncRNA and mRNA.

REFERENCES

Abdel-Ghany, S. E., Hamilton, M., Jacobi, J. L., Ngam, P., Devitt, N., Schilkey, F., et al. (2016). A survey of the sorghum transcriptome using single-molecule long reads. *Nat. Commun.* 7 (1), 1–11. doi: 10.1038/ncomms11706

Alamancos, G. P., Pages, A., Trincado, J. L., Bellora, N., and Eyras, E. (2015). Leveraging transcript quantification for fast computation of alternative splicing profiles. *RNA* 21 (9), 1521–1531. doi: 10.1261/rna.051557.115

Broadbent, K. M., Broadbent, J. C., Ribacke, U., Wirth, D., Rinn, J. L., and Sabeti, P. C. (2015). Strand-specific RNA sequencing in Plasmodium falciparum malaria identifies developmentally regulated long non-coding RNA and circular RNA. *BMC Genomics* 16 (1), 1–22. doi: 10.1186/s12864-015-1603-4

Cabrera-Quio, L. E., Herberg, S., and Pauli, A. (2016). Decoding sORF translation - from small proteins to gene regulation. *RNA Biol.* 13 (11), 1051–1059. doi: 10.1080/15476286.2016.1218589

Chappell, L., Ross, P., Orchard, L., Russell, T. J., Otto, T. D., Berriman, M., et al. (2020). Refining the transcriptome of the human malaria parasitePlasmodium falciparumusing amplification-free RNA-seq. *BMC Genomics* 21 (1), 1–19. doi: 10.1186/s12864-020-06787-5

Eddy, S. R. (2009). A new generation of homology search tools based on probabilistic inference. *Genome Inform* 23 (1), 205–211. doi: 10.1142/9781848165632_0019

Eid, J., Fehr, A., Gray, J., Luong, K., Lyle, J., Otto, G., et al. (2009). Real-time DNA sequencing from single polymerase molecules. *Science* 323 (5910), 133–138. doi: 10.1126/science.1162986

Elkon, R., Ugalde, A. P., and Agami, R. (2013). Alternative cleavage and polyadenylation: extent, regulation and function. *Nat. Rev. Genet.* 14 (7), 496–506. doi: 10.1038/nrg3482

Fesenko, I., Kirov, I., Kniazev, A., Khazigaleeva, R., Lazarev, V., Kharlampieva, D., et al. (2019). Distinct types of short open reading frames are translated in plant cells. *Genome Res.* 29 (9), 1464–1477. doi: 10.1101/gr.253302.119

Finn, R. D., Coggill, P., Eberhardt, R. Y., Eddy, S. R., Mistry, J., Mitchell, A. L., et al. (2016). The Pfam protein families database: towards a more sustainable future. *Nucleic Acids Res.* 44 (D1), D279–D285. doi: 10.1093/nar/gkv1344

Friedrich, S., and Sonnhammer, E. L. L. (2020). Fusion transcript detection using spatial transcriptomics. *BMC Med. Genomics* 13 (1), 1–11. doi: 10.1186/s12920-020-00738-5

Frith, M. C., Forrest, A. R., Nourbakhsh, E., Pang, K. C., Kai, C., Kawai, J., et al. (2006). The abundance of short proteins in the mammalian proteome. *PloS Genet.* 2 (4), e52. doi: 10.1371/journal.pgen.0020052

Gardner, M. J., Hall, N., Fung, E., White, O., Berriman, M., Hyman, R. W., et al. (2002). Genome sequence of the human malaria parasite Plasmodium falciparum. *Nature* 419 (6906), 498–511. doi: 10.1038/nature01097

Hsu, P. Y., and Benfey, P. N. (2018). Small but Mighty: Functional Peptides Encoded by Small ORFs in Plants. *Proteomics* 18 (10), 1700038. doi: 10.1002/pmic.201700038

Jing, Q., Cao, L., Zhang, L., Cheng, X., Gilbert, N., Dai, X., et al. (2018). Plasmodium falciparum var Gene Is Activated by Its Antisense Long Noncoding RNA. *Front. Microbiol.* 9, 3117. doi: 10.3389/fmicb.2018.03117

Kastenmayer, J. P., Ni, L., Chu, A., Kitchen, L. E., Au, W. C., Yang, H., et al. (2006). Functional genomics of genes with small open reading frames (sORFs) in S. cerevisiae. *Genome Res.* 16 (3), 365–373. doi: 10.1101/gr.4355406

Kong, L., Zhang, Y., Ye, Z. Q., Liu, X. Q., Zhao, S. Q., Wei, L., et al. (2007). CPC: assess the protein-coding potential of transcripts using sequence features and support vector machine. *Nucleic Acids Res.* 35 (Web Server issue), W345–W349. doi: 10.1093/nar/gkm391

Krzywinski, M., Schein, J., Birol, I., Connors, J., Gascoyne, R., Horsman, D., et al. (2009). Circos: an information aesthetic for comparative genomics. *Genome Res.* 19 (9), 1639–1645. doi: 10.1101/gr.092759.109

Ladoukakis, E., Pereira, V., Magny, E. G., Eyre-Walker, A., and Couso, J. P. (2011). Hundreds of putatively functional small open reading frames in Drosophila. *Genome Biol.* 12 (11), R118. doi: 10.1186/gb-2011-12-11-r118

Lee, C., Zeng, J., Drew, B. G., Sallam, T., Martin-Montalvo, A., Wan, J., et al. (2015). The mitochondrial-derived peptide MOTS-c promotes metabolic homeostasis and reduces obesity and insulin resistance. *Cell Metab.* 21 (3), 443–454. doi: 10.1016/j.cmet.2015.02.009

Li, A., Zhang, J., and Zhou, Z. (2014). PLEK: a tool for predicting long non-coding RNAs and messenger RNAs based on an improved k-mer scheme. *BMC Bioinf.* 15:311. doi: 10.1186/1471-2105-15-311

Li, Y., Baptista, R. P., and Kissinger, J. C. (2020). Noncoding RNAs in Apicomplexan Parasites: An Update. *Trends Parasitol.* 36 (10), 835–849. doi: 10.1016/j.pt.2020.07.006

Liao, Q., Shen, J., Liu, J. F., Sun, X., Zhao, G. G., Chang, Y. Z., et al. (2014). Genome-wide identification and functional annotation of Plasmodium falciparum long noncoding RNAs from RNA-seq data. *Parasitol. Res.* 113 (4), 1269–1281. doi: 10.1007/s00436-014-3765-4

Ma, C., Shao, M. F., and Kingsford, C. (2018). SQUID: transcriptomic structural variation detection from RNA-seq. *Genome Biol.* 19 (1), 52. doi: 10.1186/s13059-018-1421-5

Martinez, T. F., Chu, Q., Donaldson, C., Tan, D., Shokhirev, M. N., and Saghatelian, A. (2020). Accurate annotation of human protein-coding small open reading frames. *Nat. Chem. Biol.* 16 (4), 458–45+. doi: 10.1038/s41589-019-0425-0

Miles, A., Iqbal, Z., Vauterin, P., Pearson, R., Campino, S., Theron, M., et al. (2016). Indels, structural variation, and recombination drive genomic diversity in Plasmodium falciparum. *Genome Res.* 26 (9), 1288–1299. doi: 10.1101/gr.203711.115

Miravet-Verde, S., Ferrar, T., Espadas-Garcia, G., Mazzolini, R., Gharrab, A., Sabido, E., et al. (2019). Unraveling the hidden universe of small proteins in bacterial genomes. *Mol. Syst. Biol.* 15 (2), e8290. doi: 10.15252/msb.20188290

Mourier, T., Carret, C., Kyes, S., Christodoulou, Z., Gardner, P. P., Jeffares, D. C., et al. (2008). Genome-wide discovery and verification of novel structured RNAs in Plasmodium falciparum. *Genome Res.* 18 (2), 281–292. doi: 10.1101/gr.6836108

Orr, M. W., Mao, Y. H., Storz, G., and Qian, S. B. (2020). Alternative ORFs and small ORFs: shedding light on the dark proteome. *Nucleic Acids Res.* 48 (3), 1029–1042. doi: 10.1093/nar/gkz734

Patraquim, P., Mumtaz, M. A. S., Pueyo, J. I., Aspden, J. L., and Couso, J. P. (2020). Developmental regulation of canonical and small ORF translation from mRNAs. *Genome Biol.* 21 (1), 1–26. doi: 10.1186/s13059-020-02011-5

Raabe, C. A., Sanchez, C. P., Randau, G., Robeck, T., Skryabin, B. V., Chinni, S. V., et al. (2010). A global view of the nonprotein-coding transcriptome in Plasmodium falciparum. *Nucleic Acids Res.* 38 (2), 608–617. doi: 10.1093/nar/gkp895

Rhoads, A., and Au, K. F. (2015). PacBio Sequencing and Its Applications. *Genomics Proteomics Bioinf.* 13 (5), 278–289. doi: 10.1016/j.gpb.2015.08.002

Ruiz-Orera, J., and Alba, M. M. (2019). Translation of Small Open Reading Frames: Roles in Regulation and Evolutionary Innovation. *Trends Genet.* 35 (3), 186–198. doi: 10.1016/j.tig.2018.12.003

Salmela, L., and Rivals, E. (2014). LoRDEC: accurate and efficient long read error correction. *Bioinformatics* 30 (24), 3506–3514. doi: 10.1093/bioinformatics/btu538

Sberro, H., Fremin, B. J., Zlitni, S., Edfors, F., Greenfield, N., Snyder, M. P., et al. (2019). Large-Scale Analyses of Human Microbiomes Reveal Thousands of Small, Novel Genes. *Cell* 178 (5), 1245–124+. doi: 10.1016/j.cell.2019.07.016

Segonzac, C., and Monaghan, J. (2019). Modulation of plant innate immune signaling by small peptides. *Curr. Opin. Plant Biol.* 51, 22–28. doi: 10.1016/j.pbi.2019.03.007

Sharon, D., Tilgner, H., Grubert, F., and Snyder, M. (2013). A single-molecule long-read survey of the human transcriptome. *Nat. Biotechnol.* 31 (11), 1009–1014. doi: 10.1038/nbt.2705

Shen, Y. J., Venu, R. C., Nobuta, K., Wu, X. H., Notibala, V., Demirci, C., et al. (2011). Transcriptome dynamics through alternative polyadenylation in developmental and environmental responses in plants revealed by deep sequencing. *Genome Res.* 21 (9), 1478–1486. doi: 10.1101/gr.114744.110

Siegel, T. N., Hon, C. C., Zhang, Q., Lopez-Rubio, J. J., Scheidig-Benatar, C., Martins, R. M., et al. (2014). Strand-specific RNA-Seq reveals widespread and developmentally regulated transcription of natural antisense transcripts in Plasmodium falciparum. *BMC Genomics* 15, 150. doi: 10.1186/1471-2164-15-150

Sun, L., Luo, H., Bu, D., Zhao, G., Yu, K., Zhang, C., et al. (2013). Utilizing sequence intrinsic composition to classify protein-coding and long non-coding transcripts. *Nucleic Acids Res.* 41 (17), e166. doi: 10.1093/nar/gkt646

van der Pluijm, R. W., Tripura, R., Hoglund, R. M., Pyae Phyo, A., Lek, D., Ul Islam, A., et al. (2020). Triple artemisinin-based combination therapies versus artemisinin-based combination therapies for uncomplicated Plasmodium falciparum malaria: a multicentre, open-label, randomised clinical trial. *Lancet* 395 (10233), 1345–1360. doi: 10.1016/S0140-6736(20)30552-3

van Dijk, E. L., Auger, H., Jaszczyszyn, Y., and Thermes, C. (2014). Ten years of next-generation sequencing technology. *Trends Genet.* 30 (9), 418–426. doi: 10.1016/j.tig.2014.07.001

Weirather, J. L., Afshar, P. T., Clark, T. A., Tseng, E., Powers, L. S., Underwood, J. G., et al. (2015). Characterization of fusion genes and the significantly expressed fusion isoforms in breast cancer by hybrid sequencing. *Nucleic Acids Res.* 43 (18), e116. doi: 10.1093/nar/gkv562

White, N. J., Pukrittayakamee, S., Hien, T. T., Faiz, M. A., Mokuolu, O. A., and Dondorp, A. M. (2014). Malaria. *Lancet* 383 (9918), 723–735. doi: 10.1016/s0140-6736(13)60024-0

Wisniewski, J. R., Zougman, A., Nagaraj, N., and Mann, M. (2009). Universal sample preparation method for proteome analysis. *Nat. Methods* 6 (5), 359–362. doi: 10.1038/nmeth.1322

Wu, T. D., and Watanabe, C. K. (2005). GMAP: a genomic mapping and alignment program for mRNA and EST sequences. *Bioinformatics* 21 (9), 1859–1875. doi: 10.1093/bioinformatics/bti310

Yeoh, L. M., Goodman, C. D., Mollard, V., McHugh, E., Lee, V. V., Sturm, A., et al. (2019). Alternative splicing is required for stage differentiation in malaria parasites. *Genome Biol.* 20 (1), 1–13. doi: 10.1186/s13059-019-1756-6

Yin, X. Q., Jing, Y. Y., and Xu, H. M. (2019). Mining for missed sORF-encoded peptides. *Expert Rev. Proteomics* 16 (3), 257–266. doi: 10.1080/14789450.2019.1571919

Conflict of Interest: The authors declare that the research was conducted in the absence of any commercial or financial relationships that could be construed as a potential conflict of interest.

frontiers in Cellular and Infection Microbiology

ORIGINAL RESEARCH
published: 24 February 2021
doi: 10.3389/fcimb.2021.617461

Schistosoma japonicum Cystatin Alleviates Sepsis Through Activating Regulatory Macrophages

Hong Xie[1,2†], Lingqin Wu[1,3†], Xingzhi Chen[1,2], Shifang Gao[1], Huihui Li[1,2], Yuan Yuan[1,2], Jinbao Liang[1], Xiaoli Wang[1,2], Shuying Wang[1,3], Changyan Xu[1,2], Liang Chu[4], Bin Zhan[5], Rui Zhou[3,6] and Xiaodi Yang[1,2*]*

[1] Anhui Key Laboratory of Infection and Immunity of Bengbu Medical College, Bengbu, China, [2] Department of Basic Medical College, Bengbu Medical College, Bengbu, China, [3] Department of Pediatric, First Affiliated Hospital of Bengbu Medical College, Bengbu, China, [4] Department of General Surgery, Second Affiliated Hospital of Bengbu Medical College, Bengbu, China, [5] National School of Tropical Medicine, Baylor College of Medicine, Houston, TX, United States, [6] Anhui Province Key Laboratory of Immunology in Chronic Diseases of Bengbu Medical College, Bengbu, China

OPEN ACCESS

Edited by:
Xiaojun Chen,
Nanjing Medical University, China

Reviewed by:
Jilong Shen,
Anhui Medical University, China
Xi Sun,
Sun Yat-sen University, China

***Correspondence:**
Xiaodi Yang
yxd_qf@bbmc.edu.cn
Rui Zhou
zhourui@bbmc.edu.cn

[†]These authors share first authorship

Specialty section:
This article was submitted to Parasite and Host, a section of the journal Frontiers in Cellular and Infection Microbiology

Received: 14 October 2020
Accepted: 14 January 2021
Published: 24 February 2021

Citation:
Xie H, Wu L, Chen X, Gao S, Li H, Yuan Y, Liang J, Wang X, Wang S, Xu C, Chu L, Zhan B, Zhou R and Yang X (2021) Schistosoma japonicum Cystatin Alleviates Sepsis Through Activating Regulatory Macrophages. Front. Cell. Infect. Microbiol. 11:617461. doi: 10.3389/fcimb.2021.617461

Multi-organ failure caused by the inflammatory cytokine storm induced by severe infection is the major cause of death for sepsis. *Sj*-Cys is a cysteine protease inhibitor secreted by *Schistosoma japonicum* with strong immunomodulatory functions on host immune system. Our previous studies have shown that treatment with *Sj*-Cys recombinant protein (r*Sj*-Cys) attenuated inflammation caused by sepsis. However, the immunological mechanism underlying the immunomodulation of *Sj*-Cys for regulating inflammatory diseases is not yet known. In this study, we investigated the effect of *Sj*-Cys on the macrophage M2 polarization and subsequent therapeutic effect on sepsis. The r*Sj*-Cys was expressed in yeast *Pichia pastoris*. Incubation of mouse bone marrow-derived macrophages (BMDMs) with yeast-expressed r*Sj*-Cys significantly activated the polarization of macrophages to M2 subtype characterized by the expression of $F4/80^+$ $CD206^+$ with the elated secretion of IL-10 and TGF-β. Adoptive transfer of r*Sj*-Cys treated BMDMs to mice with sepsis induced by cecal ligation and puncture (CLP) significantly improved their survival rates and the systemic clinical manifestations of sepsis compared with mice receiving non-treated normal BMDMs. The therapeutic effect of *Sj*-Cys-induced M2 macrophages on sepsis was also reflected by the reduced pathological damages in organs of heart, lung, liver and kidney and reduced serological levels of tissue damage-related ALT, AST, BUN and Cr, associated with downregulated pro-inflammatory cytokines (IFN-gamma and IL-6) and upregulated regulatory anti-inflammatory cytokines (IL-10 and TGF-β). Our results demonstrated that *Sj*-Cys is a strong immunomodulatory protein with anti-inflammatory features through activating M2 macrophage polarization. The findings of this study suggested that *Sj*-Cys itself or *Sj*-Cys-induced M2 macrophages could be used as therapeutic agents in the treatment of sepsis or other inflammatory diseases.

Keywords: cysteine protease inhibitor, *Schistosoma japonicum*, sepsis, macrophage, immunomodulation, adoptive transfer

INTRODUCTION

Sepsis is a complex syndrome caused by a dysregulated host response to infection, leading to life-threatening organ dysfunction and failure (Singer et al., 2016). It remains a major cause of death throughout the world (Rudd et al., 2020; Yang et al., 2020b) regardless of appropriate antibiotic treatment and supportive care (Seymour et al., 2017; Williams et al., 2019; Baghdadi et al., 2020). Difficulties in developing drugs to treat sepsis also reflect the extreme complexity and variability of the serious condition (Fink and Shaw Warren, 2014; Huang et al., 2019). The progression of sepsis can be roughly categorized into two distinct but concomitant stages termed systemic inflammatory response syndrome (SIRS) and compensatory anti-inflammatory response syndrome (CARS) (Singer et al., 2016). SIRS is initiated by innate immune cells such as macrophages which release inflammatory cytokines upon the detection of pathogens or activation by LPS released by infected gram-negative bacteria, to mobilize host immune system to clean the infection (Ge et al., 2019; Huang et al., 2019). This stage is also referred to as the cytokine storm and is thought to be responsible for lethal organ damage during the early stage of sepsis (Guo et al., 2019; Sackett et al., 2019). On the other hand, CARS is a systemic deactivation of the immune system tasked with restoring homeostasis from an inflammatory state, which is related to the production of Th2 and regulatory cytokines such as IL-4, IL-10 and TGF-β (Ward et al., 2008). The timing and balance of SIRS and CARS responses have a powerful influence on clinical outcomes in sepsis.

Macrophages are common phagocytic cells for clearing invaded pathogens or apoptotic innate cells. The phenotype and function of macrophages may be polarized by microenvironment into M1-type (classically activated macrophage) or M2-type (alternatively activated macrophage). M1 macrophages are stimulated by IFN-gamma to promote inflammation by secreting pro-inflammatory cytokines IL-6, IL-12, and TNF-alpha. Th2 cells produced IL-4 can convert macrophages into M2-type that inhibit inflammation by secreting Arginase-I, IL-10 and TGF-β mainly involved in wound healing and tissue repair (Ley, 2017). Multiple studies have shown that M1 macrophages are associated with the SIRS stage of sepsis and are involved in the pathology and mortality in patients with sepsis. Thereby increasing M2 cells population and prolonging the presence of this macrophage subtype in the systemic microenvironment could be developed as a strategy to reduce organ damage and to increase tissue repair in sepsis condition (Xu et al., 2014; Liang et al., 2019; Takakura and Zandi-Nejad, 2019; Yang et al., 2019b; Jin et al., 2020). Additional studies also confirmed that M2 macrophages conferred a therapeutic effect on peritonitis-induced sepsis (Mehta et al., 2004) while M1-related inflammatory factor level was associated with the mortality of sepsis (Bozza et al., 2007).

Extensive experimental and epidemiological evidence suggest that helminth infections or helminth-derived products effectively modulate host immune responses to reduce deleterious inflammatory immune responses and stimulate regulatory responses, thereby exerting a therapeutic effect on inflammatory diseases (Ziegler et al., 2015; Chen et al., 2016; Jang et al., 2017; Jiang et al., 2018; Xu et al., 2018; Jin et al., 2019; Ryan et al., 2020). It has been observed that chronic infection of *Schistosoma japonicum* promoted macrophages from M1 to M2 polarization (Zhu et al., 2014; Giri and Cheng, 2019) and had a protective effect on sepsis (Du et al., 2011a). This protective effect on sepsis could be replicated in mice adoptively transferred with ex vivo programmed M2 macrophages (Du et al., 2011). The further study identified that *S. japonicum* soluble egg antigen (SEA) had the similar effect as *S. japonicum* infection to boost M2 polarization through STAT6 and PI3K pathway (Du et al., 2011). However, although the concept of worm therapy has been described as safe and effective, the application of living parasites or the derived raw materials still bears the risk of safety and side effects (Togre et al., 2018). Thus, therapeutic intervention by applying defined helminth-secreted protein with immunomodulation functions should be more practical and feasible to treat inflammatory diseases. It was found that *S. japonicum* adult worm secreted cysteine protease inhibitor or cystatin (*Sj*-Cys) played a significant role in immunomodulation of host immune system to reduce inflammatory responses as a survival strategy for the fluke living inside host (Chen et al., 2017), and has been successfully used to treat inflammatory bowel diseases (Wang et al., 2016b; Bisht et al., 2019), and collagen-induced arthritis (Liu et al., 2016) in mouse models. Our previous studies have identified that treatment with *Sj*-Cys significantly reduced the pathology caused by LPS-induced (Wan et al., 2018) or bacterial infestation-induced (Li et al., 2017) sepsis in mice with less inflammation and tissue damage through stimulating anti-inflammatory cytokines and inhibiting Th1 pro-inflammatory cytokines. In particular, treatment with *Sj*-Cys significantly reduced sepsis-induced cardiomyopathy (Gao et al., 2020). However, the immunological mechanism and targeted immune cells underlying the immunomodulation and therapeutic effect of *Sj*-Cys on sepsis remains unknown. Due to the important role of M2 macrophages in maintaining immune homeostasis from an inflammatory state to tissue repair, we would like to investigate whether treatment with *Sj*-Cys induces M2 macrophage polarization and whether *Sj*-Cys induced M2 polarization is involved in the therapeutic mechanism on sepsis. In this study, we induced sepsis with cecal ligation and puncture (CLP) in a mouse model. The mice with CLP-induced sepsis were adaptively transferred with *in vitro Sj*-Cys-induced M2 macrophages. We successfully determined that *Sj*-Cys stimulated bone marrow-derived macrophages (BMDMs) to differentiate to M2 and *Sj*-Cys-induced M2 macrophages had significant therapeutic effect on sepsis in adoptively transferred mice characterized with less tissue damage, lower pro-inflammatory cytokines and higher regulatory cytokines compared to mice transferred with normal BMDMs, indicating the M2 macrophage polarization is an important mechanism for the therapeutic effect of *Sj*-Cys on sepsis and other inflammatory diseases.

MATERIALS AND METHODS

Expression and Purification of Recombinant *Sj*-Cys Protein (r*Sj*-Cys)

DNA encoding the full-length *Sj*-Cys (GenBank accession# FJ617450) was synthesized by Zoobio Biotechnology, China,

and then subcloned into yeast expression vector pPIC9k using EcoRI and NotI sites. The correct insert and reading frame of the constructed recombinant plasmid *Sj*-Cys/pPIC9k was confirmed by double-stranded DNA sequencing. The plasmid *Sj*-Cys/pPIC9k was linearized with SacI and then transformed into *P. pastoris* GS115 by electroporation. The expression of r*Sj*-Cys with His-tag at C-terminus was induced with 0.5% methanol for 120 h. The expressed r*Sj*-Cys secreted in the medium was purified with immobilized metal affinity chromatography (IMAC) using a nickel column (Thermo, USA) as previously described (Zhan et al., 2005). The concentration of purified r*Sj*-Cys was measured using an enhanced BCA Protein Assay Kit (Beyotime, China). The purity of r*Sj*-Cys was measured with SDS-PAGE and the His-tag protein was confirmed by Western blotting with the anti-His antibody.

Animals

The specific-pathogen-free male BALB/c mice with weight of 18-20 g, were purchased from the Animal Center of Anhui Medical University. All animal study protocols and procedures were reviewed and approved by the Animal Care and Use Committee of Bengbu Medical College and complied with the National Institutes of Health Guidelines for the Care and Use of Experimental Animals. All efforts were made to minimize the suffering of animals.

Murine Model of Sepsis

A clinically relevant rodent model of sepsis was created by CLP as previously described (Li et al., 2017). Briefly, mice were anesthetized by intraperitoneal injection of 200 μL of 4% chloral hydrate (MACKLIN, China). The abdominal cavity was opened with a midline incision. The cecum was isolated, ligated (1.0 cm from the apex), and punctured with a 22-gauge needle, then returned to the abdominal cavity. The opened abdominal cavity was closed with sutures.

Induction of Mouse Bone Marrow-Derived Macrophages (BMDMs)

Bone marrow cells were collected from sacrificed donor mice by flushing bone marrow cavities of femurs and tibias with complete DMEM medium (HyClone, USA) containing 10% fetal bovine serum (FBS) (EVERY GREEN, China) and penicillin (100 U/ml)/streptomycin (100 μg/ml) (Beyotime, China). The collected bone marrow cells were seeded in a 100 mm Petri dish and incubated with complete DMEM at 37°C, 5% CO_2 for 4 h to collect adherent cells. The collected adherent cells were continuously co-cultured with murine macrophage colony-stimulating factor (M-CSF) (R&D Systems, USA) at 20 ng/ml for 7 days to stimulate the maturation of macrophages. Seven days after the culture, the matured bone marrow-derived macrophages (BMDMs) were examined using FITC-conjugated rat anti-mouse F4/80 (BioLegend, USA) and APC-conjugated rat anti-mouse CD11b (BioLegend, USA) staining.

Macrophage Polarization

To determine the effect of r*Sj*-Cys on the macrophage polarization, a total of 1×10^6 BMDMs obtained above were incubated with r*Sj*-Cys (2 ug/ml). The same number of BMDMs were incubated with LPS (100 ng/ml) (Solarbio, China) as M1 polarization control, and with IL-4 (10 ng/ml) + IL-10 (10 ng/ml) (R&D Systems, USA) as M2 polarization control. After being incubated for 24 h, cells from each group were measured for M1 marker (CD86) and M2 marker (CD206) by flow cytometry. For flow cytometry assay, BMDMs were fixed with fixable viability dye efluor 510 (BioLegend, USA) first in the dark for 10 min at RT to differentiate live/dead cells. After being washed with 2 ml PBS containing 1% FBS, the cells were collected by centrifuging at 500×g for 5 min at RT. After Fc receptors being blocked with α-CD16/32 (BioLegend, USA) for 10 min at RT, the cells were stained with FITC-conjugated rat anti-mouse F4/80 (BioLegend, USA) and APC-conjugated rat anti-mouse CD86 (Thermo Fisher Scientific, USA) for 30 min at 4°C. The cells were fixed and permeabilized using a Thermo Fixation/Permeabilization Kit (Thermo Fisher Scientific, USA) as per manufacturer's instructions, then stained with PE-conjugated rat anti-mouse CD206 (BioLegend, USA) for 30 min at 4°C. The isotype-matched immunoglobulins (BioLegend, USA; Thermo Fisher Scientific, USA) and FMO were used as control for non-specific staining as baseline. The flow cytometry was performed with a flow cytometer DxP Athena (CYTEK, USA) and the data were analyzed using FlowJo-V10 software (BD Biosciences, USA).

Adoptive Transfer of r*Sj*-Cys-Treated BMDMs to Mice With CLP-Induced Sepsis

A total of 56 mice were given CLP surgery to induce sepsis, then randomly divided into 4 groups; another 14 mice served as the blank control group. Thirty minutes after surgery, one group of 14 mice received intravenously with 1×10^6 BMDMs treated with r*Sj*-Cys. Other three groups with the same number of mice received BMDMs treated with LPS, or LPS + r*Sj*-Cys, or PBS, respectively, as controls. Four mice from each group were euthanized 12 h after the macrophage transfer, blood was collected from each euthanized mouse and sera were obtained for serological tests, heart, lung, liver and kidney tissues were collected for histopathologic analysis. The survival rate was observed for 72 h for the left 10 mice from each group.

Serological Test

The levels of alanine transaminase (ALT), aspartate transaminase (AST), blood urea nitrogen (BUN) and creatinine (Cr) in sera were used as biomarkers for tissue damage, cell disruption or failed functions of tissues including liver and kidney (Tesch, 2010; Kwo et al., 2017) in mice with sepsis. These biomarkers were measured in sera of experimental mice (4 of each group) by automatic chemistry analyzer (Beckman Coulter, USA) to evaluate sepsis-caused tissue injury.

Cytokine Measurement

The concentrations of pro-inflammatory (IFN-gamma and IL-6) and regulatory (IL-10 and TGF-β) cytokines in the culture supernatants of BMDMs incubated with r*Sj*-Cys and other controls or in the sera collected from mice 12 h after macrophage transfer were determined using specific ELISA detection kits (Mouse IFN-gamma ELISA Kit, Mouse IL-6

ELISA Kit and Mouse IL-10 ELISA Kit from Dakewe Biotech, China and Mouse TGF-beta 1 ELISA Kit from ABclonal, USA) according to the manufacturer's procedures. In order to remove the exogenously added IL-10 in the culture medium, the culture supernatant in the group with added IL-10 was removed after 24 h of culture, and cells were washed with PBS 3 times. The culture was continued with medium without IL-10 for another 24 h before harvested for IL-10 measurement.

Histopathologic Analysis

Mouse heart, lung, liver and kidney were collected from four mice in each group euthanized 12 h after sepsis induction and receiving treated BMDMs. These tissues were fixed with 4% paraformaldehyde for 24 h, embedded in paraffin, sectioned to a thickness of 4 μm and stained with hematoxylin and eosin. Histological pathology was scored using a semi-quantitative scale as previously described. Briefly, the severity of heart damage was scored 0–4 as follows: 0 = normal; 1 = moderate (normal arrangement of myocardial fibers, punctate myocardial cell edema, degeneration, and necrosis); 2 = severe (normal arrangement of myocardial fibers, scattered myocardial cell edema, degeneration, and necrosis); 3 = extremely severe (loose arrangement of myocardial fibers, sheet-like myocardial cell edema, degeneration, and necrosis); and 4 = critical (loose arrangement of muscle fibers, breakage, and dissolution of myocardial fibers, diffuse edema, degeneration and necrosis of myocardial cells) (Li et al., 2017). Lung injury was determined by the alveolar congestion, tissue hemorrhage, inflammatory cell infiltration and scored 0–4 as follows: 0 = no pathology; 1 = mild (< 25% lung involvement); 2 = moderate (25–50% lung involvement); 3 = severe (50–75% lung involvement); 4 = extremely severe (> 75% lung involvement) (Yang et al., 2019a). Liver injury was determined as hepatocyte edema and tissue congestion/hemorrhage, inflammatory cell infiltration and scored as 0 = no pathology; 1 = mild (< 25% liver involvement); 2 = moderate (25–50% liver involvement); 3 = severe (50–75% liver involvement); 4 = very severe (> 75% lung involvement) (Wang et al., 2019). The degree of kidney injury was scored as follows: 0 = no pathology; 1 = mild (areas of tubular epithelial cell swelling, vacuolar degeneration, necrosis and desquamation involving < 25% of cortical tubules); 2 = moderate with tissue damaged involved > 25% but < 50%; 3 = severe (similar changes involving > 50% but < 75% of cortical tubules); 4 = extremely severe (similar changes involving > 75% of cortical tubules) (Li et al., 2019).

Statistical Analysis

Statistical analysis was performed using SPSS 26.0 software (Chicago, USA). Data were expressed as mean ± SEM. Data with normal distribution and uniform variance were analyzed using unpaired, two-tailed Student's *t*-test with Bonferroni adjustment, or ANOVA for multiple comparisons. A *P*-value less than 0.05 was considered as statistically significant.

RESULTS

Expression of r*Sj*-Cys in Yeast

The r*Sj*-Cys with His-tag at C-terminus was successfully expressed as a soluble protein in *P. pastoris* GS115 under induction with 0.5% methanol for 120 h and purified with IMAC using a nickel column. The purified r*Sj*-Cys migrated as about 12 kDa on SDS-PAGE, the similar size as predicted by sequence (12.4 kDa). A small portion of degradation was observed at lower band (~11 kDa). The purified His-tagged r*Sj*-Cys was recognized by the anti-His antibody on Western blot (**Figure 1**). The smaller band was also recognized by the anti-His antibody, indicating it is a recombinant protein-derived product.

r*Sj*-Cys Induced M2 Macrophage Polarization

BMDMs were obtained by co-incubating with M-CSF (20 ng/ml) for 7 days. Flow cytometry measurement with a complete gating strategy (**Figure 2A**) to differentiate dead cells and adhere cells confirmed that more than 95% cells were labeled with $CD11b^{+}F4/80^{+}$, indicating most of the mouse bone marrow cells have been converted to BMDM cells (**Figure 2B**).

After being incubated with r*Sj*-Cys at 2 ug/ml for 24 h, 47.08 ± 4.59% BMDMs expressed CD206 which is significantly higher than BMDMs incubated with PBS (32.30 ± 2.72%) or LPS (33.32 ± 1.99%), however, incubation with r*Sj*-Cys did not affect the expression of CD86 on BMDMs compared with PBS control, indicating r*Sj*-Cys significantly stimulated M2 macrophage polarization, but not M1. In the control groups, M1 polarization (CD86) was strongly induced by LPS (100 ng/ml), and the IL-4 + IL-10 (each 10 ng/ml) induced M2 polarization (CD206). Interestingly, r*Sj*-Cys itself not only induced macrophage M2 polarization, but also significantly inhibited LPS-induced M1 polarization, however, the r*Sj*-Cys-induced M2 polarization was not affected in the presence of LPS (**Figures 2C–E**).

The cytokine profiles in the culture supernatants of each incubation group also showed that r*Sj*-Cys induced BMDMs to secrete M2 macrophages-related IL-10 and TGF-β, and LPS was not able to inhibit r*Sj*-Cys induced M2-related cytokines (IL-10 and TGF-β). Incubation of BMDMs with r*Sj*-Cys also induced M1-related cytokines IFN-gamma and IL-6 compared to PBS control, however, co-incubation with r*Sj*-Cys reduced LPS-induced M1 cytokines (IFN-gamma and IL-6) (**Figure 3**).

Adoptive Transfer of r*Sj*-Cys Treated-BMDMs Mitigated CLP-Induced Sepsis in Mouse

To evaluate the therapeutic effect of r*Sj*-Cys treated-BMDMs on sepsis, mice with CLP-induced sepsis were adoptively transferred with r*Sj*-Cys treated-BMDMs, the survival rate in each group was observed and the pathological improvement was identified in tissues of the treated mouse. All mice with CLP-induced sepsis without macrophage transfer or receiving LPS-treated BMDMs died within 24 h, however, 80% of mice adoptively transferred with rSj-Cys treated BMDMs survived up to 72 h while only 20% of mice receiving non-treated BMDMs survived (**Figure 4A**).

Histological examination showed significant damage in the hearts, lungs, livers, and kidneys of mice with CLP-induced sepsis. Specifically, all tissues showed varying degree of edema

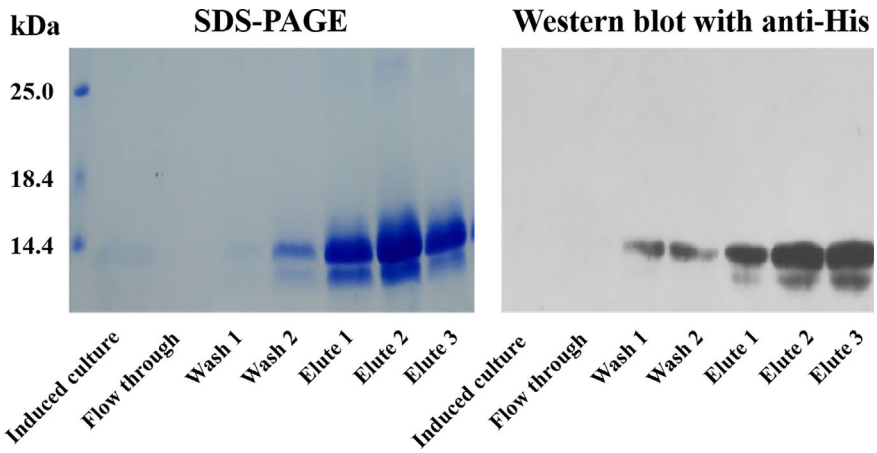

FIGURE 1 | IMAC purification of recombinant *Sj*-Cys expressed in *P. pastoris* GS115. The r*Sj*-Cys with His-tag at C-terminus was expressed as a soluble protein in the culture medium. After binding on the nickel column, r*Sj*-Cys was eluted in a buffer containing imidazole. The purified protein was recognized by the anti-His antibody.

and swelling, inflammatory cell infiltration, disrupted or disordered tissue structure, hemorrhages, and congestion (**Figures 4B, C**). The amount of ALT, AST, BUN and Cr also remained at high levels in the sera of mice with sepsis (**Figure 4D**), further indicating the tissue damage caused by serious infection and sepsis.

After being passively transferred with r*Sj*-Cys-treated BMDMs, the mice with sepsis revealed significantly reduced tissue damage and inflammatory cell infiltration in all tissues of heart, lung, liver and kidney compared with tissues of mice receiving untreated-BMDMs or PBS only. Strikingly, sepsis mice receiving LPS-treated BMDMs showed significantly more serious damage in all tissues compared with mice receiving untreated BMDMs or PBS control groups (**Figures 4B, C**). However, the LPS-treated BMDMs exacerbated pathology was significantly reduced in all tissues of mice when receiving LPS-treated BMDMs co-incubated with r*Sj*-Cys, indicating *Sj*-Cys mitigated LPS-induced inflammation and tissue damage. The levels of ALT, AST, BUN, and Cr in serum were also greatly decreased in mice after receiving r*Sj*-Cys-treated BMDMs compared to mice receiving untreated BMDMs or PBS only, reflecting the reduced injury or damage of tissue cells (**Figure 4D**).

r*Sj*-Cys Treated-BMDMs Downregulated Pro-Inflammatory Cytokines and Upregulated Regulatory Cytokines in Mice With Sepsis

To further understand the potential immunological mechanism underlying the therapeutic effect of r*Sj*-Cys treated BMDMs on sepsis in mice, the cytokine profile was measured in the serum of each treated mouse. As shown in **Figure 5**, the levels of inflammatory cytokines IFN-gamma and IL-6 were significantly reduced in mice with CLP-induced sepsis when receiving r*Sj*-Cys-treated BMDMs compared with sepsis mice receiving untreated BMDMs or PBS control. The mice receiving LPS-treated BMDMs showed even high production of IFN-gamma and IL-6 than the mice receiving non-treated BMDMs. On the other hand, the levels of regulatory cytokines IL-10 and TGF-β were significantly increased in sera of sepsis mice receiving r*Sj*-Cys-treated BMDMs compared with control mice receiving untreated or LPS-treated BMDMs or PBS only. The results further suggested that r*Sj*-Cys promoted M2 macrophage polarization which upregulated regulatory cytokines and downregulated pro-inflammatory cytokines production in donor mice, thus coffering a therapeutic effect on sepsis-induced inflammation and pathology.

DISCUSSION

In this article, we described a regulatory macrophage induced by the helminth immunomodulatory protein *Sj*-Cys and demonstrated its ability to efficiently suppress inflammatory responses in experimental CLP-induced sepsis. More and more evidence has shown that helminth infection causes damage on host, at meanwhile, it plays important roles in modulating host immune responses through secreting some proteins with immunomodulatory functions to reduce inflammation as a survival strategy (Venugopal et al., 2017; Ding et al., 2020). As a bystander effect, helminth infection or helminth-derived proteins enable to reduce host hypersensitivity to some allergens or autoantigen, therefore have been used to treat inflammatory diseases such as allergic asthma (Park et al., 2011; Aranzamendi et al., 2013; Ziegler et al., 2015; Sun et al., 2019a) or inflammatory bowel diseases (Du et al., 2011b; Ziegler et al., 2015; Sotillo et al., 2017; Xu et al., 2019). The identified mechanisms for helminth-induced immunomodulation are usually related to induce host Th2 and regulatory T cell (Treg) responses so as to reduce pro-inflammatory cytokines and

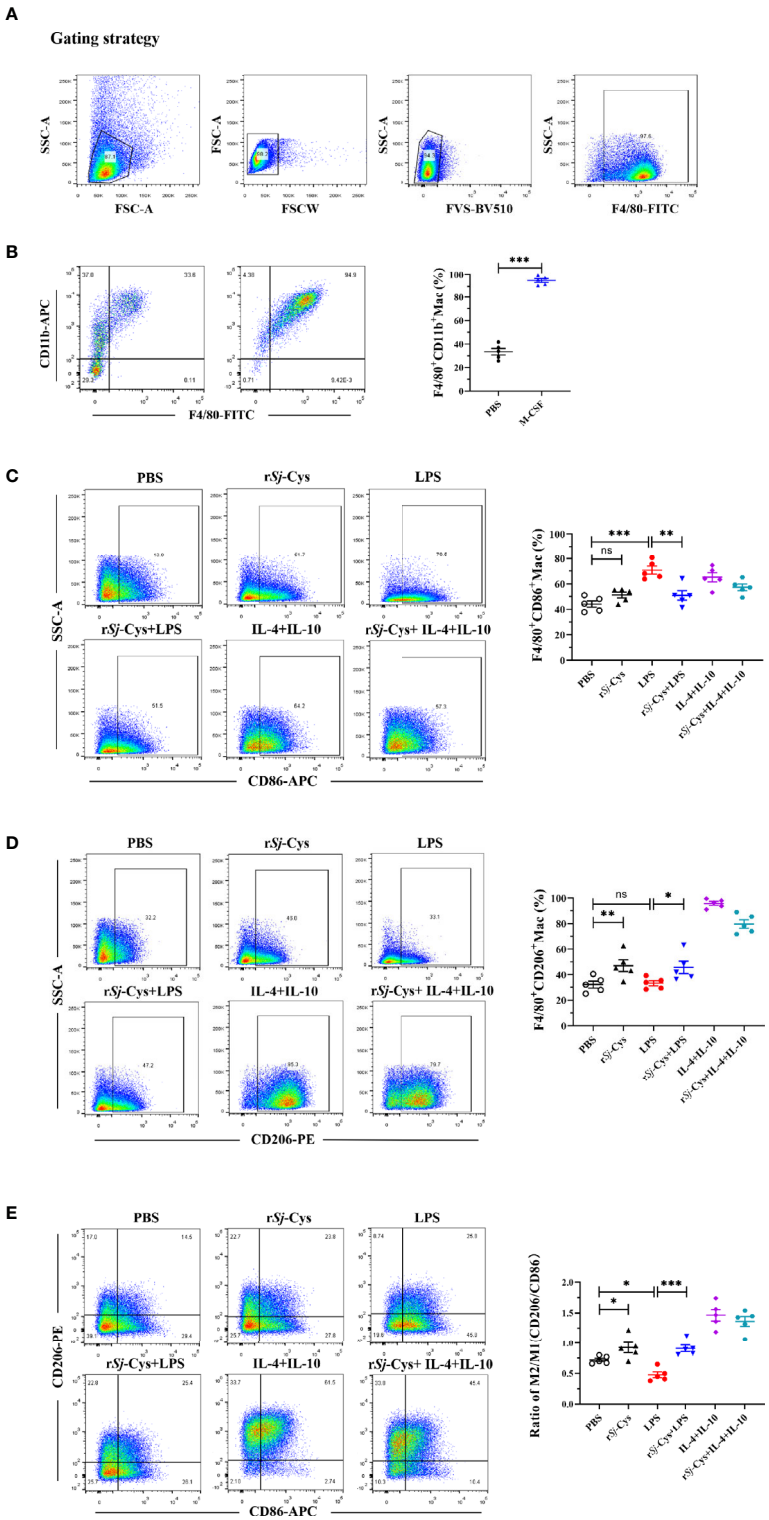

FIGURE 2 | r*Sj*-Cys induced M2 macrophage polarization and reduced LPS-induced M1 macrophages phenotype *in vitro*. **(A)** The flow cytometry experiments were repeated by adding live/dead cell staining, and re-gated to differentiate dead cells, adhere cells and to block Fc. **(B)** BMDMs were obtained by incubating mouse bone marrow cells (adherent) with M-CSF for 7 days. The mature BMDMs were defined as $CD11b^{+}F4/80^{+}$ subpopulations using FACS. **(C–E)** BMDMs were incubated with r*Sj*-Cys (2 ug/ml), LPS (100 ng/ml), IL-4 (10 ng/ml) + IL-10 (10 ng/ml), r*Sj*-Cys + LPS, r*Sj*-Cys + IL-4 + IL-10, or PBS, respectively, for 24 h. The M1 (CD86) and M2 (CD206) markers were detected using FACS. n = 5. Data are expressed as mean ± SEM, ns, not significant, $^{*}P < 0.05$, $^{**}P < 0.01$, $^{***}P < 0.001$, $^{****}P < 0.0001$.

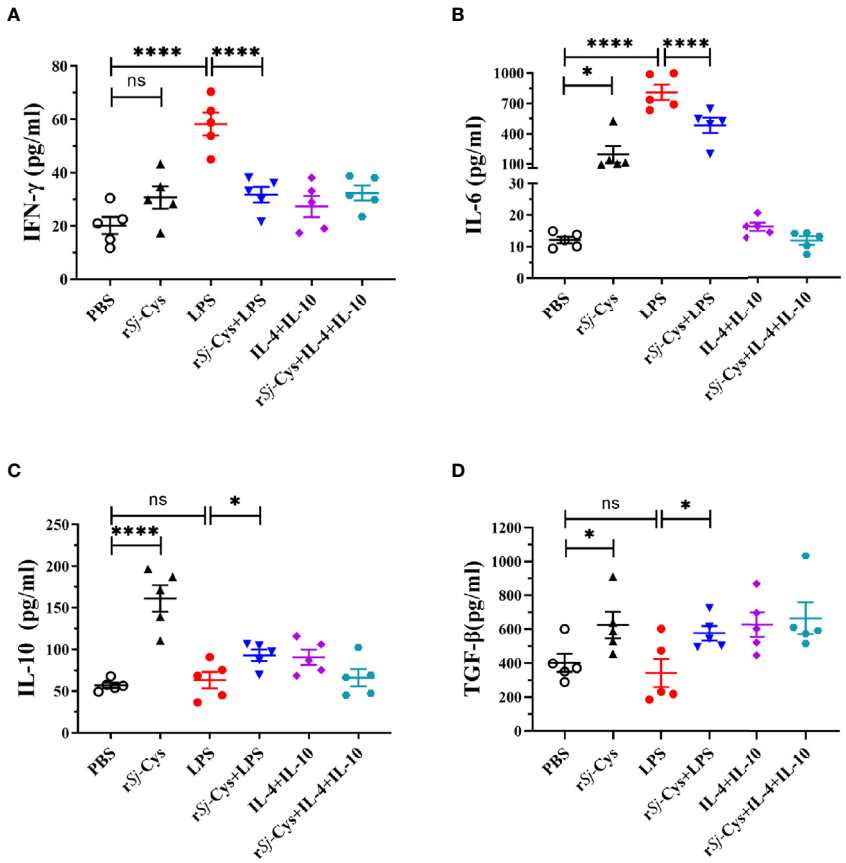

FIGURE 3 | r*Sj*-Cys induced BMDMs to secrete M2 macrophage-related cytokines IL-10 and TGF-β. Mature BMDMs were stimulated with PBS, r*Sj*-Cys (2 ug/ml), LPS (100 ng/ml), IL-4 (10 ng/ml) + IL-10 (10 ng/ml), r*Sj*-Cys + LPS, or r*Sj*-Cys + IL-4 + IL-10 for 24 h. The levels of M2-related cytokines IL-10 **(C)**, TGF-β **(D)**, and M1-related cytokines IFN-gamma **(A)**, IL-6 **(B)** were measured in the supernatant by ELISA. n = 5. The results are presented as mean ± SEM, ns, not significant, $^{*}P < 0.05$, $^{**}P < 0.01$, $^{***}P < 0.001$, $^{****}P < 0.0001$.

subsequent inflammation (Shevach, 2009; Maruyama et al., 2011; Velavan and Ojurongbe, 2011; Gao et al., 2012; Kobpornchai et al., 2020).

Recent studies indicated that innate immune cells are involved in immunomodulation mediated by parasitic worms (Chen et al., 2016; Jiang et al., 2018; Jin et al., 2019; Cai et al., 2020), but little is known about the specific immune cells targeted by helminth immunomodulatory proteins or the mechanisms conferring suppression of ongoing inflammatory immune responses (Chuah et al., 2014). Macrophage cells are not only involved in the direct process of specific immune responses as antigen presenting cells, but also act as innate immune cells to clear pathogens or senescent/apoptotic cells through phagocytosis (Mosser and Edwards, 2008). In recent year, macrophages have been identified to play important roles in maintaining immune homeostasis by regulating the polarization of M1 or M2 subtype macrophages. The M1 macrophages stimulate inflammation by secreting pro-inflammatory cytokines and chemokines to promote clearing of invaded pathogens, while M2 reduce inflammation by secreting anti-inflammatory cytokines to play important roles in immunosuppressive function, wound healing and tissue repair (Wynn et al., 2013; Francos-Quijorna et al., 2016).

In our previous studies, we demonstrated that *Sj*-Cys protein suppressed inflammation when applied to mice with sepsis induced by CLP operation in a mouse model (Wan et al., 2018). In this study, we showed that the r*Sj*-Cys-modulated regulatory macrophages are sufficient to replicate the anti-inflammatory effects of r*Sj*-Cys. To gain insight into the immunomodulatory properties of r*Sj*-Cys, the effect of *Sj*-Cys on the induction of different macrophage subpopulations (M1 and M2) has been explored in the study. Our results showed that incubation of r*Sj*-Cys with BMDMs significantly stimulated M2 macrophage polarization (47.08% expressed CD206, **Figures 2C–E**) associated with the secretion of regulatory cytokines IL-10 and TGF-β (**Figure 3**). Interestingly, incubation of r*Sj*-Cys with BMDMs even inhibited the secretion of LPS-induced pro-inflammatory cytokines IFN-gamma and IL-6, and the addition of LPS could not prevent r*Sj*-Cys-treated BMDMs from the secretion of IL-10 and TGF-β, (**Figure 3**), indicating r*Sj*-Cys is able to inhibit bacterial infection-induced inflammation. It is well known that IL-10 and TGF-β play an important role in

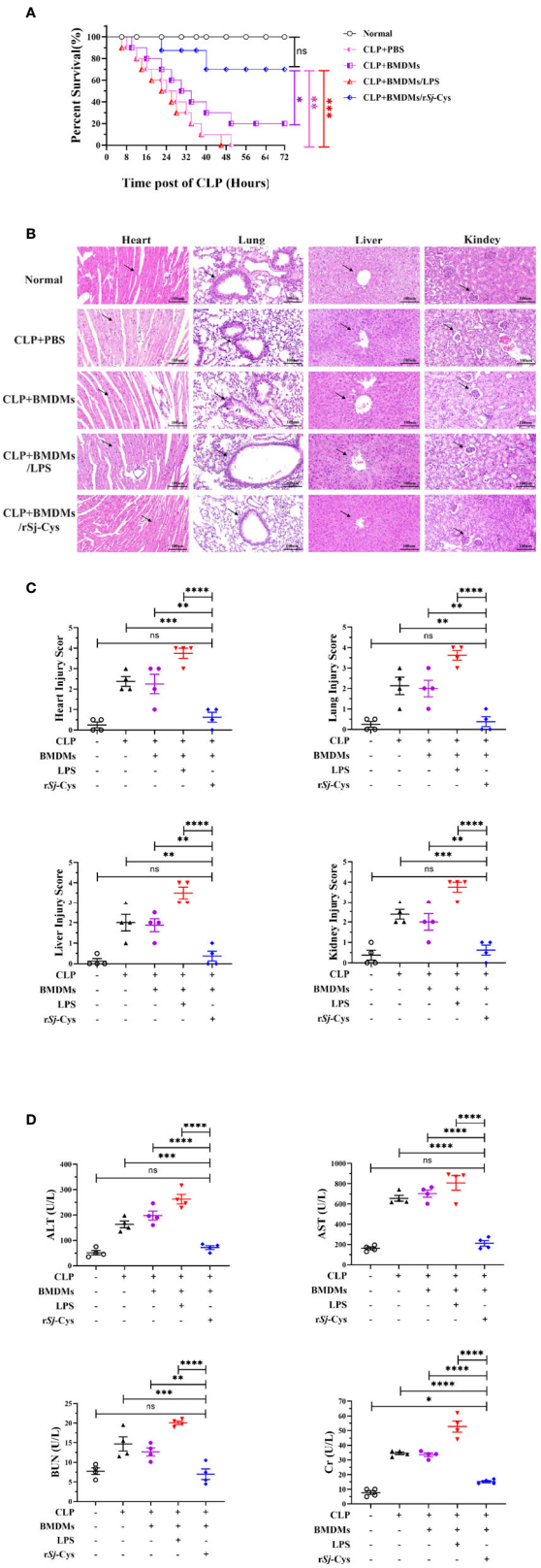

FIGURE 4 | Continued

FIGURE 4 | Adoptive transfer of rSj-Cys treated-BMDMs mitigated pathology caused by CLP-induced sepsis. **(A)** Mice adoptively transferred with r*Sj*-Cys-treated BMDMs significantly increased their survival rate up to 72 h (80%) compared to mice receiving PBS (0%), LPS-treated BMDMs (0%), or untreated BMDMs (20%) during the same observation period (n = 10). **(B, C)** The results of histopathology of heart, lung, liver and kidney stained with H&E staining from mice 12 h after CLP and transferred with BMDMs treated with r*Sj*-Cys, LPS or untreated BMDMs (n = 4). The pathological score comparison was shown on the right. The magnification ×400, scale bar = 100 μm. **(D)** The levels of ALT, AST, BUN, and Cr were measured in the sera from mice 12 h after receiving CLP and differently treated BMDMs (n = 4). The results are presented as mean ± SEM. ns, not significant, $^{*}P < 0.05$, $^{**}P < 0.01$, $^{***}P < 0.001$, $^{****}P < 0.0001$.

establishing tolerance and suppression of inflammation diseases (Murray et al., 2014; Li et al., 2018; Yan et al., 2020). IL-10 is a particularly noteworthy cytokine because it has anti-inflammatory properties and influences in the activity of several cell types of the immune system, thereby regulating the immune network (Verma et al., 2016; Mazer et al., 2019; Saraiva et al., 2020). The TGF-β is a pleiotropic cytokine with important immunoregulatory functions to reduce activities related to immune disorders (Branchett and Lloyd, 2019). Results in this study confirm that *Sj*-Cys not only stimulates the polarization of M2 macrophage, but also inhibits macrophage's pro-inflammatory responses to LPS, further indicating the ability of r*Sj*-Cys to stimulate M2 macrophage regulatory property and reverse LPS-induced M1 differentiation and inflammation caused by sepsis or other bacterial infection.

To verify whether r*Sj*-Cys-induced M2 macrophages are involved in the therapeutic effect of r*Sj*-Cys on sepsis, the mice with CLP-induced sepsis were adoptively transferred with r*Sj*-Cys-treated BMDMs. The results revealed that the 72 h survival rate of mice with CLP-induced sepsis was significantly improved after being transferred with r*Sj*-Cys-treated BMDMs (80%) compared with mice receiving non-treated normal BMDMs (20%) or LPS-treated BMDMs (mimicking sepsis condition) or PBS only (0%) (**Figure 4A**), confirming that the therapeutic effect of *Sj*-Cys can be conducted by *Sj*-Cys-induced M2 macrophages. The therapeutic effect of *Sj*-Cys-induced M2 macrophages on sepsis was also reflected by the reduced pathological damages in organs of heart, lung, liver and kidney caused by sepsis (**Figures 4B, C**) and reduced serological levels of tissue injury-related enzymes or proteins including ALT, AST, BUN and Cr (**Figure 4D**). The cytokine profile in sera of mice receiving *Sj*-Cys-induced M2 macrophages also showed significantly upregulated anti-inflammatory IL-10 and TGF-β and down-regulated pro-inflammatory IFN-gamma and IL-6. This inhibitory cytokine profile could be derived from the direct secretion of transferred M2 macrophages or subsequent inhibitory immune responses induced by transferred M2 subtype in recipient mice. All mice with sepsis adoptively transferred with LPS-activated BMDMs demonstrated more severe inflammation and tissue damage, aggravating the bacterial infection caused inflammation. Our results are consistent with the previous finding that systemic inflammation of sepsis leads to partial activation of BMDM, deteriorating the inflammation and pathological damage (Zhu et al., 2014).

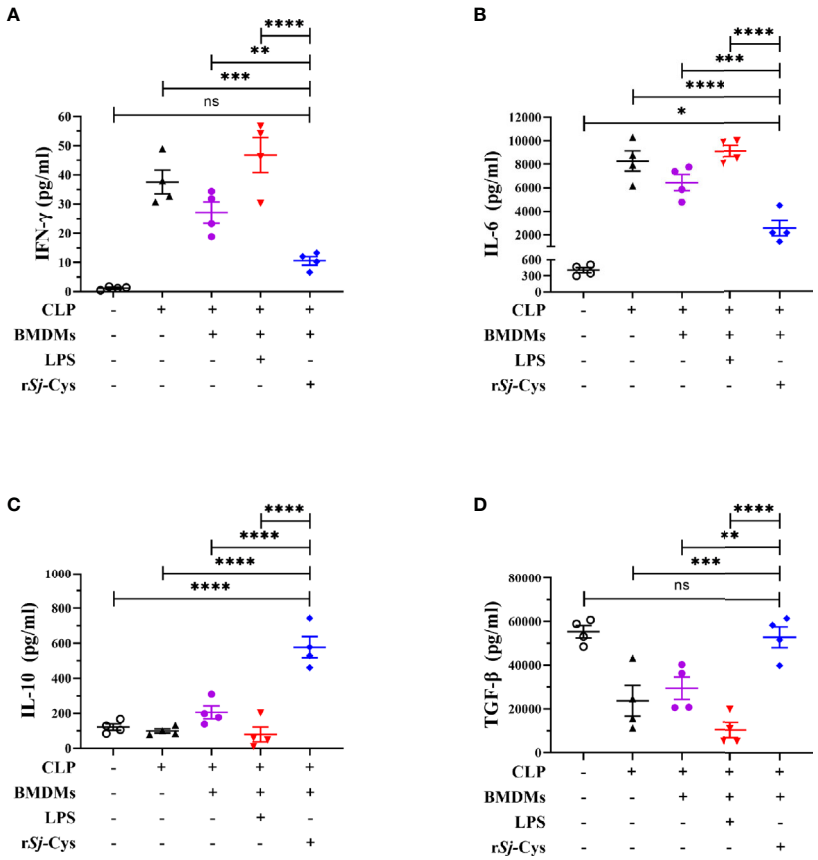

FIGURE 5 | r*Sj*-Cys treated-BMDMs downregulated pro-inflammatory cytokines and upregulated regulatory cytokines in mice with sepsis. The levels of IFN-gamma **(A)**, IL-6 **(B)**, IL-10 **(C)**, and TGF-β **(D)** were measured in the sera of mice in each group using ELISA. n = 4. The results are presented as mean ± SEM. ns, not significant, $^{*}P < 0.05$, $^{**}P < 0.01$, $^{***}P < 0.001$, $^{****}P < 0.0001$.

All results in this study provide the evidence at the first time that r*Sj*-Cys-induced M2 macrophage polarization was involved in the therapeutic effects of r*Sj*-Cys on sepsis-caused inflammation and tissue damages, providing another immunological mechanism pathway for immunomodulatory functions of helminth-secreted proteins except for the Treg regulatory pathway. However, the M2 macrophage-secreted regulatory cytokines IL-10 and TGF-β could further stimulate Treg responses (Wang et al., 2016a). It is also identified that helminth-secreted proteins stimulated Treg response through up-regulating PD-1 in $CD4^+$ T cells (Cheng et al., 2018). A recent study also showed that helminth-derived proteins stimulated Treg differentiation through activating dendritic cells (Sun et al., 2019b). It is unknown if PD-1 or dendritic cells pathways are involved in the r*Sj*-Cys-initiated immunomodulation.

The finding of the therapeutic effect of r*Sj*-Cys-induced M2 on the inflammatory sepsis in this study provides evidence that a therapeutic approach for the treatment of inflammatory disorders based on cells modulated by a single parasitic molecule may be feasible. Such an approach would be attractive because it allows the exploitation of helminth immunomodulatory therapy without the risk of living worms or the side effects of direct application of worm-derived proteins. Cell-based therapies constitute a promising approach in which cells are differentiated into an immunosuppressive or regulatory phenotype in administered patients (Ledesma-Soto et al., 2015; Kang et al., 2019). Several basic and clinical immunotherapy studies have been performed with adoptive cells, such as T cells, NK cells, dendritic cells, to targeting cancer (Magalhaes et al., 2019; Wculek et al., 2019; Xiao et al., 2019). Cell immunotherapy studies advance not only in the field of cancer but also in inflammatory disease. Adoptive transfer of helminth protein induced M2 (Ziegler et al., 2015; Reyes et al., 2016) or SNX10 deficiency induced M2 macrophages (You et al., 2016) ameliorated inflammatory bowel diseases in wild-type mice. There is evidence that mesenchymal stem/stromal cells (MSCs) could be used as a therapy for sepsis and acute respiratory distress syndrome (Byrnes et al., 2021). Adoptive transfer of macrophages containing antimicrobial peptides was successfully used for the treatment of multidrug-resistant bacteria-induced sepsis in mice (Hou et al., 2020). Inhibition of mitophagy promoted macrophage activation favored bactericidal clearance, adoptive transfer of these macrophages to mice with sepsis resulted in better survival (Patoli et al., 2020). It was also showed that adoptive transfer of polarized M2c macrophages reduced acute rejection to liver transplantation

in rat (Yang et al., 2020a). The macrophages have been evaluated as good candidates for cell-based therapeutic intervention not only for inflammatory diseases, but also for autoimmune diseases (De Dios Ruiz-Rosado et al., 2017).

Our results further confirmed the strong immunomodulatory functions of *Sj*-Cys, especially on the polarization of macrophages to regulatory M2 subtype. Adoptive transfer of *Sj*-Cys-induced M2 macrophages significantly mitigated the inflammation and tissue damage in mice with sepsis, providing a novel therapeutic approach for the treatment of inflammatory disorders.

DATA AVAILABILITY STATEMENT

The original contributions presented in the study are included in the article/supplementary material. Further inquiries can be directed to the corresponding authors.

ETHICS STATEMENT

The animal study was reviewed and approved by The Animal Care and Use Committee of Bengbu Medical College.

AUTHOR CONTRIBUTIONS

XY, RZ, HX, and LW conceived and designed the study. HX, LW, SG, JL, SW, and CX performed the experiments. XC, HL, YY, XW, and LC analyzed the data. HX and LW wrote the manuscript. BZ, XY, and RZ critically revised the manuscript. All authors contributed to the article and approved the submitted version.

FUNDING

This study was supported by the Science Foundation of Anhui Province (2008085MH260 and gxbjZD15); the Program of Natural Science Foundation of the Anhui Higher Education Institutions (KJ2019A0383, KJ2020A0554, KJ2020A0566 and KJ2020A0572); 512 Talents Development Project of Bengbu Medical College (by51201205 and by51201306); the Science Foundation of Bengbu Medical College (BYTM2019002, BYLK201818 and BYKY2019033ZD); the Postgraduate Scientific Research Innovation Program of Bengbu Medical College (Byycx1903) and the National University Students' Innovation and Entrepreneurship Training Program (201910367002 and 202010367006).

REFERENCES

Aranzamendi, C., de Bruin, A., Kuiper, R., Boog, C. J. P., van Eden, W., Rutten, V., et al. (2013). Protection against allergic airway inflammation during the chronic and acute phases of *Trichinella spiralis* infection. *Clin. Exp. Allergy* 43, 103–115. doi: 10.1111/cea.12042

Baghdadi, J. D., Brook, R. H., Uslan, D. Z., Needleman, J., Bell, D. S., Cunningham, W. E., et al. (2020). Association of a care bundle for early sepsis management with mortality among patients with hospital-onset or community-onset sepsis. *JAMA Intern. Med.* 180, 707–716. doi: 10.1001/jamainternmed.2020.0183

Bisht, N., Khatri, V., Chauhan, N., and Kalyanasundaram, R. (2019). Cystatin from filarial parasites suppress the clinical symptoms and pathology of experimentally induced colitis in mice by inducing T-Regulatory cells, B1-cells, and alternatively activated macrophages. *Biomedicines* 31, 7(4)–7(85. doi: 10.3390/biomedicines7040085

Bozza, F. A., Salluh, J. I., Japiassu, A. M., Soares, M., Assis, E. F., Gomes, R. N., et al. (2007). Cytokine profiles as markers of disease severity in sepsis: A multiplex analysis. *Crit. Care* 11, R49. doi: 10.1186/cc5783

Branchett, W. J., and Lloyd, C. M. (2019). Regulatory cytokine function in the respiratory tract. *Mucosal Immunol.* 12, 589–600. doi: 10.1038/s41385-019-0158-0

Byrnes, D., Masterson, Ã. C. H., and Laffey, J. G. (2021). Mesenchymal stem /stromal cells therapy for sepsis and acute respiratory distress syndrome. *Semin. Respir. Crit. Care Med.* 42 (1), 20–39. doi: 10.1055/s-0040-1713422

Cai, J., Huang, L., Wang, L. J., Zheng, M. H., and Liu, H. (2020). The role of macrophage polarization in parasitic infections: A review. *Zhongguo Xue Xi Chong Bing Fang Zhi Za Zhi* 32, 432–435. doi: 10.16250/j.32.1374.2019252

Chen, Z., Tang, H., Liang, Y., Yang, W., Wu, J., Hu, X., et al. (2016). Recombinant *Trichinella spiralis* 53-kDa protein activates M2 macrophages and attenuates the LPS-induced damage of endotoxemia. *Innate Immun.* 22, 419–432. doi: 10.1177/1753425916651984

Chen, L., He, B., Hou, W., and He, L. (2017). Cysteine protease inhibitor of *Schistosoma japonicum* - a parasite-derived negative immunoregulatory factor. *Parasitol. Res.* 116, 901–908. doi: 10.1007/s00436-016-5363-0

Cheng, Y., Zhu, X., Wang, X., Zhuang, Q., Huyan, X., Sun, X., et al. (2018). *Trichinella spiralis* infection mitigates collagen-induced arthritis via programmed death 1-mediated immunomodulation. *Front. Immunol.* 9:1566. doi: 10.3389/fimmu.2018.01566

Chuah, C., Jones, M. K., Burke, M. L., Mcmanus, D. P., Owen, H. C., and Gobert, G. N. (2014). Defining a pro-inflammatory neutrophil phenotype in response to *schistosome* eggs. *Cell. Microbiol.* 16, 1666–1677. doi: 10.1111/cmi.12316

De Dios Ruiz-Rosado, J., Diana, M. S., Frank, R. A., Miriam, R. S. M., Guerau-De-Arellano, M., Santiago, P. S., et al. (2017). Helminth-induced Ly6C^{hi} monocyte-derived alternatively activated macrophages suppress experimental autoimmune encephalomyelitis. *Sci. Rep.* 7, 1–13. doi: 10.1038/srep40814

Ding, J., Liu, X., Bai, X., Wang, Y., Li, J., Wang, C., et al. (2020). *Trichinella spiralis*: Inflammation modulator. *J. Helminthol.* 94, e193. doi: 10.1017/S0022149X20000802

Du, L. L., Liang, Y. B., Tang, H., Chen, Z.B., Li, Z. Y., Wu, J. G., et al. (2011a). The protective effect of chronic *Schistosoma japonica* infestation against sepsis in mice. *Chin. Crit. Care Med.* 23, 290–293. doi: 10.3760/cma.j.issn.1003-0603.2011.05.011

Du, L., Tang, H., Ma, Z., Xu, J., Gao, W., Chen, J., et al. (2011b). The protective effect of the recombinant 53-kDa protein of *Trichinella spiralis* on experimental colitis in mice. *Dig. Dis. Sci.* 56, 2810–2817. doi: 10.1007/s10620-011-1689-8

Fink, M. P., and Shaw Warren, H. (2014). Strategies to improve drug development for sepsis. *Nat. Rev. Drug Discov.* 13, 741–758. doi: 10.1038/nrd4368

Francos-Quijorna, I., Amo-Aparicio, J., Martinez-Muriana, A., and López-Vales, R. (2016). IL-4 drives microglia and macrophages toward a phenotype conducive for tissue repair and functional recovery after spinal cord injury. *Glia* 64, 2079–2092. doi: 10.1002/glia.23041

Gao, Y., Lin, F., Su, J., Gao, Z., Li, Y., Yang, J., et al. (2012). Molecular mechanisms underlying the regulation and functional plasticity of FOXP3 regulatory T cells. *Genes Immun.* 13, 1–13. doi: 10.1038/gene.2011.77

Gao, S., Li, H., Xie, H., Wu, S., Yuan, Y., Chu, L., et al. (2020). Therapeutic efficacy of *Schistosoma japonicum* cystatin on sepsis-induced cardiomyopathy in a mouse model. *Parasit. Vectors.* 13 (1), 260. doi: 10.1186/s13071-020-04104-3

Ge, Y., Xu, X., Liang, Q., Xu, Y., and Huang, M. (2019). α-Mangostin suppresses NLRP3 inflammasome activation via promoting autophagy in LPS-stimulated murine macrophages and protects against CLP-induced sepsis in mice. *Inflamm. Res.* 68, 471–479. doi: 10.1007/s00011-019-01232-0

Giri, B. R., and Cheng, G. (2019). Host miR-148 regulates a macrophage-mediated immune response during *Schistosoma japonicum* infection. *Int. J. Parasitol.* 49, 993–997. doi: 10.1016/j.ijpara.2019.08.002

Guo, L., Meng, M., Wei, Y., Lin, F., Jiang, Y., Cui, X., et al. (2019). Protective effects of live combined B. Subtilis and E. Faecium in polymicrobial sepsis through modulating activation and transformation of macrophages and mast cells. *Front. Pharmacol.* 9:1506. doi: 10.3389/fphar.2018.01506

Hou, X., Zhang, X., Zhao, W., Zeng, C., Deng, B., Mccomb, D. W., et al. (2020). Vitamin lipid nanoparticles enable adoptive macrophage transfer for the treatment of multidrug-resistant bacterial sepsis. *Nat. Nanotechnol.* 15, 41–46. doi: 10.1038/s41565-019-0600-1

Huang, M., Cai, S., and Su, J. (2019). The pathogenesis of sepsis and potential therapeutic targets. *Int. J. Mol. Sci.* 20:5376. doi: 10.3390/ijms20215376

Jang, J. C., Li, J., Gambini, L., Batugedara, H. M., Sati, S., Lazar, M. A., et al. (2017). Human resistin protects against endotoxic shock by blocking LPS-TLR4 interaction. *Proc. Natl. Acad. Sci. U. S. A.* 114, E10399–E10408. doi: 10.1073/pnas.1716015114

Jiang, J., Yin, H., Sun, Y., Huang, H., and Hu, X. (2018). *Clonorchis sinensis* cyclophilin A immunization protected mice from CLP-induced sepsis. *Int. Immunopharmacol.* 59, 347–353. doi: 10.1016/j.intimp.2018.03.039

Jin, X., Yang, Y., Bai, X., Shi, H., Zhang, W., Zhang, Z., et al. (2019). Dendritic cells treated by *Trichinella spiralis* muscle larval excretory/secretory products alleviate TNBS-induced colitis in mice. *Int. Immunopharmacol.* 70, 378–386. doi: 10.1016/j.intimp.2019.02.028

Jin, Z., Zhu, Z., Liu, S., Hou, Y., Tang, M., Zhu, P., et al. (2020). TRIM59 protects mice from sepsis by regulating inflammation and phagocytosis in macrophages. *Front. Immunol.* 11, 263. doi: 10.3389/fimmu.2020.00263

Kang, S. A., Park, M. K., Park, S. K., Choi, J. H., Lee, D. I., Song, S. M., et al. (2019). Adoptive transfer of *Trichinella spiralis*-activated macrophages can ameliorate both Th1- and Th2-activated inflammation in murine models. *Sci. Rep.* 9, 1–17. doi: 10.1038/s41598-019-43057-1

Kobpornchai, P., Flynn, R. J., Reamtong, O., Rittisoonthorn, N., Kosoltanapiwat, N., Boonnak, K., et al. (2020). A novel cystatin derived from *Trichinella spiralis* suppresses macrophage-mediated inflammatory responses. *PLoS Negl. Trop. Dis.* 14 (4), e0008192. doi: 10.1371/journal.pntd.0008192

Kwo, P. Y., Cohen, S. M., and Lim, J. K. (2017). ACG clinical guideline: Evaluation of abnormal liver chemistries. *Am. J. Gastroenterol.* 112, 18–35. doi: 10.1038/ajg.2016.517

Ledesma-Soto, Y., Callejas, B. E., Terrazas, C. A., Reyes, J. L., Espinoza-Jiménez, A., González, M. I., et al. (2015). Extraintestinal helminth infection limits pathology and proinflammatory cytokine expression during DSS-induced ulcerative colitis: A role for alternatively activated macrophages and prostaglandins. *BioMed. Res. Int.* 2015:563425. doi: 10.1155/2015/563425

Ley, K. (2017). M1 means kill; M2 means heal. *J. Immunol.* 199, 2191–2193. doi: 10.4049/jimmunol.1701135

Li, H., Wang, S., Zhan, B., He, W., Chu, L., Qiu, D., et al. (2017). Therapeutic effect of *Schistosoma japonicum* cystatin on bacterial sepsis in mice. *Parasit. Vectors* 10, 222. doi: 10.1186/s13071-017-2162-0

Li, Y., Xie, Z., Wang, Y., and Hu, H. (2018). Macrophage M1/M2 polarization in patients with pregnancy-induced hypertension. *Can. J. Physiol. Pharmacol.* 96 (9), 922–928. doi: 10.1139/cjpp-2017-0694

Li, Y. F., Xu, B. Y., An, R., Du, X. F., Yu, K., Sun, J. H., et al. (2019). Protective effect of anisodamine in rats with glycerol-induced acute kidney injury. *BMC Nephrol.* 20, 223. doi: 10.1186/s12882-019-1394-y

Liang, X., Li, T., Zhou, Q., Pi, S., Li, Y., Chen, X., et al. (2019). Mesenchymal stem cells attenuate sepsis-induced liver injury via inhibiting M1 polarization of Kupffer cells. *Mol. Cell Biochem.* 452, 187–197. doi: 10.1007/s11010-018-3424-7

Liu, F., Cheng, W., Pappoe, F., Hu, X., Wen, H., Luo, Q., et al. (2016). *Schistosoma japonicum* cystatin attenuates murine collagen-induced arthritis. *Parasitol. Res.* 115, 3795–3806. doi: 10.1007/s00436-016-5140-0

Magalhaes, I., Carvalho-Queiroz, C., Hartana, C. A., Kaiser, A., Lukic, A., Mints, M., et al. (2019). Facing the future: challenges and opportunities in adoptive T cell therapy in cancer. *Expert Opin. Biol. Ther.* 19, 811–827. doi: 10.1080/14712598.2019.1608179

Maruyama, T., Konkel, J. E., Zamarron, B. F., and Chen, W. J. (2011). The molecular mechanisms of Foxp3 gene regulation. *Semin. Immunol.* 23, 418–423. doi: 10.1016/j.smim.2011.06.005

Mazer, M., Unsinger, J., Drewry, A., Walton, A., Osborne, D., Blood, T., et al. (2019). IL-10 has differential effects on the innate and adaptive immune systems of septic patients. *J. Immunol. (Baltimore Md.: 1950)* 203 (8), 2088–2099. doi: 10.4049/jimmunol.1900637

Mehta, A., Brewington, R., Chatterji, M., Zoubine, M., Kinasewitz, G. T., Peer, G. T., et al. (2004). Infection-induced modulation of M1 and M2 phenotypes in circulating monocytes: Role in immune monitoring and early prognosis of sepsis. *Shock* 22, 423–430. doi: 10.1097/01.shk.0000142184.49976.0c

Mosser, D. M., and Edwards, J. P. (2008). Exploring the full spectrum of macrophage activation. *Nat. Rev. Immunol.* 8, 958–969. doi: 10.1038/nri2448

Murray, P. J., Allen, J. E., Biswas, S. K., Fisher, E. A., Gilroy, D. W., Goerdt, S., et al. (2014). Macrophage activation and polarization: nomenclature and experimental guidelines. *Immunity* 41, 14–20. doi: 10.1016/j.immuni.2014.06.008

Park, H. K., Cho, M. K., Choi, S. H., Kim, Y. S., and Yu, H. S. (2011). *Trichinella spiralis*: Infection reduces airway allergic inflammation in mice. *Exp. Parasitol.* 127, 539–544. doi: 10.1016/j.exppara.2010.10.004

Patoli, D., Lagrost, L., and Thomas, C. (2020). Inhibition of mitophagy drives macrophage activation and anti-bacterial defense during sepsis. *Clin. Invest.* 130 (11), 5858–5874. doi: 10.1172/JCI130996

Reyes, J. L., Lopes, F., Leung, G., Mancini, N. L., Matisz, C. E., Wang, A., et al. (2016). Treatment with cestode parasite antigens results in recruitment of $CCR2^+$ myeloid cells, the adoptive transfer of which ameliorates colitis. *Infect. Immun.* 84, 3471–3483. doi: 10.1128/IAI.00681-16

Rudd, K. E., Johnson, S. C., Agesa, K. M., Shackelford, K. A., Tsoi, D., Kievlan, D. R., et al. (2020). Global, regional, and national sepsis incidence and mortality 1990–2017: analysis for the Global Burden of Disease Study. *Lancet* 395, 200–211. doi: 10.1016/S0140-6736(19)32989-7

Ryan, S. M., Eichenberger, R. M., Ruscher, R., Giacomin, P. R., and Loukas, A. (2020). Harnessing helminth-driven immunoregulation in the search for novel therapeutic modalities. *PLoS Pathog.* 16, 1–20. doi: 10.1371/journal.ppat.1008508

Sackett, S. D., Otto, T., Mohs, A., Sander, L. E., Strauch, S., Streetz, K. L., et al. (2019). Myeloid cells require gp130 sign-aling for protective anti-inflammatory functions during sepsis. *FASEB J.* 33, 6035–6044. doi: 10.1096/fj.201802118R

Saraiva, M., Saraiva, M., Vieira, P., Vieira, P., Vieira, P., O'Garra, A., et al. (2020). Biology and therapeutic potential of interleukin-10. *J. Exp. Med.* 217 (1), e20190418. doi: 10.1084/jem_20190418

Seymour, C. W., Gesten, F., Prescott, H. C., Friedrich, M. E., Iwashyna, T. J., Phillips, G. S., et al. (2017). Time to treatment and mortality during mandated emergency care for sepsis. *N. Engl. J. Med.* 376, 2235–2244. doi: 10.1056/NEJMoa1703058

Shevach, E. M. (2009). Mechanisms of $Foxp3^+$ T regulatory cell-mediated suppression. *Immunity* 30, 636–645. doi: 10.1016/j.immuni.2009.04.010

Singer, M., Deutschman, C. S., Seymour, C., Shankar-Hari, M., Annane, D., Bauer, M., et al. (2016). The third international consensus definitions for sepsis and septic shock (sepsis-3). *JAMA - J. Am. Med. Assoc.* 315, 801–810. doi: 10.1001/jama.2016.0287

Sotillo, J., Ferreira, I., Potriquet, J., Laha, T., Navarro, S., Loukas, A., et al. (2017). Changes in protein expression after treatment with *Ancylostoma caninum* excretory/secretory products in a mouse model of colitis. *Sci. Rep.* 7, 1–11. doi: 10.1038/srep41883

Sun, S., Li, H., Yuan, Y., Wang, L., He, W., Xie, H., et al. (2019a). Preventive and therapeutic effects of *Trichinella spiralis* adult extracts on allergic inflammation in an experimental asthma mouse model. *Parasit. Vectors* 12, 1–10. doi: 10.1186/s13071-019-3561-1

Sun, X. M., Guo, K., Hao, C. Y., Zhan, B., Huang, J. J., and Zhu, X. (2019b). *Trichinella spiralis* excretory-secretory products stimulate host regulatory T cell differentiation through activating dendritic cells. *Cells* 8, 1404. doi: 10.3390/cells8111404

Takakura, A., and Zandi-Nejad, K. (2019). Lactate-induced activation of HCA2 improves survival in mice with sepsis. *FASEB J.* 33, 7625–7634. doi: 10.1096/fj.201801982R

Tesch, G. H. (2010). Review: Serum and urine biomarkers of kidney disease: A pathophysiological perspective. *Nephrology* 15, 609–616. doi: 10.1111/j.1440-1797.2010.01361.x

Togre, N., Bhoj, P., Amdare, N., Goswami, K., Tarnekar, A., and Shende, M. (2018). Immunomodulatory potential of recombinant filarial protein, rWbL2,

and its therapeutic implication in experimental ulcerative colitis in mouse. *Immunopharmacol. Immunotoxicol.* 40, 483–490. doi: 10.1080/08923973.2018.1431925

Velavan, T. P., and Ojurongbe, O. (2011). Regulatory T cells and parasites. *J. BioMed. Biotechnol.* 2011, 520940. doi: 10.1155/2011/520940

Venugopal, G., Mueller, M., Hartmann, S., and Steinfelder, S. (2017). Differential immunomodulation in human monocytes versus macrophages by filarial cystatin. *PLoS One* 12, 1–16. doi: 10.1371/journal.pone.0188138

Verma, R., Balakrishnan, L., Sharma, K., Khan, A. A., Advani, J., Gowda, H., et al. (2016). A network map of Interleukin-10 signaling pathway. *J. Cell Commun. Signal* 10, 61–67. doi: 10.1007/s12079-015-0302-x

Wan, Y. K., Li, H. H., Zuo, L., Wang, X. L., Wang, L. Y., He, W. X., et al. (2018). Intervention with *Schistosoma japonicum* cysteine protease inhibitor for treatment of lipopolysaccharide-induced sepsis in mice. *J. South. Med. Univ.* 38, 625–629. doi: 10.3969/j.issn.1673-4254.2018.05.20

Wang, S., Gao, X., Shen, G., Wang, W., Li, J., Zhao, J., et al. (2016a). Interleukin-10 deficiency impairs regulatory T cell-derived neuropilin-1 functions and promotes Th1 and Th17 immunity. *Sci. Rep.* 6, 24249. doi: 10.1038/srep24249

Wang, S., Xie, Y., Yang, X., Wang, X., Yan, K., Zhong, Z., et al. (2016b). Therapeutic potential of recombinant cystatin from *Schistosoma japonicum* in TNBS-induced experimental colitis of mice. *Parasit. Vectors* 9, 1–13. doi: 10.1186/s13071-015-1288-1

Wang, L., Cao, Y., Gorshkov, B., Zhou, Y., Yang, Q., Xu, J., et al. (2019). Ablation of endothelial Pfkfb3 protects mice from acute lung injury in LPS-induced endotoxemia. *Pharmacol. Res.* 146:104292. doi: 10.1016/j.phrs.2019.104292

Ward, N. S., Casserly, B., and Ayala, A. (2008). The Compensatory Anti-inflammatory Response Syndrome (CARS) in Critically Ill Patients. *Clin. Chest Med.* 29, 617–625. doi: 10.1016/j.ccm.2008.06.010

Wculek, S. K., Amores-Iniesta, J., Conde-Garrosa, R., Khouili, S. C., Melero, I., and Sancho, D. (2019). Effective cancer immunotherapy by natural mouse conventional type-1 dendritic cells bearing dead tumor antigen. *J. Immunother. Cancer* 7, 100. doi: 10.1186/s40425-019-0565-5

Williams, P. C. M., Waichungo, J., Gordon, N. C., Sharland, M., Murunga, S., Kamau, A., et al. (2019). The potential of fosfomycin for multi-drug resistant sepsis: An analysis of in vitro activity against invasive paediatric gram-negative bacteria. *J. Med. Microbiol.* 68, 711–719. doi: 10.1099/jmm.0.000973

Wynn, T. A., Chawla, A., and Pollard, J. W. (2013). Macrophage biology in development, homeostasis and disease. *Nature* 496, 445–455. doi: 10.1038/nature12034

Xiao, L., Cen, D., Gan, H., Sun, Y., Huang, N., Xiong, H., et al. (2019). Adoptive transfer of NKG2D CAR mRNA-engineered natural killer cells in colorectal cancer patients. *Mol. Ther.* 27, 1114–1125. doi: 10.1016/j.ymthe.2019.03.011

Xu, L., Yang, F., Lin, R., Han, C., Liu, J., and Ding, Z. (2014). Induction of M2 polarization in primary culture liver macrophages from rats with acute pancreatitis. *PLoS One* 9, e108014. doi: 10.1371/journal.pone.0108014

Xu, J., Liu, Z., Zhan, W., Jiang, R., Yang, C., Zhan, H., et al. (2018). Recombinant *Ts*P53 modulates intestinal epithelial barrier integrity via upregulation of ZO-1 in LPS-induced septic mice. *Mol. Med. Rep.* 17, 1212–1218. doi: 10.3892/mmr.2017.7946

Xu, J., Liu, M., Yu, P., Wu, L., and Lu, Y. (2019). Effect of recombinant *Trichinella spiralis* cysteine proteinase inhibitor on TNBS-induced experimental inflammatory bowel disease in mice. *Int. Immunopharmacol.* 66, 28–40. doi: 10.1016/j.intimp.2018.10.043

Yan, K., Wang, B., Zhou, H., Luo, Q., Shen, J., Xu, Y., et al. (2020). dAmelioration of type 1 diabetes by recombinant fructose-1,6-bisphosphate aldolase and cystatin derived from *Schistosoma japonicum* in a murine moel. *Parasitol. Res.* 119, 203–214. doi: 10.1007/s00436-019-06511-7

Yang, C., Xia, W., Liu, X., Lin, J., and Wu, A. (2019a). Role of TXNIP/NLRP3 in sepsis-induced myocardial dysfunction. *Int. J. Mol. Med.* 44, 417–426. doi: 10.3892/ijmm.2019.4232

Yang, X., Yin, Y., Yan, X., Yu, Z., Liu, Y., and Cao, J. (2019b). Flagellin attenuates experimental sepsis in a macrophage-dependent manner. *Crit. Care* 23, 106. doi: 10.1186/s13054-019-2408-7

Yang, P., Zhang, X., Lin, Z., Wang, Q., Guo, D., Zhang, P., et al. (2020a). Adoptive transfer of polarized M2c macrophages ameliorates acute rejection in rat liver transplantation. *Am. J. Transl. Res.* 12, 2614–2626.

Yang, W. S., Kang, H. D., Jung, S. K., Lee, Y. J., Oh, S. H., Kim, Y. J., et al. (2020b). A mortality analysis of septic shock, vasoplegic shock and cryptic shock classified by the third international consensus definitions (Sepsis-3). *Clin. Respir. J.* 14, 857–863. doi: 10.1111/crj.13218

You, Y., Zhou, C., Li, D., Cao, Z. L., Shen, W., Li, W. Z., et al. (2016). Sorting nexin 10 acting as a novel regulator of macrophage polarization mediates inflammatory response in experimental mouse colitis. *Sci. Rep.* 6, 1–9. doi: 10.1038/srep20630

Zhan, B., Liu, S., Perally, S., Xue, J., Fujiwara, R., Brophy, P., et al. (2005). Biochemical characterization and vaccine potential of a heme-binding glutathione transferase from the adult hookworm *Ancylostoma caninum*. *Infect. Immun.* 73, 6903–6911. doi: 10.1128/IAI.73.10.6903-6911.2005

Zhu, J., Xu, Z., Chen, X., Zhou, S., Zhang, W., Chi, Y., et al. (2014). Parasitic antigens alter macrophage polarization during *Schistosoma japonicum* infection in mice. *Parasit. Vectors* 7, 1–9. doi: 10.1186/1756-3305-7-122

Ziegler, T., Rausch, S., Steinfelder, S., Klotz, C., Hepworth, M. R., Kühl, A. A., et al. (2015). A novel regulatory macrophage induced by a helminth molecule instructs IL-10 in $CD4^+$ T cells and protects against mucosal inflammation. *J. Immunol.* 194, 1555–1564. doi: 10.4049/jimmunol.1401217

Conflict of Interest: The authors declare that the research was conducted in the absence of any commercial or financial relationships that could be construed as a potential conflict of interest.

frontiers in Cellular and Infection Microbiology

ORIGINAL RESEARCH
published: 25 February 2021
doi: 10.3389/fcimb.2021.626368

Detection of DENV-2 and Insect-Specific Flaviviruses in Mosquitoes Collected From Jeddah, Saudi Arabia

Yuan Fang[1,2,3,4,5,6], *Ernest Tambo*[7*], *Jing-Bo Xue*[1,2,3,4,5,6], *Yi Zhang*[1,2,3,4,5,6*], *Xiao-Nong Zhou*[1,2,3,4,5,6] *and Emad I. M. Khater*[7,8]

[1] National Institute of Parasitic Diseases, Chinese Center for Disease Control and Prevention, Shanghai, China, [2] Chinese Center for Tropical Diseases Research, Shanghai, China, [3] WHO Collaborating Centre for Tropical Diseases, Shanghai, China, [4] National Center for International Research on Tropical Diseases, Ministry of Science and Technology, Shanghai, China, [5] Key Laboratory of Parasite and Vector Biology, Ministry of Health, Shanghai, China, [6] National Institute of Parasitic Diseases, Chinese Center for Disease Control and Prevention-Shenzhen Center for Disease Control and Prevention Joint Laboratory for Imported Tropical Disease Control, Shanghai, China, [7] Public Health Pests Laboratory, Municipality of Jeddah Governorate, Jeddah, Saudi Arabia, [8] Department of Entomology, Faculty of Science, Ain Shams University, Cairo, Egypt

OPEN ACCESS

Edited by:
Tianmu Chen,
Xiamen University, China

Reviewed by:
Estanislao Nistal-Villan,
San Pablo CEU University, Spain
Kokouvi Kassegne,
Shanghai Jiao Tong University, China

***Correspondence:**
Yi Zhang
zhangyi@nipd.chinacdc.cn
Ernest Tambo
tambo0711@gmail.com

Specialty section:
This article was submitted to Virus and Host, a section of the journal Frontiers in Cellular and Infection Microbiology

Received: *05 November 2020*
Accepted: *18 January 2021*
Published: *25 February 2021*

Citation:
Fang Y, Tambo E, Xue J-B, Zhang Y, Zhou X-N and Khater EIM (2021) Detection of DENV-2 and Insect-Specific Flaviviruses in Mosquitoes Collected From Jeddah, Saudi Arabia. Front. Cell. Infect. Microbiol. 11:626368. doi: 10.3389/fcimb.2021.626368

Background: Mosquito-borne diseases are rapidly spreading due to increasing international travel and trade. Routine mosquito surveillance and screening for mosquito-borne pathogens can be early indicators for local disease transmission and outbreaks. However, arbovirus detection in mosquito vectors has rarely been reported in Saudi Arabia.

Methods: A total of 769,541 *Aedes* and *Culex* mosquitoes were collected by Black Hole traps during routine mosquito surveillance in the first half of 2016. *Culex. quinquefasciatus* and *Ae. aegypti* were the most prevalent species observed. Twenty-five and 24 randomly selected pools of *Ae. aegypti* and *Cx. quinquefasciatus*, respectively, were screened for arboviruses by RT-PCR.

Results: Dengue 2 (DENV-2) and four strains of insect-specific flaviviruses, including one of cell-fusing agent virus (CFAV) and three of Phlebotomus-associated flavivirus (PAFV) were detected in pools of *Ae. aegypti*. We also detected 10 strains of Culex flavivirus (CxFV) in pools of *Cx. quinquefasciatus*. Phylogenetic analysis using whole genome sequences placed the DENV strain into the cosmopolitan 1 sub-DENV-2 genotype, and the CxFVs into the African/Caribbean/Latin American genotype. These analyses also showed that the DENV-2 strain detected in the present study was closely related to strains detected in China in 2014 and in Japan in 2018, which suggests frequent movement of DENV-2 strains among these countries. Furthermore, the phylogenetic analysis suggested at least five introductions of DENV-2 into Saudi Arabia from 2014 through 2018, most probably from India.

Conclusions: To our knowledge, this study reports the first detection of four arboviruses DENV, CFAV, PAFV, and CxFV in mosquitoes in Saudi Arabia, which shows that they are co-circulating in Jeddah. Our findings show a need for widespread mosquito-based arbovirus surveillance programs in Saudi Arabia, which will improve our understanding of

the transmission dynamics of the mosquito-borne arboviruses within the country and help early predict and mitigate the risk of human infections and outbreaks.

Keywords: *Aedes aegypti*, Culex flavivirus, *Culex quinquefasciatus*, dengue virus, insect specific flavivirus

INTRODUCTION

Mosquitoes are the most important arthropod disease vectors in the world. They transmit malaria parasites, lymphatic filariasis nematodes, dengue virus (DENV), Chikungunya virus (CHIKV), Zika virus (ZIKV) virus, Japanese Encephalitis virus, St. Louis Encephalitis virus, Lacrosse Encephalitis virus, Eastern Equine Encephalitis virus, Western Encephalitis virus, West Nile virus (WNV), Mayaro virus, yellow fever virus, Venezuelan Encephalitis virus and many others worldwide. It is estimated that every year, approximately 700 million people are diagnosed with a mosquito-borne disease and approximately one million deaths are attributed to mosquito-borne diseases (Caraballo and King, 2014). Although the disease burden of malaria and filariasis has gradually been alleviated (WHO, 2018), the rapid spread of mosquito-borne arboviruses and associated epidemics, especially DENV, CHIKV, and ZIKV, present serious threats to public health worldwide (Roth et al., 2014). In addition, novel mosquito-transmitted arboviruses are emerging (Pybus et al., 2002).

At least four arboviruses have been detected in Saudi Arabia: DENV, Alkhurma hemorrhagic fever virus, Rift Valley fever virus, and Crimean-Congo hemorrhagic fever virus (Al-Saeed et al., 2017). DENV is currently the most prevalent. Interestingly, Saudi Arabia was traditionally a DENV-free country (Alhaeli et al., 2016); however, the recent DENV outbreaks in Jeddah, Makkah (Mecca), and Madinah in the western region (Heilman et al., 2014; Organji et al., 2017; Mohammed et al., 2018), and in Jazan in the southwestern region (Alhaeli et al., 2016; Hashem et al., 2018) suggest widespread circulation and transmission of the virus in the country. DENV-1 and DENV-2 were the most prevalent serotypes circulating during the first reported DENV outbreak in Saudi Arabia in 1994 (Fakeeh and Zaki, 2001; Zaki et al., 2008). DENV-3 was first detected in 1996 and was the dominant serotype in the dengue epidemic of 1997 (Fakeeh and Zaki, 2001). DENV-3 was not detected again for several years, but was probably circulating at low levels until it was detected again in 2004 in Jeddah (Zaki et al., 2008) and Makkah (Khan et al., 2008). Recent studies have shown that the three serotypes have been sporadically transmitted in Jeddah and Makkah (Al-Saeed et al., 2017; Organji et al., 2017). Furthermore, the DENV-4 serotype was found in serum samples from blood donors in Makkah that were collected between March 2015 and August 2016 (Ashshi, 2017), and DENV-4 infection was detected in a few cases from Jeddah in 2015 (Al-Saeed et al., 2017). Thus, all four DENV serotypes may be currently co-circulating in Saudi Arabia, and, periodical active surveillance in the *Ae. aegypti*-prone cities is needed, especially in Jeddah and Makkah, which constitute the Makkah Almokarramah (Holy) region.

The first documented DENV outbreak in Saudi Arabia was in Jeddah (289 confirmed cases) in 1994 (Fakeeh and Zaki, 2001). Jeddah is the second largest city in Saudi Arabia, and has a mean annual temperature range of 22°C–34°C, and a rainy season at the end of the year. The hot and humid climate of Jeddah is suitable for mosquito breeding. In addition, as a coastal city, Jeddah is rich in underground water and water sanitation is underdeveloped, which creates plenty of *Culex* mosquito larval habitats and is ideal for *Cx. quinquefasciatus*, the primary vector of RVFV and WNV (Franklinos et al., 2019). Owing to fresh-water scarcity, people largely depend on water storage devices as well as air-conditioning, which creates most of the *Ae. aegypti*-preferred larval water containers (natural and man-made) associated with human dwellings and activities. The city of Jeddah contains a major Saudi Arabian seaport and harbor, as well as the main airport on the Red Sea and is less than 100 km from the Holly City of Makkah. Millions of Muslim pilgrims from DENV-endemic countries travel through Jeddah to reach the Holy City of Makkah for the Holy Hajj and Umrah ceremonies every year. These pilgrims increase the chances of introducing DENV and other mosquito-borne pathogens into the city of Jeddah (Zaki et al., 2008; Alhaeli et al., 2016). The presence of high densities of competent mosquito vector in field populations, especially *Ae. aegypti*, in Jeddah puts this city at high risk of transmission of mosquito-borne viruses, especially DENV. Notably, more than 73% (3161 cases in total) of the laboratory-confirmed dengue cases in Saudi Arabia in 2015 were detected in Jeddah (Hashem et al., 2018). Moreover, the DENV antibody prevalence among the residents of Jeddah in 2015 was 47.8% (927/1939) (Jamjoom et al., 2016).

The recent studies by Alikhan et al. (2014) have observed that the relative abundance of *Ae. aegypti* in and around Jeddah is increasing (Alikhan et al., 2014), which suggests that the risk of *Ae. aegypti*-borne diseases is also increasing. Furthermore, insecticide resistance to deltamethrin was detected in field populations of *Ae. aegypti* in Jeddah and Makkah (Al Nazawi et al., 2017), making the control of this vector difficult within these cities. To the best of our knowledge, mosquito-borne disease surveillance in Saudi Arabia is currently limited to DENV, and this mainly focuses on screening serum of clinically suspected cases in endemic areas. Mosquito-based arboviral surveillance programs have not been implemented and infection rates in mosquito vectors are not routinely investigated in Saudi Arabia. It is currently unknown whether mosquito-borne arboviruses than DENV exist in Saudi Arabia. Thus, establishing mosquito-based arboviral surveillance is urgently needed to understand the dynamics of mosquito-borne disease transmission in this region. In the present study, we used mosquito samples from routine surveillance in Jeddah in the first half of 2016 to estimate the infection rates of alphaviruses, flaviviruses, and orthobunyaviruses in mosquitoes, and used molecular phylogeny to study the genotypes and the possible geographical origins of these arboviruses.

MATERIALS AND METHODS

Mosquito Sampling

Routine mosquito surveillance was conducted in Jeddah from January to June in 2016. The main purpose was to collect mosquitoes from various vulnerable municipalities for speciation and detection of viruses, especially DENV and other arboviruses that might be associated with mosquito species (family Culicidae) present in Jeddah. Mosquitoes were collected with Black Hole strap (BioTrap Co., Ltd, Seoul. S. Korea) which uses UV-LED lamps and photocatalysis to permanently produce carbon dioxide (CO_2) to lure mosquitoes and a fan to suck them up into the collection bag. The collection was carried out over a 24-h cycle from Sunday to Thursday and transferred in air-conditioned vehicles to the laboratory for sorting at 9:00–11:00 AM daily. The specimens were placed on ice and identified using standard taxonomic keys (Mattingly and Knight, 1956; Knight and Stone, 1977; Harbach and Knight, 1980; Harbach, 1985; Reinert, 2000; Rueda, 2004; Al-Ahmad et al., 2011). Ambiguous specimens were confirmed by molecular methods (Fang et al., 2017). Owing to the large number of adult mosquitoes collected daily, the mosquitoes were randomly sampled by species, date, and collection locality and pooled with a maximum of 20 per pool. Pooled mosquitoes were stored in 2-ml sterile Eppendorf tubes and frozen at −86°C for further nucleic acid extraction. As a preliminary mosquito-borne virus survey, a total of 450 *Ae. aegypti* in 25 pools from 12 municipalities and a total of 407 *Cx. quinquefasciatus* in 24 pools from 10 municipalities in Jeddah were randomly selected among sentinel sites and processed for virus detection. Survey sites are shown in **Figure 1**, from a map generated by using ArcGIS 10.1 ArcMap software (ESRI, Redlands, CA, USA).

RNA Extraction and Target Gene Sequencing

Pools of mosquitoes were transferred into new tubes containing 450 µl of TRIzol (Invitrogen, Carlsbad, CA, USA) and homogenized in a frozen block using a Mixer Mill (Jingxin,

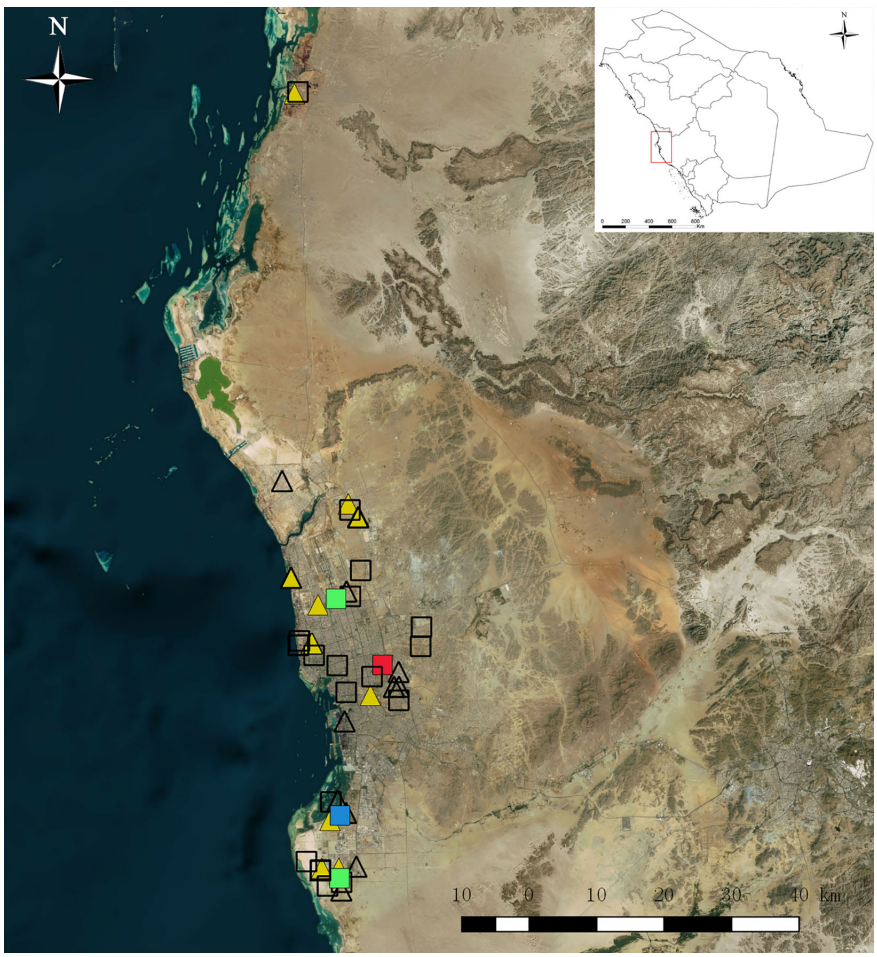

FIGURE 1 | Map of mosquito collection sites in 2016 in Jeddah, Saudi Arabia. Squares represent collection sites of *Aedes aegypti*, triangles represent sites of *Culex quinquefasciatus*. Color symbols filled with red, yellow, green, and blue represent dengue virus, Culex flavivirus, Phlebotomus-associated flavivirus (PAFV), and co-cell fusing agent virus & PAFV detection, respectively.

Shanghai, China) with one 3-mm and one 5-mm stainless-steel bead added. The samples were then centrifuged at full speed (12,700 × *rpm*) for 10 mins at 4°C. Then, 350 µl of the supernatant from each homogenate was added to the processing cartridge and placed into the MagNA Pure 96 System (Roche, Basel, Switzerland) for automated RNA extraction as described in a previous study (Fang et al., 2018). First-strand cDNA was synthesized by reverse transcription polymerase chain reaction (PCR) using the PrimeScript RT reagent kit with gDNA eraser (TAKARA BIO, Shiga, Japan). After the RT reactions, PCR amplification targeting mosquito 18S rRNA was implemented with the primers 18S417 and 18S920c (Hoffmann et al., 2004) to verify RNA integrity in each pool. If the control amplification was successful, the cDNA was amplified by semi-nested PCR using a set of primers (cFD2 and MAMD, cFD2 and FS778) for detection of the partial *NS5* gene of flaviviruses as reported previously (Scaramozzino et al., 2001). Alphavirus and orthobunyavirus in mosquito samples were amplified using the primer sets α6533f/α6999c (Bryant et al., 2005) and BCS82C/BCS332V (Kuno et al., 1996), respectively. The amplified products were separated by agarose gel electrophoresis, then purified and sequenced in both directions by Sangon Biotech (Shanghai, China). Sequences were compared with those available in the GenBank database using the BLAST program.

Whole-Genome Sequencing

For further analysis of the molecular characteristics and possible pathogenetic mechanisms of the viruses, the Primer Premier 5.0 (Premier Biosoft International, Palo Alto, CA, USA) was used to design primers for amplifying the complete genome of DENV and CxFV. DENV whole-genome sequencing was designed using the genomic sequence of an Indian isolate (RGCB921/2011) as reference. To sequence the full-length genome of CxFV, primers were designed from the Chinese strain PA3_17-6E-P-Cxp-C-1-3 (MN318426). The resulting PCR products were sequenced and subsequently used to design new Saudi-isolate-specific primers.

Comparison of Virus-Deduced Amino Acid Sequences

The whole genomes of DENV and CxFV sequenced in this study were translated into amino acid sequences and aligned with other homologous sequences retrieved from GenBank using MEGA v7.0 [31]. Amino acid substitutions unique to the newly sequenced strains and those different from their closest sequences were observed.

Phylogenetic Analysis

Multiple sequence alignments were generated using the virus sequences obtained in the present study and homologous sequences were retrieved from GenBank using ClustalW2 (Larkin et al., 2007) with default settings and were manually adjusted as necessary. Neighbor-joining trees were established following the Kimura's two-parameter distance model (Kimura, 1980) with 1,000 bootstrap replications using MEGA v7.0 (Kumar et al., 2016). Based on the Akaike Information Criterion, the best-fit model for the alignment was determined using Modeltest 3.7 in cooperation with PAUP* v4.0b10 (Wilgenbusch and Swofford, 2003). Consequently, maximum likelihood and Bayesian likelihood trees were constructed under the GTR+I+G model for the DENV-2 whole genome, DENV-2 *E* gene, and CxFV whole genome, and the TrN+I+G model for the ISFV *NS5* gene. The neighbor-joining and maximum likelihood trees were constructed using MEGA v7.0 with 1,000 bootstraps. The Bayesian tree was constructed with MrBayes v3.2.1 (Ronquist et al., 2012) on the CIPRES portal (www.phylo.org/) (Miller et al., 2010) and run for 10 million generations, with the first 25% of generations discarded as burn-in. The trees were visualized using Figtree v1.4.2 (http://tree.bio.ed.ac.uk/software/figtree/).

Infection Rate Calculation

The size of the pools of collected mosquitoes varied considerably; therefore, infection rates were calculated using bias-corrected maximum likelihood estimation (MLE) and minimum infection rate (MIR) using the Excel add-in PooledInfRate v.4 statistical software package (Biggerstaff, 2006). The rates are expressed as the number of infected mosquitoes per 1,000 collected mosquitoes.

RESULTS

Mosquito Adult Species Collected

A total of 29,678 *Aedes* spp. and 739,863 *Culex* spp. were collected at Jeddah from January to June in 2016 (**Figure 2A**). Fourteen species belonging to four genera were found in the 2,499 identified mosquitoes (**Figure 2B**). Among them, *Cx. quinquefasciatus* accounted for 44.78% (1,119/2,499), *Ae. aegypti* accounted for 17.65% (441/2,499), *Cx. pipiens* accounted for 15.85% (396/2,499), *Anopheles dthali* accounted for 6.56% (164/2,499), and *Cx. sitiens* accounted for 5.36% (134/2,499). Nine other species, *Ae. vexan arabiensis*, *Cx. tritaeniorhynchus*, *Cx. poicilipes*, *Cx. theileri*, *Cx. mattingly*, *Cx. tigripes*, *Cx. perexiguus*, *Cx. laticinctus*, and *Ochlerotatus caspius* were collected, but in extremely limited numbers.

Detection of Flavivirus in Mosquito Pools Collected in Jeddah

Twenty-five pools of *Ae. aegypti* from 12 municipalities and 24 pools of *Cx. quinquefasciatus* from 10 municipalities were randomly selected for virus detection. Control amplifications of the 18S rRNA mosquitoes were successful in all detected pools. The BLAST homology results showed that 14 pools were positive for flavivirus *NS5*, whereas neither alphavirus nor orthobunyavirus were detected. One pool of *Ae. aegypti* was DENV-2 positive, two pools of *Ae. aegypti* were Phlebotomus-associated flavivirus (PAFV) positive and one pool of *Ae. aegypti* was co-positive for PAFV and CFAV. CxFV was detected in 10 pools of *Cx. quinquefasciatus*. All generated sequences were deposited in GenBank (GenBank accession numbers: MN294937–MN294953). Details regarding virus species, host species, collection information, and GenBank accession numbers are listed in **Table 1**. The collection locations of flavivirus-positive pools are shown in **Figure 1**.

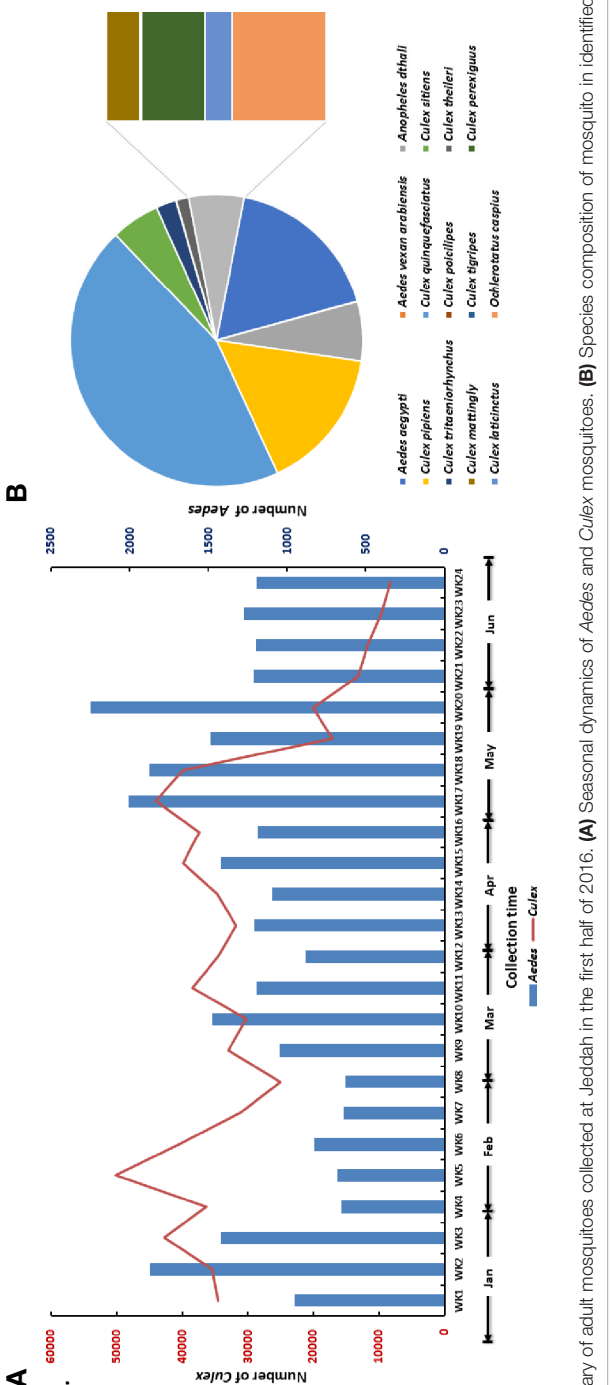

FIGURE 2 | Summary of adult mosquitoes collected at Jeddah in the first half of 2016. **(A)** Seasonal dynamics of *Aedes* and *Culex* mosquitoes. **(B)** Species composition of mosquito in identified mosquitoes.

Sequence Analysis and Phylogenetic Characterization of the DENV-2 Strain Isolated From Jeddah

The newly detected DENV-2 strain was isolated from an *Ae. aegypti* pool collected from the Bani-Malek-4 District, Al-Sharafyia municipality, Jeddah, in February 2016. The length of the whole genome of DENV-2 (SA-AS-BM4-16-2-A9 strain, MN294937) was 10,723 nt, with an open reading frame coding for 3,392 amino acids flanked by 96 nt and 451 nt at the 5′UTR and 3′UTR, respectively. The complete genome was amplified by a total of 17 pairs of overlapping primers (see Supplemental Material **Table S1**). In the BLAST results, the complete genome shared the highest nucleotide identity (98.91%) with the Indian isolate RGCB921/2011 (KY427085) collected in 2011, whereas the genome was slightly distant from that detected in Jeddah in 2014 (Jeddah-2014 strain, KJ830750) with an identity of 97.19%. In the phylogenetic tree based on DENV-2 complete genomes of 106 strains from various sources, six previously described genotypes (Sylvatic, American, American/Asian, Asian 1, Asian 2, and Cosmopolitan) clustered independently with strong bootstrap support (**Figure 3**). Both DENV-2 strains with complete genomes from Saudi Arabia belonged to the Cosmopolitan genotype. Specifically, the two strains were clustered within the Cosmopolitan 1 (C1) sub-genotype which includes strains from India and Sri Lanka in Southeast Asia and Burkina Faso in West Africa. There were 10 other DENV-2 strains with complete envelope (*E*) gene sequences available in GenBank. When combined with the two DENV-2 strains with whole genomes, in the phylogenetic tree of the DENV-2 *E* gene (**Figure 4**), the Saudi strains fell into two lineages. Except the 237 isolate (AM746226) which was isolated in 1994 clustered in the Cosmopolitan 2 (C2) lineage, the other strains were clustered within the C1 lineage. The 237 isolate was closely clustered with sequences from Burkina Faso, and sister to the strain from Indonesia (GQ398258) which was detected in 1975.

Comparing the deduced amino acid sequences of the SA-JD-AS-BM4-16-2-A9 and Saudi-2014 strains, there were 33 non-synonymous changes distributed in capsid (C, 3 positions), pre-membrane (prM, 2 positions), E (3 positions), non-structure 1 (NS1, 2 positions), NS2A (3 positions), NS2B (1 position), NS3 (3 positions), NS4A (1 position), NS4B (3 positions), and NS5 (11 positions) proteins. Most of the changes were observed in the NS5 region of the viral protein with only 1–3 substitutions observed in other proteins. The details of the differences of each position are provided in Supplemental Material **Table S2**. Among them, five amino acid substitutions were found to be unique in the SA-JD-AS-BM4-16-2-A9 strain, (i.e., different from the other DENV-2 strains), including ^{103}Gly→Ser, ^{265}Arg→Ile, ^{284}Ile→Val, ^{3119}Cys→Phe, and ^{3307}Val→Gly.

It was concluded that the six substitutions on the E protein inducing the Cosmopolitan genotype were separated from other genotypes (Twiddy et al., 2002). Of these substitutions of the 12 Saudi DENV-2 E protein sequences, substitutions on ^{71}Glu→Ala, ^{149}His→Asn, and ^{462}Ile→Val were observed in all strains. ^{390}Asn→Ser and ^{164}Ile→Val substitutions were detected in all strains except for the 237 isolate (AM746226), whereas the

TABLE 1 | Summary of the flaviviruses detected from different mosquito pools, captured in Jeddah, Saudi Arabia, in the first half of 2016.

Strain	Virus	Host	Collection date	Collection site	Geographic location		GenBank ID	
					Municipality	District	*NS5*	Whole genome
SA-JD-AS-BM4-16-2-A9	DENV-2	*Aedes aegypti*	2-Feb-2016	building under-construction	Al-Sharafyia	Bani-Malek-4	MN294939	MN294937
SA-JD-AJ-AA-16-2-A13	PAFV	*Ae. aegypti*	25-Feb-2016	building under-construction	Al-Janoub	Al-Ajwad	MN294940	
SA-JD-JA-AK-16-9-A16	PAFV	*Ae. aegypti*	9-Mar-2016	building under-construction	Jeddah Aljadeeda	Al-Khalidyia-2	MN294941	
SA-JD-JA-AM-16-4-A22	PAFV	*Ae. aegypti*	19-Apr-2016	car tire workshop	Al-Matar	Al-Nuzha-2	MN294942	
SA-JD-JA-AK-16-9-A16	CFAV	*Ae. aegypti*	9-Mar-2016	building under-construction	Jeddah Aljadeeda	Al-Khalidyia-2	MN294943	
SA-JD-Th-Th-16-2-C1	CxFV	*Culex quinquefasciatus*	12-Jan-2016	human dwelling (house)	Thuwal	Thuwal	MN294944	
SA-JD-AJ-PFN-16-6-C2	CxFV	*Cx. quinquefasciatus*	6-Jan-2016	human dwelling (house)	Al-Janoub	Prince Fawaz North	MN294945	
SA-JD-JA-AS-16-1-C6	CxFV	*Cx. quinquefasciatus*	18-Jan-2016	building under-construction	Jeddah Aljadeeda	Al-Shatea-1	MN294946	
SA-JD-AJ-AJ-16-1-C7	CxFV	*Cx. quinquefasciatus*	31-Jan-2016	building under-construction	Al-Janoub	Al-Jawhara	MN294947	MN294938
SA-JD-Ta-AS-16-2-C11	CxFV	*Cx. quinquefasciatus*	29-Feb-2016	dwelling	Tayibah	Al-Salehyia	MN294948	
SA-JD-Ta-AH-16-3-C12	CxFV	*Cx. quinquefasciatus*	3-Mar-2016	botanical nursery	Tayibah	Al-Hamdanyia	MN294949	
SA-JD-Ub-AN-16-3-C13	CxFV	*Cx. quinquefasciatus*	3-Mar-2016	human dwelling (house)	Ubhor	Al-Naeem-1	MN294950	
SA-JD-AJ-AJ-16-4-C14	CxFV	*Cx. quinquefasciatus*	4-Apr-2016	building under-construction	Al-Jameaa	Al-Jameaa	MN294951	
SA-JD-Ub-AS-16-4-C16	CxFV	*Cx. quinquefasciatus*	19-Apr-2016	building under-construction	Ubhor	Al-Shatea-6	MN294952	
SA-JD-JA-AK-16-5-C19	CxFV	*Cx. quinquefasciatus*	15-May-2016	building under-construction	Jeddah Al-Jadeeda	Al-Khalidyia-2	MN294953	

CFAV, cell fusing agent virus; CxFV, Culex flavivirus; DENV, dengue virus; NS5, non-structural 5; PAFV, Phlebotomus-associated flavivirus.

^{129}Ile→Val substitution was only observed in the 237 isolate. This discrepancy was probably due to the differences between the two sub-genotypes (C1 and C2) of the Cosmopolitan genotype.

Sequence Analysis and Phylogenetic Characterization of CxFV Genotypes

The length of the CxFV (SA-JD-AJ-AJ-16-1-C7 strain, MN294938) whole genome was 10,799 nt, amplified by a total of 11 overlapping primers (Supplemental Material **Table S3**), with an open reading frame coding for 3,362 amino acids flanked by 71 and 639 nt at the 5′UTR and 3′UTR, respectively. It was closely related to the Mexican CxFV-Mex07 strain (MH719098) with a similarity of 97.57%. In the phylogenetic tree of the CxFV whole genome (**Figure 5**), those isolated from Asia and the USA, and those from Africa, the Caribbean, and Latin America formed two separate clades that represented two genotypes. The SA-JD-AJ-AJ-16-1-C7 strain was clustered within the African/Caribbean/Latin American genotype. As expected, all 10 Saudi CxFVs with *NS5* sequences were clustered in the clade of CxFVs from Africa, the Caribbean, and Latin America in the ISFV *NS5* tree (**Figure 6**).

At the deduced polyprotein level, the Saudi-CxFV strain (SA-JD-AJ-AJ-16-1-C7, MN294938) and its most closely related strain from Mexican (CxFV-Mex07, EU879060) exhibited 17 amino acid substitutions evenly distributed in both structural and non-structural proteins, including C (2 positions), prM (1 position), E (2 positions), NS1 (1 position), NS2A (1 position), NS2B (2 positions), NS3 (3 positions), NS4B (2 positions), and NS5 (3 positions) proteins (Supplemental Material **Table S4**). Among them, eight substitutions were unique in the Saudi CxFV strain: ^{3}Lys→Arg, ^{325}Asn→Ser, ^{868}Ser→Ala, ^{1285}Ser→Phe, ^{1468}Ala→Val, ^{1902}Arg→Thr, ^{2404}Ser→Ala, and ^{2983}Leu→Phe.

Phylogenetic Analysis of PAFV and CFAV Sequences

We compared the 261-nt *NS5* sequence of the three flavivirus-positive pools from *Ae. aegypti* against genomic sequences in GenBank using BLAST. The small *NS5*-specific sequence fragments of the three flavivirus pools detected in *Ae. aegypti* showed over 99.36% identity with two short sequences amplified from *Ae. aegypti* (PoMoFlav_R1026 strain, HQ676625, 180 nt) and the sand fly *Phlebotomus perniciosus* (Alg_F19 strain, FJ817075, 157nt). In the phylogenetic tree of the ISFV *NS5* gene (**Figure 6**), they formed a sister clade with other ISFVs isolated from *Aedes* species. The BLAST homology search results showed that, at the nucleotide level, another *NS5* sequence from one of the three PAFV-positive pools in *Ae. aegypti* exhibited 96.17% identity with the CFAV Galveston strain from the USA (NC_001564). In the phylogenetic tree of the ISFV *NS5* gene (**Figure 6**), this sequence was clustered within the CFAV lineage.

Infection Rates of Flaviviruses in Mosquitoes

The infection rates of flaviviruses in mosquitoes from Jeddah, estimated by bias-corrected MLE and MIR, are shown in **Table 2**. The overall MLE values (with 95% confidence intervals) of

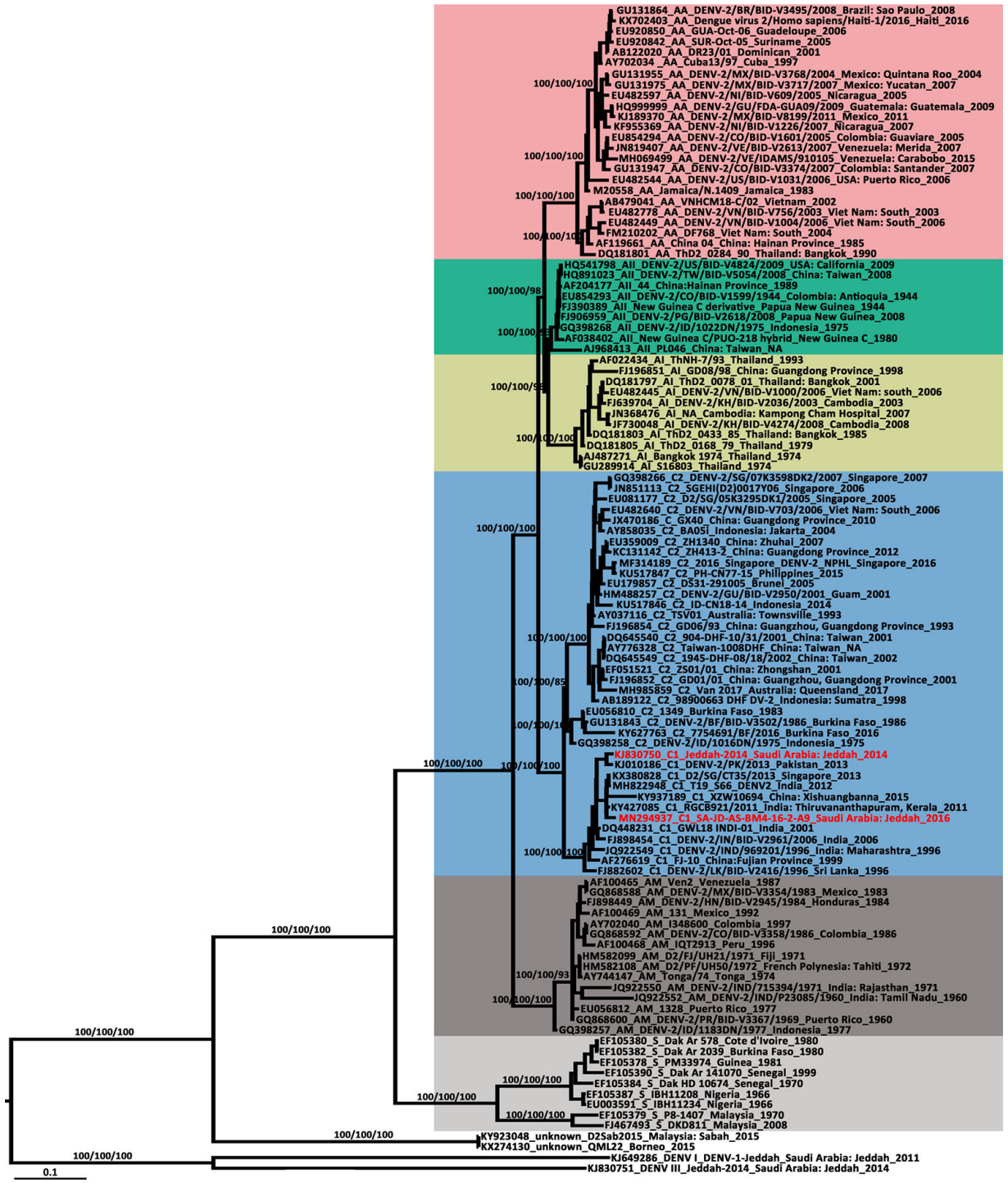

FIGURE 3 | Phylogenetic tree generated by Bayesian analysis of dengue virus 2 (DENV-2) complete genome. The GenBank accession number, virus genotype, strain, collection country and year are noted. The DENV-2 sequences from Saudi Arabia are marked in red. Bootstrap values (1,000 replicates, not shown for less than 75%) of Bayesian analyses, maximum likelihood and neighbor-joining are shown above the main lineages. The scale-bar indicates 0.1 substitutions per site. Sequences referable to the same genotype are shaded with the same colors in the tree. AA, American/Asian; AI, Asian 1; AII, Asian 2; AM, American; C, Cosmopolitan; S, Sylvatic.

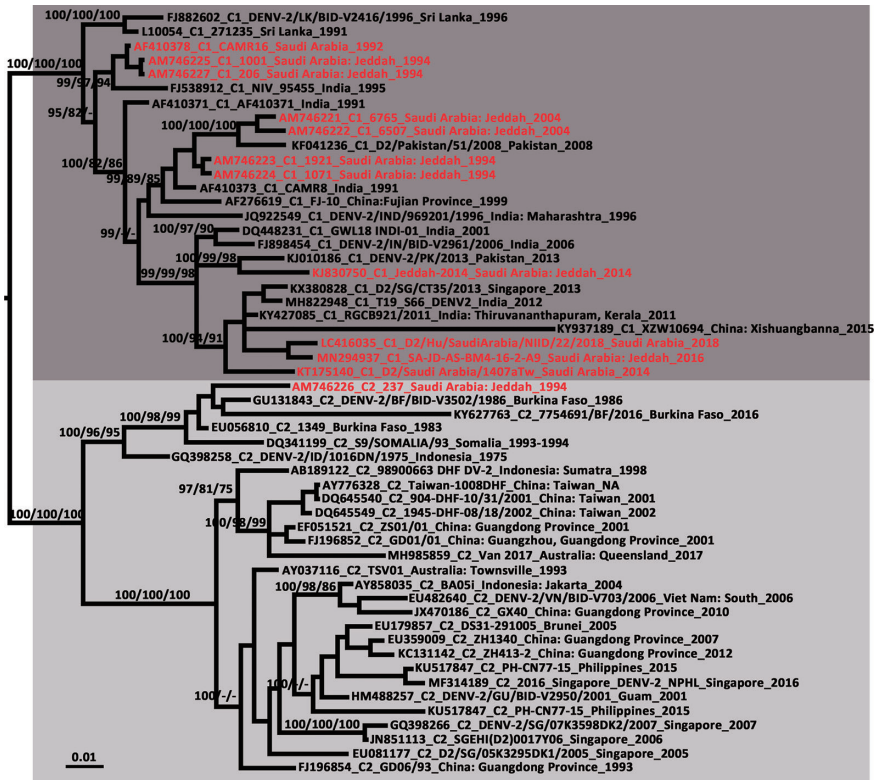

FIGURE 4 | Phylogenetic tree generated by Bayesian analysis of dengue virus 2 (DENV-2) Cosmopolitan genotype complete envelope gene. The GenBank accession number, virus sub-genotype, strain, collection country and year are noted. The DENV-2 sequences from Saudi Arabia are marked in red. Bootstrap values (1,000 replicates, not shown for less than 75%) of Bayesian analyses, maximum likelihood and neighbor-joining are shown above/below the main lineages. The scale-bar indicates 0.01 substitutions per site. Dark gray and light gray indicate DENV-2 Cosmopolitan 1 sub-genotype and DENV-2 Cosmopolitan 2 sub-genotype, respectively. C1, Cosmopolitan 1 sub-genotype; C2, Cosmopolitan 2 sub-genotype.

DENV, PAFV, and CFAV, expressed as the number of infected mosquitoes per 1,000 *Ae. aegypti*, were 2.22 (0.13–10.80), 6.93 (1.84–18.84), and 2.22 (0.13–10.80), respectively. The MLE of the CxFV per 1,000 in *Cx. quinquefasciatus* was 30.39 (15.75–54.61).

DISCUSSION

DENV-2 consists of six genotypes: sylvatic, American, Cosmopolitan, Asian 1/Asian 2, and Asian/American, in evolutionary order (Waman et al., 2016). In the phylogenetic tree of the DENV-2 whole genome (**Figure 3**), the SA-JD-AS-BM4-16-2-A9 strain belonged to the DENV-2 Cosmopolitan genotype and was further classified into the C1 sub-genotype. The C1 sub-genotype mainly circulates in the Indian subcontinent (Kumar et al., 2010). Based on the tree, this sub-genotype probably originated from India, spreading eastward to the Yunnan and Fujian Provinces, China, southward to Sri Lanka and Singapore, and radiating westward toward Pakistan and Saudi Arabia. The other sub-genotype of the Cosmopolitan genotype is the C2 sub-genotype, which has been reported in a diverse range of geographical areas worldwide (Twiddy et al., 2002).

From the tree based on the *E* gene of DENV-2 Cosmopolitan genotype (**Figure 4**), 12 strains that were detected in Saudi Arabia using the complete *E* gene available in GenBank were dispersed in five different clusters of the Cosmopolitan genotype. The 12 strains were collected over 25 years. Eleven of them belonged to the C1 sub-genotype, whereas one was classified to the C2 sub-genotype. The tree indicates at least five independent DENV-2 introduction events into Saudi Arabia (**Figure 4**). Three of them occurred before 1994 and two occurred before 2014. Almost all of them were related to the strains from the Indian subcontinent, supporting the speculation that the prevalence of DENV in Saudi Arabia is mainly associated with religious pilgrimages and Umrah (Alhaeli et al., 2016; El-Kafrawy et al., 2016; Al-Saeed et al., 2017). Jeddah governorate is a major coastal city and harbor on the Red Sea. The newly-detected strain SA-JD-AS-BM4-16-2-A9 was obtained from mosquitoes collected in a building under construction in the Bani-Malek-4 District, Al-Sharafyia Municipality, which is only 15 km away from the King Abdulaziz International Airport. Notably, in the phylogenetic tree, it is clustered with the strain D2/Hu/SaudiArabia/NIID/22/2018 (LC416035) detected from a Japanese traveler returning from Saudi Arabia in 2018 (Matsui et al., 2019), and was sister to the strain D2/Saudi Arabia/1407aTw_Saudi Arabia (KT175140)

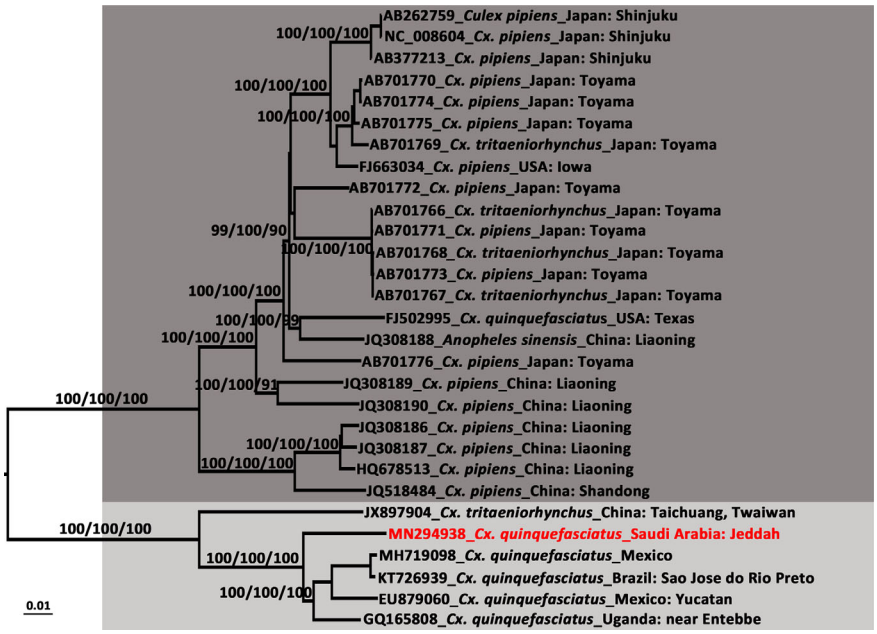

FIGURE 5 | Phylogenetic tree generated by Bayesian analysis of Culex flavivirus (CxFV) complete genome. The GenBank accession number, host species and origin are noted. The CxFV sequences obtained in this study are marked in red. Bootstrap values (1,000 replicates, not shown for less than 75%) of Bayesian analyses, maximum likelihood and neighbor-joining are shown above the main lineages. The scale-bar indicates 0.01 substitutions per site. Dark gray and light gray indicate CxFV Asian/USA genotype and Africa/Caribbean/Latin America genotype, respectively.

isolated from a suspected dengue patient from Taiwan, China, in 2014, who had traveled to Saudi Arabia (Chang et al., 2016). It can be inferred that this 'newly' detected DENV-2 strain was probably introduced by pilgrims or working expats in Saudi Arabia before 2014, subsequently evolving and circulating in local areas. This strain and its relatives not only infected local vectors but also spread from Saudi Arabia to other countries before it was even detected in Saudi Arabia, reflecting the lack of mosquito-borne disease surveillance in Saudi Arabia. It is important to note that seasonal pilgrimage and Umrah are important factors for introduction of DENV into Saudi Arabia. However, millions of expats from Africa and Asian dengue-endemic countries (Southeast Asia and Indian subcontinent) live and work in Saudi Arabia, which is also a major mechanism of virus introduction/exportation.

The potentially high transmission capacity of the strain SA-JD-AS-BM4-16-2-A9 is indicated by the discovery of the earliest detected strain in this cluster in India in 2011. In the next four years, its relatives spread to Singapore (2013), Saudi Arabia (2014), and China (2015) (**Figure 4**). Among the four serotypes, DENV-2 has been associated with severe dengue cases and is usually the most frequent cause of dengue outbreaks worldwide (Ricohesse, 2003; Cologna et al., 2005). However, only *E* gene sequences for both strains exported from Saudi Arabia were available in GenBank. No unique substitutions on the E protein of these three strains were observed. Full viral genome sequencing is an important tool for understanding both viral evolution and the mechanisms underlying viral virulence (Christenbury et al., 2010). Thus, further research is required to clarify whether the unique substitutions of the strain SA-JD-AS-BM4-16-2-A9 detected here at the whole genome level are functionally important in terms of increasing virulence, affecting dispersal patterns, or increasing the selection pressure on the host, vector, or both. The substitution of ^{390}Asn→Ser on the E protein was observed in all 11 DENV-2 C1 strains from Saudi Arabia. This substitution has previously been implicated in altering virulence and cellular tropism, and may lead to changes in transmissibility (Sánchez and Ruiz, 1996; Leitmeyer et al., 1999; Twiddy et al., 2002).

In the phylogenetic tree of the DENV-2 whole genome (**Figure 3**), each genotype formed a distinct clade, except two strains from Borneo (D2Sab2015 strain, KY923048; and QML22 strain, KX274130). Both were imported to Australia in 2015 and were temporarily classified as DENV-2 based on serologic tests but are highly divergent and basal to all other genotypes of DENV-2 (Liu et al., 2016; Pyke et al., 2017). Their phylogenetic position, as confirmed in the present study, is distant from human and sylvatic strains. However, both of their nucleotide sequences had ~76.50% identity compared to other DENV-2 strains, which is a bit more than the threshold of sequence differences between serotypes (65–70%) (Green and Rothman, 2006). In addition, in 2014, the most divergent DENV-1 was recorded from a viremic patient who had visited the rainforest of Brunei, Borneo and then returned to Australia (Pyke et al., 2016). Given that a series of highly divergent DENV strains have been found in Borneo in recent years, Borneo probably has a high DENV diversity.

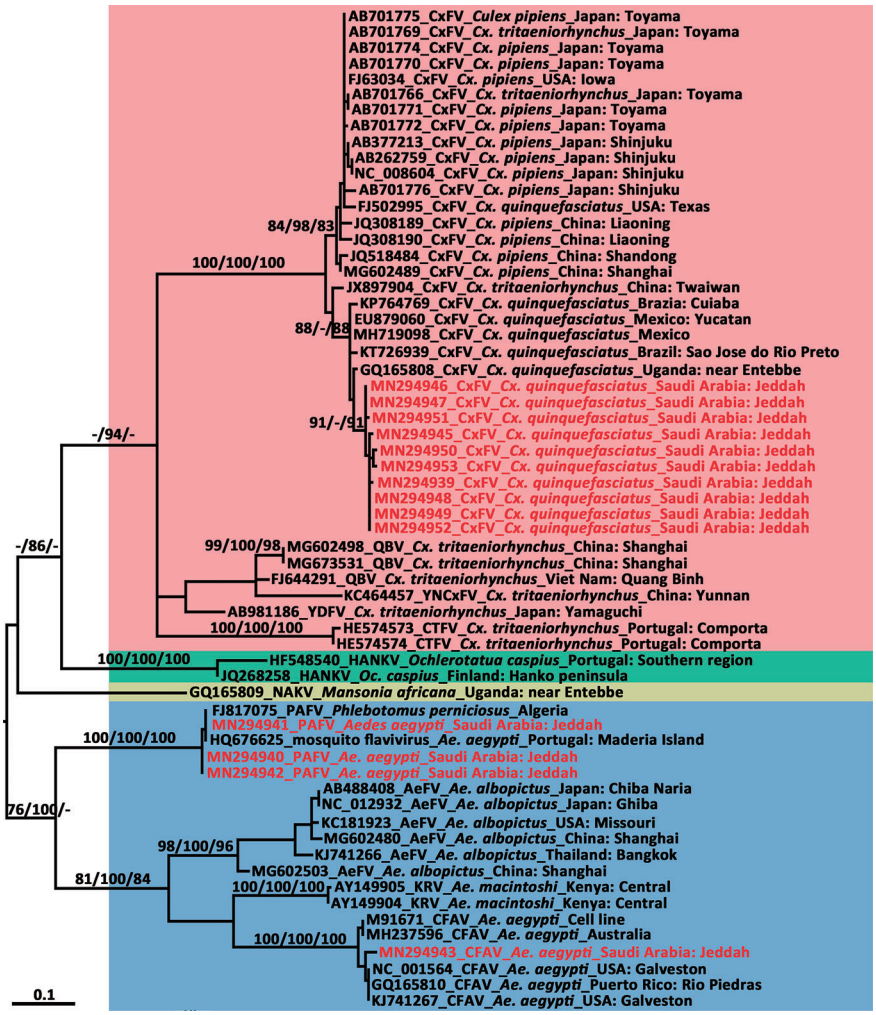

FIGURE 6 | Phylogenetic tree generated by maximum likelihood analysis of insect-specific flavivirus (ISFV) partial non-structural 5 gene. Sequences referable to the same host-genus (except for the Phlebotomus-associated flavivirus) are shown with the same colors in the tree. The ISFV sequences obtained in this study are marked in red. Bootstrap values (1,000 replicates, not shown for less than 75%) of maximum likelihood; Bayesian analyses and neighbor-joining are shown above the main lineages. The bar indicates 0.1 substitutions per site. AEFV, Aedes flavivirus; CFAV, cell fusing agent virus; CTFV, Culex theileri flavivirus; CxFV, Culex flavivirus; HANKV, Hanko virus; KRV, Kamiti River virus; NAKV, Nakiwogo virus; PAFV, Phlebotomus-associated flavivirus; QBV, Quang Binh virus; SCxFV, Spanish Culex flavivirus; YDFV, Yamadai flavivirus; YNCxFV, Yunnan Culex flavivirus.

TABLE 2 | Maximum likelihood estimation (MLE) and minimum infection rate (MIR) of flavivirus in mosquitoes from Jeddah, Saudi Arabia in the first half 2016.

Detected virus	No. individuals	No. pools	No. PP	PP rate (%)	MLE (95% CI)	MIR (95% CI)
Aedes aegypti						
DENV-2	450	25	1	4.00	2.22 (0.13–10.80)	2.22 (0.00–6.57)
PAFV	450	25	3	12.00	6.93 (1.84–18.84)	6.67 (0.00–14.19)
CFAV	450	25	1	4.00	2.22 (0.13–10.80)	2.22(0.00–6.57)
Culex quinquefasciatus						
CxFV	407	24	10	41.67	30.39 (15.75–54.61)	24.57 (9.53–39.61)

CFAV, cell fusing agent virus; CI, confidence interval; CxFV, Culex flavivirus; DENV, dengue virus; PAFV, Phlebotomus-associated flavivirus; PP, positive pool.

The estimated infection rate of DENV in *Ae. aegypti* was 2.22 per 1,000 individuals in Jeddah. However, this result is probably underestimated because we did not use the homogenate of mosquito pools to infect mosquito cell lines. A relatively low viral load in mosquitoes is difficult to detect by direct RNA isolation. In addition, although the mosquito samples were transported at low temperature, the viral RNA might have degraded with the cycles of freezing and thawing and long-distance transportation.

Insect-specific flaviviruses (ISFVs) are flaviviruses that have been detected in mosquitoes with no-known vertebrate host (Cook et al., 2012). Many ISFVs have been detected in this century (Crabtree et al., 2003; Cook et al., 2006; Hoshino et al., 2007; Crabtree et al., 2009; Chen et al., 2013). There were 14 strains of ISFVs belonging to CxFV, PAFV, and CFAV reported in the present study. Culex flavivirus is the most diverse and prevalent ISFV detected so far and can be divided into two genotypes. One is prevalent in Asia and the USA and is mainly detected in *Cx. pipiens* but is also found in *Cx. quinquefasciatus*, *Cx. tritaeniorhynchus*, and *An. sinensis*; the other is distributed in Africa, the Caribbean, and Latin America, sharing the same host (*Cx. quinquefasciatus*) (Bittar et al., 2016). Sequence alignment and phylogenetic analysis of the *NS5* gene of 10 Saudi CxFV strains showed that they have more than 96.56% (96.56–99.62%) nucleotide identity and were clustered in the clade that included strains from Africa, the Caribbean, and Latin America. Here, the African/Caribbean/Latin American genotype was detected in the Middle East, indicating that this CxFV genotype could be transmitted and sustained in geographically distant countries. The prevalence of CxFV in *Cx. quinquefasciatus* was high in Jeddah. Among the 24 pools of *Cx. quinquefasciatus*, 10 were positive for CxFV. The MLE infection rate was 30.39 per 1,000 mosquitoes, which is much higher than that in the *Cx. pipiens* (1.34) population from Shanghai, China (Fang et al., 2018). The MIR (24.57) of CxFV in Jeddah is comparable to that in the Yucatan Peninsula of Mexico (20.8) (Farfan-Ale et al., 2009), whereas it was 4.7 per 1,000 in Guatemala, which is near the Yucatan Peninsula (Morales-Betoulle et al., 2008). It has been reported that infection with CxFV may increase the WNV infection rate (Kent et al., 2010; Newman et al., 2011). Whereas; some other studies showed that prior infection of ISFVs will suppress subsequent replication of mosquito-borne flaviviruses associated with human diseases (Hobsonpeters et al., 2013; Goenaga et al., 2015). Further study is needed to investigate whether the presence of ISFVs represent a potential threat to human or animal health.

Phlebotomus-associated flavivirus was first recorded in samples of *P. perniciosus* collected in Algeria between August 2006 and July 2007 (Moureau et al., 2010). PAFV was named after the genus of its host species, similar to other ISFVs, but is the sole ISFV that was not named after a mosquito genus. Two strains of 'mosquito flavivirus' were detected in *Ae. aegypti* from Madeira Island, Portugal in 2010 and 2013 (Osório et al., 2014). Together with the three strains detected in the present study, these strains were clustered as a monophyletic clade distinct from other Aedes flaviviruses based on the phylogenetic analysis of a partial *NS5* gene (**Figure 6**). Since this ISFV was first detected in sand flies, and the name 'mosquito flavivirus' would be confused with other flaviviruses, we designated the three new ISFV strains as PAFV. Most ISFV vectors are genus- or species-specific. CxFVs have diverse hosts and are not only restricted to *Culex* species but were also once found in *An. sinensis* (Liang et al., 2015), representing intergeneric infection. Moreover, PAFVs have been detected in both *P. perniciosus* and *Ae. aegypti*, indicating trans-family diffusion. Most of the physiological and ecological dynamics of ISFVs, including their maintenance cycles in nature, remain unknown (Hoshino et al., 2009). PAFVs have been found in the Mediterranean and Red Sea regions (Moureau et al., 2010; Osório et al., 2014), which might indicate that these habitats are suitable for the transmission of PAFV and provides evidence to suggest that the transmission of ISFVs in sympatric species is potentially linked to a common source of infection, especially through feeding (Cook et al., 2009; Calzolari et al., 2016). However, the sequences of PAFVs available in GenBank for strains from Algeria and Portugal are short (<200 nt in length). We did not successfully sequence the whole genome of PAFV, mainly owing to the low concentration of PAFV RNAs in vectors collected from Jeddah and the lack of a reference genome. Nevertheless, it is important to obtain the whole genome of PAFV to further analyze its trans-family diffusion in insects and the underlying infectious mechanisms.

Cell-fusing agent virus was the first ISFV detected, and was found in an *Ae. aegypti* cell line in 1975 (Stollar and Thomas, 1975). A strain of CFAV co-detected with PAFV in a pool of *Ae. aegypti* was observed in the present study. Since the pool contained 18 mosquitoes, it is possible that the two different ISFVs infected two or more individuals of *Ae. aegypti*; however, the possibility that the two ISFVs co-infected the same mosquito cannot be ruled out. It was reported that mosquitoes infected with ISFVs might be more susceptible to pathogenic flaviviruses (Crabtree et al., 2009; Vazquez et al., 2012). Whether the effect of superinfection exists in ISFVs is unclear. Other CFAVs have been found in Galveston, USA and Puerto Rico, and in the present study were detected in Jeddah. Although these CFAV isolates are geographically distant, the latitude of their collection sites is comparable. This indicates that the distribution of CFAVs might be influenced by climate, similar to the two CxFV genotypes (Bittar et al., 2016).

One major limitation of our study is the small sample size of mosquitoes used for virus detection. Among the 49 mosquito pools, 14 were flavivirus-positive, whereas the actual mosquito-borne virus in Jeddah is probably more diverse and of higher prevalence. Since the potential in the supernatant of mosquito homogenate viruses have not been cultivated in mosquito or human cell lines and might degrade during long-term storage for direct RNA extraction, the low concentration or titer of a given virus in mosquito homogenates would influence the results of pathogen detection. In addition, we did not detect any DENV-1, DENV-3, or DENV-4 in the tested samples, possibly owing to the low circulation of these viruses and a small sample size of host mosquitoes, but they might co-circulate in local areas. Wider sampling and virus isolation for mosquito-borne disease surveillance in Jeddah and other regions of Saudi Arabia should be carried out for a more comprehensive understanding of the virus diversity, infection rates, transmission routes, virulence, and pathogen mechanisms in this region.

In conclusion, one human-pathogen DENV and three different ISFVs, including CFAV, PAFV, and CxFV, were detected in local dominant mosquito vector species *Ae. aegypti* and *Cx. quinquefasciatus* of Jeddah, western Saudi Arabia. To the best of our knowledge, this study is the first to report viral detection in field-caught mosquitoes in Saudi Arabia. The newly detected DENV strain belonged to the C1 sub-genotype of DENV-2, possessing five unique amino acid substitutions. The phylogenetic analyses

revealed that most introduction events of DENV-2 to Saudi Arabia were related to strains from the Indian subcontinent, indicating that the DENV prevalent in Saudi Arabia is associated with religious pilgrimages and resident working expats from Asian dengue-endemic countries. The phylogenetic analyses further indicated that relatives of the detected DENV-2 strain in Jeddah were probably exported to Taiwan, China and Japan in 2014 and 2018, which suggests that DENV prevalence in Jeddah is probably more complex than previously thought, and will become even worse with the increasing frequency of international travel by air and sea, especially without efficient surveillance of mosquito-borne diseases. Strategies for mosquito-borne pathogen control should not only focus on the pilgrims and travelers from DENV-endemic areas for the potential risk of DENV introduction into Saudi Arabia but also on prevention of the exportation of locally circulating virus genotypes to other countries when these visitors return home. The high prevalence of CxFV in *Cx. quinquefasciatus* from Jeddah suggests that CxFV is widespread in this region, which may increase the risk of infection with WNV (Kent et al., 2010; Newman et al., 2011), representing a potential threat to human or animal health. The preliminary findings reported herein with randomly selected small mosquito samples highlight that wide-ranging, systematic, and continuous molecular monitoring of mosquito-borne circulating viruses in vectors is urgently needed. This would provide a comprehensive understanding of virus diversity, geographic distribution, evolution, shifts in circulating genotypes, and infection rates in Jeddah and other regions of Saudi Arabia and allow for accurate and timely estimations of the true disease burden and prevalence of dengue and other emerging/re-emerging mosquito-borne pathogens. This is essential to support the decision-making process regarding appropriate prevention and control strategies in Saudi Arabia, the Arabian Peninsula, and the whole Middle East region.

DATA AVAILABILITY STATEMENT

The datasets presented in this study can be found in online repositories. The names of the repository/repositories and accession number(s) can be found in the article/**Supplementary Material**.

AUTHOR CONTRIBUTIONS

YF: conceptualization, methodology, writing original draft preparation, and writing review and edited. ET: conceptualization, methodology, investigation, project administration, and writing review and edited. J-BX: methodology and software. YZ: conceptualization, funding acquisition, and writing review and edited. X-NZ: funding acquisition, and wrote—review and edited. EK: conceptualization, methodology, investigation, and writing review and edited. All authors contributed to the article and approved the submitted version.

FUNDING

The Special Foundation of Basic Science and Technology Resources Survey of Ministry of Science and Technology of China (grant no. 2017FY101200), the Project of Basic Platform of National Science and Technology Resources of the Ministry of Sciences and Technology of China (No. TDRC-2019-194-30).

ACKNOWLEDGMENTS

Thanks to the Public Health Pests Laboratory (PHPL) staff and administrators, Department of Environmental Health, Municipality of Jeddah Governorate, Ministry of Health and Municipalities for their support for mosquito sample provision and taxonomic identification, and the Golden Eyes Establishment, Jeddah, for the operationalization of this PHPL project.

SUPPLEMENTARY MATERIAL

The Supplementary Material for this article can be found online at: https://www.frontiersin.org/articles/10.3389/fcimb.2021.626368/full#supplementary-material

REFERENCES

Al-Ahmad, A. M., Sallam, M. F., Khuriji, M. A., Kheir, S. M., and Azarihamidian, S. (2011). Checklist and pictorial key to fourth-instar larvae of mosquitoes (Diptera: Culicidae) of Saudi Arabia. *J. Med. Entomol.* 48, 717–737. doi: 10.1603/ME10146

Al-Nazawi, A. M., Aqili, J., Alzahrani, M., Mccall, P. J., and Weetman, D. (2017). Combined target site (kdr) mutations play a primary role in highly pyrethroid resistant phenotypes of *Aedes aegypti* from Saudi Arabia. *Parasitol. Vectors* 10, 161. doi: 10.1186/s13071-017-2096-6

Alhaeli, A., Bahkali, S., Ali, A., Househ, M. S., and El-Metwally, A. A. (2016). The epidemiology of Dengue fever in Saudi Arabia: A systematic review. *J. Infect. Public Health* 9, 117–124. doi: 10.1016/j.jiph.2015.05.006

Alikhan, M., Al Ghamdi, K., and Mahyoub, J. A. (2014). *Aedes* mosquito species in western Saudi Arabia. *J. Insect Sci.* 14, 69. doi: 10.1673/031.014.69

Al-Saeed, M. S., El-Kafrawy, S. A., Farraj, S. A., Al-Subhi, T. L., Othman, N. A., Alsultan, A., et al. (2017). Phylogenetic characterization of circulating Dengue and Alkhumra Hemorrhagic Fever viruses in western Saudi Arabia and lack of evidence of Zika virus in the region: a retrospective study 2010–2015. *J. Med. Virol.* 89, 1339–1346. doi: 10.1002/jmv.24785

Ashshi, A. (2017). The prevalence of dengue virus serotypes in asymptomatic blood donors reveals the emergence of serotype 4 in Saudi Arabia. *Virol. J.* 14:107. doi: 10.1186/s12985-017-0768-7

Biggerstaff, B. J. (2006). *PooledInfRate, version 3.0: a Microsoft® Excel® add-in to compute prevalence estimates from pooled samples* (Fort Collins, CO: CDC).

Bittar, C., Machado, D. C., Vedovello, D., Ullmann, L. S., Rahal, P., Junior, J. P. A., et al. (2016). Genome sequencing and genetic characterization of *Culex* flavirirus (CxFV) provides new information about its genotypes. *Virol. J.* 13, 158. doi: 10.1186/s12985-016-0614-3

Bryant, J. E., Crabtree, M. B., Nam, V. S., Yen, N. T., Duc, H. M., and Miller, B. R. (2005). Isolation of arboviruses from mosquitoes collected in northern Vietnam. *Am. J. Trop. Med. Hyg.* 73, 470–473. doi: 10.4269/ajtmh.2005.73.470

Calzolari, M., Ze-Ze, L., Vazquez, A., Sanchez Seco, M. P., Amaro, F., and Dottori, M. (2016). Insect-specific flaviviruses, a worldwide widespread group of viruses

only detected in insects. *Infect. Genet. Evol.* 40, 381–388. doi: 10.1016/j.meegid.2015.07.032

Caraballo, H., and King, K. (2014). Emergency department management of mosquito-borne illness: malaria, dengue, and West Nile virus. *Emerg. Med. Pract.* 16, 1–23.

Chang, S., Yang, C., Hsu, T., Su, C., Lin, C., and Shu, P. (2016). Laboratory-based surveillance and molecular characterization of dengue viruses in Taiwan 2014. *Am. J. Trop. Med. Hyg.* 94, 804–811. doi: 10.4269/ajtmh.15-0534

Chen, Y. Y., Lin, J. W., Fan, Y. C., Tu, W. C., Chang, G. J., and Chiou, S. S. (2013). First detection of the Africa/Caribbean/Latin American subtype of *Culex* flavivirus in Asian country, Taiwan. *Comp. Immunol. Microbiol. Infect. Dis.* 36, 387–396. doi: 10.1016/j.cimid.2013.02.001

Christenbury, J., Aw, P., Hoe Ong, S., Schreiber, M., Chow, A., Gubler, D., et al. (2010). A method for full genome sequencing of all four serotypes of the dengue virus. *J. Virol. Methods* 169, 202–206. doi: 10.1016/j.jviromet.2010.06.013

Cologna, R., Armstrong, P. M., and Ricohesse, R. (2005). Selection for virulent dengue viruses occurs in humans and mosquitoes. *J. Virol.* 79, 853–859. doi: 10.1128/JVI.79.2.853-859.2005

Cook, S., Bennett, S., Holmes, E., De Chesse, R., Moureau, G., and De Lamballerie, X. (2006). Isolation of a new strain of the flavivirus cell fusing agent virus in a natural mosquito population from Puerto Rico. *J. Gen. Virol.* 87, 735–748. doi: 10.1099/vir.0.81475-0

Cook, S., Moureau, G., Harbach, R. E., Mukwaya, L., Goodger, K., Ssenfuka, F., et al. (2009). Isolation of a novel species of flavivirus and a new strain of *Culex* flavivirus (Flaviviridae) from a natural mosquito population in Uganda. *J. Gen. Virol.* 90, 2669–2678. doi: 10.1099/vir.0.014183-0

Cook, S., Moureau, G., Kitchen, A., Gould, E. A., De Lamballerie, X., Holmes, E. C., et al. (2012). Molecular evolution of the insect-specific flaviviruses. *J. Gen. Virol.* 93, 223–234. doi: 10.1099/vir.0.036525-0

Crabtree, M. B., Sang, R. C., Stollar, V., Dunster, L. M., and Miller, B. R. (2003). Genetic and phenotypic characterization of the newly described insect flavivirus, Kamiti River virus. *Arch. Virol.* 148, 1095–1118. doi: 10.1007/s00705-003-0019-7

Crabtree, M. B., Nga, P. T., and Miller, B. R. (2009). Isolation and characterization of a new mosquito flavivirus, Quang Binh virus, from Vietnam. *Arch. Virol.* 154, 857–860. doi: 10.1007/s00705-009-0373-1

El-Kafrawy, S. A., Sohrabsayed, S., Ela, S. A., Abd-Alla, A. M. M., Alhabbab, R., Farraj, S. A., et al. (2016). Multiple introductions of dengue 2 virus strains into Saudi Arabia from 1992 to 2014. *Vector Borne Zoonotic Dis.* 16, 391–399. doi: 10.1089/vbz.2015.1911

Fakeeh, M., and Zaki, A. M. (2001). Virologic and serologic surveillance for dengue fever in Jeddah, Saudi Arabia 1994-1999. *Am. J. Trop. Med. Hyg.* 65, 764–767. doi: 10.4269/ajtmh.2001.65.764

Fang, Y., Shi, W., and Zhang, Y. (2017). Molecular phylogeny of *Anopheles hyrcanus* group members based on ITS2 rDNA. *Parasitol. Vectors* 10, 417. doi: 10.1186/s13071-017-2351-x

Fang, Y., Zhang, Y., Zhou, Z., Shi, W., Xia, S., Li, Y. Y., et al. (2018). Co-circulation of *Aedes* flavivirus, *Culex* flavivirus, and Quang Binh virus in Shanghai, China. *Infect. Dis. Poverty* 7, 75. doi: 10.1186/s40249-018-0457-9

Farfan-Ale, J. A., Lorono-Pino, M. A., Garcia-Rejon, J. E., Hovav, E., Powers, A. M., Lin, M., et al. (2009). Detection of RNA from a novel West Nile-like virus and high prevalence of an insect-specific flavivirus in mosquitoes in the Yucatan Peninsula of Mexico. *Am. J. Trop. Med. Hyg.* 80, 85–95. doi: 10.4269/ajtmh.2009.80.85

Franklinos, L. H. V., Jones, K. E., Redding, D. W., and Abubakar, I. (2019). The effect of global change on mosquito-borne disease. *Lancet Infect. Dis.* 19, e302–e312. doi: 10.1016/S1473-3099(19)30161-6

Goenaga, S., Kenney, J. L., Duggal, N. K., Delorey, M. J., Ebel, G. D., Zhang, B., et al. (2015). Potential for co-infection of a mosquito-specific flavivirus, Nhumirim Virus, to block West Nile virus transmission in mosquitoes. *Viruses* 7, 5801–5812. doi: 10.3390/v7112911

Green, S., and Rothman, A. L. (2006). Immunopathological mechanisms in dengue and dengue hemorrhagic fever. *Curr. Opin. Infect. Dis.* 19, 429–436. doi: 10.1097/01.qco.0000244047.31135.fa

Harbach, R. E., and Knight, K. L. (1980). *Taxonomists" glossary of mosquito anatomy* (Marlton, New Jersey, the USA: Plexus Publishing Inc).

Harbach, R. (1985). Pictorial keys to the genera of mosquitoes, subgenera of *Culex* and the species of *Culex* (*Culex*) occurring in Southwestern Asia and Egypt, with a note on the subgeneric placement of *Culex deserticola* (Diptera: Culicidae). *Mosq. Syst.* 17, 83–107.

Hashem, A. M., Sohrab, S. S., El-Kafrawy, S. A., El-Ela, S. A., Abd-Alla, A. M. M., Farraj, S. A., et al. (2018). First complete genome sequence of circulating dengue virus serotype 3 in Jeddah, Saudi Arabia. *New Microbes New Infect.* 21, 9–11. doi: 10.1016/j.nmni.2017.09.005

Heilman, J. M., De Wolff, J., Beards, G. M., and Basden, B. J. (2014). Dengue fever: a Wikipedia clinical review. *Open Med.* 8, e105–e115.

Hobsonpeters, J., Yam, A. W. Y., Lu, J., Setoh, Y. X., May, F. J., Kurucz, N., et al. (2013). A new insect-specific flavivirus from northern Australia suppresses replication of West Nile virus and Murray Valley encephalitis virus in co-infected mosquito cells. *PloS One* 8. doi: 10.1371/journal.pone.0056534

Hoffmann, P. R., Woodrow, R. J., Calimlim, P. S., Sciulli, R., Effler, P. V., Miyamoto, V., et al. (2004). West Nile virus surveillance: a simple method for verifying the integrity of RNA in mosquito (Diptera: Culicidae) pools. *J. Med. Entomol.* 41, 731–735. doi: 10.1603/0022-2585-41.4.731

Hoshino, K., Isawa, H., Tsuda, Y., Yano, K., Sasaki, T., Yuda, M., et al. (2007). Genetic characterization of a new insect flavivirus isolated from *Culex pipiens* mosquito in Japan. *Virology* 359, 405–414. doi: 10.1016/j.virol.2006.09.039

Hoshino, K., Isawa, H., Tsuda, Y., Sawabe, K., and Kobayashi, M. (2009). Isolation and characterization of a new insect flavivirus from *Aedes albopictus* and *Aedes flavopictus* mosquitoes in Japan. *Virology* 391, 119–129. doi: 10.1016/j.virol.2009.06.025

Jamjoom, G., Azhar, E., Kao, M., and M Radadi, R. (2016). Seroepidemiology of Asymptomatic Dengue Virus Infection in Jeddah, Saudi Arabia. *Virology (Auckl)* 7, 1–7. doi: 10.4137/VRT.S34187

Kent, R. J., Crabtree, M. B., and Miller, B. R. (2010). Transmission of West Nile virus by *Culex quinquefasciatus* Say infected with Culex flavivirus Izabal. *PloS Negl. Trop. Dis.* 4, e671. doi: 10.1371/journal.pntd.0000671

Khan, N. A., Azhar, E. I., El-Fiky, S., Madani, H. H., Abuljadial, M. A., Ashshi, A. M., et al. (2008). Clinical profile and outcome of hospitalized patients during first outbreak of dengue in Makkah, Saudi Arabia. *Acta Trop.* 105, 39–44. doi: 10.1016/j.actatropica.2007.09.005

Kimura, M. (1980). A simple method for estimating evolutionary rates of base substitutions through comparative studies of nucleotide sequences. *J. Mol. Evol.* 16, 111–120. doi: 10.1007/BF01731581

Knight, K. L., and Stone, A. (1977). *A catalog of the mosquitoes of the world (Diptera: Culicidae)* (College Park, MD: Thomas Say Foundation and Entomology Society American).

Kumar, S., Patil, J., Dayaraj, C., Cherian, S., Barde, P., M Walimbe, A., et al. (2010). Evolution, dispersal and replacement of American genotype dengue type 2 viruses in India, (1956–2005): selection pressure and molecular clock analyses. *J. Gen. Virol.* 91, 707–720. doi: 10.1099/vir.0.017954-0

Kumar, S., Stecher, G., and Tamura, K. (2016). MEGA7: molecular evolutionary genetics analysis version 7.0 for bigger datasets. *Mol. Biol. Evol.* 33, 1870–1874. doi: 10.1093/molbev/msw054

Kuno, G., Mitchell, C. J., Chang, G. J., and Smith, G. C. (1996). Detecting bunyaviruses of the Bunyamwera and California serogroups by a PCR technique. *J. Clin. Microbiol.* 34, 1184–1188. doi: 10.1128/JCM.34.5.1184-1188.1996

Larkin, M. A., Blackshields, G., Brown, N. P., Chenna, R., Mcgettigan, P. A., Mcwilliam, H., et al. (2007). Clustal W and Clustal X version 2.0. *Bioinformatics* 23, 2947–2948. doi: 10.1093/bioinformatics/btm404

Leitmeyer, K., Vaughn, W., Watts, DM., Salas, R., Villalobos, I., Chacon, D., et al. (1999). Dengue virus structural differences that correlate with pathogenesis. *J. Virol.* 73, 4738–4747. doi: 10.1128/JVI.73.6.4738-4747.1999

Liang, W., He, X., Liu, G., Zhang, S., Fu, S., Wang, M., et al. (2015). Distribution and phylogenetic analysis of *Culex* flavivirus in mosquitoes in China. *Arch. Virol.* 160, 2259–2268. doi: 10.1007/s00705-015-2492-1

Liu, W., Pickering, P., Duchene, S., Holmes, E., and G. Aaskov, J. (2016). Highly divergent dengue virus type 2 in traveler returning from Borneo to Australia. *Emerg. Infect. Dis.* 22, 2146–2148. doi: 10.3201/eid2212.160813

Matsui, T., Kinoshita, N., Maeki, T., Kutsuma, S., Nakamura, K., Nakamoto, T., et al. (2019). Dengue virus type 2 infection in a traveler returning from Saudi Arabia to Japan. *Jpn. J. Infect. Dis.* 72, 340–342. doi: 10.7883/yoken.JJID.2018.537

Mattingly, P. F., and Knight, K. L. (1956). The Mosquitoes of Arabia. I. *Bull. Br. Mus. Nat. Hist.* 4, 89–141.

Miller, M. A., Pfeiffer, W., and Schwartz, T. (2010). "Creating the CIPRES Science Gateway for inference of large phylogenetic trees," in *Proceedings of the*

gateway computing environments workshop (GCE), vol. 1–8. (New Orleans: Louisiana). doi: 10.1109/GCE.2010.5676129

Mohammed, M. S., Abakar, A. D., Nour, B. Y., and Dafalla, O. M. (2018). Molecular surveillance of dengue infections in Sabya governate of Jazan region, Southwestern Saudi Arabia. *Int. J. Mosq. Res.* 5, 125–132.

Morales-Betoulle, M. E., Monzon Pineda, M. L., Sosa, S. M., Panella, N., Lopez, M. R., Cordon-Rosales, C., et al. (2008). *Culex* flavivirus isolates from mosquitoes in Guatemala. *J. Med. Entomol.* 45, 1187–1190. doi: 10.1093/jmedent/45.6.1187

Moureau, G., Ninove, L., Izri, A., Cook, S., De Lamballerie, X., and Charrel, R. N. (2010). Flavivirus RNA in phlebotomine sandflies. *Vector Borne Zoonotic Dis.* 10, 195–197. doi: 10.1089/vbz.2008.0216

Newman, C. M., Cerutti, F., Anderson, T. K., Hamer, G. L., Walker, E. D., Kitron, U. D., et al. (2011). *Culex* flavivirus and West Nile virus mosquito coinfection and positive ecological association in Chicago, United States. *Vector Borne Zoonotic Dis.* 11, 1099–1105. doi: 10.1089/vbz.2010.0144

Organji, S. R., Abulreesh, H. H., and Osman, G. E. (2017). Circulation of dengue virus serotypes in the City of Makkah, Saudi Arabia, as determined by reverse transcription polymerase chain reaction. *Can. J. Infect. Dis. Med. Microbiol.* 2017, 1646701. doi: 10.1155/2017/1646701

Osório, H. C., Zé-Zé, L., Amaro, F., and Alves, M. J. (2014). Mosquito surveillance for prevention and control of emerging mosquito-borne diseases in Portugal—2008–2014. *Int. J. Environ. Res. Public Health* 11, 11583–11596. doi: 10.3390/ijerph111111583

Pybus, O. G., Rambaut, A., Holmes, E. C., and Harvey, P. H. (2002). New inferences from tree shape: numbers of missing taxa and population growth rates. *Syst. Biol.* 51, 881–888. doi: 10.1080/10635150290102582

Pyke, A. T., Moore, P. R., Taylor, C. T., Hallmendelin, S., Cameron, J. N., Hewitson, G. R., et al. (2016). Highly divergent dengue virus type 1 genotype sets a new distance record. *Sci. Rep.* 6, 22356. doi: 10.1038/srep22356

Pyke, A. T., Huang, B., Warrilow, D., Moore, P. R., Mcmahon, J., and Harrower, B. (2017). Complete genome sequence of a highly divergent dengue virus type 2 strain, imported into Australia from Sabah, Malaysia. *Genome Announc.* 5, e00546–e00517. doi: 10.1128/genomeA.00546-17

Reinert, J. E. (2000). New classification for the composite genus *Aedes* (Diptera: Culicidae: Aedini), elevation of subgenus *Ochlerotatus* to generic rank, reclassification of the other subgenera, and notes on certain subgenera and species. *J. Am. Mosq. Contr.* 16, 175–188.

Ricohesse, R. (2003). Microevolution and virulence of Dengue viruses. *Adv. Virus Res.* 59, 315–341. doi: 10.1016/S0065-3527(03)59009-1

Ronquist, F., Teslenko, M., Van Der Mark, P., Ayres, D. L., Darling, A., Hohna, S., et al. (2012). MrBayes 3.2: efficient Bayesian phylogenetic inference and model choice across a large model space. *Syst. Biol.* 61, 539–542. doi: 10.1093/sysbio/sys029

Roth, A., Mercier, A., Lepers, C., Hoy, D., Duituturaga, S. E., Benyon, E., et al. (2014). Concurrent outbreaks of dengue, chikungunya and Zika virus infections –an unprecedented epidemic wave of mosquito-borne viruses in the Pacific 2012–2014. *Eurosurveillance* 19, 20929. doi: 10.2807/1560-7917.ES2014.19.41.20929

Rueda, L. M. (2004). Pictorial keys for the identification of mosquitoes (Diptera: Culicidae) associated with dengue virus transmission. *Zootaxa* 589, 1–60. doi: 10.11646/zootaxa.589.1.1

Sánchez, I. J., and Ruiz, B. H. (1996). A single nucleotide change in the E protein gene of dengue virus 2 Mexican strain affects neurovirulence in mice. *J. Gen. Virol.* 77, 2541–2545. doi: 10.1099/0022-1317-77-10-2541

Scaramozzino, N., Crance, J. M., Jouan, A., Debriel, D. A., Stoll, F., and Garin, D. (2001). Comparison of flavivirus universal primer pairs and development of a rapid, highly sensitive heminested reverse transcription-PCR assay for detection of flaviviruses targeted to a conserved region of the NS5 gene sequences. *J. Clin. Microbiol.* 39, 1922–1927. doi: 10.1128/JCM.39.5.1922-1927.2001

Stollar, V., and Thomas, V. L. (1975). An agent in the *Aedes aegypti* cell line (Peleg) which causes fusion of *Aedes albopictus* cells. *Virology* 64, 367–377. doi: 10.1016/0042-6822(75)90113-0

Twiddy, S. S., Farrar, J., Chau, N. V. V., Wills, B., Gould, E. A., Gritsun, T. S., et al. (2002). Phylogenetic relationships and differential selection pressures among genotypes of dengue-2 virus. *Virology* 298, 63–72. doi: 10.1006/viro.2002.1447

Vazquez, A., Sanchezseco, M. P., Palacios, G., Molero, F., Reyes, N., Ruiz, S., et al. (2012). Novel flaviviruses detected in different species of mosquitoes in spain. *Vector Borne Zoonotic Dis.* 12, 223–229. doi: 10.1089/vbz.2011.0687

Waman, V. P., Kolekar, P., Ramtirthkar, M. R., Kale, M. M., and Kulkarni-Kale, U. (2016). Analysis of genotype diversity and evolution of Dengue virus serotype 2 using complete genomes. *Peer J.* 4, e2326. doi: 10.7717/peerj.2326

WHO (2018). *World malaria report 2018* (Geneva, Switzerland: World Health Organization).

Wilgenbusch, J. C., and Swofford, D. (2003). Inferring evolutionary trees with PAUP*. *Curr. Protoc. Bioinformatics* 6, 6.4. doi: 10.1002/0471250953.bi0604s00

Zaki, A., Perera, D., Jahan, S. S., and Cardosa, M. J. (2008). Phylogeny of dengue viruses circulating in Jeddah, Saudi Arabia: 1994 to 2006. *Trop. Med. Int. Health* 13, 584–592. doi: 10.1111/j.1365-3156.2008.02037.x

Conflict of Interest: The authors declare that the research was conducted in the absence of any commercial or financial relationships that could be construed as a potential conflict of interest.

The reviewer KK declared a past co-authorship with one of the authors X-NZ to the handling editor.

frontiers in Cellular and Infection Microbiology

ORIGINAL RESEARCH
published: 25 February 2021
doi: 10.3389/fcimb.2021.630797

Genome-Wide Scans for Ghanaian *Plasmodium falciparum* Genes Under Selection From Local and Chinese Host Populations

Shan-Mei Shi[1], *Tian-Qi Shi*[1], *Shen-Bo Chen*[1], *Yan-Bing Cui*[1], *Kokouvi Kassegne*[1,2], *Moses Okpeku*[3], *Jun-Hu Chen*[1,2,4*] *and Hai-Mo Shen*[1*]

[1] National Institute of Parasitic Diseases, Chinese Center for Disease Control and Prevention, Key Laboratory of Parasite and Vector Biology of the Chinese Ministry of Health, National Centre for International Research on Tropical Diseases, WHO Collaborating Center for Tropical Diseases, Shanghai, China, [2] School of Global Health, Chinese Centre for Tropical Diseases Research, Shanghai Jiao Tong University School of Medicine, Shanghai, China, [3] Discipline of Genetics, School of Life Science, University of Kwazulu-Natal, Durban, South Africa, [4] National Institute of Parasitic Diseases, Chinese Centre for Disease Control and Prevention-Shenzhen Centre for Disease Control and Prevention Joint Laboratory for Imported Tropical Disease Control, Shanghai, China

OPEN ACCESS

Edited by:
Xiaojun Chen,
Nanjing Medical University, China

Reviewed by:
Wenyue Xu,
Army Medical University, China
Iris Bruchhaus,
Bernhard Nocht Institute for Tropical Medicine (BNITM), Germany

***Correspondence:**
Jun-Hu Chen
chenjh@nipd.chinacdc.cn
Hai-Mo Shen
shenhm@nipd.chinacdc.cn

Specialty section:
This article was submitted to Parasite and Host, a section of the journal Frontiers in Cellular and Infection Microbiology

Received: 18 November 2020
Accepted: 07 January 2021
Published: 25 February 2021

Citation:
Shi S-M, Shi T-Q, Chen S-B, Cui Y-B, Kassegne K, Okpeku M, Chen J-H and Shen H-M (2021) Genome-Wide Scans for Ghanaian Plasmodium falciparum Genes Under Selection From Local and Chinese Host Populations. Front. Cell. Infect. Microbiol. 11:630797. doi: 10.3389/fcimb.2021.630797

Initial malarial infection mostly causes symptomatic illness in humans. Infection that is not fatal induces complete protection from severe illness and death, and thus complete protection from severe illness or death is granted with sufficient exposure. However, malaria parasite immunity necessitates constant exposure. Therefore, it is important to evaluate lowered immunity and recurrent susceptibility to symptomatic disease in lower transmission areas. We aimed to investigate selection pressure based on transmission levels, antimalarial drug use, and environmental factors. We whole genome sequenced (WGS) *P. falciparum* clinical samples from Chinese hosts working in Ghana and compared the results with the WGS data of isolates from native Ghanaians downloaded from pf3k. The *P. falciparum* samples were generally clustered according to their geographic origin, and Chinese imported samples showed a clear African origin with a slightly different distribution from the native Ghanaian samples. Moreover, samples collected from two host populations showed evidence of differences in the intensity of selection. Compared with native Ghanaian samples, the China-imported isolates exhibited a higher proportion of monoclonal infections, and many genes associated with RBC invasion and immune evasion were found to be under less selection pressure. There was no significant difference in the selection of drug-resistance genes due to a similar artemisinin-based combination therapy medication profile. Local selection of malarial parasites is considered to be a result of differences in the host immunity or disparity in the transmission opportunities of the host. In China, most *P. falciparum* infections were imported from Africa, and under these circumstances, distinct local selective pressures may be caused by varying acquired immunity and transmission intensity. This study revealed the impact of host switching on the immune system, and it may provide a better understanding of the mechanisms that enable clinical immunity to malaria.

Keywords: *Plasmodium falciparum*, Ghana, imported malaria, variant surface antigen, positive selection, acquired immunity

INTRODUCTION

Malarial parasites have yielded to the selection pressure of host immune systems after coexisting and interacting with their hosts for over 150 million years. (Carter and Mendis, 2002). It is well known that the immune system of a human host can block parasite development at different stages; but, malarial parasites have long been evolving in response to threats from multiple immune mechanisms (Rénia and Goh, 2016). It is expected that new immune escape mechanisms will constantly be uncovered. Although not always, initial malaria infection tends to cause symptomatic illness in humans. (Ryg-Cornejo et al., 2016). In this process, infants may develop lethal febrile illness, but adults acquire complete protection from severe illness or death, even though some believe that sterile immunity can never be achieved (Simon et al., 2015).

Over the last decade, the number of malaria cases globally has reduced by at least half, and many of the malaria endemic countries around the world will navigate gradual elimination with predictable results (Ariey et al., 2019). Similar to other pathogens, parasite immunity is acquired through constant exposure. Therefore, research has focused on lowered immunity and recurrent susceptibility to symptomatic disease in lower transmission areas (Barry and Hansen, 2016). During this long-term fight between humans and malaria, almost all surface antigens of the parasite have been tested for vaccine development, and their extensive polymorphisms from geographical distribution are considered to slow down the development of acquired immunity (Doolan et al., 2009; Barry and Arnott, 2014).

Researchers noted that selection pressure on parasites varies with location due to several reasons, including varying transmission ecology, innate susceptibility of mosquitoes or human hosts, degrees of acquired immunity in humans, and drug pressure in certain areas (Crompton et al., 2014). Duffy et al. emphasized that in highly endemic areas, malaria faces genotype competition due to superinfections, with stronger host acquired immune responses (Duffy et al., 2015). More genome-wide analyses of *P. falciparum* confirmed this conclusion and revealed a significant global population structure (Manske et al., 2012; Zhu et al., 2019).

After decades of efforts to control this illness, China has reduced its malaria burden from 2,961/100,000 population in 1970 to 0 in 2017, and aims to eliminate malaria nationwide (Feng et al., 2018). Today, the burden weighs mostly in Sub-Saharan Africa, where the largest prevalence rates are found (Mbacham et al., 2019; Papaioannou et al., 2019). Researchers reported 8,653 P. falciparum imported cases from 2011 to 2015. These cases were imported from 41 sub-Saharan countries into China, leading to 98 deaths, mostly of Chinese laborers (Lai et al., 2016).

Abbreviations: ACTs, artemisinin-based combination therapies; iHS, integrated haplotype score; PCA, Principal component analysis; PfEMP1, *P. falciparum* erythrocyte membrane protein 1; RBCs, red blood cells; RIFINs, repetitive interspersed families of polypeptides; STEVOR, subtelomeric variant open reading frame; VSAs, variant surface antigens; XP-EHH, cross-population extended haplotype homozygosity.

To test whether differences in selection emerge due to different hosts, patterns relating to both transmission level and drug use and environmental variations, Ghanaian *P. falciparum* samples from two different human host populations were analyzed. Clinical isolates from Chinese patients who either worked or have worked in Ghana were whole genome sequenced (WGS) and compared with the WGS data from native Ghana residents downloaded from pf3k (https://www.malariagen.net/projects/pf3k). Our clinical isolates were collected during a large-scale outbreak of imported malaria in 2013 (Li et al., 2015). Isolated parasites resembled those from the Ghanaian population. Our comparative analysis also revealed extensive genetic diversity, different selection signatures, and host adaptation-focused genomic plasticity.

In this study, we scanned the difference in *P. falciparum* genes under selection pressure to evaluate the impact of declining transmission on clinical immunity. Samples collected from two host populations showed evidence of differences in selection intensity. The imported population exhibited a higher proportion of monoclonal infections, and many genes associated with RBC invasion and immune evasion were found to be under low selection pressure. Our results deepen our understanding of factors that might drive clinical immunity against malaria.

MATERIALS AND METHODS

Sampling *P. falciparum* Parasites and Genome Sequencing

A malaria outbreak comprising 874 patients was reported in Shanglin County, China in 2013, and 871 of these patients were confirmed to be overseas laborers who had returned from Ghana. Blood samples were collected from these imported cases; all samples tested microscopically positive, and a PCR confirmed single *P. falciparum* infection. However, after rapid on-site disposal and treatment, only nine samples with high parasite density were retained for follow-up sequencing. DNA was extracted from blood samples using the QIAGEN DNeasy Blood & Tissue Kit (Qiagen, UK), and sheared into 500 bp fragments to construct the libraries with Covaris S2 (Covaris, Inc., USA) instrument. All libraries on Illumina X-10 were sequenced and generated an average of 109M (34–540 M) paired-end reads of 150 bp. All Illumina raw sequencing reads were submitted to the Chinese National Sharing Service Platform for Parasite Resources. In addition, we downloaded the *P. falciparum* 3D7 reference sequence from the PlasmoDB database (Aurrecoechea et al., 2008).

All sequenced raw reads were filtered by removing the adapter and low-quality sequences with Trimmomatic-3.0 (Bolger et al., 2014) and mapped to the 3D7 reference sequence using Burrows-Wheeler Aligner (Li and Durbin, 2010). Genotyping was performed using in-house R script based on GATK4 best-practice workflows and recalibrated with pf3k standard known-site files (Mckenna et al., 2010). High-quality single nucleotide polymorphism (SNP) data were derived by excluding SNPs with >5% missing calls in each sample; missing calls were defined as positions with <2 reads. We

downloaded high-quality SNP data from 92 indigenous Ghana *P. falciparum* isolates collected in 2013 from the PF3k project to build the reference data set (Amenga-Etego, 2012; Mensah-Brown et al., 2015).

Population Structure, Genetics Analysis, and Selection Tests

We assessed the population structure using both, the global collection and our imported isolates. Principal component analysis (PCA, Person n-1) was performed using the R4.02 package. Analysis of the ancestry shared between individual isolates was performed using the ADMIXTURE package (Alexander and Lange, 2011) to check the relationship between the China-imported and native Ghanaian isolates and their respective populations. In these analyses, the SNP dataset was filtered to exclude each locus with a minor allele frequency (MAF) of <5% for all positions, which had been restricted to loci that appeared at least once in both our samples and the references.

In this study, we used the within-isolate F_{WS} fixation index to determine the within-infection genomic diversity in relation to the total population using the bahlolab/moimix R package (Lee, 2015). Isolates with an F_{WS} score of 1 were considered as a single predominant genotype. Two of the samples in our study had genetically mixed infections (F_{WS} <0.95), analogous to inbreeding coefficient. We then checked the heterozygosity calls to evaluate genotypic errors. For two or more segregating allele loci across the two samples, we discarded the minority calls (the allele with low read depth) and retained the major allele only. Without hypnozoite-induced relapses, genetic complexity was considered to not likely affect our genetic analysis process.

In the population genetics section, we followed the evolution analysis pipeline from an earlier study, in which genome-wide variation was undertaken on clinical isolates from highly endemic regions of Guinea and compared with those of Gambia (Mobegi et al., 2014). We estimated the nucleotide diversity ($\hat{\pi}$), Watterson's estimator ($\hat{\theta}$ ω), genetic differentiation (F_{ST}), and Tajima's D value across all of the genes in ARLEQUIN-Ver3.5 (Excoffier and Lischer, 2010) on the SNP dataset of both populations.

Meanwhile, we used the integrated haplotype score (iHS) test to calculate the standardized log ratio of integrated extended-haplotype homozygosity on nine imported samples in Selscan-Ver1.10a (Szpiech and Hernandez, 2014). The XP-EHH test was also performed using the same software to obtain the standardized log ratio of the integrated site-specific EHH between the China-imported and the native Ghanaian populations.

RESULTS

Genomic Data Summary

Variant call format (VCF) files of 92 indigenous Ghanaian *P. falciparum* isolates collected in 2013 were downloaded from the PF3k project (www.malariagen.net/pf3k) to build the reference data set. After the quality control process was completed, a total of nine samples with high-quality genomic data was included in the analysis. The samples generated paired-end reads with an average read length of 150 bp. A variable proportion of reads from the nine isolate samples were mapped to the *P. falciparum* 3D7 reference. An average of 95% convergence in the whole genome was defined as high-quality consensus base calls. Using the GATK Genotype, we uncovered a total of 109,173 SNP loci, of which <5% contained missing calls (**Table 1**).

Complexity of Infection

We checked the within-sample parasite diversity of the imported samples to determine the proportion of single-genotype isolates. An F_{WS} value of >0.95 indicates that an infection predominantly contains a single genotype; thus, a higher proportion of imported samples were monoclonal infections. The distribution of F_{WS} scores was similar across isolates, ranging from 0.73 to 0.97 (mean 0.92). Seven isolates had F_{WS} values above 0.95, indicating that the samples were centered on single genotypes. Within each isolate, the majority allele at each SNP was included in the population-based allele frequency analysis.

Population Structure of *P. falciparum* Isolates

We applied PCA to the SNPs to compare the population structures with reference samples from around the world (**Figures 1A, B**). The *P. falciparum* samples clustered generally according to their geographic origin, and the samples collected from different hosts were divided along the major axis. The imported cases showed a clear African origin, and a similar, yet by no means identical, distribution with the native Ghanaian samples. The ADMIXTURE analysis identified several parts that correspond to each component of the samples (**Figure 1C**). In accordance with the general assumption, the imported samples

TABLE 1 | Sequencing and mapping summary statistics for nine China imported samples.

Sample ID	Total Reads	Mapped ratio (%)	Average coverage depth (X)	Genome covrage >1x (%)	Covrage >10x (%)	F_{WS}
Ah_28	56,712,364	16.25	51.09	99.16	92.47	0.7400
D_Pf4_1	81,054,920	7.42	29.57	98.10	81.62	0.9594
PFDL_15	49,232,000	4.97	5.73	95.05	9.46	0.9724
PFDL_17	50,636,206	5.49	8.27	97.69	27.00	0.9552
PFGX_121	47,107,990	6.48	9.86	98.84	41.81	0.8587
PFGX_154	55,644,848	9.35	20.63	98.78	86.74	0.9587
PFGX_212	47,977,732	4.46	4.29	90.18	5.06	0.9692
PFGX_316	58,322,570	2.44	6.69	96.97	18.04	0.9766
PFGX_81	56,278,848	5.46	8.62	97.32	30.34	0.9598

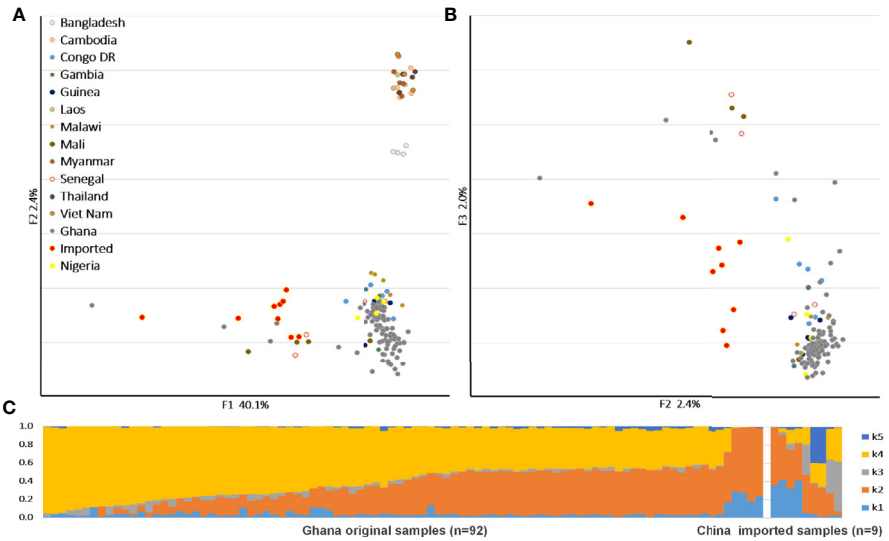

FIGURE 1 | Parasite population structure in nine China-imported samples relative to the reference. **(A)** Principal component analysis (PCA) plots illustrating the genetic differentiation between populations around the world. **(B)** Within Ghanaian population, samples collected from different hosts were divided along the secondary axis. **(C)** ADMIXTURE bar plot illustrates the population structure within Ghanaian populations from local and Chinese hosts at an optimized cluster value of K = 5.

appeared as a mixture of all the components and demonstrated the full range of the Ghana isolates, but the native Ghanaian samples comprised only K2, K4, and a few K1 components. Components K3 and K5 were almost absent in native samples, implying a higher degree of acquired immunity in African hosts.

Genomic Scan for Differentiation Between Populations

In a total of 5,602 genes, we estimated the average $\hat{\pi}$ and $\hat{\theta}\omega$ values to b 0.0013 and 0.0016, respectively. As expected, the mean values were significant lower than the native Ghanaian samples (P<0.0001, one-tailed z-test); the $\hat{\pi}$ and $\hat{\theta}\omega$ values were estimated to be 0.0017 and 0.0035, respectively. The variation profile of some gene families, particularly those associated with RBC invasion and immunity, exhibited greater genetic diversity than all gene backgrounds (**Figure 2A**), such as *rifin* (0.0116) and *var* (0.012). Based on a putative drug-resistance gene list from previous studies (Gamo et al., 2010; Plouffe et al., 2016; Cowell et al., 2018), we checked the diversity of these genes from Chinese and Ghanaian hosts. For 37 of the most common drug-resistance genes (**Supplementary Table 1**), the average $\hat{\pi}$ value was 0.0007 in imported samples and 0.0013 in native samples.

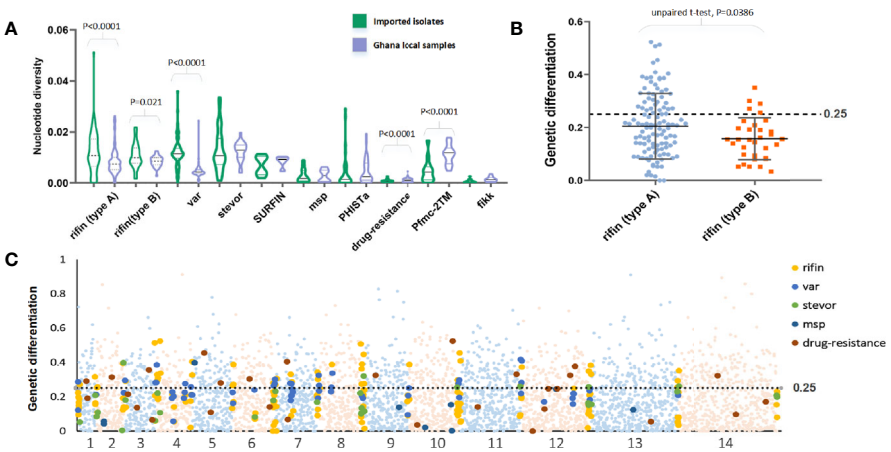

FIGURE 2 | F_{ST} value of all genes summarizing the difference between China-imported samples (n=9) and native Ghanaian (n=92) reference samples. **(A)** The variation profile of some gene families exhibited greater genetic diversity between imported and local samples. **(B)** F_{ST} value of each gene from two subgroups of the *rif* family showed significant differences. **(C)** F_{ST} value in all genes for pairs of populations to explore genomic effects of local and overseas hosts.

We calculated the F_{ST} value in individual genes for pairs of populations to explore the genomic effects from local and overseas hosts (**Figure 2C**). Although these two populations should be considered to have the same Ghanaian lineage, they still exhibited considerable differences for each gene (mean F_{ST} = 0.13, median = 0.33); 1252 genes had F_{ST} values >0.25. Among the high F_{ST} value genes, those associated with the organism membrane (GO:0044279 and GO:0044218), protein binding (GO:0005515), and important processes, such as stimulus response (GO:0050896) and interspecies interaction (GO:0044419), were found to be significantly enriched. For the variant surface antigen (VSA) genes, only a small part (54 *rif*, 7 *stevor*, but no *var*) appeared in the high F_{ST} value list, which is in accord with the fact that receptor adhesion phenotypes of RBCs normally depend on a few specific variant surface antigens that are expressed. For example, two subgroups of the *rif* family showed significant (P = 0.038, *t*-test) differences in the F_{ST} test (**Figure 2B**). RIFINs mediate the resetting of pRBCs and demonstrate stronger geographic differences, whereas B-RIFINs showed lower variability in molecules and expression. Meanwhile, 13 drug-resistance genes such like *mdr1*, *apiap2*, and *crt* showed higher F_{ST} values, reflecting the differences in treatment policy between the two countries (Ehrlich et al., 2020).

We identified signatures of selection pressure in individual genes to reveal divergence between different host populations (**Supplementary Table 2**). Not surprisingly, the two Tajima's D values were mostly negative, with an average of -0.66 and -1.58 in imported and local samples, respectively (median = -0.85 and -1.76), and mean value of imported samples were significantly higher than local samples (P <0.0001, z-test for paired samples). The background of all genes was consistent with earlier studies that described a historical population expansion of *P. falciparum* in Africa (Loy et al., 2017), and the lower mean value in native Ghanaian samples also suggested stronger selection pressure from African hosts. Similar to the gene background, the mean Tajima's D value was less negative in drug-resistant genes from the imported group (mean =-0.45, median =-1.17) compared with that from the native group (mean =-1.6, median =-1.44) (**Figure 3A**), which also occurred in some other infection-related gene families, such as *2TM* (mean =-0.57 and -1.05, median = -0.61 and -1.04), *fikk* (mean =-0.68 and -1.31, median =-0.93 and -1.52), and *msp1* (mean = – -0.39 and – -1.18, median = – -0.58 and – -1.69) (Bachmann et al., 2015). However, not much difference within VSA gene families was detected (**Figure 3B**) (average for *rif*, *var*, and *stevor* were -1.06, -1.35, and -1.01 in the imported group and -1.35, -1.47, and -1.27 in the native group, respectively).

Scan for Evidence of Directional Selection

In this study, we used the iHS statistic to detect incomplete sweeps and identified SNPs above the top 1% value of the randomly expected distribution at the whole-genome level (**Table 2** and **Supplementary Table 3**). Usually, in the *Plasmodium* genome, the top selected SNP locus is associated with RBC invasion and immune evasion genes. In our imported population, we found that the top 1% SNPs involved 329 genes, including 46 *var*, 5 *msp*, 66 *rif*, and 12 *stevor* (**Figure 4A**). In addition, most of these gene family members are present in the top 5% list (59 *var*, 130 *rif*, and 26 *stevor* in 788 genes), and these genes are located close to each other on the chromosome. This condition is common in malarial parasites because positive selection could increase the prevalence of both, the selected variant as well as of nearby variants, and local regions of extended haplotypes were generated. For the drug-resistance genes, only four genes, *mcp1*, *pi3k*, *ap2tf*, and *K13*, showed higher iHS values (**Table 2** and **Supplementary Table 1**) and reflected the unrestricted use of artemisinin-based combination therapies (ACTs) in African countries (Gallien et al., 2013; Tun et al., 2015; Velasco et al., 2017).

XP-EHH was also applied to compare the average haplotype length associated with each SNP between the imported and native Ghanaian references. The selection signals were

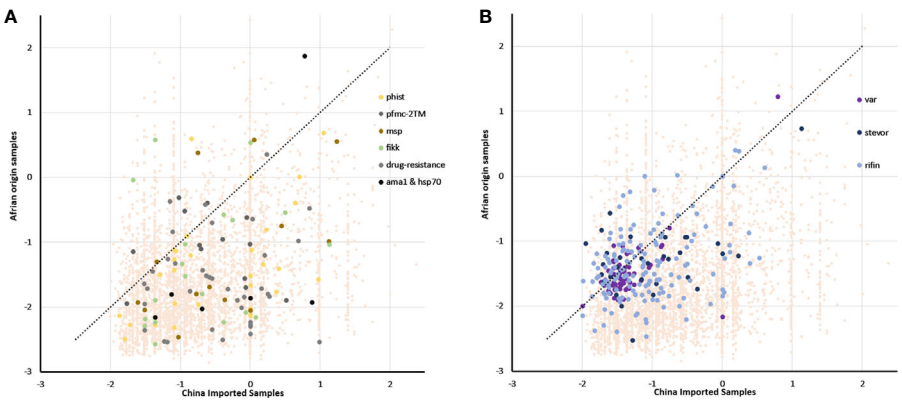

FIGURE 3 | Tajima's D value of all genes summarizing the difference of balanced selection between China-imported samples (n=9) and native Ghanaian (n=92) reference samples. The lower mean value in local samples suggested a stronger selection pressure from African hosts. **(A)** Some important genes/gene families showed the same trend as that of the gene background, and these genes/gene families include phist, 2TM, msp1, and drug-resistance genes. **(B)** Unlike the background, there was not much difference in variant surface antigen (VSA) gene families between the imported and local groups.

TABLE 2 | Notable *P. falciparum* genes with their associated positive selection statistics.

Chromosome	Gene	Product	π	Tajima's D test	FST	Top |ihs| value	Top XP-EHH value
Mosquito transmission							
13	PF3D7_1335900	thrombospondin-related	0.012	0.472	0.244	2.542	
Liver Stage Infection							
3	PF3D7_0304600	Circumsporozoite protein	0.005	0.222	0.350	3.595	
Erythrocytic stage evasion							
2	PF3D7_0206800	merozoite surface protein 2	0.009	-1.335	0.150	2.881	
4	PF3D7_0421300	PfEMP1	0.013	-1.397	0.401	2.627	2.436
6	PF3D7_0617600	stevor	0.009	-0.947	0.115	2.806	2.461
7	PF3D7_0711700	PfEMP1	0.013	-1.374	0.534	3.550	2.460
9	PF3D7_0930300	merozoite surface protein 1	0.005	0.060	0.312	2.676	
9	PF3D7_0937500	rifin	0.015	-1.314	0.326	2.509	2.653
9	PF3D7_0900100	PfEMP1	0.010	-1.668	0.220	2.810	2.903
11	PF3D7_1149900	stevor	0.025	-1.160	0.655	3.109	2.483
12	PF3D7_1255100	rifin	0.010	-0.878	0.400	2.982	3.234
12	PF3D7_1255000	rifin	0.013	-0.941	0.373	2.529	3.221
13	PF3D7_1300200	rifin	0.010	-1.841	0.396	2.803	2.785
Drug-resistance							
1	PF3D7_0108400	mitochondrial carrier protein	0.001	-1.478	0.116	3.0285	
5	PF3D7_0515300	phosphatidylinositol 3-kinase	0.001	-1.074	0.674	2.732	
6	PF3D7_0613800	AP2 domain TF	0.002	-0.546	0.110	3.613	-3.701
13	PF3D7_1343700	kelch protein K13	0.000	-0.552	0.368	2.642	

obviously stronger in native Ghanaian samples and concentrated in VSA genes (68 VSA in 96 genes) (**Table 2** and **Supplementary Table 4**). In imported isolates, in addition to VSA, these stronger selection signals were also located in some gene families, such as *pfmc-2TM* and *surfin*. However, unlike the local samples, these top signals of selection encompassed multiple genes, rendering it difficult to focus on specific genes (**Figure 4B**).

DISCUSSION

Malarial parasites have already coexisted with their hosts for over 150 million years. Throughout their life cycle, these parasites exhibit great immune evasion ability, even if they are at the asymptomatic liver stage, by using sophisticated system of proteins to avoid immune recognition (WHO, 2016) in the

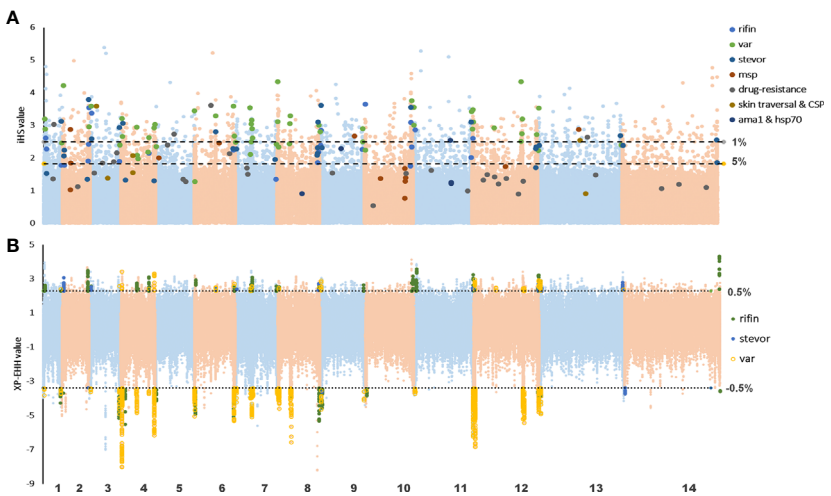

FIGURE 4 | Haplotype-based detected positive selection in China-imported samples. **(A)** Genome-wide scan of standardized |iHS| for single nucleotide polymorphisms (SNPs) with a minor allele frequency (MAF) of at least 5% in imported samples. Dashed lines indicate the top 1% and 5% of |iHS| values (|iHS| score >2.49 and 1.82, respectively). SNPs from important gene or gene families with top values were listed. **(B)** Genome-wide scan of standardized XP-EHH for SNPs with a MAF of at least 5% in China-imported samples, using native Ghanaian samples as the reference population. Dashed lines indicate the top 1% of XP-EHH values (± 0.5%, XP-EHH score >2.29 or <-3.39 in imported/local populations). SNPs from the VAS gene family with top ranking values were listed.

blood stage. Various immune evasion strategies comprise a major obstacle to the development of effective therapeutics. In as early as the 1950s, MacGregor et al. found that antibodies were a key component of antimalarial immunity (Preston et al., 2014). Decades later, researchers have characterized many immune targets and potential vaccine candidates and identified antigen-specific immune responses associated with malaria infection protection. Many studies have focused on biomolecular, genetic, and immune strategies in both hosts and parasites to better understand protective anti-*Plasmodium* immunity, but there is still a long way to go (WHO, 2016).

To date, malaria is one of the major causes of death in the African continent; the African continent accounts for about four-fifths of all cases of the world in 2017 alone, with 4% of these cases occurring in Ghana (Xu and Liu, 2016). Meanwhile, half a world away, the malaria burden in China has been dramatically reduced from 2961/100,000 in 1970 to 0.1/100,000 in 2014, and eventually down to 0 in 2017 (Zhou et al., 2016). The elimination progress soon hit a barrier since now imported malaria cases have been reported in almost all provinces in China. In 2013, a malaria outbreak (874 cases in total) was reported in the Guangxi province of China, most occurring in miners returned from Ghana (Wang et al., 2017). In response, Shanglin County conducted mass malaria screening and found an attack rate of 216/1,000 that was much higher than expected.

In the last 10 years, the number of malaria cases has fallen sharply worldwide. Malarial immunity is acquired through constant exposure, and in lower transmission areas, more studies have focused on declining immunity in communities and the recurrent susceptibility to symptomatic disease. For example, Fowkes et al. reported that rebounds of malarial infections occurred in low transmission areas (Chen et al., 2018). For similar reasons, the lack of acquired immunity in Chinese citizens increased their susceptibility to *P. falciparum*. Thus, we scanned the differences in genes under selection pressure between Chinese and Ghanaian hosts to reveal the impact of declining transmission on clinical immunity. We expected the samples to cluster according to their geographic origin and exhibit more detail in the population structure. We also hypothesized that the imported population should exhibit a higher proportion of monoclonal infections, and many genes/gene families associated with RBC invasion and immune evasion are under less selection pressures. In the native Ghanaian population, we suspected the samples to encounter a strong acquired immunity response from local human hosts and cause strong positive selection. Therefore, we expected to observe signals of extended haplotype homozygosity on immune evasion related genes. We also estimated that there would be no significant difference in the selection of drug-resistance genes due to the same ACT-based medication profile in both countries.

Our results are consistent with these assumptions. In the global population structure, samples were clustered according to their geographic origin, and imported isolates, which could be regarded as part of the Ghanaian population, maintained slight diversity to the reference sequence. It was quite unexpected that overall genetic diversity was lower in imported samples (the mean $\hat{\pi}$ values in the imported and native samples were 0.0013 and 0.0017, respectively); even though we assumed low selection pressure from Chinese hosts would enable parasites to mutate faster. However, when it comes to genes associated with RBC invasion and immunity, greater diversity was exhibited in imported samples than local ones, such as *rif* (0.0116), *var* (0.012), and *stevor* (0.013). The VSA gene families exhibited the greatest diversity in the parasite, and our observations were consistent with previous studies (Volkman et al., 2007). Highly polymorphic proteins have been used to mediate antigenic variation and help malaria parasites escape immune clearance (Julien and Wardemann, 2019). We found a higher proportion of monoclonal infections, and the average F_{WS} scores were higher than those in a local study during the same period (mean values of 0.81 and 0.74 in the Kintampo and Navrongo provinces of Ghana, respectively) (Duffy et al., 2015). A high ratio of monoclonal infection could be due to a low entomological inoculation rate or clonal parasite population. Chinese laborers normally worked in small enclosed spaces, with less chance of superinfection or co-transmission.

As we delved into evolutionary analysis, we could see natural selection acting at the gene level. The host immune response along with its genetic background is essential for malaria prevention. Clinical immunity to malaria is definitely acquired, even though the process might be slow in areas of stable transmission. The significantly higher average Tajima's D values (P <0.0001, z-test for paired samples) of imported samples demonstrated a lack of acquired immunity in Chinese citizens, while 3,934 genes showed negative values. However, in local samples, almost all genes were under directional selection (5,253 genes with negative values). This difference revealed that continued exposure to malarial antigens maintains immunity. For example, sporozoites use microneme (SPECT-1, PLP1, and TRAP) and some circumsporozoite (CSP) proteins to overcome skin and hepatic immune defenses during their invasion (Lo et al., 2016; Ryg-Cornejo et al., 2016; WHO, 2016). In these related genes, we detected stronger selective pressure in native Ghanaian samples (mean D value -0.002 in imported and -0.36 in local group), consistent with the background.

Meanwhile, in the erythrocyte stage, the key evasion mechanism is sequestration, which is mediated by proteins, such as PfEMP-1, RIFIN, and STEVOR that allow iRBC adherence to the vascular endothelium, thereby avoiding clearance (Langhorne et al., 2008; Wahlgren et al., 2017) and sequestering the cells in the microvasculature of various organs. As part of the immune evasion system, the VSA family did not encounter stronger selection, and the difference in Tajima's D test on VSA gene families was quite narrow. While the XP-EHH test showed stronger selection in both populations concentrated in the VSA family, these signatures of selection were scattered in different individual genes, such as *crt* (PF3D7_0709000), in the local host group and imported group. Therefore, our results indicate that, with their tremendous genetic diversity, the VSA families launched different genes for particular hosts to ensure antigenic variation, maintain stable function, and demonstrate regional characteristics.

CONCLUSIONS

Local selection of malaria parasites is considered to be due to differences in host immunity or disparities in transmission opportunities of the host. In China, most *P. falciparum* infections were imported from Africa, and under these circumstances, distinct local selective pressures may be caused by varying acquired immunity and transmission intensity levels. Against the background of similar structures, samples collected from two host populations showed evidence of differences in selection intensity. Compared with native Ghanaian samples, the China-imported population exhibited a higher proportion of monoclonal infections, and many genes/gene families associated with RBC invasion and immune evasion were under low-level selection pressures. There was no significant difference in the selection of drug-resistance genes due to a similar ACTs-based therapy. Our results deepen our understanding of factors that might drive clinical immunity against malaria.

DATA AVAILABILITY STATEMENT

All data supporting these findings are contained within the manuscript and supplementary tables. All Illumina raw sequencing reads were submitted to the Chinese National Sharing Service Platform for Parasite Resources (URL: https://www.tdrc.org.cn/portal-tdrc/a/freeLoginmatmain/matmain/form?id=207872). Sequencing data are available from the corresponding author upon reasonable request.

ETHICS STATEMENT

The study was conducted based on the principles expressed in the Declaration of Helsinki. Following the study protocol, potential risks and benefits were explicitly explained to participants. Blood collection was performed with written informed consent of the participants and following institutional ethical guidelines that were reviewed and approved by the ethics committee at the National Institute of Parasitic Diseases, Chinese Center for Disease Control and Prevention.

AUTHOR CONTRIBUTIONS

J-HC and H-MS conceived and designed the experiments. S-MS, T-QS, S-BC, and Y-BC conducted the experiments. S-MS, T-QS, and H-MS analyzed the data. KK contributed reagents and materials. MO contributed to the analysis tool. S-MS and H-MS drafted the manuscript. MO and J-HC revised the manuscript critically in regard to intellectual content. All authors contributed to the article and approved the submitted version.

FUNDING

This work was supported by the National Research and Development Plan of China (Grant No. 2018YFE0121600) and the National Sharing Service Platform for Parasite Resources (Grant No. TDRC-2019-194-30), the Project of Shanghai Science and Technology Commission (Grant No. 18490741100), the Foundation of National Science and Technology Major Program (Grant no. 2018ZX10734–404, 2016ZX10004222–004, and 2012ZX10004-220), and the National Natural Science Foundation of China (81101266). The funding bodies had no role in the design of the study, collection, analysis, and interpretation of data, or in writing of the manuscript.

ACKNOWLEDGMENTS

We acknowledge the patients who participated in this study and the management team of the various health facilities from Anhui, Guangxi Provinces, and Dalian City.

SUPPLEMENTARY MATERIAL

The Supplementary Material for this article can be found online at: https://www.frontiersin.org/articles/10.3389/fcimb.2021.630797/full#supplementary-material

Supplementary Table 1 | 37 drug-resistance/putative genes summary with |iHS| and XP-EHH value.

Supplementary Table 2 | 5,602 *P. falciparum* genes with population genetic statistics (nucleotide diversity, Watterson's estimator, Tajima's D test, and F_{ST} *test*).

Supplementary Table 3 | Genes with top 1% in integrated haplotype score.

Supplementary Table 4 | Genes with top 1% (±0.5%) cross population extended haplotype homozygosity value in imported/local populations.

REFERENCES

Alexander, D. H., and Lange, K. (2011). Enhancements to the ADMIXTURE algorithm for individual ancestry estimation. *BMC Bioinf.* 12, 246. doi: 10.1186/1471-2105-12-246

Amenga-Etego, N.-K. L. (2012). *Plasmodium falciparum population genetics in northern Ghana* (UK: Oxford University).

Ariey, F., Gay, F., and Ménard, R. (2019). *Malaria Control and Elimination* (New York, NY: Humana Press). doi: 10.1007/978-1-4939-9550-9

Aurrecoechea, C., Brestelli, J., Brunk, B. P., Dommer, J., Fischer, S., Gajria, B., et al. (2008). PlasmoDB: a functional genomic database for malaria parasites. *Nucleic Acids Res.* 37, 539–543. doi: 10.1093/nar/gkn814

Bachmann, A., Scholz, J., Janßen, M., Klinkert, M.-Q., Tannich, E., Bruchhaus, I., et al. (2015). A comparative study of the localization and membrane topology of members of the RIFIN, STEVOR and Pf MC-2TM protein families in Plasmodium falciparum-infected erythrocytes. *Malar J.* 14, 274. doi: 10.1186/s12936-015-0784-2

Barry, A. E., and Arnott, A. (2014). Strategies for designing and monitoring malaria vaccines targeting diverse antigens. *Front. Immunol.* 5, 359. doi: 10.3389/fimmu.2014.00359

Barry, A., and Hansen, D. (2016). Naturally acquired immunity to malaria. *Parasitology* 143, 125–128. doi: 10.1017/S0031182015001778

Bolger, A. M., Lohse, M., and Usadel, B. (2014). Trimmomatic: a flexible trimmer for Illumina sequence data. *Bioinformatics* 30, 2114–2120. doi: 10.1093/bioinformatics/btu170

Carter, R., and Mendis, K. N. (2002). Evolutionary and historical aspects of the burden of malaria. *Clin. Microbiol Rev.* 15, 564–594. doi: 10.1128/CMR.15.4.564-594.2002

Chen, T.-M., Zhang, S.-S., Feng, J., Xia, Z.-G., Luo, C.-H., Zeng, X.-C., et al. (2018). Mobile population dynamics and malaria vulnerability: a modelling study in the China-Myanmar border region of Yunnan Province, China. *Infect. Dis. Poverty* 7, 36. doi: 10.1186/s40249-018-0423-6

Cowell, A. N., Valdivia, H. O., Bishop, D. K., and Winzeler, E. A. (2018). Exploration of *Plasmodium vivax* transmission dynamics and recurrent infections in the Peruvian Amazon using whole genome sequencing. *Genome Med.* 10, 52. doi: 10.1186/s13073-018-0563-0

Crompton, P. D., Moebius, J., Portugal, S., Waisberg, M., Hart, G., Garver, L. S., et al. (2014). Malaria immunity in man and mosquito: insights into unsolved mysteries of a deadly infectious disease. *Annu. Rev. Immunol.* 32, 157–187. doi: 10.1146/annurev-immunol-032713-120220

Doolan, D. L., Dobaño, C., and Baird, J. K. (2009). Acquired immunity to malaria. *Clin. Microbiol. Rev.* 22, 13–36. doi: 10.1128/CMR.00025-08

Duffy, C. W., Assefa, S. A., Abugri, J., Amoako, N., Owusu-Agyei, S., Anyorigiya, T., et al. (2015). Comparison of genomic signatures of selection on Plasmodium falciparum between different regions of a country with high malaria endemicity. *BMC Genomics* 16, 1. doi: 10.1186/s12864-015-1746-3

Ehrlich, H. Y., Jones, J., and Parikh, S. (2020). Molecular Surveillance of Antimalarial Partner Drug Resistance in Sub-Saharan Africa: A Spatial-Temporal Evidence Mapping Study. *Lancet Microbe* 1 (5), e209–e217. doi: 10.2139/ssrn.3534203

Excoffier, L., and Lischer, H. E. (2010). Arlequin suite ver 3.5: a new series of programs to perform population genetics analyses under Linux and Windows. *Mol. Ecol. Resour* 10, 564–567. doi: 10.1111/j.1755-0998.2010.02847.x

Feng, J., Zhang, L., Huang, F., Yin, J.-H., Tu, H., Xia, Z.-G., et al. (2018). Ready for malaria elimination: zero indigenous case reported in the People's Republic of China. *Malar J.* 17, 315. doi: 10.1186/s12936-018-2444-9

Gallien, S., Taieb, F., Hamane, S., De Castro, N., and Molina, J. (2013). Autochthonous falciparum malaria possibly transmitted by luggage-carried vector in Paris, France, February 2013. *Eurosurveillance* 18, 20600. doi: 10.2807/1560-7917.ES2013.18.40.20600

Gamo, F.-J., Sanz, L. M., Vidal, J., De Cozar, C., Alvarez, E., Lavandera, J.-L., et al. (2010). Thousands of chemical starting points for antimalarial lead identification. *Nature* 465, 305. doi: 10.1038/nature09107

Julien, J.-P., and Wardemann, H. (2019). Antibodies against Plasmodium falciparum malaria at the molecular level. *Nat. Rev. Immunol.* 19 (12), 761–775. doi: 10.1038/s41577-019-0209-5

Lai, S., Wardrop, N. A., Huang, Z., Bosco, C., Sun, J., Bird, T., et al. (2016). Plasmodium falciparum malaria importation from Africa to China and its mortality: an analysis of driving factors. *Sci. REP-UK* 6, 39524. doi: 10.1038/srep39524

Langhorne, J., Ndungu, F. M., Sponaas, A.-M., and Marsh, K. (2008). Immunity to malaria: more questions than answers. *Nat. Immunol.* 9, 725–732. doi: 10.1038/ni.f.205

Lee, S. (2015). Assessing clonality in malaria parasites using massively parallel sequencing data. *F1000Research* 4, 1043.

Li, H., and Durbin, R. (2010). Fast and accurate long-read alignment with Burrows-Wheeler transform. *Bioinformatics* 26, 589–595. doi: 10.1093/bioinformatics/btp698

Li, Z., Yang, Y., Xiao, N., Zhou, S., Lin, K., Wang, D., et al. (2015). Malaria imported from Ghana by returning gold miners, Chin. *Emerging Infect. Dis.* 21, 864. doi: 10.3201/eid2105.141712

Lo, E., Nguyen, J., Oo, W., Hemming-Schroeder, E., Zhou, G., Yang, Z., et al. (2016). Examining *Plasmodium falciparum* and *P. vivax* clearance subsequent to antimalarial drug treatment in the Myanmar-China border area based on quantitative real-time polymerase chain reaction. *BMC Infect. Dis.* 16, 154. doi: 10.1186/s12879-016-1482-6

Loy, D. E., Liu, W., Li, Y., Learn, G. H., Plenderleith, L. J., Sundararaman, S. A., et al. (2017). Out of Africa: origins and evolution of the human malaria parasites Plasmodium falciparum and Plasmodium vivax. *Int. J. Parasitol* 47, 87–97. doi: 10.1016/j.ijpara.2016.05.008

Manske, M., Miotto, O., Campino, S., Auburn, S., Almagro-Garcia, J., Maslen, G., et al. (2012). Analysis of *Plasmodium falciparum* diversity in natural infections by deep sequencing. *Nature* 487, 375–379. doi: 10.1038/nature11174

Mbacham, W. F., Ayong, L., Guewo-Fokeng, M., and Makoge, V. (2019). "Current situation of malaria in Africa," in *Malaria Control and Elimination* (Springer), 29–44. doi: 10.1007/978-1-4939-9550-9_2

Mckenna, A., Hanna, M., Banks, E., Sivachenko, A., Cibulskis, K., Kernytsky, A., et al. (2010). The Genome Analysis Toolkit: a MapReduce framework for analyzing next-generation DNA sequencing data. *Genome Res.* 20, 1297–1303. doi: 10.1101/gr.107524.110

Mensah-Brown, H. E., Amoako, N., Abugri, J., Stewart, L. B., Agongo, G., Dickson, E. K., et al. (2015). Analysis of erythrocyte invasion mechanisms of Plasmodium falciparum clinical isolates across 3 malaria-endemic areas in Ghana. *J. Infect. Dis.* 212, 1288–1297. doi: 10.1093/infdis/jiv207

Mobegi, V. A., Duffy, C. W., Amambua-Ngwa, A., Loua, K. M., Laman, E., Nwakanma, D. C., et al. (2014). Genome-wide analysis of selection on the malaria parasite *Plasmodium falciparum* in West African populations of differing infection endemicity. *Mol. Biol. Evol.* 31, 1490–1499. doi: 10.1093/molbev/msu106

Papaioannou, I., Utzinger, J., and Vounatsou, P. (2019). Malaria-anemia comorbidity prevalence as a measure of malaria-related deaths in sub-Saharan Africa. *Sci. Rep.* 9, 1–9. doi: 10.1038/s41598-019-47614-6

Plouffe, D. M., Wree, M., Du, A. Y., Meister, S., Li, F., Patra, K., et al. (2016). High-throughput assay and discovery of small molecules that interrupt malaria transmission. *Cell Host Microbe* 19, 114–126. doi: 10.1016/j.chom.2015.12.001

Preston, M. D., Campino, S., Assefa, S. A., Echeverry, D. F., Ocholla, H., Amambua-Ngwa, A., et al. (2014). A barcode of organellar genome polymorphisms identifies the geographic origin of Plasmodium falciparum strains. *Nat. Commun.* 5, 1–7. doi: 10.1038/ncomms5052

Rénia, L., and Goh, Y. S. (2016). Malaria parasites: the great escape. *Front. Immunol.* 7, 463. doi: 10.3389/fimmu.2016.00463

Ryg-Cornejo, V., Ioannidis, L. J., Ly, A., Chiu, C. Y., Tellier, J., Hill, D. L., et al. (2016). Severe malaria infections impair germinal center responses by inhibiting T follicular helper cell differentiation. *Cell Rep.* 14, 68–81. doi: 10.1016/j.celrep.2015.12.006

Simon, A. K., Hollander, G. A., and Mcmichael, A. (2015). Evolution of the immune system in humans from infancy to old age. *Proc. Biol. Sci.* 282, 20143085–20143085. doi: 10.1098/rspb.2014.3085

Szpiech, Z. A., and Hernandez, R. D. (2014). Selscan: an efficient multi-threaded program to perform EHH-based scans for positive selection. *Mol. Biol. Evol.*, msu211. doi: 10.1093/molbev/msu211

Tun, K. M., Imwong, M., Lwin, K. M., Win, A. A., Hlaing, T. M., Hlaing, T., et al. (2015). Spread of artemisinin-resistant Plasmodium falciparum in Myanmar: a cross-sectional survey of the K13 molecular marker. *Lancet Infect. Dis.* 15, 415–421. doi: 10.1016/S1473-3099(15)70032-0

Velasco, E., Gomez-Barroso, D., Varela, C., Diaz, O., and Cano, R. (2017). Non-imported malaria in non-endemic countries: a review of cases in Spain. *Malar J.* 16, 260. doi: 10.1186/s12936-017-1915-8

Volkman, S. K., Sabeti, P. C., Decaprio, D., Neafsey, D. E., Schaffner, S. F., Milner, D. A., et al. (2007). A genome-wide map of diversity in Plasmodium falciparum. *Nat. Genet.* 39, 113–119. doi: 10.1038/ng1930

Wahlgren, M., Goel, S., and Akhouri, R. R. (2017). Variant surface antigens of *Plasmodium falciparum* and their roles in severe malaria. *Nat. Rev. Microbiol* 15, 479–491. doi: 10.1038/nrmicro.2017.47

Wang, D., Cotter, C., Sun, X., Bennett, A., Gosling, R. D., and Xiao, N. (2017). Adapting the local response for malaria elimination through evaluation of the 1-3-7 system performance in the China–Myanmar border region. *Malar J.* 16, 54. doi: 10.1186/s12936-017-1707-1

WHO (2016). *WHO malaria terminology*.

Xu, J.-W., and Liu, H. (2016). The relationship of malaria between Chinese side and Myanmar's five special regions along China–Myanmar border: a linear regression analysis. *Malar J.* 15, 368. doi: 10.1186/s12936-016-1413-4

Zhou, S., Li, Z., Cotter, C., Zheng, C., Zhang, Q., Li, H., et al. (2016). Trends of imported malaria in China 2010–2014: analysis of surveillance data. *Malar J.* 15, 39. doi: 10.1186/s12936-016-1093-0

Zhu, S. J., Hendry, J. A., Almagro-Garcia, J., Pearson, R. D., Amato, R., Miles, A., et al. (2019). The origins and relatedness structure of mixed infections vary with local prevalence of P. falciparum malaria. *Elife* 8, e40845. doi: 10.7554/eLife.40845

Conflict of Interest: The authors declare that the research was conducted in the absence of any commercial or financial relationships that could be construed as a potential conflict of interest.

frontiers in Cellular and Infection Microbiology

ORIGINAL RESEARCH
published: 26 February 2021
doi: 10.3389/fcimb.2021.587150

The Role of Tim-3 on dNK Cells Dysfunction During Abnormal Pregnancy With *Toxoplasma gondii* Infection

Teng Li[1†], Lijun Cui[1†], Xiaoyan Xu[1†], Haixia Zhang[1], Yuzhu Jiang[1], Liqin Ren[2], Chunyan Yang[3], Xianbing Liu[1] and Xuemei Hu[1]*

[1] Department of Immunology, Binzhou Medical University, Yantai, China, [2] Medicine & Pharmacy Research Center, Binzhou Medical University, Yantai, China, [3] School of Stomatology, Binzhou Medical University, Yantai, China

Vertical transmission of *Toxoplasma gondii* (*T. gondii*) infection during gestation can result in severe complications such as abortion, congenital malformation, fetal teratogenesis, etc. Immune inhibitory molecule Tim-3 was discovered to be expressed on some decidual immune cells and participates in the maintenance of maternal-fetal tolerance. Dysregulation of Tim-3 expression on decidual NK (dNK) cells was observed in several cases of pregnancy complications, whereas the role of Tim-3 on dNK cells during *T. gondii* infection remains unclear. In the present study, *T. gondii* infected Tim-3$^{-/-}$ pregnant mice, and anti-Tim-3 neutralizing antibody treated and infected human dNK cells were successfully established to explore the role of Tim-3 in dysfunction of dNK cells during abnormal pregnancy. Our results illustrated that Tim-3$^{-/-}$ pregnant mice displayed more worse pregnancy outcomes with *T. gondii* infection compared to infected WT pregnant mice. Also, it demonstrated that Tim-3 expression on dNK cells was significantly down-regulated following *T. gondii* infection. Data suggested a remarkable activation of dNK cells in Tim-3$^{-/-}$ mice and anti-Tim-3 neutralizing antibody treated and infected groups, with higher ratios of activating receptor NKG2D to inhibitory receptor NKG2A or KIR2DL4, IFN-γ/IL-10, and increased granule production compared with that of the infected group. Mechanism analysis proved that *T. gondii*-induced Tim-3 down-regulation significantly activated the phosphatidylinositol-3-kinase (PI3K)-AKT and JAK-STAT signaling pathway, by which the GranzymeB, Perforin, IFN-γ, and IL-10 production were further up-regulated. Our research demonstrated that the decrease of Tim-3 on dNK cells caused by *T. gondii* infection further led to dNK cells function disorder, which finally contributed to the development of abnormal pregnancy outcomes.

Keywords: *Toxoplasma gondii*, dNK cells, Tim-3, inhibitory molecule, abnormal pregnancy outcomes

OPEN ACCESS

Edited by:
Jun Feng,
National Institute of Parasitic Diseases, China

Reviewed by:
Daniel Adesse,
Oswaldo Cruz Foundation (Fiocruz), Brazil
Qingfeng Zhang,
Tongji University, China

***Correspondence:**
Xuemei Hu
xue-mei-hu@163.com

†These authors have contributed equally to this work

Specialty section:
This article was submitted to Parasite and Host, a section of the journal Frontiers in Cellular and Infection Microbiology

Received: *25 July 2020*
Accepted: *15 January 2021*
Published: *26 February 2021*

Citation:
Li T, Cui L, Xu X, Zhang H, Jiang Y, Ren L, Yang C, Liu X and Hu X (2021) The Role of Tim-3 on dNK Cells Dysfunction During Abnormal Pregnancy With Toxoplasma gondii Infection. Front. Cell. Infect. Microbiol. 11:587150. doi: 10.3389/fcimb.2021.587150

INTRODUCTION

Toxoplasma gondii (*T. gondii*) is an obligate intracellular parasite which is capable of infecting all species of warm-blooded animals *via* the ingestion of tissue cysts or sporulated oocysts (Robert-Gangneux and Dardé, 2012). Although *T. gondii* can be controlled in subjects with healthy immune systems, it can cause life-threatening damage for patients with immunocompromised states (Yarovinsky, 2014). As a pathogen of human TORCH syndrome (toxoplasmosis, rubella, cytomegalovirus, herpes simplex, and other agents), the vertical transmission of *T. gondii* from an infected mother to her fetus can lead to devastating consequences such as pregnancy loss or severe disease in the neonate, including blindness, developmental delay, or neurological manifestations (Arora et al., 2017). Successful reproduction depends on the homeostasis of maternal-fetal tolerance (Mold and McCune, 2012). The specialized immune microenvironment is sustained by the dynamic orchestration of immune cells (dNK cells, macrophages and Treg cells), cytokines and enzymatic factors (Erlebacher, 2013). In the first trimester of gestation, dNK cells represent the largest population, comprising 70% of decidual immune cells (Trundley and Moffett, 2004). The dNK cells modulate maternal-fetal tolerance by maintaining stable functional molecule expression (NKG2A and KIR2DL4) and cytokines production (Rouas-Freiss et al., 1997; Fu et al., 2017). Increasing evidence suggests that abnormal changes in the function of dNK cells are closely related to adverse pregnancy outcomes such as preeclampsia and fetal growth restriction (Moretta et al., 2000a; Koopman et al., 2003). KIR2DL4 belongs to the killer cell immunoglobulin-like receptor (KIR) family of decidual NK cells, which interact with soluble HLA-G. The interaction between dNK inhibitory receptors (KIR2DL4, ILT-2) and their ligand HLA-G on invading trophoblasts allows the extensive remodeling of the maternal vasculature during the early weeks of pregnancy and inhibits the killing activity of NK cells to HLA-G positive trophoblasts (Yan et al., 2007; Ferreira et al., 2017). C-type lectin-like receptor NKG2A is also one of the inhibitory receptors of dNK cells, which has a higher affinity to HLA-E than CD94/NKG2C-activating receptor (El et al., 2009). Compared to normal pregnancy, the recurrent spontaneous abortion (RSA) group showed decreased expression of NKG2A on dNK (Sotnikova et al., 2014). Our previous studies have reported an excessive activation of dNK cells after *T. gondii* infection with imbalance between inhibitory receptors (NKG2A, KIR2DL4) and activating receptors NKG2D (Liu et al., 2013; Xu et al., 2013; Liu et al., 2014). Besides, IFN-γ-producing dNK cells counts were significantly increased following *T. gondii* infection (Liu et al., 2014; Zhang et al., 2015). However, the detailed mechanism of dNK cells dysfunction in *T. gondii* infection remains unknown and requires further study.

T cell immunoglobulin domain and mucin domain 3 (Tim-3) is known as an inhibitory molecule that transduces negative signals into T cell triggering apoptosis or exhaustion (Zhu et al., 2005). Recently, Tim-3 is found to be highly expressed on decidual immune cells, especially on dNK cells (Sun et al., 2016). Alteration of Tim-3 expression on dNK cells has been proven in several pregnancy failure and preeclampsia cases, identifying Tim-3 as a key mediator of dNK cells maintaining successful pregnancy (Miko et al., 2013; Meggyes et al., 2015; Li et al., 2017a). However, whether *T. gondii* infection could influence Tim-3 expression on dNK cells and subsequently lead to adverse pregnancy outcomes has not yet been investigated. In a previous experiment, we observed that *T. gondii* infection significantly induced downregulation of Tim-3 on dNK cells, and Tim-$3^{-/-}$ pregnant mice exhibited more worse pregnancy outcomes compared with the WT group after infection. These findings indicated that Tim-3 expression may play an important role in adverse pregnancy outcomes by *T. gondii* infection. However, whether the change of Tim-3 expression after *T. gondii* infection leads to dNK cells dysfunction and then contributes to adverse pregnancy outcomes remains unclear. In the present study, Tim-$3^{-/-}$ pregnant mice and Tim-3 neutralizing antibodies were used to fully elucidate the specific role of Tim-3 on dNK cells dysfunction following *T. gondii* infection.

MATERIALS AND METHODS

Animal Models

C57BL/6 mice (WT mice; 6 to 8 week-old females and 8 to 10 week-old males) were purchased from Pengyue Laboratory Animal Technology Co., Ltd (Jinan, China). Tim-3-deficient (Tim-$3^{-/-}$) C57BL/6 mice were obtained from Bioray Laboratories Inc (Shanghai, China). All mice were maintained in the specific pathogen-free animal house of Binzhou Medical University at 22°C-26°C with 50%-60% humidity and a 12 h light/12 h dark cycle, with access to abundant sterilized water and food (Jiangsu Biological Engineering Co., Ltd., China). Female mice were housed five per cage, and male mice were housed one per cage for a week to facilitate acclimatization to new environment. Subsequently, females and males were housed in cages at a 2:1 overnight, and female mice with vaginal plugs (gestational day, gd 0) were segregated and randomized into uninfected, *T. gondii* infected, and *T. gondii* infected-Tim-$3^{-/-}$ groups. At gd 7, the infected group was intraperitoneally injected with 400 tachyzoites (RH strain) resuspended in 200 μl PBS, and the uninfected mice were injected with the same amount of PBS into the abdominal cavity.

Scanning Electron Microscopy (SEM)

Mice were sacrificed on gd 11. All fetuses were carefully removed and washed 5-6 times in phosphate buffer (0.1 M), and fixed in 2.5% phosphate buffered glutaraldehyde for 2 days at 4°C. Thereafter, immobilized fetuses were dehydrated using a graded ethanol series every 15 min in each step. The samples were dried by the critical point technique (Quorum K850), attached to specimen holders and coated with gold particles by ion sputter coater (Quorum Q150RS). All samples were placed on sample stages and observed with a scanning electron microscope (ZEISS EVO LS15) operated at 10 KV. All images were obtained using SmarSEM user interface software.

Obtention of Tim-3$^{-/-}$ Mice

Mouse tails were used to extract genomic DNA, and polymerase chain reaction (PCR) was conducted to synthesize cDNA. After initial denaturation for 3 min at 94°C, PCR was performed with 30 amplification cycles of denaturation for 30 s at 94°C, annealing for 30 s at 56°C, and extension for 60 s at 72°C, followed by a final extension for 8 min at 72°C and maintenance at 16°C. The primers for PCR amplification were as follows:

Tim-3-PCR-S, 5′-GGCTGGCTCAAACTCACTACA-3′; Tim-3-PCR-A, 5′-CGGACAATGATAACATGGAAA-3′. Then PCR products were sequenced (Shanghai Majorbio Bio-Pharm Technology Co., Ltd), and we distinguished the homozygotes from heterozygotes or WT mice by analyzing the DNA chromatogram. A sufficient number of Tim-3$^{-/-}$ mice were obtained and bred for use in the present study.

Preparation of *T. gondii* Tachyzoites (RH Strain)

HEp-2 cells were obtained from the Cell Research Institute of the Chinese Academy of Sciences (Shanghai, China) and were used to maintain *T. gondii* tachyzoites in minimum essential medium (MEM; Hyclone) containing 5% fetal bovine serum (FBS; Gibco) and 100 IU/mL penicillin/streptomycin (Sigma-Aldrich). HEp-2 cells were centrifuged at 1500 rpm (433×*g*) for 10 min after culture, and the clear supernatants were then centrifuged at 4000 rpm (3082×*g*) to purify the tachyzoites. MEM was used to resuspend the tachyzoites. Then tachyzoites were counted by Neubauer chamber and cultured with new HEp-2 cells. The experiment was carried out in BSL-2 laboratories. All the labwares, consumables, and liquids contaminated by the parasites were collected and sterilized by high-pressure sterilizer.

Cell Preparation of Mice

Mice uteri and placentas were carefully dissected from pregnant mice at gd 11 and were washed twice in cold PBS. Tissues were then cut into small pieces and prepared for cell dispersion by GentleMACS dissociator (Miltenyi Biotech). Sterile nets (48 μm) were used to obtain single cell suspensions. Mononuclear cells were collected from the white film layer after Ficoll density gradient centrifugation in mouse lymphocyte separation medium (TBD Science), and were then analyzed with flow cytometry. The mice cadavers were stored in a -20°C freezer and disposed of by professional organizations.

Collection of Human Clinical Sample

The sample collection for this study was approved by the Ethics Committee of Binzhou Medical University, and all voluntary abortions had occurred in the Department of Obstetrics and Gynecology of Yantai Affiliated Hospital of Binzhou Medical University and the Yantai Hospital of Traditional Chinese Medicine. Decidual tissues of first trimester (gestational age of 6 to 8 weeks) were obtained from healthy pregnant women, and any evidence of threatened abortion or any pregnancy complications during gestation was excluded. Among these patients, those with abnormal chromosome abortuses, anatomic abnormalities of uterus and cervical, endocrine, and metabolic disease (diabetes, hyperthyroidism, and hypothyroidism), infection of chlamydia and ureaplasma in cervical mucus, or positive for anticardiolipin antibodies were excluded. Tissues were immediately rinsed with sterile saline solution 5-8 times, and decidual tissues were collected in Dulbecco's modified Eagle's medium/high glucose medium (Hyclone) supplemented with 100 IU/mL penicillin/streptomycin (Sigma-Aldrich).

Isolation of Human dNK Cells

Decidual samples were immediately washed 5-6 times in Roswell Park Memorial Institute (RPMI) medium to remove the blood and then cut into small pieces. Tissues were maintained in C tubes containing 0.1% collagenase type IV (Sigma-Aldrich) and 25 IU/mL DNase-I (Sigma-Aldrich). Single cell suspensions were obtained by GentleMACS dissociator (Miltenyi Biotech) and were filtered through 48 μm nylon mesh filters. Then the mononuclear cells were isolated *via* density gradient centrifugation using human lymphocyte separation medium (TBD Science) at 2000 rpm (771×*g*) for 20 min at 20°C according to the manufacturer's instructions. dNK cells were washed once by PBS and purified using a human CD3 positive selection kit and CD56 positive selection kit (Stem Cell Science) according to the manufacturer's instructions with >95% purity ensured for experiments. Approximately 1.5×10^6 purified human $CD3^-CD56^+$ dNK cells were obtained and divided equally into uninfected, infected, and Tim-3-neutralized infected groups. $CD3^-CD56^+$ dNK cells were incubated with 10 μg/mL anti-Tim-3 monoclonal antibody mAb (Thermo Fisher Scientific) in the Tim-3-neutralized infected group for 2 h, following which *T. gondii* tachyzoites were added to the Tim-3-neutralized infected group and the infected group at a 2:1 ratio (*T. gondii*: cells). All samples were cultured in RPMI medium supplemented with 10% FBS (FBS, Gibco) and 100 IU/mL penicillin/streptomycin (Sigma-Aldrich) for 36 h at 37°C in a humidified 5% CO_2 incubator.

Flow Cytometry

For surface staining, the following fluorochrome-conjugated mAbs were used: Tim-3 (clone RMT3-23, Biolegend), CD122 (clone TM-b1), CD3e (clone 145-2C11), NKG2A (clone 16a11), NKG2D (clone CX5, all from Thermo Fisher Scientific) were used *in vivo*. Isolated murine decidual mononuclear cells were incubated with mAbs above at 4°C in the dark for 30 min and then washed with PBS. *In vitro*, cells were stained with human-specific mAbs CD3 (clone OKT3), Tim-3 (clone 8B. 2C12), NKG2D (clone 5C6, all from Thermo Fisher Scientific), KIR2DL4 (clone mAb33, Biolegend) and CD56 (clone HCD56, Biolegend). For staining of intracellular granules Perforin, GranzymeA and GranzymeB, cells were firstly surface stained, subsequently fixed and permeabilized in 1× Fix/Perm buffer (Thermo Fisher Scientific) for 25 min according to the manufacturer's protocol. After washing with buffer, cells were incubated with anti-Perforin (clone ebioOMAK-D), GranzymeA (clone GzA-3G8.5), GranzymeB (clone NGZB, all from Thermo Fisher Scientific) mAbs for 40 min at 4°C in the dark and then were washed with buffer. Human specific mAb GranzymeA

(clone CB9, Biolegend), GranzymeB (clone GB11, BD bioscience) and Perforin (clone dG9, BD bioscience) were also used *in vitro*. For analysis of the intracellular cytokines, cells were initially stimulated for 4 h with a leukocyte activation cocktail (BD bioscience). Thereafter, the cells were collected and incubated with surface staining mAbs at 4°C for 40 min in the dark and then washed with buffer. The cells were fixed and permeabilized in 1× Fix/Perm buffer (Thermo Fisher Scientific) for 30 min at 4°C according to the protocol. After being washed twice, cells were incubated with mouse-specific mAbs IL-10 (clone JES5-16E3, BD bioscience) and IFN-γ (clone XMG1.2, BD bioscience) or human-specific IL-10 (clone JES3-19F1, BD bioscience) and IFN-γ (clone 4S.B3, BD bioscience) at 4°C in the dark for 40 min and washed with buffer. Analysis was performed using a FACScanto™ II instrument (Becton Dickinson).

Immunofluorescence

Purified human $CD3^-CD56^+$ dNK cells from uninfected, infected, and Tim-3-neutralized infected groups were air-dried onto Poly-L-lysine coated slides. After fixation in 4% paraformaldehyde for 30 min, slides were then blocked with goat serum for 1 h at room temperature. dNK cells were incubated overnight at 4°C with anti-Tim-3 (1/200, Abcam), anti-NKG2D (1/200, Abcam), anti-GranzymeA, anti-GranzymeB and anti-Perforin (1/200, all from Proteintech) or for 45 min with anti-CD56 (clone HCD56, Biolegend) and anti-KIR2DL4 (clone mAb33, Biolegend) antibody. After being washed three times with PBS, cells were then incubated with appropriate concentrations of secondary antibodies for 1 h at 37° C. Cy3 rabbit anti-goat IgM (1/500, Bioss) was used as the secondary antibody for anti-Tim-3 antibody, and Cy3 donkey anti-rabbit IgG (1/500, Bioss) was used as secondary antibody for anti-NKG2D, anti-GranzymeA, anti-GranzymeB and anti-Perforin. Subsequently, dNK cells were stained with the DAPI (nucleic acid stain 4',6-diamidino-2-phenylindole) for 15 min and washed 3 times with PBS. Finally, confocal microscopy of cells was performed using Zeiss LSM880.

Western Blot Analysis

$CD3^-CD56^+$ dNK cells from the three groups were incubated for 36 h before harvesting. Equal amounts of protein from total-cell lysates were separated by 12% SDS-PAGE (Beyotime) and transferred onto polyvinylidene fluoride (PVDF) membranes (Millipore). The membranes were then blocked at room temperature for 2.5 h in 7% nonfat dry milk in TBS-T buffer. Membranes were incubated with gentle rocking 1.5 h at room temperature with primary antibodies for Tim-3 (1/2000, Proteintech), GranzymeB (1/2000, Abcam), Perforin (1/1000, Proteintech), GranzymeA (1/600, Proteintech), PI3K (1/500, Proteintech), AKT (1/500, SAB), pAKT (1/500, SAB), STAT1 (1/500, Proteintech), STAT3 (1/600, Proteintech), pSTAT1 (1/500, Abcam), pSTAT3 (1/600, Abcam), IL-10 (1/500, Abcam), IFN-γ (1/500, Proteintech) and GAPDH (1/40000, Proteintech) as a loading control. Membranes were washed with TBS-T 5 times for 10 min each, then incubated with the appropriate secondary antibody for 2 h at room temperature. Then immune complex was visualized with an enhanced chemiluminescence (ECL) detection kit (F. Hoffmann-La Roche, Ltd., Switzerland). Protein expression levels were determined by Image J software (Rawak Software, Inc., Germany).

Histopathology

Mouse placentas and uteri of gd 11 were removed after treatments and washed thrice. After immediate fixation in 4% paraformaldehyde, tissues were washed in running water and placed in a graded ethanol and then were paraffin embedded using standard methods. Paraffin sections were cut to a thickness of 5 μm and stained with hematoxylin and eosin dye (H&E; Shanghai Novland Co., Ltd., China) according to the manufacturer's instructions. Images of paraffin embedded sections were recorded at 40 × magnification and are presented with 50 μm scale bars.

Statistical Analysis

Data are presented as the means ± SD. Statistical analyses were performed using the GraphPad Prism 5 Statistics software package. Unpaired *t* tests were used to identify differences. $p< 0.05$ was regarded as significant and $p< 0.01$ was considered as extremely significant.

RESULTS

Tim-$3^{-/-}$ Pregnant Mice Exhibited More Worse Pregnancy Outcomes Than WT Pregnant Mice After *T. gondii* Infection

All mice were sacrificed and dissected on gd 11 to observe the pregnancy outcomes among three groups. We observed abnormal pregnancy outcomes caused by *T. gondii* infection, with erected fur, spiritual malaise, and inflammatory hyperemia of placentas in infected mice compared with the uninfected group (**Figures 1A, B**). Compared with infected WT mice, *T. gondii* infected Tim-$3^{-/-}$ pregnant mice had sluggish responses, along with trembling and significant placental bleeding (**Figures 1B, C**). The fetuses of the infected WT group exhibited abnormal bleeding manifestations as well as a higher rate of abnormalities than those of the uninfected group (**Figures 1A, B**); in addition, decreased fetal and placental weights were observed in the fetuses of infected WT mice (**Figure 1D**). Fetuses of the infected Tim-$3^{-/-}$ pregnant group were almost shapeless and smaller, with distinct developmental delays compared with infected WT fetuses (**Figures 1B, C**). The worse abnormal pregnancy outcomes in infected Tim-$3^{-/-}$ pregnant mice were based on the decrease in fetal and placental weights and higher rate of abnormal fetuses in comparison with infected WT group (**Figure 1D**). We further observed the intrauterine development of embryos of three groups by scanning electron microscopy (SEM). Fetuses from the Tim-$3^{-/-}$ infected mice had the smallest size among the three groups (**Figures 1E–G**), which is in line with our previous observations of fetal weight. Caused by infection of *T. gondii*, the fetuses in infected WT group exhibited smaller body and delayed formed paddle-shaped handplate and footplate (**Figures 1E, F**). The spinal development of infected fetuses was not as good as that of normal fetuses (**Figures 1E, F**). And the physical condition of the Tim-$3^{-/-}$ infected fetuses was

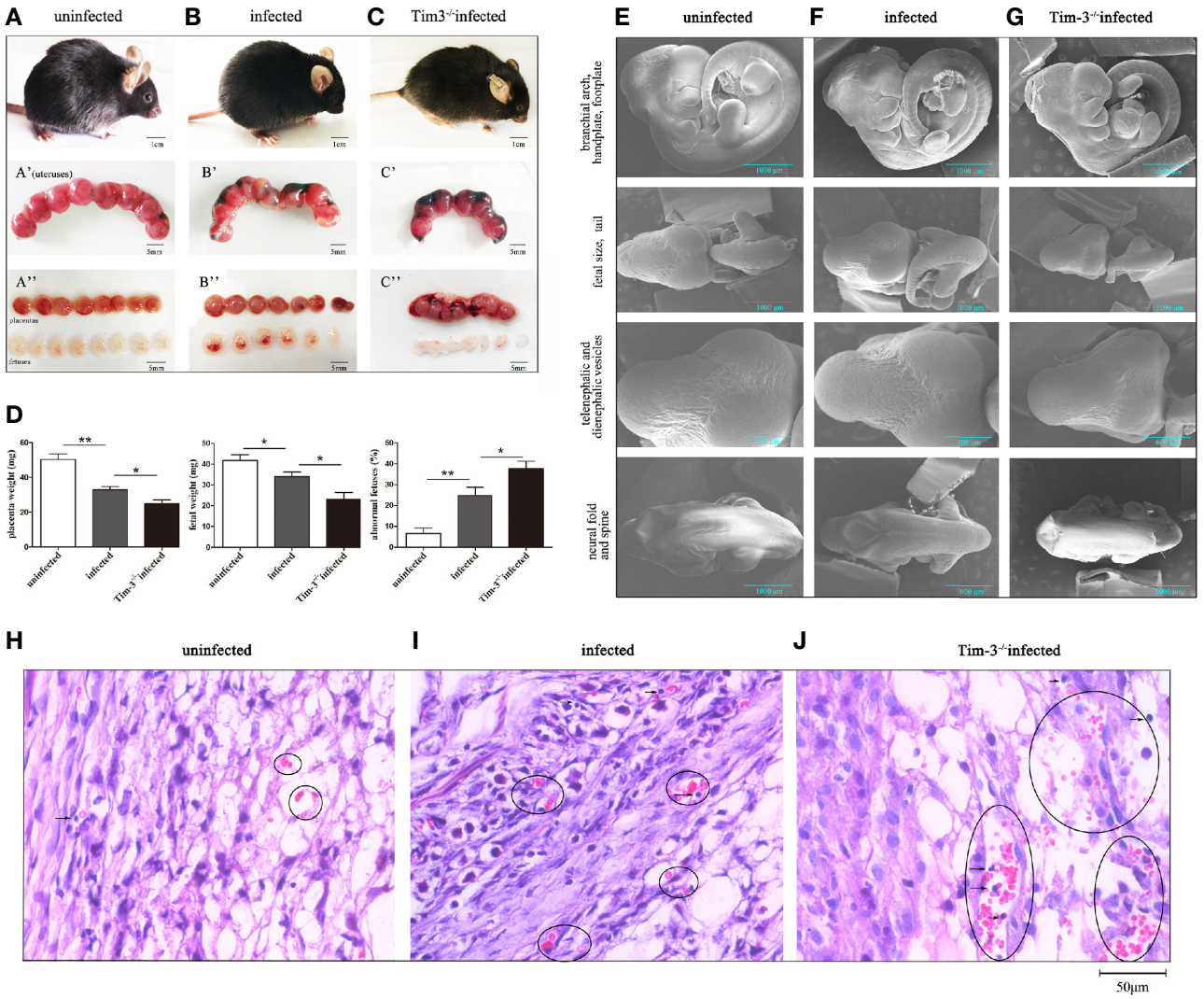

FIGURE 1 | The impact of Tim-3 on adverse pregnancy outcomes caused by *T. gondii* infection in mice. **(A)** Uninfected pregnant mice were in good condition, the placentas and fetuses developed normally. **(B)** *T. gondii* infected pregnant mice exhibited spiritual malaise, with inflammatory hyperemia of placentas and fetuses. **(C)** *T. gondii* infected Tim-3$^{-/-}$ pregnant mice had sluggish responses, their fetuses were smaller and shapeless. Scale bar of A, B, C was 1 cm. Scale bar of A', A'', B', B'', C' and C'' were 5 mm. **(D)** The weights of placentas and fetuses, and fetal abnormalities rates were calculated in uninfected, infected, Tim-3$^{-/-}$ infected mice. The abnormal fetuses included stillbirths and resorption sites. The rates of abnormal fetus were calculated as the ratio of stillbirths and resorption sites to the total number of implantation sites. (Data are presented as means ± SD. N=10 mice per group, $^{*}p < 0.05$, $^{**}p < 0.01$, by the unpaired *t*-test). **(E)** Scanning electron microscopy images of fetuses from uninfected mice, the fetuses were healthy and well developed. **(F)** Fetuses of infected mice exhibited delayed hand-plates and foot-plates development. **(G)** Fetuses of infected Tim-3$^{-/-}$ mice displayed obvious intrauterine growth restriction in head, body size, hand-plates and foot-plates development. Scale bar, 1000μm and 600μm. **(H-J)** Hematoxylin and eosin (H & E) staining of uninfected, infected and Tim-3$^{-/-}$ infected mouse placentas. Obvious hemorrhaging and lymphocytes infiltration were showed by black circles. Scale bar, 50μm.

even worse, which was evidently indicated by their significantly smaller bodies, rarely formed paddle-shaped handplate and footplate, as well as smaller size of head compared with the findings in infected WT mice (**Figures 1F, G**). Paraffin embedded sections showed increased lymphocyte infiltration of the WT group placenta caused by *T. gondii* infection, and more severe damages in placentas of infected Tim-3$^{-/-}$ group were found than WT infected mice, as evidenced by obvious hemorrhage and lymphocyte infiltration (**Figures 1H–J**). We found no differences in pregnancy outcomes between uninfected Tim-3$^{-/-}$ mice and WT mice.

Tim-3 Expression on dNK Cells Decreased After *T. gondii* Infection

To investigate the role of Tim-3 expression during *T. gondii* infection, Tim-3 expression levels on dNK cells in decidual lymphocytes and murine decidual lymphocytes were analyzed by flow cytometry, western blot, and confocal laser-

scanning microscope. The results demonstrated that Tim-3 expression levels on dNK cells were significantly decreased both in human dNK cells (**Figures 2A, B, E–G**) and in mice dNK cells (**Figures 2C, D**) after *T. gondii* infection compared with the uninfected group. In addition, the downstream molecules modulated by Tim-3 were detected through western blot analysis. Results showed that PI3K and pAKT were all increased with *T. gondii* infection compared with the uninfected group, and were further up-regulated in infected Tim-3-neutralized human dNK cells (**Figure 2H**), which confirmed the PI3K and pAKT as downstream molecules regulated by Tim-3 (**Figures 2H-J**).

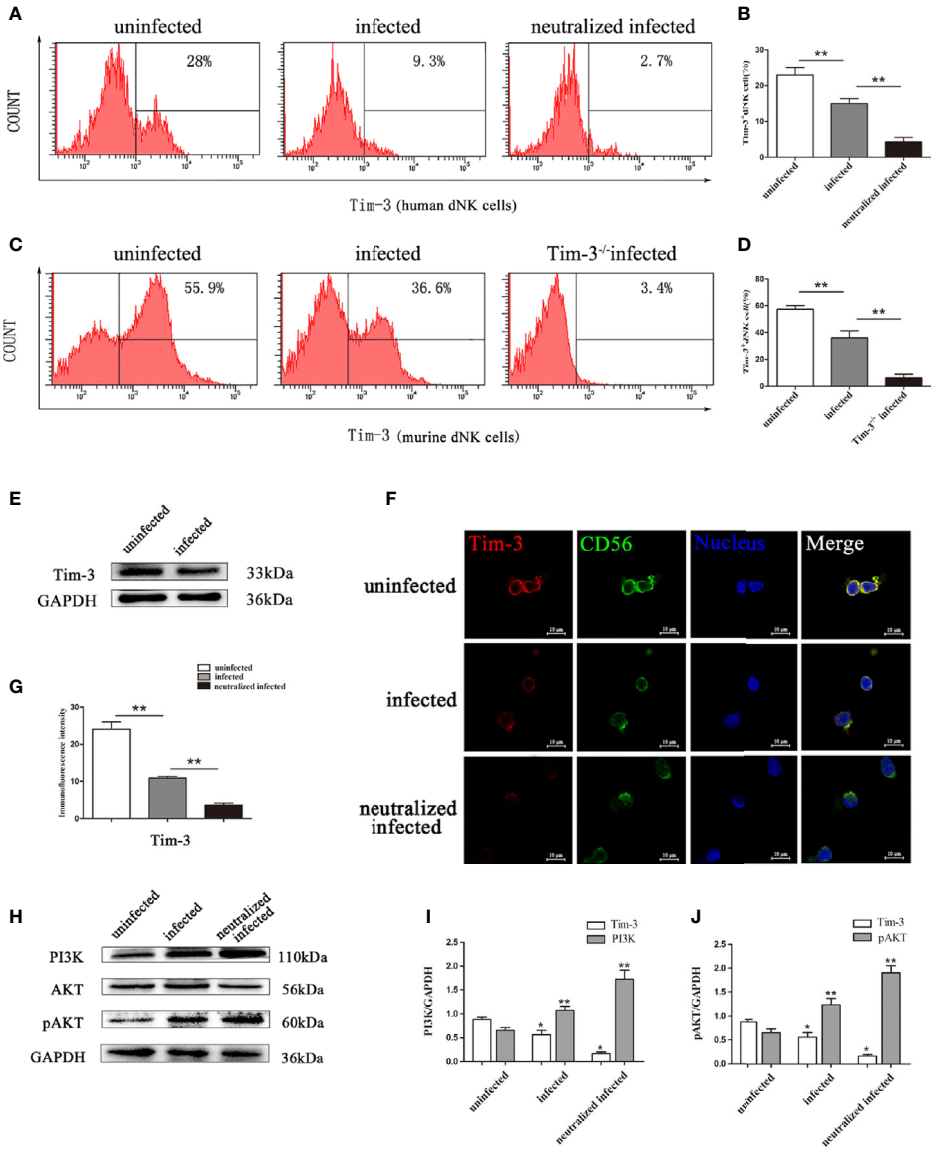

FIGURE 2 | Changes of Tim-3 expressions on dNK cells due to *T. gondii* infection. **(A)** Expression levels of Tim-3 on human $CD3^-CD56^{bright}$ dNK cells in uninfected, infected, and anti-Tim-3 neutralized infected groups using flow cytometry. **(B)** Histograms analysis of Tim-3 expression changes on human dNK cells in the three groups. (Means ± SD; N=6 human samples per group, $^*p < 0.05$, $^{**}p < 0.01$, by unpaired *t*-test). **(C)** Expression of Tim-3 on mice $CD3^-CD122^+$ dNK cells in uninfected, infected, and Tim-$3^{-/-}$ mice infected groups were detected by flow cytometry. **(D)** Histograms analysis of Tim-3 expression changes on mice dNK cells in uninfected, infected, and Tim-$3^{-/-}$ mice infected groups. (Means ± SD, N=8 mice per group, $^*p < 0.05$, $^{**}p < 0.01$, by unpaired *t*-test). **(E)** Western blot analysis of Tim-3 expression in uninfected human dNK cells and infected groups. **(F)** Immunofluorescent photographs of Tim-3 (red), CD56 (green) expression on the purified human $CD3^-CD56^{bright}$ dNK cells from uninfected, infected, and Tim-3-neutralized and infected groups. The 4 ', 6-diamidino-2-phenylindole were used to stain nuclei (blue). Scale bar, 10μm. **(G)** Histograms analysis of Tim-3 expressions changes on human dNK cells by immunofluorescent intensity among three groups. **(H)** Representative depictions of Tim-3 downstream molecules PI3K, AKT and pAKT expressions in uninfected, infected, and Tim-3-neutralized infected human dNK cells by western blot. **(I, J)** The histograms analysis of Tim-3, PI3K and pAKT among three groups. (Means ± SD; N=6 human samples per group, $^*p < 0.05$, $^{**}p < 0.01$, by unpaired *t*-test).

Down-Regulation of Tim-3 Expression by *T. gondii* Infection Was Associated With the Balance Between Inhibitory and Activating Receptors on dNK Cells

We then detected the dNK cells receptors both *in vitro* and *in vivo*. Results found that up-regulation of inhibitory receptor KIR2DL4 (*in vitro*, **Figures 3A, B, F**), NKG2A (*in vivo*, **Figures 3H, J**) and activating receptor NKG2D (*in vitro*, **Figures 3C, D, G**; *in vivo*, **Figures 3I, K**), with high ratios of NKG2D/KIR2DL4 and NKG2D/NKG2A on dNK cells in the *T. gondii* infected group (**Figures 3E, L**). Besides, anti-Tim-3 neutralized infected human dNK cells and *T. gondii* infected Tim-3$^{-/-}$ pregnant mice were used to further explore the effect of Tim-3 down-regulation on the balance between inhibitory and activating receptors. In the Tim-3 neutralized infected group, NKG2D expression was up-regulated and the imbalance of NKG2D/KIR2DL4 on dNK cells was further aggravated compared with infected cells (**Figures 3A-G**). Moreover, the expression of inhibitory receptor NKG2A and activating receptor NKG2D on murine dNK cells increased in infected Tim-3$^{-/-}$ mice; however, the ratio of NKG2D/NKG2A was significantly higher than that of WT infected mice (**Figures 3H-L**).

Tim-3 Down-Regulation by *T. gondii* Infection Altered the GranzymeA, GranzymeB, and Perforin Expressions of dNK Cells

Granules production was analyzed in the three groups to explore the impact of Tim-3 in modulating dNK cells function. *In vitro*, the GranzymeA, GranzymeB and Perforin expressions of dNK cells were analyzed by flow cytometry, western blot, and immunofluorescence respectively (**Figures 4A-K**, **5A-F**). The data revealed that the expressions of GranzymeA, GranzymeB and Perforin in CD3$^-$CD56$^+$ NK cells were increased markedly with *T. gondii* infection compared to the uninfected group (**Figures 4A-K**, **5A-F**). Interestingly, the GranzymeA, GranzymeB, and Perforin production of human dNK in Tim-3 neutralized group were all distinctly higher than those of infected dNK cells (**Figures 4A-K**, **5A-F**). In accordance with the result *in vitro*, the expression levels of GranzymeA, GranzymeB and Perforin in mice dNK cells increased after *T. gondii* infection, and further increased in infected Tim-3$^{-/-}$ mice (**Figures 5G-L**).

Down-Regulation of Tim-3 by *T. gondii* Infection Affected IL-10 and IFN-γ Production in dNK Cells

In the present study, flow cytometry and western blot were used to elucidate the relationship between Tim-3 expression and cytokine production of dNK cells. Results showed that the IL-10 and IFN-γ secretion increased in infected Tim-3-neutralized human dNK cells compared with that of the infected group (**Figures 6A, B, G, J, K**). While the ratio of IFN-γ/IL-10 were higher in infected Tim-3-neutralized cells than that of infected group (**Figure 6C**). *In vivo*, IL-10 and IFN-γ expression of dNK cells were both decreased in Tim-3$^{-/-}$ infected mice (**Figures 6D, E**) but IFN-γ/IL-10 ratios were higher than that of infected WT mice (**Figure 6F**).

To investigate how the mechanism of Tim-3 regulates the expression of IL-10 and IFN-γ in dNK cells, the expression of key molecules of JAK-STAT signaling pathway were examined by western blot. The pSTAT3 expression increased following *T. gondii* infection and were further up-regulated in infected Tim-3-neutralized human dNK cells. This result suggested that enhanced pSTAT3 may take part in the change of IL-10 induced by down-regulated Tim-3 after *T. gondii* infection (**Figure 6G, I, J**). In addition, the pSTAT1 expression related to IFN-γ synthesis was elevated with *T. gondii* infection and further increased in infected Tim-3-neutralized human dNK cells (**Figure 6H, K**).

DISCUSSION

As one of the common causative agents of prenatal infections during pregnancy, *T. gondii* infection evokes a strong immune response in maternal-fetal interface and leads to adverse pregnancy outcomes (Wong and Remington, 1994; Li et al., 2017b). Our previous studies have reported that the dysfunctions of decidual immune cells such as dNK cells, macrophages, Tregs, and DCs in response to *T. gondii* infection result in abnormal pregnancy outcomes (Zhang et al., 2012a; Li et al., 2017b; Xu et al., 2017). Our results also demonstrated that *T. gondii* infection induces an imbalance of dNK receptors and abnormal cytokines secretion, which excessively activated dNK cells and further led to adverse outcomes of pregnancy (Liu et al., 2013; Xu et al., 2013). However, the detailed mechanism underlying *T. gondii* infection-induced dNK dysfunction is still unclear. The newly defined immunosuppressive molecule Tim-3 has been found to be consistently expressed on dNK cells and reportedly modulates the function of dNK cells (Li et al., 2016; Li et al., 2017a). Emerging evidence has demonstrated that Tim-3 expression plays an important role in sustaining normal pregnancy (Zhan et al., 2018). Researchers have found that the changes in Tim-3 expression on dNK cells result in pregnancy complications such as preeclampsia and miscarriage (Meggyes et al., 2015; Sun et al., 2016; Li et al., 2017a). However, the effect of *T. gondii* infection on Tim-3 expression of dNK cells requires further investigation. Interestingly, the results of the present study showed that the Tim-3 expression on dNK cells was significantly decreased after *T. gondii* infection. To explore the mechanism of Tim-3 down-regulation on dNK cells dysfunction in abnormal pregnancy caused by *T. gondii* infection, Tim-3$^{-/-}$ infected pregnant mice models were successfully established. The results revealed that Tim-3$^{-/-}$ infected pregnant mice exhibited far worse pregnancy outcomes compared with infected WT mice. This finding suggested that Tim-3 expression may play an important role in abnormal pregnancy outcomes involving *T. gondii* infection. In the present study, *in vitro* and *in vivo* experiments were performed to further uncover the mechanism of Tim-3 in modulating dNK cells function during *T. gondii* infection. Previous studies have proved that the function of dNK cells was precisely regulated by the balance of activating and inhibitory receptors (Moretta et al., 2000b). KIR2DL4 and NKG2A are both inhibitory receptors and

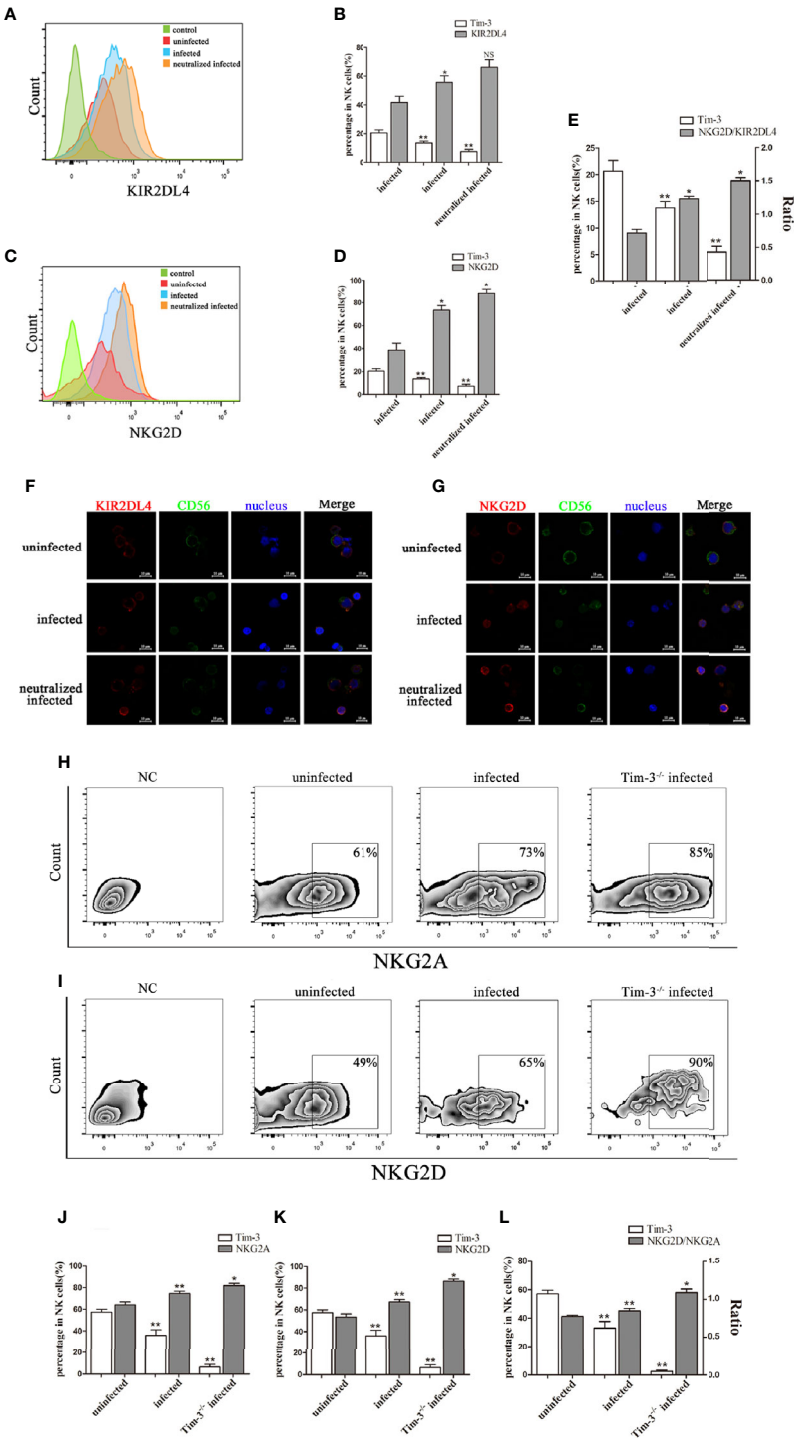

FIGURE 3 | Reduction of Tim-3 expression by *T. gondii* infection is associated with the imbalance of inhibitory and activating receptors on dNK cells. **(A, C)** Flow cytometry analysis revealed that expression of Tim-3, KIR2DL4, NKG2D on human dNK cells were altered in uninfected, infected, and anti-Tim-3 neutralized infected cells from patients who underwent induced abortion. **(B, D, E)** Statistical analysis of Tim-3, KIR2DL4 and NKG2D expression and ratios of NKG2D/KIR2DL4 on human dNK cells among three groups. (Means ± SD; N=6 human samples per group, $*p < 0.05$, $**p < 0.01$, by unpaired *t*-test. NS, Not Statistically Significant) **(F, G)** Representative immunofluorescent photographs of KIR2DL4 (red), CD56 (green) and NKG2D (red) expression in uninfected, infected, and anti-Tim-3 neutralized infected human dNK cells. Nuclei (blue) were stained by 4', 6-diamidino-2-phenylindole. Representative expression changes of inhibitory receptor NKG2A. **(H, J)** and activating receptor NKG2D **(I, K)** on mice dNK cells from uninfected, infected and Tim-3$^{-/-}$ infected mice. **(L)** Histogram analysis of Tim-3 and ratios of NKG2D/NKG2A in three groups. (Means ± SD; N=8 mice per group, *in vivo*, $*p < 0.05$, $**p < 0.01$, by unpaired *t*-test).

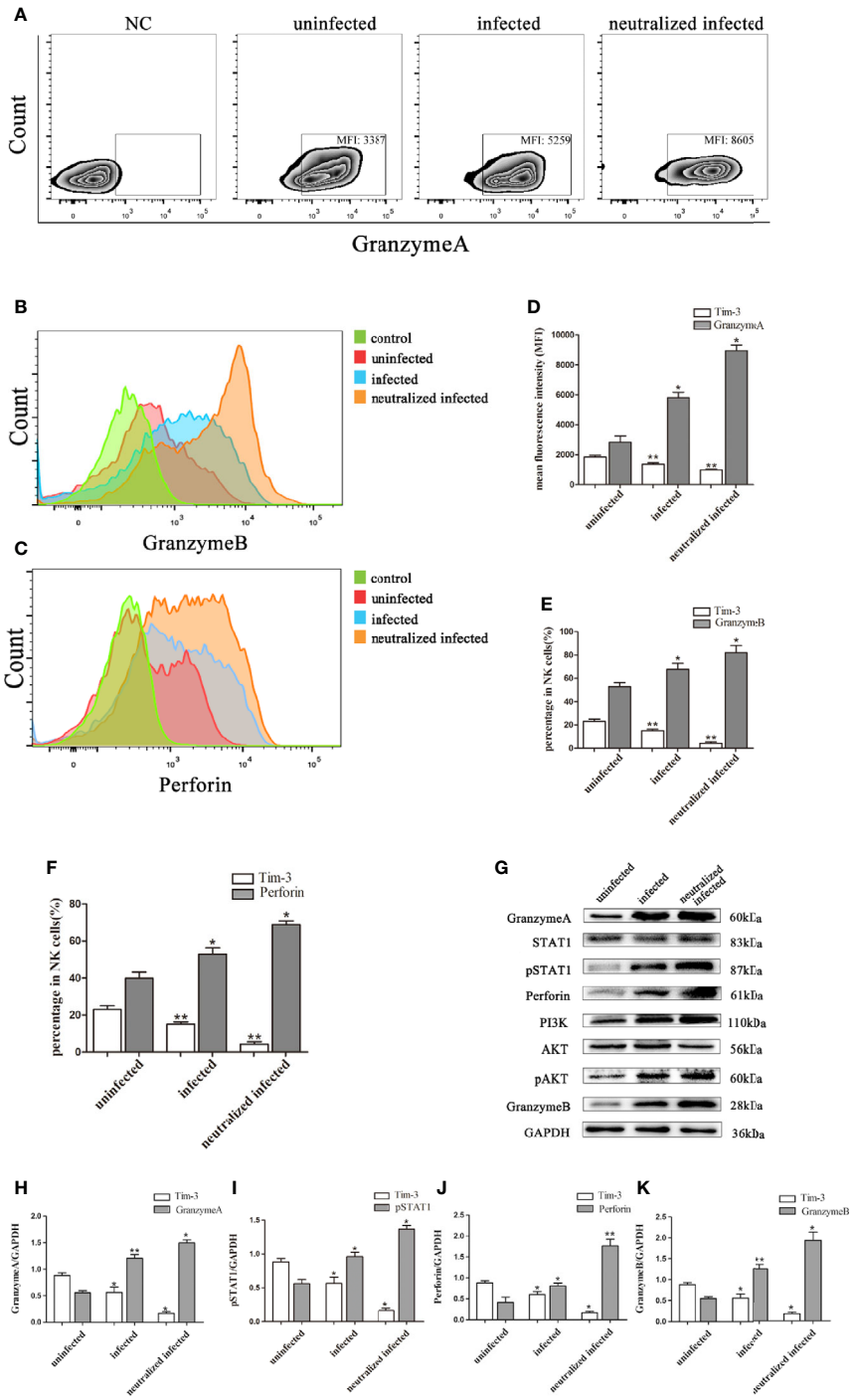

FIGURE 4 | Tim-3 down-regulation by *T. gondii* infection altered the GranzymeA, GranzymeB and Perforin expressions of human dNK cells. **(A-F)** Representative flow cytometry and histograms analysis of GranzymeA **(A, D)**, GranzymeB **(B, E)** and Perforin **(C, F)** levels of human dNK cells in the uninfected, infected, and neutralized infected groups. (Means ± SD; N=6 human samples per group, $^{*}p < 0.05$, $^{**}p < 0.01$, by unpaired *t*-test). **(G)** Western blot analysis of signaling pathway of Perforin and GranzymeB. Since GranzymeB is also modulated by PI3K-AKT signaling pathway and the experiments were performed at the same time, the data of PI3K, AKT and pAKT in **Figure 4G** were reused from the data of **Figure 2H**. **(H-K)** Histograms analysis of GranzymeA, pSTAT1, Perforin and GranzymeB in uninfected, infected, and anti-Tim-3 neutralized infected groups. (Means ± SD; N=6 human samples per group, $^{*}p < 0.05$, $^{**}p < 0.01$, by unpaired *t*-test).

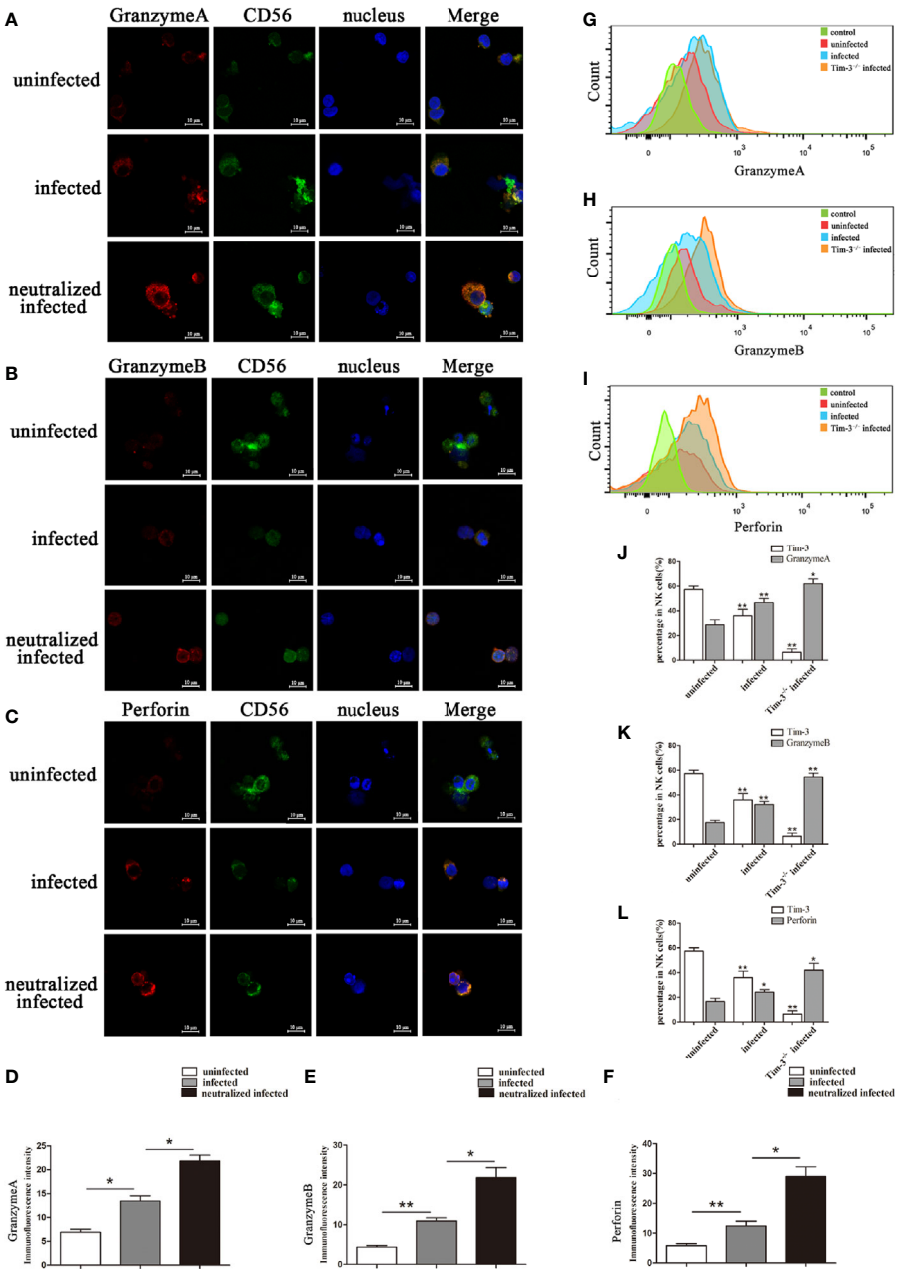

FIGURE 5 | Representative confocal micrographs of GranzymeA, GranzymeB and Perforin in human dNK cells and flow cytometry analysis of mice dNK cells. **(A-F)** Representative immunofluorescent photographs and immunofluorescent intensity analysis of GranzymeA (red), CD56 (green), GranzymeB (red) and Perforin (red) expression in uninfected, infected, and anti-Tim-3 neutralized infected huamn dNK cells. Nuclei were blue and stained using 4', 6-diamidino-2-phenylindole. Scale bar, 10μm. (Means ± SD; N=6 human samples per group, $*p < 0.05$, $**p < 0.01$, by unpaired *t*-test). **(G-L)** In uninfected, infected and Tim-3$^{-/-}$ infected mice, dNK cells expression of GranzymeA **(G, J)**, GranzymeB **(H, K)** and Perforin **(I, L)** levels were analyzed by flow cytometry and compared by unpaired *t*-test. (Means ± SD; N=8 mice per group, $*p < 0.05$, $**p < 0.01$, by unpaired *t*-test).

sustain the tolerance function of dNK cells in pregnancy, by antagonizing the activating function of NKG2D (Rouas-Freiss et al., 1997; Moretta et al., 2000a; Moretta et al., 2000b). Recently, research has demonstrated that the over-expression of NKG2D elicited an enhanced local cytotoxic response by NK cells which was associated with preeclampsia (Liu et al., 2017; Vinnars et al., 2018). In our previous research, we observed that *T. gondii* infection disturbed the balance of NKG2D and KIR2DL4 (NKG2A *in vivo*) on dNK cells, which is an important aspect of dNK cells dysfunction in *T. gondii*-mediated adverse pregnancy (Liu et al., 2013; Xu et al., 2013). However, the specific mechanism of the imbalanced receptor expression has

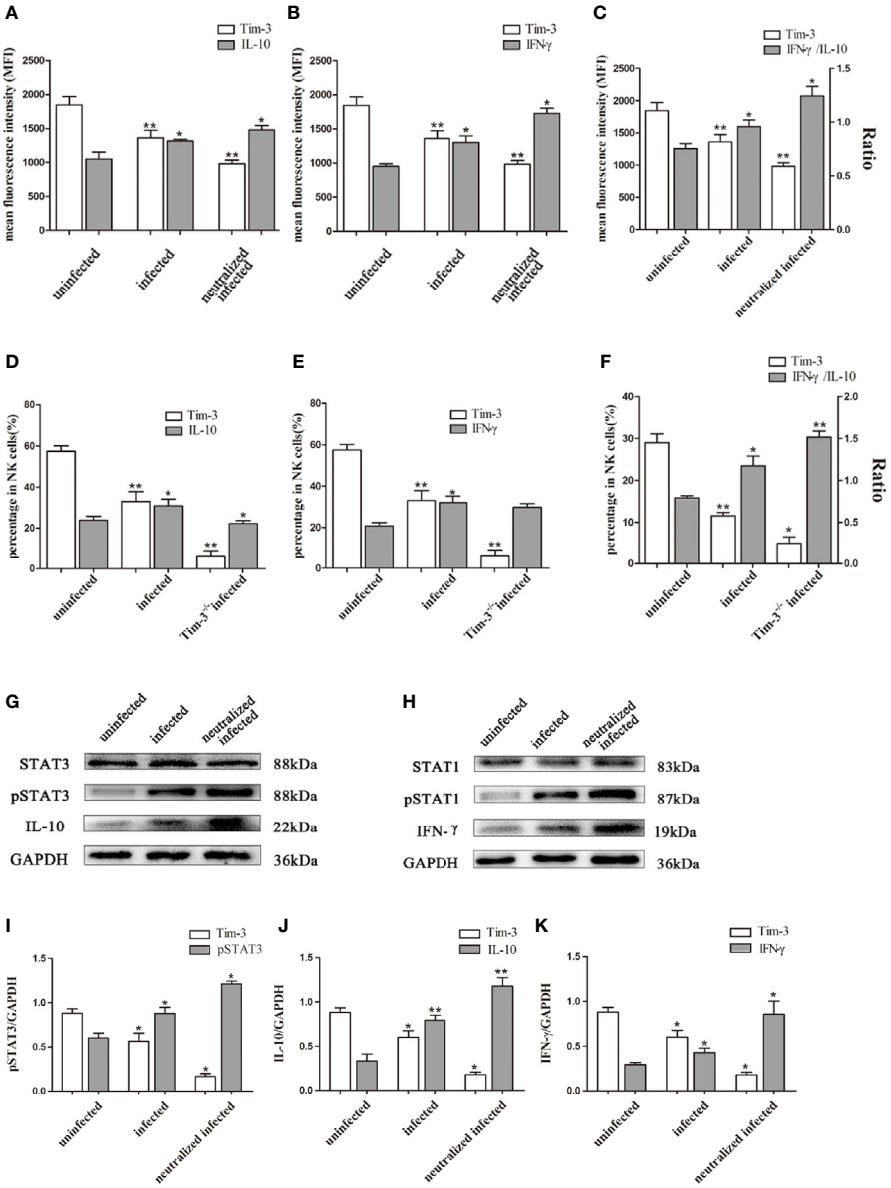

FIGURE 6 | Down-regulation of Tim-3 by *T. gondii* infection affected IL-10 and IFN-γ secretion in dNK cells. **(A-C)** The human dNK cells expression levels of Tim-3, IL-10 **(A)**, IFN-γ **(B)** and IFN-γ/IL-10 ratios **(C)** among uninfected, infected, and anti-Tim-3 neutralized infected groups were detected by flow cytometry. **(D-F)** Tim-3, IL-10 **(D)**, IFN-γ **(E)** expression changes and ratios of IFN-γ/IL-10 **(F)** in uninfected, infected, and Tim-3$^{-/-}$ infected mice dNK cells were showed by flow cytometry. (Means ± SD; N=6 human samples per group, *in vitro*; N=8 mice per group, *in vivo*, $^{*}p < 0.05$, $^{**}p < 0.01$, by unpaired *t*-test). **(G)** STAT3 and pSTAT3 involved in the regulation of IL-10 secretion were detected by western blot among uninfected, infected, and anti-Tim-3 neutralized infected groups. **(H)** STAT1 and pSTAT1 which were associated with IFN-γ expression in dNK cells were detected by western blot in uninfected, infected, and anti-Tim-3 neutralized infected groups. The data of STAT1 and pSTAT1 in **Figure 5H** reused the data in **Figure 4G** for Perforin and IFN-γshares the same upstream molecules STAT1 and pSTAT1, and the detection was conducted simultaneously. **(I-K)** Histograms analysis of pSTAT3, IL-10 and IFN-γ in uninfected, infected, and anti-Tim-3 neutralized infected groups. (Means ± SD; N=6 human samples per group, $^{*}p < 0.05$, $^{**}p < 0.01$, by unpaired *t*-test).

not yet been investigated. In this study, human dNK cells were purified and cultured with *T. gondii*, and Tim-3 was blocked with Tim-3 neutralizing antibody. The result indicated that NKG2D/KIR2DL4 ratios of dNK cells were considerably higher in Tim-3-neutralized group following *T. gondii* infection than that of the infected group. This demonstrated that the down-regulation of Tim-3 expression on dNK cells after *T. gondii* infection could result in an imbalance of inhibitory and activating receptors. In accordance with the results *in vitro*, the present study declared that the NKG2D/NKG2A ratio of dNK cells was increased after *T. gondii* infection and further enhanced in Tim-3$^{-/-}$ infected mice. Considering the different abnormal pregnancy outcomes between Tim-3$^{-/-}$ infected mice and WT infected mice, we could deduce that the down-regulation of Tim-3 expression on dNK

cells after *T. gondii* infection caused an imbalance between inhibitory and activating receptors, thereby contributing to abnormal pregnancy outcomes.

The cytotoxic molecules GranzymeA, GranzymeB and Perforin are constitutively produced by NK cells (Trapani et al., 1998; Shirshev et al., 2017; Gulic et al., 2018). Researchers have found that dysfunctional dNK cells release excessive GranzymeB and Perforin which induce pregnancy failure (Trapani et al., 1998; Gulic et al., 2018). And our precious study revealed that *T. gondii* infection could up-regulate cytotoxic production such as GranzymeA, GranzymeB and Perforin at maternal-fetal interface (Xu et al., 2017; Zhang et al., 2018). In this study, the increased expression of Granzymes and Perforin in dNK cells were demonstrated after *T. gondii* infection *in vivo* and *in vitro*. Furthermore, results showed significantly higher expression of GranzymeA, GranzymeB, and Perforin in infected Tim-3-neutralized dNK cells and Tim-$3^{-/-}$ infected mice than that of infected dNK cells, which demonstrated that the reduction of Tim-3 on dNK cells further enhanced GranzymeA, GranzymeB, and Perforin production. According to the severe pregnancy outcomes of infected Tim-$3^{-/-}$ mice, it was concluded that decreased Tim-3 on dNK cells caused by *T. gondii* infection led to excessive cytotoxic production by dNK cells, which participate in the development of pregnancy failure.

Besides, dNK cells can also secrete many cytokines such as IL-10 and IFN-γ that participate in maternal-fetal tolerance (Trundley and Moffett, 2004). Dysregulation of IL-10 has been widely confirmed in pregnancy complications such as preeclampsia, recurrent spontaneous abortion, and preterm birth (Murphy et al., 2005; Yamada et al., 2005; Makris et al., 2006). It is known that IL-10 in dNK cells plays a key role in sustaining maternal-fetal tolerance function of dDCs (Miyazaki et al., 2003). Coversely, excessive IFN-γ secretion of dNK could provoke pregnancy failure by inducing aberrant recruitment of $CD49b^{+}$ NK cells (Li et al., 2014). Additionally, emerging evidence has proven that over-expression of IFN-γ affects immune-regulation in maternal-fetal interface and leads to recurrent pregnancy loss and implantation failure (Wilczyński et al., 2003). Our previous study has revealed that the *T. gondii* infection induced excessive secretion of IFN-γ by dNK cells (Zhang et al., 2015). And we found that the IFN-γ/IL-10 ratios in placenta supernatant from *T. gondii* infected mice were higher than normal pregnant mice (Zhang et al., 2012b). In current research, the IFN-γ/IL-10 ratios in dNK cell were obviously increased after *T. gondii* infection both *in vivo* and *in vitro*, and further up-regulated in infected Tim-3-neutralized dNK and infected Tim-$3^{-/-}$ mice. This suggested that the decrease of Tim-3 on dNK cells could up-regulate ratios of IFN-γ/IL-10 and impact the tolerance function of dNK cells. On the basis of these findings, *T. gondii* infection-induced down-regulation of Tim-3 could result in dysfunction of dNK cells due to the up-regulation of IFN-γ/IL-10 ratio, and finally contribute to adverse pregnancy outcomes.

However, the detailed mechanism of Tim-3 modulating the cytokines (IFN-γ, IL-10) synthesis, Perforin, and GranzymeB production had not been confirmed during *T. gondii* infection. AKT in NK cells has been identified as a downstream molecular modulated by Tim-3 (Li et al., 2017a). Also, AKT is proved as a key molecular in PI3K-AKT-mTOR pathway modulating the GranzymeB expression and IFN-γ production by NK cells (Nandagopal et al., 2014; Li et al., 2017a). To further explore the pathways *via* which Tim-3 regulates cytokines secretion and cytotoxic production of dNK cells, the AKT, pAKT, PI3K, GranzymeB, IFN-γ expression in infected human dNK cells and in Tim-3 neutralized human dNK cells were analyzed with western blot. The results demonstrated that *T. gondii* infection increased the expression of PI3K and pAKT, leading to significant up-regulation of GranzymeB and IFN-γ expression, and the PI3K and pAKT being further up-regulated with significantly higher expression of GranzymeB and IFN-γ in Tim-3 neutralized infected dNK cells. Based on these data, it was revealed that *T. gondii*-mediated Tim-3 reduction could lead to activation of PI3K-AKT signaling pathway and further enhanced the production of GranzymeB and IFN-γ in dNK cells. In addition, pSTAT1 is also considered an important regulator of IFN-γ and Perforin production by NK cells (Miyagi et al., 2007). The phophorylation of STAT1 could up-regulate the Perforin and IFN-γ production of NK cells (Vargas-Hernández et al., 2018). Besides, pSTAT3 is considered an important regulator during the synthesis of IL-10 (Braunschweig et al., 2011). Our western blot results showed that the expression levels of pSTAT1 and pSTAT3 were all up-regulated in induced *T. gondii* infection and were even higher in infected Tim-3 neutralized dNK cells. Combining the western blot analysis of IFN-γ, Perforin, IL-10, pSTAT1, and pSTAT3, we confirmed that the inflammatory effector (IFN-γ, Perforin) and anti-inflammatory factor IL-10 were separately correlated with phosphorylation level of STAT1 and pSTAT3. Many effector proteins are injected into host cells during *T. gondii* infection and modulate cell functions (Koshy et al., 2012). *T. gondii* was found to activate the host STAT (signal transducer and activator of transcription) signaling pathway by enhancing phosphorylation level. And our research confirmed that phosphorylation of STAT1 and STAT3 of dNK cells was increased after *T. gondii* infection. Many studies proved that parasite rhoptry protein ROP16 participated in modulating STAT3 and STAT6 phosphorylation of infected host cells (Yamamoto et al., 2009; Butcher et al., 2011; Hunter and Sibley, 2012). However, we found that pSTAT1 and pSTAT3 expression was further increased in infected Tim-3 neutralized dNK cells, which suggests that Tim-3 as an important modulator of pSTAT1 and pSTAT3. This result indicated that the reduction of Tim-3 caused by *T. gondii* infection could enhance pSTAT1 and pSTAT3 expression, then leading to changes in cytokines (IL-10, IFN-γ) secretion and Perforin production. Upon invasion, *T. gondii* parasites down-regulated the Tim-3 expression of dNK cells, and the reduction of Tim-3 further modulating the cytokines and granules production by activating the PI3K-AKT and JAK-STAT signaling pathway.

In summary, *T. gondii* infection-mediated Tim-3 reduction resulted in the imbalance of dNK cells receptors, cytotoxic

granules overproduction, and abnormal cytokine secretion through activating PI3K-AKT and JAK-STAT signaling pathways, leading to the dysfunction of dNK cells which participated in the development of abnormal pregnancy outcomes. The present investigation also offers a new understanding about the immune molecular mechanisms underlying aberrant pregnancy outcomes caused by *T. gondii* infection.

DATA AVAILABILITY STATEMENT

The raw data supporting the conclusions of this article will be made available by the authors, without undue reservation.

ETHICS STATEMENT

The studies involving human participants were reviewed and approved by the Ethics Committee of Binzhou Medical University (Shandong, China) for sample collection from women undergoing voluntary termination of gestation. The patients/participants provided their written informed consent to participate in this study. The animal study was reviewed and approved by the Ethics Committee of Binzhou Medical University (Shandong, China). This study was conducted in strict accordance with the requirements of the Guide for the Care and Use of Laboratory Animals of Binzhou Medical University. All experimental procedures were performed under sodium pentobarbital anesthesia to minimize the suffering of laboratory animals.

AUTHOR CONTRIBUTIONS

TL, LC, XX, and XH designed the experiments. LC, LR, and CY contributed to sample collection. TL, XL, HZ, and YJ analyzed the data. TL, LC, XX, and XH wrote the manuscript. TL, LC, XX, and XH edited the manuscript. XH was the corresponding author. All authors contributed to the article and approved the submitted version.

FUNDING

This work was supported by funds from the National Natural Science Foundation of China (NO. 81871680, NO. 81702029, and NO. 81672049) and the Taishan Scholar Foundation of Shandong province (NO. ts201712066). The content of this manuscript in part has been presented at the 17th International Congress of Immunology.

REFERENCES

Arora, N., Sadovsky, Y., Dermody, T. S., and Coyne, C. B. (2017). Microbial vertical transmission during human pregnancy. *Cell Host Microbe* 21, 561–567. doi: 10.1016/j.chom.2017.04.007

Braunschweig, A., Poehlmann, T. G., Busch, S., Schleussner, E., and Markert, U. R. (2011). Signal transducer and activator of transcription 3 (STAT3) and Suppressor of Cytokine Signaling (SOCS3) balance controls cytotoxicity and IL-10 expression in decidual-like natural killer cell line NK-92. *Am. J. Reprod. Immunol.* 66, 329–335. doi: 10.1111/j.1600-0897.2011.00989.x

Butcher, B. A., Fox, B. A., Rommereim, L. M., Kim, S. G., Maurer, K. J., Yarovinsky, F., et al. (2011). *Toxoplasma gondii* rhoptry kinase ROP16 activates STAT3 and STAT6 resulting in cytokine inhibition and arginase-1-dependent growth control. *PloS Pathog.* 7, e1002236. doi: 10.1371/journal.ppat.1002236

El, C. H., Tabiasco, J., Berrebi, A., Parant, O., Aguerre-Girr, M., Piccinni, M. P., et al. (2009). Effector functions of human decidual NK cells in healthy early pregnancy are dependent on the specific engagement of natural cytotoxicity receptors. *J. Reprod. Immunol.* 82 (2), 142–147. doi: 10.1016/j.jri.2009.06.123

Erlebacher, A. (2013). Immunology of the maternal-fetal interface. *Annu. Rev. Immunol.* 31, 387–411. doi: 10.1146/annurev-immunol-032712-100003

Ferreira, L. M. R., Meissner, T. B., Tilburgs, T., and Strominger, J. L. (2017). HLA-G: At the interface of maternal-fetal tolerance. *Trends Immunol.* 38 (4), 272–286. doi: 10.1016/j.it.2017.01.009

Fu, B., Zhou, Y., Ni, X., Tong, X., Xu, X., and Dong, Z. (2017). Natural killer cells promote fetal development through the secretion of growth-promoting factors. *Immunity* 47, 1100–1113. doi: 10.1016/j.immuni.2017.11.018

Gulic, T., Laskarin, G., Dominovic, M., Glavan Gacanin, L., Babarović, E., and Rubesa, Z. (2018). Granulysin-mediated apoptosis of trophoblasts in blighted ovum and missed abortion. *Am. J. Reprod. Immunol.* 80, e12978. doi: 10.1111/aji.12978

Hunter, C. A., and Sibley, L. D. (2012). Modulation of innate immunity by *Toxoplasma gondii* virulence effectors. *Nat. Rev. Microbiol.* 10, 766–778. doi: 10.1038/nrmicro2858

Koopman, L. A., Kopcow, H. D., Rybalov, B., Boyson, J. E., Orange, J. S., and Schatz, F. (2003). Human decidual natural killer cells are a unique NK cell subset with immunomodulatory potential. *J. Exp. Med.* 98, 1201–1212. doi: 10.1084/jem.20030305

Koshy, A. A., Dietrich, H. K., Christian, D. A., Melehani, J. H., Shastri, A. J., Hunter, C. A., et al. (2012). Toxoplasma co-opts host cells it does not invade. *PloS Pathog.* 8, e1002825. doi: 10.1371/journal.ppat.100282

Li, Z. Y., Chao, H. H., Liu, H. Y., Song, Z. H., Li, L. L., and Zhang, Y. J. (2014). IFN-γ induces aberrant CD49b^{+}NK cell recruitment through regulating CX3CL1: a novel mechanism by which IFN-γ provokes pregnancy failure. *Cell Death Dis.* 5, e1512. doi: 10.1038/cddis.2014.470

Li, Y. H., Zhou, W. H., Tao, Y., Wang, S. C., Jiang, Y. L., and Zhang, D. (2016). The Galectin-9/Tim-3 pathway is involved in the regulation of NK cell function at the maternal-fetal interface in early pregnancy. *Cell Mol. Immunol.* 13, 73–81. doi: 10.1038/cmi.2014.126

Li, Y., Zhang, J., Zhang, D., Hong, X., Tao, Y., and Wang, S. (2017a). Tim-3 signaling in peripheral NK cells promotes maternal-fetal immune tolerance and alleviates pregnancy loss. *Sci. Signal* 10, (498). doi: 10.1126/scisignal.aah4323

Li, Z., Zhao, M., Li, T., Zheng, J., Liu, X., and Jiang, Y. (2017b). Decidual macrophage functional polarization during abnormal pregnancy due to *Toxoplasma gondii* : Role for LILRB4. *Front. Immunol.* 8:1013. doi: 10.3389/fimmu.2017.01013

Liu, Y., Zhang, L., Gao, M., Zhang, F., Xu, X., Liu, X., et al. (2013). Changes of Inhibitory Receptors on NK-92 cells and HLA-G on BeWo cells with *Toxoplasma gondii* infection. *Inflammation* 36, 1440–1447. doi: 10.1007/s10753-013-9684-1

Liu, X., Zhao, M., Yang, X., Han, M., Xu, X., and Jiang, Y. (2014). *Toxoplasma gondii* infection of decidual CD1c^{+} dendritic cells enhances cytotoxicity of decidual natural killer cells. *Inflammation* 37 (4), 1261–1270. doi: 10.1007/s10753-014-9853-x

Liu, J., Song, G., Lin, X., Pang, X., and Meng, T. (2017). Upregulated unique long 16 binding protein 1 detected in preeclamptic placenta affects human extravillous trophoblast cell line (HTR-8/SVneo) invasion by modulating the

function of uterine natural killer cells. *Exp. Ther. Med.* 13, 1447–1455. doi: 10.3892/etm.2017.4143

Makris, A., Xu, B., Yu, B., Thornton, C., and Hennessy, A. (2006). Placental deficiency of interleukin-10 (IL-10) in preeclampsia and its relationship to an IL-10 promoter polymorphism. *Placenta* 27, 445–451. doi: 10.1016/j.placenta.2005.05.003

Meggyes, M., Lajko, A., Palkovics, T., Totsimon, A., Illes, Z., and Szereday, L. (2015). Feto-maternal immune regulation by Tim-3/galectin-9 pathway and PD-1 molecule in mice at day 14.5 of pregnancy. *Placenta* 36, 1153–1160. doi: 10.1016/j.placenta.2015.07.124

Miko, E., Meggyes, M., Bogar, B., Schmitz, N., Barakonyi, A., and Varnagy, A. (2013). Involvement of Galectin-9/Tim-3 pathway in the systemic inflammatory response in early-onset preeclampsia. *PloS One* 8, e71811. doi: 10.1371/journal.pone.0071811

Miyagi, T., Gil, M. P., Wang, X., Louten, J., Chu, W. M., and Biron, C. A. (2007). High basal STAT4 balanced by STAT1 induction to control type 1 interferon effects in natural killer cells. *J. Exp. Med.* 204, 2383–2396. doi: 10.1084/jem.20070401

Miyazaki, S., Tsuda, H., Sakai, M., Hori, S., Sasaki, Y., and Futatani, T. (2003). Predominance of Th2-promoting dendritic cells in early human pregnancy decidua. *J. Leukoc. Biol.* 74, 514–522. doi: 10.1189/jlb.1102566

Mold, J. E., and McCune, J. M. (2012). Immunological tolerance during fetal development: from mouse to man. *Adv. Immunol.* 115, 73–111. doi: 10.1016/B978-0-12-394299-9.00003-5

Moretta, A., Biassoni, R., Bottino, C., Mingari, M. C., and Moretta, L. (2000a). Natural cytotoxicity receptors that trigger human NK-cell-mediated cytolysis. *Immunol. Today* 21, 228–234. doi: 10.1016/s0167-5699(00)01596-6

Moretta, L., Biassoni, R., Bottino, C., Mingari, M. C., and Moretta, A. (2000b). Human NK-cell receptors. *Immunol. Today* 21, 420–422. doi: 10.1016/s0167-5699(00)01673-x

Murphy, S. P., Fast, L. D., Hanna, N. N., and Sharma, S. (2005). Uterine NK cells mediate inflammation-induced fetal demise in IL-10-null mice. *J. Immunol.* 175, 4084–4090. doi: 10.4049/jimmunol.175.6.4084

Nandagopal, N., Ali, A. K., Komal, A. K., and Lee, S. H. (2014). The Critical Role of IL-15-PI3K-mTOR pathway in natural killer cell effector functions. *Front. Immunol.* 5:187:187. doi: 10.3389/fimmu.2014.00187

Robert-Gangneux, F., and Dardé, M. L. (2012). Epidemiology of and diagnostic strategies for Toxoplasmosis. *Clin. Microbiol. Rev.* 25, 264–296. doi: 10.1128/CMR.05013-11

Rouas-Freiss, N., Gonçalves, R. M., Menier, C., Dausset, J., and Carosella, E. D. (1997). Direct evidence to support the role of HLA-G in protecting the fetus from maternal uterine natural killer cytolysis. *Proc. Natl. Acad. Sci. U.S.A.* 94, 11520–11525. doi: 10.1073/pnas.94.21.11520

Shirshev, S. V., Nekrasova, I. V., Gorbunova, O. L., and Orlova, E. G. (2017). Hormonal regulation of NK cell cytotoxic activity. *Dokl Biol. Sci.* 472, 28–30. doi: 10.1134/S0012496617010021

Sotnikova, N., Voronin, D., Antsiferova, Y., and Bukina, E. (2014). Interaction of decidual $CD56^+$ NK with trophoblast cells during normal pregnancy and recurrent spontaneous abortion at early term of gestation. *Scandinavian J. Immunol.* 80 (3), 198–208. doi: 10.1111/sji.12196

Sun, J., Yang, M., Ban, Y., Gao, W., Song, B., and Wang, Y. (2016). Tim-3 is upregulated in NK cells during early pregnancy and inhibits NK cytotoxicity toward trophoblast in Galectin-9 dependent pathway. *PloS One* 11, e0147186. doi: 10.1371/journal.pone.0147186

Trapani, J. A., Jans, P., Smyth, M. J., Froelich, C. J., Williams, E. A., and Sutton, V. R. (1998). Perforin-dependent nuclear entry of granzyme B precedes apoptosis, and is not a consequence of nuclear membrane dysfunction. *Cell Death Differ* 5, 488–496. doi: 10.1038/sj.cdd.4400373

Trundley, A., and Moffett, A. (2004). Human uterine leukocytes and pregnancy. *Tissue Antigens* 63, 1–12. doi: 10.1111/j.1399-0039.2004.00170.x

Vargas-Hernández, A., Mace, E. M., Zimmerman, O., Zerbe, C. S., Freeman, A. F., and Rosenzweig, S. (2018). Ruxolitinib partially reverses functional natural killer cell deficiency in patients with signal transducer and activator of transcription 1 (STAT1) gain-of-function mutations. *Allergy Clin. Immunol.* 141, 2142–2155.e5. doi: 10.1016/j.jaci.2017.08.040

Vinnars, M. T., Björk, E., Nagaev, I., Bremme, K., Holmlund, U., and Sverremark-Ekström, E. (2018). Enhanced Th1 and inflammatory mRNA responses upregulate NK cell cytotoxicity and NKG2D ligand expression in human pre-eclamptic placenta and target it for NK cell attack. *Am. J. Reprod. Immunol.* 80, e12969. doi: 10.1111/aji.12969

Wilczyński, J. R., Tchórzewski, H., Banasik, M., Głowacka, E., Wieczorek, A., and Lewkowicz, P. (2003). Lymphocyte subset distribution and cytokine secretion. *Eur. J. Obstet Gynecol Reprod. Biol.* 109, 8–15. doi: 10.1016/s0301-2115(02)00350-0

Wong, S. Y., and Remington, J. S. (1994). Toxoplasmosis in pregnancy. *Clin. Infect. Dis.* 18, 853–861. doi: 10.1093/clinids/18.6.853

Xu, X., Zhao, M., Liu, X., Jiang, Y., Zhang, H., and Zhai, X. (2013). *Toxoplasma gondii* infection regulates the balance of activating and inhibitory receptors on decidual natural killer cells. *PloS One* 8 (2), e55432. doi: 10.1371/journal.pone.0055432

Xu, X., Zhang, J., Zhan, S., Li, Z., Liu, X., and Zhang, H. (2017). TGF-β1 improving abnormal pregnancy outcomes induced by *Toxoplasma gondii* infection: Regulating NKG2D/DAP10 and killer subset of decidual NK cells. *Cell Immunol.* 317, 9–17. doi: 10.1016/j.cellimm.2017.04.004

Yamada, H., Shimada, S., Morikawa, M., Iwabuchi, K., Kishi, R., Onoe, K., et al. (2005). Divergence of natural killer cell receptor and related molecule in the decidua from sporadic miscarriage with normal chromosome karyotype. *Mol. Hum. Reprod.* 11, 451–457. doi: 10.1093/molehr/gah181

Yamamoto, M., Standley, D. M., Takashima, S., Saiga, H., Okuyama, M., Kayama, H., et al. (2009). A single polymorphic amino acid on *Toxoplasma gondii* kinase ROP16 determines the direct and strain-specific activation of STAT3. *J. Exp. Med.* 206, 2747–2760. doi: 10.1084/jem.20091703

Yan, W. H., Lin, A., Chen, B. G., Zhou, M. Y., Dai, M. Z., Chen, X. J., et al. (2007). Possible roles of KIR2DL4 expression on uNK cells in human pregnancy. *Am. J. Reprod. Immunol.* 57, 233–242. doi: 10.1111/j.1600-0897.2007.00469.x

Yarovinsky, F. (2014). Innate immunity to *Toxoplasma gondii* infection. *Nat. Rev. Immunol.* 14, 109–121.2014. doi: 10.1038/nri3598

Zhan, S., Zheng, J., Zhang, H., Zhao, M., Liu, X., and Jiang, Y. (2018). LILRB4 decrease on uDCs exacerbate abnormal pregnancy outcomes following *Toxoplasma gondii* infection. *Front. Microbiol.* 9:588:588. doi: 10.3389/fmicb.2018.00588

Zhang, H., Hu, X., Liu, X., Zhang, R., Fu, Q., and Hu, X. (2012a). The Treg/Th17 imbalance in *Toxoplasma gondii*-infected pregnant mice. *Am. J. Reprod. Immunol.* 67, 112–121. doi: 10.1111/j.1600-0897.2011.01065.x

Zhang, R., Zhang, H., Liu, X., Fu, Q., Xu, X., and Hu, X. (2012b). The immunoprotective role of interleukin-10 in abnormal pregnancy outcome induced by *Toxoplasma gondii* Infection. *Gynecol Obstet Invest.* 73, 223–229. doi: 10.1159/000333310

Zhang, L., Zhao, M., Jiao, F., Xu, X., Liu, X., and Jiang, Y. (2015). Interferon gamma is involved in apoptosis of trophoblast cells at the maternal-fetal interface following *Toxoplasma gondii* infection. *Int. J. Infect. Dis.* 30, 10–16. doi: 10.1016/j.ijid.2014.10.027

Zhang, D., Sun, X., Ren, L., Yang, C., Liu, X., and Zhang, H. (2018). Proteomic profiling of human decidual immune proteins during *Toxoplasma gondii* infection. *J. Proteomics* 186, 28–37. doi: 10.1016/j.jprot.2018.07.011

Zhu, C., Anderson, A. C., Schubart, A., Xiong, H., Imitola, J., and Khoury, S. J. (2005). The Tim-3 ligand galectin-9 negatively regulates T helper type 1 immunity. *Nat. Immunol.* 6, 1245–1252. doi: 10.1038/ni1271

Conflict of Interest: The authors declare that the research was conducted in the absence of any commercial or financial relationships that could be construed as a potential conflict of interest.

frontiers in Cellular and Infection Microbiology

ORIGINAL RESEARCH
published: 11 March 2021
doi: 10.3389/fcimb.2021.640993

Monitoring Mosquito-Borne Arbovirus in Various Insect Regions in China in 2018

Yuan Fang[1,2,3,4,5], *Wei Zhang*[6], *Jing-Bo Xue*[1,2,3,4,5] *and Yi Zhang*[1,2,3,4,5]*

[1] National Institute of Parasitic Diseases, Chinese Center for Disease Control and Prevention, Shanghai, China, [2] Chinese Center for Tropical Diseases Research, Ministry of Science and Technology, Shanghai, China, [3] Key Laboratory of Parasite and Vector Biology, Ministry of Health, Shanghai, China, [4] WHO Collaborating Centre for Tropical Diseases, Shanghai, China, [5] National Center for International Research on Tropical Diseases, Ministry of Science and Technology, Shanghai, China, [6] Zichuan District Center for Disease Control and Prevention, Zibo, China

Background: Increases in global travel and trade are changing arbovirus distributions worldwide. Arboviruses can be introduced by travelers, migratory birds, or vectors transported *via* international trade. Arbovirus surveillance in field-collected mosquitoes may provide early evidence for mosquito-borne disease transmission.

Methods: During the seasons of high mosquito activity of 2018, 29,285 mosquitoes were sampled from seven sentinel sites in various insect regions. The mosquitoes were analyzed by RT-PCR for alphaviruses, flaviviruses, and orthobunyaviruses.

Results: We detected three strains of Japanese encephalitis virus (JEV), five strains of Getah virus (GETV), and 45 strains of insect-specific flaviviruses including Aedes flavivirus (AeFV, 1), Chaoyang virus (CHAOV, 1), Culex flavivirus (CxFV, 17), Hanko virus (HANKV, 2), QuangBinh virus (QBV, 22), and Yunnan Culex flavivirus (YNCxFV, 2). Whole genomes of one strain each of GETV, CxFV, CHAOV, and AeFV were successfully amplified. Phylogenetic analysis revealed that the new JEV strains detected in the Shanghai and Hubei Provinces belong to the GI-b strain and are phylogenetically close to the NX1889 strain (MT134112) isolated from a patient during a JE outbreak in Ningxia in 2018. GETVs were found in Inner Mongolia, Hubei, and Hainan and belonged to Group III. They were closely related to strains isolated from swine. HANKV was recorded for the first time in China and other ISFVs were newly detected at several sentinel sites. The bias-corrected maximum likelihood estimation value for JEV in Jinshan, Shanghai was 4.52/1,000 (range 0.80–14.64). Hence, there is a potential risk of a JEV epidemic in that region.

Conclusion: GI-b is the dominant circulating JEV genotype in nature and poses a health risk to animals and humans. The potential threat of widespread GETV distribution as a zoonosis is gradually increasing. The present study also disclosed the dispersion and host range of ISFVs. These findings highlight the importance of tracing the movements of the vectors and hosts of mosquito-borne pathogens in order to prevent and control arbovirus outbreaks in China.

Keywords: Japanese encephalitis virus, Getah virus, insect-specific flavivirus, *Culex*, *Anopheles*

OPEN ACCESS

Edited by:
Tianmu Chen,
Xiamen University, China

Reviewed by:
William Marciel de Souza,
University of São Paulo Ribeirão Preto, Brazil
Renli Zhang,
Shenzhen Center for Disease Control and Prevention, China

***Correspondence:**
Yi Zhang
zhangyi@nipd.chinacdc.cn

Specialty section:
This article was submitted to Virus and Host, a section of the journal Frontiers in Cellular and Infection Microbiology

Received: *13 December 2020*
Accepted: *05 February 2021*
Published: *11 March 2021*

Citation:
Fang Y, Zhang W, Xue J-B and Zhang Y (2021) Monitoring Mosquito-Borne Arbovirus in Various Insect Regions in China in 2018. Front. Cell. Infect. Microbiol. 11:640993. doi: 10.3389/fcimb.2021.640993

INTRODUCTION

Mosquito-borne diseases are prevalent worldwide. Emergent and established tropical diseases are spreading faster than expected. Dengue outbreaks have occurred in China over the last decade. These occurred in Yunnan [2013, (Zhang et al., 2014)], Guangdong [2014, (Xiao et al., 2016)], Fujian [2016, (Han et al., 2018)], and Zhejiang [2017, (Yan et al., 2018)] and of them emerged in heretofore dengue-free or low endemic areas. The number and spatial distribution of dengue cases in China in 2019 reached an unprecedented level. Morbidity was 1.63/100,000 and was second in severity only to that of the major dengue outbreak of 2014 (Liu, 2020). Summer monsoons and climate change have substantial impacts on dengue control and prevention in southeastern China (Liu et al., 2020a). Japanese encephalitis (JE) has been effectively controlled by vaccination. However, JE outbreaks have been recorded in adults in Shanxi [2006, (Wang et al., 2007)], Hubei [2009–2010, (Hu et al., 2013)], Shandong [2013 (Tao et al., 2014; Li et al., 2019)], Gansu [2018, (Tian and Yang, 2019)], and Ningxia [2018, (Liu et al., 2020b)]. The potential resurgence of malaria (Feng et al., 2020) and the emergence of Zika (Song et al., 2017), Chikungunya (Wu et al., 2012), and West Nile (Cao et al., 2019) virus threaten public health.

Before disease outbreaks occur, viruses colonize in field mosquitoes and circulate in nature. Mosquito-borne disease outbreaks reflect inadequate mosquito-borne pathogen surveillance. Documenting the dynamics of pathogen-bearing mosquitoes in the field might herald imminent mosquito-borne disease outbreaks (Masetti et al., 2008). Sporadic mosquito pathogen detection has been conducted in China to a limited extent. In addition, baseline surveys have not yet been performed in certain areas. Hence, surveys are needed to determine the geographic distribution of arboviruses in various regions of China. The mosquito surveillance system in China has focused mainly on vector diversity and abundance (Wu et al., 2017; Guo et al., 2019). To the best of our knowledge, however, only a few districts have sustained longitudinal mosquito-borne pathogen surveillance. Moreover, large-scale latitudinal surveillance is uncommon. In 2018, we established seven sentinel sites in China based on ecological niches for mosquito-borne pathogen surveillance. Alphaviruses, flaviviruses, and orthobunyaviruses were detected and their endemic risks were evaluated in target areas.

METHODS

Mosquito Sampling

Sentinel sites were established in various insect regions (IR) of China according to geographical insect division (Shen et al., 2013). The areas included Jining, Shandong Province (Northern China IR), Hohhot, Inner Mongolia Autonomous Region (Northeastern China IR), Jin'an and Jinshan Districts, Shanghai Municipality (Eastern China), Sanya City and Qionghai County in Hainan Province (Southern China Hainan sub-IR), and Zaoyang County in Hubei Province (Changjiang-Huaihe IR). **Figure 1** is a sentinel site map generated by ArcGIS v. 10.1 ArcMap software (ESRI, Redlands, CA, USA). Mosquitoes were collected from July to October 2018 using UV light traps (Kungfu Dude Mosquito & Fly Trap, Wuhan Ji Xing Medical Technology Co., Wuhan, China) and the labor hour method (Fang et al., 2019). The collection sites covered various ecological characteristics and included residential areas, gardens, office workplaces, schools, and livestock. Both sampling methods were performed twice monthly at 15-day intervals. Aedine larvae and pupae were collected from positive containers during a Breteau Index survey, brought to a laboratory, and reared until adult emergence. Mosquitoes were identified according to a national key using morphological characteristics (Lu, 1997). Ambiguous specimens were confirmed by molecular methods (Fang et al., 2017). Mosquitoes were pooled by species and collection date, method, and location and stored at -80°C until further testing. There was a maximum of 100 individuals per pool.

Nucleic Acid Extraction and Polymerase Chain Reaction

RNA extraction, cDNA synthesis, and RNA integrity assessment were performed as previously described (Fang et al., 2018). PCR amplification to detect alphaviruses, flaviviruses, and orthobunyaviruses was performed as described by Fang et al. (2021a). For additional genotype identification, the primer sets JEV-Ef/JEV-Er (Gao et al., 2013) and CxFV-E-F/CxFV-E-R (Saiyasombat et al., 2010) amplified the *E* genes of JEV and CxFV, respectively. The *E2* gene of the Getah virus (GETV) was amplified by the primer sets GETVE2F/GETVE2R (Zhai et al., 2008). The PCR products were visualized on 1% or 2% agarose gel in 0.5× Tris-acetate-EDTA buffer with Goldview. Positive products were purified, cloned and sequenced by Sangon (Shanghai, China).

Whole-Genome Sequencing

Primer Premier v. 5.0 (Premier Biosoft International, Palo Alto, CA, USA) was used to analyze the molecular characteristics and putative pathogenesis mechanisms of the viruses. It designed primers to amplify the complete genomes of the Getah (GETV), Chaoyang (CHAOV), and Quang Binh (QBV) viruses and Culex flavivirus (CxFV) using the local SC201807 (MK693225), HLD15 (NC_017086), JM17156/China/2017 (MH827524), and DG1064 (JQ308188) isolates, respectively, as references. The PCR products were sent for Sanger sequencing and applied towards the design of the subsequent primers.

Phylogenetic Analysis

PCR product sequences were compared with those deposited in the GenBank database using the BLAST program. Multiple sequence alignments were generated with ClustalW2 using fragments of the homologous NS5, JEV E, and GETV E2 genes available in GenBank and the sequences obtained in this study. Default ClustalW2 settings were manually adjusted as required (Larkin et al., 2007). Neighbor-joining (NJ) trees were plotted following Kimura's two-parameter (K2P) distance model (Kimura, 1980) and 1,000 bootstrap replicates in MEGA v. 7.0 (Kumar et al., 2016). Based on the Akaike Information Criterion (AIC), a best-fit alignment model was determined with Modeltest v. 3.7 and PAUP* v. 4.0b10 (Wilgenbusch and Swofford, 2003). The maximum likelihood (ML) and Bayesian

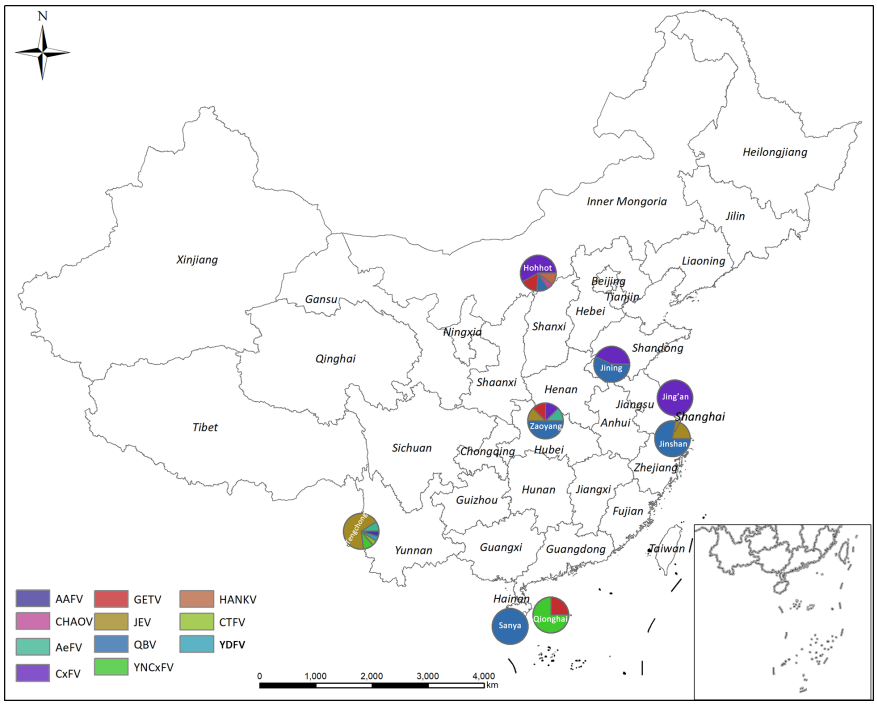

FIGURE 1 | Arbovirus distributions by mosquito pathogen surveillance sentinel site in China in 2018. AAFV, Anopheles-associated flavivirus; AeFV, Aedes flavivirus; CHAOV, Chaoyang virus; CTFV, Culex theileri flavivirus; CxFV, Culex flavivirus; HANKV, Hanko virus; JEV, Japanese encephalitis virus; QBV, Quang Binh virus; YDFV, Yamadai flavivirus; YNCxFV, Yunnan Culex flavivirus.

likelihood trees were plotted using the GTR+I+G model for flavivirus *NS5* and the Japanese encephalitis virus (JEV) *E* genes. The ML and Bayesian likelihood trees were plotted using the GTR+G model for the GETV *E2* and the Culex flavivirus (CxFV E) genes. The ML tree was plotted with MEGA v. 7.0 using 1,000 bootstrap replicates. The Bayesian tree was plotted with MrBayes v. 3.2.1 (Ronquist et al., 2012) and run for 10 million generations of which 25% were discarded as burn-in. The trees were unrooted for the least biased topology and visualized in Figtree v. 1.4.2 (http://tree.bio.ed.ac.uk/software/figtree/).

Infection Rate Calculation

Mosquito pool sizes varied considerably. Therefore, infection rates were calculated using a bias-corrected maximum likelihood estimation (MLE) and a minimum infection rate (MIR) in the Excel add-in PooledInfRate v. 4 statistical software package (Biggerstaff, 2006). Rates were expressed as the number of infected mosquitoes per 1,000 collected.

RESULTS

Detection of Mosquito-Borne Pathogens From Samples

A total of 29,285 mosquitoes including *Anopheles sinensis*, *Culex* spp., *Aedes albopictus*, and *Armigeres subalbatus* were collected at the seven sentinel sites during the mosquito activity season of 2018. All samples in 870 pools were tested for the presence of mosquito-borne pathogens. Collection data for each sentinel site are listed in **Table S1**. *Cx.* spp. including *Cx. pipiens*, *Cx. tritaeniorhychus*, and *Cx. quinquefasciatus* predominated (27,949 in 623 pools) and accounted for 95.44% of the total. They were followed by *An. sinensis* (1.66%, 486/47 pools), *Ae. albopictus* (2.43%, 713/183 pools), and *Ar. subalbatus* (0.47%, 137/17 pools). Intact RNA was successfully extracted from all mosquito pools and confirmed by 18S rRNA amplification (Hoffmann et al., 2004). Forty-eight flavivirus and five GETV strains were recovered by successful amplification of the partial flavivirus *NS5* and the alphavirus *NSP1* gene, respectively. The 48 flavivirus strains comprised one Aedes flavivirus (AeFV), one Chaoyang virus (CHAOV), 16 Culex flavivirus (CxFV), three JEV, two Hankovirus (HANKV), 22 Quang Binh virus (QBV), and three Yunnan Culex flavivirus (YNCxFV) strains. The *E* genes of JEV and CxFV were successfully amplified in three and nine positive pools, respectively. Four positive amplification and sequence determination results were obtained for the GETV *E2* gene. No orthobunyaviral RNA sequences were detected. The species names, collection information, host species, and GenBank accession numbers of the arbovirus strains obtained here are shown in **Table 1**.

AeFV was present in one pool of *Ae. albopictus* from Zaoyang, Hubei Province. CHAOV was present in one pool of *Cx. pipiens*

TABLE 1 | Mosquito-borne viruses detected at different sentinel sites during the mosquito activity seasons of 2018.

Strain	Virus	Host	Collection date	Geographic location	GenBank ID		
					NS5	*E*	Whole genome
HB_C9_18-7-HZ-Aea-B-4-JG-1	AeFV	*Aedes albopictus*	7-Jul-2018	China: Zaoyang, Hubei Province	MW246700		
NM,JA_F7_18-8L-NH-Cxp-Y-2-1	CHAOV	*Culex pipiens*	25-Aug-2018	China: Hohhot, Inner Mongolia	MW246701		MW246770
HB_F3_18-8E-HZ-C-Y-5-1	CxFV	*Cx. tritaeniorhynchus*	13-Aug-2018	China: Zaoyang, Hubei Province	MW246702		
JN,SY,TC_F3_18-8L-S-J-Cxt-Y-4-1		*Cx. tritaeniorhynchus*	24-Aug-2018	China: Jining, Shandong Province	MW246703	MW246760	
JS,JA_A4_18-9E-SJ-Cxp-Y-1-1		*Cx. pipiens*	10-Sep-2018	China: Jining, Shandong Province	MW246704	MW246767	MW246772
JS,JA_A9_18-9L-SJ-Cxp-Y-3-1		*Cx. pipiens*	26-Sep-2018	China: Jining, Shandong Province	MW246705	MW246768	
JS,JA_D9_18-10M-JA-Cxp-C-4		*Cx. pipiens*	11-Oct-2018	China: Jin'an, Shanghai Municipality	MW246706		
NM,JA_A3_18-9M-NH-Cxp-Y-1-1		*Cx. pipiens*	14-Sep-2018	China: Hohhot, Inner Mongolia	MW246707		
NM,JA_C3_18-8M-NH-Cxp-Y-1-1		*Cx. pipiens*	14-Aug-2018	China: Hohhot, Inner Mongolia	MW246708	MW246761	
NM,JA_C5_18-8E-NH-Cxp-Y-2-1		*Cx. pipiens*	10-Aug-2018	China: Hohhot, Inner Mongolia	MW246709		
NM,JA_C6_18-7L-NH-Cxp-Y-1-1		*Cx. pipiens*	25-Jul-2018	China: Hohhot, Inner Mongolia	MW246710		
NM,JA_D5_18-7L-NH-Cxp-Y-2-1		*Cx. pipiens*	25-Jul-2018	China: Hohhot, Inner Mongolia	MW246711		
NM,JA_D7_18-8M-NH-Cxp-Y-1-1		*Cx. pipiens*	14-Aug-2018	China: Hohhot, Inner Mongolia	MW246712		
NM,JA_E11_18-8M-NH-Cxp-Y-3-1		*Cx. pipiens*	14-Aug-2018	China: Hohhot, Inner Mongolia	MW246713	MW246762	
NM,JA_E12_18-8M-NH-Cxp-Y-3-1		*Cx. pipiens*	14-Aug-2018	China: Hohhot, Inner Mongolia	MW246714	MW246763	
NM,JA_E7_18-8M-NH-Cxp-Y-2-3		*Cx. pipiens*	14-Aug-2018	China: Hohhot, Inner Mongolia	MW246715	MW246764	
NM,JA_G2_18-8L-NH-Cxp-Y-3		*Cx. pipiens*	25-Jul-2018	China: Hohhot, Inner Mongolia	MW246716	MW246765	
NM,JA_G3_18-8L-NH-Cxp-Y-2-4		*Cx. pipiens*	25-Jul-2018	China: Hohhot, Inner Mongolia	MW246717	MW246766	
NM,JA_E12_18-8M-NH-Cxp-Y-3-1	GETV	*Cx. pipiens*	14-Aug-2018	China: Hohhot, Inner Mongolia	MW246718	MW246755	
NM,JA_F2_18-8L-NH-Cxp-Y-1-1		*Cx. pipiens*	25-Jul-2018	China: Hohhot, Inner Mongolia	MW246719	MW246753	MW246769
NM,JA_G4_18-8L-NH-Cxp-Y-2-4		*Cx. pipiens*	25-Jul-2018	China: Hohhot, Inner Mongolia	MW246720	MW246756	
HB_A3_18-7E-HZ-ANS-Y-1-1		*Anopheles sinensis*	16-Jul-2018	China: Zaoyang, Hubei Province	MW246721	MW246754	
JS,QH_G7_18-7L-QH-Cxt-5-4		*Cx. tritaeniorhynchus*	24-Jul-2018	China: Qionghai city, Hainan Province	MW246722		
HB_B4_18-7E-HZ-C-Y-5-4	JEV	*Cx. tritaeniorhynchus*	19-Jul-2018	China: Zaoyang, Hubei Province	MW246723	MW246759	
JS,QH_B4_18-7E-JS-Cxt-C-9-6		*Cx. tritaeniorhynchus*	4-Jul-2018	China: Jinshan, Shanghai Municipality	MW246724	MW246757	
JS,QH_D3_18-8E-JS-Cxt-C-8-4		*Cx. tritaeniorhynchus*	7-Aug-2018	China: Jinshan, Shanghai Municipality	MW246725	MW246758	
NM,JA_C7_18-7L-NH-Cxp-Y-1-1	HANKV	*Cx. pipiens*	25-Jul-2018	China: Hohhot, Inner Mongolia	MW246726		
NM,JA_E2_18-8M-NH-Cxp-Y-2-1		*Cx. pipiens*	14-Aug-2018	China: Hohhot, Inner Mongolia	MW246727		
JS,JA_A5_18-9E-SJ-Cxp-Y-2-1	QBV	*Cx. pipiens*	10-Sep-2018	China: Jining, Shandong Province	MW246728		
JS,JA_A7_18-9L-SJ-Cxp-Y-1-1		*Cx. pipiens*	26-Sep-2018	China: Jining, Shandong Province	MW246729		
JS,JA_C12_18-10E-SJ-Cxp-3-1		*Cx. pipiens*	10-Oct-2018	China: Jining, Shandong Province	MW246730		
JN,SY,TC_E2_18-8E-S-J-Cxp-Y-4-1		*Cx. tritaeniorhynchus*	6-Aug-2018	China: Jining, Shandong Province	MW246731		
HB_E10_18-8E-HZ-A-Y-2-1		*An. sinensis*	13-Aug-2018	China: Zaoyang, Hubei Province	MW246732		
HB_E2_18-7L-HZ-C-S-1		*Cx. tritaeniorhynchus*	24-Jul-2018	China: Zaoyang, Hubei Province	MW246733		
HB_E5_18-8E-HZ-C-Y-1-1		*Cx. tritaeniorhynchus*	13-Aug-2018	China: Zaoyang, Hubei Province	MW246734		
HB_E7_18-8E-HZ-A-Y-1-1		*An. sinensis*	13-Aug-2018	China: Zaoyang, Hubei Province	MW246735		
JN,SY,TC_B5_18-7E-H-S-Cxt-Y-5		*Cx. tritaeniorhynchus*	10-Jul-2018	China: Sanya, Hainan Province	MW246736		
JN,SY,TC_B6_18-7E-H-S-Cxt-Y-5		*Cx. tritaeniorhynchus*	10-Jul-2018	China: Sanya, Hainan Province	MW246737		
JN,SY,TC_B7_18-7E-H-S-Cxt-Y-5		*Cx. tritaeniorhynchus*	10-Jul-2018	China: Sanya, Hainan Province	MW246738		
JN,SY,TC_B8_18-7E-H-S-Cxt-Y-5		*Cx. tritaeniorhynchus*	10-Jul-2018	China: Sanya, Hainan Province	MW246739		
JN,SY,TC_D1_18-7L-H-S-Cxt-Y-5		*Cx. tritaeniorhynchus*	10-Jul-2018	China: Sanya, Hainan Province	MW246740		
JS,JA_H6_18-10E-JS-Cxt-C-2-1		*Cx. tritaeniorhynchus*	8-Oct-2018	China: Jinshan, Shanghai Municipality	MW246741		MW246771
JS,QH_A7_18-7E-JS-Cxt-C-8-5		*Cx. tritaeniorhynchus*	4-Jul-2018	China: Jinshan, Shanghai Municipality	MW246742		
JS,QH_B5_18-7E-JS-Cxt-C-9-7		*Cx. tritaeniorhynchus*	4-Jul-2018	China: Jinshan, Shanghai Municipality	MW246743		
JS,QH_B8_18-7E-JS-Cxt-C-10-1		*Cx. tritaeniorhynchus*	4-Jul-2018	China: Jinshan, Shanghai Municipality	MW246744		
JS,QH_C3_18-7M-JS-Cxt-C-8-1		*Cx. tritaeniorhynchus*	16-Jul-2018	China: Jinshan, Shanghai Municipality	MW246745		

(Continued)

TABLE 1 | Continued

Strain	Virus	Host	Collection date	Geographic location	GenBank ID		
					NS5	*E*	Whole genome
JS,QH_D7_18-8E-JS-Cxt-C-8-8	YNCxFV	*Cx. tritaeniorhynchus*	7-Aug-2018	China: Jinshan, Shanghai Municipality	MW246746		
JS,QH_E11_18-8L-JS-Cxt-C-3-1		*Cx. tritaeniorhynchus*	23-Aug-2018	China: Jinshan, Shanghai Municipality	MW246747		
NM,JA_C12_18-7L-NH-Cxp-Y-1-3		*Cx. pipiens*	25-Jul-2018	China: Hohhot, Inner Mongolia	MW246748		
NM,JA_D8_18-8M-NH-Cxp-Y-1-2		*Cx. pipiens*	14-Aug-2018	China: Hohhot, Inner Mongolia	MW246749		
JS,QH_F10_18-7L-H-Q-Cxt-Y-1-1		*Cx. tritaeniorhynchus*	24-Jul-2018	China: Qionghai, Hainan Province	MW246750		
JS,QH_F2_18-7E-H-Q-Cxt-Y-1-1		*Cx. tritaeniorhynchus*	10-Jul-2018	China: Qionghai, Hainan Province	MW246751		
JS,QH_F5_18-7E-H-Q-Cxt-Y-5-1		*Cx. tritaeniorhynchus*	10-Jul-2018	China: Qionghai, Hainan Province	MW246752		

AeFV, Aedes flavivirus, CHAOV, Chaoyang virus; CxFV, Culex flavivirus; E, Envelope gene; GETV, Getah virus; HANKV, Hanko virus; JEV, Japanese encephalitis virus; NS5, Non-structural 5 gene, YNCxFV, Yunnan Culex flavivirus.

from Hohhot, Inner Mongolia. CxFVs were found in two pools of *Cx. tritaeniorhynchus* and 14 pools of *Cx. pipiens*, distributed in Hohhot, Inner Mongolia (11), Zaoyang, Hubei Province (1), Jining, Shandong Province (3), and Jin'an, Shanghai (1). JEV was found in three pools of *Cx. tritaeniorhynchus* from Zaoyang, Hubei (1) and Jinshan, Shanghai (2). HANKV was found in two pools of *Cx. pipiens* from Hohhot, Inner Mongolia. QBV was found in five pools of *Cx. pipiens*, two pools of *An. sinensis*, and 15 pools of *Cx. tritaeniorhynchus* from Jining, Shandong Province (4), Zaoyang, Hubei Province (4), Hohhot, Inner Mongolia (2), Sanya, Hainan Province (5), and Jinshan, Shanghai Municipality (7). YNCxFV was found in three pools of *Cx. tritaeniorhynchus* from Qionghai, Hainan Province. GETV was found in three pools of *Cx. pipiens*, one pool of *An. sinensis*, and one pool of *Cx. tritaeniorhynchus* from Hohhot, Inner Mongolia (3), Zaoyang County, Hubei Province (1), and Qionghai City, Hainan Province (1). The arbovirus distributions at each sentinel site are shown in **Figure 1**.

The phylogenetic tree based on the *NS5* gene (**Figure 2**) showed that the *Flaviviridae* consisted of four clusters including mosquito-borne and tick-borne flaviviruses, no-known vector flaviviruses, and Insect specific flaviviruses (ISFVs). Each flavivirus had an independent lineage with high bootstrap values. Three mosquito-borne flavivirus-positive sequences were clustered in the JEV lineage while the other 44 sequences were scattered in the ISFV cluster. The CHAOV was genetically close to the mosquito-borne flavivirus clade and distant from the ISFV clade.

Molecular Characterization and Phylogenetic Analysis Based on JEV *E* Genes

For the JEV *E* gene, 99.36%–99.74% nucleotide sequence identity and 99.61%–100% amino acid sequence identity were determined for the newly detected Shanghai and Hubei strains. They had 87.76%–88.14% and 97.68%–97.76% similarity to the vaccine strain SA14-14-2 in terms of their nucleotide and amino acid levels, respectively. In the *E* gene tree (**Figure 3**), the newly detected Shanghai and Hubei strains fell into the GI-b cluster. They were genetically close and formed a cluster related to the strain obtained in Shanghai in 2016 (HP4A_16-7-H-Cut-C-5-2 strain, MT134112). However, they were distantly related to the strains circulating in Shanghai and Hubei before 2010. The deduced differences in amino acids among the E protein sequences were aligned to compare the newly detected strains against the vaccine strain (SA14-14-2) currently used in China. Relative to the SA14-14-2-derived strain (SA14), four amino acid substitutions were observed in the newly detected JEV strains, namely, E129 (Thr→Met), E222 (Ala→Ser), E327 (Ser→Thr), and E366 (Ala-Ser). There were no differences between the novel and vaccine strains in terms of their key amino acid sites related to antigenicity. All JEV strains carried the dominant haplotype SKSS based on the E123, E209, E227, and E408 sites in the E protein previously defined based on predicted positive selections (Han et al., 2014).

JEV *E* gene tree topologies (**Figure 3**) identified five major clades corresponding to genotypes I–V. GI comprised two

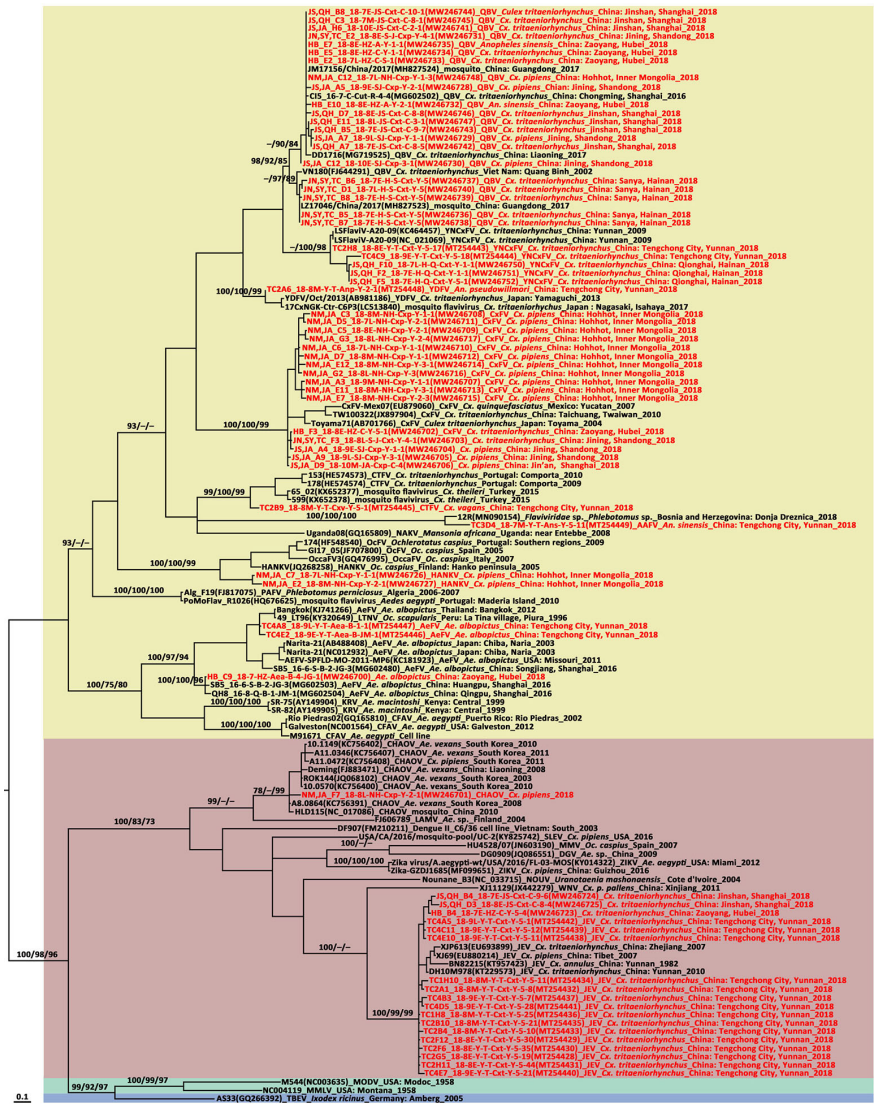

FIGURE 2 | Phylogenetic tree generated by Bayesian analysis of partial non-structural five gene sequences of flavivirus. The virus strain, GenBank accession number, host, collection country and year are noted. The flavivirus sequences obtained in this study are marked in red. Bootstrap values (1,000 replicates, not shown for less than 75%) of maximum likelihood; Bayesian analyses and neighbor-joining are shown above the main lineages. The bar indicates 0.1 substitutions per site. Sequences shaded sky blue represent tick-borne flavivirus, those shaded aquamarine represent no-known vector flavivirus, those shaded khaki represent infect specific flavivirus, those shaded rose-brown represent mosquito-borne flavivirus. AAFV, Anopheles associated flavivirus; AeFV, Aedes flavivirus; CFAV, cell fusing agent virus; CTFV, Culex theileri flavivirus; CxFV, Culex flavivirus; DGV, Donggang virus; HANKV, Hanko virus; JEV, Japanese encephalitis virus; KRV, Kamiti River virus; LTNV, La Tina virus; MMLV, Montana myotis leukoencephalitis virus; MODV, Modoc virus; NAKV, Nakiwogo virus; PAFV, Phlebotomus associated flavivirus; QBV, Quang Binh flavivirus; OcFV, Ochlerotatus caspius flavivirus; SLEV, Santa Louis encephalitis virus; TBEV, tick-borne encephalitis virus; WNV, West Nile virus; YDFV, Yamadai flavivirus; YNCxFV, Yunnan Culex flavivirus.

distinct clades representing the GI-a and GI-b subgenotypes. All newly detected strains were clustered together and belonged to the GI-b genotype. They had high similarity and clustered with the sequences obtained in Shanghai in 2016 and the NX1889 strain (MT134112) isolated from a JE patient during an outbreak in Ningxia in 2018 (Liu et al., 2020b). A sequence comparison on JEV E gene revealed 98.51%–98.78% nucleotide and 99.61%–100% amino acid sequence identities between the newly obtained JEV strains and the NX1889 strain.

Molecular Characterization and Phylogenetic Analysis Based on the GETV *E* Genes

The GETV *E2* gene was successfully amplified in four of five GETV positive pools. There were 98.50%–99.84% nucleotide and 98.82%–99.76% amino acid sequence identities among the newly detected Inner Mongolia and Hubei strains. The GETV strains identified here had 98.58%–98.74% nucleotide and 99.05%–

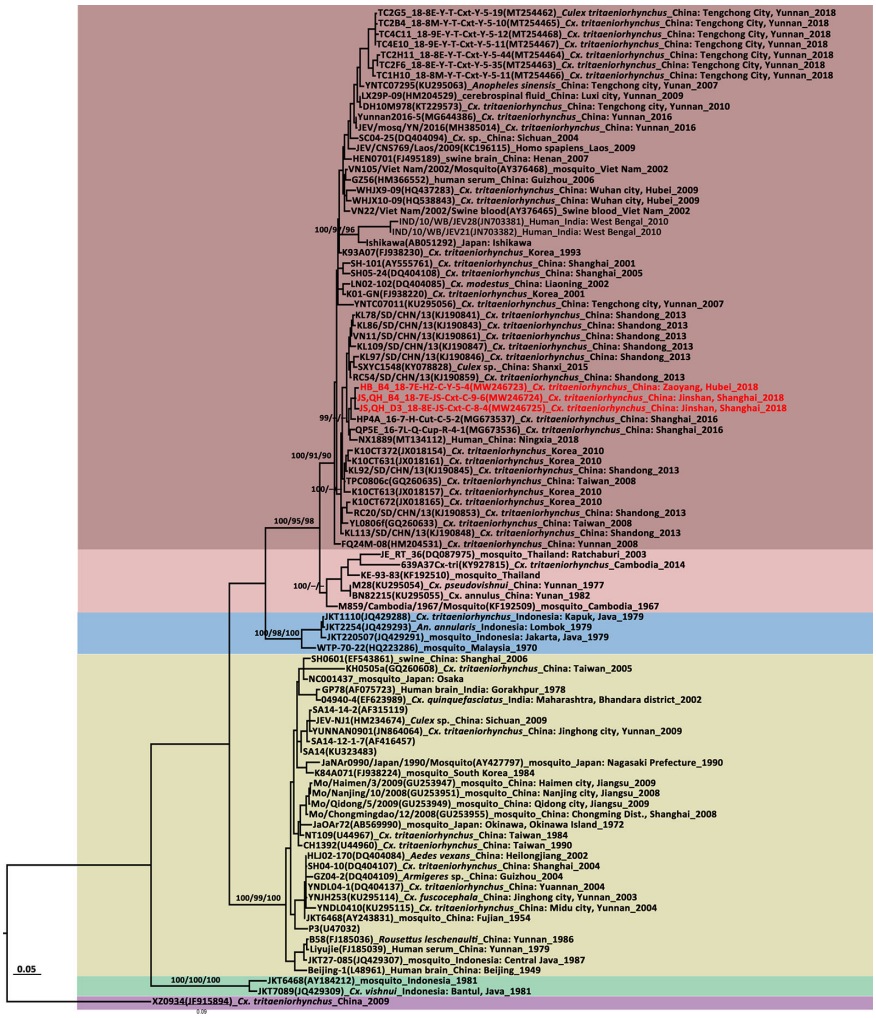

FIGURE 3 | Maximum likelihood phylogenetic analysis of Japanese encephalitis virus (JEV) envelope gene sequences. The virus strain, GenBank accession number, host, collection country and year are noted. The JEV sequences obtained in this study are marked in red. The numbers above each branch represent the bootstrap support of the maximum likelihood, neighbor-joining, and Bayesian analyses, respectively, based on 1,000 replicates. The scale-bar indicates 0.05 substitutions per site. Sequences shaded misty rose represent the GI-a genotype, those shaded rose-brown represent the GI-b genotype, those shaded sky blue represent the GII genotype, those shaded khaki represent the GIII genotype, those shaded aquamarine represent the GIV genotype, and those shaded thistle represent the GV genotype.

99.53% amino acid sequence similarities to the vaccine strain MI-110 (Japan, LC079086) based on an analysis of the E2 protein-coding region sequences. The GETV *E2* gene tree topologies (**Figure 4**) identified four distinct clades corresponding to groups I–IV. The newly obtained strains fell into two sublineages of Group III. The HB_A3_18-7E-HZ-ANS-Y-1-1, NM,JA_E12_18-8M-NH-Cxp-Y-3-1, and NM, JA_G4_18-8L-NH-Cxp-Y-2-4 strains were close to those identified in swine (HNPDS-2) and mosquito (JL17/08) samples collected in Henan and Jilin Provinces. The NM, JA_F2_18-8L-NH-Cxp-Y-1-1 strain was close to the swine sample (SC201807) obtained in Sichuan. The three GETV strains from Inner Mongolia were distributed in two sublineages and were distantly related to the strain from neighboring Mongolia. GETV was first detected in a single pool of *Cx. pipiens* (NMDK1813-1 strain) collected in Inner Mongolia in 2018 (Cheng et al., 2020). The NMDK1813-1 strain was close to the GS10-2 (EU015070) strain from Gansu Province (Cheng et al., 2020). GETV was detected in samples from Hubei (ES26) (Gao et al., 2015) collected in 2010. The phylogenetic analysis suggests that the ES26 strain was genetically close to HB0234 strain from Hubei (Gao et al., 2015). It's a pity that there were no available NMDK1813-1 strain and ES26 strain sequences available on GenBank.

The GETV *E2* gene is 1,266 nt long and encodes a 422-aa glycoprotein. The deduced amino acid differences between the E2 protein sequences and those of the vaccine derived strain (MI-110) currently used in Japan were aligned and compared. Six amino acid residues in the newly detected GETV strains differed from those of the MI-110 strain, namely, E75 (Met→Ile),

FIGURE 4 | Phylogenetic tree generated by Bayesian analysis of Getah virus (GETV) envelope gene. The virus strain, GenBank accession number, host, collection country and year are noted. The GETV sequences obtained in this study are marked in red. Bootstrap values (1,000 replicates, not shown for less than 75%) of Bayesian analyses, maximum likelihood and neighbor-joining are shown above the main lineages. The scale-bar indicates 0.005 substitutions per site. Sequences shaded sky blue represent the GETV Group I, those shaded aquamarine represent Group II, those shaded khaki represent Group III, those shaded rose-brown represent Group IV.

E86 (His→Tyr), E97 (Met→Ile), E194 (Glu→Gly), E248 (Leu→Ser), and E323 (Asp→Glu). Comparison of the E2 protein amino acids showed that Gly at locus 194 was unique to MI-110 whereas the Glu substitution at E194 (Glu→Gly) was observed in all other strains.

The length of the entire genome of the newly detected GETV (NM,JA_F2_18-8L-NH-Cxp-Y-1-1 strain, MT254427) was 11,689 bp. It comprised 5'UTR (78 nt), two ORFs encoding non-structural proteins (7,404 nt) and structural proteins (3,762 nt), 3'UTR (401 nt), and a 26S RNA junction region located between the non-structural and structural protein coding regions (44 nt; 7,483–7,526). The complete genome was amplified with 11 pairs of overlapping primers (**Table S2**). The virus isolated from *Cx. pipiens* had 99.73% and 99.84% similarities at the nucleotide and amino acid levels, respectively, to the SC201807 strain isolated from mixed infected pig reproductive and respiratory syndrome blood in Sichuan in 2018 (Jiang et al., 2019).

Molecular Characterization and Phylogenetic Analysis Based on the CHAOV *NS5* Genes

In the flavivirus *NS5* tree, CHAOVs distributed in the mosquito-borne flavivirus clade and were remote from ISFVs. CHAOVs were previously detected in Liaoning Province, China (Wang et al., 2009). This record of CHAOV is the first for Inner Mongolia.

The complete genome of the NM,JA_F2_18-8L-NH-Cxp-Y-1-1 strain was 10,679 nt and consisted of an ORF encoding 3,436 amino acids flanked by 99 and 272 nucleotides at the 5′UTR and 3′UTR ends, respectively. The complete genome was amplified with 11 pairs of overlapping primers (**Table S3**).

Compared to the genome sequences of other CHAOV strains, the newly discovered NM,JA_F2_18-8L-NH-Cxp-Y-1-1 strain had 98.91% identity to HLD115 (NC_017086) detected in mosquitoes from Hulu Island, Liaoning Province, China in 2010. It had 97.90% nucleotide similarity to the prototype Deming (FJ883471) strain from Liaoning, China and 97.87% nucleotide similarity to the ROK144 strain (JQ068102) from South Korea. Similarity of the four CHAOV strains to the whole genome available on GenBank was 99.7%–99.9% at the amino acid level.

Sequence Analysis and Phylogenetic Characterization of ISFVs

AeFV was detected in a pool of *Ae. albopictus* from Zaoyang, Hubei Province. Phylogenetic analysis revealed a close genetic relationship between it and the strains from Shanghai. This

AeFV record was the first for Hubei Province. In China, AeFVs were already detected in mosquito samples collected in Shanghai Municipality in 2016 (Fang et al., 2018) and Yunnan Province in 2018 (Fang et al., 2021b). Sixteen CxFVs were observed at four sentinel sites. The CxFV *E* gene was successfully amplified in nine strains. The CxFVs in the *E* gene phylogenetic tree (**Figure 5**) were divided into two genotypes. All newly detected CxFVs were clustered in the Asia/USA genotype clade whereas those obtained from Shandong and Shanghai were distantly related to those from Inner Mongolia. To the best of our knowledge, these records of CxFV are firsts for Hubei and Inner Mongolia. The whole JS,JA_A4_18-9E-SJ-Cxp-Y-1-1 genome was 10,799 bp long and comprised an ORF encoding 3,364 amino acids flanked by 71 and 636 nucleotides at the 5′UTR and 3′UTR ends, respectively. Eleven overlapping primers (**Table S4**) amplified the complete CxFV genome. A genome-wide comparison showed that the JS,JA_A4_18-9E-SJ-Cxp-Y-1-1 strain from Shandong Province had 99.6% nucleotide and 99.67% amino acid identities with the DG1064 strain (JQ308188.1) from *An. sinensis* in Liaoning Province.

Two *Cx. pipiens* pools from Inner Mongolia were positive for HANKV. They had 98.09% similarity with each other and shared 80.47%–87.88% nucleotide sequence identity with the partial *NS5* genes of strains from Europe. This HANKV record is a first for China. It was already detected in Finland, Spain, Italy, and Portugal (Blitvich and Firth, 2015). Hence, this virus has a broad geographical distribution and a wide host range.

QBVs have been detected at five sentinel sites in this study including Shandong, Hubei, Hainan, Inner Mongolia, and Shanghai. This record of QBV was a first for all the aforementioned sites except Shanghai. The *NS5* gene sequence similarity was 86.36%–100% among QBV strains. The strains JS, JA_A5_ 18-9E-SJ-Cxp-Y-2-1 from Jining and QBV_JN,SY, TC_B6_18-7E-H-S-Cxt-Y-5 from Sanya City had only 87.50% similarity. QBVs in the *NS5* tree were divided into two clusters. The strains from Sanya City in Hainan Province gathered with the QBV prototype strain from Vietnam. The strains from Hubei, Shanghai, Inner Mongolia, and Shandong clustered with that from Shanghai. JM17156 (MH827524) and LZ17046 (MH827523) were isolated from mosquitoes collected in Guangdong but had only 91.60% nucleotide sequence similarity and were remote from each other in the phylogenetic tree. The boundary of the two QBV lineages is probably located between 21°N and 22°N.

We elucidated the complete genome of the novel JS,JA_H6_18-10E-JS-Cxt-C-2-1 strain. It was 10,785 nt long and had an ORF encoding 3,360 amino acids flanked by 85 and 620 nucleotides at the 5′UTR and 3′UTR ends, respectively. The complete genome was amplified with 10 pairs of overlapping primers (**Table S5**). A whole-genome sequence comparison of JS,JA_H6_18-10E-JS-Cxt-C-2-1 and the other four representative QBV strains showed 88.4%–99.5% nucleotide sequence identity. The deduced amino acid sequence identities were in the range of 97.1–99.8%. JS, JA_H6_18-10E-JS-Cxt-C-2-1 had 99.5% genetic identity with the DD1716 strain detected in *Cx. tritaeniorhynchus* in Dandong City,

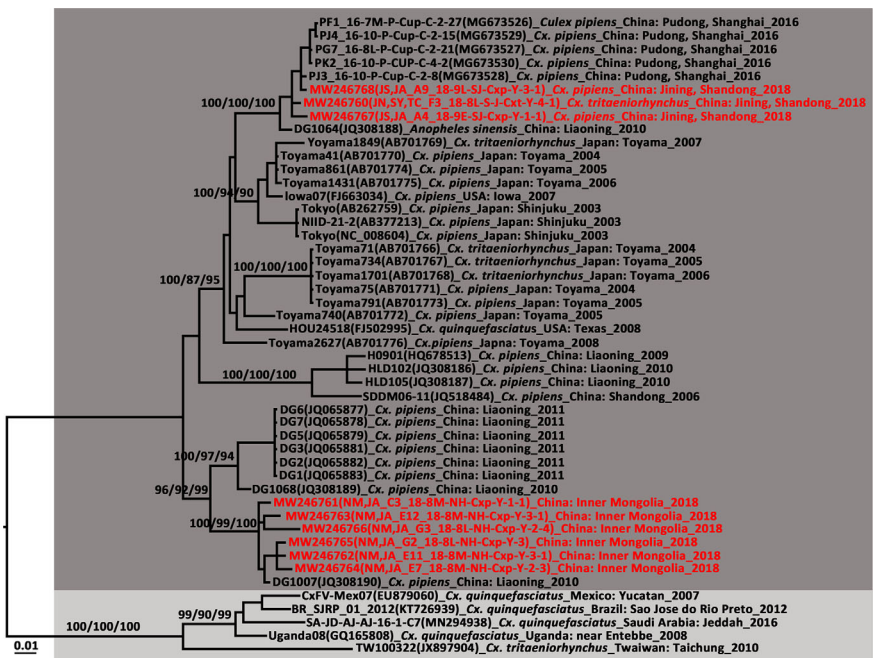

FIGURE 5 | Phylogenetic tree generated by Bayesian analysis of Culex flavivirus (CxFV) complete genome. The virus strain, GenBank accession number, host, collection country and year are noted. The CxFV sequences obtained in this study are marked in red. Bootstrap values (1,000 replicates, not shown for less than 75%) of Bayesian analyses, maximum likelihood and neighbor-joining are shown above the main lineages. The scale-bar indicates 0.01 substitutions per site. Dark grey and light grey indicate CxFV Asian/USA genotype and Africa/Caribbean/Latin America genotype, respectively.

Liaoning Province, China. However, it had only 89.79% nucleotide sequence identity with the VN180 strain.

Three newly identified YNCxFVs were obtained from three pools of *Cx. tritaeniorhynchus* collected in Qionghai, Hainan Province, China and they had 98.47%–98.85% nucleotide identity. This YNCxFV record is the first outside Yunnan Province. The phylogenetic analysis showed that the newly detected strains were close to those obtained from *Cx. tritaeniorhynchus* in Tengchong County, Yunnan Province in 2018. The partial *NS5* gene had 90.53%–100% nucleotide sequence identity with those for YNCxFV in GenBank.

Arbovirus Infection Rates in Mosquitoes

The arbovirus infection rates in the mosquitoes collected from the sentinel sites were estimated by bias-corrected MLE and MIR and are shown in **Table 2**. For JEV, the overall bias-corrected MLE values expressed as number of infected mosquitoes per 1,000 *Cx. tritaeniorhynchus* were 4.52 (0.80–14.64) and 0.35 (0.02–1.69) in Jinshan and Zaoyang, respectively. The GETV MLE per 1,000 individuals were 0.14 (0.04–0.37, *Cx. pipiens*), 3.72 (0.21–17.36, *An. sinensis*), and 0.75 (0.04–3.60, *Cx. tritaeniorhynchus*) in Hohhot, Zaoyang, and Qionghai, respectively. JEV and GETV were detected in samples collected in July and August 2018.

Bias-corrected MLE for the CHAOV, AeFV, and YNCxFV infection rates were 0.05 (0.00–0.22), 6.50 (0.38–30.94), and 2.22 (0.60–5.95) per 1,000 individuals in Hohhot, Zaoyang, and Qionghai, respectively. Bias-corrected MLE for the CxFV and QBV infection rates were in the ranges of 0.35–14.13 and 0.09–61.25, respectively.

TABLE 2 | Bias-corrected maximal likelihood estimations (MLE) and minimum infection rates (MIR) of mosquito-borne flaviviruses at various sentinel sites during the mosquito activity seasons of 2018.

Survey areas	Detected virus	host	No. individuals	No. PP	No. pools	Positive pool rate (%)	Bias Corrected MLE (95% *CI*)	MIR (95% *CI*)
Hohhot, Inner Mongolia	GETV	*Culex pipiens*	22049	3	225	1.33	0.14 (0.04–0.37)	0.14 (0.00–0.29)
	CHAOV	*Cx. pipiens*	22049	1	225	0.44	0.05 (0.00–0.22)	0.05 (0.00–0.13)
	CxFV	*Cx. pipiens*	22049	11	225	4.89	0.51 (0.27–0.88)	0.50 (0.20–0.79)
	QBV	*Cx. pipiens*	22049	2	225	0.89	0.09 (0.02–0.30)	0.09 (0.00–0.22)
	OcFV	*Cx. pipiens*	22049	2	225	0.89	0.09 (0.02–0.30)	0.09 (0.00–0.22)
Zaoyang, Hubei	GETV	*Anopheles sinensis*	273	1	28	3.57	3.60 (0.21–17.36)	3.66 (0.00–10.83)
	JEV	*Cx. tritaeniorhynchus*	2475	1	83	1.20	0.35 (0.02–1.69)	0.35 (0.00–1.83)
	QBV	*Cx. tritaeniorhynchus*	2475	2	83	2.41	0.70 (0.13–2.28)	0.70 (0.00–1.66)
	QBV	*An. sinensis*	273	2	28	7.14	7.12 (1.34–22.69)	7.33 (0.00–17.44)
	CxFV	*Cx. tritaeniorhynchus*	2475	1	83	1.20	0.35 (0.02–1.69)	0.35 (0.00–1.03)
	AeFV	*Aedes albopictus*	152	1	40	2.50	6.50 (0.38–30.94)	6.58 (0.00–19.43)
Jining, Shandong	QBV	*Cx. tritaeniorhynchus*	217	1	16	6.25	4.35 (0.27–20.66)	4.61 (0.00–13.62)
	QBV	*Cx. pipiens*	146	3	20	15.00	21.53 (5.89–57.53)	20.55 (0.00–43.56)
	CxFV	*Cx. tritaeniorhynchus*	217	1	16	6.25	4.38 (0.27–20.89)	4.61 (0.00–13.62)
	CxFV	*Cx. pipiens*	146	2	20	10.00	14.13 (2.59–46.19)	13.70 (0.00–32.55)
Jinshan, Shanghai	JEV	*Cx. tritaeniorhynchus*	452	2	69	2.90	4.48 (0.80–14.64)	4.42 (0.00–10.54)
	QBV	*Cx. tritaeniorhynchus*	452	2	69	2.90	16.27 (7.24–31.94)	15.49 (4.10–26.87)
Jing'an, Shanghai	CxFV	*Cx. pipiens*	208	1	69	1.45	4.93 (0.28–24.22)	4.81 (0.00–14.21)
Qionghai, Hainan	GETV	*Cx. tritaeniorhynchus*	1351	1	44	2.27	0.75 (0.04–3.60)	0.74 (0.00–2.18)
	YNCxFV	*Cx. tritaeniorhynchus*	1351	3	44	6.82	2.22 (0.60–5.95)	2.21 (0.00–4.71)
Sanya, Hainan	CxFV	*Cx. tritaeniorhynchus*	191	5	10	50.00	61.25 (21.50–248.10)	26.18 (3.53–48.82)

AeFV, Aedes flavivirus, CHAOV, Chaoyang virus; CI, confidence interval; CxFV, Culex flavivirus; GETV, Getah virus; HANKV, Hanko virus; JEV, Japanese encephalitis virus; gene, PP, positive pool, YNCxFV, Yunnan Culex flavivirus.

DISCUSSION

Climate change, biogeography, and human and avian behavior have been implicated in the spread of arbovirus. To the best of knowledge, our study is the first to record HANKV in China. Moreover, this work research reports for the first time the presence of AeFV, CHAOV, CxFV, QBV, and YNCxFV at multiple sentinel sites.

Hohhot, Inner Mongolia had a high mosquito density and the richest arbovirus diversity in this study. GETV, CxFV, HANKV, QBV, and CHAOV were detected at this location. Zaoyang was second to Hohhot in terms of mosquito abundance and it harbored JEV, GETV, AeFV, QBV, and CxFV. Tengchong in Yunnan Province was another sentinel site of the mosquito-borne disease surveillance in 2018. For a putative focal point of a JE epidemic has been found there, the results were published separately (Fang et al., 2021b).

JEV

As JEV naturally circulates, JE outbreaks sporadically occurred in China. The main reason for the observed increase in the number of reported JE cases between 2016 and 2018 was that the incidence rose in the subpopulation aged ≥ 40 years (Wu et al., 2020). Furthermore, the JE outbreaks occurred mainly in the north-central regions but not in the provinces wherein JEV was strongly endemic as of the early 2000s (Zheng et al., 2012).

A phylogenetic analysis of the *E* gene showed that JEV is divided into the GI–GV genotypes. GI is further subdivided into GI-a and GI-b. The latter gradually replaced GIII over the past 30 years (Schuh et al., 2014; Do et al., 2016). GI was more efficiently amplified than GIII in mosquito and porcine cells whereas the latter was more efficiently amplified in human rhabdomyosarcoma clones (Han et al., 2014). However, GI has been implicated in three recent human JE outbreaks. A few cases in the JE outbreak in India in 2010 were associated with GI but most involved GIII (Sarkar et al., 2012; Han et al., 2014). The JEV strain isolated from *Cx.* spp. during the 2010 JE outbreak in South Korea belonged to GI, although no human sequences were available (Seo et al., 2013). JEVs isolated from human and *Cx. tritaeniorhynchus* samples collected during the 2018 outbreak in Ningxia, China belonged to GI-b but no GIII was detected (Liu et al., 2020b). The phylogenetic tree based on the *E* gene demonstrated that the newly detected JEV strains gathered with the Ningxia strain and there were no amino acid substitutions on the E protein. High nucleotide identities were observed among the JEV strains obtained from Ningxia, Hubei, and Shanghai. Hence, frequent, long-range JEV transmission has occurred within China probably *via* migratory birds and windblown mosquitoes. The E proteins in the newly detected JEV strains differed from that in the live attenuated SA14-14-2 vaccine at E129 (Thr→Met), E222 (Ala→Ser), E327 (Ser→Thr), and E366 (Ala-Ser). No divergences were detected among them in terms of their key amino acid sites related to antigenicity. The E protein is a major constituent of the mature virion surface and is under constant selection pressure. It plays critical roles in infectivity and immunity (Schuh et al., 2014). It remains to be determined whether these mutations are associated with host adaptation. The vaccines currently used in China are derived from GIII. They confer protection against GI-GIV but not against GV (Cao et al., 2016). Thus, surveillance must be sustained to characterize circulating JEVs on a genetic level and avoid potential vaccine failure.

The JEV infection rate in *Cx. tritaeniorhynchus* from Jinshan District, Shanghai Municipality was 4.52/1,000 (0.80–14.64). The prevalence of West Nile virus (WNV) constituting an "epidemic risk" was > 5/1,000 mosquitoes (Tao et al., 2014). There were no data for JEV. Thus, considering the data of WNV, the Jinshan District is at potential risk of JEV epidemics.

As JEV constantly circulates in nature, it continues to pose a serious threat to public health. The vaccination program has altered the JEV endemic status and populations at risk in various areas. Hence, the JEV prevention strategy is suggested to be modified accordingly. Consistent immunization programs are required for children. Targeted JE vaccination should be administered to adults in areas to which JE is highly endemic. Domestic pigs must be relocated to communal facilities away from human habitation and irrigated rice production regions. The living conditions of people in remote rural areas require improvement to reduce the risk of viral spillover from the animal reservoir to the human population.

GETV

GETV was first isolated from *Cx. gelidus* in Malaysia in 1955 (Karabatsos, 1985). Phylogenetic analyses suggested that GETV emerged ~145 years ago and gradually evolved into four groups (Li et al., 2017b). GETV is active in Southeast Asia and Eurasia and transmitted by *Cx.* spp. to pigs and horses (Li et al., 2017b). There were frequent GETV outbreaks in Japan during the 1980s (Kamada et al., 1980). An inactivated whole-virus vaccine derived from MI-110 (Nisseiken, Japan) isolated in 1978 was developed. Two vaccine doses were administered to racehorses in Japan to prevent GETV infection (Bannai et al., 2015). However, unexpected GETV outbreaks occurred in vaccinated racehorses in Miho in 2014–2015 (Nemoto et al., 2015; Bannai et al., 2016). The reason was mainly for a single vaccine dose might not suffice to protect racehorses in areas with high GETV infection rates (Bannai et al., 2015; Bannai et al., 2017). There have been seven major GETV outbreaks. Five involved racehorses in Japan (Kamada et al., 1980; Bannai et al., 2015; Bannai et al., 2016), one affected horses in India (Brown and Timoney, 1998), and one concerned pigs in China in 2017 (Yang et al., 2018).

In China, GETV was first isolated from *Cx.* sp. in Hainan Province, in 1964 (Li et al., 1992). It was detected in mosquitoes from Hebei (2002), Shanghai (2005), Yunnan (2005), Gansu (2006, (Zhai et al., 2008)), Guizhou [2008, (Li et al., 2017b)], Hubei [2010, (Gao et al., 2015)], Shanxi [2012, (Zheng et al., 2015)], Sichuan [2012, (Li et al., 2017a)], Jilin [2017, (Liu et al., 2019)], and Inner Mongolia [2018, (Cheng et al., 2020)]. The first vertebrate GETV was isolated in Taiwan in 2002 (Chang et al., 2006). The number of cases of GETV-affected mammals has rapidly increased over the last decade. These included pigs in Henan [2011, (Zhou et al., 2018)], Hunan [2017, (Yang et al., 2018)], Anhui [2017 (available on GenBank but unpublished)], Sichuan [2018, (Jiang et al., 2019)], and Guangdong [2018, (Xing et al., 2020)], blue foxes in Shandong

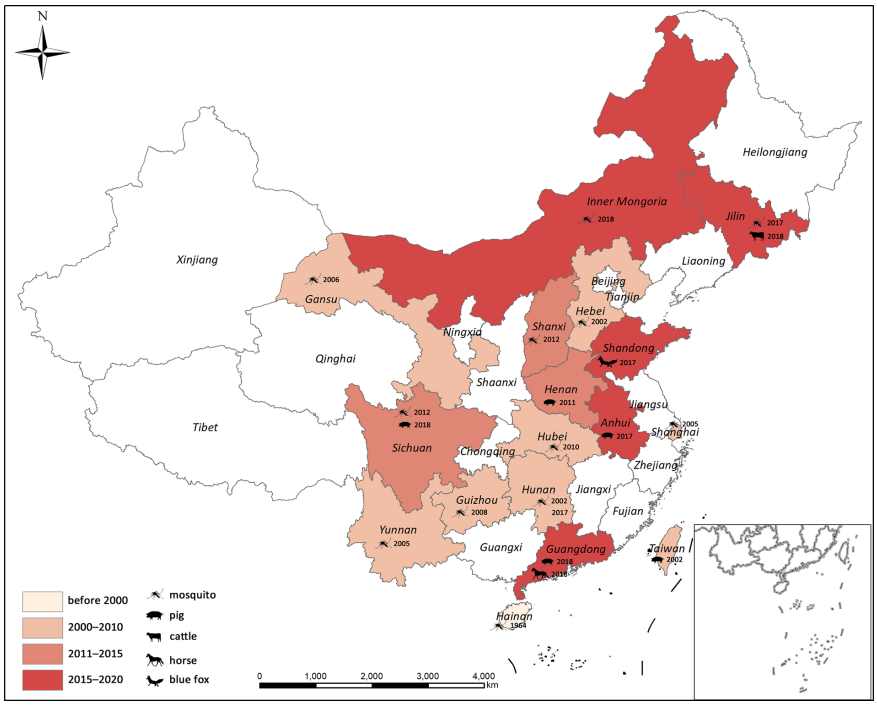

FIGURE 6 | Geographical distribution of GETV in China. Years correspond to the first GETV detection in each province.

[2017, (Shi et al., 2019)], beef cattle in Jilin [2018, (Liu et al., 2019)], and horses in Guangdong [2018, (Lu et al., 2019)]. A GETV outbreak occurred on a swine farm in Hunan Province in June and July 2017 and caused many fetal mummies, stillbirths, and piglet deaths (Yang et al., 2018). In contrast, mosquito-borne GETV has not yet been recorded in Hunan. Sudden onset of fever, caused by GETV, was reported for racehorses at a training center in Guangdong in 2018, while no GETV infection was detected in archived equine serum samples collected between 2014 and 2018 (Lu et al., 2019). To date, GETV records have covered 17 provinces in China (**Figure 6**) and most of them were reported within the last decade. Several serological surveys revealed widespread GETV occurrence in humans and domestic animals in the Asia-Pacific region (Fukunaga et al., 2000; Liang et al., 2010; Li et al., 2018). Frequent GETV detection in various vertebrates and mosquitoes over a wide geographical area suggests that this virus may cause an epidemic in China. Thus, it is important to conduct research on the molecular evolution and infection rate dynamics of GETV in its vectors and natural hosts.

The GETV *E2* phylogenetic tree revealed that vector and amplifying host sequences were in close proximity to each other. Thus, there is a potential risk of GETV epidemics in domestic animals. In addition, the GETV strains collected within the same province were distributed in two distinct Group III clusters. For this reason, GETV is frequently transmitted in China. The GETV infection rates in *Cx. tritaeniorhynchus* were 2.31/1,000 and 1.60/1,000 when the pathogen was detected in blue fox (Shi et al., 2019) and beef cattle (Liu et al., 2019), respectively. In Zaoyang, the GETV infection rate was 3.60/1,000 *An. Sinensis.* Inner Mongolia has the largest grassland in China and animal husbandry is a major industry there. This region raises domestic livestock such as cattle, sheep, swine, and horses. It is at high risk of a GETV epidemic as it has a high concentration of GETV vectors and host animals. All three GETV strains from Inner Mongolia were observed in *Cx. pipiens*. This mosquito species breeds in dirty water and is common in urban and suburban areas. Hence, *Cx. pipiens* harboring GETV intensify its potential threat to the public health.

GETV is prevalent and widespread in China. However, its harm to livestock may have been minimized as most mammalian GETV cases are subclinical. Serious clinical GETV symptoms and death have occurred in piglets (Yang et al., 2018) and ponies (Bannai et al., 2015; Bannai et al., 2016). The presence of GETV on pig breeding farms adjacent to horse and cattle farms merits close attention as pigs may amplify GETV in nature (Kumanomido et al., 1988). In addition, it is urgently required to develop a universally applicable vaccine for the prevention and control of GETV in domestic animals in China.

ISFVs

The ISFVs detected in the present study included AeFV, CHAOV, CxFV, HANKV, QBV, and YNCxFV and most of them were new local records. The CHAOV sister to Lammi virus (LAMV) clustered with the mosquito-borne human flavivirus pathogens and were distant from the ISFV clade (**Figure 2**). CHAOV was first isolated from *Ae. vexans* in Liaoning, China in 2008 (Wang et al., 2009). It was then detected in *Ae. vexans*, *Ae. albopictus*, *Cx. pipiens*, and *Ar. subalbatus* in South Korea during vector surveillance between 2008 and 2011 (Takhampunya et al., 2014). Here, it was also found in Inner Mongolia. The three

CHAOV records ranged from 35°N to 42°N. Extremely low sequence diversity between the CHAOV strains and the whole genome available in GenBank suggests that CHAOV only recently spread to Northeast Asia, has a brief history, and is evolving slowly. CHAOV may only replicate in mosquito vectors and not in mammalian or avian hosts (Lee et al., 2013). Similar pathological traits were reported for LAMV (Huhtamo et al., 2009), Nounane (NOUV) (Junglen et al., 2009), and Marisma mosquito (MMV) (Vazquez et al., 2012) viruses infecting various cell lines. It is unknown why CHAOV, LAMV, Donggang virus, NOUV, and MMV phylogenetically resemble mosquito-borne zoonotic flaviviruses but have no recognized vertebrate hosts.

Phylogenetic analysis of the CxFV *E* gene demonstrated that the newly detected CxFVs belong to the Asia/USA genotype but clustered in two lineages (**Figure 5**). The Shanghai and Jining strains were close to the Shanghai strain detected in 2016. The Inner Mongolia strains were clustered and phylogenetically distant from the others. The CxFV *E* tree (**Figure 5**) revealed that the Asia/USA genotype was localized mainly above 30°N latitude. The zone between 30°N and 32°N is the boundary of *Cx. pipiens* and *Cx. quinquefasciatus* in China (Lu, 1997). The Africa/Caribbean/Latin American genotype was found in *Cx. quinquefasciatus* from Mexico, Brazil, and Saudi Arabia. CxFV has not yet been isolated from *Cx. quinquefasciatus* in mainland China. Here, CxFV was not found in *Cx. quinquefasciatus* collected from Hainan or Yunnan Province. QBV was first isolated from samples collected in Vietnam in 2002 (Crabtree et al., 2009). It was then detected in mosquito samples collected from Chongming Island in Shanghai Municipality in 2016 (Fang et al., 2018). Here, QBV was observed at Jining, Zaoyang, Sanya City, Jinshan, and Hohhot. Hence, it is widespread in China. The primary QBV vector is *Cx. tritaeniorhynchus*. In this study, it was also detected in *An. sinensis* and *Cx. pipiens*. In previous studies (Zuo et al., 2014; Fang et al., 2021b), YNCxFV was restricted to Yunnan Province. In the present study, it was also detected in *Cx. tritaeniorhynchus* from Qionghai, Hainan Province. The taxonomic value of YNCxFV is debatable as the nucleotide identity between YNCxFV and QBV was only 83% (Zuo et al., 2014). The threshold for members species of *Flavivirus* was 84% (Kuno et al., 1998). For the partial *NS5* gene, the lowest intraspecies QBV identity was 87.50%. The interspecies similarity between QBVs and YNCxFVs was in the range of 82.40–87.88%. In the *NS5* phylogenetic tree (**Figure 2**), the YNCxFV sequences formed a sister lineage to the group containing the QBV sequences. Moreover, both species overlapped in terms of geographic distribution and mosquito host. Thus, it remains to be established *via* cytopathy and neutralization tests whether YNCxFV is an independent ISFV species. AeFV has been widespread in Japan, Thailand, USA, Peru, and Italy (Blitvich and Firth, 2015). In China, it was first detected in samples collected from Shanghai in 2016 (Fang et al., 2018). It was then observed in Yunnan (Fang et al., 2021b) and Hubei in 2018. *Aedes albopictus* is the primary vector of AeFV. HANKVs were distributed in Finland, Spain, Italy, and Portugal (Blitvich and Firth, 2015). The present study was the first to report HANKVs in *Cx. pipiens* in Asia. There is broad genetic diversity among HANKV strains (83.52%–98.09%) as they have a wide geographic span. The wide dispersion and host range of ISFVs support the hypothesis that ISFV transmission in sympatric species may be linked to a common infection source such as food (Calzolari et al., 2016).

The main limitation of our study was that no mosquito virus homogenate supernatants were cultivated in mosquito or vertebrate cell lines. The low viral titers measured in the mosquito homogenates may have skewed the pathogen detection data. Consequently, the real natural arbovirus infection rates may have been underestimated. In future work, we will try to isolate them and conduct further analysis.

In conclusion, monitoring the presence of viral pathogens in mosquitoes can forecast the risks of arbovirus epidemics. The newly detected JEV strains and the Ningxia strain were 100% identical in terms of their E protein at the amino acid level. The JEV infection rate in Jinshan District approached epidemic proportions. GETV was prevalent in more than half the provinces of China. Mammalian GETV infection and outbreaks have been reported in recent years. Hence, attention must be paid to the putative threat that GETV could pose to animal and human health. Reports of ISFV cases have dramatically increased in recent decades. It is now known that ISFVs have wide geographic and host ranges. Though it appears that ISFVs can only replicate in mosquito cells, their possible roles in mammalian pathogenesis cannot be ruled out. It also remains to be determined whether ISFV-infected mosquitoes escape vector competence or pathogenic flavivirus superinfection can occur. The present study showed that wide-ranging, systematic, and continuous monitoring of mosquito-borne circulating viruses is urgently needed in China. This surveillance program could elucidate viral diversity, geographic distribution, evolution, genotype shift, and infection rates. It would also facilitate accurate and timely estimates of actual pathogen burdens and predict the prevalence of dengue and other emerging and existing mosquito-borne pathogens.

DATA AVAILABILITY STATEMENT

The original contributions presented in the study are included in the article/**Supplementary Material**. Further inquiries can be directed to the corresponding author.

AUTHOR CONTRIBUTIONS

YF: conceived the study, performed molecular work, data analysis, and write the manuscript. WZ: performed molecular work. J-BX: drew map of mosquito collection sites for the virus detection. YZ: conceived the study and performed data analysis. All authors contributed to the article and approved the submitted version.

FUNDING

This research was funded by "The Special Foundation of Basic Science and Technology Resources Survey of Ministry of Science

and Technology of China (No. 2017FY101203)", "The Fifth Round of Three-Year Public Health Action Plan of Shanghai (No. GWV-10.1-XK13)", and "The Project of Basic Platform of National Science and Technology Resources of the Ministry of Sciences and Technology of China (No. TDRC-2019-194-30)".

ACKNOWLEDGMENTS

The authors thank the staff of Zaoyang County, Qionghai County, Sanya City, Jinshan District, Jing'an District, Hubei Provincial, Hainan Provincial Centers for Disease Control and Prevention, Shandong Institute of Parasitic Diseases, and Inner Mongolia Autonomous Region Comprehensive Center for Disease Control and Prevention, China.

SUPPLEMENTARY MATERIAL

The Supplementary Material for this article can be found online at: https://www.frontiersin.org/articles/10.3389/fcimb.2021.640993/full#supplementary-material

REFERENCES

Bannai, H., Nemoto, M., Ochi, A., Kikuchi, T., Kobayashi, M., Tsujimura, K., et al. (2015). Epizootiological investigation of Getah virus infection among racehorses in Japan in 2014. *J. Clin. Microbiol.* 53, 2286–2291. doi: 10.1128/JCM.00550-15

Bannai, H., Ochi, A., Nemoto, M., Tsujimura, K., Yamanaka, T., and Kondo, T. (2016). A 2015 outbreak of Getah virus infection occurring among Japanese racehorses sequentially to an outbreak in 2014 at the same site. *BMC Vet. Res.* 12, 98. doi: 10.1186/s12917-016-0741-5

Bannai, H., Nemoto, M., Niwa, H., Murakami, S., Tsujimura, K., Yamanaka, T., et al. (2017). Geospatial and temporal associations of Getah virus circulation among pigs and horses around the perimeter of outbreaks in Japanese racehorses in 2014 and 2015. *BMC Vet. Res.* 13, 187. doi: 10.1186/s12917-017-1112-6

Biggerstaff, B. J. (2006). PooledInfRate, version 3.0: a Microsoft® Excel® add-in to compute prevalence estimates from pooled samples. *Fort Collins CO: CDC.*

Blitvich, B. J., and Firth, A. E. (2015). Insect-specific flaviviruses: a systematic review of their discovery, host range, mode of transmission, superinfection exclusion potential and genomic organization. *Viruses* 7, 1927–1959. doi: 10.3390/v7041927

Brown, C. M., and Timoney, P. J. (1998). Getah virus infection of Indian horses. *Trop. Anim. Health Prod.* 30, 241–252. doi: 10.1023/A:1005079229232

Calzolari, M., Ze-Ze, L., Vazquez, A., Sanchez Seco, M. P., Amaro, F., and Dottori, M. (2016). Insect-specific flaviviruses, a worldwide widespread group of viruses only detected in insects. *Infect. Genet. Evol.* 40, 381–388. doi: 10.1016/j.meegid.2015.07.032

Cao, L., Fu, S., Gao, X., Li, M., Cui, S., Li, X., et al. (2016). Low protective efficacy of the current Japanese encephalitis vaccine against the emerging genotype 5 Japanese encephalitis virus. *PloS Negl. Trop. Dis.* 10, e0004686. doi: 10.1371/journal.pntd.0004686

Cao, L., Fu, S., Lu, Z., Tang, C., Gao, X., Li, X., et al. (2019). Detection of West Nile Virus Infection in Viral Encephalitis Cases, China. *Vector Borne Zoonotic Dis.* 19, 45–50. doi: 10.1089/vbz.2018.2275

Chang, C., Huang, C., Huang, T., Deng, M., Jong, M., and Wang, F. (2006). Isolation and characterization of a Sagiyama virus from domestic pigs. *J. Vet. Diagn. Invest.* 18, 156–161. doi: 10.1177/104063870601800203

Cheng, R., Nan, X., Fan, N., Fu, S., Si, X., Zhang, L., et al. (2020). Emerging of Japanese encephalitis virus and Getah virus from specimen of mosquitoes in Inner Mongolia Autonomous Region. *Chin. J. Epidemiol.* 41, 571–579.

Crabtree, M. B., Nga, P. T., and Miller, B. R. (2009). Isolation and characterization of a new mosquito flavivirus, Quang Binh virus, from Vietnam. *Arch. Virol.* 154, 857–860. doi: 10.1007/s00705-009-0373-1

Do, L. P., Bui, T. M., and Phan, N. T. (2016). Mechanism of Japanese encephalitis virus genotypes replacement based on human, porcine and mosquito-originated cell lines model. *Asian Pac. J. Trop. Med.* 9, 333–336. doi: 10.1016/j.apjtm.2016.03.007

Fang, Y., Shi, W., and Zhang, Y. (2017). Molecular phylogeny of *Anopheles hyrcanus* group members based on ITS2 rDNA. *Parasitol. Vectors* 10, 417. doi: 10.1186/s13071-017-2351-x

Fang, Y., Zhang, Y., Zhou, Z., Shi, W., Xia, S., Li, Y., et al. (2018). Co-circulation of Aedes flavivirus, Culex flavivirus, and Quang Binh virus, in Shanghai, China. *Infect. Dis. Poverty* 7, 75. doi: 10.1186/s40249-018-0457-9

Fang, Y., Zhang, Y., Zhou, Z. B., Xia, S., Shi, W. Q., Xue, J. B., et al. (2019). New strains of Japanese encephalitis virus circulating in Shanghai, China after a ten-year hiatus in local mosquito surveillance. *Parasitol. Vectors* 12, 22. doi: 10.1186/s13071-018-3267-9

Fang, Y., Ernest, T., Xue, J., Zhang, Y., Zhou, X., and Khater, E. (2021a). Detection of DENV-2 and insect-specific flaviviruses in mosquitoes collected from Jeddah, Saudi Arabia. *Front. Cell Infect. Microbiol.* 11, 626368. doi: 10.3389/fcimb.2021.626368

Fang, Y., Li, X.-S., Zhang, W., Xue, J.-B., Wang, J.-Z., Yin, S.-Q., et al. (2021b). A potential epidemic focus of Japanese encephalitis at the China-Myanmar border. *Infect. Dis. Poverty*.

Feng, J., Tu, H., Zhang, L., Xia, Z., and Zhou, S. (2020). Vital Surveillances: Imported malaria cases–China–2018. *China CDC Wkly.* 2, 277–284. doi: 10.46234/ccdcw2020.072

Fukunaga, Y., Kumanomido, T., and Kamada, M. (2000). Getah virus as an equine pathogen. *Vet. Clin. North Am. Equine Pract.* 16, 605–617. doi: 10.1016/S0749-0739(17)30099-8

Gao, X., Liu, H., Wang, H., Fu, S., Guo, Z., and Liang, G. (2013). Southernmost Asia is the source of Japanese encephalitis virus (genotype 1) diversity from which the viruses disperse and evolve throughout Asia. *PloS Negl. Trop. Dis.* 7, e2459. doi: 10.1371/journal.pntd.0002459

Gao, X., Fu, S., Zou, W., Peng, Y., Liu, H., and Cao, Y. (2015). Investigation of arbovirus in some areas of Hubei Provinc. *Chin. J. Vector Biol. Control* 26, 133–136.

Guo, Y., Wu, H., Liu, X., Yue, Y., Ren, D., Zhao, N., et al. (2019). National vectors surveillance report on mosquitoes in China. *Chin. J. Vector Biol. Control* 30, 128–133.

Han, N., Adams, J., Chen, P., Guo, Z. Y., Zhong, X. F., Fang, W., et al. (2014). Comparison of genotypes I and III in Japanese encephalitis virus reveals distinct differences in their genetic and host diversity. *J. Virol.* 88, 11469–11479. doi: 10.1128/JVI.02050-14

Han, L., Yu, X., Guan, S., ZHou, W., Wang, Y., Zheng, L., et al. (2018). The epidemiological and clinical features of 403 cases with dengue fever in Fuzhou City. *Chin. J. Infect. Dis.* 36, 411–416.

Hoffmann, P. R., Woodrow, R. J., Calimlim, P. S., Sciulli, R. H., Effler, P. V., Miyamoto, V., et al. (2004). West Nile virus surveillance: A simple method for verifying the integrity of RNA in mosquito (Diptera: Culicidae) pools. *J. Med. Entomol.* 41, 731–735. doi: 10.1603/0022-2585-41.4.731

Hu, Q., Chen, B., Zhu, Z., Tian, J., Zhou, Y., Zhang, X., et al. (2013). Recurrence of Japanese encephalitis epidemic in Wuhan, China–2010. *PloS One* 8, e52687. doi: 10.1371/journal.pone.0052687

Huhtamo, E., Putkuri, N., Kurkela, S., Manni, T., Vaheri, A., Vapalahti, O., et al. (2009). Characterization of a novel flavivirus from mosquitoes in northern europe that is related to mosquito-borne flaviviruses of the tropics. *J. Virol.* 83, 9532–9540. doi: 10.1128/JVI.00529-09

Jiang, C., Li, F., Zeng, Y., Peng, K., Zhang, R., Du, P., et al. (2019). Isolation, identification and genetic evolution analysis of pig-derived Getah virus from Sichuan, China. *Chin. J. Zoonoses* 35, 805–813.

Junglen, S., Kopp, A., Kurth, A., Pauli, G., Ellerbrok, H., and Leendertz, F. H. (2009). A new flavivirus and a new vector: characterization of a novel flavivirus isolated from uranotaenia mosquitoes from a tropical rain forest. *J. Virol.* 83, 4462–4468. doi: 10.1128/JVI.00014-09

Kamada, M., Ando, Y., Fukunaga, Y., Kumanomido, T., Imagawa, H., Wada, R., et al. (1980). Equine Getah virus infection: isolation of the virus from

racehorses during an enzootic in Japan. *Am. J. Trop. Med. Hyg.* 29, 984–988. doi: 10.4269/ajtmh.1980.29.984

Karabatsos, N. (1985). *International catalogue of arboviruses, including certain other viruses of vertebrates* (San Antonio, Texas: American Society of Tropical Medicine and Hygiene).

Kimura, M. (1980). A simple method for estimating evolutionary rates of base substitutions through comparative studies of nucleotide sequences. *J. Mol. Evol.* 16, 111–120. doi: 10.1007/BF01731581

Kumanomido, T., Wada, R., Kanemaru, T., Kamada, M., Hirasawa, K., and Akiyama, Y. (1988). Clinical and virological observations on swine experimentally infected with Getah virus. *Vet. Microbiol.* 16, 295–301. doi: 10.1016/0378-1135(88)90033-8

Kumar, S., Stecher, G., and Tamura, K. (2016). MEGA7: molecular evolutionary genetics analysis version 7.0 for bigger datasets. *Mol. Biol. Evol.* 33, 1870–1874. doi: 10.1093/molbev/msw054

Kuno, G., Chang, G. J., Tsuchiya, K. R., Karabatsos, N., and Cropp, C. B. (1998). Phylogeny of the genus Flavivirus. *J. Virol.* 72, 73–83. doi: 10.1128/JVI.72.1.73-83.1998

Larkin, M. A., Blackshields, G., Brown, N. P., Chenna, R., McGettigan, P. A., McWilliam, H., et al. (2007). Clustal W and Clustal X version 2.0. *Bioinformatics* 23, 2947–2948. doi: 10.1093/bioinformatics/btm404

Lee, J. S., Grubaugh, N. D., Kondig, J. P., Turell, M. J., Kim, H., Klein, T. A., et al. (2013). Isolation and genomic characterization of Chaoyang virus strain ROK144 from Aedes vexans nipponii from the Republic of Korea. *Virology* 435, 220–224. doi: 10.1016/j.virol.2012.10.020

Li, X. D., Qiu, F. X., Yang, H., Rao, Y. N., and Calisher, C. H. (1992). Isolation of Getah virus from mosquitos collected on Hainan Island, China, and results of a serosurvey. *Southeast Asian J. Trop. Med. Public Health* 23, 730–734.

Li, W., Pan, M., Zhou, X., Lin, S., Liu, X., Fu, S., et al. (2017a). First isolatin and identification of Getah virus SC1210 in Sichuan. *Chin. J. Exp. Clin. Virol.* 31, 2–7.

Li, Y., Liu, H., Fu, S., Li, X., Guo, X., Li, M., et al. (2017b). From discovery to spread: The evolution and phylogeny of Getah virus. *Infect. Genet. Evol.* 55, 48–55. doi: 10.1016/j.meegid.2017.08.016

Li, Y., Fu, S., Guo, X., Li, X., Li, M., Wang, L., et al. (2018). Serological survey of Getah virus in domestic animals in Yunnan Province, China. *Vector Borne Zoonotic Dis.* 19, 59–61. doi: 10.1089/vbz.2018.2273

Li, X., Gao, X., Fu, S., Wang, H., Lu, Z., He, Y., et al. (2019). An outbreak of Japanese encephalitis in adults in Northern China: A population-based study. *Vector Borne Zoonotic Dis.* 19, 26–34. doi: 10.1089/vbz.2017.2251

Liang, Y., Zhang, L., Liu, Y., Dong, Y., and Wang, Z. (2010). Serological survey of Getah virus among healthy population in She county, Hebei Province, China. *Hebei Med. J.* 32, 3079–3080.

Liu, H., Zhang, X., Li, L., Shi, N., Sun, X., Liu, Q., et al. (2019). First isolation and characterization of Getah virus from cattle in northeastern China. *BMC Vet. Res.* 15, 320. doi: 10.1186/s12917-019-2061-z

Liu, K., Hou, X., Ren, Z., Lowe, R., Wang, Y., Li, R., et al. (2020a). Climate factors and the East Asian summer monsoon may drive large outbreaks of dengue in China. *Environ. Res.* 183, 109190. doi: 10.1016/j.envres.2020.109190

Liu, W., Fu, S., Ma, X., Chen, X., Wu, D., Zhou, L., et al. (2020b). An outbreak of Japanese encephalitis caused by genotype Ib Japanese encephalitis virus in China: A laboratory and field investigation. *PloS Negl. Trop. Dis.* 14, e0008312. doi: 10.1371/journal.pntd.0008312

Liu, Q. (2020). Dengue fever in China: new epidemical trend, challenges and strategies for prevention and control. *Chin. J. Vector Biol. Control* 31, 1–6.

Lu, G., Ou, J., Ji, J., Ren, Z., Hu, X., Wang, C., et al. (2019). Emergence of Getah virus infection in horse with fever in China. *Front. Microbiol.* 10, 1416. doi: 10.3389/fmicb.2019.01416

Lu, B. (1997). *Fauna Sinica. Insect Vol. 8, Diptera: Culicidae 1* (Beijing, China: Science Press).

Masetti, A., Rivasi, F., and Bellini, R. (2008). Mosquito-based survey for the detection of flaviviruses and filarial nematodes in *Aedes albopictus* and other anthropophilic mosquitoes collected in northern Italy. *New Microbiol.* 31, 457–465.

Nemoto, M., Bannai, H., Tsujimura, K., Kobayashi, M., Kikuchi, T., Yamanaka, T., et al. (2015). Getah Virus Infection among Racehorses, Japa. *Emerg. Infect. Dis.* 21, 883. doi: 10.3201/eid2105.141975

Ronquist, F., Teslenko, M., van der Mark, P., Ayres, D. L., Darling, A., Hohna, S., et al. (2012). MrBayes 3.2: efficient Bayesian phylogenetic inference and model choice across a large model space. *Syst. Biol.* 61, 539–542. doi: 10.1093/sysbio/sys029

Saiyasombat, R., Dorman, K. S., Garcia-Rejon, J. E., Lorono-Pino, M. A., Farfan-Ale, J. A., and Blitvich, B. J. (2010). Isolation and sequence analysis of Culex flavivirus from *Culex interrogator* and *Culex quinquefasciatus* in the Yucatan Peninsula of Mexico. *Comp. Immunol. Microbiol. Infect. Dis.* 155, 983–986. doi: 10.1007/s00705-010-0665-5

Sarkar, A., Taraphdar, D., Mukhopadhyay, S. K., Chakrabarti, S., and Chatterjee, S. (2012). Molecular evidence for the occurrence of Japanese encephalitis virus genotype I and III infection associated with acute encephalitis in patients of West Bengal, Indi. *Virol. J.* 9, 271. doi: 10.1186/1743-422X-9-271

Schuh, A. J., Ward, M. J., Brown, A. J. L., and Barrett, A. D. T. (2014). Dynamics of the emergence and establishment of a newly dominant genotype of Japanese encephalitis virus throughout Asia. *J. Virol.* 88, 4522–4532. doi: 10.1128/JVI.02686-13

Seo, H. J., Kim, H. C., Klein, T. A., Ramey, A. M., Lee, J. H., Kyung, S. G., et al. (2013). Molecular detection and genotyping of Japanese encephalitis virus in mosquitoes during a 2010 outbreak in the Republic of Korea. *PloS One* 8, e55165. doi: 10.1371/journal.pone.0055165

Shen, X., Liu, X., Ren, Y., Shen, Q., Liu, X., and Zhang, S. (2013). The multivariate similarity clustering analysis and geographical division of insect fauna in China. *Acta Entomol. Sin.* 56, 896–906.

Shi, N., Li, L.-X., Lu, R.-G., Yan, X.-J., and Liu, H. (2019). Highly Pathogenic Swine Getah Virus in Blue Foxes, Eastern China. *Emerg. Infect. Dis.* 25, 1252–1254. doi: 10.3201/eid2506.181983

Song, S., Li, Y., Fu, S., Liu, H., Li, X., Gao, X., et al. (2017). Could zika virus emerge in Mainland China? Virus isolation from nature in *Culex quinquefasciatu*. *Emerg. Microbes Infect.* 6, e93. doi: 10.1038/emi.2017.80

Takhampunya, R., Kim, H. C., Tippayachai, B., Lee, D., Lee, W., Chong, S., et al. (2014). Distribution and Mosquito Hosts of Chaoyang Virus, a Newly Reported Flavivirus from the Republic of Kore–2011. *J. Med. Entomol.* 51, 464–474. doi: 10.1603/ME13033

Tao, Z., Liu, G., Wang, M., Wang, H., Lin, X., Song, L., et al. (2014). Molecular epidemiology of Japanese encephalitis virus in mosquitoes during an outbreak in China. *Sci. Rep.* 4, 4908. doi: 10.1038/srep04908

Tian, Y., and Yang, L. (2019). Epidemiological situation of Japanese encephalitis in Qinzhou District, Tianshui, Gansu Province, during 2016–2018. *Chin. J. Vector Biol. Control* 30, 232.

Vazquez, A., Sanchezseco, M. P., Palacios, G., Molero, F., Reyes, N., Ruiz, S., et al. (2012). Novel Flaviviruses Detected in Different Species of Mosquitoes in Spain. *Vector Borne Zoonotic Dis.* 12, 223–229. doi: 10.1089/vbz.2011.0687

Wang, H., Takasaki, T., Fu, S., Sun, X., Zhang, H., Wang, Z., et al. (2007). Molecular epidemiological analysis of Japanese encephalitis virus in China. *J. Gen. Virol.* 88, 885–894. doi: 10.1099/vir.0.82185-0

Wang, Z., An, S., Wang, Y., Han, Y., and Guo, J. (2009). A new virus of flavivirus Chaoyang virus isolated in Liaoning Province. *Chin. J. Public Health* 25, 769–772.

Wilgenbusch, J. C., and Swofford, D. (2003). Inferring evolutionary trees with PAUP*. *Curr. Protoc. Bioinf.* 6, 6.4. doi: 10.1002/0471250953.bi0604s00

Wu, D., Wu, J., Zhang, Q., Zhong, H., Ke, C., Deng, X., et al. (2012). Chikungunya outbreak in Guangdong Province, China. *Emerg. Infect. Dis.* 18, 493. doi: 10.3201/eid1803.110034

Wu, H., Lu, L., Meng, F., Guo, Y., and Liu, Q. (2017). Reports on national surveillance of mosquitoes in China-2015. *Chin. J. Vector Biol. Control* 28, 409–415.

Wu, D., Yin, Z., Li, J., Shi, W., Wang, H., Fu, S., et al. (2020). Epidemiology of Japanese encephalitis in China–2018. *Chin. J. Vaccines Immun.* 26, 1–4.

Xiao, J., He, J., Deng, A., Lin, H., Song, T., Peng, Z., et al. (2016). Characterizing a large outbreak of dengue fever in Guangdong Province, China. *Infect. Dis. Poverty* 5, 44. doi: 10.1186/s40249-016-0131-z

Xing, C., Jiang, J., Lu, Z., Mi, S., He, B., Tu, C., et al. (2020). Isolation and characterization of Getah virus from pigs in Guangdong province of China. *Transbound Emerg. Dis.* 00, 1–5. doi: 10.1111/tbed.13567

Yan, H., Ding, Z., Yan, J., Yao, W., Pan, J., Yang, Z., et al. (2018). Epidemiological characterization of the 2017 dengue outbreak in Zhejiang, China and molecular characterization of the viruses. *Front. Cell Infect. Microbiol.* 8, 216. doi: 10.3389/fcimb.2018.00216

Yang, T., Li, R., Hu, Y., Yang, L., Zhao, D., Du, L., et al. (2018). An outbreak of Getah virus infection among pigs in China. *Transbound Emerg. Dis.* 65, 632–637. doi: 10.1111/tbed.12867

Zhai, Y., Wang, H., Sun, X., Fu, S., Wang, H., Attoui, H., et al. (2008). Complete sequence characterization of isolates of Getah virus (genus Alphavirus, family Togaviridae) from China. *J. Gen. Virol.* 89, 1446–1456. doi: 10.1099/vir.0.83607-0

Zhang, F., Zhao, H., Li, L., Jiang, T., Hong, W., Wang, J., et al. (2014). Severe dengue outbreak in Yunnan, China. *Int. J. Infect. Dis.* 27, 4–6. doi: 10.1016/j.ijid.2014.03.1392

Zheng, Y., Li, M., Wang, H., and Liang, G. (2012). Japanese encephalitis and Japanese encephalitis virus in Mainland China. *Rev. Med. Virol.* 22, 301–322. doi: 10.1002/rmv.1710

Zheng, Y., Cao, Y., Fu, S., Cheng, J., Zhao, J., Dai, P., et al. (2015). Isolation and identification of mosquito-borne arboviruses in Yuncheng city, Shanxi provinc. *Chin. J. Epidemiol.* 2015, 368–373.

Zhou, F., Cui, D., Wang, A., Wang, X., Chang, H., Chen, L., et al. (2018). Isolation and identification of the first Getah virus (GETV) strain HNJZ-S1 from clinically suspected PRRS case of pig herd in Henan Province, China. *Chin. J. Virol.* 34, 59–66.

Zuo, S., Zhao, Q., Guo, X., Zhou, H., Cao, W., and Zhang, J. (2014). Detection of Quang Binh virus from mosquitoes in China. *Virus Res.* 180, 31–38. doi: 10.1016/j.virusres.2013.12.005

Conflict of Interest: The authors declare that the research was conducted in the absence of any commercial or financial relationships that could be construed as a potential conflict of interest.

frontiers in Medicine

ORIGINAL RESEARCH
published: 15 March 2021
doi: 10.3389/fmed.2021.602442

Assessment of Malaria Microscopy Competency at Primary Health Institutions in the Chongqing Municipality

Luo Fei, Zhou Shuang, Yuan Yi, Li Shan-Shan, Tan Yan*, Xu Jing-Ru and Zhou Yang*

Chongqing Center for Disease Control and Prevention, Chongqing, China

Background: In April 2019, Chongqing passed the national malaria elimination assessment. However, around 30 imported malaria cases are still being reported every year, and *Anopheles sinensis* was widely distributed in Chongqing, meaning the risk of malaria resurgence still exists. Early diagnosis and treatment for malaria cases are effective measures to prevent malaria resurgence. The primary health institutions are the first station where potential malaria cases may seek treatment. The competency with which primary health institutions diagnose malaria will directly affect the timeliness of malaria diagnosis. Nowadays, most primary health institutions in Chongqing use microscopy to confirm malaria cases. This study assessed the microscopy competence of primary health institutions, studied and analyzed the results, and provided a scientific basis for malaria prevention and control after malaria elimination in Chongqing.

Methods: According to the stratified sampling principle, four plasmodium microscopy technicians (156 in total) were selected from each of the 39 districts/counties of Chongqing to test the plasmodium microscopy competence. Descriptive statistical analysis, correlation analysis, spatial self-correlation analysis, and ROC curve analysis were carried out on the test results.

Result: The average of the technicians' test scores was 4.33 ± 0.47 (min: 3, mid: 4.5, max: 5); The spatial clustering of the scores was significant (MoranI $= 0.338$, $Z = 3.618$, $P < 0.01$). The test scores were positively correlated with the "level of work institutions" ($R = 0.21$, $P < 0.01$) but were negatively correlated with "age" ($R = -0.31$, $P < 0.01$). The highest Sensitivity of the technicians' microscopy was in qualitative diagnosis (98.92%, CI: 98.00–99.69%). The Delong's test showed that the diagnostic efficiency of the technicians' microscopy to *P. falciparum* was the best ($P < 0.01$), however to *P. ovale* was the worst ($P < 0.01$).

Conclusion: The microscopy technicians in primary health institutions in Chongqing have good microscopy competency in qualitative diagnosis, but there were deficiencies in the identification of plasmodium species. Township level health institutions in Central China have weaker microscopy than those in other areas.

Keywords: malaria, microscopy, competency assessment of malaria microscopy, plasmodium species identification, Chongqing municipality

OPEN ACCESS

Edited by:
Jun Feng,
National Institute of Parasitic Diseases, China

Reviewed by:
Mengyuan Lyu,
Sichuan University, China
Yang Liu,
Sichuan Center for Disease Control and Prevention, China
Shaosen Zhang,
Lilly, China

****Correspondence:***
Tan Yan
275488121@qq.com
Zhou Shuang
15264835@qq.com

Specialty section:
This article was submitted to Infectious Diseases - Surveillance, Prevention and Treatment, a section of the journal Frontiers in Medicine

Received: *03 September 2020*
Accepted: *04 February 2021*
Published: *15 March 2021*

Citation:
Fei L, Shuang Z, Yi Y, Shan-Shan L, Yan T, Jing-Ru X and Yang Z (2021) Assessment of Malaria Microscopy Competency at Primary Health Institutions in the Chongqing Municipality. Front. Med. 8:602442. doi: 10.3389/fmed.2021.602442

BACKGROUND

Malaria is one of the most serious parasitic diseases. According to WHO, there were 2.28 million malaria cases and 405,000 deaths worldwide in 2018, and 93% of the cases were in Africa (1). In 2019, a total of 2,674 malaria cases were reported in China, including 19 deaths. The median interval from onset to diagnosis was 2 days (2).

Chongqing has launched the Malaria Elimination Plan in 2010 which includes implementation of comprehensive malaria control and prevention activities (3). After 10 years of implementation, Chongqing passed the national malaria elimination assessment in April 2019. In the last decade, Chongqing has reported about 30 imported cases annually and 125 imported cases from Africa, accounting for 84.46%. After achieving the goal of malaria elimination, the next objective for Chonqing is to prevent malaria resurgence caused by imported cases and the occurrence of severe death cases. In order to achieve this, it is necessary to make sure that no malaria case be misreported in Chonqing. There are about 30 imported malaria cases still reported every year in Chonqing, and Anopheles sinensis strain is widely distributed in Chongqing, meaning the risk of malaria resurgence still exists (4, 5). Early diagnosis and treatment for malaria cases are effective measures to prevent malaria resurgence and the occurrence of severe cases and deaths (6–9). The primary health institutions are the first station where potential malaria cases may seek treatment. The malaria diagnosis competency of the primary health institutions will directly affect the timeliness of malaria diagnosis (10, 11). In 2019, 38 malaria cases and two deaths were reported. The median interval from onset to diagnosis was 2 days; only 39.19% of the cases were within 24 h (12). Microscopy of plasmodium is an important approach to confirm patients and is also the gold standard for the diagnosis of malaria (13). A well-trained technician may realize high sensitivity and specificity when using microscopy to detect Plasmodium from blood slides whose parasitemia threshold could be 50 count/UL (13, 14). However, the efficiency of malaria microscopy is affected by the quality of the microscope and the competency of the technician, both of which have a great influence on the timely and accurate diagnosis of malaria cases (15–17). Nowadays, most primary health institutions in Chongqing use microscopy to confirm malaria cases. Therefore, it is important to know the current status of malaria microscopy in the primary health institutions. This study carried out the malaria microscopy competency test on technicians in primary health institutions in Chongqing to understand the current status of their competency with malaria microscopy in the qualitative analysis of plasmodium blood slides and plasmodium species identification. The test also analyzed related factors affecting their performance, so as to accurately improve the malaria diagnosis competency of primary health institutions, provide a scientific basis for the improvement measures of malaria early diagnosis, and reduce the occurrence of severe and deadly malaria cases.

METHODS

Study Area and Objects

Chongqing is located in southwest China in the upper reaches of the Yangtze River. It covers an area of 82,400 km^2. There are 38 districts/counties and one economic development zone in Chonqing. Its permanent population is 31.24 million, and the urbanization rate is 66.8%. The landform is mainly composed of hills and mountains, of which 76% are mountains. It has a subtropical monsoon humid climate. The Yangtze River runs through the whole territory, with a flow path of 691 km, and joins the Jialing River and Wujiang River (18).

The first step in the national "*Malaria Elimination Assessment Program (2014 Edition)*" and the principle of stratified sampling means that all 39 district/county level CDCs have participated in the study. Two to three clinical medical institutions were randomly selected according to the actual situation of each district and county. The second step involved one microscopic technician being randomly selected from 39 CDCs, and three microscopic technicians being randomly selected from the selected health institutions, making up four people from each district/county to participate in the malaria microscopy competence test.

Design of Microscopy Competence Test

The malaria microscopy competency single blind tests were conducted separately in each district/county from 2014 to 2017 with one bind. There were four sets of standard blood slides for tests that were provided by the Malaria Diagnostic Reference Laboratory of Chongqing CDC. The blood slides were made in line with the requirements of the national "*Malaria Elimination Assessment Program (2014 Edition)*" and the WHO "Operating Manual for Microscopy and Evaluation of Plasmodium" (15). Each set of standard blood slides was composed of three *P. falciparum* slides classified by the density of plasmodium with three levels that were high (≥84,000 counts/ul), medium (≥2,800 counts/ul), and low (≥500 counts/ul), one *P.* vivax slide, one *P. ovale* slide, and one negative slide. The parasitemia of four *P. vivax* slides and four *P. ovale* slides were 10,072–13,280 counts/ul and 2,293–3,072 counts/ul. The positive slides were made by the malaria patients' blood which was stored in the sample bank of Chongqing CDC. The negative slides were made using a healthy person's blood. All of the blood samples were confirmed by NEST-PCR and the blood slides were double checked by technicians who had acquired a WHO malaria microscopy competency level one certification to guarantee correct diagnosis. Only the blood slides with the same diagnosis of NEST-PCR and microscopy were used in this research. When the microscopy competency test was conducted, each technician would randomly select one set, and took five blood films from the set. The microscopy of plasmodium must be completed within 1.5 h. Five points were awarded if all were correct. One point was deducted for one qualitative error and 0.5 point was deducted for one species error.

Statistical Analysis

The test results and patient information were collected and sorted, and a database in the Excel 2016. R.4.02.application was used for statistical analysis. The districts and counties of Chongqing were divided into five geographical "urban areas": "Western Chongqing," "Central Chongqing," "Southern Chongqing," "Northeast Chongqing," and "Southeast Chongqing." One factor analysis of variance was conducted for the scores. The judgment results of each blood film were recorded and scored according to the design principles. The "Kendall" correlation analysis was carried out on the variables of "score," "gender," "age," "working unit level," and "professional qualification grade" of the technicians. The average scores of 39 districts/counties were calculated, and the "overall self-correlation" analysis was done with ArcMpa16.0, and the "Clustering Distribution Map" was plotted.

The qualitative diagnosis of microscopy and sensitivity, specificity, positive predictive value, negative predictive value, and Youden index in different plasmodium determinations were calculated and the ROC curve was plotted, which was to be paired and compared using "Delong's test." When calculating the diagnostic indexes of different species, the positive determination of the blood film of the species was considered valid, while the negative or other species determination was considered invalid.

RESULT

General

A total of 156 microscopic technicians from 39 districts/counties participated in the test, including 56 males (35.90%) and 100 females (64.10%), with a male to female ratio of 0.56; the age of the technicians was between 19 and 64 years and the average age was 34.89 ± 8.91, of which 56 (35.90%) were under 30 years old. 85 (54.50%) were at County-level medical institutions; 78 (50%) had junior technical qualifications. In the assessment results, there were 13 (8.30%) technicians with one qualitative error, 75 (48.10%) with one species identification error, 43 (27.60%) with two species identification errors, and eight (5.10%) with three species identification errors. The average score was 4.33 ± 0.47; the lowest was 3, the highest was 5, and the median was 4.5 (**Table 1**).

TABLE 1 | Summary of the subjects.

Items		Count	Proportion
Gender	Male	56	35.90%
	Female	100	64.10%
Age	34.89 ± 8.91 (Range: 19–64, Mid: 33)		
Age group	<30	56	35.90%
	≥30	54	34.62%
	≥40	46	29.49%
Work units	County CDC	40	25.64%
	County hospitals	85	54.49%
	Town hospitals	31	19.87%
Technical qualifications	Junior	78	50.00%
	Senior	11	7.05%
	Intermediate	67	42.95%
Total of Qualitative errors slides	0	143	91.67%
	1	13	8.33%
Total of species errors slides	0	30	19.23%
	1	75	48.08%
	2	43	27.56%
	3	8	5.13%
Scores	4.33 ± 0.47 (Range: 4.33–5, Mid: 4.5)		
	3.0	3	1.92%
	3.5	15	9.62%
	4.0	43	27.56%
	4.5	67	42.95%
	5.0	28	17.95%

Regional Distribution

Among the 38 districts/counties and one economic development zone, Shapingba District and Wuxi County got the highest average score of 4.875, followed by Jiulongpo District with 4.75. Dazu District got the lowest score of 3.625. The results of global spatial self-correlation analysis showed that the scores had significant spatial clustering (MoranI = 0.338, $z = 3.618$, $P < 0.01$). From the clustering distribution map based on the average scores of all districts/counties, we can see that the highest scores occurred in Western Chongqing, the urban area, and Northeast Chongqing, and the low scores were concentrated in the central part of Chongqing. The results showed that there were significant differences in scores among the geographical distribution regions ($F = 3.475$, $P = 0.012$). There was no significant difference between the "Urban area" (4.51) and "Northeast Chongqing" (4.49) ($F = 0.728$, $P = 0.41$), and the lowest score was *4.08* in Central Chongqing, which was much lower than that in other regions ($P < 0.05$), see **Figure 1**.

Diagnostic Competence

The sensitivity of microscopy was the highest in qualitative diagnosis (98.92%, CI: 98.00–99.69%) and the lowest in *P. ovale* diagnosis (15.94%, CI: 8.70–24.64). The highest specificity of diagnosis occurs in *P. ovale,* 96.20% (96.20%, CI: 94.66–97.61%) and the lowest in *P. vivax* (77.22%, CI: 73.87–80.74%). The negative predictive value and positive predictive value of qualitative diagnosis were the highest, respectively, 94.70 and 99.07%. The lowest negative predictive value was 78.54% for *P. falciparum* and 28.95% for *P. ovale.* The highest Youden Index was 0.9434 for qualitative diagnosis and 0.1214 for *P. ovale*, see **Table 2**.

The area under ROC curve for qualitative diagnosis, diagnosis of *P. falciparum*, *P. vivax,* and *P. ovale* were, respectively, 0.9717, 0.8413, 0.7823, and 0.5607 for technician microscopy. See **Figure 2**.

Delong's test was used to compare the ROC curves microscopy for diagnosis of different plasmodium species. The results showed that the diagnostic efficiency of *P. falciparum* was significantly higher than that of other species ($P < 0.01$), see **Table 3**.

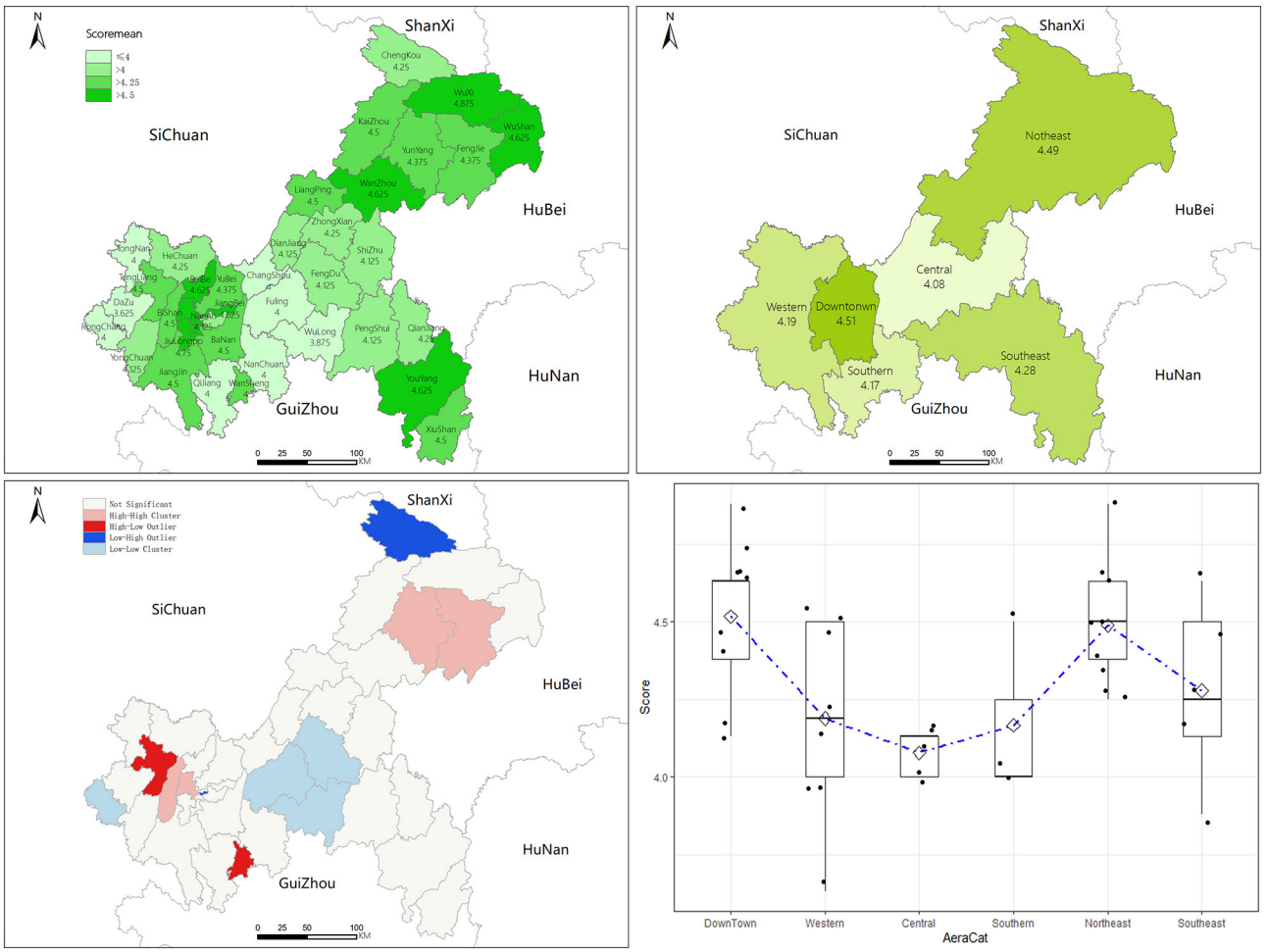

FIGURE 1 | Geographic information analysis map and statistical analysis chart of the test scores.

TABLE 2 | Indexes of the technicians' microscopy.

Items	Sensitivity (%)	95% CI of sensitivity (%)	Specificity (%)	95% CI of specificity	NPV (%)	PPV (%)	Youden index
Qualitative	98.92	(98.00–99.69)	95.42	(91.60–95.42)	94.70	99.07	0.9434
P. f	75.57	(71.53–79.35)	92.69	(90.08–95.04)	78.54	91.46	0.6826
P. v	79.23	(72.68–84.70)	77.22	(73.87–80.74)	92.38	51.60	0.5645
P. o	15.94	(8.70–24.64)	96.20	(94.66–97.61)	92.18	28.95	0.1214

Correlation Analysis

The variables were encoded: Gender: 0 = female, 1 = male; units: 1 = township medical institutions, 2 = county-level medical institutions, 3 = county-level CDC; qualification: 1 = junior, 2 = intermediate, 3 = senior; age group: 1 = under 30, 2 = 30–40, 3 = above 40. "Kendall" correlation analysis showed that the score of technicians was positively correlated with unit level ($r = 0.21$, $P < 0.01$) and negatively correlated with age ($r = -0.31$, $P < 0.01$). There was a positive correlation between technical qualification and age ($r = 0.5$, $P < 0.01$), see **Figure 3**.

DISCUSSION

The results of this study showed that the overall microscopy competency was the best in qualitative diagnosis, and the sensitivity and specificity microscopy were at a high level. There were differences in scores amongst different regions. The scores in the urban area and Northeast Chongqing were significantly higher than those in other regions, and the lowest score was in Central Chongqing. The reason could be that the number of malaria cases reported in the urban area of Chongqing accounts for about 60% of the total cases in Chongqing (12, 19, 20), and

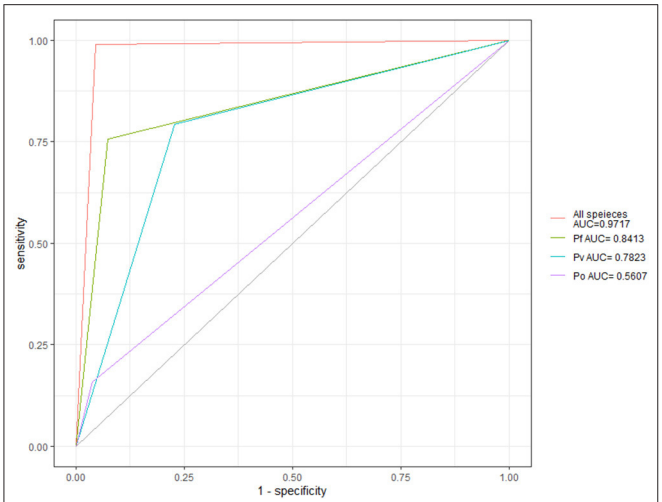

FIGURE 2 | The technicians' microscopy ROC curve for different plasmodium species.

TABLE 3 | DeLong's test on the technicians' microscopy ROC.

DeLong' test	Area under curve (AUC)	*Z*-value	*P*
P. f vs. *P. v*	0.8412 vs. 0.7823	2.75	<0.01
P. f vs. *P. o*	0.8412 vs. 0.5607	10.87	<0.01
P. v vs. *P. o*	0.7823 vs. 0.5607	7.81	<0.01

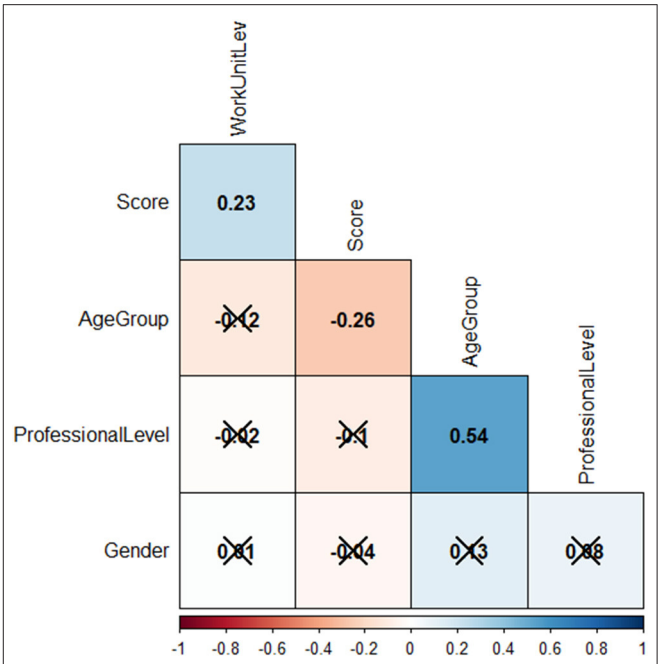

FIGURE 3 | Correlation analysis matrix to the technicians. × indicates $P > 0.05$.

the economic, social, and health development indexes in the urban area are also higher than those in other areas (21–23). Although the quality of malaria microscopy is more affected by the competency of the technician (14, 24, 25), the local economic and social development and the number of imported malaria cases may also be factors affecting the microscopy competency of the primary health institutions.

The results showed that the qualitative diagnostic efficiency of plasmodium microscopy was the highest, followed by *P. falciparum*. The scores of the identification of *P. vivax* and *P. ovale* were quite low; the positive predictive value was only 51.60 and 28.95%. Morphological identification of P. vivax and *P. ovale* by microscopy has always been difficult, and requires rich experience and technical training from the technician (26, 27). That's why, in this study, there were many misjudgments in the identification between the two. The treatments for *P. vivax* and *P. Ovale* are basically identical (6, 28); although the confusion between the two species will not have a significant impact on the treatment of patients, the earlier detection, earlier diagnosis, and earlier treatment of imported *P. vivax* malaria are of great significance to prevent the malaria resurgence of imported cases after the elimination of malaria in China (2, 29). At present, there is little research on the transmission competency of *A. sinensis* to *P. ovale*, and there is no clear evidence that imported *P. ovale* can exist in local *Anopheles sinensis* and infect humans. The primary doctors may neglect management of imported *P. ovale*; if *P. vivax* were misdiagnosed as *P. ovale*, the risk of malaria resurgence will increase. In recent years, the number of imported cases of *P. ovale* malaria cases has increased year on year (20, 29, 30), which is related to the establishment of malaria reference laboratories nationwide to carry out PCR reviews for each reported case since the implementation of the malaria elimination action plan. Compared with other detection methods, PCR detection can more accurately distinguish various types of plasmodium species (25, 27, 31–33). In 2012, the malaria reference laboratory was established in Chongqing CDC. All malaria cases reported by health institutions in Chongqing need to collect blood samples and send them to the reference laboratory for PCR review (3, 34). Therefore, a malaria reference laboratory is an important technical support for accurate diagnosis of malaria cases and an important means to prevent the transmission of imported malaria.

In the correlation analysis of technician's personal characteristics, it was found that the higher the level of work unit, the higher the score. Technicians from the township level health institutions had lower scores, and their microscopy competencies were relatively lower. The study also found that older technicians scored lower. Under normal circumstances, the technician's competency of plasmodium microscopy will increase with age; rich microscopy experience leads to better competence (13, 26, 35). However, there were no local malaria cases reported in Chongqing from 2011, and there were only about 30 imported cases each year in last decade. Seventy

percentage of the cases were reported by provincial, municipal, and county-level health institutions, and only about 8% of the cases were reported in the primary township level health Institutions (12). This situation makes it difficult for doctors and laboratory staff of township health institutions to receive malaria patients or see positive blood film in field work. As the age of the technician increases, their experience will not increase due to a lack of practice, on the contrary, it will be forgotten. In recent years, based on the principle of training young malaria prevention and control personnel, Chongqing has held a parasite microscopy competition every year, requiring all participants dispatched be under 35 years (36, 37), which indirectly leads to the training of primary malaria microscopy technicians focusing on young people. The likelihood of receiving malaria patients at the township level is low, and the microscopy technician may easily quit (22, 38). These factors will lead to the decline of the microscopy competence of primary microscopy technicians. At the same time, with the increase of age, the diagnostic competency of microscopy technicians will decrease. In contrast, Rapid Diagnostic Test (RDT) is more convenient and faster than plasmodium microscopy in the areas lacking equipment, technicians, and technologies, and has lower requirements on the technicians' competence (33, 39), so is more suitable to be widely used in primary health institutions in Chongqing.

Study Limitation

Due to limitations imposed by funds and manpower, only four microscopy technicians from three kinds of health institutions from each district/county were selected to participate in the test, and the sampling volume was small. Due to the lack of good blood samples *P. malariae* was not included in the test. The competency tested was limited to the microscopy technician's competence of the blood film reading, not the competence of film preparation. In this study, we failed to collect complete data for utilizing social, economic, and health resources, and did not conduct further study on the influence of these factors on the competency of microscopy in various regions.

CONCLUSIONS

The microscopy technicians in primary health institutions in Chongqing have good microscopy competency in qualitative diagnosis, but there were deficiencies in the identification of plasmodium species. Township level health institutions in Central China have weaker microscopy than those in other areas.

DATA AVAILABILITY STATEMENT

The raw data supporting the conclusions of this article will be made available by the authors, without undue reservation.

ETHICS STATEMENT

The study was reviewed and approved by the Ethical Committee of Chongqing center for disease control and prevention. All participants provided written informed consent for the study.

AUTHOR CONTRIBUTIONS

LF conceived the study, collected and analyzed the data, and drafted the manuscript. YY and LS-S provided suggestions for improving the quality of the data. TY, ZY, and XJ-R provided the test blood slides and collected the scores. ZS initiated the study. All authors contributed to the writing of the manuscript and approved the submitted version of the manuscript. All authors read and approved the final manuscript.

ACKNOWLEDGMENTS

We gratefully acknowledge all technicians and institutions participated in this study.

REFERENCES

1. *World Malaria Report 2020*. Geneva: World Health Organization (2020).
2. Zhang L, Feng J, Xia ZZ, Zhou SS. Epidemiological characteristics of malaria and progress on its elimination in China in 2019. *Chin J Parasitol Parasit Dis.* (2020) 38:133–8. doi: 10.12140/j.issn.1000-7423.2020.02.001
3. Luo F, Zhou S, Xiao BZ, Li SS, Yuan Y. Mid-term assessment report of malaria elimination action plan in Chongqing. *China Trop Med.* (2018) 4:312–4. doi: 10.13604/j.cnki.46-1064/r.2018.04.04
4. Zhou XN, Zhang SS, Xu JF, Xia ZG, Wang RB, Qian YJ, et al. Risk Assessment for Malaria Elimination in P. R. China. *ChinJ Parasitol Parasit Dis*. (2014) 32:414–18. doi: 10.12140/j.issn.1000-7423.2014.06.002
5. Chen TM. *Study on Indicators and Modelling of Risk Assessment on Malaria Re-establishment*. Shanghai: Chinese Center for Disease Control and Prevention; National Institute of Parasitic Disease (2018).
6. *Guidelines For The Treatment of Malaria.* Italy: World Healteh Organzation. (2015).
7. Zhang Q, Di QL, Sun JL, Zhang ZK, Lai SJ, Zhou S, et al. Epidemiological analysis of the deaths of malaria in China, 2005-2014. *Chin J Prev Med*. (2016) 4:302–5. doi: 10.3760/cma.j.issn.0253-9624.2016.04.004
8. Moonen B, Cohen JM, Tatem AJ, Cohen J, Smith DL. A framework for assessing the feasibility of malaria elimination. *Malar J.* (2010) 9:322. doi: 10.1186/1475-2875-9-322
9. Ponçon N, Tran A, Toty C, Fontenille LD. A quantitative risk assessment approach for mosquito-borne diseases: malaria re-emergence in southern France. *Malar J.* (2008) 7:147. doi: 10.1186/1475-2875-7-147
10. Chen I, Thanh HNT, Lover A, Lover A, Thao PT, Luu TV, et al. Malaria risk factors and care-seeking behaviour within the private sector among high-risk populations in Vietnam: a qualitative study. *Malar J.* (2017) 16:414. doi: 10.1186/s12936-017-2060-0
11. Yin J, Yan H, Li M, Yan H, Ruan Y, Zhang XQ, et al. Competency and challenges in malaria microscopy in China. *Biosci Trends.* (2017) 11:702–5. doi: 10.5582/bst.2017.01275
12. Luo F, Zhou S, Yuan Y, Huang WL, Li SS. Epidemiologica analysis and control strategy discussion for overseas imported malaria cases reported in Chongqing City from 2011 to 2015. *Chin J Schisto Control.* (2017) 29:310–14. doi: 10.16250/j.32.1374.2017050
13. Ngasala B, Mutemi DD, Mwaiswelo RO. Diagnostic performance of malaria rapid diagnostic test and microscopy compared with PCR for detection of plasmodium falciparum infections among primary schoolchildren in Kibiti

District, Eastern Tanzania: an area with moderate malaria transmission. *Am J Trop Med Hyg.* (2019) 101:809–11. doi: 10.4269/ajtmh.19-0394
14. Payne D. Use and limitations of light microscopy for diagnosing malaria at the primary health care level. *Bull World Health Organ.* (1988) 66:621–6. doi: 10.1146/annurev.pu.09.050188.002115
15. *Malaria Microscopy Quality Assurance Manual-Version 3.* Italy: World Health Organization (2016).
16. Kahama-Maro J, D'Acremont V, Mtasiwa D, Genton B, Lengeler C. Low quality of routine microscopy for malaria at different levels of the health system in Dar es Salaam. *Malar J.* (2011) 10:332. doi: 10.1186/1475-2875-10-332
17. Ngasala B, Bushukatale S. Evaluation of malaria microscopy diagnostic performance at private health facilities in Tanzania. *Malar J.* (2019) 18:375. doi: 10.1186/s12936-019-2998-1
18. *Introduction to Chongqing.* Available online at: http://www.cq.gov.cn/zqfz/zhsq/sqjj/202007/t20200727_7727103.html (accessed September 03, 2020).
19. Jiang SG, Wu CG, Li JY, Yan W, Li Y. Malaria situation and control effect in Chongqing municipality from 1951 to 2004. *Parasit Infect Dis.* (2005) 3:105–10. doi: 10.3969/j.issn.1672-2116.2005.03.003
20. Zhou CB, Li Q, Chen X, Shen T, Luo F. Analysis on the epidemiological characteristics of malaria in Chongqing city from 2005 to 2015. *J Trop Med.* (2017) 17:106–8. doi: 10.3969/j.issn.1672-3619.2017.01.031
21. *Statistical Yearbook to Chongqing.* Availabe online at: http://tjj.cq.gov.cn/zwgk_233/tjnj/2019/indexch.htm (accessed September 03, 2020).
22. Meng QY, Zhang QY, Liu X, Wen T, Ma Y. The spatial-temporal pattern analysis of health human resources allocation differences in Chongqing between 2005 and 2017. *Chin Health Serv Manag.* (2020) 5:359–63.
23. Wu SZ, Si GT. Spatial structure and characteristics of the urban economic networks an empirical study of the main Urban districts of Chongqing. *J Chongqing Jiaotong Univ.* (2020) 20:67–75.
24. Odhiambo F, Buff AM, Moranga C, Moseti CM, Wesongah JO, Lowther SA, et al. Factors associated with malaria microscopy diagnostic performance following a pilot quality-assurance programme in health facilities in malaria low-transmission areas of Kenya, 2014. *Malar J.* (2017) 16:371. doi: 10.1186/s12936-017-2018-2
25. Emrah R, Plul BJ, Turgut I, Aysegul TO. Investigation of pregnancy-associated malaria by microscopy, rapid diagnostic test and PCR in Bandundu, the Democratic Republic of Congo. *Trans R Soc Trop Med Hyg.* (2018) 112:8–13. doi: 10.1093/trstmh/try016
26. Shittu O, Opeyemi OA, Ajibaye O, Omotesho BO, Fakayode O. Evaluation of the clinical proficiency of RDTs, microscopy and nested PCR in the diagnosis of symptomatic malaria in Ilorin, North-Central, Nigeria. *Open Access Macedon J Med Sci.* (2018) 6:1032–40. doi: 10.3889/oamjms.2018.218
27. Li M, Yan H, Zhou HJ, Fen XY, Xia ZG, Zhou SS. World Health Organization-external competency assessment of malaria microscopists in China. *Chin J Parasitol Parasit Dis.* (2018) 5:499–503. doi: 10.12140/j.issn.1000-7423.2018.05.018
28. *Application of Antimalarials. WS/T485-2016.* BeiJing: National Health Commission; PRC (2016).
29. Fen J, Zhou SS. From control to elimination: the historical retrospect of malaria control and prevention in China. *Chin J Parasitol Parasit Dis.* (2019) 37:505–13. doi: 10.12140/j.issn.1000-7423.2019.05.001
30. Liao ZW, Wang SQ. Prevalence and prevention of major tropical diseases in China, 2000-2019. *China Trop Med.* (2020) 20:193–201. doi: 10.13604/j.cnki.46-1064/r.2020.03.01
31. Jiao BX, Huang WH, Chen ZH, Li XW, Yang XL, He YQ, et al. Practical evaluation of three testing methods on the diagnosis and curative effect of malaria. *China Med Herald.* (2012) 10:98–9. doi: 10.3969/j.issn.1673-7210.2012.27.040
32. Li M, Xia ZZ, Zhou SS. Analysis of inconsistence of Plasmodium detection in some malaria cases. *Chin J Parasitol Parasit Dis.* (2019) 37:464–71. doi: 10.12140/j.issn.1000-7423.2019.04.017
33. Zhu WJ, Ling XX, Shang WR, Du YQ. High value of rapid diagnostic tests to diagnose malaria within children: a systematic review and meta-analysis. *J Glob Health.* (2020) 10:010411. doi: 10.7189/jogh.10.010411
34. Luo F, Zhou S, Xiao BZ, Li SS, Yuan Y, Huang WL, et al. Evaluation on implementation effect of malaria elimination project supported by global fund in Chongqing. *China Health Industry.* (2017) 18. doi: 10.16659/j.cnki.1672-5654.2017.18.026
35. Yin JH, Yan H, Li M, Fang W, Huang F, Jiang W, et al. Malaria diagnosis reference laboratory: analysis of malaria detecting ability under microscope in the external quality assurance program. *Int J Med Parasit Dis.* (2015) 3:173–5. doi: 10.3760/cma.j.issn.1673-4122.2015.03.012
36. Zhang SS, Xia ZZ, Yin JH, Yan H, Zhou SS, Li SZ, et al. Analysis report of the national technique competition for diagnosis of parasitic diseases in 2012:I.capability analysis of plasmodium detection. *Chin J Parasitol Parasit Dis.* (2013) 2:131–4. doi: 10.12140/j.issn.1000-7423.2013.03.011
37. Zhu ZL, Hao YW, Tian T, Xue CZ, Tu H, Han S, et al. Assessment of ability of professionals in parasitic disease control and prevention techniques in China, 2017. *Chin J Schisto Control.* (2018) 5:518–22. doi: 10.16250/j.32.1374.2018112
38. Wu CG, Jiang SG, Luo F, Luo XJ, Xiao BZ, Xie J. Feasibility of malaria elimination in Chongqing. *J Pathogen Biol.* (2011) 6:769–71. doi: 10.13350/j.cjpb.2011.10.024
39. Anthony M. Rapid diagnostic tests for malaria parasites. *Clin Microbiol Rev.* (2002) 1:66–78. doi: 10.1128/CMR.15.1.66-78.2002

Conflict of Interest: The authors declare that the research was conducted in the absence of any commercial or financial relationships that could be construed as a potential conflict of interest.

frontiers in Public Health

ORIGINAL RESEARCH
published: 18 March 2021
doi: 10.3389/fpubh.2021.664971

A Household-Based Cross-Sectional Survey of Knowledge, Awareness and Practice Regarding Malaria in Western Area Rural District, Sierra Leone

Lili Wang[1], *Jianhai Yin*[2*], *Canjun Zheng*[3*], *Samuel Juana Smith*[4], *Esther Ngegba*[1], *Xiaoxia Huang*[5], *Anitta Kamara*[4], *Xia Chen*[6], *Xu Wang*[2], *Wei Luo*[7] *and Biao Kan*[6]

[1] *Center for Global Public Health, Chinese Center for Disease Control and Prevention, Beijing, China,* [2] *National Institute of Parasitic Diseases, Chinese Center for Disease Control and Prevention, Chinese Center for Tropical Diseases Research, Shanghai, China,* [3] *Division of Infectious Diseases, Chinese Center for Disease Control and Prevention, Beijing, China,* [4] *National Malaria Control Program, Ministry of Health and Sanitation, Freetown, Sierra Leone,* [5] *National Institute for Viral Disease Control and Prevention, Chinese Center for Disease Control and Prevention, Beijing, China,* [6] *National Institute for Communicable Disease Control and Prevention, Chinese Center for Disease Control and Prevention, Beijing, China,* [7] *National Center for AIDS/STD Control and Prevention, Chinese Center for Disease Control and Prevention, Beijing, China*

OPEN ACCESS

Edited by:
Tianmu Chen,
Xiamen University, China

Reviewed by:
Hui Liu,
Yunnan Institute of Parasitic Diseases, China
Ying Liu,
Henan Provincial Center for Disease control and Prevention, China

***Correspondence:**
Jianhai Yin
yinjh@nipd.chinacdc.cn
Canjun Zheng
zhengcj@chinacdc.cn

Specialty section:
This article was submitted to Infectious Diseases - Surveillance, Prevention and Treatment, a section of the journal Frontiers in Public Health

Received: *06 February 2021*
Accepted: *25 February 2021*
Published: *18 March 2021*

Citation:
Wang L, Yin J, Zheng C, Smith SJ, Ngegba E, Huang X, Kamara A, Chen X, Wang X, Luo W and Kan B (2021) A Household-Based Cross-Sectional Survey of Knowledge, Awareness and Practice Regarding Malaria in Western Area Rural District, Sierra Leone. Front. Public Health 9:664971. doi: 10.3389/fpubh.2021.664971

Sierra Leone is a highly endemic area for malaria, and the implementation of the National Malaria Strategic Plan (2016–2020) has reached its midpoint in 2018. To provide more specific guidance for interventions in the future, a household-based cross-sectional survey was conducted to elucidate the knowledge, awareness and practices regarding malaria and malarial control measures among the general public. Three communities (Grafton, Jui, and Kossoh) in the Western Area Rural District that were in close proximity to Sierra Leone's capital city of Freetown were included. Households were randomly selected and interviewed with a structured questionnaire covering malaria infection, diagnosis, treatment and prevention, as well as knowledge of malaria prevention. As a result, a total of 262 qualified questionnaires were included. The average cost for meals per day is ∼30,000 Leones in each household. The rate of awareness, indicated by reporting having heard of malaria, was 98.1% (257/262), and 86.6% (227/262) of the respondents knew that mosquito bites are the main route of transmission. In addition, 80.9% (212/262) of the respondents sought health advice or treatment for the illness, and a similar percentage of respondents had been tested for malaria, mostly with rapid diagnostic tests (RDTs). A high demand for long-lasting insecticidal nets (72.1%) matched the serious shortage (61.8%, 162/262), and of the households that reported a lack of nets, 66 had children younger than 5 years old. In conclusion, public awareness of malaria prevention is high, based on this survey, although there was a limited use of preventive measures in these three communities and the malaria burden was still high. Therefore, the public's knowledge of malaria should be sustained and reinforced, and the distribution and use of malaria prevention measures should be promoted to supprt the achievement of the planned objectives.

Keywords: malaria, KAP survey, Western Area Rural District, Sierra Leone, national malaria strategic plan

INTRODUCTION

Malaria is endemic in Sierra Leone; the entire population is at risk of exposure because Sierra Leone is an area of stable malarial endemicity, and almost cases were infected with *Plasmodium falciparum* (1). Sierra Leone's high malaria disease burden accounted for ∼48% of outpatient morbidity and ∼38% of mortality in children younger than 5 years according to the national Malaria Indicator Survey conducted in 2016 (2). Although significant progress with regard to reducing mortality has been made, it is still a major public health concern. The control of malaria remains a priority in the national health agenda of Sierra Leone.

A multipronged strategy to control malaria, including vector control interventions, diagnostic testing, treatment with quality-assured artemisinin-based combination therapies, and standardized case management training manuals for community and facility treatment providers, has been developed and implemented in Sierra Leone based on the World Health Organization (WHO) recommendations (3). The goals are for 80% of the population to have appropriate levels of knowledge and uptake/practice of malaria prevention and management strategies, all the at-risk population to have access to the appropriate preventive interventions, 80% of individuals with suspected malaria cases to have access to confirmatory diagnostic testing, and all individuals with malaria to receive effective treatment by 2018, according to the current Sierra Leone National Malaria Strategic Plan (2016–2020) (SL-NMSP) (3).

The awareness of malaria symptoms, transmission, prevention and treatments is closely related to the implementations of malaria control programs (4–6). A knowledge, awareness and practices (KAP) survey about malaria could help policy makers better understand the current situation and guide malaria control strategies. Therefore, this study is conducted to determine the knowledge, awareness and practices regarding malaria and its control measures in the general public through a household-based survey at the midpoint of the implementation of the SL-NMSP.

TABLE 1 | The distribution of medical sectors people seeking health advice or treatment in the three communities in the Western Area Rural District, Sierra Leone, 2018.

Medical sector	Community			Total
	Grafton	Jui	Kossoh	
Public sector only	68	29	56	153
Private medical sector only	15	5	23	43
Both sectors	2	10	3	15
Don't answer	1	0	0	1
Total	86	44	82	212

MATERIALS AND METHODS

Study Site

Three communities (Grafton, Jui, and Kossoh) in Western Area Rural District within close proximity to Sierra Leone's capital city Freetown were included in this household-based survey on malaria. This district is home to a very religiously and ethnically diverse population. Grafton is a trade center. Jui and Kossoh are neighborhood towns. Kossoh town is surrounded by a large forest reserve, and its major industries are farming and coal mining.

Participants, Questionnaire, and Data Collection

A total of 300 households in the three designated communities were randomly selected as survey respondents using a cluster sampling design. One adult member from each selected household was interviewed with a structured questionnaire covering demographic information, economic status, basic knowledge of malaria, and malaria prevention and control practices. When medicines were discussed, packages of various drugs were displayed to the participants.

The survey was conducted in collaboration with the National Malaria Control Program of the Ministry of Health and

TABLE 2 | The detail of public or private medical sectors people selected for health care seeking in the three communities in the Western Area Rural District, Sierra Leone, 2018.

	Public medical sectors						Private medical sectors							
Community	Government hospital	Government health center	Mobile clinic	Community health worker	Other public sector	Subtotal	Private hospital	Private clinic	Mission/Faith-based hospital	Mission/faith-based clinic	Pharmacy	Mobile clinic	Other private medical sector	Subtotal
Grafton	38	14	11	3	4	70	9	0	0	0	1	5	2	17
Jui	37	1	1	0	0	39	2*	1	1	10*	2	0	0	16
Kossoh	40	12	2	3	2	59	14*	0	0	6*	7	0	0	27

**There was one respondent seeking advice or treatment both in the private sectors of private hospital and Mission/Faith-based Clinic in each community.*

TABLE 3 | Malaria diagnosis and anti-malarial medicine taking in the three communities in the Western Area Rural District, Sierra Leone, 2018.

Question and answer	Community			Total	Percentage
	Grafton	Jui	Kossoh		
1. When you and your family suspected you were infected with malaria, did you always go to see a health worker/doctor?					
Yes	92	40	89	221	84.4%
No	12	1	7	20	7.6%
Don't answer	4	6	11	21	8.0%
1.1 How often?					
Every time	45	6	45	96	43.4%
Most of time	33	29	20	82	37.1%
Seldom	11	4	11	26	11.8%
Only when they showed severe condition	3	1	13	17	7.7%
2. When you or any member of your family suspected that they had malaria, did the health worker/doctor conduct a malaria test?					
Yes	88	44	78	210	80.2%
No	16	2	13	31	11.8%
Don't answer	4	1	16	21	8.0%
3. Did the Doctor/health worker explain to you the test to be done?					
Yes	64	25	55	144	55.0%
No	27	4	26	57	21.8%
Don't remember	9	17	5	31	11.8%
Don't answer	8	1	21	30	11.5%
4. What type of test did they say they were going to perform?					
RDT	57	17	69	143	54.6%
Microscopy	2	1	2	5	1.9%
Don't remember	41	27	8	76	29.0%
Don't answer	8	2	28	38	14.5%
5. When you and your family were infected with malaria, did you take the anti-malarial medicine?					
Every time	54	6	48	108	41.2%
Most of time	37	37	20	94	35.9%
Seldom	12	3	11	26	9.9%
Never	1	0	1	2	0.8%
Only when they showed severe condition	0	0	15	15	5.7%
Don't answer	4	1	12	17	6.5%
6. What anti-malarial medicines did you take?					
Sp/Fansidar	4	2*	0	6	2.3%
Combination with Artemisinin	2	1	0	3	1.1%
Artesunate+Lumafantrine	58#,&,@	32*,$,%	61#	151	57.6%
Artesunate+Amodiaquine	19#,@	14	21#	54	20.6%
Amodiaquine	6Φ	2$	1	9	3.4%
Quinine	0	1%	1	2	0.8%
Others: specify	29&,@,Φ	0	10	39	14.9%
Don't answer	2	0	16	18	6.9%
7. When did (NAME(S)) take the anti-malarial medicine?					
Same day after fever	92	44	74	210	80.2%
Next day after fever	13	3	8	24	9.2%
Two day after fever	0	0	0	0	0.0%
Three or more day after fever	1	0	8	9	3.4%
Don't know	1	0	1	2	0.8%
Don't answer	1	0	16	17	6.5%

(Continued)

TABLE 3 | Continued

Question and answer	Community			Total	Percentage
	Grafton	Jui	Kossoh		
8. Are the antimalarial drugs FREE which you and your family took?					
Yes, they are free for all	38	12	20	70	26.7%
No, only for children, pregnant women and breast-feeding women	2	4	3	9	3.4%
None is FREE	67	31	71	169	64.5%
Don't answer	1	0	13	14	5.3%
9. When you and your family were infected with malaria, did you take the full dosage of antimalarial drugs which was prescribed by doctor/health worker?					
Yes, take full dosages every time	93	35	81	209	79.8%
No, sometimes some dosage was left	15	8	10	33	12.6%
No, some dosages were left every time	0	3	1	4	1.5%
Don't answer	0	1	15	16	6.1%
9.1 If not all drugs taken, please explain why:					
We got recovery before finishing all of them	15	9	9	33	89.2%
The drugs made me have headache, nausea	0	0	0	0	0.0%
I am too busy to remember taking all the dosage	0	1	1	2	5.4%
Others: specify	0	1	1	2	5.4%
Don't answer	0	0	0	0	0.0%

[*] *There were two respondents reported taking both Sp/Fansidar and Artesunate + Lumafantrine.*
[#] *There were six respondents in Grafton and three respondents in Kossoh reported taking both Artesunate + Lumafantrine and Artesunate + Amodiaquine.*
[&] *There were three respondents reported taking both Artesunate + Lumafantrine and other.*
[@] *There was one respondent reported taking both Artesunate + Lumafantrine and Artesunate + Amodiaquine and other.*
[$] *There were two respondents reported taking both Artesunate + Lumafantrine and Amodiaquine.*
[%] *There was one respondent reported taking both Artesunate + Lumafantrine and Quinine.*
[Φ] *There was one respondent reported taking both Amodiaquine and other.*

Sanitation, Sierra Leone, in December 2018, at the midpoint of the SL-NMSP (3). Local staff from Sierra Leone-China Friendship Biological Safety Laboratory (7) were trained in prior to their involvement in the administration of the survey.

Data Analysis

Data was input and cross-checked by EpiData version 3.1 (8, 9). Then, descriptive statistics and percentages were presented using Microsoft Excel 2010 software. Differences in distribution among three communities were evaluated using the chi-square (χ^2) test or Fisher's exact test by SPSS software version 20.0 (IBM, USA) and $P < 0.05$ was considered statistically significant.

RESULTS

A total of 300 households were investigated, and 262 qualified questionnaires from 108, 47, and 107 households in Grafton, Jui, and Kossoh communities, respectively, were finally included in the analysis after checking for questionnaire completion and logic. The survey covered 1,645 residents, with ∼6 persons per family. The average cost of meals per day was ∼30,000 Leones in each household (one US dollar was equal to 8,000 Leones in December 2018).

Malaria Infection, Diagnosis, and Treatment

A total of 929 persons in 202 households reported having had a fever in 2018. Among them, 406 persons from 97 households, 228 persons from 46 households, and 295 persons from 89 households in Grafton, Jui, and Kossoh communities, respectively, reported having suffered malaria. Moreover, 129 persons from 64 households reported having suffered malaria once, and 146 persons from 66 households reported having suffered malaria being twice, and 61 persons from 26 households being three times, and 275 persons from 91 households being more than three times, respectively.

Moreover, ∼80.9% (212/262) of the respondents reported seeking professional advice or treatment for the illness from any source ($P < 0.001$, Fisher's exact test) (**Table 1**). Additionally, 72.2% (153/212) of the respondents reported preferring to seek

TABLE 4 | Malaria prevention practices in the three communities in the Western Area Rural District, Sierra Leone, 2018.

Question and answer	Community			Total	Percentage
	Grafton	Jui	Kossoh		
1. Do you have a mosquito treated bed nets in your home?					
Yes	79	37	72	188	71.8%
No	29	10	35	74	28.2%
2. Did you sleep under a mosquito net last night?					
Yes	66	25	55	146	55.7%
No	36	19	51	106	40.5%
Don't answer	6	3	1	10	3.8%
3. Is there anyone in your household who did not sleep under treated bed nets last night?					
Yes	69	37	56	162	61.8%
No	29	7	48	84	32.1%
Don't answer	10	3	3	16	6.1%
4. Are there enough treated bed nets in your household?					
Yes	25	8	32	65	24.8%
No	73	39	73	189	72.1%
Don't answer	6	0	2	8	3.1%
5. Do all children under 5 years in your household sleep under treated bed nets at night?					
Yes	39	25	38	102	38.9%
No	26	13	27	66	25.2%
No children under 5	41	8	41	90	34.4%
Don't answer	2	1	1	4	1.5%
6. Where did you get the treated bed nets?					
Government Hospital/Health Center	58	32*	40#	130	49.6%
Mobile Clinic	1	0	0	1	0.4%
Community Health Center	5	8	27	40	15.3%
Private Hospital/Clinic	0	7*	1	8	3.1%
Pharmacy	0	1	0	1	0.4%
Shop	1	1	8#	10	3.8%
Traditional Healer	0	0	0	0	0.0%
Others	24	2	0	26	9.9%
Don't answer	19	2	32	53	20.2%
7. Did you spray insecticide to kill mosquitoes in your house?					
Often	9	8	16	33	12.6%
Sometimes	12	13	12	37	14.1%
Seldom	15	9	24	48	18.3%
Never	72	17	54	143	54.6%
Don't answer	0	0	1	1	0.4%
8. Did you spray insecticide to kill mosquitoes outside your house?					
Often	0	1	4	5	1.9%
Sometimes	2	2	2	6	2.3%
Seldom	6	5	9	20	7.6%
Never	100	38	87	225	85.9%
Don't answer	0	1	5	6	2.3%
9. Does your house have doors or windows screen which could stop the mosquitoes to go into the house?					
Yes	6	14	38	58	22.1%
No	102	33	67	202	77.1%
Don't answer	0	0	2	2	0.8%

(Continued)

TABLE 4 | Continued

Question and answer	Community			Total	Percentage
	Grafton	Jui	Kossoh		
10. Do you and your family often stay outside of the house at night (such as for walk, exercises, enjoy the cool air, work, etc)					
Often	57	41	86	184	70.2%
Sometimes	38	4	9	51	19.5%
Seldom	8	1	6	15	5.7%
Never	4	1	4	9	3.4%
Don't answer	1	0	2	3	1.1%

*There were six respondents reported taking the treated bed nets from Government Hospital/Health Center and Private Hospital/Clinic both.
#There was one respondent reported taking the treated bed nets from Government Hospital/Health Center and shop both.

advice and treatment from the public medical sector (including government hospital, government health center, mobile clinic, community health worker, other public sector) only ($P = 0.001$, Fisher's exact test). And 20.3% (43/212) and 7.1% (15/212) were found to seek assistance from the private sector (including private hospital, private clinic, mission/faith-based hospital, mission/faith-based clinic, pharmacy, mobile clinic, other private medical sector) only or any sector (**Tables 1**, **2**).

Furthermore, 84.4% (221/262) of the respondents reported that they and their family members always visited a health care worker or doctor when they suspected they had contracted malaria ($P = 0.071$, Fisher's exact test). Among the individuals who went to see a health care worker or doctor, they reported visiting a professional every time (43.4%, 96/221) or most of the times (37.1%, 82/221) they suspected they had contracted malaria ($\chi^2 = 37.219$, $P < 0.000$) (**Table 3**).

As recalled by the respondents, the health care worker or doctor performed a malaria test when they visited because they suspected that they had contracted malaria (80.2%, 210/262) ($\chi^2 = 15.854$, $P = 0.003$), and the malaria rapid diagnostic tests (RDT) was the most commonly used test (54.6%, 143/262); however, approximately half of the respondents (55.0%, 144/262) reported that the doctors or health care workers did not explain the test to them (**Table 3**).

Most respondents took anti-malarial medicine every time (41.2%, 108/262) or almost every time (35.9%, 94/262) they were diagnosed with malaria, and ∼79.8% (209/262) of them took the full course of treatment every time as prescribed by the doctor or health care worker. Artesunate and lumefantrine (57.6%, 151/262) and artesunate and amodiaquine (20.6%, 54/262) were the top two choices of combination therapy. The most common reason given for the early termination of a course of treatment was having recovered prior to finishing all the doses (89.2%, 33/37). Moreover, ∼80.2% (210/262) of the respondents reported starting anti-malarial medicine on the same day that they noted the fever, and ∼64.5% (169/262) of them responded that the anti-malarial medicine were not free (**Table 3**).

Malaria Prevention Measures

In this survey, 188 households had long-lasting insecticidal nets (LLINs) ($\chi^2 = 2.282$, $P = 0.340$), but more nets were required because 189 respondents said that they did not have enough LLINs in their households ($P = 0.102$, Fisher's exact test), so resulting in children under the age of 5 years in 66 households not having LLINs to sleep under ($P = 0.120$, Fisher's exact test). Only 146 respondents had slept under nets the night before the survey ($P = 0.073$, Fisher's exact test). Furthermore, some members in 162 households with nets did not sleep under LLINs ($\chi^2 = 18.179$, $P = 0.001$), which could lead to cross-infection. Half of the LLINs were distributed by the governmental hospital/health centers (49.6%, 130/262) and community health centers (15.3%, 40/262) (**Table 4**).

In addition, a total of 143 households never sprayed insecticide indoors to kill mosquitoes ($\chi^2 = 19.945$, $P = 0.007$), and 225 households never sprayed insecticide outside ($P = 0.073$, Fisher's exact test). Furthermore, more than three quarters of the respondents (77.1%, 202/262) reported that they did not have a door or window screen to prevent mosquitoes from entering their houses ($P < 0.001$, Fisher's exact test). Additionally, most families (89.7%, 235/262) reported staying outside of the house at night ($P < 0.001$, Fisher's exact test) (**Table 4**).

Knowledge of Malaria

In this survey, almost all the respondents had heard about malaria (98.1%, 257/262) ($P = 0.214$, Fisher's exact test) and knew that the main route of transmission was through mosquito biting (86.6%, 227/262) ($\chi^2 = 5.045$, $P = 0.081$). Fever (44.3%, 116/262) ($\chi^2 = 4.845$, $P = 0.092$), body aches or joint pain (38.9%, 102/262) ($\chi^2 = 1.189$, $P = 0.566$), and loss of appetite (36.6%, 96/262) ($\chi^2 = 2.928$, $P = 0.237$) were the top three clinical manifestations they reported. A total of 173 respondents reported that they would always go to see a doctor or health care worker when they suspected they had malaria ($\chi^2 = 1.323$, $P = 0.530$), while 48 interviewees said they would take some of the anti-malarial medicine kept in their houses first ($\chi^2 = 15.322$, $P < 0.001$). The expensive costs (mentioned by 176 respondents) was the main factor preventing people from visiting the doctor or health care worker ($\chi^2 = 0.059$, $P = 0.969$). Sleeping under LLINs (198) ($\chi^2 = 1.432$, $P = 0.499$) and keeping their surrounding clean (84) ($\chi^2 = 5.982$, $P = 0.051$) were the most common methods of malaria prevention employed (**Table 5**).

TABLE 5 | Knowledge of malaria transmission, symptom and prevention in the three communities in the Western Area Rural District, Sierra Leone, 2018.

Question and answer	Community			Total	Percentage
	Grafton	Jui	Kossoh		
1. Have you or any member of your family ever heard of an illness called malaria?					
Yes	107	47	103	257	98.1%
No	1	0	4	5	1.9%
2. In your opinion, what cause malaria?*					
Mosquito bites	89	45	93	227	86.6%
Eating immature sugarcane	0	0	0	0	0.0%
Eating dirty food	6	0	1	7	2.7%
Drinking beer/palm Wine	0	0	0	0	0.0%
Drinking dirty water	11	1	4	16	6.1%
Getting soaked with rain	0	0	0	0	0.0%
Cold or changing weather	1	0	1	2	0.8%
Witchcraft I. injections/drugs	0	0	1	1	0.4%
Eating oranges or mangos	0	1	1	2	0.8%
Eating plenty oil	2	1	0	3	1.1%
Sharing razors/blades	1	0	0	1	0.4%
Don't answer	9	2	10	21	8.0%
3. Can you tell any symptoms of malaria?*					
Fever	48	27	41	116	44.3%
Excessive sweating	11	2	6	19	7.3%
Feeling cold	36	7	29	72	27.5%
Headache	33	11	11	55	21.0%
Nausea and vomiting	11	10	10	31	11.8%
Dizziness	19	13	34	66	25.2%
Loss of appetite	35	22	39	96	36.6%
Body ache or joint pain	46	16	40	102	38.9%
Body weakness	31	25	32	88	33.6%
Refusing to eat or drink	0	1	1	2	0.8%
Jaundice	0	3	3	6	2.3%
Dark urine	14	1	11	26	9.9%
Others	5	0	5	10	3.8%
Don't answer	0	0	1	1	0.4%
4. What should you do when you suspect getting malaria infection?*					
Must go to see the doctor/health worker	67	32	74	173	66.0%
Take some anti-malarial drugs kept in house	26	1	11	48	18.3%
Not necessary to see the doctor/health worker and take drugs	3	0	0	3	1.1%
Go to see the doctor/health worker only when shown severe condition	2	0	13	15	5.7%
Others: Specify.	9	1	8	18	6.9%
Don't answer	1	3	3	7	2.7%
5. What are the reasons you think that someone would not go to see the doctor/health worker when he or she gets malaria infection?*					
We are all used to it and no necessary to see the doctor	0	1	1	2	0.8%
Prayers could make us recover	0	0	0	0	0.0%
They are strong enough and could recover even if they do not see the doctor	0	0	0	0	0.0%

(Continued)

TABLE 5 | Continued

Question and answer	Community			Total	Percentage
	Grafton	Jui	Kossoh		
They have anti-malarial drugs and take it when necessary	1	11	7	19	7.3%
It is unnecessary to see the doctor/health worker for recovering from malaria	1	1	0	2	0.8%
It is too expensive to see the doctor/health worker	73	32	71	176	67.2%
It is too far to go to see the doctor/health worker	0	1	2	3	1.1%
Other reasons	33	0	21	54	20.6%
Don't answer	4	2	7	13	5.0%
6. How can someone protect themselves against malaria?*					
Sleep under treated bed net	78	38	82	198	75.6%
Untreated mosquito net	1	0	0	1	0.4%
Use mosquito repellent	2	1	1	4	1.5%
Use mosquito insecticide spray (Shelltox)	12	5	3	20	7.6%
Take preventive medication	0	9	2	11	4.2%
Indoor residual spray (IRS)	0	3	4	7	2.7%
Use mosquito coils	7	3	5	15	5.7%
Cut grass around house	6	4	1	11	4.2%
Eliminate stagnant water	8	4	9	21	8.0%
Keep surroundings clean	42	9	33	84	32.1%
Don't drink dirty water	1	0	2	3	1.1%
Contaminated food	3	0	4	7	2.7%
Use mosquito screens on windows and doors	0	1	5	6	2.3%
Others: specify	14	0	10	24	9.2%
Don't answer	1	1	1	3	1.1%
7. Where do you think the mosquito larvae live? DO NOT PROMPT ANSWER					
In water	61	33	59	153	58.4%
In weed	0	2	2	4	1.5%
In rubbish	24	6	24	54	20.6%
I don't know	19	0	17	36	13.7%
Don't answer	4	6	5	15	5.7%

**It is a multiple-choice question.*

DISCUSSION

Malaria remains one of the most serious public health issues and is responsible for high proportions of morbidity and mortality in Sierra Leone. In the present study, overall high levels of knowledge regarding the causes of malaria, prevention mechanisms and symptoms, and active seeking of treatment for malaria from health care providers were found among Sierra Leoneans, similar to the results in the MIS 2013 and 2016 (2, 10); these results with regards to knowledge and practices support malaria control (11–13).

Globally, vector control is the most commonly accomplished through the use of LLINs and indoor residual spraying (IRS), with the aim of reducing the transmission by preventing human–vector contact and killing vector mosquitoes (14, 15). The goal was for the entire at-risk population to employ preventive measures, including the use of LLINs, IRS and larval source management, by 2017 in Sierra Leone. However, 72.1% of the respondents required more nets, which may explain the high percentage (61.8%, 162/262) of households and the high proportion of children under 5 years old who did not sleep under the nets at night according to this survey. This indicates a large gap in obtaining and using nets by the most vulnerable groups who are not benefiting as much as hoped from preventive malaria interventions. Moreover, screens for doors and windows that are cost-effective to install and maintain are a supplementary

public health intervention to prevent humans from being bitten by mosquito vectors indoors, thereby significantly reducing the transmission of malaria. However, screens seem to have been neglected in the regular malaria control campaigns (16, 17), resulting in fewer than 25% of households having door or window screen in this survey, and a general low awareness of the role of screens. In addition, a low level of implementation of IRS and outside spraying and a high level of engagement in activities outside of the house at night were found, despite the presence of many mosquitoes. Therefore, how to improve residents' outdoor protection, or reduce outdoor activities at night, as well as to further improve the awareness and correct use of protective measures, can become an important content of the future malaria campaign.

The early diagnosis and prompt treatment of malaria reduces the transmission of the disease and prevents deaths. It is critical for people to seek diagnosis and care as soon as they experience any symptoms of malaria. It is encouraging that more than 80% of the respondents reported that they visited the doctor in a timely manner, and a similar percentage of respondents reported being tested for malaria, usually with RDTs not microscopy, which is the standard method for malaria diagnosis. However, approximately three-quarters of the respondents said that the doctors did not interpret the test results for the patients. Therefore, a good opportunity to provide health education and promote malaria control and prevention is being missed. A home-based RDT that could be performed by trained family members rather than at a healthcare facility may improve the timeliness of the diagnosis of malaria (18–20). Moreover, the reported adherence to completing the course of antimalarial treatment was close to 80% at the clinic or if self-administration at home. Reasons for the lack of adherence were reported to be sickness after the first dose, insufficient food to take the medicine, forgetting to take the medicine, and poor instructions provided by the community health center (CHC) (21). In addition, the cost of medical treatment and the distance from the hospital must also be considered.

However, there were some limitations of this study. First, this was a small-sample cross-sectional study conducted in three communities, and the findings are not yet nationally representative. Second, the collected data were based on respondent recall, and the data may be biased. Therefore, the results of the study highlight the need for more extensive investigations of the KAP regarding malaria in Sierra Leone.

CONCLUSION

In conclusion, in these three communities, public awareness of malaria prevention measures was relatively high in this survey, but the malaria burden was still higher than because the limited use of preventive measures against malaria potentially. Thus, the existing knowledge of malaria should be sustained and reinforced, and the availability and use of malaria prevention measures should be promoted to achieve the goals of the SL-NMSP.

DATA AVAILABILITY STATEMENT

The raw data supporting the conclusions of this article will be made available by the authors, without undue reservation.

ETHICS STATEMENT

The studies involving human participants were reviewed and approved by the Sierra Leone Ethics and Scientific Review Committee. Written informed consent to participate in this study was provided by the participants' legal guardian/next of kin.

AUTHOR CONTRIBUTIONS

JY and CZ conceived the study, developed questionnaire, and conducted fieldwork. LW and JY analyzed data and wrote the manuscript. SS and BK contributed to the study design. EN and AK conducted fieldwork and supervised fieldwork. XH, XC, XW, and WL contributed to data collation and cross-checking. All authors read and approved the final draft.

FUNDING

This study was supported by Sierra Leone-China Second Phase of the Fixed Biological Safety Laboratory Technical Cooperation Project and the National Science and Technology Major Program of China (No. 2018ZX10101002–002).

ACKNOWLEDGMENTS

We appreciate the Sierra Leonean staff for their wonderful work in the Sierra Leone-China Friendship Biological Safety Laboratory.

REFERENCES

1. World Health Organization. *World Malaria Report 2018*. Geneva: World Health Organization (2018).
2. *Sierra Leone Malaria Indicator Survey*. Freetown, Sierra Leone: NMCP, SSL, CRS, and ICF International (2016).
3. *Sierra Leone Malaria Control Strategic Plan (2016-2020)*. Freetown, Sierra Leone: National Malaria Control Programme (2015).
4. Naing PA, Maung TM, Tripathy JP, Oo T, Wai KT, Thi A. Awareness of malaria and treatment-seeking behaviour among persons with acute undifferentiated fever in the endemic regions of Myanmar. *Trop Med Health*. (2017) 45:31. doi: 10.1186/s41182-017-0070-9
5. Mathania MM, Kimera SI, Silayo RS. Knowledge and awareness of malaria and mosquito biting behaviour in selected sites within Morogoro and Dodoma regions Tanzania. *Malar J*. (2016) 15:287. doi: 10.1186/s12936-016-1332-4
6. Alelign A, Petros B. Knowledge, attitudes and practices of malaria transmission and preventive measures in Woreta town, Northwest Ethiopia. *BMC Res Notes*. (2018) 11:491. doi: 10.1186/s13104-018-3607-z
7. Wang LL, Wang XC, Pang MF, Hu XQ, Qi XP, Dong XP. The practice of the public health cooperation in the republic of sierra leone: contributions and experiences. *China CDC Weekly*. (2020) 2:28–31. doi: 10.46234/ccdcw2020.007

8. Lauritsen JM, Bruus M. *EpiData (Version 3). A Comprehensive Tool for Validated Entry and Documentation of Data*. Odense, Denmark: The EpiData Association (2003–2008).
9. Lauritsen JM, Bruus M, Myatt MA. *EpiData (Version 1.0-1.5). A Tool for Validated Entry and Documentation of Data*. County of Funen Denmark and Brixton Health UK (2001).
10. *Sierra Leone Malaria Indicator Survey*. Freetown, Sierra Leone: NMCP, SSL, CRS, and ICF International (2013).
11. Yasuoka J, Kikuchi K, Nanishi K, Ly P, Thavrin B, Omatsu T, et al. Malaria knowledge, preventive actions, and treatment-seeking behavior among ethnic minorities in Ratanakiri Province, Cambodia: a community-based cross-sectional survey. *BMC Public Health.* (2018) 18:1206. doi: 10.1186/s12889-018-6123-0
12. Balami AD, Said SM, Zulkefli NAM, Norsa'adah B, Audu B. Knowledge, motivation, self-efficacy, and their association with insecticidal net use among pregnant women in a secondary health centre in Maiduguri, Nigeria. *Malar J.* (2018) 17:359. doi: 10.1186/s12936-018-2518-8
13. Moscibrodzki P, Dobelle M, Stone J, Kalumuna C, Chiu YM, Hennig N. Free versus purchased mosquito net ownership and use in Budondo sub-county, Uganda. *Malar J.* (2018) 17:363. doi: 10.1186/s12936-018-2515-y
14. Bhatt S, Weiss DJ, Cameron E, Bisanzio D, Mappin B, Dalrymple U, et al. The effect of malaria control on *Plasmodium falciparum* in Africa between 2000 and 2015. *Nature.* (2015) 526:207–11. doi: 10.1038/nature15535
15. Killeen GF, Smith TA, Ferguson HM, Mshinda H, Abdulla S, Lengeler C, et al. Preventing childhood malaria in Africa by protecting adults from mosquitoes with insecticide-treated nets. *PLoS Med.* (2007) 4:e229. doi: 10.1371/journal.pmed.0040229
16. Kirby MJ, Ameh D, Bottomley C, Green C, Jawara M, Milligan PJ, et al. Effect of two different house screening interventions on exposure to malaria vectors and on anaemia in children in The Gambia: a randomised controlled trial. *Lancet.* (2009) 374:998–1009. doi: 10.1016/S0140-6736(09)60871-0
17. Killeen GF, Masalu JP, Chinula D, Fotakis EA, Kavishe DR, Malone D, et al. Control of malaria vector mosquitoes by insecticide-treated combinations of window screens and eave baffles. *Emerg Infect Dis.* (2017) 23:782–9. doi: 10.3201/eid2305.160662
18. Elmardi KA, Malik EM, Abdelgadir T, Ali SH, Elsyed AH, Mudather MA, et al. Feasibility and acceptability of home-based management of malaria strategy adapted to Sudan's conditions using artemisinin-based combination therapy and rapid diagnostic test. *Malar J.* (2009) 8:39. doi: 10.1186/1475-2875-8-39
19. Thiam S, Thwing J, Diallo I, Fall FB, Diouf MB, Perry R, et al. Scale-up of home-based management of malaria based on rapid diagnostic tests and artemisinin-based combination therapy in a resource-poor country: results in Senegal. *Malar J.* (2012) 11:334. doi: 10.1186/1475-2875-11-334
20. Ranasinghe S, Ansumana R, Lamin JM, Bockarie AS, Bangura U, Buanie JA, et al. Attitudes toward home-based malaria testing in rural and urban Sierra Leone. *Malar J.* (2015) 14:80. doi: 10.1186/s12936-015-0582-x
21. Gerstl S, Dunkley S, Mukhtar A, Baker S, Maikere J. Successful introduction of artesunate combination therapy is not enough to fight malaria: results from an adherence study in Sierra Leone. *Trans R Soc Trop Med Hyg.* (2010) 104:328–35. doi: 10.1016/j.trstmh.2009.12.008

Conflict of Interest: The authors declare that the research was conducted in the absence of any commercial or financial relationships that could be construed as a potential conflict of interest.

frontiers in Cellular and Infection Microbiology

MINI REVIEW
published: 19 March 2021
doi: 10.3389/fcimb.2021.647020

Phylogenomics of Tick Inward Rectifier Potassium Channels and Their Potential as Targets to Innovate Control Technologies

Perot Saelao [1,2†], Paul V. Hickner [1,2†], Kylie G. Bendele [1,2] and Adalberto A. Pérez de León [1,2‡]*

[1] USDA-ARS Knipling-Bushland U.S. Livestock Insects Research Laboratory, Kerrville, TX, United States, [2] Veterinary Pest Genomics Center, Kerrville, TX, United States

This study was conducted to enhance the identification of novel targets to develop acaricides that can be used to advance integrated tick-borne disease management. Drivers for the emergence and re-emergence of tick-borne diseases affecting humans, livestock, and other domestic animals in many parts of the world include the increased abundance and expanded geographic distribution of tick species that vector pathogens. The evolution of resistance to acaricides among some of the most important tick vector species highlights the vulnerability of relying on chemical treatments for tick control to mitigate the health burden of tick-borne diseases. The involvement of inward rectifier potassium (Kir) channels in homeostasis, diuresis, and salivary gland secretion in ticks and other pests identified them as attractive targets to develop novel acaricides. However, few studies exist on the molecular characteristics of Kir channels in ticks. This bioinformatic analysis described Kir channels in 20 species of hard and soft ticks. Summarizing relevant investigations on Kir channel function in invertebrate pests allowed the phylogenomic study of this class of ion channels in ticks. How this information can be adapted to innovate tick control technologies is discussed.

Keywords: phylogenomic, tick, Kir, Acari, evolution

OPEN ACCESS

Edited by:
Jun Feng,
National Institute of Parasitic Diseases, China

Reviewed by:
Shahid Karim,
University of Southern Mississippi, United States
Carlos Termignoni,
Federal University of Rio Grande do Sul, Brazil

***Correspondence:**
Perot Saelao
Perot.Saelao@usda.gov

[†]These authors have contributed equally to this work

[‡]Present address
Adalberto A. Pérez de León, USDA-ARS San Joaquin Valley Agricultural Sciences Center, Parlier, CA, United States

Specialty section:
This article was submitted to Parasite and Host, a section of the journal Frontiers in Cellular and Infection Microbiology

Received: *28 December 2020*
Accepted: *16 February 2021*
Published: *19 March 2021*

Citation:
Saelao P, Hickner PV, Bendele KG and Pérez de León AA (2021) Phylogenomics of Tick Inward Rectifier Potassium Channels and Their Potential as Targets to Innovate Control Technologies. Front. Cell. Infect. Microbiol. 11:647020. doi: 10.3389/fcimb.2021.647020

INTRODUCTION

Ticks (Acari) are obligate blood feeding parasites and vectors of a diverse array of pathogens including bacteria, protozoa, and viruses that cause diseases among humans, livestock, and other domestic animals (Sonenshine and Roe, 2013). The health burden of tick-borne disease (TBD) increased globally (Paules et al., 2018; Madison-Antenucci et al., 2020). In the United States alone, the number of human TBD cases more than doubled increasing from 22,527 to 48,610 between 2004 and 2016 (Rosenberg et al., 2018). Several species of hard and soft ticks are vectors of the diverse pathogens causing tick-borne diseases (Brites-Neto et al., 2015). Recent studies have implicated ticks in Alpha-Gal Syndrome, a potentially life-threatening allergy to red meat that is induced by the sugar alpha-gal from a feeding tick (Crispell et al., 2019). The application of technological advances is helping explain the global diversity of ticks and their ability to transmit pathogens (Dantas-Torres, 2018; Yang and Han, 2018).

Drivers for the emergence and re-emergence of tick-borne diseases affecting humans, livestock, and other domestic animals in many parts of the world include the increased abundance and expanded geographic distribution of tick species that vector pathogens. *Dermacentor variabilis*, the principal vector of *Rickettsia rickettsii* causing Rocky Mountain spotted fever in North America, expanded its range northward into Canada surviving the milder winters associated with variability in climatic patterns (Sonenshine, 2018). Due to its expanding geographic distribution and vector biology, *Ixodes scapularis* has become one of the most important disease vectors in North America where it transmits *Borrelia burgdorferi*, *Babesia microti*, and Powassan virus, causing Lyme disease, human babesiosis, and Powassan virus disease, respectively (Eisen and Eisen, 2018).

In addition, *Amblyomma americanum* and *Amblyomma maculatum* have expanded their range northward, extending the geographic range of additional tick species that threaten livestock (Sonenshine, 2018). Detection of the Asian longhorned tick, *Haemaphysalis longicornis*, in the United States (U.S.) in 2017 highlights the involvement of invasive tick species in the emergence of tick-borne diseases (Rainey et al., 2018). *Ha. longicornis* is a known vector of pathogens that affect humans, livestock, and other domestic animals (Beard et al., 2018). Control of tick populations, treatment of host infestations, and reduction of exposure to tick bites are critical for tick-borne disease management (Pérez De León et al., 2014).

The evolution of resistance to acaricides among some of the most important tick vector species highlights the vulnerability of relying on chemical treatments for tick control to mitigate the health burden of tick-borne diseases. In the U.S. for example, bovine babesiosis, or cattle tick fever, was eradicated by eliminating the one-host fever tick vectors, *Rhipicephalus microplus* and *R. annulatus*, through efforts of the Cattle Fever Tick Eradication Program including the systematic treatment of cattle with acaricides (Guerrero et al., 2014). However, the spread of resistance to acaricides approved for use by the Cattle Fever Tick Eradication Program among fever ticks causing outbreaks raises the specter for the emergence of bovine babesiosis in the U.S. (Thomas et al., 2020). Resistance to commonly used commercial acaricides in the three-host ticks *R. sanguineus* and *Amblyomma mixtum*, which are known vectors of human tick-borne diseases, stresses the need to innovate tick control technologies (Rodriguez-Vivas et al., 2017; Higa et al., 2020).

Discovering unique molecular targets facilitates the development of safer acaricides with new modes of action (Meng and Sluder, 2018). Previous research identified the inward rectifier potassium (Kir) channels as attractive targets to develop novel acaricides because of their involvement in homeostasis, diuresis, and salivary gland secretion in ticks and other pests (Li et al., 2019; Li et al., 2020). However, few studies exist on the molecular characteristics of Kir channels in ticks. Here, a bioinformatic analysis described Kir channels in 20 species of hard and soft ticks. Summarizing relevant investigations on Kir channel function in invertebrate pests allowed the phylogenomic study of this class of ion channels in ticks. The adaptation of this information to innovate tick control technologies is discussed.

KIR CHANNEL STRUCTURE AND GENOME REPERTOIRES

Inward rectifier potassium (Kir) channels were named due to their ability to facilitate the inward movement of K+ ions at hyperpolarizing membrane voltages more readily than the outward movement of K+ ions at depolarizing membrane voltages, a function which has been compared to an electrical diode wherein current flows in only one direction (Nishida and Mackinnon, 2002; Tao et al., 2009). The S4 voltage sensor region found in voltage-gated K^+, Na^+, and Ca^{2+} channels is absent in Kir channels; therefore, Kir channels are refractory to changes in membrane potential associated with the inward movement of other cations (Nishida and Mackinnon, 2002; Hibino et al., 2010). The outward movement of K^+ is inhibited by intracellular cations and polyamines that enter the pore from the cytoplasmic side but cannot pass through, thus blocking the channel and preventing the outward flow of K^+ (Nishida and Mackinnon, 2002; Hibino et al., 2010). These properties allow Kir channels to maintain resting membrane potential and regulate action potential duration (Hibino et al., 2010).

Kir channels are formed by the assembly of four identical or similar protein subunits, each with two transmembrane domains flanking a re-entrant loop region forming the channel pore, and N- and C-terminal cytoplasmic regions (Nichols and Lopatin, 1997; Hibino et al., 2010). The subunits are organized such that one transmembrane α-helix (TM1) is on the outside of the channel while the other (TM2) is on the inside near the pore (Hibino et al., 2010). The pore-forming region includes a selectivity filter that confers passage of K^+ but excludes Na^+ (Doyle et al., 1998). In Eukaryotes, the selectivity filter is characterized by a seven-residue motif TXGYGFR, where X is an aliphatic amino acid, and F is sometimes replaced by a different residue (Tao et al., 2009).

Sixteen genes encoding Kir channel subunits have been identified in mammals. They belong to seven subfamilies (Kir1 to Kir7) comprising four functional groups: classical, G protein-gated, ATP-sensitive, and K^+-transport channels (Hibino et al., 2010; Walsh, 2020). In mammals, Kir channels are expressed by diverse tissues comprising the nervous, muscle, cardiovascular, and urinary systems (Walsh, 2020). Consequently, abnormal function of Kir channels has been implicated in human diseases affecting these organ systems (Zangerl-Plessl et al., 2019). Mutations that cause trafficking defects associated with Kir channel dysfunction have been identified and primarily occur in two "hotspots": in and around the TM1 domain and in a segment of the C-terminal cytoplasmic region (Zangerl-Plessl et al., 2019).

Compared to mammals, insects possess a smaller repertoire of Kir channels, ranging in number from three to six genes in the species studied thus far (Lai et al., 2020). Based on phylogenetic

analysis, there are at least three different subtypes of insect Kir channels. *Drosophila melanogaster* (Luan and Li, 2012) and *Nilaparvata lugens* (Ren et al., 2018) each have three (Kir1-Kir3), while *Aedes aegypti* has four due to a duplication in Kir2 (*Kir2A* and *Kir2B*) (Piermarini et al., 2013). However, the aphids *Acyrthosiphon pisum* and *Aphis glycines* have only two (Kir1 and Kir2), suggesting a loss of Kir3 during aphid evolution (Piermarini et al., 2018). A recent study of Kir channels revealed a possible fourth subtype in Lepidoptera (Kir4), which was not found in the Diptera, Heteroptera, and Homoptera included in the study (Lai et al., 2020).

BIOINFORMATICS OF KIR CHANNELS IN TICKS

Screening of the NCBI databases produced a single Kir channel subunit gene in 20 tick species ranging from 474 to 492 amino acids in length (**Table 1**). All are apparently full-length, having start and stop codons, except for *Ornithodoros erraticus* and *O. moubata*, which did not have stop codons. Their length, however, was similar to the Kir channels in *O. rostratus* and *O. turicata* and likely represent full-length or near full-length proteins. Kir channels in *R. annulatus* and *R. microplus* were manually annotated from their respective genome assemblies and have coding sequences with six exons spanning 7,014 and 9,318 nucleotides, respectively. Despite improvements in sequencing technologies that have led to the generation of several high-quality tick genome assemblies in recent years (Miller et al., 2018; Jia et al., 2020), the lack of genome assemblies prevented the screening of all 20 tick species for additional Kir channel genes.

Based on phylogenetic analysis of the Kir channel subunits in a soft tick (*O. turicata*), two hard ticks (*I. scapularis* and *R. microplus*), two Diptera (*D. melanogaster* and *Ae. aegypti*) and two Lepidoptera (*Manduca sexta* and *Danaus plexippus*), the tick Kir channels belong to the Kir1 clade in insects (**Figure 1A**). Amino acid percent identity of tick Kirs to *D. melanogaster* Kir1 ranged from 50 to 51%. The relationships among all 20 tick Kir channel subunits are consistent with recent systematic analysis of ticks based on 18S and 28S rRNA genes and whole mitochondrial genomes (Mans et al., 2019). The soft ticks (Argasidae) and hard ticks (Ixodidae) are separated into two distinct clades, with *Ornithodoros* spp. representing the soft ticks and the remaining

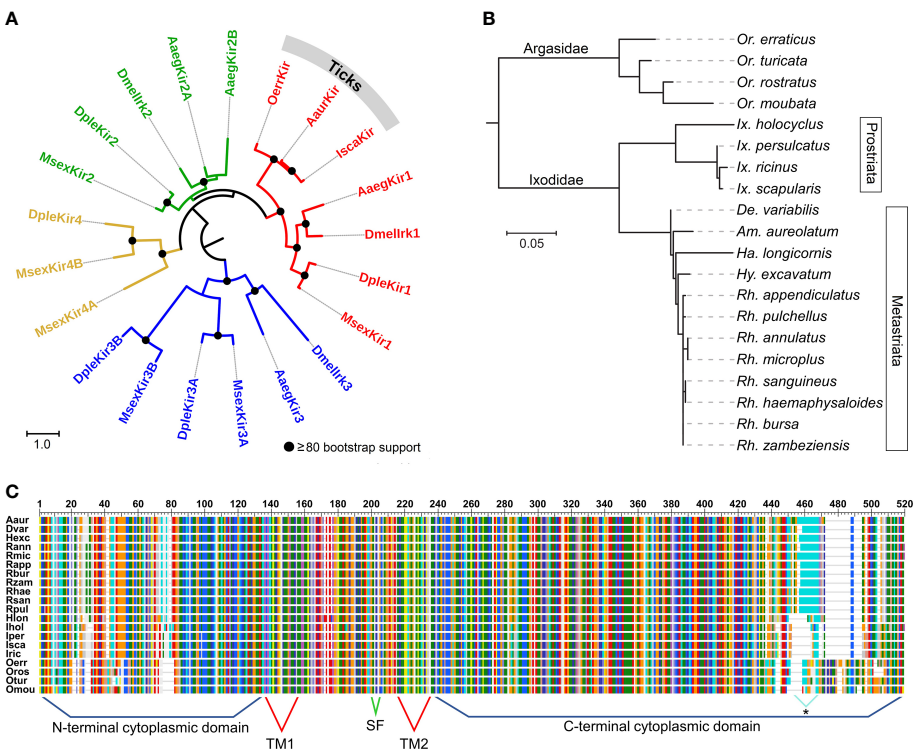

FIGURE 1 | Phylogenetic relationships and protein features of tick and insect Kir channels. **(A)** Estimated phylogenetic relationships of three tick Kir channels with those in D. melanogaster (Dmel), Aedes aegypti (Aaeg), Manduca sexta (Msex) and Danaus plexippus (Dple). The multiple alignment was conducted using the L-INS-I method in MAFFT v7.475 (Katoh et al., 2019). The phylogenies **(A, B)** were estimated using the maximum likelihood method and LG substitution model in RaxML v8.2.11 (Stamatakis, 2014). Bootstrap support was estimated using 500 replications. The trees are rooted at the midpoint. **(B)** Estimated phylogenetic relationships among 20 tick Kir channel proteins. **(C)** Multiple sequence alignment of 20 tick Kir channels illustrating the predicted transmembrane (TM) and cytoplasmic domains, and the K+ selectivity filter (SF). The C-terminus of the Metastriata ticks, except Ha. longicornis (Hlon) contains long stretches of glutamine repeats. Multiple alignment conducted using MAFFT v7.475 (Katoh et al., 2019).

TABLE 1 | Summary of tick Kir channel proteins identified in the NCBI databases. All were from transcriptome shotgun assemblies (TSA database) except *Rh. annulatus* and *Rh. Microplus*, which were acquired from their respective genome assemblies.

Species	Common name	NCBI accession	Length
Amblyomma aureolatum		GFAC01003848	490
Dermacentor variabilis	American dog tick	GGTZ01000785	486
Haemaphysalis longicornis	Asian longhorned tick	GIKJ01016725	480
Hyalomma excavatum		GEFH01003741	488
Ixodes holocyclus	Australian paralysis tick	GIBQ01000735	474
Ixodes persulcatus	Taiga tick	GBXQ01023957	479
Ixodes ricinus	Castor bean tick	GFVZ01130232	479
Ixodes scapularis	Black-legged tick	GGIX01123694	479
Ornithodoros erraticus		GFWV01008518	492
Ornithodoros moubata	African hut tampan	GFJQ01004171	486
Ornithodoros rostratus		GCJJ01005425	485
Ornithodoros turicata	Relapsing fever tick	GDIE01101609	489
Rhipicephalus annulatus	Cattle fever tick	WOVY00000000	488
Rhipicephalus appendiculatus	Brown ear tick	GEDV01010278	487
Rhipicephalus bursa		GFZJ01000158	487
Rhipicephalus haemaphysaloides		GIJA01021829	488
Rhipicephalus microplus	Southern cattle fever tick	WOVZ00000000	490
Rhipicephalus pulchellus	Zebra tick	GACK01008623	488
Rhipicephalus sanguineus	Brown dog tick	GINV01002203	488
Rhipicephalus zambeziensis		GFPF01010722	487

being hard ticks (**Figure 1B**). The soft and hard ticks differ in their feeding strategies, wherein the soft ticks are fast-feeding, and the hard ticks are long-feeding, and adaptations associated with these different feeding strategies have been described (Mans and Neitz, 2004). The divergence observed between the hard and soft tick Kir channels could reflect the physiological demands of the different feeding strategies. The Ixodidae Kir subunits formed two clades representing the Prostriata (Ixodes) and the Metastriata (all other Ixodidae), which can be separated based on morphological characteristics of the anal grooves.

A multiple sequence alignment shows the vast majority of variation to be in the N- and C-terminal domains of the protein, which flank the more highly conserved transmembrane region (**Figure 1C**). All of the tick Kir channels examined in the present study have the K^+ selectivity filter motif of TIGYGSR, except for *O. moubata* which has the motif TIGYGFR (**Figure S1**). The C-terminal domain of the Prostriata ticks, with the exception of *Ha. longicornis*, is characterized by microsatellite repeats (CAG and CAA) coding for runs of glutamine (Q), ranging from 10 to 13 residues in length (**Figures 1C** and **S1**). The role of this highly variable region of the N-terminal domain has yet to be determined.

KIR CHANNELS AS TARGETS FOR NOVEL CONTROL MEASURES

Hematophagous arthropods overcome extreme physiological challenges during and after blood feeding, most notably, post-prandial diuresis (Beyenbach, 2003; Benoit and Denlinger, 2010); therefore, inhibition of renal function could provide a means to control blood feeding arthropods and the pathogens they transmit (Piermarini et al., 2017). A series of experiments aimed at understanding insect renal physiology led to the discovery of Kir channels as key components of diuresis in insect Malpighian tubules. Among these studies were gene expression analyses showing relatively high expression of Kir channels in Malpighian tubules and functional characterization of Kir1 and Kir2 subtypes using *Drosophila* S2 and *Xenopus* oocyte heterologous expression systems (Döring et al., 2002; Piermarini et al., 2013).

The identification of small molecule inhibitors has proven to be invaluable for *in vivo* and *in vitro* analyses of Kir channels and could lead to the development of novel insecticides. The small molecule inhibitors of mammalian Kir channels, VU590 and VU573, (Raphemot et al., 2011; Denton et al., 2013) were found to modulate the activity of *Ae. aegypti* Kir1 (VU590 and VU573) and Kir2B (VU573) and cause renal failure and/or mortality in *Ae. aegypti* (Piermarini et al., 2013; Raphemot et al., 2014). One of the major concerns during the development of insecticides is the effect on non-target species such as humans and beneficial insects. A small molecule inhibitor of mosquito Kir1 (VU041) was identified by high-throughput screening that does not inhibit most mammalian Kir channels (exception Kir2.1) and is not lethal to honey bees when applied topically at the concentrations tested (Swale et al., 2016). Further, VU041 was effective in reducing fecundity in insecticide resistant and wild-type strains of *Ae. aegypti* and *An. gambiae* (Swale et al., 2016).

In addition to Malpighian tubules, there is growing evidence that Kir channels perform vital functions in the salivary glands, which are essential for osmoregulation, blood feeding, and pathogen transmission in hematophagous arthropods, making them attractive targets for disruption (Ribeiro, 1987; Sauer et al., 1995; Sauer et al., 2000; Swale et al., 2017; Nuttall, 2019). Bioactive factors produced in the salivary glands enable the acquisition of a blood meal at the host interface and facilitate the transmission of tick-borne pathogens to vertebrate hosts (Kazimírová and Stibraniova, 2013).

A recent study on the role of Kir channels in tick salivary gland function provided evidence that pharmacological

inhibition of these ion channels reduces the secretory activity of salivary glands in the lone star tick, *Amblyomma americanum* (Li et al., 2019). The reduced secretory capacity of the salivary gland was directly correlated with a dramatic reduction of blood ingestion during feeding. This study identified small-molecule modulators of Kir channel function (VU041, VU625, and VU688) that were previously shown to be inhibitors of mosquito Kir channels (Raphemot et al., 2014; Swale et al., 2016). Similarly, small molecule inhibitors reduced salivary gland secretion (VU041, VU590, VU937, and VU063) and blood meal ingestion (VU041 and VU063) in the horn fly, *Haematobia irritans* (Li et al., 2020). Although four inhibitors (VU041, VU590, VU937, and VU063) caused mortality, VU041 was the highest at 82 ± 11% (Li et al., 2020).

A recent study suggests an insecticide targeting a Kir channel has been developed and been in use for several years. Flonicamid (N-cyanomethyl-4-trifluoromethylnicotinamide) is an insecticide that is highly effective against aphids, but not against other insects, including some coleopterans, lepidopterans, and dipterans (Morita et al., 2014). It is structurally similar to neonicotinoid insecticides, which target nicotinic acetylcholine receptors (Ren et al., 2018). However, flonicamid had no activity against nicotinic acetylcholine receptors, acetylcholine esterase or sodium channels (Morita et al., 2014). The mode of action remained elusive until recently, when a study showed flonicamid had a similar effect on the *Nilaparvata lugens* Kir1 channel as VU590 (Ren et al., 2018), which is a potent inhibitor of Kir1 in *Ae. aegypti* (Rouhier et al., 2014). Flonicamid also inhibited renal excretion in *Culex pipiens* and, taken together, suggests its mode of action is by inhibiting the insect Kir1 subtype (Ren et al., 2018). Curiously, flonicamid showed little efficacy against *Ha. longicornis* after spray application at 50 ppm concentration (Park et al., 2019). This lack of activity is likely due to a failure to inhibit the *Ha. longicornis* Kir channel, thus demonstrating the need for identification of tick Kir channel inhibitors.

CONCLUSION

This review highlights the importance of Kir channels as potential targets for inhibition of renal and salivary gland function in arthropod pests and vectors of disease. Furthermore, we describe the Kir channel subunits in 20 tick species, thus providing the framework for *in vitro* functional analyses and screening of small molecule inhibitors. Recent efforts have only begun to shed light on the importance of Kir channels in tick physiology, especially their role in the regulation of blood feeding. Many gaps in our knowledge regarding the functional, temporal, spatial, and molecular characteristics of ticks still exist today. This review highlights the critical need for follow-up studies that can help elucidate these key aspects of tick Kir channel biology. The evidence for Kir channels as potential targets of insecticides and acaricides is mounting. These findings hold the potential to identifying targets for tick-borne pathogen intervention and control measures. Continued research elucidating the functional mechanisms of Kir channels and other membrane bound proteins, promises to bring an exciting new era in targeted pharmacological interventions. Although studies on the physiological role and molecular basis of Kir channel function in mammals and insects have provided critical groundwork, Kir channels in ticks remain understudied.

AUTHOR CONTRIBUTIONS

PS and AL conceived this work. PS, PH, and AL wrote the manuscript. PS, PH, and KB screened the NCBI databases for Kir sequences. All authors contributed to the article and approved the submitted version.

FUNDING

This study was funded by the United States Department of Agriculture's Agricultural Research Service (USDA-ARS) under project number: 3094-32000-042-00D.

ACKNOWLEDGMENTS

USDA is an equal opportunity employer and provider.

SUPPLEMENTARY MATERIAL

The Supplementary Material for this article can be found online at: https://www.frontiersin.org/articles/10.3389/fcimb.2021.647020/full#supplementary-material

REFERENCES

Beard, C. B., Occi, J., Bonilla, D. L., Egizi, A. M., Fonseca, D. M., Mertins, J. W., et al. (2018). Multistate infestation with the exotic disease–vector tick *Haemaphysalis longicornis*—United States, August 2017–September 2018. *Morbid Mortal. Wkly. Rep.* 67, 1310–1313. doi: 10.15585/mmwr.mm6747a3

Benoit, J. B., and Denlinger, D. L. (2010). Meeting the challenges of on-host and off-host water balance in blood-feeding arthropods. *J. Insect Physiol.* 56, 1366–1376. doi: 10.1016/j.jinsphys.2010.02.014

Beyenbach, K. W. (2003). Transport mechanisms of diuresis in Malpighian tubules of insects. *J. Exp. Biol.* 206, 3845–3856. doi: 10.1242/jeb.00639

Brites-Neto, J., Duarte, K. M. R., and Martins, T. F. (2015). Tick-borne infections in human and animal population worldwide. *Vet. World* 8, 301. doi: 10.14202/vetworld.2015.301-315

Crispell, G., Commins, S. P., Archer-Hartman, S. A., Choudhary, S., Dharmarajan, G., Azadi, P., et al. (2019). Discovery of alpha-gal-containing antigens in North American tick species believed to induce red meat allergy. *Front. Immunol.* 10, 1056. doi: 10.3389/fimmu.2019.01056

Dantas-Torres, F. (2018). Species concepts: what about ticks? *Trends Parasitol.* 34, 1017–1026 doi: 10.1016/j.pt.2018.09.009.

Denton, J. S., Pao, A. C., and Maduke, M. (2013). Novel diuretic targets. *Am. J. Physiol. Renal Physiol.* 305, F931–F942. doi: 10.1152/ajprenal.00230.2013

Döring, F., Wischmeyer, E., Kühnlein, R. P., Jäckle, H., and Karschin, A. (2002). Inwardly Rectifying K+ (Kir) Channels in Drosophila a crucial role of cellular milieu factors for kir channel function. *J. Biol. Chem.* 277, 25554–25561. doi: 10.1074/jbc.M202385200

Doyle, D. A., Cabral, J. M., Pfuetzner, R. A., Kuo, A., Gulbis, J. M., Cohen, S. L., et al. (1998). The structure of the potassium channel: molecular basis of K+ conduction and selectivity. *Science* 280, 69–77. doi: 10.1126/science.280.5360.69

Eisen, R. J., and Eisen, L. (2018). The blacklegged tick, *Ixodes scapularis*: an increasing public health concern. *Trends Parasitol.* 34, 295–309. doi: 10.1016/j.pt.2017.12.006

Guerrero, F. D., Pérez De León, A., Rodriguez-Vivas, R., Jonsson, N., Miller, R., and Andreotti, R. (2014). "Acaricide research and development, resistance and resistance monitoring," in *Biology of Ticks*, eds. D Sonenshine and R Roe. (New York: Oxford University Press)353–374.

Hibino, H., Inanobe, A., Furutani, K., Murakami, S., Findlay, I., and Kurachi, Y. (2010). Inwardly rectifying potassium channels: their structure, function, and physiological roles. *Physiol. Rev.* 90, 291–366. doi: 10.1152/physrev.00021.2009

Higa, L. D. O. S., Piña, F. T. B., Da Silva Rodrigues, V., Garcia, M. V., Salas, D. R., Miller, R. J., et al. (2020). Evidence of acaricide resistance in different life stages of *Amblyomma mixtum and Rhipicephalus microplus* (Acari: Ixodidae) collected from the same farm in the state of Veracruz, Mexico. *Prev. Vet Med.* 174, 104837. doi: 10.1016/j.prevetmed.2019.104837

Jia, N., Wang, J., Shi, W., Du, L., Sun, Y., Zhan, W., et al. (2020). Large-scale comparative analyses of tick genomes elucidate their genetic diversity and vector capacities. *Cell* 182, 1328–1340. e1313. doi: 10.1016/j.cell.2020.07.023

Katoh, K., Rozewicki, J., and Yamada, K. D. (2019). MAFFT online service: multiple sequence alignment, interactive sequence choice and visualization. *Briefings in bioinformatics* 20, 1160–1166. doi: 10.1093/bib/bbx108

Kazimírová, M., and Stibraniova, I. (2013). Tick salivary compounds: their role in modulation of host defences and pathogen transmission. *Front. Cell. Infect. Microbiol.* 3, 43.

Lai, X., Xu, J., Ma, H., Liu, Z., Zheng, W., Liu, J., et al. (2020). Identification and Expression of Inward-Rectifying Potassium Channel Subunits in *Plutella xylostella*. *Insects* 11, 461. doi: 10.3390/insects11080461

Li, Z., Macaluso, K. R., Foil, L. D., and Swale, D. R. (2019). Inward rectifier potassium (Kir) channels mediate salivary gland function and blood feeding in the lone star tick, Amblyomma americanum. *PLoS Neglect. Trop. Dis.* 13, e0007153. doi: 10.1371/journal.pntd.0007153

Li, Z., Guerrero, F., Pérez De León, A. A., Foil, L. D., and Swale, D. R. (2020). Small-Molecule Inhibitors of Inward Rectifier Potassium (Kir) Channels Reduce Bloodmeal Feeding and Have Insecticidal Activity Against the Horn Fly (Diptera: Muscidae). *J. Med. Entomol.* 57, 1131–1140 doi: 10.1093/jme/tjaa015

Luan, Z., and Li, H.-S. (2012). Inwardly rectifying potassium channels in Drosophila. *Acta Physiologica Sinica* 64, 515–519.

Madison-Antenucci, S., Kramer, L. D., Gebhardt, L. L., and Kauffman, E. (2020). Emerging Tick-Borne Diseases. *Clin. Microbiol. Rev.* 33, e00083. doi: 10.1128/CMR.00083-18

Mans, B. J., Featherston, J., Kvas, M., Pillay, K.-A., De Klerk, D. G., Pienaar, R., et al. (2019). Argasid and ixodid systematics: implications for soft tick evolution and systematics, with a new argasid species list. *Ticks tick-borne Dis.* 10, 219–240. doi: 10.1016/j.ttbdis.2018.09.010

Mans, B. J., and Neitz, A. W. (2004). Adaptation of ticks to a blood-feeding environment: evolution from a functional perspective. *Insect Biochem. Mol. Biol.* 34, 1–17. doi: 10.1016/j.ibmb.2003.09.002

Meng, C. Q., and Sluder, A. E. (2018). *Ectoparasites: drug discovery against moving targets* (Weinheim, Germany: Wiley Online Library).

Miller, J. R., Koren, S., Dilley, K. A., Harkins, D. M., Stockwell, T. B., Shabman, R. S., et al. (2018). A draft genome sequence for the *Ixodes scapularis* cell line, ISE6. *F1000Research* 7. doi: 10.12688/f1000research.13635.1

Morita, M., Yoneda, T., and Akiyoshi, N. (2014). Research and development of a novel insecticide, flonicamid. *J. Pesticide Sci.* 39, 179–180. doi: 10.1584/jpestics.J14-05

Nichols, C., and Lopatin, A. (1997). Inward rectifier potassium channels. *Annu. Rev. Physiol.* 59, 171–191. doi: 10.1146/annurev.physiol.59.1.171

Nishida, M., and Mackinnon, R. (2002). Structural basis of inward rectification: cytoplasmic pore of the G protein-gated inward rectifier GIRK1 at 1.8 Å resolution. *Cell* 111, 957–965. doi: 10.1016/S0092-8674(02)01227-8

Nuttall, P. A. (2019). Tick saliva and its role in pathogen transmission. *Wiener klinische Wochenschrift*, 1–12. doi: 10.1007/s00508-019-1500-y

Park, G. H., Kim, H. K., Lee, W. G., Cho, S. H., and Kim, G. H. (2019). Evaluation of the acaricidal activity of 63 commercialized pesticides against *Haemaphysalis longicornis* (Acari: Ixodidae). *Entomological Res.* 49, 330–336. doi: 10.1111/1748-5967.12367

Paules, C. I., Marston, H. D., Bloom, M. E., and Fauci, A. S. (2018). Tickborne diseases—confronting a growing threat. *N. Engl. J. Med.* 379, 701–703. doi: 10.1056/NEJMp1807870

Pérez De León, A. A., Teel, P. D., Li, A., Ponnusamy, L., and Roe, R. M. (2014). Advancing integrated tick management to mitigate burden of tick-borne diseases. *Outlooks Pest Manage.* 25, 382–389. doi: 10.1564/v25_dec_10

Piermarini, P. M., Rouhier, M. F., Schepel, M., Kosse, C., and Beyenbach, K. W. (2013). Cloning and functional characterization of inward-rectifying potassium (Kir) channels from Malpighian tubules of the mosquito *Aedes aegypti*. *Insect Biochem. Mol. Biol.* 43, 75–90. doi: 10.1016/j.ibmb.2012.09.009

Piermarini, P. M., Esquivel, C. J., and Denton, J. S. (2017). Malpighian tubules as novel targets for mosquito control. *Int. J. Environ. Res. Public Health* 14, 111. doi: 10.3390/ijerph14020111

Piermarini, P. M., Inocente, E. A., Acosta, N., Hopkins, C. R., Denton, J. S., and Michel, A. P. (2018). Inward rectifier potassium (Kir) channels in the soybean aphid *Aphis glycines*: Functional characterization, pharmacology, and toxicology. *J. Insect Physiol.* 110, 57–65. doi: 10.1016/j.jinsphys.2018.09.001

Rainey, T., Occi, J. L., Robbins, R. G., and Egizi, A. (2018). Discovery of *Haemaphysalis longicornis* (Ixodida: Ixodidae) parasitizing a sheep in New Jersey, United States. *J. Med. Entomol.* 55, 757–759. doi: 10.1093/jme/tjy006

Raphemot, R., Lonergan, D. F., Nguyen, T. T., Utley, T., Lewis, L. M., Kadakia, R., et al. (2011). Discovery, Characterization, and Structure–Activity Relationships of an Inhibitor of Inward Rectifier Potassium (Kir) Channels with Preference for Kir2. 3, Kir3. X, and Kir7. 1. *Front. Pharmacol.* 2, 75.

Raphemot, R., Rouhier, M. F., Swale, D. R., Days, E., Weaver, C. D., Lovell, K. M., et al. (2014). Discovery and Characterization of a Potent and Selective Inhibitor of *Aedes aegypti* Inward Rectifier Potassium Channels. *PLoS One* 9, e110772. doi: 10.1371/journal.pone.0110772

Ren, M., Niu, J., Hu, B., Wei, Q., Zheng, C., Tian, X., et al. (2018). Block of Kir channels by flonicamid disrupts salivary and renal excretion of insect pests. *Insect Biochem. Mol. Biol.* 99, 17–26. doi: 10.1016/j.ibmb.2018.05.007

Ribeiro, J. (1987). Role of saliva in blood-feeding by arthropods. *Annu. Rev. Entomol.* 32, 463–478. doi: 10.1146/annurev.en.32.010187.002335

Rodriguez-Vivas, R., Ojeda-Chi, M., Trinidad-Martinez, I., and De León, A. P. (2017). First documentation of ivermectin resistance in *Rhipicephalus sanguineus* sensu lato (Acari: Ixodidae). *Vet. Parasitol.* 233, 9–13. doi: 10.1016/j.vetpar.2016.11.015

Rosenberg, R., Lindsey, N. P., Fischer, M., Gregory, C. J., Hinckley, A. F., Mead, P. S., et al. (2018). Vital signs: trends in reported vectorborne disease cases—United States and Territories 2004–2016. *Morbid, Mortal. Weekly Rep.* 67, 496. doi: 10.15585/mmwr.mm6717e1

Rouhier, M. F., Raphemot, R., Denton, J. S., and Piermarini, P. M. (2014). Pharmacological validation of an inward-rectifier potassium (Kir) channel as an insecticide target in the yellow fever mosquito *Aedes aegypti*. *PLoS One* 9, e100700. doi: 10.1371/journal.pone.0100700

Sauer, J., Mcswain, J., Bowman, A., and Essenberg, R. (1995). Tick salivary gland physiology. *Annu. Rev. Entomol.* 40, 245–267. doi: 10.1146/annurev.en.40.010195.001333

Sauer, J., Essenberg, R., and Bowman, A. (2000). Salivary glands in ixodid ticks: control and mechanism of secretion. *J. Insect Physiol.* 46, 1069–1078. doi: 10.1016/S0022-1910(99)00210-3

Sonenshine, D. E. (2018). Range expansion of tick disease vectors in North America: implications for spread of tick-borne disease. *Int. J. Environ. Res. Public Health* 15, 478. doi: 10.3390/ijerph15030478

Sonenshine, D. E., and Roe, R. M. (2013). Ticks, people, and animals. *Biology of Ticks* (New York: Oxford University Press), 3–16.

Stamatakis, A. (2014). RAxML version 8: a tool for phylogenetic analysis and post-analysis of large phylogenies. *Bioinformatics* 30, 1312–1313. doi: 10.1093/bioinformatics/btu033

Swale, D. R., Engers, D. W., Bollinger, S. R., Gross, A., Inocente, E. A., Days, E., et al. (2016). An insecticide resistance-breaking mosquitocide targeting inward

rectifier potassium channels in vectors of Zika virus and malaria. *Sci. Rep.* 6, 36954–36954. doi: 10.1038/srep36954

Swale, D. R., Li, Z., Guerrero, F., De León, A., and Foil, L. D. (2017). Role of inward rectifier potassium channels in salivary gland function and sugar feeding of the fruit fly, *Drosophila melanogaster*. *Pesticide Biochem. Physiol.* 141, 41–49. doi: 10.1016/j.pestbp.2016.11.005

Tao, X., Avalos, J. L., Chen, J., and Mackinnon, R. (2009). Crystal structure of the eukaryotic strong inward-rectifier K+ channel Kir2. 2 at 3.1 Å resolution. *Science* 326, 1668–1674.

Thomas, D. B., Klafke, G., Busch, J. D., Olafson, P. U., Miller, R. A., Mosqueda, J., et al. (2020). Tracking the increase of acaricide resistance in an invasive population of Cattle Fever Ticks (Acari: Ixodidae) and implementation of real-time PCR assays to rapidly genotype resistance mutations. *Ann. Entomological Soc. America* 113, 298–309. doi: 10.1093/aesa/saz053

Walsh, K. B. (2020). Screening Technologies for Inward Rectifier Potassium Channels: Discovery of New Blockers and Activators. *SLAS DISCOVERY: Advancing Sci. Drug Discov.* 25, 420–433.

Yang, L. H., and Han, B. A. (2018). Data-driven predictions and novel hypotheses about zoonotic tick vectors from the genus Ixodes. *BMC Ecol.* 18, 1–6. doi: 10.1186/s12898-018-0163-2

Zangerl-Plessl, E.-M., Qile, M., Bloothooft, M., Stary-Weinzinger, A., and Van Der Heyden, M. A. (2019). Disease Associated Mutations in KIR Proteins Linked to Aberrant Inward Rectifier Channel Trafficking. *Biomolecules* 9, 650. doi: 10.3390/biom9110650

Conflict of Interest: Any mention of trade names or commercial products in this publication is solely for the purpose of providing specific information and does not imply a recommendation or endorsement by the U.S. Department of Agriculture. The USDA is an equal opportunity provider and employer.

The authors declare that the research was conducted in the absence of any commercial or financial relationships that could be construed as a potential conflict of interest.

frontiers in Cellular and Infection Microbiology

ORIGINAL RESEARCH
published: 24 March 2021
doi: 10.3389/fcimb.2021.653843

Therapeutic Efficacy of Excretory-Secretory Products of *Trichinella spiralis* Adult Worms on Sepsis-Induced Acute Lung Injury in a Mouse Model

Huihui Li[1,2], *Dapeng Qiu*[3], *Huijuan Yang*[1,2], *Yuan Yuan*[1,2], *Lingqin Wu*[1,2], *Liang Chu*[3], *Bin Zhan*[4], *Xiaoli Wang*[1,2], *Yan Sun*[1,2], *Wei Xu*[1,2] *and Xiaodi Yang*[1,2*]

[1] *Department of Basic Medical College, Bengbu Medical College, Bengbu, China,* [2] *Anhui Key Laboratory of Infection and Immunity of Bengbu Medical College, Bengbu, China,* [3] *Department of Orthopedics, Second Affiliated Hospital of Bengbu Medical College, Bengbu, China,* [4] *National School of Tropical Medicine, Baylor College of Medicine, Houston, TX, United States*

OPEN ACCESS

Edited by:
Xiaojun Chen,
Nanjing Medical University, China

Reviewed by:
Xin Ping Zhu,
Capital Medical University, China
Shannon Moonah,
University of Virginia, United States

***Correspondence:**
Xiaodi Yang
yxd_qf@bbmc.edu.cn

Specialty section:
This article was submitted to Parasite and Host, a section of the journal Frontiers in Cellular and Infection Microbiology

Received: *15 January 2021*
Accepted: *08 March 2021*
Published: *24 March 2021*

Citation:
Li H, Qiu D, Yang H, Yuan Y, Wu L, Chu L, Zhan B, Wang X, Sun Y, Xu W and Yang X (2021) Therapeutic Efficacy of Excretory-Secretory Products of Trichinella spiralis Adult Worms on Sepsis-Induced Acute Lung Injury in a Mouse Model. Front. Cell. Infect. Microbiol. 11:653843. doi: 10.3389/fcimb.2021.653843

Acute lung injury (ALI) is a common complication of systemic inflammation or sepsis with high morbidity and mortality. Although many studies have confirmed that helminth-derived proteins had strong immunomodulatory functions and could be used to treat inflammatory diseases, there is no report on the therapeutic effect of excretory-secretory products of *Trichinella spiralis* adult worms (*Ts*-AES) on sepsis-induced ALI. In this study, the therapeutic efficacy of *Ts*-AES on sepsis-induced ALI and the underlying immunological mechanism and the signaling pathway were investigated. The results indicated that after being treated with *Ts*-AES, the survival rate of mice with CLP-induced sepsis was significantly increased to 50% for 72 hours after CLP surgery compared to PBS control group with all mice died. The sepsis-induced ALI was largely mitigated characterized by reduced inflammation cell infiltration and pathological changes in lung tissue, with decreased lung injury scores and lung wet/dry weight ratio. The therapeutic efficacy of *Ts*-AES is associated with stimulated Tregs response with increased regulatory cytokines IL-10 and TGF-β and downregulated pro-inflammatory cytokines (TNF-α, IL-6, IL-1β). The expression of HMGB1, TLR2 and MyD88 in lung tissue was inhibited after treatment of *Ts*-AES. Our results demonstrated that *Ts*-AES play an important role in immunomodulation and confer a therapeutic effect on sepsis-induced ALI through inhibiting pro-inflammatory cytokines. The activation of Tregs and increased level of regulatory cytokines IL-10 and TGF-β are possibly involved in the immunomodulatory functions of *Ts*-AES through HMGB1/TLR2/MyD88 signal pathway. The findings suggest *Ts*-AES is a potential therapeutic agent for prevention and treatment of sepsis-induced ALI and other inflammatory diseases.

Keywords: excretory-secretory products, *Trichinella spiralis*, sepsis, acute lung injury, cecal ligation and puncture, immunomodulation

INTRODUCTION

Sepsis is life-threatening organ dysfunction caused by a dysregulated severe host immune response to an infection (Singer et al., 2016). It can lead to multiple organ injuries and even death affecting the lives of millions of people around the world (Butt et al., 2016; Novosad et al., 2016; Rello et al., 2017). Acute lung injury (ALI) occurs earliest in sepsis and is a main cause of death (Rubenfeld et al., 2005; Rudd et al., 2020). Although there are various therapeutic strategies for ALI which include the administration of nitric ox surfactant and glucocorticoids, none of them reduces the mortality in sepsis-induced ALI (Li et al., 2020). Thus, searching for novel and more effective therapeutic approaches is an urgent need for the treatment of sepsis-induced ALI and reducing the ALI-caused death.

High mobility group box 1 protein (HMGB1), a highly conserved nuclear DNA–binding protein, is a late inflammatory cytokine that activates macrophages and dendritic cells to produce inflammatory cytokines, playing a key role in triggering the inflammatory response in the pathogenesis of ALI and sepsis (Deng et al., 2018; Li and Lu, 2021; Xie et al., 2021). During sepsis, HMGB1 is secreted into the extracellular milieu after stimulating by bacterial endotoxin or pro-inflammatory cytokines. TLRs (TLR2 and TLR4) are reportedly the primary receptors of HMGB1 that transmit intracellular signals by Myd88 to stimulate the secretion of pro-inflammatory cytokines, which in turn promote HMGB1 secretion as a positive feedback loop during the inflammatory process (Lee et al., 2014). It has been shown that HMGB1 was elevated in the sera of septic patients, suppressing HMGB1 levels by pharmacological intervention and reducing CLP-induced sepsis mortality (Rosas-Ballina et al., 2009; Valdés-Ferrer et al., 2013; Deng et al., 2019; Wang J. et al., 2020). These findings suggest that HMGB1 could be a therapeutic target for preventing inflammation and ALI in sepsis.

Since the hygiene hypothesis was proposed by Strachan in 1989 (Strachan, 1989), an increasing number of experiments and epidemiological studies have revealed the inverse correlation between the inflammation, autoimmune or allergic diseases with helminth infections (van Riet et al., 2007; Zaccone et al., 2008; Erb, 2009; Osada and Kanazawa, 2010; Smallwood et al., 2017). Parasitic helminths co-evolve with mammalian hosts and develop some strategies such as activating host Th2-dominant immune response and regulatory T cell response to survive within hosts (O'Regan et al., 2014; Passos et al., 2017; Hernández-Ancheyta et al., 2018). Further evidences have showed that helminths regulated the local or systemic immune response of host through secreting some biofunctional proteins in excretory-secretory (ES) products. For instance, the ES products of *Marshallagia marshalli* had anti-inflammatory potentials on allergic airway inflammation in mice (Shirvan et al., 2016), and ES products of *Brugia malayi* attenuated development of streptozotocin-induced type 1 diabetes in mice associated with the decreased production of pro-inflammatory cytokines and increased production of IL-10 (Amdare et al., 2015).

Trichinella spiralis is one of the most widespread zoonotic parasitic nematodes in the world. Its life cycle is completed within a single host including three stages: muscle larvae inside skeletal striated muscle cells, adult worms in the small intestine, and newborn larvae in the lymphatic vessels and bloodstream. During the chronic phase of the *T. spiralis* infection, the adult worms or muscle larvae secrete or release ES products into host to activate regulatory network elements to reduce host immune attack as a survival strategy (Bai et al., 2012; Sofronic-Milosavljevic et al., 2015; Kosanović et al., 2019). ES products derived from different developmental stages of *T. spiralis* may act different immunomodulatory effects (Yang et al., 2014; Jin et al., 2019a). Many experimental studies have shown that infection with *T. spiralis* or exposure to ES products of *T. spiralis* induced a strong Th2/Treg response correlated with the stimulation of anti-inflammatory cytokines (IL-4, IL-5, and IL-13) and regulatory cytokines (IL-10, TGF-β), as well as the inhibition of pro-inflammatory cytokines (TNF-α, IL-6 and IL-1β) (Han et al., 2019; Sun et al., 2019b; Ding et al., 2020). *T. spiralis* ES has been successfully used for the treatment of inflammatory bowel diseases (Yang et al., 2014; Jin et al., 2019a; Wang Z. et al., 2020), allergic asthma (Sun et al., 2019a) and sepsis (Du et al., 2014) in mouse models.

In this study, we explored the therapeutic effect of ES products from *T. spiralis* adult worms (*Ts*-AES) on CLP-induced septic ALI in BALB/c mice and we found that treatment with *Ts*-AES significantly improved the survival rate against systematic sepsis and reduced the sepsis-induced ALI in mouse model, providing a potential treatment method to control sepsis-induced ALI and death.

MATERIALS AND METHODS

Animals

Male specific pathogen-free BALB/c mice (6-8 weeks old with weight of 18-22 g), female ICR mice (6-8 weeks old with weight of 25-30 g) and female Wistar mice (6 weeks old with weight of 180-220 g) were purchased from the Animal Center of Bengbu Medical College and maintained under controlled temperature of 20-25°C, relative humidity of 40-55% and a 12:12 h light/dark cycle. All animals received a normal rodent diet and free access to water. All experiments were performed in accordance with protocols approved by Animal Care and Use Committee of Bengbu Medical College (approval no: LAEC-2014-039).

Preparation of *Ts*-AES

T. spiralis muscle larvae were isolated from the muscles of infected female ICR mice by a previously described method of modified pepsin-hydrochloric acid digestion (Gu et al., 2013) as a source for infection. Each Wistar rat was orally infected with 12,000 muscle larvae of *T. spiralis* (Martínez-Gómez et al., 2009; Sun et al., 2019b) and the adult worms were collected from intestines of mice 106 hours post infection. The collected adult worms were washed with phosphate-buffered saline (PBS) for three times and then cultured in RPMI-1640 medium

(Hyclone, Logan, UT, USA) supplemented with 100 U/mL penicillin and 100 μg/mL streptomycin (Gibco, Grand Island, NY, USA) at 37°C, 5% CO_2 for 48 h. The culture supernatant containing *Ts*-AES was collected and concentrated by centrifugating and buffer exchanged into PBS. The potential contaminated endotoxin in *Ts*-AES products was removed using a ToxOut™ High Capacity Endotoxin Removal Kit (BioVision, Palo Alto, California, USA) and confirmed using ToxinSensor™ Chromogenic Limulus Amebocyte Lysate (LAL) Endotoxin Assay Kit (GenScript Biotechnology, Nanjing, China) following the manufacturer's protocol. The protein concentration of the prepared *Ts*-AES was determined by Bicinchoninic Acid Protein Assay Kit (Beyotime Biotechnology, Shanghai, China) and then stored at -80°C until use.

Sepsis Induced by Cecal Ligation and Puncture (CLP)

Sepsis model was established on the basis of the cecal ligation and puncture (CLP) (Rittirsch et al., 2009). Briefly, Male BALB/c mice were fasted for 12 h with drinking water only. A 0.8-cm midline incision was made for each mouse to expose the cecum under anesthesia with intraperitoneal injection of 4% chloral hydrate (0.2 ml/20 g) (**Figures 1A, B**). The cecum was isolated and ligated tightly with a 3.0 silk at 1.5 cm from the tip (**Figures 1C, D**). A through-and-through puncture was made on the cecum using an 18-gauge needle and a small amount of feces was extruded (**Figure 1E**). The cecum was returned back to the abdominal cavity and each opened layer was closed with 4.0 silk sutures (**Figures 1F, G**). Following CLP, 200 μl of sterile saline was injected sub-dermally to each mouse for fluid resuscitation (**Figure 1H**). The same laparotomy was operated for sham control group without cecum ligation and puncture.

Treatment of Sepsis With *Ts*-AES

BABL/c mice were randomly divided into 4 groups with 16 mice each: (i) sham-operated (mice underwent the same procedure, except for ligation and puncture of the cecum) with PBS (Sham +PBS), (ii) CLP with PBS (CLP+PBS), (iii) CLP treated with *Ts*-AES (CLP+AES), (iv) Sham-operated treated with *Ts*-AES (Sham+AES). CLP+PBS and CLP+AES groups were CLP operated and then treated intraperitoneally with PBS or 15 μg of *Ts*-AES in a total volume of 200 μl 30 min after surgery, respectively. Sham+PBS and Sham+AES groups were performed sham surgery without ligation and puncture of the cecum and given with the same amount of PBS or *Ts*-AES after surgery, respectively. Six mice in each group were sacrificed 12 h after surgery and treatment for measuring the level of inflammatory cytokines in blood and lung and pathological change in lung tissue. The remaining 10 mice were observed for general physical conditions and survival rate for 72 h. The survival rates were determined using Kaplan-Meier method.

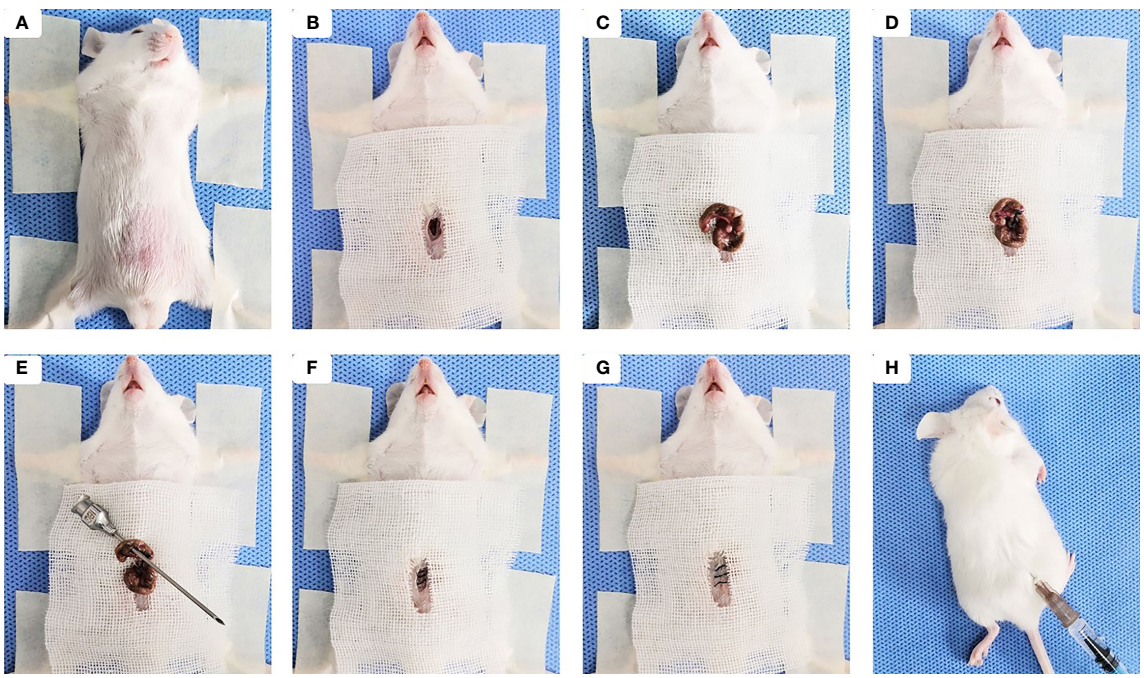

FIGURE 1 | Sepsis-induced ALI was established by the cecal ligation and puncture (CLP). **(A)** The mouse was placed in a supine position under anesthesia, then the abdominal area was shaved, cleaned, and disinfected. **(B)** Skin midline incision was made. **(C)** The cecum was isolated. **(D)** The cecum was ligated tightly with silk at 1.5 cm from the tip. **(E)** Cecal puncture (a through-and-through) was made after cecum ligation. **(F)** The cecum was returned back to the abdominal cavity and muscle layer was closed. **(G)** The skin incision was disinfected after suturing. **(H)** 200 μl of sterile saline was injected sub-dermally to each mouse.

Detection of Cytokines in Sera Using Enzyme-Linked Immunosorbent Assay (ELISA)

Six mice from each group were anesthetized with 4% chloral hydrate and blood samples were collected from the fundus venous plexus 12 h after surgery. The sera were collected from the blood samples by centrifuging at 4000 rpm for 15 min. The serological levels of the pro-inflammatory cytokines (TNF-α, IL-6, IL-1β) and regulatory cytokines (IL-10 and TGF-β) were determined using LEGEND MAX™ ELISA kits (Dakewe Biotech, Beijing, China) according to the manufacturer's instructions.

Lung Collection for Pathological Observation

After blood samples were collected 12 hours after surgery, the six mice from each group were euthanized with cervical dislocation and the lung tissues were collected by postmortem bilateral thoracotomy. The left lungs were frozen at -80°C until use for quantitative real time PCR (qRT-PCR) and western blot analysis. The right lungs were collected for the determination of lung wet/dry weight ratio and histopathological changes. Superior and middle lobes of right lung were collected and the wet weight of the tissue was weighed immediately, then the lung tissues were dried out by baking in a hot air oven at 70°C for 48 h and weighed. The lung wet/dry weight ratio was calculated to assess tissue edema. The inferior and postcaval lobes of right lung samples were fixed in 4% paraformaldehyde neutral buffer solution and cut into 5 μm sections and stained with hematoxylin and eosin (HE). The stained sections were observed under microscope (Olympus, Tokyo, Japan). The histological lung injury was scored as 0-4 based on 4 criteria: 1) alveolar hemorrhage and congestion; 2) alveolar edema; 3) alveolar or vascular wall neutrophil infiltration or aggregation; and 4) alveolar septum thickening, according to lesion severity as shown in **Table 1** (Meng et al., 2018; Shao et al., 2019).

Quantitative Real Time PCR (qRT-PCR)

Total RNA was extracted from left lung samples using TRIzol™ Reagent (Invitrogen, Carlsbad, CA, USA) and reversely transcribed to cDNA by using the Superscript First Strand cDNA Synthesis Kit (Thermo Fisher Scientific Inc., Waltham, MA, USA) according to the manufacturer's instructions. A quantitative analysis of the relative mRNA expression of different cytokines (TNF-α, IL-6, IL-1β, IL-10 and TGF-β), HMGB1, TLR2 and MyD88 in murine lung tissues were determined in triplicate using SYBR Green Super Mix Kit (Takara Bio Inc., Tokyo, Japan) on a Roche LightCycler® 96 real-time PCR system (Roche Molecular Systems, Inc., USA). The relative mRNA expression was calculated with the comparative $\triangle$Cq method using the formula $2^{-\triangle\triangle Cq}$ compared to GAPGH housekeeper gene control. The primers listed in **Table 2** were designed and synthesized by Sangon Biotech (Shanghai, China) for testing each gene expression.

Detection of HMGB1, TLR2, and MyD88 Expression in Lung Tissue by Western Blotting

The protein of left lung samples was isolated by dissolving tissue with RIPA buffer containing 0.1% phenylmethylsulfonyl fluoride (PMSF) and centrifuged at 12000 rpm for 20 min at 4°C. The proteins were separated using 12% SDS-PAGE and transferred onto polyvinylidene difluoride (PVDF) membranes. The membranes were blocked with 5% nonfat dry milk in Tris-buffered saline containing 0.05% Tween-20 (TBST), and then incubated overnight at 4°C with following primary antibodies: anti-β-actin (1:2000), anti-HMGB1(1:1000) anti-MyD88 (1:1000), (Cell Signaling Technology, Danvers, Massachusetts, USA) and anti-TLR2(1:1500) (Abcam, Cambridge, UK), respectively. Goat anti-mouse IgG was used as secondary antibody (Merck Millipore, Basilica, Massachusetts, USA) at 1:8,000 dilution for 1 h at 37°C. Immunoreactive protein bands were visualized using a Bio-Rad ChemiDoc XRS+ Chemiluminescence imaging system (Bio-Rad, Hercules, CA, USA). Semi-quantitatively analyses on developed bands were performed by ImageJ software.

Flow Cytometry

Spleen was collected from each euthanized mouse 12 hours after surgery and treatment, the single cell suspension was prepared in PBS containing 2% FBS for staining. The cell surfaces were blocked with rat anti-mouse CD16/CD32 antibody for 15 min at 4°C, and then incubated with PE-Cy7-anti-CD3Ɛ, FITC-anti-CD4 and APC-anti-CD25 antibodies (Biolegend, London, United Kingdom) for surface marker staining. After washing, fixation, permeabilization and a second blocking, the intracellular labeling of Foxp3 protein was performed by incubating the cells with PE-anti-Foxp3 antibody for 30 min on ice in the dark. The isotype-matched immunoglobulins (Biolegend, London, United Kingdom) and FMO were used as

TABLE 1 | Lung injury score parameters.

Index	Alveolar hemorrhage and congestion	Alveolar edema	Alveolar or vascular wall neutrophil infiltration or aggregation	Alveolar septum thickening
0	None or very mild lesions			
1	Mild lesions (<25% lung involvement)			
2	Moderate lesions (25–50% lung involvement)			
3	Severe lesions (50–75% lung involvement)			
4	Very severe lesions (>75% lung involvement)			

TABLE 2 | The primers of qRT-PCR.

Primer	Forward	Reverse
TNF-α	ACGGCATGGATCTCAAAGAC	GTGGGTGAGGAGCACGTAGT
IL-6	CCGGAGAGGAGACTTCACAG	TCCACGATTTCCCAGAGAAC
IL-1β	TCTTTGAAGAAGAGCCCATCC	CTAATGGGAACGTCACACAC
TGF-β	CTGGATACCAACTACTGCTTCAG	TTGGTTGTAGAGGGCAAGGACCT
IL-10	CCAAGCCTTATCGGAAATGA	TTTTCACAGGGGAGAAATCG
TLR2	TGCAAGTACGAACTGGACTTCT	CCAGGTAGGTCTTGGTGTTCATT
HMGB1	GGCGAGCATCCTGGCTTATC	AGGCAGCAATATCCTTCTCATAC
MyD88	ACTGGCCTGAGCAACTAGGA	CGTGCCACTACCTGTAGCAA
GAPDH	ACCCAGAAGACTGTGGATGG	CACATTGGGGGTAGGAACAC

control for non-specific staining as baseline. The cells were washed twice with fluorescence-activated cell sorting staining buffer and analyzed by DxP Athena™ flow cytometer (CYTEK, USA). All the results were analyzed using FlowJo® 7.6 software (Treestar, Ashland, OR, USA).

Statistical Analysis

All data were presented as the mean ± standard deviation (SD), and statistical analyses were performed using GraphPad Prism 5.0 software (GraphPad Inc., La Jolla, CA, USA). Comparison of the same parameters in multiple datasets or more than two groups was done using one-way analysis of variance (ANOVA). The difference in survival rates among four groups was compared using Kaplan-Meier survival analysis. $P < 0.05$ was considered as statistically significant.

RESULTS

Ts-AES Improved the Survival Rate of Septic Mice

Ts-AES was used to treat sepsis in a CLP-induced sepsis mouse model, to determine whether it improves the survival rate of septic mice. As shown in **Figure 2**, all mice died 72 h after CLP operation treated with PBS only (CLP+PBS). However, the 72 hours survival rate for septic mice treated intraperitoneally with 15 μg of *Ts*-AES (CLP+AES) increased to 50% with significant difference compared to CLP group without treatment (CLP+PBS) ($P<0.05$). All mice in sham groups with or without *Ts*-AES treatment survived for 72 h period. This result suggests that treatment with *Ts*-AES significantly improves the survival rate of mice with sepsis.

Ts-AES Reduced Sepsis-Caused Acute Lung Injury (ALI)

The lung tissue structure and pathological changes of mice 12 h after CLP surgery and treatment were determined by histochemical staining of lung tissue sections. The results showed that Sham+PBS group and Sham+AES group had no evidence of inflammation with normal arrangement of the lung structure. However, the lung tissue in CLP+PBS group showed alveolar congestion, structural disruption and thickened alveolar septum with the inflammatory cell infiltration, showing typical pathology of acute lung injury (ALI) (**Figure 3A**) with high lung injury scores and high ratio of wet/dry weight (**Figures 3B, C**). After treatment with *Ts*-AES, the lung injury caused by sepsis was significantly mitigated with significantly reduced inflammatory cell infiltration, lung injury scores compared to mice with CLP-induced sepsis without treatment (CLP+PBS) (**Figures 3A, B**). The sepsis inflammation caused pulmonary edema was also significantly reduced in CLP group treated with *Ts*-AES compared to CLP group treated with PBS only based on the reduced ratio of wet/dry weight ($P<0.05$) (**Figure 3C**). These results suggest that treatment with *Ts*-AES significantly attenuates the lung tissue pathology caused by sepsis and reduces the water content of lung tissue and pulmonary edema in septic ALI mice caused by inflammatory congestion and infiltration.

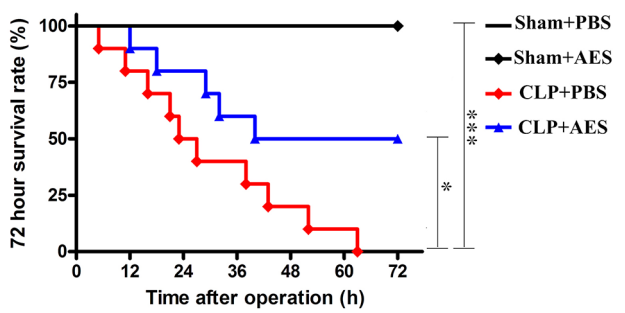

FIGURE 2 | *Ts*-AES treatment improved the survival rate of mice with CLP-induced sepsis. After CLP or sham operation, mice were injected intraperitoneally with *Ts*-AES or PBS. The survival rate was determined using Kaplan Meier method and compared by log-rank test (n = 10 mice per group). *$P < 0.05$, ***$P < 0.001$.

Ts-AES Inhibited Pro-inflammatory Cytokines and Induced IL-10 and TGF-β in Septic Mice

Sepsis was characterized by surged pro-inflammatory cytokines in the blood circulation (Hübner et al., 2013) which induced acute lung injury. We examined the serological levels of some pro-inflammatory cytokines in mice of each group and revealed that TNF-α, IL-6 and IL-1β were significantly increased in septic mice 12 h after CLP operation (CLP+PBS). However, treatment with *Ts*-AES significantly reduced their serological levels of TNF-α, IL-6 and IL-1β (CLP+AES) compared to those without treatment (CLP+PBS) (**Figure 4**). We also found that treatment with *Ts*-AES stimulated the secretion of IL-10 and TGF-β in sera of septic mice (CLP+AES) compared to CLP group without treatment (CLP+PBS). Treatment with *Ts*-AES had no effect on the serological levels of pro-inflammatory cytokines (TNF-α, IL-6, IL-1β) or regulatory cytokines (IL-10 and TGF-β) in sham surgery groups with or without *Ts*-AES treatment (Sham+AES or Sham+PBS). These data indicated that *Ts*-AES inhibited inflammatory cytokines in septic mice associated with increased serological levels of regulatory cytokines IL-10 and TGF-β.

The similar effects of *Ts*-AES treatment on these cytokines were also identified in lung tissue by measuring their mRNA levels. The qRT-PCR results showed that the mRNA expression levels of pro-inflammatory cytokines TNF-α, IL-6 and IL-1β were significantly reduced in lung tissue of septic mice treated with *Ts*-AES (CLP+AES) compared to the septic mice treated with PBS only (CLP+PBS). The reduced mRNA expression levels of pro-inflammatory cytokines were correlated with the increased regulatory cytokines IL-10 and TGF-β mRNA expression levels in lung tissues of septic mice treated with *Ts*-AES (CLP+AES) compared with the CLP group without treatment (CLP+PBS) (**Figure 5**). However, there was no change of mRNA levels for either pro-inflammatory cytokines or regulatory cytokines in lung tissue of sham surgery mice with

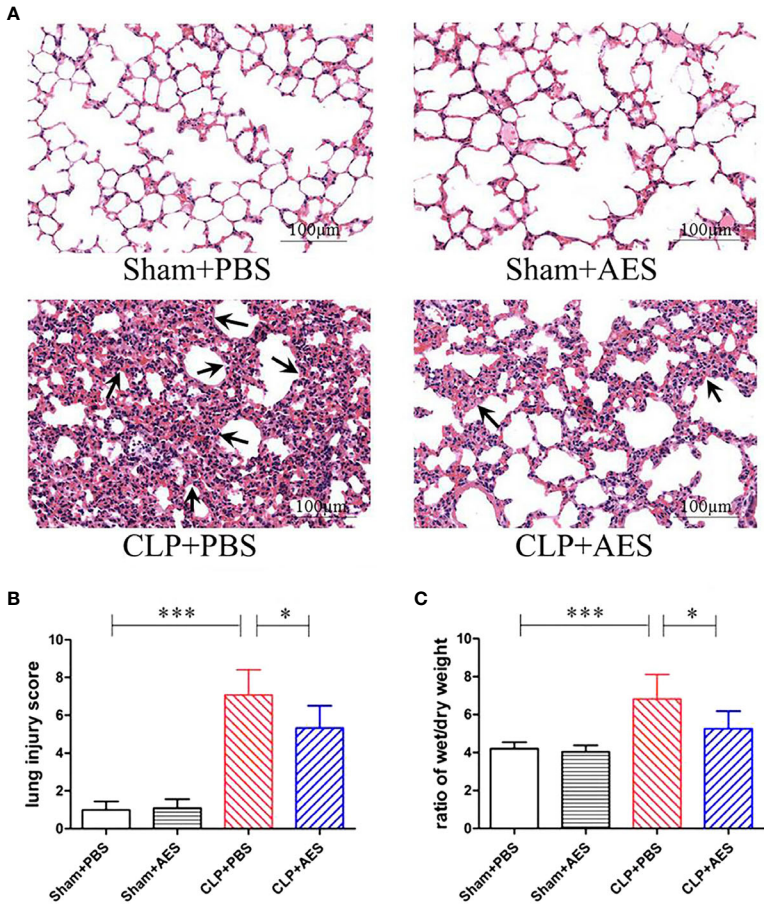

FIGURE 3 | Treatment with *Ts*-AES reduced ALI caused by CLP-induced sepsis. **(A)** Representative lung tissue sections in different groups exhibiting alveolar structural disruption and alveolar septum thickening with the inflammatory cell infiltration in septic mice (CLP+PBS). However, the lung tissue pathological changes caused by sepsis were significantly attenuated in CLP mice treated with *Ts*-AES (CLP+AES) (×200; Scale-bars: 100 μm). The arrows indicate thickened alveolar septum. **(B)** The improved lung injury score after being treated with *Ts*-AES (CLP+AES) compared with CLP+PBS. **(C)** Pulmonary edema assessed by wet/dry weight ratio of lung tissue was significantly reduced in CLP mice treated with *Ts*-AES compared with CLP mice without treatment. The results are shown as the means ± SD for each group (n = 6). $^{*}P < 0.05$, $^{***}P < 0.001$.

or without *Ts*-AES treatment. The results suggest that treatment with *Ts*-AES directly inhibits pro-inflammatory cytokine expression and stimulates the expression of regulatory cytokines that is correlated with the improvement of acute lung injury caused by CLP-induced sepsis.

Treatment With *Ts*-AES Stimulated Regulatory T-Cells (Tregs)

Many studied have demonstrated that Tregs play a key role in modulating the inflammatory responses to relieve the sepsis-related immunopathology (Xu et al., 2020). To further examine whether the reduced inflammation and acute lung injury in septic mice treated with *Ts*-AES was associated with the activation of Treg response, the Tregs with surface expressions of CD3Ɛ, CD4 and CD25 and the intracellular expression of Foxp3 were examined in lymphocytes isolated from the spleens of mice using flow cytometry. As shown in **Figure 6**, Treatment with *Ts*-AES induced $CD3Ɛ^{+}CD4^{+}CD25^{+}Foxp3^{+}$ Tregs in splenocytes from septic mice (CLP+AES) compared with those in septic mice without treatment (CLP+PBS). The severe infection itself also stimulated $CD3Ɛ^{+}CD4^{+}CD25^{+}Foxp3^{+}$ Tregs in the spleen cells from septic mice (CLP+PBS), but the increase of Tregs is more significant after treatment with *Ts*-AES. The results further suggest that *Ts*-AES modulate host immune system by stimulating regulatory T cell response. The results are correlated with the reduced pro-inflammatory cytokines and elevated regulator cytokines IL-10 and TGF-β in sera and lung tissues measured above.

Ts-AES Alleviated Sepsis-Induced ALI *via* HMGB1/TLR2/MyD88 Signaling Pathway

HMGB1 is a regulatory protein in nucleus related to activate the family of Toll-like receptors (TLRs) (Park et al., 2004; Yu et al., 2006) and TLR/MyD88 is an important signaling pathway involved in the inflammation (Kumar, 2020). To determine whether the HMGB1/TLR2/MyD88 signaling pathway is involved in the

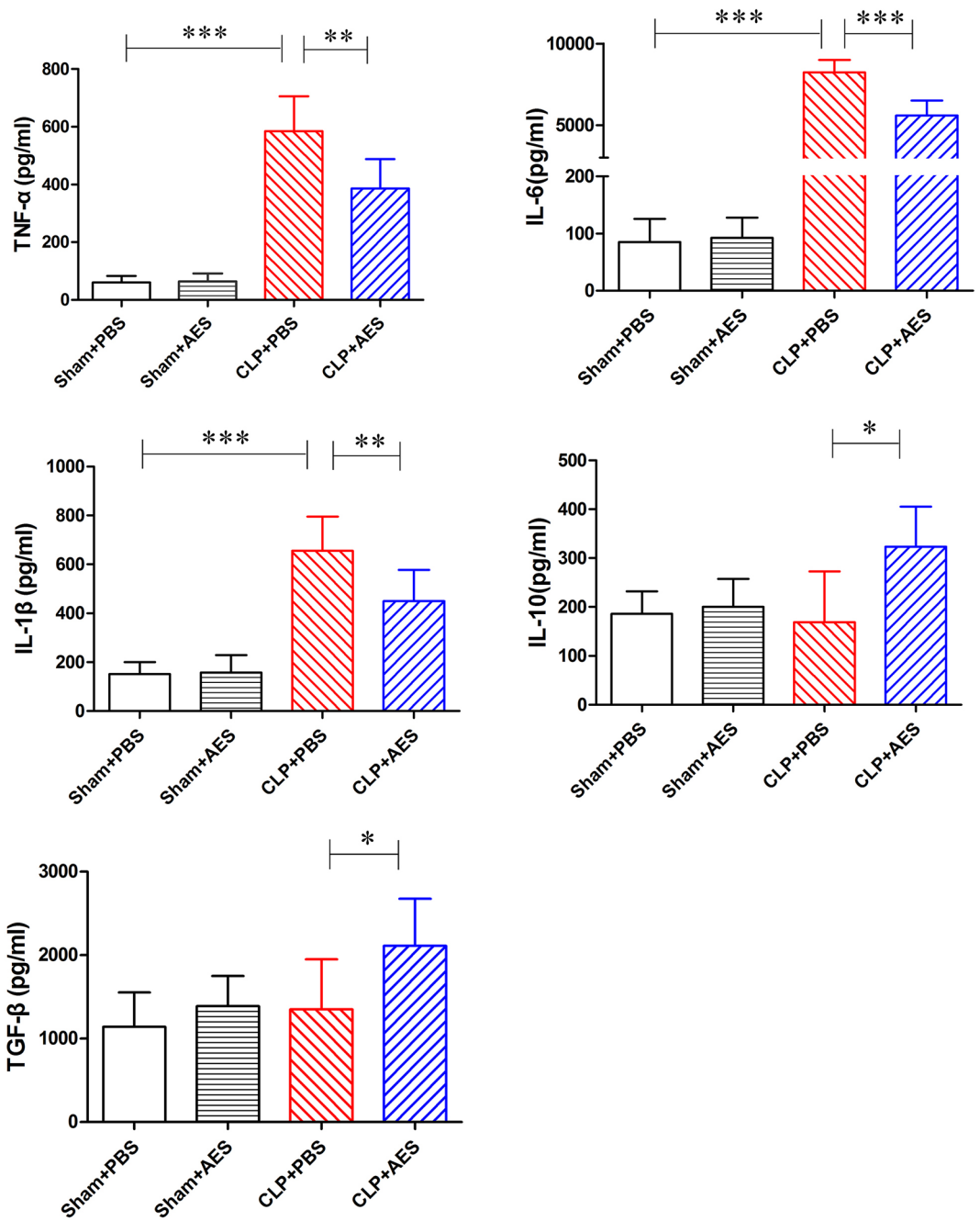

FIGURE 4 | Treatment with *Ts*-AES reduced the inflammatory cytokines TNF-α, IL-6, IL-1β and stimulated regulatory cytokines IL-10 and TGF-β in sera of CLP-induced septic mice. The levels of these cytokines in sera of mice were measured by ELISA 12 h after the surgery. The results were shown as the mean ± SD for each group (n = 6). $^{*}P < 0.05$, $^{**}P < 0.01$, $^{***}P < 0.001$.

therapeutic effect of *Ts*-AES on sepsis-induced ALI, we evaluated protein and mRNA expression levels of HMGB1, TLR2 and MyD88 in lung tissue 12 h after CLP surgery. The elevated levels of HMGB1, TLR2 and MyD88 proteins were observed in lung tissue of mice 12 h after CLP operation in CLP+PBS group compared with the mice in sham groups with or without treatment of *Ts*-AES. Treatment with *Ts*-AES significantly reduced the protein expression levels of HMGB1, TLR2 and MyD88 in lung tissues of septic mice (CLP+AES) compared with mice without *Ts*-AES treatment (CLP+PBS) (**Figure 7A**). However, there was no significant difference in protein expression of HMGB1, TLR2 and MyD88 in lung tissue between Sham+PBS group and

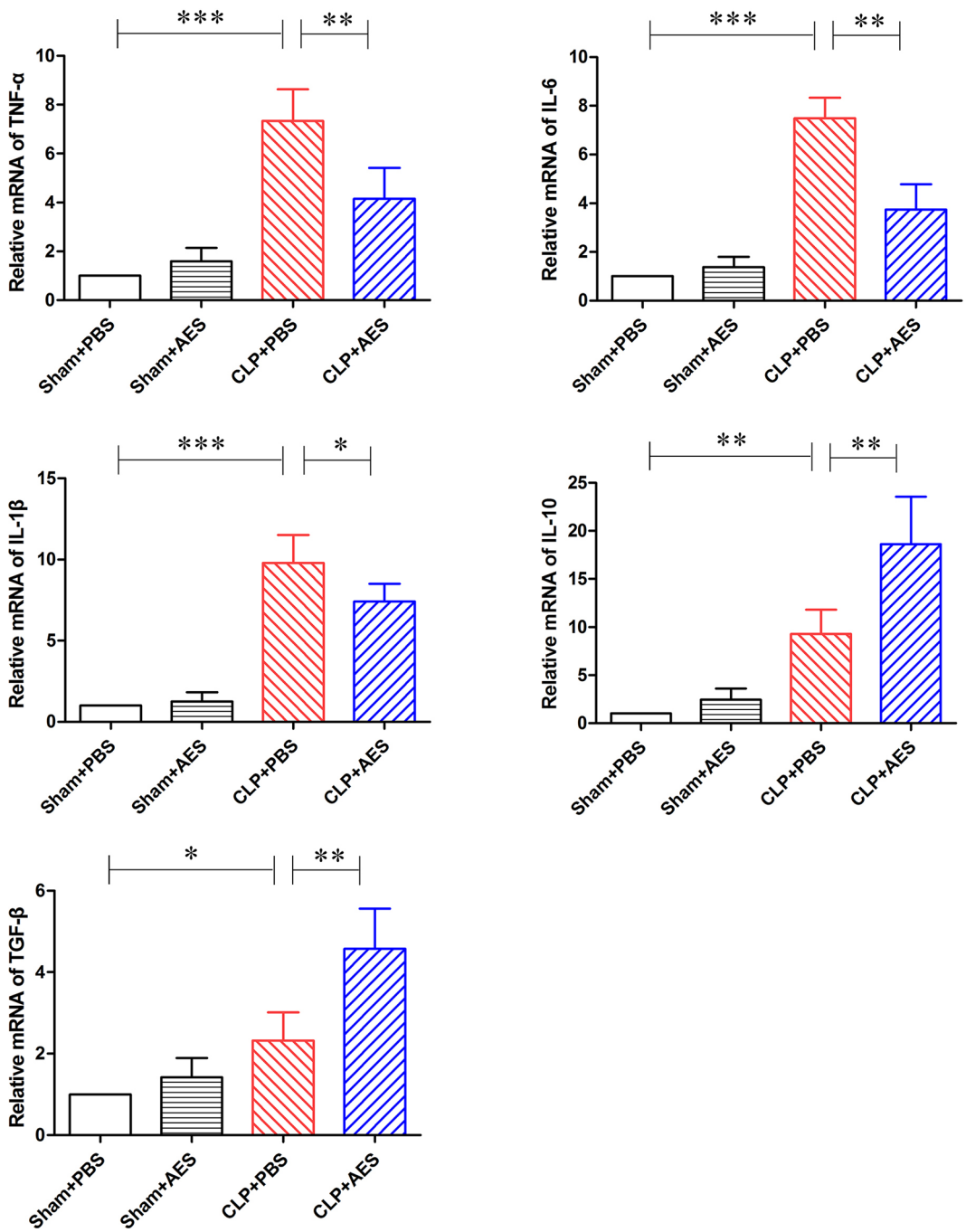

FIGURE 5 | Treatment with *Ts*-AES reduced the mRNA expression levels of pro-inflammatory cytokine (TNF-α, IL-6 and IL-1β) and increased the mRNA expression levels of regulatory cytokine (IL-10 and TGF-β) in lung tissues of septic mice. The results were shown as the means ± SD for each group (n=6). $^{*}P < 0.05$, $^{**}P < 0.01$, $^{***}P < 0.001$.

Sham+AES group. The mRNA expression levels of HMGB1, TLR2 and MyD88 detected in lung tissue showed a similar pattern to the proteins measured in lung tissue (**Figure 7B**). These results indicate that *Ts*-AES could alleviate sepsis-induced acute lung injury possibly through inhibiting HMGB1, TLR2 and MyD88 pathway.

DISCUSSION

Sepsis is overwhelming immune responses upon systemic infection that trigger inflammatory storm throughout the body to cause multiple organ damage. The lung is particularly

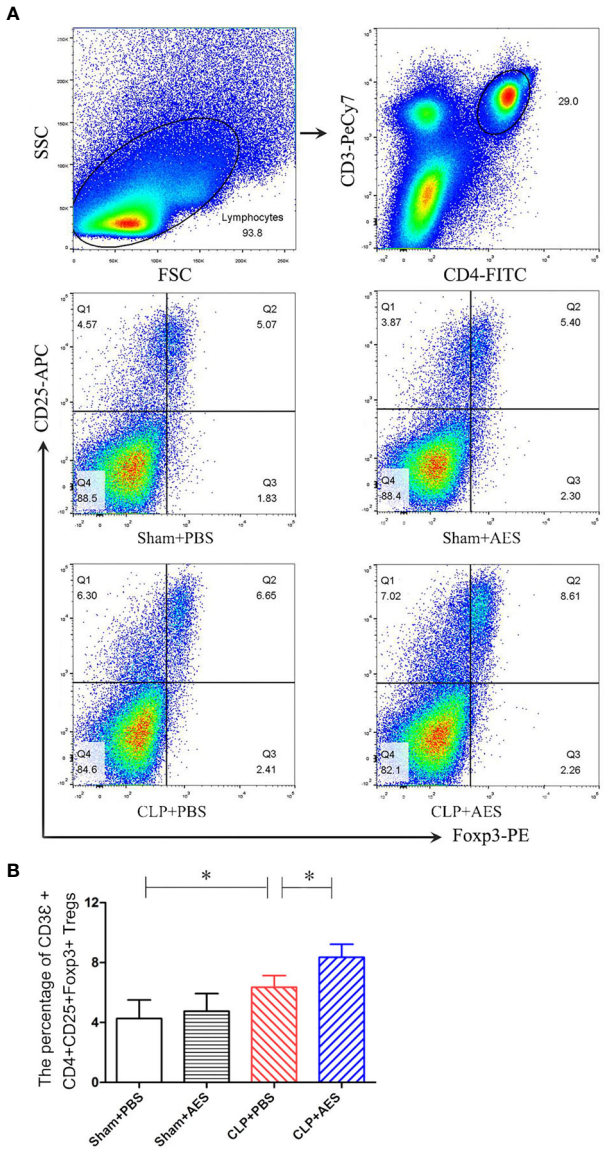

FIGURE 6 | Treatment with *Ts*-AES increased percentage of $CD3\varepsilon^+CD4^+CD25^+Foxp3^+$ Tregs in the spleen lymphocytes of mice with CLP-induced sepsis. The percentage of $CD3\varepsilon^+CD4^+CD25^+Foxp3^+$ Tregs in the splenocytes of mice was gated and counted. **(A)** Representative three-dimension scatter diagrams of $CD3\varepsilon^+CD4^+CD25^+Foxp3^+$ Tregs in the splenocytes of mice in each group. **(B)** The percentage of $CD3\varepsilon^+CD4^+CD25^+Foxp3^+$ Tregs in the splenocytes of mice in each group. The results were shown as the means ± SD for each group (n = 6). $^*P < 0.05$.

susceptible to acute injury during sepsis. Studies have found that more than 50% of patients with sepsis develop ALI or acute respiratory distress syndrome (ARDS) confirmed both in animal and clinical observations (Carvelli et al., 2019). In this study, we confirmed septic ALI in a CLP-induced sepsis mouse model characterized by structure damage and inflammatory cell infiltration, pulmonary edema in lung tissue accompanied by the increased levels of pro-inflammatory cytokines, which closely mimicked the pathophysiological characteristics of acute lung injury observed in clinical patients.

The ES products of helminth have been regarded as key molecules secreted by helminth in regulating host inflammation, cell apoptosis, protein degradation and antigen presentation (Crowe et al., 2017; Smallwood et al., 2017; Pan et al., 2018; Sun et al., 2019a). Previous studies have determined that *Ts*-AES enabled to induce strong Tregs responses, characterized by increased $CD4^+CD25^+Foxp3^+$ and $CD4^+CD25^-Foxp3^+$ Treg cells accompanied by high levels of IL-10 and TGF-β (Sun et al., 2019b). Treatment with *Ts*-AES significantly alleviated Th1-dominated colonic inflammation and pathology in DSS-induced colitis in mice (Yang et al., 2014). In this study, we would like to determine whether *Ts*-AES modulate the immune response against systemic sepsis and protect mice from septic acute lung injury.

The early phase of sepsis is characterized by excessive inflammation with the manifestation of systemically boosted production of pro-inflammatory cytokines, including TNF-α, IL-6 and IL-1β (Sackett et al., 2019). The pro-inflammatory cytokine storm can induce lung endothelial cell activation, leukocyte migration, and capillary leakage that result in lung edema to further hinder alveolar cell perfusion and oxygen exchange, thus causing ALI (Chaudhry et al., 2013). In this study, we observed that 12 hours after CLP operation, the mRNA expression levels of pro-inflammatory cytokines (TNF-α, IL-6 and IL-1β) in lung tissues were significantly increased and the structure of lung tissue was damaged including alveolar congestion and thickened alveolar septum with the inflammatory cell infiltration, which is consistent with the increased levels of TNF-α, IL-6 and IL-1β in sera. Treatment with 15 μg of *Ts*-AES significantly improved survival rate of mice with CLP-induced sepsis up to 50% at 72-hour time point after CLP operation compared with septic mice without treatment that all died at the same time point ($P<0.05$). Histochemical staining of lung tissue identified that the pathology of sepsis-caused ALI was significantly reduced in mice treated with *Ts*-AES, with reduced inflammatory cell infiltration and congestion, reduced wet/dry weight ratio of lung tissue, less lung tissue damage and structural disruption, and improved lung injury scores, compared to lung tissues of septic mice without treatment (**Figures 3A–C**). The reduced pathology of sepsis-caused ALI was correlated with reduced levels of pro-inflammation cytokines such as TNF-α, IL-6 and IL-1β in blood and their mRNA transcriptional level directly in lung tissue.

As we know, Treg cells play a key role in the induction of immune homeostasis and tolerance mainly through the secretion of IL-10 and TGF-β to exert regulatory influence on the immune system (Smallwood et al., 2017). In this study, we identified that the proportion of $CD3\varepsilon^+CD4^+CD25^+Foxp3^+$ Tregs in the spleen cells were increased in septic mice upon the treatment of *Ts*-AES after CLP operation, which is correlated with the increased levels of IL-10 and TGF-β and decreased levels of pro-inflammatory cytokines (TNF-α, IL-6 and IL-1β) in sera and lung tissue, indicating that *Ts*-AES act as an inhibitory immunomodulator in the case of excessive inflammatory infection, possibly through stimulating Tregs and Treg cell-secreted IL-10 and TGF-β to reduce sepsis-induced acute lung injury and therefore improve the survival rate of mice with septic ALI. We observe in this study that

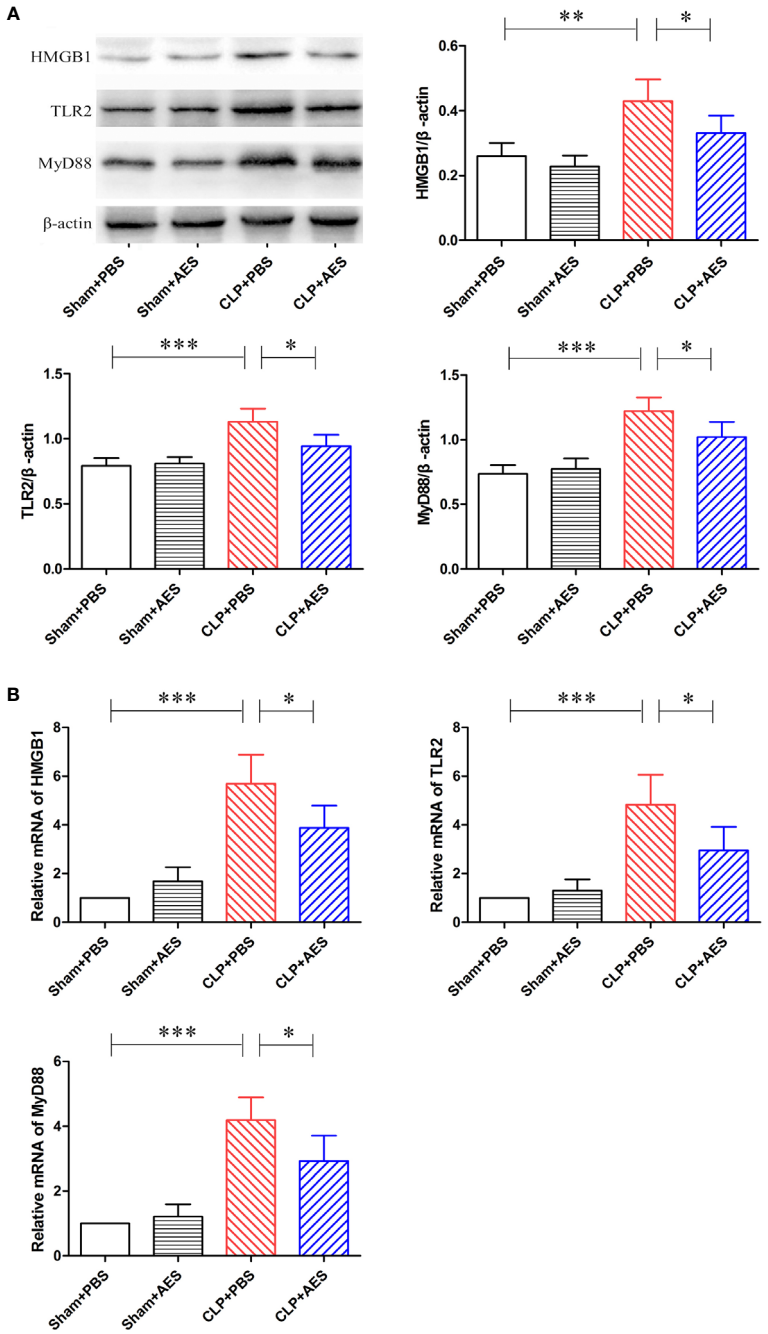

FIGURE 7 | Treatment with *Ts*-AES reduced the protein expression levels of HMGB1, TLR2 and MyD88, β-actin was measured as a control **(A)**, and the mRNA expression levels of HMGB1, TLR2 and MyD88 in lung tissues of septic mice **(B)**. The results were shown as the means ± SD for each group (n = 6). $^{*}P < 0.05$, $^{**}P < 0.01$, $^{***}P < 0.001$.

septic infection itself also increased Tregs (**Figure 6B**), however, it has been suggested the increased Tregs in inflammatory diseases, such as colitis, sepsis, the function of Tregs is typically impaired in these diseases, and the impaired Tregs are usually unable to restrict the excessive inflammation (Yang et al., 2014; Xu et al., 2020).

During the early onset of sepsis, the innate immune system is activated through toll-like receptors (TLRs) through pathogen-associated molecular patterns (PAMPs) signaling pathway. Activation of TLRs induces the rapid release of early pro-damage signals, including damage-associated molecular patterns (DAMPs) that are referred to as alarmins, into the circulation.

High Mobility Group Box 1 protein (HMGB1) is a major alarmin which is passively released from injured or necrotic cells in sepsis (Tian et al., 2020). HMGB1 is typically found in the nucleus of many cells including immune, endothelial and epithelial cells where it is bound to DNA. After being stimulated by bacterial endotoxin or pro-inflammatory cytokines in the case of sepsis, HMGB1 was acetylated and released as a cytokine mediator of inflammation through receptors for advanced glycation end products (RAGEs) and TLRs (TLR2 and TLR4) to stimulate excessive release of pro-inflammatory cytokines (Park et al., 2004; Yu et al., 2006; Kang et al., 2010; Andersson and Tracey, 2011). In this study we found that the protein expression levels and the mRNA expression levels of HMGB1, TLR2 and MyD88 in lung tissue are significantly increased associated with the high levels of pro-inflammatory cytokines in sera and lung tissues 12 hours after CLP operation. After being treated with *Ts*-AES, protein expression levels and the mRNA expression levels of HMGB1, TLR2 and MyD88 in lung tissues were significantly decreased. Our results further confirm that severe infection of bacteria in sepsis stimulates inflammatory immune responses through HMGB1/TLR2/MyD88 activation signal pathway as shown for other helminth-derived proteins (Li et al., 2017; Ilic et al., 2018; Gao et al., 2020).

In this study we have demonstrated *Ts*-AES play an important role in modulating host immune response possibly through stimulating Tregs response and promoting secretion of IL-10 and TGF-β, thereby suppressing the production of pro-inflammatory cytokines. The immunomodulation of *Ts*-AES is taken effect possibly through inhibiting the HMGB1/TLR2/MyD88 activation signal pathway. However, there are still a lot that are not clear and need to be further explored, for example, what the effective cells to which HMGB1/TLR2/MyD88 activation signal pathway regulates, macrophages, dendritic cells or other immune cells? It needs to be further investigated.

There are some concerns for using *Ts*-AES as therapeutic reagents to reduce systemic infection-caused lung and other organ injury, one of the concerns is that administration of *Ts*-AES could induce antibody response that may reduce the efficacy of *Ts*-AES. However, the administration of *Ts*-AES was through intraperitoneal injection without using any adjuvant in this study. As we know, intraperitoneal administration without adjuvant within limited time period could not effectively induce much antibody response. However, it would be expected to reduce efficacy if *Ts*-AES are used repeatedly or for a long time period due to the potential antibody production that would neutralize the efficacy of *Ts*-AES. Another concern is for the complicated composition of *Ts*-AES. *Ts*-AES is a complex pool of various molecules secreted or excreted by worms, it is difficult to be accepted by using this complex as therapeutic reagents because of the possible side-effects or immune interference. It is also difficult to make large-scale manufacture of *Ts*-AES that limits its use in clinical treatment. It is important to identify the effective components in *Ts*-AES that are involved in the regulatory activation of immune cells. Shotgun LC-MS/MS approach identified more than 280 protein components in *Ts*-AES with 4 proteins having potential regulatory functions including cysteine protease inhibitor, serine protease, 53 kDa excretory-secretory protein, and glutathione-S-transferase (Yang et al., 2017; Wang Z. et al., 2020). Recent studies have confirmed that recombinant *T. spiralis* cysteine protease inhibitor relieved TNBS-induced experimental inflammatory bowel disease by inducing Th2-type immune response and balanced the Th1-type immune response induced by TNBS administration (Xu et al., 2019). Serine protease of *Ts*-AES alleviated TNBS-induced colitis by increasing the population of Th2 and Treg cells (Pang et al., 2020). Recombinant *T. spiralis* 53-kDa excretory-secretory protein exhibited anti-inflammatory properties and rescued mice from LPS-induced damage of endotoxemia (Chen et al., 2016). Recombinant *T. spiralis* glutathione-S-transferase decreased the LPS-induced elevated level of pro-inflammatory cytokines of dendritic cells and enhanced the level of regulatory cytokines IL-10 and TGF-β (Jin et al., 2019b). The identification of the immunomodulatory molecules in *Ts*-AES will make it possible to develop effective therapeutic drugs for inflammatory and immune diseases. The related research on *Ts*-AES is under investigation in our laboratory.

CONCLUSIONS

In this study we have presented results demonstrating that *Ts*-AES strongly alleviate excessive inflammation *via* stimulating Tregs response and inhibiting the HMGB1/TLR2/MyD88 signal pathway, and protect mice from ALI induced by sepsis. Therefore, *Ts*-AES could be considered as a potential therapeutic agent for the treatment of severe infection or other inflammatory/auto immune diseases.

DATA AVAILABILITY STATEMENT

The original contributions presented in the study are included in the article/supplementary material. Further inquiries can be directed to the corresponding author.

ETHICS STATEMENT

The animal study was reviewed and approved by Animal Care and Use Committee of Bengbu Medical College (approval no: LAEC-2014-039).

AUTHOR CONTRIBUTIONS

XY, HL, and BZ conceived and designed the study. HL, DQ, HY, XW, LW, YS, and WX performed the experiments. HL, YY, and LC analyzed the data. HL wrote the manuscript. BZ and XY critically revised the manuscript. All authors contributed to the article and approved the submitted version.

FUNDING

This study was supported by the Science Foundation of Anhui Province (no. 2008085MH260, gxbjZD15); Program of Natural Science Foundation of the Anhui Higher Education Institutions (no. KJ2020A0554, KJ2020A0572); 512 Talents Development Program of Bengbu Medical College (no. by51201205, by51201306); the innovation and entrepreneurship training program for college students (no. 201910367025, S202010367040).

REFERENCES

Amdare, N., Khatri, V., Yadav, R. S., Tarnekar, A., Goswami, K., and Reddy, M. V. (2015). *Brugia malayi* soluble and excretory-secretory proteins attenuate development of streptozotocin-induced type 1 diabetes in mice. *Parasite Immunol.* 37 (12), 624–634. doi: 10.1111/pim.12283

Andersson, U., and Tracey, K. J. (2011). HMGB1 is a therapeutic target for sterile inflammation and infection. *Annu. Rev. Immunol.* 29, 139–162. doi: 10.1146/annurev-immunol-030409-101323

Bai, X., Wu, X., Wang, X., Guan, Z., Gao, F., Yu, J., et al. (2012). Regulation of cytokine expression in murine macrophages stimulated by excretory/secretory products from Trichinella spiralis in vitro. *Mol. Cell Biochem.* 360 (1-2), 79–88. doi: 10.1007/s11010-011-1046-4

Butt, Y., Kurdowska, A., and Allen, T. C. (2016). Acute Lung Injury: A Clinical and Molecular Review. *Arch. Pathol. Lab. Med.* 140 (4), 345–350. doi: 10.5858/arpa.2015-0519-RA

Carvelli, J., Piperoglou, C., Bourenne, J., Farnarier, C., Banzet, N., Demerlé, C., et al. (2019). Imbalance of circulating innate lymphoid cell subpopulations in patients with septic shock. *Front. Immunol.* 10, 2179. doi: 10.3389/fimmu.2019.02179

Chaudhry, H., Zhou, J., Zhong, Y., Ali, M. M., McGuire, F., Nagarkatti, P. S., et al. (2013). Role of cytokines as a double-edged sword in sepsis. *In Vivo* 27 (6), 669–684.

Chen, Z. B., Tang, H., Liang, Y. B., Yang, W., Wu, J. G., Hu, X. C., et al. (2016). Recombinant Trichinella spiralis 53-kDa protein activates M2 macrophages and attenuates the LPS-induced damage of endotoxemia. *Innate Immun.* 22 (6), 419–432. doi: 10.1177/1753425916651984

Crowe, J., Lumb, F. E., Harnett, M. M., and Harnett, W. (2017). Parasite excretory-secretory products and their effects on metabolic syndrome. *Parasite Immunol.* 39 (5), e12410. doi: 10.1111/pim.12410

Deng, M., Tang, Y., Li, W., Wang, X., Zhang, R., Zhang, X., et al. (2018). The Endotoxin Delivery Protein HMGB1 Mediates Caspase-11-Dependent Lethality in Sepsis. *Immunity* 16;49 (4), 740–753.e7. doi: 10.1016/j.immuni.2018.08.016

Deng, M., Scott, M. J., Fan, J., and Billiar, T. R. (2019). Location is the key to function: HMGB1 in sepsis and trauma-induced inflammation. *J. Leukoc. Biol.* 106 (1), 161–169. doi: 10.1002/JLB.3MIR1218-497R

Ding, J., Liu, X., Bai, X., Wang, Y., Li, J., Wang, C., et al. (2020). *Trichinella spiralis*: inflammation modulator. *J. Helminthol.* 21 (94), e193. doi: 10.1017/S0022149X20000802

Du, L., Liu, L., Yu, Y., Shan, H., and Li, L. (2014). *Trichinella spiralis* excretory-secretory products protect against polymicrobial sepsis by suppressing MyD88 via mannose receptor. *BioMed. Res. Int.* 2014, 898646. doi: 10.1155/2014/898646

Erb, K. J. (2009). Can helminths or helminth-derived products be used in humans to prevent or treat allergic diseases? *Trends Immunol.* 30 (2), 75–82. doi: 10.1016/j.it.2008.11.005

Gao, S., Li, H., Xie, H., Wu, S., Yuan, Y., Chu, L., et al. (2020). Therapeutic efficacy of *Schistosoma japonicum* cystatin on sepsis-induced cardiomyopathy in a mouse model. *Parasit. Vectors* 13 (1), 260. doi: 10.1186/s13071-020-04104-3

Gu, Y., Wei, J., Yang, J., Huang, J., Yang, X., and Zhu, X. (2013). Protective immunity against *Trichinella spiralis* infection induced by a multi-epitope vaccine in a murine model. *PloS One* 8 (10), e77238. doi: 10.1371/journal.pone.0077238

Han, C., Yu, J., Zhang, Z., Zhai, P., Zhang, Y., Meng, S., et al. (2019). Immunomodulatory effects of *Trichinella spiralis* excretory-secretory antigens on macrophages. *Exp. Parasitol.* 196, 68–72. doi: 10.1016/j.exppara.2018.10.001

Hernández-Ancheyta, L., Salinas-Tobón, M. D. R., Cifuentes-Goches, J. C., and Hernández-Sánchez, J. (2018). *Trichinella spiralis* muscle larvae excretory-secretory products induce changes in cytoskeletal and myogenic transcription factors in primary myoblast cultures. *Int. J. Parasitol.* 48 (3-4), 275–285. doi: 10.1016/j.ijpara.2017.10.002

Hübner, M. P., Layland, L. E., and Hoerauf, A. (2013). Helminths and their implication in sepsis-a new branch of their immunomodulatory behaviour? *Pathog. Dis.* 69 (2), 127–141. doi: 10.1111/2049-632X.12080

Ilic, N., Gruden-Movsesijan, A., Cvetkovic, J., Tomic, S., Vucevic, D. B., Aranzamendi, C., et al. (2018). *Trichinella spiralis* Excretory-Secretory Products Induce Tolerogenic Properties in Human Dendritic Cells via Toll-Like Receptors 2 and 4. *Front. Immunol.* 9, 11. doi: 10.3389/fimmu.2018.00011

Jin, X., Yang, Y., Bai, X., Shi, H., Zhang, W., Zhang, Z., et al. (2019a). Dendritic cells treated by *Trichinella spiralis* muscle larval excretory/secretory products alleviate TNBS-induced colitis in mice. *Int. Immunopharmacol.* 70, 378–386. doi: 10.1016/j.intimp.2019.02.028

Jin, X., Yang, Y., Liu, X., Shi, H., Cai, X., Luo, X., et al. (2019b). Glutathione-S-transferase of *Trichinella spiralis* regulates maturation and function of dendritic cells. *Parasitology* 146 (14), 1725–1732. doi: 10.1017/S003118201900115X

Kang, R., Tang, D., Schapiro, N. E., Livesey, K. M., Farkas, A., Loughran, P., et al. (2010). The receptor for advanced glycation end products (RAGE) sustains autophagy and limits apoptosis, promoting pancreatic tumor cell survival. *Cell Death Differ.* 17 (4), 666–676. doi: 10.1038/cdd.2009.149

Kosanović, M., Cvetković, J., Gruden-Movsesijan, A., Vasilev, S., Svetlana, M., Ilić, N., et al. (2019). *Trichinella spiralis* muscle larvae release extracellular vesicles with immunomodulatory properties. *Parasite Immunol.* 41 (10), e12665. doi: 10.1111/pim.12665

Kumar, V. (2020). Toll-like receptors in sepsis-associated cytokines storm and their endogenous negative regulators as future immunomodulatory targets. *Int. Immunopharmacol.* 89 (Pt B), 107087. doi: 10.1016/j.intimp.2020.107087

Lee, S. A., Kwak, M. S., Kim, S., and Shin, J. S. (2014). The role of high mobility group box 1 in innate immunity. *Yonsei Med. J.* 55 (5), 1165–1176. doi: 10.3349/ymj.2014.55.5.1165

Li, L., and Lu, Y. Q. (2021). The regulatory role of high-mobility group protein 1 in sepsis-related immunity. *Front. Immunol.* 22 (11), 601815. doi: 10.3389/fimmu.2020.601815

Li, H., Wang, S., Zhan, B., He, W., Chu, L., Qiu, D., et al. (2017). Therapeutic effect of *Schistosoma japonicum* cystatin on bacterial sepsis in mice. *Parasit. Vectors* 10 (1), 222. doi: 10.1186/s13071-017-2162-0

Li, L., Huang, Q., Wang, D. C., Ingbar, D. H., and Wang, X. (2020). Acute lung injury in patients with COVID-19 infection. *Clin. Transl. Med.* 10 (1), 20–27. doi: 10.1002/ctm2.16

Martínez-Gómez, F., Santiago-Rosales, R., and Ramón Bautista-Garfias, C. (2009). Effect of Lactobacillus casei Shirota strain intraperitoneal administration in CD1 mice on the establishment of *Trichinella spiralis* adult worms and on IgA anti-T. Spiralis production. *Vet. Parasitol.* 162 (1-2), 171–175. doi: 10.1016/j.vetpar.2009.02.010

Meng, P. Z., Liu, J., Hu, P. S., and Tong, F. (2018). Protective effect of dexmedetomidine on endotoxin-induced acute lung injury in rats. *Med. Sci. Monit.* 24, 4869–4875. doi: 10.12659/MSM.908887

Novosad, S. A., Sapiano, M. R., Grigg, C., Lake, J., Robyn, M., Dumyati, G., et al. (2016). Vital Signs: Epidemiology of Sepsis: Prevalence of Health Care Factors and Opportunities for Prevention. *MMWR Morb. Mortal. Wkly. Rep.* 65 (33), 864–869. doi: 10.15585/mmwr.mm6533e1

O'Regan, N. L., Steinfelder, S., Venugopal, G., Rao, G. B., Lucius, R., Srikantam, A., et al. (2014). *Brugia malayi* microfilariae induce a regulatory monocyte/macrophage phenotype that suppresses innate and adaptive immune

responses. *PloS Negl. Trop. Dis.* 8 (10), e3206. doi: 10.1371/journal.pntd.0003206

Osada, Y., and Kanazawa, T. (2010). Parasitic helminths: new weapons against immunological disorders. *J. BioMed. Biotechnol.* 2010, 743758. doi: 10.1155/2010/743758

Pan, W., Xu, H. W., Hao, W. T., Sun, F. F., Qin, Y. F., Hao, S. S., et al. (2018). The excretory-secretory products of *Echinococcus granulosus* protoscoleces stimulated IL-10 production in B cells via TLR-2 signaling. *BMC Immunol.* 19 (1), 29. doi: 10.1186/s12865-018-0267-7

Pang, J., Ding, J., Zhang, L., Zhang, Y., Yang, Y., Bai, X., et al. (2020). Effect of recombinant serine protease from adult stage of *Trichinella spiralis* on TNBS-induced experimental colitis in mice. *Int. Immunopharmacol.* 86, 106699. doi: 10.1016/j.intimp.2020.106699

Park, J. S., Svetkauskaite, D., He, Q., Kim, J. Y., Strassheim, D., Ishizaka, A., et al. (2004). Involvement of toll-like receptors 2 and 4 in cellular activation by high mobility group box 1 protein. *J. Biol. Chem.* 279 (9), 7370–7377. doi: 10.1074/jbc.M306793200

Passos, L. S., Gazzinelli-Guimarães, P. H., Oliveira Mendes, T. A., Guimarães, A. C., Silveira Lemos, D. D., Ricci, N. D., et al. (2017). Regulatory monocytes in helminth infections: insights from the modulation during human hookworm infection. *BMC Infect. Dis.* 17 (1), 253. doi: 10.1186/s12879-017-2366-0

Rello, J., Valenzuela-Sánchez, F., Ruiz-Rodriguez, M., and Moyano, S. (2017). Sepsis: A Review of Advances in Management. *Adv. Ther.* 34 (11), 2393–2411. doi: 10.1007/s12325-017-0622-8

Rittirsch, D., Huber-Lang, M. S., Flierl, M. A., and Ward, P. A. (2009). Immunodesign of experimental sepsis by cecal ligation and puncture. *Nat. Protoc.* 4 (1), 31–36. doi: 10.1038/nprot.2008.214

Rosas-Ballina, M., Goldstein, R. S., Gallowitsch-Puerta, M., Yang, L., Valdés-Ferrer, S. I., Patel, N. B., et al. (2009). The selective alpha7 agonist GTS-21 attenuates cytokine production in human whole blood and human monocytes activated by ligands for TLR2, TLR3, TLR4, TLR9, and RAGE. *Mol. Med.* 15 (7-8), 195–202. doi: 10.2119/molmed.2009.00039

Rubenfeld, G. D., Caldwell, E., Peabody, E., Weaver, J., Martin, D. P., Neff, M., et al. (2005). Incidence and outcomes of acute lung injury. *N. Engl. J. Med.* 53 (16), 1685–1693. doi: 10.1056/NEJMoa050333

Rudd, K. E., Johnson, S. C., Agesa, K. M., Shackelford, K. A., Tsoi, D., Kievlan, D. R., et al. (2020). Global, regional, and national sepsis incidence and mortality 1990-2017: analysis for the Global Burden of Disease Study. *Lancet* 395 (10219), 200–201. doi: 10.1016/S0140-6736(19)32989-7

Sackett, S. D., Otto, T., Mohs, A., Sander, L. E., Strauch, S., Streetz, K. L., et al. (2019). Myeloid cells require gp130 signaling for protective anti-inflammatory functions during sepsis. *FASEB J.* 33 (5), 6035–6044. doi: 10.1096/fj.201802118R

Shao, Z., Li, Q., Wang, S., and Chen, Z. (2019). Protective effects of PNU-282987 on sepsis-induced acute lung injury in mice. *Mol. Med. Rep.* 19 (5), 3791–3798. doi: 10.3892/mmr.2019.10016

Shirvan, S. P., Borji, H., Movassaghi, A., Khakzad, M., Farzin, H., Maleki, M., et al. (2016). Anti-inflammatory potentials of excretory/secretory (ES) and somatic products of *Marshallagia marshalli* on allergic airway inflammation in BALB/c mice. *Iran J. Parasitol.* 11 (4), 515–526.

Singer, M., Deutschman, C. S., Seymour, C. W., Shankar-Hari, M., Annane, D., Bauer, M., et al. (2016). The Third International Consensus Definitions for Sepsis and Septic Shock (Sepsis-3). *JAMA* 315 (8), 801–810. doi: 10.1001/jama.2016.0287

Smallwood, T. B., Giacomin, P. R., Loukas, A., Mulvenna, J. P., Clark, R. J., and Miles, J. J. (2017). Helminth immunomodulation in autoimmune disease. *Front. Immunol.* 8, 453. doi: 10.3389/fimmu.2017.00453

Sofronic-Milosavljevic, L., Ilic, N., Pinelli, E., and Gruden-Movsesijan, A. (2015). Secretory products of *Trichinella spiralis* muscle larvae and immunomodulation: implication for autoimmune diseases, allergies, and malignancies. *J. Immunol. Res.* 2015, 523875. doi: 10.1155/2015/523875

Strachan, D. P. (1989). Hay fever, hygiene, and household size. *BMJ* 299 (6710), 1259–1260. doi: 10.1136/bmj.299.6710.1259

Sun, S., Li, H., Yuan, Y., Wang, L., He, W., Xie, H., et al. (2019a). Preventive and therapeutic effects of *Trichinella spiralis* adult extracts on allergic inflammation in an experimental asthma mouse model. *Parasit. Vectors* 12 (1), 326. doi: 10.1186/s13071-019-3561-1

Sun, X. M., Guo, K., Hao, C. Y., Zhan, B., Huang, J. J., and Zhu, X. (2019b). *Trichinella spiralis* excretory-secretory products stimulate host regulatory T cell differentiation through activating dendritic cells. *Cells* 8 (11), 1404. doi: 10.3390/cells8111404

Tian, T., Yao, D., Zheng, L., Zhou, Z., Duan, Y., Liu, B., et al. (2020). Sphingosine kinase 1 regulates HMGB1 translocation by directly interacting with calcium/calmodulin protein kinase II-δ in sepsis-associated liver injury. *Cell Death Dis.* 11 (12), 1037. doi: 10.1038/s41419-020-03255-6

Valdés-Ferrer, S. I., Rosas-Ballina, M., Olofsson, P. S., Lu, B., Dancho, M. E., Li, J., et al. (2013). High-mobility group box 1 mediates persistent splenocyte priming in sepsis survivors: evidence from a murine model. *Shock* 40 (6), 492–495. doi: 10.1097/SHK.0000000000000050

van Riet, E., Hartgers, F. C., and Yazdanbakhsh, M. (2007). Chronic helminth infections induce immunomodulation: consequences and mechanisms. *Immunobiology* 212 (6), 475–490. doi: 10.1016/j.imbio.2007.03.009

Wang, J., Li, R., Peng, Z., Hu, B., Rao, X., and Li, J. (2020). HMGB1 participates in LPS–induced acute lung injury by activating the AIM2 inflammasome in macrophages and inducing polarization of M1 macrophages via TLR2, TLR4, and RAGE/NF–κB signaling pathways. *Int. J. Mol. Med.* 45 (1), 61–80. doi: 10.3892/ijmm.2019.4402

Wang, Z., Hao, C., Zhuang, Q., Zhan, B., Sun, X., Huang, J., et al. (2020). Excretory/Secretory products from *Trichinella spiralis* adult worms attenuated DSS-induced colitis in mice by driving PD-1-mediated M2 macrophage polarization. *Front. Immunol.* 2 (11), 563784. doi: 10.3389/fimmu.2020.563784

Xie, K., Chen, Y. Q., Chai, Y. S., Lin, S. H., Wang, C. J., and Xu, F. (2021). HMGB1 suppress the expression of IL-35 by regulating Naïve CD4+ T cell differentiation and aggravating Caspase-11-dependent pyroptosis in acute lung injury. *Int. Immunopharmacol.* 91, 107295. doi: 10.1016/j.intimp.2020.107295

Xu, J., Liu, M., Yu, P., Wu, L., and Lu, Y. (2019). Effect of recombinant *Trichinella spiralis* cysteine proteinase inhibitor on TNBS-induced experimental inflammatory bowel disease in mice. *Int. Immunopharmacol.* 66, 28–40. doi: 10.1016/j.intimp.2018.10.043

Xu, T., Zhao, J., Wang, X., Meng, Y., Zhao, Z., Bao, R., et al. (2020). CXCL4 promoted the production of CD4+CD25+FOXP3+treg cells in mouse sepsis model through regulating STAT5/FOXP3 pathway. *Autoimmunity* 53, 289–296. doi: 10.1080/08916934.2020.1777283

Yang, X., Yang, Y., Wang, Y., Zhan, B., Gu, Y., Cheng, Y., et al. (2014). Excretory/secretory products from *Trichinella spiralis* adult worms ameliorate DSS-induced colitis in mice. *PloS One* 9 (5), e96454. doi: 10.1371/journal.pone.0096454

Yang, X. D., Tao, Z. Y., Cheng, Y., Wu, Q., Wang, X. L., Song, D., et al. (2017). [Component analysis of excretory/secretory protein from *Trichinella spiralis* adult worm]. *Zhongguo Ji Sheng Chong Xue Yu Ji Sheng Chong Bing Za Zhi.* 35 (1), 24–29.

Yu, M., Wang, H., Ding, A., Golenbock, D. T., Latz, E., Czura, C. J., et al. (2006). HMGB1 signals through toll-like receptor (TLR) 4 and TLR2. *Shock* 26 (2), 174–179. doi: 10.1097/01.shk.0000225404.51320.82

Zaccone, P., Burton, O. T., and Cooke, A. (2008). Interplay of parasite-driven immune responses and autoimmunity. *Trends Parasitol.* 24 (1), 35–42. doi: 10.1016/j.pt.2007.10.006

Conflict of Interest: The authors declare that the research was conducted in the absence of any commercial or financial relationships that could be construed as a potential conflict of interest.

frontiers in Cellular and Infection Microbiology

ORIGINAL RESEARCH
published: 24 March 2021
doi: 10.3389/fcimb.2021.638785

Emergence and Autochthonous Transmission of Dengue Virus Type I in a Low-Epidemic Region in Southeast China

Yi Zhang[1†], Hongyi Chen[2†], Jingen Wang[3†], Shumei Wang[2†], Jing Wu[1], Yang Zhou[1], Xinyu Wang[1], Feibing Luo[4], Xianglin Tu[2], Qiubo Chen[3], Yanxia Huang[2], Weihua Ju[2], Xuping Peng[2], Jianfeng Rao[2], Li Wang[2], Ning Jiang[1,5], Jingwen Ai[1*] and Wenhong Zhang[1,5,6]*

[1] Department of Infectious Diseases, National Clinical Research Center for Aging and Medicine, Huashan Hospital, Fudan University, Shanghai, China, [2] Department of Infectious Disease, Nanchang Ninth Hospital, Nanchang, China, [3] Department of Infectious Disease, Zhangshu People's Hospital, Yichun, China, [4] Department of Infectious Disease, Fengcheng People's Hospital, Yichun, China, [5] State Key Laboratory of Genetic Engineering, School of Life Science, Fudan University, Shanghai, China, [6] Key Laboratory of Medical Molecular Virology (MOE/MOH) and Institutes of Biomedical Sciences, Shanghai Medical College, Fudan University, Shanghai, China

OPEN ACCESS

Edited by:
Xiaojun Chen,
Nanjing Medical University, China

Reviewed by:
Kalichamy Alagarasu,
National Institute of Virology (ICMR), India
Arindam Mondal,
Indian Institute of Technology Kharagpur, India

***Correspondence:**
Jingwen Ai
jingwenai1990@126.com
Ning Jiang
Ningjiang@fudan.edu.cn

[†]These authors have contributed equally to this work

Specialty section:
This article was submitted to Virus and Host, a section of the journal Frontiers in Cellular and Infection Microbiology

Received: *07 December 2020*
Accepted: *01 March 2021*
Published: *24 March 2021*

Citation:
Zhang Y, Chen H, Wang J, Wang S, Wu J, Zhou Y, Wang X, Luo F, Tu X, Chen Q, Huang Y, Ju W, Peng X, Rao J, Wang L, Jiang N, Ai J and Zhang W (2021) Emergence and Autochthonous Transmission of Dengue Virus Type I in a Low-Epidemic Region in Southeast China. Front. Cell. Infect. Microbiol. 11:638785. doi: 10.3389/fcimb.2021.638785

Background: Dengue fever is a mosquito-borne febrile illness. Southeast Asia experienced severe dengue outbreaks in 2019, and over 1000 cases had been reported in Jiangxi, a previously known low-epidemic region in China. However, the emergence of a dengue virus epidemic in a non-epidemic region remains unclear.

Methods: We enrolled 154 dengue fever patients from four hospitals in Jiangxi, from April 2019 to September 2019. Real-time PCR, NS1 antigen rapid test, and IgM, IgG tests were performed, and 14 samples were outsourced to be sequenced metagenomically.

Results: Among the 154 cases, 42 were identified as imported and most of them returned from Cambodia. A total of 113 blood samples were obtained and 106 were identified as DENV-1, two as DENV-2, and five were negative through RT-PCR. All DENV-1 strains sequenced in this study were all classified to one cluster and owned a high similarity with a Cambodia strain isolated in 2019. The evolutionary relationships of amino acid were consistent with that of nucleotide genome result. The sequence-based findings of Jiangxi strains were consistent with epidemiological investigation.

Conclusion: Epidemiological analysis demonstrated that the emergence of dengue cases led to autochthonous transmission in several cities in Jiangxi, a low-epidemic region before. This study emphasized future prevention and control of dengue fever in both epidemic and non-epidemic regions.

Keywords: dengue fever, outbreak, transmission, metagenomic sequencing, prevention

INTRODUCTION

Dengue fever is a mosquito-borne febrile illness affecting more than 100 countries in tropical and subtropical areas (Bhatt et al., 2013; Guzman et al., 2016). The introduction of *Aedes* is linked to the circulation of four serotypes of dengue viruses (DENV 1-4) globally (Guzman et al., 2016). High temperatures, humid climate, mosquitoes, globalization, and domestic or international travel

increase the incidence and transmission of dengue infection (Murray et al., 2013). In most patients, dengue fever is self-limiting; however, severe dengue fever cases such as dengue hemorrhagic fever and dengue shock syndrome (DHF/DSS) could pose a life-threatening danger to infected patients (Guzman et al., 2016).

Southeast Asia experienced a severe dengue outbreak in 2019. Dengue fever remains a significant public health problem in Cambodia, with more than 10000 cases annually and have affected more than 20000 cases by July 2019 (Cousien et al., 2019). The Philippines declared a 'National epidemic' after the death toll from dengue fever surpassed 1000 people, most of whom were children aged < 10 years (Dyer, 2019). The Philippines reported more than 249,000 dengue fever cases, almost twice as many as those reported in 2018 (WHO, 2019). Further, dengue cases continue to surge across other southeast Asian countries (Vietnam, Bangladesh, Malaysia, Myanmar, Singapore, etc.) (**Supplementary Table 1**). The situation will deteriorate with increasing travel from cities to rural areas and from southeast Asia to other countries, giving rise to serious pandemic events (Lai et al., 2018; Masika et al., 2020).

Since the 1970s, several outbreaks have occurred in southern China, including Guangdong, Fujian, Hainan, and Yunnan provinces (Huang et al., 2014; Zhang et al., 2014; Wang et al., 2015; Li et al., 2016; Sun et al., 2017). Reemergence and autochthonous transmission originating from travelers have been reported in Hubei and Zhejiang in China (Wang et al., 2015). In China, the overall rise in the dengue fever cases has been observed (**Supplementary Figure 1**). Jiangxi, a southwest province in China, is adjacent to Fujian and Zhejiang in the east and Guangdong in the south. Located in a subtropical region, Jiangxi has a humid climate and receives plenty of sunshine and rainfall. Previously, only scattered cases of imported dengue fever cases from southeast Asia have been identified; however, this province have experienced an outbreak since June 2019.

Over 1000 dengue fever cases have been reported in Jiangxi Province in 2019. However, the emergence of a dengue virus outbreak in a non-epidemic province remains unclear. To further investigate the origin of the 2019 Jiangxi dengue outbreak, we analyzed the clinical and epidemiological characteristics of dengue fever in Jiangxi using metagenomic next-generation sequencing.

MATERIALS AND METHODS

Participant Enrollment and Specimen

We recruited participants with clinically diagnosed or laboratory-confirmed dengue virus infections from four hospitals in Jiangxi Province, China, from April 2019 to September 2019. The participating medical facilities included Nanchang Ninth Hospital, Zhangshu People's Hospital, Fengcheng People's Hospital, and Nanchang Xian People's Hospital. Blood samples on the day of admission were collected from the participants who provided their informed consent, and all recruited patients or their guardians provided their authorization for the collection of clinical data. Laboratory-confirmed cases were identified if a blood sample tested positive by either the non-structural protein (NS1) rapid test, NS1-capture enzyme linked immunosorbent assay, IgM/IgG antibody test, or reverse transcription polymerase chain reaction (RT-PCR). In contrast, clinically diagnosed cases were identified based on various symptoms, including fever, muscle or joint pains, rash, bleeding, or gastrointestinal symptoms. We collected the patients' medical records, including clinical presentations, laboratory results, treatment regimens, epidemiological history, and follow-up monitoring. To further compare the viral phylogenic analysis, two blood samples were retrieved from Huashan Hospital, Shanghai. Ethical approval was obtained from the ethical committee of Huashan Hospital.

Etiology Tests and RT-PCR Relative Quantification

At the beginning of this outbreak, we carried out rapid NS1 antigen and antibody IgM and IgG tests in some samples to assist diagnosis apart from RT-PCR (**Supplementary Table 2**). Since the local hospitals did not perform antibody tests in Fengcheng and Zhangshu patients and no enough volume of some samples, the antibody data are missing.

All obtained blood samples were prepared for RT-PCR test. We extracted total viral RNA from 200 μL of patients' serum using TaKaRa MiniBEST Viral RNA/DNA Extraction Kit (TaKaRa, Japan). RNA was converted to cDNA using the TaKaRa PrimeScript RT Master Mix kit (TaKaRa, Japan). We performed real-time PCR using the BioGerm Dengue kit (BioGerm, Shanghai, China) with Taqman Probe (Haddar et al., 2020), including DENV-1/2 and DENV-3/4.

Metagenomic Next-Generation Sequencing

A total of 14 samples from Jiangxi with relatively high dengue virus copies and two samples from Huashan Hospital were prepared for high-throughput sequencing. Then, 60 μL cDNA of each sample and a blank control were purified with 60 μL magnetic beads (MGI, Shenzhen, China). Purified cDNA samples were fragmented into approximately 150 bp (Covaris M220 Focused-ultrasonicator, Massachusetts, US), followed by end-repair, A-tailing addition, adaptor-ligation, and PCR amplification (MGIEasy Cell-free DNA Library Prep Kit, MGI, Shenzhen, China). Qualified cDNA libraries were sequenced by a single-end 100 bp sequencing strategy on the MGISEQ-200 platform (MGI, Shenzhen, China).

Alignment and SNP Detection

Low-quality and short (average base quality < 20, length < 100 bp) reads were discarded, and reads derived from human genome sequences were filtered with Tophat2 (Kim et al., 2013). For genetic polymorphism analysis, sequenced reads were aligned to the reference isolate DENV-1 genome MF033254 using Bowtie2 with no more than 2 mismatches, and then only the uniquely mapped reads were used for genotyping analysis (Langmead and Salzberg, 2012). The Samtools mpileup and bcftools algorithms were used to generate consensus sequences for each sample. Meanwhile, amino acid sequences were aligned to DENV-1 amino acid sequence NP059433 using the multiple sequence alignment algorithm ClustalX2 (Chenna et al., 2003). A total of 56 complete dengue virus type I genomes isolated from 1956 to

2019 and respective amino acid sequences were both downloaded from the NCBI database.

Phylogenic Tree Construction and Evolutionary Analysis

The phylogenetic tree was constructed according to the detected SNPs of all 69 sequenced and published dengue nucleotide sequences. As suggested by jModelTest (v2.1.10), we estimated the substitution rate based on the Maximum-likelihood method under the GTR+γ+I substitution model (Darriba et al., 2012). The evolutionary distances were calculated based on the similarity of the SNP genotypes and validated by at least 1000 bootstrap analyses using MEGA X (Kumar et al., 2018). The evolutionary distances results were used to annotate the phylogenetic tree in iTOL v 4 (Letunic and Bork, 2019). We used the '*ape*' package in RStudio v 1.2 to analyze similarities of dengue amino acid based on polymorphic sites detected in amino acid sequences. We have uploaded the metagenomic next-generation sequence data to NCBI SRA database under accession number SRP269041.

Epidemiological Investigations

We collected epidemiological data concerning the mosquito's density (Breteau Index) and climate characteristics from previously published studies (Wu et al., 2017; Guo et al., 2019; Zhao et al., 2020). Further, we recorded the monthly average temperature and rain value and flight information in Jiangxi.

Statistical Analysis

For baseline characteristics and clinical presentations, numbers and percentages were used. Figures were constructed using the RStudio v 1.2 and GraphPad Prism 8.

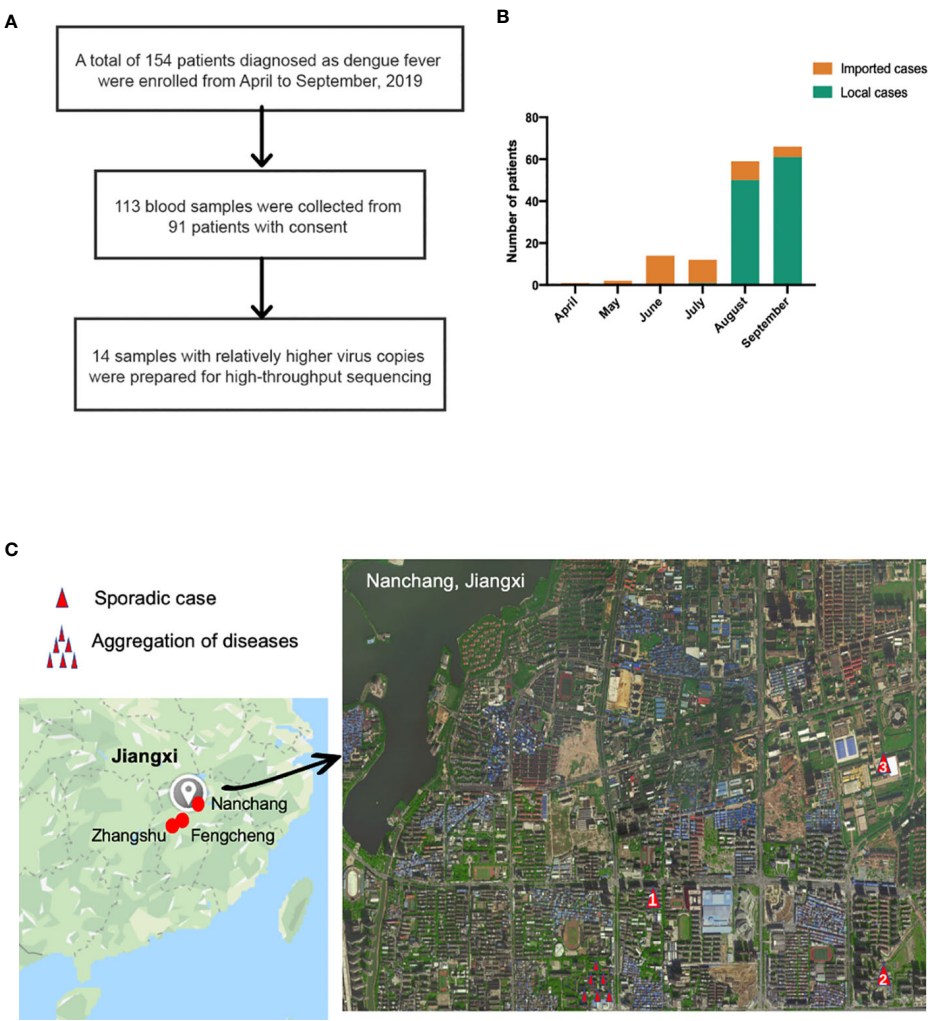

FIGURE 1 | **(A)** Sample enrollment and study flowchart; **(B)** The number of local and imported cases from April to September **(C)** Isolation sites in Jiangxi. Red circles in the left in Jiangxi represented isolation cities: Nanchang, Fengcheng and Zhangshu. For the enlarged Nanchang map, the single red triangle indicated sporadic cases in Nanchang while several triangle symbols meant aggregation of dengue fever. Panel **(C)** was based on maps from https://www.google.com/maps.

RESULTS

Clinical and Epidemiologic Characteristics of Enrolled Patients

A total of 154 patients were enrolled (**Figure 1A**) in the study from April to September 2019, and the baseline characteristics are shown in **Table 1**. Ninety-three, forty-nine, and twelve cases were collected from Nanchang, Zhangshu, and Fengcheng, respectively. Among the 154 cases, forty-two cases were identified as imported cases back from other countries; the majority (39/42) of which came from Cambodia. One hundred and nine cases were identified as local cases, and three cases were domestic cases from other provinces to Jiangxi. We observed a majority of DENV cases in August and September, with 125 cases reported, compared with 1, 2, 14, and 12 cases reported in April, May, June, and July, respectively. As shown in **Figure 1B**, the imported cases appeared in April while local cases emerged in July and increased rapidly in August and September, and small outbreaks were observed in a localized area in Nanchang (**Figure 1C**). The mean onset time (symptoms onset to admission) of enrolled patients was five days (range, 0–15). Approximately 94.16% (145/154) of patients presented with fever, and the proportion of rash, headache, and muscle pains was 31.37%, 20.13%, and 22.08%, respectively. We did not observe mucosal and gastrointestinal bleeding, a disorder of consciousness, shock, or respiratory failure. Overall, the clinical symptoms of all enrolled patients were mild, with no severe symptoms reported. All patients were later relieved during the follow-up monitoring.

TABLE 1 | Baseline characteristics of enrolled dengue fever patients.

Characteristics	N
Sex	
Male(n)	90
Female(n)	64
Age range (years)	4-84
Epidemic characteristics	
Imported cases (n)	42
Cambodia(n)	39
Philippines(n)	1
Thailand(n)	1
Malaysia(n)	1
Domestic input to Jiangxi	3
Local cases	109
Travelling to epidemic area (n, %)	80, 51.95%
History of mosquito bites (n, %)	136, 88.31%
Onset time (mean, range (d))	5(0-15)
Clinical presentations	
Fever (n)	145
Headache (n)	31
Muscle pains (n)	34
Joint pains (n)	6
Rash (n)	48
Mucosal and gastrointestinal bleeding (n)	0
Disorder of consciousness (n)	0
Shock (n)	0
Respiratory failure (n)	0
Clinical outcomes	
Relieved	154, 100%

Etiological Examination of Dengue Virus During Jiangxi Dengue Outbreak

Overall, 113 samples collected from 91 patients from Jiangxi were analyzed using DENV real-time PCR. A total of 106 samples were identified as DENV-1, two serum samples from one patient were identified as DENV-2, and five samples tested negative. The positive rate of dengue NS1 antigen was 100.00% (37/37), whereas the positive rate of dengue antibody IgM and IgG was 50.00% (11/22) and 13.63% (3/22), respectively.

Phylogenic and Molecular Analyses of Dengue Virus During Jiangxi Dengue Transmission

We investigated the nucleotide evolutionary relationships of the dengue virus during the Jiangxi dengue outbreak, with 56 published dengue virus genomes (**Figure 2A**). As illustrated in **Figure 2**, 69 selected sequences were separated into three groups, referring to DENV-1 Genotype I, IV, V, respectively. Sixteen DENV-1 genomes sequenced in this study were classified as DENV-1 Genotype I. Theses sequences owned high similarity to the genome from Cambodia (GenBank MN923099.1). All other Cambodia DENV strains and other southeast Asian DENV strains, including Thailand, Laos, Malaysia DENV isolates, had the same ancestor with the sequenced genomes in our study.

To learn the origin and high-resolution molecular characteristics of this dengue outbreak, we conducted phylogenetic analyses of 16 genomes. A total of 114 SNPs among 16 genomes were detected, indicating the existence of epidemic transmission and microevolution in Jiangxi. **Figure 2B** showed that Zhangshu virus strains, FC02 and FC03, were located in the upper branch. DENV genome NC 03, 04, 10, and 11 from Nanchang were classified into the lower branch. Three pairs of DENV genomes (NC03, NC04; ZS02, ZS17, and ZS07, ZS23) were found to be identical (**Figure 3**). The sequence-based findings were consistent with an epidemiological investigation into this transmission. NC03 and NC04 were from patients living in the same village in Nanchang, Jiangxi while ZS02, ZS17, and ZS07, ZS23 were from patients living in villages that were located within two kilometers.

To reveal evolutionary differences among amino acid sequences and functional changes, we next performed a phylogenetic analysis of 69 amino acid sequences, and showed that the evolutionary relationships are consistent with that of nucleotide genome results (**Supplementary Figure 2**). Sixty-nine amino acid sequences were classified into three categories: DENV-1 Genotype I, IV, V from upper to lower branches. Fourteen sequences collected from Jiangxi and two from Shanghai were closely related to the sequence of a traveler back from Cambodia in 2019 (GenBank MN923099.1). Analysis of detailed alterations of amino acids revealed that compared with the reference amino acid sequence from Singapore in 2016, 20 synonymous amino acid alterations were found in 16 DENV-1 sequences involved in this outbreak (**Supplementary Table 4**). Three out of 20 codon alterations in all 16 sequences were annotated with functional changes (**Table 2**).

The three altered positions were located in NP059433 position 2437 (AUG→AUA, Methionine →Isoleucine), 2750 (UAC→CAC,

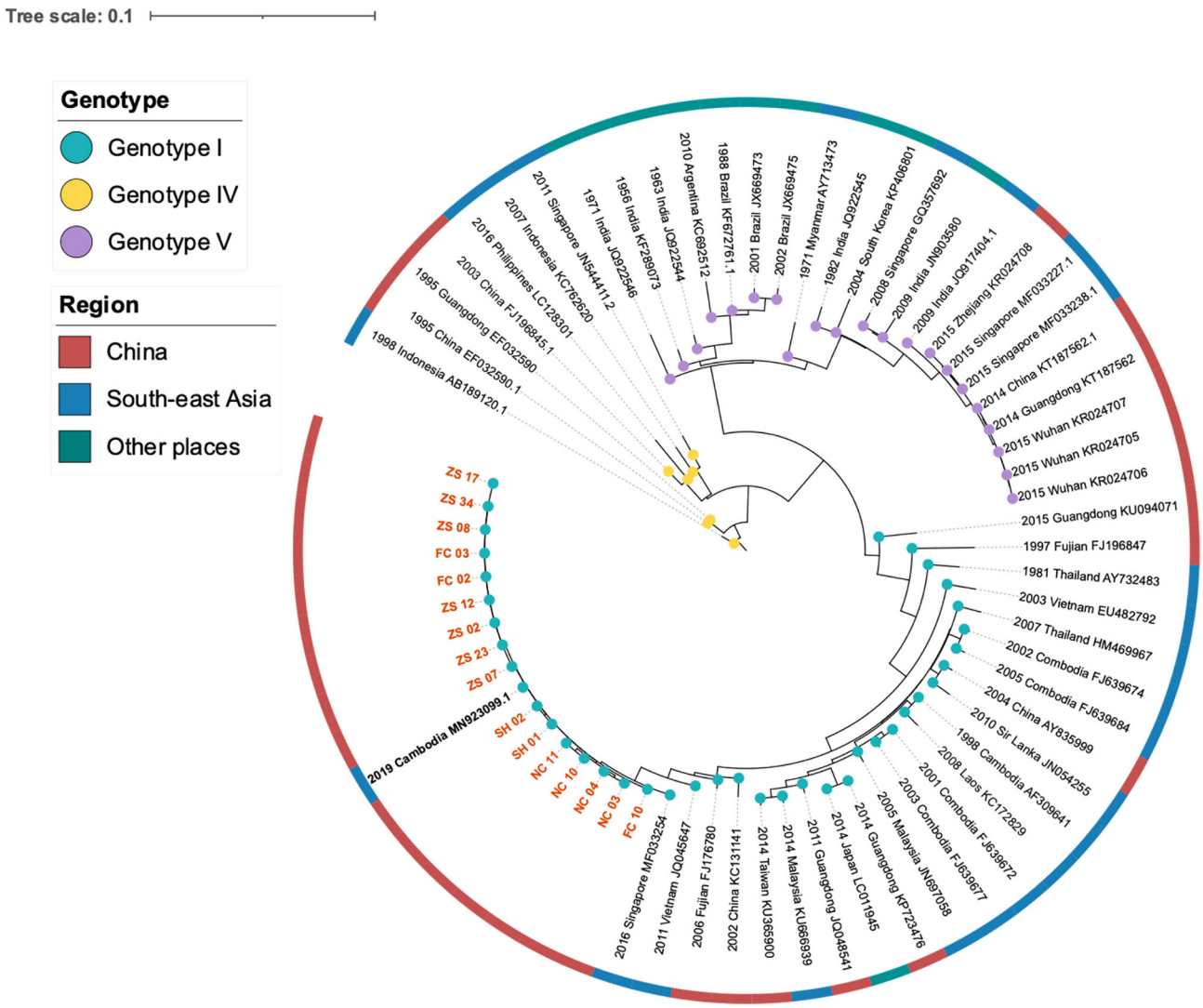

FIGURE 2 | Phylogeny and isolation resources profile of dengue virus type I strains. The colored blue, yellow and purple nodes refereed to DENV Genotype I, IV, V respectively. The dark red, blue and green color strip outside the circular tree indicated isolation resourced of these strains: China, South-east Asia and other places separately. Orange bold branch symbols meant virus we sequenced in this study and the black bold symbol is the strain isolated from a traveler back from Cambodia.

Tyrosine→ Histidine), and 3902 (CAU→TAU, Histidine→ Tyrosine). Altered positions 2437 and 2750 were located in NS1 protein, whereas 3902 was located in NS2A protein.

Mosquito's Density and Climate Characteristics of Jiangxi

Based on epidemiological investigations, the average monthly temperature and rain value indicated that Jiangxi had experienced water shortages in 2019, and the July to October temperatures were the highest since 1961 (http://www.ecns.cn/news/2019-11-08/detail-ifzqrxfh5725155.shtml). Surprisingly, Breteau Index, which represents mosquito density (Aryaprema and Xue, 2019) (**Figure 4**) showed no differences from previous years.

DISCUSSION

This work analyzed the clinical and epidemiology characteristics of 154 dengue fever cases in Jiangxi, a low-epidemic region in south-east China and molecular data of virus strains. The data present clear findings: (i) dengue virus strains shared close phylogenetic relationships (ii) the emergence of dengue cases led to autochthonous transmission in several cities in Jiangxi.

Although phylogenic and evolutionary analyses illustrated a high similarity of the dengue virus strains, a total of 97 synonymous mutations and 17 non-synonymous mutations were detected among 16 strains, suggesting fast variations of dengue virus during transmission. Moreover, comparison to referenced NP059433

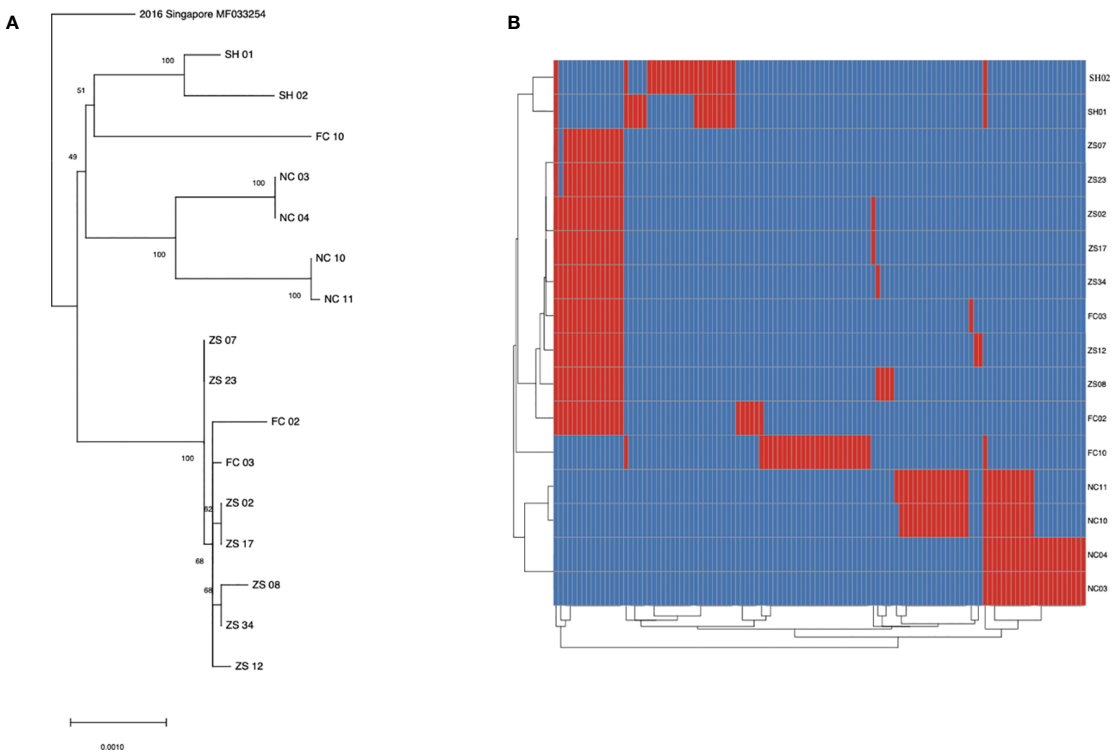

FIGURE 3 | SNP analysis among 16 sequenced dengue virus strains. **(A)** phylogenic tree constructed using 16 virus strains isolated from Jiangxi and Shanghai. The ZS, NC and FC referred to isolates from Zhangshu, Nanchang and Fengcheng separately. The SH 01 and 02 included two isolates from Shanghai. **(B)** A total of 114 SNPs was shown among 16 sequenced genomes were shown. Blue stripes indicated referenced single nucleotide polymorphisms and red ones indicated substitutions in sequenced genomes.

TABLE 2 | Three common non-synonymous amino acid mutations in 16 sequenced samples comparing to reference sequence NP059433.

Reference Amino acid sequence	Position	Protein	Reference codon	Altered codon	Reference amino acid	Alteredamino acid
NP059433	2437	NS1	G	A	AUG (Methionine)	AUA (Isoleucine)
NP059433	2750	NS1	T	C	UAC (Tyrosine)	CAC (Histidine)
NP059433	3902	NS2A	C	T	CAU (Histidine)	TAU (Tyrosine)

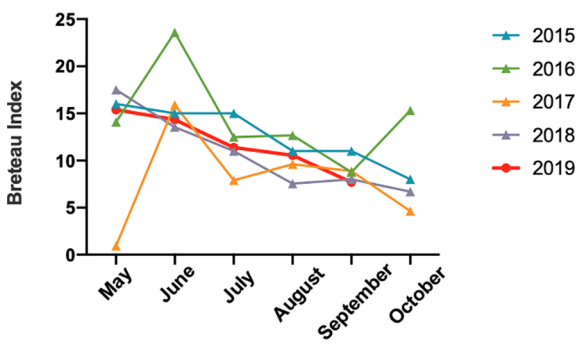

FIGURE 4 | The mosquito Breteau Index of Jiangxi from May to October between 2015 and 2019.

revealed three common alterations of amino acids, further suggesting the evolution of dengue virus. The locations of the three altered amino acids were correlated with early viral RNA replication and innate immune system activation (Guzman et al., 2016).

We evaluated the mosquito density to investigate the conversion of Jiangxi into a dengue fever epidemic region, but did not show obvious change compared with those in previous years. For climate change, we found that the summer in 2019 experienced a higher temperature and water shortages. According to previous reports, high temperatures and humid climate could increase the incidence and transmission of dengue fever (Ebi and Nealon, 2016). Thus, the higher temperature in 2019 might accelerate the dengue outbreak.

From clinical data, the cases from April to June were all imported cases and most of them were back from Cambodia. Local cases emerged in July and increased rapidly in August and September. What's more, a new airline connecting Preah Sihanouk,

Cambodia, and Nanchang, Jiangxi, has been operational since June 1, 2019. Combined with epidemiologic information of travelers in Jiangxi last year, we deduced that the emergence of the Jiangxi dengue outbreak might be linked to the Cambodia dengue wave. Further, the phylogenetic tree showed a high similarity of Jiangxi strains and Cambodia strain, and this evidence provided further evidence of our conclusion based on the clinical and epidemiological evaluation. We speculate that the new airline between Nanchang and Cambodia may be the contributory factor of a continuous movement of dengue virus-infected individuals traveling from Cambodia, therefore causing a sharp rise in the DENV infection cases in Jiangxi since June 2019. Air travel was reported to have a measurable impact on the importation of dengue virus to China, and prediction of dengue virus importation could help prevent and control the spread of the disease (Findlater et al., 2019; Wilson, 2019).

The aggregation of diseases in a small village in Nanchang, after a few sporadic cases in the nearby areas, revealed disease transmission pattern. It emphasized on the importance of regional prevention and control of dengue fever in this era of rapid growth of worldwide traffic. Additionally, areas previously considered non-epidemic should not be neglected.

As dengue fever have an incubation period from 3 to 14 days (Guzman et al., 2016), it is challenging for healthcare staff to control the disease in time, especially imported cases. Any place, especially humid tropical and subtropical areas that receive travelers and visitors from dengue fever epidemic areas should institute stringent prevention and control strategies. The silent majority carriers in the incubation period were found to be major sources of dengue virus transmission (Ferguson et al., 2018). What's more, live attenuated vaccine (CYD-TDV) has been used and candidate dengue vaccinations are currently proven to be effective in endemic populations (Biswal et al., 2019; Biswal et al., 2020; Deng et al., 2020; Tricou et al., 2020).

It has seemed that, during the human fight against the mosquito-borne virus, our deep understanding of diseases has failed to provide us with the satisfying tool to eliminate or, at least, prevent outbreaks of the disease. Therefore, this phenomenon suggests the great necessity of continuously studying the disease's epidemic traits and the possible underlying reasons.

This study has several limitations. First, we collected serum samples from July to September since the emergence of local transmission; thus, samples before July could not be included in the analysis. Second, metagenomic next-generation sequencing was performed successfully in genomes with relatively higher viral copies, whereas other samples failed to produce enough reads for analysis because of low viral loads. The limited sample size and sequenced data hinder precise and clear determination of the transmission route.

CONCLUSIONS

In conclusion, this study demonstrated that the emergence of dengue cases led to autochthonous transmission in several cities in Jiangxi. With increasing globalization, there is a need for more stringent disease prevention and control measures in regions with visitors and travelers from dengue fever epidemic areas.

DATA AVAILABILITY STATEMENT

The datasets presented in this study can be found in online repositories. The names of the repository/repositories and accession number(s) can be found in the article/ **Supplementary Material**.

AUTHOR CONTRIBUTIONS

This study was designed and supervised by JA, WZ and NJ. YZha, JA and NJ wrote the paper. YZha and JWu conducted RT-PCR, antigen and antibody tests. YZho carried out metagenomic library construction. HC, SW, XW, XT, YH, WJ, XP, JR, LW, JWa, QC and FL collected and analyzed clinical and epidemiologic data. All authors contributed to the article and approved the submitted version.

FUNDING

This study was supported by National Natural Science Foundation of China [grant number 82041010], Key Technologies Research and Development Program for Infectious Diseases of China [2018ZX10305-409-001-003] and Shanghai Youth Science and Technology Talents Sailing Project [20YF1404300].

ACKNOWLEDGMENTS

We thank the patients for cooperating with our investigation and acknowledge the professionalism and compassion demonstrated by all the healthcare workers involved in patients' care. We thank BGI platform for providing metagenomic next-generation sequencing in this study. We thank MATRIDX for assisting in molecular diagnosis in dengue fever.

SUPPLEMENTARY MATERIAL

The Supplementary Material for this article can be found online at: https://www.frontiersin.org/articles/10.3389/fcimb.2021.638785/full#supplementary-material

REFERENCES

Aryaprema, V. S., and Xue, R. D. (2019). Breteau index as a promising early warning signal for dengue fever outbreaks in the Colombo District, Sri Lanka. *Acta Trop.* 199, 105155. doi: 10.1016/j.actatropica.2019.105155

Bhatt, S., Gething, P. W., Brady, O. J., Messina, J. P., Farlow, A. W., Moyes, C. L., et al. (2013). The global distribution and burden of dengue. *Nature* 496, 504–507. doi: 10.1038/nature12060

Biswal, S., Reynales, H., Saez-Llorens, X., Lopez, P., Borja-Tabora, C., Kosalaraksa, P., et al. (2019). Efficacy of a Tetravalent Dengue Vaccine in Healthy Children

and Adolescents. *N. Engl. J. Med.* 381, 2009–2019. doi: 10.1056/NEJMoa1903869

Biswal, S., Borja-Tabora, C., Martinez Vargas, L., Velásquez, H., Theresa Alera, M., Sierra, V., et al. (2020). Efficacy of a tetravalent dengue vaccine in healthy children aged 4–16 years: a randomised, placebo-controlled, phase 3 trial. *Lancet* 395, 1423–1433. doi: 10.1016/S0140-6736(20)30414-1

Chenna, R., Sugawara, H., Koike, T., Lopez, R., Gibson, T. J., Higgins, D. G., et al. (2003). Multiple sequence alignment with the Clustal series of programs. *Nucleic Acids Res.* 31, 3497–3500. doi: 10.1093/nar/gkg500

Cousien, A., Ledien, J., Souv, K., Leang, R., Huy, R., Fontenille, D., et al. (2019). Predicting Dengue Outbreaks in Cambodia. *Emerg. Infect. Dis.* 25, 2281–2283. doi: 10.3201/eid2512.181193

Darriba, D., Taboada, G. L., Doallo, R., and Posada, D. (2012). jModelTest 2: more models, new heuristics and parallel computing. *Nat. Methods* 9 (8), 722. doi: 10.1038/nmeth.2109

Deng, S. Q., Yang, X., Wei, Y., Chen, J. T., Wang, X. J., and Peng, H. J. (2020). A Review on Dengue Vaccine Development. *Vaccines (Basel)* 8 (1), 63. doi: 10.3390/vaccines8010063

Dyer, O. (2019). Dengue: Philippines declares national epidemic as cases surge across South East Asia. *BMJ.* 366, l5098. doi: 10.1136/bmj.l5098

Ebi, K. L., and Nealon, J. (2016). Dengue in a changing climate. *Environ. Res.* 151, 115–123. doi: 10.1016/j.envres.2016.07.026

Ferguson, N. M., ten Bosch, Q. A., Clapham, H. E., Lambrechts, L., Duong, V., Buchy, P., et al. (2018). Contributions from the silent majority dominate dengue virus transmission. *PLoS Pathog.* 14 (5). doi: 10.1371/journal.ppat.1006965

Findlater, A., Moineddin, R., Kain, D., Yang, J., Wang, X., Lai, S., et al. (2019). The use of air travel data for predicting dengue importation to China: A modelling study. *Travel Med. Infect. Dis.* 31, 101446. doi: 10.1016/j.tmaid.2019.07.002

Guo, Y.-H., Wu, H.-X., Liu, X.-B., Yue, Y.-J., Ren, D.-S., Zhao, N., et al. (2019). National vector surveillance report on mosquitoes in China, 2018. *Chin. J. Vector Biol. Control* 30 (2), 134–138. doi: 10.11853/j.issn.1003.8280.2019.02.003

Guzman, M. G., Gubler, D. J., Izquierdo, A., Martinez, E., and Halstead, S. B. (2016). Dengue infection. *Nat. Rev. Dis. Primers* 2. doi: 10.1038/nrdp.2016.55

Haddar, C., Verhoeven, P. O., Bourlet, T., Pozzetto, B., and Pillet, S. (2020). Brief comparative evaluation of six open one-step RT-qPCR mastermixes for the detection of SARS-CoV-2 RNA using a Taqman probe. *J. Clin. Virol.* 132, 104636. doi: 10.1016/j.jcv.2020.104636

Huang, X. Y., Ma, H. X., Wang, H. F., Du, Y. H., Su, J., Li, X. L., et al. (2014). Outbreak of dengue Fever in central China, 2013. *BioMed. Environ. Sci.* 27, 894–897. doi: 10.3967/bes2014.125

Kim, D., Pertea, G., Trapnell, C., Pimentel, H., Kelley, R., and Salzberg, S. L. (2013). TopHat2: accurate alignment of transcriptomes in the presence of insertions, deletions and gene fusions. *Genome Biol.* 14, R36. doi: 10.1186/gb-2013-14-4-r36

Kumar, S., Stecher, G., Li, M., Knyaz, C., and Tamura, K. (2018). MEGA X: Molecular Evolutionary Genetics Analysis across Computing Platforms. *Mol. Biol. Evol.* 35, 1547–1549. doi: 10.1093/molbev/msy096

Lai, S., Johansson, M. A., Yin, W., Wardrop, N. A., van Panhuis, W. G., Wesolowski, A., et al. (2018). Seasonal and interannual risks of dengue introduction from South-East Asia into China, 2005-2015. *PLoS Negl. Trop. Dis.* 12, e0006743. doi: 10.1371/journal.pntd.0006743

Langmead, B., and Salzberg, S. L. (2012). Fast gapped-read alignment with Bowtie 2. *Nat. Methods* 9, 357–359. doi: 10.1038/nmeth.1923

Letunic, I., and Bork, P. (2019). Interactive Tree Of Life (iTOL) v4: recent updates and new developments. *Nucleic Acids Res.* 47, W256–W259. doi: 10.1093/nar/gkz239

Li, M. T., Sun, G. Q., Yakob, L., Zhu, H. P., Jin, Z., and Zhang, W. Y. (2016). The Driving Force for 2014 Dengue Outbreak in Guangdong, China. *PLoS One* 11, e0166211. doi: 10.1371/journal.pone.0166211

Masika, M. M., Korhonen, E. M., Smura, T., Uusitalo, R., Vapalahti, K., Mwaengo, D., et al. (2020). Detection of dengue virus type 2 of Indian origin in acute febrile patients in rural Kenya. *PLoS Negl. Trop. Dis.* 14, e0008099. doi: 10.1371/journal.pntd.0008099

Murray, K. O., Rodriguez, L. F., Herrington, E., Kharat, V., Vasilakis, N., Walker, C., et al. (2013). Identification of dengue fever cases in Houston, Texas, with evidence of autochthonous transmission between 2003 and 2005. *Vector Borne Zoonotic Dis.* 13, 835–845. doi: 10.1089/vbz.2013.1413

Sun, J., Lu, L., Wu, H., Yang, J., Xu, L., Sang, S., et al. (2017). Epidemiological trends of dengue in mainland China, 2005–2015. *Int. J. Infect. Dis.* 57, 86–91. doi: 10.1016/j.ijid.2017.02.007

Tricou, V., Sáez-Llorens, X., Yu, D., Rivera, L., Jimeno, J., Villarreal, A. C., et al. (2020). Safety and immunogenicity of a tetravalent dengue vaccine in children aged 2–17 years: a randomised, placebo-controlled, phase 2 trial. *Lancet* 395, 1434–1443. doi: 10.1016/S0140-6736(20)30556-0

Wang, W., Yu, B., Lin, X. D., Kong, D. G., Wang, J., Tian, J. H., et al. (2015). Reemergence and Autochthonous Transmission of Dengue Virus, Eastern China, 2014. *Emerg. Infect. Dis.* 21, 1670–1673. doi: 10.3201/eid2109.150622

WHO. (2019). *WHO Philippines Dengue Outbreak Report 8: 4 October 2019* (Geneva: World Health Organization).

Wilson, M. E. (2019). Arbovirus on board - Predicting dengue importation into China. *Travel Med. Infect. Dis.* 31, 101476. doi: 10.1016/j.tmaid.2019.101476

Wu, H.-X., Liang, L., Meng, F.-x., Guo, Y.-h., and Liu, Q.-y. (2017). Reports on national surveillance of mosquitoes in China,2006-2015. *Chin. J. Vector Biol. Control* 28 (5), 409–415. doi: 10.11853/j.issn.1003.8280.2018.02.001

Zhang, F. C., Zhao, H., Li, L. H., Jiang, T., Hong, W. X., Wang, J., et al. (2014). Severe dengue outbreak in Yunnan, China, 2013. *Int. J. Infect. Dis.* 27, 4–6. doi: 10.1016/j.ijid.2014.03.1392

Zhao, N., Guo, Y.-h., Wu, H.-x., Liu, X.-b., Yue, Y.-j., Ren, D.-s., et al. (2020). National vector surveillance report on mosquitoes in China, 2019. *Chin. J. Vector Biol. Control* 31 (4), 395–400. doi: 10.11853/j.issn.1003.8280.2020.04.003

Conflict of Interest: The authors declare that the research was conducted in the absence of any commercial or financial relationships that could be construed as a potential conflict of interest.

frontiers in Cellular and Infection Microbiology

ORIGINAL RESEARCH
published: 25 March 2021
doi: 10.3389/fcimb.2021.645944

Epidemiology of *Leishmania* Carriers in Tan Chang County, Gansu Province, China

Shuai Han[1,2,3,4,5], *Sheng-bang Chen*[6], *Zhang-hong Yang*[7], *Yu Feng*[6] *and Wei-ping Wu*[1,2,3,4,5]*

[1] National Institute of Parasitic Diseases, Chinese Center for Disease Control and Prevention, Shanghai, China, [2] Chinese Center for Tropical Diseases Research, Shanghai, China, [3] Key Laboratory of Parasite and Vector Biology, Ministry of Health, Shanghai, China, [4] WHO Collaborating Centre for Tropical Diseases, Shanghai, China, [5] National Center for International Research on Tropical Diseases, Ministry of Science and Technology, Shanghai, China, [6] Gansu Province Center for Disease Control and Prevention, Lanzhou, China, [7] Tan Chang County Center for Disease Control and Prevention, Longnan, China

OPEN ACCESS

Edited by:
Khalid B. Beshir,
London School of Hygiene and Tropical Medicine, United Kingdom

Reviewed by:
Canjun Zheng,
Chinese Center For Disease Control and Prevention, China
Yang Liu,
Sichuan Center for Disease Control and Prevention, China

***Correspondence:**
Wei-ping Wu
wuwp@nipd.chinacdc.cn

Specialty section:
This article was submitted to Parasite and Host, a section of the journal Frontiers in Cellular and Infection Microbiology

Received: 24 December 2020
Accepted: 10 March 2021
Published: 25 March 2021

Citation:
Han S, Chen S-b, Yang Z-h, Feng Y and Wu W-p (2021) Epidemiology of Leishmania Carriers in Tan Chang County, Gansu Province, China. Front. Cell. Infect. Microbiol. 11:645944. doi: 10.3389/fcimb.2021.645944

Background: Leishmaniasis is a regional infectious disease caused by the bite of *Leishmania*-carrying sandflies. The clinical symptoms include prolonged fever, spleen enlargement, anemia, emaciation, leukopenia, and increased serum globulin levels. If not appropriately treated, patients may die of complications caused by leishmaniasis within 1–2 years after the onset of the illness. Therefore, further investigation of the mechanisms of infection by this pathogen is required. Here, an epidemiological study of *Leishmania* carriers was conducted. The potential mechanism of infection through domestic animals as carriers of the parasite was investigated to identify potential reservoir hosts for *Leishmania.*

Methods: The rK-39 strip test was performed on blood samples from previously infected patients. Blood samples were collected from the patients and their families. The blood, liver, spleen, and diaphragm muscle samples were collected from livestock. To perform nested polymerase chain reaction (PCR), DNA was extracted and the internal transcribed spacer sequence was used. The amplified products were then subjected to restriction fragment length polymorphism and phylogenetic analyses.

Results: Among previously infected patients, 40% (12/30) showed positive results in the rK-39 strip test. The nested PCR positive rates for previously infected patients/relatives and livestock samples were 86% (77/90) and 80% (8/10), respectively. Moreover, the phylogenetic analysis showed that the pathogen was *Leishmania infantum*. Dogs, patients, and domesticated animals carrying *Leishmania* were found to be a potential source of infection for leishmaniasis.

Conclusions: The results of this study provide a basis for developing disease prevention and control strategies for leishmaniasis.

Keywords: Kala-azar, *Leishmania*, host, nested PCR, rk39

INTRODUCTION

Kala-azar, also known as visceral leishmaniasis (VL), is a regional infectious disease caused by the bite of *Leishmania*-carrying sandflies. Clinical symptoms include prolonged irregular fever, spleen enlargement, anemia, emaciation, leukopenia, and increased serum globulin levels. If not treated appropriately, most patients would die of VL-related complications within 1–2 years after the onset of illness (Desjeux, 1996; Boelaert et al., 2000; Alvar et al., 2006). The annual incidence of VL is around 200,000–400,000 cases globally; of these cases, over 90% are distributed in six countries including India, Bangladesh, Sudan, South Sudan, Ethiopia, and Brazil (Guerin et al., 2002; de Vries et al., 2015). Kala-azar is a disease that can be easily overlooked and whose severity is often underestimated (Singh et al., 2006; Mosleh et al., 2008; Zijlstra, 2016). Therefore, a trend of kala-azar outbreaks has been noticed in recent years (Wang et al., 2010).

In China, 650 endemic VL cases were reported in the 1950s. The disease was eliminated from the major epidemic areas of the country by the end of the 1950s. Currently, there are about 200 to 500 VL cases in China each year and these cases are sparsely distributed in different rural areas. The endemic areas have been classified into three types according to geography, pathogen, and medium: plain, mountainous, and desert areas (Lu et al., 1994; Wang et al., 2012). The Longnan Region in the Gansu Province is one of the current endemic areas for leishmaniasis in China and the pathogen found within this region is *Leishmania infantum* (Wang et al., 2000; Li and Gao, 2001; Yu et al., 2015; Zheng et al., 2017). The mountainous type of VL is endemic to Tan Chang County, situated in the northwestern part of the Longnan Region, Gansu Province. Tan Chang County is one of the primary locations of VL incidents (Wei et al., 2008) and the patient population within this county primarily consists of children. According to the Infectious Disease Report System, 87 VL cases have been reported in Tan Chang County since 2006, with an increasing number of patients identified each year. Although these VL cases are often sparsely distributed and most patients reside in small villages such as Shawan, Xinzhai, Guanting, and Lianghekou, the disease has continued to spread without intermission, and the number of patients and the size of the affected area are increasing each year.

Previously, dogs were thought to be the major animal source of infection for kala-azar (Smeyne et al., 1995; Dantas-Torres, 2007). However, studies on *Leishmania*-infected dogs suggested that most carrier dogs do not show any symptoms of the disease. Rather, they appear to be asymptomatic or not show any signs of infection (Boelaert et al., 2000; Caldas et al., 2002; Wang et al., 2007). Therefore, asymptomatic animals carrying the parasite may play a substantial role in transmitting the disease (Molina et al., 1994; Bern et al., 2007; Ferreira et al., 2009; Fu et al., 2009; Topno et al., 2010; Moreno et al., 2014; Gao et al., 2015; Esteva et al., 2017). Accurate estimation and confirmation of the number of leishmaniasis-affected asymptomatic dogs are critical for controlling the disease (Ashford et al., 1998; Zhang et al., 2008). Some researchers have proposed that the areas where the disease is endemic may be the ones from which the disease originated (Xiong and Jin, 2003). Given that local residents regularly take dogs with them into the mountains for hunting or guarding crops, *Leishmania* parasites can be regularly found in dogs that roam in the mountains. An analysis of the potential animal reservoirs suggests that the source of infection may originate from certain wild animals that reside within the mountains; hence, the possibility of additional animal hosts in the wilderness cannot be excluded (Jin et al., 2007; Souza et al., 2014). Because of local geographical features, houses generally consist of two stories, with the ground level designated for livestock rearing and the second level designated for living. As a result, villagers regularly come into contact with domesticated animals on a daily basis, which makes these domesticated animals another potential host for *Leishmania* (Bhattarai et al., 2010; Singh et al., 2013).

In recent years, as the number of domesticated dogs has increased along with population mobility, leishmaniasis has shown a tendency to spread again. Therefore, to understand the current status of the leishmaniasis epidemic in Tan Chang County and to identify potential hosts for *Leishmania*, a scientific investigation of the distribution of hosts and the associated infection status was conducted in Tan Chang County in December 2014.

Abbreviations: EDTA, Ethylenediaminetetraacetic acid; kDNA, kinetoplast DNA; PBS, phosphate-buffered saline; PCR, Polymerase chain reaction; RFLP, restriction fragment length polymorphism; rRNA, ribosomal RNA; VL, Visceral leishmaniasis.

MATERIALS AND METHODS

Collection of Blood Samples From Patients and Their Relatives, and of Blood and Tissue Samples From Livestock

To examine the kala-azar awareness and the patients' treatment conditions, patients identified by local records were provided with a questionnaire where they were asked about their living habits and environment. All questionnaires were answered anonymously. Written informed consent was obtained from all adult participants that answered the questionnaire and from whom blood samples were collected. In the case of child participants, written informed consent was obtained from the parents or guardians for questionnaire participation and blood sample collection.

In total, 29 households across five villages were included in this study based on the national notifiable disease report system database (**Table 1**; **Figure 1**). Blood samples (3 mL) were collected from patients and their relatives living in the same house (for a total of 90 samples) using 6-mL EDTA blood collection tubes (BD Vacutainer; Becton Dickinson, Franklin Lakes, NJ, USA). Tubes were kept at 4°C until analysis.

The 29 households containing previously infected patients typically reared livestock and dogs, with an average of 1.3 livestock per household (38/29) and 0.7 dogs per household (21/29), which was significantly higher than the numbers in other households in these five villages.

Local slaughterhouses were also selected for blood sample collection with the approval and supervision of the Animal

TABLE 1 | Distribution of Visceral Leishmaniasis Cases in the Tan Chang County (up to 2014).

Village	Population (from 5th National Census)	Number of patients with visceral leishmaniasis									
		2006	2007	2008	2009	2010	2011	2012	2013	2014	Total
Shawan	24778	2	3		4	5	4	1	2	5	26
Guanting	6713				2		2			2	6
Lianghekou	12361				1	1	3	2	4	2	13
Xinzhai	12425			6	3	5	7	4	1	4	30
Xinchengzi	6129						2		1		3
Nanyang	13486						2			1	3
Lichuan	11816					1					1
Hadapu	13118							1			1
Shizi	5905							1			1
Chela	11721									1	1
Unknown										2	2
Total		2	3	6	10	12	20	9	8	17	87

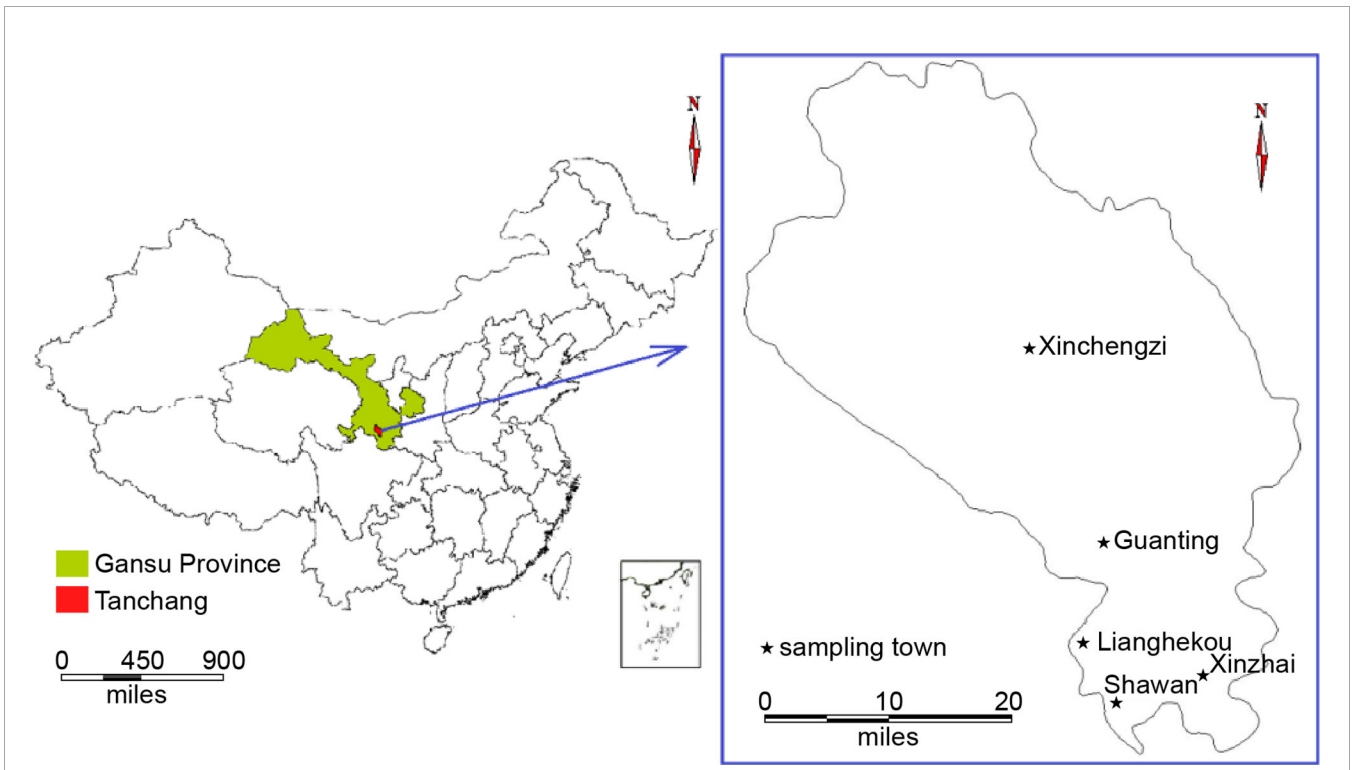

FIGURE 1 | Distribution of selected villages for blood sample collection.

Husbandry and Veterinary Department of Tan Chang County. The blood (3 mL), liver, spleen, and diaphragm muscle tissue samples (5 g) were collected from nine livestock pigs. Specifically, liver samples from three sheep and two pigs, blood samples from two pigs, spleen sample from one pig, and diaphragm muscle sample from one pig were collected. Notably, this study did not involve any animal raising or animal sacrifice, and the collections were scheduled in advance and did not change the routine procedures used at the slaughterhouses.

rK39 Strip Test

Whole blood (20 μL) was dripped onto the sample application site of an rK39 strip (InBios, Seattle, WA, USA) on a sample application pad. Next, 1–2 drops of PBS were added, and the strip was laid flat for 5–10 min. All strips were then visually examined.

DNA Extraction

DNA was extracted using an SE Blood DNA Kit (Omega Bio-Tek, Norcross, GA, USA) following the manufacturer's instructions. Each DNA extraction required 300 μL of whole blood. The obtained DNA was kept at −20°C until use.

Nested PCR

DNA from blood samples was extracted using the SE Blood DNA Kit (Omega Bio-Tek) according to the protocol in the instructions manual (Wang et al., 2006). The conserved internal transcribed

spacer (*ITS*)-1 gene between the genes encoding for *SSU* rRNA and 5.8S rRNA was used as the target gene in this analysis (Schonian et al., 2003). Nested PCR was performed as described by Ferreira et al. using the reported amplification protocol and primers (Katakura et al., 1998; Carvalho Ferreira et al., 2014). The primers were synthesized by Invitrogen Trading Co., Ltd, Shanghai, China. In the first round of PCR, the reaction volume was 50 μL, containing 1 μL of DNA template, 25 μL of MAX PCR Master Mix (Takara Biotechnology Co., Ltd, Dalian, China), and 1 μL of each primer; the concentration of primers used in each reaction was 10 μM. The primers were as follows: forward, 5′-CTGGATCA TTTTCCGATG-3′ and reverse, 5′-TGATACCACTTATCGC ACTT-3′. For every reaction, a positive control (*L. infantum* MHOM/CN/08/JS-1 DNA) and negative controls were used. Conditions for the nested PCR were as follows: initial denaturation at 94°C for 5 min; 30 cycles of denaturation at 94°C for 30 s, annealing at 53°C for 30 s, and extension at 72°C for 30 s; and a final extension at 72°C for 5 min. The amplification products from the first round of PCR were then diluted 1:40 and used as a template for the second round of PCR performed in a reaction volume of 25 μL, including 12.5 μL of MAX PCR Master Mix and 1 μL of each primer (10 μM; sequences: forward, 5′-CATTTTCCGATGATTACACC-3′ and reverse, 5′-CGTTCTTCAACGAAATAGG-3′). The reaction conditions were the same as those in the first round of PCR. The expected size of the PCR product was approximately 280–330 bp. The product from the second round of PCR (5 μL) was loaded onto a 1.5% agarose gel and subjected to electrophoresis. The PCR products were then visualized using a gel imager.

Restriction Fragment Length Polymorphism Analysis

Positive nested PCR products were digested using the restriction endonuclease *Hae*III (1 μL, 50 ng/μL; TaKaRa Biotechnology Co., Ltd.) in a 20-μL reaction containing 2 μL of 10× M buffer and 1 μg or less of DNA. The mixture was incubated at 37°C in a water bath for 1 h; 5 μL of the digested product was subjected to electrophoresis on 1.5% agarose gels, and RFLP analysis was then performed. If the RFLP analysis of different nested PCR products showed the exact same RFLP pattern, the products were categorized as having originated from the same visceral *Leishmania* species. Different positive nested PCR products were sent to Life Technologies Co. Ltd., Shanghai, China for sequencing.

Phylogenetic Analysis and Cladogram Construction

The sequences were edited using the DNAstar software (DNASTAR Inc., Madison, WI, USA). BLAST (National Center of Biotechnology Information, NCBI) was used to identify published sequences homologous to the target sequence and to determine *Leishmania* species. The sequence alignments and phylogenetic analyses of the aligned sequences were performed using ClustalW and the neighbor-joining method, respectively, in the MEGA 5.0 software package (DNASTAR Inc.).

RESULTS

rK39 Strip Test Results

Among previously infected patients, 40% (12/30) showed positive results for the rK-39 strip test (**Table 2**). The rK39 strip test was not performed on relatives of previously infected patients.

Assessment of *L. infantum* Infection Rates Using Nested PCR Analysis

As expected, 285-bp bands (**Figure 2**) indicated the target gene amplified by nested PCR, and no bands of other sizes were present. Data collected from previously infected patients and relatives indicated that the infection rate by *L. infantum* was 86% (77/90). The infection rate in animal blood and tissue samples was 80% (8/10). Liver samples from a sheep and a pig were negative for the infection. Thus, these data suggested that previously infected patients and their relatives (even without VL symptoms), and domestic livestock may serve as potential hosts for *L. infantum* parasites.

RFLP Analysis

The RFLP analysis indicated exact matches for all PCR products following restriction digestion (**Figure 3**). The fragments had a length of 161, 69, and 55 bp, suggesting that all the bands originated from the same *Leishmania* species.

Phylogenetic Analysis

The GR-6, GD-2, and LS-Y (MHOM/CN/08/JS-1) target sequences all belonged to the same group on the phylogenetic tree, indicating that local villagers and domesticated livestock were infected by the same type of *L. infantum*. Additionally, the sequences from GR-6 and GD-2 belonged to the same cluster, offering further evidence that the infection of people and domesticated livestock was related (**Figure 4**).

DISCUSSION

Herein, a case study of *Leishmania* carriers and the potential infection route of the parasites through domestic animals was performed to investigate the potential reservoir hosts for the

TABLE 2 | Test results of patients previously infected with visceral leishmaniasis and their relatives.

Sample population	rK39 test			Nested PCR test		
	Number	Positive number	Positive rate	Number	Positive number	Positive rate
Patient	30	12	40.00%	30	28	93.33%
Patient relatives	N/A	N/A	N/A	60	49	81.67%
Total	30	12	40.00%	90	77	85.56%
χ^2						2.2028
p-value						0.1377

N/A, not available.

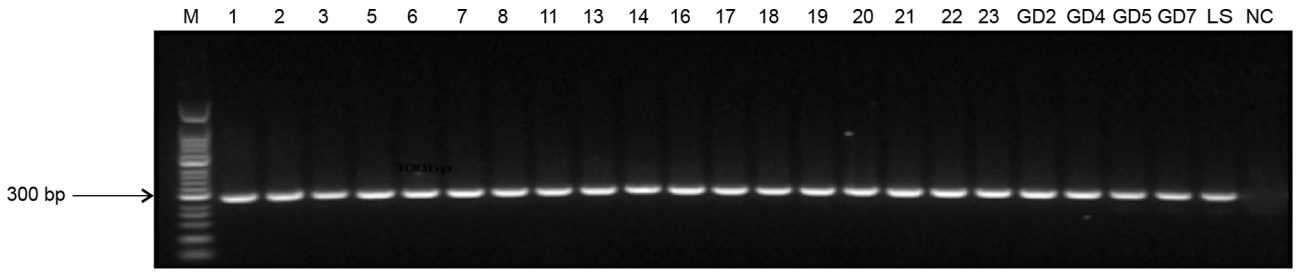

FIGURE 2 | Nested PCR amplification of *ITS* genes from *Leishmania* species. M, 50-bp DNA marker; 1–23, DNA extracted from patient blood samples and samples from their family members; GD2–GD7, DNA extracted from animal tissues of pigs; LS, positive control; NC, negative control.

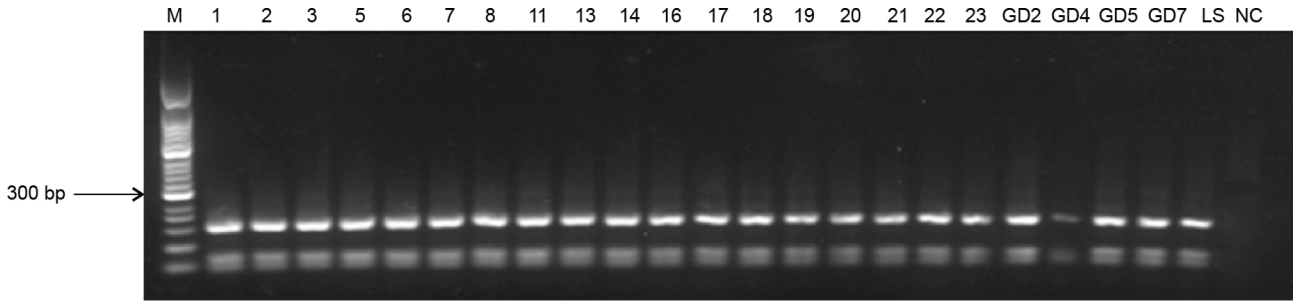

FIGURE 3 | RFLP profiles of *ITS* genes amplified from *Leishmania* digested with *Hae*III. M, 50-bp marker; 1–23, blood samples from infected patients and their families; GD2–GD7, blood and tissue samples from domesticated pigs; LS, positive control; NC, negative control.

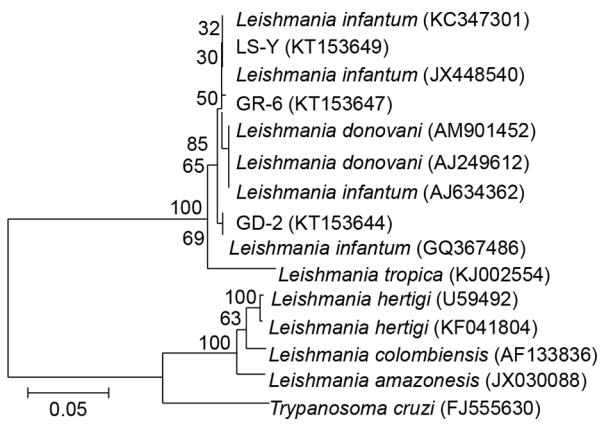

FIGURE 4 | Phylogenetic analysis of *ITS* genes in *Leishmania*. LS-Y (MHOM/CN/08/JS-1), positive control; GR-6, blood from kala-azar patient; GD-2, animal tissue from pigs.

parasites. Our data demonstrated that domesticated livestock may serve as carriers for *Leishmania* and provide insights into the origins of the infection in different families and individuals from Tan Chang County, China.

According to Xiong and Jin, (2003) the mountainous type of leishmaniasis and its local spread pattern in this region suggested that this type represented the natural cause of the epidemic in humans and dogs. It was believed that the parasite was passed to dogs from natural wildlife and subsequently spread from dogs to humans. When the parasite was transmitted from one host to another or between different hosts, the lifecycle of the sandfly played a pivotal role (Ashford et al., 1998), allowing parasites to spread among local wildlife and maintaining the presence of *Leishmania* in its natural habitat, while at the same time transmitting it to humans and dogs and causing visceral leishmaniasis.

The villages in Tan Chang County are fairly spread out. Moreover, the unique characteristics of the residential houses create perfect conditions for sandflies to thrive and spread (Li et al., 2004). The results of the rK39 strip test for previously infected patients showed a high positive rate, suggesting that they still produced *L. infantum*-related antibodies (Molinet et al., 2013; Regina-Silva et al., 2014). Locally, the numbers of domesticated sheep and pigs are fairly high, and with the improvement in the quality of life, the number of pet dogs has also increased. Patients previously infected with *L. infantum* had on average 1.3 (38/29) livestock animals and 0.7 (21/29) dogs per household, and these numbers are significantly higher than the local average. Studies of the transmission dynamics of visceral *Leishmania* by Stauch et al. (2011) in India indicated that asymptomatic carriers are the main factor in the spread of the disease (Bern et al., 2007; Fu et al., 2009; Stauch et al., 2011;

Tiwary et al., 2017). Furthermore, we cannot exclude the possibility that asymptomatic domesticated *Leishmania*-carrying animals may also be a major factor affecting the maintenance of the *Leishmania* epidemic in this endemic region. As the lifestyle of local villagers includes frequent contact with and close proximity to domesticated animals, the risk of parasite transmission is greatly increased.

The standard test for leishmaniasis is the rK39 strip test (Maia et al., 2012; Srividya et al., 2012; Georgiadou et al., 2015). However, this test can only be used on symptomatic patients and cannot detect asymptomatic carriers (Burns et al., 1993; Guan et al., 2001; Matlashewski et al., 2013; Molinet et al., 2013; Regina-Silva et al., 2014). Thus, an alternative method for the detection of asymptomatic carriers is needed. The *ITS-1* sequence located between the genes encoding *SSU* rRNA and 5.8S rRNA is not transcribed into RNA. During evolution, this region has accumulated many mutations, and the degree of variation in ITS-1 sequence can reflect the genetic relationships during biological evolution. Therefore, sequence analysis of *ITS-1* is widely used in evolutionary research for the classification of various biological systems (Villalba and Ramirez, 1982; Villalba et al., 1985). Leite et al. (2010) used a combination of *ITS-1* nested PCR and Kinetoplast DNA PCR in asymptomatic dogs infected with *L. infantum* to assess the efficacy of the hybrid test. This analysis showed that *ITS-1* nested PCR analysis of conjunctiva swab samples exhibited high sensitivity (up to 83.3%), whereas that of samples from dog blood displayed a relatively lower sensitivity (56.7%). The sensitivity of both of these tests is much higher than that of the kDNA PCR hybrid test (13.3%). Pilatti et al. (2009) also performed *ITS-1* nested PCR in symptomatic dogs and observed a sensitivity of 73.9%. Thus, these data showed that *ITS-1* nested PCR displays a fairly high sensitivity for detection of *L. infantum* in symptomatic and asymptomatic dogs (Di Muccio et al., 2012; Ajaoud et al., 2013).

In this study, rK39 strip tests showed 40.00% positivity (12/30) in blood samples from patients previously infected with VL, which indicates that these previously infected patients still presented symptoms of kala-azar. Nested PCR on DNA extracted from these blood samples was also used to assess the *L. infantum* infection status in previously infected patients and their relatives. Our results showed that the infection rate was 86% (77/90), suggesting that local residents may have a widespread history of sandfly bites and are asymptomatic carriers at high risk of developing the disease. Moreover, the infection rate in animal blood and tissue samples was 80% (8/10), and our phylogenetic analysis showed that GR-6, GD-2, and LS-Y (MHOM/CN/08/JS-1) belonged to the same cluster, indicating that local villagers and domesticated livestock were both infected with the same strain of *L. infantum*. Additionally, GR-6 and GD-2 belonged to the same cluster, suggesting that the *Leishmania* infections in humans and domestic animals were linked.

Given that the time of sampling did not coincide with the sandfly transmission season, it was suspected that symptom-free patients and domesticated livestock might also be potential hosts for *Leishmania*. Indeed, it was found that not only dogs, but also other livestock, could be animal *Leishmania* hosts. Thus, this study has expanded the current understanding of the types of *Leishmania* hosts and may facilitate the implementation of targeted preventive measures to effectively control the disease. However, because of the small sample size and long storage time of the samples used in our study, we cannot yet confirm the presence of *Leishmania* in all tested hosts and patient groups, and further studies are required.

CONCLUSIONS

This report provides insights into the potential mechanism of infection by *Leishmania* and identifies potential factors promoting the spread of leishmaniasis, which is an overlooked disease with no current prevention strategies. The treatment of patients with leishmaniasis is very challenging due to the lack of knowledge about the disease transmission and the asymptomatic nature of the pathogen. rK39 strip test results, nested PCR, and phylogenetic analyses demonstrated that the patients and domesticated livestock were infected by the same type of *L. infantum*. Thus, dogs, patients, and livestock carrying *Leishmania* could be potential sources of infection. Therefore, implementation of directed control and epidemic monitoring might help in preventing leishmaniasis outbreaks in endemic regions.

DATA AVAILABILITY STATEMENT

The datasets presented in this study can be found in online repositories. The names of the repository/repositories and accession number(s) can be found below: https://www.ncbi.nlm.nih.gov/genbank/, KT153649 https://www.ncbi.nlm.nih.gov/genbank/, KT153647 https://www.ncbi.nlm.nih.gov/genbank/, KT153644.

ETHICS STATEMENT

The studies involving human participants were reviewed and approved by National Institute of Parasitic Diseases, Chinese Center for Disease Control and Prevention. Written informed consent to participate in this study was provided by the participants' legal guardian/next of kin.

AUTHOR CONTRIBUTIONS

SH, W-pW, and YF conceived and designed the experiments. SH, W-pW, S-bC, and Z-hY collected the samples and

performed the experiments. SH and W-pW were the major contributors in purchasing reagents and materials, data collection and analysis, and writing the manuscript. All authors contributed to the article and approved the submitted version.

FUNDING

This work was supported by the Research Project of Shanghai Municipal Health Commission(No.202040052) and National Key Technology Research and Development Program (No. 2014BAI13B05).

ACKNOWLEDGMENTS

We thank Prof. Jun-Yun Wang (National Institute of Parasitic Diseases, Chinese Center for Disease Control and Prevention) for providing the standard strain of *L. infantum* (MHOM/CN/08/JS-1). We thank the CDCs of Gansu Province and Tan Chang County for their help with fieldwork.

REFERENCES

Ajaoud, M., Es-sette, N., Hamdi, S., El-Idrissi, A. L., Riyad, M., and Lemrani, M. (2013). Detection and molecular typing of*Leishmania tropica* from *Phlebotomus sergenti* and lesions of cutaneous leishmaniasis in an emerging focus of Morocco. *Parasit. Vectors* 6, 217. doi: 10.1186/1756-3305-6-217

Alvar, J., Yactayo, S., and Bern, C. (2006). Leishmaniasis and poverty. *Trends Parasitol.* 22, 552–557. doi: 10.1016/j.pt.2006.09.004

Ashford, D. A., David, J. R., Freire, M., David, R., Sherlock, I., Eulálio, M. C., et al. (1998). Studies on control of visceral leishmaniasis: impact of dog control on canine and human visceral leishmaniasis in Jacobina, Bahia, Brazil. *Am. J. Trop. Med. Hyg.* 59, 53–57. doi: 10.4269/ajtmh.1998.59.53

Bern, C., Haque, R., Chowdhury, R., Ali, M., Kurkjian, K. M., Vaz, L., et al. (2007). The epidemiology of visceral leishmaniasis and asymptomatic leishmanial infection in a highly endemic Bangladeshi village. *Am. J. Trop. Med. Hyg.* 76, 909–914. doi: 10.4269/ajtmh.2007.76.909

Bhattarai, N. R., van Der Auwera, G., Rijal, S., Picado, A., Speybroeck, N., Khanal, B., et al. (2010). Domestic animals and epidemiology of visceral leishmaniasis, Nepal. *Emerg. Infect. Dis.* 16, 231–237. doi: 10.3201/eid1602.090623

Boelaert, M., Criel, B., Leeuwenburg, J., Van Damme, W., Le Ray, D., and Van der Stuyft, P. (2000). Visceral leishmaniasis control: a public health perspective. *Trans. R Soc. Trop. Med. Hyg.* 94, 465–471. doi: 10.1016/s0035-9203(00)90055-5

Burns, J. M. Jr., Shreffler, W. G., Benson, D. R., Ghalib, H. W., Badaro, R., and Reed, S. G. (1993). Molecular characterization of a kinesin-related antigen of *Leishmania chagasi* that detects specific antibody in African and American visceral leishmaniasis. *Proc. Natl. Acad. Sci. U.S.A.* 90, 775–779. doi: 10.1073/pnas.90.2.775

Caldas, A. J., Costa, J. M., Silva, A. A., Vinhas, V., and Barral, A. (2002). Risk factors associated with asymptomatic infection by Leishmania chagasi in north-east Brazil. *Trans. R Soc. Trop. Med. Hyg.* 96, 21–28. doi: 10.1016/s0035-9203(02)90227-0

Carvalho Ferreira, A. L., Carregal, V. M., de Almeida Ferreira, S., Leite, R. S., and de Andrade, A. S. (2014). Detection of *Leishmania infantum* in 4 different dog samples by real-time PCR and ITS-1 nested PCR. *Diagn. Microbiol. Infect. Dis.* 78, 418–421. doi: 10.1016/j.diagmicrobio.2013.10.015

Dantas-Torres, F. (2007). The role of dogs as reservoirs of Leishmania parasites, with emphasis on *Leishmania* (Leishmania) *infantum* and *Leishmania* (Viannia) *braziliensis*. *Vet. Parasitol.* 149, 139–146. doi: 10.1016/j.vetpar.2007.07.007

de Vries, H. J., Reedijk, S. H., and Schallig, H. D. (2015). Cutaneous leishmaniasis: recent developments in diagnosis and management. *Am. J. Clin. Dermatol.* 16, 99–109. doi: 10.1007/s40257-015-0114-z

Desjeux, P. (1996). Leishmaniasis. Public health aspects and control. *Clin. Dermatol.* 14, 417–423. doi: 10.1016/0738-081x(96)00057-0

Di Muccio, T., Veronesi, F., Antognoni, M. T., Onfri, A., Piergili Fioretti, D., and Gramiccia, M. (2012). Diagnostic value of conjunctival swab sampling associated with nested PCR for different categories of dogs naturally exposed to *Leishmania infantum* infection. *J. Clin. Microbiol.* 50, 2651–2659. doi: 10.1128/JCM.00558-12

Esteva, L., Vargas, C., and Vargas de Leon, C. (2017). The role of asymptomatics and dogs on leishmaniasis propagation. *Math Biosci.* 293, 46–55. doi: 10.1016/j.mbs.2017.08.006

Ferreira, M. G., Fattori, K. R., Souza, F., and Lima, V. M. (2009). Potential role for dog fleas in the cycle of *Leishmania* spp. *Vet. Parasitol.* 165, 150–154. doi: 10.1016/j.vetpar.2009.06.026

Fu, Q., Wu, W. P., Tong, S. X., Israyil, O., Zhang, S., and Iskender, K. (2009). Study on time-space clustering regarding the distribution of visceral leishmaniasis in Kashgar Region, Xinjiang. *Zhonghua liu xing bing xue za zhi = Zhonghua liuxingbingxue zazhi* 30, 6–9. doi: 10.3969/j.issn.1673-5234.2008.10.012

Gao, C. H., Wang, J. Y., Zhang, S., Yang, Y. T., and Wang, Y. (2015). Survey of wild and domestic mammals for infection with *Leishmania infantum* following an outbreak of desert zoonotic visceral leishmaniasis in Jiashi, People's Republic of China. *PloS One* 10, e0132493. doi: 10.1371/journal.pone.0132493

Georgiadou, S. P., Makaritsis, K. P., and Dalekos, G. N. (2015). Leishmaniasis revisited: Current aspects on epidemiology, diagnosis and treatment. *J. Transl. Int. Med.* 3, 43–50. doi: 10.1515/jtim-2015-0002

Guan, L. R., Qu, J. Q., Cai, J. J., Matsumoto, Y., and Chang, K. P. (2001). Detection of canine visceral leishmaniasis by rK 39 antigen dipstick method. *Chin. J. Parasitol. Parasit. Dis.* 19, 58. doi: 10.3969/j.issn.1000-7423.2001.01.018

Guerin, P. J., Olliaro, P., Sundar, S., Boelaert, M., Croft, S. L., Desjeux, P., et al. (2002). Visceral leishmaniasis: current status of control, diagnosis, and treatment, and a proposed research and development agenda. *Lancet Infect. Dis.* 2, 494–501. doi: 10.1016/S1473-3099(02)00347-X

Jin, C. F., Hong, Y. M., and Xiong, G. H. (2007). Progress of research in visceral leishmania origins of canines and wildlife in China. *Int. J. Med. Parasit. Dis.* 34, 227–230. doi: 10.3760/cma.j.issn.1673-4122.2007.05.001

Katakura, K., Kawazu, S., Naya, T., Nagakura, K., Ito, M., Aikawa, M., et al. (1998). Diagnosis of kala-azar by nested PCR based on amplification of the Leishmania mini-exon gene. *J. Clin. Microbiol.* 36, 2173–2177. doi: 10.1128/JCM.36.8.2173-2177.1998

Leite, R. S., Ferreira Sde, A., Ituassu, L. T., de Melo, M. N., and de Andrade, A. S. (2010). PCR diagnosis of visceral leishmaniasis in asymptomatic dogs using conjunctival swab samples. *Vet. Parasitol.* 170, 201–206. doi: 10.1016/j.vetpar.2010.02.020

Li, G. R., and Gao, B. (2001). Mountainous type of kala-azar in the western region of China. *J. Pract. Parasit. Dis.* 9, 29–31. doi: 10.3969/j.issn.1672-2116.2001.01.016

Li, D. M., Chen, Y., Wei, L. S., and Si, E. C. (2004). Endemic status and preventive strategy of kala-azar in the Longnan region of Gansu Province. *Endemic. Dis. Bull. (China)* 19, 95–96. doi: 10.3969/j.issn.1000-3711.2004.03.050

Lu, H. G., Zhong, L., Guan, L. R., Qu, J. Q., Hu, X. S., Chai, J. J., et al. (1994). Separation of Chinese Leishmania isolates into five genotypes by kinetoplast and chromosomal DNA heterogeneity. *Am. J. Trop. Med. Hyg.* 50, 763–770. doi: 10.4269/ajtmh.1994.50.763

Maia, Z., Lirio, M., Mistro, S., Mendes, C. M., Mehta, S. R., and Badaro, R. (2012). Comparative study of rK39 Leishmania antigen for serodiagnosis of visceral leishmaniasis: systematic review with meta-analysis. *PloS Negl. Trop. Dis.* 6, e1484. doi: 10.1371/journal.pntd.0001484

Matlashewski, G., Das, V. N., Pandey, K., Singh, D., Das, S., Ghosh, A. K., et al. (2013). Diagnosis of visceral leishmaniasis in Bihar India: comparison of the

rK39 rapid diagnostic test on whole blood versus serum. *PloS Negl. Trop. Dis.* 7, e2233. doi: 10.1371/journal.pntd.0002233

Molina, R., Amela, C., Nieto, J., San-Andrés, M., González, F., Castillo, J. A., et al. (1994). Infectivity of dogs naturally infected with *Leishmania infantum* to colonized *Phlebotomus perniciosus*. *Trans. R Soc. Trop. Med. Hyg.* 88, 491–493. doi: 10.1016/0035-9203(94)90446-4

Molinet, F. J., Ampuero, J. S., Costa, R. D., Noronha, E. F., and Romero, G. A. (2013). Specificity of the rapid rK39 antigen-based immunochromatographic test Kalazar Detect(r) in patients with cutaneous leishmaniasis in Brazil. *Mem. Inst. Oswaldo Cruz.* 108, 0074–02762013000300293. doi: 10.1590/S0074-02762013000300006

Moreno, I., Alvarez, J., Garcia, N., de la Fuente, S., Martinez, I., Marino, E., et al. (2014). Detection of anti-*Leishmania infantum* antibodies in sylvatic lagomorphs from an epidemic area of Madrid using the indirect immunofluorescence antibody test. *Vet. Parasitol.* 199, 264–267. doi: 10.1016/j.vetpar.2013.10.010

Mosleh, I. M., Geith, E., Natsheh, L., Abdul-Dayem, M., and Abotteen, N. (2008). Cutaneous leishmaniasis in the Jordanian side of the Jordan Valley: severe under-reporting and consequences on public health management. *Trop. Med. Int. Health* 13, 855–860. doi: 10.1111/j.1365-3156.2008.02063.x

Pilatti, M. M., Ferreira Sde, A., de Melo, M. N., and de Andrade, A. S. (2009). Comparison of PCR methods for diagnosis of canine visceral leishmaniasis in conjunctival swab samples. *Res. Vet. Sci.* 87, 255–257. doi: 10.1016/j.rvsc.2009.02.005

Regina-Silva, S., Fortes-Dias, C. L., Michalsky, E. M., França-Silva, J. C., Quaresma, P. F., da Rocha Lima, A. C., et al. (2014). Evaluation of parasitological examination, kDNA polymerase chain reaction and rK39-based immunochromatography for the diagnosis of visceral leishmaniasis in seropositive dogs from the screening-culling program in Brazil. *Rev. Soc. Bras. Med. Trop.* 47, 462–468. doi: 10.1590/0037-8682-0064-2014

Schonian, G., Nasereddin, A., Dinse, N., Schweynoch, C., Schallig, H. D., Presber, W., et al. (2003). PCR diagnosis and characterization of Leishmania in local and imported clinical samples. *Diagn. Microbiol. Infect. Dis.* 47, 349–358. doi: 10.1016/s0732-8893(03)00093-2

Singh, S. P., Reddy, D. C., Rai, M., and Sundar, S. (2006). Serious underreporting of visceral leishmaniasis through passive case reporting in Bihar, India. *Trop. Med. Int. Health* 11, 899–905. doi: 10.1111/j.1365-3156.2006.01647.x

Singh, N., Mishra, J., Singh, R., and Singh, S. (2013). Animal reservoirs of visceral leishmaniasis in India. *J. Parasitol.* 99, 64–67. doi: 10.1645/GE-3085.1

Smeyne, R. J., Chu, T., Lewin, A., Bian, F., Sanlioglu, S., Kunsch, C., et al. (1995). Local control of granule cell generation by cerebellar Purkinje cells. *Mol. Cell Neurosci.* 6, 230–251. doi: 10.1006/mcne.1995.1019

Souza, T. D., Turchetti, A. P., Fujiwara, R. T., Paixao, T. A., and Santos, R. L. (2014). Visceral leishmaniasis in zoo and wildlife. *Vet. Parasitol.* 200, 233–241. doi: 10.1016/j.vetpar.2013.12.025

Srividya, G., Kulshrestha, A., Singh, R., and Salotra, P. (2012). Diagnosis of visceral leishmaniasis: developments over the last decade. *Parasitol. Res.* 110, 1065–1078. doi: 10.1007/s00436-011-2680-1

Stauch, A., Sarkar, R. R., Picado, A., Ostyn, B., Sundar, S., Rijal, S., et al. (2011). Visceral leishmaniasis in the Indian subcontinent: modelling epidemiology and control. *PloS Negl. Trop. Dis.* 5, e1405. doi: 10.1371/journal.pntd.0001405

Tiwary, P., Singh, S. K., Kushwaha, A. K., Rowton, E., Sacks, D., Singh, O. P., et al. (2017). Establishing, Expanding, and Certifying a Closed Colony of Phlebotomus argentipes (Diptera: Psychodidae) for Xenodiagnostic Studies at the Kala Azar Medical Research Center, Muzaffarpur, Bihar, India. *J. Med. Entomol.* 54, 1129–1139. doi: 10.1093/jme/tjx099

Topno, R. K., Das, V. N., Ranjan, A., Pandey, K., Singh, D., Kumar, N., et al. (2010). Asymptomatic infection with visceral leishmaniasis in a disease-endemic area in Bihar, India. *Am. J. Trop. Med. Hyg.* 83, 502–506. doi: 10.4269/ajtmh.2010.09-0345

Villalba, E., and Ramirez, J. L. (1982). Ribosomal DNA of *Leishmania brasiliensis*: number of ribosomal copies and gene isolation. *J. Protozool.* 29, 438–441. doi: 10.1111/j.1550-7408.1982.tb05428.x

Villalba, E., Dorta, B., and Ramirez, J. L. (1985). Comparative study of the ribosomal RNA from Leishmania and Trypanosoma. *J. Protozool.* 32, 49–53. doi: 10.1111/j.1550-7408.1985.tb03012.x

Wang, Z. J., Xiong, G. H., and Guang, L. R. (2000). The achievements of preventive measures and treatment of kala-azar epidemiology in new China. *Chin. J. Epidemiol.* 21, 51–54. doi: 10.3760/j.issn:0254-6450.2000.01.017

Wang, J. Y., Chen, S. B., Gao, C. H., Jin, C. F., Feng, Y., Zhang, C. J., et al. (2006). Survey on the Leishmania infantum asymptomatic infection in dogs in Wenxian county of Gansu province. *Chin. J. Zoonoses* 8, 734–737. doi: 10.3969/j.issn.1002-2694.2006.08.011

Wang, J. Y., Feng, Y., Gao, C. H., Jin, C. F., Chen, S. B., Zhang, C. J., et al. (2007). Asymptomatic Leishmania infection in human population of Wenxian County, Gansu Province. *Chin. J. Parasitol. Parasit. Dis.* 25, 62–64. doi: 10.3969/j.issn.1000-7423.2007.01.014

Wang, J. Y., Gao, C. H., Yang, Y. T., Chen, H. T., Zhu, X. H., Lv, S., et al. (2010). An outbreak of the desert sub-type of zoonotic visceral leishmaniasis in Jiashi, Xinjiang Uygur Autonomous Region, People's Republic of China. *Parasitol. Int.* 59, 331–337. doi: 10.1016/j.parint.2010.04.002

Wang, J. Y., Cui, G., Chen, H. T., Zhou, X. N., Gao, C. H., and Yang, Y. T. (2012). Current epidemiological profile and features of visceral leishmaniasis in people's republic of China. *Parasit. Vectors* 5:31. doi: 10.1186/1756-3305-5-31

Wei, X., Yang, G. R., Liu, Y. F., Li, W. C., Jiao, C. H., Xiao, X. D., et al. (2008). Symptom analysis of 350 case reports of kala-azar in Longnan city, Gansu Province. *Endemic. Dis. Bull. (China)* 23, 22–24. doi: 10.3969/j.issn.1000-3711.2008.03.007

Xiong, G. H., and Jin, C. F. (2003). Study of sand fly and leishmania disease in relation to economic development of western region of China. *Chin. J. Parasitol. Parasit. Dis.* 21, 119–122. doi: 10.3969/j.issn.1000-7423.2006.04.013

Yu, D. W., Ding, G. W., Ge, P. F., and Feng, Y. (2015). Li F. A Retrospective Analysis on the Prevalence of Visceral Leishmaniasis in Gansu Province during 2005–2014. *Zhongguo Ji Sheng Chong Xue Yu Ji Sheng Chong Bing Za Zhi* 33, 208–211. doi: 10.3969/j.issn.1000-7423.2015.03.011

Zhang, F. N., Chen, Q. L., and Xiao, Y. (2008). Endemic status of Sichuan Province in 2006–2007 and analysis of preventive measures. *Chin. J. Zoonoses* 24, 1085–1086. doi: 10.3969/j.issn.1002-2694.2008.11.026

Zheng, C. J., Xue, C. Z., Wu, W. P., and Zhou, X. N. (2017). Epidemiological characteristics of Kala-azar disease in China, during 2005-2015. *Zhonghua Liu Xing Bing Xue Za Zhi* 38, 431–434. doi: 10.3760/cma.j.issn.0254-6450.2017.04.004

Zijlstra, E. E. (2016). Visceral leishmaniasis: a forgotten epidemic. *Arch. Dis. Child.* 101, 561–567. doi: 10.1136/archdischild-2015-309302

Conflict of Interest: The authors declare that the research was conducted in the absence of any commercial or financial relationships that could be construed as a potential conflict of interest.

frontiers in Public Health

ORIGINAL RESEARCH
published: 16 April 2021
doi: 10.3389/fpubh.2021.649170

A PCR-Based Technique to Track the Geographic Origin of *Plasmodium falciparum* With 23-SNP Barcode Analysis

Fengyue Hu[1†], *Qicheng Zou*[1†], *Yinyue Li*[1], *Guoding Zhu*[2,3], *Huayun Zhou*[2,3], *Meihua Zhang*[2,3], *Fang Tian*[1], *Yaobao Liu*[2,3*] and *Feng Lu*[1,4,5*]

[1] Jiangsu Key Laboratory of Experimental and Translational Non-coding RNA Research, School of Medicine, Yangzhou University, Yangzhou, China, [2] National Health Commission Key Laboratory of Parasitic Disease Control and Prevention, Jiangsu Institute of Parasitic Diseases, Wuxi, China, [3] Jiangsu Provincial Key Laboratory on Parasite and Vector Control Technology, Jiangsu Institute of Parasitic Diseases, Wuxi, China, [4] Department of Clinical Laboratory, Affiliated Hospital of Yangzhou University, Yangzhou, China, [5] Jiangsu Key Laboratory of Zoonosis, Jiangsu Co-Innovation Center for Prevention and Control of Important Animal Infectious Diseases and Zoonoses, Yangzhou, China

Increased population movement has increased the risk of reintroducing parasites to elimination areas and also dispersing drug-resistant parasites to new regions. Therefore, reliable and repeatable methods to trace back to the source of imported infections are essential. The recently developed 23-single-nucleotide polymorphism (SNP) barcode from organellar genomes of mitochondrion (*mt*) and apicoplast (*apico*) provides a valuable tool to locate the geographic origin of *Plasmodium falciparum*. This study aims to explore the feasibility of using the 23-SNP barcode for tracking *P. falciparum* by polymerase chain reaction and sequencing, while providing geographical haplotypes of isolates that originated from Central Africa. Based on 23-SNP barcode analysis, SNPs were found at seven loci; 27 isolates were confirmed to have originated in West Africa, and this study also showed four isolates from Central Africa (Equatorial Guinea, 3; Republic of Congo, 1) that originated in East Africa. This study provides the sequence data from Central Africa and fills 23-SNP barcode data gaps of sample origins.

Keywords: *Plasmodium falciparum*, mitochondrion, apicoplast, SNP, barcode

OPEN ACCESS

Edited by:
Xiaojun Chen,
Nanjing Medical University, China

Reviewed by:
Surendra Kumar Prajapati,
Henry M. Jackson Foundation for the Advancement of Military Medicine (HJF), United States
Jian Li,
Tinnitus Hub Ltd., United Kingdom
Takafira Mduluza,
University of Zimbabwe, Zimbabwe

***Correspondence:**
Feng Lu
lufeng981@hotmail.com
Yaobao Liu
yaobao0721@163.com

†These authors have contributed equally to this work

Specialty section:
This article was submitted to Infectious Diseases - Surveillance, Prevention and Treatment, a section of the journal Frontiers in Public Health

Received: *04 January 2021*
Accepted: *12 March 2021*
Published: *16 April 2021*

Citation:
Hu F, Zou Q, Li Y, Zhu G, Zhou H, Zhang M, Tian F, Liu Y and Lu F (2021) A PCR-Based Technique to Track the Geographic Origin of Plasmodium falciparum With 23-SNP Barcode Analysis. Front. Public Health 9:649170. doi: 10.3389/fpubh.2021.649170

INTRODUCTION

Malaria is a serious public health problem in tropical and subtropical areas, with an estimated 228 million cases of malaria occurring worldwide [(1), available online at: https://www.who.int/publications/i/item/9789241565721]. Among the five species of *Plasmodium* that infect humans, *Plasmodium falciparum* is the most dangerous one, causing high levels of mortality and morbidity worldwide, particularly in sub-Saharan Africa. With today's ease of transmissibility, the emergence and spread of artemisinin-resistant *P. falciparum* threatens malaria eradication (2–4). Increased population movement has increased the risk of reintroducing parasites to elimination areas and dispersing drug-resistant parasites to new regions. To facilitate a better response for this new challenge and to understand it well, except drug sensitivity monitoring, the geographic origins of imported malaria need be tracked accurately and in good time. Reliable and repeatable methods to trace back to the source of imported infections are therefore essential.

In the past decade, the single-nucleotide polymorphism (SNP) barcode has been developed as a forceful genotyping technique to investigate the origin of *Plasmodium* (5). The first *P. falciparum* molecular barcode was composed of 24 SNPs, which in combination created a unique and concise signature to differentiate recrudescence from reinfection from malaria parasites or to monitor distribution and frequency of specific parasites in patients (6). However, these nuclear SNPs are constrained by a lack of geographic specificity and frequent recombination. The establishment of a 23-SNP barcode using polymorphisms from mitochondrion (*mt*) and apicoplast (*apico*) genomes provides evidence that they are non-recombining and coinherited and are capable of identifying the geographic origin of *P. falciparum* strains (7). The 23-SNP barcoding strategy was 92% accurate in identifying the continental origin of *P. falciparum* samples from West and East Africa, Southeast Asia, Oceania, and South America (7). However, feasible and conventional methods for the 23-SNP barcode are lacking, and information about the haplotypes of isolates from Central Africa is rare. To conquer such a plight, we designed a simple 23-SNP barcode based on polymerase chain reaction (PCR) and sequencing, and assayed the samples from *P. falciparum* malaria cases imported from sub-Saharan Africa.

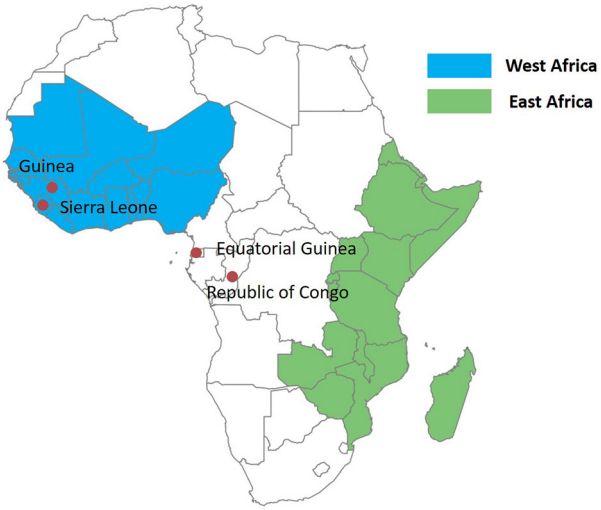

FIGURE 1 | Map of Africa showing the countries where *Plasmodium falciparum* isolates were imported from: Equatorial Guinea ($n = 29$), Guinea ($n = 1$), the Republic of Congo ($n = 1$), Sierra Leone ($n = 1$).

MATERIALS AND METHODS

Study Sites and Participants

The study was carried out in Jiangsu Province, China, where only imported malaria cases have been reported since 2013. The study was approved by the institutional review board of Jiangsu Institute of Parasitic Diseases (IRB00004221), Wuxi, China. Samples were collected from imported malaria cases. Imported cases were identified based on the travel history of the patients (travel to a malaria-endemic country within the previous month of illness onset); the last country visited with ongoing malaria transmission was taken as the potential location of infection (8). All of the malaria cases were routinely confirmed by microscopy and PCR through the malaria diagnosis reference laboratory in Jiangsu Institute of Parasitic Diseases. The 32 samples included in this study are a subset of the 765 imported malaria samples analyzed earlier (3); 21 mutated isolates were selected for this study. In addition, 11 isolates with wild-type *Pf kelch13* from Equatorial Guinea were also random selected for this barcode assay. Together, 32 samples, including 30 samples from Central Africa (29 samples from Equatorial Guinea, 1 from Guinea), and 2 samples from West Africa (Republic of Congo, Sierra Leone) as reference, were enrolled in this study (**Figure 1**). **Figure 1** was produced using Microsoft Excel and SPSS software 26.0 for Windows.

PCR and Sequencing of the Targets

Genomic DNA of *P. falciparum* isolates was extracted from the whole blood samples on the QIAcube Connect platform, using a QIAamp DNA Blood Kit (Qiagen, Valencia, CA) according to the manufacturer's instructions. From the 200 μL of input whole blood sample, a final 100 μL of elution volume was obtained. The gDNA was used for PCR amplification with gene-specific primers to amplify SNP loci targets within the *mt* and *apico P. falciparum* genomes. Primers were designed manually on the basis of geographically informative barcoding; the reference sequences used in this study were from the database of GenBank (https://www.ncbi.nlm.nih.gov/nucleotide/); AY282930 (5,949 bp) was selected as the reference sequence for *mt*, and X95276 (1–14,009 bp) combined the reverse sequence of X95275 (14,010–29,430 bp) for *apico* (9) (Appendix 1 in **Supplementary Material**).

A total of 10 sets of primers that covered the sites of the 23-SNP barcode were included in this study; detailed primer sequences are shown in **Table 1**, and the target sequences are shown (**Figure 2** and Appendix 2 in **Supplementary Material**). Amplifications were performed in a reaction mixture that contained 25 μL of 2× PCR buffer for KOD FX, 10 μL of 2 mM dNTPs, 1.5 μL each of 10 μM Primer-F and Primer-R, 3 μL of template DNA, 1 μL of 1.0 U/μL KOD FX, and 8 μL of double-distilled water. The PCR was performed with initial denature at 98°C for 2 min, and 35 cycles of 98°C for 10 s, 58°C for 30 s, and 68°C for 2 min and ending with a final extension of 5 min at 68°C. The PCR products were purified and sequenced. Double-strand capillary sequencing of PCR products was performed on an Applied Biosystems 3,730 sequence analyzer with the sequencing primers (**Table 1**). The deduced amino acid sequences were aligned and analyzed with the Lasergene® software (DNASTAR, Madison, WI).

RESULTS

The reference *mt* and *apico* sequences were selected from the complex database and were shown to be well-correlated to the loci of the barcode designed (7). With the designed primers, the 32 isolates were amplified and sequenced successfully (**Figure 3**); however, the sequencing peak chromatograms showed one

TABLE 1 | Primers used for polymerase chain reaction (PCR) amplification and sequencing of *mt/apico*.

	Primer sequence (5′ → 3′)	Amplified position	Amplicon
mt	F: AAGCTTTTGGTATCTCGTAATGTAGAA R*: TTAGCAATAACATTCCTGATGTAATGA SF1: CCTTCTCGCCATTTGATAGC SR1: GGCGAACCTTCTTACCGTTAT	*mt*772, *mt*853, *mt*973, *mt*1283, *mt*2383	1–2,650
apico 1	F: TTAGTTAATAATCCAGAAACCCATTT R*: GTGGATATTCTTTACATACAGA	*apico*15131	14,392–15,247
2	F: TGCCTGAGTGGTTAAAAGGAA R*: Ccctgtttacatacaggtg	*apico*2122	1,473–2,278
3	F: TCTTTGACCCCCTTGTTTTG R*: ctaatgaaggattaacttgtgg	*apico*20831, *apico*21188	19,599–21,277
4	F*: Gaagctgtacatccttct R: Tatatttaaattacctgattggaa	*apico*23803	23,595–24,104
5	F*: AAGTACATCCTTTAATATTTAGAGG R*: CCTATAACTATATCACCATATTTAGG	*apico*4370, *apico*4878, *apico*4945, *apico*5005	3,857–5,257
6	F*: GTAGGTACTAAAAGTAATAATTATATATC R*: TATTATTTTACAATTAAAATAACCTAAAC	*apico*5715, *apico*6361, *apico*6832	5,415–7,054
7	F*: CAACATATAAATTTAGGTACTATAGG R: GAGGTTTATATCCAATATTAAAAGG	*apico*9003, *apico*9096	8,785–9,778
8	F: CCAAAATTTATAATAAAGGTTCG R: ATCCAACTTCCTATAGGTTTA SF2: ACTAGAAGGGGTAAATGATA Sr2: TATCATTTACCCCTTCTAGT	*apico*11066, *apico*11619, *apico*11671	10,497–12,414
9	F*: AATTCGATTGGCATTTCACC R: GGATTCATGCTCCGAAGGTA	*apico*26659	26,347–27,183

*F, forward; R, reverse; S, sequencing. F and R pairs were used in PCR amplifications; SF, SR, and primers with *labels were used in the sequencing reactions.*

sample with a double peak at the two special loci indicated in mixed haplotype infections. For the five loci of *mt* genomes, including *mt*772, *mt*853, *mt*973, *mt*1283, and *mt*2383, the wild-type was shown except in one isolate with a double peak at *mt772* mentioned previously. A total of 18 loci of the *apico* genomes were selected for the barcode, with six loci including *apico*2122, *apico*6832, *apico*20831, *apico*21188, *apico*23803, and *apico*26659 with different alleles (**Figures 2**, **3**). The haplotype analysis of *mt*/*apico* among all 32 samples in this study revealed seven distinct haplotypes. **Figure 4** and Appendix 3 (**Supplementary Material**) show the number of haplotypes identified in samples from each country for the seven haplotypes identified therein. A single mutation at G_{26659} of *mt*/*apico* (haplotype 9) was the most prevalent haplotype (22/29) in Equatorial Guinea, which is unique to West Africa. In addition, haplotype 9 was also found in the isolates from Guinea and Sierra Leone. Among isolates from Equatorial Guinea, the C_{23803} single mutation (haplotype 8) was found in two isolates, and the $A_{21188}G_{26659}$ double mutations (haplotype 7) were observed in one isolate, corresponding to the barcodes published for West Africa. Meanwhile, the isolate CWX, with 23-SNP barcode identified in this study was consisted with the results analyzed with whole-genome sequencing (3).

The $A_{20831}G_{26659}$ double mutations (haplotype 12), the $T_{6832}G_{26659}$ double mutations (haplotype 13), and the C_{2122} single mutation (haplotype 14) identified in some of the isolates correspond to the barcodes published for East Africa. Haplotype 12 and haplotype 14 were observed in two isolates and one isolate from Equatorial Guinea, respectively. Haplotype 13 was found in only one isolate from the Republic of Congo. In addition, the mixed genotype of the wild-type and position *mt*772, *apico*26659 mutations, was found in one sample from Equatorial Guinea.

DISCUSSION

The Greater Mekong Subregion is the cradle of now widespread resistance to previous frontline antimalarial drugs (10). There is a significant risk that the artemisinin-resistant phenotypes within the Greater Mekong Subregion may similarly spread to other endemic regions. Therefore, the geographic origin of the parasites is important for monitoring the global emergence and spread of resistance and may prevent or delay the spread of artemisinin resistance from South East Asia to sub-Saharan Africa (11, 12).

With the establishment of sequence-based genome-wide polymorphisms in *P. falciparum* parasites, it is becoming feasible to design panels of SNP-based genotyping assays in tracing parasite geographic origin. Highly polymorphic microsatellites are useful to characterize community-, country-, or region-level genetic diversity over relatively short periods of time, as often required in outbreak investigations. However, it is difficult to standardize the interpretation of microsatellite assays across laboratories (13). The genomes of *mt* and *apico*, which have uniparental inheritance and do not recombine with each other,

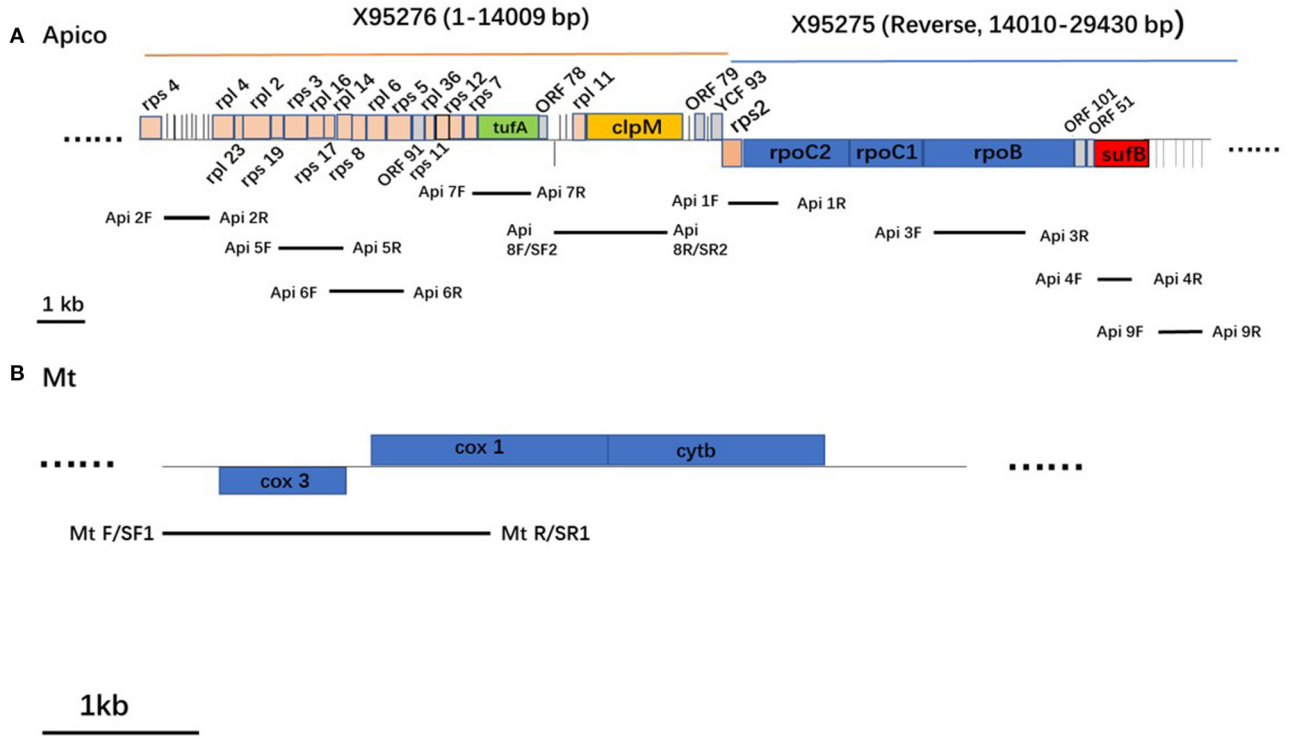

FIGURE 2 | Schematic representation of the apicoplast genome **(A)** and mitochondrion genome **(B)** in *Plasmodium falciparum*. Protein coding genes are boxed and color-coded. tRNAs are represented by vertical lines. Genes shown above the horizontal line in each genome are transcribed left to right, and those below are transcribed from right to left.

could provide more stable region-specific genotypes than nuclear genome SNPs. As a result, Preston et al. (7) developed a 23-SNP barcode using polymorphisms from *mt*/*apico* to identify the geographic origin of *P. falciparum* strains. In the study, 151 SNPs in *mt* and 488 in *apico* were identified from 711 *P. falciparum* samples in five geographic regions: West Africa, East Africa, Southeast Africa, Southeast Africa, Oceania, and South America, and a 23-SNP barcode was designed to trace the origin and dispersal of parasite strains across and between continents (7).

PCR-based approaches are inexpensive ways of extracting genomic data from samples containing very small quantities of parasite DNA, excluding the interference of host DNA. PCR-based approaches that genotype small collections of SNPs or a limited number of amplicons are of great value for timely genetic analysis of clinical samples collected directly from sporadic cases. In this study, we chose the method that used a 23-SNP barcode based on single-step PCR (ssPCR) and sequencing because it is a low-cost, rapid, and easy method to perform in the laboratory. This study presented the feasible application of PCR and sequencing in examining the 23-SNP barcode from *mt*/*apico*, effectively identifying the geographic origin of *P. falciparum* strains imported to China.

In this study, 10 fragments were amplified with 10 sets of primers by ssPCR, and the amplification efficiency of *mt* was much higher than *apico* (**Figure 3A**). Molecular targets are involved in malaria diagnosis assays; 18S rRNA genes are the most common; meanwhile, *mt* and *apico* are also an obvious target for malaria diagnosis (14, 15). Normally, the 18S rRNA gene of *P. falciparum* has 7-fold the amount of nuclear genomes, while *mt* and *apico* are ∼20-fold and between 1- and 15-fold, respectively. All of them can be used to classify samples with mixed infections; however, ssPCR targeting 18S rRNA still showed similar sensitivity with targeting *mt* and even higher than the *apico* genome-based classification. Of the 23-SNP barcode, a total of 13 loci were polymorphic and composed of African haplotypes (7), and only seven loci were found to be polymorphic in this study. Then, it could also select specific loci for amplification and attempt to predict the geographic source. Our results confirm the relatively low efficiency of the amplification of *apico* targets. Although the limit of detection was not tested, we recommend using whole blood, high-efficiency enzymes, and DNA enrichment if necessary.

We not only supported a feasible method for the 23-SNP barcode assay, but we also listed the clear sequence references of the targets and genome of *apico* (Appendices 1, 2 in **Supplementary Material**). For the accurate demand of the assay, the reference sequences must contain the original design (7); even a single deletion/insertion will make the analysis change completely. The genome of *P. falciparum* 3D7 was the first reference genome published in *Plasmodium* research; however, the *apico* was not sequenced in the original genome project, and the *apico* from the *P. falciparum* isolate C10 was used

FIGURE 3 | Agarose gel electrophoresis of polymerase chain reaction **(A)** and sequencing wave of the target loci with wild-type **(B)**, mutant type **(C)**, and mixed type **(D)** compared to the reference *Plasmodium falciparum* 3D7. Gray shading marked in the sequencing waves indicates the target loci.

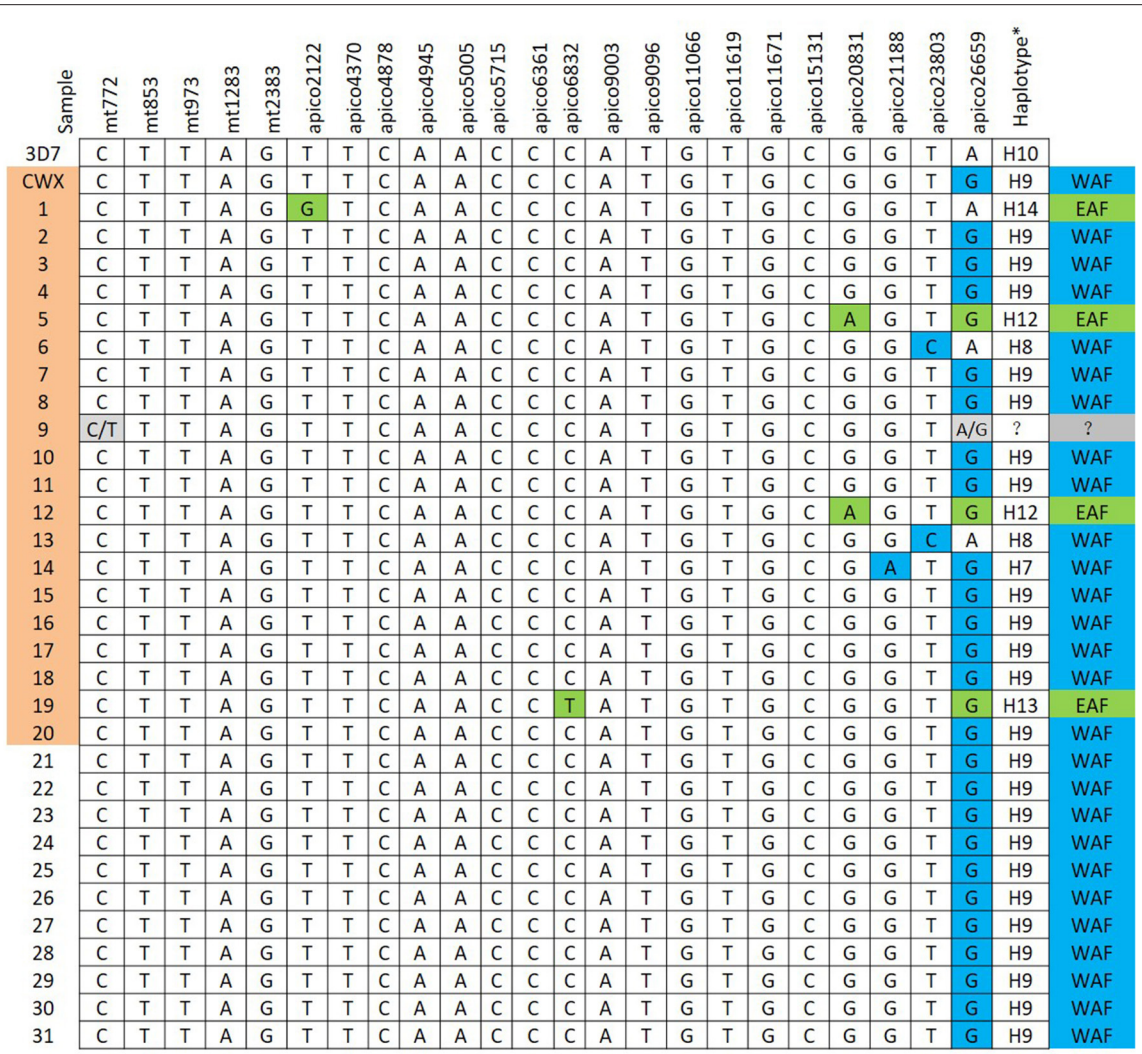

Sample	mt772	mt853	mt973	mt1283	mt2383	apico2122	apico4370	apico4878	apico4945	apico5005	apico5715	apico6361	apico6832	apico9003	apico9096	apico11066	apico11619	apico11671	apico15131	apico20831	apico21188	apico23803	apico26659	Haplotype*	
3D7	C	T	T	A	G	T	T	C	A	A	C	C	C	A	T	G	T	G	C	G	G	T	A	H10	
CWX	C	T	T	A	G	T	T	C	A	A	C	C	C	A	T	G	T	G	C	G	G	T	G	H9	WAF
1	C	T	T	A	G	G	T	C	A	A	C	C	C	A	T	G	T	G	C	G	G	T	A	H14	EAF
2	C	T	T	A	G	T	T	C	A	A	C	C	C	A	T	G	T	G	C	G	G	T	G	H9	WAF
3	C	T	T	A	G	T	T	C	A	A	C	C	C	A	T	G	T	G	C	G	G	T	G	H9	WAF
4	C	T	T	A	G	T	T	C	A	A	C	C	C	A	T	G	T	G	C	G	G	T	G	H9	WAF
5	C	T	T	A	G	T	T	C	A	A	C	C	C	A	T	G	T	G	C	A	G	T	G	H12	EAF
6	C	T	T	A	G	T	T	C	A	A	C	C	C	A	T	G	T	G	C	G	G	C	A	H8	WAF
7	C	T	T	A	G	T	T	C	A	A	C	C	C	A	T	G	T	G	C	G	G	T	G	H9	WAF
8	C	T	T	A	G	T	T	C	A	A	C	C	C	A	T	G	T	G	C	G	G	T	G	H9	WAF
9	C/T	T	T	A	G	T	T	C	A	A	C	C	C	A	T	G	T	G	C	G	G	T	A/G	?	?
10	C	T	T	A	G	T	T	C	A	A	C	C	C	A	T	G	T	G	C	G	G	T	G	H9	WAF
11	C	T	T	A	G	T	T	C	A	A	C	C	C	A	T	G	T	G	C	G	G	T	G	H9	WAF
12	C	T	T	A	G	T	T	C	A	A	C	C	C	A	T	G	T	G	C	A	G	T	G	H12	EAF
13	C	T	T	A	G	T	T	C	A	A	C	C	C	A	T	G	T	G	C	G	G	C	A	H8	WAF
14	C	T	T	A	G	T	T	C	A	A	C	C	C	A	T	G	T	G	C	G	A	T	G	H7	WAF
15	C	T	T	A	G	T	T	C	A	A	C	C	C	A	T	G	T	G	C	G	G	T	G	H9	WAF
16	C	T	T	A	G	T	T	C	A	A	C	C	C	A	T	G	T	G	C	G	G	T	G	H9	WAF
17	C	T	T	A	G	T	T	C	A	A	C	C	C	A	T	G	T	G	C	G	G	T	G	H9	WAF
18	C	T	T	A	G	T	T	C	A	A	C	C	C	A	T	G	T	G	C	G	G	T	G	H9	WAF
19	C	T	T	A	G	T	T	C	A	A	C	C	T	A	T	G	T	G	C	G	G	T	G	H13	EAF
20	C	T	T	A	G	T	T	C	A	A	C	C	C	A	T	G	T	G	C	G	G	T	G	H9	WAF
21	C	T	T	A	G	T	T	C	A	A	C	C	C	A	T	G	T	G	C	G	G	T	G	H9	WAF
22	C	T	T	A	G	T	T	C	A	A	C	C	C	A	T	G	T	G	C	G	G	T	G	H9	WAF
23	C	T	T	A	G	T	T	C	A	A	C	C	C	A	T	G	T	G	C	G	G	T	G	H9	WAF
24	C	T	T	A	G	T	T	C	A	A	C	C	C	A	T	G	T	G	C	G	G	T	G	H9	WAF
25	C	T	T	A	G	T	T	C	A	A	C	C	C	A	T	G	T	G	C	G	G	T	G	H9	WAF
26	C	T	T	A	G	T	T	C	A	A	C	C	C	A	T	G	T	G	C	G	G	T	G	H9	WAF
27	C	T	T	A	G	T	T	C	A	A	C	C	C	A	T	G	T	G	C	G	G	T	G	H9	WAF
28	C	T	T	A	G	T	T	C	A	A	C	C	C	A	T	G	T	G	C	G	G	T	G	H9	WAF
29	C	T	T	A	G	T	T	C	A	A	C	C	C	A	T	G	T	G	C	G	G	T	G	H9	WAF
30	C	T	T	A	G	T	T	C	A	A	C	C	C	A	T	G	T	G	C	G	G	T	G	H9	WAF
31	C	T	T	A	G	T	T	C	A	A	C	C	C	A	T	G	T	G	C	G	G	T	G	H9	WAF

FIGURE 4 | Geographically informative barcode of *Plasmodium falciparum* mitochondrion and apicoplast genome single-nucleotide polymorphism (SNPs). The sample sequence results from the 23-SNP loci were compared to the geographically informative haplotype barcodes previously defined (7). WAF, West Africa; EAF, East Africa. Sample information: 18: Guinea, 19: Republic of Congo, 20: Sierra Leone; others originated from Equatorial Guinea. CWX and 1–20 samples marked with color were isolates with *PfK13* mutation. *Haplotypes are based on the reference (7).

(GenBank X95275.2, X95276.2) (9) until version 3.1 of the *P. falciparum* genome including a complete *apico* genome was uploaded (16, 17). We checked the database carefully and found X95276 (1–14,009 bp) combined with the reverse sequence of X95275 (14,010–29,430 bp) was well-confirmed with the loci selected in the design. Our sorted data supplied good reference for the later relative study.

In the present study, parasites were screened from origins that are not yet included in the network (WAF: Burkina Faso, Gambia, Ghana, and Mali; EAF: Kenya, Malawi, and Uganda) (7). Most of the malaria imported cases in this study were acquired in the central–western part of sub-Saharan Africa (Equatorial Guinea and Republic of Congo), and two isolates from West Africa were selected as control (Guinean and Sierra Leonean). Based on 23-SNP barcode analysis, West African isolates as well as the 25 isolates from Equatorial Guinea were confirmed to have the same haplotypes as those originating in West Africa. Surprisingly, the geographic origins of three isolates from Equatorial Guinea and one isolate from the Republic of Congo were East Africa. In addition, one isolate from Equatorial Guinea showed mixed haplotypes, indicating either heteroplasmy or multiclonal infections, in which it was difficult to infer the geographical origin for the parasites with multiple *mt* and *apico* genomes. The confused results consisted of the prediction that the 23-SNP barcode may lack the genetic resolution to distinguish between ongoing autochthonous transmission and malaria infections imported from one or more nearby locations (7). However, they are better suited to tracing the origin and dispersal of parasite strains across and between continents. With limited samples, this study still could provide the sequence data

from Central Africa and fill data gaps in sample origins that are not yet included in the network.

Previous studies revealed the highly conserved structure of *mt* and *apico* in the genus *Plasmodium* (18, 19). The ratio of NS/S substitutions, which can be used to gauge the intensity and directionality of natural selection, are generally quite low for both organelle genomes, indicative of the strong purifying selection on NS sites, but see Preston et al. (7) and Wicke et al. (20) for exceptions to this trend (21). In this study, NS/S ratios were quite low for *mt*; this points to the highly conserved structure of *mt* in *P. falciparum*. In addition, *apico* genes had a higher NS/S ratio than *mt*, corresponding to the previously published study by Preston et al. (7). Pressure from antimalarial drugs may account for the high NS/S ratio of the *apico* SNPs. As translationally active organelles, *Plasmodium mt* and *apico* have been validated as important drug targets.

The *apico* genome encodes ∼30 proteins, and most are ribosome subunits. Apicoplast has been identified in interactions with the delayed death phenotype caused by antibiotics, which may inhibit the *apico* housekeeping functions (22). Ribosomes of the *Plasmodium apico* and *mt* have been validated as targets for antibiotic action (23). It has also been reported that the artemisinin-exposed persistent forms restructured the mitochondrial–nuclear associations in *P. falciparum* (24). In contrast, rapid killing of malaria parasites by artemisinin is thought to result from depolarization of the mitochondrial membrane (25). The *Plasmodium mt* genome encodes only three protein-coding genes; however, each parasite has multiple genomes in *mt*, which may allow suboptimal mutant genes to preadapt to drug resistance even without strong drug-selective pressure. Studies into the mutant genes of *mt* and *apico* with drug pressure are rare; conclusive evidence is still lacking. In this study, the selected 32 isolates were from Chinese travelers who had returned from African countries. CWX has been reported as an artemisinin-resistant strain (3), and the 1–20 isolates have been confirmed to have the *Pfkelch13* mutant genotype. The other 11 isolates (21-31) showed *Pfkelch13* wild-type in another study. However, for the limited number of Kelch13 mutant samples, drug assays were not included and also out of the focus of the study. Multiple surveys of populations subjected to drug pressure are necessary to confirm the haplotypes and drug pressure.

In conclusion, this study provides a practical and highly valuable method to trace back to the geographic origins of *P. falciparum* malaria based on PCR and sequencing using the 23-SNP barcode from *mt*/*apico*. As population mobility has increased, the risk of reintroducing parasites to elimination areas and dispersing drug-resistant parasites to new regions has also increased, malaria control programs should be prepared to respond to this.

DATA AVAILABILITY STATEMENT

The raw data supporting the conclusions of this article will be made available by the authors, without undue reservation, to any qualified researcher.

ETHICS STATEMENT

The studies involving human participants were reviewed and approved by The Institutional Review Board of Jiangsu Institute of Parasitic Diseases. The patients/participants provided their written informed consent to participate in this study. Written informed consent was obtained from the individual(s) for the publication of any potentially identifiable images or data included in this article.

AUTHOR CONTRIBUTIONS

FH and QZ performed the experiments and wrote the manuscript. GZ, HZ, and MZ helped with the sample collection and conformation. YLi and FT designed the experiments and analyzed the data. FL and YLiu conceived the experiments, provided advice on data interpretation, and edited the paper. All authors contributed to the article and approved the submitted version.

FUNDING

This work was supported by the National Key R&D Program of China (2020YFC1200105), the National Natural Science Foundation of China (82072297 and 81601790), the Six Talent Peaks Project in Jiangsu Province (2019-YY-065), and the high level talent support project of Yangzhou University.

SUPPLEMENTARY MATERIAL

The Supplementary Material for this article can be found online at: https://www.frontiersin.org/articles/10.3389/fpubh.2021.649170/full#supplementary-material

REFERENCES

1. World Health Organazation. *World Malaria Report 2019* (2019). Available online at: https://www.who.int/publications/i/item/9789241565721 (accessed December 4, 2019).
2. Fairhurst RM, Dondorp AM. Artemisinin-resistant *Plasmodium falciparum* malaria. *Microbiol Spectrum.* (2016) 4:EI10-0013-2016. doi: 10.1128/9781555819453.ch22
3. Lu F, Culleton R, Zhang M, Ramaprasad A, von Seidlein L, Zhou H, et al. Emergence of indigenous artemisinin-resistant Plasmodium falciparum in Africa. *N Engl J Med.* (2017) 376:991–3. doi: 10.1056/NEJMc1612765
4. Ménard D, Khim N, Beghain J, Adegnika AA, Shafiul-Alam M, Amodu O, et al. A worldwide map of *Plasmodium falciparum* K13-propeller polymorphisms. *N Engl J Med.* (2016) 374:2453–64. doi: 10.1056/NEJMoa1513137
5. Manske M, Miotto O, Campino S, Auburn S, Almagro-Garcia J, Maslen G, et al. Analysis of *Plasmodium falciparum* diversity in natural infections by deep sequencing. *Nature.* (2012) 487:375–9. doi: 10.1038/nature11174

6. Rachel D, Volkman SK, Danny DA, Mahesh N, Neafsey DE, Park DJ, et al. A general SNP-based molecular barcode for Plasmodium falciparum identification and tracking. *Malaria J.* (2008) 7:223. doi: 10.1186/1475-2875-7-223
7. Preston MD, Campino S, Assefa SA, Echeverry DF, Ocholla H, Amambua-Ngwa A, et al. A barcode of organellar genome polymorphisms identifies the geographic origin of *Plasmodium falciparum* strains. *Nat Commun.* (2014) 5:4052. doi: 10.1038/ncomms5052
8. Lai S, Sun J, Ruktanonchai NW, Zhou S, Yu J, Routledge I, et al. Changing epidemiology andchallenges of malaria in China towards elimination. *Malar J.* (2019) 18:107. doi: 10.1186/s12936-019-2736-8
9. Wilson RJ, Denny PW, Preiser PR, Rangachari K, Roberts K, Roy A, et al. Complete gene map of the plastid-like DNA of the malaria parasite *Plasmodium falciparum*. *J MolBiol.* (1996) 261:155–72. doi: 10.1006/jmbi.1996.0449
10. Tulloch J, David B, Newman R, Meek SJL. Artemisinin-resistant malaria in the Asia-Pacific region. *Lancet.* (2013) 381:e16–7. doi: 10.1016/S0140-6736(12)61820-0
11. Nag, S. MD, Dalgaard PE, Kofoed J, Ursing M, Crespo, Andersen LO, et al. High throughput resistance profiling of *Plasmodium falciparum* infections based on custom dual indexing and Illumina next generation sequencing-technology. *Sci Rep.* (2017) 7:2398. doi: 10.1038/s41598-017-02724-x
12. Taylor SM, Parobek CM, DeConti DK, Kayentao K, Coulibaly SO, Greenwood BM, et al. Absence of putative artemisinin resistance mutations among *Plasmodium falciparum* in Sub-Saharan Africa: a molecular epidemiologic study. *JID.* (2015) 211:680–8. doi: 10.1093/infdis/jiu467
13. Baniecki ML, Faust AL, Schaffner SF, Park DJ, Galinsky K, Daniels RF, et al. Development of a Single Nucleotide Polymorphism Barcode to Genotype Plasmodium vivax Infections. *PLoS Negl Trop Dis.* (2015) 9:e0003539. doi: 10.1371/journal.pntd.0003539
14. Haanshuus CG, Mohn SC, Mørch K, Langeland N, Blomberg B, Hanevik K, et al. A novel, single-amplification PCR targeting mitochondrial genome highly sensitive and specific in diagnosing malaria among returned travellers in Bergen, Norway. *Malar J.* (2013) 12:26. doi: 10.1186/1475-2875-12-26
15. Oriero CE, van Geertruyden JP, Jacobs J, D'Alessandro U, Nwakanma D. Validation of an apicoplast genome target for the detection of *Plasmodium species* using polymerase chain reaction and loop mediated isothermal amplification. *Clin Microbiol Infect.* (2015) 21:686.e1–7. doi: 10.1016/j.cmi.2015.02.025
16. Hunt M, Silva ND, Otto TD, Parkhill J, Keane JA, Harris SR, et al. Circlator: automated circularization of genome assemblies using long sequencing reads. *Genome Biol.* (2015) 16:294. doi: 10.1186/s13059-015-0849-0
17. Böhme U, Otto TD, Sanders M, Newbold CI, Berriman M, Llinas M, et al. Progression of the canonical reference malaria parasite genome from 2002-2019. *Wellcome Open Res.* (2019) 4:58. doi: 10.12688/wellcomeopenres.15194.1
18. Hikosaka K, Watanabe Y, Kobayashi F, Waki S, Kita K, Tanabe K. Highly conserved gene arrangement of the mitochondrial genomes of 23 Plasmodium species. *Parasitol Int.* (2011) 60:175–80. doi: 10.1016/j.parint.2011.02.001
19. Nobuko A, Tetsuo H, Hideya M, Palacpac NMQ, Akira K, Kawai S, et al. The Plasmodium apicoplast genome: conserved structure and close relationship of P. ovale to rodent malaria parasites. *Mol Biol Evol Lett.* (2012) 29:2095–9. doi: 10.1093/molbev/mss082
20. Wicke S, Schäferhoff B, dePamphilis CW, Müller KF. Disproportional plastome-wide increase of substitution rates and relaxed purifying selection in genes of carnivorous Lentibulariaceae. *Mol Biol Evol.* (2014) 31:529–45. doi: 10.1093/molbev/mst261
21. Smith DR. Mutation rates in plastid genomes: they are lower than you might think. *Genome Biol.* (2015) 7:1227–34. doi: 10.1093/gbe/evv069
22. Yeh E, DeRisi JL. Chemical rescue of malaria parasites lacking an apicoplast defines organelle function in blood-stage *Plasmodium falciparum*. *PLoS Biol.* (2011) 9:e1001138. doi: 10.1371/journal.pbio.1001138
23. Gupta A, Shah P, Haider A, Gupta K, Siddiqi MI, Ralph SA, et al. Reduced ribosomes of the apicoplast and mitochondrion of *Plasmodium* spp. and predicted interactions with antibiotics. *Open Biol.* (2014) 45:140045. doi: 10.1098/rsob.140045
24. Connelly SV, Manzella-Lapeira J, Levine ZC, Brzostowski J, Krymskaya L, Rahman RS, et al. Restructured mitochondrial-nuclear interaction in *P. falciparum* dormancy and persister survival of artemisinin exposure. *bioRxiv [Preprint].* (2020). doi: 10.1101/2020.09.28.314435
25. Antoine T, Fisher N, Amewu R, O'Neill PM, Ward SA, Biagini GA, et al. Rapid kill of malaria parasites by artemisinin and semi-synthetic endoperoxides involves ROS-dependent depolarization of the membrane potential. *J Antimicrob Chemother.* (2014) 694:1005–16. doi: 10.1093/jac/dkt486

Conflict of Interest: The authors declare that the research was conducted in the absence of any commercial or financial relationships that could be construed as a potential conflict of interest.

frontiers in Cellular and Infection Microbiology

ORIGINAL RESEARCH
published: 21 April 2021
doi: 10.3389/fcimb.2021.631508

Fast Expansion of the Asian-Pacific Genotype of the Chikungunya Virus in Indonesia

Yusnita Mirna Anggraeni[1*†], *Triwibowo Ambar Garjito*[1,2*†], *Mega Tyas Prihatin*[1], *Sri Wahyuni Handayani*[1], *Kusumaningtyas Sekar Negari*[1], *Ary Oktsari Yanti*[1], *Muhammad Choirul Hidajat*[1], *Dhian Prastowo*[1], *Tri Baskoro Tunggul Satoto*[3], *Sylvie Manguin*[2], *Laurent Gavotte*[4] *and Roger Frutos*[5]

[1] Institute for Vector and Reservoir Control Research and Development, National Institute of Health Research and Development, the Ministry of Health of Indonesia, Salatiga, Indonesia, [2] HSM, University of Montpellier, CNRS, IRD, Montpellier, France, [3] Department of Parasitology, Faculty of Medicine, Public Health and Nursing, Gadjah Mada University, Yogyakarta, Indonesia, [4] Espace-DEV, University of Montpellier, Montpellier, France, [5] Cirad, UMR 17, Intertryp, Montpellier, France

OPEN ACCESS

Edited by:
Xiaoxiao Wang,
Zhejiang Center for Disease Control and Prevention (Zhejiang CDC), China

Reviewed by:
Barry Alto,
University of Florida, United States
Padet Siriyasatien,
Chulalongkorn University, Thailand

***Correspondence:**
Yusnita Mirna Anggraeni
yusnita.ma@litbang.kemkes.go.id
Triwibowo Ambar Garjito
triwibowo@litbang.kemkes.go.id

[†]These authors have contributed equally to this work

Specialty section:
This article was submitted to Virus and Host, a section of the journal Frontiers in Cellular and Infection Microbiology

Received: 20 November 2020
Accepted: 22 March 2021
Published: 21 April 2021

Citation:
Anggraeni YM, Garjito TA, Prihatin MT, Handayani SW, Negari KS, Yanti AO, Hidajat MC, Prastowo D, Satoto TBT, Manguin S, Gavotte L and Frutos R (2021) Fast Expansion of the Asian-Pacific Genotype of the Chikungunya Virus in Indonesia. Front. Cell. Infect. Microbiol. 11:631508. doi: 10.3389/fcimb.2021.631508

Chikungunya is repeatedly affecting Indonesia through successive outbreaks. The Asian genotype has been present in Asia since the late 1950s while the ECSA-IOL (East/Central/South Africa - Indian Ocean Lineage) genotype invaded Asia in 2005. In order to determine the extension of the circulation of the chikungunya virus (CHIKV) in Indonesia, mosquitoes were collected in 28 different sites from 12 Indonesian provinces in 2016-2017. The E1 subunit of the CHIKV envelope gene was sequenced while mosquitoes were genotyped using the mitochondrial *cox*1 (cytochrome C oxidase subunit 1) gene to determine whether a specific population was involved in the vectoring of CHIKV. A total of 37 CHIKV samples were found in 28 *Aedes aegypti*, 8 *Aedes albopictus* and 1 *Aedes butleri* out of 15,362 samples collected and tested. These viruses, like all Indonesian CHIKV since 2000, belonged to a genotype we propose to call the Asian-Pacific genotype. It also comprises the Yap isolates and viruses having emerged in Polynesia, the Caribbean and South America. They differ from the CHIKV of the Asian genotype found earlier in Indonesia indicating a replacement. These results raise the question of the mechanisms behind this fast and massive replacement.

Keywords: chikungunya, *Aedes aegypti*, *Aedes albopictus*, genotyping, Indonesia

INTRODUCTION

The chikungunya virus (CHIKV) is an arbovirus, member of the genus *Alphavirus* in the family *Togaviridae*. CHIKV is a positive-strand RNA virus, 60-70 nm in diameter, spherical, and enveloped. The genome length is ca.12 kb, capped in 5', with a polyA tail in the 3' end. The genome has two open reading frames encoding two polyproteins: a non-structural polyprotein and a structural polyprotein. The polyproteins can be cleaved by proteases into four non-structural proteins: nsP1, nsP2, nsP3, nsP4; and five structural proteins (C, E3, E2, 6K, E1) (Higashi et al., 1967; Simizu et al., 1984; Powers et al., 2001; Khan et al., 2002). CHIKV was isolated for the first time in the Mokande plateau between Tanzania and Mozambique, in the Eastern part of the current

Democratic Republic of Congo in 1958 (Osterrieth and Blanes-Ridaura, 1960; Osterrieth et al., 1961). Since then, chikungunya outbreaks were documented in South Africa, and Zimbabwe in 1956-1977; the Democratic Republic of Congo, Zambia, Senegal, Uganda, Nigeria, Angola and Republic of Central Africa in 1958-2000; and Equatorial Guinea in 2002 (Jupp and McIntosh, 1988; Powers and Logue, 2007; Desdouits et al., 2015; Zeller et al., 2016). CHIKV was introduced in Asia at two different times. The first expansion in Asia corresponded to the initial divergence of the Asian genotype from the ECSA (East/Central/South African) genotype, itself having diverged from the West African genotype (Hammon et al., 1960; Powers et al., 2000; Caglioti et al., 2013; Lo Presti et al., 2014). Chikungunya was for the first time reported in Asia, specifically in Thailand, in 1958 and early 1960 (Hammon et al., 1960; Weaver and Lecuit, 2015). The second Asian expansion corresponded to the emergence of the ECSA A226V mutant, also known as the Indian Ocean Lineage or IOL, which evolved from the ECSA genotype in Kenya in 2004 (Tsetsarkin et al., 2011; Coffey et al., 2014).

This re-emerging CHIKV, which displayed a higher affinity for *Aedes albopictus* and more precisely changes in the extrinsic incubation period (Tsetsarkin et al., 2007; Tsetsarkin and Weaver, 2011), became even more transmissible and virulent after additional mutations in Kerala, India (Tsetsarkin and Weaver, 2011; Agarwal et al., 2016). It spread eastward to cover continental Southeast Asia (Sam et al., 2009; Rianthavorn et al., 2010; Tsetsarkin et al., 2011; Duong et al., 2012). Currently, the ECSA-IOL genotype, circulates in many Asian countries (Sam et al., 2012; Chen et al., 2016; Sam, 2018).

In order to map the presence of vector-borne diseases and potential vectors in Indonesia, the Ministry of Health launched a large program of screening throughout the country. Part of the program was to identify which chikungunya virus was circulating in Indonesia, ECSA-IOL or Asian, or both, and where, and to genotype the vectors most likely involved in this circulation. We report in this article the results of this screening and the characterization of a genotype present all over Indonesia, which we propose to name the Asian-Pacific genotype.

MATERIALS AND METHODS

Sampling Sites

In 2016-2017, larvae suspected to be *Ae. aegypti* and *Ae. albopictus* mosquitoes were collected from the field as previously described (IVRCRD, 2016) in 28 locations in 12 different Indonesian provinces: Riau, Riau Islands, Banten, Yogyakarta, Central Kalimantan, East Kalimantan, South Sulawesi, Southeast Sulawesi, Central Sulawesi, Maluku, North Maluku, Southeast Maluku, and West Papua (**Supplementary Tables 1**, **2**, **Supplementary Figure 1**). In this work only the samples used for CHIKV detection were considered. Three additional virus samples from human patients were obtained from the National Chikungunya Survey Program after a chikungunya outbreak in Magelang, province of Jateng (Central Java) in 2014 (**Table 1**). This sampling program was part of a larger initiative from the Ministry of Health to map viruses and vectors in Indonesia. The same standardized sampling methods were thus used for collecting mosquitoes for each objective, i.e. each individual virus (IVRCRD, 2016).

Mosquito Collection

Collected larvae of *Ae. aegypti* and *Ae. albopictus* were reared individually until emergence of adults and then identified using standard taxonomic keys for *Stegomyia* (Rueda, 2004). Adults of *Aedes butleri* were collected by morning resting. Samples were segregated according to locality and date. Adult mosquitoes were stored individually in 1.5 ml microtubes with RNALater and stored at -80°C. Aliquots (head and thorax) were pooled for up to 25 individuals in 1.5-ml microtubes containing 250 μl of RNALater (Ambion-Thermo Fisher Scientific, Waltham, USA) to facilitate virus screening and minimize the number of RT-PCR reactions and stored at -80°C until further analysis. The pooling was conducted as follows:

1. Mosquitoes were stored individually in RNAlater.
2. An aliquot sample of each mosquito (head and thorax) was taken and the rest of the mosquito was kept individually.
3. Aliquot samples were pooled by up to 25 based on location and species. Specimen from different species or different locations were not mixed in the same pool.
4. An RT-PCR detection was ran on the pools.
5. When a pool was positive for CHIKV, a second aliquot sample of each of the mosquitoes making this pool was taken but this time each sample was analyzed individually by RT-PCR for the presence of CHIKV.

Chikungunya Virus Detection

Chikungunya virus detection was carried out by one-step RT-PCR, selective for the E1 gene as previously described (Gopal, 2016). Excised head and thorax of each mosquito were homogenized in a sterile homogenizer and RNAs were extracted by the silica-based methods (RNA-easy minikit, Qiagen, Hilden, Germany). A single-step RT-PCR was performed using consensus primers (CHIK1: 5'-ACC GGC GTC TAC CCA TTC ATG T-3'; CHIK2: 5'GGG CGG GTA GTC CAT GTT GTA GA-3'). Master mix was prepared using Superscript III on step RT-PCR with platinum *Taq* DNA polymerase (Invitrogen, Life Technologies, Carlsbad, USA). The products were electrophoresed in alternate lanes in 2% agarose gels. Amplicons, 330-bp in size, were purified using Applied Biosystems ExoSAP-IT™ (Thermo Fisher Scientific, Vilnius, Lithuania). The detection was first conducted on each pool and, for the positive pools only, a second detection was done on each of the individual specimen present in these pools to identify those bearing the virus.

Mosquito Genotyping

In order to map the different genotypes of potential mosquito vectors, the sequencing of the *cox1* (cytochrome c oxidase subunit) mitochondrial gene was performed. The amplification of the *cox*1 gene was conducted using the primers CI-N-2087 (5'-AAT TTC GGT CAG TTA ATA ATA TAG-3') and TY-J-1460 (5'-TAC AAT TTA TCG CCT AAA CTT CAG CC-3') as previously

TABLE 1 | Description of the samples used for sequencing.

Virus		CHIKV-positive *Aedes*		Location	
Virus	**ChikV code**	**Species**	**Sample**	**District**	**Province**
ChikV	a023	***Aedes albopictus***	**14_Aal**	Muna	South east Sulawesi
ChikV	a027	***Aedes aegypti***	**15_Aae**	Muna	South east Sulawesi
ChikV	a30	***Aedes aegypti***	**16_Aae**	Muna	South east Sulawesi
ChikV	a044	***Aedes aegypti***	**17_Aae**	Muna	South east Sulawesi
ChikV	10	***Aedes aegypti***	**9-18_Aae**	Fak-Fak	West Papua
ChikV	12	***Aedes butleri***	**012_Abt**	Bengkalis	Riau
ChikV	85	***Aedes aegypti***	**8_Aae**	South east Maluku	Maluku
ChikV	a070	***Aedes aegypti***	**6_Aae**	South east Maluku	Maluku
ChikV	a150	***Aedes albopictus***	**5_Aal**	South east Maluku	Maluku
ChikV	b084	***Aedes aegypti***	**3_Aae**	South east Maluku	Maluku
ChikV	a20	***Aedes aegypti***	**37_Aae**	South east Maluku	Maluku
ChikV	a024	***Aedes aegypti***	**15-18_Aae**	South Halmahera	North Maluku
ChikV	a050	***Aedes aegypti***	**13-11_Aae**	South Halmahera	North Maluku
ChikV	a072	***Aedes aegypti***	**19_Aae**	South Halmahera	North Maluku
ChikV	a085	***Aedes albopictus***	**22-30_Aal**	South Halmahera	North Maluku
ChikV	a71	***Aedes aegypti***	**2_Aae**	Lebak	Banten
ChikV	a078	***Aedes aegypti***	**ktg_H05_Aae**	Pulang Pisau	Central Kalimantan
NA	NA	***Aedes aegypti***	**10_Aae**	Bantul	Yogyakarta
		CHIKV-negative *Aedes*		**Location**	
		Species	**Sample**	**District**	**Province**
		Ae.aegypti	**pl1_Aae**	Palu	Central Sulawesi
		Ae.aegypti	**pl26_Aae**	Palu	Central Sulawesi
		Ae.albopictus	**sls11_Aal**	Maros	South Sulawesi
		Ae.albopictus	**sls16_Aal**	Maros	South Sulawesi
		Ae.aegypti	**19_18_1_Aae**	Fak-Fak	West Papua
		Ae.aegypti	**tb131_Aae**	Batam	Riau islands
		Ae.aegypti	**mlk38_Aae**	Ambon	Maluku
		Ae.aegypti	**mlk40_Aae**	Ambon	Maluku
		Ae.aegypti	**mlk73_Aae**	Ambon	Maluku
		Ae.aegypti	**mlk654_Aae**	Ambon	Maluku
		Ae.aegypti	**mlk48_Aae**	Ambon	Maluku
		Ae. aegypti	**15-18_1_Aae**	South Halmahera	North Maluku
		Ae. aegypti	**13_11_1_Aae**	South Halmahera	North Maluku
		Ae. aegypti	**19_1_Aae**	South Halmahera	North Maluku
		Ae. albopictus	**ktg28_Aal**	Pulang Pisau	Central Kalimantan
		Ae. aegypti	**11_Aae**	Serang	Banten
		Ae.aegypti	**blp3_Aae**	Balikpapan	East Kalimantan
		Ae.aegypti	**jgj5_Aae**	Bantul	Yogyakarta

described (Rueanghiran et al., 2011). PCR reactions were carried out using the GoTaq® Green Master Mix (Promega, Madison, WI, USA). The conditions for PCR amplification of the *cox*1 gene were as follows: 1 cycle at 94°C for 1 min for initial denaturation, followed by five cycles of 94°C for 30 s, 45°C for 40 s and 72°C for 1 min. This was then followed by 35 cycles of 94°C for 30 s, 44°C for 40 s and 72°C for 1 min, and by a final extension step at 72°C for 10 min (Rueanghiran et al., 2011). The products were electrophoresed in alternate lanes in 2% agarose gels. Amplicons, 650-bp in size, were purified using Applied Biosystems ExoSAP-IT™ (Thermo Fisher Scientific, Vilnius, Lithuania).

DNA Sequencing

Cycle sequencing was performed using the primers listed above and an Applied Biosystems BigDye™ Terminator v.3.1 Cycle Sequencing Kit (Life Technologies Cooperation, Austin, TX, USA). To remove unincorporated BigDye® terminators and salts, cycle sequencing products were purified using a BigDye® Xterminator Purification Kit (Life technologies, Bedford, MA, USA). Sequence data were obtained using a DNA sequencer (Applied Biosystems® 3500 Genetic Analyzer) and analyzed using the Sequencing Analysis 6 program (Applied Biosystems). All sequences have been deposited in Genbank under the accession numbers MW265951 to MW265970, MW270068 to MW270085 and MW270131 to MW270147.

Phylogenetic Analyses

Sequences were aligned using MUSCLE in the SeaView package (Gouy et al., 2010). Multiple alignments and phylogenetic analyses were performed using the SeaView package (Gouy et al., 2010). The *Aedes cox*1 gene tree was built using the maximum likelihood method under the GTR+G model with 1,000 bootstrap repeats. The CHIKV E1 gene tree was built using the maximum likelihood method under the GTR model with 1,000 bootstrap repeats. Proteins trees were built using the maximum likelihood method under the LG model with 500 bootstrap repeats.

Polymorphism Analyses

Polymorphism was analyzed using DNASp 6.12.03 (Rozas et al., 2017). The parameters considered were N: Number of samples, h: Number of haplotypes, S: Number of polymorphic sites, η: (Eta) Number of mutations, π: (Pi) Polymorphism at the nucleotide level, θ: (Theta) Watterson estimator of polymorphism (from Eta), ηs: Number of singletons, ηp: Number of parsimony significant sites, Ka/Ks ratio, Tajima's D statistics, Fu and Li D* statistics and Fu and Li F* statistics. The haplotype relationship was computed and constructed as a distance map based on median-joining network using PopART version 1.7 (http://popart.otago.ac.nz/) (Bandelt et al., 1999; Clement et al., 2002; French et al., 2014).

RESULTS

Mosquito Sampling and Chikungunya Virus Detection

Mosquito collections were conducted in 28 different locations in 12 provinces and a total of 15,362 mosquitoes, 11,776 *Ae. aegypti*, 3,421 *Ae. albopictus* and 165 *Ae. butleri* were collected (**Supplementary Table 1**). Other *Aedes* species were found, i.e. *Aedes lineatopennis, Aedes parasimilis, Aedes vexans, Aedes* sp. (*Verallina* sp.), *Aedes amesti, Aedes andamanensis, Aedes aurantius, Aedes poicilius, Aedes flavipennis, Aedes quadrifolium,* and *Aedes longirostris*. However, with the exception of one *Ae. butleri* individual from Bengkalis in the province of Riau, all were negative for CHIKV (**Supplementary Table 1**). *Aedes aegypti* was more frequent than *Ae. albopictus* in 17 locations, whereas *Ae. albopictus* was more frequent in 6 sampling sites (**Supplementary Table 1**). Only one place, Kulon Progo in Yogyakarta province, did not yield any *Ae. aegypti* sample and only one place, Bombana in Southeast Sulawesi, did not yield any *Ae. albopictus* sample (**Supplementary Table 1**). Mosquitoes were pooled by species and location for up to 25 individuals. A total of 1,190 pools tested for CHIKV, 800 pools (11,776 mosquitoes) for *Ae. aegypti*, 354 pools (3,421 mosquitoes) for *Ae. albopictus* and 36 pools (165 mosquitoes) of *Ae. butleri*. CHIKV was found in 25 *Ae. aegypti*, 8 *Ae. albopictus* and 1 *Ae. butleri* pools. Out of 33 pools of *Ae. aegypti* from Pulang Pisau (Central Kalimentan) only one was CHIKV-positive, but 4 out of the 25 mosquitoes making this pool were CHIKV-positive. All other CHIKV-positive pools contained only one CHIKV-infected mosquito (**Supplementary Table 1**). A total of 37 mosquitoes from these positive pools were found infected with CHIKV, including 28 *Ae. aegypti*, 8 *Ae. albopictus*, and 1 *Ae. butleri* (**Supplementary Table 1**). The infection rate (IR) was 0.24%, 0.23% and 0.6% for *Ae. aegypti*, *Ae. albopictus*, and *Ae. butleri*, respectively. However, owing to the limited number of specimens obtained for *Ae. butleri* and the difference in collection method, the IR for this species must be considered with caution.

cox1 Phylogeny of *Aedes aegypti* and *Aedes albopictus* Mosquitoes

The *cox*1 genes of 29 *Ae. aegypti* samples (14 CHIKV-positive and 15 CHIKV-negative) and of 6 *Ae. albopictus* mosquitoes (3 CHIKV-positive and 3 CHIKV-negative) were sequenced (**Table 1**). No correlation was found for *Ae. aegypti* between the cox1 haplotype and the presence of CHIKV. The *cox*1 phylogenetic tree of *Ae. aegypti* mosquitoes showed a monophyletic topology with limited structuration (**Supplementary Figure 2**). The CHIKV-positive sample ktg_H05_Aae from Pulang Pisau in Central Kalimantan branched separately with a bootstrap of 70. The samples mlk48_Aae and mlk654 from Maluku clustered separately with a bootstrap of 57. Finally, a group comprising the CHIKV-negative samples mlk73_Aae, 11_Aae and the CHIKV-positive mosquitoes 3_Aae, 6_Aae, 10_Aae, 15_Aae, 37_Aae, 9-18_Aae and 13-11_Aae separated with a bootstrap value of 63 (**Supplementary Figure 2**). With the exception of 11_Aae from Banten (West Java), all other samples from this last group were from Eastern Indonesia, i.e. Southeast Sulawesi, Maluku and West Papua (**Table 1**). *Aedes albopictus* samples fell into two different clusters depending on whether they were CHIKV-positive or -negative with a rather high bootstrap value, i.e. 85 (**Supplementary Figure 2**). However, the number of samples is too low to draw any trend and reach any significant conclusion.

Envelope Gene (E1) Phylogeny of the Isolated Chikungunya Viruses

The 17 CHIKV samples from mosquitoes collected in 2016-2017 for this work were included in a phylogenetic analysis with the 3 human CHIKV samples from Magelang/Jateng collected in 2014, with all CHIKV sequences from Indonesia present in Genbank, and sequences from the Asian, ECSA and West African genotypes (**Supplementary Figure 3**, **Supplementary Table 2**). All samples from this work clustered into two related populations derived from the Asian genotype (**Supplementary Figure 3**). A first population, cluster 1, comprised the samples 9C, a023, a027, a044, a070, a072, a078, a085, b084, a30 and a71. The second population, cluster 2, comprised the samples 10, 12, 85, a20, a150, a024 and a050. These clusters were characterized by weak bootstraps indicating that they were not genetically distinct from each other (**Supplementary Figure 3**). They corresponded to different locations and mosquito species, including *Ae. butleri*, suggesting that they were not linked to specific geographical clusters or vector populations. The three viruses isolated from human patients in 2014 did not correspond to the exact same populations as the mosquito samples but were very close. The samples B14 and 8F from clinical cases in Magelang, Province of Jateng, Central Java, in 2014 were identical to human isolates from totally different provinces, such as Banten, Bali and Jambi collected 2011, 2014 and 2015, respectively (**Supplementary Figure 3**, **Table 1**, **Supplementary Table 2**). The sample C7 from Magelang, Province of Jateng, Central Java, obtained in 2014 was related, but still different, to human samples from the Eastern tip of Java (East Java) in 2011 and to the cluster 2 of mosquito samples from this work (**Supplementary Figure 3**, **Supplementary Table 2**). When compared to the Asian genotype reference sequences, the E1 gene sequences from this work, and almost all Indonesian CHIKV sequences from Genbank, grouped within a single population comprising also CHIKVs from Yap Island, French Polynesia, Caribbean islands and South America (**Supplementary Figure 3**, **Supplementary Table 2**). This population was genetically distinct from known Asian genotype reference sequences

(**Supplementary Figure 3**, **Supplementary Table 2**). Within the ECSA references, two 2011 Indonesian samples from West Kalimantan (KJ729851, KJ729852), one Indonesian sample from unknown exact location (KC862329) and five samples from Taiwan having been imported from Indonesia (KU561427, KU561428, KU561430, KU561431, KU561432) grouped with a CHIKV isolate of 2009 from Malaysia (HQ148971) and a 2011 isolate from Cambodia (JQ861254). They were all identical to the 2009 Malaysian sample suggesting the occurrence of imported cases (**Supplementary Figure 3**, **Supplementary Table 2**). The West African (HM045785) references (HM045785, MK028837, JQ943720) branched as expected in an ancestral position (**Supplementary Figure 3**, **Supplementary Table 2**). The sequences from this work as well as several reference sequences from Indonesia were truncated gene version and in particular did not cover the amino acid 226, which distinguishes ECSA from ECSA-IOL. Therefore, a full-length gene phylogenetic analysis was conducted with Indonesian samples and reference sequences from the ECSA, ECSA-IOL, Asian and West African (**Supplementary Figure 5**) present in Genbank. This full-length gene analysis confirmed what was seen with the truncated gene. The ancestral genotype is the West African genotype from which the ECSA genotype emerged (bootstrap = 98). The Asian genotype emerged from the ECSA genotype (bootstrap = 55) and gave rise to the Asian-Pacific genotype (bootstrap = 96). The ECSA-IOL genotype emerged independently from the ECSA genotype (bootstrap = 90). The haplotype mapping provided also a clear view of the evolution the different genotypes and the divergence of the Asian-Pacific genotype from the Asian one (**Supplementary Figure 5**). The analysis of polymorphism confirmed the existence of the Asian-Pacific as a population displaying a specific dynamic (**Table 2**). The Asian-Pacific genotype displayed a Pi value, which represents the polymorphism at the nucleotide level, clearly lower than that of the Asian genotype, even though the number of samples was far higher (98 vs. 7) (**Table 2**). The Tajima's D, Fu and Li's D* and Fu and Li's F* statistics of the Asian-Pacific genotype were -1.50497, -3.25593, -3.04089, respectively, indicating a selective sweep and a population in expansion. In particular, the Fu and Li's F* statistics displayed a value of -3.04089 significant at 0.02 which is indicative of a population in recent active expansion. The ECSA-IOL genotype displayed a similar trend, indicating also a population in expansion (**Table 2**). The full-length protein tree yielded the same topology as the gene phylogeny (**Supplementary Figure 6**). Four discriminating mutations, i.e. mutations linked to genotypes, were present (**Supplementary Figure 7**). The position 98 was characterized by an alanine (A) for the African genotypes, i.e. West African, ECSA and ECSA-IOL, and a threonine (T) for the Asian genotypes, i.e. Asian and Asian-Pacific. The position 145 was discriminative for the Asian-Pacific genotype, which was characterized by an alanine (A) whereas the Asian genotype displayed a serine (S) or a tyrosine (Y), and the ECSA and ECSA-IOL genotypes were characterized by a threonine (T). Interestingly, the Western African genotype displayed also an alanine (A) at this position. The position 225 was also discriminating the African genotypes characterized by an alanine (A) from the Asian genotypes, which displayed a serine (S). The position 226 is known for discriminating the ECSA and ECSA-IOL genotypes with an alanine (A) and a valine (V), respectively. The Asian genotypes, i.e. Asian and Asian-Pacific, displayed an alanine (A) at this position.

DISCUSSION

CHIKV has been introduced in Asia at two different times. The first occurrence corresponded in the late 1950s to the deployment of the ECSA genotype (East/Central/South Africa), which gave rise to the Asian genotype (Hammon et al., 1960). The second occurrence was also due to the ECSA genotype, which in 2004 yielded the A226V mutant, also known as the Indian Ocean Lineage or IOL, which invaded the Indian Ocean in 2005 before spreading to India, Thailand, Cambodia, Singapore and Malaysia (Sam et al., 2009; Hapuarachchi et al., 2010; Rianthavorn et al., 2010; Tsetsarkin et al., 2011; Duong et al., 2012). However, the dynamic of CHIKV was not clearly established in Indonesia, which has been exposed to several chikungunya outbreaks over the past decades (MoH Indonesia, 2007; Harapan et al., 2019). This work brings some clarification on this dynamic.

The first conclusion is that a replacement of the Asian genotype of CHIKV by the Asian-Pacific genotype occurred in Indonesia between 1985 and 2000. This replacement is visible in both mosquitoes (our work) and humans (references and our work). Unfortunately, there is no sequence available from the 1985-2000 period to narrow down the time of occurrence of the replacement and try to identify the causes. No chikungunya cases were reported in Indonesia between 1985 and 2000. Until 1985, all CHIKVs sequenced in Indonesia belonged to the Asian genotype. This Asian genotype was present in several Asian countries. However, after 2000 almost exclusively the Asian-Pacific genotype was present in Indonesia. It is found all over the country until now.

TABLE 2 | Polymorphism analysis of the chikungunya E1 sequences.

Genotype	N	h	S	η	π	θ	ηs	ηp	Ka/Ks	Tajima's D	Fu & Li's D*	Fu & Li's F*
ECSA	6	5	27	27	0.01719	0.01480	5	22	0.082	1.01925	1.11048	1.19180
ECSA-IOL	10	8	10	11	0.00292	0.00487	9	1	0.030	-1.79074*	-1.93522	-2.13705
Asian	7	6	25	25	0.01109	0.01277	16	9	0.070	-0.74824	-0.56450	-0.61115
Asian-Pacific	98	50	64	65	0.00845	0.01579	30	34	0.036	-1.50497	-3.25593*	-3.04089**

*Significant at 0.05.

**Significant at 0.02.

N, Number of samples; h, Number of haplotypes; S, Number of polymorphic sites; η, (Eta) Number of mutations; π, (Pi) Polymorphism at the nucleotide level; θ, (Theta) Watterson estimator of polymorphism (from Eta); ηs, Number of singletons; ηp, Number of parsimony significant sites.

Few ECSA-IOL samples were detected but no Asian genotype could be found in databases after 2000. The Asian-Pacific genotype expanded in the Caribbean, South America, and Polynesia in 2013-2014, starting a pandemic (Lanciotti and Valadere, 2014; Leparc-Goffart et al., 2014; Nhan et al., 2014; Aubry et al., 2015; Diaz-Quinonez et al., 2016; Lanciotti and Lambert, 2016; Freitas et al., 2018; Wimalasiri-Yapa et al., 2019). The Caribbean isolates were found to be closer to the Yap Island isolates (Lanciotti and Valadere, 2014). The CHIKV contamination in French Polynesia was traced back to the Caribbean (Nhan et al., 2014) indicating a worldwide human-borne mobility. These massive Caribbean, South American and Polynesian epidemics were caused by what was initially described as an Asian genotype (Lanciotti and Valadere, 2014; Nhan et al., 2014). However, it is not the Asian genotype present since the 1960s that was responsible, but instead the distinct genotype we characterized as the Asian-Pacific genotype. This genotype was already present in Indonesia, and perhaps in other Asian-Pacific countries, long before the 2013 Caribbean and Polynesian outbreaks. It is not clear where this genotype appeared at the first place, in Yap Island or Micronesia, in the Pacific area or in Asia. Interestingly, this Asian-Pacific genotype developed in Indonesia while at the same time other Asian countries, mostly continental, i.e. India, Thailand, Cambodia, Singapore and Malaysia, were invaded by the ECSA-IOL genotype (Sam et al., 2009; Hapuarachchi et al., 2010; Rianthavorn et al., 2010; Tsetsarkin et al., 2011; Duong et al., 2012; Fu et al., 2019; Intayot et al., 2019; Zakotnik et al., 2019; Chansaenroj et al., 2020; Pyke et al., 2020). The reason for this duality is not known but would be worth investigating. A systematic review conducted in 2019 on CHIKV infection in Indonesia showed that out 130 sequences available, 120 (92.3%) were of what the authors named the Asian genotype and 10 (7.7%) belonged to the ECSA-IOL genotype (Harapan et al., 2019). All ECSA-IOL viruses in Indonesia were closely related to other CHIKV outbreaks in Southeast Asia countries during the same period but did not last beyond 2011 (Harapan et al., 2019). This is in agreement with the data reported in this work that indicate that the ECSA-IOL lineage was imported in Indonesia in 2009 through introduction for other countries but was never able to establish. It was quickly outcompeted by the Asian-Pacific genotype. However the reason for this lack of establishment of the ECSA-IOL genotype is not known. It would be important for the management of this disease to identify the drivers leading for the expansion of ECSA-IOL in one part of Asia and of the Asian-Pacific genotype in the other part.

The invasive capacity of the Asian-Pacific genotype demonstrated in Indonesia, but also in the Caribbean, South America and Polynesia (Lanciotti and Valadere, 2014; Leparc-Goffart et al., 2014; Nhan et al., 2014; Aubry et al., 2015; Diaz-Quinonez et al., 2016; Lanciotti and Lambert, 2016; Freitas et al., 2018; Wimalasiri-Yapa et al., 2019) raises the question of its selective advantage. The homogeneity of the Asian-Pacific genotype and its characterization as a population in expansion following a selective sweep along with its almost exclusive presence in Indonesia, its fast expansion in other continents and the absence of the Asian genotype in Indonesia strongly suggest the existence of a selective advantage. The presence of a selected marker at position 145 is certainly an indication of this pressure. However, it is not possible to determine at this stage what this selective advantage is. A higher transmissibility is a likely hypothesis but further analyses are needed to formally establish what this selective advantage could be. The invasiveness of IOL was due to a higher affinity for *Ae. albopictus* and a wide transportation by this mosquito species through international trade (Benedict et al., 2007). IOL showed invasiveness in the Indian Ocean and in Continental South and Southeast Asia where it replaced the initial Asian genotype (Sam et al., 2009; Hapuarachchi et al., 2010; Rianthavorn et al., 2010; Tsetsarkin et al., 2011; Duong et al., 2012; Quyen et al., 2017). Conversely, the invasiveness of the Asian-Pacific genotype does not seem to be related to the mosquito species since it can be transmitted by *Ae. aegypti, Ae. albopictus, Ae. hensilli, Ae. polynesiensis* and, perhaps by *Ae. butleri*, making it at higher risk of global dispersion. However, the presence of CHIKV in *Ae. butleri*, which is not a recognized vector, is not a proof of a transmission. Further analyses, such as testing saliva samples (Hall-Mendelin et al., 2010) would help determining the actual status of *Ae. butleri* as a vector of CHIKV.

The diversity of vectors was also found to be very low in Indonesia. *Aedes aegypti* samples, whether CHIKV-positive or not, belonged to the same population. This suggests that in parallel to the uniformity of CHIKV in Indonesia, there might also be a uniformity of *Ae. aegypti* vectors with a single population occupying the country. However, the number of samples is not high enough to bring a definitive conclusion and a larger genotyping study must be conducted at the scale of the whole country to determine the structure of the *Ae. aegypti* populations. This dynamic of *Aedes* vectors is not only of importance for chikungunya but also for dengue, Zika fever and other arbovirus diseases transmitted by the same mosquito species. Another issue raised by this work is the confirmation of the vertical transmission of CHIKV in *Ae. aegypti* under natural conditions. This had already been reported in *Ae. aegypti* populations from Delhi and Haryana states in India (Jain et al., 2016). This work is therefore a confirmation of the occurrence of natural vertical transmission in *Ae. aegypti* and it is the first report of natural vertical transmission of CHIKV in *Ae. albopictus*. Natural vertical transmission in *Ae. albopictus* was suspected but not demonstrated (Grandadam et al., 2011; Bellini et al., 2012). Previous works have investigated the rate of vertical transmission in *Ae. aegypti* and *Ae. albopictus* under experimental conditions (Agarwal et al., 2014; Chompoosri et al., 2016; Honório et al., 2019) but it is not possible to compare these data with those reported in this work under natural conditions. However, since all *Ae. aegypti* and *Ae. albopictus* mosquitoes analyzed in this work were adults having emerged from collected larvae, the calculated IRs, i.e. 0.24% and 0.23% for *Ae. aegypti* and *Ae. albopictus*, respectively, also correspond to the observed vertical transmission rate. The natural vertical transmission of CHIKV is an important aspect to consider in the dynamic of chikungunya fever.

The Asian-Pacific genotype of CHIKV described in Indonesia raises the question of the mechanisms behind this fast and massive replacement. Further studies must be conducted on the impact of the observed mutations on the rate of transmissibility. Societal aspects, which could favor the expansion of the virus, should also be investigated. Indonesia being an archipelago with no permanent contact between populations from different islands, trade and people mobility must be analyzed. Although IOL invaded largely Continental South and Southeast Asia owing to intensive international trade and people mobility, it does not seem to have invaded Indonesia. Further studies are therefore needed to understand why, unlike what happened on the continent, it is the Asian-Pacific genotype that expanded and is now dominating in Indonesia. Beyond chikungunya, these investigations will be useful to understand the dynamic of other arbovirus diseases, such as dengue, which are among the most widely distributed and fast-spreading diseases worldwide.

DATA AVAILABILITY STATEMENT

The datasets presented in this study can be found in online repositories. The names of the repository/repositories and accession number(s) can be found below: https://www.ncbi.nlm.nih.gov/genbank/, MW265951 to MW265970, https://www.ncbi.nlm.nih.gov/genbank/, MW270068 to MW270085, https://www.ncbi.nlm.nih.gov/genbank/, MW270131 to MW270147.

ETHICS STATEMENT

The studies involving human participants were reviewed and approved by Health research ethics committee, national institute of health research and development (HREC-NIHRD), Ministry of Health of Republic of Indonesia. The patients/participants provided their written informed consent to participate in this study.

AUTHOR CONTRIBUTIONS

YA, TG, MH, MP, DP, SH, and TS conceived and designed the field studies. YA, TG, MH, MP, AY, KN, DP, and SH prepared samples. YA, MP, TG, and KN ran molecular analyses and laboratory experiments. TG, LG, and RF analyzed the data. TG and RF wrote the manuscript. SM and LG provided critics and significant revisions to the manuscript. All authors contributed to the article and approved the submitted version.

FUNDING

The research was supported by the Institute for Vector and Reservoir Control Research and Development (IVRCRD), National Institute of Health Research and Development (NIHRD), Ministry of Health of the Republic of Indonesia (MoH RI). LG, SM, and RF were supported by the Université de Montpellier, IRD, ISEM, and CIRAD, Montpellier, France and by the French-Indonesian PHC Nusantara projects Zika &Co and SOCIAL.

SUPPLEMENTARY MATERIAL

The Supplementary Material for this article can be found online at: https://www.frontiersin.org/articles/10.3389/fcimb.2021.631508/full#supplementary-material

Supplementary Figure 1 | Map of the sampling locations in Indonesia.

Supplementary Figure 2 | cox1 gene phylogeny of *Aedes aegypti* and *Aedes albopictus* mosquitoes. The tree was built using the maximum-likelihood (ML) method under the GTR+G model with 1,000 bootstrap repeats. Red: CHIKV-positive *Ae. albopictus* samples; Green: CHIKV-negative *Ae. albopictus* samples; Blue: CHIKV-positive *Ae. aegypti* samples; Purple: CHIKV-negative *Ae. aegypti* samples. The tree was rooted on the cox1 gene of *Culex quinquefasciatus* used as outgroup (beige).

Supplementary Figure 3 | Phylogenetic analysis of the partial E1 gene of chikungunya viruses. The tree was built using the maximum-likelihood (ML) method under the GTR model with 1,000 bootstrap repeats. The tree was rooted on the E1 gene of the O'nyong-nyong virus (HM045785) used as outgroup. Purple: West African genotype; Dark blue: ECSA genotype (ECSA + ECSA-IOL); Orange: Asian genotype; Dark green: Asian-Pacific genotype samples from this work; Light green: Reference Asian-Pacific sequences.

Supplementary Figure 4 | Phylogenetic analysis of the full-length E1 gene of chikungunya viruses. The tree was built using the maximum-likelihood (ML) method under the GTR model with 1,000 bootstrap repeats. The tree was rooted on the E1 gene of the O'nyong-nyong virus (HM045785) used as outgroup. Purple: West African genotype; Light blue: ECSA genotype; Dark blue: ECSA-IOL genotype; Orange: Asian genotype; Green: Asian-Pacific genotype.

Supplementary Figure 5 | Haplotype network of the full-length E1 gene. The haplotype relationship was computed and constructed as a distance map based on median-joining network using PopART version 1.7. Purple: West African genotype; Light blue: ECSA genotype; Dark blue: ECSA-IOL genotype; Orange: Asian genotype; Green: Asian-Pacific genotype.

Supplementary Figure 6 | Distribution tree of the full-length E1 protein sequence of chikungunya viruses. The tree was built using the maximum-likelihood (ML) method under the LG model with 500 bootstrap repeats. The tree was rooted on the E1 protein of the O'nyong-nyong virus (HM045785) used as outgroup. Purple: West African genotype; Light blue: ECSA genotype; Dark blue: ECSA-IOL genotype; Orange: Asian genotype; Green: Asian-Pacific genotype.

Supplementary Figure 7 | Alignment of the full-length E1 protein sequences of chikungunya viruses.

REFERENCES

Agarwal, A., Dash, P. K., Singh, A. K., Sharma, S., Gopalan, N., Rao, P. V. L., et al. (2014). Evidence of experimental vertical transmission of emerging novel ECSA genotype of Chikungunya Virus in *Aedes aegypti*. *PloS Negl. Trop. Dis.* 8, e2990. doi: 10.1371/journal.pntd.0002990

Agarwal, A., Sharma, A. K., Sukumaran, D., Parida, M., and Dash, P. K. (2016). Two novel epistatic mutations (E1: K211E and E2: V264A) in structural

proteins of Chikungunya virus enhance fitness in *Aedes aegypti*. *Virology* 497, 59–68. doi: 10.1016/j.virol.2016.06.025

Aubry, M., Teissier, A., Roche, C., Richard, V., Yan, A. S., Zisou, K., et al. (2015). Chikungunya outbreak, French Polynesia 2014. *Emerg. Infect. Dis.* 21, 724–726. doi: 10.3201/eid2104.141741

Bandelt, H., Forster, P., and Röhl, A. (1999). Median-joining networks for inferring intraspecific phylogenies. *Mol. Biol. Evol.* 16, 37–48. doi: 10.1093/oxfordjournals.molbev.a026036

Bellini, R., Medici, A., Calzolari, M., Bonilauri, P., Cavrini, F., Sambri, V., et al. (2012). Impact of Chikungunya virus on *Aedes albopictus* females and possibility of vertical transmission using the actors of the 2007 outbreak in Italy. *PloS One* 7, e28360. doi: 10.1371/journal.pone.0028360

Benedict, M. Q., Levine, R. S., Hawley, W. A., and Lounibos, L. P. (2007). Spread of the tiger: global risk of invasion by the mosquito *Aedes albopictus*. *Vector Borne Zoo Dis.* 7, 76–85. doi: 10.1089/vbz.2006.0562

Caglioti, C., Lalle, E., Castilletti, C., Carletti, F., Capobianchi, M. R., and Bordi, L. (2013). Chikungunya virus infection: an overview. *New Microbiol.* 36, 211–227.

Chansaenroj, J., Wanlapakorn, N., Ngamsaithong, C., Thongmee, T., Siriyasatien, P., Vongpunsawad, S., et al. (2020). Genome sequences of chikungunya virus isolates from an outbreak in southwest Bangkok in 2018. *Arch. Virol.* 165, 445–450. doi: 10.1007/s00705-019-04509-1

Chen, R., Puri, V., Fedorova, N., Lin, D., Hari, K. L., Jain, R., et al. (2016). Comprehensive genome scale phylogenetic study provides new insights on the global expansion of Chikungunya virus. *J. Virol.* 90, 10600–10611. doi: 10.1128/JVI.01166-16

Chompoosri, J., Thavara, U., Tawatsin, A., Boonserm, R., Phumee, A., Sangkitporn, S., et al. (2016). Vertical transmission of Indian Ocean Lineage of chikungunya virus in *Aedes aegypti* and *Aedes albopictus* mosquitoes. *Parasites Vectors* 9, 1–13. doi: 10.1186/s13071-016-1505-6

Clement, M., Snell, Q., Walker, P., Posada, D., and Crandall, K. (2002). TCS: Estimating gene genealogies. *Parallel DIS. Process. Symp. Int. Proc.* 2, 184. doi: 10.1109/IPDPS.2002.1016585

Coffey, L. L., Failloux, A. B., and Weaver, S. C. (2014). Chikungunya virus–vector interactions. *Viruses* 6, 4628–4663. doi: 10.3390/v6114628

Desdouits, M., Kamgang, B., Berthet, N., Tricou, V., Ngoagouni, C., Gessain, A., et al. (2015). Genetic characterization of Chikungunya virus in the Central African Republic. *Infect. Genet. Evol.* 33, 25–31. doi: 10.1016/j.meegid.2015.04.006

Diaz-Quinonez, J. A., Escobar-Escamilla, N., Ortíz-Alcántara, J., Vázquez-Pichardo, M., de la Luz Torres-Rodríguez, M., Nuñez-León, A., et al. (2016). Identification of Asian genotype of chikungunya virus isolated in Mexico. *Virus Genes* 52, 127–129. doi: 10.1007/s11262-015-1275-9

Duong, V., Andries, A. C., Ngan, C., Sok, T., Richner, B., Asgari-Jirhandeh, N., et al. (2012). Reemergence of Chikungunya virus in Cambodia. *Emerg. Infect. Dis.* 18, 2066–2069. doi: 10.3201/eid1812.120471

Freitas, A. R. R., Alarcón-Elbal, P. M., Paulino-Ramírez, R., and Donalisio, M. R. (2018). Excess mortality profile during the Asian genotype chikungunya epidemic in the Dominican Republic 2014. *Trans. R. Soc. Trop. Med. Hyg.* 112, 443–449. doi: 10.1093/trstmh/try072

French, N., Yu, S., Biggs, P., Holland, B., Fearnhead, P., Binney, B., et al. (2014). "Evolution of Campylobacter species in New Zealand," in *Campylobacter Ecology and Evolution*. Eds. S. K. Sheppard and G. Méric (Norfolk, England: Caister Academic Press), 221–240.

Fu, J. Y. L., Chua, C. L., Vythilingam, I., Sulaiman, W. Y. W., Wong, H. V., Chan, Y. F., et al. (2019). An amino acid change in nsP4 of chikungunya virus confers fitness advantage in human cell lines rather than in *Aedes albopictus*. *J. Gen. Virol.* 100, 1541–1553. doi: 10.1099/jgv.0.001338

Gopal, S. D. V. R. (2016). Isolation and diagnosis of chikungunya virus causing outbreaks in Andhra Pradesh, India. *Clin. Microbiol.* 5, 4(Suppl). doi: 10.15380/2277-5706.JCSR.12.044

Gouy, M., Guindon, S., and Gascuel, O. (2010). SeaView version 4: a multiplatform graphical user interface for sequence alignment and phylogenetic tree building. *Mol. Biol. Evol.* 27, 221–224. doi: 10.1093/molbev/msp259

Grandadam, M., Caro, V., Plumet, S., Thiberge, J. M., Souarès, Y., Failloux, A. B., et al. (2011). Chikungunya virus, southeastern France. *Emerg. Infect. Dis.* 17, 910. doi: 10.3201/eid1705.101873

Hall-Mendelin, S., Ritchie, S. A., Johansen, C. A., Zborowski, P., Cortis, G., Dandridge, S., et al. (2010). Exploiting mosquito sugar feeding to detect mosquito-borne pathogens. *Proc. Natl. Acad. Sci.* 107, 11255–11259. doi: 10.1073/pnas.1002040107

Hammon, W. M., Rundnick, A., and Sather, G. E. (1960). Viruses associated with epidemic hemorrhagic fevers of the Philippines and Thailand. *Science* 131, 1102–1103. doi: 10.1126/science.131.3407.1102

Hapuarachchi, H. C., Bandara, K. B. A. T., Sumanadasa, S. D. M., Hapugoda, M. D., Lai, Y. L., Lee, K. S., et al. (2010). Re-emergence of Chikungunya virus in South-east Asia: virological evidence from Sri Lanka and Singapore. *J. Gen. Virol.* 91, 1067–1076. doi: 10.1099/vir.0.015743-0

Harapan, H., Michie, A., Mudatsir, M., Nusa, R., Yohan, B., Wagner, A. L., et al. (2019). Chikungunya virus infection in Indonesia: A systematic review and evolutionary analysis. *BMC Infect. Dis.* 19, 1–20. doi: 10.1186/s12879-019-3857-y

Higashi, N., Matsumoto, A., Tabata, K., and Nagatomo, Y. (1967). Electron microscope study of development of Chikungunya virus in green monkey kidney stable (VERO) cells. *Virology* 33, 55–69. doi: 10.1016/0042-6822(67)90093-1

Honório, N. A., Wiggins, K., Eastmond, B., Câmara, D. C. P., and Alto, B. W. (2019). Experimental vertical transmission of chikungunya virus by Brazilian and Florida *Aedes albopictus* populations. *Viruses* 11, 353. doi: 10.3390/v11040353

Intayot, P., Phumee, A., Boonserm, R., Sor-Suwan, S., Buathong, R., Wacharapluesadee, S., et al. (2019). Genetic characterization of chikungunya virus in field-caught *Aedes aegypti* mosquitoes collected during the recent outbreaks in 2019, Thailand. *Pathogens* 8, 121. doi: 10.3390/pathogens8030121

IVRCRD (2016). *Manual on mosquitoes field sampling methods (in Bahasa Indonesia). 2nd edition* (Salatiga: NIHRD-IVRCRD. NIHRD-MoH Indonesia), 176.

Jain, J., Kushwah, R. B. S., Singh, S. S., Sharma, A., Adak, T., Singh, O. P., et al. (2016). Evidence for natural vertical transmission of chikungunya viruses in field populations of *Aedes aegypti* in Delhi and Haryana states in India—a preliminary report. *Acta Trop.* 162, 46–55. doi: 10.1016/j.actatropica.2016.06.004

Jupp, P., and McIntosh, B. (1988). "The arboviruses: epidemiology and ecology," in *Medical Entomology, a textbook on public health and veterinary problems caused by arthropods*. Ed. T. Monath (Boca Raton, Florida: CRC Press), 137–157.

Khan, A. H., Morita, K., Parquet, M. D., Hasebe, F., and Mathenge, E. G. (2002). Complete nucleotide sequence of chikungunya virus and evidence for an internal polyadenylation site. *J Gen Virol.* 83 (12), 3075–3084. doi: 10.1099/0022-1317-83-12-3075

Lanciotti, R. S., and Lambert, A. J. (2016). Phylogenetic analysis of chikungunya virus strains circulating in the Western Hemisphere. *Am. J. Trop. Med. Hyg.* 94, 800–803. doi: 10.4269/ajtmh.15-0375

Lanciotti, R. S., and Valadere, A. M. (2014). Transcontinental movement of Asian genotype chikungunya virus. *Emerg. Infect. Dis.* 20, 1400–1402. doi: 10.3201/eid2008.140268

Leparc-Goffart, I., Nougairede, A., Cassadou, S., Prat, C., and De Lamballerie, X. (2014). Chikungunya in the Americas. *Lancet* 383, 514. doi: 10.1016/S0140-6736(14)60185-9

Lai, A., Cella, E., Zehender, G., and Ciccozzi, M. (2014). Chikungunya virus, epidemiology, clinics and phylogenesis: A review. *Asian Pacif. J. Trop. Med.* 7, 925–932. doi: 10.1016/S1995-7645(14)60164-4

MoH Indonesia (2007). *Health profile of Indonesia 2005* (Jakarta: Ministry of Health Republic of Indonesia), 283.

Nhan, T. X., Claverie, A., Roche, C., Teissier, A., Colleuil, M., Baudet, J. M., et al. (2014). Chikungunya virus imported into French Polynesia 2014. *Emerg. Infect. Dis.* 20, 1773–1774. doi: 10.3201/eid2010.141060

Osterrieth, P., and Blanes-Ridaura, G. (1960). Recherches sur le virus Chikungunya au Congo belge. *Ann. Soc. Belg. Med. Trop.* 40, 199–203.

Osterrieth, P., Rathe, E., and Deleplanque-Liegeois, P. (1961). Isolément simultané des virus de la fièvre jaune et de chikungunya à Bili (Haut-Uélé, Congo Belge). *Ann. Soc. Belge. Med. Trop.* 3, 207–212.

Powers, A. M., and Logue, C. H. (2007). Changing patterns of chikungunya virus: Re-emergence of a zoonotic arbovirus. *J. Gen. Virol.* 88 (9), 2363–2377. doi: 10.1099/vir.0.82858-0

Powers, A. M., Brault, A. C., Tesh, R. B., and Weaver, S. C. (2000). Re-emergence of chikungunya and o'nyong-nyong viruses: Evidence for distinct geographical lineages and distant evolutionary relationships. *J. Gen. Virol.* 81, 471–479. doi: 10.1099/0022-1317-81-2-471

Powers, A., Brault, A., Shirako, Y., Strauss, E., Kang, W., and Strauss, J. (2001). Evolutionary relationships and systematics of the alphaviruses. *J. Virol.* 75, 10118–10131. doi: 10.1128/JVI.75.21.10118-10131.2001

Pyke, A. T., McMahon, J., Burtonclay, P., Nair, N., and De Jong, A. (2020). Genome sequences of chikungunya virus strains from Bangladesh and Thailand. *Microbiol. Resour. Announc.* 9, e01452–e01 19. doi: 10.1128/MRA.01452-19

Quyen, N. T. H., Kien, D. T. H., Rabaa, M., Tuan, N. M., Vi, T. T., Hung, N. T., et al. (2017). Chikungunya and Zika virus cases detected against a backdrop of endemic dengue transmission in Vietnam. *Am. J. Trop. Med. Hyg.* 97, 146–150. doi: 10.4269/ajtmh.16-0979

Rianthavorn, P., Prianantathavorn, K., Wuttirattanakowit, N., Theamboonlers, A., and Poovorawan, Y. (2010). An outbreak of chikungunya in southern Thailand from 2008 to 2009 caused by African strains with A226V mutation. *Intern. J. Infect. Dis.* 14, e161–e165. doi: 10.1016/j.ijid.2010.01.001

Rozas, J., Ferrer-Mata, A., Sánchez-DelBarrio, J. C., Guirao-Rico, S., Librado, P., Ramos-Onsins, S. E., et al. (2017). DnaSP 6: DNA sequence polymorphism analysis of large data sets. *Mol. Biol. Evol.* 34, 3299–3302. doi: 10.1093/molbev/msx248

Rueanghiran, C., Apiwathnasorn, C., Sangthong, P., Samung, Y., and Ruangsittichai, J. (2011). Utility of a set of conserved mitochondrial cytochrome oxidase subunit I gene primers for *Mansonia annulata* identification. *Southeast Asian J. Trop. Med. Public Health* 42, 1381–1387.

Rueda, L. M. (2004). Pictorial keys for the identification of mosquitoes (Diptera: Culicidae) associated with dengue virus transmission. *Zootaxa* 589, 1–60. doi: 10.11646/zootaxa.589.1.1

Sam, I. C., Chan, Y. F., Chan, S. Y., Loong, S. K., Chin, H. K., Hooi, P. S., et al. (2009). Chikungunya virus of Asian and Central/East African genotypes in Malaysia. *J. Clin. Virol.* 46, 180–183. doi: 10.1016/j.jcv.2009.07.016

Sam, I. C., Loong, S. K., Michael, J. C., Chua, C. L., Sulaiman, W. Y. W., Vythilingam, I., et al. (2012). Genotypic and phenotypic characterization of Chikungunya virus of different genotypes from Malaysia. *PloS One* 7, e50476. doi: 10.1371/journal.pone.0050476

Sam, J. I. C. (2018). "Chikungunya and Zika virus in Asia," in *Chikungunya and Zika viruses: global emerging health threats*. Eds. S. Higgs, D. L. Vanlandingham and A. M. Powers (London, UK: Academic Press), 135–176.

Simizu, B., Yamamoto, K., Hashimoto, K., and Ogata, T. (1984). Structural proteins of Chikungunya virus. *J. Virol.* 51, 254–258. doi: 10.1128/JVI.51.1.254-258.1984

Tsetsarkin, K. A., and Weaver, S. C. (2011). Sequential adaptive mutations enhance efficient vector switching by Chikungunya virus and its epidemic emergence. *PloS Pathog.* 7, e1002412. doi: 10.1371/journal.ppat.1002412

Tsetsarkin, K. A., Vanlandingham, D. L., McGee, C. E., and Higgs, S. (2007). A single mutation in chikungunya virus affects vector specificity and epidemic potential. *PloS Pathog.* 3, e201. doi: 10.1371/journal.ppat.0030201

Tsetsarkin, K. A., Chen, R., Leal, G., Forrester, N., Higgs, S., Huang, J., et al. (2011). Chikungunya virus emergence is constrained in Asia by lineage-specific adaptive landscapes. *PNAS* 108, 7872–7877. doi: 10.1073/pnas.1018344108

Weaver, S., and Lecuit, M. (2015). Chikungunya Virus and the Global Spread of a Mosquito-Borne Disease. *N. Engl. J. Med.* 372 (13), 1231–1239. doi: 10.1056/NEJMra1406035

Wimalasiri-Yapa, B. R., Stassen, L., Huang, X., Hafner, L. M., Hu, W., Devine, G. J., et al. (2019). Chikungunya virus in Asia–Pacific: a systematic review. *Emerg. Microbes Infect.* 8, 70–79. doi: 10.1080/22221751.2018.1559708

Zakotnik, S., Korva, M., Knap, N., Robnik, B., Gorišek Miksić, N., and Avšič Županc, T. (2019). Complete Coding Sequence of a Chikungunya Virus Strain Imported into Slovenia from Thailand in Late 2018. *Microbiol. Resour. Announc.* 8 (37), e00581–19. doi: 10.1128/MRA.00581-19

Zeller, H., Van Bortel, W., and Sudre, B. (2016). Chikungunya: Its history in Africa and Asia and its spread to new regions in 2013-2014. *J. Infect. Dis.* 214 (Suppl 5), S436–S440. doi: 10.1093/infdis/jiw391

Conflict of Interest: The authors declare that the research was conducted in the absence of any commercial or financial relationships that could be constructed as a potential conflict of interest.

frontiers in Cellular and Infection Microbiology

ORIGINAL RESEARCH
published: 23 April 2021
doi: 10.3389/fcimb.2021.644576

Surveillance of Antimalarial Drug-Resistance Genes in Imported *Plasmodium falciparum* Isolates From Nigeria in Henan, China, 2012–2019

Dongyang Zhao[†], *Hongwei Zhang*[†], *Penghui Ji*, *Suhua Li*, *Chengyun Yang*, *Ying Liu*, *Dan Qian*, *Yan Deng*, *Hao Wang*, *Deling Lu*, *Ruimin Zhou*[*] *and Yuling Zhao*[*]

Department of Parasite Disease Control and Prevention, Henan Provincial Center for Disease Control and Prevention, Henan Key Laboratory of Infectious Disease Microbiology, Zhengzhou, China

Malaria remains a major public health issue in Nigeria, and Nigeria is one of the main sources of imported malaria in China. Antimalarial drug resistance is a significant obstacle to the control and prevention of malaria globally. The molecular markers associated with antimalarial drug resistance can provide early warnings about the emergence of resistance. The prevalence of antimalarial drug resistant genes and mutants, including *PfK13*, *Pfcrt*, *Pfmdr1*, *Pfdhfr*, and *Pfdhps*, was evaluated among the imported *Plasmodium falciparum* isolates from Nigeria in Henan, China, from 2012 to 2019. Among the 167 imported *P. falciparum* isolates, the wild-type frequency of *PfK13*, *Pfcrt*, *Pfmdr1*, *Pfdhfr*, and *Pfdhps* was 98.7, 63.9, 34.8, 3.1, and 3.1%, respectively. The mutation of *PfK13* was rare, with just two nonsynonymous (S693F and Q613H) and two synonymous mutations (C469C and G496G) identified from four isolates. The prevalence of *Pfcrt* mutation at codon 74–76 decreased year-by-year, while the prevalence of *pfmdr1* 86Y also decreased significantly with time. The prevalence of *Pfdhfr* and *Pfdhps* mutants was high. Combined mutations of *Pfdhfr* and *Pfdhps* had a high prevalence of the quadruple mutant $I_{51}R_{59}N_{108}$-G_{437} (39.0%), followed by the octal mutant $I_{51}R_{59}N_{108}$-$V_{431}A_{436}G_{437}G_{581}S_{613}$ (17.0%). These molecular findings update the known data on antimalarial drug-resistance genes and provide supplemental information for Nigeria.

Keywords: Plasmodium falciparum, drug resistance, Pf*K13*, *Pfcrt*, *Pfmdr1*, *Pfdhfr*, *Pfdhps*, Nigeria

OPEN ACCESS

Edited by:
Jun Feng,
National Institute of Parasitic Diseases, China

Reviewed by:
Carlo Severini,
National Institute of Health (ISS), Italy
Didier Menard,
Institut Pasteur, France
Yaming Cao,
China Medical University, China
Olusola Ojurongbe,
Ladoke Akintola University of Technology, Nigeria

****Correspondence:***
Ruimin Zhou
zrm920@126.com
Yuling Zhao
819482937@qq.com

[†]*These authors have contributed equally to this work*

Specialty section:
This article was submitted to Parasite and Host, a section of the journal Frontiers in Cellular and Infection Microbiology

Received: *21 December 2020*
Accepted: *31 March 2021*
Published: *23 April 2021*

Citation:
Zhao D, Zhang H, Ji P, Li S, Yang C, Liu Y, Qian D, Deng Y, Wang H, Lu D, Zhou R and Zhao Y (2021) Surveillance of Antimalarial Drug-Resistance Genes in Imported Plasmodium falciparum Isolates From Nigeria in Henan, China, 2012–2019. Front. Cell. Infect. Microbiol. 11:644576. doi: 10.3389/fcimb.2021.644576

INTRODUCTION

Globally, malaria incidence and mortality have substantially reduced since 2010, and an increasing number of countries are moving toward malaria elimination. In 2016, the World Health Organization (WHO) identified 21 countries that had the potential to eliminate malaria by 2020, including China (WHO, 2018). In Henan Province, there has been no local malaria case since 2012

(Liu et al., 2014), while in 2017, no indigenous malaria cases were reported in China for the first time (Zhang et al., 2018). However, malaria remains the major public problem in sub-Saharan Africa, and Nigeria had the greatest burden of global malaria cases (27%) and malaria deaths (23%) worldwide in 2019 (WHO, 2020).

Efficacious antimalarial medicines are critical to malaria control and elimination. However, the emergence of antimalarial drug resistance increases the burden of malaria, and is one of the recurring challenges in the global fight against malaria. Monitoring antimalarial drug efficacy is necessary to provide information for treatment policies, as well as to mitigate the impact of resistance and prevent its spread. Therapeutic efficacy studies (TESs) and integrated drug efficacy surveillance (iDES) are common and reliable measures to obtain data on treatment efficacy, and the molecular markers associated with parasite resistance can provide supplemental information for TESs and iDES.

Chloroquine (CQ), as the first-line therapy for *Plasmodium falciparum* malaria, was the most common antimalarial in Africa from the 1940s to the 2000s (Nuwaha, 2001). CQ was replaced by artemisinin-based combination therapies (ACTs) in most African countries from the late 1990s to 2000s with the spread of chloroquine resistance (Flegg et al., 2013). However, CQ remains the first-line treatment for *P. vivax* in most endemic countries (WHO, 2019), while ACTs have been recommended by the WHO as the first-line treatment for uncomplicated *P. falciparum* malaria in nearly all areas, as well as for chloroquine-resistant (CQR) *P. vivax* malaria (WHO, 2015). Artemether-lumefantrine (AL), artesunate-amodiaquine (AS-AQ), and dihydroartemisinin-piperaquine (DHA-PPQ) are used as the first-line treatment for *P. falciparum* in most African countries (WHO, 2019). Sulfadoxine-pyrimethamine (SP) is recommended for the intermittent preventive treatment of malaria in pregnant women and infants (IPTp and IPTi) by the WHO (WHO, 2010).

CQR was first reported at the Thailand-Cambodia border in 1957 (Mehlotra et al., 2001; Ridley, 2002) and then confirmed in Africa in 1979 (Campbell et al., 1979). The emergence of artemisinin resistance (ART-R) in *P. falciparum* was first reported in Cambodia and later became widespread in the Greater Mekong sub-region (GMS) (Noedl et al., 2008; Dondorp et al., 2009; Yeung et al., 2009). Currently, resistance to the partner drugs of artemisinin (ART) is also common in the GMS, which affects the efficacy of ACTs. The *P. falciparum* chloroquine resistance transporter gene (*Pfcrt*) is the most reliable molecular marker of CQR, and has also been considered to be associated with resistance to ACT partner drugs, such as piperaquine (Ross et al., 2018), amodiaquine (Sá et al., 2009), lumefantrine (Sisowath et al., 2009), and mefloquine (Picot et al., 2009). The polymorphism of the Kelch 13 (*K13*) propeller domain in *P. falciparum* has been identified as a molecular marker of partial ART resistance (Ariey et al., 2014). Many non-synonymous mutations in *PfK13* have been identified (WHO, 2018); however, only a few *PfK13* mutations have been validated, and all of them have been identified in the GMS in Southeast Asia (Ménard et al., 2016). Some mutations in *PfK13* were also identified in Africa, although these have not been validated *in vivo* or *in vitro* (Taylor et al., 2014). A recent study confirmed the *de novo* emergence and clonal expansion of an ART-R *PfK13* R561H lineage in Rwanda (Uwimana et al., 2020). These findings have substantial implications for the treatment and control of malaria in Africa. *P. falciparum* multidrug resistance 1 gene (*Pfmdr1*) has been linked with the efficacy of chloroquine, mefloquine, amodiaquine, lumefantrine, artemisinin, and others (Humphreys et al., 2007; Somé et al., 2010). The polymorphisms of *Pfmdr1* at codons N86Y, Y184F, S1034C, N1042D, and D1246Y have also been shown to be linked with antimalarial drug resistance (Picot et al., 2009; Kamugisha et al., 2012). The *Pfmdr1* mutations N86Y and D1246Y, together with the *Pfcrt* mutations, can reduce the efficacy of CQ (Sá et al., 2009). The mutations of *P. falciparum* dihydrofolate reductase (*Pfdhfr*) at codons A16V, N51I, C59R, S108N/T, and I164L have been reported to be related with pyrimethamine resistance (McCollum et al., 2006). Moreover, polymorphisms of *P. falciparum* dihydropteroate synthase (*Pfdhps*) at codons S436A/F, A437G, K540E, A581G, and A613S/T are considered to be associated with sulphadoxine resistance (Vinayak et al., 2010). The quintuple mutation composed of the *pfdhfr* triple mutant 51I59R108N and the *Pfdhps* double mutant 437G540E has been reported to reduce the efficacy of SP in IPTp and IPTi (Gosling et al., 2009; Nankabirwa et al., 2010).

In Nigeria, ACTs have been recommended by the National malaria drug policy since 2005 because of the failure of CQ treatment (FMoH, 2005). However, CQ is still used to treat malaria because it is both accessible and cheap. Currently, AL and AS-AQ, as the recommended ART-based combinations, are adopted for the treatment of uncomplicated malaria in Nigeria, and the most recent TES showed that the cure rate was more than 95% (Sowunmi et al., 2017). At present, pregnant Nigerian women are also recommended to receive 3+ doses of SP to prevent malaria (NPC and ICF, 2019).

Nigeria is one of the main sources of imported malaria in China. It is important to understand the efficacy of antimalarial drugs for these imported cases. Therefore, in this study, we performed molecular surveillance of antimalarial drug-resistant genes in *P. falciparum* isolates imported from Nigeria in Henan Province, China, to determine their haplotypes and prevalence.

MATERIALS AND METHODS

Sample Characteristics

All of the information on imported malaria cases in Henan Province was collected from the Disease Surveillance Information Report Management system of China Center for Disease Control and Prevention. A total of 1,522 imported malaria cases were reported in Henan Province during 2012–2019, with no indigenous cases. Nigeria is one of the main sources of imported malaria in Henan Province, and 201 of the total cases originated from here. Among these 201 cases, 167 cases were infected with *P. falciparum*. With the exception of one patient who was Nigerian working in China, the other 200 cases were Chinese people who traveled to Nigeria and returned with malaria infection. One case was female, and the others were male. The youngest was 19 years old and the oldest was 62 years old.

The average age was 38.11 ± 9.188 years, and most cases were concentrated in the 21–50 years age group (86.6%, 174/201). Most of the patients were migrant workers (84.6%, 170/201).

DNA Extraction and Amplification

The patients were diagnosed with malaria initially by blood smear microscopy and/or rapid diagnosis test (RDT) in the local hospital or County Centers for Disease Control and Prevention. The whole blood and blood smear samples of the cases were collected before antimalarial treatment and deposited in the Sample Resource Library in Henan Provincial Reference Laboratory for Malaria Diagnosis. All of the cases were confirmed to be infected with malaria parasite species using nested polymerase chain reaction (PCR) and blood smear microscopy performed at the Henan Provincial Reference Laboratory for Malaria Diagnosis (Yin et al., 2015). The genomic DNA was extracted from blood samples using QIAamp DNA Blood Mini Kits (Qiagen, USA) following the manufacturer's instructions.

The target genes of *PfK13*, *Pfcrt*, *Pfmdr1*, *Pfdhfr*, and *Pfdhps* were amplified using nested PCR previously described (Zhou et al., 2016; Zhou et al., 2019). The primer sequences and conditions are shown in **Supplementary Material**. The amplification of the *Pfcrt* gene amplified covered the codons C72S, V73V, M74I, N75E, and K76T. The *Pfmdr1* gene contained the codons N86Y, Y184F, S1034C, N1042D, and D1246Y. The *Pfdhfr* gene was amplified to identify the polymorphism at codons A16S, N51I, C59R, S108N, and I164L. The *Pfdhps* gene covered the codons I431V, S436A, A437G, K540E, A581G, and A613S. Bidirectional sequencing of the secondary PCR products was performed by Sangon Biotech Co Ltd (Shanghai, China).

Data Analysis

ChromasPro software v. 1.5 (https://technelysium.com.au/wp/chromaspro/) was used to assemble the forward and reverse sequences of the genes. MEGA7 (Molecular Evolutionary Genetics Analysis, https://www.megasoftware.net/show_eua) software was used to identify the mutations by comparing with their reference genomes. The reference genomes of *PfK13*, *Pfcrt*, *Pfmdr1*, *Pfdhfr*, and *Pfdhps* were from the *P. falciparum* 3D7 strain obtained from Genbank (Genbank ID: Pf3D7_1343700, Pf3D7_0709000, Pf3D7_0523000, PF3D7_0417200, and PF3D7_1324800, respectively). The data were analyzed using SSPS v.21.0 (Statistical Product and Service Solutions). The difference was compared using Chi-square or Fisher's exact test, and a two-sided p value of <0.05 was considered statistically significant.

RESULTS

K13-Propeller

The 850 bp fragments of the *K13*-propeller domain were successfully sequenced from 157 samples among 167 P. *falciparum* isolates. Two non-synonymous and two synonymous mutations were identified from four isolates: S693F, Q613H, C469C, and G496G. The total mutant prevalence was 2.5% (4/157). Two synonymous mutations were detected in 2014 and 2016, and one non-synonymous mutation was identified in 2017 and 2019.

Pfcrt

A total of 158 out of 167 isolates were successfully sequenced on *Pfcrt*. The codons 72 and 73 were all wild type. The mutant prevalence of codons 74, 75, and 76 was 36.1% (57/158), 36.1% (57/158), and 35.4% (56/158), respectively, during 2012–2019 (**Table 1**). Four haplotypes of *Pfcrt* were identified, wild-type CVMNK (63.9%, 101/158), CVIET (32.3%, 51/158), CVIEK (0.6%, 1/158), and CV M/I N/E K/T (3.2%, 5/158) (**Table 2**). The mutant prevalence of *Pfcrt* 74I, 75E, and 76T decreased with time, and the differences showed statistical significance (74I and 75E: $\chi^2 = 9.837$, $p = 0.020$; 76T: $\chi^2 = 8.260$, $p = 0.041$) (**Figure 1A**).

Pfmdr1

The fragments of *Pfmdr1* were successfully obtained from 158 isolates. No mutation was found at codons 1034 and 1042, and only two isolates had mutation at codon D1246Y. One T1192L mutant was identified for the first time in our study. The mutant prevalence of N86Y and Y184F was 13.9% (22/158) and 63.3% (100/158), respectively, during 2012–2019 (**Table 1**). Five haplotypes of *Pfmdr1* were found, including wild-type NYSND, two single mutant haplotypes N**F**SND and NYSND-T1192**L**, and two double mutant haplotypes **YF**SNLD and **Y**YSN**Y** (**Table 2**). The mutant prevalence of *Pfmdr1* 86Y decreased significantly with time ($\chi^2 = 23.704$, $p = 0.000$) (**Figure 1B**).

Pfdhfr

Pfdhfr was successfully amplified from 159 P. *falciparum* isolates. Only five isolates were wild type, and the other 154 isolates had mutations among five codons N51I, C59R, S108N, S120R, and I164L. The mutations at codons N51I, C59R, and S108N were common, accounting for 91.8% (146/159), 92.5% (147/159), and 96.9% (154/159), respectively (**Table 1**). The *Pfdhfr* S120R and I164L mutants were identified from just one isolate each. The *Pfdhfr* S120R mutant was newly identified in this study. No *Pfdhfr* A16V mutant was found, although there was no statistical difference in the mutant prevalence among these codons during 2012–2019 (**Figure 1C**). Seven haplotypes of *Pfdhfr* were found, including wild-type, single, double, triple, and quadruple mutant haplotypes. However, the triple mutation, $I_{51}R_{59}N_{108}$ haplotype, was the most common, accounting for 88.1% (140/159) (**Table 2**).

Pfdhps

Among the 159 successfully sequenced samples, five isolates were free of mutations, and the other 154 isolates had mutations among six codons E424G, I431V, S436A/F, A437G, A581G, and A613S. There were two types of mutations at codon 436, S436A (75 isolates), and S436F (4 isolates). The mutant S436F always appeared with *Pfdhps* 613S. No *Pfdhps* K540E mutant was found. The mutation at codon A437G (86.2%, 137/159) was the most prevalent, followed by S436A/F (49.7%, 79/159), A613S (28.9%, 46/159), I431V (27.0%, 43/159), and A581G (21.4%, 34/159) (**Table 1**). Only one E424G mutant was found and was newly identified in this study. There was statistical difference about the mutant prevalence at codon S436A/F during 2012–2019 ($\chi^2 = 13.152$, $p = 0.004$) (**Figure 1D**). The prevalence of *Pfdhps* A613S

TABLE 1 | Mutant prevalence of the *Pfcrt*, *Pfmdr1*, *Pfdhfr*, and *Pfdhps* genes detected in *Plasmodium falciparum* isolates returned from Nigeria during 2012–2019.

Gene	SNP	Prevalence of mutation[a] (%)								
		Total	2012	2013	2014	2015	2016	2017	2018	2019
Pfcrt	M74I	36.1 (57/158)	72.2(13/18)	35.7 (5/14)	42.3 (11/26)	38.5 (5/13)	20.0 (3/15)	34.6 (9/26)	26.7(4/15)	22.6(7/31)
	N75E	36.1 (57/158)	72.2(13/18)	35.7 (5/14)	42.3 (11/26)	38.5 (5/13)	20.0 (3/15)	34.6 (9/26)	26.7(4/15)	22.6(7/31)
	K76T	35.4 (56/158)	66.7(12/18)	35.7 (5/14)	42.3 (11/26)	38.5 (5/13)	20.0 (3/15)	34.6 (9/26)	26.7(4/15)	22.6(7/31)
Pfmdr1[b]	N86Y	13.9 (22/158)	38.9 (7/18)	28.6 (4/14)	23.1 (6/26)	23.1 (3/13)	6.7 (1/15)	0 (0/26)	0(0/15)	3.2(1/31)
	Y184F	63.3 (100/158)	77.8 (14/18)	64.3 (9/14)	61.5 (16/26)	76.9 (10/13)	53.3 (8/15)	50 (13/26)	60.0(9/15)	67.7(21/31)
	D1246Y	1.3 (2/158)	0 (0/18)	7.1 (1/14)	3.8 (1/26)	0 (0/13)	0 (0/15)	0 (0/26)	0(0/15)	0(0/31)
Pfdhfr[c]	N51I	91.8 (146/159)	100 (18/18)	78.6 (11/14)	100 (26/26)	84.6 (11/13)	86.7 (13/15)	100 (27/27)	86.7(13/15)	87.1(27/31)
	C59R	92.5 (147/159)	100 (18/18)	92.9 (13/14)	96.2 (25/26)	69.2 (9/13)	93.3 (14/15)	96.2 (26/27)	86.7(13/15)	93.5(29/31)
	S108N	96.9 (154/159)	100 (18/18)	92.9 (13/14)	100 (26/26)	92.3 (12/13)	100 (15/15)	100 (27/27)	93.3(14/15)	93.5(29/31)
	I164L	0.6 (1/159)	5.6 (1/18)	0 (0/14)	0 (0/26)	0 (0/13)	0 (0/15)	0 (0/27)	0(0/15)	0(0/31)
Pfdhps[d]	I431V	27.0 (43/159)	22.2 (4/18)	28.6 (4/14)	19.2 (5/26)	23.1 (3/13)	26.7 (4/15)	37.0 (10/27)	33.3(5/15)	25.8(8/31)
	S436A	47.2 (75/159)	38.9 (7/18)	64.3 (9/14)	15.4 (4/26)	30.8 (4/13)	60 (9/15)	66.7 (18/27)	53.3(8/15)	51.6(16/31)
	S436F	2.5 (4/159)	5.6 (1/18)	0 (0/14)	7.7 (2/26)	0 (0/13)	0 (0/15)	0 (0/27)	0(0/15)	3.2(1/31)
	A437G	86.2 (137/159)	77.8 (14/18)	85.7 (12/14)	84.6 (22/26)	100 (13/13)	73.3 (11/15)	88.9 (24/27)	100(15/15)	83.9(26/31)
	A581G	21.4 (34/159)	16.7 (3/18)	14.3 (2/14)	11.5 (3/26)	23.1 (3/13)	26.7 (4/15)	25.9 (7/27)	33.3(5/15)	22.6(7/31)
	A613S	28.9 (46/159)	22.2 (4/18)	14.3 (2/14)	19.2 (5/26)	30.8 (4/13)	33.3 (5/15)	33.3 (9/27)	40.0(6/15)	35.5(11/31)

[a]*including the mixed mutation.*
[b]*T1192L mutant was identified from one isolate in 2019.*
[c]*S120R mutant was identified from one isolate in 2015.*
[d]*E424G mutant was identified from one isolate in 2015.*

TABLE 2 | Haplotypes of *Pfcrt*, *Pfmdr1*, *Pfdhfr*, and *Pfdhps* genes detected in *Plasmodium falciparum* isolates returned from Nigeria during 2012–2019.

Gene (No.)	Haplotypes	No. (%)
Pfcrt (n=158)	Wild-type $C_{72}V_{73}M_{74}N_{75}K_{76}$	101 (63.9)
	Double mutant haplotype CV**IE**K	1 (0.6)
	Triple mutant haplotype CV**IET**	51 (32.3)
	Mixed triple mutant haplotype CV **M/I N/E K/T**	5 (3.2)
Pfmdr1 (n=158)	Wild-type $N_{86}Y_{184}S_{1034}N_{1042}D_{1246}$	55 (34.8)
	Single mutant haplotype N**F**SND	80 (50.6)
	Single mutant haplotype NYSND-T1192**L**	1 (0.6)
	Double mutant haplotype **YF**SND	20 (12.7)
	Double mutant haplotype **Y**YSN**Y**	2 (1.3)
Pfdhfr (n=159)	Wild-type $A_{16}N_{51}C_{59}S_{108}I_{164}$	5 (3.1)
	Single mutant haplotype ANC**N**I	1 (0.6)
	Double mutant haplotype A**I**C**N**I	5 (3.1)
	Double mutant haplotype AN**RN**I	6 (3.8)
	Double mutant haplotype ANC**N**I-S120**R**	1 (0.6)
	Triple mutant haplotype A**IRN**I	140 (88.1)
	Quadruple mutant haplotype A**IRNL**	1 (0.6)
Pfdhps (n=159)	Wild-type $I_{431}S_{436}A_{437}K_{540}A_{581}A_{613}$	5 (3.1)
	Single mutant haplotype IS**G**KAA	70 (40.0)
	Single mutant haplotype I**A**AKAA	11 (6.9)
	Double mutant haplotype I**AG**KAA	11 (6.9)
	Double mutant haplotype **VA**AKAA	2 (1.3)
	Double mutant haplotype I**F**AKA**S**	4 (2.5)
	Double mutant haplotype IS**G**K**G**A	2 (1.3)
	Triple mutant haplotype **VAG**KAA	8 (5.0)
	Triple mutant haplotype **V**S**G**K**G**A	1 (0.6)
	Triple mutant haplotype I**AG**KA**S**	12 (7.5)
	Triple mutant haplotype IS**G**K**G**A-E424G	1 (0.6)
	Quadruple mutant haplotype **VAG**K**G**A	2 (1.3)
	Quadruple mutant haplotype **VAG**KA**S**	2 (1.3)
	Quadruple mutant haplotype **V**S**G**K**GS**	1 (0.6)
	Quintuple mutant haplotype **VAG**K**GS**	27 (17.0)

increased yearly, but there was no significant difference (χ^2 = 4.100, p = 0.251). In addition to the wild type (ISAKAA), there were 14 mutant types, including two single mutant haplotypes (ISGKAA, IAAKAA), four double mutant haplotypes (IAGKAA, VAAKAA, IFAKAS, ISGKGA), four triple mutant haplotypes (VAGKAA, VSGKGA, IAGKAS, ISGKGA-E424G), three quadruple mutant haplotypes (VAGKGA, VAGKAS, VSGKGS), and one quintuple mutant haplotype (VAGKGS). The single mutant haplotype ISGKAA (40.0%) was the most common, followed by the quintuple mutant haplotype VAGKGS (17.0%), and the triple mutant haplotype IAGKAS (7.5%) (**Table 2**).

Combined Haplotypes of *Pfdhfr* and *Pfdhps*

Among the 167 P. *falciparum* isolates, 159 samples were successfully sequenced for *Pfdhfr* and *Pfdhps*. The results of sequencing demonstrated that only one isolate was free of mutations, and eight isolates had single-gene mutations, *Pfdhfr* or *Pfdhps*. The other 150 isolates (94.3%) had mutations in two genes simultaneously. The most frequent mutation was the quadruple mutant $I_{51}R_{59}N_{108}$- G_{437}, accounting for 39.0%, followed by $I_{51}R_{59}N_{108}$- $V_{431}A_{436}G_{437}G_{581}S_{613}$ (17.0%) and $I_{51}R_{59}N_{108}$- A_{436} (6.9%). As no *Pfdhps* K540E mutants were detected, the combination of the *Pfdhfr* triple mutant $I_{51}R_{59}N_{108}$ and the *Pfdhps* double mutant $G_{437}E_{540}$ was not observed (**Table 3**).

DISCUSSION

ACTs are currently considered the most effective treatment for uncomplicated falciparum malaria globally. However, the emergence and radical spread of ACT resistance represents a significant threat to malaria control and elimination. Until now, previously validated *PfK13* mutants, including F446I, N485Y, M476I, Y493H, R539T, I543T, P553L, R561H, and C580Y (the most common), have been mainly identified in Southeast Asia

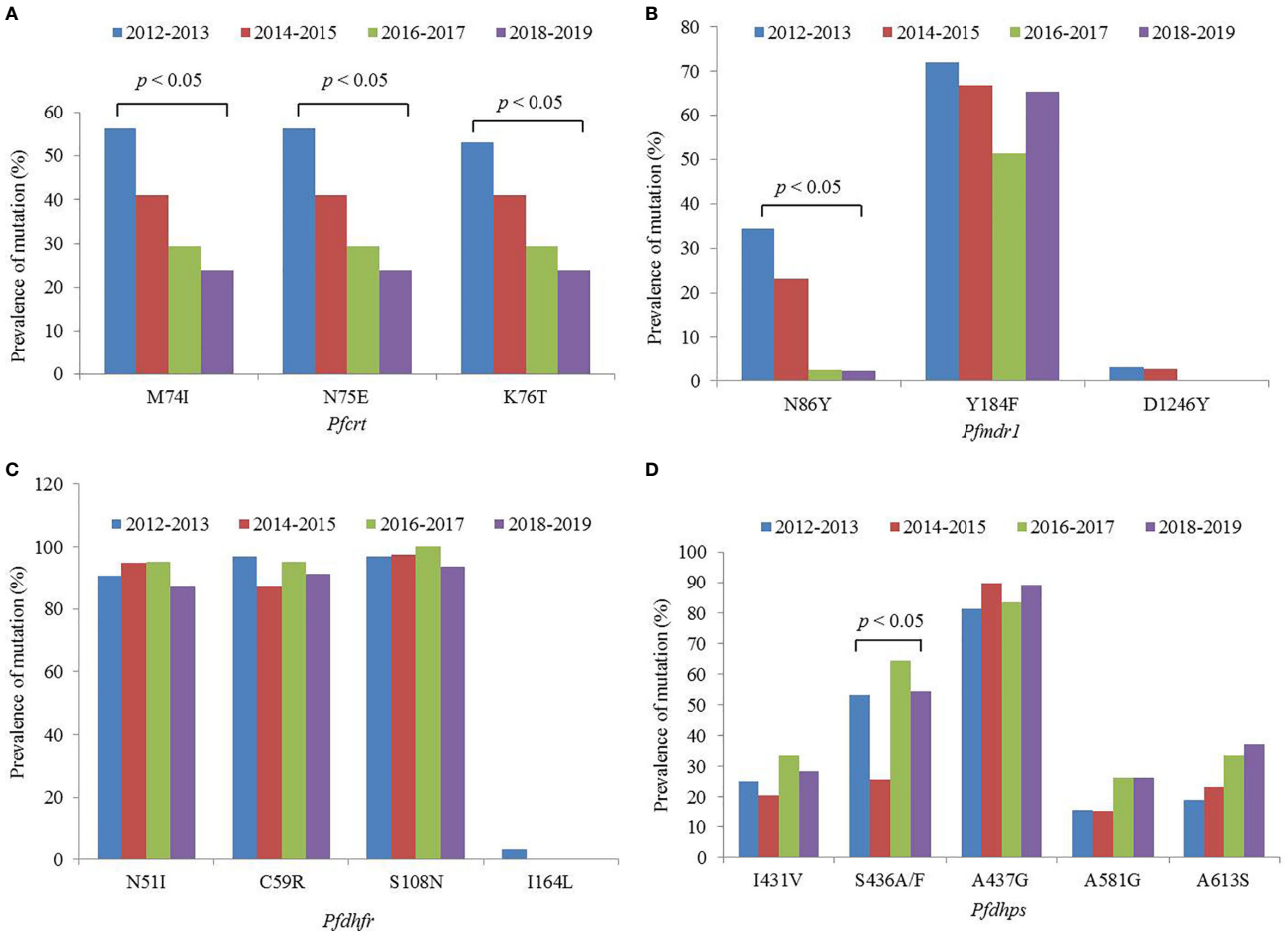

FIGURE 1 | Mutant prevalence of the **(A)** *Pfcrt*, **(B)** *Pfmdr1*, **(C)** *Pfdhfr*, and **(D)** *Pfdhps* genes detected in *Plasmodium falciparum* isolates returned from Nigeria, 2012–2019.

(WHO, 2018). Meanwhile, a few *PfK13* mutations have been reported in African *P. falciparum* isolates, including A557S, V566I, A567T, S576L, A578S, and L589I; however, none of them conferred the ART-R *in vivo* or *in vitro* (Taylor et al., 2014). The confirmation of *PfK13* R561H in Rwanda would have an important impact on the ART-R in Africa (Uwimana et al., 2020). Moreover, delayed clearance of ACTs has been reported among a few cases in Nigeria (Ajayi and Ukwaja, 2013; Wundermann and Osiki, 2017). Several mutations of *PfK13* have also been described in Nigerian isolates, including one non-synonymous mutation G665C discovered in southwestern Nigeria (Oboh et al., 2018), and six mutations (E433G, F434I, F434S, I684N, I684T, and E688K) identified in northern Nigeria, among which E433G and E688K were identified from isolates with the delayed clearance (Abubakar et al., 2020). The study performed in southwestern Nigeria in 2014 identified eight non-synonymous mutations in *PfK13*, including G496S, R539F, I543V, V566K, D584I, C580Y, and a deletion variant A557; the C580Y mutant was suspected by allelic discrimination in two samples with mixed genotypes (Tola et al., 2020). In this study, two non-synonymous mutations, S693F and Q613H, were identified in two isolates. However, none of these mutations detected in Nigerian isolates has been fully validated *in vivo* or *in vitro* for resistance to ART. Given the cases with delayed clearance to ACTs, and the fact that the *PfK13* C580Y mutation has been reported in Nigeria, urgent monitoring of the efficacy of antimalarial drugs is required to obtain an early warning signal, update the treatment policy and stop the spread of ACTs-resistance.

An increasing number of studies have shown that CQ sensitivity is recovered as a consequence of CQ withdrawal (Mwanza et al., 2016; Lu et al., 2017; Ndam et al., 2017). In Nigeria, CQ was replaced with ACTs in 2005 (FMoH, 2005). In this study, the prevalence of the *Pfcrt* mutation reduced from 72.2% in 2012 to 22.6% in 2019, and decreased steadily, and *significantly year-by-year* (**Figure 1A**). *The study of* Tola *et al.* reported that the prevalence of mutant *Pfcrt* (CVIET) was 45% in 2014 in southwestern Nigeria (Tola et al., 2020), and Lu *et al.* reported that the prevalence of *Pfcrt* 76T was 46.9% in Nigeria during 2011–2014 (Lu et al., 2017), and the prevalence of mutant *Pfcrt* was 41.9% in Nigeria during 2012–2015 in our published study (Zhou et al., 2016), the results of the three studies

TABLE 3 | Combination of the *Pfdhfr* and *Pfdhps* genes detected from *Plasmodium falciparum* isolates returned from Nigeria during 2012–2019.

Haplotypes	No. (%)
$I_{51}R_{59}N_{108}$- $V_{431}A_{436}G_{437}G_{581}S_{613}$	27 (17.0)
$I_{51}R_{59}N_{108}$- $V_{431}A_{436}G_{437}G_{581}$	2 (1.3)
$I_{51}R_{59}N_{108}$- $V_{431}A_{436}G_{437}S_{613}$	2 (1.3)
$I_{51}R_{59}N_{108}$- $V_{431}G_{437}G_{581}S_{613}$	1 (0.6)
$I_{51}R_{59}N_{108}$- $V_{431}A_{436}G_{437}$	6 (3.8)
$I_{51}R_{59}N_{108}$- $A_{436}G_{437}S_{613}$	9 (5.7)
$I_{51}R_{59}N_{108}$- $V_{431}G_{437}G_{581}$	1 (0.6)
$I_{51}R_{59}N_{108}$- $A_{436}G_{437}$	7 (4.4)
$I_{51}R_{59}N_{108}$- $F_{436}S_{613}$	4 (2.5)
$I_{51}R_{59}N_{108}$- $V_{431}A_{436}$	2 (1.3)
$I_{51}R_{59}N_{108}$- $G_{437}G_{581}$	2 (1.3)
$I_{51}R_{59}N_{108}$- A_{436}	11 (6.9)
$I_{51}R_{59}N_{108}L_{164}$- G_{437}	1 (0.6)
$I_{51}R_{59}N_{108}$- G_{437}	62 (39.0)
$I_{51}N_{108}$- $G_{424}G_{437}G_{581}$	1 (0.6)
$I_{51}N_{108}$- $A_{436}G_{437}$	2 (1.3)
$I_{51}N_{108}$- G_{437}	2 (1.3)
$R_{59}N_{108}$- G_{437}	2 (1.3)
$R_{59}N_{108}$- $A_{436}G_{437}$	2 (1.3)
$R_{59}N_{108}$- $V_{431}A_{436}G_{437}$	1 (0.6)
$R_{59}N_{108}$- $A_{436}G_{437}S_{613}$	1 (0.6)
$N_{108}R_{120}$- $A_{436}G_{437}S_{613}$	1 (0.6)
N_{108}- G_{437}	1 (0.6)
$I_{51}R_{59}N_{108}$	4 (2.5)
$V_{431}A_{436}G_{437}$	1 (0.6)
$A_{436}G_{437}S_{613}$	1 (0.6)
G_{437}	2 (1.3)
Wildtype	1 (0.6)

performed in Nigeria were similar. However, there are few recent data on the prevalence in Nigeria. In this study, the molecular monitoring of *Pfcrt* took place over an 8-year period, from 2012 to 2019, and provided sufficient information to observe the reversal of CQR in Nigeria. It is possible that the mutant prevalence of *Pfcrt* will reduce further, leading to full recovery of the sensitivity to CQ. Moreover, the dynamics of population genetics may also account for the recovered sensitivity of CQ, in that as the corresponding antimalarial drug is withdrawn, the wild type gene might segregate and increase in population.

Pfmdr1 gene is considered to be associated with the efficacy of multiple antimalarial drugs. Meanwhile, *Pfmdr1* and *Pfcrt* are assumed to be associated with resistance to ACT partner drugs, such as amodiaquine, lumefantrine, and mefloquine (Otienoburu et al., 2019). *Pfmdr1* has also been found to be closely associated with chloroquine resistance, especially between the *Pfmdr1* N86Y and *Pfcrt* K76T (Duraisingh and Cowman, 2005), and the prevalence of *Pfmdr1* 86Y reduced with the withdrawal of chloroquine (Gupta et al., 2018). Indeed, in this study, a significant decrease in the prevalence of *Pfmdr1* 86Y was observed from 38.9% in 2012 to 3.2% in 2019. The literature review also reported that the prevalence of *Pfmdr1* 86Y reduced significantly in all of the studied countries (Otienoburu et al., 2019), which was confirmed by the current study. The prevalence of *Pfmdr1* 184F was high in this study, at 63.3% during 2012–2019. The study performed in 2007–2008 showed that the frequency of 184F was 69.0% in Nigeria (Oladipo et al., 2015). Therefore, it can be considered that the prevalence of *Pfmdr1* 184F might be maintained at a certain level for a long time in Nigeria. The prevalence of *Pfmdr1* 86Y and 184F obtained from isolates imported from Angola was 11.7 and 30.9%, respectively, during 2012–2017 (Zhou et al., 2019). In Mozambique, the frequency of *Pfmdr1* 86Y and 184F was 3.1 and 46.7%, respectively, in 2015 (Gupta et al., 2018). In other countries, the prevalence of *Pfmdr1* 86Y has been shown to be lower, whereas that of *Pfmdr1* 184F has been found to vary considerably; these observations may be related to the medication strategy of individual countries.

Pfdhfr and *Pfdhps* were used to monitor resistance of SP, and the level of SP resistance was considered to be related to the number of combined mutations within the two genes. The level of resistance can be divided into three groups: the quadruple mutant, *Pfdhfr* $I_{51}R_{59}N_{108}$-*Pfdhps* G_{437}, is considered to be "partially resistant," the quintuple mutant, *Pfdhfr* $I_{51}R_{59}N_{108}$-*Pfdhps* $G_{437}E_{540}$, is considered to be "fully resistant," and the sextuple mutant, *Pfdhfr* $I_{51}R_{59}N_{108}$-$G_{437}E_{540}G_{581}/S_{613}$, is considered to be "super resistant" (Naidoo et al., 2013). In this study, *Pfdhfr* $I_{51}R_{59}N_{108}$ was very common (88.1%); meanwhile, the *Pfdhps* gene had 15 haplotypes, among which the single mutant G_{437} had the highest prevalence, followed by the quintuple mutant $V_{431}A_{436}G_{437}G_{581}S_{613}$. No *Pfdhps* K540E mutants were found. The combined mutants of the two genes showed that the quadruple mutant, *Pfdhfr* $I_{51}R_{59}N_{108}$-*Pfdhps* G_{437}, was common (39.0%) and classified as "partially resistant." Because the *Pfdhps* K540E mutant was not identified in this study, the quintuple mutant *Pfdhfr* $I_{51}R_{59}N_{108}$-*Pfdhps* $G_{437}E_{540}$ was not identified. However, 17.0% of isolates in Nigeria comprised the octal mutant *Pfdhfr* $I_{51}R_{59}N_{108}$-*Pfdhps* $V_{431}A_{436}G_{437}G_{581}S_{613}$. Moreover, the *Pfdhps* I431V mutant was discovered recently and it has been identified in Nigeria, Cameroon, and Equatorial Guinea (Chauvin et al., 2015; Oguike et al., 2016). It has also been reported that the prevalence of *Pfdhps* 431V is 8.3, 16.7, and 6.3% in Nigeria, Cameroon, and Equatorial Guinea, respectively (Xu et al., 2019). However, the frequency of *Pfdhps* 431V reached 27.0% in this study. *Pfdhps* 431V has always been found together with other mutants, among which *Pfdhps* $V_{431}A_{436}G_{437}G_{581}S_{613}$ was the most common. The effects of *Pfdhps* 431V on SP resistance need further study. Although no data were obtained from pregnant women or children, our findings provide supplementary information for SP resistance in Nigeria. It is necessary to monitor SP resistance continuously using the two genes to guide the IPT strategy.

There are some limitations to this study. First, the samples were passively obtained from migrants returning from Nigeria; thus, the sampling was not planned, and the sample size was not controlled. Second, the exact information about which part of Nigeria these individuals worked/lived in was unavailable. Third, although the individuals were all cured, detailed information about the treatment process and the use of antimalarial drugs was not incomplete. Fourth, the individuals were almost all Chinese people who returned from Nigeria with malaria; therefore, the prevalence of mutations among them might differ from those among native Nigerians.

This study evaluated polymorphisms and prevalence of antimalarial drug-resistance genes in imported *P. falciparum* cases from Nigeria to Henan Province, China. The mutation of *Pf K13*, associated with ACTs, was rare, and no validated mutation was found. The prevalence of *Pfcrt* and *Pfmdr1* mutants

associated with the resistance of ACT partner drugs reduced gradually. Moreover, the prevalence of *Pfdhfr* and *Pfdhps* mutations was high. At present, ACTs are still effective for those returning from Nigeria with *P. falciparum* malaria infected in Henan Province. However, the validated *PfK13* R561H mutation recently observed in Rwanda has substantial implications for ART-R in Africa (Uwimana et al., 2020). The routine molecular surveillance of antimalarial drugs is more important and imperative for the imported malaria cases, especially those from Africa, and will be helpful to rationalize drug guidance for local authorities in China.

DATA AVAILABILITY STATEMENT

The raw data supporting the conclusions of this article will be made available by the authors, without undue reservation.

ETHICS STATEMENT

The studies involving human participants were reviewed and approved by the Ethical Committee of Henan Province Center for Disease Control and Prevention. The patients/participants provided their written informed consent to participate in this study.

AUTHOR CONTRIBUTIONS

DZ, RZ, and YZ conceived and designed the study. HZ, SL, and CY performed the experiments. DZ was responsible for the data analysis and drafted the manuscript. SL and YL participated in the sample collection. PJ and DQ contributed to the data collection. RZ and YZ revised the manuscript. YD, HW, and DL provided the administrative coordination. All authors contributed to the article and approved the submitted version.

FUNDING

The study was supported by Science and Technology Project of Henan Province (**No.** 182102310631) and Henan Provincial Medical Science and Technology Project (**No.** 2018020515, **No.** 2018020509). The funders had no role in study design, data collection and analysis, decision to publish, or preparation of the manuscript.

ACKNOWLEDGMENTS

We would like to thank all the patients who participated in this study and the staff of the hospitals and centers for disease control and prevention in Henan Province.

SUPPLEMENTARY MATERIAL

The Supplementary Material for this article can be found online at: https://www.frontiersin.org/articles/10.3389/fcimb.2021.644576/full#supplementary-material

REFERENCES

Abubakar, U. F., Adam, R., Mukhtar, M. M., Muhammad, A., Yahuza, A. A., and Ibrahim, S. S. (2020). Identification of Mutations in Antimalarial Resistance Gene Kelch13 From Plasmodium Falciparum Isolates in Kano, Nigeria. *Trop. Med. Infect. Dis.* 5 (2), 85. doi: 10.3390/tropicalmed5020085

Ajayi, N. A., and Ukwaja, K. N. (2013). Possible Artemisinin-Based Combination Therapy-Resistant Malaria in Nigeria: A Report of Three Cases. *Rev. Da Sociedade Bras. Medicina Tropical.* 46 (4), 525–527. doi: 10.1590/0037-8682-0098-2013

Ariey, F., Witkowski, B., Amaratunga, C., Beghain, J., Langlois, A.-C., Khim, N., et al. (2014). A Molecular Marker of Artemisinin-Resistant Plasmodium Falciparum Malaria. *Nature* 505 (7481), 50–55. doi: 10.1038/nature12876

Campbell, C. C., Chin, W., Collins, W. E., Teutsch, S. M., and Moss, D. M. (1979). Chloroquine-Resistant *Plasmodium Falciparum* From East Africa: Cultivation and Drug Sensitivity of the Tanzanian I/CDC Strain From an American Tourist. *Lancet* 2 (8153), 1151–1154. doi: 10.1016/s0140-6736(79)92383-3

Chauvin, P., Menard, S., Iriart, X., Nsango, S. E., Tchioffo, M. T., Abate, L., et al. (2015). Prevalence of Plasmodium Falciparum Parasites Resistant to Sulfadoxine/Pyrimethamine in Pregnant Women in Yaoundé, Cameroon: Emergence of Highly Resistant Pfdhfr/ Pfdhps Alleles. *J. Antimicrob. Chemother.* 70 (9), 2566–2571. doi: 10.1093/jac/dkv160

Dondorp, A. M., Nosten, F., Yi, P., Das, D., Phyo, A. P., Tarning, J., et al. (2009). Artemisinin Resistance in *Plasmodium Falciparum* Malaria. *N Engl. J. Med.* 361 (5), 455–467. doi: 10.1056/NEJMoa0808859

Duraisingh, M. T., and Cowman, A. F. (2005). Contribution of the Pfmdr1 Gene to Antimalarial Drug-Resistance. *Acta Trop.* 94, 181–190. doi: 10.1016/j.actatropica.2005.04.008

Flegg, J. A., Metcalf, C. J. E., Gharbi, M., Venkatesan, M., Shewchuk, T., Sibley, C. H., et al. (2013). Trends in Antimalatial Drug Use in Africa. *Am. J. Trop. Med. Hyg.* 89 (5), 857–865. doi: 10.4269/ajtmh.13-0129

FMoH (2005). *National Antimalarial Treatment Guidelines Policy Federal Ministry of Health, National Malaria and Vector Control Division* (Abuja-Nigeria, Nigeria: Federal Ministry of Health).

Gosling, R. D., Gesase, S., Mosha, J. F., Carneiro, I., Hashim, R., Lemnge, M., et al. (2009). Protective Efficacy and Safety of Three Antimalarial Regimens for Intermittent Preventive Treatment for Malaria in Infants: A Randomised, Double-Blind, Placebo-Controlled Trial. *Lancet* 374 (9700), 1521–1532. doi: 10.1016/S0140-6736(09)60997-1

Gupta, H., Macete, E., Bulo, H., Salvador, C., Warsame, M., Carvalho, E., et al. (2018). Drug-Resistant Polymorphisms and Copy Numbers in Plasmodium Falciparum, Mozambiqu. *Emerg. Infect. Dis.* 24 (1), 40–48. doi: 10.3201/eid2401.170864

Humphreys, G. S., Merinopoulos, I., Ahmed, J., Whitty, C. J. M., Mutabingwa, T. K., Sutherland, C. J., et al. (2007). Amodiaquine and Artemether-Lumefantrine Select Distinct Alleles of the Plasmodium Falciparum Mdr1 Gene in Tanzanian Children Treated for Uncomplicated Malaria. *Antimicrob. Agents Chemother.* 51 (3), 991–997. doi: 10.1128/AAC.00875-06

Kamugisha, E., Jing, S., Minde, M., Kataraihya, J., Kongola, G., Kironde, F., et al. (2012). Efficacy of Artemether-Lumefantrine in Treatment of Malaria Among Under-Fives and Prevalence of Drug Resistance Markers in Igombe-Mwanza, North-Western Tanzania. *Malaria J.* 11, 58. doi: 10.1186/1475-2875-11-58

Liu, Y., Zhou, R., Qian, D., Yang, C., and Zhang, H. (2014). Analysis of Malaria Epidemiological Characteristics in Henan Province From 2005 to 2013. *Zhongguo Ji Sheng Chong Xue Yu Ji Sheng Chong Bing Za Zhi* 32, 419–422. (in Chinese).

Lu, F., Zhang, M., Culleton, R. L., Xu, S., Tang, J., Zhou, H., et al. (2017). Return of Chloroquine Sensitivity to Africa? Surveillance of African Plasmodium

Falciparum Chloroquine Resistance Through Malaria Imported to China. *Parasites Vectors* 10 (1), 355. doi: 10.1186/s13071-017-2298-y

McCollum, A. M., Poe, A. C., Hamel, M., Huber, C., Zhou, Z., Shi, Y. P., et al. (2006). Antifolate Resistance in Plasmodium Falciparum: Multiple Origins and Identification of Novel Dhfr Alleles. *J. Infect. Dis.* 194 (2), 189–197. doi: 10.1086/504687

Mehlotra, R. K., Fujioka, H., Roepe, P. D., Janneh, O., Ursos, L. M., Jacobs-Lorena, V., et al. (2001). Evolution of a Unique *Plasmodium Falciparum* Chloroquine-Resistance Phenotype in Association With *Pfcrt* Polymorphism in Papua New Guinea and South America. *Proc. Natl. Acad. Sci. U. S. A.* 98 (22), 12689–12694. doi: 10.1073/pnas.221440898

Ménard, D., Khim, N., Beghain, J., Adegnika, A. A., Shafiul-Alam, M., Amodu, O., et al. (2016). A Worldwide Map of Plasmodium Falciparum K13-Propeller Polymorphisms. *N Engl. J. Med.* 374 (25), 2453–2464. doi: 10.1056/NEJMoa1513137

Mwanza, S., Joshi, S., Nambozi, M., Chileshe, J., Malunga, P., Kabuya, J.-B., et al. (2016). The Return of Chloroquine-Susceptible Plasmodium Falciparum Malaria in Zambia. *Malar. J.* 15 (1), 584. doi: 10.1186/s12936-016-1637-3

Naidoo, I., and Roper, C. (2013). Mapping 'Partially Resistant', 'Fully Resistant', and 'Super Resistant' Malaria. *Trends Parasitol.* 29 (10), 505–515. doi: 10.1016/j.pt.2013.08.002

Nankabirwa, J., Cundill, B., Clarke, S., Kabatereine, N., Rosenthal, P. J., Dorsey, G., et al. (2010). Efficacy, Safety, and Tolerability of Three Regimens for Prevention of Malaria: A Randomized, Placebo-Controlled Trial in Ugandan Schoolchildren. *PloS One* 5 (10), e13438. doi: 10.1371/journal.pone.0013438

National Population Commission (NPC) [Nigeria] and ICF (2019). *The 2018 Nigeria Demographic and Health Survey Key Findings* (Abuja, Nigeria and Rockville, Maryland, USA: NPC and ICF).

Ndam, N. T., Basco, L. K., Ngane, V. F., Ayouba, A., Ngolle, E. M., Deloron, P., et al. (2017). Reemergence of Chloroquine-Sensitive Pfcrt K76 Plasmodium Falciparum Genotype in Southeastern Cameroon. *Malar. J.* 16 (1), 130. doi: 10.1186/s12936-017-1783-2

Noedl, H., Se, Y., Schaecher, K., Smith, B. L., Socheat, D., and Fukuda, M. M. (2008). Evidence of Artemisinin-Resistant Malaria in Western Cambodia. *N Engl. J. Med.* 359 (24), 2619–2620. doi: 10.1056/NEJMc0805011

Nuwaha, F. (2001). The Challenge of Chloroquine-Resistant Malaria in Sub-Saharan Africa. *Health Policy Plann.* 16 (1), 1–12. doi: 10.1093/heapol/16.1.1

Oboh, M. A., Ndiaye, D., Antony, H. A., Badiane, A. S., Singh, U., Ali, N. A., et al. (2018). Status of Artemisinin Resistance in Malaria Parasite Plasmodium Falciparum From Molecular Analyses of the Kelch13 Gene in Southwestern Nigeria. *BioMed. Res. Int.* 2018, 2305062. doi: 10.1155/2018/2305062

Oguike, M. C., Falade, C. O., Shu, E., Enato, I. G., Watila, I., Baba, E. S., et al. (2016). Molecular Determinants of Sulfadoxinepyrimethamine Resistance in Plasmodium Falciparum in Nigeria and the Regional Emergence of Dhps 431V. *Int. J. Parasitol. Drugs Drug Resist.* 6 (3), 220–229. doi: 10.1016/j.ijpddr.2016.08.004

Oladipo, O. O., Wellington, O. A., and Sutherland, C. J. (2015). Persistence of Chloroquine-Resistant Haplotypes of Plasmodium Falciparum in Children With Uncomplicated Malaria in Lagos, Nigeria, Four Years After Change of Chloroquine as First-Line Antimalarial Medicine. *Diagn. Pathol.* 10, 41. doi: 10.1186/s13000-015-0276-2

Otienoburu, S. D., Suay, I., Garcia, S., Thomas, N. V., Srisutham, S., Björkman, A., et al. (2019). An Online Mapping Database of Molecular Markers of Drug Resistance in Plasmodium Falciparum: The ACT Partner Drug Molecular Surveyor. *Malar. J.* 18 (1), 12. doi: 10.1186/s12936-019-2645-x

Picot, S., Olliaro, P., de Monbrison, F., Bienvenu, A.-L., Price, R. N., and Ringwald, P. (2009). A Systematic Review and Meta-Analysis of Evidence for Correlation Between Molecular Markers of Parasite Resistance and Treatment Outcome in Falciparum Malaria. *Malar. J.* 8, 89. doi: 10.1186/1475-2875-8-89

Ridley, R. G. (2002). Medical Need, Scientific Opportunity and the Drive for Antimalarial Drugs. *Nature* 415 (6872), 686–693. doi: 10.1038/415686a

Ross, L. S., Dhingra, S. K., Mok, S., Yeo, T., Wicht, K. J., Kümpornsin, K., et al. (2018). Emerging Southeast Asian Pfcrt Mutations Confer Plasmodium Falciparum Resistance to the First-Line Antimalarial Piperaquine. *Nat. Commun.* 9 (1), 3314. doi: 10.1038/s41467-018-05652-0

Sá, J. M., Twu, O., Hayton, K., Reyes, S., Fay, M. P., Ringwald, P., et al. (2009). Geographic Patterns of Plasmodium Falciparum Drug Resistance Distinguished by Differential Responses to Amodiaquine and Chloroquine. *Proc. Natl. Acad. Sci. U. S. A.* 106 (45), 18883–18889. doi: 10.1073/pnas.0911317106

Sisowath, C., Petersen, I., Veiga, M. I., Mårtensson, A., Premji, Z., Björkman, A., et al. (2009). In Vivo Selection of Plasmodium Falciparum Parasites Carrying the Chloroquine-Susceptible Pfcrt K76 Allele After Treatment With Artemether-Lumefantrine in Africa. *J. Infect. Dis.* 199 (5), 750–757. doi: 10.1086/596738

Somé, A. F., Seré, Y. Y., Dokomajilar, C., Zongo, I., Rouamba, N., Greenhouse, B., et al. (2010). Selection of Known Plasmodium Falciparum Resistance-Mediating Polymorphisms by Artemether-Lumefantrine and Amodiaquine-Sulfadoxine-Pyrimethamine But Not Dihydroartemisinin-Piperaquine in Burkina Faso. *Antimicrob. Agents Chemother.* 54 (5), 1949–1954. doi: 10.1128/AAC.01413-09

Sowunmi, A., Akano, K., Ntadom, G., Ayede, A. I., Ibironke, F. O., Aderoyeje, T., et al. (2017). Therapeutic Efficacy and Effects of Artemisinin-Based Combination Treatments on Uncomplicated Plasmodium Falciparum Malaria-Associated Anaemia in Nigerian Children During Seven Years of Adoption as First-Line Treatments. *Infect. Dis. Poverty* 6 (1), 36. doi: 10.1186/s40249-016-0217-7

Taylor, S. M., Parobek, C. M., DeConti, D. K., Kayentao, K., Coulibaly, S. O., Greenwood, B. M., et al. (2014). Absence of Putative Artemisinin Resistance Mutations Among Plasmodium Falciparum in Sub-Saharan Africa: A Molecular Epidemiologic Study. *J. Infect. Dis.* 211 (5), 680–688. doi: 10.1093/infdis/jiu467

Tola, M., Ajibola, O., Idowu, E. T., Omidiji, O., Awolola, S. T., and Amambua-Ngwa, A. (2020). Molecular Detection of Drug Resistant Polymorphisms in Plasmodium Falciparum Isolates From Southwest, Nigeria. *BMC Res. Notes* 13 (1), 497. doi: 10.1186/s13104-020-05334-5

Uwimana, A., Legrand, E., Stokes, B. H., Ndikumana, J. M., Warsame, M., Umulisa, N., et al. (2020). Emergence and Clonal Expansion of In Vitro Artemisinin-Resistant Plasmodium Falciparum Kelch13 R561H Mutant Parasites in Rwanda. *Nat. Med.* 26, 1602–1608. doi: 10.1038/s41591-020-1005-2

Vinayak, S., Alam, M. T., Mixson-Hayden, T., McCollum, A. M., Sem, R., Shah, N. K., et al. (2010). Origin and Evolution of Sulfadoxine Resistant Plasmodium Falciparum. *PloS Pathog.* 6 (3), e1000830. doi: 10.1371/journal.ppat.1000830

World Health Organization (2010). *Global Report on Antimalarial Drug Efficacy and Drug Resistance: 2000-2010*. Available at: https://www.who.int/publications/i/item/9789241500470.

World Health Organization (2015). *Guidelines for the Treatment of Malaria. 3rd ed* (WHO).

World Health Organization (2018). *Artemisinin Resistance and Artemisininbased Combination Therapy Efficacy*. Available at: https://www.who.int/publications/i/item/status-report-on-artemisinin-resistance-and-act-efficacy.

World Health Organization (2018). *World Malaria Report 2017*. Available at: https://www.who.int/publications/i/item/9789241565523.

World Health Organization (2019). *Artemisinin Resistance and Artemisinin-Based Combination Therapy Efficacy*. Available at: https://www.who.int/publications/i/item/status-report-on-artemisinin-resistance-and-act-efficacy.

World Health Organization (2020). *World Malaria Report 2020*. Available at: https://www.who.int/publications/i/item/9789240015791.

Wundermann, G., and Osiki, A. (2017). Currently Observed Trend in the Resistance of Malaria to Artemisinin Based Combination Therapy in Nigeria – a Report of 5 Cases. *Int. J. Trop. Dis. Health* 21 (2), 1–5. doi: 10.9734/IJTDH/2017/30914

Xu, C., Sun, H., Wei, Q., Li, J., Xiao, T., Kong, X., et al. (2019). Mutation Profile of Pfdhfr and Pfdhps in Plasmodium Falciparum Among Returned Chinese Migrant Workers From Africa. *Antimicrob. Agents Chemother.* 63 (5), e01927–e01918. doi: 10.1128/AAC.01927-18

Yeung, S., Socheat, D., Moorthy, V. S., and Mills, A. J. (2009). Artemisinin Resistance on the Thai–Cambodian Border. *Lancet* 374 (9699), 1418–1419. doi: 10.1016/S0140-6736(09)61856-0

Yin, J., Yan, H., Huang, F., Li, M., Xiao, H., Zhou, S., et al. (2015). Establishing a China Malaria Diagnosis Reference Laboratory Network for Malaria Elimination. *Malar. J.* 14, 40. doi: 10.1186/s12936-015-0556-z

Zhang, L., Feng, J., Zhang, S., Xia, Z., and Zhou, S. (2018). The Progress of National Malaria Elimination and Epidemiological Characteristics of Malaria in China in 2017. *Zhongguo Ji Sheng Chong Xue Yu Ji Sheng Chong Bing Za Zhi* 36, 201–209. (in Chinese).

Zhou, R., Yang, C., Li, S., Zhao, Y., Liu, Y., Qian, D., et al. (2019). Molecular Surveillance of Drug Resistance of Plasmodium Falciparum Isolates Imported From Angola in Henan Province, China. *Antimicrob. Agents Chemother.* 63 (10), e00552–e00519. doi: 10.1128/AAC.00552-19

Zhou, R., Zhang, H., Yang, C., Liu, Y., Zhao, Y., Li, S., et al. (2016). Molecular Mutation Profile of Pfcrt in Plasmodium Falciparum Isolates Imported From Africa in Henan Province. *Malar. J.* 15 (1), 265. doi: 10.1186/s12936-016-1306-6

Conflict of Interest: The authors declare that the research was conducted in the absence of any commercial or financial relationships that could be construed as a potential conflict of interest.

frontiers in Cellular and Infection Microbiology

ORIGINAL RESEARCH
published: 17 May 2021
doi: 10.3389/fcimb.2021.673966

In Vivo and *In Vitro* Genome-Wide Profiling of RNA Secondary Structures Reveals Key Regulatory Features in *Plasmodium falciparum*

Yanwei Qi[1†], Yuhong Zhang[1†], Guixing Zheng[2], Bingxia Chen[3], Mengxin Zhang[3], Jian Li[4], Tao Peng[5], Jun Huang[1] and Xinhua Wang[6*]*

[1] Department of Pathogenic Biology and Immunology, School of Basic Medical Sciences, Guangzhou Medical University, Guangzhou, China, [2] Department of Blood Transfusion, The First Affiliated Hospital of Guangzhou Medical University, Guangzhou Medical University, Guangzhou, China, [3] The Third Clinical School, Guangzhou Medical University, Guangzhou, China, [4] State Key Laboratory of Cellular Stress Biology, Innovation Center for Cell Signaling Network, School of Life Sciences, Xiamen University, Xiamen, China, [5] Sino-French Hoffmann Institute, State Key Laboratory of Respiratory Disease, School of Basic Medical Science, Guangzhou Medical University, Guangzhou, China, [6] The First Affiliated Hospital of Guangzhou Medical University, Guangzhou Medical University, Guangzhou, China

OPEN ACCESS

Edited by:
Xiaojun Chen,
Nanjing Medical University,
China

Reviewed by:
Lubin Jiang,
Institut Pasteur of Shanghai,
Chinese Academy of Sciences
(CAS), China
Fangli Lu,
Sun Yat-Sen University,
China

***Correspondence:**
Yanwei Qi
qiyanwei@gzhmu.edu.cn
Xinhua Wang
xinhuaw@gzhmu.edu.cn

[†]These authors have contributed
equally to this work

Specialty section:
This article was submitted to
Parasite and Host,
a section of the journal
Frontiers in Cellular
and Infection Microbiology

Received: 28 February 2021
Accepted: 26 April 2021
Published: 17 May 2021

Citation:
Qi Y, Zhang Y, Zheng G,
Chen B, Zhang M, Li J,
Peng T, Huang J and Wang X (2021)
In Vivo and In Vitro Genome-Wide
Profiling of RNA Secondary Structures
Reveals Key Regulatory Features
in Plasmodium falciparum.
Front. Cell. Infect. Microbiol. 11:673966.
doi: 10.3389/fcimb.2021.673966

It is widely accepted that the structure of RNA plays important roles in a number of biological processes, such as polyadenylation, splicing, and catalytic functions. Dynamic changes in RNA structure are able to regulate the gene expression programme and can be used as a highly specific and subtle mechanism for governing cellular processes. However, the nature of most RNA secondary structures in *Plasmodium falciparum* has not been determined. To investigate the genome-wide RNA secondary structural features at single-nucleotide resolution in *P. falciparum*, we applied a novel high-throughput method utilizing the chemical modification of RNA structures to characterize these structures. Structural data from parasites are in close agreement with the known 18S ribosomal RNA secondary structures of *P. falciparum* and can help to predict the *in vivo* RNA secondary structure of a total of 3,396 transcripts in the ring-stage and trophozoite-stage developmental cycles. By parallel analysis of RNA structures *in vivo* and *in vitro* during the *Plasmodium* parasite ring-stage and trophozoite-stage intraerythrocytic developmental cycles, we identified some key regulatory features. Recent studies have established that the RNA structure is a ubiquitous and fundamental regulator of gene expression. Our study indicate that there is a critical connection between RNA secondary structure and mRNA abundance during the complex biological programme of *P. falciparum*. This work presents a useful framework and important results, which may facilitate further research investigating the interactions between RNA secondary structure and the complex biological programme in *P. falciparum*. The RNA secondary structure characterized in this study has potential applications and important implications regarding the identification of RNA structural elements, which are important for parasite infection and elucidating host-parasite interactions and parasites in the environment.

Keywords: *Plasmodium falciparum*, RNA secondary structure, *in vivo*, *in vitro*, mRNA

INTRODUCTION

RNA, a multitasking biomolecule, plays important roles in many aspects of cellular and physiological processes, such as the regulation of transcription, RNA processing and stability including splicing events, and translation (Wan et al., 2011; Mortimer et al., 2014). As the carrier of genetic information for translation into proteins, RNA molecules can fold into a wide array of complicated and exquisite secondary and tertiary structures *via* complex patterns of intramolecular base pairing formed by Watson-Crick-base pairing (Vandivier et al., 2016). These complex secondary and tertiary structures of RNAs play important roles in regulating such processes as catalytic and ligand sensing, the regulation of mRNA maturation, translation and turnover, alternative polyadenylation and alternative splicing (Ding et al., 2014).

Due to the multiple functions of RNA structural elements changed by base pairing and folding, they can be considered another layer of the genetic code that is only beginning to be understood (Bevilacqua et al., 2016). Characterizing these complex global RNA structures, especially *in vivo*, is essential to achieve a mechanistic understanding of the function and regulation of RNA transcripts. However, it remains challenging to understand the role and mechanism of mRNA secondary structure-based regulation, especially the long-standing challenges in RNA structure modelling. Although structural studies can examine global patterns of RNA structures in a single sample, these RNA structures are not static *in vivo*. At the same time, RNA structure can be refolded by RNA binding proteins or have posttranscriptional covalent modifications that result in drastic changes in secondary structure in response to changes in the prevailing physicochemical environment of the cell and the effects of various stimuli (Vandivier et al., 2016). These studies may help to identify additional temperature sensors (RNA thermometers), enzymes (ribozymes), ligand-binding sensors (riboswitches) or other environmentally responsive structural elements in various organisms, although not in *Plasmodium* parasites.

Investigation of RNA secondary structures associated with specific biological events is therefore essential to understanding the functions and roles of these RNA molecules. The secondary structure of RNA is relatively stable and is present across the length of an mRNA, including the CDS and UTRs (Mignone et al., 2002). A number of studies using global RNA structure-probing approaches have explored the RNA structurome in different species, such as mouse cell lines (Spitale et al., 2015), yeast (Kertesz, 2010; Talkish et al., 2014), human cells (Wan et al., 2014), *Arabidopsis thaliana* (Zheng et al., 2010; Li et al., 2012b; Ding et al., 2014; Incarnato et al., 2014), *Drosophila melanogaster* and *Caenorhabditis elegans* (Li et al., 2012a), zebrafish (Kaushik et al., 2018), *Yersinia pseudotuberculosis* (Righetti et al., 2016), and, recently *Oryza sativa* (Su et al., 2018). However, a comprehensive whole-genome analysis of RNA secondary structures has not been obtained for *Plasmodium* parasites. Furthermore, a thorough analysis of secondary structure correlations between different developmental stages has never been accomplished. In this study, we applied the novel biochemical approach icSHAPE which, to the best of our knowledge, enables the first global view of RNA secondary structures in the major human pathogen *Plasmodium falciparum* for all four bases *in vivo* and *in vitro* at the ring stage and trophozoite stage of parasite development.

Malaria is caused by any one of five species of protozoan parasites, namely, *P. falciparum*, *P. vivax*, *P. malariae*, *P. ovale*, and *P. knowlesi*, and is one of the most important tropical parasitic diseases with high morbidity and mortality rates, especially in many developing countries. In 2019, approximately 229 millions cases of malaria and 409,000 deaths were reported in endemic countries each year, especially in the sub-Saharan African region (World Health Organization, 2020). Various measures have been employed to control the disease, including vector control, bed-nets, and chemotherapy, but these methods have achieved only limited success (Choi et al., 2019). Given the lack of effective vaccines, the widespread resistance to anti-malaria drugs in current use (Capela et al., 2019), and poorly understood molecular mechanisms, it has become an urgently important to identify and develop new effective strategies to control malaria.

The major strength of this study is that it explained the landscape of the RNA secondary structure associated with parasite development at single-nucleotide resolution. Our analysis profiled the structure of more than 3,396 (*in vivo*) and 2,024 (*in vitro*) transcripts in the ring-stage and trophozoite-stage developmental cycles. In this study, we showed that (1) RNA secondary structures in *P. falciparum* have common characteristics similar to those of other diverse organisms, such as UTR regions, CDS regions, noncoding RNAs, and malaria mitochondrion. (2) Structural changes are dramatically different in the ring and trophozoite stages but less pronounced in the ring stage than in the trophozoite stage. (3) Comparing the *in vivo* and *in vitro* structures indicates the important role of RNA-binding protein (RBP) in structure formation. (4) Combined with transcriptome data, RNA secondary structure changes were significantly associated with transcriptome changes. Therefore, our results make it possible to obtain a framework for understanding how malaria parasites develop through changes in RNA structure *in vivo* and potential use for further investigations. Our results imply that there is a critical connection between the RNA secondary structure and the complex biological programme of *Plasmodium falciparum*, but the mechanism governing this process needs to be further elucidated.

MATERIALS AND METHODS

Parasite Culture and Synchronized

The *P. falciparum* strain 3D7 was cultured in human O^+ erythrocytes at 5% hematocrit under standard *in vitro* conditions as previously described (Trager and Jensen, 1976). Cultures were synchronized twice at ring stage with 5% D-sorbitol treatments performed 8 hours apart (Lambros and Vanderberg, 1979). The cultures were expanded to accommodate harvesting of at least 200 mL of culture at each planned time-point. Cultures (~8% parasitemia in 5% hematocrit) were harvested 48 hours (ring stage) and 72 hours (trophozoite stage) after the first sorbitol

treatment. Next, the cells were harvested at 2000 rpm for 3 min to obtain packed RBCs. The packed RBCs were lysed by a 0.05% saponin solution, and parasite pellets were washed twice using phosphate-buffered saline (pH 7.4). The remaining pellets were used for icSHAPE library construction, and total RNA was extracted directly, or conversely, parasites were stored in 10 mL of TRIzol reagent at −80°C prior to RNA extraction.

In Vivo and *In Vitro* NAI-N_3 Chemical Probing and RNA Sample Extraction

For *in vivo* NAI-N_3 modification of parasite RNAs, the washed parasites pellets were treated as described previously (Flynn et al., 2016) before total RNA extraction. The parasites pellets were equally divided into three parts, one part for NAI-N_3 *in vivo* modification and the two other parts for the DMSO control. NAI-N_3 concentration/times were chosen as in our experiment described in the following section to provide a similar overall level of modification for samples *in vivo*. Briefly, almost all PBS was removed from the pelleted parasite, the parasite pellet was resuspended in 200 μl of 100 mM NAI-N_3 solution or 200 μl of DMSO solution, and the suspension was immediately mixed by inversion and incubated at 37°C with end-over-end rotation for 15 min. Before use, the 100 mM NAI-N_3 was thawed completely to 37°C. The reaction was stopped by quickly placing the pellets on ice and collecting them by centrifugation at 14,000 g at 4°C for 30 s. Next, the supernatants were removed, and the pellets were transferred to 15-ml tubes and resuspended in 10 ml of prewarmed TRIzol Reagent. Total RNA was isolated as recommended by the manufacturer's protocol followed by phenol/chloroform extraction and ethanol precipitation. The RNA yield was measured using a Nanodrop spectrophotometer, and RNA quality was assessed by 1% agarose gel analysis. We ensured that clear 18S and 28S rRNA bands were present. We needed to construct total RNA/polyA-selected RNA *in vivo* SHAPE RNA libraries. In this study, polyA mRNA was obtained using the NEBNext® Poly-A mRNA Magnetic Isolation Module (NEB).

For *in vitro* NAI-N_3 probing, we also needed to construct total RNA/ribosomal *in vitro* SHAPE RNA libraries. For total RNA/ribosomal *in vitro* SHAPE RNA libraries, no additional processing was needed. For polyA-selected *in vitro* SHAPE libraries, polyA selection was performed first using polyT oligomagnetic beads before NAI-N_3 *in vitro* modification was undertaken. Heat-denatured total RNA or polyA+ RNA samples were obtained from DMSO-treated pellets at 95°C for 2 min and were later transferred to ice to cool. The NAI-N_3 final concentration and times for *in vitro* modification were 100 mM and 37°C for 10 min. The reactions were stopped by moving the samples to ice, and the samples were purified using a Zymo RNA Clean & Concentrator-5 column according to the manufacturer's protocol.

Quantification of Modifications by Primer Extension and Resolution by Capillary Electrophoresis

Incubation time and NAI-N_3 concentration can strongly affect single-hit kinetics; therefore, we focused on optimizing these two parameters, although it is possible that other factors, such as temperature and buffer conditions, could also affect these kinetics (Ding et al., 2015). We took a time course (5 min, 10 min, 15 min and 30 min) of *in vivo* NAI-N_3 modification as an example for a region of 18S rRNA in *P. falciparum* by capillary electrophoresis for at least three times. Seven micrograms of total RNA (non-polyA-selected) was treated with DNase (NEB) to remove residual genomic DNA in the RNA sample. Next, the DNA-free total RNA was reverse-transcribed using SuperScript III (Invitrogen) by a colour-coded fluorescently FAM-labelled oligonucleotide in the 271-bp-293-bp region of the 18S rRNA gene. The PCR programme was as follows: samples were heated to 65°C for 5 min, maintained on ice for at least 2 min, and incubated at 50°C for 1 h followed by 95°C for 5 min, and the samples were maintained at 4°C after the reaction ended. The reverse-transcribed cDNA products were electrophoresed using an ABI 3730XL DNA Sequencer. The results were presented by GeneMarker (V2.7.0, SoftGenetics, LLC.)

Determination of Fragmentation Time by Primer Extension Electropherograms

Total RNA was extracted from parasite lysates without any chemical reagent modification. In a 20-μL reaction, ~2 μg of total RNA was fragmented using RNA fragmentation reagents (Ambion) for the proper time at 70°C. After the end of the experiment, 10× stop solution was added to each sample, and the samples were immediately placed on ice. Next, fragmented RNA was purified with a Zymo RNA Clean & Concentrator-5 column. The purified fragmented RNA was reverse-transcribed by primer extension with gene-specific colour-coded fluorescently FAM-labelled oligonucleotides (5'-ACCCTAACATCAAAAGCT GATAGG-3'), as described above. The length of every fragment was assessed using an ABI 3730XL DNA Sequencer (Applied Biosystems). The results were shown by GeneMarker (V2.7.0, SoftGenetics, LLC.).

RNA-Seq Illumina Library Construction

For RNA-seq library construction, the NEBNext Ultra Directional RNA Library Prep Kit (NEB) was used to prepare a validated strand-specific, polyA-selected RNA sequencing library according to the manufacturer's instructions in the kit. Briefly, mRNA was purified from 3 μg of total RNA using the Poly(A) mRNA Magnetic Isolation Module. Fragmentation was carried out at 94°C for 7 min in NEBNext First Strand Synthesis Reaction Buffer. First strand cDNA was synthesized using random primers and ProtoScript II Reverse Transcriptase (with 0.1 μg/μl actinomycin D and murine RNase inhibitor). Second strand cDNA was synthesized using Second Strand Synthesis Enzyme Mix and incubated at 16°C for 1 h. Next, the double-stranded cDNA was purified using 1.8X Agencourt AMPure XP Beads. End prep of a cDNA library was performed by NEBNext End Prep Enzyme Mix at 20°C for 30 min followed by 65°C for 30 min. NEBNext adaptors were ligated to the cDNAs with the function of Blunt/TA Ligase Master Mix at 20°C for 15 min, and fragments measuring 150–200 bp were purified

using AMPure XP beads. The samples were later treated with 3 μl NEBNext USER Enzyme at 37°C for 15 min before PCR amplification. Library amplification was performed using NEBNext Q5 Hot Start HiFi PCR Master Mix, NEBNext Universal PCR Primer for Illumina, and Index (X) Primer. The primer and oligonucleotide sequences used in the experiment are shown in **Supplementary Table 1**. The PCR machine was programmed as follows: initial denaturation at 98°C for 30 s, denaturation at 98°C for 10 s and annealing/extension at 65°C for 75 s for 12 cycles. The end step was final extension at 65°C for 5 min. The PCR products were purified using an AMPure XP system before the quality of the libraries was assessed using an Agilent Bioanalyzer 2100, and the libraries were sequenced on an Illumina HiSeq 2000 at Vazyme Biotech Co., Ltd. (Nanjing, China) and GENEWIZ company (Suzhou, China). Paired-end reads were mapped to the *P. falciparum* 3D7 assembly release-33 downloaded from PlasmoDB (http://plasmodb.org/common/downloads/Current_Release/Pfalciparum3D7/). Next, read counts were collected, and gene expression levels among different samples were estimated.

icSHAPE Deep-Sequencing Illumina Library Construction

For the icSHAPE library, we used the methods developed by Ryan A Flynn et al. as described previously (Flynn et al., 2016), with some modifications. For total RNA/ribosomal RNA libraries, no additional processing was needed. For polyA-selected libraries, polyA selection was performed first using polyT oligo magnetic beads. Briefly, DNA-free mRNA, which was purified from total RNA using polyT oligo magnetic beads, was subjected to a biotin click reaction with the modification reagent NAI-N_3 at 37°C in a thermomixer for 2 h at 1,000 r.p.m. with 4 U/μl RiboLock RNase inhibitor. Fragmentation was performed using RNA fragmentation reagent (Ambion) at 70°C for 3 min. Next, purified fragmented RNA was end-repaired by T4 polynucleotide kinase (NEB) and incubated at 37°C for 1 h. A 3'-biotin RNA linker or a 3'-ddC RNA linker were ligated to the end-repaired RNA samples by T4 RNA ligase 1. After each above step, the reaction was purified by a Zymo RNA Clean & Concentrator-5 column according to the manufacturer's protocol.

First strand cDNA was subsequently synthesized using 1 μl of 1 μM RT primer (with a 4-nt barcode for separate samples in one sequencing lane). After reverse transcription, isolation by MyOneC1 streptavidin beads and size selection (>70 nt) of NAI-N_3-modified molecules from cDNA products, the concentrated cDNA samples were purified with a Zymo DNA Clean & Concentrator-5 column. The size-selected cDNA was circularized by 5 U/μl CircLigase II (Epicentre) and incubated at 60°C for 2 h. Amplification was performed using NEBNext High-Fidelity 2X PCR Master Mix, Solexa-P5 primer, and Solexa-P3 primer. The qPCR machine was programmed as follows: 98°C for 45 s, 98°C for 15 s, 65°C for 20 s, and 72°C for 30 s. For the *in vivo* and *in vitro* NAI-N_3-treated samples, 14 cycles were employed, and for DMSO-treated samples, 11 cycles were employed. Finally, the PCR-amplified library was gel size-selected using 10% TBE PAGE to obtain a size between 200 bp and 300 bp. The primer and oligonucleotide sequences used in the experiment are shown in **Supplementary Table 1**.

Final icSHAPE library material was quantified on a Bioanalyzer High Sensitivity DNA Chip 2100 (Agilent) and Qubit and was sent for deep sequencing and Illumina HiSeq analysis at Vazyme Biotech Co., Ltd. (Nanjing, China) and GENEWIZ Company (Suzhou, China).

Sequencing Data Analysis

The quality of all PF data from Illumina's HiSeq sequencer was assessed by FastQC (Babraham Bioinformatics), and the percentages of reads with Q20, Q30, and GC content were calculated. All sequenced libraries were collapsed to remove PCR duplicates, reads containing adapters, reads containing polyN, and low-quality scores.

All downstream analyses were based on clean data with barcodes (1-13 bases in each read) removed by using Trimmomatic (Bolger et al., 2014), and reads with bases < 35 nt were discarded after barcode removal. All the clipped sequenced libraries were later mapped to the *P. falciparum* genome and transcriptome (build release-33 downloaded from PlasmoDB on June 26th, 2017 http://plasmodb.org/common/downloads/Current_Release/Pfalciparum3D7/) using bowtie (Langmead et al., 2009) implemented with mismatch = 0 (bases from 1-28 nt) and default parameters. The '-1 positions' of each sequencing read represented the reverse transcription stop, which corresponded to modified nucleotides in the NAI-N_3 group and intrinsic/fragmentation modified in the DMSO control group. The number of times a base was mapped as '-1 positions' was counted by Perl scripts and bed tools (Quinlan and Hall, 2010). All icSHAPE profiles of all mapped RNA species were sorted into different files by chromosome for the two experiments at the two developmental stages at the ring stage and trophozoite stage. All reads mapped to the genome and transcriptome from different libraries were normalized by the total number of RT stops in each library [NAI-N_3 *in vivo*, NAI-N_3 *in vitro*, and DMSO control] and sequencing depth. The icSHAPE signals/scores for each RNA position were calculated as the ratio of NAI-N_3/DMSO numbers of modified nucleotides after all reverse transcription stops were normalized by the amount of all reads in each library (Talkish et al., 2014). To reduce the potential overestimation of structural signals of bases with low/zero coverage, a small number 5 was added to the numbers of modified nucleotides, which were normalized by sequencing depth (Wan et al., 2014). The final analysis of the icSHAPE sums was performed with Microsoft Excel 2013 and Student's t-tests using R.

Computation of the RNA Secondary Structures With icSHAPE Scores

An increasing number of online web services or software can be used for the prediction of RNA secondary structure (Jin et al., 2011). In our research, colour coding by icSHAPE signalling was performed using online ViennaRNA Web Services (http://rna.tbi.univie.ac.at/) with five different colours. Specifically, the coloured base pair was placed into the known regions of the

18S rRNA secondary structure, and the experimental single/double results were subsequently checked against the known ways of pairing. For the RNA secondary structure profile, all selected secondary structure models were generated using RNAstructure 6.1 12 on a Windows operating system (http://rna.urmc.rochester.edu/RNAstructure.html) with and without hard constraints due to the extracted icSHAPE score profiles of all single RNAs that were calculated (After testing and comparing on the known regions of 18S rRNA, we concluded that in RNAstructure software, the parameter of threshold for force single stranded was 1.5, and the threshold for chemical modification was 1.0, for our icSHAPE scores profiles.) In our approach, the nucleotides that have icSHAPE scores above a specified threshold (1.5) are forced to be single-stranded. Otherwise, the positions are treated as being inaccessible to chemical modification, i.e., double-stranded or crowded by specific protein. We also used the current best parameters (read shape reactivity - pseudo energy constraints with slope = 1.8, intercept =-0.613) for icSHAPE-directed RNA structure prediction. Alternatively, webserver tools were also used at http://rna.urmc.rochester.edu/RNAstructureWeb/. RNA structures were drawn and coloured using StructureEditor.

RESULTS

Determination of the Conditions for Single-Hit Kinetics and Fragmentation Time by Primer Extension Electropherograms

To obtain the single-nucleotide resolution and genome-wide RNA secondary structural features in *P. falciparum*, NAI-N_3 should be titrated to single-hit kinetics in structure probing. In our pilot experiments, we used capillary electrophoresis (CE) (Vasa et al., 2008), which has extended the amenable length to 500 nt, to confirm the NAI-N_3-labelled 18S 5' end rRNA structure and compare those structures with the known secondary structure of PF 18S rRNAs (Wong et al., 2014) (**Supplementary Figure 1**). Our results showed that we obtained nearly identical secondary structure for the 5' end of 18S rRNA as previously reported (**Supplementary Figure 1**). These results show that the 15-min time point is the optimal duration for NAI-N_3 modification, as it is the longest time point for which single-hit kinetics still occur as revealed by consistency with the known structure. The 30-min time point is too long, as revealed by the significant of loss modified points and the increase of shorter length bands. Next, we used this condition for all the following *in vivo* RNA modifications. IcSHAPE *in vivo* libraries were subsequently prepared using RNA from pellets treated with 100 mM NAI-N_3 for 15 min, and control pellets not treated with NAI-N_3 but with DMSO solution.

Appropriate fragment sizes have a critical role in ensuring the highest signal to-noise ratio and are need for efficient obtaining meaningful reads and modification sites *via* RT-PCR and sequencing. Short RNAs (measuring~100 nt) are the most common strategies that have been optimized to achieve single-hit kinetics of chemical modification, which can result in ~10% of all transcriptions being structurally informative (Merino et al., 2005). For this purpose, we first determined the fragmentation time by primer extension electropherogram experiments (**Supplementary Figure 2**). The results showed that the 3-min time point was the optimal fragment time for obtaining ~100 nt short RNAs. The 4-min time point is too long, as revealed by significant loss of ~100 nt short RNAs.

Comparison of icSHAPE Data to Known RNA Structures

To evaluate the accuracy of our NAI-N_3-labelledicSHAPE approach, we first used capillary electrophoresis-based probing to compare NAI-N_3 modifications from icSHAPE with those from conventional gel-based modification read-outs. These results indicated strong agreement for the special regions of 18S rRNA tested (**Figures 1A, B**). Second, we mapped our icSHAPE scores to well-studied RNA molecules (**Figure 1C** and **Supplementary Figure 3**). The secondary structure of *P. falciparum* A-type 18S small subunit ribosomal RNA (http://www.rna.ccbb.utexas.edu) has been published (Cannone et al., 2002); therefore, we used this known RNA secondary structure as a model to compare with our icSHAPE modification RNA secondary structure according to our icSHAPE scores. *In vitro* RNA icSHAPE libraries prepared using RNA from *in vitro* NAI-N_3 modification with no ribosomal removal were sequenced to produce an average of 14.5 million reads in the 2092-bp region of *P. falciparum* A-type 18S small subunit ribosomal RNA. The icSHAPE scores for each site on 18S rRNA are depicted in **Supplementary Table 2**. Colour coding by icSHAPE signal was performed using online ViennaRNA Web Services (http://rna.tbi.univie.ac.at/) with five different colours according to the icSHAPE scores generated from icSHAPE-seq (icSHAPE scores < 1.5 were marked in red; icSHAPE scores 1.5-2.0 were marked in yellow; icSHAPE scores 2.0-2.5 were marked in green; icSHAPE scores 2.5-3.0 were marked in blue; icSHAPE scores > 3.0 were marked in purple). The coloured base pair was placed into the known regions of the 18S rRNA secondary structure, and the experimental single/double results were subsequently checked against the known ways of pairing.

In the known secondary RNA structure of entire 18S A-type rRNA (length of 2,092 nt, located on chromosome 5), approximately 41.0% of bases are single-stranded, 55.2% of bases are double-stranded, and 3.8% (80 nt) are indeterminate. In the entire 18S A-type rRNA, 43.9% (the icSHAPE score is above 1.5, indicating that this position is single-stranded) of the bases that show high *in vivo* icSHAPE scores (defined as 1.5) in our data set correspond to single-stranded regions in the phylogenetic structure (41.0%), whereas 56.1% (the icSHAPE score is below 1.5, indicating that this position is a double strand) of the bases that show low *in vivo* icSHAPE scores in our dataset correspond to base-paired regions in the phylogenetic structure (55.2%) and presumably are protected by either ribosomal proteins or non-canonical base-pairing tertiary RNA structures. Our data showed that there is a high correlation between icSHAPE scores and the known 18S A-type RNA

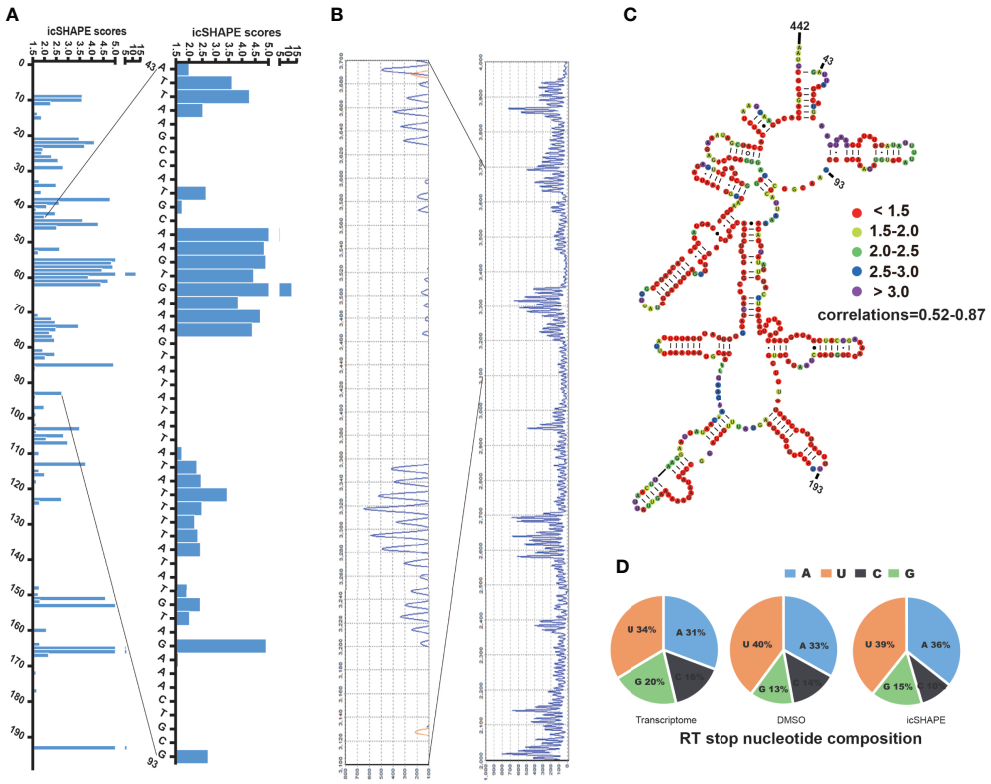

FIGURE 1 | icSHAPE scores accurately maps the region 43–442bp of P. falciparum 18S small subunit rRNA (blood stage) icSHAPE scores accurately maps the region 43–442bp of *Plasmodium falciparum* 18S small subunit ribosomal RNA (blood stage) and agrees with capillary electrophoresis-based *in vivo* structure probing. **(A)** icSHAPE scores for nucleotides 1-193 is shown on the left. The sites of nucleotides which showed have the scores above 1.5, this score means this position is single-strand. **(B)** The gel from 18S A-type rRNA NAI-N_3 modification read-out by capillary electrophoresis-based probing, which was done here near the 5' end (100bp-300bp), which consist with the region on the 1-193 of the 18S rRNA. **(C)** Nucleotides 43–442 of the 18S A-type small subunit ribosomal RNA, colour-coded according to icSHAPE scores. The whole secondary structure of 18S A-type small subunit ribosomal RNA are showed in **Supplementary Figure 3**. **(D)** Reverse transcription stop distribution for the transcriptome of 18S A-type rRNA on chromosome 5, DMSO-treated RNA control libraries or icSHAPE-treated RNAs libraries in the same regions of 18S rRNA. All of the three stop distributions are highly concordant, icSHAPE *in vivo* treatment no enriches for any sequencing reads mapping to four bases compared to untreated control, except a slight enrichment in NAI-N_3 library for As and Us.

secondary structure. We set the sites with icSHAPE scores above 1.5 to be localized to regions of single-stranded RNA and were consistent with traditional primer extension analysis and known RNA secondary structures. NAI-N_3 modification has no specific RT stops with almost equal numbers of four bases, consistent with the known absent or minor (Spitale et al., 2015) (with a very slight enrichment in NAI-N_3 samples for As and Us) base-specificity of NAI-N_3 (**Figure 1D**). Overall, the reactivities from our icSHAPE libraries are consistent with the known structural mapping of 18S rRNA, which is the closest *in vivo* model.

Overview of the *P. falciparum* RNA Structurome

To obtain a genome-wide profile of the single-nucleotide resolution RNA secondary structure during the intraerythrocytic developmental cycle of *P. falciparum*, we performed icSHAPE, as depicted in **Supplementary Figure 4**. *P. falciparum* 3D7 synchronized twice with 5% D-sorbitol was cultured in a 37°C incubator to keep the majority of the parasite population at the same stage. Smears were made by Giemsa staining and used for microscopic observation of parasite morphology at each time point.

The transcripts, with reverse transcription stop coverage no less than 2 and background base density higher than 200 as described previously (Spitale et al., 2015), were analysed. The detailed data in the icSHAPE libraries and RNA-seq libraries are displayed in **Supplementary Table 3**. We obtained an average of 55.38% mappability and 78.3 million qualified fragments per sample in the icSHAPE library (**Supplementary Table 3**). The results are highly reproducible across two biological replicates.

Finally, 2,044 and 1,701 valid structural profiles for transcripts (35.2% and 29.4% of the ratio of all transcripts respectively) were obtained from *in vivo* and *in vitro* 37°C treated polyA-selected RNA ring stage libraries, among which the majority were mRNAs as shown in **Figures 2A–C** (and also in **Supplementary Table 4**). In addition 1,374 and 329 valid structural profiles for transcripts (23.7% and 5.69% of the ratio of all transcripts respectively, with reverse transcription stop coverage no less than 2) were obtained from *in vivo* and

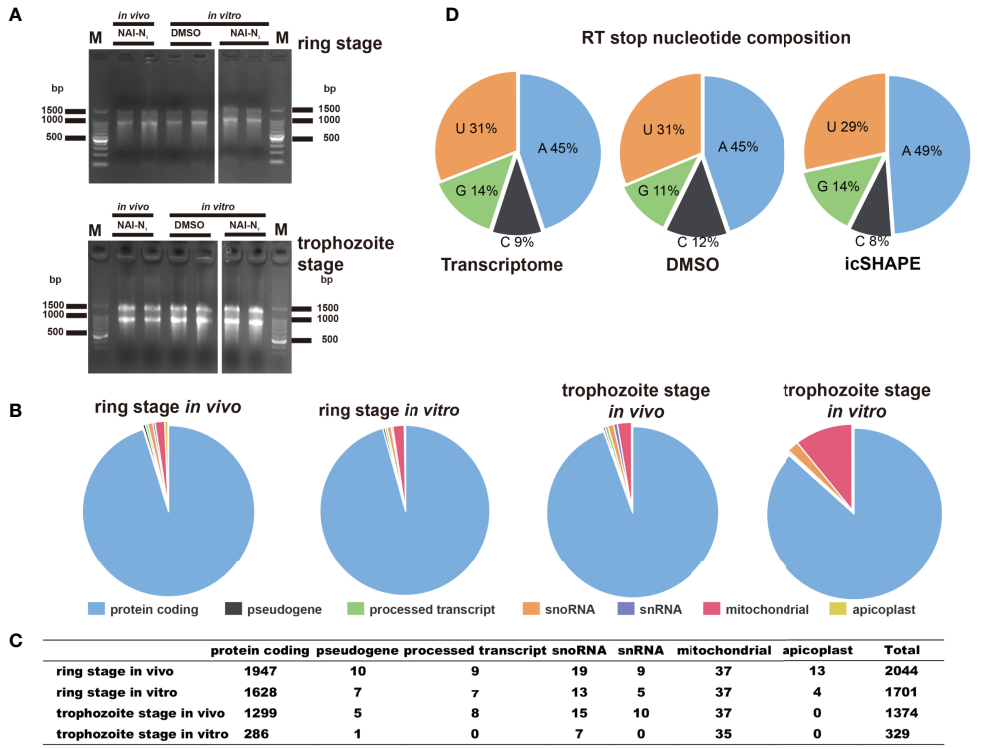

C

	protein coding	pseudogene	processed transcript	snoRNA	snRNA	mitochondrial	apicoplast	Total
ring stage in vivo	1947	10	9	19	9	37	13	2044
ring stage in vitro	1628	7	7	13	5	37	4	1701
trophozoite stage in vivo	1299	5	8	15	10	37	0	1374
trophozoite stage in vitro	286	1	0	7	0	35	0	329

FIGURE 2 | icSHAPE is capable of measuring the RNA structure profiles of thousands of RNAs simultaneously *in vivo* and *in vitro*. icSHAPE is capable of measuring the RNA structure profiles of thousands of RNAs simultaneously *in vivo*. **(A)** Evaluation of RNA quality of two biological replicates between stages and conditions *in vivo* modification, *in vitro* modification, and DMSO control samples in agarose gel. **(B, C)** The total number of structural profiles for transcripts was classified into different classes of RNAs from a total number of 2044 transcripts for the ring stage library at 37 degree *in vivo*, 1701 transcripts for the ring stage library at 37 degree *in vitro*, 1374 transcripts for the trophozoite stage library at 37 degree *in vivo*, and 329 transcripts for the trophozoite stage library at 37 degree *in vitro*. This figure combines results from both two biological replicates. **(D)** Reverse transcription stop distribution for the whole transcriptome, DMSO-treated RNA control libraries or icSHAPE-treated RNAs libraries. All of the three stop distributions are highly concordant, icSHAPE *in vivo* treatment no enriches for any sequencing reads mapping to four bases compared to untreated control, except a slight enrichment in NAI-N_3 library for As.

in vitro 37°C treated polyA-selected RNA trophozoite stage libraries (**Supplementary Table 4**). All of the three reverse transcription stop distributions for the whole transcriptome, DMSO-treated RNA control libraries or icSHAPE-treated RNAs libraries were highly concordant. The icSHAPE *in vivo* treatment did not enrich any sequencing reads mapping to four bases compared to the untreated control, except for a slight enrichment in the NAI-N_3 library for As (**Figure 2D**).

While polyA purification was undertaken in those polyA-selected RNA libraries before library construction, it strongly reduced the reads mapped to the tRNAs and rRNAs. We mapped the structural profiles by icSHAPE score data *in vivo* and *in vitro* from selected regions of 110 mRNAs (the top 110 structural profiles for transcripts that have the highest reverse transcription stop coverage, **Supplementary Table 5**) across parasites that have 5' untranslated regions (UTRs) and 3' UTR regions longer than 200 nt: 5' UTR (200 nt upstream of the start codon); coding sequence region (CDS region, 110 nt downstream of the start codon and 110 nt upstream of the stop codon); and 3' UTR (100 nt downstream of the stop codon) (Kertesz, 2010). Next, we used the obtained structural profiles by icSHAPE scores to investigate three global properties of parasite transcripts to evaluate the hypothesis that robustness of the periodic structure signal might influence translation and alternative splicing.

Distribution of icSHAPE Reactivity Profiles *In Vivo* and *In Vitro* Across the CDS Regions and UTR Regions

The average icSHAPE score of the transcripts *in vivo* and *in vitro* across the CDS regions and UTR regions to quantify the distribution of icSHAPE reactivity profiles in the ring and trophozoite stage development. **Figure 3** shows that RNAs are more folded or crowded by a specific protein *in vivo* (low icSHAPE scores), and the extent of folding varies in different regions of RNAs in ring stage and trophozoite stage. In the ring stage, the 5' UTRs exhibited noticeable but partial unfolding, with the largest variation being observed between the CDS regions and the 3' UTRs. These three different regions of RNAs have nearly the same icSHAPE scores *in vivo*, but the CDS region has higher icSHAPE scores than the 5' UTR and 3' UTR when the RNA structure is modified *in vitro*. Then, we compared the average icSHAPE score collected from three

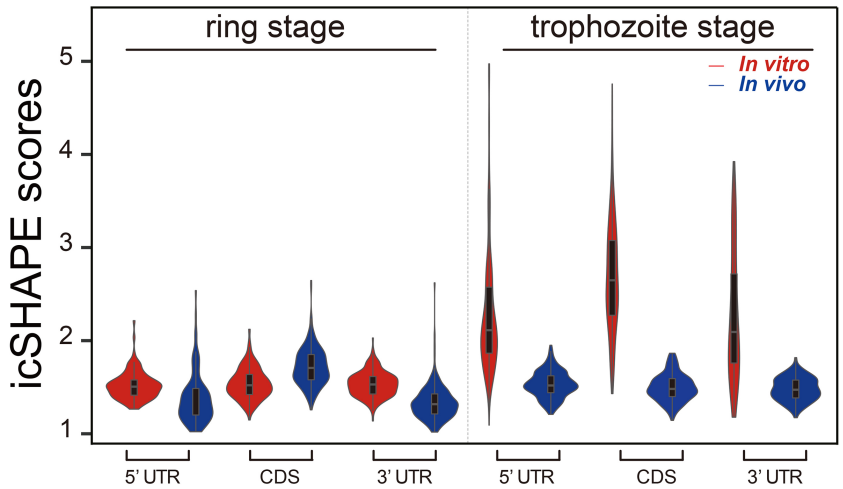

FIGURE 3 | icSHAPE reveals new features of mRNA secondary structures that located 5-UTR, CDS region and 3-UTR region *in vivo* and *in vitro* icSHAPE reveals new features of mRNA secondary structures that located 5-UTR, CDS region and 3-UTR region. The average icSHAPE score *in vivo* and *in vitro* across the CDS regions and UTR regions to quantify the distribution of icSHAPE reactivity profiles in the trophozoite stage development. The figure showed that RNAs are less folded *in vivo* (low icSHAPE scores), and the extent of unfolding varies in different regions of RNAs. The 5' UTRs exhibited noticeable but partial unfolding, with the largest variation compared to the CDS regions and 3' UTRs. Those three different regions of RNAs have nearly the same icSHAPE scores *in vivo*, but the CDS region have the highest icSHAPE scores than the 5' UTR and 3' UTR when the RNA structure were modified *in vitro*.

different regions of RNAs in trophozoite stage, the results also exhibited higher icSHAPE scores *in vitro* than that *in vivo*. Collectively, our data suggest that RNAs are more folded or crowded by a specific protein *in vivo*.

We examined the average icSHAPE score *in vivo* and *in vitro* across the CDS regions and UTR regions to quantify the distribution of icSHAPE reactivity profiles. Due to some nucleotides that were crowded *in vivo* and/or protein binding, or experimental limitations, we observed that icSHAPE scores from *in vivo* and *in vitro* are different. In our research, we found that RNAs are more folded or crowded *in vivo* (low icSHAPE scores), consistent with previous reports (Rouskin et al., 2014; Spitale et al., 2015), and the extent of unfolding was determined to vary in different regions of RNAs (**Figures 4A, B**). It has been revealed that the scale and distribution of RNA structural dynamics under *in vitro* conditions, which are refolded entirely by genome sequencing, are different from those under *in vivo* conditions, in which RNA molecular folding occurs depending on the context of the intracellular environment (Schroeder et al., 2002). Similar results were observed in metazoans (Li et al., 2012a) and humans (Wan et al., 2014), in which UTRs are, on average, more structured than coding regions. However, this global trend is different than that in yeast (Kertesz, 2010) and in *E. coli* (Del Campo et al., 2015), in which UTRs are less structured than CDSs.

Structure Analysis Across the CDS Regions and UTR Regions *In Vivo*

We performed structure analysis across the CDS regions and UTR regions *in vivo*. By PARS technology, Yue Wan et al. (Wan et al., 2014) were used to analyse more than 3,000 secondary structure human messenger RNAs, and found that it is more complicated and complex RNA secondary structures in the UTR regions than the CDS regions. Structures from the UTR, especially the 5' UTR, have an important role in the process of development due to their interaction with regulatory proteins. To explore this hypothesis in our experiment, we focused on two structured 5' UTRs and on the structured 3' UTR for more detailed functional analyses (**Figures 4A, B**). **Figure 4** shows the icSHAPE signal *in vivo* from the ring stage and trophozoite stage libraries. We compared the average icSHAPE score collected from the four genomic features. The results exhibited significant differences from one region to another region in the RNA structure.

Metagene analysis of the transcripts, which aligned at their start and stop codons, shows that *P. falciparum* CDS regions have a propensity to form double-stranded structure (lower icSHAPE scores) to a level that is similar to the structural propensity of the 5'- and 3'-untranslated regions (UTRs). Additionally, our data indicated that lower icSHAPE scores in the sites from nt -25 to -21 in trophozoite stage than in the other sites of 5'UTR region of the transcriptome. This low icSHAPE scores means that those regions are more structured or protein binding sites of mRNA secondary structures. These positions may provide candidate sites for the functional conformation of mRNA, but require further investigation.

We next investigated whether a correlation is shared between intrinsic mRNA secondary structure propensity around the translation start/stop site and whether the efficiency of protein translation correlates with mRNA abundance. In **Figures 4A, B**, we also found that nt -1 to 4 and the last four base pairs of the CDS region of the transcriptome had significantly (Student's t-test, $P < 0.05$) higher icSHAPE scores than average, consistent with previous findings (Ding et al., 2014; Righetti et al., 2016).

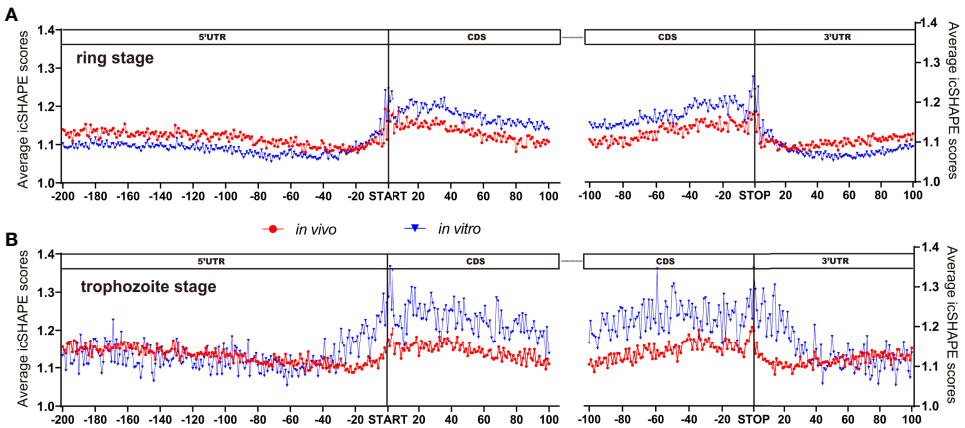

FIGURE 4 | icSHAPE reveals new features of mRNA secondary structures that located 5-UTR, CDS region and 3-UTR region. (Ring stage and trophozoite stage *in vivo* and *in vitro* compare) Average icSHAPE scores in selected regions of the whole expressed transcripts across the ring stage (**A** for ring stage and **B** for trophozoite stage) of parasites that have 5' and 3' UTR regions longer than 200 nt: 5' UTR region (200 nt upstream of the start codon); CDS initial region (100 nt downstream of the start codon); CDS final region (100 nt upstream of the stop codon); and 3' UTR region (100 nt downstream of the stop codon) are displayed. The start and stop codons of mRNA transcripts are indicated by grey bars; The first 4 nt immediately upstream of the start codon show significantly higher reactivity than the average icSHAPE scores across the first 100 nt of the CDS with Significantly different (Student's t-test, $P < 0.05$).

Notably, the start and stop codons of each transcript exhibit higher icSHAPE scores, indicating reduced tendency for double-stranded conformation and easily increased accessibility for the expression of transcripts.

mRNA Structure Correlates With mRNA Abundance in *P. falciparum*

It is clear that mRNA structure is important for a variety of biological processes, including maintenance of RNA half-life and stability (Carrier and Keasling, 1997). We next asked whether the RNA secondary structure of the CDS correlates with mRNA abundance in the parasites. To quantify the transcriptome, we performed RNA-seq (**Supplementary Table 6**) with the parasites sample under the same condition as those used for treatment with NAI-N_3 which exhibited high reproducibility between biological replicates.

Comparison of the average icSHAPE score over the CDS revealed a very clear correlation with the mRNA abundance with this combined approach (**Figure 5**). A higher icSHAPE scores, those positions are treated as that they were more accessible to chemical modification, means that those regions are in the presence of a single strand. A lower icSHAPE scores, the positions are treated as that they were unaccessible to chemical modification, indicate the presence of a double strand or those regions are crowded by a specific protein. Our data in **Figure 5** showed that the most abundant transcripts exhibited higher icSHAPE scores. Collectively, our data indicate that it's has unfolding of structured in those most abundant transcripts and open their double-strand with reduced tendency for double-stranded conformation in order to increase the accessibility for the following of ribosomal protein binding easily. In the other hand, due to some nucleotides which were crowded *in vivo* and/or protein binding, they were not chemically reactive, and no complete coverage was be provided in our experiment for this long transcript, the Pearson correlations in our results seem not high but with reasonable. Therefore, we hypothesized that the RNA structure could regulate the activation/repression of gene expression in *P. falciparum*. Combined analysis of icSHAPE with transcriptome data demonstrated that stage-specific RNA structure plays an important role in the regulation of gene expression in *P. falciparum*.

DISCUSSION

In this study, to the best of our knowledge, we presented for the first global view of the genome-scale landscape of RNA secondary structures of the major human pathogen *P. falciparum* for all four bases *in vivo* and *in vitro* at two developmental stages at single-nucleotide resolution. The major strength of this scarcity of our RNA secondary structure was its potential use and important implications for understanding parasite gene expression and development. Recent studies have established RNA structure as a ubiquitous and fundamental regulator of gene expression (Mustoe et al., 2018) that can be used as an extremely specific and subtle mechanism for fine tuning a variety of cellular processes (Vandivier et al., 2016) within picoseconds to seconds (Ganser et al., 2019). On the other hand, *Plasmodium* parasites have 4 to 8 nucleus-encoded, structurally distinct, and differentially transcribed rRNA genes in different developmental stages (Gunderson et al., 1987; Qi et al., 2015). This finding also prompted us to identify the RNA secondary structure as an important factor that contributes to posttranslational control, especially in *Plasmodium* parasites.

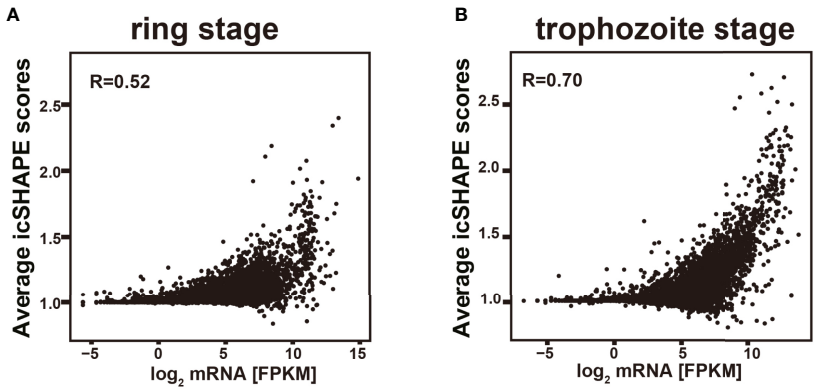

FIGURE 5 | Relationship of icSHAPE and expression abundant (FPKM) from RNA-seq analysis. Comparison of the average icSHAPE scores over the whole transcripts CDS regions revealed a clear correlation with the mRNA abundance. Dependence of the average icSHAPE scores on the mRNA abundance of the whole transcripts from ring stage at 37 degree **(A)**, and also the trophozoite stage at 37 degree **(B)**. Pearson correlation coefficient (R) is showed in each panel.

Prior to NAI-N_3 treatment, NAI-N_3 was titred to single-hit kinetics in structure probing at the different temperatures to ensure that on average, any one copy of any RNA molecule was methylated only once. The major difference between the *in vivo* and *in vitro* conditions for SHAPE mapping is the cell walls and membranes encasing the transcriptomes of these organisms (Lee et al., 2017), especially the parasites that are located in the RBCs. For mapping RNA structures using either nuclease (RNase S1/ RNase V1) or DMS, NAI-N_3 chemical probes, single-hit kinetics are one of the key factors (Kwok et al., 2015), because the over/no modification and/or cleavage of each site can cause conformational changes that lead to erroneous conclusions for specific structures. Moreover, the cell walls and cell membranes encasing the transcriptomes of different organisms are different, which makes the single-hit kinetics for diverse organisms different. Finally, we observed that modifying RNA inside parasite cells with 100 mM NAI-N_3 for 15 min yielded a good-quality RNA secondary structure at 37°C. This method can also be used for other organisms, especially for organisms still without characterized RNA secondary structures.

With the development of high-throughput sequencing techniques over the past half-decade, methods for RNA structure probing have improved from single-gene analysis to whole-transcriptome interrogation. Therefore, we can produce a map of the 'RNA structurome' in a given organism to investigate the structural landscape of eukaryotic transcriptomes and highlight the relationship between some specific RNA structures and functions (Kwok et al., 2015). Chemical modification or RNase digestion are two usually powerful methods that have been used most extensively to map RNA structure *in vivo* and *in vitro* (Lucks et al., 2011; Mortimer et al., 2014; Wildauer et al., 2014; Lee et al., 2017). Recently, a new chemoaffinity structure probing methodology, icSHAPE (*in vivo* click selective 2-hydroxyl acylation and profiling experiment), using a novel bifunctional chemical probe, NAI-N_3, for *in vivo* RNA structure profiling in the genome has become a well-established tool for the analysis of RNA structure, and labelling each accessible single-stranded nucleotide provides a higher-resolution picture of the secondary structure of each transcript (Spitale et al., 2015).

Using the new chemoaffinity structure probing methodology icSHAPE, we generated a map of the 'RNA structurome' in *Plasmodium*, investigated the structural landscape of transcriptomes and highlighted the relationship between some specific RNA structures and their functions. Comparison of the static snapshots of our RNA structurome analysis in two developmental stages showed that the RNA structurome at two developmental stages possessed dynamic developmental responsive reorganization, long-range structures and higher-order architectures across the *Plasmodium* transcriptome. There was only 329 valid structural profiles for transcripts were obtained from *in vitro* 37°C treated polyA-selected RNA trophozoite stage libraries for the following reasons. First, the structural profiles that we define to valid structural profiles for transcripts are based on the transcripts which the reverse transcription stop coverage no less than 2 and background base density higher than 200. This is stricter than previously research. Second, the main reasons of less structural profiles from protein coding RNAs at the trophozoite stage compared to the ring stage is the low number of raw reads in trophozoite stage. Lower number of raw reads, less structural profiles. For the current study, we would like to focus on resolution and genome-wide RNA secondary structural in *P. falciparum* and the connection between RNA secondary structure and mRNA abundance during the complex biological program of *P. falciparum*. We therefore have not performed additional *in vitro* icSHAPE experiments (trophozoite stage) even with low coverage. *In vitro* structural profiles from protein coding RNAs at the trophozoite stage is for further investigation.

Although there is significant global correspondence between our icSHAPE-modified RNA structures and known structures, there are still some differences between icSHAPE and known

structures; one reason for the differences is the noise in our approach, and the other reason is the known inaccuracies of folding algorithms (Kertesz, 2010). Therefore, these NAI-N_3-independent stops occurred at known endogenously modified rRNA nucleotides; thus, we conclude that icSHAPE can successfully and accurately map chemically modified nucleotides on large RNAs on a genome-wide basis from *Plasmodium* parasites. Due to some nucleotides that were crowded *in vivo* and/or protein binding or experimental limitations, they were not chemically reactive, and no complete coverage was provided in our single experiment for this long transcript. Our partial but accurate RNA secondary structure can provide important information at some vital position of each transcript. Our icSHAPE results are strongly correlated with the results from our capillary electrophoresis-based probing method, and it can be used for accurate mapping of the RNA secondary structure. Our *in vivo* icSHAPE data are in excellent agreement with known RNA structures.

Although icSHAPE RNA secondary data were obtained from two stages of the *Plasmodium* and many genes expressed in other asexual developmental stages or mosquito/liver stages could not be obtained here, this study still provides important information on RNA secondary structure and the changes in structures between the two stages. Our study may have had several limitations. The depth was not enough to cover all of the whole transcripts, and larger studies with longer follow-up are needed to obtain RNA secondary structure information from the very low-level transcripts. Recently, a method named hiCLIP (Sugimoto et al., 2015) (RNA hybrid and individual nucleotide resolution ultraviolet crosslinking and immunoprecipitation), uses crosslinking and proximity ligation to determine a special RNA structures bound by special double-stranded RNA-binding proteins. This method may be a good choice for the determination of low-level transcripts or transcripts with complex RNA duplexes.

At present, researchers have found that mutations in many RNA helicases may lead to cancers (Fuller-Pace, 2013; Sullenger and Nair, 2016). Therefore, the application of the RNA secondary structure determination methods to these diverse problems and our parasites field will help us to identify some basic mechanisms of gene expression and potential therapeutic opportunities for treating diseases and parasites. Our findings also open avenues for the influence of specific RNA structural features on gene expression. It has yielded insights into the regulatory roles of RNA secondary structure in many organisms and cellular conditions (Wan et al., 2011; Strobel et al., 2018; Aw et al., 2020).

The development of *Plasmodium* parasites requires two hosts and completes 11 different stages. Therefore, there is a quick efficient response to various environmental changes. In the future, *in vivo* RNA structure studies under different stress conditions, such as temperature (Fang and McCutchan, 2002), the host body of nutrient supply (Mancio-Silva et al., 2017), amino acid (Babbitt et al., 2012) and glucose concentration in the blood (Fang et al., 2004), could provide clues about the structural characteristics of these dynamic mRNAs and their regulatory roles (Kwok et al., 2015).

In summary, our study presents the first icSHAPE-enabled transcriptome-wide secondary structure map and adds to the accumulating evidence that there is a critical connection between RNA structure and the complex biological programme of *P. falciparum*. Our results showed that the average icSHAPE score over the CDS revealed a very clearly correlation with the mRNA abundance. This means that stage specific RNA structure also play an important role in the regulation of gene expression in *P. falciparum*.

DATA AVAILABILITY STATEMENT

The datasets presented in this study can be found in online repositories. The names of the repository/repositories and accession number(s) can be found in the National Center for Biotechnology Information (NCBI) Sequence Read Archive under the BioProject ID PRJNA625343.

AUTHOR CONTRIBUTIONS

YQ designed and performed the experiments, analysed data, prepared figures, writing, review, and editing original draft. YZ and GZ designed and performed the experiments, analysed data, and prepared figures. BC and MZ prepared figures and performed analysis. JL, TP, and JH review and editing. XW designed and supervised the study. All authors performed data quantification, discussed the results, and commented on the manuscript. All authors contributed to the article and approved the submitted version.

FUNDING

This research was funded by Natural Science Foundation of China (Grant number: 81902087), Guangdong Natural Science Fund Project (Grant number: 2017A030310535), and China postdoctoral Science Foundation (Grant number: 2016M592474).

ACKNOWLEDGMENTS

The authors would like to thank Jianbing Mu at National Institutes of Health, USA for his discussion and technical assistance.

SUPPLEMENTARY MATERIAL

The Supplementary Material for this article can be found online at: https://www.frontiersin.org/articles/10.3389/fcimb.2021.673966/full#supplementary-material

Supplementary Figure 1 | Determination of the conditions for single-hit kinetics Determination of the conditions for single-hit kinetics. Time course of NAI-N_3 modification and capillary electrophoresis data accurately maps to known

structures. Lysis parasites were NAI-N_3 treated for different durations (5 min, 10min, 15 min and 30 min) with the final NAI-N_3 concentration was 100 mM. The 18S A-type rRNA NAI-N_3 modification read-out was assessed by capillary electrophoresis-based probing, which was done here near the 5' end (200bp-250bp, the region between two orange peaks). "5 min", "10min", "15 min" and "30 min" show the parasite lysis were incubated with 100mM NAI-N_3 for 5 min, 10min, 15 min and 30 min at 37°C water bath respectively. "Control" show the parasite lysis were incubated with DMSO for 30 min at 37°C water bath. The red-blue stripe below "15 min" indicate the double-(red) or single-stranded (blue) RNA in this region.

Supplementary Figure 2 | Determination of fragmentation time by primer extension electropherograms Determination of fragmentation time by primer extension electropherograms. Appropriate sizes of fragments are need for efficient obtain modification sites *via* RT-PCR and sequencing. Short RNAs, ~100 nt, are the most strategies that have been optimized to achieve single-hit kinetics of chemical modification. "1 min", "2min", "3 min" and "4 min" show the total RNA were fragmented for 1 min, 2min, 3 min and 4 min at 70°C PCR machine respectively. "Control" show the total RNA were no fragmented. The orange pink is GeneScan 500LIZ size standard, provides 5 single-stranded labeled fragments of: 50, 75, 100, 139 and 150 nucleotides.

Supplementary Figure 3 | Secondary structure of *Plasmodium falciparum* 18S small subunit ribosomal RNA (blood stage) *in vivo* NAI-N_3 modification identified by icSHAPE.

Supplementary Figure 4 | Overview of the icSHAPE approach in our experiment Overview of the icSHAPE approach used for temperature-responsive *in vivo* and *in vitro* RNA structurome of *Plasmodium falciparum* in our experiment. P. falciparum was cultured in human O+ erythrocytes at 5% hematocrit at 37°C. Cultures were synchronized twice at ring stage with 5% D-sorbitol treatments performed 8 hours apart. We performed to culture parasites at 48/72 (ring stage/trophozoite stage) hours after the first synchronization experiment. Then parasites were lysis by 1% saponin, following by RNA structure modification by NAI-N_3 or extract total RNA from parasite directly. During NAI-N_3 modification, we set a DMSO-treated negative control sample for that the DMSO sample can provides an 'input' sample. *In vitro* RNA structure experiments were done by treating the total RNA from DMSO-treated sample with NAI-N_3. After library preparation and Illumina sequencing, the count of mapping reads from sequencing generated NAI-N_3 *in vitro*, NAI-N_3 *in vivo*, and DMSO-treated control profiles. Finally, visualization the RNA secondary structure at difference stages and find the relationship between RNA secondary structure and gene expression.

REFERENCES

Aw, J. G. A., Lim, S. W., Wang, J. X., Lambert, F. R. P., Tan, W. T., Shen, Y., et al. (2020). Determination of Isoform-Specific RNA Structure With Nanopore Long Reads. *Nat. Biotechnol.* 39 (3), 336–346. doi: 10.1038/s41587-020-0712-z

Babbitt, S. E., Altenhofen, L., Cobbold, S. A., Istvan, E. S., Fennell, C., Doerig, C., et al. (2012). *Plasmodium falciparum* Responds to Amino Acid Starvation by Entering Into a Hibernatory State. *Proc. Natl. Acad. Sci. U. S. A.* 109 (47), E3278–E3287. doi: 10.1073/pnas.1209823109

Bevilacqua, P. C., Ritchey, L. E., Su, Z., and Assmann, S. M. (2016). Genome-Wide Analysis of RNA Secondary Structure. *Annu. Rev. Genet.* 50 (1), 235–266. doi: 10.1146/annurev-genet-120215-035034

Bolger, A. M., Lohse, M., and Usadel, B. (2014). Trimmomatic: A Flexible Trimmer for Illumina Sequence Data. *Bioinformatics* 30 (15), 2114–2120. doi: 10.1093/bioinformatics/btu170

Cannone, J. J., Subramanian, S., Schnare, M. N., Collett, J. R., D'Souza, L. M., Du, Y., et al. (2002). The Comparative RNA Web (CRW) Site: An Online Database of Comparative Sequence and Structure Information for Ribosomal, Intron, and Other Rnas. *BMC Bioinf.* 3, 2. doi: 10.1186/1471-2105-3-2

Capela, R., Moreira, R., and Lopes, F. (2019). An Overview of Drug Resistance in Protozoal Diseases. *Int. J. Mol. Sci.* 20 (22), 5748. doi: 10.3390/ijms20225748

Carrier, T. A., and Keasling, J. D. (1997). Controlling Messenger RNA Stability in Bacteria: Strategies for Engineering Gene Expression. *Biotechnol. Prog.* 13 (6), 699–708. doi: 10.1021/bp970095h

Choi, L., Pryce, J., and Garner, P. (2019). Indoor Residual Spraying for Preventing Malaria in Communities Using Insecticide-Treated Nets. *Cochrane Database Syst. Rev.* 5:CD012688. doi: 10.1002/14651858.CD012688.pub2

Del Campo, C., Bartholomaus, A., Fedyunin, I., and Ignatova, Z. (2015). Secondary Structure Across the Bacterial Transcriptome Reveals Versatile Roles in mRNA Regulation and Function. *PLoS Genet.* 11 (10), e1005613. doi: 10.1371/journal.pgen.1005613

Ding, Y., Kwok, C. K., Tang, Y., Bevilacqua, P. C., and Assmann, S. M. (2015). Genome-Wide Profiling of In Vivo RNA Structure At Single-Nucleotide Resolution Using Structure-Seq. *Nat. Protoc.* 10 (7), 1050–1066. doi: 10.1038/nprot.2015.064

Ding, Y., Tang, Y., Kwok, C. K., Zhang, Y., Bevilacqua, P. C., and Assmann, S. M. (2014). In Vivo Genome-Wide Profiling of RNA Secondary Structure Reveals Novel Regulatory Features. *Nature* 505 (7485), 696–700. doi: 10.1038/nature12756

Fang, J., and McCutchan, T. F. (2002). Thermoregulation in a Parasite's Life Cycle. *Nature* 418 (6899):742. doi: 10.1038/418742a

Fang, J., Sullivan, M., and McCutchan, T. F. (2004). The Effects of Glucose Concentration on the Reciprocal Regulation of rRNA Promoters in *Plasmodium falciparum*. *J. Biol. Chem.* 279 (1), 720–725. doi: 10.1074/jbc.M308284200

Flynn, R. A., Zhang, Q. C., Spitale, R. C., Lee, B., Mumbach, M. R., and Chang, H. Y. (2016). Transcriptome-Wide Interrogation of RNA Secondary Structure in Living Cells With Icshape. *Nat. Protoc.* 11 (2), 273–290. doi: 10.1038/nprot.2016.011

Fuller-Pace, F. V. (2013). DEAD Box RNA Helicase Functions in Cancer. *RNA Biol.* 10 (1), 121–132. doi: 10.4161/rna.23312

Ganser, L. R., Kelly, M. L., Herschlag, D., and Al-Hashimi, H. M. (2019). The Roles of Structural Dynamics in the Cellular Functions of Rnas. *Nat. Rev. Mol. Cell Biol.* 20 (8), 474–489. doi: 10.1038/s41580-019-0136-0

Gunderson, J. H., Sogin, M. L., Wollett, G., Hollingdale, M., de la Cruz, V. F., Waters, A. P., et al. (1987). Structurally Distinct, Stage-Specific Ribosomes Occur in *Plasmodium*. *Science* 238 (4829), 933–937. doi: 10.1126/science.3672135

Incarnato, D., Neri, F., Anselmi, F., and Oliviero, S. (2014). Genome-Wide Profiling of Mouse RNA Secondary Structures Reveals Key Features of the Mammalian Transcriptome. *Genome Biol.* 15, 491. doi: 10.1186/s13059-014-0491-2

Jin, Y., Yang, Y., and Zhang, P. (2011). New Insights Into RNA Secondary Structure in the Alternative Splicing of Pre-Mrnas. *RNA Biol.* 8 (3), 450–457. doi: 10.4161/rna.8.3.15388

Kaushik, K., Sivadas, A., Vellarikkal, S. K., Verma, A., Jayarajan, R., Pandey, S., et al. (2018). RNA Secondary Structure Profiling in Zebrafish Reveals Unique Regulatory Features. *BMC Genomics* 19 (1), 147. doi: 10.1186/s12864-018-4497-0

Kertesz, M. (2010). Genome-Wide Measurement of RNA Secondary Structure in Yeast. *Nature* 467, 103–107. doi: 10.1038/nature09322

Kwok, C. K., Tang, Y., Assmann, S. M., and Bevilacqua, P. C. (2015). The RNA Structurome: Transcriptome-Wide Structure Probing With Next-Generation Sequencing. *Trends Biochem. Sci.* 40 (4), 221–232. doi: 10.1016/j.tibs.2015.02.005

Lambros, C., and Vanderberg, J. P. (1979). Synchronization of *Plasmodium falciparum* Erythrocytic Stages in Culture. *J. Parasitol.* 65 (3), 418–420.

Langmead, B., Trapnell, C., Pop, M., and Salzberg, S. L. (2009). Ultrafast and Memory-Efficient Alignment of Short DNA Sequences to the Human Genome. *Genome Biol.* 10 (3), R25. doi: 10.1186/gb-2009-10-3-r25

Lee, B., Flynn, R. A., Kadina, A., Guo, J. K., Kool, E. T., and Chang, H. Y. (2017). Comparison of SHAPE Reagents for Mapping RNA Structures Inside Living Cells. *RNA* 23 (2), 169–174. doi: 10.1261/rna.058784.116

Li, F., Zheng, Q., Ryvkin, P., Dragomir, I., Desai, Y., Aiyer, S., et al. (2012a). Global Analysis of RNA Secondary Structure in Two Metazoans. *Cell Rep.* 1 (1), 69–82. doi: 10.1016/j.celrep.2011.10.002

Li, F., Zheng, Q., Vandivier, L. E., Willmann, M. R., Chen, Y., and Gregory, B. D. (2012b). Regulatory Impact of RNA Secondary Structure Across the Arabidopsis Transcriptome. *Plant Cell* 24 (11), 4346–4359. doi: 10.1105/tpc.112.104232

Lucks, J. B., Mortimer, S. A., Trapnell, C., Luo, S. J., Aviran, S., Schroth, G. P., et al. (2011). Multiplexed RNA Structure Characterization With Selective 2 '-Hydroxyl Acylation Analyzed by Primer Extension Sequencing (SHAPE-Seq). *Proc. Natl. Acad. Sci. U. S. A.* 108 (27), 11063–11068. doi: 10.1073/pnas.1106501108

Mancio-Silva, L., Slavic, K., Grilo Ruivo, M. T., Grosso, A. R., Modrzynska, K. K., Vera, I. M., et al. (2017). Nutrient Sensing Modulates Malaria Parasite Virulence. *Nature* 547 (7662), 213–216. doi: 10.1038/nature23009

Merino, E. J., Wilkinson, K. A., Coughlan, J. L., and Weeks, K. M. (2005). RNA Structure Analysis At Single Nucleotide Resolution by Selective 2'-Hydroxyl Acylation and Primer Extension (SHAPE). *J. Am. Chem. Soc.* 127 (12), 4223–4231. doi: 10.1021/ja043822v

Mignone, F., Gissi, C., Liuni, S., and Pesole, G. (2002). Untranslated Regions of Mrnas. *Genome Biol.* 3 (3), REVIEWS0004. doi: 10.1186/gb-2002-3-3-reviews0004

Mortimer, S. A., Kidwell, M. A., and Doudna, J. A. (2014). Insights Into RNA Structure and Function From Genome-Wide Studies. *Nat. Rev. Genet.* 15 (7), 469–479. doi: 10.1038/nrg3681

Mustoe, A. M., Busan, S., Rice, G. M., Hajdin, C. E., Peterson, B. K., Ruda, V. M., et al. (2018). Pervasive Regulatory Functions of mRNA Structure Revealed by High-Resolution Shape Probing. *Cell* 173 (1), 181–195.e118. doi: 10.1016/j.cell.2018.02.034

Qi, Y., Zhu, F., Eastman, R. T., Fu, Y., Zilversmit, M., Pattaradilokrat, S., et al. (2015). Regulation of *Plasmodium yoelii* Oocyst Development by Strain- and Stage-Specific Small-Subunit Rrna. *MBio* 6 (2), e00117. doi: 10.1128/mBio.00117-15

Quinlan, A. R., and Hall, I. M. (2010). Bedtools: A Flexible Suite of Utilities for Comparing Genomic Features. *Bioinformatics* 26 (6), 841–842. doi: 10.1093/bioinformatics/btq033

Righetti, F., Nuss, A. M., Twittenhoff, C., Beele, S., Urban, K., Will, S., et al. (2016). Temperature-Responsive In Vitro RNA Structurome of Yersinia Pseudotuberculosis. *Proc. Natl. Acad. Sci. U. S. A.* 113 (26), 7237–7242. doi: 10.1073/pnas.1523004113

Rouskin, S., Zubradt, M., Washietl, S., Kellis, M., and Weissman, J. S. (2014). Genome-Wide Probing of RNA Structure Reveals Active Unfolding of mRNA Structures In Vivo. *Nature* 505 (7485), 701–705. doi: 10.1038/nature12894

Schroeder, R., Grossberger, R., Pichler, A., and Waldsich, C. (2002). RNA Folding In Vivo. *Curr. Opin. Struct. Biol.* 12 (3), 296–300. doi: 10.1016/s0959-440x(02)00325-1

Spitale, R. C., Flynn, R. A., Zhang, Q. C., Crisalli, P., Lee, B., Jung, J. W., et al. (2015). Structural Imprints In Vivo Decode RNA Regulatory Mechanisms. *Nature* 519 (7544), 486–490. doi: 10.1038/nature14263

Strobel, E. J., Yu, A. M., and Lucks, J. B. (2018). High-Throughput Determination of RNA Structures. *Nat. Rev. Genet.* 19 (10), 615–634. doi: 10.1038/s41576-018-0034-x

Sugimoto, Y., Vigilante, A., Darbo, E., Zirra, A., Militti, C., D'Ambrogio, A., et al. (2015). hiCLIP Reveals the In Vivo Atlas of mRNA Secondary Structures Recognized by Staufen 1. *Nature* 519 (7544), 491–494. doi: 10.1038/nature14280

Sullenger, B. A., and Nair, S. (2016). From the RNA World to the Clinic. *Science* 352 (6292), 1417–1420. doi: 10.1126/science.aad8709

Su, Z., Tang, Y., Ritchey, L. E., Tack, D. C., Zhu, M., Bevilacqua, P. C., et al. (2018). Genome-Wide RNA Structurome Reprogramming by Acute Heat Shock Globally Regulates mRNA Abundance. *Proc. Natl. Acad. Sci. U. S. A.* 115 (48), 12170–12175. doi: 10.1073/pnas.1807988115

Talkish, J., May, G., Lin, Y., Woolford, J. L. Jr., and McManus, C. J. (2014). Mod-Seq: High-Throughput Sequencing for Chemical Probing of RNA Structure. *RNA* 20 (5), 713–720. doi: 10.1261/rna.042218.113

Trager, W., and Jensen, J. B. (1976). Human Malaria Parasites in Continuous Culture. *Science* 193 (4254), 673–675. doi: 10.1126/science.781840

Vandivier, L. E., Anderson, S. J., Foley, S. W., and Gregory, B. D. (2016). The Conservation and Function of RNA Secondary Structure in Plants. *Annu. Rev. Plant Biol.* 67, 463–488. doi: 10.1146/annurev-arplant-043015-111754

Vasa, S. M., Guex, N., Wilkinson, K. A., Weeks, K. M., and Giddings, M. C. (2008). Shapefinder: A Software System for High-Throughput Quantitative Analysis of Nucleic Acid Reactivity Information Resolved by Capillary Electrophoresis. *Rna-a Publ. RNA Soc.* 14 (10), 1979–1990. doi: 10.1261/rna.1166808

Wan, Y., Kertesz, M., Spitale, R. C., Segal, E., and Chang, H. Y. (2011). Understanding the Transcriptome Through RNA Structure. *Nat. Rev. Genet.* 12 (9), 641–655. doi: 10.1038/nrg3049

Wan, Y., Qu, K., Zhang, Q. C., Flynn, R. A., Manor, O., Ouyang, Z., et al. (2014). Landscape and Variation of RNA Secondary Structure Across the Human Transcriptome. *Nature* 505 (7485), 706–709. doi: 10.1038/nature12946

Wildauer, M., Zemora, G., Liebeg, A., Heisig, V., and Waldsich, C. (2014). Chemical Probing of RNA in Living Cells. *Methods Mol. Biol.* 1086, 159–176. doi: 10.1007/978-1-62703-667-2_9

Wong, W., Bai, X. C., Brown, A., Fernandez, I. S., Hanssen, E., Condron, M., et al. (2014). Cryo-EM Structure of the *Plasmodium falciparum* 80S Ribosome Bound to the Anti-Protozoan Drug Emetine. *Elife* 3, e03080. doi: 10.7554/eLife.03080

World Health Organization (2020). *World Malaria Report 2020* (Geneva: WHO Press).

Zheng, Q., Ryvkin, P., Li, F., Dragomir, I., Valladares, O., Yang, J., et al. (2010). Genome-Wide Double-Stranded Rna Sequencing Reveals the Functional Significance of Base-Paired RNAs in Arabidopsis. *PLoS Genet.* 6 (9), e1001141. doi: 10.1371/journal.pgen.1001141

Conflict of Interest: The authors declare that the research was conducted in the absence of any commercial or financial relationships that could be construed as a potential conflict of interest.

frontiers in Medicine

METHODS
published: 08 June 2021
doi: 10.3389/fmed.2021.685926

Assessment of Mosquito Collection Methods for Dengue Surveillance

Triwibowo Ambar Garjito[1], Lulus Susanti[1], Mujiyono Mujiyono[1], Mega Tyas Prihatin[1], Dwi Susilo[1], Sidiq Setyo Nugroho[1], Mujiyanto Mujiyanto[1], Raden Ajeng Wigati[1], Tri Baskoro Tunggul Satoto[2], Sylvie Manguin[3], Laurent Gavotte[4] and Roger Frutos[5]**

[1] Institute for Vector and Reservoir Control Research and Development, National Institute of Health Research and Development, The Ministry of Health of Indonesia, Salatiga, Indonesia, [2] Department of Parasitology, Faculty of Medicine, Public Health and Nursing, Gadjah Mada University, Yogyakarta, Indonesia, [3] HSM, Univ. Montpellier, CNRS, IRD, Montpellier, France, [4] Espace-Dev, University of Montpellier, Montpellier, France, [5] Cirad, UMR 17, Intertryp, Montpellier, France

Several methods exist to collect and assess the abundance of dengue vector mosquitoes, i.e., morning adult collection, pupal collection, ovitraps, human landing, and larval collection. Several of these methods are officially implemented to monitor mosquito density and make decisions on treatments for dengue control. This monitoring is also constrained by the need to conduct this assessment on a "one point/one day" process, meaning that once the threshold of 100 households is reached, the assessment is made, and the collectors teams move to another place, thus preventing the use of long-term sampling methods. This diversity of methods might be a source of variability and lack of statistical significance. There is also a lack of published data regarding the efficacy of these methods. Furthermore, the *Stegomyia* indices are shown to be not reliable for assessing the risk of dengue outbreaks. A mosquito survey was, thus, conducted in 39 locations corresponding to 15 dengue endemic provinces in Indonesia by using the different adult and larval collection methods recommended nationwide. A total of 44,675 mosquitoes were collected. The single larva method was the most efficient. Out of a total of 89 dengue-positive pools, the most frequently encountered virus was DENV2, which made up half of the positive samples, followed by DENV3 and DENV1, respectively. Factor analysis of mixed data showed that no correlation could be found between any methods and the presence of dengue virus in mosquitoes. Moreover, no correlation could be found between any methods and the incidence of dengue. There was no consistency in the efficacy of a given method from one site to another. There was no correlation between any of the parameters considered, i.e., method, incidence of dengue, location, and the presence of dengue virus in mosquitoes.

Keywords: ***Aedes aegypti***, ***Aedes albopictus***, **dengue, collection methods, dengue incidence, Indonesia**

OPEN ACCESS

Edited by:
Xiaoxiao Wang, Zhejiang Center for Disease Control and Prevention (Zhejiang CDC), China

Reviewed by:
Rafael Maciel-de-Freitas, Oswaldo Cruz Foundation (Fiocruz), Brazil
Aishah Hani Azil, National University of Malaysia, Malaysia

****Correspondence:***
Triwibowo Ambar Garjito
triwibowo@litbang.kemkes.go.id
Roger Frutos
roger.frutos@cirad.fr

Specialty section:
This article was submitted to Infectious Diseases - Surveillance, Prevention and Treatment, a section of the journal Frontiers in Medicine

Received: *26 March 2021*
Accepted: *27 April 2021*
Published: *08 June 2021*

Citation:
Garjito TA, Susanti L, Mujiyono M, Prihatin MT, Susilo D, Nugroho SS, Mujiyanto M, Wigati RA, Satoto TBT, Manguin S, Gavotte L and Frutos R (2021) Assessment of Mosquito Collection Methods for Dengue Surveillance. Front. Med. 8:685926. doi: 10.3389/fmed.2021.685926

INTRODUCTION

Dengue is the most rapidly spreading arboviral disease worldwide (1). Recent studies estimate that 55–100 million dengue cases are reported annually with 3.9 billion people at risk (2, 3). Indonesia is an hyperendemic dengue country; i.e., all four serotypes are circulating with the highest number of dengue cases in Southeast Asia (4, 5). Dengue incidence in Indonesia has increased

significantly over the last four decades from 0.05/100,000 in 1968 to 78.8/100,000 in 2016 (6). The dengue virus is transmitted to humans by the bite of infected *Aedes aegypti* mosquitoes, the main vector, and *Ae. albopictus,* the secondary vector. These species are anthropophilic; i.e., they live in human environments and breed in various sites, such as water containers, flowerpots, birdbaths, disposed water-holding vessels, waste disposal areas, small containers, discarded tires, natural holes in vegetation, etc. (7–10). Both are present in urban and suburban areas. With no treatment and while an effective vaccine is still under study, vector control remains the only effective way to prevent and control dengue.

Vector surveillance methods have remained mostly unchanged for more than three decades (11). Larval survey is the most widely adopted dengue vector surveillance method to locate larval habitats and to measure the abundance of *Ae. aegypti* and *Ae. albopictus* (12, 13). The *Stegomyia* indices, i.e., house index (HI), container index (CI), and Breteau index (BI), to which a specific free larval index (FLI) is added in Indonesia, are used for calculating mosquito abundance and for predicting the risk of dengue transmission (11). The FLI is defined as the number of houses without larva x 100/total number houses. The FLI is, thus, the reverse of the HI. However, previous studies demonstrated the lack of correlation between *Stegomyia* indices and the risk of dengue outbreak (12, 14–18), although a correlation was found between human population density and incidence of dengue (18). This sounds logical owing to the anthropophilic behavior of these vectoring mosquitoes. Several methods for collecting mosquitoes are officially recommended by the Ministry of Health, i.e., morning adult collection, pupal collection, ovitraps, whole night collection using human landing, and larval collection. Because the *Stegomyia* indices, exclusively based on larval collection, are not reliable predictors, other predictors must be sought. The diversity of methods endorsed by the Ministry might be a source of variability. Furthermore, there is a lack of published data regarding the effectiveness of these methods (12, 19–22). A major constraint associated with the monitoring of mosquitoes is that the decision for treatment or absence of treatment is made on a one point/one day basis, meaning that agents in charge of the survey issue the assessment conclusion once the threshold of 100 households is reached and move to another place. They do not conduct long-term capture and sampling. Methods of insect collection influence the reliability of entomological indices. We report here a large-scale comparative analysis of various methods of insect collection to assess their relative effectiveness and reliability to determine whether entomological descriptors can be envisioned to determine the risk of dengue outbreak or if other kinds of descriptors should be considered.

Abbreviations: HI, House Index; CI, Container Index; BI, Breteau Index; FAMD, Factor Analysis of Mixed Data.

METHODS

Study Sites

The study was conducted in 39 locations corresponding to 39 districts/municipalities in 15 dengue endemic provinces in Indonesia (**Figure 1**). These provinces include Aceh, West Sumatra, Lampung, Bangka-Belitung, Banten, West Kalimantan, South Kalimantan, North Sulawesi, West Java, East Java, Southeast Sulawesi, Maluku, West Nusa Tenggara, East Nusa Tenggara, and North Maluku. This study is part of the Indonesia national project, Rikhus Vektora led by the Ministry of Health which started in 2016.

Study Design

A mosquito survey was performed in all study sites from July to August 2016 during the rainy season. Larva collection was performed in at least 100 households taken at random in each study site according to the recommendations for the calculation of the *Stegomyia* indices. Adult collection of *Aedes* mosquitoes were performed in the morning (morning resting) on mosquitoes resting inside houses using manual aspirators. Adult mosquitoes were also collected outside using standard procedures for all night human-landing collection methods from 6 p.m. to 6 a.m. All methodologies used in this study are described in the Ministry of Health guidelines (22). All methodologies investigated must be compatible with the "one point/one day" process of decision making. This "one point/one day" concept means that collectors do not stay in the same sampling site over a long period of time. As soon as the threshold of 100 households is reached, they calculate the *Stegomyia* indices and move to another sampling site. Long-term sampling methods are not suitable. Field data collections for larva and adult *Aedes* mosquitoes were performed by trained collectors in collaboration with local volunteers, local authorities, and staff from district/municipality dengue control programs.

Single Larva and Rearing Methods

At least 100 households were taken at random in each study site for larval and pupal sampling. All artificial and natural water containers in and around each household were inspected for mosquito larvae and pupae. At least one larva (second, third, and/or fourth instars) and pupae (if any) from each positive container were collected with pipettes and tea strainers. Water from large containers was first removed with a water hose and then sieved with tea strainers. Larvae or pupae were then collected on a white plastic tray. Immature stages were pipetted and placed in a plastic clip with water, labeled, and taken to the field laboratory. Data on infected containers and households were used for calculating the *Stegomyia* indices. This corresponds to the single larva method routinely implemented for mosquito monitoring. For the rearing method, immature mosquitoes (pupae and larvae) were reared in 250-ml plastic cups covered with gauze under room temperature. Larvae were fed on tetrabit fish food until adult mosquitoes emerged. Emerged adult mosquitoes from the same household and species were then killed in a freezer (−20°C) or by using ethyl acetate for 5–10 min and immediately stored in 1.5-ml vial tubes with RNALater

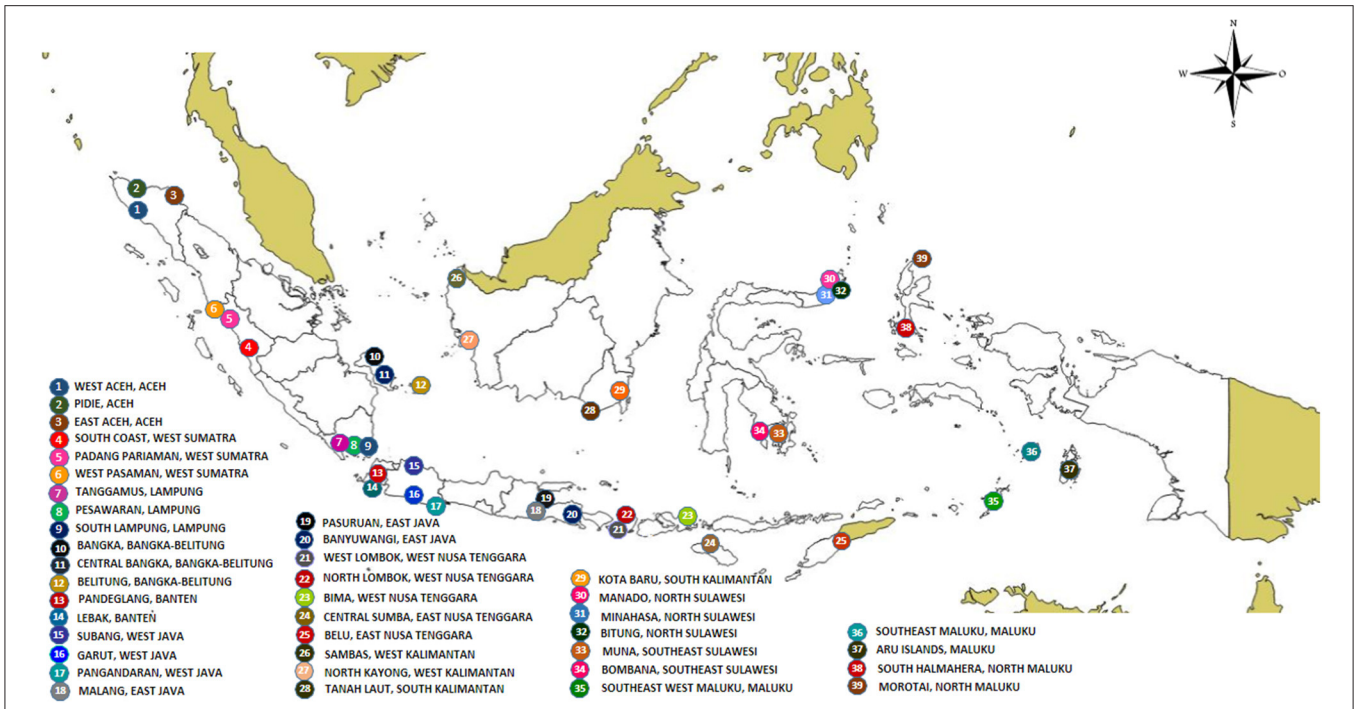

FIGURE 1 | Map of the sampling sites throughout Indonesia.

(Qiagen, Hilden, Germany) by pools of up to 25 specimens. Mosquitoes from different households or different species were not pooled together. Immature stages that did not yield adults by the fourth day were pooled based on location (maximum 25 larvae per tube).

Adult Mosquito Collection Methods

Two adult mosquito sampling methods were conducted simultaneously in all study sites, i.e., morning resting and human landing collection, to which a third one, an animal-baited trap, was added in one location (Malang, East Java).

(1) Morning resting collections were made by eight collectors using hand nets and aspirators. Collections were conducted from 7 to 9 a.m. and included any resting locations within the house. All adult mosquitoes were placed into labeled paper caps and taken to the field laboratory for further analysis.
(2) Human landing collections were performed by eight local volunteers as collectors in three selected houses in each study site for sampling adult mosquitoes using mouth aspirators. They were all trained before collecting mosquitoes. Three teams of two people sampled outdoors (up to 5 m from the house) and indoors. Each collector sat on a chair while exposing the legs. Sampling was conducted all night from 6 p.m. to 6 a.m. The teams rotated and changed roles regularly every 2 h with a 2-h break. Although the targeted *Aedes* mosquitoes are diurnal, Indonesia law does not allow human landing collection during daytime. Therefore, collections had to be conducted at night. This introduces a strong bias in the sampling, but because it is what surveillance teams do in accordance with the law, this method was nevertheless considered. Mosquitoes that have been collected per hour were then taken to the field laboratory for species identification and further analysis.
(3) An animal-baited trap was conducted by using tame animals, i.e., cows, placed inside a net all night. Mosquito collections were carried out for 15 min/h inside the nets by three collectors. Collected mosquitoes were then similarly preserved as for the human landing collection method.

All mosquitoes from these three collecting methods identified as *Ae. aegypti* and *Ae. albopictus* were then killed with ethyl acetate, pooled up to 25 mosquitoes in labeled 1.5-ml vial tubes with RNAlater (Qiagen, Hilden, Germany) and preserved based on the same cold chain management as above for larvae.

Detection of Dengue Virus From Mosquitoes

The *Ae. aegypti* and *Ae. albopictus* mosquito pools were homogenized in 1.5-ml tubes containing 200 µl PBS 1x by using pellet pestles. RNA was extracted using QIAamp® Viral RNA Mini Kit (Qiagen®, Courtaboeuf, France). RNA was extracted from 200-µl homogenized samples following the manufacturer's instructions. All RNA extracted samples were analyzed for dengue detection using Lanciotti's protocol (23). The nested RT-PCR for dengue was performed using SimpliAmp Thermal Cycler Applied Biosystems™ (ThermoFisher Scientific®, United States). Amplification of dengue RNA was carried out with following specific primers: D1 (5′-TCA ATA TGC TGA AAC GCG CGA GAA ACC G-3′), D2 (5′-TTG CAC CAA CAG

TCA ATG TCT TCA GGT TC-3′), TS1 (5′-CGT CTC AGT GAT CCG GGG G-3′), TS2 (5′-CGC CAC AAG GGC CAT GAA CAG-3′), TS3 (5′-TAA CAT CAT CAT GAG ACA GAG C-3′), and TS4 (5′-CTC TGT TGT CTT AAA CAA GAG A-3′). The first amplification of dengue virus was performed using Superscript III one-step RT-PCR kit (Invitrogen, Carlsbad, CA). The cycling conditions consisted of an initial 95°C denaturation step for 2 min, followed by 40 cycles of 95°C denaturation for 30 s, 60°C annealing for 1 min, and 72°C extension for 1 min 30 s, and a final extension step 72°C for 10 min. Samples were then stored at 4°C. First-step PCR products were run on 2% agarose gel under 120 V current for 1 h. Visualization was done using SYBR® safe DNA gel stain (Invitrogen, Carlsbad, CA, USA) under UV condition in a GelDoc system. The presence of the 511-bp control band indicated a dengue virus (DENV) positive sample. Subsequent genotyping was conducted by using the first step PCR product with thermal cycle setting as follow: initial denaturation step at 95°C for 2 min, followed by 10 cycles of denaturation step at 95°C for 30 s, 60°C annealing for 1 min, and an extension step at 72°C for 1 min and 30 s. The final extension step was conducted at 72°C for 10 min. Subsequently, samples were stored at 4°C. Multiplex genotyping reactions yielded a single specific band with the size of 482 bp for DENV-1, 119 bp for DENV-2, 290 bp for DENV-3, and 389 bp for DENV-4. All field samples were tested for the presence of dengue virus after being pooled by 25 individuals of the same species.

Dengue Incidence Data

The incidence, number of new dengue cases per total population for the time of the study, was obtained from the district health center in each district.

Statistical Analyses

A first factor analysis of mixed data (FAMD) (24) was conducted using the incidence data, the number of mosquitoes, and the number of positive pools for each dengue serotype as quantitative parameters and mosquito species, methods of collection, and provinces as qualitative parameters. The effectiveness of the collection methods (qualitative data) against mosquito species (quantitative data) was assessed using a second FAMD. These analyses were performed using the R software with FactoMineR (25).

RESULTS

Mosquito Sampling

A total of 44,675 mosquitoes were collected from 39 locations (**Figure 1**, **Supplementary Table 1**). Out of these 44,675 mosquitoes collected, 32,525 (72.8%) were *Ae. aegypti* and 10,300 (23.1%) were *Ae. albopictus*, and 1,850 (4.1%) were undetermined. When considering the method of capture, the highest number of captured individuals was, as expected, obtained when targeting larvae. The single larva method was the most efficient in terms of number of individuals collected. A total of 36,500 larvae were collected with this method out of which 27,475 were *Ae. aegypti*, 7,775 were *Ae. albopictus* and 1,250 were not identified. Out of 6,450 larvae collected and reared, 4,325 were *Ae. aegypti,* 1,575 were *Ae. albopictus*, and 550 were not identified. With both larval methods, a bias was observed in favor of *Ae. aegypti*, which represented 75.27% and 37.05% of all samples for the single lava and rearing methods, respectively. Very different results were obtained with the adult capture method. From the three methods used, human landing was the most efficient even though a bias was introduced by the legal obligation to perform this approach by night. Out of 1,325 adult mosquitoes captured, 325 were *Ae. aegypti*, 975 were *Ae. albopictus* and 25 were not identified. The animal-baited trap method yielded only 25 mosquitoes, all being *Ae. albopictus*. The ratio between *Ae. aegypti* and *Ae. albopictus* was reversed with this time a bias in favor of *Ae. albopictus*. It represented 73.58% and 53.33% for the human landing and morning resting methods, respectively. The animal baited trap method yielded only *Ae. albopictus*, but considering the very low number of mosquitoes captured, i.e., 25, this is not significant.

Distribution of Dengue Virus

A total of 89 pools were positive for dengue virus. The most frequently encountered virus was DENV2 ($n = 44$), which made up half of the positive samples. DENV3 and DENV1 followed with 20 and 17 positive pools, respectively. DENV4 was detected in only one pool. Combinations were also detected. Eight pools contained a combination of DENV1 and DENV2, whereas the combination of DENV1 and DENV3 was found in only one pool. Another single pool contained the triple combination DENV1–DENV2–DENV3. With respect to the geographic distribution, a strong imbalance was observed. A large part of the detected dengue viruses, i.e., 56 (63%), were found in mosquitoes collected in the province of Aceh. All four dengue virus serotypes and all positive combinations were found in this province. The other provinces where positive pools were detected were West Sumatra ($n = 5$), Lampung ($n = 6$), Bangka-Belitung ($n = 4$), West Kalimantan ($n = 2$), South Kalimantan ($n = 1$), North Sulawesi ($n = 2$), East Java ($n = 7$), and Maluku ($n = 6$). A strong imbalance was also observed when considering the nature of the positive samples. Mosquito larvae were almost the exclusive source of virus, i.e., 93.3% ($n = 83$) with 70.8% ($n = 63$) found with the single larva method and 22.5% ($n = 20$) for the rearing method. Only six pools (6.7%) of adult mosquitoes were found positive with the human landing method totalizing two pools (2.3%), and four pools (4.4%) were found positive in mosquitoes collected with the morning resting method. An imbalanced result was also found regarding the mosquito species with 76.4% ($n = 68$) of the positive pools corresponding to *Ae. aegypti* and 23.6% ($n = 21$) corresponding to *Ae. albopictus*.

Correlation Assessment

A FAMD was performed to determine the potential correlation between the various parameters considered: mosquito species, province, number of mosquitoes, collection method, dengue virus, and dengue incidence (**Figure 2A**). The only correlation that could be found was between the province and the incidence (**Figure 2A**). However, the global level of explanation was low (20%) indicating a lack of correlation between any of

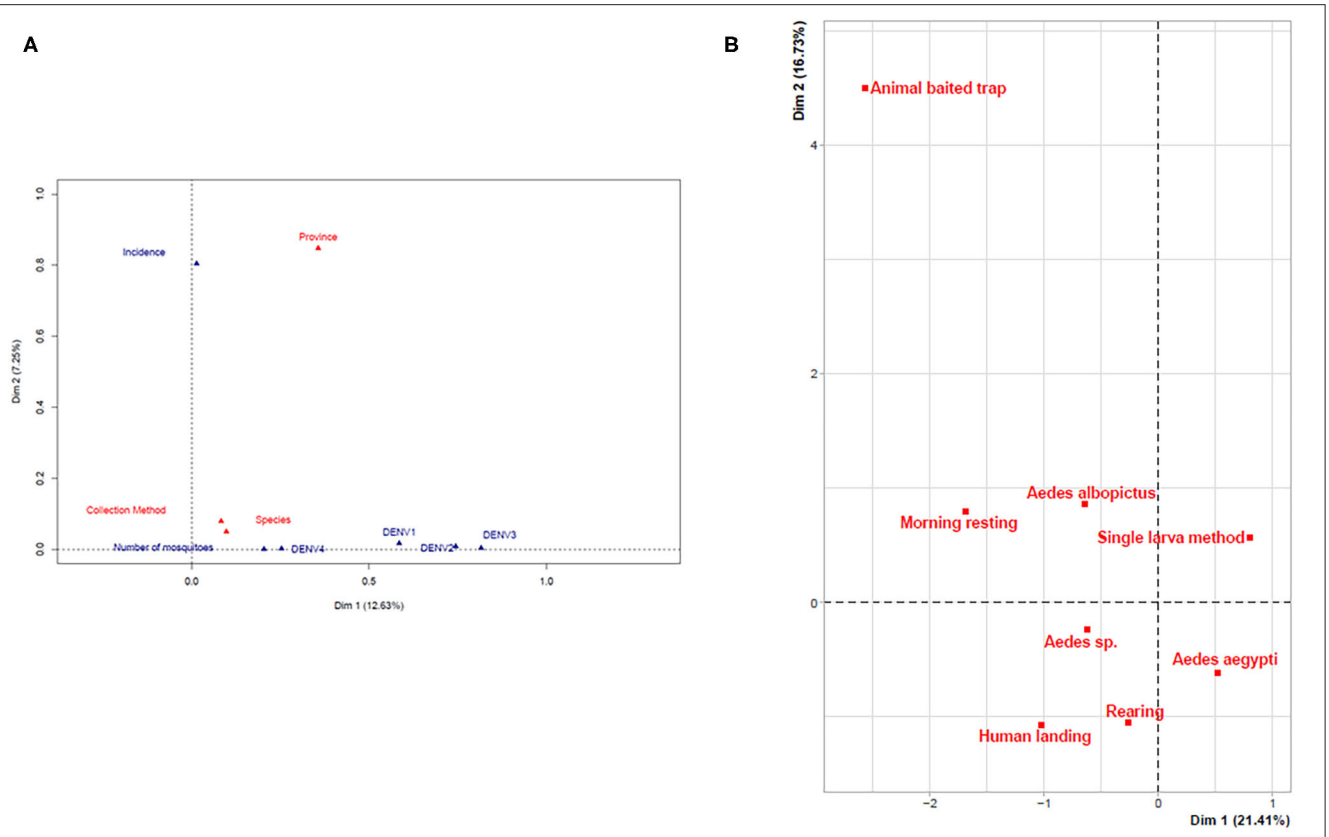

FIGURE 2 | Multivariate analysis of parameters. **(A)** Global factor analysis of mixed data. **(B)** FAMD assessment of the effectiveness of the collection methods.

the parameters with the exception of province and incidence of dengue. A similar result was found when comparing the different collection methods with the mosquito species. The only, but rather weak, correlation that could be found was the preferred association of the larval methods with *Ae. aegypti* and the adult methods with *Ae. albopictus* (**Figure 2B**, **Supplementary Table 1**).

DISCUSSION

In the absence of commercialized vaccines and of any medical treatment, the management of dengue relies only on mosquito control and on prevention. Finding efficient and reliable descriptors for assessing the risk of dengue outbreaks is, thus, a priority in all dengue-endemic countries. The main tools currently in use for assessing this risk of dengue outbreak are the *Stegomyia* indices (15, 26), which rely on the calculation of the relative density of mosquito larvae present in containers and in households through the CI, HI, and BI (26, 27). However, these indices were shown to display no correlation with dengue infection rates and are, thus, not reliable descriptors (16, 18, 28, 29).

Because the *Stegomyia* indices are not reliable descriptors, they must be replaced by other descriptors. They could be replaced by other entomological indices provided that these other entomological indices are reliable. Entomological indices are, by definition, based on the capture of insects. Therefore, it is essential to assess whether the collection methods are reliable and reproducible and do not generate biases. This is independent from the calculation model applied. It is an intrinsic trait of the collection method itself. If not, entomological indices cannot be used as predictors. They must also be compatible with the logistical and administrative constraint of the "one point/one day" nature of the operational monitoring and decision process. This operational constraint is essential. Agents conducting mosquito surveys do not spend all their time at the same place and make their calculations and assessments and release their conclusions usually within 1 day. They move to another place as soon as the threshold of 100 households needed for calculation of the official *Stegomyia* indices is reached. The window for deciding on treatment is also narrow because treatments must be effective before outbreaks occur. Long-term assessments within a single place are scientific experimentations for the purpose of understanding biological processes or developing techniques and methodology but are not adapted to fast decision making. They are not suitable for use under such conditions. This constraint is even more important in large countries such as Indonesia. As a consequence, trapping methods, which are long-term methods based on cumulated data, are not favored.

The methods implemented being used to generate descriptors must be reliable regardless of the location and local conditions. We, therefore, conducted this large-scale study to assess the procedures endorsed by the Ministry of Health guidelines within a very large study involving many sampling sites corresponding to different urbanistic and geographical conditions. This work is, to our knowledge, the most extensive one with 44,675 mosquitoes collected in 39 different sampling locations over Indonesia within a short 2-month period, allowing thus a robust statistical analysis. The main conclusion of this work is that it is not only the *Stegomyia* indices, but any kind of entomological indices that might be at best of very limited use. Not only could no correlation be found between any methods and the presence of dengue virus in mosquitoes, but no correlation could be found between any of the methods and the incidence of dengue. The higher proportion of *Ae. albopictus* found in the human landing method might be related to the fact that this species is more crepuscular than *Ae. aegypti*. No consistency was found for any given method from one place to another. Finally, there was no consistency in the efficiency of a given method for detecting dengue. The single-larva and rearing methods yielded 63% of all dengue-positive samples in the sole province of Aceh. However, the incidence of dengue in Aceh is not the highest among all provinces and is rather the average. Provinces displaying the highest incidence, such as Bangka-Belitung, South Kalimantan, or North Sulawesi, did not yield any dengue-positive larvae. The only single positive pool in these provinces was found in South Kalimantan among morning resting adults. This lack of correlation between incidence and dengue infection rate in mosquitoes is also a drawback for methods associating the capture of adults and the direct detection of dengue virus in the sampled mosquitoes (30–32).

The use of *Stegomyia* indices and the monitoring of mosquitoes are today the main means of assessment of the risk of dengue outbreaks and efficiency of mosquito control. Previous studies demonstrated the lack of correlation of the *Stegomyia* indices with the risk of dengue outbreaks and dengue incidence (12, 14–18). In this work, we further demonstrate the lack of consistency of the various collection methods officially recommended and the lack of correlation with the recorded dengue incidence. Altogether, this indicates that entomological approaches do not provide reliable indicators of risks of dengue outbreak. The risk with these methods is mostly misleading interpretation and misguided decisions and allocation of resources. The assessment of the risk of dengue outbreaks should be reconsidered from a different angle.

CONCLUSIONS

A previous study found that a factor positively correlated with the incidence of dengue was the human population density (18). This provides an angle for further research. *Ae. aegypti* and *Ae. albopictus* are both anthropophilic species, and the human environment is, thus, a major driver of their demography and distribution. The measurement and prediction of the risk of dengue outbreaks should be considered from the angle of urbanism and human societal factors. Efforts should be devoted to the development of novel societal indices. It is even more important to communicate on this issue because dengue endemic countries worldwide, as well as WHO, still base their recommendations and dengue management procedures on entomological indices.

DATA AVAILABILITY STATEMENT

The datasets presented in this study can be found in online repositories. The names of the repository/repositories and accession number(s) can be found in the article/**Supplementary Material**.

ETHICS STATEMENT

The studies involving human participants were reviewed and approved by the Ethical Commission Board of the NIHRD, Ministry of Health, Indonesia (No. LB.02.01/5.2/KE.003/2016 and No. LB.02.01/5.2/KE.020/2017). The patients/participants provided their written informed consent to participate in this study.

AUTHOR CONTRIBUTIONS

TG, LS, TS, RW, and MP conceived and designed the field studies. MujiyonoM, SN, and DS prepared samples. TG and MP ran molecular analyses and laboratory experiments. TG, LG, and RF analyzed the data. MujiyantoM prepared the map. TG and RF wrote the manuscript. SM, LG, and RF provided critiques and significant revisions to the manuscript. All authors contributed to the article and approved the submitted version.

FUNDING

The research was supported by the Institute for Vector and Reservoir Control Research and Development, National Institute of Health Research and Development, Ministry of Health Indonesia. SM, LG, and RF were supported by the Université de Montpellier, IRD, Espace-Dev, and CIRAD, Montpellier, France. The project was supported in part by the French-Indonesian Nusantara projects Zika & Co and SOCIAL.

ACKNOWLEDGMENTS

Authors express their gratitude to all field mosquito collectors, the experts, and technical team and validators of the Rikhus Vektora project for great support. The authors would also like to thank the head of Laboratory Data Management NIHRD, MoH Indonesia who have permitted to do further analyses. The authors also gratefully acknowledge especially Widiarti, Mochammad Choirul Hidajat, Dhian Prastowo, Riyani Setyaningsih, Yusnita Mirna Anggraeny, Siti Alfiah, Evi Sulistyorini, Lasmiati, Sapto Prihasto Siswoko, Warido,

Valentinus Widiratno, Rima Tunjungsari Dyah Ayuningtyas, Fahmay Dwi Ayuningrum, Ary Octsari Yanti, Sekar Negari Kusumaningtyas, Jeri Cahyandaru, Indira Diah Utami, Happy Anita Putri, Syarifah Nurhayati, Senja Rahayu Kinanti, Wahyu Sri Kunto, and other members of the IVRCRD-NIHRD, MoH Indonesia for all support of fieldwork and laboratory work.

SUPPLEMENTARY MATERIAL

The Supplementary Material for this article can be found online at: https://www.frontiersin.org/articles/10.3389/fmed.2021.685926/full#supplementary-material

Supplementary Table 1 | Sampling localities and characteristics of samples.

REFERENCES

1. World Health Organization. *Global Strategy for Dengue Prevention and Control 2012-2020*. World Health Organization, Geneva (2012).
2. Ritchie SA. Dengue vector bionomics: why *Aedes aegypti* is such a good vector. In: Gubler DJ, Ooi EE, Subhash Vasudevan JF, editor. *Dengue and Dengue Hemorrhagic Fever. 2nd ed*. Boston, MA: CAB International (2014). p. 455–80. doi: 10.1079/9781845939649.0455
3. Nadjib M, Setiawan E, Putri S, Nealon J, Beucher S, Hadinegoro R, et al. Economic burden of dengue in Indonesia. *PLoS Negl Trop Dis.* (2019) 13:e0007038. doi: 10.1371/journal.pntd.0007038
4. Maula AW, Utarini A. Ten-years trend of dengue research in Indonesia and South-east Asian countries: a bibliometric analysis. *Glob Health Action*. (2018) 11:1504398. doi: 10.1080/16549716.2018.1504398
5. World Health Organization. *Treatment, Prevention and Control Global Strategy for Dengue Prevention and Control 2012-2020*. (2012). Available online at: http://apps.who.int/iris/bitstream/10665/75303/I/9789241504034_eng.pdf
6. MoH-Indonesia. *Situasi Demam Berdarah Dengue di Indonesia*. Pusat data dan Informasi Kementerian Kesehatan RI (2018). Available online at: https://pusdatin.kemkes.go.id/download.php?file=download/pusdatin/infodatin/InfoDatin-Situasi-Demam-Berdarah-Dengue.pdf
7. Sutherst RW. Global change and human vulnerability to vector-borne diseases. *Clin Microbiol Rev*. (2004) 17:136–73. doi: 10.1128/CMR.17.1.136-173.2004
8. Mulligan K, Elliott SJ, Schuster-Wallace C. The place of health and the health of place: Dengue fever and urban governance in Putrajaya, Malaysia. *Health Place*. (2012) 18:613–20. doi: 10.1016/j.healthplace.2012.01.001
9. de Mendonca HFMS, Ferreira AL, dos Santos CB, Rezende HR, Ferreira GEM, Leite GR, et al. Breeding sites of *Aedes aegypti* in metropolitan vacant lots in Greater Vitória, State of Espírito Santo, Brazil. *Rev Soc Bras Med Trop*. (2011) 44:243–6. doi: 10.1590/S0037-86822011000200022
10. Hawley WA. The biology of *Aedes albopictus*. *J Am Mosq Control Assoc Suppl.* (1988) 1:1–39.
11. Kusriastuti R, Sutomo S. Evolution of dengue prevention and control programme in Indonesia DF / DHF Disease Burden. *Dengue Bull*. (2005) 29:1–7.
12. Resende MC De, Silva IM, Ellis BR, Eiras ÁE. A comparison of larval, ovitrap and MosquiTRAP surveillance for *Aedes* (*Stegomyia*) *aegypti*. *Mem Inst Oswaldo Cruz*. (2013) 108:1024–30. doi: 10.1590/0074-02760130128
13. Nathan MB. Critical review of *Aedes aegypti* control programs in the Caribbean and selected neighboring countries. *J Am Mosq Control Assoc*. (1993) 9:1–7.
14. Focks D. *A Review of Entomological Sampling Methods and Indicators for dengue Vectors*. WHO (2003).
15. Bowman LR, Runge-Ranzinger S, McCall PJ. Assessing the relationship between vector indices and dengue transmission: a systematic review of the evidence. *PLoS Negl Trop Dis.* (2014) 8:e2848. doi: 10.1371/journal.pntd.0002848
16. Chang FS, Tseng YT, Hsu PS, Chen CD, Lian IB, Chao DY. Re-assess vector indices threshold as an early warning tool for predicting dengue epidemic in a dengue non-endemic country. *PLoS Negl Trop Dis.* (2015) 9:e0004043. doi: 10.1371/journal.pntd.0004043
17. Cromwell EA, Stoddard ST, Barker CM, Van Rie A, Messer WB, Meshnick SR, et al. The relationship between entomological indicators of *Aedes aegypti* abundance and dengue virus infection. *PLoS Negl Trop Dis.* (2017) 11:e0005429. doi: 10.1371/journal.pntd.0005429
18. Garjito TA, Hidajat MC, Kinansi R, Setyaningsih R, Anggraeni YM, Mujiyanto M, et al. *Stegomyia* indices and risk of dengue transmission: a lack of correlation. *Front Public Health*. (2020). 8:328. doi: 10.3389/fpubh.2020.00328
19. Morrison AC, Astete H, Chapilliqun F, Ramirez-Prada G, Diaz G, Getis A, et al. Evaluation of a sampling methodology for rapid assessment of *Aedes aegypti* infestation levels in Iquitos, Peru. *J Med Entomol*. (2004) 41:502–10. doi: 10.1603/0022-2585-41.3.502
20. Focks D, Chadee DD. Pupal survey at epidemioogically significant surveillance method for *Aedes aegypti*: an example using data from Trinidad. *Am J Trop Med Hyg*. (1997) 56:159–67. doi: 10.4269/ajtmh.1997.56.159
21. WHO. *Malaria Entomology and Vector Control: Tutor's Guide*. (2013). Available online at: http://whqlibdoc.who.int/hq/2003/WHO_CDS_CPE_SMT_2
22. IVRCRD. *Manual on Mosquitoes Field Sampling Methods (In Bahasa Indonesia)*. Available online at: http://www.b2p2vrp.litbang.kemkes.go.id/publikasi/download/59
23. Lanciotti RS, Calisher CH, Gubler DJ, Chang GJ, Vorndam AV. Rapid detection and typing of dengue viruses from clinical samples by using reverse transcriptase-polymerase chain reaction. *J Clin Microbiol*. (1992) 30:545–51. doi: 10.1128/JCM.30.3.545-551.1992
24. Pagès J. Analyse factorielle de donnees mixtes. *Revue Statistique Appliquée*. (2004) 4:93–111.
25. Lê S, Josse J, Husson F. FactoMineR: an R package for multivariate analysis. *J Stat Softw*. (2008) 25:1–18. doi: 10.18637/jss.v025.i01
26. World Health Organization. *Dengue: Guidelines for Diagnosis, Treatment, Prevention and Control*. (2009). Available online at: https://www.who.int/rpc/guidelines/9789241547871/en/
27. Pan American Health Organization. *Dengue and Dengue Hemorrhagic Fever in the Americas: Guidelines for Prevention and Control* (1994).
28. Wijayanti SP, Sunaryo S, Suprihatin S, McFarlane M, Rainey SM, Dietrich I, et al. Dengue in Java, Indonesia: relevance of mosquito indices as risk predictors. *PLoS Negl Trop Dis.* (2016) 10:e0004500. doi: 10.1371/journal.pntd.0004500
29. Agha SB, Tchouassi DP, Bastos AD, Sang R. Assessment of risk of dengue and yellow fever virus transmission in three major Kenyan cities based on *Stegomyia* indices. *PLoS Negl Trop Dis.* (2017) 11:e0005858. doi: 10.1371/journal.pntd.0005858
30. Muller DA, Frentiu FD, Rojas A, Moreira LA, O'Neill SL, Young PR. A portable approach for the surveillance of dengue virus-infected mosquitoes. *J Virol Methods*. (2012) 183:90–3. doi: 10.1016/j.jviromet.2012.03.033
31. Lau SM, Chua TH, Sulaiman WY, Joanne S, Lim YAL, Sekaran SD, et al. A new paradigm for *Aedes* spp. surveillance using gravid ovipositing sticky trap and NS1 antigen test kit. *Parasites Vectors*. (2017). 10:151. doi: 10.1186/s13071-017-2091-y

32. Wasik D, Mulchandani A, Yates MV. Point-of-use nanobiosensor for detection of dengue virus NS1 antigen in adult *Aedes aegypti*: a potential tool for improved dengue surveillance. *Anal. Chem.* (2018) 90:679–84. doi: 10.1021/acs.analchem.7b03407

Conflict of Interest: The authors declare that the research was conducted in the absence of any commercial or financial relationships that could be construed as a potential conflict of interest.

frontiers in Medicine

ORIGINAL RESEARCH
published: 17 June 2021
doi: 10.3389/fmed.2021.593623

Immune Response, Viral Shedding Time, and Clinical Characterization in COVID-19 Patients With Gastrointestinal Symptoms

Huan Yang[1†], *Xiangyu Xi*[2,3†], *Weimin Wang*[3*] and *Bing Gu*[4*]

[1] Xuzhou Key Laboratory of Laboratory Diagnostics, School of Medical Technology, Xuzhou Medical University, Xuzhou, China, [2] The First Affiliated Hospital of Suzhou University, Suzhou, China, [3] Xuzhou Infectious Disease Hospital, Xuzhou, China, [4] Laboratory Medicine, Guangdong Provincial People's Hospital, Guangdong Academy of Medical Sciences, Guangzhou, China

OPEN ACCESS

Edited by:
Jun Feng,
National Institute of Parasitic Diseases, China

Reviewed by:
Hamed Akbari,
Kerman University of Medical Sciences, Iran
Sina Vakili,
Shiraz University of Medical Sciences, Iran

***Correspondence:**
Weimin Wang
1045470899@qq.com
Bing Gu
binggu2015@xzhmu.edu.cn

[†]These authors have contributed equally to this work

Specialty section:
This article was submitted to Infectious Diseases – Surveillance, Prevention and Treatment, a section of the journal Frontiers in Medicine

Received: 14 August 2020
Accepted: 26 May 2021
Published: 17 June 2021

Citation:
Yang H, Xi X, Wang W and Gu B (2021) Immune Response, Viral Shedding Time, and Clinical Characterization in COVID-19 Patients With Gastrointestinal Symptoms. Front. Med. 8:593623. doi: 10.3389/fmed.2021.593623

Background and Aims: Gastrointestinal (GI) symptoms are frequently observed in coronavirus disease (COVID-19) symptoms. Previous studies have mainly focused on epidemiology and characteristics in patients with GI symptoms, little is known about the roles of the immune response in susceptibility to and severity of infection. Here, we analyzed COVID-19 cases to determine immune response and clinical characteristics in COVID-19 patients with GI symptoms.

Methods: Based on the presence of GI symptoms, 79 patients in Xuzhou were divided into GI and non-GI groups. A retrospective study investigating the clinical characteristics, selected laboratory abnormalities, immune response, treatment, and clinical outcome was performed to compare patients with or without GI symptoms.

Results: Approximately 25% of patients reported at least one GI symptom. Our results showed significantly higher rates of fatigue, increased LDH, increased CK, higher percentage increase neutrophil-to-lymphocyte ratio (NLR), lymphopenia, and bilateral pneumonia in patients with GI symptoms. No significant changes in serum amylase (SAA), immunoglobulin (Ig) G, IgM, C-reactive protein (CRP), procalcitonin (PCT), interleukin-6 (IL-6), viral shedding time, liver injury, and kidney injury between the two groups were observed. The clinical type on admission of patients with GI symptoms reported significantly higher rates of critical disease type (20 vs. 3.3%; $p = 0.033$). However, the survival rate did not differ between the two groups.

Conclusions: Increase in total lymphocytes and NLR as well as the elevation of CRP, SAA, PCT, IL-6, CK, and LDH were closely associated with COVID-19 with GI symptoms, implying reliable indicators COVID-19 patients with GI symptoms were more likely to develop into a severe disease.

Keywords: COVID-19, gastrointestinal symptoms, immune response, clinical characterization, epidemiology

INTRODUCTION

The coronavirus disease 2019 (COVID-19) outbreak started in December 2019 in China has spread sharply all over the world (1). Although COVID-19 presents most commonly with respiratory symptoms, early reports have described GI symptoms in patients diagnosed with COVID-19 (2). Clinical observations have shown that patients with COVID-19, especially severe patients, have significantly reduced lymphocyte counts and increased neutrophils, and are accompanied by a large accumulation of cytokines, indicating an imbalance in the immune system (3). The epidemiological, clinical dynamic profile among observed in patients with COVID-19 with GI symptoms has begun to emerge (4–6), but the characteristics of the immune response in COVID-19 patients with GI symptoms are still not clear.

An immune response in COVID-19 patients with GI symptoms is urgently needed to guide clinical diagnosis, treatment, infection control, and vaccine design. IgM antibodies are indicators of current or recent infections and the earliest signs after exposure to pathogens. IgG antibodies are the most common antibodies to the disease, indicating that the disease or past infection has recovered. Therefore, the testing of SARS-CoV-2 IgG and IgM antibodies not only helps to diagnose COVID-19, but also helps to assess the infection status. However, the production of antibodies and their protective effects on the prognosis of COVID-19 patients with GI symptoms need to be clarified.

Increasing clinical data have indicated the NLR as a powerful predictive and prognostic indicator for severe COVID-19 (7, 8). However, the NLR in COVID-19 patients with GI symptoms and its relation to disease status and outcome remains to be determined.

IL-6 is a typical pro-inflammatory factor that causes cytokine storms, and IL-6 blocking strategies have been successfully used in the treatment of various chronic inflammatory diseases (9). Therefore, we monitored serum IL-6 levels in patients with COVID-19 to better understand prognosis and to implement effective treatment. CRP, SAA, and procalcitonin (PCT) are usually early indicators of acute viral infection.

METHODS

Data Collection

We enrolled a total of 79 patients with COVID-19 following the Declaration of Helsinki, which was confirmed by detecting SARS-CoV-2 RNA in throat swab samples using a SARS-CoV-2 nucleic acid detection kit according to the manufacturer's protocol (Shanghai BioGerm Medical Biotechnology Co.,Ltd). All patients were initially admitted to the Affiliated Hospital of Xuzhou Medical University and Xuzhou Infectious Disease Hospital from 26 January to 16 February, 2020.

A retrospective study investigating patients age, sex, medical history, symptoms, comorbid conditions, severity assessment on admission, laboratory findings, immune response parameter, chest CT findings, treatment, efficacy, and clinically-relevant hospitalization outcomes was performed.

The definition of positive GI symptoms requires patients to present at least one of the following symptoms: nausea, vomiting, or diarrhea. GI symptoms are recorded on admission, to exclude the effects of other drug treatments and external factors. COVID-19 patients are divided into four subtypes according to their symptoms. The severity of the disease is determined according to the diagnosis and treatment plan of SARS-CoV-2 in China (Sixth Edition). Mild patients have very mild symptoms, and imaging does not show signs of pneumonia. The common type has fever and respiratory symptoms, while imaging shows evidence of pneumonia. Severe patients present obvious clinical symptoms, shortness of breath and other symptoms, and changes in clinical indicators. The pulse oxygen saturation is <93% in the resting state, and the lung imaging progressed significantly within 24–48 h, reaching a degree of 50%. Critical patients have respiratory failure, require mechanical ventilation or non-invasive ventilation, or present shock or other organ failure, and require ICU monitoring and treatment.

Laboratory Examination of Blood Samples

Approximately 3–5 mL of peripheral blood was obtained with a collection tube from the subjects in each group, serum samples were separated at 2,000 rpm for 20 min centrifugation. Serum cytokines were tested using enzyme-linked immunosorbent assay (ELISA). CRP was tested using i-CHROMA immunofluorescence assay. IgG and IgM antibodies were tested using quantum dot fluorescence immunoassay technology. PCT were tested by chemiluminescence analysis.

COVID-19 Treatment

There is currently no targeted or specific treatment for COVID-19. We have attempted many treatment approaches, including antiviral therapy, antibiotics, steroid hormones, oxygen therapy, Traditional Chinese medicine treatment, probiotics, immunoglobulin treatment. For antibiotic treatment, we have attempted one or more antibiotics, which included moxifloxacin hydrochloride tablets, levofloxacin hydrochloride, ceftriaxone, cefoperazone, biapenem, daptomycin, and linezolid. We used lopinavir, ritonavir, and interferon-α as antiviral treatments. Probiotics were used to regulate the gut microbe and thus, we used *Bacillus* subtilis dual live bacteria capsules to relieve GI symptoms. Traditional Chinese medicine (TCM) treatment can regulate immunity. Lianhua Qingwen granules, Huoxiang Zhengqi capsules, and Chinese herbal decoctions. Immune globulin was used to treat patients at a dose of 20 g/day. Glucocorticoids such as methylprednisolone and inhaled budesonide were not used in patients with non-severe COVID-19 patients.

Statistical Analysis

Variables are described by frequency and percentages, compared using the chi-squared ($\chi 2$) or Fisher exact tests. Normality of distribution was analyzed by Shapiro-Wilk test. When data had a normal distribution, statistical significance of differences between groups was calculated, followed by unpaired *t*-test and non-parametric test when appropriate. All statistical analyses were

TABLE 1 | Epidemiological characteristics of patients with COVID-19 with and without GI symptoms.

Characteristic	Group A: GI symptoms ($n = 20$)	Group B: No GI symptoms ($n = 59$)	*P*-value
Age (≥45 years old)	11 (55%)	24 (40.6%)	0.265
Sex (male)	8 (40%)	27 (45.7%)	0.654
Sex (female)	12 (60%)	32 (54.2%)	0.654
Past medical history			
Any	8 (40%)	29 (49.1%)	0.478
Hypertension	5 (25%)	10 (16.9%)	0.643
Diabetes	2 (10%)	8 (13.5%)	0.980
Cancer	1 (5%)	1 (1.7%)	0.445
Hyperthyresis	0	1 (1.7%)	>0.999
Coronary heart disease	0	3 (5%)	0.567
Cerebrovascular disease	0	4 (6.7%)	0.545
Pregnancy	0	1 (1.7%)	>0.999
Exposure history			
Contact with the epidemic area	5 (25%)	10 (16.9%)	0.643
Contact with patients	3 (15%)	30 (50.8%)	0.005
Family cluster	9 (45%)	17 (28.8%)	0.183
Clinical subtype on admission			
Critical	4 (20%)	2 (3.3%)	0.033
Coventional	16 (80%)	54 (91.5%)	0.32
Light	0	3 (5%)	0.567

TABLE 2 | Clinical characteristics and selected laboratory abnormalities of patients with COVID-19 with and without GI symptoms.

Characteristic	Group A: GI symptoms ($n = 20$)	Group B: No GI symptoms ($n = 59$)	*P*-value
Fever >38.5°C	9 (45%)	15 (25.4%)	0.100
Sore throat	6 (30%)	6 (10.1%)	0.076
Muscle ache	3 (15%)	1 (1.7%)	0.079
Headache	4 (20%)	5 (8.5%)	0.320
Fatigue	13 (65%)	14 (23.7%)	0.001
Chills	1 (5%)	5 (8.5%)	0.985
Dyspnea	10 (50%)	20 (33.8%)	0.200
Cough	14 (70%)	40 (67.7%)	0.855
Sputum production	9 (45%)	23 (38.9%)	0.636
Co-infection (*Enterobacter aerogenes, Enterococcus gallinarum,* Urinary Tract Infection)	0	5 (8.5%)	0.416
Selected abnormal laboratory findings			
Hyperglycemia (3.8–6.2 mmol/L)	11 (55%)	31 (52.5%)	0.849
Coagulopathy (PT 9.4–12.5 s, D-dimer 0–2.4 μg/mL)	4 (20%)	25 (42.3%)	0.073
Anemia (Hb115–150 g/L)	1 (5%)	6 (10.1%)	0.804
CK increased (20–200 U/L)	5 (25%)	1 (1.7%)	0.004
LDH inceased (110–240 U/L)	9 (45%)	12 (20.3%)	0.031
Liver injury (ALT 9–50 U/L, AST 15–40 U/L)	1 (5%)	5 (8.5%)	0.985
Kidney injury (Urea nitrogen 1.7–8.3 mmol/L, Creatinine 40–97 umol/L)	2 (10%)	2 (3.4%)	0.565
Chest X—ray/CT findings			
Normal	0	3 (5%)	0.567
Unilateral pneumonia	2 (10%)	15 (25.4%)	0.256
Bilateral pneumonia	18 (90%)	36 (61%)	0.0160
Multiple mottling and ground- glass opacity	18 (90%)	48 (81.3%)	0.581

performed using SPSS version 23.0 software. $P \leq 0.05$ was considered statistically significant.

RESULTS

A total of 79 patients with confirmed COVID-19 were enrolled from 26 January 2020 to 16 February 2020 in Xuzhou, among which 20 (25%) patients presented at least one GI tract symptom GI symptoms were as follows: 14 patients experienced diarrhea six patients had vomiting symptoms. Of the 20 COVID-19 patients with GI symptoms, eight were males and 12 females, with a mean age of 46.7 years (range 26–69). As outlined in **Table 1**, there were no age and sex differences between In addition, COVID-19 patients with GI symptoms were not significantly correlated with any medical history, including hypertension, diabetes or cancer (**Table 1**). Five (25%) patients had a history of exposure to Wuhan three (15%) patients had a history of contact with patients with COVID-19 and nine (45%) patients were exposed to a positive family cluster (**Table 1**). The proportion of critical disease type was significantly higher in patients with COVID-19 with GI symptoms than in those without GI symptoms (20 vs. 3.3%, $p = 0.033$).

As outlined in **Table 2**, clinical symptoms such as fatigue (65 vs. 23.7%; $p = 0.001$) were also more frequent in patients with GI symptoms than in those without GI symptoms. Although there were no statistical differences, COVID-19 patients with GI symptoms had higher rate of fever >38.5°C, sore throat and muscle ache. The percentage of patients with higher CK (25 vs. 1.7%; $p = 0.004$) and LDH (45 vs. 20.3%; $p = 0.031$) was significantly higher in COVID-19 patients with GI symptoms than in those without GI symptoms. However, other abnormal laboratory findings revealed no significant differences in the rate of hyperglycemia, coagulopathy, anemia, liver injury, and kidney injury between patients with GI symptoms and those without. Additionally, Chest CT findings showed that patients with GI symptoms had significantly higher rates of bilateral pneumonia (90 vs. 61%; $p = 0.016$).

Next, to compare the immune response induced by SARS-CoV-2 in COVID-19 patients between with GI symptoms and in those without GI symptoms, we investigated the protein expression of pro-inflammatory cytokines IL-6, the SARS-CoV-2

IgM and IgG antibody, lymphocyte, NLR (cut off 3.04), CRP, SAA, and PCT. The percentages of increased NLR (55.5 vs. 31.7%; $p = 0.049$), lymphopenia (55.5 vs. 31.7%; $p = 0.049$), increased SAA (75 vs. 38.5%; $p = 0.059$), increased CRP (58.3 vs. 26.9%; $p = 0.061$), and increased IgG antibody (84.2 vs. 76.7%; $p = 0.743$) and IgM antibody (73.6 vs. 60.4%; $p = 0.316$) were higher in COVID-19 patients with GI symptoms than in those without GI symptoms, although some test results showed no significant differences. However, the SARS-CoV-2 IgM, IL-6, and PCT were not differences between patients with GI symptoms and those without (**Figure 1**). We further analyzed the absolute expression level of IL-6, and the SARS-CoV-2 IgM and IgG antibodies, NLR, CRP, SAA, and PCT (**Figure 2**). Among COVID-19 patients with GI symptoms, the median level of IgM, IgG, IL-6, SAA, CRP, PCT, and NLR were 209.15 IU/mL, 470.36 IU/mL, 15.7 pg/mL, 120.6 mg/mL, 37.1 mg/mL, 0.76 ng/mL, and 8.76, respectively. In addition, for COVID-19 patients without GI symptoms, the median levels of IgM, IgG, IL-6, SAA, CRP, PCT, and NLR were 195.1 IU/mL, 521.1 IU/mL, 10.1 pg/mL, 71.8 mg/mL, 15.4 mg/mL, 0.268 ng/mL, and 6.35, respectively. Except for IgG, there was a similar tendency for a stronger immune response in COVID-19 patients with GI symptoms than in those without GI symptoms, although there were no statistically significant differences between patients with GI symptoms and those without. In sum, COVID-19 patients with GI symptoms experienced a more severe immune system disorder.

The median duration of viral shedding was similar between patients with GI symptoms and without (**Figure 3**). For COVID-19 with GI symptoms patients, the median duration of viral shedding was 16.1 days, and the median duration of viral shedding was 15.6 days in patients without GI symptoms.

COVID-19 patients with GI symptoms receiving oxygen, antibiotics, antivirals, immunoglobulins, hormones, TCM and probiotics treatment accounted for 95, 90, 100, 10, 45, 60%, and 0, respectively (**Table 3**). No significant differences in rates of treatment with oxygen, antibiotics, antivirals, immunoglobulins, TCM and probiotics treatment, except for hormone treatment (45 vs. 19%; $p = 0.031$). At the end of observation, all patients were discharged.

DISCUSSION

In this study involving two tertiary hospitals in Xuzhou, we found that nearly 25% of hospitalized patients with SARS-CoV-2 infection presented at least one GI symptom. Vomiting and diarrhea were the most common symptoms in these patients. Patients diagnosed with COVID-19 may only have GI symptoms. Therefore, in order to control the epidemic, it is necessary to rigorously screen patients and take appropriate treatment measures. Patients diagnosed with COVID-19 with GI symptoms patients, may be misdiagnosed which favors diffusion of the virus. These close contacts will not be isolated, and may lead to widespread spread of the virus and improper treatment of diagnosed patients. Patients suspected of COVID-19 presenting with GI symptoms, should be carefully managed as the ability of the virus bind to ACE2 receptor of the GI tract has been identified (10). Patients with GI symptoms have reported greater fatigue. The percentage of increased CK and LDH was significantly higher in patients presenting GI symptoms. LDH levels have been positively associated with the COVID-19 severity (11). Increased CK and LDH are indicators of heart damage, therefore, patients with GI symptoms should be monitored for heart disease. Patients with GI symptoms on admission are associated with the clinical types indicating significantly higher rates of critical type disease. Therefore, patients with GI symptoms should receive greater attention for the development of critical disease. It was consistent with other report that patients with COVID-19 with GI symptoms had significantly higher critical types than those without GI symptoms (6).

Lymphocytes and specific lymphocyte subsets played an important role in the maintenance of the immune system function. Lymphocytes and the subsets alterations were associated with the clinical characteristics and treatment efficacy of COVID-19, and critically ill patients showed a significant reduction in levels of lymphocytes, monocytes, CD4 + T cells, CD8 + T cells, CD3 cells, CD19 cells, and natural killer (NK) cells (12–14). The association between lymphopenia and the severity of COVID-19 implied as the depletion of lymphocytes with had occurred, especially CD4+T and CD8+T cells. Thus, it is important to clarify the different characteristics of lymphocytes in COVID-19 patients with GI symptoms and without. However, this study observed levels of total lymphocytes and did not detect its subsets. We found that lymphopenia was significantly higher in COVID-19 patients with GI symptoms than in those without, indicating immune system disorders during the course of SARS-CoV-2 infection with GI symptoms. This was not consistent with the findings by Luo et al. who reported that lymphocyte counts in COVID-19 patients with GI symptoms were similar in those without GI symptoms in Wuhan, China (14). For reasons that are not entirely clear, these differences may be related to the region and the number of patients. The high NLR is a reliable indicator for predicting the incidence of early more severe disease (15). Our results showed that patients with GI symptoms had higher levels of NLR than those without GI symptoms, suggesting that COVID-19 patients with GI symptoms and high NLR levels were more likely to develop into severe patients. In total, our study demonstrated the association between GI symptoms and lymphopenia, and provided important insights on the immunopathogenesis of SARS-CoV-2 infection with GI symptoms.

The SARS-CoV-2 specific IgM and IgG antibodies in patients provided the basis for disease diagnosis. In addition, patients with severe disease frequently presented a stronger IgG response and a higher titer of total antibodies, which was associated with worse outcome (7). However, some studies have reported that there was no direct correlation between antibody concentration and disease severity (13). Therefore, whether SARS-CoV-2 specific IgM and IgG antibodies in patients was pathogenic or protective required further study. Our study showed that there was no difference between COVID-19 patients with GI symptoms and those without IgM and IgG antibody levels. The IgM and IgG antibody responses in COVID- 19 patients, still require elucidation.

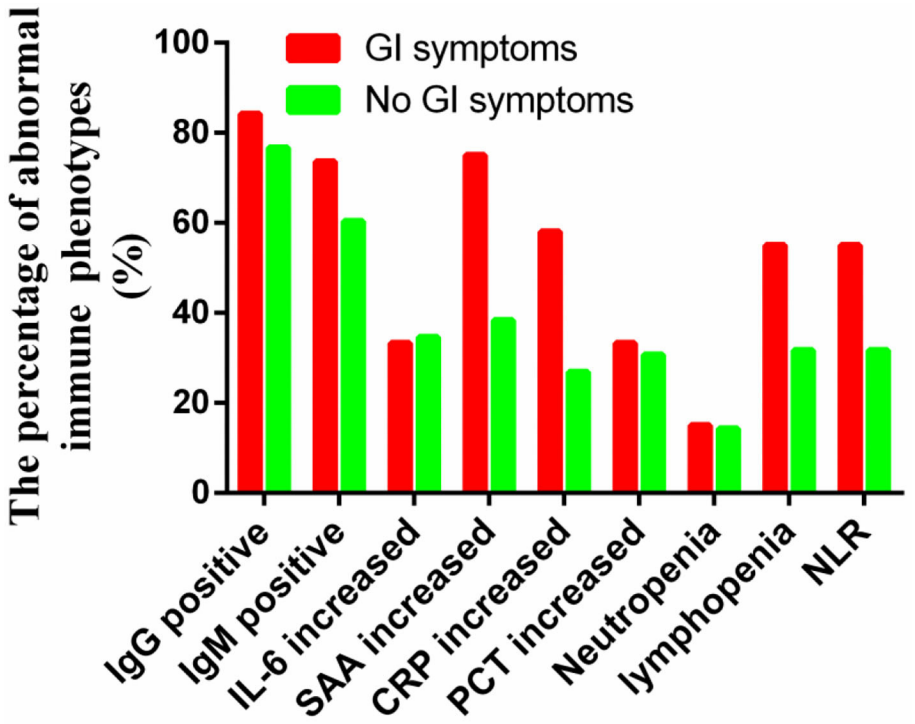

FIGURE 1 | Immune response phenotype in COVID-19 patients with and without GI symptoms according to the percentage of abnormal indicators.

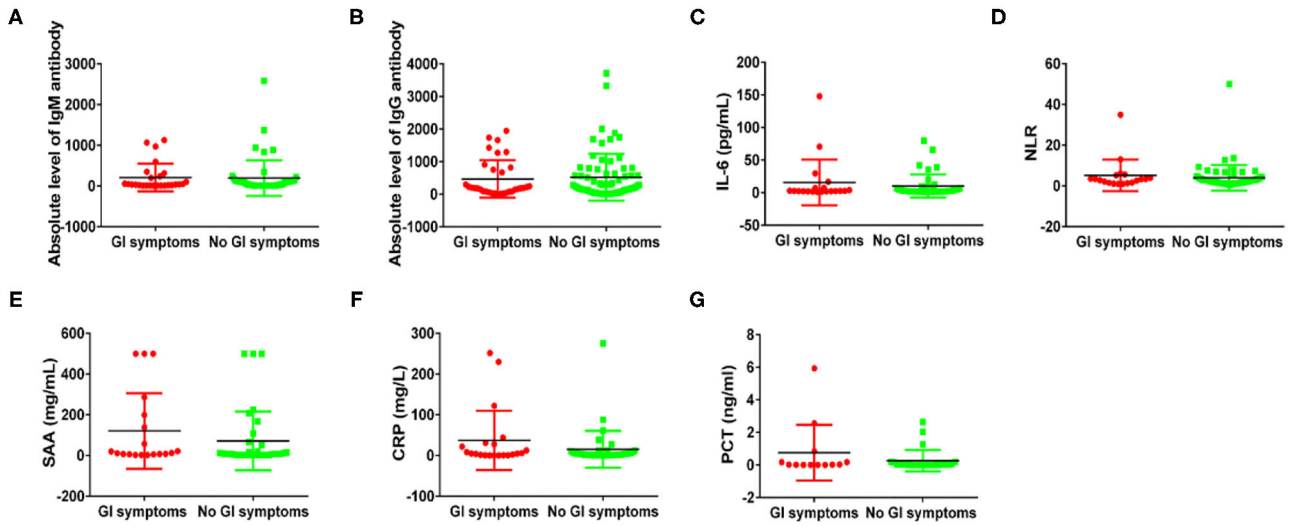

FIGURE 2 | Immune response phenotyping in COVID-19 patients with and without GI symptoms according to the expression level. Comparing IgM levels **(A)**, IgG levels **(B)**, IL-6 levels **(C)**, NLR levels **(D)**, SAA levels **(E)**, CRP levels **(F)**, and PCT levels **(G)** between patients with and without GI symptoms.

Infammatory markers such as CRP and PCT were associated with the COVID-19 severity. It has been reported that the levels of CRP were significantly increased in severe cases compared to non-severe COVID-19 patients (16). SAA can improve inflammation by activating chemokines and inducing chemotaxis (17), and were significantly related to COVID-19 severity. The PCT concentration of severe patients was significantly higher than that of non-severe patients (18). Although there was no significant difference, the percentage of increased SAA, increased PCT, and increased CRP and their concentrations were higher in COVID-19 patients with GI symptoms, which indicated patients with GI symptoms presented more intense inflammation. In the

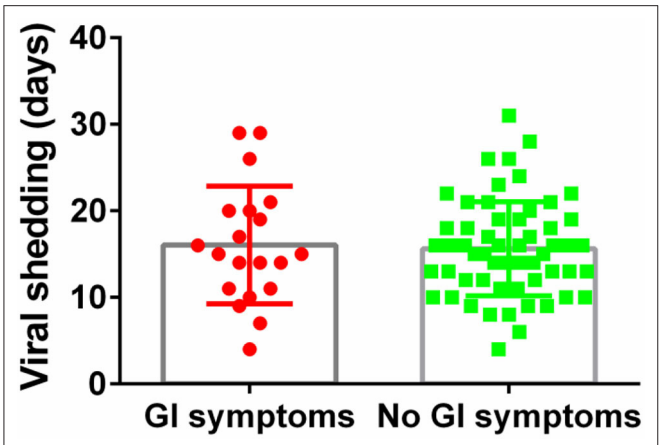

FIGURE 3 | Viral shedding days between patients with and without GI symptoms.

TABLE 3 | Treatment and Clinical outcome in patients with COVID-19 with and without GI symptoms.

Variable	GI symptoms ($n = 20$)	No GI symptoms ($n = 59$)	*P*-value
Treatment			
Antiviral therapy	20 (100%)	59 (100%)	>0.999
Antibiotic treatment	18 (90%)	41 (69.5%)	0.068
Hormones	9 (45%)	12 (19%)	0.031
Oxygen therapy	19 (95%)	58 (98.3%)	0.445
Traditional Chinese medicine treatment	12 (60%)	22 (37.2%)	0.076
Probiotics treatment	0	3 (5%)	0.567
Immunoglobulin treatment	2 (10%)	1 (1.7%)	0.156
Clinical outcome			
Discharge from hospital	20 (100%)	59 (100%)	>0.999
Staying in hospital	0	0	
Death	0	0	

fight against SARS-CoV-2, excessive secretion of IL-6 could cause acute and severe systemic inflammatory cytokine storms (19). Although no clear correlation has been found between COVID-19 patients with GI symptoms and IL-6 levels, IL-6 may become a potential target for immunotherapy for COVID-19 pneumonia.

In our study, the SARS-CoV-2 viral duration in COVID-19 patients with GI symptoms and without was similar, which means they were equally effective in spreading COVID-19. For COVID-19 patients with only GI symptoms, nucleic acid testing for virus is the gold standard for diagnosis. According to the latest version of the Chinese guidelines (20), after discharge from the hospital, patients should remain isolated and receive close medical observation by doctors for an additional 14 days. Our study showed that the average viral shedding time for the COVID-19 patients with GI symptoms was 16 days, so medical observation require longer periods.

It should be noted that there were some limitations of this study. First, our study is was limited by its small sample size, thereby it is not known whether our findings could be generalized. Nevertheless, our cohort is representative of two tertiary care hospitals containing different COVID-19 diseases spectrums. Furthermore, the quantitative viral load was not available for our patients, so the kinetics of viral shedding and the magnitude of antibody response during COVID-19 disease progression remained unknown in this study. Peripheral lymphocyte subset alteration showed an obvious association with the clinical characteristics of COVID-19, our study did not monitor lymphocyte subsets, including CD4+T cells, CD8+T cells and B cells. Although multiple immune indicators were detected, there was no continuous monitoring of dynamic immune responses.

In conclusion, we reported, the immune response, viral shedding time and clinical characterization in of COVID-19 patients with GI symptoms. Although we did not find a correlation between the presence of GI symptoms and hospitalization outcomes, we noted that the rate of critical disease type was increased in COVID-19 patients with GI symptoms. The percentage of increased CK and LDH was significantly higher in COVID-19 patients with GI symptoms than in those without GI symptoms. Fortunately, COVID-19 patients with GI symptoms did not tend to present more serious liver or kidney damage. In addition, COVID-19 patients with GI symptoms showed more intense immune response, including increased NLR, lymphopenia, increased SAA and increased CRP levels, although there was no significant difference in the levels of specific IgG or IgM antibodies. Based on the characteristics of the immune response of patients with GI symptoms, it is suggested that immunotherapy such as antagonistic cytokines may be used to treat COVID-19 patients. Further study on the immunopathogenesis of SARS- CoV-2 infection with GI symptoms is warranted. Immunotherapy and other TCM, probiotics, antiviral, anti-inflammatory, antioxidant, oxygen inhalation, respiratory support, and protective effects of organ failure may be available, cost-effective, and of tolerable toxicity.

DATA AVAILABILITY STATEMENT

The original contributions presented in the study are included in the article/supplementary material, further inquiries can be directed to the corresponding author/s.

ETHICS STATEMENT

Written informed consent was obtained from the individual(s), and minor(s)' legal guardian/next of kin, for the publication of any potentially identifiable images or data included in this article.

AUTHOR CONTRIBUTIONS

HY analyzed the data and drafted the paper. XX processed and collected data. WW and BG revised and proofreaded

articles. All authors contributed to the article and approved the submitted version.

FUNDING

This research was supported by National key research and development plan public safety risk prevention and emergency technology equipment key special novel coronavirus-infected pneumonia emergency project (2020YFC0848100), the National Natural Science Foundation of China (81871734, 81471994), the Xuzhou Science and Technology planning Project (KC20116), Natural Science Research Project of Higher Education Institutions in Jiangsu Province (20KJB310013) and Xuzhou Medical University Excellent Talent Introduction Project (D2019030).

ACKNOWLEDGMENTS

The authors would like to thank the researchers who help us get better understanding of the SARS-CoV-2 and the medical doctors who work in the frontiers to save lives all over the world.

REFERENCES

1. Li Q, Guan X, Wu P, Wang X, Zhou L, Tong Y, et al. Early transmission dynamics in Wuhan, China, of novel coronavirus-infected pneumonia. *N Engl J Med*. (2020) 382:1199–207. doi: 10.1056/NEJMoa2001316
2. Xiao F, Tang M, Zheng X, Liu Y, LI X, Shan H. Evidence for gastrointestinal infection of SARS-CoV-2. *Gastroenterology*. (2020) 158:1831–3.e3. doi: 10.1053/j.gastro.2020.02.055
3. Qin C, Zhou L, Hu Z, Zhang S, Yang S, Tao Y, et al. Dysregulation of immune response in patients with COVID-19 in Wuhan, China. *Clin Infect Dis*. (2020) 71:762–8. doi: 10.1093/cid/ciaa248
4. Walker DR, Joyce CH, Kelly EH,Thomas RM, Ahmad NB, Christopher CT, Shen L, et al. Prevalence and characteristics of gastrointestinal symptoms in patients with SARS-CoV-2 infection in the United States: a multicenter cohort study. *Gastroenterology*. (2020) 159:765–7.e2. doi: 10.1053/j.gastro.2020.04.045
5. Zhou ZL, Zhao N, Shu Y, Han SB, Chen B, Shu XG. Effect of gastrointestinal symptoms on patients infected with COVID-19. *Gastroenterology*. (2020) 158:2294–7. doi: 10.1053/j.gastro.2020.03.020
6. Jin X, Lian JS, Hu GH, Gao J, Zheng L, Zhang YM, et al. Epidemiological, clinical and virological characteristics of 74 cases of coronavirus infected disease 2019. (COVID-19) with gastrointestinal symptoms. *Gut*. (2020) 69:1002–9. doi: 10.1136/gutjnl-2020-320926
7. Zhang B, Zhou X, Zhu C, Song Y, Feng F, Qiu Y, et al. Immune phenotyping based on neutrophil-to-lymphocyte ratio and IgG predicts disease severity and outcome for patients with COVID-19. *medRxiv*. (2020) 7:1–7. doi: 10.1101/2020.03.12.20035048
8. Liu J, Li S, Liu J, Lang B, Wang X, Wang H, et al. Longitudinal characteristics of lymphocyte responses and cytokine profiles in the peripheral blood of SARS-CoV-2 infected patients. *medRxiv*. (2020) 55:1–10. doi: 10.1016/j.ebiom.2020.102763
9. Dennis MG, Kassem S, Anthony OR, Charlie B. The role of cytokines including Interleukin-6 in COVID-19 induced pneumonia and macrophage activation syndrome-like disease. *Autoimmun Rev*. (2020) 19:102537. doi: 10.1016/j.autrev.2020.102537
10. Du ML, Cai GS, Chen F,David CC, Zhang Z, Wang ML. Multiomics evaluation of gastrointestinal and other clinical characteristics of SARS-CoV-2 and COVID-19. *Gastroenterology*. (2020) 158:2298–301.e7. doi: 10.1053/j.gastro.2020.03.045
11. Sulmaz G, Reza T, Kanran BL, Seyyed MAK, Shahla R, Nazanin Z, et al. Laboratory features of severe vs. non-severe COVID−19 patients in Asian populations: a systematic review and meta-analysis. Ghahramani et al. *Eur J Med Res*. (2020). doi: 10.1186/s40001-020-00432-3
12. Wang F, Nie JY, Wang HZ, Zhao Q, Xiong Y, Deng LP, et al. Characteristics of peripheral lymphocyte subset alteration in COVID-19 pneumonia. *J Infect Dis*. (2020) 221:1762–9. doi: 10.1093/infdis/jiaa150
13. Zhao J, Yuan Q, Wang H, Liu W, Liao XJ, Su YY, et al. Antibody response to SARS-CoV-2 in patients of novel coronavirus disease 2019. *Clin Infect Dis*. (2020) 71:2027–34. doi: 10.1093/cid/ciaa344
14. Luo SH, Deng ZQ, Zhang XC, Pan ZY, Xu HB. Clinical characteristics and outcomes of 2019 novel coronavirus disease patients presenting with initial gastrointestinal symptoms in Wuhan, China: a retrospective cohort study. *J Gastroenterol Hepatol*. (2020) 36:694–9. doi: 10.1111/jgh.15199
15. Liu J, Liu Y, Xiang P, Pu L, Xiong HF, Li CS, et al. Neutrophil-to-Lymphocyte ratio predicts severe illness patients with 2019. novel coronavirus in the early stage. *medRxiv*. (2020) 18:1–12. doi: 10.1101/2020.02.10.20021584
16. Zhang F, Ouyang L, Gong YL, Li JH, Wei XY, Chu YQ, et al. Clinical features of 81 hospitalized patients with 2019 novel coronavirus-infected pneumonia in Jingzhou, China: a descriptive study. *SSRN Electron*. (2020). doi: 10.2139/ssrn.3544834
17. Sack GH. Serum amyloid a –a review. *Mol Med*. (2018) 24:1–27. doi: 10.1186/s10020-018-0047-0
18. Hamed A, Reza T, Kamran BL, Hamid A, Sina V, Fatemah A, et al. The role of cytokine profile and lymphocyte subsets in the severity of coronavirus disease 2019. (COVID-19): a systematic review and meta-analysis. *Life Sci*. (2020) 258:118167. doi: 10.1016/j.lfs.2020.118167
19. Han H, Ma QF, Li C, Liu R, Zhao L, Wang W, et al. Profiling serum cytokines in COVID-19 patients reveals IL-6 and IL-10 are disease severity predictors. *Emerg Microb Infect*. (2020) 9:1123–30. doi: 10.1080/22221751.2020.1770129
20. National Health Commission of the People's Republic of China. *The Notice of Launching Guideline on Diagnosis and Treatment of the Novel Coronavirus Pneumonia*. 7th ed. Available online at: http://www.nhc.gov.cn/yzygj/s7653p/202003/46c9294a7dfe4cef80dc7f5912eb1989.shtml (accessed March 4, 2020).

Conflict of Interest: The authors declare that the research was conducted in the absence of any commercial or financial relationships that could be construed as a potential conflict of interest.

frontiers in Cellular and Infection Microbiology

REVIEW
published: 21 June 2021
doi: 10.3389/fcimb.2021.665444

Development of miRNA-Based Approaches to Explore the Interruption of Mosquito-Borne Disease Transmission

Tie-Long Xu[1,2,3], *Ya-Wen Sun*[2,3], *Xin-Yu Feng*[2,3,4], *Xiao-Nong Zhou*[2,3,4]* *and Bin Zheng*[2,3,4]*

[1] Evidence-Based Medicine Research Center, Jiangxi University of Chinese Medicine, Nanchang, China, [2] National Institute of Parasitic Diseases, Chinese Center for Disease Control and Prevention, and WHO Collaborating Center for Tropical Diseases, Shanghai, China, [3] Key Laboratory of Parasite and Vector Biology, Ministry of Public Health, Shanghai, China, [4] School of Global Health, Chinese Center for Tropical Diseases Research, Shanghai Jiao Tong University School of Medicine, Shanghai, China

OPEN ACCESS

Edited by:
Lubin Jiang,
Institut Pasteur of Shanghai (CAS), China

Reviewed by:
Fabrizio Lombardo,
Sapienza University of Rome, Italy
Maria Luisa Simões,
Johns Hopkins University, United States

***Correspondence:**
Xiao-Nong Zhou
zhouxn1@chinacdc.cn
Bin Zheng
cdcipdzhengbin@126.com

Specialty section:
This article was submitted to Parasite and Host, a section of the journal Frontiers in Cellular and Infection Microbiology

Received: 08 February 2021
Accepted: 02 June 2021
Published: 21 June 2021

Citation:
Xu T-L, Sun Y-W, Feng X-Y, Zhou X-N and Zheng B (2021) Development of miRNA-Based Approaches to Explore the Interruption of Mosquito-Borne Disease Transmission. Front. Cell. Infect. Microbiol. 11:665444. doi: 10.3389/fcimb.2021.665444

MicroRNA (miRNA or miR)-based approaches to interrupt the transmission of mosquito-borne diseases have been explored since 2005. A review of these studies and areas in which to proceed is needed. In this review, significant progress is reviewed at the level of individual miRNAs, and miRNA diversification and relevant confounders are described in detail. Current miRNA studies in mosquitoes include four steps, namely, identifying miRNAs, validating miRNA-pathogen interactions, exploring action mechanisms, and performing preapplication investigations. Notably, regarding the *Plasmodium* parasite, mosquito miRNAs generally bind to mosquito immunity- or development-related mRNAs, indirectly regulating *Plasmodium* infection; However, regarding arboviruses, mosquito miRNAs can bind to the viral genome, directly modifying viral replication. Thus, during explorations of miRNA-based approaches, researchers need select an ideal miRNA for investigation based on the mosquito species, tissue, and mosquito-borne pathogen of interest. Additionally, strategies for miRNA-based approaches differ for arboviruses and protozoan parasites.

Keywords: miRNAs, mosquito, *Plasmodium*, interruption, miRNA-based approach, mosquito-borne diseases

BACKGROUND

Insecticide-based interventions [e.g., long-lasting insecticide-treated bed nets (LLINs) and indoor residual spraying (IRS)] are important components of integrated mosquito management programs designed to block the transmission of mosquito-borne diseases. The insecticides used in these interventions exert strong selection pressure on resistance and lead to the evolution and spread of mosquito resistance, representing a major concern in mosquito-borne disease control programs (Xu et al., 2014). The World Health Organization (WHO) claims that innovative vector control tools are urgently needed (World Health Organization, 2012). MicroRNAs (miRNAs) are single-stranded, conserved, and small endogenous noncoding RNAs that have important regulatory functions at the posttranscriptional level in diverse organisms (Bartel, 2004; Bartel, 2009). The regulation of

miRNAs is indispensable for various processes, including apoptosis, development, differentiation, viral infection, and so on (Bartel, 2004; Bartel, 2009). More importantly, the functions of miRNAs can be explored and utilized. For instance, miR-15, miR-16, miR-34, and Let-7 have been patented and approved for cancer diagnosis or treatment (Mishra et al., 2016). Given their characteristics and functions, miRNAs represent one possibility for establishing a new tool, namely, miRNA-based approaches. Thus, numerous studies on mosquito miRNAs have been performed since 2005 (Wang et al., 2005) with the ultimate goal of utilizing miRNA-based approaches for disease control (Liu et al., 2017; Feng et al., 2018a). The development of a mosquito miRNA-based approach is presumed to always follow the research roadmap of identifying mosquito miRNAs, observing miRNA-pathogen interaction, exploring action mechanisms, performing preapplication investigations and conducting clinical or field trials. Advances at each step of the roadmap need to be outlined to provide important insight into potential applications.

THE MOSQUITO MIRNA DATABASES ANALYZED

Publications focused on investigating mosquito global miRNA profiles were selected for extraction of information, including the authors, publication year, study materials, methods, miRNA names, canonical sequences, and so on. Then, this information was supplemented during the review of the other included papers. Approximately 1635 mature or predicted miRNAs were collected. Of the 1635 miRNAs, 853 (52.17%) were limited to identification and lacked any additional study information. The remaining 782 (47.83%) were further investigated; thus, they were tracked by their annotated names for study development.

Overall, the miRNAs of 24 mosquito species, including 2 species of *Aedes* (Li et al., 2009; Akbari et al., 2013; Gu et al., 2013; Campbell et al., 2014; Hu et al., 2015; Maharaj et al., 2015; Liu et al., 2015; Liu Y. X. et al., 2016; Batz et al., 2017; Su et al., 2017; Zhang et al., 2017), 2 species of *Culex* (Skalsky et al., 2010; Hong et al., 2014), and 20 species of *Anopheles* mosquitoes (Wang et al., 2005; Chatterjee and Chaudhuri, 2006; Mead and Tu, 2008; Dritsou et al., 2014; Liu et al., 2014; Allam et al., 2016; Liu et al., 2017; Carissimo et al., 2018; Feng et al., 2018a; Bruno et al., 2019), were studied. The study materials involved almost every possible type, including mosquito genome sequences obtained from websites; whole mosquitoes at all developmental stages; mosquitoes at different blood feeding states, ages, pathogen infection statuses, diapause statuses or insecticide resistance states; mosquito tissues except for legs; and even mosquito cell nuclei and cytoplasm (**Tables 1–6**).

STEPS OF THE RESEARCH ROADMAP

Progress in studying individual miRNAs with annotated names in the database was tracked (**Tables 1–7** and **S1**), and an overview of study advances is provided in **Figure 1**. The exploration of miRNA-based approaches proceeded through the following four steps along the proposed research roadmap: identifying mosquito miRNAs (**Tables 1–5**); validating pathogen- miRNA interactions (**Tables 6** and **S1**); exploring the mechanism of action, which refers mainly to target prediction and verification (**Tables 7** and **S1**); and performing preapplication investigations (Liu P. et al., 2016). These steps involved the 20 items listed in **Figure 1**, for example, interactions between miRNAs and *Plasmodium*, dengue virus (DENV), Zika virus (ZIKA), Chikungunya virus (CHIKV), *Wolbachia*, West Nile virus (WNV), Palm Creek virus (PCV), Japanese Encephalitis virus (JEV), and o'nyong'nyong virus (ONNV).

However, no clinical or field trial has been reported, indicating that the miRNA-based approach may have encountered a bottleneck of application in mosquito-borne disease prevention and control, although several attempts to establish application models have been conducted (Heiss et al., 2011; Tsetsarkin et al., 2015; Tsetsarkin et al., 2016a; Tsetsarkin et al., 2016b). The details of significant progress achieved at each step are reviewed below.

ADVANCES AT EACH STEP OF THE RESEARCH ROADMAP

Identification of miRNA Profiles in Mosquitoes

The first step in the research roadmap is to understand mosquito miRNA profiles. Currently, studies of mosquito miRNA profiles focus mainly on mosquito miRNA identification (Mead and Tu, 2008; Skalsky et al., 2010; Gu et al., 2013; Jain et al., 2014; Castellano et al., 2015; Etebari et al., 2015; Hu et al., 2015; Allam et al., 2016; Su et al., 2017; Carissimo et al., 2018; Feng et al., 2018a) with the detection of spatial and temporal expression patterns (Jain et al., 2014; Yen et al., 2018), the functional arm between the 5' and 3' ends (Skalsky et al., 2010; Biryukova et al., 2014; Etebari et al., 2015), the production of miRNAs with varying lengths and sequences (i.e., isomiRs) (Skalsky et al., 2010; Biryukova et al., 2014; Castellano et al., 2015; Nouzova et al., 2018), and miRNA clusters (Biryukova et al., 2014). At this step in the roadmap, variations in the spatial and temporal expression of miRNAs have been observed by analyzing several factors. (i) Mosquito species: For example, miR-282-5p was found to be conserved in *Ae. aegypti* and *An. gambiae* but not in *Cx. quinquefasciatus* (Gu et al., 2013) (**Table 2**). Additionally, miR-1175-3p expression has been found to display opposite trends (upregulated or downregulated by blood feeding) in *Aedes albopictus* and *Anopheles gambiae*, and the corresponding molecular mechanisms may also be different in each species (Winter et al., 2007; Su et al., 2017) (**Table 4**). (ii) Sexes: For example, miR-989-5p was found to be restricted in female *Anopheles coluzzii* (Bruno et al., 2019) (**Table 3**). (iii) Developmental stages: Notably, miR-1-3p was found to be enriched in the pupa of female *Anopheles stephensi* (Jain et al., 2015) compared to the larvae and adult (**Table 4**). (iv) Blood feeding and insecticide resistance statuses: The expression of miR-

TABLE 1 | The generally most highly expressed miRNAs in mosquitoes.

miRNA names	References and study materials
miR-1-3p	*Ae. aegypti* (Yen et al., 2018), adult carcasses of *Ae. aegypti* (Akbari et al., 2013)
miR-10-5p	*An. gambiae* (Biryukova et al., 2014), *An. sinensis* (Feng et al., 2018a)
miR-124-3p	*Ae. aegypti*, *Cx. quinquefasciatus* and *An. gambiae* (Behura et al., 2011)
miR-125-5p	*Ae. aegypti*, *Cx. quinquefasciatus* and *An. gambiae* (Behura et al., 2011)
miR-133-3p	*Ae. aegypti*, *Cx. quinquefasciatus* and *An. gambiae* (Behura et al., 2011)
miR-14-3p	*Ae. aegypti*, *Cx. quinquefasciatus* and *An. gambiae* (Behura et al., 2011), *An. sinensis* (Feng et al., 2018a)
miR-143	*Ae. aegypti* saliva (Maharaj et al., 2015)
miR-184-3p	*Ae. albopictus*, *Cx. quinquefasciatus*, *Ae. albopictus* cell, *An. gambiae*, *Ae. aegypti*, nucleus and the cytoplasm of *Ae. aegypti* cells, *An. stephensi*, *An. sinensis* (Biryukova et al., 2014; Mayoral et al., 2014; Shrinet et al., 2014; Hu et al., 2015; Su et al., 2017; Feng et al., 2018a; Nouzova et al., 2018)
miR-1889-5p	nucleus of *Wolbachia* infected *Ae. aegypti* cells, nucleus and cytoplasm of *Ae. aegypti* cell (Mayoral et al., 2014)
miR-1891-5p	*An. sinensis* (Feng et al., 2018a)
miR-210-3p	*Ae. aegypti*, *Cx. quinquefasciatus* and *An. gambiae* (Behura et al., 2011)
miR-263a-5p/-3p	*Ae. aegypti* and *An. stephensi* (Hu et al., 2015), *An. gambiae* (Biryukova et al., 2014)
miR-263b-5p/-3p	*Ae. aegypti* and *An. stephensi* (Hu et al., 2015)
miR-275-3p/-5p	nucleus and cytoplasm of *Ae. aegypti* cells infected or uninfected with *Wolbachia* (Mayoral et al., 2014) *Ae. albopictus* midgut (Su et al., 2017), *An. sinensis* (Feng et al., 2018a)
miR-276-3p	*An. sinensis* (Feng et al., 2018a), nucleus and the cytoplasm of *Ae. aegypti* cells (Mayoral et al., 2014), *An. gambiae* (Bryant et al., 2019)
miR-277-3p	*An. sinensis* (Feng et al., 2018a), *An. coluzzii* saliva (Bruno et al., 2019)
miR-278-3p/5p	*Ae. aegypti, Cx. quinquefasciatus* and *An. gambiae* (Behura et al., 2011)
miR-281-3p/-5p	*An. sinensis* (Feng et al., 2018a), *An. gambiae* (Biryukova et al., 2014)
miR-287	*Ae. aegypti*, *Cx. quinquefasciatus* and *An. gambiae* (Behura et al., 2011)
miR-2940-5p	*Ae. albopictus* (Skalsky et al., 2010)
miR-2941-3p	*Ae. aegypti* embryos (Hu et al., 2015)
miR-2943-5p	*Ae. aegypti* and *An. stephensi* embryos (Hu et al., 2015)
miR-2945-3p	*Ae. aegypti* and *An. stephensi* embryos (Hu et al., 2015)
miR-2946-3p	*Ae. aegypti* embryos (Hu et al., 2015)
miR-305-5p	*Ae. aegypti*, *Cx. quinquefasciatus*, and *An. gambiae* (Behura et al., 2011)
miR-306-5p	*Ae. aegypti*, *Cx. quinquefasciatus*, and *An. gambiae* (Behura et al., 2011)
miR-307-3p	*Ae. aegypti*, *Cx. quinquefasciatus*, and *An. gambiae* (Behura et al., 2011)
miR-316-5p	*An. sinensis* (Feng et al., 2018a)
miR-317-3p	*Cx. quinquefasciatus*, *Ae. albopictus* C7/10 cells (Skalsky et al., 2010), nucleus and cytoplasm of *Ae. aegypti* cells infected or uninfected with *Wolbachia* (Mayoral et al., 2014), *Ae. albopictus* midgut (Su et al., 2017)
miR-34-5p	*Ae. aegypti*, *Cx. quinquefasciatus* and *An. gambiae* (Behura et al., 2011)
miR-5	*Ae. aegypti*, *Cx. quinquefasciatus* and *An. gambiae* (Behura et al., 2011)
miR-5706	*Ae. albopictus* (Su et al., 2017)
miR-6	*Ae. aegypti*, *Cx. quinquefasciatus* and *An. gambiae* (Behura et al., 2011)
miR-8-3p	*Ae. aegypti*, *Cx. quinquefasciatus An. gambiae* (Skalsky et al., 2010; Behura et al., 2011; Biryukova et al., 2014), C7/10 cells (Skalsky et al., 2010), *Ae. albopictus* (Su et al., 2017), *An. sinensis* (Feng et al., 2018a)
miR-9c	*An. sinensis* (Feng et al., 2018a)
bantam-3p/-5p	*An. gambiae* (Biryukova et al., 2014; Bryant et al., 2019)
let-7-5p	*An. gambiae* (Winter et al., 2007), *Cx. pipiens* (Meuti et al., 2018)
miR-iab-4-5p	*Ae. aegypti*, *Cx. quinquefasciatus* and *An. gambiae* (Behura et al., 2011)

Here, the term "most highly expressed miRNAs" refers to the miRNAs with the greatest abundance among many miRNAs detected in the same sequencing library. During the exploration of miRNA-based approaches, more attention should be devoted to highly expressed mosquito miRNAs.

999-3p was found to be downregulated in deltamethrin-resistant *Culex pipiens* (Hong et al., 2014) (**Table 4**). (v) Tissues: For example, miR-998-5p was found to be specifically expressed in the ovary of *An. gambiae* (Lampe and Levashina, 2018) (**Table 5**), and miR-8-3p was found to be particularly enriched in the salivary glands in *An. coluzzii* (Bruno et al., 2019) but in the fat body in *Aedes aegypti* (Bryant et al., 2010) (**Table 5**). Moreover, in addition to these specificities, miRNAs may even exhibit cellular cytoplasm- or nucleus- specificity (Mayoral et al., 2014) (**Table 5**).

More examples based on individual miRNAs are noted in **Tables 2–5**. Overall, the expression levels of miRNAs are regulated by complicated factors, including mosquito species, sexes, developmental stages, tissues or organs, aging, blood feeding, and so on (**Tables 2–5**). In addition to differences in expression levels, the preferred or functional arm also varies among these factors in terms of the change in 5p/3p ratio or even dominant arm shifts (Skalsky et al., 2010; Biryukova et al., 2014; Castellano et al., 2015). For example, the 5p/3p ratios of miR-956-3p and miR-219-5p are significantly reduced by blood feeding (Biryukova et al., 2014). Moreover, isomiR production based on acylation, uridylation, adenine and uracil extension/addition can be induced by blood feeding and insecticide resistance (Skalsky et al., 2010; Biryukova et al., 2014).

miRNA-Pathogen Interactions in the Mosquitoes

The second step in the research roadmap always begins with an observation of statistical correlations between miRNA regulation and pathogen infection in mosquitoes. The pathogens primarily include *Plasmodium*, DENV, CHIKV, *Wolbachia*, Zika virus, WNV, JEV, PCV and ONNV (**Table 6**). The miRNA abundance may vary upon pathogen infection in mosquitoes according to differences in the studied material, e.g., miR-10-5p is upregulated in CHIKV-infected *Ae. aegypti* (Dubey et al., 2017); conversely, it is downregulated in DENV-infected *Ae. aegypti* (Liu et al., 2015; Etebari et al., 2015) (**Table 6**). More importantly, a few miRNAs were found to exhibit similar regulation patterns in different independent studies, and the repeatability of these results makes them more reliable (**Table 6**), as described in the following

TABLE 2 | Species-specific miRNAs in mosquitoes.

miRNA names	Study material and references
Conserved insect miRNAs	
miR-iab-8-5p	eight arthropod species but not mosquitoes (Jain et al., 2014)
miR-133-5p	eight arthropod species but not mosquitoes (Jain et al., 2014)
miR-190-3p	eight arthropod species but not mosquitoes (Jain et al., 2014)
miR-2944a-5p	insect (Allam et al., 2016)
miR-2944b-5p	insect (Allam et al., 2016)
miR-2779	eight arthropod species but not mosquitoes (Jain et al., 2014)
miR-2796-5p	eight arthropod species but not mosquitoes (Jain et al., 2014)
miR-2796-3p	eight arthropod species but not mosquitoes (Jain et al., 2014)
Conserved mosquito miRNAs	
miR-1174-3p	mosquito (Winter et al., 2007; Skalsky et al., 2010), e.g., *An. funestus* (Allam et al., 2016), *An. gambiae* (Winter et al., 2007)
miR-1175-5p/-3p	mosquito e.g., *Ae. albopictus* (Gu et al., 2013), *An. funestus* (Allam et al., 2016), *An. gambiae* (Winter et al., 2007)
miR-137-3p	mosquito (Lucas et al., 2015a; Lucas et al., 2015b)
miR-1890-3p	mosquito (Li et al., 2009; Skalsky et al., 2010; Liu et al., 2015; Lucas et al., 2015b), e.g., *Ae. albopictus* (Gu et al., 2013), *Ae. aegypti* (Lucas et al., 2015b)
miR-1891-5p	mosquito (Skalsky et al., 2010), e.g., *Ae. albopictus* (Gu et al., 2013; Liu et al., 2015)
miR-210-3p	mosquito, e.g., *An. funestus* (Allam et al., 2016) and *Ae. albopictus* (Gu et al., 2013)
miR-278-3p	mosquito, e.g., *An. funestus* (Allam et al., 2016)
miR-275-3p	mosquito, e.g., *An. funestus* (Allam et al., 2016)
miR-2941-3p	mosquito (Allam et al., 2016), e.g., *Ae. albopictus* (Gu et al., 2013), *Ae. aegypti* and *An. stephensi* (Hu et al., 2015), insect
miR-2942-3p	mosquito (Allam et al., 2016)
miR-2943-5p	insect (Allam et al., 2016), mosquito (Skalsky et al., 2010; Gu et al., 2013), *Ae. albopictus* (Gu et al., 2013), *Ae. aegypti* and *An. stephensi* (Hu et al., 2015)
miR-2945-3p	mosquitoes (Skalsky et al., 2010)
miR-2946-3p	*Aedes* and *Culex* spp (Gu et al., 2013)., *Ae. aegypti*, *An. stephensi* (Hu et al., 2015), *Ae. albopictus* (Gu et al., 2013)
miR-305-5p	mosquito, e.g., *An. funestus* (Allam et al., 2016)
miR-307-3p	mosquito, e.g., *An. funestus* (Allam et al., 2016)
miR-315–5p	mosquito (Lucas et al., 2015a; Lucas et al., 2015b)
miR-34–3p	mosquito (Lucas et al., 2015a; Lucas et al., 2015b)
miR-989-3p	mosquito, e.g., *An. gambiae* (Winter et al., 2007)
Conserved miRNAs in different subspecies	
miR-1889-3p/-5p	*Aedes* and *Culex* spp (Li et al., 2009; Gu et al., 2013; Liu et al., 2015).
miR-282-5p	mosquito, e.g., *Ae. aegypti* and *An. gambiae* but not in *Cx. quinquefasciatus* (Gu et al., 2013)
miR-2940-5p	*Aedes* and *Culex* spp (Gu et al., 2013).
miR-2952	*Cx. quinquefasciatus* (Skalsky et al., 2010)
miR-927-5p	mosquito, e.g., *An. funestus* (Allam et al., 2016), *Ae. aegypti* and *An. gambiae* (but not *Cx. quinquefasciatus*) (Gu et al., 2013)
miR-971-3p	*An. stephensi* (Jain et al., 2014; Hu et al., 2015) [not in *Ae. albopictus* (Su et al., 2017)]

The term "specific" here indicates that the miRNA is restricted to the corresponding mosquito subject. During the exploration of miRNA-based approaches, special attention should be devoted to mosquito-specific miRNAs. Species-specific miRNA may be chosen to establish miRNA-based approaches, and for different mosquito species, the candidate miRNAs for study may differ.

examples below. The miR-10-5p, -125-5p, -143, -275-3p, -277-3p, -308-5p, and -927-5p have been consistently shown to be upregulated upon CHIKV infection (**Table 6**). Downregulation of miR-133-3p, -14-3p, -252-5p, -275-3p, miR-306-3p, -71-3p, -957-3p, -970-3p, -980-3p, or let-7-5p has been observed upon *Plasmodium* infection (**Table 6**). Upregulation of miR-1767, -34-5p, or -622 and downregulation of miR-1-3p, -275-3p, -317-3p, -4448, -8-3p, or bantam-5p have been detected upon DENV infection. Upregulation of miR-125-5p, -252-5p, -277-3p, -281-3p, -2940-5p, -2941-3p, -308-5p, or let-7-5p and downregulation of miR-210-3p, -2945-3p, or -989-3p have been observed upon *Wolbachia* infection. Notably, miR-2940-5p, -375-3p, -87-3p, -988-5p, and -999-3p are consistently regulated by CHIKV and DENV, which may provide insight into coregulation by these two pathogens and the subsequent codevelopment of miRNA-based approaches for transmission control. More specifically, miR-2940-5p is inversely regulated by DENV and *Wolbachia*, consistent with the results that *Wolbachia* uses miRNA-2940-5p to inhibit DENV infection in *Ae. aegypti* (Hussain et al., 2011; Zhang et al., 2013) (**Table 6**).

As in the first study step in the roadmap, in addition to differences in expression levels, changes in 5p/3p ratio, dominant arm shifts, and isomiR production can be modified by pathogen infection (Etebari et al., 2015).

JEV, PCV and ONNV pathogens do not appear in the summary presented in **Table 6**. Except for a study showing that miR-124 inhibits JEV replication in PK15 porcine kidney epithelial cells (Yang et al., 2016), no report that has indicated that miRNAs are statistically correlated with JEV infection in mosquito or mosquito cells. PCV and ONNV infection exert

TABLE 3 | Sex-specific miRNAs in adult mosquitoes.

Female-specific or enriched miRNAs	Study material and reference	Male-specific or enriched miRNAs	Study material and reference
miR-100-5p	*An. stephensi* (Jain et al., 2015)	miR-1-5p	*An. stephensi* (Jain et al., 2015)
miR-10357-5p	*An. coluzzii* (Bruno et al., 2019)	miR-100-5p	*An. anthropophagus* (Liu et al., 2014)
miR-10358-5p	*An. coluzzii* (Bruno et al., 2019)	miR-1000-5p	*An. anthropophagus* (Liu et al., 2014)
miR-10359-5p	*An. coluzzii* (Bruno et al., 2019)	miR-10381	*An. coluzzii* (Bruno et al., 2019)
miR-10359-3p	*An. coluzzii* (Bruno et al., 2019)	miR-124-3p	*An. anthropophagus* (Liu et al., 2014)
miR-10360-5p	*An. coluzzii* (Bruno et al., 2019)	miR-125-5p	*An. anthropophagus* (Liu et al., 2014)
miR-10362-5p	*An. coluzzii* (Bruno et al., 2019)	miR-125-3p	*An. anthropophagus* (Liu et al., 2014)
miR-10371-5p	*An. coluzzii* (Bruno et al., 2019)	miR-137-3p	*An. anthropophagus* (Liu et al., 2014)
miR-11-3p	*An. stephensi* (Jain et al., 2015)	miR-184-5p	*An. anthropophagus* (Liu et al., 2014)
miR-1174-3p	*An. coluzzii* (Bruno et al., 2019)	miR-1891-5p	*Ae. aegypti*, *An. stephensi* (Hu et al., 2015)
miR-1174-5p	*An. coluzzii* (Bruno et al., 2019)	miR-193-3p	*An. anthropophagus* (Liu et al., 2014)
miR-1175-5p	*An. stephensi* (Jain et al., 2015)	miR-219-5p	*An. coluzzii* (Bruno et al., 2019)
miR-1175-3p	*An. anthropophagus* (Liu et al., 2014), *An. coluzzii* (Bruno et al., 2019)	miR-2765-5p	*An. stephensi* (Jain et al., 2015; Allam et al., 2016)
miR-283-5p	*An. coluzzii* (Bruno et al., 2019)	miR-277-3p	*An. anthropophagus* (Liu et al., 2014)
miR-307-3p	*An. anthropophagus* (Liu et al., 2014)	miR-282-5p	*An. anthropophagus* (Liu et al., 2014)
miR-305-5p	*An. funestus* (Allam et al., 2016)	miR-7-5p	*An. anthropophagus* (Liu et al., 2014), *An. stephensi* (Jain et al., 2015)
miR-315-5p	*An. anthropophagus* (Liu et al., 2014)	miR-981-3p	*An. anthropophagus* (Liu et al., 2014), *An. coluzzii* (Bruno et al., 2019)
miR-79-5p	*An. Anthropophagus* (Liu et al., 2014)	—	—
miR-929-5p	*An. anthropophagus* (Liu et al., 2014)	—	—
miR-980-3p	*An. coluzzii* (Bruno et al., 2019)	—	—
miR-988-3p	*An. anthropophagus* (Liu et al., 2014), *An. coluzzii* (Bruno et al., 2019)	—	—
miR-989-3p	*An. anthropophagus* (Liu et al., 2014), *An. stephensi* (Jain et al., 2015; Allam et al., 2016), *Ae. aegypti* (Allam et al., 2016), *An. coluzzii* (Bruno et al., 2019)	—	—
miR-989-5p	*An. coluzzii* (Bruno et al., 2019)	—	—

The term "specific" here indicates that miRNA is restricted to one sex or is more abundant in one sex than in the other sex. The symbol "—" indicates that no related evidence is available regarding the corresponding sex of the mosquito.

remarkably limited effects on the mosquito miRNA profile; therefore, miRNAs may not play an important role in the interaction of PCV with *Ae. aegypti* (Lee et al., 2017) or ONNV with *Anopheles coluzzii* (Carissimo et al., 2018). Thus, researchers are currently unable to select a miRNA as an ideal candidate to establish a miRNA-based approach for the control of three mosquito-borne diseases.

After statistical correlations between miRNA alterations and pathogen infection being observed, their causal relationship should be confirmed (**Tables 7** and **S1**). Overexpression or suppression of a miRNA is the most widely used approach to study causality (Jones-Rhoades et al., 2006). Eighteen miRNAs have been validated to exert promotive or inhibitory effects on CHIKV (Maharaj et al., 2015; Dubey et al., 2019), DENV (Hussain et al., 2013; Zhang et al., 2013; Yan et al., 2014; Zhou et al., 2014; Su et al., 2017; Su et al., 2019; Avila-Bonilla et al., 2020), WNV (Slonchak et al., 2014), *Plasmodium* (Jain et al., 2014; Dennison et al., 2015; Lampe et al., 2019; Dong et al., 2020), *Wolbachia* (Hussain et al., 2011; Zhang et al., 2014), or JEV (Yang et al., 2016) infections *via* these types of experiments (**Table 7**). Notably, miR-2940-5p restricts the replication of both WNV and DENV in mosquitoes (Zhang et al., 2013; Slonchak et al., 2014), and miR-375-3p exerts the opposite effect on DENV-2 and CHIKV (Hussain et al., 2013; Maharaj et al., 2015). It is easy to find that the upregulating and downregulating miRNAs in response to pathogen infection co-exist in the mosquito (**Table 7**). No miRNA has been reported to induce multi-antipathogen effects on the two kinds of flaviviruses and *Plasmodium* protozoans. A more detailed description of the progress achieved by studies examining miRNA-pathogen interactions in mosquitoes is presented in **Table S1**.

Exploration of the Mechanism of Action

Research on the mechanism of action mostly focuses on the prediction and verification of miRNA targets or functions through genetic disruption methods. Bioinformatic analysis tools, such as TargetScan, PITA and RNAhybrid, are always used for target prediction. The verification methods usually include the transfection of miRNA-specific antagomirs into mosquito cells, miRNA mimic/inhibitor microinjection in mosquitoes, real-time quantitative polymerase chain reaction (qRT-PCR), or luciferase assays (Liu B. et al., 2016; Ma et al., 2017; Nouzova et al., 2018; Yen et al., 2019; Avila-Bonilla et al., 2020; Fu et al., 2020). The most recent method applied to elucidate the targets and biological functions of mosquito miRNAs is high-throughput sequencing of covalent ligation of endogenous Argonaute-bound RNAs isolated by crosslinking and immunoprecipitation (CLEAR-CLIP). In this assay, the

TABLE 4 | Stage- or status-specific miRNAs.

miRNA names	Study materials and expression levels in certain stages or statuses*					
	Egg[&]	Larva[&]	Pupa[&]	Adult[&]	Blood feeding[#]	Other stages[$]
miR-1-3p	—	—	***An. stephensi*** (Jain et al., 2015)	—	***Ae. aegypti* fat body 24 h PBM** (Zhang et al., 2017)**, *Ae. aegypti*** (Hussain et al., 2013), ***An. stephensi*** (Jain et al., 2014), *An. anthropophagus* midgut (Liu et al., 2017)	***Ae. albopictus* nondiapause pharate larva** (Batz et al., 2017), *Cx. pipiens* DR-strain (Hong et al., 2014)
miR-1-5p	—	—	***An. stephensi*** (Jain et al., 2015)	***An. stephensi*** (Jain et al., 2015)	—	—
miR-10-3p	—	—	—	—	*An. gambiae* (Fu et al., 2017)	—
miR-10-5p	***An. sinensis*** (Feng et al., 2018b)	—	—	***An. stephensi*** (Jain et al., 2015)	—	—
miR-100-5p	—	—	—	***An. stephensi*** (Jain et al., 2015)	***Ae. aegypti at* 12 *h* PBM** (Bryant et al., 2010), *An. anthropophagus* midguts (Liu et al., 2017)	*Cx. pipiens* DR strain (Hong et al., 2014)
miR-1000-5p	—	—	—	—	***An. gambiae*** (Biryukova et al., 2014), ***An. anthropophagus* midguts** (Liu et al., 2017), ***Ae. aegypti* fat body at 48 h PBM** (Zhang et al., 2017)	—
miR-11-3p	—	—	—	***An. stephensi*** (Jain et al., 2015)**, *An. sinensis*** (Feng et al., 2018b)	***Ae. aegypti* midgut** (Li et al., 2009), ***An. stephensi*** (Jain et al., 2014), ***An. anthropophagus*** (Liu et al., 2017), ***Ae. aegypti* fat body 72 h PBM** (Zhang et al., 2017)	*Cx. pipiens* DR strain (Hong et al., 2014)
miR-11-5p	—	—	—	—	***Ae. aegypti* fat body at 48 h PBM** (Zhang et al., 2017)	—
miR-1174-5p	—	—	—	—	—	*Cx. pipiens* DR strain (Hong et al., 2014)
miR-1174-3p	—	***An. sinensis*** (Feng et al., 2018b) ***An. stephensi*** (Jain et al., 2015)	—	—	***An. gambiae* midguts** (Winter et al., 2007), ***Ae. aegypti* and *An. gambiae*** (Jain et al., 2014), ***Ae. aegypti* fat body at 48 h PBM** (Zhang et al., 2017), *An. gambiae* (Fu et al., 2017), *An. anthropophagus* midguts (Liu et al., 2017), *Ae. albopictus* midguts (Su et al., 2017)	—
miR-1175-5p	—	***An. funestus*** (Allam et al., 2016) ***An. sinensis*** (Feng et al., 2018b)	—	***An. sinensis*** (Feng et al., 2018b)	*Ae. albopictus* midguts (Su et al., 2017)	*Cx. pipiens* DR strain (Hong et al., 2014)
miR-1175-3p	—	***An. sinensis*** (Feng et al., 2018b)	—	***An. sinensis*** (Feng et al., 2018b)	***An. gambiae* midgut** (Winter et al., 2007), ***Aedes* spp.** (Jain et al., 2014), *Ae. albopictus* midgut (Su et al., 2017)	—
miR-12-5p	—	—	—	—	**leftover of *An. gambiae*** (Winter et al., 2007), *An. anthropophagus* midguts (Liu et al., 2017), *Ae. albopictus* midguts (Su et al., 2017)	—
miR-124-3p	***An. sinensis*** (Feng et al., 2018b)	—	—	—	—	old *Cx. pipiens* (Meuti et al., 2018)
miR-125-5p	—	***An. funestus*** (Allam et al., 2016)	—	—	***Ae. aegypti* 12 *h* PBM** (Bryant et al., 2010), ***An. anthropophagus* midguts** (Liu et al., 2017), ***Ae. aegypti* fat body at 72 h PBM** (Zhang et al., 2017)	*Cx. pipiens* DR strain (Hong et al., 2014)
miR-127	—	—	—	—	—	*Cx. pipiens* DR strain (Hong et al., 2014)
miR-13-3p	—	—	—	—	*An. anthropophagus* midguts (Liu et al., 2017)	*Cx. pipiens* DR strain (Hong et al., 2014)
miR-13-5p	—	—	—	—	***Ae. aegypti* fat body at 48 h PBM** (Zhang et al., 2017)	
miR-133-3p	***An. funestus*** (Allam et al., 2016)	***An. funestus*** (Allam et al., 2016)	***An. stephensi*** (Jain et al., 2015)	—	***Ae. aegypti* fat body at 48 h PBM** (Zhang et al., 2017)	*Cx. pipiens* DR strain (Hong et al., 2014)

(Continued)

TABLE 4 | Continued

miRNA names	Study materials and expression levels in certain stages or statuses*					
	Egg[&]	Larva[&]	Pupa[&]	Adult[&]	Blood feeding[#]	Other stages[$]
miR-133-5p	—	—	***An. stephensi*** (Jain et al., 2015)	***An. stephensi*** (Jain et al., 2015)	—	—
miR-137-3p	—	—	—	—	*An. anthropophagus* midguts (Liu et al., 2017)	—
miR-137-5p	***An. funestus*** (Allam et al., 2016)	***An. funestus*** (Allam et al., 2016)	—	—	—	—
miR-14-5p	—	—	—	—	—	***Ae. albopictus*** **nondiapause pharate larva** (Batz et al., 2017)
miR-14-3p	***An. funestus*** (Allam et al., 2016)	***An. funestus*** (Allam et al., 2016)	—	—	***Ae. aegypti*** (Hussain et al., 2013), *An. anthropophagus* midguts (Liu et al., 2017)	old or DR *Cx. pipiens* (Hong et al., 2014; Meuti et al., 2018)
miR-1767	—	—	—	—	**midguts of *Ae. albopictus*** (Su et al., 2017)	—
miR-184-3p	***An. funestus*** (Allam et al., 2016)	—	—	—	***Ae. aegypti*** (Li et al., 2009), ***Ae. aegypti*** **fat body at 72 h PBM** (Zhang et al., 2017), fat body of *Ae. aegypti* and *An. gambiae* (Fu et al., 2017), *An. anthropophagus* midguts (Liu et al., 2017), *Ae. albopictus* midguts (Su et al., 2017), *Aedes aegypti* (Nouzova et al., 2018)	—
miR-1889-5p	—	—	—	—	***Ae. aegypti*** **fat body at 36 h PBM** (Zhang et al., 2017)	—
miR-1890-3p	—	—	***Ae. aegypti***, ***An. stephensi*** (Hu et al., 2015; Jain et al., 2015; Allam et al., 2016; Batz et al., 2017)	—	***Ae. aegypti*** **fat body at 36 h PBM** (Zhang et al., 2017)	***Ae. albopictus*** **diapause oocyte** (Batz et al., 2017), *Cx. pipiens* DR strain (Hong et al., 2014)
miR-1891-5p	—	—	***An. sinensis*** (Feng et al., 2018b)	***An. stephensi*** (Jain et al., 2015)	—	*Cx. pipiens* DR strain (Hong et al., 2014)
miR-190-5p	—	—			***Ae. aegypti*** **midgut** (Li et al., 2009), *An. Stephensi* (Jain et al., 2014)	*Cx. pipiens* DR strain (Hong et al., 2014)
miR-190-3p	—	—	***An. stephensi*** (Jain et al., 2015)	***An. stephensi*** (Jain et al., 2015)	*An. Stephensi* (Jain et al., 2014)	—
miR-193-5p	—	—			***Ae. albopictus*** **midguts** (Su et al., 2017)	—
miR-193-3p	—	—	***An. stephensi*** (Jain et al., 2015) ***An. funestus*** (Allam et al., 2016) ***An. sinensis*** (Feng et al., 2018b)	—	—	—
miR-1951	—	—	—	—	***Ae. albopictus*** **midguts** (Su et al., 2019)	—

(Continued)

TABLE 4 | Continued

miRNA names	Study materials and expression levels in certain stages or statuses*					
	Egg[&]	Larva[&]	Pupa[&]	Adult[&]	Blood feeding[#]	Other stages[$]
miR-210-3p	***An. stephensi*** (Mead and Tu, 2008)			***An. stephensi*** (Mead and Tu, 2008; Jain et al., 2015)	***Ae. aegypti* fat body at 48 h PBM** (Zhang et al., 2017)	***Cx. pipiens* DR strain** (Hong et al., 2014)
miR-219-5p	—	—	—	***An. stephensi*** (Jain et al., 2015)	—	—
miR-2491-3p	—	—	***An. sinensis*** (Feng et al., 2018b)	—	—	—
miR-252-5p	—	—	—	—	***Ae. aegypti* fat body at 6 h PBM** (Zhang et al., 2017)	*Cx. pipiens* DR strain (Hong et al., 2014)
miR-252-3p	—	—	—	—	***Ae. aegypti* fat body at 6 h PBM** (Zhang et al., 2017)	
miR-263a-5p	—	—	—	—		*Cx. pipiens* DR strain (Hong et al., 2014)
miR-275-3p	—	—	—	—	***An. stephensi*** (Jain et al., 2014), ***An. anthropophagus* midguts** (Liu et al., 2017), ***Ae. aegypti* fat body at 48h PBM** (Zhang et al., 2017), ***An. gambiae*** (Lampe and Levashina, 2018), *Ae.albopictus* midgut (Su et al., 2017)	old *Cx. pipiens* (Meuti et al., 2018), *Cx. pipiens* DR-strain (Hong et al., 2014)
miR-275-5p	—	—	—	—	*Ae. aegypti* fat body at 24 h PBM (Zhang et al., 2017)	
miR-276-3p	—	—	—	—	*An.anthropophagus* midgut (Liu et al., 2017), *Ae.aegypti* fat body at 24h PBM (Zhang et al., 2017)	*Cx. pipiens* DR strain (Hong et al., 2014)
miR-276-5p	—	—	—	—	***Ae. aegypti* fat body at 24 h PBM** (Zhang et al., 2017), ***An. gambiae* midgut** (Lampe and Levashina, 2018), *An. gambiae* head (Lampe and Levashina, 2018)	
miR-2765-5p	—	—	—	***An. stephensi*** (Jain et al., 2015) *An. funestus* (Allam et al., 2016)	—	—
miR-277-3p		***An. funestus*** (Allam et al., 2016)	***An. stephensi*** (Jain et al., 2015)	***An. stephensi*** (Jain et al., 2015)	*An. anthropophagus* midguts (Liu et al., 2017)	old or DR *Cx. pipiens* (Hong et al., 2014; Meuti et al., 2018)
miR-2779	—	—	—		—	—
miR-278-3p		***An. funestus*** (Allam et al., 2016)			***Ae.aegypti* fat body at 48h PBM** (Zhang et al., 2017), *An.anthropophagus* midgut (Liu et al., 2017)	*Cx. pipiens* DR strain (Hong et al., 2014)
miR-278-5p	—	—	—	—	***Ae. aegypti* fat body at 6 h PBM** (Zhang et al., 2017), fat body of *Ae. aegypti* (Fu et al., 2017)	
miR-279-3p	***An. gambiae*** (Allam et al., 2016)	***An. gambiae*** (Allam et al., 2016)	—	—	***Ae.aegypti* fat body at 24h PBM** (Zhang et al., 2017), *An.anthropophagus* midgut (Liu et al., 2017)	*Cx. pipiens* DR strain (Hong et al., 2014)
miR-2796-3p	***An. funestus*** (Allam et al., 2016)	—	—	—	—	—
miR-281-3p		***An. sinensis*** (Feng et al., 2018b)		***An. sinensis*** (Feng et al., 2018b)	***An. stephensi*** (Jain et al., 2014), ***Ae. aegypti* fat body at 48 h PBM** (Zhang et al., 2017)	***Cx. pipiens* DR strain** (Hong et al., 2014)
miR-281-5p	***An. gambiae*** (Allam et al., 2016)	***An. gambiae*** (Allam et al., 2016)		***An. sinensis*** (Feng et al., 2018b)	***An. stephensi*** (Jain et al., 2014), ***Ae. aegypti* fat body at 48 h PBM** (Zhang et al., 2017), *Ae. aegypti* (Li et al., 2009), *Ae. albopictus* midgut (Su et al., 2017)	

(Continued)

TABLE 4 | Continued

miRNA names	Study materials and expression levels in certain stages or statuses*					
	Egg[&]	Larva[&]	Pupa[&]	Adult[&]	Blood feeding[#]	Other stages[$]
miR-282-5p	—	—		***An. stephensi*** (Jain et al., 2015)	—	***Ae. albopictus*** **diapause pharate larva** (Batz et al., 2017)
miR-283-5p		***Ae. albopictus*** (Batz et al., 2017)		—	*Ae. albopictus* midguts (Su et al., 2017)	
miR-2840	—	—	—	—	—	***Cx. pipiens*** **DR strain** (Hong et al., 2014)
miR-285-3p	—	—	***An. stephensi*** (Jain et al., 2015)	—	—	*Cx. pipiens* DR strain (Hong et al., 2014)
miR-286-3p	—	—	***An. stephensi*** (Jain et al., 2015)		fat body of *Ae. aegypti* (Fu et al., 2017)	
miR-2940-3p	—	—	—	—	***Ae. aegypti*** **fat body at 36 h PBM** (Zhang et al., 2017)	
miR-2940-5p	—	—	—	—	***Ae. aegypti*** (Hussain et al., 2013)	
miR-2941-3p	—	—	—	—	***Ae. aegypti*** **fat body at 48 h PBM** (Zhang et al., 2017), *Ae. albopictus* midguts (Su et al., 2017)	***Cx. pipiens*** **DR strain** (Hong et al., 2014)
miR-2942-3p	—	***Ae. albopictus*** (Puthiyakunnon et al., 2013)	—	—	—	***Ae. albopictus*** **nondiapause pharate larva** (Batz et al., 2017), *Cx. pipiens* DR strain (Hong et al., 2014)
miR-2943-5p	***An.anthropophagus*** (Liu et al., 2014) ***An. sinensis*** (Feng et al., 2018b)	—	—	—	—	—
miR-2944a-5p	—	—	—	—	***An. gambiae*** (Fu et al., 2017)	—
miR-2945-3p	—	—	—	—	***Ae. aegypti*** **fat body at 36 h PBM** (Zhang et al., 2017)	—
miR-2946-3p	—	—	—	—	***Ae. aegypti*** **fat body at 48 h PBM** (Zhang et al., 2017)	—
miR-2951-5p	—	—	—	—	**midgut of *Ae. albopictus*** (Su et al., 2017)	*Cx. pipiens* DR strain (Hong et al., 2014)
miR-2952	—	—	—	—	—	***Cx. pipiens*** **DR strain** (Hong et al., 2014)
miR-2981	—	—	—	—	—	*Cx. pipiens* DR strain (Hong et al., 2014)
miR-2c-3p	—	—	—	—	—	*Cx. pipiens* DR strain (Hong et al., 2014; Guo et al., 2017)
miR-309a-3p	***An. funestus*** (Hu et al., 2015; Allam et al., 2016)		***An. stephensi*** (Jain et al., 2015)		—	old *Cx. pipiens* (Meuti et al., 2018), ***Cx. pipiens*** **DR strain** (Hong et al., 2014)

(Continued)

TABLE 4 | Continued

miRNA names	Study materials and expression levels in certain stages or statuses*					
	Egg[&]	Larva[&]	Pupa[&]	Adult[&]	Blood feeding[#]	Other stages[$]
	Ae. aegypti*, *An. stephensi (Hu et al., 2015)					
miR-305-5p	—	***An. funestus*** (Allam et al., 2016)	***An. funestus*** (Allam et al., 2016)	***An. funestus*** (Allam et al., 2016)	***Ae. aegypti*** (Bryant et al., 2010), ***An. Stephensi*** (Jain et al., 2014), ***Ae.aegypti* fat body at 48 h PBM** (Zhang et al., 2017), ***An. gambiae* midgut** (Lampe and Levashina, 2018), *An.anthropophagus* midgut (Liu et al., 2017)	*Cx. pipiens* DR strain (Hong et al., 2014)
miR-305-3p	—	—	—	—	*Ae. aegypti* fat body at 24 h PBM (Zhang et al., 2017)	**nondiapausing *Cx. pipiens*** (Meuti et al., 2018)
miR-306-5p	—	—	—	—	***Ae. aegypti*** (Li et al., 2009), ***An. stephensi*** (Jain et al., 2014), ***Ae. aegypti* fat body at 72 h PBM** (Zhang et al., 2017), ***An. gambiae* ovary** (Nouzova et al., 2018), *An.anthropophagus* midgut (Liu et al., 2017)	***Cx. pipiens* DR strain** (Hong et al., 2014)
miR-306-3p	—	—	—	—	*Ae. aegypti* fat body at 72 h PBM (Zhang et al., 2017)	—
miR-307-3p	—	—	—	—	*An. anthropophagus* midguts (Liu et al., 2017)	*Cx. pipiens* DR strain (Hong et al., 2014)
miR-308-3p	—	—	—	—	***An. gambiae*** (Biryukova et al., 2014), ***Ae. aegypti* fat body at 24h PBM** (Zhang et al., 2017)	—
miR-308-5p	—	—	—	—	***Ae. aegypti* fat body at 72 h PBM** (Zhang et al., 2017)	—
miR-315-5p	—	—	*An. stephensi* (Jain et al., 2015)		**midgut of *An. anthropophagus*** (Liu et al., 2017)	—
miR-315-3p	—	—	—	—	**midgut of *An. anthropophagus*** (Liu et al., 2017)	—
miR-316-5p	***An. funestus*** (Allam et al., 2016)	***An. funestus*** (Allam et al., 2016)	—	—	***Ae. aegypti* fat body at 48 h PBM** (Zhang et al., 2017)	***Cx. pipiens* DR strain** (Hong et al., 2014)
miR-317-3p	—	***An. stephensi*** (Jain et al., 2015) ***An. funestus*** (Allam et al., 2016) ***An. sinensis*** (Feng et al., 2018b)		***An. stephensi*** (Jain et al., 2015) ***An. funestus*** (Allam et al., 2016) ***An. sinensis*** (Feng et al., 2018b)	***An. gambiae* midguts** (Winter et al., 2007), ***Ae. aegypti* midguts** (Li et al., 2009; Su et al., 2017), ***Ae. aegypti*** (Hussain et al., 2013; Nouzova et al., 2018), ***Ae. aegypti* fat body at 36 h PBM** (Zhang et al., 2017), *Ae. albopictus* midguts (Su et al., 2017)	***Cx. pipiens* DR strain** (Hong et al., 2014)
miR-33-5p	—	—	—	—	—	*Cx. pipiens* DR strain (Hong et al., 2014)
miR-34-3p	—	—	—	—	***Ae. aegypti* fat body at 48 h PBM** (Zhang et al., 2017)	—
miR-34-5p	—	***An. stephensi*** (Jain et al., 2015) ***An. funestus*** (Allam et al., 2016) ***An. sinensis*** (Feng et al., 2018b)	—	***An. stephensi*** (Jain et al., 2015) ***An. funestus*** (Allam et al., 2016) ***An. sinensis*** (Feng et al., 2018b)	***Ae. aegypti* midgut** (Li et al., 2009; Su et al., 2017), ***Ae. aegypti* fat body at 24 h PBM** (Zhang et al., 2017), *An. anthropophagus* midguts (Liu et al., 2017), *Ae. albopictus* midguts (Su et al., 2017)	—
miR-375-3p	—	***An. stephensi*** (Jain et al., 2015)	***Ae. aegypti*** (Nouzova et al., 2018)	***An. stephensi*** (Jain et al., 2015)	***Ae. aegypti*** (Hussain et al., 2013), ***Ae. albopictus* midguts** (Su et al., 2017), ***Ae. aegypti* fat body at 48 h PBM** (Zhang et al., 2017), ***Cx. pipiens*** (Meuti et al., 2018)	**nondiapausing *Cx. pipiens*** (Meuti et al., 2018) *Cx. pipiens* DR strain (Hong et al., 2014)

(Continued)

TABLE 4 | Continued

miRNA names	Study materials and expression levels in certain stages or statuses*					
	Egg[&]	Larva[&]	Pupa[&]	Adult[&]	Blood feeding[#]	Other stages[$]
miR-375-5p	—	—	—	—	—	***Cx. pipiens*** **DR strain** (Hong et al., 2014)
miR-3809-3p	—	—	—	—	***Ae. albopictus*** **midguts** (Su et al., 2017)	old *Cx. pipiens* (Meuti et al., 2018)
miR-3809-5p	—	—	—	—	***Ae. albopictus*** **midguts** (Su et al., 2017)	—
miR-424-3p	—	—	—	—	***Ae. albopictus*** **midguts** (Su et al., 2017)	—
miR-4448	—	—	—	—	***Ae. albopictus*** **midguts** (Su et al., 2017)	***Cx. pipiens*** **DR strain** (Hong et al., 2014)
miR-4728-5p	—	—	—	—	***Ae. albopictus*** **midguts** (Su et al., 2017)	—
miR-493-3p	—	—	—	—	—	***Cx. pipiens*** **DR strain** (Hong et al., 2014)
miR-4968-3p	—	***An. sinensis*** (Feng et al., 2018b)	—	—	—	—
miR-622	—	—	—	—	***Ae. albopictus*** **midguts** (Su et al., 2017)	—
miR-7-5p	—	***An. stephensi*** (Jain et al., 2015)	—	—	***An. gambiae*** (Biryukova et al., 2014)	*Cx. pipiens* DR strain (Hong et al., 2014)
miR-71-3p	—	—	—	—	***Ae. aegypti*** **fat body at 48 h PBM** (Zhang et al., 2017), *An. anthropophagus* midguts (Liu et al., 2017), *Ae. albopictus* midguts (Su et al., 2017)	*Cx. pipiens* DR strain (Hong et al., 2014)
miR-79-3p	—	—	—	—	***Ae. aegypti*** **fat body at 6 h PBM** (Zhang et al., 2017)	*Cx. pipiens* DR strain (Hong et al., 2014)
miR-79-5p	—	—	—	—	*An. anthropophagus* midguts (Liu et al., 2017)	
miR-8-3p	—	***An. funestus*** (Allam et al., 2016)	***Ae. aegypti*** (Bryant et al., 2010)	—	***An. anthropophagus*** **midguts** (Liu et al., 2017)**, *Ae. aegypti*** **fat body at 24 h PBM** (Zhang et al., 2017), *Ae. aegypti* midguts (Li et al., 2009), *Ae. aegypti* (Bryant et al., 2010), *Ae.albopictus* (Su et al., 2017)	old *Cx. pipiens* (Meuti et al., 2018), *Cx. pipiens* DR strain (Hong et al., 2014)
miR-87-3p	*An. funestus* (Allam et al., 2016)	—	*An. funestus* (Allam et al., 2016)	—	***Ae. aegypti*** **fat body at 48 h PBM** (Zhang et al., 2017)	*Cx. pipiens* DR strain (Hong et al., 2014)
miR-927-5p	—	—	—	***An. stephensi*** (Jain et al., 2015)	***Ae. aegypti*** **fat body at 48 h PBM** (Zhang et al., 2017)	—
miR-927-3p	***An. funestus*** (Allam et al., 2016)	***An. funestus*** (Allam et al., 2016)	—	***An. stephensi*** (Jain et al., 2015)	—	—
miR-929-3p	—	—	—	—	*An. stephensi* (Jain et al., 2014)	—
miR-929-5p	—	—	—	***An. stephensi*** (Jain et al., 2015), *An. funestus* (Allam et al., 2016)	***Ae. aegypti*** **fat body at 48 h PBM** (Zhang et al., 2017)	—
miR-92a-3p	—	*An. funestus* (Allam et al., 2016)	—	—	—	—
miR-932-5p	—	—	—	—	***An. anthropophagus*** **midguts** (Liu et al., 2017), *An. Stephensi* (Jain et al., 2014)	*Cx. pipiens* DR strain (Hong et al., 2014)
miR-956-3p	—	—	—	—	***An. gambiae*** (Biryukova et al., 2014), *Ae.albopictus* and *Ae. aegypti* (Su et al., 2017)	

(Continued)

TABLE 4 | Continued

miRNA names	Study materials and expression levels in certain stages or statuses*					
	Egg[&]	Larva[&]	Pupa[&]	Adult[&]	Blood feeding[#]	Other stages[$]
miR-957-3p	—	—	—	—	***An.anthropophagus* midguts** (Liu et al., 2017), ***Ae.aegypti* fat body at 48h PBM** (Zhang et al., 2017)	***Ae. albopictus* diapause oocyte** (Batz et al., 2017), *Cx. pipiens* DR strain (Hong et al., 2014)
miR-965-3p	—	—	—	*An. stephensi* (Jain et al., 2015)	—	***Cx. pipiens* DR strain** (Hong et al., 2014)
miR-970-3p	***An. funestus*** (Allam et al., 2016)	***An. funestus*** (Allam et al., 2016)	—	—	***Ae. aegypti* fat body at 36h PBM** (Zhang et al., 2017), *An.anthropophagus* midgut (Liu et al., 2017)	*Cx. pipiens* DR strain (Hong et al., 2014)
miR-976-5p	—	—	—	—	***Ae. albopictus* and *Ae. aegypti*** (Su et al., 2017)	—
miR-980-3p	—	—	—	***An. stephensi*** (Jain et al., 2015)	—	—
miR-981-3p	—	—	—	—	***An. anthropophagus* gut (**Liu et al., 2017), ***Ae.aegypti* fat body at 48h PBM** (Zhang et al., 2017)	*Cx. pipiens* DR strain (Hong et al., 2014)
miR-988-5p	—	—	***An. stephensi*** (Jain et al., 2015)	***An. stephensi*** (Jain et al., 2015)	***Ae. aegypti* fat body at 72 h PBM** (Zhang et al., 2017)	—
miR-988-3p	—	—	—	—	*An. gambiae* (Fu et al., 2017)	—
miR-989-3p	—	—	—	***An. stephensi*** (Jain et al., 2015)	***Ae. aegypti*** (Li et al., 2009), ***An. stephensi*** (Jain et al., 2014), ***An. anthropophagus* midguts** (Liu et al., 2017), ***Ae. aegypti* fat body at 24 h PBM** (Zhang et al., 2017), *Ae. albopictus* (Su et al., 2017), *An. gambiae* ovaries (Lampe and Levashina, 2018)	***Cx. pipiens* DR strain** (Hong et al., 2014)
miR-993-5p	—	—	—	***An. stephensi*** (Jain et al., 2015)	—	—
miR-993-3p	***An. funestus*** (Allam et al., 2016)	***An. funestus*** (Allam et al., 2016)	—	—	***Ae. aegypti* fat body at 36 h PBM** (Zhang et al., 2017)	*Cx. pipiens* DR strain (Hong et al., 2014)
miR-996-3p	***An. funestus*** (Allam et al., 2016)	***An. stephensi*** (Jain et al., 2015) ***An. funestus*** (Allam et al., 2016)	—	***An. stephensi*** (Jain et al., 2015)	***Ae. aegypti* fat body at 72 h PBM** (Zhang et al., 2017), *An. anthropophagus* midgut (Liu et al., 2017)	—
miR-996-5p	—	—	—	—	*An. anthropophagus* midgut (Liu et al., 2017)	—
miR-988-3p	—	—	—	—	***Ae. aegypti*** (Li et al., 2009), ***Ae. aegypti* fat body at 72 h PBM** (Zhang et al., 2017)	
miR-998-3p	***An. funestus*** (Allam et al., 2016)	—	***An. stephensi*** (Jain et al., 2015)	—	*Ae. albopictus* (Su et al., 2017)	*Cx. pipiens* DR strain (Hong et al., 2014)
miR-999-3p	—	—	—	—	***Ae. aegypti* fat body at 24 h PBM** (Zhang et al., 2017)	*Cx. pipiens* DR strain (Hong et al., 2014)
miR-9a-5p	—	—	—	—	—	*Cx. pipiens* DR strain (Hong et al., 2014)
miR-iab-4-3p	—	—	***An. stephensi*** (Jain et al., 2015)		—	—
miR-iab-4-5p	—	—	—	—	***Ae. aegypti* fat body at 72 h PBM** (Zhang et al., 2017)	
bantam-3p	—	—	***An. stephensi*** (Jain et al., 2015)	—	***Ae. aegypti* fat body at 6h PBM** (Zhang et al., 2017), *An.anthropophagus* midgut (Liu et al., 2017)	***Ae.albopictus* oocyte** (Batz et al., 2017)

(Continued)

TABLE 4 | Continued

miRNA names	Study materials and expression levels in certain stages or statuses*					
	Egg[&]	Larva[&]	Pupa[&]	Adult[&]	Blood feeding[#]	Other stages[$]
bantam-5p	—	—	***Ae. aegypti*** (Bryant et al., 2010)	—	***Ae. aegypti*** (Hussain et al., 2013)	—
let-7-5p	*An. funestus* (Mead and Tu, 2008; Allam et al., 2016)	***An. funestus*** (Allam et al., 2016)	***Ae. albopictus*** (Gu et al., 2013)**, *An. stephensi*** (Jain et al., 2015)	—	***Ae. aegypti* gut at 12 h PBM** (Bryant et al., 2010), ***Ae. aegypti* fat body at 6 h PBM** (Zhang et al., 2017), *An. anthropophagus* midguts (Liu et al., 2017), *Ae. albopictus* (Su et al., 2017)	—

*The "study materials" are written in two styles, namely **bold** and nonbold, which indicates that the miRNAs are upregulated and downregulated, respectively. "—", no evidence of upregulation or downregulation is available. [&]The term "specific" here indicates that miRNAs are upregulated or downregulated in one mosquito development stage when compared with the others. [#]The term "specific" here indicates that the miRNA is upregulated or downregulated in blood-feeding mosquitoes compared with non-blood-feeding mosquitoes, in one study (Zhang et al., 2017), the comparisons were conducted at the time points 72 post eclosion, 6, 12, 24, 36, 48 and 72h post blood meal (PBM). [$]The term "specific" here indicates that the miRNA is upregulated or downregulated in one group compared with the opposite group. DR, deltamethrin-resistant.

miRNA and its target mRNA are joined in the purified RNA-induced silencing complex (RISC) complex to form one chimeric molecule. Analysis of the chimeric miRNA-target molecule among the RNA molecules associated with Argonaute (AGOs) proteins facilitates the systematic identification of miRNA-target interactions (Dong et al., 2020).

The miRNAs noted in bold in **Table S1** have been confirmed to contribute to blood digestion (Bryant et al., 2010; Jain et al., 2014), egg development (Bryant et al., 2010; Puthiyakunnon et al., 2013; Jain et al., 2014; Lucas et al., 2015a; Zhang et al., 2017), ovary development (Ling et al., 2017), larval eclosion (Puthiyakunnon et al., 2013; Feng et al., 2018b), reproduction (Zhang et al., 2016; Fu et al., 2017), the stability and nuclear translocation of AGO1 (Hussain et al., 2013), lipid accumulation (Batz et al., 2017), metabolism (Ling et al., 2017), host-pathogen interactions (Yan et al., 2014; Lucas et al., 2015b; Dubey et al., 2019; Yen et al., 2019), and insecticide resistance (Hong et al., 2014) (**Table S1**).

In the canonical mechanism of action of miRNAs, mature miRNAs guide the RISC to the 3' untranslated regions (UTRs) of target mRNAs *via* complementary base pair interactions, thus regulating the expression of target genes (Hammond et al., 2000; Lee et al., 2002; Lee et al., 2003). Most miRNA-target (mRNA) interactions are consistent with the canonical action mechanism; however, exceptions have been identified for miRNA-virus interactions (e.g., DENV and CHIKV) in terms of the target type or regulatory outcome. First, during arbovirus infection, mosquito miRNAs can directly bind to the 3'-UTR of the viral genome (not necessary an mRNA), regulating virus replication (Yan et al., 2014; Lucas et al., 2015b; Dubey et al., 2019; Yen et al., 2019), which differs from the canonical mechanism of action. However, the mechanisms underlying mosquito miRNA-*Plasmodium* interactions are always consistent with the canonical mechanism of action, namely, miRNAs generally bind to mosquito immunity- or development-related mRNAs, indirectly regulating pathogen infection (Jain et al., 2014; Dennison et al., 2015; Dong et al., 2020) (**Table S1**). However, the exact mechanism of translational or viral repression remains unclear (Winter et al., 2007). Second, miRNAs always negatively regulate their targets by inducing mRNA cleavage (Yekta et al., 2004) or degradation (Eichhorn et al., 2014), or by repressing translation (Fabian and Sonenberg, 2012); however, positive regulation by miRNAs is repeatedly observed in mosquitoes (Hussain et al., 2013; Zhou et al., 2014; Maharaj et al., 2015; Su et al., 2019). In addition to repressing gene expression, miRNAs can also induce the expression of genes with complementary promoter sequences, switching these genes from repressed to activated (Hussain et al., 2013; Zhou et al., 2014; Maharaj et al., 2015; Su et al., 2019).

More interestingly, the miRNA-target interaction may involve a complex network. A network was observed among clusters of miR-2-3p, miR-13-3p, miR-71-5p, CYP9J35 (a target of miR-2-3p and -13-3p), and CYP325BG3 (a target of miR-71-5p) in insecticide resistant *Cx. pipiens* (Hong et al., 2014).

Moreover, infection with one pathogen affects coinfection with another pathogen in mosquitoes, especially for *Wolbachia* or engineered mosquito densoviruses (MDVs), which can modify host miRNA profiles or use a specific host miRNA to manipulate pathogen invasion in mosquitoes (Osei-Amo et al., 2012; Maharaj et al., 2015; Liu P. et al., 2016).

Preapplication Investigation

Of the 1635 putative or mature miRNAs reported in mosquitoes, only a few have advanced to the step of preapplication investigations, and the names of these miRNAs are italicized in **Table S1**. The first attempt to establish an application is to exploit the vector specificity and stability of MDVs, which are restricted to mosquitoes. Anti-miRNA sponges targeting endogenous let-7-5p and miR-210-3p were introduced into MDVs in *Ae. aegypti* (noted as **AaeDV**-based vectors in **Figure 1**), and both sponges downregulated the expression levels of these miRNAs. According to the study, this recombinant vector is useful to purposefully inhibit or promote

TABLE 5 | Tissue-, organ- or cell compartment- specific miRNAs.

miRNA names	Study materials and enriched tissues, organs, or cell compartments							
	Ovary[&]	Salivary glands[&]	Midgut[&]	Brain[&]	Fat body[&]	Thorax[&]	Cell cytoplasm[#]	Cell nucleus[#]
miR-1-3p	–	–	–	–	–	–	infected cells (Mayoral et al., 2014)	*Ae. aegypti* cells (Mayoral et al., 2014)
miR-10-3p	*An. gambiae* (Nouzova et al., 2018)	–	–	–	–	–	–	–
miR-10-5p	*An. gambiae* (Lampe and Levashina, 2018)	–	–	–	–	–	*Ae. aegypti* cells (Mayoral et al., 2014)	–
miR-100-5p	–	–	–	–	–	–	–	–
miR-10355-3p	*An. gambiae* (Bryant et al., 2019)	–	–	–	–	–	–	–
miR-10355-5p	*An. gambiae* (Bryant et al., 2019)	–	–	–	–	–	–	–
miR-10365-5p	*An. gambiae* (Bryant et al., 2019)	–	–	–	–	–	–	–
miR-10367-5p	*An. gambiae* (Bryant et al., 2019)	–	–	–	–	–	–	–
miR-10368-3p	*An. gambiae* (Bryant et al., 2019)	–	–	–	–	–	–	–
miR-10365-3p	–	*An. coluzzii* (Bruno et al., 2019)	–	–	–	–	–	–
miR-10376-3p	–	–	–	–	–	–	–	–
miR-11-3p	–	*An. coluzzii* (Bruno et al., 2019)	–	–	–	–	–	–
miR-1174-3p	–	–	–	*An. gambiae* (Bryant et al., 2020)	–	–	–	–
miR-1174-5p	–	–	–	–	–	–	–	–
miR-1175-5p	*An. gambiae* (Bryant et al., 2019)	–	–	–	–	–	*Ae. aegypti* cells (Mayoral et al., 2014)	–
miR-1175-3p	*An. gambiae* (Bryant et al., 2019)	–	–	–	–	–	*Ae. aegypti* cells (Mayoral et al., 2014)	–
miR-12-5p	*An. gambiae* (Bryant et al., 2019)	*An. coluzzii* (Bruno et al., 2019)	*An. gambiae* (Winter et al., 2007; Bryant et al., 2019)	–	–	–	–	*Ae. aegypti* cells (Mayoral et al., 2014)

(Continued)

TABLE 5 | Continued

miRNA names	Study materials and enriched tissues, organs, or cell compartments							
	Ovary[&]	Salivary glands[&]	Midgut[&]	Brain[&]	Fat body[&]	Thorax[&]	Cell cytoplasm[#]	Cell nucleus[#]
miR-12-3p	*An. gambiae* (Bryant et al., 2019)	*An. coluzzii* (Bruno et al., 2019)	*An. gambiae* (Winter et al., 2007; Bryant et al., 2019)	—	—	—	—	*Ae. aegypti* cells (Mayoral et al., 2014)
miR-124-3p	—	—	—	*An. gambiae* (Lampe and Levashina, 2018)	—	—	—	—
miR-12414-3p	*An. gambiae* (Bryant et al., 2019)	—	—	—	—	—	—	—
miR-125-5p		*An. coluzzii* (Bruno et al., 2019)	—	—	—	—	*Ae. aegypti* cells (Mayoral et al., 2014)	—
miR-133-3p	—	—	—	—	—	—	—	—
miR-137-3p	—	—	—	—	—	—	*Ae. aegypti* cells (Mayoral et al., 2014)	—
miR-14-3p	—	—	—	—	*Ae. aegypti* (Bryant et al., 2010)	—	—	—
miR-1889-3p	—	*An. coluzzii* (Bruno et al., 2019)	—	—	—	—	infected cells (Mayoral et al., 2014)	*Ae. aegypti* cells (Mayoral et al., 2014)
miR-1889-5p	—	*An. coluzzii* (Bruno et al., 2019)	—	—	—	—	—	—
miR-1891-3p	—	—	—	—	*An. gambiae* (Bryant et al., 2019)	—	—	—
miR-1891-5p	*An. gambiae* (Bryant et al., 2019)	—	*An. gambiae* (Bryant et al., 2019)	—	—	—	—	—
miR-210-3p	—	—	—	*An. gambiae* (Lampe and Levashina, 2018)			*Ae. aegypti* cells (Mayoral et al., 2014)	
miR-252-5p	—	—	—	—	—	—	—	—
miR-252-3p	—	—	—	—	—	—	—	—
miR-275-3p	—	—	—	*An. gambiae* (Lampe and Levashina, 2018)	—	—	—	—
miR-275-5p	—	*An. coluzzii* (Bruno et al., 2019)	—	—	—	—	—	—
miR-276-5p	—	—	—	*An. gambiae* (Nouzova et al., 2018; Lampe and Levashina, 2018)	*An. gambiae* (Nouzova et al., 2018)	—	—	—

(Continued)

TABLE 5 | Continued

miRNA names	Study materials and enriched tissues, organs, or cell compartments							
	Ovary[&]	Salivary glands[&]	Midgut[&]	Brain[&]	Fat body[&]	Thorax[&]	Cell cytoplasm[#]	Cell nucleus[#]
miR-2765-5p	*An. gambiae* (Bryant et al., 2019)	—	—	—	—	—	—	—
miR-277-3p	—	—	—	—	—	*An. gambiae* (Winter et al., 2007)	—	—
miR-279-3p	*An. gambiae* (Lampe and Levashina, 2018)	—	—	—	—	—	—	—
miR-281-3p	*An. gambiae* (Lampe and Levashina, 2018)	*An. coluzzii* (Bruno et al., 2019)	*An. gambiae* (Nouzova et al., 2018; Bryant et al., 2019)	*An. gambiae* (Lampe and Levashina, 2018)	—	—	—	—
miR-281-5p		*An. coluzzii* (Bruno et al., 2019)	*An. gambiae* (Nouzova et al., 2018; Bryant et al., 2019)	—	—	—	*Ae. aegypti* cells (Mayoral et al., 2014)	*Ae. aegypti* cells (Mayoral et al., 2014)
miR-282-5p	—	—	—	—	—	—	*Ae. aegypti* cells (Mayoral et al., 2014)	
miR-283-5p	—	*An. coluzzii* (Bruno et al., 2019)	*An. gambiae* (Winter et al., 2007; Bryant et al., 2019)	—	—	*An. gambiae* (Winter et al., 2007)	—	—
miR-285-3p	—	—	—	—	—	—		
miR-286-3p	*Ae. aegypti* (Akbari et al., 2013)	—	—	—	—	—		
miR-2945-3p	—	—	*Ae. albopictus* (Su et al., 2017)	—	—	—	—	—
miR-2c-3p	—	*An. coluzzii* (Bruno et al., 2019)	—	—	—	—	—	—
miR-305-5p	*An. gambiae* (Lampe and Levashina, 2018)	—	—	—	—	—	*Ae. aegypti* cells (Mayoral et al., 2014)	*Ae. aegypti* cells (Mayoral et al., 2014)
miR-306-5p	*An. gambiae* (Nouzova et al., 2018)	—	—	—	—	—	—	—
miR-3069	—	—	—	—	—	—	—	—
miR-307-3p	—	*An. coluzzii* (Bruno et al., 2019)		*An. gambiae* (Lampe and Levashina, 2018)	*An. gambiae* (Lampe and Levashina, 2018)	—	—	—
miR-308-3p	—	*An. coluzzii* (Bruno et al., 2019)	—	—	—	—	—	—

(Continued)

TABLE 5 | Continued

miRNA names	Study materials and enriched tissues, organs, or cell compartments							
	Ovary[&]	Salivary glands[&]	Midgut[&]	Brain[&]	Fat body[&]	Thorax[&]	Cell cytoplasm[#]	Cell nucleus[#]
miR-309a-3p	*An.gambiae* (Bryant et al., 2019)	—	—	—	—	—	—	—
miR-375-5p	—	*An. coluzzii* (Bruno et al., 2019)	—	—	—	—	—	—
miR-375-3p	—	*An. coluzzii* (Bruno et al., 2019)	—	—	—	—	—	—
miR-7-5p	—	—	—	*An. gambiae* (Lampe and Levashina, 2018)	—	—	—	—
miR-71-3p	—	—	—	—	—	—	infected cells (Mayoral et al., 2014)	—
miR-79-5p	—	—	—	—	—	—	infected cells (Mayoral et al., 2014)	—
miR-8-3p	—	*An. coluzzii* (Bruno et al., 2019)	—	—	*Ae. aegypti* (Bryant et al., 2010)	—	*Ae.aegypti* cells (Mayoral et al., 2014)	
miR-927-5p	—	—	—	—	—	—	—	—
miR-927-3p	—	—	—	—	—	—	—	—
miR-932-5p	—	—	—	—	—	—	*Ae.aegypti* cells (Mayoral et al., 2014)	
miR-956-3p	—	—	*An. gambiae* (Bryant et al., 2020)	—	—	—	—	—
miR-957-5p	—	—	—	—	*An. gambiae* (Bryant et al., 2019)	—	—	—
miR-965-3p	—	*An. coluzzii* (Bruno et al., 2019)	—	—	—	—	—	—
miR-970-3p	—	—	—	—	—	—	infected cells (Mayoral et al., 2014)	infected cells (Mayoral et al., 2014)
miR-980-3p	—	*An. coluzzii* (Bruno et al., 2019)	—	—	—	—	—	—
miR-981-3p	—	*An. coluzzii* (Bruno et al., 2019)	—	—	—	—	—	—

(Continued)

TABLE 5 | Continued

miRNA names	Study materials and enriched tissues, organs, or cell compartments							
	Ovary[&]	Salivary glands[&]	Midgut[&]	Brain[&]	Fat body[&]	Thorax[&]	Cell cytoplasm[#]	Cell nucleus[#]
miR-989-3p	*An. stephensi*, *Ae. aegypti* (Mead and Tu, 2008), *An. gambiae* (Lampe and Levashina, 2018; Bryant et al., 2019)	—	*An. gambiae* (Winter et al., 2007)	—	—	—	—	—
miR-993-3p	—	—	—	—	*An. gambiae* (Bryant et al., 2019)	—	—	—
miR-998-3p	*An. gambiae* (Lampe and Levashina, 2018)	—	—	—	—	—	—	—
miR-998-5p	*An. gambiae* (Lampe and Levashina, 2018)	—	—	—	—	—	—	—

[&]The term "specific" here indicates that the miRNA is enriched in the corresponding tissue compared with the other tissues from one mosquito species. [#]The term "specific" here indicates that the miRNA is enriched in either the cytoplasm or nucleus in comparison between the two cell compartments; and for reference (Mayoral et al., 2014), the pathogen used for infection was Wolbachia. "—", no evidence shows that the miRNA is more abundant in these comparisons.

TABLE 6 | Alterations in miRNA abundance in response to infection with different pathogens in various mosquito samples.

miRNA names	Study materials* and changes in expression levels upon pathogen infection						
	CHIKV infection	*Plasmodium* infection	DENV infection	*Wolbachia* infection	ZIKA infection	WNV infection	BTV infection
miR-1-3p	*Ae. albopictus* cells (Shrinet et al., 2014)	***An. anthropophagus* midgut** (Liu et al., 2017), *An. stephensi* (Jain et al., 2014)	*Ae. albopictus* midgut (Su et al., 2017), *Ae. albopictus* (Liu et al., 2015)	***Ae. aegypti* cell cytoplasm** (Mayoral et al., 2014), *Ae. aegypti* cell nucleus (Mayoral et al., 2014)	***Ae. aegypti*** (Saldana et al., 2017)	—	—
miR-1-5p	—	—	—	—	***Ae. aegypti*** (Saldana et al., 2017)	—	—
miR-10-5p	***Ae.aegypti* saliva, *Ae. albopictus* saliva** (Maharaj et al., 2015)**, *Ae. aegypti*** (Dubey et al., 2017)	***An. anthropophagus* midguts** (Liu et al., 2017), *An. stephensi* (Jain et al., 2014)	*Ae. aegypti* (Liu et al., 2015; Etebari et al., 2015), C6/36 cells (Avila-Bonilla et al., 2017)	*Ae. aegypti* cell nucleus (Mayoral et al., 2014)	—	—	—
miR-100-5p	***Ae. albopictus* cells** (Shrinet et al., 2014), ***Ae. aegypti* saliva**, ***Ae. albopictus* saliva** (Maharaj et al., 2015), *Ae. aegypti* (Saldana et al., 2017)	***An. anthropophagus* midguts** (Liu et al., 2017), *An. stephensi* (Jain et al., 2014)	***Ae. albopictus*** (Yan et al., 2014)	***Ae. aegypti* cell cytoplasm and nucleus** (Mayoral et al., 2014)	—	—	—
miR-1000-5p	***Ae.aegypti* saliva** (Maharaj et al., 2015), *Ae. albopictus* cells (Shrinet et al., 2014)	*An. anthropophagus* midguts (Liu et al., 2017), ***An. stephensi*** (Jain et al., 2014)	***Ae. albopictus* midgut** (Su et al., 2017), *Ae. aegypti* (Campbell et al., 2014)	***Ae. aegypti* cell cytoplasm and nucleus** (Mayoral et al., 2014)	—	—	—
miR-109	*Ae. aegypti* saliva (Maharaj et al., 2015)	—	—	—	—	—	—
miR-11-3p	*Ae. albopictus* cells (Shrinet et al., 2014), *Ae. aegypti* saliva (Maharaj et al., 2015)	***An. anthropophagus* midguts** (Liu et al., 2017), *An. stephensi* (Jain et al., 2014)	—	*Ae. aegypti* cell cytoplasm (Mayoral et al., 2014)	—	—	—
miR-11-5p	***Ae. albopictus* cells** (Shrinet et al., 2014)	—	—	*Ae. aegypti* cell nucleus (Mayoral et al., 2014)	—	—	—
miR-115	*Ae. aegypti* saliva (Maharaj et al., 2015)	—	—	—	—	—	—
miR-117	***Ae. aegypti* saliva** (Maharaj et al., 2015)	—	—	—	—	—	—

(Continued)

TABLE 6 | Continued

miRNA names	Study materials* and changes in expression levels upon pathogen infection						
	CHIKV infection	***Plasmodium* infection**	**DENV infection**	***Wolbachia* infection**	**ZIKA infection**	**WNV infection**	**BTV infection**
miR-1174-3p	*Ae. aegypti* saliva (Maharaj et al., 2015)	***An. stephensi*** (Jain et al., 2014), *An. gambiae* (Winter et al., 2007)	*Ae. albopictus* midgut (Su et al., 2017)	*Ae. aegypti* cell cytoplasm (Mayoral et al., 2014)	—	—	—
miR-1175-5p	—	*An. stephensi* (Jain et al., 2014)	***Ae. albopictus* midgut** (Su et al., 2017)	***Ae. aegypti* cell nucleus** (Mayoral et al., 2014), *Ae. aegypti* cell cytoplasm (Mayoral et al., 2014)	—	—	—
miR-1175-3p	*Ae. albopictus* cells (Shrinet et al., 2014), *Ae. aegypti* saliva (Maharaj et al., 2015)	***An. anthropophagus* midguts** (Liu et al., 2017), *An. gambiae* (Winter et al., 2007), *An.stephensi* (Jain et al., 2014)	***Ae. albopictus* midgut** (Su et al., 2017), *Ae. aegypti* (Campbell et al., 2014)	*Ae. aegypti* cell cytoplasm (Mayoral et al., 2014)	—	—	—
miR-11900			*Ae. aegypti* cells (Miesen et al., 2016; Zhang et al., 2017)	—	—	—	—
miR-12-5p	***Ae. aegypti* saliva** (Maharaj et al., 2015), *Ae. albopictus* cells (Shrinet et al., 2014)	***An. anthropophagus* midguts** (Liu et al., 2017), *An. stephensi* (Jain et al., 2014)	*Ae. albopictus* midguts (Su et al., 2017)	***Ae. aegypti* cells** (Osei-Amo et al., 2012)	—	—	—
miR-12-3p	—	—	—	***Ae. aegypti* cell nucleus and cytoplasm** (Mayoral et al., 2014)	—	—	—
miR-124-3p	—	***An. stephensi*** (Jain et al., 2014)	*Ae. aegypti* (Campbell et al., 2014), C6/36 cells (Avila-Bonilla et al., 2017)	***Ae. aegypti* cell nucleus and cytoplasm** (Mayoral et al., 2014)	—	—	—
miR-1247	***Ae. aegypti* saliva** (Maharaj et al., 2015)	—	—	—	—	—	—
miR-125-5p	***Ae. albopictus* cells** (Shrinet et al., 2014)**, *Ae. aegypti* saliva, *Ae. albopictus* saliva** (Maharaj et al., 2015)	***An. anthropophagus* midguts** (Liu et al., 2017), *An. stephensi* (Jain et al., 2014)	—	***Ae. aegypti*** (Hussain et al., 2013)**, *Ae. aegypti* cell cytoplasm and nucleus** (Mayoral et al., 2014)	—	—	—
miR-125-3p	***Ae. albopictus* cells** (Shrinet et al., 2014)	*An. stephensi* (Jain et al., 2014)	—	—	—	—	—
miR-127	***Ae. albopictus* saliva** (Maharaj et al., 2015)		—	—	—	—	—
miR-13-3p	***Ae. aegypti* saliva** (Maharaj et al., 2015), C6/36 cells (Shrinet et al., 2014), *Ae. albopictus* saliva (Maharaj et al., 2015)	***An. anthropophagus* midgut** (Liu et al., 2017), *An. stephensi* (Jain et al., 2014)	—	—	—	—	*Ae. albopictus* cells (Xing et al., 2016)
miR-13-5p	*Ae. albopictus* cells (Shrinet et al., 2014)	*An. stephensi* (Jain et al., 2014)	—	—	—	—	
miR-133-3p	***Ae. aegypti* saliva, *Ae. albopictus* saliva** (Maharaj et al., 2015), *Ae. albopictus* cells (Shrinet et al., 2014)	*An. stephensi* (Jain et al., 2014), *An. anthropophagus* midgut (Liu et al., 2017)	—	—	—	—	*Ae. albopictus* cells (Xing et al., 2016)
miR-133-5p		*An. stephensi* (Jain et al., 2014)	—	—	—	—	—
miR-137-3p	***Ae.albopictus* saliva** (Maharaj et al., 2015), *Ae. albopictus* cells (Shrinet et al., 2014)	***An. stephensi* iBF at 42h** (Jain et al., 2014), ***An. anthropophagus* midguts** (Liu et al., 2017), *An. stephensi* iBF at 5d (Jain et al., 2014)	—	—	—	—	—

(Continued)

TABLE 6 | Continued

miRNA names	Study materials* and changes in expression levels upon pathogen infection						
	CHIKV infection	***Plasmodium* infection**	**DENV infection**	***Wolbachia* infection**	**ZIKA infection**	**WNV infection**	**BTV infection**
miR-14-3p	***Ae. aegypti* saliva, *Ae. albopictus* saliva** (Maharaj et al., 2015), *Ae. albopictus* cells (Shrinet et al., 2014)	*An. stephensi* (Jain et al., 2014), *An. anthropophagus* midguts (Liu et al., 2017)	—	***Ae. aegypti* cell cytoplasm** (Mayoral et al., 2014)	—	—	—
miR-143	***Ae. aegypti* saliva, *Ae. albopictus* saliva** (Maharaj et al., 2015)	—	—	—	—	—	—
miR-15-3p	—	—	**HEK293 and HeLa cells** (Smith et al., 2017)	—	**HEK293 and HeLa cells** (Smith et al., 2017)	**HEK293 and HeLa cells** (Smith et al., 2017)	—
miR-157	***Ae. albopictus* saliva** (Maharaj et al., 2015)	—	—	—	—	—	—
miR-1571	***Ae. aegypti* saliva** (Maharaj et al., 2015)	—	—	—	—	—	—
miR-1767		—	***Ae. albopictus* midgut** (Su et al., 2017; Su et al., 2019)	—	—	—	—
miR-184-3p	***Ae. albopictus* saliva** (Maharaj et al., 2015)**, C6/36 cells** (Dubey et al., 2017), *Ae. aegypti* saliva (Maharaj et al., 2015)	***An. anthropophagus* midguts** (Liu et al., 2017), *An. stephensi* (Jain et al., 2014)	***Ae. albopictus*** (Liu et al., 2015), *Ae. albopictus* midguts (Su et al., 2017)	—	—	—	—
miR-1889-3p	—	—	***Ae. albopictus* and C6/36 cells** (Yan et al., 2014), *Ae. albopictus* (Liu et al., 2015)	***Ae. aegypti* cell cytoplasm** (Mayoral et al., 2014)	—	—	—
miR-1889-5p	***Ae. aegypti* saliva** (Maharaj et al., 2015)	—	—	*Ae. aegypti* cell cytoplasm (Mayoral et al., 2014)	—	—	***Ae. albopictus* cells** (Xing et al., 2016)
miR-1890-3p	***Ae. aegypti* saliva** (Maharaj et al., 2015), *Ae. albopictus* cells (Shrinet et al., 2014)	***An. anthropophagus* midguts** (Liu et al., 2017), *An. stephensi* (Jain et al., 2014)	—	***Ae. aegypti* cell cytoplasm** (Mayoral et al., 2014)	—	—	—
miR-1891-5p	***Ae. aegypti* saliva**, ***Ae. albopictus* saliva** (Maharaj et al., 2015), *Ae. albopictus* cells (Shrinet et al., 2014)	*An. stephensi* (Jain et al., 2014)	***Ae. albopictus* midgut** (Su et al., 2017), C6/36 cells, *Ae. albopictus* (Yan et al., 2014)	*Ae. aegypti* (Hussain et al., 2011)	—	—	—
miR-190-5p	*Ae. albopictus* cells (Shrinet et al., 2014)	*An. stephensi* (Jain et al., 2014)	**C6/36 cells** (Avila-Bonilla et al., 2017)	*Ae. aegypti* cell cytoplasm (Mayoral et al., 2014)	—	—	—
miR-190-3p	—	*An. stephensi* (Jain et al., 2014)	—	—	—	—	—
miR-193-5p	—	—	***Ae. albopictus*** (Su et al., 2019)	—	—	—	—
miR-193-3p	*Ae. albopictus* cells (Shrinet et al., 2014)	—	—	—	—	—	—
miR-1951		—	***Ae. albopictus* midgut** (Su et al., 2019)	—	—	—	—
miR-210-3p	***Ae. aegypti* saliva** (Maharaj et al., 2015), *Ae. albopictus* saliva (Maharaj et al., 2015)	*An. stephensi* (Jain et al., 2014), *An. anthropophagus* midguts (Liu et al., 2017)	**C6/36 cells** (Avila-Bonilla et al., 2017)	*Ae. aegypti* (Hussain et al., 2011), C6/36 cells cytoplasm (Mayoral et al., 2014)	—	—	—
miR-210-5p	*Ae. albopictus* cells (Shrinet et al., 2014)	—	*Ae. aegypti* (Campbell et al., 2014)	—	—	—	—
miR-214	***Ae.aegypti* saliva** (Maharaj et al., 2015), *Ae. albopictus* saliva (Maharaj et al., 2015)	—	—	—	—	—	—

(Continued)

TABLE 6 | Continued

miRNA names	Study materials* and changes in expression levels upon pathogen infection						
	CHIKV infection	***Plasmodium* infection**	**DENV infection**	***Wolbachia* infection**	**ZIKA infection**	**WNV infection**	**BTV infection**
miR-219-5p	*Ae. albopictus* cells (Shrinet et al., 2014)	—	—	***Ae. aegypti* cell cytoplasm** (Mayoral et al., 2014)	—	—	—
miR-229	***Ae. aegypti* saliva** (Maharaj et al., 2015)	—	—	—	—	—	—
miR-23	***Ae. aegypti* saliva** (Maharaj et al., 2015)	—	—	—	—	—	—
miR-2308	***Ae. albopictus* saliva** (Maharaj et al., 2015)	—	—	—	—	—	—
miR-242	***Ae. aegypti* saliva** (Maharaj et al., 2015)	—	—	—	—	—	—
miR-249	***Ae. albopictus* saliva, *Ae. aegypti* saliva** (Maharaj et al., 2015)	—	—	—	—	—	—
miR-252-5p	***Ae. aegypti* saliva** (Maharaj et al., 2015), *Ae. albopictus* saliva (Maharaj et al., 2015)	*An. stephensi* (Jain et al., 2014), *An. anthropophagus* midgut (Liu et al., 2017)	**C6/36 cells** (Yan et al., 2014), C6/36 cells (Avila-Bonilla et al., 2017)	***Ae. aegypti*** (Hussain et al., 2011), ***Ae. aegypti* cell cytoplasm** (Mayoral et al., 2014)	—	—	—
miR-252-3p	—	—	*Ae. albopictus* cells (Shrinet et al., 2014)	—	—	—	—
miR-263a-3p	—	—	C6/36 cells (Avila-Bonilla et al., 2017)	—	—	—	—
miR-263a-5p	—	—	—	—	*Ae. aegypti* (Saldana et al., 2017)	—	—
miR-275-3p	***Ae. albopictus* cells** (Shrinet et al., 2014)**, *Ae. aegypti* saliva, *Ae.albopictus* saliva** (Maharaj et al., 2015)	*An. stephensi* (Jain et al., 2014), *An. anthropophagus* midgut (Liu et al., 2017)	*Ae. albopictus* (Liu et al., 2015), C7/10 cells, *Ae. albopictus* midgut (Su et al., 2017)	—	—	—	—
miR-275-5p	***Ae. albopictus* cells** (Shrinet et al., 2014)	—	—	—	—	—	—
miR-276-3p	***Ae. aegypti* saliva, *Ae. albopictus* saliva** (Maharaj et al., 2015)	***An. anthropophagus* midguts** (Liu et al., 2017), *An. stephensi* (Jain et al., 2014)	***Ae. albopictus* midgut** (Su et al., 2017), *Ae. aegypti* (Etebari et al., 2015), *Ae. albopictus (*Liu et al., 2015)	***Ae. aegypti* cell cytoplasm** (Mayoral et al., 2014)	—	—	—
miR-276-5p	—	*An. stephensi* (Jain et al., 2014)	***Ae. albopictus*** (Liu et al., 2015), ***Ae. albopictus* midguts** (Su et al., 2019), *Ae. aegypti* (Campbell et al., 2014), *Ae. albopictus* midgut (Su et al., 2017)	—	—	—	*Ae. albopictus* cells (Xing et al., 2016)
miR-2765-5p	*Ae. albopictus* cells (Shrinet et al., 2014)	—	—	***Ae. aegypti* cell nucleus** (Mayoral et al., 2014)	—	—	—
miR-277-3p	***Ae. albopictus* cells** (Shrinet et al., 2014), ***Ae. aegypti* saliva, *Ae. albopictus* saliva** (Maharaj et al., 2015)	***An. anthropophagus* midguts** (Liu et al., 2017), *An. stephensi* (Jain et al., 2014)	*Ae. albopictus* (Liu et al., 2015)	***Ae. aegypti*** (Hussain et al., 2011)**, *Ae. aegypti* cell nucleus** (Mayoral et al., 2014)	—	—	—
miR-278-3p	*Ae. albopictus* cells (Shrinet et al., 2014)	***An. anthropophagus* midguts** (Liu et al., 2017), *An. stephensi* (Jain et al., 2014)	—	*Ae. aegypti* cell cytoplasm (Mayoral et al., 2014)	—	—	*Ae. albopictus* cells (Xing et al., 2016)
miR-278-5p	***Ae. albopictus* cells** (Shrinet et al., 2014), ***Ae. aegypti*** (Dubey et al., 2017)	—	—	*Ae. aegypti* cell cytoplasm (Mayoral et al., 2014)	—	—	—

(Continued)

TABLE 6 | Continued

miRNA names	Study materials* and changes in expression levels upon pathogen infection						
	CHIKV infection	***Plasmodium* infection**	**DENV infection**	***Wolbachia* infection**	**ZIKA infection**	**WNV infection**	**BTV infection**
miR-279-3p	***Ae.aegypti* saliva** (Maharaj et al., 2015), *Ae. albopictus* cells (Shrinet et al., 2014), *Ae. albopictus* saliva (Maharaj et al., 2015)	***An. anthropophagus* midgut** (Liu et al., 2017), *An. stephensi* (Jain et al., 2014)	—	—	—	—	—
miR-2796-5p	*Ae. albopictus* cells (Shrinet et al., 2014)	*An. stephensi* (Jain et al., 2014)	***Ae. albopictus*** (Liu et al., 2015)	—	—	—	—
miR-2779	*Ae. aegypti* (Dubey et al., 2017)	—	—	—	—	—	—
miR-28	***Ae. albopictus* saliva** (Maharaj et al., 2015)	—	—	—	—	—	—
miR-281-3p	—	*An. stephensi* (Jain et al., 2014)	***Ae. albopictus*** (Zhou et al., 2014)	***Ae. aegypti*** (Hussain et al., 2011), ***Ae. aegypti* cell cytoplasm** (Mayoral et al., 2014)	—	—	—
miR-281-5p	***Ae. albopictus* saliva** (Maharaj et al., 2015), *Ae. aegypti* saliva (Maharaj et al., 2015)	*An. stephensi* (Jain et al., 2014)	*Ae. albopictus* (Liu et al., 2015; Su et al., 2017)	*Ae. aegypti* cell nucleus (Mayoral et al., 2014)	—	—	—
miR-282-5p	—	—	*Ae. albopictus* (Su et al., 2017)	***Ae. aegypti* cell nucleus** (Mayoral et al., 2014)	—	—	—
miR-283-5p	***Ae. albopicts* midgut** (Maharaj et al., 2015), ***Ae. albopictus* cells** (Shrinet et al., 2014)	***An. anthropophagus* midguts** (Liu et al., 2017)	—	—	—	—	—
miR-285-3p	***Ae. aegypti* saliva** (Maharaj et al., 2015), *Ae. albopic- tus* saliva (Maharaj et al., 2015), *Ae. aegypti* (Dubey et al., 2017)	*An. stephensi* (Jain et al., 2014)	—	***Ae. aegypti* cell cytoplasm** (Mayoral et al., 2014)	—	—	***Ae. albopictus* cells** (Xing et al., 2016)
miR-286b-5p	—	—	C6/36 cells (Avila-Bonilla et al., 2017)	—	—	—	—
miR-286a-3p	—	—	C6/36 cells (Avila-Bonilla et al., 2017)	—	—	—	—
miR-2940-3p	—	—	*Ae. albopictus* (Liu et al., 2015)	—	***Ae. aegypti*** (Saldana et al., 2017)	—	—
miR-2940-5p	*Ae. albopictus* cells (Shrinet et al., 2014), *Ae. aegypti* saliva (Maharaj et al., 2015)	***An. gambiae*** (Biryukova et al., 2014)	*Ae. albopictus* (Liu et al., 2015)	***Ae. aegypti* and *Aedes aegypti* cells** (Hussain et al., 2011; Zhang et al., 2013; Mayoral et al., 2014; Asad et al., 2018)	—	C6/36 cells (Slonchak et al., 2014)	—
miR-2941-3p	*Ae. albopictus* cells (Shrinet et al., 2014)	—	***Ae. albopictus*** (Su et al., 2019), *Ae. albopictus* (Liu et al., 2015), *Ae. albopictus* midgut (Liu et al., 2016)	***Ae. aegypti*** (Hussain et al., 2011)**, *Aedes aegypti* cell nucleus and cytoplasm** (Mayoral et al., 2014)	*Ae. aegypti* (Saldana et al., 2017)	—	—
miR-2943-5p	—	—	***Ae. albopictus* midgut** (Liu et al., 2016)	***Ae. aegypti*** (Hussain et al., 2011)	—	—	—
miR-2944a-5p	***Ae. albopictus* cells** (Shrinet et al., 2014)	***An. stephensi*** (Shrinet et al., 2014)	—	—	—	—	—

(Continued)

TABLE 6 | Continued

miRNA names	Study materials* and changes in expression levels upon pathogen infection						
	CHIKV infection	***Plasmodium* infection**	**DENV infection**	***Wolbachia* infection**	**ZIKA infection**	**WNV infection**	**BTV infection**
miR-2945-3p	***Ae. aegypti* saliva** (Maharaj et al., 2015), *Ae. albopictus* cells (Shrinet et al., 2014)	***An. stephensi*** (Jain et al., 2014)	**C6/36 cells** (Yan et al., 2014)**, *Ae. albopictus*** (Liu et al., 2015), *Ae. aegypti* (Campbell et al., 2014)	*Ae. aegypti* (Hussain et al., 2011), *Ae. aegypti* cells (Mayoral et al., 2014)	—	—	—
miR-2946-3p	*Ae. aegypti* saliva (Maharaj et al., 2015)	—	—	***Ae. aegypti* cells** (Mayoral et al., 2014)	*Ae. aegypti* (Saldana et al., 2017)	—	***Ae. albopictus* cells** (Xing et al., 2016)
miR-2951-5p	*Ae. aegypti* (Dubey et al., 2017)	—	—	—	—	—	—
miR-2a-3p	—	—	**C6/36 cells** (Avila-Bonilla et al., 2017)	—	—	—	—
miR-3	***Ae. aegypti* saliva** (Maharaj et al., 2015)	—	—	—	—	—	—
miR-305-5p	***Ae. aegypti* saliva** (Maharaj et al., 2015), *Ae. albopictus* cell (Shrinet et al., 2014), *Ae.albopictus* saliva (Maharaj et al., 2015)	***An. gambiae* midguts** (Dennison et al., 2015)**, *An. anthropophagus* midguts** (Liu et al., 2017), *An. stephensi* (Jain et al., 2014)	*Ae. aegypti* (Campbell et al., 2014)	*Ae. aegypti* cells (Mayoral et al., 2014)	—	—	—
miR-305-3p	—	*An. stephensi* (Jain et al., 2014)	—	—	—	—	—
miR-306-5p	***Ae. aegypti* saliva** (Maharaj et al., 2015), *Ae. albopictus* cells (Shrinet et al., 2014)	*An. stephensi* (Jain et al., 2014), *An. anthropophagus* midguts (Liu et al., 2017)	*Ae. albopictus* (Liu et al., 2015)	***Ae. aegypti* cell cytoplasm** (Mayoral et al., 2014), *Ae. aegypti* cell nucleus (Mayoral et al., 2014)	*Ae. aegypti* (Saldana et al., 2017)	—	—
miR-3069	*Ae. aegypti* saliva (Maharaj et al., 2015)	—	—	—	—	—	—
miR-307-3p	***Ae. aegypti* saliva** (Maharaj et al., 2015)	—	—	—	—	—	—
miR-308-3p	—	***An. anthropophagus* midguts** (Liu et al., 2017), *An. stephensi* (Jain et al., 2014)	*Ae. aegypti* (Campbell et al., 2014)	—	*Ae. aegypti* (Saldana et al., 2017)	—	*Ae. albopictus* cells (Xing et al., 2016)
miR-308-5p	**C6/36 cells** (Shrinet et al., 2014)**, *Ae. aegypti* saliva** (Maharaj et al., 2015)	—	—	***Ae. aegypti*** (Hussain et al., 2011)**, *Ae. aegypti* cell nucleus** (Mayoral et al., 2014)	***Ae. aegypti*** (Saldana et al., 2017)	—	—
miR-309a-3p	***Ae. aegypti* saliva, *Ae. albopictus* saliva** (Maharaj et al., 2015)	***An. anthropophagus* midgut** (Liu et al., 2017), *An. stephensi* (Jain et al., 2014)	—	—	—	—	—
miR-31-5p	***Ae. aegypti* saliva** (Maharaj et al., 2015)	***An. anthropophagus* midguts** (Liu et al., 2017)	—	—	—	—	—
miR-315-5p	***Ae. aegypti* saliva, *Ae. albopictus* saliva** (Maharaj et al., 2015)	*An. stephensi* (Jain et al., 2014)	—	—	—	—	—
miR-315-3p		*An. anthropophagus* midguts (Liu et al., 2017)	—	—	—	—	—
miR-317-3p	***Ae. aegypti* saliva** (Maharaj et al., 2015), ***Ae. aegypti*** (Dubey et al., 2017), *Ae. albopictus* saliva (Maharaj et al., 2015)	***An. gambiae*** (Biryukova et al., 2014), *An. stephensi* (Jain et al., 2014), *An. anthropophagus* midguts (Liu et al., 2017)	*Ae. albopictus* (Liu et al., 2015), *Ae. albopictus* midgut (Su et al., 2017)	***Ae. aegypti*** (Hussain et al., 2011), *Ae. aegypti* cell cytoplasm (Mayoral et al., 2014)	—	—	—

(Continued)

TABLE 6 | Continued

miRNA names	Study materials* and changes in expression levels upon pathogen infection						
	CHIKV infection	***Plasmodium* infection**	**DENV infection**	***Wolbachia* infection**	**ZIKA infection**	**WNV infection**	**BTV infection**
miR-317-5p	***Ae. albopictus* cells** (Shrinet et al., 2014)	—	—	—	—	—	—
miR-320	***Ae. aegypti* saliva** (Maharaj et al., 2015)	—	—	—	—	—	—
miR-33-5p	***Ae. aegypti* saliva** (Maharaj et al., 2015), *Ae. albopictus* cell (Shrinet et al., 2014)	—	***Ae. albopictus*** (Yan et al., 2014)	***Ae. aegypti* cell cytoplasm** (Mayoral et al., 2014)	—	**HEK293 cells** (Slonchak et al., 2015)	—
miR-3368-5p	—	—	*Ae. aegypti* (Campbell et al., 2014)	—	—	—	—
miR-34-3p	***Ae. aegypti* cells** (Shrinet et al., 2014)	—	—	***Ae. aegypti* cell cytoplasm** (Mayoral et al., 2014), *Ae. aegypti* cell nucleus (Mayoral et al., 2014)	—	—	—
miR-34-5p	***Ae. aegypti* saliva** (Maharaj et al., 2015), ***Ae. aegypti*** (Dubey et al., 2017), *Ae. aegypti* cells (Shrinet et al., 2014), *Ae. albopictus* saliva (Maharaj et al., 2015)	***An. anthropophagus* midguts** (Liu et al., 2017), *An. gambiae* (Winter et al., 2007), *An. stephensi* (Jain et al., 2014)	***Ae. aegypti*** (Campbell et al., 2014), ***Ae. albopictus* midgut** (Su et al., 2017), ***Ae. albopictus*** (Su et al., 2019)	***Ae. aegypti*** (Hussain et al., 2011), *Ae. aegypti* cell nucleus (Mayoral et al., 2014)	—	—	*Ae. albopictus* cells (Xing et al., 2016)
miR-341	***Ae. aegypti* saliva** (Maharaj et al., 2015)	—	—	—	—	—	—
miR-3722-5p	—	—	*Ae. aegypti* (Campbell et al., 2014)	—	—	—	—
miR-375-3p	*Ae. albopictus* cells (Shrinet et al., 2014), *Ae. aegypti* saliva (Maharaj et al., 2015)	***An. anthropophagus* midguts** (Liu et al., 2017), *An. stephensi* (Jain et al., 2014)	*Ae. albopictus* midgut (Su et al., 2017)	—	*Ae. aegypti* (Saldana et al., 2017)	—	—
miR-359	***Ae. aegypti* saliva** (Maharaj et al., 2015)	—	—	—	—	—	—
miR-360	***Ae. aegypti* saliva** (Maharaj et al., 2015)	—	—	—	—	—	—
miR-40	***Ae. aegypti* saliva** (Maharaj et al., 2015)	—	—	—	—	—	—
miR-402	***Ae. aegypti* saliva** (Maharaj et al., 2015)	—	—	—	—	—	—
miR-408	***Ae. aegypti* saliva** (Maharaj et al., 2015)	—	—	—	—	—	—
miR-4110-5p	—	—	***Ae. albopictus* midgut** (Su et al., 2019)	—	—	—	—
miR-424-3p	—	—	***Ae. albopictus* midgut** (Su et al., 2019)	—	—	—	—
miR-4275-5p	—	—	*Ae. aegypti* (Campbell et al., 2014)	—	—	—	—
miR-4448	—	—	*Ae. albopictus* midgut (Su et al., 2017), *Ae. albopictus* midgut (Su et al., 2019)	—	—	—	—
miR-446	***Ae. aegypti* saliva** (Maharaj et al., 2015)	—		—	—	—	—
miR-4682	***Ae. aegypti* saliva** (Maharaj et al., 2015)	—		—	—	—	—
miR-47	***Ae. aegypti* saliva** (Maharaj et al., 2015)	—		—	—	—	—

(Continued)

TABLE 6 | Continued

miRNA names	Study materials* and changes in expression levels upon pathogen infection						
	CHIKV infection	***Plasmodium* infection**	**DENV infection**	***Wolbachia* infection**	**ZIKA infection**	**WNV infection**	**BTV infection**
miR-4728-5p		—	***Ae. albopictus* midgut** (Su et al., 2017)	—	—	—	—
miR-5	***Ae. aegypti* saliva, *Ae. albopictus* saliva** (Maharaj et al., 2015)	—		—	—	—	—
miR-5108-5p		—	*Ae. aegypti* (Campbell et al., 2014)	—	—	—	—
miR-5119-5p		—	***Ae. aegypti*** (Campbell et al., 2014)	—	—	—	—
miR-5706		—	***Ae. albopictus* midgut** (Su et al., 2019)	—	—	—	—
miR-576	***Ae. aegypti* saliva** (Maharaj et al., 2015)	—	—	—	—	—	—
miR-6	***Ae. aegypti* saliva** (Maharaj et al., 2015)	—	—	—	—	—	—
miR-62	*Ae. albopictus* saliva (Maharaj et al., 2015)	—	—	—	—	—	—
miR-620	***Ae. aegypti* saliva** (Maharaj et al., 2015)	—	—	—	—	—	—
miR-622		—	***Ae. albopictus* midgut** (Su et al., 2017; Su et al., 2019)	—	—	—	—
miR-69	***Ae. aegypti* saliva** (Maharaj et al., 2015)	—	—	—	—	—	—
miR-7-5p	C6/36 cells (Shrinet et al., 2014)	*An. stephensi* (Jain et al., 2014)	—	***Ae. aegypti* cell nucleus** (Mayoral et al., 2014)	—	—	*Ae. albopictus* cells (Xing et al., 2016)
miR-71-5p	***Ae. aegypti*** (Dubey et al., 2017)	*An. stephensi* (Jain et al., 2014)	—		***Ae. aegypti*** (Saldana et al., 2017)	—	—
miR-71-3p	***Ae. aegypti* saliva** (Maharaj et al., 2015), C6/36 cells (Shrinet et al., 2014), *Ae. albopictus* saliva (Maharaj et al., 2015)	*An. stephensi* (Jain et al., 2014), *An. anthropophagus* midguts (Liu et al., 2017)	*Ae. albopictus* midgut (Su et al., 2017)	***Ae. aegypti* cell cytoplasm** (Mayoral et al., 2014)	—	—	—
miR-778	***Ae. aegypti* and *Ae. albopictus* midgut** (Maharaj et al., 2015)	—	—	—	—	—	—
miR-79-5p	—	—	—	***Ae. aegypti* cell cytoplasm** (Mayoral et al., 2014)	—	—	—
miR-8-3p	***Ae. albopictus* saliva** (Maharaj et al., 2015), *Ae. albopictus* cells (Shrinet et al., 2014)	*An. stephensi* (Jain et al., 2015; Guo et al., 2017)	*Ae. albopictus* (Liu et al., 2015), C7/10 cells, *Ae. albopictus* midgut (Su et al., 2017)	***Ae. aegypti*** (Hussain et al., 2011), *Ae. aegypti* cell cytoplasm (Mayoral et al., 2014)	—	—	—
miR-8-5p	***Ae. albopictus* cells** (Shrinet et al., 2014)	*An. stephensi* (Jain et al., 2014)	*Ae. albopictus* (Liu et al., 2015)	*Ae. aegypti* cell cytoplasm (Mayoral et al., 2014)	—	—	—
miR-80	*Ae.aegypti* saliva (Maharaj et al., 2015)	—	—	—	—	—	—
miR-87-3p	***Ae. aegypti* saliva** (Maharaj et al., 2015), *Ae. albopictus* cells (Shrinet et al., 2014)	*An. anthropophagus* midgut (Liu et al., 2017)	***Ae. albopictus* midgut** (Su et al., 2017), **C6/36 cells** (Avila-Bonilla et al., 2017)	—	—	—	—
miR-87-5p	—	—	*Ae. albopictus* midgut (Su et al., 2019)	—	—	—	—

(Continued)

TABLE 6 | Continued

miRNA names	Study materials* and changes in expression levels upon pathogen infection						
	CHIKV infection	***Plasmodium* infection**	**DENV infection**	***Wolbachia* infection**	**ZIKA infection**	**WNV infection**	**BTV infection**
miR-927-5p	***Ae. albopictus* cell** (Shrinet et al., 2014), ***Ae. aegypti* midgut, *Ae. albopictus* midgut** (Maharaj et al., 2015)	*An. stephensi* (Jain et al., 2014)	*Ae. albopictus* (Liu et al., 2015), **C6/36 cells** (Avila-Bonilla et al., 2017; Avila-Bonilla et al., 2020)	—	—	—	—
miR-927-3p	—	*An. stephensi* (Jain et al., 2014)	***Ae. albopictus* midgut** (Su et al., 2017)	—	—	—	***Ae. albopictus* cells** (Xing et al., 2016)
miR-929-5p	—	*An. stephensi* (Jain et al., 2014)	—	—	—	—	—
miR-92b-3p	—	—	C6/36 cells (Avila-Bonilla et al., 2017)	—	—	—	—
miR-92a-3p	—	***An. gambiae*** (Dennison et al., 2015)	—	—	—	***Cx.Quinquefasciatus*** (Skalsky et al., 2010)	—
miR-932-3p	—		—	**mosquito cell nucleus** (Mayoral et al., 2014)	—	—	—
miR-932-5p	***Ae. aegypti* saliva** (Maharaj et al., 2015), C6/36 cells (Shrinet et al., 2014), *Ae. albopictus* saliva (Maharaj et al., 2015)	***An. stephensi*** (Jain et al., 2014)	*Ae. aegypti* (Campbell et al., 2014)	*Ae. aegypti* cell cytoplasm (Mayoral et al., 2014)	—	—	—
miR-956-3p	—	—	*Ae. albopictus* midgut (Su et al., 2017)	—	—	—	—
miR-957-3p	***Ae. aegypti* saliva**, ***Ae. albopictus* saliva** (Maharaj et al., 2015)	*An. stephensi* (Jain et al., 2014), *An. anthropophagus* midgut (Liu et al., 2017)	*Ae. albopictus* (Liu et al., 2015)	—	—	*Cx.Quinquefasciatus* (Skalsky et al., 2010)	—
miR-965-3p	—	—	—	***Ae. aegypti* cell nucleus and cytoplasm** (Mayoral et al., 2014)	—	—	—
miR-970-3p	***Ae. aegypti* saliva** (Maharaj et al., 2015)	*An. stephensi* (Jain et al., 2014), *An. anthropophagus* midguts (Liu et al., 2017)	**C6/36 cells** (Avila-Bonilla et al., 2017)	—	—	—	—
miR-976-5p			***Ae. albopictus* midgut** (Su et al., 2019)	—	—	—	—
miR-980-3p	***Ae.aegypti* saliva** (Maharaj et al., 2015), *Ae. albopictus* cells (Shrinet et al., 2014)	*An. stephensi* (Jain et al., 2014), *An. anthropophagus* midgut (Liu et al., 2017)	—	—	*Ae. aegypti* (Saldana et al., 2017)	***Cx.quinquefasciatus*** (Skalsky et al., 2010)	*Ae. albopictus* cells (Xing et al., 2016)
miR-980-5p	***Ae. albopictus* cells** (Shrinet et al., 2014)	—	—	—	—	—	—
miR-981-3p	—	***An. anthropophagus* midguts** (Liu et al., 2017), *An. stephensi* (Jain et al., 2014)	—	—	—	—	—
miR-988-5p	*Ae. albopictus* cells (Shrinet et al., 2014)		*Ae. albopictus* midgut (Su et al., 2017)	—	—	—	—
miR-988-3p	***Ae. albopictus* cells** (Shrinet et al., 2014)	*An. stephensi* (Jain et al., 2014)	—	*Ae. aegypti* (Hussain et al., 2011)	—	—	—
miR-989-3p	*Ae. aegypti* (Dubey et al., 2017)	***An. gambiae* midgut** (Winter et al., 2007; Dennison et al., 2015), *An. gambiae* leftover (Winter et al., 2007)	***Ae. albopictus* midgut** (Su et al., 2019), *Ae. albopictus* midguts (Liu et al., 2016), *Ae. albopictus* (Su et al., 2017)	*Ae. aegypti* (Hussain et al., 2011), *Ae. aegypti* cell nucleus and cytoplasm (Mayoral et al., 2014)	***Ae. aegypti*** (Saldana et al., 2017)	*Cx.quinquefasciatus* (Skalsky et al., 2010)	—

(Continued)

TABLE 6 | Continued

miRNA names	Study materials* and changes in expression levels upon pathogen infection						
	CHIKV infection	*Plasmodium* infection	DENV infection	*Wolbachia* infection	ZIKA infection	WNV infection	BTV infection
miR-993-5p	—	*An. stephensi* (Jain et al., 2014)	—	—	—	—	—
miR-993-3p	—	*An. stephensi* (Jain et al., 2014)	***Ae. albopictus* midgut** (Liu et al., 2015)	—	—	—	—
miR-996-3p	***Ae. albopictus* saliva** (Maharaj et al., 2015), C6/36 cells (Shrinet et al., 2014), *Ae. aegypti* saliva (Maharaj et al., 2015)	*An. stephensi* (Jain et al., 2014)	—	***Ae. aegypti* cell cytoplasm** (Mayoral et al., 2014)	—	—	—
miR-996-5p	—	***An. anthropophagus* midgut** (Liu et al., 2017)	—	—	—	—	—
miR-988-5p	—	—	—	***Ae. aegypti* cell nucleus** (Mayoral et al., 2014)	—	—	—
miR-988-3p	—	—	—	***Ae. aegypti* cell cytoplasm** (Mayoral et al., 2014)	—	—	—
miR-998-3p	***Ae. albopictus* cells** (Shrinet et al., 2014), ***Ae. aegypti* saliva** (Maharaj et al., 2015), *Ae. aegypti* (Dubey et al., 2017)	***An. anthropophagus* midguts** (Liu et al., 2017), *An. stephensi* (Jain et al., 2014)	***Ae. albopictus* midgut** (Su et al., 2017)		—	—	—
miR-998-5p	***Ae. albopictus* cells** (Shrinet et al., 2014)	—	—	—	—	—	—
miR-999-3p	*Ae. albopictus* cells (Shrinet et al., 2014), *Ae. aegypti* saliva, *Ae. albopictus* saliva (Maharaj et al., 2015)	*An. stephensi* (Jain et al., 2014)	*Ae. aegypti* (Campbell et al., 2014)	—	—	—	—
miR-9a-5p	—	—	C6/36 cells (Avila-Bonilla et al., 2017)	—	—	—	—
miR-iab-4-5p	—	***An. anthropophagus* midguts** (Liu et al., 2017)	—	—	—	—	—
miR-iab-8-5p	*Ae. albopictus* cells (Shrinet et al., 2014)	—	—	—	—	—	—
bantam-3p	***Ae. aegypti* saliva** (Maharaj et al., 2015), C6/36 cells (Shrinet et al., 2014), *Ae. albopictus* saliva (Maharaj et al., 2015)	***An. anthropophagus* midguts** (Liu et al., 2017), *An. stephensi* (Jain et al., 2014)	*Ae. aegypti* (Campbell et al., 2014)	***Ae. aegypti* cell nucleus** (Mayoral et al., 2014)	—	—	—
bantam-5p	—	*An. stephensi* (Jain et al., 2014)	*Ae. aegypti* (Etebari et al., 2015), *Ae. albopictus* (Liu et al., 2015)	***Ae. aegypti* cell nucleus** (Mayoral et al., 2014), *Ae. aegypti* cell cytoplasm (Mayoral et al., 2014)	—	—	—
let-7-5p	*Ae. albopictus* cells (Shrinet et al., 2014), *Ae. albopictus* saliva (Maharaj et al., 2015)	*An. stephensi* (Jain et al., 2014), *An. anthropophagus* midguts (Liu et al., 2017)	***Ae. albopictus*, C6/36 cells** (Yan et al., 2014), *Ae. aegypti* (Campbell et al., 2014), *Ae. albopictus* (Liu et al., 2015; Su et al., 2017)	***Ae. aegypti* cells** (Hussain et al., 2011)**, nucleus, cytoplasm of cells** (Mayoral et al., 2014)	—	—	—

The "study materials" are written in two styles, namely **bold and nonbold, which means that the miRNAs are upregulated or downregulated upon infection with the corresponding microbes or pathogens infection, respectively. "—", no related data on upregulation or downregulation is available.*

the expression of endogenous miRNAs and subsequently regulate pathogen infection in mosquitoes (Liu P. et al., 2016). This study is similar to a study research that used a plasmid construction technique to express artificial miRNAs that inhibit JEV (Wu et al., 2011) and DENV (Xie et al., 2013) *in vitro* or impede mosquito reproduction and embryonic development (Biedler et al., 2014).

Given the specificity of miRNA-virus interactions in which mosquito miRNAs can directly inhibit the virus *via* complementary base pair interactions, methods to introduce

TABLE 7 | miRNAs with validated targets that exert promotive or inhibitory effects on pathogens.

miRNA names	Validated targets	Validated promotive or inhibitory effect on pathogens
miR-12-5p	MCM6 and MCT1 (Osei-Amo et al., 2012)	Facilitating the *Wolbachia* infection (Osei-Amo et al., 2012; Maharaj et al., 2015), enhancing CHIKV infection (Maharaj et al., 2015)
miR-125-5p	—	Enhancing CHIKV infection (Maharaj et al., 2015)
miR-2944a-5p	vps-13 and CHIKV (Dubey et al., 2019)	Repressing CHIKV replication (Dubey et al., 2019)
miR-184-3p	AAEL002512, AAEL005741 (Zhang et al., 2017)	Inhibiting CHIKV infection (Maharaj et al., 2015)
miR-375-3p	Cactus, kinesin, prohibitin, DEAD box ATP-depen-dent RNA helicase, REL1, hypothetical protein (Hussain et al., 2013)	Enhancing DENV-2 infection (Hussain et al., 2013), repressing CHIKV replication (Maharaj et al., 2015).
miR-1767	—	Enhancing DENV-2 replication (Su et al., 2019)
miR-252-5p	DENV E protein gene (Yan et al., 2014)	Inhibiting DENV replication (Yan et al., 2014)
miR-281-3p	5'-UTR of DENV-2 (Zhou et al., 2014)	Enhancing DENV-2 replication (Zhou et al., 2014)
miR-4448	—	Inhibiting DENV-2 infection (Su et al., 2019)
miR-4728-5p	—	Enhancing DENV infections (Su et al., 2017)
miR-927-5p	FLN (Avila-Bonilla et al., 2020)	Reguating antimicrobial peptides, promoting DENV infection (Avila-Bonilla et al., 2020)
miR-2940-5p	AaDnmt 2 (Zhang et al., 2013), metalloprotease m41 FtsH gene (Slonchak et al., 2014), AaArgM3 (Zhang et al., 2014)	Facilitating *Wolbachia* infection (Hussain et al., 2011; Zhang et al., 2014) and subsequent inhibition of DENV replication (Zhang et al., 2013), restricting WNV replication (Slonchak et al., 2014)
miR-276-5p	Branched-chain amino acid transferase (Lampe et al., 2019)	Enhancing DENV-2 infection (Su et al., 2019), prolonging AA catabolism, and then inhibiting development of sporozoites (Lampe et al., 2019)
miR-137-3p	—	Inhibiting *Plasmodium* infection (Jain et al., 2014)
miR-14-3p	3'UTR-binding sites of GCE mRNA (Qu et al., 2017)	*P. falciparum* and gut microbiota agonist (Dong et al., 2020)
miR-305-5p	—	*P. falciparum* and gut microbiota agonist (Dennison et al., 2015; Dong et al., 2020)
miR-124-3p	Dynamin 2 (Yang et al., 2016), PGRP-LD (Feng et al., 2018b)	Inhibiting JEV infection (Yang et al., 2016)
miR-34-5p	Activation of type I interferon signaling (Smith et al., 2017)	Role in vector competence (Winter et al., 2007), inhibits multiple flaviviruses (Smith et al., 2017)

MCT1, monocarboxylate transporter; MCM6, DNA replication licensing; UTR, untranslated region; FLN, cytoskeleton; AaArgM3, protein arginine methyltransferase 3.

sequences complementary to mosquito miRNAs (noted as miRNA-targeting approaches in **Figure 1**) into arboviruses have been established (Heiss et al., 2011; Tsetsarkin et al., 2015; Tsetsarkin et al., 2016a; Tsetsarkin et al., 2016b). The introduction of a single copy of a miRNA target sequence into the DENV genome was shown to lead to the reduction of DENV 4 replication *in vivo* and *in vitro* (Heiss et al., 2011; Tsetsarkin et al., 2015), consistent with the results of a similar study with another pathogen, JEV (Yen et al., 2013). More interestingly, multiple insertions of heterologous target sequences of different miRNAs into the virus were shown to increase virus attenuation, whereas the insertion of two or three copies of homologous sequence (the same miRNAs) into the virus did not increase virus attenuation (Tsetsarkin et al., 2016a; Tsetsarkin et al., 2016b).

The two preapplication investigations indicate the possible application of miRNA-based approaches, e.g., 1) expressing a miRNA inhibitor in vector mosquitoes by establishing genetically modified mosquitoes, subsequently reducing the fitness between mosquitoes and pathogens and interrupting the transmission of mosquito-borne pathogens (Heiss et al., 2011; Tsetsarkin et al., 2015; Tsetsarkin et al., 2016a; Tsetsarkin et al., 2016b); and 2) inserting specific miRNA target sequences into the flavivirus genome, resulting in selective tissue-specific attenuation and nonhuman-range restriction of live attenuated vaccine viruses (Tsetsarkin et al., 2016a; Tsetsarkin et al., 2016b).

CONCLUDING REMARKS

Currently, miRNA-based approaches employ four steps that address 20 aspects as listed in **Figure 1**. These exploratory studies are limited because of the bottleneck at the preapplication investigation step (**Figure 1**) and require further advances towards field or clinical applications. Twenty-four

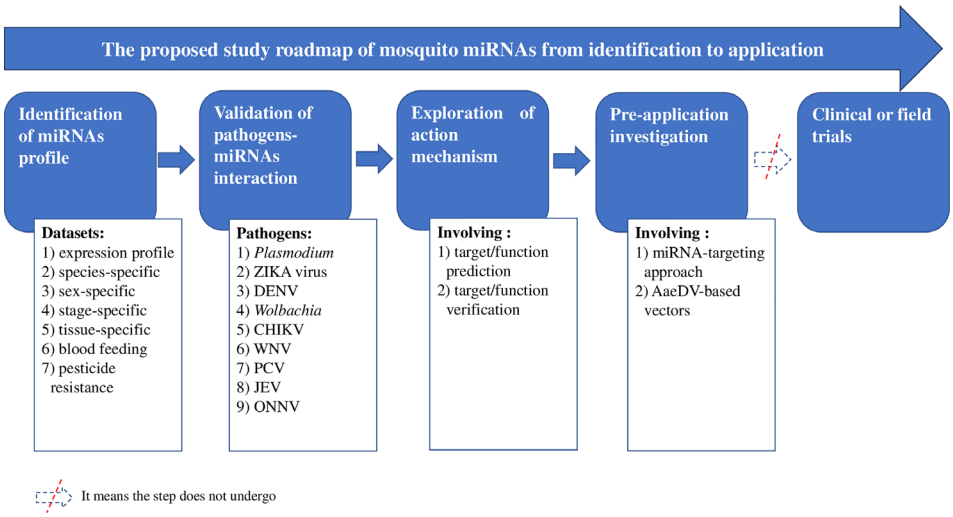

FIGURE 1 | Overall advances in studies of mosquito miRNAs. ZIKA, Zika virus; DENV, Dengue virus; CHIKV, Chikungunya virus; WNV, West Nile virus; ONNV, o'nyong'nyong virus; JEV, Japanese encephalitis virus; PCV, Palm Creek virus; AaeDVs, *Ae. aegypti* densoviruses.

mosquito species have been analyzed for miRNA-related studies. The study materials have ranged widely, from entire mosquitoes to the cytoplasm or nucleus of mosquito cells, from eggs to adult mosquitoes, or from sugar-fed to pathogen-infected mosquitoes (**Tables 1–6**).

The expression of miRNAs is regulated by complex factors, including mosquito species, sex, developmental stage, tissue or organ, age, blood feeding status, pathogen infection status and pathogen type (**Tables 2–7**). Thus, miRNA expression levels detected in entire mosquitoes may lead to biased results, and for one arbovirus, some miRNAs may promote infection in mosquitoes, while for another arbovirus, miRNAs may inhibit infection (**Table 7**). Thus, during the exploration of miRNA-based approaches for the interruption of mosquito-borne disease transmission, an irrational approach is to commonly define a miRNA as solely inhibiting or promoting pathogen infection in mosquitoes, when the actual effects of a miRNA depend on those complex factors. Most importantly, the results presented here

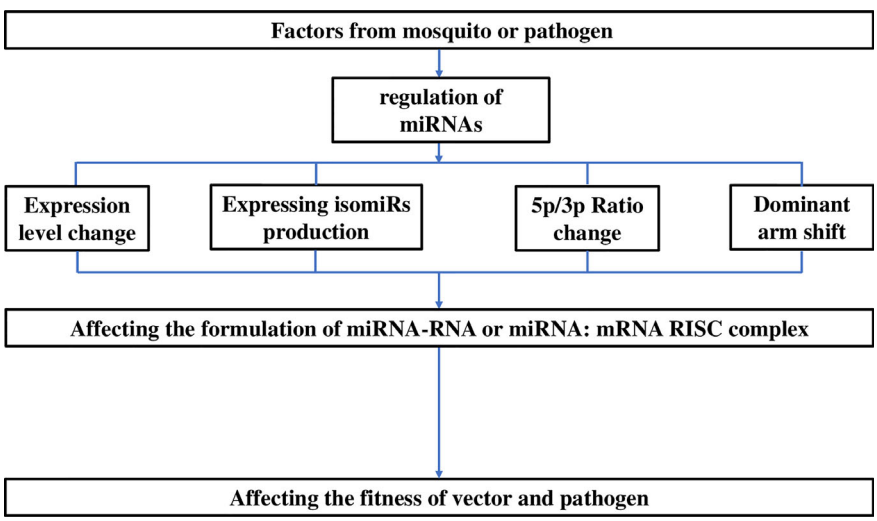

FIGURE 2 | Responses of miRNAs to characteristics of mosquitoes or pathogens and subsequent miRNA-pathogen interactions in mosquitoes. The responses involve modifications in the expression level, isomiR production, or 5p/3p ratio or shift in dominant arm, and any of these alterations can affect the fitness between the vector and pathogen. During modification by miRNAs, the functional component is the formation of the miRNA-target RISC complex. For arboviruses, the complex can be composed of miRNAs and the virus genome (miR-RNA complex) in mosquitoes, directly regulating pathogen infection; however, for *Plasmodium* parasites, it is always composed of miRNAs and mosquito immunity-related mRNAs (miR-mRNA complex), indirectly regulating the infection.

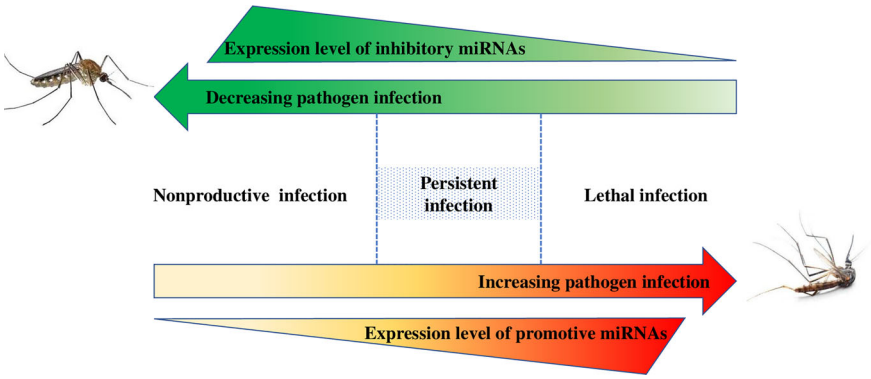

FIGURE 3 | Causal relationship between mosquito miRNAs and pathogen infection. The manipulation by miRNAs is mediated *via* a network. The inhibitory miRNAs and promotive miRNAs always coexist in mosquitoes, inhibiting or promoting pathogen infection, respectively. These miRNAs can balance the miRNA-pathogen interaction, maintain persistent infection and preventing considerable harm to the mosquito.

indicate that the selection of a candidate miRNA according to unique conditions or objectives during miRNA-based approach development is crucial. The current statuses of individual miRNAs presented in **Tables 1–7** and **S1** provide guidance for selection.

As described above, the main variations in miRNAs attributed to the mosquito species or infecting pathogen include changes in the expression level, isomiR production, or 5p/3p ratio or even a shift in the dominant arm. In our opinion, these variations in miRNAs might collectively or individually affect the formulation of miRNA-target RISC complexes, and subsequently influence the fitness between the mosquito and pathogen (Winter et al., 2007). And for mosquito miRNA-arbovirus interactions, the targets of miRNAs can be RNA genomes of arboviruses, which are always mRNA obeying the canonical action mechanism. These viewpoints are presented in **Figure 2**.

Moreover, although the canonical action mechanism of miRNAs always results in repression, the mosquito miRNA-target interaction can lead to two possible forms of regulation, namely, repression or enhancement of pathogen infection in mosquitoes. Both upregulation and downregulation of miRNAs in response to pathogen infection widely coexist in the mosquito, subsequently promoting and inhibiting pathogen infection, respectively. In our opinion, these findings suggest that inhibitory and inducing miRNA expressions are essential to balance the miRNA-pathogen interaction, maintaining persistent infection and preventing considerable harm to the mosquito (**Figure 3**).

Currently, the antiviral effects of mosquito miRNAs on pathogens in combination with genetic engineering and molecular biology techniques may allow the use of these miRNA-based approaches as new tools to interrupt the transmission of mosquito-borne diseases. In this review, the significant progress achieved at the level of individual miRNAs facilitates the selection of an abundant, specific and effective mosquito miRNA (see **Tables 1–7** and **S1**) that can be referenced for further research with different and specific objectives to increase the pace of development of applications and overcome the bottleneck (Tsetsarkin et al., 2015). More importantly, mosquito miRNAs can directly bind to the arbovirus genome, modifying viral replication. However, regarding the *Plasmodium* parasite, mosquito miRNAs generally bind to mosquito immunity or development-related mRNAs, indirectly regulating *Plasmodium* infection. Hence, the strategies for miRNA-based approaches differ for arboviruses and protozoan parasites.

AUTHOR CONTRIBUTIONS

Conceptualization and formal analysis: T-LX. Data curation: T-LX, Y-WS, and X-YF.

Supervision: BZ and X-NZ. Writing-original draft: T-LX. Writing-review & editing: BZ and X-NZ. All authors contributed to the article and approved the submitted version.

FUNDING

BZ received a grant from the National Science and Technology Major Program of China (No. 2018ZX10734-404). This project was financially supported by Ministry of Science and Technology of the People's Republic of China. The funder had no role in study design, data collection and analysis, decision to publish, or preparation of the manuscript.

ACKNOWLEDGMENTS

The ideas presented here were developed during the completion of research projects funded by the Belt and Road Young Scientist Research Exchange Program (No. 17430741900).

SUPPLEMENTARY MATERIAL

The Supplementary Material for this article can be found online at: https://www.frontiersin.org/articles/10.3389/fcimb.2021.665444/full#supplementary-material

REFERENCES

Akbari, O. S., Antoshechkin, I., Amrhein, H., Williams, B., Diloreto, R., Sandler, J., et al. (2013). The Developmental Transcriptome of the Mosquito *Aedes Aegypti*, an Invasive Species and Major Arbovirus Vector. *G3* 3, 1493–1509. doi: 10.1534/g3.113.006742

Allam, M., Spillings, B. L., Abdalla, H., Mapiye, D., Koekemoer, L. L., and Christoffels, A. (2016). Identification and Characterization of microRNAs Expressed in the African Malaria Vector *Anopheles Funestus* Life Stages Using High Throughput Sequencing. *Malaria J.* 15, 542. doi: 10.1186/s12936-016-1591-0

Asad, S., Hussain, M., Hugo, L., Osei-Amo, S., Zhang, G., Watterson, D., et al. (2018). Suppression of the Pelo Protein by *Wolbachia* and Its Effect on Dengue Virus in Aedes Aegypti. *PloS Negl. Trop. Dis.* 12, e0006405. doi: 10.1371/journal.pntd.0006405

Avila-Bonilla, R. G., Yocupicio-Monroy, M., Marchat, L. A., De Nova-Ocampo, M. A., Del Angel, R. M., and Salas-Benito, J. S. (2017). Analysis of the miRNA Profile in C6/36 Cells Persistently Infected With Dengue Virus Type 2. *Virus Res.* 232, 139–151. doi: 10.1016/j.virusres.2017.03.005

Avila-Bonilla, R. G., Yocupicio-Monroy, M., Marchat, L. A., Perez-Ishiwara, D. G., Cerecedo-Mercado, D. A., Del Angel, R. M., et al. (2020). miR-927 Has Pro-Viral Effects During Acute and Persistent Infection With Dengue Virus Type 2 in C6/36 Mosquito Cells. *J. Gen. Virol.* 101, 8. doi: 10.1099/jgv.0.001441

Bartel, D. P. (2004). MicroRNAs: Genomics, Biogenesis, Mechanism, and Function. *Cell* 116, 281–297. doi: 10.1016/S0092-8674(04)00045-5

Bartel, D. P. (2009). MicroRNAs: Target Recognition and Regulatory Functions. *Cell* 136, 215–233. doi: 10.1016/j.cell.2009.01.002

Batz, Z. A., Goff, A. C., and Armbruster, P. A. (2017). MicroRNAs Are Differentially Abundant During *Aedes Albopictus* Diapause Maintenance But Not Diapause Induction. *Insect Mol. Biol.* 26, 721–733. doi: 10.1111/imb.12332

Behura, S. K., Haugen, M., Flannery, E., Sarro, J., Tessier, C. R., Severson, D. W., et al. (2011). Comparative Genomic Analysis of *Drosophila* Melanogaster and Vector Mosquito Developmental Genes. *PloS One* 6, e21504. doi: 10.1371/journal.pone.0021504

Biedler, J. K., Qi, Y., Pledger, D., Macias, V. M., James, A. A., and Tu, Z. (2014). Maternal Germline-Specific Genes in the Asian Malaria Mosquito *Anopheles Stephensi*: Characterization and Application for Disease Control. *G3* 5, 157–166. doi: 10.1534/g3.114.015578

Biryukova, I., Ye, T., and Levashina, E. (2014). Transcriptome-Wide Analysis of microRNA Expression in the Malaria Mosquito Anopheles Gambiae. *BMC Genomics* 15, 557. doi: 10.1186/1471-2164-15-557

Bruno, A., Alessio, C., Carmine, F., Francesco, S., Vladimir, B., Marco, D. L., et al. (2019). MicroRNAs From Saliva of Anopheline Mosquitoes Mimic Human Endogenous miRNAs and may Contribute to Vector-Hostpathogen Interactions. *Sci. Rep.* 9, 2955. doi: 10.1038/s41598-019-39880-1

Bryant, B., Macdonald, W., and Raikhel, A. S. (2010). microRNA miR-275 Is Indispensable for Blood Digestion and Egg Development in the Mosquito *Aedes Aegypti*. *Proc. Natl. Acad. Sci. U. S. A.* 107, 22391–22398. doi: 10.1073/pnas.1016230107

Bryant, W. B., Mills, M. K., Olson, B. J., and Michel, K. (2019). Small RNA-Seq Analysis Reveals Mirna Expression Dynamics Across Tissues in the Malaria Vector, Anopheles Gambiae. *G3* 9, 1507–1517. doi: 10.1534/g3.119.400104

Bryant, W. B., Ray, S., and Mills, M. K. (2020). Global Analysis of Small non-Coding RNA Populations Across Tissues in the Malaria Vector, *Anopheles Gambiae*. *Insects* 11, 7. doi: 10.3390/insects11070406

Campbell, C. L., Harrison, T., Hess, A. M., and Ebel, G. D. (2014). MicroRNA Levels Are Modulated in *Aedes Aegypti* After Exposure to Dengue-2. *Insect Mol. Biol.* 23, 132–139. doi: 10.1111/imb.12070

Carissimo, G., Pain, A., Belda, E., and Vernick, K. D. (2018). Highly Focused Transcriptional Response of *Anopheles Coluzzii* to O'nyong Nyong Arbovirus During the Primary Midgut Infection. *BMC Genomics* 19, 526. doi: 10.1186/s12864-018-4918-0

Castellano, L., Rizzi, E., Krell, J., Di Cristina, M., Galizi, R., Mori, A., et al. (2015). The Germline of the Malaria Mosquito Produces Abundant miRNAs, endo-siRNAs, piRNAs and 29-Nt Small RNAs. *BMC Genomics* 16, 100. doi: 10.1186/s12864-015-1257-2

Chatterjee, R., and Chaudhuri, K. (2006). An Approach for the Identification of microRNA With an Application to Anopheles Gambiae. *Acta Biochim. Polonica* 53, 303–309. doi: 10.18388/abp.2006_3343

Dennison, N. J., BenMarzouk-Hidalgo, O. J., and Dimopoulos, G. (2015). MicroRNA-Regulation of *Anopheles Gambiae* Immunity to *Plasmodium* Falciparum Infection and Midgut Microbiota. *Dev. Comp. Immunol.* 49, 170–178. doi: 10.1016/j.dci.2014.10.016

Dong, S., Fu, X., Dong, Y., Simoes, M. L., Zhu, J., and Dimopoulos, G. (2020). Broad Spectrum Immunomodulatory Effects of *Anopheles Gambiae* microRNAs and Their Use for Transgenic Suppression of Plasmodium. *PloS Pathog.* 16, e1008453. doi: 10.1371/journal.ppat.1008453

Dritsou, V., Deligianni, E., Dialynas, E., Allen, J., Poulakakis, N., Louis, C., et al. (2014). Non-Coding RNA Gene Families in the Genomes of *Anopheline* Mosquitoes. *BMC Genomics* 15, 1038. doi: 10.1186/1471-2164-15-1038

Dubey, S. K., Shrinet, J., Jain, J., Ali, S., and Sunil, S. (2017). *Aedes Aegypti* microRNA miR-2b Regulates Ubiquitin-Related Modifier to Control Chikungunya Virus Replication. *Sci. Rep.* 7, 17666. doi: 10.1038/s41598-017-18043-0

Dubey, S. K., Shrinet, J., and Sunil, S. (2019). *Aedes Aegypti* microRNA, miR-2944b-5p Interacts With 3'UTR of Chikungunya Virus and Cellular Target vps-13 to Regulate Viral Replication. *PloS Negl. Trop. Dis.* 13, e0007429. doi: 10.1371/journal.pntd.0007429

Eichhorn, S. W., Guo, H., McGeary, S. E., Rodriguez-Mias, R. A., Shin, C., Baek, D., et al. (2014). mRNA Destabilization Is the Dominant Effect of Mammalian microRNAs by the Time Substantial Repression Ensues. *Mol. Cell* 56, 104–115. doi: 10.1016/j.molcel.2014.08.028

Etebari, K., Osei-Amo, S., Blomberg, S. P., and Asgari, S. (2015). Dengue Virus Infection Alters Post-Transcriptional Modification of microRNAs in the Mosquito Vector Aedes Aegypti. *Sci. Rep.* 5, 15968. doi: 10.1038/srep15968

Fabian, M. R., and Sonenberg, N. (2012). The Mechanics of miRNA-Mediated Gene Silencing: A Look Under the Hood of Mirisc. *Nat. Struct. Mol. Biol.* 19, 586–593. doi: 10.1038/nsmb.2296

Feng, X., Wu, J., Zhou, S., Wang, J., and Hu, W. (2018b). Characterization and Potential Role of microRNA in the Chinese Dominant Malaria Mosquito *Anopheles Sinensis* (Diptera: Culicidae) Throughout Four Different Life Stages. *Cell Bioscience* 8, 29. doi: 10.1186/s13578-018-0227-1

Feng, X., Zhou, X., Zhou, S., Wang, J., and Hu, W. (2018a). Analysis of microRNA Profile of *Anopheles Sinensis* by Deep Sequencing and Bioinformatic Approaches. *Parasites Vectors* 11, 172. doi: 10.1186/s13071-018-2734-7

Fu, X., Dimopoulos, G., and Zhu, J. (2017). Association of microRNAs With Argonaute Proteins in the Malaria Mosquito *Anopheles Gambiae* After Blood Ingestion. *Sci. Rep.* 7, 6493. doi: 10.1038/s41598-017-07013-1

Fu, X., Liu, P., Dimopoulos, G., and Zhu, J. (2020). Dynamic miRNA-mRNA Interactions Coordinate Gene Expression in Adult Anopheles Gambiae. *PloS Genet.* 16, e1008765. doi: 10.1371/journal.pgen.1008765

Gu, J., Hu, W., Wu, J., Zheng, P., Chen, M., James, A. A., et al. (2013). miRNA Genes of an Invasive Vector Mosquito, Aedes Albopictus. *PloS One* 8, e67638. doi: 10.1371/journal.pone.0067638

Guo, Q., Huang, Y., Zou, F., Liu, B., Tian, M., Ye, W., et al. (2017). The Role of miR-2~13~71 Cluster in Resistance to Deltamethrin in *Culex Pipiens* Pallens. *Insect Biochem. Mol. Biol.* 84, 15–22. doi: 10.1016/j.ibmb.2017.03.006

Hammond, S. M., Bernstein, E., Beach, D., and Hannon, G. J. (2000). An RNA-directed Nuclease Mediates Post-Transcriptional Gene Silencing in *Drosophila* Cells. *Nature* 404, 293–296. doi: 10.1038/35005107

Heiss, B. L., Maximova, O. A., and Pletnev, A. G. (2011). Insertion of microRNA Targets Into the Flavivirus Genome Alters Its Highly Neurovirulent Phenotype. *J. Virol.* 85, 1464–1472. doi: 10.1128/JVI.02091-10

Hong, S., Guo, Q., Wang, W., Hu, S., Fang, F., Lv, Y., et al. (2014). Identification of Differentially Expressed microRNAs in *Culex Pipiens* and Their Potential Roles in Pyrethroid Resistance. *Insect Biochem. Mol. Biol.* 55, 39–50. doi: 10.1016/j.ibmb.2014.10.007

Hu, W., Criscione, F., Liang, S., and Tu, Z. (2015). MicroRNAs of Two Medically Important Mosquito Species: *Aedes Aegypti* and Anopheles Stephensi. *Insect Mol. Biol.* 24, 240–252. doi: 10.1111/imb.12152

Hussain, M., Frentiu, F. D., Moreira, L. A., O'Neill, S. L., and Asgari, S. (2011). *Wolbachia* Uses Host microRNAs to Manipulate Host Gene Expression and Facilitate Colonization of the Dengue Vector *Aedes Aegypti*. *Proc. Natl. Acad. Sci. U. S. A.* 108, 9250–9255. doi: 10.1073/pnas.1105469108

Hussain, M., Walker, T., O'Neill, S. L., and Asgari, S. (2013). Blood Meal Induced microRNA Regulates Development and Immune Associated Genes in the Dengue Mosquito Vector, Aedes Aegypti. *Insect Biochem. Mol. Biol.* 43, 146–152. doi: 10.1016/j.ibmb.2012.11.005

Jain, S., Rana, V., Shrinet, J., Sharma, A., Tridibes, A., Sunil, S., et al. (2014). Blood Feeding and *Plasmodium* Infection Alters the miRNome of Anopheles Stephensi. *PloS One* 9, e98402. doi: 10.1371/journal.pone.0098402

Jain, S., Rana, V., Tridibes, A., Sunil, S., and Bhatnagar, R. K. (2015). Dynamic Expression of miRNAs Across Immature and Adult Stages of the Malaria Mosquito Anopheles Stephensi. *Parasites Vectors* 8, 179. doi: 10.1186/s13071-015-0772-y

Jones-Rhoades, M. W., Bartel, D. P., and Bartel, B. (2006). MicroRNAs and Their Regulatory Roles in Plants. *Annu. Rev. Plant Biol.* 57, 19–53. doi: 10.1146/annurev.arplant.57.032905.105218

Lampe, L., Jentzsch, M., Kierszniowska, S., and Levashina, E. A. (2019). Metabolic Balancing by miR-276 Shapes the Mosquito Reproductive Cycle and *Plasmodium* Falciparum Development. *Nat. Commun.* 10, 5634. doi: 10.1038/s41467-019-13627-y

Lampe, L., and Levashina, E. A. (2018). Microrna Tissue Atlas of the Malaria Mosquito Anopheles Gambiae. *G3* 8, 185–193. doi: 10.1534/g3.117.300170

Lee, Y., Ahn, C., Han, J., Choi, H., Kim, J., Yim, J., et al. (2003). The Nuclear RNase III Drosha Initiates microRNA Processing. *Nature* 425, 415–419. doi: 10.1038/nature01957

Lee, M., Etebari, K., Hall-Mendelin, S., van den Hurk, A. F., Hobson-Peters, J., Vatipally, S., et al. (2017). Understanding the Role of microRNAs in the Interaction of *Aedes Aegypti* Mosquitoes With an Insect-Specific Flavivirus. *J. Gen. Virol.* 98, 1892–1903. doi: 10.1099/jgv.0.000832

Lee, Y., Jeon, K., Lee, J. T., Kim, S., and Kim, V. N. (2002). MicroRNA Maturation: Stepwise Processing and Subcellular Localization. *EMBO J.* 21, 4663–4670. doi: 10.1093/emboj/cdf476

Li, S., Mead, E. A., Liang, S., and Tu, Z. (2009). Direct Sequencing and Expression Analysis of a Large Number of miRNAs in *Aedes Aegypti* and a Multi-Species Survey of Novel Mosquito Mirnas. *BMC Genomics* 10, 581. doi: 10.1186/1471-2164-10-581

Ling, L., Kokoza, V. A., Zhang, C., Aksoy, E., and Raikhel, A. S. (2017). MicroRNA-277 Targets Insulin-Like Peptides 7 and 8 to Control Lipid Metabolism and Reproduction in Aedes Aegypti Mosquitoes. *Proc. Natl. Acad. Sci. U. S. A.* 114, E8017–E8024. doi: 10.1073/pnas.1710970114

Liu, W., Hao, Z., Huang, L., Chen, L., Wei, Q., Cai, L., et al. (2017). Comparative Expression Profile of microRNAs in *Anopheles Anthropophagus* Midgut After Blood-Feeding and *Plasmodium* Infection. *Parasites Vectors* 10, 86. doi: 10.1186/s13071-017-2027-6

Liu, W., Huang, H., Xing, C., Li, C., Tan, F., and Liang, S. (2014). Identification and Characterization of the Expression Profile of microRNAs in Anopheles Anthropophagus. *Parasites Vectors* 7, 159. doi: 10.1186/1756-3305-7-159

Liu, P., Li, X., Gu, J., Dong, Y., Liu, Y., Santhosh, P., et al. (2016). Development of Non-Defective Recombinant Densovirus Vectors for microRNA Delivery in the Invasive Vector Mosquito, Aedes Albopictus. *Sci. Rep.* 6, 20979. doi: 10.1038/srep20979

Liu, Y. X., Li, F. X., Liu, Z. Z., Jia, Z. R., Zhou, Y. H., Zhang, H., et al. (2016). Integrated Analysis of miRNAs and Transcriptomes in *Aedes Albopictus* Midgut Reveals the Differential Expression Profiles of Immune-Related Genes During Dengue Virus Serotype-2 Infection. *Insect Sci.* 23, 377–385. doi: 10.1111/1744-7917.12339

Liu, B., Tian, M., Guo, Q., Ma, L., Zhou, D., Shen, B., et al. (2016). Mir-932 Regulates Pyrethroid Resistance in Culex Pipiens Pallens (Diptera: Culicidae). *J. Med. Entomology* 53, 1205–1210. doi: 10.1093/jme/tjw083

Liu, Y., Zhou, Y., Wu, J., Zheng, P., Li, Y., Zheng, X., et al. (2015). The Expression Profile of *Aedes Albopictus* miRNAs Is Altered by Dengue Virus Serotype-2 Infection. *Cell Bioscience* 5, 16. doi: 10.1186/s13578-015-0009-y

Lucas, K. J., Roy, S., Ha, J., Gervaise, A. L., Kokoza, V. A., and Raikhel, A. S. (2015a). MicroRNA-8 Targets the Wingless Signaling Pathway in the Female Mosquito Fat Body to Regulate Reproductive Processes. *Proc. Natl. Acad. Sci. U. S. A.* 112, 1440–1445. doi: 10.1073/pnas.1424408112

Lucas, K. J., Zhao, B., Roy, S., Gervaise, A. L., and Raikhel, A. S. (2015b). Mosquito-Specific microRNA-1890 Targets the Juvenile Hormone-Regulated Serine Protease JHA15 in the Female Mosquito Gut. *RNA Biol.* 12, 1383–1390. doi: 10.1080/15476286.2015.1101525

Maharaj, P. D., Widen, S. G., Huang, J., Wood, T. G., and Thangamani, S. (2015). Discovery of Mosquito Saliva microRNAs During CHIKV Infection. *PloS Negl. Trop. Dis.* 9, e0003386. doi: 10.1371/journal.pntd.0003386

Ma, K., Li, X., Hu, H., Zhou, D., Sun, Y., Ma, L., et al. (2017). Pyrethroid-Resistance Is Modulated by miR-92a by Targeting CpCPR4 in *Culex Pipiens* Pallens. *Comp. Biochem. Physiol. Part B Biochem. Mol. Biol.* 203, 20–24. doi: 10.1016/j.cbpb.2016.09.002

ayoral, J. G., Etebari, K., Hussain, M., Khromykh, A. A., and Asgari, S. (2014). *Wolbachia* Infection Modifies the Profile, Shuttling and Structure of microRNAs in a Mosquito Cell Line. *PloS One* 9, e96107. doi: 10.1371/journal.pone.0096107

Mead, E. A., and Tu, Z. (2008). Cloning, Characterization, and Expression of microRNAs From the Asian Malaria Mosquito, Anopheles Stephensi. *BMC Genomics* 9, 244. doi: 10.1186/1471-2164-9-244

Meuti, M. E., Bautista-Jimenez, R., and Reynolds, J. A. (2018). Evidence That microRNAs Are Part of the Molecular Toolkit Regulating Adult Reproductive Diapause in the Mosquito, Culex Pipiens. *PloS One* 13, e0203015. doi: 10.1371/journal.pone.0203015

Miesen, P., Ivens, A., Buck, A. H., and van Rij, R. P. (2016). Small RNA Profiling in Dengue Virus 2-Infected *Aedes* Mosquito Cells Reveals Viral piRNAs and Novel Host Mirnas. *PloS Negl. Trop. Dis.* 10, e0004452. doi: 10.1371/journal.pntd.0004452

Mishra, S., Yadav, T., and Rani, V. (2016). Exploring miRNA Based Approaches in Cancer Diagnostics and Therapeutics. *Crit. Rev. Oncol. Hematol.* 98, 12–23. doi: 10.1016/j.critrevonc.2015.10.003

Nouzova, M., Etebari, K., Noriega, F. G., and Asgari, S. (2018). A Comparative Analysis of Corpora Allata-Corpora Cardiaca microRNA Repertoires Revealed Significant Changes During Mosquito Metamorphosis. *Insect Biochem. Mol. Biol.* 96, 10–18. doi: 10.1016/j.ibmb.2018.03.007

Osei-Amo, S., Hussain, M., O'Neill, S. L., and Asgari, S. (2012). *Wolbachia*-Induced aae-miR-12 miRNA Negatively Regulates the Expression of MCT1 and MCM6 Genes in *Wolbachia*-infected Mosquito Cell Line. *PloS One* 7, e50049. doi: 10.1371/journal.pone.0050049

Puthiyakunnon, S., Yao, Y., Li, Y., Gu, J., Peng, H., and Chen, X. (2013). Functional Characterization of Three MicroRNAs of the Asian Tiger Mosquito, Aedes Albopictus. *Parasites Vectors* 6, 230. doi: 10.1186/1756-3305-6-230

Qu, Z., Bendena, W. G., Nong, W., Siggens, K. W., Noriega, F. G., Kai, Z. P., et al. (2017). MicroRNAs Regulate the Sesquiterpenoid Hormonal Pathway in Drosophila and Other Arthropods. *Proc. Biol. Sci.* 284, 1869. doi: 10.1098/rspb.2017.1827

Saldana, M. A., Etebari, K., Hart, C. E., Widen, S. G., Wood, T. G., Thangamani, S., et al. (2017). Zika Virus Alters the microRNA Expression Profile and Elicits an RNAi Response in *Aedes Aegypti* Mosquitoes. *PloS Negl. Trop. Dis.* 11, e0005760. doi: 10.1371/journal.pntd.0005760

Shrinet, J., Jain, S., Jain, J., Bhatnagar, R. K., and Sunil, S. (2014). Next Generation Sequencing Reveals Regulation of Distinct *Aedes* microRNAs During Chikungunya Virus Development. *PloS Negl. Trop. Dis.* 8, e2616. doi: 10.1371/journal.pntd.0002616

Skalsky, R. L., Vanlandingham, D. L., Scholle, F., Higgs, S., and Cullen, B. R. (2010). Identification of microRNAs Expressed in Two Mosquito Vectors, *Aedes Albopictus* and Culex Quinquefasciatus. *BMC Genomics* 11, 119. doi: 10.1186/1471-2164-11-119

Slonchak, A., Hussain, M., Torres, S., Asgari, S., and Khromykh, A. A. (2014). Expression of Mosquito Microrna Aae-miR-2940-5p Is Downregulated in Response to West Nile Virus Infection to Restrict Viral Replication. *J. Virol.* 88, 8457–8467. doi: 10.1128/JVI.00317-14

Slonchak, A., Shannon, R. P., Pali, G., and Khromykh, A. A. (2015). Human MicroRNA Mir-532-5p Exhibits Antiviral Activity Against West Nile Virus *Via* Suppression of Host Genes SESTD1 and TAB3 Required for Virus Replication. *J. Virol.* 90, 2388–2402. doi: 10.1128/JVI.02608-15

Smith, J. L., Jeng, S., McWeeney, S. K., and Hirsch, A. J. (2017). A MicroRNA Screen Identifies the Wnt Signaling Pathway as a Regulator of the Interferon Response During Flavivirus Infection. *J. Virol.* 91, 8. doi: 10.1128/JVI.02388-16

Su, J., Li, C., Zhang, Y., Yan, T., Zhu, X., Zhao, M., et al. (2017). Identification of microRNAs Expressed in the Midgut of *Aedes Albopictus* During Dengue Infection. *Parasites Vectors* 10, 63. doi: 10.1186/s13071-017-1966-2

Su, J., Wang, G., Li, C., Xing, D., Yan, T., Zhu, X., et al. (2019). Screening for Differentially Expressed miRNAs in *Aedes Albopictus* (Diptera: Culicidae) Exposed to DENV-2 and Their Effect on Replication of DENV-2 in C6/36 Cells. *Parasites Vectors* 12, 44. doi: 10.1186/s13071-018-3261-2

Tsetsarkin, K. A., Liu, G., Kenney, H., Bustos-Arriaga, J., Hanson, C. T., Whitehead, S. S., et al. (2015). Dual miRNA Targeting Restricts Host Range

and Attenuates Neurovirulence of Flaviviruses. *PloS Pathog.* 11, e1004852. doi: 10.1371/journal.ppat.1004852

Tsetsarkin, K. A., Liu, G., Kenney, H., Hermance, M., Thangamani, S., and Pletnev, A. G. (2016a). Concurrent micro-RNA Mediated Silencing of Tick-Borne Flavivirus Replication in Tick Vector and in the Brain of Vertebrate Host. *Sci. Rep.* 6, 33088. doi: 10.1038/srep33088

Tsetsarkin, K. A., Liu, G., Shen, K., and Pletnev, A. G. (2016b). Kissing-Loop Interaction Between 5' and 3' Ends of Tick-Borne Langat Virus Genome 'Bridges the Gap' Between Mosquito- and Tick-Borne Flaviviruses in Mechanisms of Viral RNA Cyclization: Applications for Virus Attenuation and Vaccine Development. *Nucleic Acids Res.* 44, 3330–3350. doi: 10.1093/nar/gkw061

Wang, X., Zhang, J., Li, F., Gu, J., He, T., Zhang, X., et al. (2005). MicroRNA Identification Based on Sequence and Structure Alignment. *Bioinformatics* 21, 3610–3614. doi: 10.1093/bioinformatics/bti562

World Health Organization (2012). *Global strategy for dengue prevention and control 2012-2020*. WHO. Available at: https://apps.who.int/iris/handle/10665/75303.

Winter, F., Edaye, S., Huttenhofer, A., and Brunel, C. (2007). *Anopheles Gambiae* miRNAs as Actors of Defence Reaction Against *Plasmodium* Invasion. *Nucleic Acids Res.* 35, 6953–6962. doi: 10.1093/nar/gkm686

Wu, Z., Xue, Y., Wang, B., Du, J., and Jin, Q. (2011). Broad-Spectrum Antiviral Activity of RNA Interference Against Four Genotypes of Japanese Encephalitis Virus Based on Single microRNA Polycistrons. *PloS One* 6, e26304. doi: 10.1371/journal.pone.0026304

Xie, P. W., Xie, Y., Zhang, X. J., Huang, H., He, L. N., Wang, X. J., et al. (2013). Inhibition of Dengue Virus 2 Replication by Artificial Micrornas Targeting the Conserved Regions. *Nucleic Acid Ther.* 23, 244–252. doi: 10.1089/nat.2012.0405

Xing, S., Du, J., Gao, S., Tian, Z., Zheng, Y., Liu, G., et al. (2016). Analysis of the miRNA Expression Profile in an *Aedes Albopictus* Cell Line in Response to Bluetongue Virus Infection. *Infection Genet. Evolution: J. Mol. Epidemiol. Evolutionary Genet. Infect. Dis.* 39, 74–84. doi: 10.1016/j.meegid.2016.01.012

Xu, T., Zhong, D., Tang, L., Chang, X., Fu, F., Yan, G., et al. (2014). *Anopheles Sinensis* Mosquito Insecticide Resistance: Comparison of Three Mosquito Sample Collection and Preparation Methods and Mosquito Age in Resistance Measurements. *Parasites Vectors* 7, 54. doi: 10.1186/1756-3305-7-54

Yang, S., Pei, Y., Li, X., Zhao, S., Zhu, M., and Zhao, A. (2016). miR-124 Attenuates Japanese Encephalitis Virus Replication by Targeting DNM2. *Virol. J.* 13, 105. doi: 10.1186/s12985-016-0562-y

Yan, H., Zhou, Y., Liu, Y., Deng, Y., and Chen, X. (2014). miR-252 of the Asian Tiger Mosquito *Aedes Albopictus* Regulates Dengue Virus Replication by Suppressing the Expression of the Dengue Virus Envelope Protein. *J. Med. Virol.* 86, 1428–1436. doi: 10.1002/jmv.23815

Yekta, S., Shih, I. H., and Bartel, D. P. (2004). MicroRNA-directed Cleavage of HOXB8 Mrna. *Science* 304, 594–596. doi: 10.1126/science.1097434

Yen, P. S., Chen, C. H., Sreenu, V., Kohl, A., and Failloux, A. B. (2019). Assessing the Potential Interactions Between Cellular miRNA and Arboviral Genomic RNA in the Yellow Fever Mosquito, *Aedes Aegypti*. *Viruses* 11, 6. doi: 10.3390/v11060540

Yen, P. S., James, A., Li, J. C., Chen, C. H., and Failloux, A. B. (2018). Synthetic miRNAs Induce Dual Arboviral-Resistance Phenotypes in the Vector Mosquito Aedes Aegypti. *Commun. Biol.* 1, 11. doi: 10.1038/s42003-017-0011-5

Yen, L. C., Lin, Y. L., Sung, H. H., Liao, J. T., Tsao, C. H., Su, C. M., et al. (2013). Neurovirulent Flavivirus Can be Attenuated in Mice by Incorporation of Neuron-Specific microRNA Recognition Elements Into Viral Genome. *Vaccine* 31, 5915–5922. doi: 10.1016/j.vaccine.2011.09.102

Zhang, X., Aksoy, E., Girke, T., Raikhel, A. S., and Karginov, F. V. (2017). Transcriptome-Wide microRNA and Target Dynamics in the Fat Body During the Gonadotrophic Cycle of *Aedes Aegypti*. *Proc. Natl. Acad. Sci. U. S. A.* 114, E1895–E1903. doi: 10.1073/pnas.1701474114

Zhang, G., Hussain, M., and Asgari, S. (2014). Regulation of Arginine Methyltransferase 3 by a *Wolbachia*-Induced microRNA in *Aedes Aegypti* and Its Effect on *Wolbachia* and Dengue Virus Replication. *Insect Biochem. Mol. Biol.* 53, 81–88. doi: 10.1016/j.ibmb.2014.08.003

Zhang, G., Hussain, M., O'Neill, S. L., and Asgari, S. (2013). *Wolbachia* Uses a Host microRNA to Regulate Transcripts of a Methyltransferase, Contributing to Dengue Virus Inhibition in *Aedes Aegypti*. *Proc. Natl. Acad. Sci. U. S. A.* 110, 10276–10281. doi: 10.1073/pnas.1303603110

Zhang, Y., Zhao, B., Roy, S., Saha, T. T., Kokoza, V. A., Li, M., et al. (2016). microRNA-309 Targets the Homeobox Gene SIX4 and Controls Ovarian Development in the Mosquito *Aedes Aegypti*. *Proc. Natl. Acad. Sci. U. S. A.* 113, E4828–E4836. doi: 10.1073/pnas.1609792113

Zhou, Y., Liu, Y., Yan, H., Li, Y., Zhang, H., Xu, J., et al. (2014). miR-281, an Abundant Midgut-Specific miRNA of the Vector Mosquito *Aedes Albopictus* Enhances Dengue Virus Replication. *Parasites Vectors* 7, 488. doi: 10.1186/s13071-014-0488-4

Conflict of Interest: The authors declare that the research was conducted in the absence of any commercial or financial relationships that could be construed as a potential conflict of interest.

frontiers in Cellular and Infection Microbiology

OPINION
published: 29 June 2021
doi: 10.3389/fcimb.2021.650277

Friend, Not Foe: Unveiling Vector-Bacteria Symbiosis and Its Utility as an Arboviral Intervention Strategy in the Philippines

Shaira Limson Kee[1†] *and Myles Joshua Toledo Tan*[1,2*†]

[1] *Department of Natural Sciences, University of St. La Salle, Bacolod, Philippines,* [2] *Department of Chemical Engineering, University of St. La Salle, Bacolod, Philippines*

Keywords: vector-borne disease control, dengue, Philippines, Wolbachia, symbiosis, arbovirus, mosquito, biocontrol

Edited by:
Khalid B. Beshir, London School of Hygiene and Tropical Medicine, United Kingdom

Reviewed by:
Robert P. Hirt, Newcastle University, United Kingdom

****Correspondence:***
Myles Joshua Toledo Tan
mj.tan@usls.edu.ph

[†]These authors have contributed equally to this work and share first authorship

Specialty section:
This article was submitted to Parasite and Host, a section of the journal Frontiers in Cellular and Infection Microbiology

Received: *06 January 2021*
Accepted: *14 June 2021*
Published: *29 June 2021*

Citation:
Kee SL and Tan MJT (2021) Friend, Not Foe: Unveiling Vector-Bacteria Symbiosis and Its Utility as an Arboviral Intervention Strategy in the Philippines. Front. Cell. Infect. Microbiol. 11:650277. doi: 10.3389/fcimb.2021.650277

INTRODUCTION

Humans have long studied the ecological symbiosis of organisms primarily from an anthropocentric perspective. Among these investigations are the symbiosis of bacteria and arthropods. Studies conducted in relation to this usually lean toward subjects of pathogen transmission, cure, and prevention. However, Bourtzis and Zchori-Fein, editors of *Manipulative Tenants: Bacteria Associated with Arthropods*, discuss the diversity of the symbiosis that occurs between bacteria and arthropods. They also explain that despite common negative associations between them, microbial interaction with its vector can also benefit eukaryotic organisms, including humans. In fact, some symbiotic relationships that involve bacteria are essential to the survival of arthropods. One major benefit that this relationship offers to increase the survival of humans is its purpose as a biocontrol strategy aimed toward minimizing arboviruses. This presents a significant benefit as the alarming trend of insecticide-resistant mosquitoes intensifies due to gradual adaptation to conventional control measures (Brathwaite Dick et al., 2012; Marcombe et al., 2012). Further research into symbiosis will greatly benefit countries like the Philippines whose commonly applied intervention strategy for dengue involves the use of insecticides and manual elimination of mosquito breeding sites.

FUNCTIONAL SYMBIOSIS

Symbiosis, as defined by Heinrich Anton de Bary (1878), is the living together of organisms originating from separate species (Oulhen et al., 2016). It occurs in multivariate forms and can be either endosymbiotic, like between *Pseudotrichonympha* spp. in the gut of subterranean termites and the nitrogen-fixing endosymbiont *Azobacteroides pseudotrichonymphae*, or ectosymbiotic, like between *Devescovina* spp. in the gut of dry-wood termites and the nitrogen-fixing cell surface-attached ectosymbiont *Armantifilum devescovinae* (Strassert et al., 2010; Desai and Brune, 2012). Symbionts, whether primary or secondary, play different roles in the lives of their hosts, some of which supplement metabolic functions, determine alterations, manipulate host reproduction and

protect against pathogens (Zchori-Fein and Bourtzis, 2012). These aid in increasing an organism's fitness and enable adaptive radiation to further increase its ecological niche. This is the reason why mammalian systems are more complex, and why microbial diversity is greater among mammals of the same species than among insects of the same species. However, greater diversity can be observed among different insect species than among different mammal species. This is observed to be a consequence of the greater variations found in the diet and gut physiology of insects when compared with those of mammals (Douglas, 2011). The co-existence of these organisms have been apparent in nature for a long time. As a consequence of this long history of association, a dependency on the relationship has been established in many instances such that deprivation of the symbiont results in the inability of the organism to grow and reproduce (Douglas, 2007).

IMPLICATIONS OF TRANSMISSION

The functions provided by bacteria to their hosts vary among species. This diversity among microbes was thought to arise from differences in lineage, but due to recent developments, it was discovered that these differences may not be as large as initially hypothesized. Particular genera of bacteria are constantly found in hosts that are distantly related (Zchori-Fein and Bourtzis, 2012). These are potentially effects of different bacterial transmissions that occur either vertically or horizontally. Vertical transmission involves parent-to-offspring exchange of microbes due to their presence in the reproductive organs of the host (Ricci et al., 2012). On the other hand, horizontal transmission, which occurs between individuals of different species, offers a topic of interest. This cross-colonizing capability of selected bacteria among different species can be witnessed in *Spiroplasma, Arsenophonus, Asaia* and *Wolbachia* groups (Fukatsu et al., 2001; Gómez-Valero et al., 2004; Marzorati et al., 2006; Wille and Hartman, 2009). These resilient individuals have been found to have evolved mechanisms that allow them to colonize and survive different immune systems. In fact, several studies have shown a comparison of vector competence of both aseptic (absence of endogenous bacterial flora) and septic mosquitoes. The results indicated that gut microbes can potentially reduce *Plasmodium* infection among mosquitoes and that aseptic mosquitoes have an increased susceptibility (Pumpuni et al., 1996; Gonzalez-Ceron et al., 2003; Dong et al., 2009). Along with that, the absence of *Wigglesworthia*, which is an obligate symbiont of flies, was also observed to have resulted in an increased susceptibility to parasitic infections (Pais et al., 2008). With that, microbiota can either directly or indirectly affect the vectorial competence of their hosts through interactions with parasites either by inhibitory bioactivity functions of their secretions, or by host immune system stimulation that signals the clearing of pathogenic microbes, respectively (Weiss and Aksoy, 2011; Ricci et al., 2012). Aside from this, zoonotic diseases are also influenced by changes in topography, deforestation, and agricultural land conversion. These anthropogenic changes that are commonly witnessed in the Philippines are key drivers for the proliferation of mosquitoes and their associated pathogens (Walsh et al., 1993; Guerra et al., 2006; Yasuoka and Levins, 2007; Jones et al., 2008; Olson et al., 2010; Fornace et al., 2016). An essential note to focus on is that they offer interesting implications in understanding the response of the body's immune system during host invasion. Further research will help us understand vector-borne pathogens better.

BIOCONTROL STRATEGY AGAINST ARBOVIRUSES

In the public view, increased arthropod fitness and resilience to different internal systems due to microbial symbiosis does not offer a positive subject because arthropods, primarily mosquitoes, are known as harborers of pathogens. However, this can, in fact, be a useful solution to humanity's alarming arboviral issues through the use of biocontrol strategies. Abundant research on reproductive parasites over the past 25 years have been centered on Wolbachia, an intracellular bacterium that is dependent on the cytoplasmic environment of its host (Zchori-Fein and Bourtzis, 2012). With that, Wolbachia was discovered to induce cytoplasmic incompatibility in their infected hosts. This biological process alters the reproductive functions of the host by inducing high embryonic mortality, thereby decreasing the number of viable offspring (Hoffmann et al., 1986; Vavre et al., 2000; Tram and Sullivan, 2002; Bordenstein and Werren, 2007). Research on bacterial symbionts is not solely concentrated on Wolbachia. In fact, *Pantoea agglomerans* is a bacterial symbiont of the *Anopheles* mosquito that was transformed to express anti-*Plasmodium* activity through effector proteins pelB or hlyA. Aside from this, symbiont bacteria *Rhodococcus rhodnii*, *Asaia* and *Pantoea* are also potentially effective for symbiotic control strategies (Ricci et al., 2012). Years of research and field experimentation have proven that bacteria have the ability to restrict arbovirus transmission. This serves as a promising intervention to reduce the incidence of vector-borne diseases (Sinkins, 2004; Kambris et al., 2009; McMeniman et al., 2009; Moreira et al., 2009). This can benefit countries like the Philippines (~400,000 reported cases in 2019 according to the World Health Organization) that suffer frequent dengue outbreaks. Another interesting fact is that through application of highly sensitive polymerase chain reaction (PCR) methods accompanied by DNA hybridization and sequence analysis techniques, it was revealed that Wolbachia infection is evident in up to 76% of all arthropod species (Jeyaprakash and Hoy, 2000). This means that it is common worldwide. Its widespread population emphasizes the adaptability of these microorganisms. In fact, this extensive distribution could be attributed to the evolutionary success induced by the symbiotic relationships between mosquitoes and several microorganisms (Ricci et al., 2012). This versatility can be manipulated to benefit future intervention strategies. To add, this prevalence in nature means that it can be applied anywhere around the globe as it is

not climatically restricted. Taking these factors into consideration, increasing the limited research on Wolbachia in the Philippines and integrating it into the national intervention strategy will likely produce better results than current approaches.

DISCUSSION

The wide array of symbiotic relationships displayed by arthropods and their symbionts are evidence that these associations are relatively ubiquitous and ever-evolving in nature. For instance, organisms involved in parasitism are observable in all major clades of eukaryotes. Moreover, these parasites were found to share a common ancestry with their free-living relatives. This suggests that convergence through occupying similar environmental niches and reductive evolution played a huge part in their evolution (Walochnik and Duchêne, 2016). With that, humans can utilize this interdependence and interrelatedness of organisms to innovate new forms of symbiosis, and thereby, tackle existing health issues such as arboviral diseases without resorting to eradicative measures. Just like how bacteria thrive by exchanging nutrients that are inadequately represented in the diet of their eukaryotic partners, humans can participate in this type of symbiosis, as well. By aiding these Wolbachia-infected mosquitoes, they can infect other vectors through horizontal and vertical transmissions and thereby increase their population (Laven, 1967; Zabalou et al., 2004; McMeniman et al., 2009). This can lead to greater chances of preventing the transmission of arboviral diseases (e.g. dengue, Chikungunya, Zika), and malaria, that have been proven to be inhibited by Wolbachia infection of their vectors (Moreira et al., 2009; Caragata et al., 2016).

Further knowledge on these topics opens the less ventured idea that pathogenic infections are not the sole relationship that humans share with arthropods and that mutualistic associations are also prevalent. This is not a particularly new idea since human symbiocosm has existed for many years. A good example would be bacterial species more commonly classified as "good bacteria" that live permanently through commensal or mutualistic interactions with human hosts, especially in the digestive tract. The fact that these organisms are necessary enough to have aided in the continuation of the existence of some arthropods for more than 275 million years is a point to ponder. Perhaps we, humans, may benefit from this symbiosis for our own survival. *Manipulative Tenants: Bacteria Associated with Arthropods*, along with its findings from years of research and the increasing success of field experimentation in this area, is solid proof that an efficient action plan that would utilize Wolbachia as an intervention strategy against arboviruses, particularly dengue, must be applied and disseminated throughout the Philippines in order to mitigate the concurrent issues, if not eradicate them once and for all.

AUTHOR CONTRIBUTIONS

Conceived the work: MT. Drafted the article: SK. Critically revised the manuscript: MT. All authors contributed to the article and approved the submitted version.

REFERENCES

Bordenstein, S. R., and Werren, J. H. (2007). Bidirectional Incompatibility Among Divergent Wolbachia And Incompatibility Level Differences Among Closely Related Wolbachia In Nasonia. *Heredity* 99 (3), 278–287. doi: 10.1038/sj.hdy.6800994

Brathwaite Dick, O., San Martín, J. L., Montoya, R. H., del Diego, J., Zambrano, B., and Dayan, G. H. (2012). The History of Dengue Outbreaks In The Americas. *Am. J. Trop. Med. Hyg.* 87 (4), 584–593. doi: 10.4269/ajtmh.2012.11-0770

Caragata, E., Dutra, H., and Moreira, L. (2016). Inhibition of Zika Virus by Wolbachia in Aedes Aegypti. *Microb. Cell* 3 (7), 293–295. doi: 10.15698/mic2016.07.513

Desai, M. S., and Brune, A. (2012). Bacteroidales Ectosymbionts of Gut Flagellates Shape the Nitrogen-Fixing Community in Dry-Wood Termites. *ISME J.* 6 (7), 1302–1313. doi: 10.1038/ismej.2011.194

Dong, Y., Manfredini, F., and Dand Dimopoulos, G. (2009). Implication of the Mosquito Midgut Microbiota in the Defense Against Malaria Parasites. *PloS Pathog.* 5 (5), e1000423. doi: 10.1371/journal.ppat.1000423

Douglas, A. E. (2007). Symbiotic Microorganisms: Untapped Resources for Insect Pest Control. *Trends Biotechnol.* 25 (8), 338–342. doi: 10.1016/j.tibtech.2007.06.003

Douglas, A. E. (2011). Lessons From Studying Insect Symbioses. *Cell Host Microbe* 10 (4), 359–367. doi: 10.1016/j.chom.2011.09.001

Fornace, K. M., Abidin, T. R., Alexander, N., Brock, P., Grigg, M. J., Murphy, A., et al. (2016). Association Between Landscape Factors And Spatial Patterns Ofplasmodium Knowlesiinfections In Sabah, Malaysia. *Emerg. Infect. Dis.* 22 (2), 201–2095. doi: 10.3201/eid2202.150656

Fukatsu, T., Tsuchida, T., Nicoh, N., and Koga, R. (2001). Spiroplasma Symbiont of the Pea Aphid Acyrthosiphon Pisum (Insecta: Homoptera). *Appl. Environ. Microbiol.* 67 (3), 1284–1291. doi: 10.1128/aem.67.3.1284-1291.2001

Gómez-Valero, L., Soriano-Navarro, M., Pérez-Brocal, V., Heddi, A., Moya, A., GarciaVerdugo, J. M., et al. (2004). Coexistence of Wolbachia With Buchnera Aphidicola And A Secondary Symbiont In The Aphid Cinara Cedri. *J. Bacteriol.* 186 (19), 6626–66335. doi: 10.1128/jb.186.19.6626-6633.2004

Gonzalez-Ceron, L., Santillan, F., Rodriguez, M. H., Mendez, D., and Hernandez-Avila, J. E. (2003). Bacteria in Midguts of Field-Collected Anopheles Albimanus Block Plasmodium Vivax Sporogonic Development. *J. Med. Entomol.* 40 (3), 371–374. doi: 10.1603/0022-2585-40.3.371

Guerra, C. A., Snow, R. W., and Hay, S. I. (2006). A Global Assessment of Closed Forests, Deforestation And Malaria Risk. *Ann. Trop. Med. Parasitol.* 100 (3), 189–204. doi: 10.1179/136485906x91512

Hoffmann, A. A., Turelli, M., and Simmons, G. M. (1986). Unidirectional Incompatibility Between Populations of Drosophila Simulans. *Evolution* 40 (4), 692. doi: 10.2307/2408456

Jeyaprakash, A., and Hoy, M. A. (2000). Long PCR Improves Wolbachia DNA Amplification: Wsp Sequences Found In 76% of Sixty-Three Arthropod Species. *Insect Mol. Biol.* 9 (4), 393–405. doi: 10.1046/j.1365-2583.2000.00203.x

Jones, K. E., Patel, N. G., Levy, M. A., Storeygard, A., Balk, D., Gittleman, J. L., et al. (2008). Global Trends in Emerging Infectious Diseases. *Nature* 451 (7181), 990–993. doi: 10.1038/nature06536

Kambris, Z., Cook, P. E., Phuc, H. K., and Sinkins, S. P. (2009). Immune Activation by Life-Shortening Wolbachia and Reduced Filarial Competence in Mosquitoes. *Science* 326 (5949), 134–136. doi: 10.1126/science.1177531

Laven, H. (1967). "Speciation and Evolution in Culex Pipiens," in *Genetics of Insect Vectors of Disease*. Eds. J. W. Wright and R. Pal (Amsterdam: Elsevier), 251–275.

Marcombe, S., Mathieu, R. B., Pocquet, N., Riaz, M.-A., Poupardin, R., Sélior, S., et al. (2012). Insecticide Resistance in the Dengue Vector Aedes Aegypti From Martinique : Distribution, Mechanisms and Relations With Environmental Factors. *PloS One* 7 (2), e30989. doi: 10.1371/journal.pone.0030989

Marzorati, M., Alma, A., Sacchi, L., Pajoro, M., Palermo, S., Brusetti, L., et al. (2006). A Novel Bacteroidetes Symbiont Is Localized in Scaphoideus Titanus, the Insect Vector of Flavescence Dorée in Vitis Vinifera. *Appl. Environ. Microbiol.* 72 (2), 1467–1475. doi: 10.1128/aem.72.2.1467-1475.2006

McMeniman, C. J., Lane, R. V., Cass, B. N., Fong, A. W. C., Sidhu, M., Wang, Y. F., et al. (2009). Stable Introduction of a Life-Shortening Wolbachia Infection Into the Mosquito Aedes Aegypti. *Science* 323 (5910), 141–144. doi: 10.1126/science.1165326

Moreira, L. A., Iturbe-Ormaetxe, I., Jeffery, J. A., Lu, G., Pyke, T., Hedges, L. M., et al. (2009). A Wolbachia Symbiont in Aedes Aegypti Limits Infection With Dengue, Chikungunya, and Plasmodium. *Cell* 139 (7), 1268–1278. doi: 10.1016/j.cell.2009.11.042

Olson, S. H., Gangnon, R., Silveira, G. A., and Patz, J. A. (2010). Deforestation and Malaria in Mâncio Lima County, Brazil. *Emerg. Infect. Dis.* 16 (7), 1108–1115. doi: 10.3201/eid1607.091785

Oulhen, N., Schulz, B. J., and Carrier, T. J. (2016). English Translation of Heinrich Anton De Bary's 1878 Speech, 'Die Erscheinung Der Symbiose' ('De La Symbiose'). *Symbiosis* 69 (3), 131–139. doi: 10.1007/s13199-016-0409-8

Pais, R., Lohs, C., and Wu, Y. (2008). The Obligate Mutualist Wigglesworthia Glossinidia Influences Reproduction, Digestion, and Immunity Processes of its Host, the Tsetse Fly. *Appl. Environ. Microbiol.* 74 (19), 5965–5974. doi: 10.1128/AEM.00741-08

Pumpuni, C. B., Demaio, J., Kent, M., Davis, J. R., and Beier, J. C. (1996). Bacterial Population Dynamics in Three Anopheline Species: The Impact on Plasmodium Sporogonic Development. *Am. J. Trop. Med. Hyg.* 54 (2), 214–218. doi: 10.4269/ajtmh.1996.54.214

Ricci, I., Damiani, C., Capone, A., DeFreece, C., Rossi, P., and Favia, G. (2012). Mosquito/microbiota Interactions: From Complex Relationships to Biotechnological Perspectives. *Curr. Opin. Microbiol.* 15 (3), 278–284. doi: 10.1016/j.mib.2012.03.004

Sinkins, S. P. (2004). Wolbachia and Cytoplasmic Incompatibility in Mosquitoes. *Insect Biochem. Mol. Biol.* 34 (7), 723–729. doi: 10.1016/j.ibmb.2004.03.025

Strassert, J. F. H., Desai, M. S., Radek, R., and Brune, A. (2010). Identification and Localization of the Multiple Bacterial Symbionts of the Termite Gut Flagellate Joenia Annectens. *Microbiology* 156 (7), 2068–2079. doi: 10.1099/mic.0.037267-0

Tram, U., and Sullivan, W. (2002). Role of Delayed Nuclear Envelope Breakdown and Mitosis in Wolbachia-Induced Cytoplasmic Incompatibility. *Science* 296 (5570), 1124–1126. doi: 10.1126/science.1070536

Vavre, F., Fleury, F., Varaldi, J., Fouillet, P., and Boulétreau, M. (2000). Evidence for Female Mortality in Wolbachia-Mediated Cytoplasmic Incompatibility in Haplodiploid Insects, Epidemiologic and Evolutionary Consequences. *Evolution* 54 (1), 191. doi: 10.1554/0014-3820(2000)054[0191:effmiw]2.0.co;2

Walochnik, J., and Duchêne, M. (2016). *Molecular Parasitology: Protozoan Parasites and Their Molecules* (Berlin, Germany: Springer).

Walsh, J. F., Molyneux, D. H., and Birley, M. H. (1993). Deforestation: Effects on Vector-Borne Disease. *Parasitology* 106 (S1), S55–S75. doi: 10.1017/s0031182000086121

Weiss, B., and Aksoy, S. (2011). Microbiome Influences on Insect Host Vector Competence. *Trends Parasitol.* 27 (11), 514–522. doi: 10.1016/j.pt.2011.05.001

Wille, B. D., and Hartman, G. L. (2009). Two Species of Symbiotic Bacteria Present in the Soybean Aphid (Hemiptera: Aphididae). *Environ. Entomol.* 38 (1), 110–1155. doi: 10.1603/022.038.0113

Yasuoka, J., and Levins, R. (2007). Impact of Deforestation and Agricultural Development on Anopheline Ecology and Malaria Epidemiology. *Am. J. Trop. Med. Hyg.* 76 (3), 450–460. doi: 10.4269/ajtmh.2007.76.450

Zabalou, S., Riegler, M., Theodorakopoulou, M., Stauffer, C., Savakis, C., and Bourtzis, K. (2004). Wolbachia-Induced Cytoplasmic Incompatibility as a Means for Insect Pest Population Control. *Proc. Natl. Acad. Sci.* 101 (42), 15042–15045. doi: 10.1073/pnas.0403853101

Zchori-Fein, E., and Bourtzis, K. (2012). *Manipulative Tenants: Bacteria Associated With Arthropods* (Boca Raton, FL: CRC Press).

Conflict of Interest: The authors declare that the research was conducted in the absence of any commercial or financial relationships that could be construed as a potential conflict of interest.

frontiers in Cellular and Infection Microbiology

ORIGINAL RESEARCH
published: 29 June 2021
doi: 10.3389/fcimb.2021.702081

Knockdown Resistance (*kdr*) Mutations I1532T and F1534S Were Identified in *Aedes albopictus* Field Populations in Zhejiang Province, Central China

Yuyan Wu[1†], Qinmei Liu[1†], Yunpeng Qi[2], Yinping Wu[3], Qinxiang Ni[4], Weihua Chen[5], Jinna Wang[1], Tianqi Li[1], Mingyu Luo[1], Juan Hou[1], Zhenyu Gong[1*] and Jimin Sun[1*]*

[1] Department of Infectious Diseases Control and Prevention, Zhejiang Provincial Center for Disease Control and Prevention, Hangzhou City, China, [2] Department of Infectious Diseases Control and Prevention, Jiaxing Center for Disease Control and Prevention, Jiaxing City, China, [3] Department of Vector Control and Prevention, Yiwu Center for Disease Control and Prevention, Yiwu City, China, [4] Department of Infectious Diseases Control and Prevention, Wenzhou Center for Disease Control and Prevention, Wenzhou City, China, [5] Department of Infectious Diseases Control and Prevention, Quzhou Center for Disease Control and Prevention, Quzhou City, China

Aedes albopictus is the only vector that can transmit the dengue virus in Zhejiang Province, central China, and it can develop insecticide resistance due to long-term exposure to pyrethroids. The presence of knockdown resistance (*kdr*) mutations is one of the mechanisms responsible for pyrethroid resistance, and has been reported in some *Ae. albopictus* populations in southern China. However, little is known about the DNA diversity of the voltage-gated sodium channel (VGSC) gene in *Ae. albopictus* populations in central China. Four *Ae. albopictus* field populations were collected, in Yiwu (YW), Quzhou (QZ), Wenzhou (WZ), and Jiaxing (JX) from Zhejiang Province, central China. The susceptibility of *Ae. albopictus* adults to three pyrethroids (beta-cypermethrin, deltamethrin, and permethrin) was tested using the WHO tube assay, and *Kdr* mutations were identified *via* PCR and sequencing. The relationship between *kdr* mutations and pyrethroid phenotypes was also analyzed. Of the four populations, none was sensitive to any pyrethroid tested, and the YW population showed the strongest pyrethroid resistance. Non-synonymous *kdr* mutations were detected in codons 1532 and 1534, domain III. At codon 1534, one mutant allele, TCC(S), was detected in the four populations with a frequency of 42.08%, while at codon 1532, one mutant allele, ACC(T), was detected in the JX and QZ populations, with frequencies of 4.22 and 3.03%, respectively. The F1534S mutant allele was positively correlated with both beta-cypermethrin and deltamethrin resistance phenotypes (OR > 1, P < 0.05), whereas the I1532T mutant allele was possibly negatively correlated with beta-cypermethrin, deltamethrin, and permethrin resistance phenotypes (OR < 1, P > 0.05). In conclusion, resistance and resistance mutations regarding to three pyrethroids are already present in

OPEN ACCESS

Edited by:
Jun Feng, National Institute of Parasitic Diseases, China

Reviewed by:
Hongliang Chu, Jiangsu Provincial Center for Disease Control and Prevention, China
Leng Ben, Shanghai Municipal Center for Disease Control and Prevention (SCDC), China

***Correspondence:**
Juan Hou
jhou@cdc.zj.cn
Zhenyu Gong
gongzhenyu2020@163.com
Jimin Sun
jmsun@cdc.zj.cn

[†]These authors share first authorship

Specialty section:
This article was submitted to Parasite and Host, a section of the journal Frontiers in Cellular and Infection Microbiology

Received: *29 April 2021*
Accepted: *11 June 2021*
Published: *29 June 2021*

Citation:
Wu YY, Liu QM, Qi Y, Wu YP, Ni QX, Chen WH, Wang JN, Li TQ, Luo MY, Hou J, Gong ZY and Sun JM (2021) Knockdown Resistance (kdr) Mutations I1532T and F1534S Were Identified in Aedes albopictus Field Populations in Zhejiang Province, Central China. Front. Cell. Infect. Microbiol. 11:702081. doi: 10.3389/fcimb.2021.702081

the *Ae. Albopictus* populations from Zhejiang, central China, which prompts the need to use non-insecticide-based methods of insect control.

Keywords: *Aedes albopictus*, pyrethroid, insecticide resistance, *kdr*, Central China

INTRODUCTION

Ae. albopictus, also known as the Asian tiger mosquito, is widely distributed in southern and central China (Robertson and Hu, 1988). It is perhaps the most dangerous mosquito vector species in Zhejiang Province because of its high density and primary role in transmitting Zika, chikungunya, and dengue viruses (Robertson and Hu, 1988; Yang and Fu, 2006). In 2019, 924 cases of dengue fever were reported in Zhejiang Province, China, which was 3.90-fold higher than that in 2018 (237 cases). *Ae. albopictus* is the only vector species responsible for chikungunya and dengue fever in Zhejiang Province and its surrounding areas, which needs to be controlled (Guo et al., 2016).

Elimination of larval breeding sites and insecticide application are the two main means of controlling *Aedes* species. At present, the insecticides have been employed as the principal control procedure because of its excellent quick kill effect when *Aedes*-borne diseases spread (WHO, 2013; Wang and Jiang, 2016; Wang et al., 2017). As a consequence, insecticides such as pyrethroids have been widely used by both government campaigns and citizens. According to our previous research, the consumption of pyrethroids in Hangzhou City, Zhejiang Province is 5,566 kg per liter per year (unpublished data). The long-term and heavy utilization of pyrethroids has resulted in the resistance of many populations of *Ae. albopictus*, which poses a significant challenge for its control when it triggers an outbreak of dengue fever (Hou et al., 2017).

Behavioral resistance, target insensitivity, and metabolic detoxification are related to the mechanisms of *Ae.* resistance (Hemingway and Ranson, 2000). Target sensitivity has been widely studied in *Ae. aegypti* for several decades, although little is known about it in *Ae. albopictus* (Kushwah et al., 2015; Wuliandari et al., 2015; Smith et al., 2018). Since the first report of the F1534C mutant allele in *Ae. albopictus* populations in Singapore in 2011, the F1534S and F1534L mutations were then detected in *Ae. albopictus* in Haikou and Guangdong Province, China (Kasai et al., 2011; Wang et al., 2015; Chen et al., 2016; Xu et al., 2016; Li et al., 2018). A few years later, the I1532T mutant allele was identified in populations of *Ae. albopictus* in Shanghai, and a correlation was suspected between the I1532T mutation and pyrethroid resistance caused by the F1534S mutation (Gao et al., 2018). However, the vast majority of studies on *kdr* mutations in *Ae. albopictus* was concentrated in the southern tropics, while most of the *Ae. albopictus* can be found in the subtropical regions of China, where the status of *kdr* mutations remains unclear. Zhejiang Province, located on the east coast of central China, has a subtropical monsoon climate. Although resistance against pyrethroids has been detected for several years, few studies on *kdr* mutations have been conducted in *Ae. albopictus* populations in Zhejiang.

In the present study, we investigated the insecticide resistance of *Ae. albopictus* populations collected from the north, south, east, and west of Zhejiang Province to three pyrethroids (beta-cypermethrin, deltamethrin, and permethrin), and the corresponding *kdr* mutations in these four populations were examined. The aim was to explore the occurrence, frequency, and distribution of possible *kdr* mutations in *Ae. albopictus* in a subtropical climate in central China, and to explore the relationship between *kdr* mutations and pyrethroid resistance.

MATERIALS AND METHODS

Ethics Statement

No permit was required for this field study, because no endangered or protected species were involved, and mosquito collections at breeding sites were provided by the owners.

Mosquito Sampling

The field populations of *Ae. albopictus* were collected as larvae or pupae from four sites during the 2019 active mosquito season, in Yiwu (YW), Quzhou (QZ), Wenzhou (WZ), and Jiaxing (JX), in Zhejiang Province, China (**Figure 1**). Mosquito larvae were collected from their breeding sites, such as scrap tire dumps, flowerpot trays, plastic containers, and water tanks. All larvae were brought back to the Zhejiang Provincial Center for Disease Control and Prevention Laboratory and were reared in an incubator to adults under standard conditions at (26 ± 1)°C and 65 ± 5% relative humidity with a 14:10 light:darkness period. The F1 progeny adults were used for susceptibility testing.

Insecticide Susceptibility Bioassay

Non-blood-fed female mosquitoes, 3 to 5 days post-emergence, were tested for susceptibility to three pyrethroid insecticides using WHO tube assay. Test papers containing beta-cypermethrin (0.4%), deltamethrin (0.1%), and permethrin (3%) were used for the assays, which were provided by the National Institute for Communicable Disease Control and Prevention, Chinese Center for Disease Control and Prevention (China CDC) (Chen et al., 2016; Hou et al., 2020). Silicone oil-treated papers without insecticides were used as controls. Tests using each insecticide paper and control paper were repeated at least three times according to the tube test protocol recommended by the China CDC (National Health Commission of the People's Republic of China, 2016; Hou et al., 2020). After 1 h of exposure, the mosquitoes were transferred to its recovery tube and were maintained in an 8% sucrose solution for 24 h. After 24 h, the mosquitoes were considered alive if they could fly, while they were considered dead if they were knocked down moribund or

FIGURE 1 | Map of Zhejiang Province showing the *Ae. albopictus* collection sites.

motionless. The number of dead mosquitoes was counted to calculate the 24-h mortality, and to evaluate insecticide sensitivity. If the control group mortality was between 5 and 20%, the test group mortality would be corrected by Abbott's formula, as follows: Corrected mortality (%) = (test group mortality − control group mortality)/(1-control group mortality) × 100. If the mortality of the control group was ≥20%, the bioassay would be repeated (National Health Commission of the People's Republic of China, 2016). Resistance status was classified using corrected mortality according to the WHO recommendations (WHO, 2016). There are three categories according to the corrected 24-h mortality rate: susceptibility, if mortality was between 98 and 100%; probable resistance, if mortality was between 90 and 97%; and resistance, if mortality was <90% (WHO, 2016). All mosquitoes were collected and stored in a −80°C refrigerator for DNA analysis.

DNA Extraction and *kdr* Allele Detection

Genomic DNA was extracted from individual mosquitoes using the ALLPrepQiagen Nucleic Acid Kit (Qiagen, Germany). Extracted DNA was stored at −20°C until further analysis. To identify *kdr* alleles, partial sequences of domains II, III, and IV of the voltage-gated sodium channel (VGSC) gene, which are known targets of pyrethroid and Dichloro diphenyltrichloroe thane (DDT) insecticides, were amplified using the primers aegSCF3 (5'-GTGGAACTTCACCGACTTCA-3') and aeg SCR22 (5'-TTCACGAACTTGAGCGCGTTG-3'), aegSCF7 (5'-GAGAACTCGCCGATGAACTT-3') and albSCR9 (5'-CTG ATCCTCCGTCATGAACA), and albSCF6 (5'-TCGAGAAG TACTTCGTGTCG-3') and albSCR8 (5'-AACAGCAGGA TCATGCTCTG-3'), respectively (Chen et al., 2016; Gao et al., 2018). The PCR kit was purchased from Aidlab (China). PCR was carried out in Eppendorf AG 22331 Hamburg (Eppendorf, Germany). The cycling parameters used were adapted from the methods of Kasai and Yajun Ma, including one cycle of denaturation at 94°C for 2 min, followed by 35 cycles of amplification at 94°C for 30 s, 60°C for 30 s, and 72°C for 30 s, with a final extension at 72°C for 8 min (Kasai et al., 2011; Gao et al., 2018). After electrophoresis, the PCR products were purified and directly sequenced in both directions using the same set of primers (Gao et al., 2018). Sequences were analyzed

using DNASTAR Lasergene 12.0 software to determine the codons and the corresponding genotypes (Burland, 2000).

Statistical Analysis

The frequency of a particular allele was calculated for each population as the number of alleles/(sample size × 2). Chi-squared tests were used, and the odds ratio (OR) values with 95% confidence intervals (CI) were calculated using SPSS (version 23.0, Armonk, NY: IBM Corp, USA) (Deng et al., 2017) to examine the association between *kdr* alleles and the resistance phenotypes. In this study, the dependent variable was the mosquito status, which was either dead or alive at 24-h post bioassay. Dead mosquitoes were defined as having a susceptible phenotype while live mosquitoes were defined as having a resistant phenotype. If the OR > 1, the relationship between the *kdr* allele and resistant phenotype was considered as positive. If the OR < 1, the relationship between the *kdr* allele and resistant phenotype was considered as negative (Gao et al., 2018). $P < 0.05$ was considered statistically significant.

RESULTS

Insecticide Susceptibility Tests

None of the four field populations of *Ae. albopictus* showed sensitivity to the pyrethroids tested (**Figure 2**). The range of corrected mortality was between 65.15% (YW) and 91.38% (QZ) after exposure to beta-cypermethrin, 61.67% (YW) and 86.67% (WZ) after exposure to deltamethrin, and 80.00% (YW) and 95.52% (QZ) after exposure to permethrin. The resistance of the YW population was the highest among all three pyrethroids tested, while the QZ population was relatively sensitive to beta-cypermethrin and permethrin. Among the three pyrethrin insecticides tested, permethrin caused the highest mortality in all four populations.

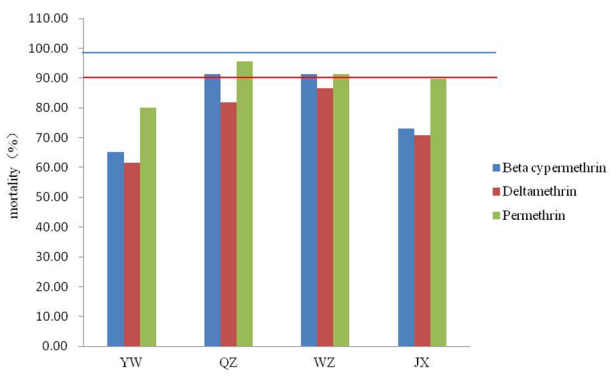

FIGURE 2 | Mortality of four *Ae. albopictus* field populations after exposure to three pyrethroids using the WHO tube bioassay. Red lines represent 90% mortality and blue lines represent 98% mortality.

Detection of *kdr* Genes in *Ae. albopictus* Field Populations

One hundred fifty-three specimens were sequenced for domains II and IV of the VGSC gene, and we found synonymous mutations in both domains, although they were not recorded in this study. Sequences of domains III were obtained from a total of 385 samples, and non-synonymous *kdr* mutations were detected at codons 1532 and 1534. At codon 1532, in addition to the wild-type codon ATC encoding isoleucine (I), another allele was detected, which was ACC, encoding threonine (T) (GenBank accession No.: MH384955 – MH384958) (Gao et al., 2018). The mutant allele I1532T was detected in the JX and QZ populations, with frequencies of 4.22 and 3.03%, respectively. Three genotypes, including the wild genotype I/I (91.86%) and the wild/mutant heterozygote I/T (8.14%) in the two populations were detected, but the mutant genotype T/T was not detected in this study.

At codon 1534, only two alleles were detected in samples obtained from the Zhejiang Province: one mutant allele TCC/S and the wildtype TTC/F (**Table 1**). The mutant allele TCC/S was found in all four populations. Overall, the allele frequencies were 57.92 and 42.08% for TTC/F and TCC/S, respectively, were obtained, and a total of three genotypes, including the wild-type genotype F/F (22.86%), wild-type/mutant heterozygote F/S (38.70%), and mutant genotype S/S (38.44%). Among the four populations, the mutant frequency was highest in YW (88.37%) and lowest in JX (42.77%).

In this study, individuals with *kdr* mutations in both codons 1532 and 1534 were detected in samples obtained from both QZ and JX. The genotypes included both wild-type (I/I+F/F), wild-type+mutant (I/I+F/S, I/I+S/S, I/T+F/F), and both mutant types (I/T+F/S, I/T+S/S) (**Table 2**).

Correlation Between Mutant *kdr* Genotypes and Resistance Phenotypes

The OR values were calculated for both mutant alleles. At codon 1532, the mutant frequency was 4.17% for susceptible individuals after exposure to beta-cypermethrin in all samples, while it was 1.72% for resistant individuals, with an OR value of 0.40 (95% CI: 0.04–3.70) (**Table 3**). The OR value was 0.54 and 0.55 in *Ae. albopitus* populations to deltamethrin and permethrin, respectively (95% CI: 0.06–5.29 and 0.07–4.72, respectively), indicating that the I1532T mutant allele might be negatively correlated with the three insecticide resistance phenotypes (**Table 3**). None of the mutant alleles at codon 1532 were found in resistant QZ individuals for all three insecticides, whereas it was found in individuals susceptible to beta-cypermethrin and permethrin (**Table 3**). No significant correlation between the I1532T mutant allele and three pyrethroids resistance phenotypes were observed, which might be caused by the relatively small sample size.

At codon 1534, the OR values were 2.28 ($P < 0.05$) and 2.23 ($P < 0.05$) in *Ae. albopitus* populations after exposure to beta-cypermethrin and deltamethrin, respectively, indicating that the F1534S mutant allele was positively correlated with both the

TABLE 1 | *Kdr* mutant allele frequency at codon 1534 from *Ae. albopictus* populations in YW, QZ, WZ, and JX from Zhejiang Province, China.

Insecticide	Population	Phenotype	N	*kdr*		Mutant (%) frequency	OR	Genotype		
				Wild TTC(F)	Mutant TCC(S)			F/F	F/S	S/S
Beta-cypermethrin	YW	R	18	5	31	86.11	0.56	1	2	15
		S	6	1	11	91.67		0	1	5
	QZ	R	5	1	9	90.00	23.0*	1	0	4
		S	16	23	9	28.13		10	4	2
	WZ	R	6	5	7	58.33	0.28	1	3	2
		S	15	5	25	83.33		0	5	10
	JX	R	24	20	28	58.33	2.05	5	10	9
		S	32	38	26	40.63		11	17	4
	Total	R	53	31	75	70.75	2.28*	8	15	30
		S	69	67	71	51.44		21	27	21
Deltamethrin	YW	R	18	0	36	100.00	/	0	0	18
		S	16	6	26	81.25		1	4	11
	QZ	R	10	5	15	75.00	6.6*	1	3	6
		S	16	22	10	31.25		8	6	2
	WZ	R	10	5	15	75.00	1.17	0	5	5
		S	16	9	23	71.88		1	7	8
	JX	R	26	29	23	44.23	1.27	6	17	3
		S	43	53	33	38.37		15	23	5
	Total	R	64	39	89	69.53	2.23*	25	40	26
		S	91	90	92	50.55		32	65	58
Permethrin	YW	R	12	4	20	91.67	0.71	0	2	10
		S	16	4	28	87.5		0	4	12
	QZ	R	3	3	3	50.00	1.46	1	1	1
		S	16	19	13	40.63		7	5	4
	WZ	R	6	9	3	25.00	0.13	3	3	0
		S	14	8	20	71.43		3	4	7
	JX	R	9	7	11	61.11	3.22*	1	5	3
		S	32	43	21	32.81		12	18	2
		R	30	21	37	61.67	1.59	5	11	14
	Total	S	78	74	82	52.56		22	31	25

N indicates the sample number. S was the susceptible phenotype; R was the resistant phenotype.
**P < 0.05.*

TABLE 2 | Number of simultaneous mutations at codon 1532 and 1534 in *Ae. albopictus* populations from QZ and JX.

Population	N	(Wild+wild) type	(Wild+mutant) type			(Mutant+mutant) type	
		I/I+F/F	I/I+F/S	I/I+S/S	I/T+F/F	I/T+F/S	I/T+S/S
QZ	66	24	19	19	2	2	0
JX	166	40	85	27	10	3	1
Total	232	64	104	46	12	5	1

N indicates the sample number.

beta-cypermethrin and deltamethrin resistance phenotype in all samples (**Table 1**). No statistically significant differences between the F1534S genotype and permethrin resistance phenotypes were found in the all samples, but a positive correlation was observed in JX.

The *kdr* mutant alleles F1534S and I1532T showed opposite effects on pyrethroid resistance. To explore the possible interactions between codons 1532 and 1534 and the resulting phenotype, all samples with the alleles I1532T+F1534, I1532T+F1534S, and I1532T+S1534 were chosen for analysis. As shown in **Figure 3**, only one sample with the I/T+S/S genotype showed resistance phenotype in three pyrethroids. A total of 83.33% (5/6) *vs.* 16.67% (1/6) of the samples with the I/T+F/F genotype were susceptible to permethrin, while almost half of the samples with I/T+F/S genotypes (2/5) had resistant phenotypes to the three pyrethroids. No statistical analysis was conducted because of the small sample size.

DISCUSSION

In the present study, four *Ae. albopticus* populations from Zhejiang Province in central China were tested for three pyrethroid insecticides (beta-cypermethrin, deltamethrin, and permethrin) using the WHO tube bioassay. The results showed that none of the populations were sensitive to any pyrethroid insecticide tested. After detecting the corresponding *kdr* mutations, we found mutations in domain III, specifically the I1532T mutation at codon 1532 and the F1534S mutations at codon 1534. Although the sequences of domains II and IV of VGSC were obtained, no non-synonymous mutations were found. Correlation analysis was conducted between the genotypes from codons 1532/1534 and the resistance phenotype in *Ae. albopictus*, indicating that the F1534S mutation was positively correlated with resistance phenotype to beta-cypermethrin (OR > 1, P < 0.05) and deltamethrin (OR > 1, P < 0.05), whereas the I1532T mutation was negatively correlated with resistance phenotype to beta-cypermethrin (OR < 1, P > 0.05), deltamethrin (OR < 1,

TABLE 3 | *Kdr* mutant allele frequency at codon 1532 of *Ae. albopictus* populations in QZ and JX.

Insecticide	Population	Phenotype	N	kdr		Mutant (%) frequency	OR	95% CI	
				Wild ATC(I)	Mutant ACC(T)			Down	Up
Beta-cypermethrin	QZ	R	5	10	0	0.00	/	/	/
		S	16	30	2	6.25			
	JX	R	24	47	1	2.08	0.66	0.06	7.49
		S	32	62	2	3.13			
	Total	R	29	57	1	1.72	0.40	0.04	3.70
		S	48	92	4	4.17			
Deltamethrin	QZ	R	10	20	0	0.00	/	/	/
		S	16	32	0	0.00			
	JX	R	26	51	1	1.92	0.54	0.06	5.36
		S	43	83	3	3.49			
	Total	R	36	71	1	1.39	0.54	0.06	5.29
		S	59	115	3	2.54			
Permethrin	QZ	R	3	6	0	0.00	/	/	/
		S	16	30	2	6.25			
	JX	R	9	17	1	5.56	0.70	0.08	6.35
		S	32	59	5	7.81			
		R	12	23	1	4.17	0.55	0.07	4.72
	Total	S	48	89	7	7.29			

N indicates the sample number. S was the susceptible phenotype; R was the resistant phenotype.

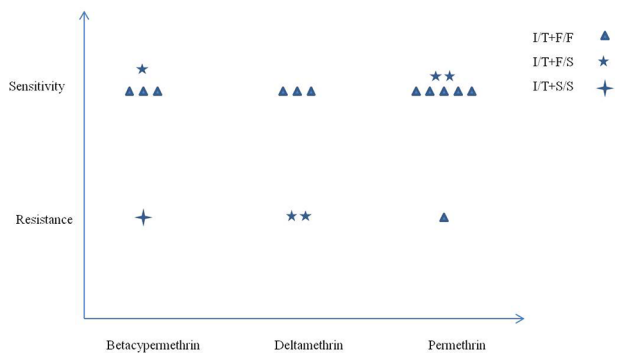

FIGURE 3 | Correlation between mutations at codons 1532 and 1534 and pyrethroid resistance in *Ae. albopictus* populations from Zhejiang Province, central China.

P > 0.05), and permethrin (OR < 1, P > 0.05), although no statistical significance was found.

Ae. albopictus is responsible for transmitting various arboviruses, leading to a high health burden in Zhejiang Province, because the only regularly conducted mosquito control measures there relied mainly on chemical insecticides (Hou et al., 2017). In the urban areas of some cities in the Zhejiang Province, most of the citizens from the residential communities signed an agreement with pest control operation companies (PCO) in the quest to kill mosquitoes twice a month during the seasons of peak mosquito activity. When dengue fever outbreaks occur, the spraying frequency increases to once daily to control the spread of the disease (Gao et al., 2018). All these measures lead to the overuse of insecticides, causing resistance in mosquitoes, as well as flies, who share the same living environment. According to the data regarding house files in 2011, 2014, and 2017, resistance to pyrethroids was very common (Wang et al., 2019).

Thus, a systematic surveillance of the insecticide resistance of *Ae. albopictus* in Zhejiang Province was carried out in 2016, and it was found that the number of cities where mosquitoes were resistant to pyrethroids, organophosphorus, and carbamates increased in 2019 (National Health Commission of the People's Republic of China, 2016; Hou et al., 2017). Compared to a previous study in 2019 in Zhejiang Province, JX and WZ showed a low mortality after exposure to all three pyrethroids, while QZ showed a low mortality after exposure to deltamethrin (National Health Commission of the People's Republic of China, 2016). These differences might be caused by the differences in sample locations. In a previous report in 2019, to obtain the resistance level of mosquitoes in the entire city, almost half of the *Ae. albopictus* populations were collected from rural and non-human settlements where no regular spray was applied. In the present study, samples were mainly collected from residential areas and parks in the urban areas where spaying was conducted regularly (Chen et al., 2016; National Health Commission of the People's Republic of China, 2016). Among the four populations, mosquitoes from YW showed the strongest resistance to all three pyrethroids, which was consistent with data obtained from previous reports (National Health Commission of the People's Republic of China, 2016; Hou et al., 2017). This might be caused by a high pressure on the city regarding the handling of large numbers of dengue patients from outside the country due to the international mobility of business personnel annually. As a result, the local government had to regularly organize large-scale mosquito control campaigns using large amounts of pyrethroid insecticides (National Health Commission of the People's Republic of China, 2016).

According to the results of this study, there were two resistance alleles, one each at codons 1532 and 1534. At codon

1534, only one mutant allele, TCC(S), was identified in mosquitoes from Zhejiang Province, central China. This was consistent with the study by Chen et al. in Shanghai and Hangzhou (both cities are from central China), but different from the results obtained from Ruili City (Yunnan Province, southern China), and Haikou City (Hainan Province, southern China), where three mutant codons, TTC(S), TGC(C), and TTG (L) were found (Chen et al., 2016; Gao et al., 2018; Lan et al., 2019). These differences should be further analyzed. We hypothesize that one influencing factor for this might be the high selection pressure on mosquitoes in Ruili and Haikou. Both cities are located in the marginal area of the tropics where *Ae.* mosquito density is high throughout the year and dengue fever outbreaks occur frequently (Li et al., 1986; Qiu and Zhao, 1988; Qiu et al., 1991; Qiu et al., 1993; Yong-hua et al., 2014; Han et al., 2015; Gao et al., 2018). Continuous use of insecticides in cities in southern China might contribute to the selection for homozygous *kdr*, where a diversity in the gene could be more conducive to the survival of the species (Brito et al., 2013). At codon 1532, the frequency of I1532T ranged from 3.03% (QZ) to 4.22% (JX). These low frequencies indicate that the mutation may have just emerged or was introduced very recently in Zhejiang Province, central China (Aguirre-Obando et al., 2017).

Few studies have reported the correlation between the *kdr* mutant allele in codon 1534 and pyrethroid resistance in *Ae. albopictus* in China. Chen et al. (2016) first identified the F1534S allele in the Haikou mosquito population and demonstrated that it was positively correlated with resistance to permethrin and beta-cypermethrin. Further, Gao et al. demonstrated that F1534S was positively correlated with resistance against permethrin and deltamethrin. In this study, our results confirmed that F1534S was significantly positively correlated with resistance against beta-cypermethrin and deltamethrin. In codon 1532, we found that the mutant allele I1532T was possibly negatively correlated with resistance against the three pyrethroids tested, with OR values ranging from 0.40 to 0.55, which were consistent with the results obtained from Shanghai City (Gao et al., 2018). However, no statistical significance was found in this study because of the relatively small sample size resulting from the low mutation frequency at codon 1532. The small sample size also made it impossible to analyze the interaction between I1532T and F1534S on the resistance phenotype. Thus, further studies with larger sample sizes are needed to study the role of I1532T in pyrethroid resistance in *Ae. albopictus*.

DATA AVAILABILITY STATEMENT

The original contributions presented in the study are included in the article/supplementary material. Further inquiries can be directed to the corresponding authors.

AUTHOR CONTRIBUTIONS

JS, ZG, and JH conceived the study and coordinated its implementation. JH, YyW, and QL participated in the experimental design. YQ, YpW, QN, WC, JW, TL, and ML collected mosquito samples. YyW and QL performed the experiments. JS and YyW interpreted the data. YyW and QL drafted the manuscript. All authors contributed to the article and approved the submitted version.

FUNDING

This work was granted by the National Critical Project for Science and Technology on Infectious Diseases of P. R. China (no. 2017ZX10303404).

REFERENCES

Aguirre-Obando, O. A., Martins, A. J., and Navarro-Silva, MárioAntônio (2017). First Report of the Phe1534Cys Kdr Mutation in Natural Populations of Aedes Albopictus From Brazil. *Parasites Vectors* 10, 160. doi: 10.1186/s13071-017-2089-5

Brito, L., Linss, J., Lima-Camara, T., Belinato, T., Peixoto, A., Lima, J., et al. (2013). Assessing the Effects of Aedes Aegypti Kdr Mutations on Pyrethroid Resistance and Its Fitness Cost. *PloS One* 8 (4), e60878. doi: 10.1371/journal.pone.0060878

Burland, T. G. (2000). DNASTAR's Lasergene Sequence Analysis Software. *Methods Mol. Biol.* 132, 71–91. doi: 10.1385/1-59259-192-2:71

Chen, H., Li, K., Wang, X., Yang, X., Lin, Yi, Fang, C., et al. (2016). First Identification of Kdr Allele F1534S in VGSC Gene and its Association With Resistance to Pyrethroid Insecticides in Aedes Albopictus Populations From Haikou City, Hainan Island, China. *Infect. Dis. Poverty* 5, 31. doi: 10.1186/s40249-016-0125-x

Deng, W. B., Zhou, Y. M., Liu, J., and Tian, S. H. (2017). *Spss 23 (Chinese Edition) Statistical Analysis Practical Course. 2th Edition* (Beijing: Electronic Industry Press).

Gao, J.-P., Chen, H.-M., Shi, H., Peng, H., and Ma, Y.-J. (2018). Correlation Between Adult Pyrethroid Resistance and Knockdown Resistance (Kdr) Mutations in Aedes Albopictus (Diptera: Culicidae) Field Populations in China. *Infect. Dis. Poverty* 7, 86. doi: 10.1186/s40249-018-0471-y

Guo, S., Ling, F., Wang, J.-n., Wu, Y.-y., Hou, J., and Gong, Z.-Y. (2016). Genetic Polymorphism Analysis of Cytochrome C Oxidase Subunit I Gene in Aedes Albopictus From Zhejiang Province, China. *Chin. J. Zoonoses* 32 (2), 133–136,147. doi: 10.3969/j.issn.1002-2694.2016.02.007

Han, J.-Z., Yin, Z.-L., and Liu, Y.-h. (2015). Ruili Characteristics of Dengue Epidemic in 2014. *China Health Ind* 15, 186–188. doi: 10.16659/j.cnki.1672-5654.2015.15.070

Hemingway, J., and Ranson, H. (2000). Insecticide Resistance in Insect Vectors of Human Disease. *Annu. Rev. Entomol* 45 (3), 71–91. doi: 10.1146/annurev.ento.45.1.371

Hou, J., Liu, Q., Wang, J., Wu, Y., Li, T., and Gong, Z. (2020). Insecticide Resistance of *Aedes Albopictus* in Zhejiang Province, China. *BioSci Trends* 14 (4), 248–254. doi: 10.5582/bst.2020.03194

Hou, J., Meng, F., Wu, Y., Wang, J., Guo, S., and Gong, Z. (2017). Resistance of Adult Aedes Albopictus to Commonly Used Insecticides in Zhejiang Province. *Chin. J. Vector Biol. Control* 28 (3), 230–232. doi: 10.11853/j.issn.1003.8280.2017.03.008

Kasai, S., Ng, L. C., Lam-Phua, S. G., Tang, C. S., Itokawa, K., Komagata, O., et al. (2011). First Detection of a Putative Knockdown Resistance Gene in Major Mosquito Vector, Aedes Albopictus. *Jpn J. Infect. Dis.* 64 (3), 217–221.

Kushwah, R. B., Dykes, C. L., Kapoor, N., Adak, T., and Singh, O. P. (2015). Pyrethroid-Resistance and Presence of Two Knockdown Resistance (Kdr) Mutations, F1534C and a Novel Mutation T1520I, in Indian Aedes Aegypti. *PloS Negl. Trop. Dis.* 9 (1), e3332. doi: 10.1371/journal.pntd.0003332

Lan, X.-m., Xu, J.-b., and Jiang, J.-y. (2019). An Analysis of Voltage-Gated Sodium Channel Gene Mutation in *Aedes Albopictus* Resistant Populations Against Pyrethroid Insecticides in Ruili, Yunnan Province, China. *Chin. J. Vector Biol. Control* 30 (2), 158–162. doi: 10.11853/j.issn.1003.8280.2019.02.010

Li, Y., Xu, J., Zhong, D., Zhang, H., Yang, W., Zhou, G., et al. (2018). Evidence for Multipleinsecticide Resistance in Urban Aedes Albopictus Populations in Southern China. *Parasit Vectors* 11 (1), 4. doi: 10.1186/s13071-017-2581-y

Li, F. S., Yang, F. R., Song, J. C., Gao, H., Tang, J. Q., Zou, C. H., et al. (1986). Etiologic and Serologic Investigations of the 1980 Epidemic of Dengue Fever on Hainan Island, China. *Am. J. Trop. Med. Hyq.* 35 (5), 1051–1054. doi: 10.4269/ajtmh.1986.35.1051

National Health Commission of the People's Republic of China (2016). *National Vector Surveillance Program [s]* (Beijing: China Center for Disease Control and prevention).

Qiu, F. X., Chen, Q. Q., Ho, Q. Y., Chen, W. Z., Zhao, Z. G., and Zhao, B. W. (1991). The First Epidemic of Dengue Hemorrhagic Fever in the People's Republic of China. *Am. J. Trop. Med. Hyq* 44 (4), 364–370. doi: 10.4269/ajtmh.1991.44.364

Qiu, F. X., Gubler, D. J., Liu, J. C., and Chen, Q. Q. (1993). Dengue in China: A Clinical Review. *Bull. World Health Organ* 71 (3–4), 349–359.

Qiu, F. X., and Zhao, Z. G. (1988). A Pandemic of Dengue Fever on the Hainan Island. Epidemiologic Investigations. *Chin. Med. J.* 101 (7), 463–467.

Robertson, R. C., and Hu, S. M. (1988). The Tiger Mosquito in Shanghai, by RC Robertson and Stephen M. *K Hu 1935 J. Am. Mosq Control Assoc.* 4, 179–183.

Smith, L. B., Kasai, S., and Scott, J. G. (2018). Voltage-Sensitive Sodium Channel Mutations S989P + V1016G in Aedes Aegypti Confer Variable Resistance to Pyrethroids, DDT and Oxadiazines. *Pest Manag Sci.* 74 (3), 737–745. doi: 10.1002/ps.4771

Wang, X. H., Chen, H. Y., Yang, X. Y., Lin, Y., Cai, F., Zhong, W. B., et al. (2015). Resistance to Pyrethroid Insecticides and Analysis of Knockdown Resistance (Kdr) Gene Mutations in Aedes Albopictus Form Haikou City. *Acad. J. Second Mil Univ* 36 (8), 832–838. doi: 10.3724/SP.J.1008.2015.00832

Wang, J. N., Hou, J., Wu, Y.-Y., Guo, S., Liu, Q.-M., Li, T.-Q., et al. (2019). Resistance of House Fly, Musca Domestica L. (Diptera: Muscidae), to Five Insecticides in Zhejiang Province, China: The Situation in 2017. *Can. J. Infect. Dis. Med. Microbiol.* 2019, 4851914. doi: 10.1155/2019/4851914

Wang, Y. Y., and Jiang, Z. K. (2016). Development and Application of Public Health Pesticides in China, 2013-2016. *Chin. J. Vector Biol. Control* 27 (5), 321–325. doi: 10.11853/j.issn.1003.8280.2016.05.001

Wang, Y. G., Liu, X., Li, C. L., Su, T. Y., Jin, J. C., Guo, Y. H., et al. (2017). A Survey of Insecticide Resistance in Aedes Albopictus (Diptera: Culicidae) During a 2014 Dengue Fever Outbreak in Guangzhou, China. *J. Econ Entomol* 110 (1), 239–244. doi: 10.1093/jee/tow254

WHO (2013). *Sustaining the Drive to Overcome the Global Impact of Neglected Tropical Diseases: Second WHO Report on Neglected Tropical Diseases* (Geneva: World Health Organization).

WHO (2016). *Monitoring and Managing Insecticide Resistance in Aedes Mosquito Populations* (Geneva: World Health Organization).

Wuliandari, J. R., Lee, S. F., White, V. L., Tantowijoyo, W., Hoffmann, A. A., and Endersby- Harshman, N. M. (2015). Association Between Three Mutations, F1565C, V1023G and S996P, in the Voltage-Sensitive Sodium Channel Gene and Knockdown Resistance in Aedes Aegypti From Yogyakarta, Indonesia. *Insects* 6 (3), 658–685. doi: 10.3390/insects6030658

Xu, J. B., Bonizzoni, M., Zhong, D. B., Zhou, G. F., Cai, S. W., Li, Y. J., et al. (2016). Multi-Country Survey Revealed Prevalent and Novel F1534S Mutation in Voltage-Gated Sodium Channel (VGSC) Gene in Aedes Albopictus. *PloS Negl. Trop. Dis.* 10 (5), e0004696. doi: 10.1371/journal.pntd.0004696

Yang, T.-c., and Fu, G.-m. (2006). Investigation on the Distribution of Dengue Vector Aedes Albopictus in Zhejiang Province. *Chin. J. Hygien IC Insecticides Equipments* 12 (3), 189–191.

Yong-hua, L. I. U., Xiao-xiong, Y. I. N., Zhao-lan, Y. A. N. G., Ping, L. I., Zheng-liu, Y. I. N., Shi, L. I., et al. (2014). Epidemiological Study on an Outbreak of Dengue Fever in Ruili, Dehong Prefecture of Yunnan Province, China. *Chin. J. Vector Biol. Control* 25 (6), 524–526. doi: 10.11853/j.issn.1003.4692.2014.06.010

Conflict of Interest: The authors declare that the research was conducted in the absence of any commercial or financial relationships that could be construed as a potential conflict of interest.

frontiers in Cellular and Infection Microbiology

ORIGINAL RESEARCH
published: 07 July 2021
doi: 10.3389/fcimb.2021.705129

Homogeneity and Possible Replacement of Populations of the Dengue Vectors *Aedes aegypti* and *Aedes albopictus* in Indonesia

OPEN ACCESS

Edited by:
Jun Feng,
National Institute of Parasitic Diseases, China

Reviewed by:
Padet Siriyasatien,
Chulalongkorn University, Thailand
Zhao Lei,
Xiamen University, China

***Correspondence:**
Triwibowo Ambar Garjito
triwibowo@litbang.kemkes.go.id
Roger Frutos
roger.frutos@cirad.fr

Specialty section:
This article was submitted to Virus and Host, a section of the journal Frontiers in Cellular and Infection Microbiology

Received: 04 May 2021
Accepted: 10 June 2021
Published: 07 July 2021

Citation:
Garjito TA, Widiarti W, Hidajat MC, Handayani SW, Mujiyono M, Prihatin MT, Ubaidillah R, Sudomo M, Satoto TBT, Manguin S, Gavotte L and Frutos R (2021) Homogeneity and Possible Replacement of Populations of the Dengue Vectors Aedes aegypti and Aedes albopictus in Indonesia. Front. Cell. Infect. Microbiol. 11:705129. doi: 10.3389/fcimb.2021.705129

Triwibowo Ambar Garjito[1*], *Widiarti Widiarti*[1], *Muhammad Choirul Hidajat*[1,2], *Sri Wahyuni Handayani*[1], *Mujiyono Mujiyono*[1], *Mega Tyas Prihatin*[1], *Rosichon Ubaidillah*[3], *Mohammad Sudomo*[4], *Tri Baskoro Tunggul Satoto*[5], *Sylvie Manguin*[6], *Laurent Gavotte*[7] *and Roger Frutos*[8*]

[1] Institute for Vector and Reservoir Control Research and Development, National Institute of Health Research and Development, The Ministry of Health of Indonesia, Salatiga, Indonesia, [2] Doctoral School of Medical Science, Faculty of Medicine, Diponegoro University, Semarang, Indonesia, [3] Research Center for Biology, Indonesian Institute of Sciences, Cibinong, Indonesia, [4] National Institute of Health Research and Development, The Ministry of Health of Indonesia, Jakarta, Indonesia, [5] Department of Parasitology, Faculty of Medicine, Public Health and Nursing, Gadjah Mada University, Yogyakarta, Indonesia, [6] HydroSciences Montpellier (UMR-HSM), IRD, CNRS, Montpellier, France, [7] Espace-Dev, University of Montpellier, Montpellier, France, [8] Cirad, UMR 17, Intertryp, Montpellier, France

Currently, *Aedes aegypti*, the principal vector of dengue virus in Indonesia, has spread throughout the archipelago. *Aedes albopictus* is also present. Invasion and high adaptability of the *Aedes* mosquitoes to all of these areas are closely related to their ecology and biology. Between June 2016 and July 2017, larval and adult mosquito collections were conducted in 43 locations in 25 provinces of Indonesia using standardized sampling methods for dengue vector surveillance. The samples collected were analyzed for polymorphism and phylogenetic relationship using the mitochondrial *cox*1 gene and the nuclear ribosomal internal transcribed spacer 2 (ITS2). Almost all *Ae. aegypti* samples collected in this study (89%) belonged to the same haplotype. A similar situation is observed with the nuclear ITS2 marker. Populations of *Ae. aegypti* characterized few years ago were genetically different. A closely related observation was made with *Aedes albopictus* for which the current populations are different from those described earlier. *Ae. aegypti* populations were found to be highly homogenous all over Indonesia with all samples belonging to the same maternal lineage. Although difficult to demonstrate formally, there is a possibility of population replacement. Although to a lower extent, a similar conclusion was reached with *Ae. albopictus*.

Keywords: *Aedes aegypti*, *Aedes albopictus*, Indonesia, *cox*1, internal transcribed spacer 2 (ITS2)

INTRODUCTION

Aedes aegypti is known as a major vector of dengue viruses (family *Flaviviridae*, genus *Flavivirus*, DENV) (Simmons et al., 2012; Kraemer et al., 2015), yellow fever virus (family *Flaviviridae*, genus *Flavivirus*, YF) (da Costa-da-Silva et al., 2005; Kraemer et al., 2015; Yohan et al., 2018), zika virus (family *Flaviviridae*, genus *Flavivirus*, ZIKV) (Ja, 2016; Olson et al., 2020), and chikungunya virus (family *Togaviridae*, genus *Alphavirus*, CHIKV) (Kraemer et al., 2015; Yohan et al., 2018). This mosquito species originates from the forest of Africa and, since the 18th century, has spread *via* transcontinental trade throughout tropical and subtropical regions (Gubler, 1997; da Costa-da-Silva et al., 2005; Gubler, 2011; Joyce et al., 2018; Tedjou et al., 2019). In Southeast Asia, *Ae. aegypti* was formally identified for the first time in Malaysia and Thailand (1907) at the early 20th century (Urdaneta-Marquez and Failloux, 2011; Parimittr et al., 2018). *Ae. aegypti* was formally identified in Indonesia in 1908 (Leicester, 1908). A local strain of *Ae. aegypti*, the Medan strain, was first reported and successfully colonized in a laboratory in the 1930s (Kuno, 2010). Currently, the species is reported to have spread throughout the archipelago (Setiati et al., 2006; IVRCRD, 2018).

Another dengue vector species is the Asian tiger mosquito, *Aedes albopictus*. This species has for long been considered as a secondary vector of several viruses (Paupy et al., 2009; Grard et al., 2014; Goubert et al., 2016; Mulyatno et al., 2018). *Ae. albopictus* originates in the forests of Southeast Asia, and has spread worlwide since the 1970s (Moncayo et al., 2004). According to the Global invasive species database (http://www.issg.org/database/), this species has been recorded as one of the worst invasive species in the world. Currently, *Ae. albopictus* can be found in Asia, Africa, Europe, North and South America, and many locations in the Pacific and Indian oceans except Antartica (Paupy et al., 2009; Kraemer et al., 2015). As an invasive species, *Ae. albopictus* plays a potential role in triggering a re-emergence of arboviruses transmission in many locations. Recently, this species played an important role in Dengue, Chikungunya, and Zika outbreaks in both endemic and invaded regions (Rezza et al., 2007; Teixeira et al., 2009; Paupy et al., 2010; McKenzie et al., 2019; Lai et al., 2020).

The invasion and adaptation to all of these areas are closely related to their ecology and biology. *Ae. aegypti* has high adaptability to urban and peridomestic areas, where it breeds in the vicinity of human dwellings in a variety of artificial and natural containers in urban and rural areas (Kusriastuti and Sutomo, 2005; Kraemer et al., 2015; IVRCRD, 2018). This species is also recognized as the most anthropophilic mosquito and has the ability to blood-feed repeatedly on humans almost on a daily basis (Ritchie, 2014). This behavior may have contributed to the capacity of *Ae. aegypti* to cause high epidemics of dengue fever in Indonesia. A total of 68,407 dengue cases (incidence: 78.85/100,000) with 493 deaths (case fatality rates (CFR): 0.72%) were reported in 2017 (MoH Indonesia, 2018; Harapan et al., 2019). *Ae. albopictus* displays a strong ecological plasticity and has shown a remarkable capacity to adapt to urban and sub-urbans under various climate conditions, displacing *Ae. aegypti* population in some areas. *Ae. albopictus* has now become a significant vector of CHIKV and DENV (Knudsen., 1995; Paupy et al., 2009; Thiberville et al., 2013; Ngoagouni et al., 2015).

While an effective multivalent dengue vaccine is still under research and not yet available, vector control and entomological surveillance are the only reliable means of prevention and control of dengue fever (Wilder-Smith et al., 2010; Thisyakorn and Thisyakorn, 2014; Chang et al., 2015; Parra et al., 2018). Updated information on the genetic diversity and evolutionary patterns among *Ae. aegypti* and *Ae. albopictus* populations is needed to provide clues for better understanding the origin, the structuration, and the distribution of populations. Moreover, this is also a prerequisite to define differences in vector competence and capacity to transmit dengue virus, in ecological adaptations and in resistance to insecticides (Gupta and Preet, 2014; Yohan et al., 2018; Naim et al., 2020). However, a comprehensive information about genetic diversity and structuration of populations of *Ae. aegypti* and *Ae. albopictus* in Indonesia is still missing.

Therefore, we investigated the genetic diversity, evolutionary relationship, and distribution of *Ae. aegypti* and *Ae. albopictus* mosquitoes collected in different locations and islands, from Western Sumatra (Aceh) to Eastern Indonesia (Papua) using the mitochondrial *cox*1 or COI gene and the internal transcribed spacer 2 (ITS2) of the ribosomal DNA as target sequences.

MATERIAL AND METHODS

Collection and Rearing of Mosquitoes

Larva, pupa, and adult mosquitoes were collected using standardized sampling methods for dengue vector surveillance (Focks and Special Program for Research and Training in Tropical Diseases (TDR), 2003; Kusriastuti and Sutomo, 2005; WHO, 2011; Ritchie, 2014; WHO, 2016; MoH Indonesia, 2018; Harapan et al., 2019). In each house, larvae and pupae from different containers were put in different plastic bags. All samples were then transported to a field laboratory. Larvae and pupae were reared in the field laboratory for 3 days until the emergence of adult mosquitoes. Mosquitoes were then morphologically identified, sorted according to locality, and preserved in 250 µl of RNAlater (Ambion-Thermo Fisher Scientific, Watham, USA). This large sampling campaign was conducted as part of a nationwide program supervised by the Ministry of Health. Mosquitoes were collected during this campaign as a cohort of samples for use in different projects. This explains why the samples were stored individually in RNAlater even though no virus detection was conducted in this work. They were then stored at −80°C until further analysis. Larvae which did not emerge after 3 days were preserved the same way as adult mosquito samples for further analysis. All mosquito samples were individual samples, and only female mosquitoes were used as samples.

DNA Extraction, Amplification and Sequencing

Whole DNA from each mosquito was individually extracted using a DNeasy® Blood & Tissue Kit (Qiagen, Hilden, Germany) according to the manufacturer's standard protocol. ITS2 and *cox*1 (COI) were selected as target sequence because they are the most used sequences for phylogenetic and population structure analyses of mosquitoes. They are present in databases. They were also used in previous works on the genotyping of *Aedes* mosquitoes in Indonesia, allowing thus for comparison. The amplification of *cox*1 was conducted using the primers CI-N-2087 (5′-AAT TTC GGT CAG TTA ATA ATA TAG-3′ and TY-J-1460 (5′-TAC AAT TTA TCG CCT AAA CTT CAG CC-3′) as previously described (Rueanghiran, et al., 2011; Ngoagouni et al., 2015). The ITS2 sequence was amplified using the primers ITS2a (5′-TGT GAA CTG CAG GAC ACA T-3′) and ITS2b (5′-TAT GCT TAA ATT CAG GGG GT-3′). PCR reactions were carried out using the GoTaq® Green Master Mix (Promega, Madison, WI, USA). The conditions for PCR amplification of the *cox*1 gene were as follows: one cycle at 94°C for 1 min for initial denaturation, followed by five cycles at 94°C for 30 s, 45°C for 40 s, and 72°C for 1 min. This was then followed by 35 cycles at 94° C for 30 s, 44°C for 40 s, and 72°C for 1 min, and by a final extension step at 72°C for 10 min (Ngoagouni et al., 2015). PCR thermocycling conditions for ITS2 were as follows: 94°C for 10 min; followed by 40 cycles of denaturation at 94°C for 1 min, annealing at 56°C for 45 s, and elongation at 72°C for 1 min; followed by a final extension step at 72°C for 10 min. PCR products were electrophoresed in 1.5% agarose gel and visualized by SYBR® safe DNA gel stain (Invitrogen, Carlsbad, CA, USA) using a Biorad Molecular Image Gel Doc XR (Biorad Laboratories Inc, California, USA). A 100-bp DNA ladder was used for calculating the size of the PCR products. Amplicons were purified using Applied Biosystems ExoSAP-IT™ (Thermo Fisher Scientific, Vilnius, Lithuania). Cycle sequencing was performed using the primers listed above and an Applied Biosystems BigDye™ Terminator v.3.1 Cycle Sequencing Kit (Life Technologies Cooperation, Austin, TX, USA). To remove unincorporated BigDye® terminators and salts, cycle sequencing products were purified using a BigDye® Xterminator Purification Kit (Life technologies, Bedford, MA, USA). Sequence data were obtained using a DNA sequencer (Applied Biosystems® 3500 Genetic Analyzer) and analyzed using the Sequencing Analysis 6 program (Applied Biosystems). All sequences have been deposited in Genbank under the accession numbers MW280620 to MW280792, MW280794 to MW280797 and MW280800 to MW280818 for *Ae. aegypti cox*1 sequences. The accession numbers for *Ae. aegypti* ITS2 sequences range from MW288143 to MW288145 and MW290431 to MW290468. The accession numbers for *Ae. albopictus cox*1 sequences are MW280793, MW280798, MW280799, and MW283303 to MW283318. The accession numbers for *Ae. albopictus* ITS2 sequences are MW287155 to MW287157. The accession numbers of the *cox*1 and ITS2 sequences of the unknown species *Aedes* sp (sls25_Asp) are MW286812 and MW293720, respectively.

Polymorphism and Phylogenetic Analysis

Sequences were analyzed for definition of haplotypes using DnaSP software v.6.12.03 (Rozas et al., 2017). The relationship between haplotypes, based on pairwise difference to generate a minimum spanning tree (MST) and minimum spanning network (MSN), was calculated and modeled using Network software and Hapstar v. 0.7. Multiple alignment and phylogenetic analysis were performed using the SaeView package (Gouy et al., 2010). Phylogenetic trees were built using maximum-likelihood (ML) with the general time reversible model with gama distributed with four discrete categories (GTR + I + G). The clade support was assessed *via* 500 bootstrap replicates.

RESULTS

Mosquito Collection

Collections were conducted in 43 districts/municipalities in 25 dengue-endemic provinces in Indonesia (**Supplementary Table 1** and **Figure 1**). These provinces were Aceh, Riau, Riau Islands, Jambi, Bangka-Belitung, Lampung, Banten, West Java, Central Java, Yogyakarta, East Java, West Kalimantan, South Kalimantan, Central Kalimantan, East Kalimantan, Bali, West Nusa Tenggara, East Nusa Tenggara, North Sulawesi, Central Sulawesi, South Sulawesi, Southeast Sulawesi, Maluku, North Maluku, and West Papua. Sampling of larva and adult mosquitoes was conducted as part of the 2nd year of the "Rikhus Vektora" project in July–August 2016 in 28 locations, the WHO project SEINO (#1611945) in September–October 2016 in six locations, and subsequently in nine locations as part of the 3rd year of "Rikhus Vektora" project in May–July 2017 (**Figure 1**). A total of 60,873 *Ae. aegypti* mosquitoes were collected: 2,184 adults, 54,251 larvae, and 4,438 adults obtained from reared larvae. With respect to *Ae. albopictus*, 16,223 mosquitoes were collected with the following breakdown: 4,957 adults, 9,638 larvae, and 1,628 adults obtained from reared larvae. From these samples 196 *Ae. aegypti* mosquitoes were sequenced: 34 adults and 162 adults obtained from reared larvae. For *Ae. albopictus*, 19 samples were sequenced, two adults and 17 adults obtained from reared larvae.

Phylogenetic Relationships of the Collected Samples

The samples collected in this work fell into three different branches, both for *cox*1 and ITS2 (**Supplementary Figure 1**). These branches corresponded to *Ae. aegypti*, *Ae. albopictus*, and another undetermined *Aedes* species. The latter sample was therefore named sls25_Asp (**Supplementary Figure 1**). The *cox*1 gene phylogeny showed the presence of two main clusters in *Ae. aegypti*, Cluster Aae1 and Cluster Aae2, with Cluster Aae1 being separated into two subclusters: Subcluster Aae1a and Subcluster Aae1b (**Supplementary Table 1** and **Supplementary Figure 1**). These clusters were separated by very low bootstrap values indicating that the tree was not well structured and that the samples belonged to the same population

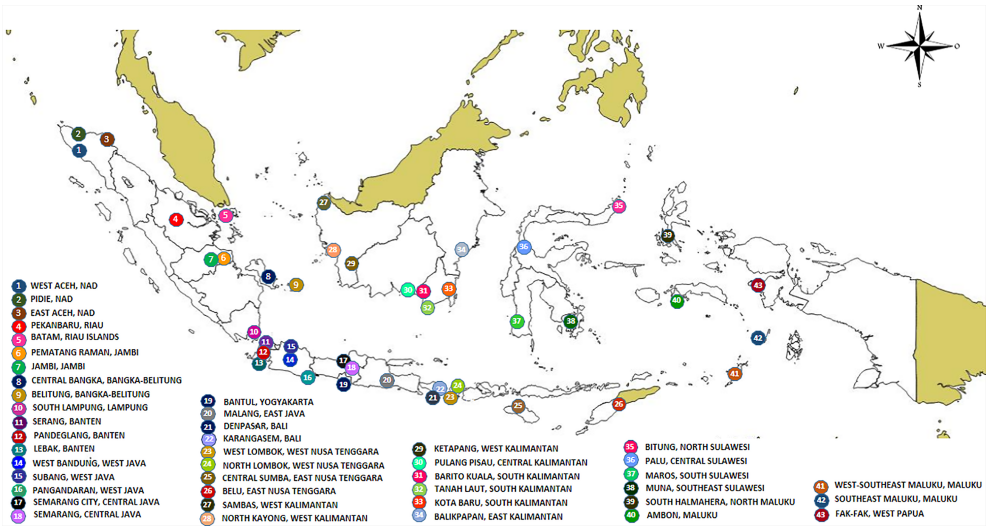

FIGURE 1 | Map of sampling sites.

(**Supplementary Figure 1**). However, with the *cox*1 gene from *Ae. albopictus*, three clusters could be identified with strong bootstraps (100), Cluster Aal1, Cluster Aal2, and Cluster Aal3 (**Supplementary Table 2** and **Supplementary Figure 1**).

Presence of a Yet Unidentified Species

The sample sls25_Asp from Maros in South Sulawesi (site No 36 in **Figure 1**) was initially misidentified in the field as *Culex quinquefasciatus*. This sample was branching apart from *Ae. aegypti* and *Ae. albopictus* for the *cox*1 gene indicating that it was neither *Ae. aegypti* nor *Ae. albopictus* (**Supplementary Figure 1**). It was also different from *Cx. quinquefasciatus* which was used as outgroup. The phylogeny of the ITS2 sequences showed a similar result. The sample sls25_Asp was different from *Ae. aegypti* and *Ae. albopictus* (**Supplementary Figure 2**). The ITS2 sequence showed a best hit with an *Aedes polynesiensis* mosquito from Fidji (AY822662) with a percentage of identity of 88.24%, whereas the *cox*1 sequence displayed a best hit with an *Ae. albopictus* sample from Vietnam (HQ398902) with 91.95% identity. However, there was no *cox*1 sequence for *Ae. polynesiensis* in Genbank, and it was thus impossible to confirm if the *cox*1 gene would also link sls25_Asp to *Ae. polynesiensis*. A morphological analysis showed that the closest species, although still with morphological differences, was *Aedes paullusi* (data not shown). There is no *cox*1 or ITS2 records for *Ae. paullusi* in databases. The *Ae. albopictus* and *Ae. polynesiensis* hits for sls25_Asp *cox*1 and ITS2 sequences, respectively, might simply be default hits due of the lack of relevant sequences in the databases.

Phylogeny and Polymorphism of *Aedes aegypti cox*1 Gene

The *cox*1 sequences from 196 samples collected for this work were compared to the only other source of *Ae. aegypti cox*1 sequences from Indonesia, a 17-sample collection from 2013 in the North Coast of Central Java (Yohan et al., 2018). These samples, identified in the tree by their accession numbers from KP869121 to KP869126 and KP334259 to KP334269, make a completely separate cluster (**Figure 2**). The genetic distance between the sequences from this work and those reported by Yohan et al. (2018) ranged from 0.4 to 3.1%. With a mutation rate of the *cox*1 gene in insects ranging from 2.4% Mya^{-1} to 3.5% Mya^{-1} (Brower, 1994; Papadopoulou et al., 2010), the time needed for the accumulation of these mutations ranges from 114,285 to 167,000 years for a mutation rate of 2.4% Mya^{-1} and from 885,714 to 1,291,667 years for a mutation rate of 3.1% Mya^{-1}. When blasting the *cox*1 sequences from this work against Genbank data, the sequences from previously *Ae. aegypti* identified from Indonesia in 2013 (Yohan et al., 2018) did not respond as best hits. However, best hits were obtained with the same score with a series of nine *cox*1 sequences of *Ae. aegypti* mosquitoes captured in Peru, Cambodia, Puerto Rico, India, Georgia, England, and Germany (**Supplementary Table 3**). Subcluster Aae2a showed two best hits both from Kenya (**Supplementary Table 3**). Subclusters Aae2b and Aae2d had only one corresponding best hit in Genbank from Mozambique and Haiti, respectively (**Supplementary Table 4**). Subcluster Aae2c showed five best hits with the same score from Egypt and Kenya (**Supplementary Table 3**). Interestingly, Subcluster Aae2e displayed four best hits with the same score, but only one was a wild-type mosquito captured in Haiti. The other three best hits corresponded to the reference strains reared in laboratory conditions of Liverpool and RED (**Supplementary Table 3**). Finally, each of the two individual samples diverging from Cluster 1, 46_Aae (IS1) and 28-1-Aae (IS2) displayed a different best hit. IS1 showed a best hit with a mosquito collected in Russia, whereas IS2 showed a best hit with *Aedes aegypti formosus*, which is considered an ancestral feral population from sub-Saharan Africa (Powell and Tabachnick, 2013; Gloria-Soria et al., 2016) (**Supplementary Table 3**). The breakdown into

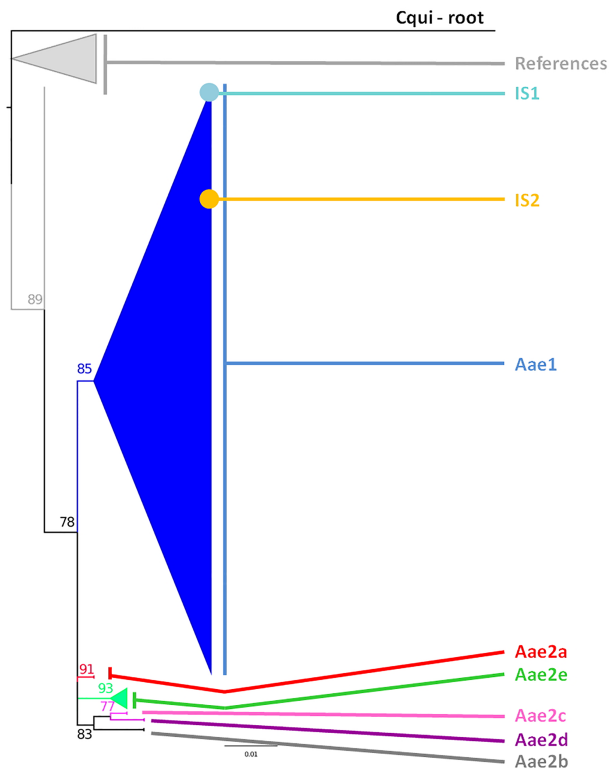

FIGURE 2 | Phylogeny of the *Aedes aegypti cox*1 gene. The phylogenetic trees were built using maximum-likelihood (ML) with the general time reversible model with gama distributed with four discrete categories (GTR + I + G). The clade support was assessed *via* 500 bootstrap replicates. The tree was rooted using the *Culex quinquefasciatus cox*1 gene (MK265737) as outgroup. The color code is that of the *cox*1 subclusters shown in **Supplementary Table 1**: light gray: References, dark blue: Subcluster Aae1, red: Subcluster Aae2a, dark gray: Subcluster Aae2b, pink: Subcluster Aae2c, purple: Subcluster Aae2d, green: Subcluster Aae2e, light blue: individual sample 1, yellow: individual sample 2, black: root. "References" correspond to the *Ae. aegypti cox*1 sequences published by Yohan et al. (2018) from samples collected in 2013 whose accession numbers are KP334259 to KP334269 and KP869121 to KP89126.

individual haplotypes showed that Cluster Aae1 comprised 176 samples out of 198 (89%) and 39 haplotypes out of 53 (73.6%) with two of them, H1 and H4, being the most represented (**Supplementary Tables 1**, **3** and **Figure 3**). H1 haplotype comprised 57 samples (32.85%) whereas the haplotype H4 contained 61 samples (34.6%) (**Supplementary Table 1**). Subcluster Aae1a comprised 16 haplotypes, including haplotype H1, and 75 samples, whereas Subcluster Aae1b contained haplotype H4 and 22 other haplotypes for a total of 102 samples (**Supplementary Table 1**).

Phylogeographic Distribution of *Aedes aegypti cox*1 Lineages

Cluster Aae1 was, as expected, present everywhere with the exception of East Aceh and North Lombok (**Supplementary Figure 3** and **Supplementary Table 1**). No correlation could be found between any cluster and any location. When considering the geographic distribution of the haplotypes, a lack of correlation was also observed (**Supplementary Figure 4**). Only a default correlation could be observed, *i.e.* rare haplotypes from a region with few samples. However, this is a sampling bias and is not significant.

Phylogeny and Polymorphism of *Aedes aegypti* ITS2

The 40 sequences were distributed into two clusters and 21 haplotypes (**Supplementary Table 1**, **Figure 4** and **Supplementary Table 5**). Cluster 1 is divided into four subclusters (1a to 1d), which displayed limited variations (**Figure 5**). As a consequence, Cluster 1 gathered 42 samples and 23 haplotypes representing all the sequence variations observed within this monophyletic group (**Figure 5**). The different haplotypes were closely related with a maximum relative distance of 11.54% (**Supplementary Table 5**). Cluster 2 comprised only four samples, each one corresponding to a different haplotype. They were very closely related with an overall variation of 0.51% (**Supplementary Table 5**).

Phylogeographic Distribution of *Aedes aegypti* ITS2 Sequences

The analysis of the polymorphism of *Ae. aegypti* ITS2 haplotype in this study showed that cluster 1 was the dominant one (**Supplementary Figure 5**). Subcluster 1a displayed the most extensive distribution, covering Sumatra (East Aceh-Aceh, Pematang Raman-Jambi, Pekan Baru-Riau, South Lampung-Lampung), Java (West Bandung-West Java, Semarang-Central Java, Bantul-Yogyakarta, Malang-East Java), Kalimantan (Sambas-West Kalimantan, Balikpapan-East Kalimantan), Bali (Karangasem), West Nusa Tenggara (Lombok), and Sulawesi (Palu-Central Sulawesi, Maros-South Sulawesi) (**Supplementary Figure 5**). Subcluster 1a showed a best hit with mosquitoes collected in Russia, Sri Lanka. The other subclusters, namely 1b, 1c, and 1d, showed a limited distribution. Subcluster 1b was only found in the Sambas-West Kalimantan region, while Subcluster 1c was identified in two locations: Batam-Riau Islands and Bantul-Yogyakarta. Subcluster 1d was found in two locations, *i.e.* Pematang Raman-Jambi and Palu-Central Sulawesi (**Supplementary Figure 5** and **Supplementary Table 5**). Cluster 2 had a more limited distribution. This cluster was found in Karangasem-Bali, Ambon-Maluku, Malang-East Java and Batam-Riau islands (**Supplementary Figure 5** and **Supplementary Table 5**).

Phylogeographic Distribution, Phylogeny and Polymorphism of *Aedes albopictus cox*1 and ITS2

The 19 *cox*1 sequences of the *Ae. albopictus* samples collected in this work were compared to those released by Maynard et al. (2017) who collected samples in Jakarta in 2012, in Waingapu (Sumba) in 2013, and in Timika (Papua) in 2015. Sequences were also compared to those released by Battaglia et al. (2016) who established a worldwide classification of *Ae. albopictus cox*1 haplogroups (Battaglia et al., 2016). The COI sequences from

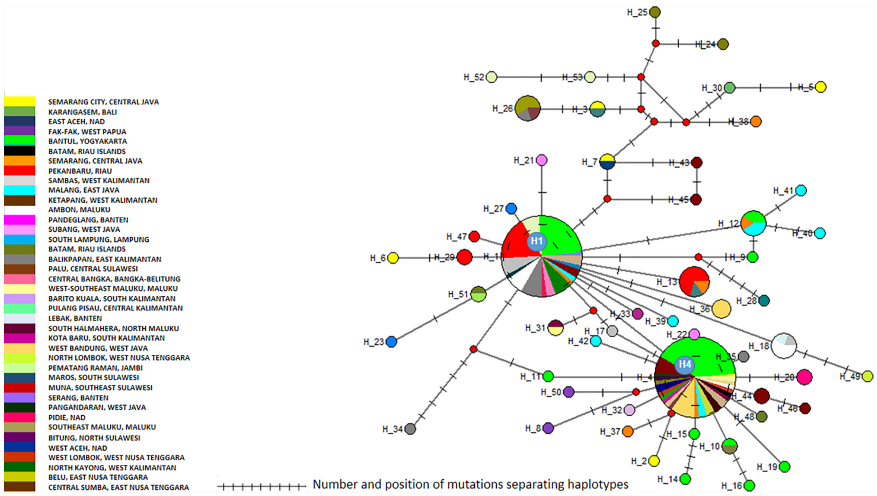

FIGURE 3 | Network of *Aedes aegypti cox*1 haplotypes. The figure represents the frequency of each haplotype of the *cox*1 gene of *Ae. aegypti* in the regions sampled. The network represents the number of mutations between the haplotypes and their location.

Maynard et al. (2017) matched perfectly the haplogroups defined by Battaglia et al. (2016) and were distributed within two different haplogroups, A2a and A1b1a. The sequences obtained in this work did not correspond to the sequences reported by Maynard et al. (2017) and did not match any of the haplogroups defined by Battaglia et al. (2016) (**Figure 6**). Out of the three clusters identified within the *Ae. albopictus* sequences reported in this work, Cluster Aal1 was closer, although clearly different, to the haplogroups A2a; Cluster Aal3 was closer, although different, to the haplogroup A1ba1; and Cluster Aal2 was not close to any haplogroup. A total of 11 different haplotypes were found (**Figure 7** and **Supplementary Table 2**). The genetic distance between the *cox*1 sequences reported in this work and those from Maynard et al. (2017) ranges from 0.4 to 1.3%, depending on the sample. The time needed to accumulate the number of mutations separating the samples from this work to those described by Maynard et al. (2017) ranges from 114,285 to 167,000 years for a mutation rate of 2.4% Mya^{-1} and from 371,428 to 542,000 years for a mutation rate of 3.5% Mya^{-1}. Cluster Aal1 was found only in Central Kalimantan, whereas the other two clusters were spread over different provinces (**Supplementary Figure 6**). However, the sample size is too small to draw any significant conclusion on the phylogeography. When blasted on databases, Cluster Aal1 and Cluster Aal2 both displayed best hits with the same *Ae. albopictus* populations from The Philippines but with differing percentage of identity ranging from 99.51 to 99.85% (**Supplementary Table 4**). Cluster Aal3 showed best hits with invasive populations of *Ae. albopictus* found in D.R. Congo, China, Thailand, Greece, Brazil, and the USA with 99.65 to 99.84% of identity (**Supplementary Table 4**). With respect to

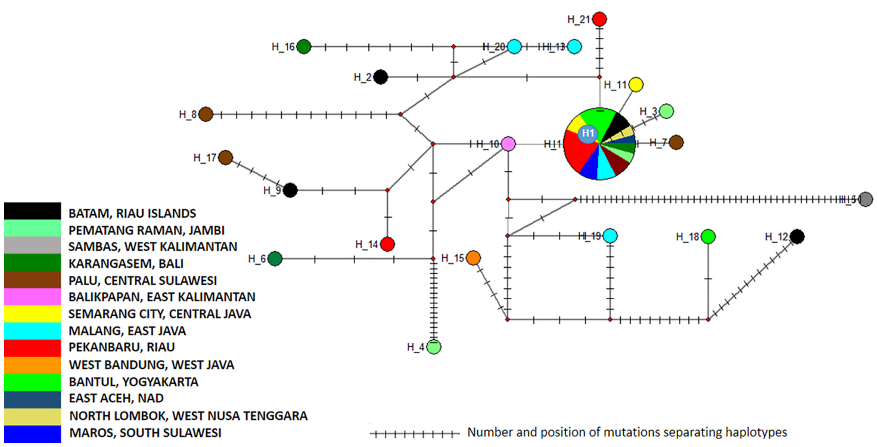

FIGURE 4 | Network of *Aedes aegypti* ITS2 sequences. The figure represents the frequency of each haplotype of the ITS2 sequence of *Ae. aegypti* in the regions sampled. The network represents the number of mutations between the haplotypes and their location.

FIGURE 5 | Phylogeny of the *Aedes aegypti* ITS2 sequences. The phylogenetic tree was built using maximum-likelihood (ML) with the general time reversible model with gama distributed with four discrete categories (GTR + I + G). The clade support was assessed *via* 500 bootstrap replicates. The tree was rooted using the *Culex quinquefasciatus* ITS2 sequence (HQ848572) as outgroup. The color code used is that of the ITS2 subclusters given in **Supplementary Table 1**.

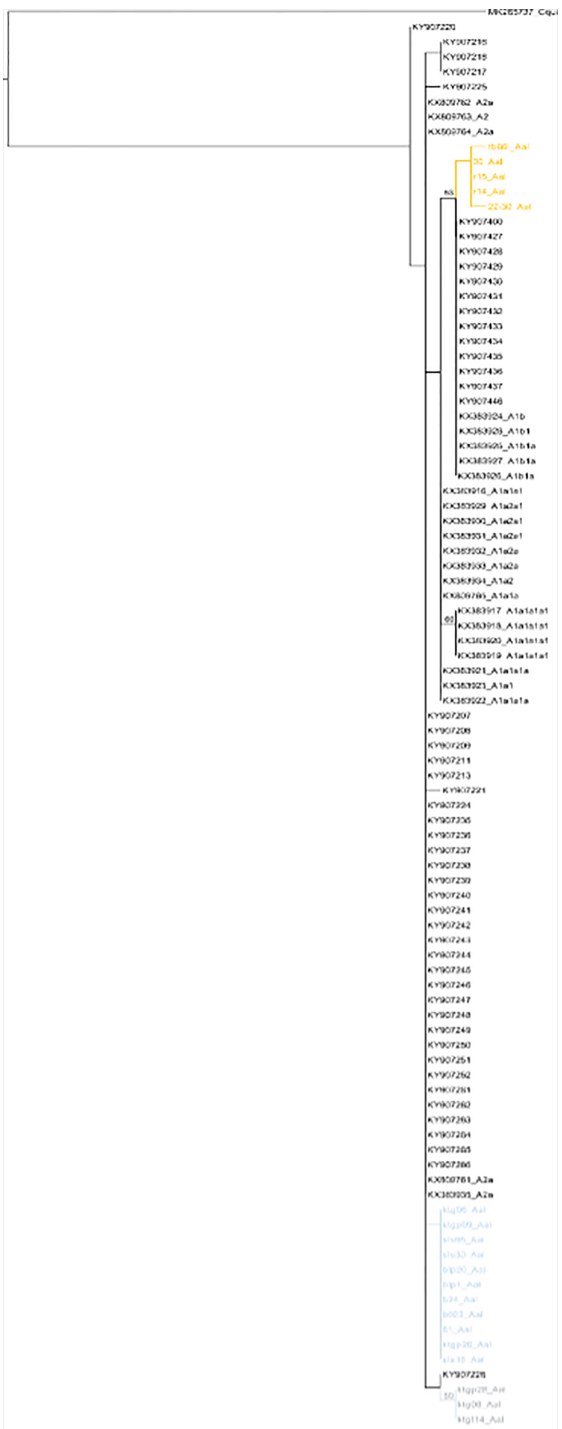

FIGURE 6 | Phylogeny of *Aedes albopictus cox*1 genes. The phylogenetic tree was built using maximum-likelihood (ML) with the general time reversible model with gama distributed with four discrete categories (GTR + I + G). The clade support was assessed *via* 500 bootstrap replicates. The tree was rooted using the *Culex quinquefasciatus cox*1 gene (MK265737) as outgroup. The color code used is that of the *cox*1 subclusters displayed in **Supplementary Table 2**. Gray: Subcluster Aal1, green: Subcluster Aal2, orange: Subcluster Aal3.

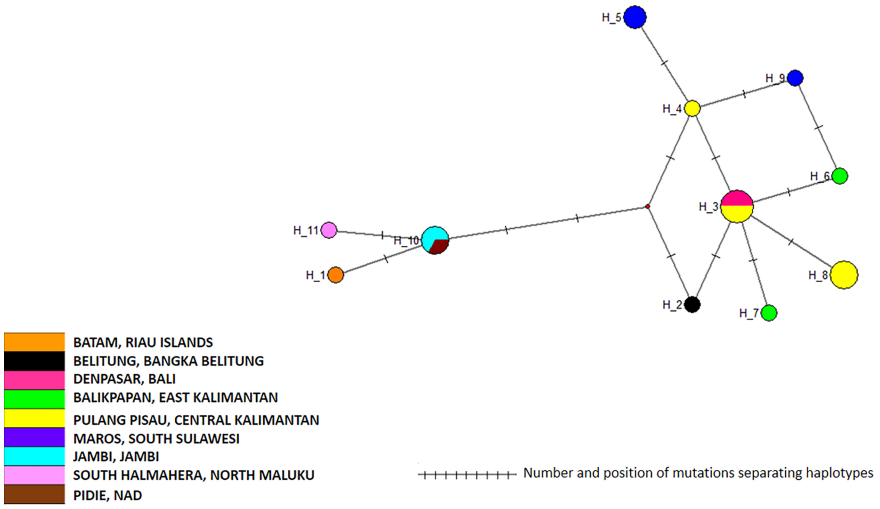

FIGURE 7 | Network of *Aedes albopictus cox*1 haplotypes. The figure represents the frequency of each haplotype of the *cox*1 gene of *Ae. albopictus* in the regions sampled. The network represents the number of mutations between the haplotypes and their location on the gene sequence.

ITS2, the number of sequences available (only three) was too small to draw a conclusion. Nevertheless, they corresponded to invasive populations of *Ae. albopictus* found in Italy, Georgia, Israel, or Sri Lanka (**Supplementary Table 6**).

DISCUSSION

Dengue, which is the fastest spreading arbovirus disease worldwide, is also the first ranking vector-borne disease in Indonesia and, thus, a national health priority. In the absence of treatment and commercially available vaccine, vector management remains the only way to control the disease. However, in order to do so, the knowledge of vector population structure is an obligate prerequisite. The capacity of vectoring a given pathogen is not correlated with the species but instead with the population. Some populations of *Ae. aegypti* or *Ae. albopictus* are more prone to disseminate a given pathogen than others (Alto et al., 2008; Reinhold et al., 2018). Therefore, a species should be regarded as a metapopulation or the combination of cross-fertile genetically distinct populations displaying differing phenotypic traits (Garjito et al., 2020). Vector competence is one of these phenotypic traits, which in *Aedes* and other mosquitoes, was shown to be related to specific populations (Beerntsen et al., 2000; Severson and Behura, 2016) and not to the species *per se*. Deciphering the structure of the vector populations is thus essential.

Although dengue is the transmissible disease ranking number one in Indonesia, there have been very limited works on the analysis of the structure of the populations of *Aedes* with only one study on *Ae. Aegypti* (Yohan et al., 2018) and one on *Ae. albopictus* (Maynard et al., 2017). In both cases, the number of sampling sites was very limited. To these must be added studies aiming at assessing the stability of populations in the framework of a *Wolbachia* release program in Yogyakarta (Rašić et al., 2015). However, in this case, the genetic diversity was assessed with microsatellites and SNPs only on a sample from the city of Yogyakarta in South Central Java (Rašić et al., 2015). This work is, to our knowledge, the first one exploring the genetic diversity of *Ae. aegypti* and *Ae. albopictus* throughout Indonesia, a huge archipelago of more than 13,000 islands spanning 5,271 km from east to west and 2,210 km from north to south.

A first conclusion from this work is the homogeneity of the *Ae. aegypti* populations found all over Indonesia. With respect to the *cox*1 sequences, all *Ae. aegypti* samples belonged to the same maternal lineage. Variations were observed and clusters were described, but they simply represent a polymorphism within a monophyletic population. All clusters identified correspond to co-circulating variants. The main difference is that one cluster, Cluster Aae2, comprised samples displaying a larger polymorphism. Cluster Aae1, and in particular the haplotypes H1 and H4, seemed to be populations with a very high colonizing and demographic potential. These two haplotypes represent each about 30% of the samples collected all over Indonesia. They represent indeed the very same population with very limited or no polymorphism at all with Cluster Aae1 making up 87% of all samples and being present everywhere in Indonesia. Considering the size and structure of Indonesia, an archipelago spanning from the Indian Ocean to the Pacific Ocean, this is unexpected. One would have instead expected patched populations differing from one island to the other. What is observed is exactly the contrary, the same population throughout the whole country.

Owing to the mutation rate of the *cox*1 gene in *Ae. aegypti* (Brower, 1994; Papadopoulou et al., 2010), the population described in this work cannot have evolved from the populations previously described. Even in the case of introgression, the maternal lineage remains the same. What is described in this case is a different maternal lineage. This indicates that the observed population is allogenic. The lack of

BLAST best hits with the previously described Indonesian populations and the occurrence of BLAST best hits with populations from other parts of the world also support this allogenic origin. Two hypotheses must then be considered to explain the massive presence of this homogeneous and allogenic population of *Ae. aegypti*. The first hypothesis is that the population described in this work has been completely missed in previous studies. Previous sampling conducted in 2013 yielded genetically different populations (Yohan et al., 2018) but were very limited and covered a limited zone (Yohan et al., 2018). This result could then be considered a consequence of a sampling bias, all mosquitoes from the previous study (Yohan et al., 2018) having been captured in a specific area, *i.e.* Northern Coastal Central Java. However, considering the extension of Cluster Aae1 throughout Indonesia and its overwhelming presence among samples (87%), it seems unlikely that it would have been missed in the 2013 sampling campaign. Furthermore, Cluster Aae1 was found to be strongly present in this same Northern Coastal Central Java area. The second hypothesis is that this allogenic population might have invaded Indonesia after the 2013 sampling. This invasion would have been very fast then, within a maximum of three years between 2013, date of the former sampling, and 2016, date of our first sampling. However, owing to the very limited information available on the previous populations, it is not possible to formally demonstrate this replacement hypothesis. Nevertheless, the ITS2 marker showed a similar trend; and considering the high potential of nuclear DNA for recombination and variation and finding the same ITS2 cluster all over Indonesia confirm the presence of a set of genetically closely related populations in Indonesia with one specific population characterized by two very closely related, monophyletic maternal haplotypes, H1 and H4. These haplotypes seem to be highly invasive most likely due to higher demographic and adaptability potentials. This also suggests that assortative mating might occur, which restricts greatly intraspecies breeding with preexisting populations.

Ae. aegypti has been shown to be highly susceptible to satyrization by *Ae. albopictus* leading to the replacement of *Ae. aegypti* populations by *Ae. albopictus* ones, thus explaining in part the invasive potential of the latter (Bargielowski and Lounibos, 2016). However, what is observed in Indonesia does not match this model despite the presence of populations of *Ae. albopictus* described as invasive in other parts of the world. What is seen in Indonesia is instead a homogeneous population of *Ae. aegypti* occupying all the archipelago and outcompeting *Ae. albopictus*. As per *Ae. aegypti*, the populations of *Ae. albopictus* collected in Indonesia do not correspond to those previously described from 2012 to 2015 (Maynard et al., 2017). Unlike populations described by Maynard et al. (2017), they also do not correspond to the haplogroups designed on samples from 2013 (Battaglia et al., 2016). They are related but not the same. Owing to the rate of mutation of the *cox*1 gene in insects, 2.4% Mya^{-1} to 3.5% Mya^{-1} depending on the model (Brower, 1994; Papadopoulou et al., 2010), the variations observed are not compatible with an evolution of previous local populations and indicate an invasion by allogenic populations. However, just as per *Ae. aegypti* the very limited number of previous studies makes it difficult to formally demonstrate a replacement.

The domestication of *Ae. aegypti* and *Ae. albopictus* is a process closely linked to the development of the human society and in particular to long distance mobility, transportation of goods, and international trade (Paupy et al., 2009). The current expansion of the *Aedes*-borne diseases is by far a consequence of the global economy. *Ae. aegypti* and *Ae. albopictus*, like all living organisms, are structured in metapopulations, which differ slightly one from the other and due to massive international transportation are distributed all over the world within the areas suitable for the survival of these species. The mobility of these populations from one place to another is a stochastic event, which depends on the place of departure, the place of arrival, the genetic and physiological traits of the populations involved, the economic situation, and the commercial exchanges and routes at a given time. This is to our knowledge the first report of such a massive homogeneity of a population of *Ae. aegypti* over such a large area.

One limitation of this work is the lack of previous data at the scale of the whole country. Only two studies have been conducted prior to our work on the genotyping of *Aedes* mosquitoes in Indonesia. There is only one report on the genotyping of *Ae. aegypti* but only on few samples and only in one restricted area in northern coastal central Java (Yohan et al., 2018). This lack of previous data prevents us from fully analyzing and concluding on the putative replacement of populations that the phylogenetic analyses suggest. Regarding the analysis of *Ae. albopictus*, the same problem occurred with only one previous study (Maynard et al., 2017) thus preventing the conduct of a fully significant comparison. On another hand, a major limitation of this work is the limited number of *Ae. albopictus* samples and sequences of ITS2. This is due to a limitation in funding which prevented the conduct of a full scale sequencing program. Further analyses of *Ae. albopictus* diversity in Indonesia should be conducted to complete the current study.

CONCLUSIONS

A general consequence of our results is that populations are changing over time, even throughout a very large archipelago. Whatever the population, established or invasive, *Ae. aegypti* and *Ae. albopictus* mosquitoes will have to breed in the human environment. Then, the best way to prevent any population of vector from thriving is certainly to implement vector control at a very local level, at maximum at the community level, essentially by eliminating breeding sites using very simple and affordable means of control such as containers and garbage removal. The strategy of prevention of dengue transmission through community participation currently recommended in Indonesia will most likely be the most successful of all. This approach named 3M for "Menutup" for covering water containers, "Menguras" for cleaning water containers, and "Mengubur" for

burying discarded containers, is implemented under the responsibility of families in each household with at least one person in charge of monitoring *Aedes* larvae in all water storage (Paupy et al., 2009; MoH Indonesia, 2015). This strategy shed light on what is most needed for the successful control of *Aedes*-borne diseases, not big science, big management or big strategies but simply information, education, people awareness and community-based management.

DATA AVAILABILITY STATEMENT

The datasets presented in this study can be found in online repositories. The names of the repository/repositories and accession number(s) can be found in the article/ **Supplementary Material**.

ETHICS STATEMENT

Specific permissions were not required for field *Aedes* larval collections. Oral consent to inspect the *Aedes* breeding places in the household was obtained from the homeowners and local government authorities. Formal approval to conduct these activities was granted by the Ethical Commission Board of the NIHRD, Ministry of Health, Indonesia (No. LB.02.01/5.2/ KE.003/2016, January 13, 2016; and No. LB.02.01/5.2/KE.020/ 2017, February 6, 2017).

AUTHOR CONTRIBUTIONS

Conceptualization: TG, W, MH, RU, MS, and TS. Data curation: TG, SH, M, and MP. Investigation: TG, SH, M, and MP. Formal analysis: TG, MP, MH, RF, and LG. Resources: TG, MP, M, MH, and SH. Methodology: TG, RF, and LG. Project administration: MH and TG. Software: RF, LG, and TG. Supervision: SM and RF. Validation: RF, SM, TG, and LG. Writing—original draft: TG and RF. Writing—review and editing: RF, SM, and TG. All authors contributed to the article and approved the submitted version.

FUNDING

The research was supported by the Institute for Vector and Reservoir Control Research and Development, National Institute of Health Research and Development, Ministry of Health Indonesia under the project Rikhus Vektora 2016–2017 and as part of the WHO project SEINO1611945 in 2016. TG, RF, SM, and TS were supported in part by the PHC Nusantara projects Zika & Co and SOCIAL, co-funded by the French Ministry of Foreign Affairs and RISTEKDIKTI under the Indonesian Ministry of Education and Culture.

ACKNOWLEDGMENTS

The authors would also like to thank the people in the study areas for cooperating during the entomological surveys, all field mosquito collectors and all technical team of the Rikhus Vektora project on disease vectors and reservoirs in 2016–2017. We also thank all team members of the WHO project SEINO 1611945 in 2016. Both projects were conducted under the supervision and coordination of the Institute for Vector and Reservoir Control Research and Development, National Institute of Health Research and Development, Ministry of Health, Republic of Indonesia.

SUPPLEMENTARY MATERIAL

The Supplementary Material for this article can be found online at: https://www.frontiersin.org/articles/10.3389/fcimb.2021.705129/full#supplementary-material

Supplementary Figure 1 | *cox*1 gene phylogeny of the collected samples. The phylogenetic trees were built using maximum-likelihood (ML) with the general time reversible model with gama distributed with four discrete categories (GTR + I + G). The clade support was assessed *via* 500 bootstrap replicates. The tree was rooted using the *Culex quinquefasciatus cox*1 gene (MK265737) as outgroup.

Supplementary Figure 2 | ITS2 phylogeny of the collected samples. The phylogenetic tree was built using maximum-likelihood (ML) with the general time reversible model with gama distributed with four discrete categories (GTR + I + G). The clade support was assessed *via* 500 bootstrap replicates. The tree was rooted using the *Culex quinquefasciatus* ITS2 sequence (HQ848572) as outgroup. The color code used is that of the ITS2 clusters of *Ae. aegypti* and *Ae. albopictus* displayed in **Supplementary Tables 1** and **2**, respectively. The color code for *Ae. aegypti* ITS2 clusters is: blue: Cluster 1a, red: Cluster 1b, orange: Cluster 1c.

Supplementary Figure 3 | Geographic distribution of *Aedes aegypti cox*1 clusters.

Supplementary Figure 4 | Geographic distribution of *Aedes aegypti cox*1 haplotypes.

Supplementary Figure 5 | Geographic distribution of *Aedes aegypti* ITS2 sequences.

Supplementary Figure 6 | Geographic distribution of *Aedes albopictus cox*1 haplotypes.

Supplementary Table 1 | Specimens and sampling localities of *Aedes aegypti.*

Supplementary Table 2 | Specimens and sampling localities of *Aedes albopictus*.

Supplementary Table 3 | Polymorphism of *Aedes aegypti cox*1 haplotypes from Indonesia.

Supplementary Table 4 | Polymorphism of *Aedes albopictus cox*1 haplotypes from Indonesia.

Supplementary Table 5 | Polymorphism of *Aedes aegypti* ITS2 haplotypes from Indonesia.

Supplementary Table 6 | Polymorphism of *Aedes albopictus* ITS2 haplotypes from Indonesia.

REFERENCES

Alto, B. W., Reiskind, M. H., and Lounibos, L. P. (2008). Size Alters Susceptibility of Vectors to Dengue Virus Infection and Dissemination. *Am. J. Trop. Med. Hyg.* 79, 688–695. doi: 10.4269/ajtmh.2008.79.688

Bargielowski, I. E., and Lounibos, L. P. (2016). Satyrization and Satyrization-Resistance in Competitive Displacements of Invasive Mosquito Species. *Insect Sci.* 23, 162–174. doi: 10.1111/1744-7917.12291

Battaglia, V., Gabrieli, P., Brandini, S., Capodiferro, M. R., Javier, P. A., Chen, X.-G., et al. (2016). The Worldwide Spread of the Tiger Mosquito as Revealed by Mitogenome Haplogroup Diversity. *Front. Genet.* 23, 208. doi: 10.3389/fgene.2016.00208

Beerntsen, B. T., James, A. A., and Christensen, B. M. (2000). Genetics of Mosquito Vector Competence. *Microbiol. Mol. Biol. Rev.* 64, 115–137. doi: 10.1128/MMBR.64.1.115-137.2000

Brower, A. V. Z. (1994). Phylogeny of *Heliconius* Butterflies Inferred From Mitochondrial Dna Sequences (Lepidoptera: Nymphalidae). *Mol. Phyl. Evol.* 3, 159–174. doi: 10.1006/mpev.1994.1018

Chang, F. S., Tseng, Y. T., Hsu, P. S., Chen, C. D., Lian, I. B., and Chao, D. Y. (2015). Re-Assess Vector Indices Threshold as an Early Warning Tool for Predicting Dengue Epidemic in a Dengue non-Endemic Country. *PloS Negl. Trop. Dis.* 9, 1–20. doi: 10.1371/journal.pntd.0004043

da Costa-da-Silva, A. L., Capurro, M. L., and Bracco, J. E. (2005). Genetic Lineages in the Yellow Fever Mosquito *Aedes (Stegomyia) aegypti* (Diptera: Culicidae) From Peru. *Mem. do Inst. Oswaldo. Cruz.* 100, 539–544. doi: 10.1590/S0074-02762005000600007

Focks, D. A. Special Program for Research and Training in Tropical Diseases (TDR) (2003). *Review of Entomological Sampling Methods and Indicators for Dengue Vectors* Vol. 28 (Geneva, Switzerland: UNICEF, UNDP, World Bank, WHO Spec Program Res Train Trop Dis), 208–389.

Garjito, T. A., Hidajat, M. C., Kinansi, R. R., Setyaningsih, R., Anggraeni, Y. M., Mujiyanto,, et al. (2020). *Stegomyia* Indices and Risk of Dengue Transmission: A Lack of Correlation. *Front. Public Health* 8, 328. doi: 10.3389/fpubh.2020.00328

Gloria-Soria, A., Ayala, D., Bheecarry, A., Calderon-Arguedas, O., Chadee, D. D., Chiappero, M., et al. (2016). Global Genetic Diversity of *Aedes aegypti*. *Mol. Ecol.* 25, 5377–5395. doi: 10.1111/mec.13866

Goubert, C., Minard, G., Vieira, C., and Boulesteix, M. (2016). Population Genetics of the Asian Tiger Mosquito *Aedes albopictus*, an Invasive Vector of Human Diseases. *Heredity. (Edinb).* 117, 125–134. doi: 10.1038/hdy.2016.35

Gouy, M., Guindon, S., and Gascuel, O. (2010). SeaView Version 4: A Multiplatform Graphical User Interface for Sequence Alignment and Phylogenetic Tree Building. *Mol. Biol. Evol.* 27, 221–224. doi: 10.1093/molbev/msp259

Grard, G., Caron, M., Mombo, I. M., Nkoghe, D., Mboui Ondo, S., Jiolle, D., et al. (2014). Zika Virus in Gabon (Central Africa)–2007: A New Threat From *Aedes albopictus*? *PloS Negl. Trop. Dis.* 8, e2681. doi: 10.1371/journal.pntd.0002681

Gubler, D. J. (1997). "Dengue and Dengue Hemorrhagic Fever: Its History and Resurgence as a Global Public Health Prolem," in *Dengue and Dengue Hemorrhagic Fever*. Eds. D. Gubler and G. Kuno (Wallingford, UK: CAB International), 1–22.

Gubler, D. J. (2011). Dengue, Urbanization and Globalization: The Unholy Trinity of the 21 St Century. *Trop. Med. Health* 39 (4 Suppl.), 3–11. doi: 10.2149/tmh.2011-S05

Gupta, S., and Preet, S. (2014). Genetic Differentiation of Invasive *Aedes albopictus* by RAPD-PCR: Implications for Effective Vector Control. *Parasitol. Res.* 113, 2137–2142. doi: 10.1007/s00436-014-3864-2

Harapan, H., Michie, A., Mudatsir, M., Sasmono, R. T., and Imrie, A. (2019). Epidemiology of Dengue Hemorrhagic Fever in Indonesia: Analysis of Five Decades Data From the National Disease Surveillance. *BMC Res. Notes* 12, 4–9. doi: 10.1186/s13104-019-4379-9

IVRCRD (2017). *Manual on Mosquitoes Field Sampling Methods (in Bahasa Indonesia). 3rd edition* (Indonesia: IVRCRD: NIHRD-MoH Indonesia, Salatiga).

IVRCRD (2018). *Final Compilation Rikhus Vectora 2015-2018* (Indonesia: IVRCRD-Salatiga, NIHRD-MoH Indonesia), 80.

Ja, D. (2016). Etymologia: *Aedes aegypti*. *Emerg. Infect. Dis.* 22, 1807–1807. doi: 10.3201/eid2210.ET2210

Joyce, A. L., Torres, M. M., Torres, R., and Moreno, M. (2018). Genetic Variability of the *Aedes aegypti* (Diptera: Culicidae) Mosquito in El Salvador, Vector of Dengue, Yellow Fever, Chikungunya and Zika. *Parasit. Vectors* 11, 1–14. doi: 10.1186/s13071-018-3226-5

Knudsen, A. B. (1995). Global Distribution and Continuing Spread of *Aedes albopictus*. *Parassitologia* 37, 91–97.

Kraemer, M., Sinka, M., Duda, K., Mylne, A., Shearer, F., Barker, C., et al. (2015). The Global Distribution of the Arbovirus Vectors *Aedes aegypti* and *Ae. albopictus*. *Elife* 4, e08347. doi: 10.7554/eLife.08347

Kuno, G. (2010). Early History of Laboratory Breeding of *Aedes aegypti* (Diptera: Culicidae) Focusing on the Origins and Use of Selected Strains. *J. Med. Entomol.* 47, 957–971. doi: 10.1603/ME10152

Kusriastuti, R., and Sutomo, S. (2005). Evolution of Dengue Prevention and Control Programme in Indonesia DF/DHF Disease Burden. *Dengue. Bull.* 29, 1–7.

Lai, Z., Zhou, T., Zhou, J., Liu, S., Xu, Y., Gu, J., et al. (2020). Vertical Transmission of Zika Virus in *Aedes albopictus*. *PloS Negl. Trop. Dis.* 14, e0008776. doi: 10.1371/journal.pntd.0008776

Leicester, G. F. (1908). The Culicidae of Malaya. *Stud. Inst. Med. Res. F. M. S.* 3, 18–261.

Maynard, A. J., Ambrose, L., Cooper, R. D., Chow, W. K., Davis, J. B., Muzari, M. O., et al. (2017). Tiger on the Prowl: Invasion History and Spatio-Temporal Genetic Structure of the Asian Tiger Mosquito *Aedes albopictus* (Skuse 1894) in the Indo-Pacific. *PloS Negl. Trop. Dis.* 11, 1–27. doi: 10.1371/journal.pntd.0005546

McKenzie, B. A., Wilson, A. E., and Zohdy, S. (2019). *Aedes albopictus* is a Competent Vector of Zika Virus: A Meta-Analysis. *PloS One* 14, e0216794. doi: 10.1371/journal.pone.0216794

MoH Indonesia. (2015). "Guidelines for Dengue Hemorrhagic Fever Control in Indonesia (in Bahasa Indonesia)," in *Directorate General Disease Prevention and Control* (Jakarta, Indonesia: Ministry of Health of Republic Indonesia).

MoH Indonesia (2018). "Dengue Hemorrhagic Fever Situation in Indonesia Tahun 2017," in *Center for Data and Information* (MoH Republic of Indonesia).

Moncayo, A. C., Fernandez, Z., Ortiz, D., Diallo, M., Sall, A., Hartman, S., et al. (2004). Dengue Emergence and Adaptation to Peridomestic Mosquitoes. *Emerg. Infect. Dis.* 10, 1790–1796. doi: 10.3201/eid1010.030846

Mulyatno, K. C., Kotaki, T., Yotopranoto, S., Rohmah, E. A., Churotin, S., Sucipto, T. H., et al. (2018). Detection and Serotyping of Dengue Viruses in Aedes aegypti and *Aedes albopictus* (Diptera: Culicidae) Collected in Surabaya, Indonesia From 2008 to 2015. *Jpn. J. Infect. Dis.* 71, 58–61. doi: 10.7883/yoken.JJID.2017.117

Naim, D. M., Kamal, N. Z. M., and Mahboob, S. (2020). Population Structure and Genetic Diversity of *Aedes aegypti* and *Aedes albopictus* in Penang as Revealed by Mitochondrial DNA Cytochrome Oxidase I. *Saudi. J. Biol. Sci.* 27, 953–967. doi: 10.1016/j.sjbs.2020.01.021

Ngoagouni, C., Kamgang, B., Nakouné, E., Paupy, C., and Kazanji, M. (2015). Invasion of *Aedes albopictus* (Diptera: Culicidae) Into Central Africa: What Consequences for Emerging Diseases? *Parasit. Vectors* 8, 191. doi: 10.1186/s13071-015-0808-3

Olson, M. F., Ndeffo-Mbah, M. L., Juarez, J. G., Garcia-Luna, S., Martin, E., Borucki, M. K., et al. (2020). High Rate of non-Human Feeding by *Aedes aegypti* Reduces Zika Virus Transmission in South Texas. *Viruses* 12, 1–20. doi: 10.3390/v12040453

Papadopoulou, A., Anastasiou, I., and Vogler, A. P. (2010). Revisiting the Insect Mitochondrial Molecular Clock: The Mid-Aegean Trench Calibration. *Mol. Biol. Evol.* 27, 1659–1672. doi: 10.1093/molbev/msq051

Parimittr, P., Chareonviriyaphap, T., Bangs, M. J., and Arunyawat, U. (2018). Genetic Variation of *Aedes aegypti* Mosquitoes Across Thailand Based on Nuclear DNA Sequences. *Agric. Nat. Resour.* 52, 596–602. doi: 10.1016/j.anres.2018.11.021

Parra, M. C. P., Fávaro, E. A., Dibo, M. R., Mondini, A., Eiras, Á. E, Kroon, E. G., et al. (2018). Using Adult *Aedes aegypti* Females to Predict Areas at Risk for Dengue Transmission: A Spatial Case-Control Study. *Acta Trop.* 182, 43–53. doi: 10.1016/j.actatropica.2018.02.018

Paupy, C., Delatte, H., Bagny, L., Corbel, V., and Fontenille, D. (2009). *Aedes albopictus*, an Arbovirus Vector: From the Darkness to the Light. *Microbes Infect.* 11, 1177–1185. doi: 10.1016/j.micinf.2009.05.005

Paupy, C., Ollomo, B., Kamgang, B., Moutailler, S., Rousset, D., Demanou, M., et al. (2010). Comparative Role of *Aedes albopictus* and *Aedes aegypti* in the Emergence of Dengue and Chikungunya in Central Africa. *Vector. Borne. Zoonotic. Dis.* 10, 259–266. doi: 10.1089/vbz.2009.0005

Powell, J. R., and Tabachnick, W. J. (2013). History of Domestication and Spread of *Aedes aegypti*–a Review. *Mem. Inst. Oswaldo. Cruz.* 108 (Suppl 1), 11–17. doi: 10.1590/0074-0276130395

Rašić, G., Endersby-Harshman, N., Tantowijoyo, W., Goundar, A., White, V., Yang, Q., et al. (2015). *Aedes aegypti* has Spatially Structured and Seasonally Stable Populations in Yogyakarta, Indonesia. *Parasit. Vectors* 8, 1–12.

Reinhold, J. M., Lazzari, C. R., and Lahondère, C. (2018). Effects of the Environmental Temperature on *Aedes aegypti* and *Aedes albopictus* Mosquitoes: A Review. *Insects* 9, 158. doi: 10.3390/insects9040158

Rezza, G., Nicoletti, L., Angelini, R., Romi, R., Finarelli, A. C., Panning, M., et al. (2007). Infection With Chikungunya Virus in Italy: An Outbreak in a Temperate Region. *Lancet* 370, 1840–1846. doi: 10.1016/S0140-6736(07)61779-6

Ritchie, S. A. (2014). "Dengue Vectors Bionomics : Why *Aedes aegypti* Such a Good Vector," in *Dengue and Dengue Hemorrhagic Fever, 2nd edition*. Eds. D. J. Gubler, E. E. Ooi and J. F. S. Vasudevan (Boston, USA: CAB International), 455–480.

Rozas, J., Ferrer-Mata, A., Sanchez-DelBarrio, J., Guirao-Rico, S., Librado, P., Ramos-Onsins, S., et al. (2017). DnaSP V6: DNA Sequence Polymorphism Analysis of Large Datasets. *Mol. Biol. Evol.* 34, 3299–3302. doi: 10.1093/molbev/msx248

Rueanghiran, C., Apiwathnasorn, C., Sangthong, P., Samung, Y., and Ruangsittichai, J. (2011). Utility of a Set of Conserved Mitochondrial Cytochrome Oxidase Subunit I Gene Primers for *Mansonia Annulata* Identification. *Southeast. Asian J. Trop. Med. Publ. Health* 42, 1381–1387.

Setiati, T. E., Wagenaar, J. F. P., de Kruif, M. D., Mairuhu, A. T. A., Van-gorp, E. C. M., and Soemantri, A. (2006). Changing Epidemiology of Dengue Haemorrhagic Fever in Indonesia. *Dengue. Bull.* 30, 1–14.

Severson, D. W., and Behura, S. K. (2016). Genome Investigations of Vector Competence in *Aedes aegypti* to Inform Novel Arbovirus Disease Control Approaches. *Insects* 7, 58. doi: 10.3390/insects7040058

Simmons, C. P., Farrar, J. J., Nguyen, V. V. C., and Wills, B. (2012). Dengue. *N. Engl. J. Med.* 366, 1423–1432. doi: 10.1056/NEJMra1110265

Tedjou, A. N., Kamgang, B., Yougang, A. P., Njiokou, F., and Wondji, C. S. (2019). Update on the Geographical Distribution and Prevalence of *Aedes aegypti* and *Aedes albopictus* (Diptera: Culicidae), Two Major Arbovirus Vectors in Cameroon. *PloS Negl. Trop. Dis.* 13, e0007137. doi: 10.1371/journal.pntd.0007137

Teixeira, M. G., Costa, M., Barreto, F., and Barreto, M. L. (2009). Dengue: Twenty-Five Years Since Reemergence in Brazil *Cad Saude Publica* 25 (Suppl 1), S7–18. doi: 10.1590/s0102-311x2009001300002

Thiberville, S. D., Moyen, N., Dupuis-Maguiraga, L., Nougairede, A., Gould, E. A., Roques, P., et al. (2013). Chikungunya Fever: Epidemiology, Clinical Syndrome, Pathogenesis and Therapy. *Antiviral Res.* 99, 345–370. doi: 10.1016/j.antiviral.2013.06.009

Thisyakorn, U., and Thisyakorn, C. (2014). Latest Developments and Future Directions in Dengue Vaccines. *Ther. Adv. Vaccines* 2, 3–9. doi: 10.1177/2051013613507862

Urdaneta-Marquez, L., and Failloux, A.-B. (2011). Population Genetic Structure of *Aedes aegypti*, the Principal Vector of Dengue Viruses. *Infect. Genet. Evol.* 11, 253–261. doi: 10.1016/j.meegid.2010.11.020

WHO (2011). *Comprehensive Guidelines for Prevention and Control of Dengue and Dengue Haemorrhagic Fever. Revised Eds* (New Delhi, India: World Health Organization: Regional Office for South-East Asia).

WHO (2016). *Entomological Surveillance for Aedes Spp. In the Context of Zika Virus: Interim Guidance for Entomologist* Vol. 10 (Geneva, Switzerland: World Health Organization).

Wilder-Smith, A., Ooi, E. E., Vasudevan, S. G., and Gubler, D. J. (2010). Update on Dengue: Epidemiology, Virus Evolution, Antiviral Drugs, and Vaccine Development. *Curr. Infect. Dis. Rep.* 12, 157–164. doi: 10.1007/s11908-010-0102-7

Yohan, B., Fauziah, Y., Sayono, S., Trimarsanto, H., and Sasmono, R. T. (2018). Genetic Diversity of *Aedes aegypti* (Diptera: Culicidae) Isolated From Five Cities in North Coast Area of Central Java, Indonesia. *Southeast. Asian J. Trop. Med. Public Health* 49, 217–226.

Conflict of Interest: The authors declare that the research was conducted in the absence of any commercial or financial relationships that could be construed as a potential conflict of interest.

frontiers in Cellular and Infection Microbiology

ORIGINAL RESEARCH
published: 07 July 2021
doi: 10.3389/fcimb.2021.633905

Presence of L1014F Knockdown-Resistance Mutation in *Anopheles gambiae s.s.* From São Tomé and Príncipe

*Hongying Zhang[1,2], Mingqiang Li[1], Ruixiang Tan[1], Changsheng Deng[1,3], Bo Huang[2], Zhibin Wu[3], Shaoqing Zheng[2], Wenfeng Guo[1,3], Fei Tuo[1], Yueming Yuan[2], Carlos Alberto Bandeira[4], D'almeida Herodes Rompão[4], Qin Xu[1,3], Jianping Song[1,3] and Qi Wang[1,3]**

[1] Artemisinin Research Center, Guangzhou University of Chinese Medicine, Guangzhou, China, [2] Science and Technology Institute, Guangzhou University of Chinese Medicine, Guangzhou, China, [3] The Ministry of Health, The First Affiliated Hospital of Guangzhou University of Chinese Medicine, Guangzhou, China, [4] National Malaria Control Programme, São Tomé and Príncipe, Guangzhou, China

OPEN ACCESS

Edited by:
Xiaojun Chen,
Nanjing Medical University, China

Reviewed by:
William Kisinza,
National Institute of Medical Research, Tanzania
Koffi Mensah Ahadji-Dabla,
University of Lomé, Togo

***Correspondence:**
Qi Wang
wangqi2019@gzucm.edu.cn

Specialty section:
This article was submitted to Parasite and Host, a section of the journal Frontiers in Cellular and Infection Microbiology

Received: 26 November 2020
Accepted: 08 June 2021
Published: 07 July 2021

Citation:
Zhang H, Li M, Tan R, Deng C, Huang B, Wu Z, Zheng S, Guo W, Tuo F, Yuan Y, Bandeira CA, Rompão DH, Xu Q, Song J and Wang Q (2021) Presence of L1014F Knockdown-Resistance Mutation in Anopheles gambiae s.s. From São Tomé and Príncipe. Front. Cell. Infect. Microbiol. 11:633905. doi: 10.3389/fcimb.2021.633905

Malaria, one of the most serious parasitic diseases, kills thousands of people every year, especially in Africa. São Tomé and Príncipe are known to have stable transmission of malaria. Indoor residual spraying (IRS) of insecticides and long-lasting insecticidal nets (LLIN) are considered as an effective malaria control interventions in these places. The resistance status of *Anopheles gambiae s.s.* from Agua Grande, Caue, and Lemba of São Tomé and Príncipe to insecticides, such as dichlorodiphenyltrichloroethane (DDT) (4.0%), deltamethrin (0.05%), permethrin (0.75%), fenitrothion (1.0%), and malathion (5.0%), were tested according to the WHO standard protocol. DNA extraction, species identification, as well as *kdr* and *ace-1^R* genotyping were done with the surviving and dead mosquitoes post testing. They showed resistance to cypermethrin with mortality rates ranging from 89.06% to 89.66%. Mosquitoes collected from Agua Grande, Caue, and Lemba displayed resistance to DDT and fenitrothion with mortality rates higher than 90%. No other species were detected in these study localities other than *Anopheles gambiae s.s*. The frequency of L1014F was high in the three investigated sites, which was detected for the first time in São Tomé and Príncipe. No *ace^{-1R}* mutation was detected in all investigated sites. The high frequency of L1014F showed that *kdr* L1014F mutation might be related to insecticide resistance to *Anopheles gambiae s.s.* populations from São Tomé and Príncipe. Insecticide resistance status is alarming and, therefore, future malaria vector management should be seriously considered by the government of São Tomé and Príncipe.

Keywords: malaria, vector control, *Anopheles gambiae*, resistance, *kdr*, *ace^{-1R}*

INTRODUCTION

Malaria, one of the most deadly parasitic diseases, has claimed thousands of people every year worldwide, especially in Africa. In 2019, nearly 229 million cases of malaria occurred worldwide with the high mortality (409,000), of which 80% occurred in sub-Saharan Africa. Malaria is thus a major limiting factor in the socio-economic development of Africa (WHO, 2018c). *Anopheles gambiae s.s.* was the only malaria vector found in São Tomé and Príncipe (Pinto et al., 2000). The country has a suitable climate and rich vegetation which is conducive for mosquito breeding and survival.

In São Tomé and Príncipe, malaria control strategies, such as long-lasting insecticidal nets (LLINs), indoor residual spraying (IRS) of insecticides, are carried out. Furthermore, intermittent preventive therapy treatment (IPT) during pregnancy, early diagnosis, and treatment using artemisinin-based combination therapy (ACT) have also been implemented (Lee et al., 2010b). Indoor residual spraying of insecticides, including dichlorodiphenyltrichloroethane (DDT), malathion, fenitrothion, deltamethrin, and cypermethrin, has been the anti-malarial intervention used. Cypermethrin was the most recommended compounds for IRS and LLINs in these late years as it is a fast-acting and low-toxicity insecticide (Graham et al., 2005). Malaria vector control dominated the anti-malaria measures in the last decade. IRS of insecticides was carried out for the 16th time in October 2019 in São Tomé and Príncipe. The evidence of malaria reduction coupled with IRS was reported in São Tomé and Príncipe (Hagmann et al., 2003; Lee et al., 2010b).

Since 2009, malaria incidence has decreased to less than 1% and morality rate fell to zero with the application of IRS using DDT and pyrethroid insecticides (Lee et al., 2010a). However, in 2018, 2978 malaria cases were reported by the National Malaria Control Programme of São Tomé and Príncipe. These cases increased in a larger extent from 2014 to 2017. Malaria positive rates were: 2.18% in Agua Grande, 1.86% in Lemba, 1.52% in Caue, 1.08% in Cantagalo, 1.01% in Me-Zochi, 0.54% in Lobata, and 0.39% in Príncipe from the database of the National Malaria Control Programme of São Tomé and Príncipe. However, no local malaria cases were found in some villages for more than three consecutive years compared with almost 30% of malaria cases in other villages.

Unfortunately, it was found that many malaria vectors are resistant to dichlorodiphenyltrichloroethane (DDT), deltamethrin, and cypermethrin used in public malaria interventions in Africa (WHO, 2018a). Out of which, resistance to pyrethroids and DDT has been reported in west and central Africa (Djogbenou et al., 2008; Kerah-Hinzoumbe et al., 2008; Moreno et al., 2008; Djegbe et al., 2011; Djogbenou et al., 2011; Namountougou et al., 2012; Aikpon et al., 2013; Nwane et al., 2013; Dery et al., 2016). In São Tomé and Príncipe, *Anopheles gambiae s.s.* mosquito mortality rates were 99% to 100% for carbamates from seven tested sites in 2014 to 2015, which meant *Anopheles gambiae s.s.* were still fully susceptible to carbamates. Target site of *kdr* L1014 had been detected with no reporting of testing for the *kdr* L1014 S in any species, and no *ace-1*^{R} had been detected (WHO, 2018a).

The crucial mechanisms of insecticide resistance are enhanced detoxification and the voltage-gated sodium channel gene, known as knockdown resistance (*kdr*) and insensitive acetylcholinesterase (*ace-1*) gene (Vulule et al., 1999; Hemingway et al., 2004). The sodium channel gene at codon 1014 (1014F, 1014S) with two amino acid changes are related to *kdr* in *Anopheles gambiae s.s.* (Martinez-Torres et al., 1998; Ranson et al., 2000). Consequently, resistance to DDT and pyrethroids is caused by target site mutations (1014F and 1014S), whereas resistance to organophosphates and carbamates caused by *ace-1* results in a single amino acid substitution, changing the position 119, from glycine to serine (Weill et al., 2004).

The increase in malaria cases in São Tomé and Príncipe indicated that the long-term use of insecticides cannot eliminate malaria. This may be because of the acquired resistance in mosquitos to insecticides. Hence, it is necessary to carry out studies on insecticide resistance and its mechanism, which may help the government to control malaria. In this study, insecticide resistance, distribution, and frequency of *kdr* (L1014F, L1014S) mutation of *Anopheles gambiae s.s.* were performed in Agua Grande, Lemba, and Caue counties of São Tomé and Príncipe.

METHODS

Study Sites

Three counties of São Tomé and Príncipe with high malaria positive rates were selected for this study (**Figure 1** and **Table 1**). São Tomé and Príncipe is an island country located near the equator, with a population of 200 thousand inhabitants. It has a tropical rainy climate of hot and humid condition all the year. It is characterized by rainy seasons (January to May and October to December) and one dry season (June to September) with a temperature ranging from 19°C to 30°C. The average rainfall ranges from 1000 to 2500 mm, whereas an average relative humidity ranges from 77% to 85% monthly. Moreover, the large planted surface area provided a favorable breeding condition for mosquitoes.

Adult Mosquito Density Survey

Adult mosquitoes were captured using the human landing catch (HLC) technique in the study counties from 9:00 PM to 2:00 AM by trained agents. At each capture site, two agents took turns during the night (each hour or between the first and the second part of the night). Each agent was equipped with a flashlight, hemolysis tubes, cotton, bags with notes on the capture point (indoor or outdoor), and the time intervals of the capture. An agent must capture the mosquito before the mosquito bites him after landing on his bare legs. In the dark, the agent turned on his flashlight as soon as he feels the mosquito landing on him and captured the mosquito before it bites the hemolysis tube and covers the tube with cotton. Once the tube clogged, the tube was introduced in the bag corresponding to the location and hour of capture. The capture was conducted at each site and at each passage in at least two capture points. At each site, the capture was done two times a week, inside the room/dwelling and outside (veranda). The collectors must rotate from 1 day to the next, depending on the location and the hours of capture. *Anopheles gambiae s.s.* were

FIGURE 1 | The map of São Tomé and Príncipe.

TABLE 1 | Characteristics of study sites.

Localities	Geographic coordinates	Periods of collection
Agua Grande	N 0.33998 E 6.72446	September to December, 2018
Caue	N 0.06685 E 6.53714	September to December, 2018
Lemba	N 0.27986 E 6.50967	September to December, 2018

then counted after identification, and the mosquito density was calculated as "number of mosquitoes/collectors •40 h".

Larva Mosquito Density Survey

Mosquito larva density surveillance was conducted using the ladle method by specific people at specific time (from 8:00 AM to 2:00 PM) and at specific mosquito breeding sites in each county. The surveying team was made up of two experienced technicians. The prospecting of mosquito breeding sites consists of, directly or when needed, taking water from the larval habitats with a ladle in order to search for larvae or nymphs. Water was taken by a ladle 15 times with 1 to 2 min between each take or 15 times with one time each 2-m distance. Take at least 1 L of water, count the number of larvae/nymphs. If the volume of water of the larval habitats is less than 1 L, calculate according to the following formula: the total number of larvae or nymphs/the volume of water (L). Larva density: number of collected larvae and nymphs/total number of take (with ladle).

Mosquito Rearing

Instar larvae of *Anopheles gambiae s.l.* collected from larva density survey was pooled together by locality. The instar larvae of *Anopheles gambiae s.l.* were reared in the insectary of Centre for Disease Control and Prevention of São Tomé and Príncipe under standard conditions of 25 ± 2°C temperature and 80 ± 10% relative humidity (RH).

Insecticide Susceptibility Assays

Three-day-old F_0 female mosquitoes were used for insecticide susceptibility tests. Insecticide bioassays were carried out according to the WHO standard protocol (WHO, 2018b). Insecticides, including DDT (4%), deltamethrin (0.05%), permethrin (0.75%), fenitrothion (1.0%), and malathion (5.0%), were tested at 25 ± 2°C temperature and 70% to 80% relative humidity.

For this, insecticide papers were bought from the Centre for Disease Control and Prevention, China. Approximately 20 to 30 female mosquitoes without blood feeding were selected randomly for each batch, three batches were tested, and exposed to on impregnated paper for 1 h, and mosquitoes knockdown were counted every 10 min. Mosquitoes were then transferred into observation tubes under standard condition and provided with a pad of cotton wool soaked in 10% sugar water (WHO, 2018b). Mosquitoes mortality rates were estimated 24-h post-exposure. Test tubes without insecticide-impregnated papers were taken as a control. Later dead and surviving mosquitoes were transferred to labeled separate Eppendorf tubes and kept at −20°C.

The DNAs from dead and surviving mosquitoes were extracted according to the manufacturer's protocol (TaKaRa, Japan, brought from China) in the laboratory of Centre for Disease Control and Prevention of São Tomé and Príncipe, and then were transferred to the laboratory of Guangzhou University of Chinese Medicine for species identification and resistance mechanism characterization.

Species Identification, *kdr* L1014F, *kdr* L1014S, and *ace-1^R* Genotyping

The PCR was performed to distinguish the species of *Anopheles gambiae* mosquitoes. The screening of *kdr* mutation, L1014F and L1014S by PCR was performed as described by Bass et al. (2007). For PCR, two common primers were used: kdr-F (5′-CATGAT CTGCCAAGATGGAA-3′), kdr-R (5′-GTTGGTGCAGACA AGGATGA-3′) S6 region. The PCR amplification was performed for 35 cycles. It included the first pre-denaturation at 95°C for 3 min, then denaturation at 95°C for 30 s, annealing at 55°C for 30 s, and extension at 72°C for 30 s. Heated for 7 min at 72°C, the refrigerator was set at 4°C. The expected band size of 172 bp distinguished the resistant allele in the sibling species.

The presence of G119S-ace1 allele was screened as previously described (Bass et al., 2010) with primers of ace-1 F (5′-GATCGTGGACACCGTGTTCG-3′) and ace-1 R (5′-AGGATG GCCCGCTGGAACAG-3′). The PCR amplification was performed for 35 cycles. It included the first pre-denaturation at 95°C for 3 min, then denaturation at 95°C for 30 s, annealing at 55°C for 30 s, and extension at 72°C for 30 s. Heated for 7 min at 72°C, the refrigerator was set at 4°C. The band size of 541 bp was expected to distinguish between the resistant allele in the sibling species.

Statistical Analysis

To check the resistance of mosquitoes according to the WHO criteria (WHO, 2018b): susceptibility of the mosquitoes is indicated for mortality rate in range of 98% to 100%.

Suspected resistance of the mosquitoes is indicated for mortality rate between 90% and 97%.

Confirmation of resistant mosquitoes is indicated for mortality rate less than 90%.

The mortality rates of the test samples were calculated by adding the number of dead mosquitoes across all exposure replicates and then expressing this as a percentage of the total number of exposed mosquitoes. The SPSS software version 24.0 was used to calculate the 95% CI mortality rates.

The genotype frequencies of *kdr* and *ace-1^R* were compared between resistant and susceptible mosquitoes using Fisher exact test.

RESULTS

Adult Mosquito Density

Mosquitoes were less abundant in the dry season (June to September), and the highest number of individuals was collected from January to May, corresponding to the rainy season, which provides suitable ecological environment for mosquito breeding.

As shown in **Table 2**, the mosquito density in Agua Grande was quite high, with a monthly value of 26.75 (outdoor) in May. The mosquito density in the study counties showed that the highest mosquito density from January to May and absolutely falling down from June to September.

Larva Mosquito Density

The mosquito larva density was higher in the rainy season (January to May), that could provide suitable ecological environment for mosquito breeding. Few larvae were collected in the dry season (June to September).

As shown in **Table 3**, the mosquito larva density in Agua Grande was higher than other counties, with a monthly value of 4.90 in January and 6.96 in February. The mosquito larva density in the study counties showed that the highest larva density from January to May and absolutely falling down from June to September.

Species Composition of *Anopheles gambiae s.l.*

The species identification was performed by PCR for the F_0 females in *Anopheles gambiae* complex (n=1009) (**Table 5**). It was found that *Anopheles gambiae s.s.* (100%) was the only species of these three study sites.

Insecticide Resistance Status

The insecticide resistance status of *An. gambiae s.s.* collected from different study sites were represented in **Table 4**. It was observed that the pyrethroid-resistant *Anopheles gambiae s.s.* were found in the three study sites with the highest mortality rates were 89.66% [CI (89.54 ± 1.34)] for 0.75% Cypermethrin and 88.57% [CI (89.17 ± 7.40)] for 0.05% Deltamethrin in Lemba. The *Anopheles gambiae s.s.*, resistant to 5% Malathion [89.71%,

TABLE 2 | Adult mosquito density survey in the study sites in 2018.

Month	Adult mosquito density (number of mosquitoes/collectors 40 h)					
	Agua Grande		Lema		Caue	
	Indoor	Outdoor	Indoor	Outdoor	Indoor	Outdoor
January	0.125	6.125	0	0.750	0	4.125
February	0	0.125	0	0	0.375	2.875
March	0	2.375	0	0.875	1.125	9.875
April	0	9.000	0.500	5.750	1.000	6.750
May	0	26.750	0.125	3.125	1.125	5.250
June	0	5.250	0	4.000	1.500	12.750
July	0	1.375	0	4.500	0.750	4.500
August	0	3.875	0	3.375	0.125	5.500
September	0.125	1.875	1.125	6.625	0.375	3.125
October	0	10.000	0	3.870	0.280	2.280
November	0.250	8.870	0	2.420	0.500	3.250
December	0	17.600	2.000	2.250	0	3.160

CI (89.65 ± 2.54)] was also observed in Caue. The mosquitoes were suspected resistant to 4% DDT and 1% Fenitrothion.

Detection of Resistance Genes

DNA was extracted from dead and surviving mosquitoes of insecticide susceptibility assays in every study site for checking *kdr* and *ace-1*^{R}. The *kdr* mutation of *Anopheles gambiae s.s.* only detected one heterozygous mutations type (TTA/TTT): leucine to phenylalanine substitution (L1014F). The mutation frequency of *kdr* (L1014F) and *ace-1*^{R} (G119S) is shown in **Table 5**. The L1014F *kdr* mutation was observed in *Anopheles gambiae s.s.* in all the three study sites with frequencies ranging from 8.33% to 43.75%, and it appeared for the first time in São Tomé and Príncipe. However, no *ace-1*^{R} mutation was detected in *Anopheles gambiae s.s.* in all the three study sites.

DISCUSSION

The study showed that the levels of insecticide resistance in *Anopheles gambiae s.s.* were high in São Tomé and Príncipe with high allelic frequencies. *Anopheles gambiae s.s.* was resistant to DDT and pyrethroids with the allele targeting the voltage-gate sodium channel. Only one species of malaria vector, i.e., *Anopheles gambiae s.s.*, was identified in this study. In this species, *kdr* allele frequencies were high at Agua Grande and Lemba, and for the first time, the high frequency *kdr* mutation of L1014F was detected in São Tomé and Príncipe.

Current status of pyrethroid resistance in *Anopheles gambiae s.s.* can also be provided to the National Malaria Control Programme of São Tomé and Príncipe from the study. The insecticide susceptibility assay results demonstrated a high level of DDT and pyrethroids resistance at study sites. It also suggested that there are many selection pressures on choosing these insecticides. Clément Kerah-Hinzoumbé et al. reported the resistance to permethrin and deltamethrin with varying concentration, and the *kdr* mutation of L1014F appeared as the S form of *Anopheles gambiae* in Chad (Kerah-Hinzoumbe et al., 2008). In Cameroon, the incidence of DDT resistance and the heterogenous levels of susceptibility to deltamethrin and permethrin were extensive in *Anopheles gambiae s.s*, it was demonstrated that, the multiple resistance mechanisms segregate in *Anopheles gambiae* which resulted in the heterogeneous resistance profiles (Nwane et al., 2013). In Cameroon, the insecticide resistance due to DDT, bendiocarb, permethrin, and deltamethrin spread widely in

TABLE 3 | Larva mosquito larva density survey in the study sites in 2018.

Month	Mosquito larva density (number of collected larvae and nymphs/total number of take)		
	Agua Grande	Lema	Caue
January	4.90	1.20	0.42
February	6.96	0.44	0.20
March	0.96	1.97	0.28
April	1.55	1.25	0
May	2.23	2.03	0
June	0.83	1.70	0
July	0	1.73	0
August	0	1.58	0
September	0.33	0.70	0
October	0.88	0.73	1.60
November	0.63	0.74	0.04
December	1.06	1.26	0.72

TABLE 4 | Susceptibility status of *Anopheles gambiae s.s.* collected in the study sites and exposed to the five classes of insecticides.

Insecticides	Study sites	Species	N	Mortality (%)	95%CI	Susceptibility status
4%DDT	Agua Grande	*Anopheles gambiae s.s.*	56	92.86	93.01 ± 2.20	Suspected resistant
	Caue	*Anopheles gambiae s.s.*	60	93.33	93.24 ± 3.26	Suspected resistant
	Lemba	*Anopheles gambiae s.s.*	69	92.75	92.89 ± 1.84	Suspected resistant
0.05% Deltamethrin	Agua Grande	*Anopheles gambiae s.s.*	82	91.46	91.23 ± 3.24	Suspected resistant
	Caue	*Anopheles gambiae s.s.*	78	84.62	85.11 ± 9.58	Resistant
	Lemba	*Anopheles gambiae s.s.*	70	88.57	89.17 ± 7.40	Resistant
0.75% Cypermethrin	Agua Grande	*Anopheles gambiae s.s.*	64	89.06	89.05 ± 2.18	Resistant
	Caue	*Anopheles gambiae s.s.*	57	89.47	89.63 ± 4.18	Resistant
	Lemba	*Anopheles gambiae s.s.*	58	89.66	89.54 ± 1.34	Resistant
1% Fenitrothion	Agua Grande	*Anopheles gambiae s.s.*	73	90.41	90.84 ± 5.01	Suspected resistant
	Caue	*Anopheles gambiae s.s.*	75	92.00	92.35 ± 2.37	Suspected resistant
	Lemba	*Anopheles gambiae s.s.*	66	90.91	91.21 ± 3.11	Suspected resistant
5% Malathion	Agua Grande	*Anopheles gambiae s.s.*	61	91.80	91.92 ± 2.28	Suspected resistant
	Caue	*Anopheles gambiae s.s.*	68	89.71	89.65 ± 2.54	Resistant
	Lemba	*Anopheles gambiae s.s.*	72	93.06	93.18 ± 1.79	Suspected resistant

N, number of mosquitoes; CI, confidence interval.

Anopheles gambiae (s.l.). From 2000 to 2017, the prevalence of *kdr* allele frequency increased steadily in all study sites in *Anopheles gambiae (s.l.)*, with the L1014F *kdr* allele frequency was the most extensive (Antonio-Nkondjio et al., 2017). Furthermore, it was reported that there was some resistance to the insecticides such as pyrethroids and DDT in the Kassena-Nankana district of Ghana in 2009 (Anto et al., 2009). In this study, the results suggested that the increase of pyrethroid resistance was greatly enhanced during last 3 years, which may be due to the selection pressure, such as mass implementation of IRS and mass distribution of LLINs. The continuous application of IRS with the pyrethroid insecticides resulted in the increase of the resistance. Therefore, we observed high frequencies of *kdr* alleles in these study sites. The *kdr* allele dominated in the mechanism of resistance to DDT and pyrethroids in experimental mosquitos.

The resistance of pyrethroid is worrying, and as per our knowledge, it can influence the current vector intervention strategies, such as pyrethroid-only in IRS and LLINs. This target site of *kdr* mutation could be the reason of high resistance to deltamethrin and permethrin in *Anopheles gambiae s.s.* in São Tomé and Príncipe. Further, the L1014S allele related to *Anopheles gambiae s.s.* resistance appeared in Congo in 2013 (Basilua Kanza et al., 2013). Similarly, the pyrethroid resistance related to *kdr* L1014F and *ace*$^{-1R}$ G119S mutation was first reported in Togo (Djegbe et al., 2018).

Here, we found that most of the malaria cases were in Agua Grande with the lowest coverage rate 64.55% of IRS, which indicated that *Anopheles gambiae s.s.* in Agua Grande may be resistant to insecticides used in IRS. From the results of this study, it is necessary to pay attention for the use of insecticides and urge the decision makers (National Malaria Control Programme of São Tomé and Príncipe) for an urgent change of resistance management program.

As we all know, study on the mechanism of Pyrethroids resistance of mosquitoes include two categories: metabolic detoxification and reduced sensitivity of the target.

Other metabolic resistance mechanisms (detoxification genes) particularly P450 monooxygenase and GST, which are primarily associated with DDT, pyrethroids, and bendiocarb resistance are really important. As the lack of the special equipments and reagents for metabolic resistance mechanisms, especially for Sao Tome and Principe, a Low-Middle Income Country, we could not

TABLE 5 | Distribution and Resistant allele frequencies in *Anopheles gambiae s.s. in* study sites from São Tomé and Príncipe.

Insecticides	Study sites	Species	*Bioassay**	N	*kdr* Genotypes		f(L1014F)	*p*	*ace*$^{-1}$ Genotypes		G119S%
					TTA/TTA	TTA/TTT			GGC/GGC	GGC/AGC	
0.75% Cypermethrin	Agua Grande	*Anopheles gambiae s.s.*	Resistant	24	3	21	0.4375	0.000$^{\triangle}$	–	–	–
			Susceptible	24	24	0	0		–	–	–
	Caue	*Anopheles gambiae s.s.*	Resistant	24	20	4	0.0833	0.109$^{\triangle}$	–	–	–
			Susceptible	24	24	0	0		–	–	–
	Lemba	*Anopheles gambiae s.s.*	Resistant	24	9	15	0.3125	0.000$^{\triangle}$	–	–	–
			Susceptible	24	24	0	0		–	–	–
5% Malathion	Agua Grande	*Anopheles gambiae s.s.*	Resistant	24	–	–	–		24	0	0
			Susceptible	24	–	–	–		24	0	0
	Caue	*Anopheles gambiae s.s.*	Resistant	24	–	–	–		24	0	0
			Susceptible	24	–	–	–		24	0	0
	Lemba	*Anopheles gambiae s.s.*	Resistant	24	–	–	–		24	0	0
			Susceptible	24	–	–	–		24	0	0

**"Resistant" refers to the mosquitoes that were alive 24 h after 1-h exposure to the insecticides in the standard WHO tube bioassay; and "susceptible" refers to the mosquitoes that were knocked down within the 24-h recovery period. $^{\triangle}$Fisher Exact test.*

monitor the metabolic resistance mechanisms in the study. However, special equipments and reagents for metabolic resistance mechanisms will be considered to bring into São Tomé and Príncipe for the future work. We found that more research should be needed and designed more rigorously to study the resistance mechanism of mosquitoes and serious intervention malaria programs in São Tomé and Príncipe.

CONCLUSION

This study showed that *Anopheles gambiae s.s.* in São Tomé and Príncipe was resistant to almost all the investigated insecticides. The increase in malaria cases in these years may be related to the resistance allele of L1014F(TTA/TTT) that was identified, representing a serious threat. Therefore, it is necessary to devise a malaria vector control strategy in Sao Tome and Principe urgently. The combined role of the mosquito resistance mechanism provides a scientific basis for local mosquito vector interventions in São Tomé and Príncipe.

DATA AVAILABILITY STATEMENT

The original contributions presented in the study are included in the article/supplementary material. Further inquiries can be directed to the corresponding author.

AUTHOR CONTRIBUTIONS

QW and JS designed, organized, and supervised the program. HZ and QW designed the study protocol, analyzed data, and wrote the manuscript. ML, RT, SZ, FT, WG, CB, and DR helped carry out the field work. BH and YY performed molecular and biochemical analyses. CD and QX revised the manuscript. All authors contributed to the article and approved the submitted version.

FUNDING

This work was supported by Natural Science Foundation of China [Grant Number 81873218] to JS and QW, Natural Science Foundation of China [Grant Number 82074301] to CD, Guangdong Provincial Science and Technology Plan Project [Grant Number 2020A0505090009] to QW and YY, Guangdong Provincial Science and Technology Plan Project [Grant Number 2021A0505030060] to JS, and Project of Traditional Chinese Medicine Bureau [Grant Number GZYYGJ2020030] to JS and CD. The funders had no role in study design, data collection and analysis, decision to publish, or preparation of the manuscript.

ACKNOWLEDGMENTS

The authors are grateful to the staff of the sentinel sites, especially Hongyan Zhou, Guozhuang Shi, and Xun Wang for their collaboration. The authors also thank the staff of the National Malaria Control Programme of São Tomé and Príncipe, the members of the Malaria Technical Committee.

REFERENCES

Aikpon, R., Agossa, F., Osse, R., Oussou, O., Aizoun, N., Oke-Agbo, F., et al. (2013). Bendiocarb Resistance in Anopheles Gambiae s.l. Populations From Atacora Department in Benin, West Africa: A Threat for Malaria Vector Control. *Parasit. Vectors* 6, 192. doi: 10.1186/1756-3305-6-192

Anto, F., Asoala, V., Anyorigiya, T., Oduro, A., Adjuik, M., Owusu-Agyei, S., et al. (2009). Insecticide Resistance Profiles for Malaria Vectors in the Kassena-Nankana District of Ghana. *Malar. J.* 8, 81. doi: 10.1186/1475-2875-8-81

Antonio-Nkondjio, C., Sonhafouo-Chiana, N., Ngadjeu, C. S., Doumbe-Belisse, P., Talipouo, A., Djamouko-Djonkam, L., et al. (2017). Review of the Evolution of Insecticide Resistance in Main Malaria Vectors in Cameroon From 1990 to 2017. *Parasit. Vectors* 10, 472. doi: 10.1186/s13071-017-2417-9

Basilua Kanza, J. P., El Fahime, E., Alaoui, S., Essassi El, M., Brooke, B., Nkebolo Malafu, A., et al. (2013). Pyrethroid, DDT and Malathion Resistance in the Malaria Vector Anopheles Gambiae From the Democratic Republic of Congo. *Trans. R. Soc. Trop. Med. Hyg.* 107, 8–14. doi: 10.1093/trstmh/trs002

Bass, C., Nikou, D., Donnelly, M. J., Williamson, M. S., Ranson, H., Ball, A., et al. (2007). Detection of Knockdown Resistance (Kdr) Mutations in Anopheles Gambiae: A Comparison of Two New High-Throughput Assays With Existing Methods. *Malaria J.* 6, 111. doi: 10.1186/1475-2875-6-111

Bass, C., Nikou, D., Vontas, J., Williamson, M. S., and Field, L. M. (2010). Development of High-Throughput Real-Time PCR Assays for the Identification of Insensitive Acetylcholinesterase (Ace-1(R)) in Anopheles Gambiae. *Pestic. Biochem. Physiol.* 96, 80–85. doi: 10.1016/j.pestbp.2009.09.004

Dery, D. B., Segbaya, S., Asoalla, V., Amoyaw, F., Amoako, N., Agyeman-Budu, A., et al. (2016). Anopheles Gambiae (Diptera: Culicidae) Susceptibility to Insecticides and Knockdown Resistance Genes Prior to Introduction of Indoor Residual Spraying in 11 Districts in Ghana. *J. Med. Entomol.* 53, 1403–1409. doi: 10.1093/jme/tjw098

Djegbe, I., Akoton, R., Tchigossou, G., Ahadji-Dabla, K. M., Atoyebi, S. M., Adeoti, R., et al. (2018). First Report of the Presence of L1014S Knockdown-Resistance Mutation in Anopheles Gambiae s.s and Anopheles Coluzzii From Togo, West Africa. *Wellcome Open Res.* 3, 30. doi: 10.12688/wellcomeopenres.13888.1

Djegbe, I., Boussari, O., Sidick, A., Martin, T., Ranson, H., Chandre, F., et al. (2011). Dynamics of Insecticide Resistance in Malaria Vectors in Benin: First Evidence of the Presence of L1014S Kdr Mutation in Anopheles Gambiae From West Africa. *Malaria J.* 10, 261. doi: 10.1186/1475-2875-10-261

Djogbenou, L., Dabire, R., Diabate, A., Kengne, P., Akogbeto, M., Hougard, J. M., et al. (2008). Identification and Geographic Distribution of the ACE-1R Mutation in the Malaria Vector Anopheles Gambiae in South-Western Burkina Faso, West Africa. *Am. J. Trop. Med. Hyg.* 78, 298–302. doi: 10.4269/ajtmh.2008.78.298

Djogbenou, L., Pasteur, N., Akogbeto, M., Weill, M., and Chandre, F. (2011). Insecticide Resistance in the Anopheles Gambiae Complex in Benin: A Nationwide Survey. *Med. Vet. Entomol.* 25, 256–267. doi: 10.1111/j.1365-2915.2010.00925.x

Graham, K., Kayedi, M. H., Maxwell, C., Kaur, H., Rehman, H., Malima, R., et al. (2005). Multi-Country Field Trials Comparing Wash-Resistance of PermaNet and Conventional Insecticide-Treated Nets Against Anopheline and Culicine Mosquitoes. *Med. Vet. Entomol.* 19, 72–83. doi: 10.1111/j.0269-283X.2005.00543.x

Hagmann, R., Charlwood, J. D., Gil, V., Ferreira, C., Do Rosario, V., and Smith, T. A. (2003). Malaria and its Possible Control on the Island of Principe. *Malaria J.* 2, 15. doi: 10.1186/1475-2875-2-15

Hemingway, J., Hawkes, N. J., Mccarroll, L., and Ranson, H. (2004). The Molecular Basis of Insecticide Resistance in Mosquitoes. *Insect Biochem. Mol. Biol.* 34, 653–665. doi: 10.1016/j.ibmb.2004.03.018

Kerah-Hinzoumbe, C., Peka, M., Nwane, P., Donan-Gouni, I., Etang, J., Same-Ekobo, A., et al. (2008). Insecticide Resistance in Anopheles Gambiae From South-Western Chad, Central Africa. *Malar. J.* 7, 192. doi: 10.1186/1475-2875-7-192

Lee, P. W., Liu, C. T., Do Rosario, V. E., De Sousa, B., Rampao, H. S., and Shaio, M. F. (2010a). Potential Threat of Malaria Epidemics in a Low Transmission Area, as Exemplified by Sao Tome and Principe. *Malar. J.* 9, 264. doi: 10.1186/1475-2875-9-264

Lee, P. W., Liu, C. T., Rampao, H. S., Do Rosario, V. E., and Shaio, M. F. (2010b). Pre-Elimination of Malaria on the Island of Principe. *Malar. J.* 9, 26. doi: 10.1186/1475-2875-9-26

Martinez-Torres, D., Chandre, F., Williamson, M. S., Darriet, F., Berge, J. B., Devonshire, A. L., et al. (1998). Molecular Characterization of Pyrethroid Knockdown Resistance (Kdr) in the Major Malaria Vector Anopheles Gambiae S.S. *Insect Mol. Biol.* 7, 179–184. doi: 10.1046/j.1365-2583.1998.72062.x

Moreno, M., Vicente, J. L., Cano, J., Berzosa, P. J., De Lucio, A., Nzambo, S., et al. (2008). Knockdown Resistance Mutations (Kdr) and Insecticide Susceptibility to DDT and Pyrethroids in Anopheles Gambiae From Equatorial Guinea. *Trop. Med. Int. Health* 13, 430–433. doi: 10.1111/j.1365-3156.2008.02010.x

Namountougou, M., Simard, F., Baldet, T., Diabate, A., Ouedraogo, J. B., Martin, T., et al. (2012). Multiple Insecticide Resistance in Anopheles Gambiae s.l. Populations From Burkina Faso, West Africa. *PloS One* 7 (11), e48412. doi: 10.1371/journal.pone.0048412

Nwane, P., Etang, J., Chouasmall Yi, U. M., Toto, J. C., Koffi, A., Mimpfoundi, R., et al. (2013). Multiple Insecticide Resistance Mechanisms in Anopheles Gambiae s.l. Populations From Cameroon, Central Africa. *Parasit. Vectors* 6, 41. doi: 10.1186/1756-3305-6-41

Pinto, J., Sousa, C. A., Gil, V., Ferreira, C., Goncalves, L., Lopes, D., et al. (2000). Malaria in Sao Tome and Principe: Parasite Prevalences and Vector Densities. *Acta Trop.* 76, 185–193. doi: 10.1016/S0001-706X(00)00100-5

Ranson, H., Jensen, B., Vulule, J. M., Wang, X., Hemingway, J., and Collins, F. H. (2000). Identification of a Point Mutation in the Voltage-Gated Sodium Channel Gene of Kenyan Anopheles Gambiae Associated With Resistance to DDT and Pyrethroids. *Insect Mol. Biol.* 9, 491–497. doi: 10.1046/j.1365-2583.2000.00209.x

Vulule, J. M., Beach, R. F., Atieli, F. K., Mcallister, J. C., Brogdon, W. G., Roberts, J. M., et al. (1999). Elevated Oxidase and Esterase Levels Associated With Permethrin Tolerance in Anopheles Gambiae From Kenyan Villages Using Permethrin-Impregnated Nets. *Med. Vet. Entomol.* 13, 239–244. doi: 10.1046/j.1365-2915.1999.00177.x

Weill, M., Malcolm, C., Chandre, F., Mogensen, K., Berthomieu, A., Marquine, M., et al. (2004). The Unique Mutation in Ace-1 Giving High Insecticide Resistance Is Easily Detectable in Mosquito Vectors. *Insect Mol. Biol.* 13, 1–7. doi: 10.1111/j.1365-2583.2004.00452.x

Who. (2018a). *Global Report on Insecticide Resistance in Malaria Vectors: 2010-2016*. (Geneva: World Health Organization).

Who. (2018b). *Test Procedures for Insecticide Resistance Monitoring in Malaria Vector Mosquitoes, 2nd ed.* (Geneva: World Health Organization).

Who. (2018c). *World Malaria Report 2018*. (Geneva: World Health Organization).

Conflict of Interest: The authors declare that the research was conducted in the absence of any commercial or financial relationships that could be construed as a potential conflict of interest.

frontiers in Cellular and Infection Microbiology

ORIGINAL RESEARCH
published: 19 August 2021
doi: 10.3389/fcimb.2021.666469

Molecular Detection of Insecticide Resistance Mutations in *Anopheles gambiae* from Sierra Leone Using Multiplex SNaPshot and Sequencing

Jianhai Yin[1], Frederick Yamba[2], Canjun Zheng[3], Shuisen Zhou[1], Samuel Juana Smith[2], Lili Wang[4], Hongmei Li[1], Zhigui Xia[1] and Ning Xiao[1]**

[1] National Institute of Parasitic Diseases, Chinese Center for Disease Control and Prevention; Chinese Center for Tropical Diseases Research; WHO Collaborating Centre for Tropical Diseases; National Center for International Research on Tropical Diseases, Ministry of Science and Technology; Key Laboratory of Parasite and Vector Biology, Ministry of Health, Shanghai, China, [2] National Malaria Control Program, Ministry of Health and Sanitation, Freetown, Sierra Leone, [3] Division of Infectious Diseases, Chinese Center for Disease Control and Prevention, Beijing, China, [4] Center for Global Public Health, Chinese Center for Disease Control and Prevention, Beijing, China

OPEN ACCESS

Edited by:
Xiaojun Chen,
Nanjing Medical University, China

Reviewed by:
Isabel Mauricio,
New University of Lisbon, Portugal
Mqoqing Gong,
Shandong Institute of Parasitic Diseases, China

***Correspondence:**
Ning Xiao
xiaoning@nipd.chinacdc.cn
Samuel Juana Smith
samueljuana@yahoo.com

Specialty section:
This article was submitted to Parasite and Host, a section of the journal Frontiers in Cellular and Infection Microbiology

Received: *10 February 2021*
Accepted: *05 August 2021*
Published: *19 August 2021*

Citation:
Yin J, Yamba F, Zheng C, Zhou S, Smith SJ, Wang L, Li H, Xia Z and Xiao N (2021) Molecular Detection of Insecticide Resistance Mutations in Anopheles gambiae from Sierra Leone Using Multiplex SNaPshot and Sequencing. Front. Cell. Infect. Microbiol. 11:666469. doi: 10.3389/fcimb.2021.666469

Vector control interventions including long-lasting insecticidal nets and indoor residual spraying are important for malaria control and elimination. And effectiveness of these interventions depends entirely on the high level of susceptibility of malaria vectors to insecticides. However, the insecticide resistance in majority of mosquito vector species across African countries is a serious threat to the success of vector control efforts with the extensive use of insecticides, while no data on insecticide resistance was reported from Sierra Leone in the past decade. In the present study, the polymerase chain reaction was applied for the identification of species of 757 dry adult female *Anopheles gambiae* mosquitoes reared from larvae collected from four districts in Sierra Leone during May and June 2018. And the mutations of *kdr*, *rdl*, *ace-1* genes in *An. gambiae* were detected using SNaPshot and sequencing. As a result, one sample from Western Area Rural district belonged to *Anopheles melas*, and 748 *An. gambiae* were identified. Furthermore, the *rdl* mutations, *kdr* west mutations and *ace-1* mutation were found. The overall frequency was 35.7%, 0.3%, 97.6% and 4.5% in A296G *rdl*, A296S *rdl*, *kdrW* and *ace-1*, respectively. The frequencies of A296G *rdl* mutation ($P < 0.001$), *kdrW* mutation ($P = 0.001$) and *ace-1* mutation ($P < 0.001$) were unevenly distributed in four districts, respectively, while no statistical significance was found in A296S *rdl* mutation ($P = 0.868$). In addition, multiple resistance patterns were also found. In conclusion, multiple mutations involved in insecticide resistance in *An. gambiae* populations in Sierra Leone were detected in the *kdrW*, A296G *rdl* and *ace-1* alleles in the present study. It is necessary to monitor vector susceptibility levels to insecticides used in this country, and update the insecticide resistance monitoring and management strategy.

Keywords: Multiple insecticide resistance, *Anopheles gambiae*, *kdr*, SNaPshot, Sierra Leone, *rdl*, *ace-1*

INTRODUCTION

Malaria is one of the most widespread infectious diseases globally, with a major burden causing the death of more than 400,000 people yearly in the past three years, most of them were reported in the WHO African Region and children aged under five years (WHO, 2018; WHO, 2019; WHO, 2020). Sierra Leone is an area of stable malaria endemicity. The high malaria disease burden in this country accounted for approximately 48% of outpatient morbidity and approximately 38% of mortality in children under five years according to the national Malaria Indicator Survey 2016 (National Malaria Control Programme (NMCP) et al., 2016).

Vector control is an essential component of malaria control and elimination. At present, long-lasting insecticidal nets and indoor residual spraying are still two core interventions for malaria vector control. The effectiveness of these interventions depends entirely on the high level of susceptibility of malaria vectors to the insecticides. However, the insecticide resistance in majority of mosquito vector species across African countries is a serious threat to the success of vector control efforts with the extensive use of insecticides (https://anopheles.irmapper.com/).

Target-site resistance is one of the most main mechanisms of insecticide resistance. Alterations in the target sites can reduce sensitivity of the target receptors to insecticide. Four main chemical classes (organochlorines, organophosphates, carbamates, and pyrethroids) are used in the vector control, and only pyrethroids are for use on nets. Moreover, mutations in the *ace-1* gene encoding the target site of acetylcholinesterase (AChE) for organophosphate and carbamate insecticides (Weill et al., 2003; Weill et al., 2004; Fournier, 2005; Djogbenou et al., 2008), the *rdl* (resistance to dieldrin) gene (Ffrench-Constant, 1994; Du et al., 2005), and the amino acid sequence in the voltage-gated sodium channel referred to as knockdown resistance (*kdr*) (resistance to DDT and pyrethroids) (Martinez Torres et al., 1998; Ranson et al., 2000; Davies et al., 2007; Donnelly et al., 2009), have been found in *Anopheles gambiae*, which is a main malaria vector in Africa. For example, pyrethroid resistance is high in *An. gambiae* in West Africa including Benin, Burkina Faso, Ghana, Mali, Nigeria, etc. (Vincent and N'Guessan, 2013), while no data was reported from Sierra Leone in the past decade.

Moreover, strategies for insecticide resistance management in vector control must be implemented on the basis of local epidemiological and entomological data. Hence, bioassays using WHO defined diagnostic doses of insecticide, dose response bioassays, biochemical assays to detect activity of enzymes associated with insecticide resistance, and molecular assays to detect known resistance alleles, have been developed to facilitate the implementation of vector control interventions (Ranson et al., 2011; Vincent and N'Guessan, 2013). Among them, the molecular assays are very sensitive, and they can detect resistant alleles at low frequencies at an early stage of resistance development, which, therefore, provide an early warning of future resistance.

In addition, the World Health Organization (WHO) supported the Sierra Leone National Malaria Control Program (NMCP) to develop an Insecticide Resistance Monitoring and Management Program (IRMMP) 2017-2020 to conduct insecticide resistance monitoring in the four pilot districts - Bo, Bombali, Kono and Western Area Rural district, in order to maintain the effectiveness of existing insecticidal vector control interventions, adhering to the existing malaria strategic plan and linking with other specific implementation documents of the NMCP and the Ministry of Health and Sanitation (MOHS), Sierra Leone.

In this study, molecular detection of mutations in the three genes of *ace-1*, *rdl* and *kdr* were performed to understand the insecticide resistance of the female *An. gambiae* to the four classes of insecticides recommended by WHO for vector control especially the pyrethroids in Sierra Leone.

MATERIALS AND METHODS

Sample Source and PCR-Species Identification

Adult female *Anopheles gambiae* mosquitoes were stored in the 1.5 ml Eppendorf tubes with cottons and silico gels (one mosquito per tube). They were reared from larvae, which were collected from natural breeding water bodies in Kayangba community from Bo district, Magbema community from Bombali district, Lebanon community from Kono district, and Bolima community from Western Area Rural district, respectively, during May and June 2018. And these four districts were selected into a four-year insecticide resistance monitoring and management program (2017-2020) which was supported by WHO to the National Malaria Control Program, Sierra Leone. Upon collection, larvae were kept in separate labelled buckets, transported to the insectary and maintained under optimal condition for mosquitoes rearing.

All adult females used for molecular characterization were morphologically identified as belonging to the *An. gambiae* complex. Genomic DNA was extracted from one mosquito respectively using the Qiagen DNA Mini Kit (Qiagen, Germany) according to the manufacturer's instruction. The identification of single specimens of the *An. gambiae* complex was performed by a PCR (Scott et al., 1993).

Multiplex PCR Amplification of Multiple Insecticide Resistance Genes

Three pairs of primers to detect *kdr* west and *kdr* east mutation, *rdl* Ala296Gly and *rdl* Ala296Ser mutation, and *ace-1* G119S mutation were used (**Table 1**) (Bass et al., 2007; Bass et al., 2015a; Bass et al., 2015b). Multiplex PCR was performed in a volume of 20 μl containing 1x GC-I buffer (Takara, Japan), 3.0 mM Mg2+ (Takara, Japan), 0.3 mM dNTP (Generay Biotech, Shanghai), 1 U Hot Star Taq polymerase (Qiagen, Germany), 1 μl of template DNA and 1 μl of primers (Sangon Biotech, Shanghai) (**Table 1**). Thermal cycler conditions were: 95°C for 2 min; 11 cycles of 94°C

TABLE 1 | Multiplex PCR primers for detection of multiple insecticide resistance genes in *An. gambiae*.

Locus	Primer	Sequence (5′→3′)	Concentration (μM)	PCR Length (bp)	Reference
ace-1	ace-1-F	GGCCGTCATGCTGTGGAT	1.5	50	Bass et al., 2015a
	ace-1-R	TGGCGGTGCCGGAGTAGA			
kdrE/kdrW	kdr-F	CATTTTTCTTGGCCACTGTAGTGAT	1	71	Bass et al., 2007
	kdr-R	CGATCTTGGTCCATGTTAATTTGCA			
A296S/A296G	rdl-F	TCATATCGTGGGTATCATTTTGGCT	1	98	
	rdl-R	CGACATCAGTGTTGTCATTGTCAAG			Bass et al., 2015b

for 20 s, 65°C for 40 s, and 72°C for 1.5 min; 24 cycles of 94°C for 20 s, 59°C for 30 s, and 72°C for 1.5 min; and finally 2 min at 72°C. Multiplex PCR products were separated by electrophoresis on 2% agarose gels stained with ethidium bromide (Sangon Biotech, Shanghai). The remaining PCR products were purified with 5 units of shrimp alkaline phosphatase (SAP) (Promega, USA) and 2 units of exonuclease I (EXO I) (Epicentre, USA) at 37°C for 1 h and 75°C for 15 min, to remove excess dNTPs and primers, respectively.

SNaPshot Single Nucleotide Extension Reaction Assay and Sequencing

SNaPshot extension primers for detection of *kdr* west (L1014F) and *kdr* east (L1014S) mutations, A296G *rdl* (Ala-Gly) and A296S *rdl* (A296S) mutations, and G119S *ace-1* (Gly-Ser) mutation were designed (**Table 2**) to anneal on the sense strand immediately adjacent to the mutation site. Each extension primer was synthesized with a different length of poly (dT) tail to allow separation of SNaPshot products on the basis of size. SNaPshot analysis was performed using an Applied Biosystems SNaPshot Multiplex Kit (Applied Biosystems Co., Ltd., USA). Extension reactions were performed in a volume of 10 μl containing 5 μl of SNaPshot Ready Multiplex Ready Reaction Mix, 1 μl of extension primer mix (**Table 2**) and 2 μl of ddH_2o. Thermal cycler conditions were: 96°C for 1 min; 28 cycles of 96°C for 10 s, 50°C for 5 s, and 60°C for 30 s. Each 10 μl of extension products were purified with 1 unit of SAP at 37°C for 1 h and 75°C for 15 min. Then, 0.5 μl of the purified extension products were mixed with 0.5 μl of Liz120 size standard, and 9 μl of Hi-Di™ formamide, and were denatured at 95°C for 5 minutes then sequenced using ABI3730XL. Analysis was performed using GeneMapper 4.1 (Applied Biosystems Co., Ltd., USA).

Data Statistics

Data was entered in Microsoft Excel 2010 and analyzed using IBM SPSS Statistic 20. Frequency counts for mutations of insecticide resistance genes in mosquitoes from different districts were compared using Pearson Chi-Square test or Fisher's exact test performed at 0.05 level of significance.

RESULTS

Sample Composition

A total of 757 adult anopheline mosquitoes reared from larvae were analyzed in the present study. In detail, 271, 253, 112, and 121 mosquitoes were from Kayangba community, Magbema community, Lebanon community, and Bolima community, respectively.

Moreover, a total of 8 samples from Kayangba (1), Magbema (1), and Bolima (6) were detected as negative results of the *An. gambiae* complex by PCR (Scott et al., 1993), and one sample belonged to *Anopheles melas*, the remaining 748 samples were *An. gambiae* (**Table 3**).

TABLE 2 | SNaPshot extension primers for the detection of multiple insecticide resistance genes mutations in *An. gambiae*.

Locus	Probe	Sequence (5′→3′)	Concentration (μM)
ace-1	ace-1-SR	TTTTCGGTGCCGGAGTAGAAGC	1.6
kdrE	kdrE-SF	TTTTTTTGGCCACTGTAGTGATAGGAAATT	0.8
A296G	A296G-SR	TTTTTTTTTTTTCATTGTCAAGACAGTAGTTACACCTAAT	0.8
kdrW	kdrW-SR	TTTTTTTTTTTTTTTTTTTCCATGTTAATTTGCATTACTTACGAC	0.8
A296S	A296S-SF	TTTTTTTTTTTTTTTTTTTTTTTTTTTTTTTTAAATGCTACACCAGCACGTGTT	1.6

TABLE 3 | PCR authentication for the members of the *An. gambiae* complex.

Community	*An. gambiae*	*An. melas*	Negative	Total
Kayangba (Bo)	270	0	1	271
Magbema (Bombali)	252	0	1	253
Lebanon (Kono)	112	0	0	112
Bolima (Western Area Rural)	114	1	6	121
Total	748	1	8	757

Mutations of Multiple Insecticide Resistance Genes

A total of 748 adult *An. gambiae* were analyzed for presence of the *rdl* mutations, *kdr* mutations and G119S *ace-1* mutation (**Table 4**). A296G *rdl* mutation, *kdrW* mutation and *ace-1* mutation were identified at all 4 geographical sites, while A296S *rdl* mutation was only found in the samples from Kayangba and Magbema communities, and no *kdrE* mutation was found at all 4 sites. The overall mutation frequency was 35.7%, 0.3%, 0.0%, 97.6% and 4.5% in A296G *rdl*, A296S *rdl*, *kdrE*, *kdrW* and *ace-1*, respectively (**Table 4**). Moreover, the frequencies of A296G *rdl* mutation (χ^2 = 377.148, *df* = 3, $P < 0.001$), *kdrW* mutation (Fisher's exact test, $P = 0.001$) and *ace-1* mutation (χ^2 = 42.989, *df* = 3, $P < 0.001$) were significantly different among four districts, respectively, while no statistical significance was found in A296S *rdl* mutation (Fisher's exact test, $P = 0.868$). In addition, there were 12 types of allelic combinations totally including the sites that test failed, and a simple homozygous resistant mutation of *kdrW* (319), or combined homozygous resistant mutation of A296G *rdl* (174), or combined heterozygous mutation of A296G *rdl* (154), were the three most common combinations (**Table 5**). And four samples are provided as examples to show the results of sequencing (**Figure 1**).

DISCUSSION

This study has analyzed the species composition in the *An. gambiae* complex and the mutations of the multiple insecticide resistance genes in *An. gambiae* in Sierra Leone, 2018. Adult female mosquitoes were reared from larvae, which were collected from several identified water bodies in four pilot districts for insecticide resistance monitoring in Sierra Leone. And only *An. gambiae* (99.9%, 748/749) and *An. melas* (0.1%, 1/749) were characterized in the present study, which is consistent with Sierra Leone's records on the species distribution of *An. gambiae* complex (National Malaria Control Programme, 2015).

Key to the success of malaria control and elimination is a strategic plan on malaria vector control informed by comprehensive monitoring and evaluation of insecticide resistance, this is becoming more important as insecticide resistance increases and spreads across Africa, but there was absence of insecticide resistance monitoring and entomological work in general in the presence of large scale use of insecticides for malaria control in Sierra Leone. Therefore, it is necessary to carry out work in this area to promote the malaria control and elimination in this country.

Currently most resistance monitoring is dependent on bioassays which detect resistance under defined insecticide concentrations and exposure times recommended by WHO, but these methods require large numbers of alive mosquitoes and lack sensitivity (Ranson et al., 2011; Vincent and N'Guessan, 2013). And several alternative methods for detecting resistance have been developed, especially molecular tests based on DNA providing an early warning of emergence of the resistance are available for target sites with high sensitivity, although they are just a complement rather than a substitute for bioassays. And

TABLE 4 | Genotypes of multiple insecticide resistance genes and their mutation frequency in the *An. gambiae*.

Community	A296G			F	A296S			F	*kdrE*				F	*kdrW*				F	*ace-1*				F
	RR	RS	SS		RR	RS	SS		RR	RS	SS	Failed		RR	RS	SS	Failed		RR	RS	SS	Failed	
Kayangba	178	81	11	0.809	0	1	269	0.002	0	0	270	0	0.000	270	0	0	0	1.000	0	7	263	0	0.013
Magbema	0	38	214	0.075	0	3	249	0.006	0	0	250	2#	0.000	227	23	0	2#	0.946	0	7	244	1#	0.014
Lebanon	1	28	83	0.134	0	0	112	0.000	0	0	112	0	0.000	108	4	0	0	0.982	0	20	92		0.089
Bolima	4	21	89	0.127	0	0	114	0.000	0	0	112	2*	0.000	111	1	0	2*	0.978	2	29	82	1*	0.145
Total	183	168	397	0.357	0	4	744	0.003	0	0	744	4	0.000	716	28	0	4	0.976	2	63	681	2	0.045

RR, homozygous resistant; RS, heterozygous; SS, homozygous susceptible; F, frequency.
*# and * indicates that the failed samples are the same samples.*

TABLE 5 | The mutations of the multiple insecticide resistance genes in *An. gambiae* from communities.

Allelic combination					Number of mosquitoes detected				Total
A296G *rdl*	A296S *rdl*	*kdrE*	*kdrW*	G119S *ace-1*	Kayangba	Magbema	Lebanon	Bolima	
C/C	G/G	T/T	T/T	G/G	10	181	68	60	319
C/C	G/G	T/T	T/T	G/A	0	5	11	25	41
C/C	G/G	T/T	T/A	G/G	0	23	4	1	28
C/C	G/G	T/T	T/T	A/A	0	0	0	1	1
C/C	G/T	T/T	T/T	G/G	1	3	0	0	4
C/C	G/G	Failed	Failed	Failed	0	1	0	1	2
C/C	G/G	Failed	Failed	G/G	0	1	0	1	2
C/G	G/G	T/T	T/T	G/A	1	2	8	3	14
C/G	G/G	T/T	T/T	G/G	80	36	20	18	154
G/G	G/G	T/T	T/T	G/A	6	0	1	1	8
G/G	G/G	T/T	T/T	G/G	172	0	0	2	174
G/G	G/G	T/T	T/T	A/A	0	0	0	1	1

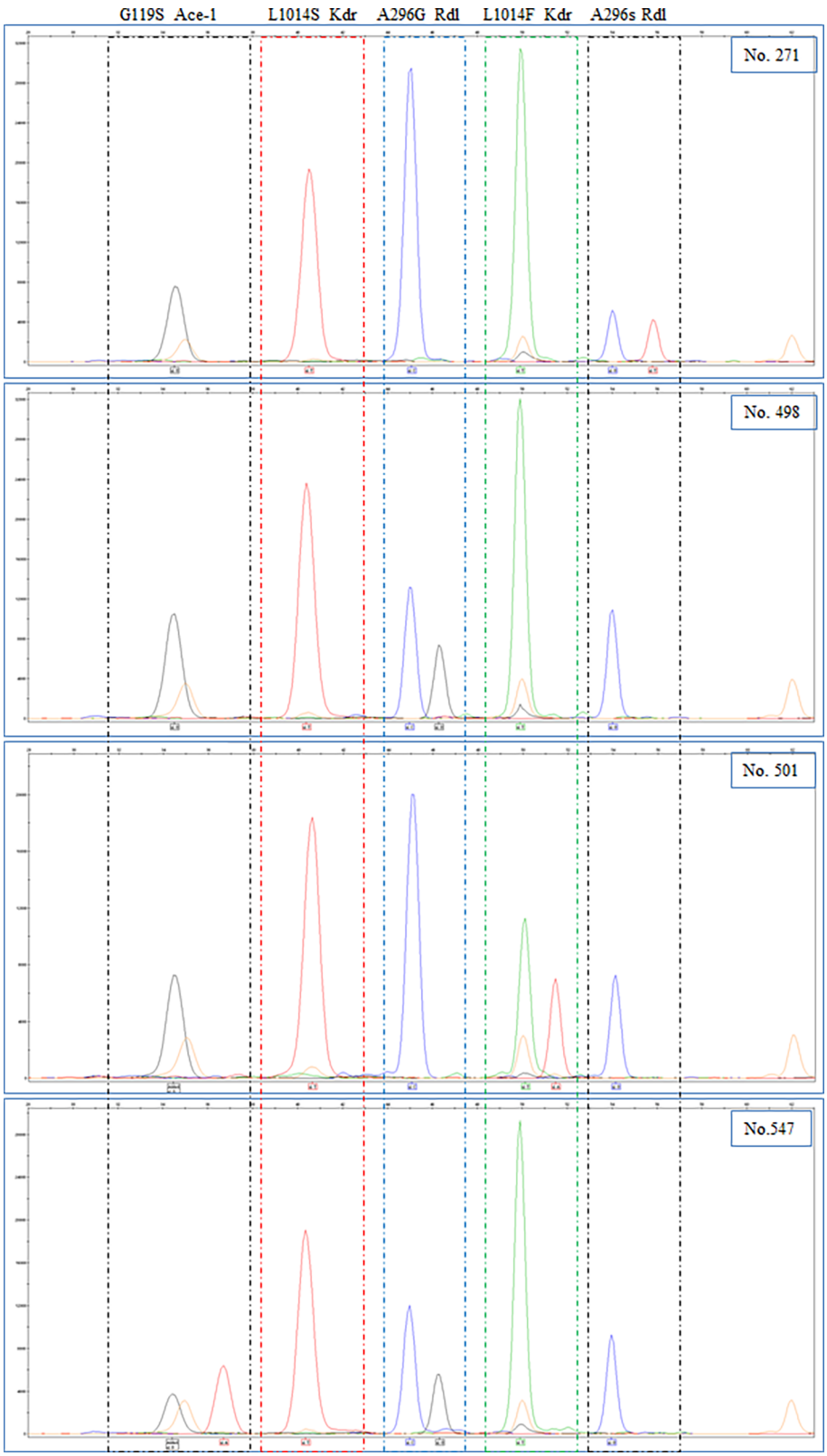

FIGURE 1 | Electropherograms of genscan analysis of the SNaPshot reaction and alleles were indicated at the bottom. (Blue peak: G; Black peak: C; Green peak: A; Red peak: T; Orange peak: size standard).

PCR or an intentional mismatched primer - PCR (IMP - PCR) followed by agarose gel electrophresis, or real - time TaqMan assays have typically been applied to the characterization of allelic mutations of the single insecticide resistance genes, respectively (Bass et al., 2010; Donnelly et al., 2016; Mavridis et al., 2018). Although reliable, these are time consuming with large numbers of samples for detection of multiple resistance mutations. The SNaPshot method used in the present study offers a specific, sensitive, inexpensive and rapid alternative to the simultaneous screening for multiple mutations and subsequent confirmation by sequencing (Quintans et al., 2004; Alina et al., 2005; Fondevila et al., 2017). This method has been extensively used in the blood group typing (Palacajornsuk et al., 2009; Latini et al., 2014; Chen et al., 2019) and common mutations in genes related to some cancers (Filippini et al., 2007; Hurst et al., 2009; Fariña Sarasqueta et al., 2011).

With regard to the frequency of mutations, a high mutation frequency of *kdrW* (97.6%) was found totally and most of them were homozygous (**Table 4**), and distributed in all four pilot sites. It supports the findings that pyrethroid resistance is predominant in *An. gambiae s.s.* in West Africa (Vincent and N'Guessan, 2013). Moreover, the *kdrW* mutation combined with one to two mutations at other three sites (A296G *rdl*, A296S *rdl*, *ace-1*) were found (**Table 5**), it revealed for the first time in Sierra Leone to our knowledge that multiple resistance patterns existed. However, standardized bioassays are still needed to test the resistance phenotype in individuals and combined with the molecular tests, to understand the real resistance status in this country. For example, there was a report that *An. gambiae s.l.* with the L1014F mutation were still susceptible to pyrethroids in Guinea Bissau (Dabire et al., 2008). Meanwhile, the failure to detect allelic mutations by molecular tests also cannot be interpreted as an absence of resistance in a population, and it reminds us that the detection system used in the present study should be further optimized. In addition, resistance mutations in different genes of A296G *rdl*, *kdrW* and *ace-1* were unevenly distributed in four pilot sites (**Table 4**). The mutation in A296G *rdl* (80.9%) was more frequent in samples from Kayangba community than other three communities. And no mutation was detected in A296S *rdl* in samples from Lebanon and Bolima communities, and very few samples were heterozygous individuals in the other two sites. Furthermore, the mutation in *ace-1* was more frequent in samples from Bolima community than other three communities.

CONCLUSIONS

High frequencies of *kdrW* alleles and uneven frequencies of A296G *rdl* and *ace-1* in *An. gambiae* populations in Sierra Leone detected in the present study prompts the need for close vector monitoring of susceptibility levels to insecticides used in this country. It provides important information to the Sierra Leone Malaria Control Programme for development of insecticide resistance monitoring and adjusting the strategy to implement in this country.

DATA AVAILABILITY STATEMENT

The original contributions presented in the study are included in the article. Further inquiries can be directed to the corresponding authors.

ETHICS STATEMENT

The project was informed to the study sites, and consent was obtained from the local authorities.

AUTHOR CONTRIBUTIONS

JY, SS, and NX conceived the study. FY and SS conducted sample collection and preparation. JY and FY performed the laboratory works. JY performed the result analysis. JY, CZ, SS, LW, and NX contributed to the study design. JY, SZ, HL, ZX, and NX contributed to experimental materials. JY drafted and revised the manuscript. All authors contributed to the article and approved the submitted version.

FUNDING

This study was supported by the National Science and Technology Major Program of China (No. 2018ZX10101002–002), Technical Reserve Programme for Global Tropical Diseases Prevention and Control (No. 131031104000160004), the Fifth Round of Three-Year Public Health Action Plan of Shanghai (No. GWV-10.1-XK13), and Sierra Leone-China Second Phase of the Fixed Biological Safety Laboratory Technical Cooperation Project.

ACKNOWLEDGMENTS

We appreciate the Consultant Medical Entomologists, staffs from National Malaria Control Program, Directorate for Environmental Health and Sanitation, Onchocerciasis Control Program, and District Health Management Teams for their wonderful work in the sample collection and other works.

REFERENCES

Alina, D., Yolanda, V., and John, P. N. (2005). Multiplexed SNP Genotyping Using Primer Single - Base Extension (SBE) and Microsphere Arrays. *Curr. Protoc. Cytom.* 13, 13–14. doi: 10.1002/0471142956.cy1304s34

Bass, C., Nikou, D., Donnelly, M. J., Williamson, M. S., Ranson, H., Ball, A., et al. (2007). Detection of Knockdown Resistance (Kdr) Mutations in Anopheles Gambiae: A Comparison of Two New High-Throughput Assays With Existing Methods. *Malar. J.* 6, 111. doi: 10.1186/1475-2875-6-111

Bass, C., Nikou, D., Vontas, J., Donnelly, M. J., Williamson, M. S., and Field, L. M. (2010). The Vector Population Monitoring Tool (VPMT): High-Throughput DNA-Based Diagnostics for the Monitoring of Mosquito Vector Populations. *Malar. Res. Treat.* 2010, 190434. doi: 10.4061/2010/190434

Bass, C., Williamson, M. S., Vontas, J., Ranson, H., Donnelly, M. J., and Field, L. M. (2015a). "Insensitive Acetylcholinesterase (Iache) Assay," in *Methods in Anopheles Research*, *2015 edition*. chapter 8.5.1.4. BEI Resources.

Bass, C., Williamson, M. S., Vontas, J., Ranson, H., Donnelly, M. J., and Field, L. M. (2015b). "Resistance to Dieldrin (Rdl) Assay," in *Methods in Anopheles Research*, *2015 edition*. chapter 8.5.1.5. BEI Resources.

Chen, D. P., Wen, Y. H., Lu, J. J., Tseng, C. P., and Wang, W. T. (2019). Rapid Rare ABO Blood Typing Using a Single PCR Based on a Multiplex SNaPshot Reaction. *J. Formos. Med. Assoc.* 118, 395–400. doi: 10.1016/j.jfma.2018.06.014

Dabire, K. R., Diabate, A., Agostinho, F., Alves, F., Manga, L., Faye, O., et al. (2008). Distribution of the Members of Anopheles Gambiae and Pyrethroid Knock-Down Resistance Gene (Kdr) in Guinea-Bissau, West Africa. *Bull. Soc Pathol. Exot.* 101 (2), 119–123.

Davies, T. G., Field, L. M., Usherwood, P. N., and Williamson, M. S. (2007). DDT, Pyrethrins, Pyrethroids and Insect Sodium Channels. *IUBMB Life* 59 (3), 151–162. doi: 10.1080/15216540701352042

Djogbenou, L., Chandre, F., Berthomieu, A., Dabire, R., Koffi, A., Alout, H., et al. (2008). Evidence of Introgression of the Ace-1(R) Mutation and of the Ace-1 Duplication in West African Anopheles Gambiae s. s. *PloS One* 3 (5), e2172. doi: 10.1371/journal.pone.0002172

Donnelly, M. J., Corbel, V., Weetman, D., Wilding, C. S., Williamson, M. S., and Black, W. (2009). Does Kdr Genotype Predict Insecticide-Resistance Phenotype in Mosquitoes? *Trends Parasitol.* 25 (5), 213–219. doi: 10.1016/j.pt.2009.02.007

Donnelly, M. J., Isaacs, A. T., and Weetman, D. (2016). Identification, Validation, and Application of Molecular Diagnostics for Insecticide Resistance in Malaria Vectors. *Trends Parasitol.* 32, 197–206. doi: 10.1016/j.pt.2015.12.001

Du, W., Awolola, T. S., Howell, P., Koekemoer, L. L., Brooke, B. D., Benedict, M. Q., et al. (2005). Independent Mutations in the Rdl Locus Confer Dieldrin Resistance to Anopheles Gambiae and An. Arabiensis. *Insect. Mol. Biol.* 14 (2), 179–183. doi: 10.1111/j.1365-2583.2005.00544.x

Fariña Sarasqueta, A., Moerland, E., de Bruyne, H., de Graaf, H., Vrancken, T., van Lijnschoten, G., et al. (2011). SNaPshot and StripAssay as Valuable Alternatives to Direct Sequencing for KRAS Mutation Detection in Colon Cancer Routine Diagnostics. *J. Mol. Diagn.* 13, 199–205. doi: 10.1016/j.jmoldx.2010.10.006

Ffrench-Constant, R. H. (1994). The Molecular and Population Genetics of Cyclodiene Insecticide Resistance. *Insect. Biochem. Mol. Biol.* 24 (4), 335–345. doi: 10.1016/0965-1748(94)90026-4

Filippini, S., Blanco, A., Fernández-Marmiesse, A., Álvarez-Iglesias, V., Ruíz-Ponte, C., Carracedo, Á., et al. (2007). Multiplex SNaPshot for Detection of BRCA1/2 Common Mutations in Spanish and Spanish Related Breast/Ovarian Cancer Families. *BMC Med. Genet.* 8, 40. doi: 10.1186/1471-2350-8-40

Fondevila, M., Børsting, C., Phillips, C., de la Puente, M., Consortium, E. N., Carracedo, A., et al. (2017). Forensic SNP Genotyping With SNaPshot: Technical Considerations for the Development and Optimization of Multiplexed SNP Assays. *Forensic Sci. Rev.* 29, 57–76.

Fournier, D. (2005). Mutations of Acetylcholinesterase Which Confer Insecticide Resistance in Insect Populations. *Chem. Biol. Interact.* 157-158, 257–261. doi: 10.1016/j.cbi.2005.10.040

Hurst, C. D., Zuiverloon, T. C., Hafner, C., Zwarthoff, E. C., and Knowles, M. A. (2009). A SNaPshot Assay for the Rapid and Simple Detection of Four Common Hotspot Codon Mutations in the PIK3CA Gene. *BMC Res. Notes* 2, 66. doi: 10.1186/1756-0500-2-66

Latini, F. R., Gazito, D., Arnoni, C. P., Muniz, J. G., de Medeiros Person, R., Carvalho, F. O., et al. (2014). A New Strategy to Identify Rare Blood Donors: Single Polymerase Chain Reaction Multiplex SNaPshot Reaction for Detection of 16 Blood Group Alleles. *Blood Transfus.* 12 (Suppl 1), s256–s263. doi: 10.2450/2013.0242-12

Martinez Torres, D., Chandre, F., Williamson, M. S., Darriet, F., Berge, J. B., Devonshire, A. L., et al. (1998). Molecular Characterization of Pyrethroid Knockdown Resistance (Kdr) in the Major Malaria Vector Anopheles Gambiae s.s. *Insect. Mol. Biol.* 7 (2), 179–184. doi: 10.1046/j.1365-2583.1998.72062.x

Mavridis, K., Wipf, N., Müller, P., Traoré, M. M., Muller, G., and Vontas, J. (2018). Detection and Monitoring of Insecticide Resistance Mutations in Anopheles Gambiae: Individual *vs* Pooled Specimens. *Genes* 9, 479. doi: 10.3390/genes9100479

National Malaria Control Programme (2015). *Sierra Leone Malaria Control Strategic Plan (2016-2020)*. 40–42.

National Malaria Control Programme (NMCP) [Sierra Leone], Statistics Sierra Leone, University of Sierra Leone, Catholic Relief Services and ICF. (2016). *Sierra Leone Malaria Indicator Survey*. Freetown, Sierra Leone: NMCP, SSL, CRS, and ICF.

Palacajornsuk, P., Halter, C., Isakova, V., Tarnawski, M., Farmar, J., Reid, M. E., et al. (2009). Detection of Blood Group Genes Using Multiplex SNaPshot Method. *Transfusion* 49, 740–749. doi: 10.1111/j.1537-2995.2008.02053.x

Quintans, B., Alvarez-Iglesias, V., Salas, A., Phillips, C., Lareu, M. V., and Carracedo, A. (2004). Typing of Mitochondrial DNA Coding Region SNPs of Forensic and Anthropological Interest Using SNaPshot Minisequencing. *Forensic Sci. Int.* 140, 241e57. doi: 10.1016/j.forsciint.2003.12.005

Ranson, H., Jensen, B., Vulule, J. M., Wang, X., Hemingway, J., and Collins, F. H. (2000). Identification of a Point Mutation in the Voltage-Gated Sodium Channel Gene of Kenyan Anopheles Gambiae Associated With Resistance to DDT and Pyrethroids. *Insect. Mol. Biol.* 9 (5), 491–497. doi: 10.1046/j.1365-2583.2000.00209.x

Ranson, H., N'Guessan, R., Lines, J., Moiroux, N., Nkuni, Z., and Corbel, V. (2011). Pyrethroid Resistance in African Anopheline Mosquitoes: What Are the Implications for Malaria Control? *Trends Parasitol.* 27 (2), 91–98. doi: 10.1016/j.pt.2010.08.004

Scott, J. A., Brogdon, W. G., and Collins, F. H. (1993). Identification of Single Specimens of the Anopheles Gambiae Complex by the Polymerase Chain Reaction. *Am. J. Trop. Med. Hyg.* 49, 520–529. doi: 10.4269/ajtmh.1993.49.520

Vincent, C., and N'Guessan, R. (2013). Distribution, Mechanism, Impact and Management of Insecticide Resistance in Malaria Vectors: A Pragmatic Review. *IntechOpen: Anopheles Mosq.: New Insights Malaria Vectors*, 579–633. doi: 10.5772/56117

Weill, M., Lutfalla, G., Mogensen, K., Chandre, F., Berthomieu, A., Berticat, C., et al. (2003). Comparative Genomics: Insecticide Resistance in Mosquito Vectors. *Nature* 423 (6936), 136–137. doi: 10.1038/423136b

Weill, M., Malcolm, C., Chandre, F., Mogensen, K., Berthomieu, A., Marquine, M., et al. (2004). The Unique Mutation in Ace-1 Giving High Insecticide Resistance Is Easily Detectable in Mosquito Vectors. *Insect. Mol. Biol.* 13 (1), 1–7. doi: 10.1111/j.1365-2583.2004.00452.x

WHO. (2018). *World Malaria Report 2018* (Geneva: World Health Organization).

WHO. (2019). *World Malaria Report 2019* (Geneva: World Health Organization).

WHO. (2020). *World Malaria Report 2020: 20 Years of Global Progress and Challenges* (Geneva: World Health Organization).

Conflict of Interest: The authors declare that the research was conducted in the absence of any commercial or financial relationships that could be construed as a potential conflict of interest.

frontiers in Cellular and Infection Microbiology

ORIGINAL RESEARCH
published: 08 September 2021
doi: 10.3389/fcimb.2021.673194

High Frequency Mutations in *pfdhfr* and *pfdhps* of *Plasmodium falciparum* in Response to Sulfadoxine-Pyrimethamine: A Cross-Sectional Survey in Returning Chinese Migrants From Africa

He Yan[1†], Jun Feng[1,2†], Jian-hai Yin[1], Fang Huang[1], Xiang-li Kong[3], Kang-ming Lin[4], Tao Zhang[5], Xin-yu Feng[1], Shui-sen Zhou[1], Jian-ping Cao[1,2] and Zhi-gui Xia[1*]*

[1] National Institute of Parasitic Diseases, Chinese Center for Disease Control and Prevention (Chinese Center for Tropical Diseases Research), NHC Key Laboratory of Parasite and Vector Biology, WHO Collaborating Centre for Tropical Diseases, National Center for International Research on Tropical Diseases, Shanghai, China, [2] School of Global Health, Chinese Center for Tropical Diseases Research, Shanghai Jiao Tong University School of Medicine, Shanghai, China, [3] Shandong Institute of Parasitic Diseases, Shandong First Medical University & Shandong Academy of Medical Sciences, Shandong, China, [4] Instit of Parasitic Diseases, Guangxi Zhuang Autonomous Region Center for Disease Control and Prevention, Guangxi, China, [5] Anhu Provincial Center for Disease Control and Prevention, Anhui, China

Background: Sulfadoxine-pyrimethamine (SP) is recommended for intermittent preventive treatment in Africa against *Plasmodium falciparum* infection. However, increasing SP resistance (SPR) of *P. falciparum* affects the therapeutic efficacy of SP, and *pfdhfr* (encoding dihydrofolate reductase) and *pfdhps* (encoding dihydropteroate synthase) genes are widely used as molecular markers for SPR surveillance. In the present study, we analyzed single nucleotide polymorphisms (SNPs) of *pfdhfr* and *pfdhps* in *P. falciparum* isolated from infected Chinese migrant workers returning from Africa.

Methods: In total, 159 blood samples from *P. falciparum*-infected workers who had returned from Africa to Anhui, Shangdong, and Guangxi provinces were successfully detected and analyzed from 2017 to 2019. The SNPs in *pfdhfr* and *pfdhps* were analyzed using nested PCR. The genotypes and linkage disequilibrium (LD) were analyzed using Haploview.

Results: High frequencies of the Asn51Ile (N51I), Cys59Arg(C59R), and Ser108Asn (S108N) mutant alleles were observed, with mutation frequencies of 97.60, 87.43, and 97.01% in *pfdhfr*, respectively. A triple mutation (IRN) in *pfdhfr* was the most prevalent haplotype (86.83%). Six point mutations were detected in *pfdhps* DNA fragment, Ile431Val (I431V), Ser436Ala (S436A), Ala437Gly (A437G), Lys540Glu(K540E), Ala581Gly(A581G), Ala613Ser(A613S). The *pfdhps* K540E (27.67%) was the most predominant allele, followed by S436A (27.04%), and a single mutant haplotype (SGKAA; 62.66%) was predominant in *pfdhps*. In total, 5 haplotypes of the *pfdhfr* gene and 13 haplotypes of the *pfdhps* gene were identified. A total of 130 isolates with 12 unique haplotypes were found in the *pfdhfr-pfdhps* combined haplotypes, most of them (n = 85, 65.38%) carried quadruple allele combinations (CIRNI-SGKAA).

OPEN ACCESS

Edited by:
Tianmu Chen, Xiamen University, China

Reviewed by:
Ruimin Zhou, National Health Commission of the People's Republic of China, China
Shaojun Long, China Agricultural University, China
Yi Cao, George Washington University, United States

***Correspondence:**
Jian-ping Cao
caojpcdc@163.com
Zhi-gui Xia
xiag@nipd.chinacdc.cn

†These authors have contributed equally to this work

Specialty section:
This article was submitted to Parasite and Host, a section of the journal Frontiers in Cellular and Infection Microbiology

Received: *27 February 2021*
Accepted: *14 June 2021*
Published: *08 September 2021*

Citation:
Yan H, Feng J, Yin J-h, Huang F, Kong X-l, Lin K-m, Zhang T, Feng X-y, Zhou S-s, Cao J-p and Xia Z-g (2021) High Frequency Mutations in pfdhfr and pfdhps of Plasmodium falciparum in Response to Sulfadoxine-Pyrimethamine: A Cross-Sectional Survey in Returning Chinese Migrants From Africa. Front. Cell. Infect. Microbiol. 11:673194. doi: 10.3389/fcimb.2021.673194

Conclusion: A high prevalence of point mutations in the *pfdhfr* and *pfdhps* genes of *P. falciparum* isolates was detected among Chinese migrant workers returning from Africa. Therefore, continuous *in vitro* molecular monitoring of Sulfadoxine-Pyrimethemine combined *in vivo* therapeutic monitoring of artemisinin combination therapy (ACT) efficacy and additional control efforts among migrant workers are urgently needed.

Keywords: *Plasmodium falciparum*, sulfadoxine-pyrimethamine, dihydropteroate synthase, dihydrofolate reductase, migrants from Africa

INTRODUCTION

Imported *Plasmodium falciparum* infections are of great concern in China during malaria elimination and post-elimination stages, because China achieved zero indigenous malaria cases in 2017 (Feng et al., 2018). Appropriate treatment for *P. falciparum* according to the national plan is important; however, some studies have demonstrated mutations in molecular markers related to artemisinin combination therapy (ACT) resistance among isolates from Africa, suggesting that careful surveillance of African parasite populations is still warranted (Feng et al., 2015a; Feng et al., 2019, Yan et al., 2020).

Sulfadoxine-pyrimethamine (SP) is a second-line antimalarial for uncomplicated *P. falciparum* malaria treatment, as recommended by the World Health Organization (WHO), which is used as an intermittent preventive treatment in pregnancy (IPTp) and as an intermittent preventive treatment in infants (IPTi) in malaria-endemic regions (Gosling et al., 2010; Konate et al., 2011). Resistance to SP is caused mainly by point mutations in *pfdhfr* (encoding dihydrofolate reductase) and *pfdhps* (encoding dihydropteroate synthase). Mutations in *pfdhfr* and *pfdhps* have been associated with decreased parasite sensitivity to the SP, because the products of these genes could incrementally increase the parasite's tolerance to the drugs *in vitro* (Chulay et al. 1984). Studies have identified point mutations in codons N51I, C59R, and S108N, I164L of *pfdhfr* located on chromosome 4 and codons I431V, S436A, A437G, K540E, A581G, and A613S of *pfdhps* located on chromosome 8, all of which were associated with *P. falciparum* SP treatment failure (Triglia et al., 1997; Berglez et al., 2004; Pearce et al., 2009). Monitoring drug resistance and the pattern of mutations is essential for early detection and subsequent prevention of the spread of drug resistance. The present study identified the polymorphisms in *pfdhfr* and *pfdhps* in *P. falciparum* among returned migrant workers from Africa in 2017–2019 reported in eastern China. The results provide a deeper understanding of the disease as well as baseline information on antimalarial drug resistance among imported *P. falciparum* in China.

MATERIALS AND METHODS

Sample Sites

Sample Collection and DNA Extraction

The study was conducted in Anhui, Shandong, and Guangxi Provinces in Eastern and Southern China, where imported *P. falciparum* cases were predominantly. Anhui Province covers 105 counties with 70.6 million people and experienced a malaria resurgence in 2005–2008 that was mainly caused by the accumulation of residual foci of *P. vivax* (Feng et al., 2015b). Shandong Province, located in eastern China, has a long coastline measuring 3,024.4 kilometers. It contains 137 counties and has a population of 97.9 million. Economic trade overseas is frequent. Another province, Guangxi, is known for its gold miners who returned from Ghana in 2013, which was mainly reported in Shanglin County (Feng et al., 2015a). The number of imported *P. falciparum* cases, especially those from Africa, has increased significantly in these three provinces, and 360 P. *falciparum* cases were reported in 2019, accounting for 18.5% of all *P. falciparum* cases nationwide (Zhang L et al., 2020).

A total of 206 *P. falciparum*-infected blood samples were collected from the travelers returning from Africa from 2017 to 2019. The samples distribution were shown as **Figure 1**. Approximately 100 μl of finger-prick blood was spotted onto a piece of 3MM Whatman filter paper (GE Healthcare, Boston, MA, USA) and air dried.

The *Plasmodium falciparum* genomic DNA from the approximately 100 μl of collected blood sample was extracted using a QIAamp DNA blood kit (QIAGEN, Valencia, CA, USA) as described previously (Yan et al., 2020). Each of the samples was labeled with a study number and stored at −4°C until extraction. Individual epidemiological information was also collected using a web-based reporting system (China Information System for Diseases Control and Prevention) and analyzed.

Detection of *pfdhfr* and *pfdhps* Polymorphisms

Point mutations at codons 16, 51, 59, 108, and 164 of the *pfdhfr* gene and codons 431, 436, 437, 540, 581, and 613 of the *pfdhps* gene were evaluated using nested PCR amplification. The sequences of the primers used for *pfdhfr* and *pfdhps* genotyping were as described previously (Zhang et al., 2014). The primary amplification was performed using the following parameters: 1 cycle of 95°C for 3 min; 35 cycles of 95°C for 30 s, 55°C for 30 s, and 65°C for 6 for 30 s, and 1 cycle of 65°C for 60 s; and 65°C for 5 min. The second amplifcation was performed using the following parameters: 1 cycle of 95°C for 3 min; 35 cycles of 95°C for 30 s, 52°C for 30 s, and 65°C for 60 s; and 1 cycle of 65°C for 5 min. 750-bp product of *pfdhps* were sent for Sanger sequencing (Shanghai Bunan Biological Co., Ltd., Shanghai, China).

Data Analysis

Sequences were analyzed using the Blast program (http://blast.ncbi.nlm.nih.gov/). Multiple nucleotide sequence alignments and

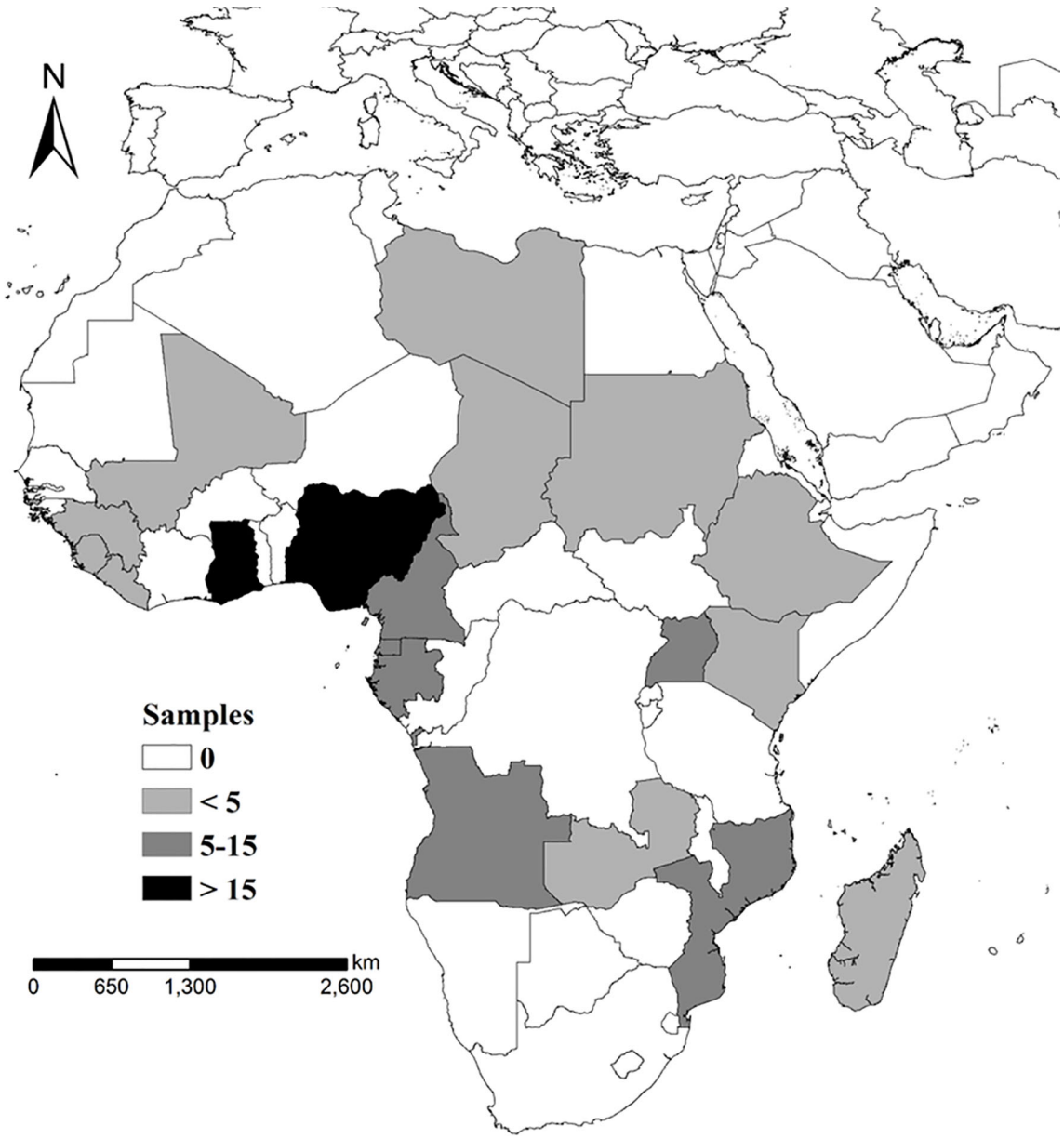

FIGURE 1 | Sample collection and distribution, samples collection sites and sample screening and follow-up analysis of subject patterns.

analysis were carried out using the MAFFT web-based tool with the Cluster Omega Sequence Alignment Editor (https://www.ebi.ac.uk/Tools/msa/clustalo/). Sequences with poor quality after three sequencing attempts or those with more than one peak at one locus were not included in the analysis. The map showing the imported of countries with number of the isolates was created by ArcGIS 10.1 (Environmental Systems Research Institute, Inc., Redlands, CA, USA). SPSS18.0 (IBM Corp., Armonk, NY, USA) was used to conduct the statistical analyses, and the Chi-squared test was employed to test the different constituent ratios of *pfdhfr* and *pfdhps* gene polymorphisms. The Fisher's precision probability test was used as the sample size is less 50; For the sample size less than five would be discarded when analyzing the geographical distribution difference. The inter and intragenic SNP Linkage disequilibrium (LD) associations of *pfdhfr* and *pfdhps* were analyzed using Haploview 15 (Patel et al., 2017).

Ethical Considerations

This study was reviewed and approved by the ethical committee of the National Institute of Parasitic Diseases, Chinese Centre for Disease Control and Prevention (NIPD, China CDC, No. 2019008).

RESULTS

Epidemiological Information

Among the 206 *P. falciparum* isolates collected in this study, 202 and 177 isolates were successfully amplified and sequenced for the *pfdhfr* and *pfdhps* genes, respectively; however, only single infections and both of *pfdhfr* and *pfdhps* successful amplicons were involved in the final analysis. Therefore, a total of 159 P. *falciparum* isolates were successfully detected and analyzed in this study (**Figure 1**). Their distribution was identified as 2 from North Africa, 23 from East Africa, 54 from West Africa, and 80 from Central Africa. Among them, the Democratic Republic of the Congo (n = 28), Nigeria (n = 27), and Angola (n = 16) were considered as the top three imported source countries. The average patient age was 42 years, and 154 patients (154/159, 96.86%) were male. The numbers of cases reported in 2017, 2018, and 2019 were 28, 58, and 73, respectively.

Prevalence of *pfdhfr* Polymorphisms

For *pfdhfr*, no polymorphism was found for codons 50 or 164. Compared with mutations N51I and C59R, S108N had a higher SNP prevalence, whereas, the difference between N51I and C59R was not significant. Only three isolates were sequenced as wild-type Asparagine-Cysteine-Serine (NCS) (accounting for 1.89%), whereas, the triple-mutant genotype, Isoleucine-Arginine-Asparagine (IRN), comprised 80.50% (n = 128), the others were NCN (n = 3, 1.89%), ICN (n = 10, 6.29%), and NRN (n = 15, 9.43%), respectively (**Table 1**).

Prevalence of *pfdhps* Polymorphisms

The SNPs of *pfdhps* were relatively scattered, S436A (27.07%) and K540E (27.67%) carried a higher allele frequency, which were statistically significant than others (the average mutant frequency was 6.92%). The frequencies of the other three alleles, I431V, A437G, and A581G, were lower than those of S436A or K540E, but higher than that of S613A, which was carried by only two isolates. In all, among 159 P. *falciparum* isolates, 13 kinds of mutants of *pfdhps* were detected. Further sequencing showed that 73 single mutant isolates, including ISA**E**AA (the bold residue represents the mutated site; n = 41, 25.79%), I**A**AKAA (n = 24, 15.09%), IS**G**KAA (n = 6, 3.77%), and ISAK**G**A (n = 2, 1.26%); 13 double mutant isolates, including I**AG**KAA (n = 7, 4.40%), **VA**AKAA (n = 2, 1.26%), ISA**EG**A (n = 2, 1.26%), I**A**AKA**S** (n = 1, 0.63%), and I**A**A**E**AA (n = 1, 0.63%); 9 triple mutant genotypes, comprising 8 examples of **VA**AK**G**A, 1 of **V**S**G**K**G**A; and only 1 quadruple mutation, as **VA**AK**GS,** were identified. There were more wild-type isolates of *pfdhps* than p*fdhfr* (63 *pfdhps* isolates, compared with three in *pfdhfr*). Three genotypes, ISAKAA (39.62%, 63/159), ISA**E**AA (25.79%, 41/159), and I**A**AKAA (15.09%, 24/159), accounted for 80.50% of all *pfdhps* genotypes (**Table 2**).

Geographical Genetic Analysis

The mutant frequency in all targeted *pfdhfr* gene fragments were all above 86.79%, and there was no significant difference (P > 0.05) among isolates from West, East, and Central Africa. For the *pfdhps* gene, the mutant genotypes carried a relatively high number of polymorphisms. The two *P. falciparum* samples from North Africa were wild-types (**Table 3**). Two of six loci were detected as site mutations in samples from East Africa, with K540E representing 69.57% (16/23) of the mutations, which was a markedly higher frequency than that for S436A (4.34%, 1/23). Each locus carried a sense mutation associated with West Africa, the mutant frequencies were 14.81% (8/54, I413V), 51.85% (28/54, S436V), 9.26% (5/54, A437G), 11.11% (6/54, K540E), 12.96% (7/54, A581G), and 5.56% (3/54, A613S). The site mutations in central African region were all different for the S436V (17.5%, 14/80, P < 0.001) and K540E (27.5%, 22/80, P = 0.017) loci, which was significantly different compared with the Western African Region isolates (P < 0.05). Moreover, the mutant frequency of K540E varied between Western and Eastern African Region isolates (P <0.01). A613S only occurred in Ghana (n = 2) and Nigeria (n = 1) in West Africa.

TABLE 1 | Prevalence of *pfdhfr* and *pfdhps* polymorphisms in imported African isolates.

Gene	Position	Wild type	Mutant type	Mutant isolates (n)	Frequency (%)
pfdhfr	51	AAT	ATT	138	86.79
	59	TGT	**C**GT	143	89.94
	108	AGC	A**A**C	156	98.11
pfdhps	431	ATA	**G**TA	12	7.55
	436	TCT	**G**CT	43	27.04
	437	GCT	G**G**T	15	9.43
	540	AAA	**G**AA	44	27.67
	581	GCG	G**G**G	14	8.81
	613	GCC	**T**CC	3	1.89

The bold values stand for mutant nucleic acid base.

TABLE 2 | Prevalence of *pfdhfr* and *pfdhps* haplotypes.

Gene	Genotype	Mutations	Sample size	Frequency (%)
pfdhfr	NCS	0	3	1.89%
	NC**N**	1	3	1.89%
	IC**N**	2	10	6.29%
	N**RN**	2	15	9.43%
	IRN	3	128	80.50%
pfdhps	ISAKAA	0	63	39.62%
	ISA**E**AA	1	41	25.79%
	I**A**AKAA	1	24	15.09%
	IS**G**KAA	1	6	3.77%
	ISAK**G**A	1	2	1.26%
	VAAKAA	2	2	1.26%
	I**AG**KAA	2	7	4.40%
	ISA**EG**A	2	2	1.26%
	I**A**AKA**S**	2	1	0.63%
	I**A**A**E**AA	2	1	0.63%
	VAAK**G**A	3	8	5.03%
	VS**G**K**G**A	3	1	0.63%
	VAAK**GS**	4	1	0.63%

The bold values stand for mutant nucleic acid base.

Linkage Disequilibrium (LD) Analysis

In total, 25 genotypes of *pfdhfr*/*pfdhps* were detected among the 159 P. *falciparum* isolates. For *pfdhfr*, no SNP was found for codons 16 or 164. Ultimately, 5 and 13 genotypes of *pfdhfr* (involving codons 51, 59, and 108) and *pfdhps* (involving codons 431, 436, 437, 540, 581, and 613) were detected and analyzed. To evaluate the SNP LD associations of *pfdhfr* and *pfdhps*, several

TABLE 3 | Geographical genetic analysis of *pfdhfr/pfdhps* genotypes.

Region	No. samples	Country	No. samples	No. of mutations	*pfdhfr/pfdhps* genotypes	No. of genotypes
North Africa	2	Libya	1	3	IRN/ISAKAA	1
		Sudan	1	3	IRN/ISAKAA	1
East Africa	23	Kenya	1	3	IRN/ISAKAA	1
		Madagascar	2	2	NRN/ISAKAA	2
		Ethiopia	3	3	IRN/ISAKAA	1
				4	IRN/IAAKAA	1
				4	IRN/ISAEAA	1
		Zambia	4	3	NRN/ISAEAA	1
				4	IRN/ISAEAA	3
		Uganda	6	4	IRN/ISAEAA	6
		Mozambique	7	2	ICN/ISAKAA	1
				4	IRN/ISAEAA	6
West Africa	54	Mali	1	3	IRN/ISAKAA	1
		Sierra Leone	2	2	NCN/IAAKAA	1
				3	IRN/ISAKAA	1
		Guinea	2	3	IRN/ISAKAA	1
				4	IRN/ISGKAA	1
		Liberia	3	1	NCN/ISAKAA	1
				4	IRN/IAAKAA	2
		Cote d'Ivoire	8	0	NCS/ISAKAA	1
				2	NRN/ISAKAA	1
				3	IRN/ISAKAA	2
				4	IRN/IAAKAA	3
				4	IRN/ISAEAA	1
		Ghana	16	1	NCS/IAAKAA	1
				2	NRN/ISAKAA	1
				3	IRN/ISAKAA	3
				3	ICN/ISAEAA	1
				3	NRN/IAAKAA	1
				4	IRN/IAAKAA	3
				4	IRN/ISAEAA	2
				4	ICN/IAGKAA	1
				4	NRN/IAAKAS	1
				5	IRN/IAAEAA	1
				5	IRN/IAGKAA	1
		Nigeria	22	2	NRN/ISAKAA	1
				3	IRN/ISAKAA	6
				4	IRN/IAAKAA	5
				4	IRN/ISAEAA	1
				5	IRN/IAGKAA	1
				5	IRN/VAAKAA	1
				5	NRN/VAAKGS	1
				6	IRN/VAAKGA	6
Central Africa	80	Chad	1	6	IRN/VSGKGA	1
		Central Africa	3	2	NRN/ISAKAA	2
				3	IRN/ISAKAA	1
		Congo	4	2	NRN/ISAKAA	2
				3	IRN/ISAKAA	2
		Equatorial Guinea	6	3	IRN/ISAKAA	3
				4	IRN/ISAKGA	1
				5	IRN/ISAEGA	1
				6	IRN/VAAKGA	1
		Gabon	10	3	IRN/ISAKAA	7
				4	IRN/ISAEAA	3
		Angola	14	2	ICN/ISAKAA	2
				2	NCN/ISGKAA	1
				3	IRN/ISAKAA	4
				4	IRN/IAAKAA	2
				4	IRN/ISAKGA	1
				4	IRN/ISAEAA	3
				4	IRN/ISGKAA	1
		Cameroon	14	3	IRN/ISAKAA	5
				4	IRN/IAAKAA	4

(Continued)

TABLE 3 | Continued

Region	No. samples	Country	No. samples	No. of mutations	*pfdhfr/pfdhps* genotypes	No. of genotypes
				4	IRN/ISAEAA	1
				5	IRN/IAGKAA	2
				5	IRN/VAAKAA	1
				6	IRN/VAAKGA	1
		DR Congo	28	2	ICN/ISAKAA	1
				2	NRN/ISAKAA	1
				3	IRN/ISAKAA	6
				3	NRN/ISAEAA	1
				3	ICN/ISAEAA	3
				4	IRN/IAAKAA	1
				4	IRN/ISGKAA	3
				4	ICN/ISAEGA	1
				4	IRN/ISAEAA	9
				5	IRN/IAGKAA	2

statistically significant associations were found among the SNPs located in both the *pfdhfr* and *pfdhps* genes (**Figure 2**). For the *pfdhfr* gene, N51I was significantly associated with the SNPs (t175c, C59R; and g323a, S108N) with a D' value of 0.84 ($P < 0.05$) and 1.0 ($P < 0.05$), respectively. Similarly, t175c was significantly associated with the g323a (0.71, $P < 0.05$). For the *pfdhps* gene, t1482g, c1486g, a1794g, and g2013t formed an LD block. The sole SNP (t1482g, S436A) was significantly associated with the SNPs (c1486g, A437G; a1794g, K540E; and g2013t, A613S) with D' values of 0.75, 1.0, and 0.73, respectively. The SNP (t152a) of the *pfdhfr* gene encoding N51I was significantly associated with c1486g, with a D' value of 0.68. No associations were detected for the other SNPs of either the *pfdhfr* or *pfdhps* genes.

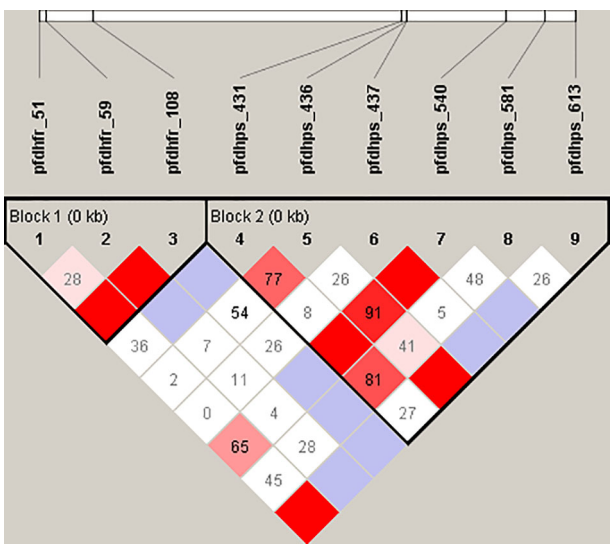

FIGURE 2 | Linkage disequilibrium (LD) analysis of *pfdhfr* and *pfdhps* SNPs. For the *pfdhfr* gene, the single amino acid mutations were N51I, C59R, and S108N, respectively. Likewise, *pfdhps* gene are related to the mutations S436A, A437G, K540E, and A613S, respectively. The dark and light red squares indicate a linkage that was statistically significant ($P < 0.05$). Cambridge blue squares indicate a linkage that is present but is not statistically significant ($P > 0.05$). A white square with indicates that no linkage is present.

DISCUSSION

The emergence and spread of Sulfadoxine-Pyrimethamine (SP) resistance has narrowed its usage to IPTp and IPTi in Africa (Rieckmann and Cheng, 2002). In 2019, the WHO covered 33 African countries for IPTp, in which at least nearly 62% of pregnant women received a first dose of IPTp (of four doses of ITPp)) (World Health Organization, 2020). The presents study aimed to determine the prevalence of SP resistance-associated *pfdhfr* and *pfdhps* genes in *P. falciparum* isolated from returned migrant workers from Africa reported in China. The study showed the *pfdhfr* triple haplotype mutation (**IRN**, including N51I, C59R, S108N) was highly prevalent, which was similar to other publications concerning African isolates (Jiang et al., 2019; Gikunju et al., 2020; Quan et al., 2020). This high prevalence was also found in the migrant workers returning to Guangxi from Ghana, suggesting that SP resistant genotype was widespread in Central and West Africa (Zhao et al., 2020). It was noted *pfdhfr* I164L, which was also associated with high resistance to cycloguanil, was detected in Ghanaian isolates, but was not found in our study (Zhao et al., 2020). It is worth noting that I164L is common in East Africa and Asia (Basuki et al., 2018,; Lynch et al., 2017), but rarely seen in Central and West Africa. One of the explanations was that this mutation site carries a high fitness cost to the parasite and therefore it is unable to survive the immune response of hosts in West Africa (Nzila et al., 2002). Further studies are needed to assess the effect of this mutation on the phenotype of parasites carrying this haplotype.

Mutations in *pfdhps* haplotypes at S436A and K540E, which are associated with decreased parasite sensitivity to Sulfadoxine drugs (Berglez et al., 2004), carried a higher allele frequency, which was also found in Uganda and Tanzania (Alifrangis et al., 2009; Mbonye et al., 2015). The WHO recommended that IPTp should not implemented in the regions when K540E exceed 50%; in our study, this mutation was present at 27.67%, which might favor the continued efficacy of IPTp treatment in these countries. Another mutation, A581G, is considered to have an important modulatory role in SP resistance. IPTp and SP could not protect pregnant women from delivering low birth weight infants when the frequency of this mutation is above 10% (Chico et al., 2015). In our study, the frequency of this mutation was 8.81% and half

of these mutated isolates were found in Nigeria. For the mutation A437G, which was associated with resistance to Sulfadoxine in endemic regions because of the drug pressure selection, showed a frequency of only 9.43% in our study, which was lower than that reported in Equatorial Guinea, Pakistan, and Iran (Rouhani et al., 2015; Yaqoob et al., 2018; Jiang et al., 2019). The I431V mutation was detected in Nigeria, Cameroon, Equatorial Guinea, and Chad. The most frequent haplotype of I431V was **VA**AK**G**A, similar to that found in isolates from Cameroon and Nigeria (Chauvin et al., 2015; Oguike et al., 2016). These haplotypes occurring in Central and West Africa suggested that SP conferred a selective advantage, and ongoing drug pressure is relative strong because SP was used as IPTp in these regions. It is noted A437G was widely spread in central and western African countries, which indicating *in vivo* SP drug resistance in these regions (Pearce et al., 2009). Some other studies combined with the clinical study indicated the *pfdhfr* triple mutant genotype was associated with SP treatment resistance (Basco et al, 2000; Naidoo et al., 2013). However, in this study, the A437G was not widely spread in central and western African region, even less than S436A, which was also different with our previous study in China-Myanmar border (Zhang et al., 2014), which may partially ascribe as the sample size limitation, the loss of drug pressure, and time passage may also the potential reason.

In our study, the frequency of the quadruple mutation **IRN**/ISA**E**AA was significantly higher in East Africa (100% in Uganda, 85.7% in Mozambique) than western and central African countries ($P < 0.01$), suggesting that the clinical implications of such haplotypes require further combined genotype and phenotype analysis. SP was limited for malaria control among the general population in many countries in Africa because of the high frequency of drug resistance developed by *P. falciparum*; therefore, we expected to obtain SP sensitive strains. Indeed, in our study, 39.62% of the isolates harbored the non-mutated *pfdhps* gene. This may be similar to the process for chloroquine, which tends to recover its effectiveness against the parasite after a long period during which its use in malaria control activities is halted (Lu et al., 2017).

CONCLUSION

This study showed a high frequency of SP-resistance associated SNPs in the *pfdhfr* and *pfdhps* genes of *P. falciparum* isolated since 2017 in returned migrant workers from Africa. The high resistance may be linked to the unsuccessful withdrawal of the SP treatment, and thus might affect the efficacy of IPTp for pregnant women and IPTi for infants. Mutations such as K540E, and the *pfdhfr-pfdhps* haplotype **IRN**/ISA**E**AA, which occurred at moderate frequencies in East Africa, such as in Uganda and Mozambique, the other regions showed as high frequency triple mutations of *pfdhfr*, but relatively scatter site mutations in *pfdhps* gene. The present data could provide the evidence for molecular surveillance in the post-elimination stage in China, focusing on the risk population among returning migrant workers from Africa, and could be used to determine the treatment policy for imported malaria in China.

DATA AVAILABILITY STATEMENT

The raw data supporting the conclusions of this article will be made available by the authors, without undue reservation.

ETHICS STATEMENT

The studies involving human participants were reviewed and approved by the ethical committee of the National Institute of Parasitic Diseases (NIPD), Chinese Centre for Disease Control and Prevention, Chinese Center for Tropical Diseases Research. The patients/participants provided their written informed consent to participate in this study.

AUTHOR CONTRIBUTIONS

HY conceived the study. J-hY, FH, X-yF, and JF performed the study and analyzed the data. JF assisted with editing the manuscript. J-pC provided strategic advice and revised the manuscript. All authors assisted with draft revisions. All authors contributed to the article and approved the submitted version.

FUNDING

The work was supported by the Key Techniques in Collaborative Prevention and Control of Major Infectious Diseases in the Belt and Road (Grant No. 2018ZX10101002-004) and the National Natural Science Foundation of China (Grant No. 81602904). The study had also been supported by "the Fifth Round of Three-Year Public Health Action Plan of Shanghai (No. GWV-10.1-XK13)".

REFERENCES

Alifrangis, M., Lusingu, J. P., Mmbando, B., Dalgaard, M. B., Vestergaard, L. S., Ishengoma, D., et al. (2009). Five-Year Surveillance of Molecular Markers of Plasmodium Falciparum Antimalarial Drug Resistance in Korogwe District, Tanzania: Accumulation of the 581G Mutation in the P. Falciparum Dihydropteroate Synthase Gene. *Am. J. Trop. Med. Hyg.* 80, 523–527. doi: 10.4269/ajtmh.2009.80.523

Basuki, S., F., Risamasu, P. M., Kasmijati, A. P., Riyanto, S., Hidayat, A., et al. (2018). Origins and Spread of Novel Genetic Variants of Sulfadoxine-Pyrimethamine Resistance in Plasmodium Falciparum Isolates In Indonesia. *Malaria J.* 17, 475. doi: 10.1186/s12936-018-2597-6

Basco, L. K., Tahar, R., Keundjian, A., and Ringwald, P. (2000). Sequence Variations in the Genes Encoding Dihydropteroate Synthase and Dihydrofolate Reductase and Clinical Response to Sulfadoxine-Pyrimethamine in Patients With Acute Uncomplicated Falciparum Malaria. *J. Infect. Dis.* 182, 624–628. doi: 10.1086/315731

Berglez, J., Iliades, P., Sirawaraporn, W., Coloe, P., and Macreadie, I. (2004). Analysis in Escherichia Coli of Plasmodium Falciparum Dihydropteroate Synthase (DHPS) Alleles Implicated in Resistance to Sulfadoxine. *Int. J. Parasitol.* 34, 95–100. doi: 10.1016/j.ijpara.2003.09.009

Chauvin, P., Menard, S., Iriart, X., Nsango, S. E., Tchioffo, M. T., Abate, L., et al. (2015). Prevalence of Plasmodium Falciparum Parasites Resistant to Sulfadoxine/Pyrimethamine in Pregnant Women in Yaounde, Cameroon: Emergence of Highly Resistant Pfdhfr/Pfdhps Alleles. *J. Antimicrob. Chemother.* 70, 2566–2571. doi: 10.1093/jac/dkv160

Chico, R. M., Cano, J., Ariti, C., Collier, T. J., Chandramohan, D., Roper, C., et al. (2015). Influence of Malaria Transmission Intensity and the 581G Mutation on the Efficacy of Intermittent Preventive Treatment in Pregnancy: Systematic Review and Meta-Analysis. *Trop. Med. Int. Health TM IH* 20, 1621–1633. doi: 10.1111/tmi.12595

Chulay, J. D., Watkins, W. M., and Sixsmith, D. G. (1984). Synergistic Antimalarial Activity of Pyrimethamine and Sulfadoxine Against Plasmodium Falciparum in Vitro. *Am. J. Trop. Med. Hyg.* 33, 325–330. doi: 10.4269/ajtmh.1984.33.325

Feng, J., Kong, X., Xu, D., Yan, H., Zhou, H., Tu, H., et al. (2019). Investigation and Evaluation of Genetic Diversity of Plasmodium Falciparum Kelch 13 Polymorphisms Imported From Southeast Asia and Africa in Southern China. *Front. Public Health* 7, 95. doi: 10.3389/fpubh.2019.00095

Feng, J., Li, J., Yan, H., Feng, X., and Xia, Z. (2015a). Evaluation of Antimalarial Resistance Marker Polymorphism in Returned Migrant Workers in China. *Antimicrob Agents Chemother* 59, 326–330. doi: 10.1128/AAC.04144-14

Feng, J., Xiao, H., Xia, Z., Zhang, L., and Xiao, N. (2015b). Analysis of Malaria Epidemiological Characteristics in the People's Republic of China 2004-2013. *Am. J. Trop. Med. Hyg.* 93, 293–299. doi: 10.4269/ajtmh.14-0733

Feng, J., Zhang, L., Huang, F., Yin, J. H., Tu, H., Xia, Z. G., et al. (2018). Ready for Malaria Elimination: Zero Indigenous Case Reported in the People's Republic of China. *Malaria J.* 17, 315. doi: 10.1186/s12936-018-2444-9

Gikunju, S. W., Agola, E. L., Ondondo, R. O., Kinyua, J., Kimani, F., LaBeaud, A. D., et al. (2020). Prevalence of Pfdhfr and Pfdhps Mutations in Plasmodium Falciparum Associated With Drug Resistance Among Pregnant Women Receiving IPTp-SP at Msambweni County Referral Hospital, Kwale County, Kenya. *Malaria J.* 19, 190. doi: 10.1186/s12936-020-03263-z

Gosling, R. D., Cairns, M. E., Chico, R. M., and Chandramohan, D. (2010). Intermittent Preventive Treatment Against Malaria: An Update. *Expert Rev. Anti Infect. Ther.* 8, 589–606. doi: 10.1586/eri.10.36

Jiang, T., Chen, J., Fu, H., Wu, K., Yao, Y., Eyi, J. U. M., et al. (2019). High Prevalence of Pfdhfr-Pfdhps Quadruple Mutations Associated With Sulfadoxine-Pyrimethamine Resistance in Plasmodium Falciparum Isolates From Bioko Island, Equatorial Guinea. *Malaria J.* 18, 101. doi: 10.1186/s12936-019-2734-x

Konate, A. T., Yaro, J. B., Ouedraogo, A. Z., Diarra, A., Gansane, A., Soulama, I., et al. (2011). Intermittent Preventive Treatment of Malaria Provides Substantial Protection Against Malaria in Children Already Protected by an Insecticide-Treated Bednet in Burkina Faso: A Randomised, Double-Blind, Placebo-Controlled Trial. *PloS Med.* 8, e1000408. doi: 10.1371/journal.pmed.1000408

Lu, F., Zhang, M., Culleton, R. L., Xu, S., Tang, J., Zhou, H., et al. (2017). Return of Chloroquine Sensitivity to Africa? Surveillance of African Plasmodium Falciparum Chloroquine Resistance Through Malaria Imported to China. *Parasites Vectors* 10, 355. doi: 10.1186/s13071-017-2298-y

Lynch, C. A., Pearce, R., Pota, H., Egwang, C., Egwang, T., Bhasin, A., et al. (2017). Travel and the Emergence of High-Level Drug Resistance in Plasmodium Falciparum in Southwest Uganda: Results From a Population-Based Study. *Malaria J.* 16, 150. doi: 10.1186/s12936-017-1812-1

Mbonye, A. K., Birungi, J., Yanow, S. K., Shokoples, S., Malamba, S., Alifrangis, M., et al. (2015). Prevalence of Plasmodium Falciparum Resistance Markers to Sulfadoxine-Pyrimethamine Among Pregnant Women Receiving Intermittent Preventive Treatment for Malaria in Uganda. *Antimicrob Agents Chemother.* 59, 5475–5482. doi: 10.1128/AAC.00507-15

Naidoo, I., and Roper, C. (1984). Mapping 'Partially Resistant', 'Fully Resistant', and 'Super Resistant' Malaria. *Trends Parasitol.* 29, 505–515. doi: 10.1016/j.pt.2013.08.002

Nzila, A. M., Mberu, E. K., Nduati, E., Ross, A., Watkins, W. M., and Sibley, C. H. (2002). Genetic Diversity of Plasmodium Falciparum Parasites From Kenya is Not Affected by Antifolate Drug Selection. *Int. J. Parasitol.* 32, 1469–1476. doi: 10.1016/S0020-7519(02)00164-9

Oguike, M. C., Falade, C. O., Shu, E., Enato, I. G., Watila, I., Baba, E. S., et al. (2016). Molecular Determinants of Sulfadoxine-Pyrimethamine Resistance in Plasmodium Falciparum in Nigeria and the Regional Emergence of Dhps 431V. *Int. J. Parasitol Drugs Drug Resist.* 6, 220–229. doi: 10.1016/j.ijpddr.2016.08.004

Patel, P., Bharti, P. K., Bansal, D., Ali, N. A., Raman, R. K., Mohapatra, P. K., et al. (2017). Prevalence of Mutations Linked to Antimalarial Resistance in Plasmodium Falciparum From Chhattisgarh, Central India: A Malaria Elimination Point of View. *Sci. Rep.* 7, 16690. doi: 10.1038/s41598-017-16866-5

Pearce, R. J., Pota, H., Evehe, M. S., Ba el, H., Mombo-Ngoma, G., Malisa, A. L., et al. (2009). Multiple Origins and Regional Dispersal of Resistant Dhps in African Plasmodium Falciparum Malaria. *PloS Med.* 6, e1000055. doi: 10.1371/journal.pmed.1000055

Quan, H., Igbasi, U., Oyibo, W., Omilabu, S., Chen, S. B., Shen, H. M., et al. (2020). High Multiple Mutations of Plasmodium Falciparum-Resistant Genotypes to Sulphadoxine-Pyrimethamine in Lagos, Nigeria. *Infect. Dis. Poverty* 9, 91. doi: 10.1186/s40249-020-00712-4

Rieckmann, K., and Cheng, Q. (2002). Pyrimethamine-Sulfadoxine Resistance in Plasmodium Falciparum Must be Delayed in Africa. *Trends Parasitol* 18, 293–294. doi: 10.1016/S1471-4922(02)02287-0

Rouhani, M., Zakeri, S., Pirahmadi, S., Raeisi, A., and Djadid, N. D. (2015). High Prevalence of Pfdhfr-Pfdhps Triple Mutations Associated With Anti-Malarial Drugs Resistance in Plasmodium Falciparum Isolates Seven Years After the Adoption of Sulfadoxine-Pyrimethamine in Combination With Artesunate as First-Line Treatment in Iran. *Infect. Genet. Evol.* 31, 183–189. doi: 10.1016/j.meegid.2015.01.020

Triglia, T., Menting, J. G., Wilson, C., and Cowman, A. F. (1997). Mutations in Dihydropteroate Synthase are Responsible for Sulfone and Sulfonamide Resistance in Plasmodium Falciparum. *Proc. Natl. Acad. Sci. U. S. A.* 94, 13944–13949. doi: 10.1073/pnas.94.25.13944

World Health Organization (2020). *World Malaria Report 2020* (Geneva: World Health Organization).

Yan, H., Kong, X., Zhang, T., Xiao, H., Feng, X., Tu, H., et al. (2020). Prevalence of Plasmodium Falciparum Kelch 13 (PfK13) and Ubiquitin-Specific Protease 1 (Pfubp1) Gene Polymorphisms in Returning Travelers From Africa Reported in Eastern China. *Antimicrob. Agents Chemother.* 20, 64. doi: 10.1128/AAC.00981-20

Yaqoob, A., Khattak, A. A., Nadeem, M. F., Fatima, H., Mbambo, G., Ouattara, A., et al. (2018). Prevalence of Molecular Markers of Sulfadoxine-Pyrimethamine and Artemisinin Resistance in Plasmodium Falciparum From Pakistan. *Malar J.* 17, 471. doi: 10.1186/s12936-018-2620-y

Zhang, L., Feng, J., Xia, Z. G., and Zhou, S. S. (2020). Epidemiological Characteristics of Malaria and Progress on Its Elimination in China in 2019. *Chin. J. Parasitol Parasit Dis.* 38, 133–138. doi: 10.12140/j.issn.1000-7423.2020.02.001

Zhang, Y., Yan, H., Wei, G., Han, S., Huang, Y., Zhang, Q., et al. (2014). Distinctive Origin and Spread Route of Pyrimethamine-Resistant Plasmodium Falciparum in Southern China. *Antimicrob. Agents Chemother.* 58, 237–246. doi: 10.1128/AAC.00972-13

Zhao, L., Pi, L., Qin, Y., Lu, Y., Zeng, W., Xiang, Z., et al. (2020). Widespread Resistance Mutations to Sulfadoxine-Pyrimethamine in Malaria Parasites Imported to China From Central and Western Africa. *Int. J. Parasitol. Drugs Drug Resist.* 12, 1–6. doi: 10.1016/j.ijpddr.2019.11.002

Conflict of Interest: The authors declare that the research was conducted in the absence of any commercial or financial relationships that could be construed as a potential conflict of interest.

frontiers in Medicine

ORIGINAL RESEARCH
published: 29 September 2021
doi: 10.3389/fmed.2021.721515

Time-Varying Effects of Meteorological Variables on Malaria Epidemiology in the Context of Interrupted Control Efforts in the Amazon Rainforest, 2000–2017

Gabriel Carrasco-Escobar[1,2]*, *Jazmin Qquellon*[1], *Diego Villa*[1], *Renato Cava*[1], *Alejandro Llanos-Cuentas*[3,4] and *Tarik Benmarhnia*[2,5]

[1] Health Innovation Laboratory, Institute of Tropical Medicine "Alexander von Humboldt", Universidad Peruana Cayetano Heredia, Lima, Peru, [2] Herbert Wertheim School of Public Health and Human Longevity Science, University of California, San Diego, La Jolla, CA, United States, [3] Facultad de Salud Pública y Administración, Universidad Peruana Cayetano Heredia, Lima, Peru, [4] Instituto de Medicina Tropical "Alexander von Humboldt", Universidad Peruana Cayetano Heredia, Lima, Peru, [5] Scripps Institution of Oceanography, University of California, San Diego, San Diego, CA, United States

OPEN ACCESS

Edited by:
Jun Feng,
National Institute of Parasitic Diseases, China

Reviewed by:
Ronald Balczon,
University of South Alabama, United States
Timothy Kudinha,
Charles Sturt University, Australia

***Correspondence:**
Gabriel Carrasco-Escobar
gabriel.carrasco@upch.pe

Specialty section:
This article was submitted to Infectious Diseases - Surveillance, Prevention and Treatment, a section of the journal Frontiers in Medicine

Received: 07 June 2021
Accepted: 27 August 2021
Published: 29 September 2021

Citation:
Carrasco-Escobar G, Qquellon J, Villa D, Cava R, Llanos-Cuentas A and Benmarhnia T (2021) Time-Varying Effects of Meteorological Variables on Malaria Epidemiology in the Context of Interrupted Control Efforts in the Amazon Rainforest, 2000–2017. Front. Med. 8:721515. doi: 10.3389/fmed.2021.721515

Successful malaria control interventions, mostly based on the training of health workers, distribution of insecticide-treated nets, and spraying, decrease malaria incidence; however, when these interventions are interrupted, a resurgence may occur. In the Peruvian Amazon, after discontinuing the control activities implemented by the PAMAFRO project (2006–2010)-a Global Fund-sponsored project for the strengthening of malaria control and surveillance in multiple countries in Latin America– malaria cases re-emerged dramatically. In parallel, meteorological factors determine the conditions suitable for the development, reproduction, and survival of mosquito vectors and parasites. This study hypothesized that interruption of malaria interventions may have modified the meteorological-malaria relationships over time (i.e., temporal changes in the dose-response between meteorological variables and malaria incidence). In this panel data analysis, we assessed the extent that relationships between meteorological variables and malaria changed temporally using data of monthly malaria incidence due to *Plasmodium vivax* or *P. falciparum* in Loreto, Peru (2000–2017). Generalized additive models were used to explore how the effects of meteorological variables changed in magnitude before, during, and after the PAMAFRO intervention. We found that once the PAMAFRO intervention had been interrupted, the estimated effects (dose-response) of meteorological variables on incidence rates decreased for both malaria parasite species. However, these fitted effect estimates did not reach their baseline levels (before the PAMAFRO period); variations of time-varying slopes between 0.45 and 2.07 times were observed after the PAMAFRO intervention. We also reported significant heterogeneity in the geographical distributions of malaria, parasite species, and meteorological variables. High malaria transmission occurred consistently in the northwestern provinces of Loreto Department. Since the end of the PAMAFRO period, a higher effect of precipitation and actual evapotranspiration was described on *P. falciparum* compared to *P. vivax*. The effect of temperature on malaria was greater over a shorter time (1-month lag or less),

compared with precipitation and actual evapotranspiration (12-month lag). These findings demonstrate the importance of sustained malaria control efforts since interruption may enhance the links between meteorological factors and malaria. Our results also emphasize the importance of considering the time-varying effect of meteorological factors on malaria incidence to tailor control interventions, especially to better manage the current and future climate change crisis.

Keywords: meteorological variables, malaria epidemiology, *Plasmodium vivax*, *Plasmodium falciparum*, interrupted malaria control intervention, Amazon rainforest

INTRODUCTION

Malaria remains a relevant public health problem, despite being a preventable and treatable infectious disease. During 2019, 229 million malaria cases were reported worldwide and ∼139 million people were at risk of acquiring malaria in Latin America, where more than 90% of cases occur in countries with Amazon rainforest, such as the Bolivarian Republic of Venezuela (53%), Brazil (20%), Colombia (10%), and Peru (5%) (1). In this area, most (75%) cases are caused by *Plasmodium vivax* species and transmitted by the primary malaria vector *Nyssorhynchus darlingi* (also known as *Anopheles darlingi*). In the Peruvian Amazon region, malaria is the most important vector-borne disease, with most cases (93.1%) located in Loreto Department (2). Although the annual incidence rates (AIR) in this area decreased from 59.18 per 1,000 inhabitants in 2005 to 11.59 in 2010, a sharp increase was observed in the subsequent years, reaching a peak of AIR of 42.69 in 2013 for both endemic species, *P. vivax* (AIR of 34.94) and *P. falciparum* (AIR of 7.75) (3), and with modest reduction in the following years. Social, economic, and weather variability were hypothesized as drivers of the rapid increase in malaria incidence in recent years (4, 5).

During the PAMAFRO project (2006–2011)—financed by external funding sources such as the World Bank and established in strategic Amazon regions such as Peru, Ecuador, Colombia, and Venezuela—malaria cases were successfully controlled. Training of community health workers for early diagnosis, monitoring, and treatment in first-level health facilities, use of long-lasting insecticide-treated nets (LLINs), and community education in prevention measures were critical to the success of the project and malaria control in these countries (6, 7). However, control interventions were neither widely distributed nor consistent over time in all districts of Loreto (3). The southern provinces of Loreto (Ramón Castilla, Requena, and Ucayali) benefited the least from this project. Even the district of Soplin (Requena Province), where the highest incidence of both malaria species was reported, did not implement community education. Simultaneously, training of health workers was only conducted during 2007–2008, the improvement of diagnosis only during 2007–2010, and the LLIN distribution during 2009–2010 (3). Regrettably, due to lack of sustainable funding, PAMAFRO strategies were discontinued in 2011, and the incidence of malaria increased markedly in all regions the following year (8, 9).

Studies have reported that intervention setbacks or interruptions affect the transmission and re-emergence of malaria (10). On Zanzibar island, Tanzania, after stopping indoor residual spraying (IRS) due to economic factors, malaria cases re-emerged drastically after a period with the lowest malaria burden (11). In the Mutasa district, Zimbabwe, reduced funding for IRS caused a resurgence of malaria (12). Political instability also disrupted control programs as demonstrated in a border area of Brazil where a change of government stopped malaria prevention activities among indigenous peoples, resulting in an outbreak during 2017 (13). Furthermore, in the context of climate change and variability, malaria incidence may be further influenced by meteorological determinants. Although previous studies evaluated the impact of meteorological factors and control interventions on malaria transmission (14, 15), none have assessed whether the dose-response effect of meteorological factors on malaria incidence varies over time (time-varying effect) and if the interruption of control intervention periods plays a role in exacerbating the trends of those time-varying effects.

Meteorological factors are essential components of the mosquito life cycle and parasite reproduction (16, 17). Mosquitoes need particular ranges of temperature (from 23° to 31°C) to transition successfully between each biological stage (18). Particularly, precipitation and humidity patterns are also crucial for adult and immature mosquito survival. For example, an increase in precipitation is often related to higher mortality in mosquito larvae (19, 20). However, rainfall also contributes to mosquito breeding sources (natural or artificial water pools), and even determines their spatial distribution (21). Lower evapotranspiration, defined as the flow of moisture from the soil that directly evaporates into the atmosphere and the water that vegetation transpires into the atmosphere, provides suitable habitat for mosquito larvae development (22). Ambient temperature is a regulator of the parasite biological cycle (23), i.e., high temperature can decrease the parasite extrinsic incubation period (EIP) inside the mosquito salivary glands and stomach (24). However, temperature affects *P. vivax* and *P. falciparum* differently (14). *P. vivax* can develop at a range of 15–30°C, showing less sensitivity to temperature changes compared to *P. falciparum,* which develops at a narrower range (18–30°C) (25). In addition, it has been hypothesized that temperature impacts *P. vivax* during the hypnozoite stage in the human liver until reactivation. The increase in temperature lengthens the latency time of temperate hypnozoite strains in the absence of other external factors such as fever due to other infections (26). In this context, documenting how dose-response relationships between

meteorological factors and malaria incidence change temporally, especially in the context of intervention interruptions, is critical to provide updated epidemiological evidence to identify preventable outbreaks.

As malaria transmission is sensitive to meteorological conditions, the use of early warning systems (EWS) offers the opportunity to take proactive measures to reduce the impact of vector-borne diseases due to the forecasting of unusual temporal or spatial trends prior to the onset of an outbreak (27). For malaria forecasting, an EWS was constructed using temperature, humidity, and precipitation (28). This system identified an increase of malaria cases during warm and humid seasons compared to cold and dry ones. The lagged effect of temperature and rainfall also described the common seasonal patterns observed in malaria epidemics (29). However, endemic infectious disease areas are characterized by extrinsic time-varying factors (public interventions, social and political conflicts) that may affect the course of an outbreak, which would require regular updates of EWS parameters (30).

In this context, our study aims to assess the time-varying relationship between malaria and climatic variables and explore retrospectively whether deviations from the baseline trends were synchronic with the interruption of control strategies (such as the PAMAFRO project). We analyzed detailed data on *P. vivax* and *P. falciparum* malaria cases at a local scale between 2000 and 2017 in the Peruvian Amazon.

METHODS

Study Design

We conducted a retrospective panel data analysis using secondary data of monthly malaria incidence in Loreto, Peru, and meteorological data derived from satellite imagery data to analyze the climate-malaria relationship over an 18-year period.

Study Area and Population

Loreto Department, in northeastern Peru, covers 28.7% of the national territory. The political-administrative organization of Loreto is divided into eight provinces and 53 districts, with Maynas being the province with the largest territorial area and population density in the department, and Iquitos (the capital of Loreto), its most populous city. We included only 49 districts because four were created after the start of the data collection in 2000. According to the National Institute of Statistics and Informatics (INEI is the Spanish acronym) and the Peru National Household Survey (ENAHO in Spanish) in 2019, the total Loreto population was 883,510 inhabitants, of which 69.6% were urban dwellers. Overall, 32.2% of the population lives in poverty (7% in extreme poverty) and only 39.6% of households accessed basic public services (water, sanitation, electricity, and telephone) (31).

The health system in Loreto is composed of public and private clinics. In 2016, Loreto had 521 healthcare facilities (2.8% of the total national facilities), where each physician had to assist an estimated 1,086 inhabitants (32). Regarding health coverage, 85.4% of the population had health insurance, of which 66.6% were affiliated with the free integral health insurance (access to health establishment belonging to the Ministry of Health of Peru [MoH]) (33). For malaria, the diagnosis is carried out exclusively by MoH. However, health access is still deficient in indigenous and rural communities in the Peruvian Amazon, mainly due to transportation and monetary barriers (34, 35). Approximately 83.3% of the population had informal employment since the most common economic activities are based on agriculture, fishing, and mining (32). The geographical location of Loreto, in the Amazon basin, has a rainy tropical climate with high levels of humidity. The maximum temperature reaches 36°C (between December and March), and the minimum is 17°C (between June and July). The humidity and rain are constant throughout the year, with greater intensity between December and May (36).

Data Sources

Malaria Passive Case Detection Data

Epidemiological surveillance of malaria in Peru, carried out by the General Directorate of Epidemiology of MoH, established mandatory weekly case reporting through NOTI software in all health facilities (37, 38). Most of the data were collected at health facilities (passive case detection). The data included malaria cases caused by *P. falciparum* and *P. vivax* species at the district- or province-level.

In Peru, the most common method for laboratory malaria diagnosis is microscopic examination of a thick and thin smear of capillary blood to identify *Plasmodium* presence and specific *Plasmodium* species, respectively. Thick and thin smear procedures (39) and treatment management (40) have been established in national guidelines provided by the Ministry of Health.

For this study, we collected monthly confirmed malaria cases classified by species during 2000–2017 in all districts of Loreto. Data from the four districts created since 2014—after data collection had begun—were included in the districts where they were formerly located. Monthly malaria incidence rates (MIR) were calculated as the ratio of malaria cases to the total population at risk of malaria.

PAMAFRO Study Description

The PAMAFRO project, sponsored by the Global Fund, focused on health worker training and community-based prevention measures and conducted four types of activities for malaria intervention throughout the Loreto region between 2006 and 2010 (41). First, improvement of malaria diagnosis, through training, monitoring, and constant evaluation of experienced and less experienced microscopists, purchase of new microscopes, and maintenance of existing microscopes (7), and implementing a diagnostic quality control system and active and passive search of cases. Second, the strengthening of malaria monitoring and treatment through the supply and availability of antimalarial drugs and inputs, treatment standardization, monitoring treatment adherence, evaluating drug efficacy, and training health workers (3). Third, community participation, through health promotion and education using graphic, radio, and audiovisual materials, formation of community groups to participate in health decision making, searching for community leaders to facilitate communication of behavioral change, and technical and financial support of community environmental

management activities and financial support for prevention campaigns. Finally, the project integrated vector control by purchasing logistical support for the distribution of LLINs in all communities, identifying and eliminating mosquito breeding sites, and applying IRS (6).

Considering that the interventions were not consistently implemented over time, we defined dichotomous variables for each intervention type to identify whether it was conducted during each year in a particular district. Other control efforts carried out by national or international institutions during periods outside of the PAMAFRO project time frame were not considered for this study.

Meteorological Data

Meteorological data for terrestrial surfaces were obtained from the TerraClimate dataset (Climatology Lab of the University of California, Merced) based on climatic aided interpolations (at ∼4-km spatial resolution) from 1958 to 2019 for several meteorological variables, which combine high-resolution spatial climatological normal from the WorldClim with time-varying data from Climate Research Unit version 4.0, and the Japanese 55-year Reanalysis (42). The meteorological variables used for the analysis were actual evapotranspiration (mm), precipitation (mm), runoff (mm), and maximum and minimum temperature (°C). The dataset was downloaded and processed using R software version 5.0.3 to produce monthly district aggregates for the meteorological variables by taking the mean cell values of the grid that pertain to each district in Loreto.

Data Analysis

A descriptive analysis was conducted, where we first analyzed graphically the annual incidence rate variation of malaria by species between 2000 and 2017 at the provincial level, comparing the variation before, during, and after the PAMAFRO intervention. Data from the new province of Putumayo (2014–2017) was merged to their parental province, Maynas province. We also estimated the mean and standard deviation of the annual incidence rates by species and the annual values of the meteorological variables at the provincial level to compare their central tendency and dispersion throughout the study period. Finally, a repeated measures correlation analysis (43) was carried out over the observed values of the meteorological variables at a district level. For studies with repeated measurements of the same groups or individuals over time, the usual technique for a correlation analysis is to aggregate the observations for each group and calculate the correlation coefficient across the aggregated data. However, this may lead to spurious results if the inter-group associations differ from the intra-groups associations (Simpson's paradox). Repeated measures correlation analysis allows for isolation of the inter-district variability to better estimate the common within-district association of the meteorological variables.

Generalized additive models (GAM) were used to apply smooth functions over time to estimate the time-varying effects (i.e., monthly specific slopes) of the meteorological variables on the malaria case count at the district level. Separate models for *P. vivax* and *P. falciparum* were constructed using the same set of selected meteorological covariates to compare the results. The selected variables were the monthly actual evapotranspiration (mm), precipitation (mm), and minimum temperature (°C). Covariate selection for each meteorological exposure model was based on *a priori* knowledge of the structural dependence between these factors. Monthly district counts of new malaria cases were modeled using a Negative binomial (NB) distribution. This distribution was chosen primarily to address the presence of over-dispersion in the counts. Further discussion about the specific distribution can be found in the **Supplementary Methods** section. In addition, we built lagged versions of the models to analyze how the lagged effects of the meteorological variables changed over time. We lagged the values of the covariates by 1, 3, 6, and 12 months and built a different time-varying coefficients model for each lag value. We refer to the model without lagging as the base model. To make the models comparable (fitted over the same data set), we filtered out the first year (2000) since for the 12 month-lagged model we had observations starting at January 2001. Consequently, we fitted all the models with observations of 204 months, from January 2001 to December 2017. We then compared the base model with the lagged models using the Akaike information criterion (AIC) to determine which configuration best fit the data.

For each parasite species, the base NB additive model for the expected cases count was specified as follows:

$$log[E(Y_{ij})] = \alpha + \delta_0(district) + \gamma_1(t) \cdot aet_{ij} + \gamma_2(t) \cdot prcp_{ij} + \gamma_3(t) \cdot mintemp_{ij} + log(pop2015_i),$$

were $E(\cdot)$ is the expectation operator, and Y_{it} is the count of malaria cases for the i-th district ($i = 1, ..., 49$) in the j-th month ($j = 1, ..., 204$). The covariates aet_{ij}, $prcp_{ij}$, and $mintemp_{ij}$ represent the values for the actual evapotranspiration, precipitation, and minimum temperature, respectively, for the i-th district in the j-th month. The parameter α is the intercept of the model. The variable t represents the continuous time over the period of study, and its values were generated by creating date-time values using the months and years of the measurements in the dataset and then converting them into numerical values. Further detail about the generation of these time values can be found in the **Supplementary Methods** section. The functions $\gamma_1(t)$, $\gamma_2(t)$, and $\gamma_3(t)$ are smooth functions over the time variable, and they act as time-varying regression coefficients for the covariates. These smooth terms in the model were approximated using *penalized regression splines*. These types of splines are penalized for their curvature complexity to prevent over-fitting. The degree of penalization is controlled by a regularization parameter, known in the GAM literature as the *smoothing parameter*, which can be estimated from the data along with the estimation of the whole model. The term $\delta_0(district)$ is a random effect term for the districts to adjust for the repeated measures at this geographic level. Finally, the log-population of the districts in 2015 was added as an offset to the models to estimate incidence rates. We did not consider population density as an additional covariate of interest as we assumed no time changes in this variable during the study period. The configuration for the lagged models is the same, but using

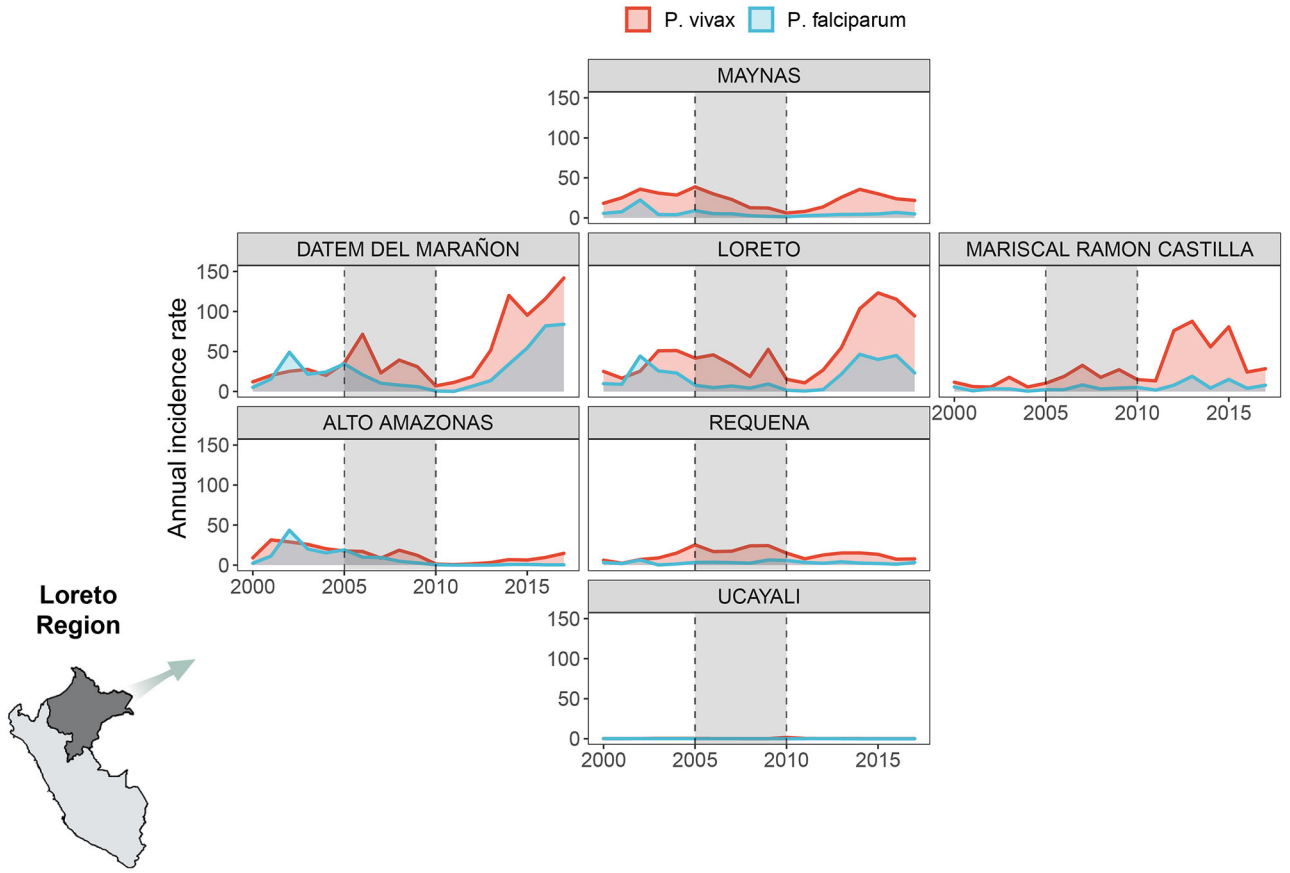

FIGURE 1 | Annual malaria incidence rates variation by parasite species. Annual malaria incidence rates variation due to *P. vivax* (red) and *P. falciparum* (light blue) in 7 provinces of Loreto Region between 2000 and 2017. We created our own grid using the geofacet R package to represent the Loreto provinces: Maynas (first row), Datem del Marañon, Loreto, Mariscal Ramon Castilla (second row from left to right), Alto Amazonas, Requena (third row from left to right), Ucayali (fourth row). The period shaded in gray represents the PAMAFRO intervention.

the lagged values of the covariates instead. The models were estimated using the implementation of the *restricted maximum likelihood* estimation algorithm done by Wood (44). The model fitting under all these specifications was done using the **mgcv** package of R software. Further details about the specifications of the GAMs are available in the **Supplementary Methods** section, but for a more comprehensive review of this topic, please refer to Wood et al. (45).

Before model fitting, we scaled the meteorological variables from 0 to 1, where 0 corresponds to the minimum observed value and 1 to the maximum. Scaling was done to obtain comparable estimates of the coefficients (i.e., standardize), and avoid convergence problems. Therefore, the value of a coefficient for a given meteorological variable at a specific point in time is the log-relative risk of the malaria incidence when the meteorological variable changes from its minimum value to its maximum.

The fitted values of the time-varying coefficients and their confidence intervals were plotted over time, highlighting the period of the PAMAFRO intervention. This strategy enabled a visual analysis of how the coefficients changed before, during, and after this period. For the base time-varying coefficients model, we built a table for the maximum and minimum fitted values and their confidence intervals on each period to facilitate analysis.

RESULTS

Malaria and Meteorological Heterogeneities

Overall, 697,916 malaria cases were analyzed in all the Loreto districts between 2000 and 2017. Most of them (76%) were caused by *P. vivax*, while 24%, by *P. falciparum*. Over time, the AIR decreased between 2006 and 2011 for both malaria species exclusively during the PAMAFRO period. **Figure 1** shows an important geographical heterogeneity of malaria epidemiology for both parasite species. At the sub-regional level, high malaria transmission occurred consistently in the northern provinces of Loreto (Loreto, Datem del Marañon, Mariscal Castilla, and Maynas) compared to the southern provinces (Requena, Alto Amazonas, and Ucayali). The highest mean AIR (per 10,000 population) of *P. vivax* malaria (**Table 1**) was in Loreto province

(Mean-M = 50.3; Standard Deviation-SD = 35.5), whereas the lowest in Ucayali (M = 0.3; SD = 0.4). The highest mean AIR of *P. falciparum* malaria was in Datem del Marañon province (M = 26.2; SD = 25.9), the lowest in Ucayali (M = 0.03; SD = 0.02).

The variability in the distribution of meteorological factors between provinces during the period of study is presented in **Table 1**. Requena had, on average, the lowest annual mean value of actual evapotranspiration (M = 82.41 mm; SD = 4.15), while Datem del Marañon had the highest (M = 86.14 mm; SD = 4.28). Both provinces also had the greatest standard deviations of the annual mean values for this variable, meaning a broader variability. Ucayali showed, on average, the lower level of annual mean precipitation (M = 160.20 mm; SD = 17.50), whereas Maynas had the highest (M = 275.59 mm; SD = 67.55). Greater dispersion is shown in the annual values for this variable compared to the others, i.e., Maynas is the province with the highest dispersion. Regarding the annual mean of maximum temperature, on average, Datem del Marañon had the lowest level (M = 30.37°C; SD = 0.34) and Ucayali had the highest (M = 32.62°C; SD = 0.25). In the case of minimum temperature, lower levels of annual means were seen in Ucayali (M = 20.74°C; SD = 0.25) and the highest levels in Mariscal Ramon Castilla (M = 21.85°C; SD = 0.20). In addition, the outbreak of malaria cases following the interruption of the control efforts was accompanied by an increasing trend of the mean levels of the maximum and minimum temperature over most of the areas of study (**Supplementary Figures 1–7**). For instance, in Datem del Marañon, one of the provinces which had a mayor outbreak, the mean minimum temperature went from ranging from 20.30° to 21.57°C before the interruption to ranging from 20.7° to 22.06°C after the control ceased, and the mean maximum temperature went from ranging from 29.55° to 30.79°C before the interruption to ranging from 29.98° to 31.33°C.

Supplementary Table 1 shows the repeated measures correlation coefficients (r) and their 95% confidence intervals for the climate variables. The most noticeable finding is the almost perfect correlation between precipitation and runoff (r = 0.99; 95% CI: [0.99, 0.99]) within the districts during the period of study. Therefore, including both variables in a model for the malaria incidence rate would have caused multi-collinearity problems. Other variables that showed moderate to strong correlation were the actual evapotranspiration and maximum temperature (r = 0.56; 95% CI: [0.55, 0.57]), and maximum temperature and minimum temperature (r = 0.44; 95% CI: [0.43, 0.46]).

Meteorological Time-Varying Effects

The fitted values of the time-varying coefficients for actual evapotranspiration, precipitation, and minimum temperature, along with their 95% confidence intervals, for both the base model for *P. vivax* and the base model for *P. falciparum* from 2001 to 2017 were plotted in **Figure 2**.

A concurrent exacerbation to a more negative effect of all meteorological variables on the log-relative risk occurs right before and right after the end of the PAMAFRO intervention (**Figure 2**). This exacerbation to a more negative

TABLE 1 | Mean and standard deviation (SD) of the annual incidence rates by parasite species and the annual values of the meteorological variables in the 7 Loreto provinces between 2000 and 2017.

Provinces	AIR		AIR		Actual Evapotranspiration		Precipitation		Runoff		Maximum Temperature		Minimum Temperature	
	P. vivax		*P. falciparum*											
	Mean	SD	Mean	SD	Mean	SD	Mean	SD	Mean	SD	Mean	SD	Mean	SD
Alto Amazonas	13.01	9.51	7.85	11.22	84.93	3.66	186.79	17.56	101.86	16.93	31.63	0.25	21.55	0.25
Datem del Marañon	48.16	42.14	26.17	25.86	86.14	4.28	197.68	18.52	111.55	17.85	30.37	0.34	21.11	0.32
Loreto	50.30	35.49	18.11	16.19	82.12	3.97	233.04	36.00	150.92	36.05	31.24	0.32	21.61	0.26
Mariscal Ramon Castilla	29.71	26.73	5.50	4.81	85.01	3.41	266.47	46.04	181.46	46.67	31.33	0.20	21.85	0.20
Maynas	23.39	9.74	5.64	4.60	80.13	3.52	275.59	67.55	195.45	67.50	30.87	0.29	21.61	0.21
Requena	13.44	6.65	3.16	1.72	82.41	4.15	210.67	31.10	128.26	30.11	31.87	0.22	21.38	0.22
Ucayali	0.26	0.37	0.03	0.02	85.80	3.37	160.20	17.50	74.41	16.62	32.62	0.25	20.74	0.25

AIR, Annual incidence rates (per 10,000 population); Precipitation, actual evapotranspiration and runoff in millimeters (mm), maximum and minimum temperature in Celsius degrees (°C).

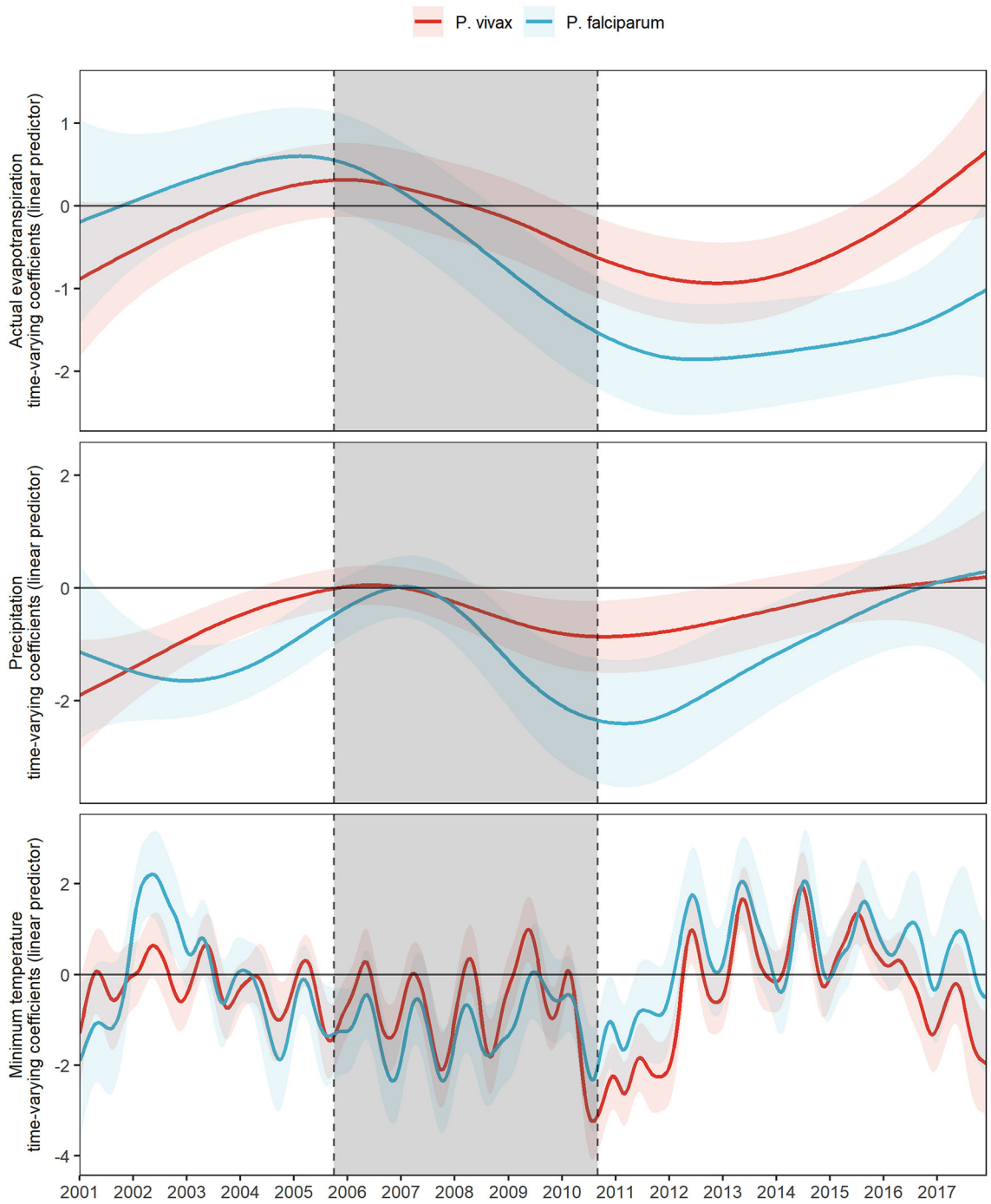

FIGURE 2 | Fitted time-varying meteorological effects on MIR by parasite species. Fitted time-varying meteorological effects due to *P. vivax* (red) and *P. falciparum* (light blue) and their 95% CI (shading of each colored curve). The period shaded in gray represents the PAMAFRO intervention.

effect seems greater for actual transpiration and precipitation for *P. falciparum* than for *P. vivax*, whereas the difference is less evident for the effects of minimum temperature. **Table 2** presents the maximum and minimum values before, during, and after the PAMAFRO intervention of the fitted coefficients of the meteorological variables on each parasite-specific model. The effect of actual evapotranspiration on *P. vivax* began to have a progressive change from being not significant throughout the intervention to a more negative effect around mid-2010 (**Figure 2** and **Table 2**). After the intervention, the minimum coefficient value was −0.94 (95% CI: [−1.43, −0.44]) at the end of 2012, and then transitioned to a non-significant effect between 2015 and

2016. On the other hand, the effect of actual evapotranspiration on *P. falciparum* transitioned from being not significant at the start of the intervention to a more negative effect around mid-2008, prior to the effect on *P. vivax*. It reached the value of −1.86 (95% CI: [−2.52, −1.19]) between 2012 and 2013, which is the minimum value throughout the whole period of study.

A similar pattern was found for precipitation, the only difference being that its effect on *P. vivax* did not intensify much in magnitude at the end of the intervention, compared with its effect on *P. falciparum*. The latter increased significantly in magnitude toward a more negative effect, reaching the value of −2.41 (95% CI: [−3.53, −1.28]) at the first quarter of 2011, right after the end of the PAMAFRO intervention. Finally, it is apparent from **Figure 2** that the effect of minimum temperature on the log-relative risk of malaria incidence presented a seasonal pattern with a stable level throughout the whole period of study. Two disruptions in the level of its effect are visible in the plot. The first one occurred between 2002 and 2003, where the effect of minimum temperature on *P. falciparum* had a substantial increase toward a more positive effect, and the second one between 2010 and 2012, where the effect on *P. vivax* increased toward a more negative effect. In the latter period, the effect of minimum temperature on *P. vivax* reached a value of −3.23 (95% CI: [−4.07, −2.40]) in 2010, the same year the intervention ended. Before 2010, the effect of minimum temperate on both parasite species tended to have a negative level, whereas, after 2012, it tended to have a positive level.

Variation of Meteorological Time-Varying Lagged Effects

Figure 3 shows the fitted coefficients and their 95% confidence interval for the meteorological variables lagged by different numbers of months. Different models were fitted for each lag value. The magnitude and direction of the lagged effects of the meteorological variables on each parasite species changed differently throughout the study, although most of the lags for each variable follow a similar trend. In the case of actual evapotranspiration, its 6-month lagged effects on *P. vivax* and *P. falciparum* intensified more over time compared to the other lags. For *P. vivax*, it was exacerbated toward a more positive effect between 2008 and 2010, following an exacerbation to a more negative effect from 2010 to 2013. For *P. falciparum,* it transitioned from null effects most of the time during the intervention to a more negative effect after the PAMAFRO intervention between 2010 and 2013.

For precipitation, the exacerbation to a more negative effect at the end of PAMAFRO was observed for the no lagged and 12-month lagged effects on *P. vivax*, and all the lagged effects, except the 6-month lagged effect on *P. falciparum*. Finally, for the minimum temperature, all the lagged effects suggest evidence of a seasonal pattern. The greatest intensification was observed on the 6-month lagged effect after the PAMAFRO intervention, from 2012 to 2014, where the effects on each parasite species increased in magnitude toward a more positive effect.

Model performance metrics were presented in **Supplementary Table 2**. For *P. vivax*, the 1-, 3-, and 6-month lagged covariates models performed better for the AIC. For instance, the 6-month lag had the best AIC value, and the 12-month lagged covariates model had the worst. The more complex model was the 3-month lagged covariates model, as it had higher degrees of freedom, and, conversely, the simpler one was the 1-month lagged covariates model. For *P. falciparum*, results were similar, but the base model, in this case, was slightly better than the 3-month lagged covariates model. The more complex model for *P. falciparum* was the model with 6-month lags, and the simpler one was the model with a 12-month lag.

DISCUSSION

By analyzing panel data of the Peruvian Amazon from 2001 to 2017, this study found a critical disruption in the baseline relationship between malaria and climate after the interruption of the malaria control period implemented by PAMAFRO. At the end of the PAMAFRO intervention, the estimated effects (dose-response) of actual evapotranspiration, precipitation, and minimum temperature on the incidence rates decreased for both malaria parasite species. Although this decrease diminished after ∼2 years, the dose-response effects did not return to baseline levels (before the PAMAFRO period). Notably, the interruption of the PAMAFRO project impacted the time-varying effects of meteorological variables such as precipitation and actual evapotranspiration more markedly for *P. falciparum* compared with *P. vivax*. These findings highlight the importance of sustaining malaria control efforts since interruption may destabilize the baseline (pre-PAMAFRO) associations between meteorological factors and malaria incidence rates. Also, the time-varying effect of meteorological factors on malaria incidence should be used to inform and update EWS in the context of climate change projections.

The effect of meteorological variables on malaria incidence, when the PAMAFRO intervention was discontinued, demonstrated that the relationship between malaria and climate intensified in a region of low malaria incidence. This emphasizes the importance of monitoring meteorological variation during the elimination process to detect early disruptions of this relationship. EWS play a pivotal role in this context when considering these time-varying effects. Previous studies have revealed the importance of implementing integrated surveillance and control systems for monitoring meteorological indicators in predicting abrupt changes in the risk of malaria in hotspots of the Amazon region (46).

The effect of meteorological variables on *P. falciparum* was longer and temporally significant compared with *P. vivax* where the decreases are potentially related to activation of the silent latent parasite stage (hypnozoite), that results in relapses (47). In addition, *P. falciparum* has been associated with minimum temperatures over time (14, 48), due to its shorter optimal developmental temperature range (15°-30°C) compared to *P. vivax* (18°-30°C) (49). High temperature shortens the parasite

TABLE 2 | Maximum and minimum fitted effects of the meteorological variables of the adjusted models for the parasite species within three periods: before, during and after the PAMAFRO intervention.

Climate variable	Before				During				After			
	Min		Max		Min		Max		Min		Max	
	Estimate	95% CI	Estimate	95% CI	Estimate	95% CI	Estimate	95% CI	Estimate	95% CI	Estimate	95% CI
P. vivax												
Actual evapotranspiration	−0.88	[−1.82, 0.06]	0.31	[−0.13, 0.76]	−0.62	[−1.11, −0.14]	0.31	[−0.13, 0.76]	−0.94	[−1.43, −0.44]	0.66	[−0.13, 1.44]
Precipitation	−1.90	[−2.88, −0.92]	−0.01	[−0.37, 0.34]	−0.87	[−1.50, −0.23]	0.05	[−0.30, 0.40]	−0.87	[−1.51, −0.23]	0.19	[−1.02, 1.40]
Minimum temperature	−1.46	[−2.29, −0.64]	0.66	[−0.03, 1.34]	−3.23	[−4.07, −2.40]	1.00	[0.28, 1.71]	−3.04	[−3.81, −2.26]	1.93	[1.17, 2.69]
P. falciparum												
Actual evapotranspiration	−0.19	[−1.43, 1.04]	0.60	[0.02, 1.18]	−1.53	[−2.20, −0.86]	0.55	[−0.04, 1.13]	−1.86	[−2.52, −1.19]	−1.01	[−2.08, 0.06]
Precipitation	−1.65	[−2.30, −1.00]	−0.48	[−1.03, 0.07]	−2.35	[−3.45, −1.25]	0.02	[−0.53, 0.57]	−2.41	[−3.53, −1.28]	0.29	[−1.72, 2.30]
Minimum temperature	−1.90	[−3.68, −0.12]	2.21	[1.28, 3.15]	−2.35	[−3.49, −1.20]	0.06	[−0.99, 1.11]	−1.88	[−2.98, −0.79]	2.07	[0.96, 3.17]

95% CI: 95% Confidence Interval.
Precipitation and actual evapotranspiration in millimeters (mm), maximum and minimum temperature in Celsius degrees (°C).

development inside the mosquito; thus the EIP is ∼9–15 days for *P. falciparum* and 8–24 days for *P. vivax* (50).

Our results were consistent with previous studies in terms of heterogeneity among meteorological variables. A predictive study reported that moderate temperature (23–24°C) was related to the highest risk of malaria at a lag of 2 weeks, with a significantly increased risk up to 4 weeks of lag (51). Intriguingly, this is consistent with the incubation period of the parasite inside a human host; the time elapsed between the mosquito bite and the manifestation of symptoms is ∼9–14 days for *P. falciparum* and 12–17 days for *P. vivax* infection (52). The parasite EIP inside the mosquito ranges between 1 and 3 weeks (50), reinforcing the seasonal relationship between temperature and malaria incidence. In addition, our study described a significantly longer effect of precipitation and evapotranspiration on malaria incidence; this could be explained by the formation of optimal mosquito breeding sites as a consequence of rainfall over the previous year (51). The development of natural breeding sources is a long-term process that depends not only on precipitation but also on vegetation and soil moisture (which control evapotranspiration) (53). In other vector-borne diseases such as dengue, there was a similar pattern of meteorological variables: the minimum temperature (26°C) with 0–5 weeks lag and precipitation (60 mm) with 8–15 weeks lag was related with increased dengue incidence (54).

Our findings are relevant for current and future climate change. Climate change causes unexpected circumstances such as land degradation and disruption, floods, and droughts that destabilize the economic growth, population health and often increase migration (23, 55), which alter the operation of control activities, as well as interactions among the environment, mosquito, and host. Mosquitoes circulate in impacted environments near human settlements, resulting in increased malaria risk (56). Also, rising global temperature is a major contributor to the increasing spread of malaria even in non-endemic areas (57, 58). In addition, governments need to monitor and enforce the implementation of malaria interventions (59). In Zambia, for example, many of the positive effects of control programs are being reduced by the negative impact of climatic conditions that favor the spread of malaria (60). These scenarios may lead to a more substantial resurgence, changes in seasonal trends, and complications for malaria control and elimination.

After a period of low malaria rates due to control interventions, malaria re-emerged due to weakening control activities, technical problems, and increasing malaria potential (61). Funding constraints are the most common cause of control program interruptions. After only 4 months of discontinuing malaria prevention activities in Uganda, malaria cases increased (62). In Venezuela, the high incidence rates of malaria continue to increase due to the catastrophic socio-economic and political crisis that decimated vector-borne disease control programs. Prolonged poverty, lack of hygiene, and malnutrition has increased population-level susceptibility to infectious diseases (63). A major contributing factor has been the massive migration of Venezuelans to neighboring countries resulting in the importation of malaria cases to border regions (64). Similar situations have been reported around the world (11, 12, 61). Despite decreases in funding from international entities and global funds, we strongly recommend that intervention be considered an ongoing and necessary expense (65). Effective control of malaria hotspots could reduce malaria mortality and morbidity (66). Changes in land cover due to human settlement may also alter the temperature and increase mosquito migration to non-endemic high altitudes, for example in Kenya (67). One study showed that mosquitoes carried by wind continued surviving, breeding, and feeding on human blood, potentially expanding malaria transmission to new altitudes (68).

We acknowledge the following limitations to this study. First, passive case detection data are recorded only for individuals overwhelmed by symptoms who seek care at health services; health personnel do not conduct active case detection in the community. Hence the results of these findings are relevant only for clinical cases, and further studies are required to understand whether the same patterns are observed for asymptomatic cases, which contribute to the maintenance of parasite transmission

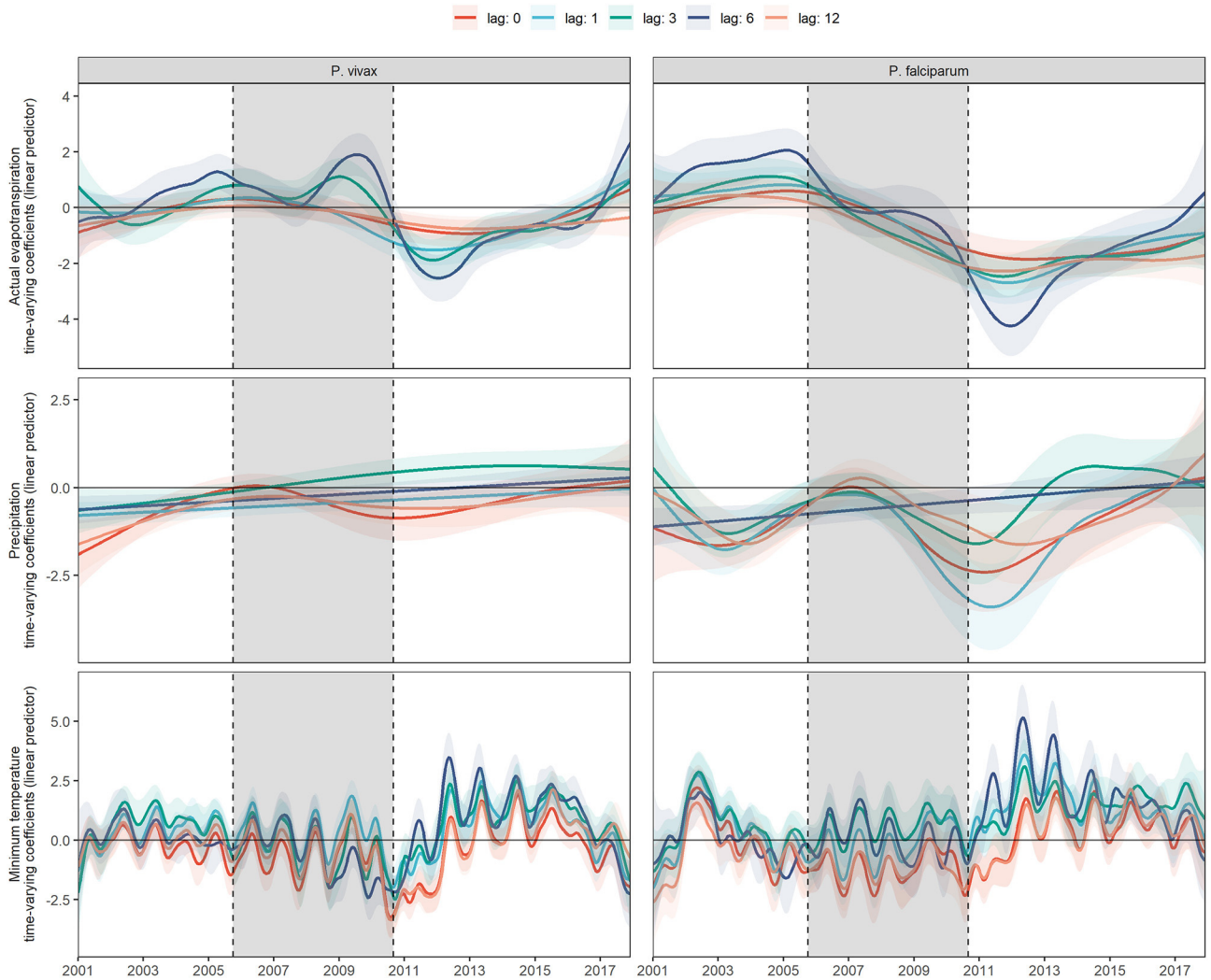

FIGURE 3 | Fitted time-varying meteorological effects on MIR by parasite species at different time lags. Fitted time-varying meteorological effects at different time lags and their 95% CI (shading of each colored curve). The period shaded in gray represents the PAMAFRO intervention.

(69). Second, limited access to remote areas in the Amazon region prevents continuous health care access to indigenous communities, thus the malaria caseload is an underestimate. Low geographic accessibility and travel time have been found to be barriers to reaching remote health facilities (35). Third, some reports have indicated that mosquito activities such as host-seeking behavior were influenced by wind speed affecting human CO_2 dispersion, and other studies reported that the mosquito movement depends on wind direction (70). However, we did not include other meteorological variables such as wind speed in this analysis. Instead, we selected meteorological variables commonly used in epidemiological malaria studies. Finally, other factors such as natural disasters or political crises were not considered for this analysis; to the best of our knowledge, no major events were reported in this area during the study period.

CONCLUSIONS

The sustainability of malaria elimination efforts deserves particular attention due to current climate change challenges. This study provided evidence of important deviations of the baseline climate-malaria trends concurrent with the interruption of malaria control interventions in the study area. These disruptions significantly affect the transmission of *P. falciparum* in comparison to *P. vivax* and provide information for tailoring future malaria control activities.

DATA AVAILABILITY STATEMENT

The data analyzed in this study is subject to the following licenses/restrictions: Dataset will be available upon request to the Peruvian Ministry of Health. Requests to access these datasets should be directed to transparencia@minsa.gob.pe.

ETHICS STATEMENT

Ethical review and approval was not required for the study on human participants in accordance with the local legislation and institutional requirements. Written informed consent from the participants' legal guardian/next of kin was not required to participate in this study in accordance with the national legislation and the institutional requirements.

AUTHOR CONTRIBUTIONS

GC-E conceived the idea of the study. GC-E, JQ, DV, and RC designed the study. DV and RC analyzed the data. GC-E wrote the article with contributions from JQ, DV, RC, AL-C, and TB. All authors contributed to the article and approved the submitted version.

ACKNOWLEDGMENTS

We thank the Ministry of Health and the Regional Directorate of Health of Loreto for providing such useful data to researchers. We thank Prof. Jan Evelyn Conn (New York State Department of Health, Wadsworth Center, Albany, NY, United States of America) for editing and proof-reading the manuscript.

SUPPLEMENTARY MATERIAL

The Supplementary Material for this article can be found online at: https://www.frontiersin.org/articles/10.3389/fmed.2021.721515/full#supplementary-material

REFERENCES

1. World Health Organization. *World Malaria Report 2020*. (2020). Available online at: https://www.who.int/teams/global-malaria-programme/reports/world-malaria-report-2020 (accessed: February 7, 2021).
2. Centro Nacional de Epidemiología Prevención y Control de Enfermedades. *Boletín Epidemiológico del Perú - SE 42*. (2019). Available online at: https://www.dge.gob.pe/portal/docs/vigilancia/boletines/2019/42.pdf (accessed on: December 1, 2020).
3. Soto-Calle V, Rosas-Aguirre A, Llanos-Cuentas A, Abatih E, Dedeken R, Rodriguez H, et al. Spatio-temporal analysis of malaria incidence in the Peruvian Amazon Region between 2002 and 2013. *Sci Rep*. (2017) 7:40350. doi: 10.1038/srep40350
4. Rosas-Aguirre A, Gamboa D, Manrique P, Conn JE, Moreno M, Lescano AG, et al. Epidemiology of *Plasmodium vivax* malaria in Peru. *Am J Trop Med Hyg*. (2016) 95:133–44. doi: 10.4269/ajtmh.16-0268
5. Chowell G, Munayco CV, Escalante AA, McKenzie FE. The spatial and temporal patterns of falciparum and vivax malaria in Peru: 1994–2006. *Malar J*. (2009) 8:142. doi: 10.1186/1475-2875-8-142
6. Rosas-Aguirre A, Guzmán-Guzmán M, Moreno-Gutierrez D, Rodriguez-Ferrucci H, Vargas-Pacherrez D, González A. Long-lasting insecticide - treated bednet ownership, retention and usage one year after their distribution in Loreto, Peru. *Rev Peru Med Exp Salud Publica*. (2011) 28:228–64. doi: 10.1590/S1726-46342011000200009
7. Rosas-Aguirre A, Gamboa D, Rodriguez H, Llanos-Zavalaga F, Aguirre K, Llanos-Cuentas A. Use of standardized blood smear slide sets for competency assessment in the malaria microscopic diagnosis in the Peruvian Amazon. *Rev Peru Med Exp Salud Publica*. (2010) 27:540–7. doi: 10.1590/S1726-46342010000400008
8. Rosas-Aguirre A. *Understanding transmission dynamics for malaria control and elimination in peru [Doctoral Dissertation]*. Université catholique de Louvain, Brussels, Belgium (2015). Available online at: https://dial.uclouvain.be/pr/boreal/object/boreal%3A165403/datastream/PDF_01/view (accessed March 10, 2021).
9. Rosas-Aguirre A, Speybroeck N, Llanos-Cuentas A, Rosanas-Urgell A, Carrasco-Escobar G, Rodriguez H, et al. Hotspots of malaria transmission in the Peruvian amazon: rapid assessment through a parasitological and serological survey. *PLoS ONE*. (2015) 10:e0137458. doi: 10.1371/journal.pone.0137458
10. Bennett A, Yukich J, Miller JM, Keating J, Moonga H, Hamainza B, et al. The relative contribution of climate variability and vector control coverage to changes in malaria parasite prevalence in Zambia 2006–2012. *Parasit Vectors*. (2016) 9:431. doi: 10.1186/s13071-016-1693-0
11. Aregawi MW, Ali AS, Al-Mafazy AW, Molteni F, Katikiti S, Warsame M, et al. Reductions in malaria and anaemia case and death burden at hospitals following scale-up of malaria control in Zanzibar, 1999–2008. *Malar J*. (2011) 10:46. doi: 10.1186/1475-2875-10-46
12. Mharakurwa S, Thuma PE, Norris DE, Mulenga M, Chalwe V, Chipeta J, et al. Malaria epidemiology and control in Southern Africa. *Acta Trop*. (2012) 121:202–6. doi: 10.1016/j.actatropica.2011.06.012
13. Mosnier E, Dusfour I, Lacour G, Saldanha R, Guidez A, Gomes MS, et al. Resurgence risk for malaria, and the characterization of a recent outbreak in an Amazonian border area between French Guiana and Brazil. *BMC Infect Dis*. (2020) 20:373. doi: 10.1186/s12879-020-05086-4
14. Fletcher IK, Stewart-Ibarra AM, Sippy R, Carrasco-Escobar G, Silva M, Beltran-Ayala E, et al. The relative role of climate variation and control interventions on malaria elimination efforts in El Oro, Ecuador: a modeling study. *Front Environ Sci*. (2020) 8:135. doi: 10.3389/fenvs.2020.00135
15. Thomson MC, Muñoz ÁG, Cousin R, Shumake-Guillemot J. Climate drivers of vector-borne diseases in Africa and their relevance to control programmes. *Infect Dis Poverty*. (2018) 7:81. doi: 10.1186/s40249-018-0460-1
16. Castro MC. Malaria transmission and prospects for malaria eradication: the role of the environment. *Cold Spring Harb Perspect Med*. (2017) 7:a025601. doi: 10.1101/cshperspect.a025601
17. Brugueras S, Fernández-Martínez B, Martínez-de la Puente J, Figuerola J, Porro TM, Rius C, et al. Environmental drivers, climate change and emergent diseases transmitted by mosquitoes and their vectors in southern Europe: a systematic review. *Environ Res*. (2020) 191:110038. doi: 10.1016/j.envres.2020.110038
18. Christiansen-Jucht CD, Parham PE, Saddler A, Koella JC, Basáñez MG. Larval and adult environmental temperatures influence the adult reproductive traits of *Anopheles gambiae s.s. Parasit Vect*. (2015) 8:456. doi: 10.1186/s13071-015-1053-5
19. Parham PE, Pople D, Christiansen-Jucht C, Lindsay S, Hinsley W, Michael E. Modeling the role of environmental variables on the population dynamics of the malaria vector *Anopheles gambiae* sensu stricto. *Malar J*. (2012) 11:271. doi: 10.1186/1475-2875-11-271
20. Paaijmans KP, Wandago MO, Githeko AK, Takken W. Unexpected high losses of *Anopheles gambiae* larvae due to rainfall. *PLoS ONE*. (2007) 2:1146. doi: 10.1371/journal.pone.0001146
21. Zeilhofer P, dos Santos ES, Ribeiro ALM, Miyazaki RD, dos Santos MA. Habitat suitability mapping of *Anopheles darlingi* in the surroundings of the Manso hydropower plant reservoir, Mato Grosso, Central Brazil. *Int J Health Geogr*. (2007) 6:7. doi: 10.1186/1476-072X-6-7
22. Le PVV, Kumar P, Ruiz MO, Mbogo C, Muturi EJ. Predicting the direct and indirect impacts of climate change on malaria in coastal Kenya. *PLoS ONE*. (2019) 14:e0211258. doi: 10.1371/journal.pone.0211258
23. Rossati A, Bargiacchi O, Kroumova V, Zaramella M, Caputo A, Garavelli Pietro L. Climate, environment and transmission of malaria. *Infez Med*. (2016) 24:93–104.

24. Patz JA, Olson SH. Malaria risk and temperature: influences from global climate change and local land use practices. *Proc Natl Acad Sci USA*. (2006) 103:5635–6. doi: 10.1073/pnas.0601493103
25. Guo C, Yang L, Ou CQ, Li L, Zhuang Y, Yang J, et al. Malaria incidence from 2005–2013 and its associations with meteorological factors in Guangdong, China. *Malar J*. (2015) 14:116. doi: 10.1186/s12936-015-0630-6
26. White MT, Shirreff G, Karl S, Ghani AC, Mueller I. Variation in relapse frequency and the transmission potential of *Plasmodium vivax* malaria. *Proc R Soc B Biol Sci*. (2016) 283:20160048. doi: 10.1098/rspb.2016.0048
27. Semenza JC, Suk JE. Vector-borne diseases and climate change: a European perspective. *FEMS Microbiol Lett*. (2018) 365:244. doi: 10.1093/femsle/fnx244
28. Maharaj R. Early warning systems for the detection of malaria outbreaks. *Indian J Med Res*. (2017) 146:560–2. doi: 10.4103/ijmr.IJMR_933_17
29. Teklehaimanot HD, Schwartz J, Teklehaimanot A, Lipsitch M. Weather-based prediction of *Plasmodium falciparum* malaria in epidemic-prone regions of Ethiopia II. Weather-based prediction systems perform comparably to early detection systems in identifying times for interventions. *Malar J*. (2004) 3:44. doi: 10.1186/1475-2875-3-44
30. Dureau J, Kalogeropoulos K, Baguelin M. Capturing the time-varying drivers of an epidemic using stochastic dynamical systems. *Biostatistics*. (2013) 14:541–55. doi: 10.1093/biostatistics/kxs052
31. Ministerio de Desarrollo e Inclusión Social. *Reporte regional de indicadores sociales del departamento de Loreto*. (2020). Available online at: http://sdv.midis.gob.pe/RedInforma/Reporte/ReportePDF?vCodTema=1 (accessed on: December 18, 2020).
32. Instituto Nacional de Estadística e Informática. *Compendio Estadístico: Loreto 2017*. (2017). Available online at: https://www.inei.gob.pe/media/MenuRecursivo/publicaciones_digitales/Est/Lib1501/libro.pdf (accessed on: December 18, 2020).
33. Instituto Nacional de Estadística e Informática. *Población afiliada a algún seguro de salud*. (2018). Available online at: http://censo2017.inei.gob.pe/publicaciones_especiales/ (accessed: December 10, 2020).
34. Brierley CK, Suarez N, Arora G, Graham D. Healthcare access and health beliefs of the indigenous peoples in remote amazonian Peru. *Am J Trop Med Hyg*. (2014) 90:180–3. doi: 10.4269/ajtmh.13-0547
35. Carrasco-Escobar G, Manrique E, Tello-Lizarraga K, Miranda JJ. Travel time to health facilities as a marker of geographical accessibility across heterogeneous land coverage in Peru. *Front Public Health*. (2020) 8:498. doi: 10.3389/fpubh.2020.00498
36. Ministerio del ambiente. SENAMHI - Loreto (2020). Available online at: https://www.senamhi.gob.pe/main.php?dp=loreto&p=pronostico-detalle (accessed on: January 31, 2021)
37. Ministerio de Salud. *Herramientas Para la Vigilancia Epidemiológica*. (2005). Available online at: https://www.dge.gob.pe/portalnuevo/publicaciones/materiales/herramientas-para-la-vigilancia-epidemiologica/ (accessed on: January 27, 2021).
38. Ministerio de Salud. Directiva sanitaria N° 046 - *MINSA/DGE-V.01 de notificación de enfermedades y eventos sujetos a vigilancia epidemiológica en salud pública*. (2013). Available online at: https://www.gob.pe/institucion/minsa/informes-publicaciones/280839-directiva-sanitaria-n-046-minsa-dge-v-01-de-notificacion-de-enfermedades-y-eventos-sujetos-a-vigilancia-epidemiologica-en-salud-publica (accessed: January 27, 2021).
39. Instituto Nacional de Salud. *Manual de procedimientos de laboratorio para el diagnóstico de malaria*. (2003). Available online at: https://www.gob.pe/institucion/minsa/informes-publicaciones/353447-manual-de-procedimientos-de-laboratorio-para-el-diagnostico-de-malaria (accessed: January 27, 2021).
40. Ministerio de Salud. *Norma técnica de salud para la atención de la malaria y malaria grave en el Perú*. (2015). Available online at: https://www.gob.pe/institucion/minsa/informes-publicaciones/280813-norma-tecnica-de-salud-para-la-atencion-de-la-malaria-y-malaria-grave-en-el-peru (accessed: January 27, 2021).
41. Pan American Health Organization. *Compartiendo Lecciones Aprendidas*. Proyecto control de la Malaria en las zonas fronterizas de la Región Andina: Un enfoque comunitario - PAMAFRO (2011). Available online at: https://www.paho.org/es/documentos/compartiendo-lecciones-aprendidas-proyecto-control-malaria-zonas-fronterizas-region (accessed on: January 25, 2021).
42. Abatzoglou JT, Dobrowski SZ, Parks SA, Hegewisch KC. TerraClimate, a high-resolution global dataset of monthly climate and climatic water balance from 1958-2015. *Sci Data*. (2018) 5:170191. doi: 10.1038/sdata.2017.191
43. Bakdash JZ, Marusich LR. Repeated measures correlation. *Front Psychol*. (2017) 8:456. doi: 10.3389/fpsyg.2017.00456
44. Wood SN. Fast stable restricted maximum likelihood and marginal likelihood estimation of semiparametric generalized linear models. *J R Stat Soc Ser B (Statistical Methodol*. (2011) 73:3–36. doi: 10.1111/j.1467-9868.2010.00749.x
45. Wood SN. *Generalized Additive Models: An Introduction With R*. 2nd ed. Chapman and Hall/CRC (2017). doi: 10.1201/9781315370279
46. Ruiz D, Ceroń V, Molina AM, Quiñones ML, Ji?enez MM, Ahumada M, et al. Implementation of malaria dynamic models in municipality level early warning systems in Colombia. Part I: description of study sites. *Am J Trop Med Hyg*. (2014) 91:27–38. doi: 10.4269/ajtmh.13-0363
47. White NJ. Determinants of relapse periodicity in *Plasmodium vivax* malaria. *Malar J*. (2011) 10:297. doi: 10.1186/1475-2875-10-297
48. Bi Y, Yu W, Hu W, Lin H, Guo Y, Zhou XN, et al. Impact of climate variability on *Plasmodium vivax* and *Plasmodium falciparum* malaria in Yunnan Province, China. *Parasit Vectors*. (2013) 6:357. doi: 10.1186/1756-3305-6-357
49. Olliaro PL, Barnwell JW, Barry A, Mendis K, Mueller I, Reeder JC, et al. Implications of *Plasmodium vivax* biology for control, elimination, and research. *Am J Trop Med Hyg*. (2016) 95:4–14. doi: 10.4269/ajtmh.16-0160
50. Thomas S, Ravishankaran S, Justin NAJA, Asokan A, Kalsingh TMJ, Mathai MT, et al. Microclimate variables of the ambient environment deliver the actual estimates of the extrinsic incubation period of *Plasmodium vivax* and *Plasmodium falciparum*: a study from a malaria-endemic urban setting, Chennai in India. *Malar J*. (2018) 17:201. doi: 10.1186/s12936-018-2342-1
51. Kim Y, Ratnam JV, Doi T, Morioka Y, Behera S, Tsuzuki A, et al. Malaria predictions based on seasonal climate forecasts in South Africa: a time series distributed lag nonlinear model. *Sci Rep*. (2019) 9:17882. doi: 10.1038/s41598-019-53838-3
52. Warrell DA, Gilles HM. *Essential Malariology*. 4th ed. New York, NY: Oxford University Press (2002).
53. Malahlela OE, Olwoch JM, Adjorlolo C. Evaluating efficacy of landsat-derived environmental covariates for predicting malaria distribution in rural villages of Vhembe District, South Africa. *Ecohealth*. (2018) 15:23–40. doi: 10.1007/s10393-017-1307-0
54. Kakarla SG, Caminade C, Mutheneni SR, Morse AP, Upadhyayula SM, Kadiri MR, et al. Lag effect of climatic variables on dengue burden in India. *Epidemiol Infect*. (2019) 147:e170. doi: 10.1017/S0950268819000608
55. Arora NK. Impact of climate change on agriculture production and its sustainable solutions. *Environ Sustain*. (2019) 2:95–6. doi: 10.1007/s42398-019-00078-w
56. Alimi TO, Fuller DO, Qualls WA, Herrera SV, Arevalo-Herrera M, Quinones ML, et al. Predicting potential ranges of primary malaria vectors and malaria in northern South America based on projected changes in climate, land cover and human population. *Parasit Vectors*. (2015) 8:431. doi: 10.1186/s13071-015-1033-9
57. Moukam Kakmeni FM, Guimapi RYA, Ndjomatchoua FT, Pedro SA, Mutunga J, Tonnang HEZ. Spatial panorama of malaria prevalence in Africa under climate change and interventions scenarios. *Int J Health Geogr*. (2018) 17:2. doi: 10.1186/s12942-018-0122-3
58. Dhimal M, Ahrens B, Kuch U. Climate change and spatiotemporal distributions of vector-borne diseases in Nepal - A systematic synthesis of literature. *PLoS ONE*. (2015) 10:e0129869. doi: 10.1371/journal.pone.0129869
59. Gething PW, Smith DL, Patil AP, Tatem AJ, Snow RW, Hay SI. Climate change and the global malaria recession. *Nature*. (2010) 465:342–5. doi: 10.1038/nature09098
60. Nawa M, Halwindi H, Hangoma P. Modelling malaria reduction in a highly endemic country: Evidence from household survey, climate, and programme data in Zambia. *J Public Health Afr*. (2020) 11:1096. doi: 10.4081/jphia.2020.1096
61. Cohen JM, Smith DL, Cotter C, Ward A, Yamey G, Sabot OJ, et al. Malaria resurgence: a systematic review and assessment of its causes. *Malar J*. (2012) 11:122. doi: 10.1186/1475-2875-11-122
62. Raouf S, Mpimbaza A, Kigozi R, Sserwanga A, Rubahika D, Katamba H, et al. Resurgence of malaria following discontinuation of indoor residual

spraying of insecticide in an area of Uganda with previously high-transmission intensity. *Clin Infect Dis*. (2017) 65:453–60. doi: 10.1093/cid/cix251
63. Grillet ME, Hernández-Villena JV, Llewellyn MS, Paniz-Mondolfi AE, Tami A, Vincenti-Gonzalez MF, et al. Venezuela's humanitarian crisis, resurgence of vector-borne diseases, and implications for spillover in the region. *Lancet Infect Dis*. (2019) 19:e149–61. doi: 10.1016/S1473-3099(18)30757-6
64. Arisco NJ, Peterka C, Castro MC. Cross-border malaria in Northern Brazil. *Malar J*. (2021) 20:135. doi: 10.1186/s12936-021-03668-4
65. Shretta R, Avanceña ALV, Hatefi A. The economics of malaria control and elimination: a systematic review. *Malar J*. (2016) 15:593. doi: 10.1186/s12936-016-1635-5
66. Scott N, Hussain SA, Martin-Hughes R, Fowkes FJI, Kerr CC, Pearson R, et al. Maximizing the impact of malaria funding through allocative efficiency: using the right interventions in the right locations. *Malar J*. (2017) 16:368. doi: 10.1186/s12936-017-2019-1
67. Kweka EJ, Kimaro EE, Munga S. Effect of deforestation and land use changes on mosquito productivity and development in western Kenya highlands: Implication for malaria risk. *Front Public Health*. (2016) 4:238. doi: 10.3389/fpubh.2016.00238
68. Sanogo ZL, Yaro AS, Dao A, Diallo M, Yossi O, Samaké D, et al. The effects of high-altitude windborne migration on survival, oviposition, and blood-feeding of the African malaria mosquito, *Anopheles gambiae* s.l. (Diptera: Culicidae). *J Med Entomol*. (2020) 58:343–9. doi: 10.1093/jme/tjaa137
69. Cheaveau J, Mogollon DC, Mohon MAN, Golassa L, Yewhalaw D, Pillai DR. Asymptomatic malaria in the clinical and public health context. *Expert Rev Anti Infect Ther*. (2019) 17:997–1010. doi: 10.1080/14787210.2019.1693259
70. Endo N, Eltahir EAB. Modelling and observing the role of wind in *Anopheles* population dynamics around a reservoir. *Malar J*. (2018) 17:48. doi: 10.1186/s12936-018-2197-5

Conflict of Interest: The authors declare that the research was conducted in the absence of any commercial or financial relationships that could be construed as a potential conflict of interest.

Publisher's Note: All claims expressed in this article are solely those of the authors and do not necessarily represent those of their affiliated organizations, or those of the publisher, the editors and the reviewers. Any product that may be evaluated in this article, or claim that may be made by its manufacturer, is not guaranteed or endorsed by the publisher.

frontiers in Cellular and Infection Microbiology

ORIGINAL RESEARCH
published: 05 October 2021
doi: 10.3389/fcimb.2021.673299

Molecular Characterization of Dengue Virus Type 1 in Zhejiang in 2019

Wenwu Yao[†], *Zhangnv Yang*[†], *Xiuyu Lou*, *Haiyan Mao*, *Hao Yan*[*] *and Yanjun Zhang*[*]

Department of Microbiology, Zhejiang Provincial Center for Disease Control and Prevention, Hangzhou, China

Dengue fever (DF) is a mosquito-borne viral disease caused by the dengue virus (DENV), which is considered one of the most important arboviruses in the world. This study aimed to determine the molecular, epidemiological, and phylogenetic characterization of 174 DENV-1 (132 indigenous cases and 42 imported cases) isolated from nine municipalities of Zhejiang province in 2019. The analyses of phylogenetics, haplotypes, and amino acid substitutions were conducted based on the full envelope (E) gene sequences. Sixty-four haplotypes were clustered into two main clades, with isolates from Wenzhou and Taizhou mainly clustered into clade I and Hangzhou and Ningbo cases clustered into clade II. Six sites of amino acid substitutions including A88T, F96L, M297V, T339S, I378L, and V436I were only observed in strains isolated from Ningbo and Hangzhou, while two sites of amino acid substitutions including V312L and V380I were observed in strains from Taizhou and Wenzhou. In our study, strains were in high homology with the strains from Southeast Asian countries, thus cases in Zhejiang were probably imported from Southeast Asian countries. The strains from different regions in Zhejiang were clustered in the same branch which may be caused by the continuous import of cases in the same country at different time periods. After the continuous outbreak in Zhejiang province, some sites of the dengue gene have mutated, and the effects need further study.

Keywords: dengue virus, phylogentic analysis, E gene, amino acid mutation, prevention

OPEN ACCESS

Edited by:
Jun Feng,
National Institute of Parasitic Diseases, China

Reviewed by:
Huda Makhluf,
National University, United States
Changwen Ke,
Guangdong Provincial Center for Disease Control and Prevention, China

***Correspondence:**
Hao Yan
hyan@cdc.zj.cn
Yanjun Zhang
yjzhang@cdc.zj.cn

[†]*These authors have contributed equally to this work*

Specialty section:
This article was submitted to Parasite and Host, a section of the journal Frontiers in Cellular and Infection Microbiology

Received: *27 February 2021*
Accepted: *14 September 2021*
Published: *05 October 2021*

Citation:
Yao W, Yang Z, Lou X, Mao H, Yan H and Zhang Y (2021) Molecular Characterization of Dengue Virus Type 1 in Zhejiang in 2019. Front. Cell. Infect. Microbiol. 11:673299. doi: 10.3389/fcimb.2021.673299

INTRODUCTION

Dengue is one of the most globally prevalent arboviruses in the word, which is caused by the dengue virus (DENV). DENV belongs to the genus *Flavivirus* of the family *Flaviviridae* (Ngwe Tun et al., 2016). Human infection with DENV is through a bite of mosquito, and the clinical symptoms range from asymptomatic infection to dengue hemorrhagic fever (DHF), dengue shock syndrome (DSS), and death (Cruz et al., 2013; Martins et al., 2014). The World Health Organization (WHO) has estimated that approximately 50–100 million dengue infections occur every year, of which 500,000 cases are DHF and 22,000 deaths. The genome of DENV is a single-stranded positive-sense RNA and approximately 11,000 nucleotides. Its genome encodes three structural proteins including C (capsid), prM/M (precursor of membrane), and envelope (E); seven nonstructural proteins, including NS1, NS2A, NS2B, NS3, NS4A, NS4B, and NS5. DENV are represented by four distinct serotypes (DENV-1, DENV-2, DENV-3, and DENV-4) (Wang et al., 2000; Conceição et al., 2010; Lee et al., 2012), and

each of the serotypes can be subclassified into several genotypes on the basis of their E gene sequences (Li et al., 2017). Many Asian countries including Singapore, Malaysia, Pakistan, India, Japan, China, and Indonesia have also reported outbreaks of DENV (Jarman et al., 2008; Holmes et al., 2009; Vu et al., 2010; Akram and Idrees, 2016; Tajima et al., 2017). Since the first reported outbreak of DENV in 1978 in China, Southeastern coastal provinces, including Guangdong, Fujian, Zhejiang, and Hainan have been affected by DENV outbreaks, where the genotypes of DENV-1, DENV-2, DENV-3, and DENV-4 were detected (Wang et al., 2009; Xiong and Chen, 2014; Chen and Liu, 2015; Sun et al., 2017).

Zhejiang province, with a population of 56 million, is one of the important members of the Yangtze River Delta. Meanwhile, as the important entry/exit port province in east China, Zhejiang has frequent exchanges and cooperation with foreign countries, especially with Southeast Asian countries, where DENV originated. Plains, hills, and mountains constitute the complex geographical features of Zhejiang, and the complex environments provide ideal conditions for the growth of mosquitoes, which is the vector for the transmission of DENV (Guo et al., 2014). In 2004, a DENV outbreak in Cixi of Zhejiang caused 83 people to get infected 18]. More cases occurred in Yiwu of Zhejiang in 2009, and 196 cases of DF were reported (Sun et al., 2011). In 2017, a historical outbreak occurred in Zhejiang province, and a total of 1,229 cases were reported, with 93.8% emerging in Hangzhou (Yan et al., 2018). In recent years, DF cases have been reported almost every year in Zhejiang.

Despite that the four serotypes of DENV have been detected in Zhejiang in recent years, the serotype 1 has gradually become the dominant serotype. Therefore, in our study, 174 cases of DENV-1 (including 132 indigenous cases and 42 imported cases) were used to conduct a molecular investigation and epidemiological and phylogenetic characterization of DENV that were detected during the dengue outbreak in Zhejiang province in 2019.

MATERIALS AND METHODS

Sample Collected

Serum samples for this study were kept in the Zhejiang provincial Centers for Disease Control and Prevention (CDC) in 2019. DV nucleotide detection and serotype identification of all DF cases were determined according to diagnostic criteria for DF (WS216-2008) of the Ministry of Health of China, and 174 cases of DENV-1 were collected in this study.

Virus Strains

DENV strains in our study were isolated from the positive serums of patients, and the *Aedes albopictus* gut cell line (C6/36) was used for virus propagation. Serum samples were diluted 10-fold with fresh MEM medium (Gibco, Waltham, MA, USA) and then inoculated with a C6/36 cell monolayer, which was incubated in MEM medium supplemented with 2% fetal bovine serum (FBS, Gibco, USA) at 28°C for 5–7 days. Cells showed typical cytopathic effects (CPE) being considered DENV positive. These culture supernatants were then stored at −80°C for use.

RNA Extraction and Sequencing

The RNeasy Mini Kit (Qiagen, Hilden, Germany) was used to extract virus RNA from 200 μl cell culture supernatants according to the manufacturer's instructions. RT-PCR was conducted using the PrimeScript™ One Step RT-PCR Kit (TaKaRa, Shiga, Japan). The full-length E genes of the 174 DENVs were amplified with the following primers: DV1-E-F (5′CAAGAACCGAAACRTGGATGTC3′) and DV1-E-R (5′ GGCTGATCGAATTCCACACAC3′). The 50-μl PCR reaction included 25 μl of 1× one-step buffer, 2 μl of PrimeScript one-step enzyme mix, 1 μl of each primer (20 μM), 4 μl of the template RNA, and 17 μl of RNase Free dH2O. RT-PCR reverse transcription reaction was initiated at 50°C for 30 min, then denaturation at 94°C for 2 min, followed by 40 cycles of denaturation step at 94°C for 30 s, and primer annealing at 53°C for 30 s, primer extension at 72°C for 2 min, and a final extension step at 72°C for 10 min. The PCR products were purified by agarose gel electrophoresis, and then sequenced by Sangon Biotech Co. (Shanghai, China).

Data Analysis

One hundred seventy-four sequences from the isolated strains were spliced in SEQMAN from the LaserGene package (DNASTAR Inc., Madison, WI, USA), and 39 reference sequences were downloaded from the GenBank database. The nucleotide sequences were aligned using the professional software Clustal W. The phylogenetic tree based on full E gene sequences was constructed by using the neighbor-joining method with the Tajima-Nei model in MEGA v.6.06. The bootstrap value was 1,000 replicates, and only values >70% are presented. Haplotype analyses for the 174 full E gene sequences were conducted using the DNAsp5.1 software. Then the sequences were divided into nine groups (Wenzhou/Hangzhou/Jinhua/Taizhou/Ningbo/Shaoxing/Jiaxing/Huzhou/Zhoushan) according to the geographic location, and haplotype network was made by Popart 1.7 software. The differences of amino acid sequence were analyzed by MEGA-x.

Ethics Statement

The authors declare that they have no conflict of interest. This study was approved by the Institutional Ethics Committee of the Zhejiang Provincial Center for Disease Control and Prevention. Informed oral consent was obtained from all of the patients recruited for the study.

RESULTS

Case Confirmation and Epidemiology of Dengue in 2019 in Zhejiang

A total of 174 DENV-1 serum samples from nine municipal Centers for Disease Control and Prevention (CDC) of Zhejiang, including Wenzhou, Hangzhou, Jinhua, Taizhou, Ningbo,

Shaoxing, Jiaxing, Huzhou, and Zhoushan, were verified by multiplex RT-PCR. Geographical distribution of 132 indigenous cases and 42 imported cases are shown in **Table 1**, and the detailed geographical distribution of cases is shown in **Table 2**. Monthly distribution of dengue fever cases in four main cites in Zhejiang Province is shown in **Figure 1**. In Ningbo and Wenzhou, cases peak was in September, while cases peaks in Hangzhou and Taizhou were in August and June, respectively.

Evolutionary Relationships of DENV-1 Haplotypes

As shown in phylogenetic networks, the 64 haplotypes were clustered into two main clades (**Figure 2**). Nucleotide diversity was 0.03336, and haplotype diversity was 0.950. Forty-one haplotypes clustered into clade I and 23 haplotypes clustered into clade II. Clade I is mainly composed of Wenzhou and Taizhou cases, and clade II is mainly composed of Hangzhou and Ningbo cases. Hap_42 (TZ 004, imported from Cambodia), connected to Hap_5, Hap_9, Hap_27, and Hap_57, was supported as the potential ancestral haplotypes. The Hap_5 and Hap_35 were the other two core haplotypes. The long branches of Hap_61, Hap_59, Hap_47, Hap_51, and Hap_48 correspond to a significant mutation.

Phylogenetic Analysis

Phylogenetic tree was obtained based on the 174 of nucleotide sequences of the E gene of DENV-1and 39 of reference sequences (**Figure 3**). The results demonstrated that 73.3% of the strains (11/15) from Hangzhou were clustered in the same branch with 39% viruses (7/18) from Ningbo. Almost all the strains found in Taizhou were clustered with strains from Wenzhou. The strains in our study were in high homology with the strains from Vietnam/1409a Tw/2014 and Singapore/2334/2014.

TABLE 1 | Demographic characteristics of dengue cases in Zhejiang Province, 2019.

City	Indigenous	Imported	Total
Wenzhou	91	13	104
Hangzhou	15		15
Taizhou	8	16	24
Ningbo	10	8	18
Jinhua	3	2	5
Zhoushan	3		3
Jiaxing		3	3
Shaoxing	1		1
Hzhou	1		1
Total	132	42	174

TABLE 2 | Distribution of countries of origin for imported dengue cases.

Original country	Cases number	Total
Cambodia	Taizhou: 004-014, 017,019,020,024; Wenzhou: 032,078,096-098,101; Jinhua: 004,005; Ningbo: 013,017; Jiaxing: 003	26
Thailand	Wenzhou: 060,062; Ningbo: 018; Jiaxing: 002	4
Malaysia	Taizhou: 002	1
Other cities in China	Wenzhou: 080-082, 087,089; Ningbo: 003,004,011,015,016; Jiaxing: 001	11

Phylogenetic analysis of strains found in Wenzhou (**Figure 3** shown by red color) was more complex, most of the strains were clustered with the two strains Vietnam/1409a Tw/2014 from Vietnam and Singapore/2334/2014 from Singapore in 2014, and some of the strains were clustered with the strains from Zhoushan, Ningbo or Taizhou.

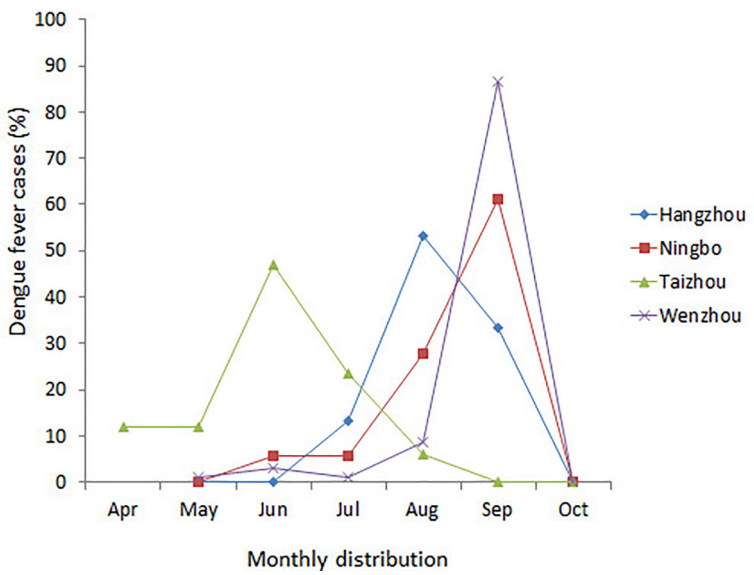

FIGURE 1 | Monthly distribution of dengue fever cases in four main cities in Zhejiang Province, China, 2019.

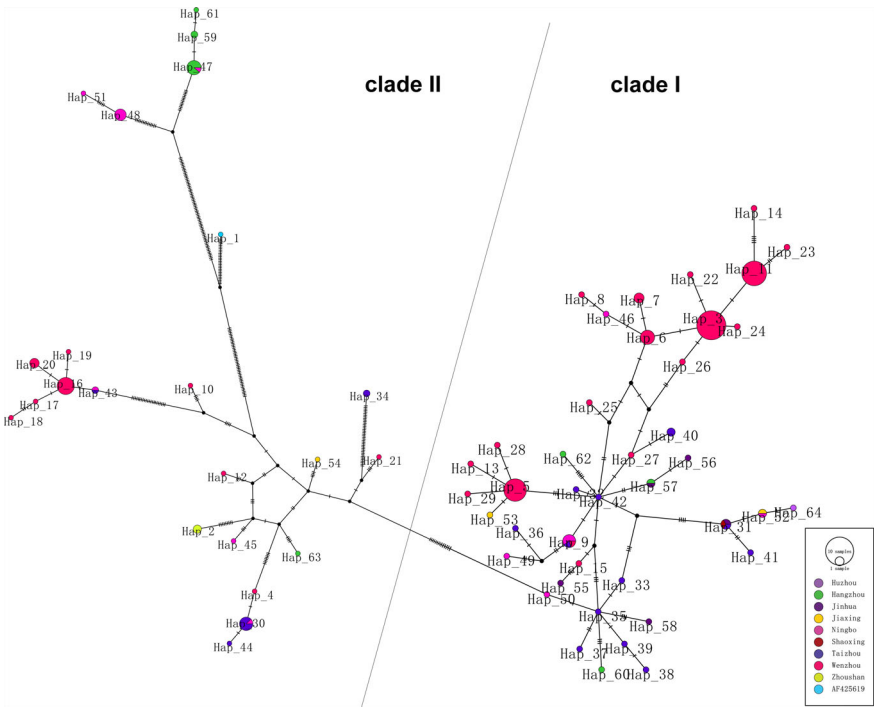

FIGURE 2 | Phylogenetic networks of 174 DENV-1 strains. Each node in the network represents a haplotype, and the circle size of the node represents the number of sequences contained in this haplotype.

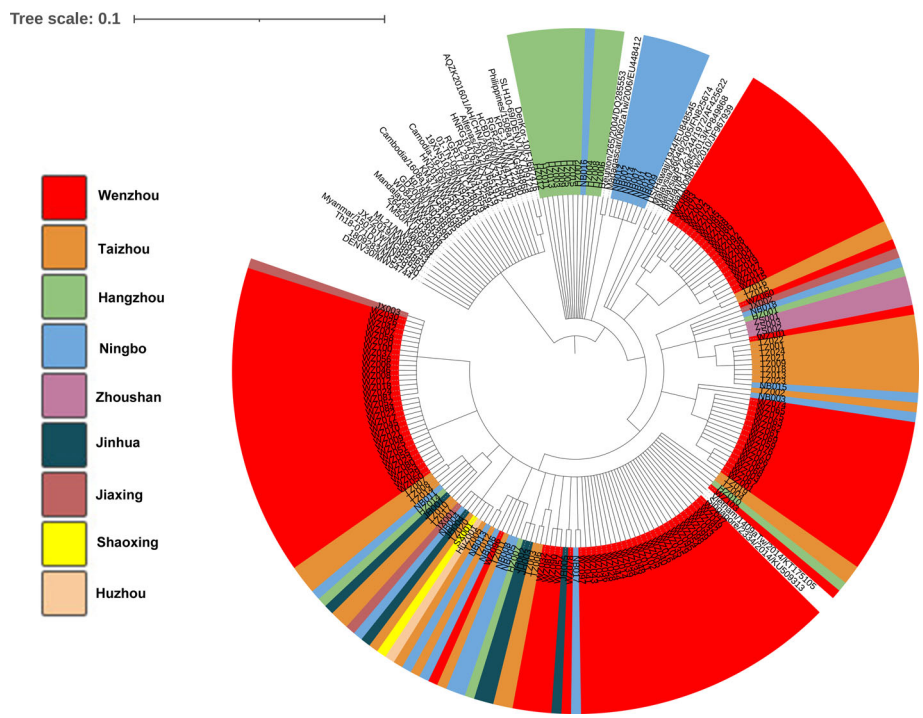

FIGURE 3 | Phylogenetic analysis of isolated DENV-1 based on the E gene. Phylogenetic tree was constructed on the basis of whole nucleotide sequences of the E protein gene of DENV-1 showing the relationship of 174 DENV-1 isolated and 39 of reference sequences.

Amino Acid Substitutions

Mainly 10 sites of the E protein amino acid substitutions were observed among the DENV-1 strains compared with the D1 Hawaii reference strain (**Table 3**). Six sites of amino acid substitutions including A88T, F96L, M297V, T339S, I378L, and V436I were observed in strains isolated from Ningbo and Hangzhou, while two sites of amino acid substitutions including V312L and V380I were observed in strains found in Taizhou and Wenzhou. Amino acid substitutions in two sites (I161T and L402F) were almost observed among the strains isolated from 4 cities (Ningbo, Hangzhou, Taizhou and Wenzhou).

DISCUSSION

Since 2004, DENV outbreak occurred in Cixi of Zhejiang and causing 83 people to get infected; cases of DF have been reported nearly every year in Zhejiang province (Xu et al., 2007). Especially in 2017, a large outbreak occurred in Zhejiang with a total of 1,229 DF cases being reported, as DENV-2 was the dominant serotype (Yan et al., 2018). However, DENV-1 has gradually become the dominant serotype since then. Zhejiang province was one of the important regions of international trade, commercial trade, and tourism; the convenient communication with the world has increased the incidence of DENV infections. In 2019, 174 cases of DENV-1 were collected from nine municipal CDC of Zhejiang, including 132 indigenous cases and 42 imported cases, with 26 of the imported cases being imported from Cambodia (**Table 2**), and the phylogenetic, molecular, and epidemiological characteristics were conducted in our study. The peak of the cases was almost in June, August, and October, which is consistent with the mosquito peak season. One hundred four out of 174 total cases (59.8%) and 13 out of 42 (31%) imported cases were come from Wenzhou. It is well known that Wenzhou is an important commercial city in China and located in the southeast of Zhejiang province. Meanwhile, Wenzhou has the ideal conditions for the life cycle of mosquitoes, including rivers, mountains, hills, and comfortable temperature. DENV is spread by mosquito bites, and the infection of DENV is closely related to the density of mosquitoes. Trade and population movements make it possible for the spread of the DENV. Those superior geographical location and frequent commercial exchanges provide conditions for the outbreaks of DENV infections.

Phylogenetic networks showed that most strains from Wenzhou and Taizhou clustered into the same clade, and more strains from Hangzhou and Ningbo clustered into

TABLE 3 | Amino acid differences in the E protein of DENV-1 strains in comparison with the D1 Hawaii reference strain (AF 425619).

Position	88	96	161	297	312	339	378	380	402	436
D1 Hawaii AF425619	A	F	I	M	V	T	I	V	L	V
NB001	T	L	T	V	–	S	L	–	F	I
NB002	T	L	T	V	–	S	L	–	F	I
NB009	T	L	T	V	–	S	L	–	F	I
NB007	T	L	T	V	–	S	L	–	F	I
NB018	T	L	T	V	–	–	–	I	F	–
NB016	T	L	T	V	–	S	L	–	F	I
HZ002	T	L	T	V	–	S	L	–	F	I
HZ004	T	L	T	V	–	S	L	–	F	I
HZ003	T	L	T	V	–	S	L	–	F	I
HZ005	T	L	T	V	–	S	L	–	F	I
HZ006	T	L	T	V	–	S	L	–	F	I
HZ009	T	L	T	V	–	S	L	–	F	I
HZ008	T	L	T	V	–	S	L	–	F	I
HZ011	T	L	T	V	–	S	L	–	F	I
TZ011	–	–	T	–	L	–	–	I	F	–
TZ014	–	–	T	–	L	–	–	I	F	–
TZ020	–	–	T	–	L	–	–	I	F	–
TZ004	–	–	T	–	L	–	–	I	F	–
TZ005	–	–	T	–	L	–	–	I	F	–
TZ007	–	–	T	–	L	–	–	I	F	–
TZ012	–	–	T	–	L	–	–	I	F	–
TZ019	–	–	T	–	L	–	–	I	F	–
TZ017	–	–	T	–	L	–	–	I	F	–
WZ100	–	–	T	–	L	–	–	I	F	–
WZ096	–	–	T	–	L	–	–	I	F	–
WZ097	–	–	T	–	L	–	–	I	F	–
WZ098	–	–	T	–	L	–	–	I	F	–
WZ099	–	–	T	–	L	–	–	I	F	–
WZ102	–	–	T	–	L	–	–	I	F	–
WZ103	–	–	T	–	L	–	–	I	F	–
WZ104	–	–	T	–	L	–	–	I	F	–

another clade (**Figure 2**). The strains founded in Wenzhou differentiate two subgroups, and one subgroup only spreads within Wenzhou. By detecting the difference of amino acid, we found an interesting phenomenon: amino acid substitutions (A88T, F96L, M297V, T339S, I378L, and V436I) only occurred in strains from Ningbo and Hangzhou, while sites of amino acid substitutions (V380I and V312L) occurred in strains from Wenzhou and Taizhou. Whether the substitutions are related to virulence still need further study. The result was consistent with the phylogenetic networks. It may be that the DENV has spread to surrounding areas after circulating in one area in a period of time. Geographically, Wenzhou and Taizhou are adjacent, while Hangzhou and Ningbo are relatively close.

The E gene encodes envelope protein, which is responsible for cell receptor binding and the key target for neutralizing antibodies and vaccine development. The amino acid substitutions in the envelope protein may influence the recognition and binding of antibodies. In our study, the phylogenetic tree was obtained based on the full E gene. The result indicated that 20 indigenous strains from Wenzhou (WZ001–WZ003, WZ059, WZ061–WZ076) and two imported strains (Taizhou002 and Ningbo003) were clustered in the same subclade with strains from Singapore (SGEHID104009Y13) and Malaysia (TM45). It demonstrated that some early cases in Wenzhou may be imported from Southeast Asian countries. Eleven strains from Hangzhou (HZ002–HZ006, HZ008, HZ009, HZ011–HZ013, HZ015) and eight strains from Ningbo (NB001, NB002, NB007, NB009, NB010, NB012, NB014) were clustered with the strains from Madagascar/0602aTw/2006 and Reunion/265/2004.

We analyzed the molecular characterization, amino acid mutation, and phylogenetic tree of 174 DENV-1 strains in Zhejiang province in 2019. The strains from Hangzhou had a close link with the virus from Ningbo; however, the strains from Wenzhou were closely related to the isolates from Taizhou. The strains in Zhejiang province were probably imported from Southeast Asian countries. The strains from different regions in Zhejiang were clustered in the same branch which may be caused by the continuous import of cases in the same country at different time periods. After the continuous outbreak in Zhejiang province, some sites of the dengue gene have mutated, and the effects need further study.

DATA AVAILABILITY STATEMENT

The raw data supporting the conclusions of this article will be made available by the authors, without undue reservation.

ETHICS STATEMENT

The studies involving human participants were reviewed and approved by Institutional Ethical Committee of Zhejiang Provincial Center for Disease Control and Prevention. Written informed consent for participation was not required for this study in accordance with the national legislation and the institutional requirements.

AUTHOR CONTRIBUTIONS

HY and YZ designed the study. HY and WY performed the data. ZY and WY analysed data. All authors contributed to the article and approved the submitted version.

FUNDING

This study was supported by Natural Science foundation of Zhejiang Province(LGF20H260003), Health Leading Talents Program of Zhejiang Province (2018(22)), Key Disciplinary of Health and Family Planning Commission of Zhejiang Province (CX-9), and Medical Science and Technology Program of Zhejiang Province (2020RC050,2020KY092, 2018KY341).

REFERENCES

Akram, M., and Idrees, M. (2016). Complete Genome Sequencing and Comparative Analysis of Three Dengue Virus Type 2 Pakistani Isolates. *Virusdisease* 27 (1), 27–33. doi: 10.1007/s13337-015-0279-3

Chen, B., and Liu, Q. (2015). Dengue Fever in China. *Lancet (London England)* 385 (9978), 1621–1622. doi: 10.1016/s0140-6736(15)60793-0

Conceição, T. M., Da Poian, A. T., and Sorgine, M. H. (2010). A Real-Time PCR Procedure for Detection of Dengue Virus Serotypes 1, 2, and 3, and Their Quantitation in Clinical and Laboratory Samples. *J. Virologic. Met.* 163 (1), 1–9. doi: 10.1016/j.jviromet.2009.10.001

Cruz, C. D., Forshey, B. M., Juarez, D. S., Guevara, C., Leguia, M., Kochel, T. J., et al. (2013). *Infect. Genet. Evol. J. Mol. Epidemiol. Evol. Genet. Infect. Dis.* 18, 220–228. doi: 10.1016/j.meegid.2013.04.029

Guo, S., Ling, F., Hou, J., Wang, J., Fu, G., and Gong, Z. (2014). Mosquito Surveillance Revealed Lagged Effects of Mosquito Abundance on Mosquito-Borne Disease Transmission: A Retrospective Study in Zhejiang, China. *PloS One* 9 (11), e112975. doi: 10.1371/journal.pone.0112975

Holmes, E. C., Tio, P. H., Perera, D., Muhi, J., and Cardosa, J.. (2009). Importation and Co-Circulation of Multiple Serotypes of Dengue Virus in Sarawak, Malaysia. *Virus Res.* 143 (1), 1–5. doi: 10.1016/j.virusres.2009.02.020

Jarman, R. G., Holmes, E. C., Rodpradit, P., Klungthong, C., Gibbons, R. V., Nisalak, A., et al. (2008). Microevolution of Dengue Viruses Circulating Among Primary School Children in Kamphaeng Phet, Thailand. *J. Virol.* 82 (11), 5494–5500. doi: 10.1128/jvi.02728-07

Lee, K. S., Lo, S., Tan, S. S., Chua, R., Tan, L. K., Xu, H., et al. (2012). Dengue Virus Surveillance in Singapore Reveals High Viral Diversity Through Multiple Introductions and in Situ Evolution. *Infect. Genet. Evol. J. Mol. Epidemiol. Evol. Genet. Infect. Dis.* 12 (1), 77–85. doi: 10.1016/j.meegid.2011.10.012

Li, G., Pan, P., He, Q., Kong, X., Wu, K., Zhang, W., et al. (2017). Molecular Epidemiology Demonstrates That Imported and Local Strains Circulated During the 2014 Dengue Outbreak in Guangzhou, China. *Virologica Sin.* 32 (1), 63–72. doi: 10.1007/s12250-016-3872-8

Martins Vdo, C., Bastos Mde, S., Ramasawmy, R., de Figueiredo, R. P., Gimaque, J. B., Braga, W. S., et al. (2014). Clinical and Virological Descriptive Study in the 2011 Outbreak of Dengue in the Amazonas, Brazil. *PloS One* 9 (6), e100535. doi: 10.1371/journal.pone.0100535

Ngwe Tun, M. M., Kyaw, A. K., Makki, N., Muthugala, R., Nabeshima, T., Inoue, S., et al. (2016). Characterization of the 2013 Dengue Epidemic in Myanmar With Dengue Virus 1 as the Dominant Serotype. *Infect. Genet. Evol. J. Mol. Epidemiol. Evol. Genet. Infect. Dis.* 43, 31–37. doi: 10.1016/j.meegid.2016.04.025

Sun, J., Lu, L., Wu, H., Yang, J., Xu, L., Sang, S., et al. (2017). Epidemiological Trends of Dengue in Mainland China, 2005-2015. *Int. J. Infect. Dis. IJID Off. Publ. Int. Soc. Infect. Dis.* 57, 86–91. doi: 10.1016/j.ijid.2017.02.007

Sun, J., Lin, J., Yan, J., Fan, W., Lu, L., Lv, H., et al. (2011). Dengue Virus Serotype 3 Subtype III, Zhejiang Province, China. *Emerging Infect. Dis.* 17 (2), 321–323. doi: 10.3201/eid1702.100396

Tajima, S., Nakayama, E., Kotaki, A., Moi, M. L., Ikeda, M., Yagasaki, K., et al. (2017). Whole Genome Sequencing-Based Molecular Epidemiologic Analysis of Autochthonous Dengue Virus Type 1 Strains Circulating in Japan in 2014. *Japanese J. Infect. Dis.* 70 (1), 45–49. doi: 10.7883/yoken.JJID.2016.086

Vu, T. T., Holmes, E. C., Duong, V., Nguyen, T. Q., Tran, T. H., Quail, M., et al. (2010). Emergence of the Asian 1 Genotype of Dengue Virus Serotype 2 in Viet Nam: *In Vivo* Fitness Advantage and Lineage Replacement in South-East Asia. *PloS Negl. Trop. Dis.* 4 (7), e757. doi: 10.1371/journal.pntd.0000757

Wang, E., Ni, H., Xu, R., Barrett, A. D., Watowich, S. J., Gubler, D. J., et al. (2000). Evolutionary Relationships of Endemic/Epidemic and Sylvatic Dengue Viruses. *J. Virol.* 74 (7), 3227–3234. doi: 10.1128/jvi.74.7.3227-3234.2000

Wang, Q., Xu, Z., Dou, F. M., Zhou, H., Wang, X. F., Yin, W. W., et al. (2009). Current Situation and Surveillance on Dengue Fever in China, 2005 - 2007. *Zhonghua liu xing bing xue za zhi = Zhonghua liuxingbingxue zazhi* 30 (8), 802–806.

Xiong, Y., and Chen, Q. (2014). Epidemiology of Dengue Fever in China Since 1978. *Nan fang yi ke da xue xue bao = J. South. Med. Univ.* 34 (12), 1822–1825.

Xu, G., Dong, H., Shi, N., Liu, S., Zhou, A., Cheng, Z., et al. (2007). An Outbreak of Dengue Virus Serotype 1 Infection in Cixi, Ningbo, People's Republic of China, 2004, Associated With a Traveler From Thailand and High Density of Aedes Albopictus. *Am. J. Trop. Med. hygiene* 76 (6), 1182–1188. doi: 10.4269/ajtmh.2007.76.1182

Yan, H., Ding, Z., Yan, J., Yao, W., Pan, J., Yang, Z., et al. (2018). Epidemiological Characterization of the 2017 Dengue Outbreak in Zhejiang, China and Molecular Characterization of the Viruses. *Front. Cell. Inf. Microbiol.* 8, 216. doi: 10.3389/fcimb.2018.00216

Conflict of Interest: The authors declare that the research was conducted in the absence of any commercial or financial relationships that could be construed as a potential conflict of interest.

Publisher's Note: All claims expressed in this article are solely those of the authors and do not necessarily represent those of their affiliated organizations, or those of the publisher, the editors and the reviewers. Any product that may be evaluated in this article, or claim that may be made by its manufacturer, is not guaranteed or endorsed by the publisher.

frontiers in Public Health

ORIGINAL RESEARCH
published: 25 October 2021
doi: 10.3389/fpubh.2021.686122

Deltamethrin Microencapsulation in Emulsion Paint Binder and Its Long-Term Efficacy Against Dengue Vector *Aedes aegypti*

B. N. Acharya[1], Rajkumar Ahirwar[1], Sunil Dhiman[2], Kavita Yadav[2], Pratibha Pandey[3] and Devanathan Sukumaran[2]*

[1] Synthetic Chemistry Division, Defence R&D Establishment, Gwalior, India, [2] Vector Management Division, Defence R&D Establishment, Gwalior, India, [3] Electron Microscopy Division, Defence R&D Establishment, Gwalior, India

OPEN ACCESS

Edited by:
Tianmu Chen,
Xiamen University, China

Reviewed by:
Ramesh C. Dhiman,
National Institute of Malaria Research (NIMR), India
Zhao Lei,
Xiamen University, China

***Correspondence:**
Sunil Dhiman
sunildhiman81@gmail.com

Specialty section:
This article was submitted to Infectious Diseases – Surveillance, Prevention and Treatment, a section of the journal Frontiers in Public Health

Received: *01 April 2021*
Accepted: *23 September 2021*
Published: *25 October 2021*

Citation:
Acharya BN, Ahirwar R, Dhiman S, Yadav K, Pandey P and Sukumaran D (2021) Deltamethrin Microencapsulation in Emulsion Paint Binder and Its Long-Term Efficacy Against Dengue Vector Aedes aegypti. Front. Public Health 9:686122. doi: 10.3389/fpubh.2021.686122

Various control interventions have been effective in the control of arthropod vectors to a certain extent; still, sustained vector control is an existing problem globally. Insecticide-based formulations have been found to be useful, however the proper delivery of active molecules to target vectors is important. Currently, synthetic pyrethroid deltamethrin (DM) has been microencapsulated in the emulsion paint binder and evaluated for long-term effectiveness against dengue vector *Aedes aegypti*. Different compositions of emulsion binder were prepared by varying the content of monomer and DM. A selection was made for the composition yielding the best combination of properties like solid content, intrinsic viscosity, and DM content. Developed formulation was tested against laboratory-reared and pathogen-free *Ae. aegypti* mosquitoes. Encapsulation of DM in emulsion binder during polymerization showed a uniform distribution. The optimized formulation was stable and did not have a considerable plasticizing effect. Scanning electron microscopy revealed that grain-like micro crystals of DM and surfactant sodium lauryl sulfate (SDS) were uniformly distributed on the formulation surface. The best optimized formulation was highly effective against dengue vector *Ae. aegypti* and found to provide efficacy for up to 18 months of application. The knockdown time (KDT) values KDT_{10} and KDT_{50} were 7.4 min (95% CI: 5.6–9.1) and 22.1 min (95% CI: 19.7–24.3) respectively, whereas 24 h corrected mortality was 90% (95% CI: 82.5–97.5) after 18 months of application (T18). The probit model used to determine knockdown values did not deviate from the linearity and displayed normal distribution of knockdown % with time for different formulations ($p \geq 0.1$). Presently developed DM microencapsulated emulsion binder was stable, smooth, and uniform. The binder displayed excellent anti-insect property and was capable of providing long-term effectiveness against dengue vectors *Ae. aegypti*. Such a formulation after field-scale evaluation could be very useful in attaining long-term protection from arthropod vectors.

Keywords: binder, emulsion, deltamethrin, insecticidal paint, dengue vector, *Aedes aegypti*

INTRODUCTION

Vector control is an outstanding problem in countries situated in tropical and sub-tropical climate zones. Arthropods such as mosquitoes, houseflies, cockroaches, and ticks spread life-threatening diseases in humans. Insecticides are effective tools for arthropod vectors control with appropriate deployment methods taking into consideration the ambient condition, especially home dwellings, hospitals, food production units, etc. The majority of vector insects rest and crawl on walls and surfaces of a building. Insecticidal paints kill insects usually by contact, therefore coating the interior and external walls and surfaces of civil constructions with insecticide paint could be a cost-effective intervention to control hematophagous insects and nuisance pests. Research on architectural paints containing insecticides, used to coat walls and ceilings of buildings, has gained attention during recent years. The development of novel technology of paint formulations in which microencapsulated insecticides in the form of active ingredients (AIs) have been embedded in the paint matrix has been found to be durable and effective against mosquitoes for a considerably long period of time (1, 2).

However, there are certain drawbacks in the existing insecticidal paint formulations and paints additives. The majority of such products are organic solvent-based and hence not very environmentally friendly (3). This is largely because insecticides are based on chemicals with carbon as the basis of their molecular structure, and therefore may not readily dissolve in aqueous formulations (4). The Weatherall Company Inc. has disclosed a dispersion (BugJuice®) containing 4.75% of the insecticide deltamethrin (DM), which can be added to any oil- or latex-based paint. However, once added, the paint must be used within 3 h otherwise the insecticide becomes ineffective. Furthermore, the users of architectural paints prefer not to mix the additives to paint as it is often difficult to achieve a homogenous mixture and sustained release over a long period of time. The process of making insecticide dispersion is complicated and the dispersion itself will contain surfactants that may adversely affect the film properties of the coating.

Waterborne paints are widely used in public and residential buildings because of their quick drying, lack of undesirable odor, good washability, excellent finish, and easy application. However, most of the synthetic insecticides are not water soluble, therefore a one pack composition where the insecticide is incorporated into the paint during manufacturing and is stable for many months is desirable. At present, Inesfly® Paint 5A IGR NG, a water-based insecticidal paint from Inesfly Corporation, is a single pack system in which insecticide and insect growth regulator are mixed in an emulsified form and homogeneous mixing is required before application (1, 2). However, to the best of our knowledge, encapsulation of DM in polymeric binder particles at the time of polymerization has not been reported. Incorporating DM at the time of polymerization has many advantages, including that the insecticide will remain uniform, stable, and its slow and sustained release will be ensured for a wide period of time due to encapsulation in polymeric binder particles. This binder formulation is used to prepare slow-release insecticidal paint. With an objective to develop single pack water-based slow-release insecticidal paint formulation, we synthesized a series of latex binders with varied monomer and DM compositions at the time of polymerization. Binder composition suitable for paint formulation was selected on the basis of lower coagulum formation during polymerization, higher solid content (%), higher intrinsic viscosity, and higher DM content in binder emulsion.

Many studies have shown that the insecticide embedded in the matrix of different surfaces can produce substantial efficacy against a variety of arthropods vectors both in laboratory and field conditions. It was found that AIs loaded into the matrix are released slowly onto the surface and hence sustain for a longer time to provide consistent efficacy. Maloney et al. (5) has reported that insecticide embedded in the matrix provided more efficacy as compared to the insecticide alone after 9 months of application. Similarly, Yadav et al. (6) has shown that tarsal exposure to insect growth regulator (IGR) labeled surface for a brief period of time and at very low concentrations drastically influenced the fecundity, fertility, and adult emergence in wild *Ae. aegypti* mosquitoes.

In the pre-text of increased geographical expansion of vectors and extraordinary transmission of arthropod vector-borne disease in new areas, the idea of using insecticidal paint-based formulations is popular. Therefore, an attempt has been made to develop and optimize an effective insecticide-based paint formulation and to establish its residual activity by evaluating against a well-known mosquito vector.

METHODS

Chemicals and Insecticide

Vinyl acetate (VA), methylmethacrylate (MMA), ethylacrylate (EA), methacrylic acid (MAA), and acrylic acid (AA) (all from Aldrich) were used as monomers. Sodium lauryl sulfate (SLS, Merck) and Triton X-100 (Aldrich) were used as emulsifiers. Ammonium persulfate (APS, Analytical grade, BDH) was used as free radical initiator. Technical grade deltamethrin (98% pure) obtained from M/S Tagros Chemical India, Chennai was used for encapsulation.

Emulsion Polymerization

Emulsion polymerization was carried out using a previously reported method with some modifications (7). Polymerization was performed in a 1 L capacity three necked glass reactor equipped with an overhead mechanical stirrer, a reflux condenser, a thermometer, and two dropping funnels through a Y-shaped connector. Copolymers of varying composition were synthesized by semi-continuous emulsion polymerization technique. Initially, the reactor was charged with 200 g de-ionized (DI) water, 2 g SLS, and 5 g Triton-X. The reactor was heated to 75°C in a water bath and the rotation of the mechanical stirrer was adjusted to 100 rpm. All the monomers were weighted and mixed before feeding to the reactor (**Table 1**). Initiator solution was prepared with 0.2 g APS in 50 g DI water. When desired temperature was achieved, 5 ml of initiator solution was added to the reactor in a single shot. Monomer mixture was fed drop wise (150 ml in 135 min) in parallel with initiator

TABLE 1 | Monomer composition, solid content, and intrinsic viscosity of the binders.

Code	Monomers										Solid content in binder emulsion (% w)	Conversion (%)	η_{int} (dL/g)	Acid content (mM)
	VA		EA		MMA		MAA		AA					
	w%	mol%	w%	mol%	w%	Mol%	w%	mol%	w%	mol%				
P1	80	82.37	20	17.69	–	–	–	–	–	–	31	72	0.563	–
P2	60	63.66	40	36.33	–	–	–	–	–	–	33	77	0.860	–
P3	50	53.87	50	46.12	–	–	–	–	–	–	34	79	0.947	–
P4	40	43.77	60	56.22	–	–	–	–	–	–	34	79	1.024	–
P5	20	22.60	80	77.39	–	–	–	–	–	–	35	81	0.586	–
P6	–	–	100	100	–	–	–	–	–	–	33	77	0.408	–
P7	55	58.35	40	36.33	–	–	5	5.30	–	–	35	81	1.194	1.9
P8	50	53.05	40	36.33	–	–	10	10.61	–	–	25	58	1.246	2.1
P9	45	48.11	45	41.19	–	–	10	10.69	–	–	36	84	1.158	5.4
P10	25	27.99	50	47.94	25	24.06	–	–	–	–	37	86	1.572	–
P11	24.5	27.14	49.2	46.86	24.5	23.33	–	–	2	2.65	36	84	2.194	0.8
P12	23.5	25.68	48.4	45.67	23.5	22.06	–	–	5	6.58	40	93	2.563	2.5
P13	22.5	24.73	22.5	21.17	48	44.95	–	–	7	9.14	33	77	1.146	4.5
P14	21.5	23.41	21.5	20.04	47	43.59	–	–	10	12.94	35	81	0.863	6.3

% w, % weight; η_{int}, Intrinsic viscosity.

solution (40 ml in 135 min). Subsequently, 5 ml of initiator solution was added in a single shot after the monomer feeding was completed. The polymerization was continued for another 2 h at the same temperature to achieve maximum conversion. Then the reactor was cooled to room temperature and polymer emulsion was filtered through cheesecloth and stored in high density polyethylene (HDPE) containers at room temperature.

Microencapsulation of Deltamethrin

For DM microencapsulation, 200 g DI water mixed with 2 g SDS (Sodium-Dodecyl-Sulfate) and 5 g of Triton-X (non-ionic surfactant) was taken in a polymerization reactor. The temperature was raised to 75°C with continuous agitation. Monomer mixture was prepared with 72.6 g EA, 34.95 g MMA, and 34.95 g VA, and 7.5 g AA. DM (1–5 g) was added to the monomer mixture and stirred to dissolve it completely. Monomer mixture containing DM was fed slowly into the reactor over a duration of 135 min. Simultaneously 0.2 g of APS in 50 ml water was fed in for the same duration of time. The reaction was held for another 2 h at 75°C for complete conversion. Then the polymer emulsion was cooled to room temperature and filtered through cheesecloth and stored in HDPE containers at room temperature.

Polymer Characterization

Polymer emulsion was broken by addition of 15% sodium chloride (NaCl) solution. The coagulated polymers were washed several times with distilled water and dried at 70°C for 24 h. Solid content of each emulsion was determined from the dry weight of coagulum and reported in percentage. Characterization of the dried polymers was carried out to determine their intrinsic viscosity (η_{int}) and acid value. The η_{int} of the copolymers was determined by Ubbelohde viscometer in a thermostat at 30 ± 1°C. The acid content in the copolymers was determined by acid-base titration of 0.5% polymer solution in methanol with standard sodium hydroxide (NaOH) solution, in the presence of phenolphthalein as indicator.

Thermal Studies

Differential scanning calorimetry (DSC) of the copolymers was carried out on DSC 1 STAR^e system (Mettler Toledo, USA) in nitrogen atmosphere from −40 to 200°C at a heating rate of 10°C/min. The sample size was between 4 and 5 mg in all the experiments. Thermo gravimetric analysis (TGA) was carried out on Pyris 1 TGA (Perkin Elmer, USA) in nitrogen atmosphere from room temperature to 600°C. The rate of heating was 20°C/min.

HPLC Quantification

Binder samples were applied on glass panels and dried for 72 h at ambient condition. Approximately 0.5 g of the dried binder sample was taken in a 100 ml beaker. To extract DM, 25 ml of HPLC grade acetonitrile was added and sonicated for 5 min. After filtration the binder sample was extracted again with 25 ml acetonitrile. Filtrates were combined and transferred in to a 50 ml volumetric flask, and volume was made up by acetonitrile. One ml of the solution was filtered through 0.22 micron syringe filter (Millipore Inc., USA) and analyzed by HPLC. HPLC system (Waters, USA) equipped with 1,525 binary pump, 2,487 tunable dual wavelength UV detector, and Rheodyne injector with 10 µl loop was used in the present study. Analysis was performed by isocratic elution (methanol and water 8:2 v/v) on XTerra MS C18 (4.6 × 250 mm, 5 µm) reverse phase HPLC column (Waters, USA). Wavelength and flow rate were set at 280 nm

TABLE 2 | Theoretical and estimated deltamethrin (DM) content in binder emulsion and glass transition temperature (Tg).

Polymer code	Solid content (w%)	Conversion (%)	DM in monomer feed (w%)	DM content in binder (w%)*	#Tg (°C)
P12	40	93	0	0	15.1
PS001	39	91	0.68	0.95	8.09
PS002	38	88	1.3	1.18	10.1
PS003	34	79	2.2	1.09	10.5
PS004	–	–	3.2	–	9.91

Determined by HPLC; #Tg, Glass Transition temperature; DM, deltamethrin.

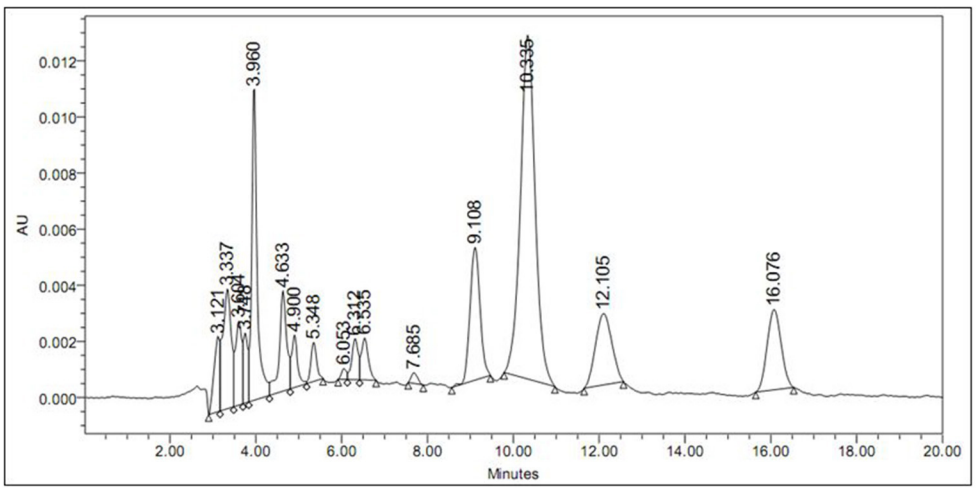

FIGURE 1 | HPLC chromatogram of binder (PS001) extract containing DM (Rt = 16.076 min).

and 1 ml/min, respectively. Standard solution was prepared by dissolving 14.78 mg of DM in 20 ml of acetonitrile. DM content was determined by comparing the corresponding peak area of sample with standard.

ESEM-EDX Characterization

Different binders were characterized by Quanta 400 environmental scanning electron microscope equipped with energy dispersive X-ray analyzer (ESEM-EDX) for their microscopic homogeneity and phase formation morphology. Small round cover slips were mounted on brass SEM stubs with double-sided adhesive tape. Small drops of binder emulsion were placed on the cover slip and dried under vacuum at room temperature and then coated with gold in a JFC-1100 sputter coating unit. These specimens were than analyzed by ESEM for morphology. Micrographs were taken at different magnifications to ascertain phase homogeneity and micro-distribution.

Preparation of Insecticidal Paint

Titanium dioxide (TiO_2), Triton X-100, and SDS were mixed in requisite quantities with DM encapsulated binder thoroughly to prepare the emulsion paint. The emulsion paint was applied on a cement surface by brush for testing of the insecticidal property of the paint. Binder without DM was used to prepare paint as control. The paint compositions were prepared using different essential components such as binder, pigment (TiO_2), and surfactants. However, the number of components other than binder was kept unaltered for all compositions to avoid any ambiguity in insecticidal properties.

Bio-Efficacy Evaluation

Developed insecticidal paint at the rate of 8 square meters per liter (2.82 g of ready-to-use paint) was applied uniformly on 15 × 15 cm^2 of cement surface and left to dry at ambient temperature for 24 h. After complete drying, anti-insect activity was determined using laboratory-reared *Ae. aegypti* mosquitoes following standard method as recommended by WHO (8). In brief, 4-to-5 day-old unfed female mosquitoes ($N \geq 41$ for each time period; ≥3 mosquitoes/replicate) were exposed to the treated surface in a WHO cone bioassay (obtained from Universiti Sains Malaysia) for 30 min; thereafter the mosquitoes were transferred into the holding cups (150 ml capacity) (1). Mosquito knockdown was recorded after five min intervals up to 60 min, whereas the mortality was observed after 24 h of exposure. The mortality was corrected by taking into account the control mortality. Test females were left at a temperature of 27 ± 2°C and a relative humidity (RH) of 80% for 24 h delayed mortality assessments. During the holding period, 10% sugar solution was provided for feeding. The painted surfaces were stored carefully in aluminum foil at room temperature and

TABLE 3 | Composition of paint formulations developed in the study.

Code	PS 002 (g)	Rutile TiO_2 (g)	Triton-X (g)	SDS (g)	Water (g)	25% Ammonia (g)	DM content w%[#]
WSRIP-1	10	10	2.5	2.5	10	0.5	0.24
WSRIP-2	15	10	2.5	2.5	10	0.5	0.44
WSRIP-3	20	10	2.5	2.5	5	0.5	0.59
Control	20*	10	2.5	2.5	5	0.5	0

**Binder P12 was used in place of PS002, [#]calculated.*

similar experiments were performed again after 6 (T6), 12 (T12), and 18 months (T18) to determine the residual efficacy.

Data Analysis

The mortality obtained in the mosquito species was corrected using Schneider-Orelli's formula (9). Knockdown time (KDT) along with slope and 95% confidence interval (CI) was determined using Log dose probit (Ldp) Line computer program. Chi-square (χ^2) test was used to check the fitment of probit, whereas the linearity of data was evaluated using linear regression. Dunnett's multiple comparisons test has been used to compare the corrected mortality at different time intervals.

RESULTS

Polymer Characterization

Solid content of an emulsion polymer indicates the actual content of polymer in the emulsion. The conversion of monomer to polymer can be calculated from actual polymer content with respect to theoretically maximum achievable polymer content, where all monomers are converted to polymers. Intrinsic viscosity (η_{int}) indicates the molecular weight of the polymer, hence longer polymer chains are formed with higher value of η_{int}, Furthermore, for binder application both percent conversion and η_{int} should be optimum to achieve the desired performance. Conversion of monomer to polymer depends upon the nature of monomers and reaction conditions. Copolymers of VA and EA (P1–P5) showed conversion between 72 and 81% and η_{int} between 0.563 and 1.024 dL/g. EA has a significant effect on both conversion and η_{int} of the resultant copolymers (P1–P5). Both the parameters displayed their optimum between 40 and 20 w% of EA in the monomer feed (**Table 1**). However, polyethylacrylate (P6) showed lower η_{int} than the VA-EA copolymers, whereas the introduction of MAA (P7–P9) marginally improved the η_{int} value. Nevertheless, the conversion for P8 was found to be 58% only. This may be due to lower EA than VA content in the monomer feed. When the feed was balanced with equal EA and VA content, 84% conversion was observed (P9), but our target for higher η_{int} was not achieved.

MAA is highly water soluble and weighs 10% of the total monomer in P8. Since EA is more hydrophobic than VA, the emulsification of MAA is enhanced by EA. Furthermore, at lower EA content in P8, the emulsification of MAA was less effective; therefore a significant amount of MAA was polymerized outside the micelles forming lumps in the reaction vessel. Hence the overall yield was low in the case of P8. Again, the acid content in P8 was also found to be low due to lumps formation. Extra-micellar polymerization of MAA was prevented and percentage conversion was increased when EA content was increased, as is evident for P9 (**Table 1**). MMA was introduced as a co-monomer and significant improvement was observed for P10 ($\eta_{int} = 1.572$ dL/g) with a good conversion of 86%. Introduction of AA as co-monomer (P11–P14) further improved η_{int} and showed an optimum value at 5 w% (P12) in the monomer composition. Acid content in polymeric binder was found to be increased with an increase in corresponding acid monomer feed from P11 to P14. It signifies that the introduction of hydrophobic MMA co-monomer prevented extra-micellar polymerization of the acid co-monomer during polymerization.

We started the synthesis of binders' (P1–P6) composition with VA and EA. Thereafter MAA was incorporated to increase the intrinsic viscosity of binders (P7–P9). Then P10–P14 MAA was replaced with MMA and AA in order to get higher intrinsic viscosity. Among the 14 binder emulsions synthesized, P12 showed optimum conversion and η_{int}, and hence was considered for microencapsulation of DM.

Deltamethrin Microencapsulation

A total of four binders were synthesized encapsulating DM ranging between 0.68 and 3.2 w% in the monomer feed (**Table 2**). DM was completely soluble in the monomer mixture. During polymerization the parameters, such as temperature, stirring speed, and monomer feed rate were the same for all DM encapsulated binders. The actual concentration of DM in binder film was estimated by HPLC. The retention time (Rt) of DM recorded at 16.076 min was free from other interferences (**Figure 1**). Hence the described method was found to be suitable to estimate DM content in all the binders. Microencapsulation of DM first increased and then decreased with increase in DM concentration in monomer feed. This may be attributed to the coagulum formation. The amount of coagulum was found to be increased with an increase in DM content in the monomer feed, as evident in **Table 2**. Increase in DM concentration in the feed caused extra-micellar polymerization, which contributed to the coagulum formation. Furthermore, the loss of DM was also found to be increased due to coagulum formation as evident from **Table 2**. Therefore, incorporation of DM in the binder has an upper limit as the entire batch is coagulating at 3.2 w% of DM content. Binder attained an optimum DM content when monomer feed contained 1.3 w% of DM, as shown in **Table 2**. Therefore, PS002 (the binder with optimum DM content) was used to prepare the paint formulations (**Table 3**).

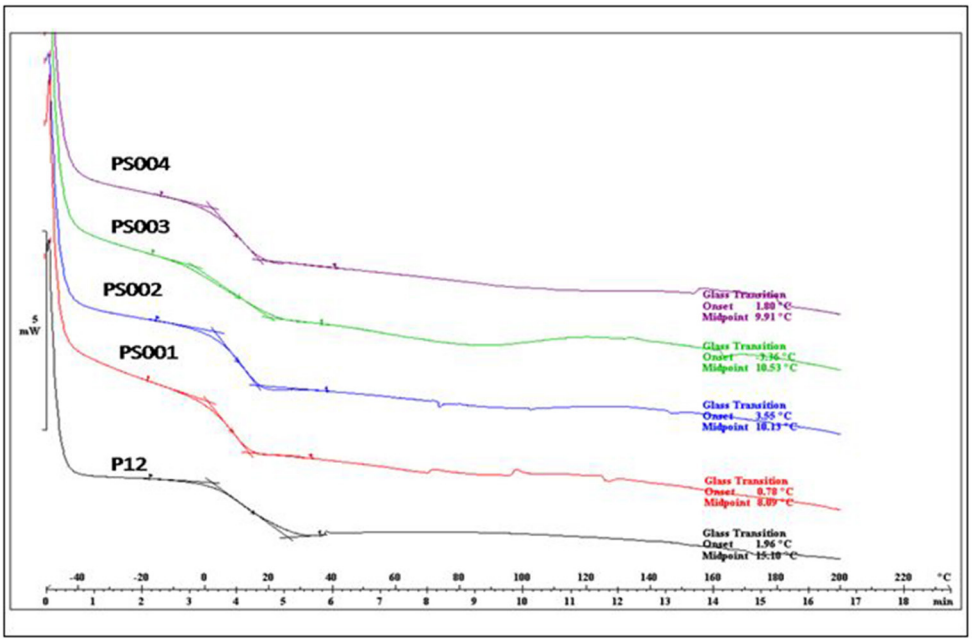

FIGURE 2 | Glass transition temperature (Tg) of binders with different concentrations of DM; P12 (0%), PS001 (0.68%), PS002 (1.3 %), PS003 (2.2%), PS004 (3.2%).

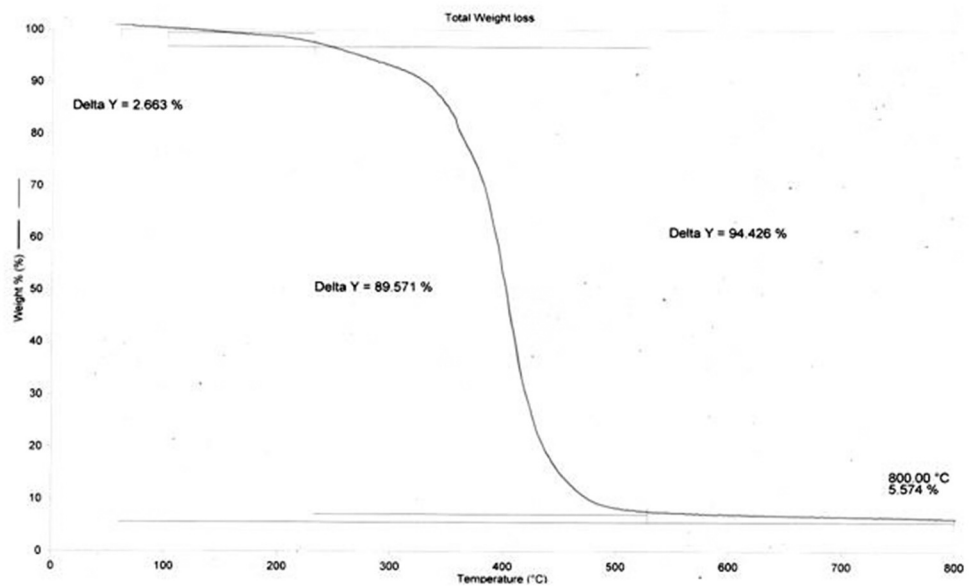

FIGURE 3 | Thermo gravimetric plot of binder PS002.

These formulations were used for preparing painted surfaces for evaluating the anti-insect activity.

Thermal Analysis

Glass transition temperature (T_g) of all the binders were determined by differential scanning calorimetry (DSC). T_g of all the DM encapsulated binders were found to range from 8 to 11°C (**Figure 2**), however T_g of binder without DM (P12) was recorded at 15.1°C. It is evident from **Table 2** that DM is modifying the T_g of the polymer matrix, however to a lesser extent, and does not have a considerable plasticizing effect. Degradation of both with DM and without DM binders followed a similar pattern in TGA. A sharp decrease in mass was observed at 400°C (**Figure 3**) which is typical of acrylic copolymers (5).

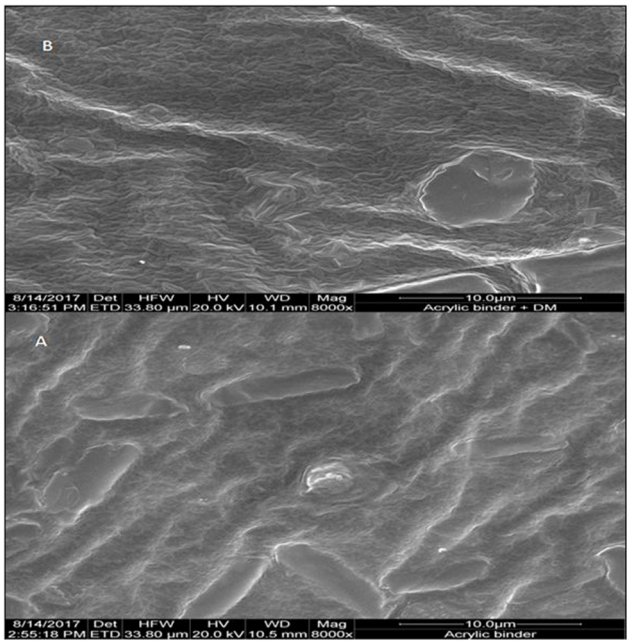

FIGURE 4 | ESEM micrographs of binders without deltamethrin P12 **(A)** and with deltamethrin PS002 **(B)**.

ESEM-EDX Characterization

ESEM pictures of binder without DM (P12) and with DM (PS002) are represented in **Figures 4A,B**, respectively, at 10 µm resolution. Cracks were observed on both P12 and PS002 binders and the surfaces were not smooth. Some grain-like micro crystals of DM and surfactant SLS were found uniformly distributed on the PS002 surface. Such structures were absent on the surface of P12.

Effectiveness of Insecticidal Paint Against Dengue Vector *Ae. aegypti*

The paint formulations as given in **Table 3** were evaluated against lab-reared and maintained *Ae. aegypti* mosquitoes in the laboratory. Among the three formulations, WSRIP-3 was found to retain the highest DM content (0.59 w%) as compared to the others. Therefore, this formulation was evaluated for up to 18 months at 6-month intervals. It was found that the DM contents (%) were 0.31, 0.24, and 0.19% after 6 (T6), 12 (T12), and 18 months (T18) of evaluation, respectively.

The percentage knockdown observed for the tested *Ae. aegypti* mosquitoes has been shown in **Figures 5**, **6**. It was found that at T0 (freshly applied formulation) the KD (%) was 98% in WSRIP-1, while it was 100% in WSRIP-2 and WSRIP-3 formulations, respectively, post 60 min of exposure (**Figure 5**). The corrected mortality (post 24 h) was also found to be 100% in all the three formulations at T0. Probit model suggested that the tested formulations showed KDT_{10} values ranging from 4.0 to 13.7 min, with KDT_{50} values ranging from 13.4 to 23.1 min at T0 (**Table 4**). Although mortality was similar in all three formulations at T0,

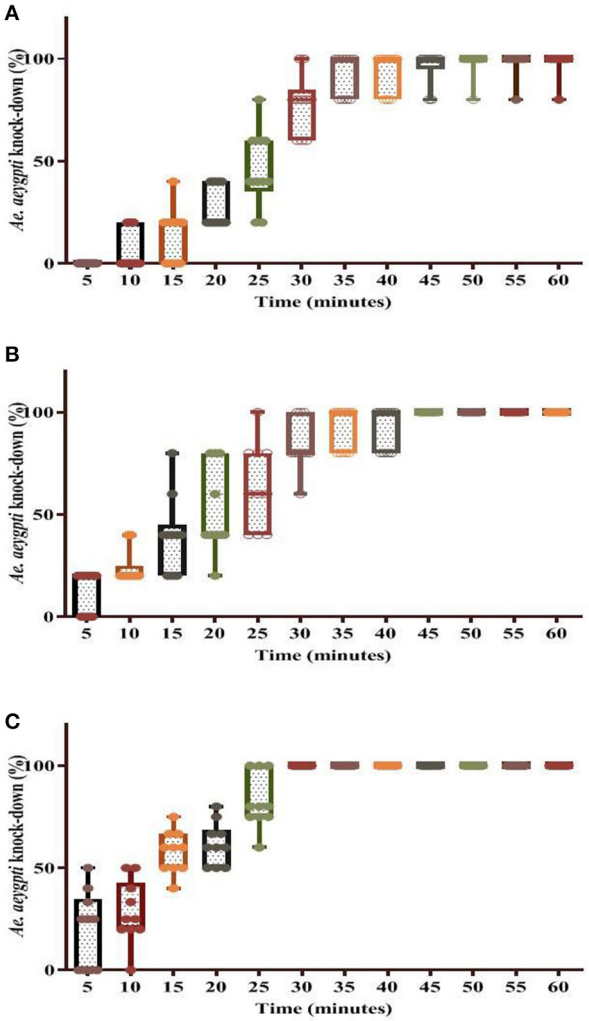

FIGURE 5 | Knockdown rate of dengue vector *Ae. aegypti* using different formulations at time T0. **(A)** WSRIP-1; **(B)** WSRIP-2; **(C)** WSRIP-3.

WSRIP-3 formulation was still more effective as compared to the other formulations as the KDT_{10} and KDT_{50} values for this formulation were 4.0 min (95% CI: 2.2–5.6) and 13.4 min (95% CI: 11.2–16.0) respectively. Considering the uptake of DM and T0 bio-efficacy, WSRIP-3 was taken for long-term efficacy evaluation.

Bio-efficacy results suggested that KD in WSRIP-3 did not decline and remained at 100%, however the corrected mortality declined non-significantly to 97.6% (95% CI: 93.5–102.5) ($p = 0.9$) at T6 (**Table 4**). Nevertheless, there was an increase in the KD_{10} and KD_{50} values to 6.8 min (95% CI: 5.2–8.3) and 15.2 min (95% CI: 13.4–16.9) respectively (**Figure 6**). At T12, percent KD and corrected mortality were found to be reduced to 98% ($KDT_{50} = 18.1$ min) and 94% (95% CI: 87.1–100.9) (compared to T0, $p = 0.2$) respectively. Furthermore, KDT_{10} and KDT_{50} values were 7.4 min (95% CI: 5.6–9.1) and 22.1 min (95% CI: 19.7–24.3) respectively, whereas 24 h corrected mortality was found to be

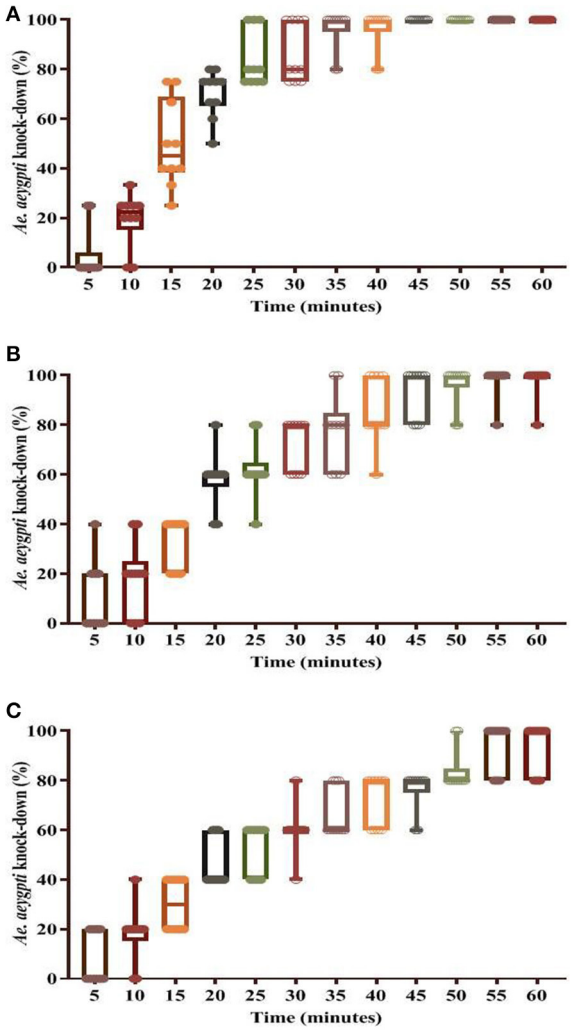

FIGURE 6 | Knockdown rate in dengue vector *Ae. aegypti* using insecticidal paint formulation (WSRIP-3). **(A)** after 6 months (T6); **(B)** after 12 months (T12); **(C)** after 18 months (T18).

90% (95% CI: 82.5–97.5) (compared to T0, $p = 0.02$) after T18. The probit model used to determine KDT values did not deviate from the linearity and displayed normal distribution of percent knockdown with time for the tested formulations at different time intervals ($p \geq 0.1$).

DISCUSSION

In the past few years, a variety of insecticidal paints have become available commercially for achieving protection from hematophagous arthropod vectors (1, 2, 5). However, their availability and use in households was primarily restricted to USA and some European countries, where such formulations were promoted against arthropod vectors that tend to feed indoors and mainly dwell on the walls and ceilings of human houses (10). The concept, although promising, did not gain much popularity in the majority of developing countries compared to the existing and less costly interventions, such as Indoor Residual Spray (IRS), which is effective but may not provide consistent efficacy for a longer time. At present, advances in paint technology have enabled researchers to guide insecticidal paint formulations to have insecticide or a mixture of insecticides embedded into the matrix which releases slowly on to the dried paint surface (10). Studies have shown that IRS is not considered to control adult *Ae. aegypti* except during outbreaks (11), therefore suitable paint formulations may provide consistent efficacy against *Aedes* vectors and other desired insects for a considerably longer time.

Presently, different compositions of emulsion binder using monomer and DM were prepared and the best optimized composition was formulated into insecticidal paint to test against known dengue vector. It is well-known that surface coating quality is a critical element in any paint formulation. Surface coating is a process where a liquid material is spread over a surface and forms a thin film. It is used for protection, aesthetic attraction, and some other functional purposes like protection from insects (12). The surface coatings, in general, are made up of four basic components: binder resin, pigments, solvent, and other additives. The main part of coating is binder resin which is the film-forming agent of the coating material. In recent years, acceptability to the water-based emulsion paints has increased, primarily due to their low cost, stability, quick drying, and quick recoatability (13). Polymer VA is widely used in the production of emulsion binder of water-based emulsion paints (14). However, the Tg of polyvinyl acetate (PVA) is 29°C, therefore it is often copolymerized with EA to obtain a softer composition for use

TABLE 4 | Knockdown and 24 h delayed mortality in susceptible *Ae. aegypti* for different formulations.

Time interval	Formulation code	Deltamethrin content w%	KD_{60min} % (*N*)	KDT_{10} (95% CI)	KDT_{50} (95% CI)	Slope (±)	χ^2 (*p*)	*R*	CM_{24h} (%)
T0	WSRIP-1	0.24#	98 (50)	13.7 (12.1–15.1)	23.1 (21.6–24.6)	5.6 ± 0.4	10.9 (0.3)	0.98	100
	WSRIP-2	0.44#	100 (50)	6.1 (4.6–7.6)	16.2 (14.3–18.0)	3.1 ± 0.3	10.7 (0.1)	0.96	100
	WSRIP-3	0.59#	100 (42)	4.0 (2.2–5.6)	13.4 (11.2–16.0)	2.8 ± 0.4	3.5 (0.3)	0.96	100
T6	WSRIP-3	0.31&	100 (41)	6.8 (5.2–8.3)	15.2 (13.4–16.9)	3.7 ± 0.4	5.4 (0.5)	0.99	97.6
T12	WSRIP 3	0.24&	98 (50)	6.9 (5.4–8.4)	18.1 (16.2–19.9)	3.1 ± 0.2	12.9 (0.2)	0.97	94
T18	WSRIP 3	0.19&	94 (50)	7.4 (5.6–9.1)	22.1 (19.7–24.3)	2.7 ± 0.2	8.6 (0.6)	0.97	90

T0, at the time of application; T6/T12/T18, 6/12/18 months post-application; CM_{24h}, Corrected mortality post 24 h exposure; KDT, knockdown time; CM_{24h}, 24 h corrected mortality; #calculated, &estimated by HPLC; p significant if <0.05.

as emulsion (15). Since lower acrylate polymers like EA have Tg below room temperature, they are typically soft and rubbery, hence a small amount of MMA was added to impart strength and hardness to the polymer film (16). A small amount of acid monomer (AA and MAA) was also used to provide adhesion and thermosetting capability to the polymer film.

Monomer composition has a significant effect on polymerization and end properties of the binder emulsion (17). Higher solid content and larger polymer molecules contribute significantly to the film forming properties of the binder emulsion. Therefore, different compositions (**Table 1**) of acrylic monomers have been used to prepare the binder emulsion in the present study. Conversion of monomer to polymer is crucial in polymerization, as the monomer not converted to polymer will remain in the binder emulsion and may adversely affect the film property (18). In the present study, the theoretical solid content of all the emulsion would have been 43% under complete conversion of monomer to polymer. Conversion of monomer to polymer was determined from percent solid content of the emulsion after polymerization with respect to theoretical solid content. However, a small part of the polymer is also lost due to formation of coagulum. Strength of the binder film depends upon the molecular weight of the polymer molecules. The file strength tends to become better with the increase in the molecular weight. Polymer η_{int} has been regarded as an indicator of its molecular weight, which increases with the increase in the molecular weight. Hence, along with the percent solid content, η_{int} was also considered as a parameter to optimize monomer composition of emulsion binder (**Table 1**).

The estimated DM contents at different time intervals were suggestive that the developed formulation has a slow-release mechanism which enables the DM to gradually release to the surface. The slow-release mechanism ensures the availability of DM on surface and hence provides considerable residual effectiveness even after 18 months of application (**Table 4**). It has been shown previously that such formulations can offer protection against a variety of arthropod vectors that play important roles in transmitting various diseases such as malaria, dengue, filaria, Zika, chikungunya, leishmaniasis, and chagas disease (10). Present results have shown that the insecticidal paint formulation provided 18 months residual efficacy by producing 94% knockdown and 90% mortality against a well-known dengue vector of the Indian region. Amelotti et al. (19) have evaluated organophosphate (Inesfly® 5A IGR™) and a pyrethroid-based insecticidal paint (Inesfly® 5A IGR NG™) formulation against *Triatoma infestans* and reported that pyrethroid formulations showed 84% while organophosphate formulation displayed 98% mortality after 12 months of the application on different surfaces (19). Similarly, Mosqueira et al. (1, 2) have shown that insecticidal paint Inesfly® 5A IGR™ has been found to be effective against malaria vector *An. gambiae* in both laboratory and field conditions. It was reported that the mortality was 93–100% after 12 months of application in laboratory (1), while 90–100% against pyrethroid-resistant mosquitoes in experimental huts in the field (2). However, the efficacy after 12 months in the treated huts was found to have decreased to 60–80% (2).

The optimized formulation presently displayed encouraging efficacy and physiochemical properties, suggesting that the formulation has the potential to be evolved commercially after evaluation for a considerably longer time in different endemic settings. Many studies have argued that the slow release of insecticides from the paint layer could make the insecticide available on the surface or the surrounding surface for a considerable time, thereby providing protection for a longer duration compared to the traditionally encouraged interventions (8). The present formulation can be further improved by using different insecticides and insect growth regulators in optimized concentrations to form a single formulation, thereby offering a combination of insecticides for application against the target insect vectors. Similar formulations have the advantage that these can be applied indoors and outdoors by any individual without any special logistic planning.

The slow-release water-based insecticidal paint formulation developed presently was stable and produced high residual mortality against dengue vector in laboratory. Although we did not evaluate it for a long time, the achieved results after 18 months are sufficient to suggest that the formulation would be effective for a longer time against different vectors. The formulation after field evaluation could be an attractive tool to control hematophagous vector abundance in human houses and other peri-domestic structures with an advantage of embellishment, mainly in rural areas. However, in addition to monitoring the long-term human safety aspects and the effect on the environment, limitations associated with the use of this product also need to be acknowledged. The formulation may not perform well in remote settings where people live in mud-plastered porous houses. Although the formulation was tested for up to 18 months for efficacy under laboratory conditions, the actual impact of environmental factors, such as sunshine, rainfall, humidity, and wind speed on the formulation also needed to be studied in field trials to better understand its actual service life.

DATA AVAILABILITY STATEMENT

The original contributions presented in the study are included in the article/supplementary material, further inquiries can be directed to the corresponding author.

AUTHOR CONTRIBUTIONS

BA and SD conceptualized and designed the study. RA and BA performed the development and physico-chemical evaluation of the formulation. SD and KY maintained the *Ae. aegypti* mosquitoes and conducted the anti-mosquito study. PP performed the microscopy study. SD and BA analyzed the data. BA and SD drafted, while DS edited the manuscript. All authors read and approved the manuscript.

ACKNOWLEDGMENTS

Authors are thankful to the Director DRDE Gwalior for necessary support and advice during this project. The DRDE accession number assigned to this manuscript is DRDE/SC/08/2020.

REFERENCES

1. Mosqueira B, Duchon S, Chandre F, Hougard JM, Carnevale P, Mas-Coma S. Efficacy of an insecticide paint against insecticide-susceptible and resistant mosquitoes - Part 1: laboratory evaluation. *Malaria J.* (2010) 9:340. doi: 10.1186/1475-2875-9-340
2. Mosqueira B, Chabi J, Chandre F, Akogbeto M, Hougard JM, Carnevale P, et al. Efficacy of an insecticide paint against malaria vectors and nuisance in West Africa - Part 2: field evaluation. *Malaria J.* (2010) 9:341. doi: 10.1186/1475-2875-9-341
3. Capello C, Fischer U, Hungerbuhler K. What are green solvents? A comprehensive framework for the environmental assessment of solvents. *Green Chem.* (2007) 9:927–34. doi: 10.1039/b617536h
4. Yang D, Cui B, Wang C, Zhao X, Zeng Z, Wang Y, et al. Preparation and characterisation of emamectin benzoate solid nanodispersion. *J Nanomater.* (2017) 6560780. doi: 10.1155/2017/6560780
5. Maloney KM, Ancca-Juarez J, Salazar R, Borrini-Mayori K, Niemierko M, Yukich JO, et al. Comparison of insecticidal paint and deltamethrin against Triatoma infestans (Hemiptera: Reduviidae) feeding and mortality in simulated natural conditions. *J Vect Ecol.* (2013) 38:6–11. doi: 10.1111/j.1948-7134.2013.12003.x
6. Yadav K, Dhiman S, Acharya B, Ghorpade RR, Sukumaran D. Pyriproxyfen treated surface exposure exhibits reproductive disruption in dengue vector *Aedes aegypti*. *PLoS Neg Trop Dis.* (2019) 13:e0007842. doi: 10.1371/journal.pntd.0007842
7. Jassal M, Acharya B N, Bajaj P. Synthesis, characterization and rheological studies of Methacrylic acid-Ethyl Acrylate-Diallyl Phthalate copolymers. *J App Polym Sci.* (2003) 89:1430–41. doi: 10.1002/app.12318
8. WHO. World Health Organisation. *Test Procedures for Insecticide Resistance Monitoring in Malaria Vectors, Bio-efficacy and Persistence of Insecticides on Treated Surfaces*. Report of the WHO Informal Consultation. Document WHO/CDS/CPC/MAL/1998.12. Geneva: World Health Organization. (1998) 1-43.
9. Puntener W. *Manual for Field Trials in Plant Protection*. 2nd ed. Agricultural Division, Basel: Ciba-Geigy Limited (1981) 205.
10. Schioler KL, Alifrangis M, Kitron U, Konradsen F. Insecticidal paints: a realistic approach to vector control? *PLoS Neg Trop Dis.* (2016) 10:e0004518. doi: 10.1371/journal.pntd.0004518
11. Das MK, Singh RK, Lal RK, Dhiman RC. Susceptibility of *Aedes aegypti* to insecticides in Ranchi city, Jharkhand state, India. *Dengue Bull.* (2011) 35:194–8.
12. Fillion R, Riahi A, Edrisy A. A review of icing prevention in photovoltaic devices by surface engineering. *Renew Sust Energ Rev.* (2014) 32:797–809. doi: 10.1016/j.rser.2014.01.015
13. Siepmann F, Siepmann J, Walther M, MacRae RJ, Bodmeier R. Polymer blends for controlled release coatings. *J Control Release.* (2008) 125:1–15. doi: 10.1016/j.jconrel.2007.09.012
14. Cao TY, Liu QP, Hu JS. Application of polymer emulsion. In: *Synthetic Principle, Property and Application of Emulsion*. 1st ed. Beijing: Chemical Industry Press (1997). p. 515–95.
15. Billmeyer FB. *Text Book of Polymer Science*. Noida: Wiley Press India (2008). p. 114–8.
16. Badran AS, Moustafa AB, Yehia AA, Shendy SMM. Emulsion polymerization of vinyl acetate initiated by potassium persulfate-cyclohexanone sodium bisulfite redox pair system. *J Poly Sci - Pt A.* (1999) 28:411–24. doi: 10.1002/pola.1990.080280215
17. Oliveira MAM, Melo PA, Nele M, Pinto JC. Suspension copolymerization of Vinyl Acetate and Methyl Methacrylate in the presence of amoxicillin. *Macromol React Eng.* (2012) 6:280–92. doi: 10.1002/mren.201100083
18. Yamak HB. Emulsion polymerization: effects of polymerization variables on the properties of vinyl acetate based emulsion polymers. In: *Polymer Science*. ed. F. Yilmaz (Croatia: Intech). (2013). p. 35–73.
19. Amelotti I, Catala S, Gorla D. Experimental evaluation of insecticidal paints against Triatoma infestans (Hemiptera: Reduviidae), under natural climatic conditions. *Parasit Vectors.* (2009) 2:30–6. doi: 10.1186/1756-3305-2-30

Conflict of Interest: The authors declare that the research was conducted in the absence of any commercial or financial relationships that could be construed as a potential conflict of interest.

frontiers in Cellular and Infection Microbiology

ORIGINAL RESEARCH
published: 26 October 2021
doi: 10.3389/fcimb.2021.673503

Molecular Mechanisms of Colistin Resistance in *Klebsiella pneumoniae* in a Tertiary Care Teaching Hospital

Yanling Liu[1†], Yiqing Lin[1†], Ziwen Wang[1], Niya Hu[1], Qiong Liu[2], Wenkai Zhou[1], Xiuzhen Li[2], Longhua Hu[3], Jian Guo[4], Xiaotian Huang[2*] and Lingbing Zeng[1*]*

[1] Department of Clinical Laboratory, The First Affiliated Hospital of Nanchang University, Nanchang, China, [2] Department of Medical Microbiology, School of Medicine, Nanchang University, Nanchang, China, [3] Department of Clinical Laboratory, The Second Affiliated Hospital of Nanchang University, Nanchang, China, [4] Department of Laboratory Medicine, Shanghai East Hospital, Tongji University School of Medicine, Shanghai, China

OPEN ACCESS

Edited by:
Xiaojun Chen,
Nanjing Medical University, China

Reviewed by:
Chaitra Shankar,
Christian Medical College & Hospital, India
Qingtian Li,
Shanghai Jiao Tong University, China
Zhipeng Qu,
University of Adelaide, Australia

***Correspondence:**
Lingbing Zeng
lingbing_zeng@163.com
Xiaotian Huang
xthuang@ncu.edu.cn
Jian Guo
guojian1110@126.com

[†]These authors have equally contributed to this work

Specialty section:
This article was submitted to Parasite and Host, a section of the journal Frontiers in Cellular and Infection Microbiology

Received: 27 February 2021
Accepted: 06 July 2021
Published: 26 October 2021

Citation:
Liu Y, Lin Y, Wang Z, Hu N, Liu Q, Zhou W, Li X, Hu L, Guo J, Huang X and Zeng L (2021) Molecular Mechanisms of Colistin Resistance in Klebsiella pneumoniae in a Tertiary Care Teaching Hospital. Front. Cell. Infect. Microbiol. 11:673503. doi: 10.3389/fcimb.2021.673503

Background: Over the last two decades, the prevalence of colistin resistance among the members of *Enterobacteriaceae* has been increasing, particularly among *Klebsiella pneumoniae* isolates; this limits the potential use of colistin and leads to worsened clinical outcomes.

Methods: We investigated the prevalence and genetic characteristics of colistin-resistant *K. pneumoniae* (COLR-KP) in clinical isolates using genomic sequencing.

Results: In total, 53 K. *pneumoniae* isolates (4.5%, 53/1,171) were confirmed as COLR-KP, of which eight isolates carried mobile colistin-resistant (*mcr*) gene. Although the overall prevalence rate (0.7%, 8/1,171) of *mcr*-like genes in clinical *K. pneumoniae* remained relatively low, the presence of *mcr* (15.1%, 8/53) among the COLR-KP isolates indicated that the mobile resistance gene was already widespread among *K. pneumoniae* isolates in hospital setting. We randomly selected 13 COLR-KP isolates (four *mcr*-bearing and nine non-*mcr*-bearing isolates) for whole-genome sequencing, including two pandrug-resistant and four sequence type 11 (ST11) isolates. Phylogenetic analysis revealed that all COLR-KP isolates were genetically diverse. Among the four *mcr*-bearing isolates, three (KP4, KP18, and KP30) were positive for *mcr-1* and one (KP23) for *mcr-8*; none of the other *mcr* genes were detected. The *mcr-1* in the KP4 and KP30 isolates were located in an *IncX4* plasmid (approximately 33 kb) and could be successfully transferred to *Escherichia coli* J53AZ^{R}. In contrast, for the *mcr-8*-bearing plasmid in KP23 (*IncFII*), colistin resistance could not be transferred by conjugation. The mcr-1-producing isolate KP18 coexists a novel plasmid-carried tigecycline resistance gene tmexCD1-toprJ1. The most common chromosomal mutation associated with colistin resistance was a T246A amino acid substitution in PmrB, which was identified in most COLR-KP isolates (11/13, 84.6%). All ST11 isolates additionally had an R256G amino acid substitution. Critical virulence factors associated with hypervirulent *K. pneumoniae* were detected in four COLR-KP isolates; these virulence factors included aerobactin, salmochelin, and yersiniabactin.

Conclusion: We found that *mcr*-bearing COLR-KP emerged in our hospital and was growing at an increasing rate. Simultaneous emergence of hypervirulence and colistin–tigecycline–carbapenem resistance in the epidemic clone ST11 *K. pneumoniae* was also observed; this highlights the significance of active and continuous surveillance.

Keywords: *Klebsiella pneumoniae*, Colistin resistance, mcr, Pan-drug resistance, Molecular mechanism

BACKGROUND

Multidrug-resistant (MDR) gram-negative bacteria present a serious threat to global public health, especially, carbapenem-resistant *Klebsiella pneumoniae* (CRKP). Colistin has been considered one of the last resorts in treating severe infections that retain activity against *K. pneumoniae* carbapenemase (KPC)-producing *K. pneumoniae*. However, the emergence and global dissemination of colistin resistance compromise the efficacy of colistin.

Colistin is a cationic peptide synthesized by Gram-positive species, and it exhibits antimicrobial activity through multiple pathways, including direct antibacterial activity, antiendotoxin colistin activity, vesicle–vesicle contact pathway, hydroxyl radical death pathway, and respiratory enzyme inhibition (Sun et al., 2018). With antimicrobials, bacteria develop a series of resistance systems, including chromosomal gene mutations and plasmid-associated resistance genes to adapt to the environment. Colistin resistance in *K. pneumoniae* is mediated by several mechanisms. Mutations in genes encoding PhoP/PhoQ and PmrA/PmrB two-component regulatory systems regulate the expression of *pmrC* and *pmrHFIJKLM* operons and are responsible for the synthesis and transfer of 4-amino-4-deoxy-L-arabinose (L-Ara4N) cationic groups to lipid A. This modification increases the positive charge on lipopolysaccharides (LPSs) and therefore, decreases colistin binding, leading to colistin resistance (Poirel et al., 2017). Alternatively, MgrB is a small transmembrane protein produced upon the activation of the PhoP/PhoQ signaling system and acts as a negative regulator of this system. It regulates the expression of *etpB*, which is related to the modification of LPS. Mutations in *mgrB* gene upregulate the expression of the PhoP/PhoQ system, thereby leading to colistin resistance. Generally, *mgrB* mutations are caused by insertion sequences (ISs; IS*5-like*, IS*1F*, IS*Kpn13*, IS*Kpn14*, and IS*10R*) or point mutations (Cannatelli et al., 2014). In addition, hyperproduction of capsular polysaccharide reduces the interactions of colistin with the bacterial surface, leading to colistin resistance (Poirel et al., 2017). Besides, horizontal transfer of plasmid-borne *mcr* gene play a significant role in the dissemination of colistin resistance among various bacteria. Since its first identification in the late 2015 (Liu et al., 2016), the determinants of transferable colistin resistance have extended further away from *mcr*-1 to include various novel alleles (Sun et al., 2018). Until now, nine novel *mcr* variants have been reported, namely, *mcr-2*, *mcr-3*, *mcr-4*, *mcr-5*, *mcr-6*, *mcr-7*, *mcr-8*, *mcr-9*, and the recently identified *mcr-10* (Wang et al., 2018; Xiang et al., 2018; Yang et al., 2018; Kieffer et al., 2019; Wang et al., 2020). Moreover, the *mcr* family has been increasingly reported in various genera of *Enterobacteriaceae* worldwide, isolated from food animals, meat and vegetables, the environment, infected patients, and asymptomatic human carriers (Skov and Monnet, 2016). All MCR proteins are characterized as phosphoethanolamine (PEtN) transferases. They catalyze the attachment of PEtN to lipid A and lead to a reduction of the negative charge of LPS through structural alterations of lipid A and a decrease in the binding of colistin, thus resulting in colistin resistance (Sun et al., 2018). However, although these alleles belong to the group of PEtN transferases, the similarities in amino acid sequences vary, reflecting different genetic origins of these *mcr* alleles. Similarly, previous studies have demonstrated the complex dissemination of these alleles across the diversified species of *Enterobacteriaceae* and plasmid reservoirs and genetic environment for *mcr*-like genes (Wang Q. et al., 2017; El-Sayed Ahmed et al., 2020). Nevertheless, limited reports have indicated the presence of *mcr-1*, *mcr-3*, *mcr-7*, and *mcr-8* in *K. pneumoniae* at a relatively low prevalence. Although several studies have elucidated colistin-resistance mechanisms from different aspects, the underlying mechanism of colistin resistance in clinical *K. pneumoniae* isolates in our hospital was unclear.

Therefore, in this study, we identified 53 colistin-resistant *K. pneumoniae* (COLR-KP) isolates between 2017 and 2019 to investigate the primary mechanisms of colistin resistance and evaluate the potential prevalence of clinical *K. pneumoniae* isolates in our hospital.

MATERIAL AND METHODS

Bacterial Isolates and Antimicrobial Susceptibility Testing

In total, 1,171 *K. pneumoniae* clinical isolates and relevant data were collected between June 2017 and November 2019 at The First Affiliated Hospital of Nanchang University, a 3,200-bed tertiary care teaching hospital in Jiangxi, China. Matrix-assisted laser desorption ionization–time of flight mass spectrometry (BioMérieux, Marcy-l'Étoile, France) was used to identify the isolates. The ethics committee of the related university hospital (approval no. 2014036) approved this study. The VITEK 2 System (BioMérieux, Marcy-l'Etoile, France) was used to assess the *in vitro* antimicrobial susceptibility. The interpretation of tigecycline-related data was based on the criteria proposed by the US Food and Drug Administration. Similarly, the minimum inhibitory concentrations (MICs) of colistin were determined using the broth microdilution method in triplicate (Sigma, St. Louis, MO, USA) according to the Clinical and Laboratory

Standards Institute guidelines (document VET01-A4) and interpreted following the European Committee on Antimicrobial Susceptibility Testing breakpoints (European Committee on Antimicrobial Susceptibility Testing. Breakpoint tables for the interpretation of MICs and zone diameters. EUCAST; 2019. Version 9.0. http://www.eucast.org/clinicalbreakpoints/). All colistin-non-susceptible isolates were defined as those with MIC >2 μg/ml.

Plasmid-Mediated Colistin-Resistance Gene Screening and Conjugation Experiments

All COLR-KP isolates were screened for the presence of *mcr-1* to *mcr-8* genes (**Supplementary Table S1**) using polymerase chain reaction (PCR) and sequenced as described in the previous literature (Wang et al., 2018). The primers are listed in **Supplementary Table S1**.

Conjugation experiments were performed for *mcr* gene-bearing COLR-KP as described previously (Wang Y. et al., 2017). Briefly, using the azide-resistant *Escherichia coli* J53 as the recipient strain, both donor and recipient strains were cultured in the exponential phase and mixed on solid LB agar using filters at a 1:10 donor/recipient ratio. After 5 h of incubation, filters were resuspended in 0.9% NaCl, and the bacterial mixture was plated onto LB agar plates supplemented with colistin (1 μg/ml) and sodium azide (100 μg/ml). Confirmation of the susceptibility of all transconjugants to antibiotics was conducted using the antibiogram, followed by the amplification of the *mcr* gene using PCR.

Whole-Genome Sequencing

Genomic DNA was extracted from overnight cultures of selected isolates using the QIAGEN DNeasy Kit (Qiagen Sciences, Germantown, MD, USA) following the protocol of the manufacturer and sent for whole-genome sequencing (WGS). Genomic libraries were prepared with an insert of approximately 350 bp using the TruSeq DNA PCR-Free Sample Preparation Kit (Illumina Inc., San Diego, CA, USA) following the instructions of the manufacturer and sequenced using the Illumina HiSeq platform using a 150-bp paired-end protocol (Annoroad Biotech Co., Beijing, China). Two of the isolates were extracted using the QIAGEN Large-Construct Kit (Qiagen Sciences, Germantown, MD, USA) and sequenced using the PacBio RS II System (Pacific Bioscience, Menlo Park, CA, USA) with a 10-kb size library and P6/C4 chemistry.

Raw reads were trimmed with Trimmomatic 0.30 to remove low-quality sequences and adapters. Genomes were *de novo* assembled using the SPAdes Genome Assembler v3.13.0 (https://github.com/ablab/spades) (Bankevich et al., 2012).

Bioinformatics Analysis

General genomic features were defined by PATRIC automatic annotation tools. Mobile antibiotic resistance genes, including plasmid-mediated colistin-resistance genes, were identified using ResFinder 3.0 (https://cge.cbs.dtu.dk/services/ResFinder/) (Zankari et al., 2012). Plasmid replicon types were determined using PlasmidFinder v2.0 (https://cge.cbs.dtu.dk/services/PlasmidFinder/) with a minimum threshold of 95% identity (Carattoli et al., 2014). ISs were identified using ISfinder (Siguier et al., 2006). *In silico* multilocus sequence typing and serotyping were confirmed using MLST v.2.11 (https://cge.cbs.dtu.dk/services/MLST/) and Kaptive Web (https://github.com/katholt/Kaptive), respectively (Wick et al., 2018). Plasmid alignment was performed using the BRIG (http://brig.sourceforge.net/) software.

Mutations in Colistin-Resistance Genes

Mutations in genes potentially involved in colistin resistance (*mgrB*, *pmrA/pmrB*, and *phoP/phoQ*) were inspected by alignment with reference genome *K. pneumoniae* subsp. *pneumoniae* MGH78578 (# NC_009648.1). The PROVEAN tool v.1.1.5 (http://provean.jcvi.org/index.php) was used to predict the effect of amino acid substitutions on protein function (Choi and Chan, 2015). PROVEAN score ≤−2.5 was deleterious for protein function, and a score >−2.5 was considered to have a neutral effect on protein function.

Comparative Genomic and Phylogenetic Analysis

All selected genomes in this study and the reference genome *K. pneumoniae* subsp. *pneumoniae* MGH78578 were annotated with RAST (Overbeek et al., 2014). Genomes were aligned, and the core genome was inferred with Roary v.3.11.2 (Page et al., 2015). A maximum-likelihood phylogenetic tree was inferred by PhyML v.3.1 using the GTR evolutionary model with 500 bootstraps (Guindon et al., 2010). The phylogenetic tree was visualized using MEGA 6.0 (Kumar et al., 2018).

RESULTS

General Characteristics of *K.pneumoniae* Isolates

During the study period, we collected 1,171 non-duplicate isolates from various clinical samples. A total of 53 *K. pneumoniae* isolates (4.5%, 53/1,171) were then confirmed as COLR-KP, of which eight carried plasmid-mediated colistin-resistant *mcr* genes. Despite the relatively low overall prevalence rate (0.7%, 8/1,171) of *mcr*-like genes in clinical *K. pneumoniae* isolates, the presence of *mcr* (15.1%, 8/53) among the COLR-KP isolates indicated that this gene was already widely disseminated among *K. pneumoniae* isolates in our hospital. Of the 53 COLR-KP isolates, 13 (four *mcr*-bearing and nine non-*mcr*-bearing isolates) were randomly selected for further characterization, with colistin MICs ranging from 8 to 128 μg/ml, as shown in **Table 1**.

Among the 13 isolates, eight were isolated from sterile specimens, including blood, urine, peritoneal fluid, and surgical wound, whereas the other five were isolated from non-sterile sputum specimen. Patients were aged 35–80 (average 64) years. All patients had a history of previous hospitalization but without exposure to colistin, none had a history of recent overseas travel.

TABLE 1 | Clinical features, resistance profiles, and sequence types of colistin-resistant *Klebsiella pneumoniae* isolates.

Isolate	Date(year)	Specimen	CRO	TZP	MEM	IPM	GN	AK	LEV	ATM	TGC	COL	ST
KP3	2018	Urine	≥64	≥128	≥16	≥16	≥16	≤8	≥8	≥64	≤2	8	11
KP4	2018	Blood	≤1	≤16	≤1	≤1	≥16	≤16	≤2	≤4	≤2	8	25
KP7	2018	Urine	≥64	≤4	≤1	≤1	≥16	≤2	4	16	≤2	128	36
KP9	2018	Sputum	≥64	≥128	≤1	≤1	≤4	≤16	≥8	≥64	≤2	32	22
KP11	2018	Sputum	≤1	≤16	≤1	≤1	≤4	≤8	≤2	≤4	≤2	16	592
KP12	2018	Sputum	≤1	≤16	≤1	≤1	≤4	≤8	≤2	≤4	≤2	16	105
KP15	2018	Sputum	≥64	≥128	≥16	≥16	≥16	≥64	≥8	≥64	≤2	8	11
KP18	2018	Surgical wound	32	≥128	≤1	≤1	≥16	≥64	≥8	≥64	≤2	16	378
KP19	2018	Sputum	≤1	≤16	≤1	≤1	≤4	≤16	≤2	≤4	≤2	16	218
KP23	2018	Surgical wound	≥64	≥128	≤1	≤1	≥16	≤16	≥8	≥64	≤2	16	11
KP30	2018	Ascites	≥64	≤4	≤1	≤1	≤1	≤2	≤0.25	16	≤2	64	294
KP67	2019	Blood	≥64	≥128	≥16	≥16	≥16	≥64	≥8	≥64	8	64	11
KP69	2019	Blood	≥64	≥128	≥16	≥16	≥16	≥64	≥8	≥64	8	64	11

ST, sequence type; BSI, bloodstream infection; UTI, urinary tract infection; CRO, ceftriaxone; TZP, piperacillin–tazobactam; MEM, meropenem; IPM, imipenem; GN, gentamicin; AK, amikacin; LEV, levofloxacin; ATM, aztreonam; TGC, tigecycline; COL, colistin.

Therefore, it was presumed that the spread of colistin resistance occurs in hospitals without colistin use. In the bloodstream isolates, designated KP4, KP67, and KP69, KP4 was recovered from a patient with severe bloodstream infection (BSI) with acute monocytic leukemia. This patient was under immunosuppression and already received combination treatments of imipenem, meropenem, teicoplanin, and voriconazole. Alternatively, patients expressing KP67 and KP69 were admitted for third-degree burn injuries, where the barrier of their skin mucosa was severely damaged.

Antimicrobial susceptibility testing revealed that of these COLR-KP isolates, four were assigned to CRKP and five were extended-spectrum beta-lactamase (ESBL)-producing isolates. Both exhibited MDR phenotypes, whereas the remaining five isolates were susceptible to most antimicrobials other than colistin. This finding was similar to previous observations of colistin resistance developed in MDR strains. This result thus indicates that colistin resistance evolved independently.

In silico MLST analysis assigned the COLR-KP isolates to nine distinct STs, of which five belonged to ST11 (5/13, 38.5%) and the rest belonged to different STs. Two of these ST11 isolates were recovered from the blood of patients with burn injury who displayed pan-resistance profiles and were resistant to all tested antimicrobial agents, including tigecycline. STs and antimicrobial-resistance profiles are shown in **Table 1**.

General Genomic Features

A summary of the genomic features of the 13 sequenced *K. pneumoniae* genomes is presented in **Table S2**. Isolates KP67 and KP69 were two completed genomes, and the rest were draft sequences. Whole-genome sizes ranged from 5,284,652 to 5,958,900 bp, with an average GC content of 57.2%. The mean number of mapped contigs was 231. The coding sequences ranged from 3,521 to 6,100, and the proteins with assignment function ranged from 3,083 to 5,189.

Antimicrobial Resistance and Virulence Genes

Four COLR-KP isolates (KP3, KP15, KP67, and KP69) were carbapenem-resistant, which belonged to ST11, and were positive for $bla_{\text{KPC-2}}$ and ESBL gene $bla_{\text{CTX-M-65}}$, corresponding to a previous national surveillance (Zhang et al., 2017). ESBL genes, mainly of the CTX-M group, including $bla_{\text{CTX-M-3}}$, $bla_{\text{CTX-M-14}}$, and $bla_{\text{CTX-M-65}}$, were identified in six of the 13 COLR-KP isolates. Isolate KP18 bore tigecycline-resistance gene *tmexCD1-toprJ1*; however, the strain remained susceptible to tigecycline while being resistant to other antimicrobials such as tetracyclines, quinolones, and aminoglycosides. These COLR-KP isolates also harbored several antimicrobial-resistance genes leading to β-lactam, aminoglycoside, fluoroquinolone, sulfonamide, and trimethoprim resistance. Four isolates also possessed multiple virulence genes, including *rmpA*, *iucABCD*, *iroBCDN*, *iutA*, and *ybt*, which have been associated with urinary tract infections, septicemia, and pneumonia. KP4 and KP67 isolates were obtained from patients with BSI who finally died of severe infection. The antimicrobial-resistance genes, virulence genes, and serotypes of COLR-KP isolates are shown in **Table 2**.

Colistin-Resistance Mechanisms

Four isolates were confirmed as *mcr*-bearing COLR-KP, of which three (KP4, KP18, and KP30) were positive for *mcr-1*and one (KP23) for *mcr-8*; none of the other *mcr* genes was detected. WGS and plasmid replicon typing revealed that *mcr-1.1* in KP4 and KP30 isolates was located in an *IncX4* plasmid (approximately 33 kb). The *mcr-1* bearing plasmid pMCR_KP18 in KP18 coexisted with an acquired novel tigecycline-resistance gene in an *IncHI1* plasmid. Conjugation experiments showed that colistin resistance could be successfully transferred from *mcr-1*-bearing isolates KP4, KP18, and KP30 to *E. coli* J53AZ$^{\text{R}}$, with the colistin MIC for the transconjugants increasing 16- and 4-fold compared with the untransformed control, respectively. PCR and sequencing analysis further revealed that the transconjugants harbored *mcr-1* gene, which demonstrated that the *mcr-1* genes in isolates KP4, KP18, and KP30 were functional in colistin resistance.

The *mcr-8*-bearing plasmid in KP23 was identified as an *IncFII* type of approximately 13 kb in size. In contrast, colistin resistance from *mcr-8*-KP23 strain could not be transferred by conjugation despite several attempts. No genes encoding conjugation-related proteins were found in the complete

TABLE 2 | Antimicrobial-resistance genes, virulence genes, and serotypes of colistin-resistant *Klebsiella pneumoniae* isolates.

Isolate	Resistance genes					Virulent				Plasmids
	β-Lactam	Fluoroquinolone	Aminoglycoside	Tigecycline (acquired)	Others	Virulence genes	wzi	Cps	O locus	Predicted plasmid elements
KP3	bla_{KPC-2}, $bla_{CTX-M-14}$, $bla_{CTX-M-55}$, $bla_{SHV-182}$, bla_{TEM-1B}	*qnrS1*	*aac(3)-IId,aadA2b, aph (3'')-Ib,aph(6)-Id*		*fosA,sul1,sul2,tet (A),dfrA1,catA2*	*ybt 9*	64	K64	O2	IncFIB(K), IncFII, IncFII, IncR,ColRNAI
KP4	$bla_{SHV-110}$, bla_{SHV-81}	-	*aac(3)-IId,aph(3'')-Ib,aph (3')-Ia,aph(3')-Id*		*sul1,sul2,dfrA1*	*iucABCD, iutA*	72	K2	O1	IncX4, IncFIA(HI1), IncFIB(K), IncFIB, IncFII, IncN
KP7	$bla_{CTX-M-3}$, bla_{SHV-11}, bla_{SHV-13}, bla_{SHV-70}, bla_{TEM-1B}	*aac(6')-Ib-cr, qnrB2,qnrB52, qnrS1,oqxA,oqxB*	*aac(3)-IId,aac(6')-Ib-cr, aadA16,aph(3'')-Ib,aph (3')-Ia,aph(6)-Id*		*fosA5,floR,mph(A), ARR-3,sul1,sul2, tet(A),dfrA27*		27	K27	O2	IncFII(K)
KP9	$bla_{CTX-M-14}$, bla_{DHA-1}, bla_{SHV-99}	*oqxA,oqxB,qnrB4*			*fosA,sul1*		9	K9	O1	IncFIA(HI1)
KP11	bla_{SHV-26}	*oqxA, oqxB*			*fosA5*	*rmpA2, iucABCD, iutA, iroBCDN*	206	K57	O3b	IncHI1B
KP12	bla_{DHA-1},$bla_{SHV-187}$	*oqxA, oqxB, qnrB4*	*aadA16*		*fosA,ARR-3, sul1, tet(B), dfrA27*	*ybt*	383	K102	O2	IncHI1B
KP15	bla_{KPC-2},$bla_{SHV-182}$,bla_{TEM-1B}	*oqxA, oqxB*	*aadA2b, aph(3'')-Ib, aph(6)-Id, rmtB*		*fosA, fosA3, sul1, sul2, tet(A), dfrA1, catA2*	*ybt 9*	64	K64	O2	IncFIB(K), IncFII, IncFII, IncR, ColRNAI
KP18	$bla_{SHV-119}$, bla_{DHA-1}	*qnrB6, qnrB4, aac (6')-Ib-cr, oqxA, oqxB*	*aph(3')-Ia, aac(6')-Ib-cr, aadA2, aadA16, aadA1, aph(6)-Id, aph(4)-Ia, armA, aac(3)-IV, aph(3'')-Ib*	*tmexCD1-toprJ1*	*fosA, msr(E), mph (A), mph(E), ARR-3, sul1, sul2, sul3, tet(A), dfrA27*		177	K125	O5	IncFIA(HI1), IncFIB (K), IncFIB(Mar), IncFIB(pKPHS1), IncFII(K), IncHI1B, IncR
KP19	bla_{SHV-33}	*oqxA, oqxB*			*fosA*	*rmpA2, iucABCD, iroBCDN, iutA, ybt 9*	77	K57	O2	
KP23	$bla_{CTX-M-3}$, $bla_{SHV-182}$, bla_{TEM-1B}	*aac(6')-Ib-cr, qnrS1*	*aac(3)-IId, aph(3')-Ia, aac (6')-Ib-cr, aph(3'')-Ib, aph (6)-Id, aadA16*		*fosA, ARR-3, sul2, tet(A), dfrA27*		385	K111	O3b	IncFII(K), IncFIA(HI1), IncR
KP30	$bla_{SHV-187}$	*oqxA,oqxB*			*fosA*	*ybt 4*	274	K30	O1	IncX4, IncHI1B
KP67	bla_{KPC-2}, $bla_{CTX-M-65}$, bla_{SHV-12}, bla_{LAP-2}, bla_{TEM-1D}	*qnrS1*	*rmtB*		*sul2, tet(A), dfrA14, CatA2*	*rmpA2, iucABCD, iutA,ybt 9*	64	K64	O2	IncHI1B, IncFII, IncR, colRNAI, repB
KP69	bla_{KPC-2}, $bla_{CTX-M-65}$, bla_{SHV-11}, bla_{TEM-1D}		*aadA2, rmtB, strA, strB*		*fosA3, sul1, sul2, tet(A), dfrA1, CatA2*	*ybt 9*	64	K64	02	IncFIB(K), IncFII (pKP91), IncR, colRNAI

sequence of pMCR_KP23. Therefore, it is suggested that the *mcr-8*-bearing plasmid in this strain was non-self-transmissible.

We also screened for common chromosomal mutations that caused resistance to colistin. All COLR-KP isolates had wild-type *phoP* and similar neutral amino acid substitution T246A in *pmrB* gene. In addition, five ST11 isolates coexisted with missense mutations in *pmrB* leading to R256G substitution. Isolate KP15 also had a missense mutation as a T157P substitution. Alterations in the PhoP/PhoQ regulator *mgrB* gene occurred in three isolates; KP12 and KP69 had complete deletion in *mgrB*, whereas the ST11 isolate KP67 had an interruption in the *mgrB* gene caused by a promoter deletion. These three isolates did not possess any *mcr* gene or other deleterious mutation. Therefore, the inactivation of *mgrB* gene might be responsible for its high colistin resistance (Hamel et al., 2020). Moreover, four *mcr*-bearing isolates had chromosomal mutations in the *pmrB*, leading to T246A substitution and absence of *phoP* mutations. KP23 isolate additionally had a deleterious R256G amino acid substitution in *pmrB* and KP 18 had two amino acid mutations in pmrA (M66I, E35A) (**Table 3**).

Comparative Genomic Analysis of COLR-KP

Comparative plasmid analysis revealed that *mcr-1*-bearing plasmids in KP4 identified in this study had >95% nucleotide identity to the plasmid pMCR_WCHEC1618 (GenBank accession no. KY463454) isolated in Sichuan, China and plasmid pIBMC*mcr1* (GenBank accession no. MF449287) isolated in Italy. Interestingly, plasmid pMCR_KP30 displayed a huge difference from KP4, which showed large fragment inversion (**Figure 1A**). In addition, an approximately 13-kb *mcr-8*-related plasmid fragment in KP23 genome showed >99.9% identity to plasmid pMCR8_095845 (GenBank accession no. CP031883; **Figure 1B**).

Furthermore, to characterize the genetic features of the COLR-KP isolates, we performed a comparative genomic analysis. We identified 9,227 gene clusters, including 4,140 core, 2,593 cloud, and 2,494 shell genes using Roary for comparative analysis. Overall, the COLR-KP isolates were genetically diverse, suggesting that the *mcr*-bearing *K. pneumoniae* isolates were also genetically diverse, and these genes were disseminated among various *K. pneumoniae* isolates, primarily by horizontal transmission (**Figure S1**). Furthermore, we compared the colistin-resistant *K. pneumoniae* genomes from different areas. The results indicated that most of the isolates were ST11 type, and acquired colistin resistance might not have shown any strain bias (**Figure 1C**).

TABLE 3 | Plasmid-mediated genes and chromosomal mutations related to colistin resistance in *Klebsiella pneumoniae* isolates.

Isolate	*mcr* gene	Chromosomal mutation*		
		mgrB	***pmrB***	**Others**
KP3			T246A, R256G	*phoQ*(V24G)
KP4	*mcr-1*		T246A	
KP7			T246A	
KP9			T246A, S203P	
KP11			T246A	
KP12		Complete deletion	T246A	
KP15			T246A, R256G, T157P	
KP18	*mcr-1*		T246A	*pmrA*(M66I,E35A)
KP19			T246A, V257A, T240M	
KP23	*mcr-8*		T246A, R256G	
KP30	*mcr-1*		T246A, M285L	
KP67		Promoter area deletion		
KP69		Complete deletion		

**Aligned with Klebsiella pneumoniae subsp. pneumoniae MGH 78578 (GenBank accession no. CP000647).*

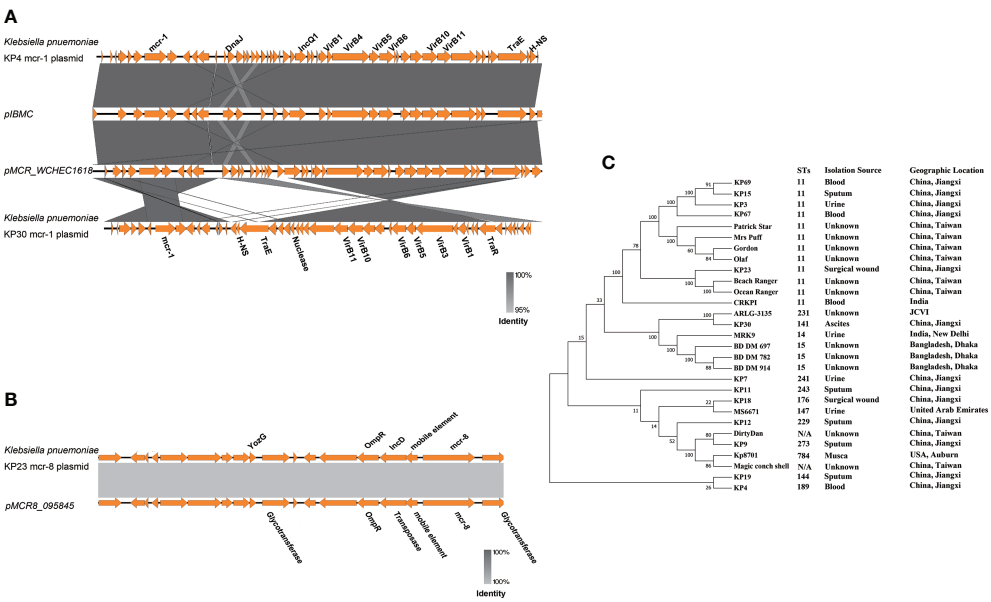

FIGURE 1 | Comparative analysis of COLR-KP. **(A)** Comparative analysis of *mcr-1* related plasmids. **(B)** Comparative analysis of *mcr-8* related plasmids. **(C)** Phylogenetic analysis of core genes for COLR-KP from different area. Core genes are those genes existed in all *K. pneumoniae* genomes in this study, which were produced by a pan genome analysis using Roary pipeline (e value = 1e-5, identity = 90, coverage = 90).

DISCUSSION

During the coronavirus disease 2019 pandemic, the problem of bacterial resistance cannot be ignored. The World Health Organization celebrated the "World Antimicrobial Awareness Week" in 2020, aiming to raise awareness regarding the problems of antimicrobial resistance and establish a united front to preserve antimicrobials and curb the development of antimicrobial resistance. Colistin is an ultimate line of refuge against lethal infections by MDR gram-negative pathogens. Unfortunately, this last-resort antibiotic has been challenged by the mobilized colistin resistance determinant *mcr* family, resulting in a rapid spread worldwide with unexpected diversity.

The overall prevalence of colistin resistance in clinical *K. pneumoniae* isolates was 4.5% (53/1,171), which is higher than that in national surveillance from the CHINET report (CHINET data, 2020. http://www.chinets.com/Data/AntibioticDrugFast). In addition, the rising prevalence trend of COLR-KP was observed with each passing year, with a significant increase from 2.8% (17/603) in 2018 to 6.3% (36/568) in 2019. However, of all patients without colistin exposure, none had a history of recent overseas travel. It is possible that the spread of colistin resistance can occur in hospitals in the absence of colistin use, which is consistent with previous study (Huang et al., 2018). The fact that the prevalence of COLR-KP increased in 2019 coincided well with the consumption of colistin in our hospital, suggesting that selective pressure from colistin use is a factor that intensifies resistance rather than a definite correlation to colistin use.

Among the COLR-KP isolates in our study, >50% were MDR, which further limited the current treatment options. Four of these isolates were KPC-producing *K. pneumoniae* ST11 clones, indicating that colistin resistance emerged among the KPC-2-producing *K. pneumoniae* pandemic ST11 clonal lineage isolates in our region. Recent clinical studies have reported that mortality rates among patients with infections caused by COLR-KPC *K. pneumoniae* isolates were higher than those among patients infected by colistin-susceptible KPC *K. pneumoniae* strains. This observation is attributable to further narrowing of available therapeutic options (Giacobbe et al., 2015).

Of particular concern were two COLR-KPC *K. pneumoniae* isolates, KP67 and KP69, which exhibited pandrug resistance (PDR) and were recovered from patients with BSI; these were resistant to all tested antimicrobials, including tigecycline. These findings suggest that colistin resistance is imparted to KPC-producing *K. pneumoniae* with minimal impact on its ability to either spread or cause invasive infection. This finding agrees with those of an earlier report (Arena et al., 2016).

The genomic features of isolates were consistent with the previously described data for other *K. pneumoniae* genomes (Wyres and Holt, 2018). MLST data showed that 13 COLR-KP isolates had diverse genetic backgrounds and five of these isolates belonged to the epidemic ST11 clone. Phylogenetic analysis also showed a genetic diversity, including those ST11 isolates. Although isolated in the same period (within a week) from the same department, the mechanisms of colistin resistance in ST11 KP67 and KP69 strains were different, indicating that the colistin resistance of these strains proceeded in a distinctly evolutionary pathway.

Of the 13 colistin-resistant KP isolates, four carried *mcr* genes, and among these, three carried *mcr-1* and one carried *mcr-8* genes. The genetic characterization of *mcr-1*-bearing plasmids showed that *mcr-1* in KP4 and KP30 was located in the transferable approximately 33-kb *IncX4* plasmid, the most prevalent version of the *mcr-1*-bearing plasmid reservoirs (Fernandes et al., 2016; Zurfluh et al., 2016). Comparative analysis revealed that the *mcr-1*-bearing plasmid pMCR_KP4 (KP4) identified in this study displayed >95% nucleotide identity to various plasmids, including pMCR_WCHEC1618 (GenBank accession no. KY463454) isolated from *E. coli* in Sichuan, located 1,490 km away from Nanchang, China, and pIBMC*mcr1* (GenBank accession no. MF449287) isolated in Italy. Interestingly, KP30 bore a different *mcr-1* plasmid, which showed a large fragment inversion. It indicated that KP30 acquires the *mcr-1* gene from a different approach. The *mcr-8.2*-bearing fragment from KP23 (pMCR_KP23), which showed a >99.9% identity to plasmid pMCR8_095845 (GenBank accession no. CP031883), was also recovered from clinical *K. pneumoniae* strain in 2016 in Sichuan, China (Ma et al., 2020).

The first identification of MCR-1-producing *K. pneumoniae* in the study hospital was in 2018, highlighting a much later emergence than that of *E. coli* in 2014 as reported previously (Quan et al., 2017). Notably, the *mcr-1*-bearing plasmid in the colistin-resistant *E. coli* was *IncX4*, which was identical to those of KP4 and KP30, implying that the *IncX4*-bearing-*mcr-1* was successfully disseminated and circulated among various species of *Enterobacteriaceae* in this hospital. Accordingly, there were questions about whether *mcr-1* was an emerging resistance trait in other countries as *mcr-1*-positive isolates were collected as early as in 2005 in France (Haenni et al., 2016).

Of a particular concern is the transfer of a plasmid with *mcr-1* into carbapenemase-producing isolates intra-hospital, which leads to nosocomial infections with PDR strains, leaving no beneficial treatment options available. In our study, we did not detect *mcr-1* gene in all KPC-2-producing COLR-CRKP isolates. Nevertheless, we detected two PDR strains resistant to all antibiotics, including tigecycline, with the colistin resistance associated with *mgrB* inactivation. These patients had no colistin exposure history before the specimen collection; consequently, tracing the origin of selective pressure for these isolates was difficult.

Plasmid pMCR_KP4 and pMCR_KP30 successfully transferred the *mcr-1* gene to *E. coli* J53AZ^{R}, which harbored an intact set of conjugative transfer genes to facilitate the transfer of plasmids among various isolates, consistent with its ability to conjugate into *E. coli* J53AZ^{R}, as described above. In contrast, the *mcr-8.2* could not be transferred from the KP23 isolate to the recipient strain by conjugation despite several attempts. Moreover, no genes encoding conjugation-related proteins were found in the sequence of pMCR_KP23; therefore, it is suggested that the *mcr-8.2*-bearing plasmid in this strain was non-self-transmissible, which is consistent with the results of a

previous report (Ma et al., 2020). Although the IS*3*-like family was detected in this plasmid, it could mobilize the intervening genetic components of *mcr-8.2* or acquire colistin resistance.

Interestingly, KP18 was an *mcr-1*-ESBL-producing isolate, which also carried a novel plasmid-borne RND-type tigecycline-resistance determinant *tmexCD1-toprJ1* (Lv et al., 2020). More recently, a research group first identified the *tmexCD1-toprJ1* located on the conjugative *IncFIA* plasmid (pHNAH8I-1) in a PDR *K. pneumoniae* isolate obtained from a chicken in Sichuan. This strain also carried both carbapenem-resistance gene $bla_{\text{NDM-1}}$ and colistin- resistance genes *mcr-1* and *mcr-8* (Lv et al., 2020). Although *tmexCD1-toprJ1* mainly spreads among *K. pneumoniae* isolates from food animals, the simultaneous appearance of mobilized colistin- and tigecycline-resistance genes in clinical isolates is an alarming evolutionary trend, which may lead to rapid horizontal transfer in hospital settings; this requires attention for a continuous and meticulous surveillance.

In the present study, the most common chromosomal mutation associated with colistin resistance was the T246A amino acid substitution in *pmrB*. This substitution was identified in most COLR-KP isolates and reported in colistin-resistant *K. pneumoniae* in a Tunisian Teaching Hospital (Jaidane et al., 2018). However, the T246A was predicted as neutral mutation that was most likely unrelated to colistin resistance, consistent with of the findings of a previous report (Longo et al., 2019). All ST11 isolates had R256G and T246A amino acid substitutions in *pmrB*, similar to that previously described in ST258 isolates (Aires et al., 2016), and the ST11 is a close variant of the international pandemic clone ST258. Furthermore, some isolates presented several new mutations as amino acid substitutions: S203P, T240M, and V257A in *PmrB*; E35A and M66I in *PmrA*; and V24G in *PhoQ*. These mutations were predicted to be neutral, with no effect on the biological functions of these proteins. The underlying mechanisms of colistin resistance in GNB are complex and not completely understood yet (El-Sayed Ahmed et al., 2020). According to our results, there still exists some unknown molecular mechanism leading to colistin resistance, which requires further investigations. However, this prediction is not definitive, and further investigation is needed to confirm the relationship between these mutations and colistin resistance.

MgrB mutation was the most frequently reported molecular mechanism of colistin resistance in *K. pneumoniae* (Cannatelli et al., 2014), whereas only three isolates possessed *mgrB* mutations in our study. The ST105 KP12 and ST11 KP69 isolates had complete deletion; the ST11 KP67 isolate had a truncated gene due to a promoter deletion. Insertional inactivation caused by diverse ISs at different locations within the *mgrB* gene was often responsible for acquired colistin resistance in *K. pneumoniae* (Nordmann et al., 2016). Some complete deletions of the *mgrB* locus had been reported as well. Of note, isolate KP67 was significantly more virulent and exhibited resistance to tigecycline and carbapenem, as well as to colistin, causing BSI.

Various resistance genes were carried by these COLR-KP isolates, which conferred resistance to carbapenems, cephalosporins, fluoroquinolones, aminoglycosides, macrolides, sulfonamides, tetracyclines, and trimethoprims. Four carbapenem-resistant COLR-KP isolates produced KPC-2 as the predominant carbapenemase in the world and China (Munoz-Price et al., 2013; Zong et al., 2020). In addition, critical virulence factors associated with the hypervirulent *K. pneumoniae*, including aerobactin (*iucABCD* and *iutA*), salmochelin (*iron* and *iroBCD*), and yersiniabactin (*ybt*), were found in the isolates KP4, KP11, KP19, and KP67. The combination of hypervirulence and high drug resistance also resulted in veritable "superbug," thus making infection control intractable.

CONCLUSION

COLR-KP emerged in our hospital and was increasing with each passing year. Although the molecular determinants of colistin resistance in *K. pneumoniae* clinical isolates in our region are still chromosomal mutations, *mcr-1* and *mcr-8* have been detected in MDR *K. pneumoniae* isolates without colistin use. Moreover, the coexistence of plasmid-borne *mcr-1* and *tmexCD1-toprJ1* in *K. pneumoniae* further threatens public health. Of a particular concern is the simultaneous emergence of hypervirulence and colistin–tigecycline–carbapenem resistance in an epidemic clone ST11 *K. pneumoniae* isolate, causing a lethal and untreatable infection.

DATA AVAILABILITY STATEMENT

The data presented in the study are deposited in the NCBI repository, accession number PRJNA718703 can be found below: https://www.ncbi.nlm.nih.gov/bioproject/?term=PRJNA718703.

ETHICS STATEMENT

The studies involving human participants were reviewed and approved by Ethics Committee of the First Affiliated Hospital of Nanchang University. The patients/participants provided their written informed consent to participate in this study.

AUTHOR CONTRIBUTIONS

XH, JG, and LZ designed the study. YLL, YQL, and XL wrote the manuscript. LZ reviewed the manuscript. NH and QL managed the strains and data collection. ZW, WZ, XL, and YQL prepared the figures and tables. All authors contributed to the article and approved the submitted version.

FUNDING

This work was supported by the National Natural Science Foundation of China (32060040 and 31760261), the Natural Science Foundation of Jiangxi Province (20202BABL216084, 20192ACBL21042, 20202BAB216045, 20192BBG, and

20204BCJL23054), the Science and Technology Research Project of Education Department of Jiangxi Province (GJJ180130), and the Major Science and Technology Project of Jiangxi Province (20181BBG70030).

ACKNOWLEDGMENTS

We thank Dr. Chong Li for providing additional bioinformatics analysis for this study.

REFERENCES

Aires, C. A., Pereira, P. S., Asensi, M. D., and Carvalho-Assef, A. P. (2016). mgrB Mutations Mediating Polymyxin B Resistance in Klebsiella Pneumoniae Isolates From Rectal Surveillance Swabs in Brazil. *Antimicrob. Agents Chemother.* 60 (11), 6969–6972. doi: 10.1128/AAC.01456-16

Arena, F., Henrici De Angelis, L., Cannatelli, A., Di Pilato, V., Amorese, M., D'Andrea, M. M., et al (2016). Colistin Resistance Caused by Inactivation of the MgrB Regulator Is Not Associated With Decreased Virulence of Sequence Type 258 KPC Carbapenemase-Producing Klebsiella Pneumoniae. *Antimicrob. Agents Chemother.* 60 (4), 2509–2512. doi: 10.1128/AAC.02981-15

Bankevich, A., Nurk, S., Antipov, D., Gurevich, A. A., Dvorkin, M., Kulikov, A. S., et al (2012). SPAdes: A New Genome Assembly Algorithm and its Applications to Single-Cell Sequencing. *J. Comput. Biol.* 19 (5), 455–477. doi: 10.1089/cmb.2012.0021

Cannatelli, A., Giani, T., D'Andrea, M. M., Di Pilato, V., Arena, F., Conte, V., et al (2014). MgrB Inactivation is a Common Mechanism of Colistin Resistance in KPC-Producing Klebsiella Pneumoniae of Clinical Origin. *Antimicrob. Agents Chemother.* 58 (10), 5696–5703. doi: 10.1128/AAC.03110-14

Carattoli, A., Zankari, E., Garcia-Fernandez, A., Voldby Larsen, M., Lund, O., Villa, L., et al (2014). In Silico Detection and Typing of Plasmids Using PlasmidFinder and Plasmid Multilocus Sequence Typing. *Antimicrob. Agents Chemother.* 58 (7), 3895–3903. doi: 10.1128/AAC.02412-14

Choi, Y., and Chan, A. P. (2015). PROVEAN Web Server: A Tool to Predict the Functional Effect of Amino Acid Substitutions and Indels. *Bioinformatics* 31 (16), 2745–2747. doi: 10.1093/bioinformatics/btv195

El-Sayed Ahmed, M. A. E., Zhong, L. L., Shen, C., Yang, Y., Doi, Y., and Tian, G. B. (2020). Colistin and its Role in the Era of Antibiotic Resistance: An Extended Revie-2019). *Emerg. Microbes Infect.* 9 (1), 868–885. doi: 10.1080/22221751.2020.1754133

Fernandes, M. R., McCulloch, J. A., Vianello, M. A., Moura, Q., Perez-Chaparro, P. J., Esposito, F., et al (2016). First Report of the Globally Disseminated IncX4 Plasmid Carrying the Mcr-1 Gene in a Colistin-Resistant Escherichia Coli Sequence Type 101 Isolate From a Human Infection in Brazil. *Antimicrob. Agents Chemother.* 60 (10), 6415–6417. doi: 10.1128/AAC.01325-16

Giacobbe, D. R., Del Bono, V., Trecarichi, E. M., De Rosa, F. G., Giannella, M., Bassetti, M., et al (2015). Risk Factors for Bloodstream Infections Due to Colistin-Resistant KPC-Producing Klebsiella Pneumoniae: Results From a Multicenter Case-Control-Control Study. *Clin. Microbiol. Infect.* 211106 (12), e1101–e1108. doi: 10.1016/j.cmi.2015.08.001

Guindon, S., Dufayard, J. F., Lefort, V., Anisimova, M., Hordijk, W., and Gascuel, O. (2010). New Algorithms and Methods to Estimate Maximum-Likelihood Phylogenies: Assessing the Performance of PhyML 3.0. *Syst. Biol.* 59 (3), 307–321. doi: 10.1093/sysbio/syq010

Haenni, M., Poirel, L., Kieffer, N., Chatre, P., Saras, E., Metayer, V., et al (2016). Co-Occurrence of Extended Spectrum Beta Lactamase and MCR-1 Encoding Genes on Plasmids. *Lancet Infect. Dis.* 16 (3), 281–282. doi: 10.1016/S1473-3099(16)00007-4

Hamel, M., Chatzipanagiotou, S., Hadjadj, L., Petinaki, E., Papagianni, S., Charalampaki, N., et al (2020). Inactivation of mgrB Gene Regulator and Resistance to Colistin is Becoming Endemic in Carbapenem-Resistant Klebsiella Pneumoniae in Greece: A Nationwide Study From 2014 to 2017. *Int. J. Antimicrob. Agents* 55 (4), 105930. doi: 10.1016/j.ijantimicag.2020.105930

Huang, B., He, Y., Ma, X., Cai, R., Zeng, J., Lu, Y., et al (2018). Promoter Variation and Gene Expression of Mcr-1-Harboring Plasmids in Clinical Isolates of Escherichia Coli and Klebsiella Pneumoniae From a Chinese Hospital. *Antimicrob. Agents Chemother.* 62 (5), e00018-18. doi: 10.1128/AAC.00018-18

Jaidane, N., Bonnin, R. A., Mansour, W., Girlich, D., Creton, E., Cotellon, G., et al (2018). Genomic Insights Into Colistin-Resistant Klebsiella Pneumoniae From a Tunisian Teaching Hospital. *Antimicrob. Agents Chemother.* 62 (2), e01601-17. doi: 10.1128/AAC.01601-17

Kieffer, N., Royer, G., Decousser, J. W., Bourrel, A. S., Palmieri, M., Ortiz de la Rosa, J. M., et al (2019). mcr-9, an Inducible Gene Encoding an Acquired Phosphoethanolamine Transferase in Escherichia Coli, and Its Origin. *Antimicrob. Agents Chemother.* 63 (9), e00965-19. doi: 10.1128/AAC.00965-19

Kumar, S., Stecher, G., Li, M., Knyaz, C., and Tamura, K. (2018). MEGA X: Molecular Evolutionary Genetics Analysis Across Computing Platforms. *Mol. Biol. Evol.* 35 (6), 1547–1549. doi: 10.1093/molbev/msy096

Liu, Y. Y., Wang, Y., Walsh, T. R., Yi, L. X., Zhang, R., Spencer, J., et al (2016). Emergence of Plasmid-Mediated Colistin Resistance Mechanism MCR-1 in Animals and Human Beings in China: A Microbiological and Molecular Biological Study. *Lancet Infect. Dis.* 16 (2), 161–168. doi: 10.1016/S1473-3099(15)00424-7

Longo, L. G. A., de Sousa, V. S., Kraychete, G. B., Justo-da-Silva, L. H., Rocha, J. A., Superti, S. V., et al (2019). Colistin Resistance Emerges in Pandrug-Resistant Klebsiella Pneumoniae Epidemic Clones in Rio De Janeiro, Brazil. *Int. J. Antimicrob. Agents* 54 (5), 579–586. doi: 10.1016/j.ijantimicag.2019.08.017

Lv, L., Wan, M., Wang, C., Gao, X., Yang, Q., Partridge, S. R., et al (2020). Emergence of a Plasmid-Encoded Resistance-Nodulation-Division Efflux Pump Conferring Resistance to Multiple Drugs, Including Tigecycline, in Klebsiella Pneumoniae. *mBio* 11 (2), e02930-19. doi: 10.1128/mBio.02930-19

Ma, K., Feng, Y., Liu, L., Yao, Z., and Zong, Z. (2020). A Cluster of Colistin- and Carbapenem-Resistant Klebsiella Pneumoniae Carrying blaNDM-1 and mcr-8.2. *J. Infect. Dis.* 221 (Suppl 2), S237–S242. doi: 10.1093/infdis/jiz519

Munoz-Price, L. S., Poirel, L., Bonomo, R. A., Schwaber, M. J., Daikos, G. L., Cormican, M., et al (2013). Clinical Epidemiology of the Global Expansion of Klebsiella Pneumoniae Carbapenemases. *Lancet Infect. Dis.* 13 (9), 785–796. doi: 10.1016/S1473-3099(13)70190-7

Nordmann, P., Jayol, A., and Poirel, L. (2016). Rapid Detection of Polymyxin Resistance in Enterobacteriaceae. *Emerg. Infect. Dis.* 22 (6), 1038–1043. doi: 10.3201/eid2206.151840

Overbeek, R., Olson, R., Pusch, G. D., Olsen, G. J., Davis, J. J., Disz, T., et al (2014). The SEED and the Rapid Annotation of Microbial Genomes Using Subsystems Technology (RAST). *Nucleic Acids Res.* 42 (Database issue), D206–D214. doi: 10.1093/nar/gkt1226

Page, A. J., Cummins, C. A., Hunt, M., Wong, V. K., Reuter, S., Holden, M. T., et al (2015). Roary: Rapid Large-Scale Prokaryote Pan Genome Analysis. *Bioinformatics* 31 (22), 3691–3693. doi: 10.1093/bioinformatics/btv421

Poirel, L., Jayol, A., and Nordmann, P. (2017). Polymyxins: Antibacterial Activity, Susceptibility Testing, and Resistance Mechanisms Encoded by Plasmids or Chromosomes. *Clin. Microbiol. Rev.* 30 (2), 557–596. doi: 10.1128/CMR.00064-16

Quan, J., Li, X., Chen, Y., Jiang, Y., Zhou, Z., Zhang, H., et al (2017). Prevalence of mcr-1 in Escherichia Coli and Klebsiella Pneumoniae Recovered From Bloodstream Infections in China: A Multicentre Longitudinal Study. *Lancet Infect. Dis.* 17 (4), 400–410. doi: 10.1016/S1473-3099(16)30528-X

Siguier, P., Perochon, J., Lestrade, L., Mahillon, J., and Chandler, M. (2006). ISfinder: The Reference Centre for Bacterial Insertion Sequences. *Nucleic Acids Res.* 34 (Database issue), D32–D36. doi: 10.1093/nar/gkj014

Skov, R. L., and Monnet, D. L. (2016). Plasmid-Mediated Colistin Resistance (Mcr-1 Gene): Three Months Later, the Story Unfolds. *Euro. Surveill.* 21 (9):30155. doi: 10.2807/1560-7917.ES.2016.21.9.30155

SUPPLEMENTARY MATERIAL

The Supplementary Material for this article can be found online at: https://www.frontiersin.org/articles/10.3389/fcimb.2021.673503/full#supplementary-material

Supplementary Figure 1 | Comparative genomics of 13 COLR-KP isolated in this study. **(A)** Pan genomic analysis of 13 COLR-KP isolates. **(B)** Phylogenetic analysis of 13 COLR-KP genomes using their core proteins. Gene matrix showed genes present (blue) or absent (blank) in the *K. pneumoniae* genomes.

Sun, J., Zhang, H., Liu, Y. H., and Feng, Y. (2018). Towards Understanding MCR-Like Colistin Resistance. *Trends Microbiol.* 26 (9), 794–808. doi: 10.1016/j.tim.2018.02.006

Wang, C., Feng, Y., Liu, L., Wei, L., Kang, M., and Zong, Z. (2020). Identification of Novel Mobile Colistin Resistance Gene Mcr-10. *Emerg. Microbes Infect.* 9 (1), 508–516. doi: 10.1080/22221751.2020.1732231

Wang, Q., Sun, J., Ding, Y., Li, X. P., Liu, Y. H., and Feng, Y. (2017). Genomic Insights Into mcr-1-Positive Plasmids Carried by Colistin-Resistant Escherichia Coli Isolates From Inpatients. *Antimicrob. Agents Chemother.* 61 (7), e00361-17. doi: 10.1128/AAC.00361-17

Wang, X., Wang, Y., Zhou, Y., Li, J., Yin, W., Wang, S., et al (2018). Emergence of a Novel Mobile Colistin Resistance Gene, mcr-8, in NDM-Producing Klebsiella Pneumoniae. *Emerg. Microbes Infect.* 7 (1), 122. doi: 10.1038/s41426-018-0124-z

Wang, Y., Zhang, R., Li, J., Wu, Z., Yin, W., Schwarz, S., et al (2017). Comprehensive Resistome Analysis Reveals the Prevalence of NDM and MCR-1 in Chinese Poultry Production. *Nat. Microbiol.* 2, 16260. doi: 10.1038/nmicrobiol.2016.260

Wick, R. R., Heinz, E., Holt, K. E., and Wyres, K. L. (2018). Kaptive Web: User-Friendly Capsule and Lipopolysaccharide Serotype Prediction for Klebsiella Genomes. *J. Clin. Microbiol.* 56 (6), e00197-18. doi: 10.1128/JCM.00197-18

Wyres, K. L., and Holt, K. E. (2018). Klebsiella Pneumoniae as a Key Trafficker of Drug Resistance Genes From Environmental to Clinically Important Bacteria. *Curr. Opin. Microbiol.* 45, 131–139. doi: 10.1016/j.mib.2018.04.004

Xiang, R., Ye, X., Tuo, H., Zhang, X., Zhang, A., Lei, C., et al (2018). Co-Occurrence of mcr-3 and blaNDM-5 Genes in Multidrug-Resistant Klebsiella Pneumoniae ST709 From a Commercial Chicken Farm in China. *Int. J. Antimicrob. Agents* 52 (4), 519–520. doi: 10.1016/j.ijantimicag.2018.07.007

Yang, Y. Q., Li, Y. X., Lei, C. W., Zhang, A. Y., and Wang, H. N. (2018). Novel Plasmid-Mediated Colistin Resistance Gene mcr-7.1 in Klebsiella Pneumoniae. *J. Antimicrob. Chemother.* 73 (7), 1791–1795. doi: 10.1093/jac/dky111

Zankari, E., Hasman, H., Cosentino, S., Vestergaard, M., Rasmussen, S., Lund, O., et al (2012). Identification of Acquired Antimicrobial Resistance Genes. *J. Antimicrob. Chemother.* 67 (11), 2640–2644. doi: 10.1093/jac/dks261

Zhang, R., Chan, E. W., Zhou, H., and Chen, S. (2017). Prevalence and Genetic Characteristics of Carbapenem-Resistant Enterobacteriaceae Strains in China. *Lancet Infect. Dis.* 17 (3), 256–257. doi: 10.1016/S1473-3099(17)30072-5

Zong, Z., Wu, A., and Hu, B. (2020). Infection Control in the Era of Antimicrobial Resistance in China: Progress, Challenges, and Opportunities. *Clin. Infect. Dis.* 71 (Supplement_4), S372–S378. doi: 10.1093/cid/ciaa1514

Zurfluh, K., Klumpp, J., Nuesch-Inderbinen, M., and Stephan, R. (2016). Full-Length Nucleotide Sequences of mcr-1-Harboring Plasmids Isolated From Extended-Spectrum-Beta-Lactamase-Producing Escherichia Coli Isolates of Different Origins. *Antimicrob. Agents Chemother.* 60 (9), 5589–5591. doi: 10.1128/AAC.00935-16

Conflict of Interest: The authors declare that the research was conducted in the absence of any commercial or financial relationships that could be construed as a potential conflict of interest.

The reviewer QL declared a past co-authorship with several of the authors, LZ and YZ, to the handling editor.

Publisher's Note: All claims expressed in this article are solely those of the authors and do not necessarily represent those of their affiliated organizations, or those of the publisher, the editors and the reviewers. Any product that may be evaluated in this article, or claim that may be made by its manufacturer, is not guaranteed or endorsed by the publisher.

frontiers in Medicine

REVIEW
published: 16 February 2022
doi: 10.3389/fmed.2022.654395

Human Genetic Host Factors and Its Role in the Pathogenesis of Chikungunya Virus Infection

Juan C. Rueda[1,2], *Mauricio Arcos-Burgos*[3], *Ana M. Santos*[2], *Daniel Martin-Arsanios*[2], *Catalina Villota-Erazo*[2,4], *Viviana Reyes*[2,4], *Santiago Bernal-Macías*[2,4], *Ingris Peláez-Ballestas*[5], *Mario H. Cardiel*[6] *and John Londono*[2,4]*

[1] Faculty of Medicine and Engineering, Universidad de La Sabana, Chía, Colombia, [2] Grupo de Espondiloartropatías, Rheumatology Department, Universidad de La Sabana, Chía, Colombia, [3] Grupo de Investigación en Psiquiatría (GIPSI), Departamento de Psiquiatría, Faculty of Medicine, Instituto de Investigaciones Médicas, Universidad de Antioquia, Medellín, Colombia, [4] Rheumatology Department, Hospital Militar Central, Bogotá, Colombia, [5] Rheumatology Unit, Hospital General de México "Doctor Eduardo Liceaga", Mexico City, Mexico, [6] Centro de Investigación Clínica de Morelia, Morelia, SC, Mexico

OPEN ACCESS

Edited by:
Xiaoxiao Wang, Zhejiang Center for Disease Control and Prevention (Zhejiang CDC), China

Reviewed by:
Mark T. Heise, University of North Carolina at Chapel Hill, United States
Pritom Chowdhury, Tea Research Association, India

***Correspondence:**
John Londono
john.londono@unisabana.edu.co

Specialty section:
This article was submitted to Infectious Diseases - Surveillance, Prevention and Treatment, a section of the journal Frontiers in Medicine

Received: *16 January 2021*
Accepted: *25 January 2022*
Published: *16 February 2022*

Citation:
Rueda JC, Arcos-Burgos M, Santos AM, Martin-Arsanios D, Villota-Erazo C, Reyes V, Bernal-Macías S, Peláez-Ballestas I, Cardiel MH and Londono J (2022) Human Genetic Host Factors and Its Role in the Pathogenesis of Chikungunya Virus Infection. Front. Med. 9:654395. doi: 10.3389/fmed.2022.654395

Chikungunya virus (CHIKV) is an alphavirus from the *Togaviridae* family that causes acute arthropathy in humans. It is an arthropod-borne virus transmitted initially by the *Aedes (Ae) aegypti* and after 2006's epidemic in La Reunion by *Ae albopictus* due to an adaptive mutation of alanine for valine in the position 226 of the E1 glycoprotein genome (A226V). The first isolated cases of CHIKV were reported in Tanzania, however since its arrival to the Western Hemisphere in 2013, the infection became a pandemic. After a mosquito bite from an infected viremic patient the virus replicates eliciting viremia, fever, rash, myalgia, arthralgia, and arthritis. After the acute phase, CHIKV infection can progress to a chronic stage where rheumatic symptoms can last for several months to years. Although there is a great number of studies on the pathogenesis of CHIKV infection not only in humans but also in animal models, there still gaps in the proper understanding of the disease. To this date, it is unknown why a percentage of patients do not develop clinical symptoms despite having been exposed to the virus and developing an adaptive immune response. Also, controversy stills exist on the pathogenesis of chronic joint symptoms. It is known that host immune response to an infectious disease is reflected on patient's symptoms. At the same time, it is now well-established that host genetic variation is an important component of the varied onset, severity, and outcome of infectious disease. It is essential to understand the interaction between the aetiological agent and the host to know the chronic sequelae of the disease. The present review summarizes the current findings on human host genetics and its relationship with immune response in CHIKV infection.

Keywords: chikungunya, genetic, host, pathogenesis, arbovirus

INTRODUCTION

Chikungunya virus (CHIKV) is an alphavirus from the *Togaviridae* family, and a member of the Semliki Forest virus antigenic complex, that together with other alphaviruses (O'nyong-nyong, Mayaro, and Ross River) causes acute arthropathy in humans (1–3). The virion has an icosahedral capsid, enclosed by a lipid envelope with a single-stranded, positive sense, RNA genome of

∼12 kilobases in length, which is arranged in two open reading frames (ORF) with a junction region in between (4, 5). The 5' ORF contains code for four non-structural proteins (nsP1-4), whereas the 3' encodes the capsid protein (C), two surface envelope glycoproteins (E1 and E2), and two small peptides designated E3 and 6k (6, 7).

A mosquito bite from an infected viremic patient is where the transmission initially starts (8). The virus replicates for a few days, before being transmitted to another person (9). Upon mosquito bite, the virus due to cellular tropism, infects fibroblasts in the dermis and macrophages, following an incubation period of 3–7 days, from where it is disseminated through lymphatics and bloodstream to joint capsule, muscle, epithelial, and endothelial cells (8). The virus replicates eliciting viremia, fever, rash, myalgia, arthralgia and arthritis (10). At this point the acute phase is established, lasting for ∼2 weeks, and characterized by the appearance of immunoglobulin type M (IgM) which usually persist up to 3 months, however long-term follow up studies have demonstrated its presence after 10 months post infection in 17 to 76% of the patients and even up to 12 months (11–13). The production of immunoglobulin type G (IgG) starts usually 7–10 days post-onset of symptoms, which will provide antiviral immunity for years (5, 8, 10, 14). After the acute phase, CHIKV infection can progress to a chronic stage where rheumatic symptoms can last for several months to years (10).

CHIKV is an arthropod-borne virus transmitted initially by the *Aedes (Ae) aegypti* and after 2006's epidemic in La Reunion by *Ae albopictus* due to an adaptive mutation of alanine for valine in the position 226 of the E1 glycoprotein genome (A226V) (5, 15). It is believed that the infection started in a sylvatic or enzootic cycle where the virus was maintained through arboreal vectors (*Ae africanus*, and *Ae furcifer*) using non-human primates (vervet monkeys) as hosts, and later spilled over to humans living nearby forested regions (16). From here on, transmission from human to human via *Ae aegypti* or *albopictus* is amplified in urban settings and spread by air travel establishing an epidemic cycle (16).

The first isolated cases of CHIKV were reported in July 1952 along the coastal plateaus of Mawia, Makonde and Rondo, what is known today as Tanzania (17). The people of this region named the disease chikungunya, which translates to "the one that bends up the joints" (18). Phylogenetic studies indicated that CHIKV originated in Africa over 500 years ago and determined that a common lineage diverged into two branches termed West African (WA) and East/Central/South African (ECSA) (1, 2, 19, 20). While the ECSA lineage spread outside Africa causing multiple urban epidemics in Asia almost 150 years ago, WA lineage maintained local outbreaks in Africa through enzootic transmission (8, 20). It was in Asia were the ECSA lineage kept circulating and evolving into a separate genotype called Asian lineage (20). In the earlies 2000, the ECSA lineage reached Kenya and from there expanded to islands in the Indian Ocean, India, and Southeast Asia creating an unprecedented epidemic and again evolving into a new lineage with the aforementioned A226V mutation (Indian Ocean Lineage or IOL) (15, 21–23). This allowed the virus to use *Ae albopictus* as a new vector which has a higher altitude tolerance and therefore increasing the disease's reach to more temperate regions like southern France and northern Italy (24–27). During the last decade CHIKV continued to cause epidemics in the Pacific Islands, Indian subcontinent, Oceania and Southeast Asia (28–30). Finally, in 2013 the CHIKV Asian lineage arrived to the Western Hemisphere with the first autochthonous cases reported in the Island of Saint Martin (31). From there, the virus rapidly spread throughout the Caribbean, Central and South America, affecting 42 countries by 2015 (32). The virus kept circulating mainly in Asia and the Americas with outbreaks being continuously reported. In Brazil for example, 712.990 cases were accumulated over a period of 4 years since 2015 (33). In the years 2016, 2017 and 2019, a maximum number of laboratory confirmed cases were reported in India (34). Also, the first large epidemic in Pakistan was reported in December of 2016 with 1018 cases reported from multiple regions of Karachi (35). Up to September 2021, according to the European Center for Disease Prevention and Control, in 2021 133.928 cases have been reported (36). Of those, 106.768 from the Americas and the Caribbean (97% from Brazil), 27.056 from Asia (93% from India) and 104 from Africa (all from the Democratic Republic of Congo) (36).

Multiple studies have discovered genetic variants in the immune response to specific pathogens, providing important insights into the genetic control of immune signaling in humans (37). Increasing evidence support the fact that host genetics drives phenotypes of infectious diseases, however a gap still exists in CHIKV infection. A characteristic feature of many human infections is that only a proportion of exposed individuals develop clinical disease (37). Mouse studies have illustrated the potential importance of host genetic effects, by showing differences between different inbred strains in bacterial loads, cytokine responses and outcomes following bacterial and mycobacterial infection (38).

In humans, genetic studies, mainly using genome-wide association studies (GWAS), have discovered genetic variants in the immune response to specific pathogens, highlighting the role of shared host signaling pathways in the pathogenesis of diverse infectious diseases and providing important insights into the genetic control of immune signaling in humans (37). These studies have found correlations between gene polymorphisms with specific phenotypes in infectious diseases. For example, in HIV and AIDS, single nucleotide polymorphisms (SNP) in HLA-C, HLA-B and HCP5 genes were associated with high viral load at set point (39, 40). Also, dengue shock syndrome was associated in Vietnamese patients with SNPs in MICB and PLCE1 genes (41). Regarding CHIKV, few studies have been conducted to elucidate host genetics and specific phenotypes of the disease. The study of the genetic effects of CHIKV infected patients will increase our knowledge and understanding of the pathogenesis of the disease as well as the bases for potential treatment targets. The present review summarizes the current findings on human host genetics and its relationship with immune response in CHIKV infection.

PATHOGENESIS

Innate Immunity

Acute CHIKV infection elicits robust innate immune responses, leading to elevation of type I IFNs and numerous

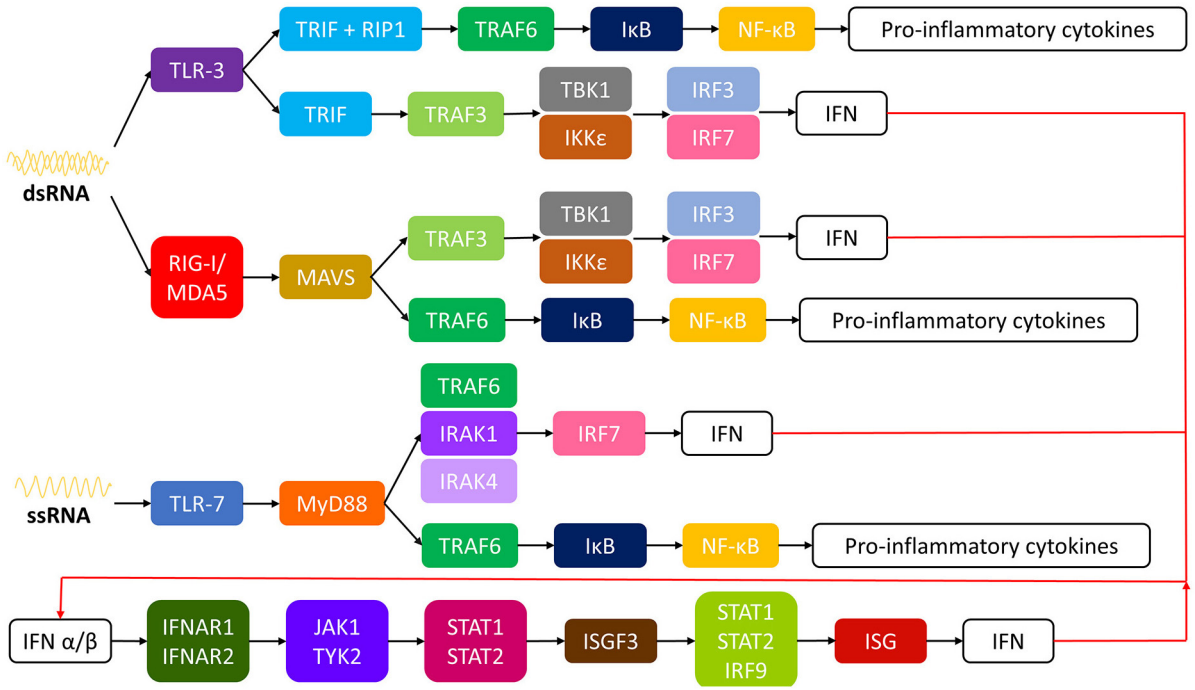

FIGURE 1 | Intracellular pathways of innate immune response to CHIKV. CHIKV, chikungunya virus; ssRNA, single-stranded RNA; dsRNA, double-stranded RNA; TLR, toll like receptor; TRIF, TIR-domain containing adapter-inducing interferon-β; RIP-1, receptor interacting protein 1; TRAF, TNF receptor associated factor; IκB, inhibitor of κB; NF-κB, nuclear factor kappa-light-chain-enhancer of activated B cells; TBK1, tank binding kinase; IRF, interferon regulator factor; IFN, interferon; IKKε, inducible IκB kinase; RIG-I, retinoic acid-inducible gene I; MDAS, melanoma differentiation-associated protein 5; MAVS, mitochondrial antivirial signaling; MyD88, myeloid differentiation primary response gene 88; IRAK, interleukin-1 receptor-associated kinase; IFNAR, interferon α/β receptor; JAK1, Janus kinase 1; TYR2, tyrosine kinase 2; STAT, signal transducer and activator of transcription; ISGF3, ISG factor 3; ISG, interferon stimulated gene.

proinflammatory chemokines, cytokines, and growth factors (42–44). Type I IFN signaling controls viral replication and pathogenesis during acute infection (45, 46). In humans, IFN-α appears early in infection and correlates with viral load (42, 47). Coincident with rising viral loads and IFN-α responses, the vast majority of infected patients experience sudden onset of clinical illness, with a small proportion of infected individuals (5–28%) remaining asymptomatic (48).

The mechanism which such immune response is initiated by CHIKV is like other emerging RNA virus infections. In a nutshell, innate immune response starts with recognition of viral RNA by pattern recognition receptors (PRRs). In the case of CHIKV, double stranded RNA (dsRNA) induce toll like receptor (TLR) 3, retinoic acid-inducible gene I (RIG-I) and melanoma differentiation-associated protein 5 (MDA5), while single-stranded RNA (ssRNA) induce TLR-7 (49–52). A signaling cascade is initiated which results in activation of nuclear factor kappa-light-chain-enhancer of activated B cells (NF-κB) and interferon regulator factors (IRFs) inducing the transcription of interferons and pro-inflammatory cytokines (49, 52–54). See **Figure 1** for more detail. The produced type I interferons (IFN α/β) bind to receptors IFNAR1 and 2 (interferon receptor α/β) inducing phosphorylation of Janus kinase 1 (JAK1) and tyrosine kinase 2 (TYK2) which leads to assembly of interferon stimulated gene factor 3 (ISGF3) complex. ISGF3 binds to interferon stimulated genes (ISGs) resulting in gene expression of IFNs (52, 53, 55, 56). As expected, CHIKV developed mechanisms to counteract the host immune response. CHIKV inhibits IFN signaling with its own nsP2 by blocking the JAK/STAT (signal transducer and activator of transcription) signaling pathway (53, 57). Also, CHIKV nsP2 inhibits RNA polymerase II by inducing the degradation of its catalytic subunit RpB1, blocking the expression of cellular genes (53, 58, 59).

Adaptive Immunity

Symptoms of acute CHIKV disease are caused by direct cellular damage and local inflammation, but the specific contributions of viral replication and the host immune response to CHIKV infection are yet to be completely unraveled (60). CHIKV infection is cytopathic and induces apoptosis, resulting in direct tissue injury. Numerous cell types, many of which are located at sites of disease, are susceptible to CHIKV, including chondrocytes, endothelial cells, fibroblasts, hepatocytes, macrophages, monocytes, muscle satellite cells, myocytes, and osteoblasts (61–64).

Monocytes and macrophages are targeted by CHIKV and contribute to virus-induced pathogenesis. Activated macrophages are the primary infiltrating cell in infected tissues (65, 66), and elevated levels of MCP-1, the major chemoattractant for monocytes and macrophages, correlate with high viral loads

in persons with acute CHIKV infection (42–44, 47, 66, 67). A meta-analysis of immune mediators from geographically distinct cohorts revealed an immune mediator signature dominated by proinflammatory cytokines, which include INF-α, INF-γ and Il-2, 2R, 6, 7, 12, 15, 17 and 18 (42).

Acute infection in humans leads to activation and proliferation of CD8+ T cells, while a CD4+T cell response is dominant during the chronic phase of CHIKV disease (68). Although activated, CD8+ T cells do not appear to mediate CHIKV clearance or disease in animals (69). In contrast, studies using mice deficient in various types of lymphocytes implicate CD4+ T cells as inflammatory mediators in infected tissues (70). However, these cells also may contribute to viral clearance (70). Tregs are involved in CHIKV pathology, as expansion of Tregs reduces CHIKV disease by selectively inhibiting CHIKV-specific CD4+ effector T cells (71). In addition, γδ T cells, which are abundant in skin, protect against CHIKV disease, as γδ T cell–deficient mice display exacerbated CHIKV infection (72). Development of CHIKV neutralizing antibodies is essential to control CHIKV viremia (69, 70). In humans, IgM levels are detected within 5–7 days after the onset of symptoms, peak several weeks after infection, and begin to wane over the next several months (14). An IgG response can be detected approximately 7–10 days after onset of illness, often after viremia has been cleared (14).

Studies of CHIKV-infected humans and animals have defined symptoms and immune responses of acute CHIVK disease, but much of the molecular interplay between virus and host remains to be established. To this date, it is unknown why a percentage of patients do not develop clinical symptoms despite having been exposed to the virus and developing an adaptive immune response (presence of positive CHIKV IgM or IgG).

HOST GENETICS AND CHIKUNGUNYA

Human Leukocyte Antigen

Virulence factors specific to the infective agent as well as host factors like innate and adaptive immune response play an important part in disease susceptibility (73–75). Regarding host factors, the HLA plays a major role in initiating immune responses; the HLA type I molecules present pathogen peptides to CD8+ lymphocyte cells, while HLA type II molecules present pathogen peptides to CD4+ lymphocyte cells (76).

HLA molecules are coded on the short arm of chromosome 6, occupying a large portion of the DNA (∼3,500 kilobases) (77). To date, HLA molecules are the most polymorphic genes in the human genome (77). These polymorphisms allow the immune system to increase the repertoire of peptides presented by HLA molecules, which in turn will affect the susceptibility to infectious diseases.

Many chronic diseases and their host's interaction with the disease have been studied to understand their immunogenetics. HLA-DR3 (HLA- DRB1*0301, DQB1*0201) and DR4 (HLA-DRB1*04, DQB1*0302) are markers for type 1 diabetes in Caucasian populations, but not among Japanese patients (78). The DRB1*07 allele is associated with protection against Dengue virus infection in the Cuban population, but not in the Sri Lankan population (79, 80). Studies have demonstrated HLA class II alleles association to susceptibility or resistance to CHIKV (**Table 1**, **Figure 2**), however none have reported associations with clinical symptoms of CHIKV infection (78, 81, 82).

A study in 73 Gabonese patients with CHIKV infection, Petitdemange et al. studied the association between killer cell immunoglobulin like receptors (KIR), their HLA-class I genotype and susceptibility to CHIKV (83). KIR receptors on the surface of natural killer (NK) cells bind to HLA-class I molecules on target cells. The KIR-HLA interaction has a functional significance in response to infectious diseases activating or inhibiting NK cells. The authors found that KIR2DL1 and its interaction with HLA-C2 (KIR2DL1-C2) granted susceptibility to CHIKV infection, while KIR2DS5 conferred protection (83). The authors believe that the expansion of highly functional NK cells and the development of a strong adaptive memory response are associated with the interplay between KIR2DL1 and HLA-C2 in CHIKV infected patients.

In a study of 21 patients from Reunion Island with chronic chikungunya, HLA-DRB1*01 and DRB1*04 alleles were frequently found among the patients who developed rheumatoid arthritis after the infection, indicating the probable involvement of HLA class II gene in chikungunya infection (87). However, details regarding the relevance of these alleles with chikungunya virus associated clinical presentations were not indicated in the study.

In India, two studies have reported the association of HLA alleles with CHIKV infection (78, 81). One study demonstrated the presence of HLA-DRB1*04-HLA-DQB1*03 haplotype with susceptibility to CHIKV infection, and the presence of HLA-DRB1*11 and HLA-DRB1*11-HLA-DQB1*03 haplotype with resistance to the infection (81). According to the authors, one explanation could be that the epitopes presented by HLA-DRB*11 modulates toward a more robust immune response to CHIKV by means of CD4 T cells.

The other study reported a lower frequency of HLA-DQB1*03:03 allele in CHIKV infected patients with statistical significance when compared to normal subjects (78). The authors suggest that the DQ*03:03 allele may stimulate diverse antiviral CD4 T-cell responses and therefore its association with protection against CHIKV. In this study, although HLA-DRB1*01 and HLA-DRB1*04 were more frequent in CHIKV infected patients, the difference was not statistically significant. In the same study, the presence of non-glutamic acid at position 86 of the peptide biding groove of DQB1genotypes was associated with infection while lower frequencies of glutamic acid at the same position was protective against CHIKV infection when compared with healthy controls. This can be explained by the fact that the presence of glutamate at the β86th position allows for accommodation of peptides with large hydrophobic amino acids, which in turn enhance the ability to bind a large number of amino acids conferring a selective advantage against CHIKV (78, 88). Taking this into account, special interest should be given to research of HLA-DRB1 alleles in CHIKV infected patients and its role in the pathophysiology of the disease.

A study on 65 patients with confirmed CHIKV infection from Colombia demonstrated the presence of five HLA class I and II

TABLE 1 | Genetic studies on host and CHIKV infection.

Country	Sample	Gene	Allele/polymorphism	Findings			Type of association	Year	Reference
				OR	CI	*p*			
India	- 101 CHIKV	HLA class II	- DQB1*03:03	0.13	0.04-0.40	0.024	Protection against CHIKV	2013	(78)
	- 104 controls	- DQB1	- Peptide binding groove DQ						
		- DRB1	*β86 non GLU	1.79	1.16-2.74	0.008	Susceptibility to CHIKV		
			*β86 GLU/GLU	0.30	0.12-0.70	0.004	Protection against CHIKV		
India	- 100 CHIKV	HLA class II	- DRB1*11	0.21	0.07-0.61	0.002	Protection against CHIKV	2014	(81)
	- 250 controls	- DQB1	- DRB1*11/DQB1*03	0.15	0.03-0.66	0.007	Protection against CHIKV		
		- DRB1	- DRB1*04/DQB1*03	1.94	1.06-3.55	0.042	Susceptibility to CHIKV		
Gabon	- 73 CHIKV	KIR	- 2DL1	NP	NP NP NP NP	0.033	Susceptibility to CHIKV	2014	(83)
	- 54 controls	HLA class I	- 2DS5	NP		0.050	Protection against CHIKV		
		- C	- C2	NP		0.023	Susceptibility to CHIKV		
		- Bw4	- 2DL1	NP		0.001	Protection against CHIKV		
			- Bw4						
			- 80Trn-3DL1						
Singapore	- 94 CHIKV	TLR-3	- RS3775292	2.16	1.31-3.42	0.002	Susceptibility to CHIKV	2015	(84)
	- 179 controls		- RS6552950	1.54	1.03-2.29	0.03	Susceptibility to CHIKV		
			- RS6552950	2.31	1.16-4.57	0.02	Susceptibility to severe disease		
India	- 101 CHIKV	CD209	- CD209 *RS4804803						(85)
	- 101 controls	OAS1	- A-G	0.16	0.03-0.97	0.037	Protection to fever	2016	
		OAS2	- OAS1 *RS1131454						
		OAS3	- G-G	0.32	0.11-0.96	0.036	Protection to oedema		
			- OAS2 *RS1732778						
			- A-A *RS15895	0.16	0.05-0.57	0.002	Protection to nausea		
			- G-A *RS15895	0.34	0.13-0.88	0.024	Protection to chills		
			- G-A	0.39					
			- OAS3 *RS2285932		0.15-0.99	0.036	Protection to red eye		
			- C-T *RS2285832	0.39	0.16-0.92	0.031	Protection to chills		
			- T	0.40	0.17-0.91	0.028	Protection to oedema		
India	- 173 CHIKV	TLR-3	- TLR-3 *RS3775290						(86)
	- 157 controls	TLR-7	- T-T	2.10	1.03-4.30	0.039	Susceptibility to CHIKV†	2017	
		TLR-8	- T-T	0.30	0.14-0.76	0.002	Protection to fever		
			- C	0.53	0.34-0.84	0.007	Protection against CHIKV†		
			- C-T	5.05	1.55-11.1	0.003	Susceptibility to joint pain		
			- TLR-7 *RS179008						
			- C-C	2.03	1.12-3.66	0.017	Susceptibility to CHIKV		
			- T-C *RS5741880	0.43	0.25-0.74	0.002	Protection against CHIKV		
			- G-T	0.43	0.23-0.76	0.030	Protection against CHIKV		
			- G-T	0.33	0.13-0.86	0.019	Protection against CHIKV†		
			- G-G *RS3853839	6.84	0.90-51.4	0.032	Susceptibility to joint pain		
			- G-C	4.33	2.23-8.53	0.000	Susceptibility to CHIKV†		
			- G-C	3.44	2.12-5.57	0.006	Susceptibility to CHIKV		
			- G-C	2.50	1.23-5.07	0.009	Susceptibility to CHIKV‡		
			- G-C	0.42	0.22-0.78	0.050	Protection to rash		
			- C-C	10.0	0.51-196	0.039	Susceptibility to CHIKV		
			- C	2.82	1.84-4.32	0.000	Susceptibility to CHIKV		
			- C *RS179010	2.28	1.19-4.35	0.010	Susceptibility to CHIKV‡		
			- C-C	2.03	1.12-.3.66	0.010	Susceptibility to CHIKV		
			- C-C	2.42	1.08-5.41	0.028	Susceptibility to CHIKV‡		
			- C-C	3.77	1.39-10.1	0.003	Susceptibility to high INFα		
			- T-C	0.43	0.25-0.74	0.002	Protection against CHIKV		
			- T-C	0.33	0.15-0.76	0.002	Protection against CHIKV‡		
			- T-T	0.36	0.17-0.76	0.002	Protection against fever		
			- TLR-8 *RS53764879						
			- G-C	3.04	1.83-5.05	0.000	Susceptibility to CHIKV		
			- G-C	2.63	1.31-5.29	0.005	Susceptibility to CHIKV‡		
			- G-C	3.31	1.60-6.84	0.000	Susceptibility to CHIKV†		
			- G	0.68	0.47-0.97	0.034	Protection against CHIKV		
			- C-C *RS3764880	0.19	0.04-0.91	0.020	Protection against CHIKV†		
			- G-G	2.04	1.06-3.90	0.031	Susceptibility to fever		

(Continued)

TABLE 1 | Continued

Country	Sample	Gene	Allele/polymorphism	Findings			Type of association	Year	Reference
				OR	CI	*p*			
Colombia	- 65 CHIKV - 100 controls	HLA-class I - A - B HLA-class II - DRB1	- A*29 - A*68 - B*35 - B*46 - DRB1*01 - DRB1*04 - DRB1*13	0.10 8.90 2.02 0.26 5.70 7.37 3.75	0.02-0.44 1.8-42.1 1.06-3.86 0.10-0.67 1.9-16.5 3.3-16.3 1.50-9.39	0.002 0.005 0.030 0.005 0.001 0.000 0.004	Protection against CHIKV Susceptibility to CHIKV Susceptibility to CHIKV Protection against CHIKV Susceptibility to CHIKV Susceptibility to CHIKV Susceptibility to CHIKV	2021	Accepted

OR, odds ratio; CI, 95% confidence interval; CHIKV, chikungunya virus infection; HLA, human leukocyte antigen; KIR, killer cell immunoglobulin like receptor; TLR, toll like receptor; OAS, 2'-5'oligoadenylate synthase; †: in females; ‡: in males.

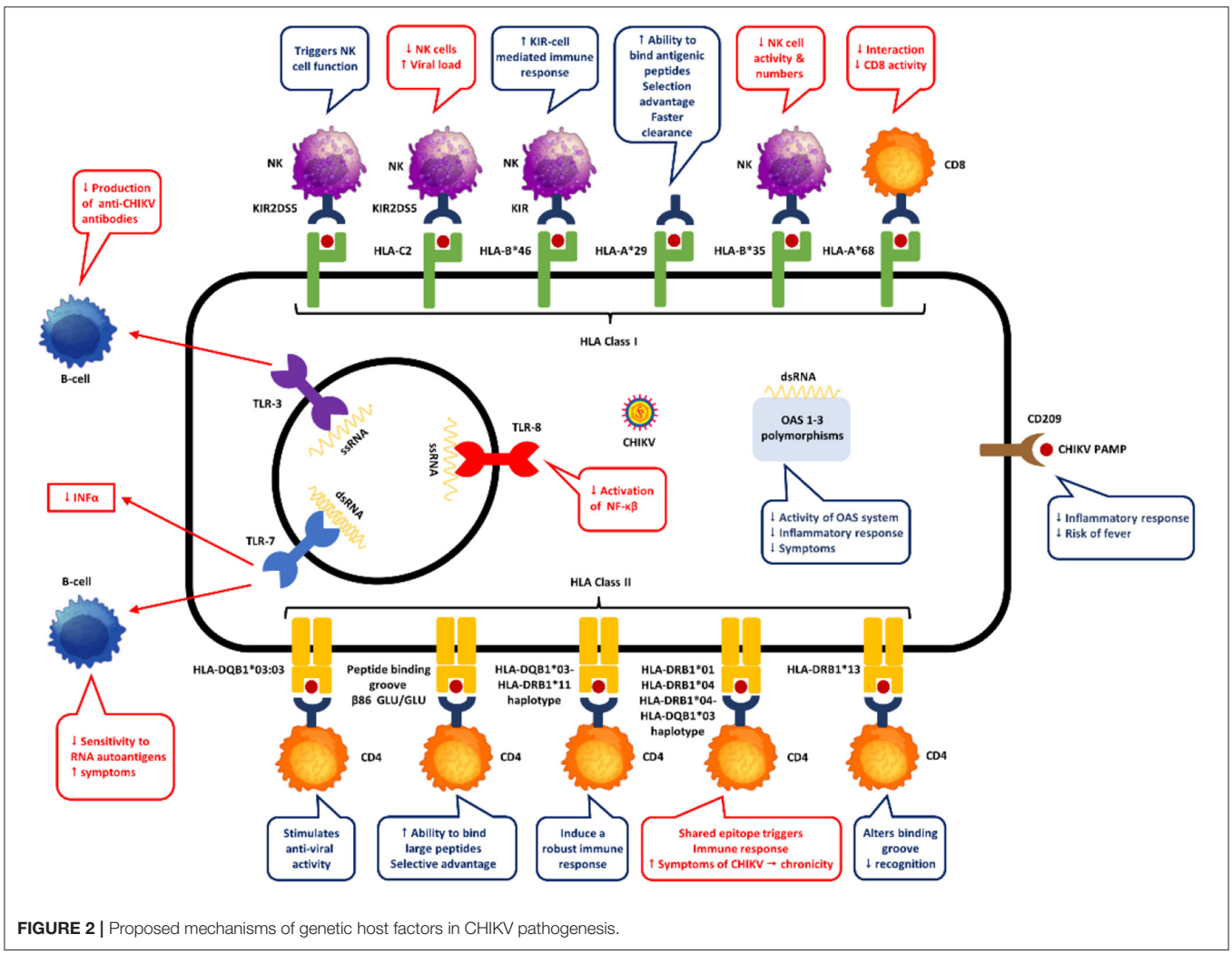

FIGURE 2 | Proposed mechanisms of genetic host factors in CHIKV pathogenesis.

alleles in CHIKV infected patients when compared to healthy subjects (accepted). Specifically, HLA-A*68, HLA-B*35, HLA-DRB1*01, HLA-DRB1*04 and HLA-DRB1*13. Of interest, HLA-A*68 and HLA-DRB1*04 had the strongest association with CHIKV infection. In fact, HLA-DRB1*04 was the only allele associated with the presence of rash in the abdomen and the face. No other alleles were statistically associated with other clinical symptoms or disability scores. Only class I alleles (HLA-A*29 and HLA-B*46) were associated with reduced risk of CHIKV infection as well as rash in the abdomen and the face (HLA-B*35). None of the HLA-DRB1 alleles showed protection for CHIKV infection. Studies have found that in HLA-A*68 a valine residue at position 245 replace the alanine present in other HLA molecules (89, 90). This distorts the α3 loop, resulting

in a less energetically favorable interaction with CD8-T cells, which could explain the susceptibility to infection in CHIKV patients. On the other hand, HLA-A*29 distinguishes from other HLA-A alleles by the presence of leucine at position 62 and glutamine at position 63 (91). This change in position 63 has the largest effect on the ability to bind antigenic peptides in the peptide binding groove of HLA-A (91). In fact, the 62–63 motif may influence the flexibility to accommodate antigenic peptides, which can confer selective advantage against CHIKV (91). In another study in human immunodeficiency virus (HIV) infected patients, the progression to AIDS was associated with the presence of HLA-B*35-HLA-Cw4 haplotype due to reduction of natural killer cell number and activity (92). A finding that could explain the susceptibility to CHIKV infection in our population. In our population, HLA-B*46 was associated with protection against CHIKV infection. HLA-B*46 is an unusual allele formed by the recombination between HLA-B*15 and HLA-C*01, which allows it to interact with KIR ligand (93). Its distinctive peptide-binding site derived from its recombination and ability to react with KIR ligands helps create a strong KIR cell mediated immune response, which in turn could explain its protection against CHIKV infection. Regarding HLA class II alleles, HLA-DRB1*01 and *04, which were associated with susceptibility to CHIKV in our population, were also found in parvovirus B19 infection by Kerr et al. (94). It is known that both DRB1*01 and *04 code for the shared epitope in residues 70 to 74 in the HLA-DRB chain (95). We hypothesize that CHIKV antigens could bind the shared epitope triggering innate immune signaling as well as production of pro-inflammatory cytokines like IL-6, TNF-α and IL-23 by dendritic cells, conferring symptomatic susceptibility to CHIKV infection. Finally, HLA-DRB1*13 has been associated with carrying an asparagine in position 37 of P9 peptide binding pocket granting electropositibity (96). This restricts the range of peptides that can be presented which is sufficient to alter recognition by the T-cell receptor, and therefore increase susceptibility to CHIKV infection.

The relationship between host genetics and disease can be variable. The presence of an allele like HLA-DRB1*13 is associated with CHIKV infection (susceptibility), on the other hand, the same allele confers protection for AIH. On the contrary, while HLA-A*29 and B*46 protect against CHIKV infection, they are associated with birdshot retinochoroidopathy and severe sacroiliitis in psoriatic arthritis, respectively. To explain the relationships between HLA variants involved in both autoimmune and infectious diseases, two hypotheses have been proposed (97). The first hypothesis states that pressure on the human genome by pathogens has led to selection of host defense genes that protects against infections. However, this advantageous selection may also increase the risk of developing autoimmune diseases. The second hypothesis suggests that pathogens can trigger autoimmunity by molecular mimicry, epitope spreading bystander activation or cryptic antigens (98).

Candidate Genes

Genes outside the HLA complex have been studied in CHIKV infection (**Table 1**, **Figure 2**). Specifically, polymorphisms of TLR genes as well the 2'-5'-oligoadenylate synthetase (OAS) gene cluster and CD209. As mentioned before, tt is well-established that the innate immune response starts with recognition of viral RNA genome by PRRs. In the case of CHIKV infection, its RNA is recognized by TLRs (3, 7 and 8), retinoic acid-inducible gene I (RIG -I) like receptors (RLRs) and melanoma differentiation-associated protein 5 (MDA5) (99). The PRRs stimulates the production of pro-inflammatory cytokines through myeloid differentiation factor 88 (MyD88) and TRAF, which in turn activates OAS genes increasing viral degradation (62). TLR-3 polymorphisms can change the ecto-domain of the receptor altering the ligand-receptor interaction, while TLR-7 polymorphisms affects TLR-7 processing and receptor expression (100–102). Studies on TLR-8 polymorphisms have demonstrated variation in transcription of TLR-8 isoforms which affects NF-κB activation as well as diverse production of TNF-α and IL-1β (103, 104).

A study found the SNP rs6552950 in the TLR-3 gene to be associated with disease severity and CHIKV-specific neutralizing antibody response and the SNP rs3775292 to disease susceptibility (84). In this study the authors demonstrated that the polymorphisms in TLR-3 gene produced a loss in TLR-3 functionality which decreased the production of anti-E2EP3 IgG anti-bodies (CHIKV specific neutralizing antibodies), reducing CHIKV clearance and eliciting severe disease (defined by maximum temperature $>38.5^{\circ}C$, a maximum pulse rate >100 beats/min or a nadir platelet count $<100 \times 10^9$/l).

Similarly, another study found three polymorphisms of TLR-7 (rs179010, rs5741880, rs3853839) and one of TLR8 (rs3764879) to be significantly associated with CHIKV infection (86). In the same study, the SNP rs3775290 from the TLR-3 gene was associated with the presence of joint pain, the SNPs rs179010, rs5741880 and rs38533839 from the TLR-7 gene with fever, joint pain, and rash, respectively. Interestingly, the SNP in the TLR-7 gene associated with fever (rs179010) was also present in patients with CHIKV infection and increased levels of IFN-α. Finally, fever was also associated with a SNP (rs3764880) in the TLR-8 gene. Studies have found that polymorphisms in TLR-7 increases B-cell sensitivity to RNA-containing autoantigens in the development of systemic autoimmunity. Specifically, rs3853839 of TLR-7 in lupus patients was associated with skin involvement like malar rash and photosensitivity (105). Also, TLR-7 and−8 polymorphisms may impair the immune response to hepatitis C virus due to less INF-α (103). Other studies have demonstrated that TLR-8 polymorphisms could produce a truncated TLR-8 with a shorter signal peptide which result in a more rapid decay of TLR-8 or may affect the protein function impairing NF-κB activation *in-vitro* (106, 107).

The OAS gene cluster and CD209 (also known as DC-SIGN: dendritic cell-specific intercellular adhesion molecule-3-grabbing non-integrin) has also been studied in CHIKV infected patients. OAS activation by INFs degrades viral RNA decreasing viral replication, while the DC-SIGN, a type II transmembrane in macrophages and dendritic cells plays an important role in innate immunity activation through recognition of high-mannose type N-glycans pathogen associated molecular patterns (PAMPs) (108–111). A study in India found that the rs4804803 of the CD209 gene is associated with susceptibility to CHIKV

infection (85). The researchers also found that the same polymorphism (rs4804803) and others from de OAS gene cluster (OAS1 rs1131454, OAS2 rs1732778 and rs15895, and OAS3 rs2285932) influence the risk of developing clinical symptoms in CHIKV infected patients. The authors hypothesize that some OAS polymorphisms reduce the activity of the OAS system, decreasing inflammatory response which could protect against developing symptoms. On the other hand, other OAS polymorphisms increase antiviral activity, reducing viral replication and therefore protecting against developing symptoms. Also, the authors believe that CD209 polymorphisms affect binding of transcription factors and the presence of G-G polymorphism influence the expression of DC-SIGN, all of which at end affects the innate and adaptive immune response of dendritic cells increasing susceptibility to CHIKV infection. Conversely, G-A polymorphisms of CD209 decreases inflammatory response which could explain its association with protection against fever.

CONCLUSION

Increasing evidence support the fact that host genetics drives phenotypes of infectious diseases, however a gap still exists in CHIKV infection. So far it has been shown that the presence of certain alleles in certain populations as well as polymorphisms in certain genes change the presentation and course of the disease. However, some important questions remain unanswered. Why some patients develop symptoms, while others do not regardless of being infected? Why some patients develop chronic symptoms? Why the host immune system responds differently to the same infectious agent? Is there a genetic predisposition to host-agent interaction? Questions that can be applied not only to CHIKV but to other infectious diseases. The door remains open for research to provide a newer insight in the host dynamics and infectious diseases, especially, by conducting association studies between inflammatory markers, clinical manifestations, with long-term follow-up are necessary to understand the repercussions that host genetic factors have on the immune response and how this is reflected in the clinical picture of the infection both acutely and chronically. Additionally, the possibility of conducting genetic studies that include not only candidate genes and HLA alleles using genome wide analysis or exome wide analysis techniques in conjunction with proteomic techniques will allow us to find possible associations that at first glance were not on the radar of the pathogenesis of the disease. The study of the genetic effects of CHIKV infected patients will increase our knowledge and understanding of the pathogenesis of the disease as well as the bases for potential treatment targets.

AUTHOR CONTRIBUTIONS

JR, MA-B, AS, DM-A, CV-E, VR, SB-M, IP-B, MC, and JL: conceptualization, supervision, funding acquisition, methodology, data curation, writing-original draft preparation, and writing-review and editing. All authors contributed to the article and approved the submitted version.

FUNDING

The study was supported by the Colombian Rheumatology Association (ASOREUMA) under grant number Acta 169 10th July 2015; Universidad de La Sabana under grant number MED-197-2015; and COLCIENCIAS doctoral scholarship under grant number 757-2016.

REFERENCES

1. Powers AM, Brault AC, Tesh RB, Weaver SC. Re-emergence of chikungunya and o'nyong-nyong viruses: evidence for distinct geographical lineages and distant evolutionary relationships. *J Gen Virol.* (2000) 81:471–9. doi: 10.1099/0022-1317-81-2-471
2. Powers AM, Logue CH. Changing patterns of chikunya virus: re-emergence of a zoonotic arbovirus. *J Gen Virol.* (2007) 88:2363–77. doi: 10.1099/vir.0.82858-0
3. Enserink M. Infectious diseases. Massive outbreak draws fresh attention to little-known virus. *Science.* (2006) 311:1085. doi: 10.1126/science.311.5764.1085a
4. Khan AH, Morita K, Parquet MDC, Hasebe F, Mathenge EGM, Igarashi A. Complete nucleotide sequence of chikungunya virus and evidence for an internal polyadenylation site. *J Gen Virol.* (2002) 83:3075–84. doi: 10.1099/0022-1317-83-12-3075
5. Thiberville S-D, Moyen N, Dupuis-Maguiraga L, Nougairede A, Gould EA, Roques P, et al. Chikungunya fever: epidemiology, clinical syndrome, pathogenesis and therapy. *Antiviral Res.* (2013) 99:345–70. doi: 10.1016/j.antiviral.2013.06.009
6. Voss JE, Vaney MC, Duquerroy S, Vonrhein C, Girard-Blanc C, Crublet E, et al. Glycoprotein organization of chikungunya virus particles revealed by X-ray crystallography. *Nature.* (2010) 468:709–12. doi: 10.1038/nature09555
7. Simizu B, Yamamoto K, Hashimoto K, Ogata T. Structural proteins of chikungunya virus. *J Virol.* (1984) 51:254–8. doi: 10.1128/jvi.51.1.254-258.1984
8. Silva LA, Dermody TS. Chikungunya virus: epidemiology, replication, disease mechanisms, and prospective intervention strategies. *J Clin Invest.* (2017) 127:737–49. doi: 10.1172/JCI84417
9. Hua C, Combe B. Chikungunya virus-associated disease. *Curr Rheumatol Rep.* (2017) 19:69. doi: 10.1007/s11926-017-0694-0
10. Vu DM, Jungkind D, LaBeaud AD. Chikungunya virus. *Clin Lab Med.* (2017) 37:371–82. doi: 10.1016/j.cll.2017.01.008
11. Grivard P, Le Roux K, Laurent P, Fianu A, Perrau J, Gigan J, et al. Molecular and serological diagnosis of chikungunya virus infection. *Pathol Biol.* (2007) 55:490–4. doi: 10.1016/j.patbio.2007.07.002
12. Chelluboina S, Robin S, Aswathyraj S, Arunkumar G. Persistence of antibody response in chikungunya. *Virusdisease.* (2019) 30:469–73. doi: 10.1007/s13337-019-0 0534-5
13. Pierro A, Rossini G, Gaibani P, Finarelli AC, Moro ML, Landini MP, et al. Persistence of anti-chikungunya virus-specific antibodies in a cohort of patients followed from the acute phase of infection after the 2007 outbreak in Italy. *New Microbes New Infect.* (2015) 7:23–5. doi: 10.1016/j.nmni.2015. 04.002
14. Kam YW, Simarmata D, Chow A, Her Z, Teng TS, Ong EKS, et al. Early appearance of neutralizing immunoglobulin G3 antibodies is associated with chikungunya virus clearance and long-term clinical protection. *J Infect Dis.* (2012) 205:1147–54. doi: 10.1093/infdis/jis033
15. Tsetsarkin KA, Vanlandingham DL, McGee CE, Higgs S. A single mutation in chikungunya virus affects vector specificity and epidemic potential. *PLoS Pathog.* (2007) 3:1895–906. doi: 10.1371/journal.ppat.0030201

16. Weaver SC, Forrester NL. Chikungunya: evolutionary history and recent epidemic spread. *Antiviral Res.* (2015) 120:32–9. doi: 10.1016/j.antiviral.2015.04.016
17. Lumsden WH. An epidemic of virus disease in Southern Province, Tanganyika Territory, in 1952-53. II. General description and epidemiology. *Trans R Soc Trop Med Hyg.* (1955) 49:33–57. doi: 10.1016/0035-9203(55)90081-X
18. Ross RW. The newala epidemic. III. The virus: isolation, pathogenic properties and relationship to the epidemic. *J Hyg.* (1956) 54:177–91. doi: 10.1017/S0022172400044442
19. Schuffenecker I, Iteman I, Michault A, Murri S, Frangeul L, Vaney MC, et al. Genome microevolution of chikungunya viruses causing the Indian Ocean outbreak. *PLoS Med.* (2006) 3:1058–70. doi: 10.1371/journal.pmed.0030263
20. Volk SM, Chen R, Tsetsarkin KA, Adams AP, Garcia TI, Sall AA, et al. Genome-scale phylogenetic analyses of chikungunya virus reveal independent emergences of recent epidemics and various evolutionary rates. *J Virol.* (2010) 84:6497–504. doi: 10.1128/JVI.01603-09
21. Tsetsarkin KA, Chen R, Leal G, Forrester N, Higgs S, Huang J, et al. Chikungunya virus emergence is constrained in Asia by lineage-specific adaptive landscapes. *Proc Natl Acad Sci.* (2011) 108:7872–7. doi: 10.1073/pnas.1018344108
22. Njenga MK, Nderitu L, Ledermann JP, Ndirangu A, Logue CH, Kelly CHL, et al. Tracking epidemic chikungunya virus into the Indian Ocean from East Africa. *J Gen Virol.* (2008) 89:2754–60. doi: 10.1099/vir.0.2008/005413-0
23. Borgherini G, Poubeau P, Staikowsky F, Lory M, Moullec NL, Becquart JP, et al. Outbreak of chikungunya on reunion island: early clinical and laboratory features in 157 adult patients. *Clin Infect Dis.* (2007) 44:1401–7. doi: 10.1086/517537
24. Tsetsarkin KA, Weaver SC. Sequential adaptive mutations enhance efficient vector switching by chikungunya virus and its epidemic emergence. *PLoS Pathog.* (2011) 7:e1002412. doi: 10.1371/journal.ppat.1002412
25. Tsetsarkin KA, Chen R, Yun R, Rossi SL, Plante KS, Guerbois M, et al. Multi-peaked adaptive landscape for chikungunya virus evolution predicts continued fitness optimization in aedes albopictus mosquitoes. *Nat Commun.* (2014) 5:4084. doi: 10.1038/ncomms5084
26. Rezza G, Nicoletti L, Angelini R, Romi R, Finarelli A, Panning M, et al. Infection with chikungunya virus in Italy: an outbreak in a temperate region. *Lancet.* (2007) 370:1840–6. doi: 10.1016/S0140-6736(07)61779-6
27. Grandadam M, Caro V, Plumet S, Thiberge JM, Souarès Y, Failloux AB, et al. Chikungunya virus, Southeastern France. *Emerg Infect Dis.* (2011) 17:910–3. doi: 10.3201/eid1705.101873
28. Hapuarachchi HC, Bandara KBAT, Sumanadasa SDM, Hapugoda MD, Lai YL, Lee KS, et al. Re-emergence of chikungunya virus in South-east Asia: virological evidence from Sri Lanka and Singapore. *J Gen Virol.* (2010) 91:1067–76. doi: 10.1099/vir.0.015743-0
29. Nhan TX, Musso D. The burden of chikungunya in the Pacific. *Clin Microbiol Infect.* (2015) 21:e47–8. doi: 10.1016/j.cmi.2015.02.018
30. Dupont-Rouzeyrol M, Caro V, Guillaumot L, Vazeille M, D'Ortenzio E, Thiberge J-M, et al. Chikungunya virus and the mosquito vector aedes aegypti in New Caledonia (South Pacific Region). *Vector-Borne Zoonotic Dis.* (2012) 12:1036–41. doi: 10.1089/vbz.2011.0937
31. Cassadou S, Boucau S, Petit-Sinturel M, Huc P, Leparc-Goffart I, Ledrans M. Emergence of chikungunya fever on the French side of Saint Martin island, october to december 2013. *Euro Surveill.* (2014) 19:20752. doi: 10.2807/1560-7917.ES2014.19.13.20752
32. The Pan American Health Organization. *Number of Reported Cases of Chikungunya Fever in the Americas, by Country or Territory Cumulative Cases. Data Source : Cases Reported by IHR NFPs to PAHO / WHO and / or Through Member States Websites or Official News Publication* (2015). Available online at: https://www.paho.org/hq/index.php?option=com_topics&view=readall&cid=5927&Itemid=40931&lang=en (accessed May 15, 2015).
33. Cunha MS, Costa PAG, Correa IA, de Souza MRM, Calil PT, da Silva GPD, et al. Chikungunya virus: an emergent arbovirus to the South American Continent and a continuous threat to the world. *Front Microbiol.* (2020) 11:1297. doi: 10.3389/fmicb.2020.01297
34. Translational Research Consortia (TRC) for Chikungunya Virus in India. Current status of chikungunya in India. *Front Microbiol.* (2021) 12:695173. doi: 10.3389/fmicb.2021.695173
35. Ali I, Dasti JI. Chikungunya virus; an emerging arbovirus in Pakistan. *J Pak Med Assoc.* (2018) 68:252–7.
36. European Centre for Disease Prevention and Control and European Food Safety Authority. *Chikungunya Worldwide Overview* (2021). Available online at: https://www.ecdc.europa.eu/en/chikungunya-monthly (accessed October 19, 2021).
37. Chapman SJ, Hill AVS. Human genetic susceptibility to infectious disease. *Nat Rev Genet.* (2012) 13:175–88. doi: 10.1038/nrg3114
38. Gingles NA, Alexander JE, Kadioglu A, Andrew PW, Kerr A, Mitchell TJ, et al. Role of genetic resistance in invasive pneumococcal infection: identification and study of susceptibility and resistance in inbred mouse strains. *Infect Immun.* (2001) 69:426–34. doi: 10.1128/IAI.69.1.426-434.2001
39. Fellay J, Ge D, Shianna KV, Colombo S, Ledergerber B, Cirulli ET, et al. Common genetic variation and the control of HIV-1 in humans. *PLoS Genet.* (2009) 5:e1000791. doi: 10.1371/journal.pgen.1000791
40. Fellay J, Shianna KV, Ge D, Colombo S, Ledergerber B, Weale M, et al. A whole-genome association study of major determinants for host control of HIV-1. *Science.* (2007) 317:944–7. doi: 10.1126/science.1143767
41. Khor CC, Chau TNB, Pang J, Davila S, Long HT, Ong RTH, et al. Genome-wide association study identifies susceptibility loci for dengue shock syndrome at MICB and PLCE1. *Nat Genet.* (2011) 43:1139–41. doi: 10.1038/ng.960
42. Teng T-S, Kam Y-W, Lee B, Hapuarachchi HC, Wimal A, Ng L-C, et al. A systematic meta-analysis of immune signatures in patients with acute chikungunya virus infection. *J Infect Dis.* (2015) 211:1925–35. doi: 10.1093/infdis/jiv049
43. Ruiz Silva M, van der Ende-Metselaar H, Mulder HL, Smit JM, Rodenhuis-Zybert IA. Mechanism and role of MCP-1 upregulation upon chikungunya virus infection in human peripheral blood mononuclear cells. *Sci Rep.* (2016) 6:32288. doi: 10.1038/srep32288
44. Her Z, Malleret B, Chan M, Ong EKS, Wong SC, Kwek DJC, et al. Active infection of human blood monocytes by chikungunya virus triggers an innate immune response. *J Immunol.* (2010) 184:5903–13. doi: 10.4049/jimmunol.0904181
45. Couderc T, Lecuit M. Chikungunya virus pathogenesis: from bedside to bench. *Antiviral Res.* (2015) 121:120–31. doi: 10.1016/j.antiviral.2015.07.002
46. Gardner CL, Burke CW, Higgs ST, Klimstra WB, Ryman KD. Interferon-alpha/beta deficiency greatly exacerbates arthritogenic disease in mice infected with wild-type chikungunya virus but not with the cell culture-adapted live-attenuated 181/25 vaccine candidate. *Virology.* (2012) 425:103–12. doi: 10.1016/j.virol.2011.12.020
47. Chow A, Her Z, Ong EKS, Chen J, Dimatatac F, Kwek DJC, et al. Persistent arthralgia induced by Chikungunya virus infection is associated with interleukin-6 and granulocyte macrophage colony-stimulating factor. *J Infect Dis.* (2011) 203:149–57. doi: 10.1093/infdis/jiq042
48. Dupuis-Maguiraga L, Noret M, Brun S, Le Grand R, Gras G, Roques P. Chikungunya disease: infection-associated markers from the acute to the chronic phase of arbovirus-induced arthralgia. *PLoS Negl Trop Dis.* (2012) 6:e1446. doi: 10.1371/journal.pntd.0001446
49. Jensen S, Thomsen AR. Sensing of RNA viruses: a review of innate immune receptors involved in recognizing RNA virus invasion. *J Virol.* (2012) 86:2900–10. doi: 10.1128/JVI.05738-11
50. Akira S, Uematsu S, Takeuchi O. Pathogen recognition and innate immunity. *Cell.* (2006) 124:783–801. doi: 10.1016/j.cell.2006.02.015
51. Dias Junior AG, Sampaio NG, Rehwinkel J. A balancing act: MDA5 in antiviral immunity and autoinflammation. *Trends Microbiol.* (2019) 27:75–85. doi: 10.1016/j.tim.2018.08.007
52. Nelemans T, Kikkert M. Viral innate immune evasion and the pathogenesis of emerging RNA virus infections. *Viruses.* (2019) 11:961. doi: 10.3390/v11100961
53. Valdés López JF, Velilla PA, Urcuqui-Inchima S. Chikungunya virus and zika virus, two different viruses examined with a common aim: role of pattern recognition receptors on the inflammatory response. *J Interf Cytokine Res.* (2019) 39:507–21. doi: 10.1089/jir.2019.0058

54. Han J. Myd88 beyond toll. *Nat Immunol.* (2006) 7:370–1. doi: 10.1038/ni0406-370
55. McNab F, Mayer-Barber K, Sher A, Wack A, O'Garra A. Type I interferons in infectious disease. *Nat Rev Immunol.* (2015) 15:87–103. doi: 10.1038/nri3787
56. Levy DE, Marié IJ, Durbin JE. Induction and function of type i and III interferon in response to viral infection. *Curr Opin Virol.* (2011) 1:476–86. doi: 10.1016/j.coviro.2011.11.001
57. Fros JJ, Liu WJ, Prow NA, Geertsema C, Ligtenberg M, Vanlandingham DL, et al. Chikungunya virus nonstructural protein 2 inhibits type I/II interferon-stimulated JAK-STAT signaling. *J Virol.* (2010) 84:10877–87. doi: 10.1128/JVI.00949-10
58. Akhrymuk I, Kulemzin SV, Frolova EI. Evasion of the innate immune response: the old world alphavirus nsP2 protein induces rapid degradation of Rpb1, a catalytic subunit of RNA polymerase II. *J Virol.* (2012) 86:7180–91. doi: 10.1128/JVI.00541-12
59. White LK, Sali T, Alvarado D, Gatti E, Pierre P, Streblow D, et al. Chikungunya virus induces IPS-1-dependent innate immune activation and protein kinase R-independent translational shutoff. *J Virol.* (2011) 85:606–20. doi: 10.1128/JVI.00767-10
60. Dhanwani R, Khan M, Alam SI, Rao PVL, Parida M. Differential proteome analysis of chikungunya virus-infected new-born mice tissues reveal implication of stress, inflammatory and apoptotic pathways in disease pathogenesis. *Proteomics.* (2011) 11:1936–51. doi: 10.1002/pmic.201000500
61. Ziegler SA, Lu L, da Rosa APAT, Xiao S-Y, Tesh RB. An animal model for studying the pathogenesis of chikungunya virus infection. *Am J Trop Med Hyg.* (2008) 79:133–9. doi: 10.4269/ajtmh.2008.79.133
62. Rudd PA, Wilson J, Gardner J, Larcher T, Babarit C, Le TT, et al. Interferon response factors 3 and 7 protect against chikungunya virus hemorrhagic fever and shock. *J Virol.* (2012) 86:9888–98. doi: 10.1128/JVI.00956-12
63. Hawman DW, Stoermer KA, Montgomery SA, Pal P, Oko L, Diamond MS, et al. Chronic joint disease caused by persistent chikungunya virus infection is controlled by the adaptive immune response. *J Virol.* (2013) 87:13878–88. doi: 10.1128/JVI.02666-13
64. Rohatgi A, Corbo JC, Monte K, Higgs S, Vanlandingham DL, Kardon G, et al. Infection of myofibers contributes to increased pathogenicity during infection with an epidemic strain of chikungunya virus. *J Virol.* (2013) 88:2414–25. doi: 10.1128/JVI.02716-13
65. Ozden S, Huerre M, Riviere J-P, Coffey LL, Afonso P V, Mouly V, et al. Human muscle satellite cells as targets of chikungunya virus infection. *PLoS ONE.* (2007) 2:e527. doi: 10.1371/journal.pone.0000527
66. Gardner J, Anraku I, Le TT, Larcher T, Major L, Roques P, et al. Chikungunya virus arthritis in adult wild-type mice. *J Virol.* (2010) 84:8021–32. doi: 10.1128/JVI.02603-09
67. Poo YS, Nakaya H, Gardner J, Larcher T, Schroder WA, Le TT, et al. CCR2 deficiency promotes exacerbated chronic erosive neutrophil-dominated chikungunya virus arthritis. *J Virol.* (2014) 88:6862–72. doi: 10.1128/JVI.03364-13
68. Wauquier N, Becquart P, Nkoghe D, Padilla C, Ndjoyi-Mbiguino A, Leroy EM. The acute phase of chikungunya virus infection in humans is associated with strong innate immunity and T CD8 cell activation. *J Infect Dis.* (2011) 204:115–23. doi: 10.1093/infdis/jiq006
69. Teo T-H, Lum F-M, Lee WWL, Ng LFP. Mouse models for chikungunya virus: deciphering immune mechanisms responsible for disease and pathology. *Immunol Res.* (2012) 53:136–47. doi: 10.1007/s12026-012-8266-x
70. Poo YS, Rudd PA, Gardner J, Wilson JAC, Larcher T, Colle M-A, et al. Multiple immune factors are involved in controlling acute and chronic chikungunya virus infection. *PLoS Negl Trop Dis.* (2014) 8:e3354. doi: 10.1371/journal.pntd.0003354
71. Lee WWL, Teo T-H, Her Z, Lum F-M, Kam Y-W, Haase D, et al. Expanding regulatory T cells alleviates chikungunya virus-induced pathology in mice. *J Virol.* (2015) 89:7893–904. doi: 10.1128/JVI.00998-15
72. Long KM, Ferris MT, Whitmore AC, Montgomery SA, Thurlow LR, McGee CE, et al. γδ T cells play a protective role in chikungunya virus-induced disease. *J Virol.* (2016) 90:433–43. doi: 10.1128/JVI.02159-15
73. Singh RK, Tiwari S, Mishra VK, Tiwari R, Dhole TN. Molecular epidemiology of chikungunya virus: mutation in E1 gene region. *J Virol Methods.* (2012) 185:213–20. doi: 10.1016/j.jviromet.2012.07.001
74. Assunção-Miranda I, Cruz-Oliveira C, Da Poian AT. Molecular mechanisms involved in the pathogenesis of alphavirus-induced arthritis. *Biomed Res Int.* (2013) 2013:1–11. doi: 10.1155/2013/973516
75. Kam YW, Ong EKS, Rénia L, Tong JC, Ng LFP. Immuno-biology of chikungunya and implications for disease intervention. *Microbes Infect.* (2009) 11:1186–96. doi: 10.1016/j.micinf.2009.09.003
76. Alberts B, Johnson A, Lewis J, Raff M, Roberts K, Walter P. *Molecular Biology of the Cell*. New York, NY: Garland Science (2002).
77. Abbas AK, Lichtman AH, Pillai S. *Cellular and Molecular Immunology*. Philadelphia, PA: Elsevier Saunders (2021).
78. Chaaithanya IK, Muruganandam N, Anwesh M, Rajesh R, Ghosal SR, Kartick C, et al. HLA class II allele polymorphism in an outbreak of chikungunya fever in middle andaman, india. *Immunology.* (2013) 140:202–10. doi: 10.1111/imm.12128
79. Sierra B, Alegre R, Pérez AB, García G, Sturn-Ramirez K, Obasanjo O, et al. HLA-A, -B, -C, and -DRB1 allele frequencies in cuban individuals with antecedents of dengue 2 disease: advantages of the cuban population for HLA studies of dengue virus infection. *Hum Immunol.* (2007) 68:531–40. doi: 10.1016/j.humimm.2007.03.001
80. Malavige GN, Rostron T, Rohanachandra LT, Jayaratne SD, Fernando N, De Silva AD, et al. HLA class I and class II associations in dengue viral infections in a Sri Lankan population. *PLoS ONE.* (2011) 6:e20581. doi: 10.1371/journal.pone.0020581
81. Thanapati S, Hande A, Das R, Gurav Y, Tripathy AS. Association of human leukocyte antigen class II allele and haplotypes in chikungunya viral infection in a western Indian population. *Trans R Soc Trop Med Hyg.* (2014) 108:277–82. doi: 10.1093/trstmh/tru030
82. Bouquillard É, Combe B. A report of 21 cases of rheumatoid arthritis following Chikungunya fever. A mean follow-up of two years. *Jt Bone Spine.* (2009) 76:654–7. doi: 10.1016/j.jbspin.2009.08.005
83. Petitdemange C, Wauquier N, Jacquet J-M, Theodorou I, Leroy E, Vieillard V. Association of HLA class-I and inhibitory KIR genotypes in gabonese patients infected by chikungunya or dengue type-2 viruses. *PLoS ONE.* (2014) 9:e108798. doi: 10.1371/journal.pone.0108798
84. Her Z, Teng T-S, Tan JJ, Teo T-H, Kam Y-W, Lum F-M, et al. Loss of TLR3 aggravates CHIKV replication and pathology due to an altered virus-specific neutralizing antibody response. *EMBO Mol Med.* (2015) 7:24–41. doi: 10.15252/emmm.201404459
85. Chaaithanya IK, Muruganandam N, Surya P, Anwesh M, Alagarasu K, Vijayachari P. Association of oligoadenylate synthetase gene cluster and DC-SIGN (*CD209*) gene polymorphisms with clinical symptoms in chikungunya virus infection. *DNA Cell Biol.* (2016) 35:44–50. doi: 10.1089/dna.2015.2819
86. Dutta SK, Tripathi A. Association of toll-like receptor polymorphisms with susceptibility to chikungunya virus infection. *Virology.* (2017) 511:207–13. doi: 10.1016/j.virol.2017.08.009
87. Bouquillard E, Combe B. Rheumatoid arthritis after chikungunya fever: a prospective follow-up study of 21 cases. *Ann Rheum Dis.* (2009) 68:1505–6. doi: 10.1136/ard.2008.097626
88. Doytchinova IA, Flower DRF. In silico identification of supertypes for class II MHCs. *J Immunol.* (2005) 174:7085–95. doi: 10.4049/jimmunol.174.11.7085
89. Guo H-C, Jardetzky TS, Garrettt TPJ, Lane WS, Strominger JL, Wiley DC. Different length peptides bind to HLA-Aw68 similarly at their ends but bulge out in the middle. *Nat.* (1992) 360:364–6. doi: 10.1038/360364a0
90. Gostick E, Cole DK, Hutchinson SL, Wooldridge L, Tafuro S, Laugel B, et al. Functional and biophysical characterization of an HLA-A*6801-restricted HIV-specific T cell receptor. *Eur J Immunol.* (2007) 37:479. doi: 10.1002/eji.200636243
91. Kuiper JJW, Venema WJ. HLA-A29 and birdshot uveitis: further down the rabbit hole. *Front Immunol.* (2020) 11:599558. doi: 10.3389/fimmu.2020.599558
92. Carrington M, Nelson GW, Martin MP, Kissner T, Vlahov D, Goedert JJ, et al. HLA and HIV-1: Heterozygote advantage and B*35-Cw*04 disadvantage. *Science.* (1999) 283:1748–52. doi: 10.1126/science.283.5408.1748
93. Hilton HG, McMurtrey CP, Han AS, Djaoud Z, Guethlein LA, Blokhuis JH, et al. The intergenic recombinant HLA-B∗46:01 has a distinctive peptidome that includes KIR2DL3 ligands. *Cell Rep.* (2017) 19:1394. doi: 10.1016/j.celrep.2017.04.059

94. Kerr JR, Mattey LD, Thomson W, Poulton KV, Ollier WER. Association of symptomatic acute human parvovirus B19 infection with human leukocyte antigen class I and II alleles. *J Infect Dis.* (2002) 186:447–52. doi: 10.1086/341947
95. Gregersen PK, Silver J, Winchester RJ. The shared epitope hypothesis. An approach to understanding the molecular genetics of susceptibility to rheumatoid arthritis. *Arthritis Rheum.* (1987) 30:1205–13. doi: 10.1002/art.1780301102
96. Hov JR, Kosmoliaptsis V, Traherne JA, Olsson M, Boberg KM, Bergquist A, et al. Electrostatic modifications of the human leukocyte antigen-DR P9 peptide-binding pocket and susceptibility to primary sclerosing cholangitis. *Hepatology*. (2011) 53:1967–76. doi: 10.1002/hep.24299
97. Matzaraki V, Kumar V, Wijmenga C, Zhernakova A. The MHC locus and genetic susceptibility to autoimmune and infectious diseases. *Genome Biol.* (2017) 18:76. doi: 10.1186/s13059-017-1207-1
98. Ercolini AM, Miller SD. The role of infections in autoimmune disease. *Clin Exp Immunol.* (2009) 155:1–15. doi: 10.1111/j.1365-2249.2008.03834.x
99. Schilte C, Couderc T, Chretien F, Sourisseau M, Gangneux N, Guivel-Benhassine F, et al. Type I IFN controls chikungunya virus via its action on nonhematopoietic cells. *J Exp Med*. (2010) 207:429–42. doi: 10.1084/jem.20090851
100. Gao Y, Guo J, Zhang F, Guo Z, Zhang LR, Wang T, et al. Evaluation of neonatal toll-like receptors 3 (c.1377C/T) and 9 (G2848A) gene polymorphisms in HBV intrauterine transmission susceptibility. *Epidemiol Infect.* (2015) 143:1868–75. doi: 10.1017/S0950268814002921
101. Kawasaki A, Furukawa H, Kondo Y, Ito S, Hayashi T, Kusaoi M, et al. TLR7 single-nucleotide polymorphisms in the 3' untranslated region and intron 2 independently contribute to systemic lupus erythematosus in Japanese women: a case-control association study. *Arthritis Res Ther.* (2011) 13:R41. doi: 10.1186/ar3277
102. Møller-Larsen S, Nyegaard M, Haagerup A, Vestbo J, Kruse TA, Børglum AD. Association analysis identifies TLR7 and TLR8 as novel risk genes in asthma and related disorders. *Thorax.* (2008) 63:1064–9. doi: 10.1136/thx.2007.094128
103. Wang C-H, Eng H-L, Lin K-H, Chang C-H, Hsieh C-A, Lin Y-L, et al. TLR7 and TLR8 gene variations and susceptibility to hepatitis C virus infection. *PLoS ONE.* (2011) 6:e26235. doi: 10.1371/journal.pone.0026235
104. Wang C-H, Eng H-L, Lin K-H, Liu H-C, Chang C-H, Lin T-M. Functional polymorphisms of TLR8 are associated with hepatitis C virus infection. *Immunology*. (2014) 141:540–8. doi: 10.1111/imm.12211
105. Wang CM, Chang SW, Wu YJJ, Lin JC, Ho HH, Chou TC, et al. Genetic variations in toll-like receptors (TLRs 3/7/8) are associated with systemic lupus erythematosus in a Taiwanese population. *Sci Rep*. (2014) 4:3792. doi: 10.1038/srep03792
106. Gantier MP, Irving AT, Kaparakis-Liaskos M, Xu D, Evans VA, Cameron PU, et al. Genetic modulation of TLR8 response following bacterial phagocytosis. *Hum Mutat*. (2010) 31:1069–79. doi: 10.1002/humu.21321
107. Oh DY, Taube S, Hamouda O, Kücherer C, Poggensee G, Jessen H, et al. A functional toll-like receptor 8 variant is associated with HIV disease restriction. *J Infect Dis*. (2008) 198:701–9. doi: 10.1086/590431
108. Silverman RH. Viral encounters with 2′,5′-oligoadenylate synthetase and RNase L during the interferon antiviral response. *J Virol.* (2007) 81:12720–9. doi: 10.1128/JVI.01471-07
109. Malathi K, Paranjape JM, Bulanova E, Shim M, Guenther-Johnson JM, Faber PW, et al. A transcriptional signaling pathway in the IFN system mediated by 2′-5′-oligoadenylate activation of RNase L. *Proc Natl Acad Sci U S A*. (2005) 102:14533–8. doi: 10.1073/pnas.0507551102
110. Bonnevie-Nielsen V, Field LL, Lu S, Zheng DJ, Li M, Martensen PM, et al. Variation in antiviral 2′,5′-oligoadenylate synthetase (2′5′AS) enzyme activity is controlled by a single-nucleotide polymorphism at a splice-acceptor site in the OAS1 gene. *Am J Hum Genet.* (2005) 76:623–33. doi: 10.1086/429391
111. Alagarasu K, Damle IM, Bachal RV, Mulay AP, Shah PS, Dayaraj C. Association of promoter region polymorphisms of CD209 gene with clinical outcomes of dengue virus infection in Western India. *Infect Genet Evol.* (2013) 17:239–42. doi: 10.1016/j.meegid.2013.04.024

Conflict of Interest: The authors declare that the research was conducted in the absence of any commercial or financial relationships that could be construed as a potential conflict of interest.

Publisher's Note: All claims expressed in this article are solely those of the authors and do not necessarily represent those of their affiliated organizations, or those of the publisher, the editors and the reviewers. Any product that may be evaluated in this article, or claim that may be made by its manufacturer, is not guaranteed or endorsed by the publisher.

Advantages of publishing in Frontiers

OPEN ACCESS
Articles are free to read for greatest visibility and readership

FAST PUBLICATION
Around 90 days from submission to decision

HIGH QUALITY PEER-REVIEW
Rigorous, collaborative, and constructive peer-review

TRANSPARENT PEER-REVIEW
Editors and reviewers acknowledged by name on published articles

Frontiers
Avenue du Tribunal-Fédéral 34
1005 Lausanne | Switzerland

Visit us: www.frontiersin.org
Contact us: frontiersin.org/about/contact

REPRODUCIBILITY OF RESEARCH
Support open data and methods to enhance research reproducibility

DIGITAL PUBLISHING
Articles designed for optimal readership across devices

FOLLOW US
@frontiersin

IMPACT METRICS
Advanced article metrics track visibility across digital media

EXTENSIVE PROMOTION
Marketing and promotion of impactful research

LOOP RESEARCH NETWORK
Our network increases your article's readership